

http://researchcommons.waikato.ac.nz/

Research Commons at the University of Waikato

Copyright Statement:

The digital copy of this thesis is protected by the Copyright Act 1994 (New Zealand).

The thesis may be consulted by you, provided you comply with the provisions of the Act and the following conditions of use:

- Any use you make of these documents or images must be for research or private study purposes only, and you may not make them available to any other person.
- Authors control the copyright of their thesis. You will recognise the author's right to be identified as the author of the thesis, and due acknowledgement will be made to the author where appropriate.
- You will obtain the author's permission before publishing any material from the thesis.

Petrogenesis of Pliocene limestones in southern Hawke's Bay, New Zealand: a contribution to unravelling the sequence stratigraphy and diagenetic pathways of cool-water shelf carbonate facies

A thesis
submitted in fulfilment
of the requirements for the degree
of
Doctor of Philosophy in Earth Sciences
at the
University of Waikato



The University of Waikato
Te Whare Wānanga o Waikato

by

Vincent Caron

THE UNIVERSITY OF WAIKATO
HAMILTON, NEW ZEALAND
2002

We have forgotten to observe. Instead of observing, we do things according to patterns.
Andrei Tarkovsky

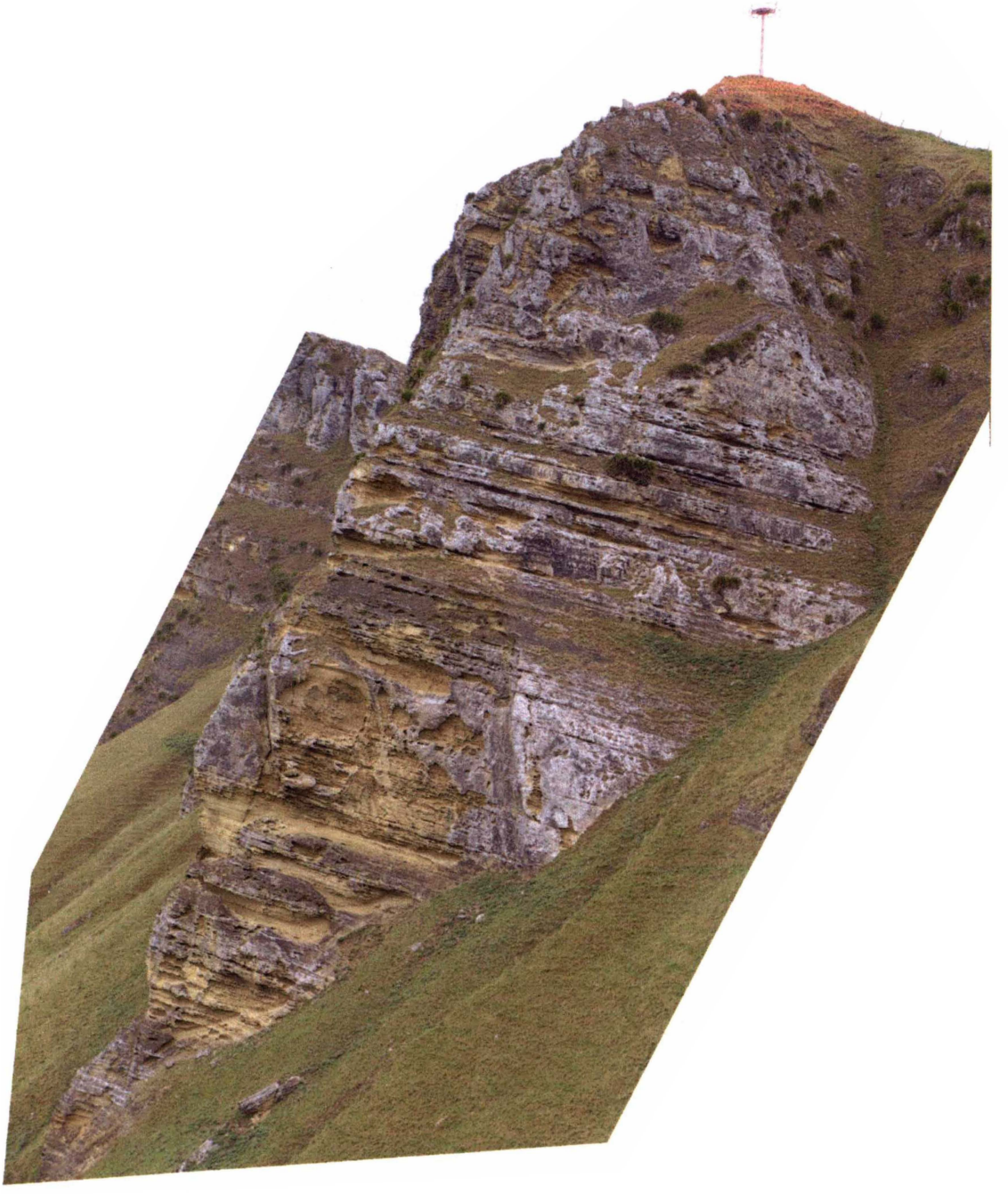

Te Mata Peak Section (~ 120 m high), Awapapa Limestone (Waipipian, mid-Pliocene), see Appendix 1 - column 9-A2 (Photo by Arne Pallentin).

ABSTRACT

Among carbonate sedimentologists, it is now appreciated that shallow-marine carbonates are not restricted to warm-water tropical settings, but can also be produced on modern cool-water shelves outside tropical latitudes. In the last two decades, many publications have not only advanced our knowledge about modern non-tropical carbonates, but have documented ancient skeletal limestones that are fossil analogues of these modern deposits. While the broad environmental and sedimentary characteristics of non-tropical deposits are becoming well established, the nature, timing, and relative importance of the various diagenetic processes affecting their evolution into limestones are yet to be fully appreciated, a topic addressed in the present study.

In New Zealand, the Plio-Pleistocene (5-1.5 Ma) Te Aute limestones in southern Hawke's Bay (eastern North Island) are non-tropical in origin, and formed in shoal areas about the margins of a forearc basin seaway adjacent to the convergent Pacific-Australian Plate boundary. Because of the dynamic tectonic setting, which led to narrowing and shallowing of the host basin over time, the studied carbonates exhibit a variety of sedimentary facies (i.e., from pure coquina to mixed carbonate-siliciclastic) and mineralogical signatures (i.e., calcite- to, more rarely, aragonite-dominated), and have undergone varying degrees of burial before being uplifted to their present position. As such, the Te Aute deposits provide a unique opportunity to: (1) decipher the suite of processes that have altered their texture and composition through time; (2) address the questions of what likely regional and more global parameters, namely tectonics and eustasy, may have driven diagenetic pathways, and how this occurred; and (3) more generally advance fundamental knowledge about models of porosity evolution in non-tropical carbonates.

The present study integrates the combined results of detailed field investigations with a variety of analytical techniques, including standard, stained, and cathodoluminescence (CL) microscopic examinations of rock thin-sections, X-ray diffraction (XRD), and elemental (ICP-OES and microprobe) and stable isotope ($\delta^{18}O$ and $\delta^{13}C$) geochemistry.

Sedimentologic analysis has identified 14 different facies types that correspond to a spectrum of depositional settings associated with both continent-attached shelves

and isolated upthrust-cored antiforms within the forearc seaway. Facies are representative of environments ranging from below storm-wave base, in outer shelf-type locations, to predominantly shallow-water shoreface-type conditions under the influence of strong tidal current flows and storm waves.

A new petrographic approach for studying cool-water carbonate diagenesis has been developed. The method entails recording the high-resolution chronological occurrence of all diagenetic features within samples, and noting their vertical and lateral distribution within sedimentary formations. It is demonstrated that the attributes of pre-compaction diagenetic suites between consecutive sedimentary discontinuities change vertically in relation to the stacking of depositional facies. This original approach, by also revealing marine-cemented condensed horizons and key surfaces otherwise unrecognized in the field, has helped unlock the cryptic sedimentary architecture within the limestones. Thus, the Te Aute deposits appear to be constructed of metre-scale (1-15 m) sequences that could be integrated into a sequence stratigraphic scheme, emphasizing that not only the production and deposition, but also the diagenesis of these carbonate deposits, were forced by glacio-eustatically and tectonically-driven processes.

In order to better explain the probable progression of diagenetic environments that moved through Te Aute limestones, concepts that classically underpin the sequence stratigraphic analysis of sedimentary successions have been used to group cement zones, revealed under cathodoluminescent (CL) light, into diagenetic discontinuity-bounded CL sequences. In most Pliocene limestones, the procedure, in combination with geochemical data, has: (1) identified recurring and correlative motifs of pre- and post-compaction CL sequence stratigraphies; (2) enabled regional mapping of CL sequences; (3) highlighted the spatial geometry and timing of emplacement of cementing aquifers; and (4) led to the construction of paleohydrologic models, invoking location of recharge areas and fluid-flow directions. Pre-compaction CL sequences formed locally from marine and more widely from oxidized meteoric (or mixed marine-meteoric) waters after exposure of limestone caps due to relative drops in sea level. Post-compaction burial CL sequences precipitated from reduced fluids recharged from areas of basin margin exposure, while the next CL sequences in the chronological suite are related to the ingress of oxidized meteoric waters as a result of uplift.

ACKNOWLEDGEMENTS

I have been fortunate and honoured to work under the supervision of Prof. Cam Nelson whose personal support and scientific guidance have significantly contributed to leading this thesis to completion. I would also like to thank Cam for careful reviews, editing, and constructive criticism of draft versions of the thesis chapters. I also wish to thank my second supervisor, Prof. Peter Kamp, for helpful comments and encouragement throughout the study.

I take this opportunity to express my gratitude to Paul Bernier (Lyon, France) who introduced me to carbonate diagenesis, and kept encouraging me over the years and always showed great interest in my work.

I also extend my gratitude to the many farmers and shepherds who, without exception, readily granted permission for access to their land and shared their knowledge of the unique Hawke's Bay landscape and its hazards.

In the three years prior to coming to New Zealand, and during the three years of this study, I have benefited from the enormous field experience of many geologists. I respectfully acknowledge this expertise, and in particular mention Bertrand Keraudren (France) and Dave Francis (New Zealand).

I am also most appreciative of the field guidance and expertise on Pliocene macrofauna provided by Alan Beu (GNS, Lower Hutt) whose initial work on the Te Aute deposits provided the regional stratigraphic basis on which this study was built. Special thanks also go to Austin Hendy and Rochelle Hansen for helping with macrofaunal and microfaunal determinations, respectively.

I express my appreciation to Steven Hood for sharing his knowledge of the diagenesis of the Te Aute limestones and for assistance in the "CL" room, and to Brian Ricketts, George Dix, Colin Mazengarb, Brad Field, Kyle Bland, and Adam Vonk for their interest, advice, and encouragement. I also thank Roger Briggs, Chairperson of Earth Sciences, for his support of this study.

This work was supported by the technical assistance of Renat Radosinsky, Annette Rodgers, and Sydney Wright, by Geoff Kilgour for rock slabbing, by Franziska Schellenberg for ICP-OES analysis, by Viviane Simard-Caron for XRD analysis and chemical staining, by Arne Pallentin for microprobe analysis, and by Helen Turner (University of Waikato), Karyn Rodgers (GNS), and Helen Neil (NIWA) for stable isotopic analysis. I thank all these people for their contribution.

A very special thanks goes to Margaret Nelson and Penelope Cooke for their support and kindness, and to Frank Bailey for his "gentillesse".

I am very much indebted to my room colleague Arne Pallentin for his many involvements in various aspects of the thesis. Not only has Arne provided assistance and advice in the field, and played an important part in the development of the ideas presented in this study, but also he has been a very appreciated companion outside the university walls.

Funding assistance for this study came from Marsden Fund contract UOW801 to the University of Waikato. I am indebted to the Marsden Fund for the provision of a scholarship supporting my living expenses while in New Zealand.

Ecrasés sous les formules chirurgicales, quelques mots aux résonnances familières pour exprimer ma reconnaissance, mon affection et mon amitié à celles et ceux qui nous ont apporté leur soutien à Viviane et à moi, exilés pour un trop long temps à mon goût sur un radeau du Pacifique Sud. Merci à vous qui avez su gardé le regard clair, compagnons de voyage, compagnons des mystères, frères voyants, soeurs de coeur, picards et bourguignons, franc-comtois, jurassiens, mosellans, ici et ailleurs.

Merci à mes parents pour leur amour, leurs encouragements, et surtout pour m'avoir appris la liberté. Une volée de pensées pour Virginie, puissent les vents les porter jusqu'à ton île de l'Atlantique.

Enfin, pour toi l'orchidée perchée dans les falaises d'Hawke's Bay, ma confidente, mon amante, mon aimante, je pose un baiser où tu sais.

CONTENTS

Abstract i
Acknowledgements iii
Table of contents v
Prologue xii

Chapter 1

STRATIGRAPHIC SEDIMENTOLOGY OF COOL-WATER PLIO-PLEISTOCENE LIMESTONES IN SOUTHERN HAWKE'S BAY, NEW ZEALAND

Abstract 1
1. Introduction 2
2. Geological and tectonic setting of the Plio-Pleistocene successions 5
3. Methods 7
    3.1. Sedimentary nomenclature 9
    3.2. Geological age: Early Pliocene (Opoitian) to Early Pleistocene (late Nukumaruan) 9

4. Lithostratigraphy 11
    4.1. Kairakau Limestone (Opoitian) 11
    4.2. Tuki Bell limestone (informal) 17
    4.3. Awapapa Limestone (Waipipian) 18
    4.4. Rotookiwa Limestone (Waipipian) 20
    4.5. Te Onepu Limestone (Mangapanian) 25
    4.6. Mason Ridge Formation (Nukumaruan) 30
    4.7. Flag Range Limestone (Nukumaruan) 37
    4.8. Matapiro Limestone (Nukumaruan) 39
    4.9. Titiokura Formation (Waipipian) 42
    4.10. Te Waka Formation (Mangapanian) 44
    4.11. Whanawhana Limestone (Nukumaruan) 48
    4.12. Sentry Box Limestone (Nukumaruan) 50
    4.13. Kereru Limestone (Nukumaruan) 52

5. Sedimentary facies 53
    5.1. Bioclastic rudstone facies (B1a, B1b, B1c, B1d) 54
    5.2. Bioclastic grainstone facies: clast-supported facies B2a and B2b 61
    5.3. Bioclastic packstone facies: mud-supported facies B3a and B3b 63
    5.4. Mixed carbonate-siliciclastic facies: interbedded grainstones and packstones (M1), interbedded grainstones and terrigenous packstones (M2), and interbedded packstones and calcareous sandstones (M3) 64
    5.5. Siliciclastic facies: S1, S2, and S3 facies 66

6. Skeletal and microfacies assemblages 69
    6.1. Skeletal assemblages 69
    6.2. Microfacies assemblages 70

6.3. Evolution of microfacies contribution to the Plio-Pleistocene limestones with time 73
6.4. XRD-ICPOES data for calcium carbonate and calcium content 75

7. The depositional model 77
7.1. Eastern setting 77
7.2. Western setting 79

8. Conclusions 81
References 85

Chapter 2

DEVELOPING CONCEPTS OF HIGH-RESOLUTION DIAGENETIC STRATIGRAPHY FOR COOL-WATER LIMESTONES: APPLICATION TO PLIOCENE TE AUTE LIMESTONES, NEW ZEALAND, AND THEIR SEQUENCE STRATIGRAPHY

Abstract 88
1. Introduction 89
2. Geological framework 90
3. Methods 96
4. Concept of diagenetic stratigraphy 96
4.1. The diagenetic sequence diagram 98
4.2. Cathodoluminescence (CL) zones and subzones 98
4.3. CL sequences 99
4.4. Diagenetic stratigraphy and sequence stratigraphy 101

5. Diagenetic stages: eogenesis-mesogenesis-telogenesis versus pre- and post-compaction terminology 102
5.1. Early diagenesis – eogenesis 102
5.2. Burial diagenesis – mesogenesis 103
5.2.1. Mechanical compaction 103
5.2.2. Chemical compaction 104
5.2.3. Pressure-dissolution and cementation 106
5.3. Late diagenesis – telogenesis 106
5.4. Pre- and post-compaction diagenesis 107
5.4.1. Specific diagenesis and pre-compaction diagenesis 108
5.4.2. Specific diagenesis and diagenetic overprint 115

6. Application of diagenetic stratigraphy concepts to Te Aute limestones 116
6.1. Patterns of pre-compaction diagenesis 116
6.1.1. Specific diagenetic patterns in metre-scale sequences 116
6.1.2. Diagenetic overprints cross sequence-bounding unconformities 123
6.2. Comment on post-compaction diagenesis 125

7. Conclusions 125
References 128

Chapter 3

DIAGENESIS OF COOL-WATER PLIO-PLEISTOCENE LIMESTONES IN SOUTHERN HAWKE'S BAY, NEW ZEALAND

Abstract 133
1. Introduction 135
2. Analytical techniques 138
2.1. Sampling 139
2.2. X-ray diffraction 139
2.3. Chemical staining 140
2.4. Cathodoluminescence 140
2.4.1. Principles 140
2.4.2. Chemical considerations 141
2.4.3. Use of cathodoluminescence in carbonate diagenetic studies 142
2.5. Isotopic analysis 143
2.5.1. Principles 143
2.5.2. Brachiopods and seawater composition 144
2.6. Trace elements 145

3. Times and environments of carbonate diagenesis 145
3.1. Diagenetic environments 145
3.2. Diagenetic stages 147

4. Diagenetic products and processes 148
4.1. Early fine acicular precipitate 148
4.1.1. Description 148
4.1.2. Diagenetic environment 149
4.2. Early inclusion-rich cement 149
4.2.1. Petrography of early turbid cements 149
4.2.2. Petrography of turbid syntaxial overgrowths 152
4.2.3. Stratigraphic position of inclusion-rich cements 155
4.2.4. Precursor mineralogy of inclusion-rich cements 155
4.2.5. Diagenetic environment 162
4.3. Clear spar cements 168
4.3.1. Cement types 168
4.3.2. Compositional zoning of clear spar cements 169
4.3.3. Chemical staining versus cathodoluminescence 170
4.3.4. Growth patterns 170
4.3.5. Pre- and post-compaction clear spar cements: PrC, PoFC, and YnfC 170
4.3.6. Diagenetic environment for PrC, PoFC, and YnfC cements 176
4.3.7. Pseudo-PrC: early blocky and "lozenge-shaped" isopachous sparry calcite 185
4.3.8. Needle cement 186
4.4. Internal sediments 189
4.4.1. Internal sediment types 189
4.4.2. Origin and evolution of the geopetal microfabrics 190
4.4.3. Microclastic internal sediments 191
4.4.4. Micropeloidal internal sediment 194

4.5. Cryptocrystalline meniscus-type cements, irregular micrite bindings, and micrite envelopes 195
4.6. Dissolution 196
4.6.1. Unaltered material 197
4.6.2. Preserved mineralogy with evidence of chemical alteration 198
4.6.3. Original mineralogy relics in neomorphic calcite 201
4.6.4. Neomorphosed skeletons with the retention of microstructures 201
4.6.5. Mouldic or "ghost" fabrics 202
4.6.6. What controls the different modes of Mg-calcite (IMC-HMC) and aragonite neomorphism? 203
4.7. Bioactivity: biological alteration and encrustation 208
4.7.1. Bioerosion 208
4.7.2. Encrustation 212
4.8. Mechanical abrasion 212
4.9. Non-carbonate cement: Glauconite and iron-oxides 213
4.10. Compaction features 214
4.10.1. Mechanical compaction 214
4.10.2. Chemical compaction 215
4.10.3. Pressure-dissolution and cementation 217
4.11. Diagenetic sequence diagrams 219

5. Carbonate diagenesis and relative sea-level changes 219
5.1. Sequence stratigraphic framework 221
5.2. Depositional setting for the Te Aute carbonates (Opoitian to early Nukumaruan) 223
5.3. Carbonate diagenesis on a high-frequency sequence scale 224
5.3.1. Carbonate diagenesis model of isolated antiforms during a relative sea-level rise: TST 228
5.3.2. Carbonate diagenesis model of isolated antiforms during a sea-level highstand: HST 232
5.3.3. Carbonate diagenesis model of isolated antiforms during a sea-level fall: RST 232
5.3.4. Carbonate diagenesis model of isolated antiforms during subaerial exposure: LST 233
5.3.5. Drowning and termination of carbonate factories 237

6. Conclusions 239
References 244

Chapter 4

INTERRELATIONSHIPS BETWEEN THE PETROGENESIS AND HIGH-RESOLUTION SEQUENCE STRATIGRAPHY OF THE PLIOCENE COOL-WATER LIMESTONES IN SOUTHERN HAWKE'S BAY, NEW ZEALAND

Abstract 254
1. Introduction 258
2. Geological and tectonic setting of the Pliocene successions 260
3. Diagenetic approach 261
3.1. Destructive versus constructive diagenesis 262
3.2. Specific diagenesis 262

4. Sequence stratigraphic approach 264
4.1. Preamble 264
4.2. Sequence stratigraphic concepts applied to the Te Aute carbonate successions 268
4.3. Modelling of the diagenetic signature of carbonate facies: an attempt to predict the diagenesis of unsampled horizons 269

5. Facies architecture, diagenesis, and sequence stratigraphy of the Pliocene sequences 271
5.1. Introduction 271
5.2. Sequence architecture 272
5.3. Key surfaces 275
5.3.1. Transgressive surface of erosion (TSE) 275
5.3.2. Maximum flooding surface (Mfs) versus mid-sequence horizon of maximum diagenetic condensation (Cdh) 279
5.3.3. Regressive surface of erosion (TSE) 281
5.3.4. Subaerially exposed surfaces 284
5.3.5. Discussion: Key surfaces and Sequence Boundary 286
5.4. Systems tracts: TST, HST, RST, FRST, LST 289
5.4.1. Transgressive systems tracts (TST) 290
5.4.2. Highstand systems tracts (HST) 291
5.4.3. Regressive systems tracts (RST) 291
5.4.4. Forced regressive systems tract (FRST) 293
5.4.5. Lowstand systems tract (LST) 293
5.4.6. Microfacies stacking within the fundamental sequence 294
5.5. Diagenetic and facies motifs in sedimentary sequences 294
5.5.1. Motif 1 295
5.5.2. Motif 2 295
5.5.3. Motif 3 295
5.5.4. Motif 4 296

6. Hypothetical framework to account for the stacking of the Pliocene sequences 296
6.1. Multiple working hypotheses 296
6.2. Tectonic forcing 298
6.3. Internal processes 298
6.4. Glacio-eustatic forcing 299

7. Sequences in the eastern limestone occurrences from late Opoitian to early Nukumaruan 300
7.1. Kairakau Limestone (late Opoitian) 300
7.1.1. Introduction 300
7.1.2. Description of the main subdivisions and their bounding surfaces 301
7.1.3. Carbonate production development within a sequence stratigraphic framework 306
7.2. Awapapa Limestone (early Waipipian) 308
7.2.1. Introduction 308
7.2.2. Description of the main subdivisions and their bounding surfaces 309
7.2.3. Carbonate production development within a sequence stratigraphic framework 311
7.3. Rotookiwa Limestone (late Waipipian) 315
7.3.1. Introduction 315
7.3.2. Description of the main subdivisions and their bounding surfaces 316

7.3.3. Carbonate production development within a sequence stratigraphic framework 318
7.4. Te Onepu Limestone (Mangapanian-early Nukumaruan) 320
7.4.1. Introduction 320
7.4.2. Description of the main subdivisions and their bounding surfaces 320
7.4.3. Carbonate production development within a sequence stratigraphic framework 321
7.5. Mason Ridge Formation (Nukumaruan) 325
7.5.1. Introduction 325
7.5.2. Description of the main subdivisions and their bounding surfaces 327
7.5.3. Summary of attributes identifying systems tracts in the Mason Ridge Formation 328
7.5.4. *Carbonate production development within a sequence stratigraphic framework* 330
7.5.5. Correlation across Ngaruroro River 331

8. Te Aute sedimentary sequences periodicities 334
8.1. Periodicity approximates 334
8.2. Pliocene climate variability from the isotopic record 334

9. Sequence development and syndepositional tectonic overprint 335
10. Conclusions 337
References 342

Chapter 5

DIAGENETIC SEQUENCE STRATIGRAPHY OF CALCITE CEMENT SUCCESSIONS IN PLIOCENE TE AUTE COOL-WATER LIMESTONES, SOUTHERN HAWKE'S BAY, NEW ZEALAND

Abstract 349
1. Introduction 351
2. Analytical methods 354
2.1. Chemical staining 354
2.2. Cathodoluminescence (CL) 354
2.3. Trace elements 355
2.4. Isotopic analysis 356

3. Concept of CL sequence stratigraphy 357
3.1. Introduction 357
3.2. CL sequences 358
3.3. Diagenetic discontinuities 359
3.3.1. Fractures 359
3.3.2. Dissolution surfaces 364
3.3.3. Renucleation surfaces 364
3.3.4. Summary of general attributes of diagenetic discontinuity surfaces 365

4. Application of the concept of CL sequence to the Te Aute limestones 365
4.1. Setting 366
4.2. CL sequences in the Early Pliocene cool-water Kairakau Limestone 367
4.2.1. Pre-d1 CL sequence (KZ) 368

4.2.2. Post-d1/Pre-d2 CL sequence (KA) 370
4.2.3. Post-d2/Pre-d3 CL sequence (KB) 373
4.2.4. Post-d3/Pre-d4 CL sequence (KC) 379
4.2.5. Post-d4 CL sequence (KD) 381
4.3. Discussion and interpretation 381
4.3.1. Regional distribution of CL sequences 381
4.3.2. Trace elements 386
4.3.3. Stable isotope data 393
4.4. Cementation history of Kairakau Limestone and origin of CL sequences 397
4.5. Comparability of diagenetic pathways for the Kairakau and Awapapa Limestones 398
4.5.1. Cementation within the Kairakau and Awapapa units 398
4.5.2. Timing of formation of CL sequences 401
4.5.3. Configuration of the burial CL sequence 402
4.5.4. Configuration of the telogenetic CL sequence 408
4.5.5. Diagenetic and fluid flow pathways 408
4.6. Comment on the CL attributes of the Waipipian-Mangapanian limestones on the western margin of the forearc basin 409

5. Sequence stratigraphic approach to cool-water carbonate diagenesis of the Te Aute Pliocene limestones 410
5.1. Introduction 410
5.2. CL sequence geometries 414
5.2.1. CL sequences within Pliocene limestones 414
5.2.2. Architecture of the Pliocene CL sequences 414
5.3. Modelling the diagenetic sequence stratigraphy of the Te Aute Pliocene carbonates: principles and definitions 421
5.3.1. Definition of diagenetic (CL) sequences 421
5.3.2. Type-A diagenetic sequence boundary 422
5.3.3. Type-B diagenetic sequence boundary 422
5.3.4. Pre-compaction type-a and type-b diagenetic discontinuities 423
5.3.5. Post-compaction type-c and type-d diagenetic discontinuities 423
5.4. Transgressive-regressive CL megasequences 426
5.4.1. Pre-compaction transgressive-regressive CL sequence 426
5.4.2. Post-compaction transgressive-regressive CL sequence 428
5.5. Variations in the attributes of CL sequences across their distribution area 429

6. Conclusions 430
References 434

Epilogue 439

Appendices – contained in the accompanying volume and on CD1.

PROLOGUE

The traditional scientific approach to carbonate sedimentology and carbonate diagenesis has been founded mainly on the study of processes and products occurring in warm shallow seas of tropical regions, which subsequently served as a tool for interpreting most limestones in the rock record (e.g., Bathurst, 1975; Tucker and Wright, 1990; Moore, 2001). However, there is now wide acceptance that modern shelf carbonates can also be widespread in cool-water shelf settings at mid- to high latitudes beyond about 30° North and South (e.g., Nelson, 1988; James and Clarke, 1997). Although the relatively more recent results of temperate carbonate research have provided new perspectives for correctly assessing the origin and significance of all ancient shelf limestones, the diagenesis of these cool-water carbonates, involving alteration and cementation of their constituents, both in surficial and burial environments, remains a poorly documented field.

Among other attributes, the relatively stable calcite mineralogy (i.e., low- and intermediate-Mg calcite) of cool-water carbonates, the rather destructive nature (dissolution, abrasion, bioerosion) of sea-floor diagenesis, and the relatively low carbonate production rates in cool-water settings, distinguish them from the preponderance of metastable minerals (i.e., high-Mg calcite and aragonite) in tropical carbonates that form at high production rates in environments where sea-floor constructive diagenesis (cementation) can be pervasive. This incomparability of processes and mineralogical composition is likely to determine contrasting diagenetic pathways within tropical and non-tropical environments. In this context, therefore, the applicability of known diagenetic concepts and models for all carbonate sediments, which are mostly derived from tropical examples, is questionable.

In New Zealand, the Plio-Pleistocene limestones in southern Hawke's Bay of eastern North Island, informally referred to here as the Te Aute limestones, are non-tropical deposits comprising typically barnacle and epifaunal mollusc-dominated carbonates formed in shoal areas about the margins of a forearc basin seaway, immediately inboard of the convergent Pacific-Australian Plate boundary located just off eastern North Island. Because of the dynamic tectonic setting, which resulted in the progressive narrowing and shallowing of the host basin over time and afforded

diversified depositional settings, the studied carbonates exhibit a variety of sedimentary facies (i.e., from pure coquina to mixed carbonate-siliciclastic) and mineralogical signatures (i.e., calcite- to, more rarely, aragonite-dominated).

Reconnaissance petrographic studies (Hood and Nelson, 1996) showed that the Te Aute limestones bear a remarkable array of diagenetic features, testimony to their journey from the sea floor (marine), through pre-burial meteoric (subaerial exposure) to burial, and post-burial meteoric (uplift) diagenetic environments. Moreover, it has been suggested that the cyclical interbedding of the limestones with siliciclastic deposits may be related to astronomically-forced sea-level fluctuations during the Plio-Pleistocene (Beu, 1995; Haywick, 2000).

Although limestones have been buried to different levels in the basin, portions of most units have been differentially uplifted because of crustal movements, and are now well exposed at the surface, thereby providing a unique field laboratory for understanding and predicting pathways and timing of carbonate diagenesis in non-tropical carbonates in relation to patterns of relative sea-level changes and regional tectonics.

This study investigates, on a range of scales (basin, outcrop, microscopic), the external (climate, tectonic, eustasy) and internal (skeletal composition, geochemistry, porosity) controls that have acted to build up the non-tropical Te Aute carbonate successions, and that, through fluid-rock interactions, have diagenetically transformed the carbonate sediments into limestones. In this context, the principal objectives of the present study are:

(1) To construct detailed stratigraphic columns through the many limestone units to determine their stratigraphic, faunal, and sedimentologic characteristics, and to assess vertical facies changes in the columns and the occurrence of intra- and inter-formational unconformities as a basis for making regional correlations and defining the internal architecture of the limestone units.

(2) To document diagenetic features and establish their environmental origin in a chronological framework, and thus determine the history of skeletal mineral alteration

and cementation in each limestone unit as a basis for making comparisons between limestones of different ages.

(3) To use cement stratigraphy to trace the geochemical evolution of the fluids responsible for the diagenetic changes, and subsequently to relate this paragenesis to regional paleohydrologic systems and patterns of relative sea-level changes associated with local tectonic movements and/or global glacio-eustasy.

(4) To integrate the full spectrum of diagenetic features and processes for the Te Aute limestones into a comprehensive model of diagenetic evolution within a modern sequence stratigraphic framework.

The thesis is formatted into five chapters bounded by this prologue and a concluding epilogue. From the outset an intention was to develop each of the chapters as essentially stand alone extended articles having the potential for future publication. Hence each chapter has its own abstract, introduction, conclusions, and reference section, along with the main body of text, figures, and tables. As a consequence of this approach a certain degree of repetition has been unavoidable, especially with respect to aspects of geological setting and locality information.

Three matters relating to reader convenience are mentioned here. First, a few key diagrams in particular chapters are repeated as fold outs contained in the pocket inside the back cover of the thesis. This enables the interested person to have ready access to those diagrams, if desired, while reading the text. Second, considering the wide scope of the study, the number of formations involved, and the nature of the diagenetic approach, some guidance is offered the reader at the title page of each chapter regarding the most relevant or key sections, figures, and tables in the chapter. These enable the philosophical and scientific outcomes of the study to be appreciated without necessarily reading in detail the more lengthy and sometimes tedious, but otherwise essential descriptive information in the chapters such as, for example, the descriptive attributes of facies, diagenetic fabrics, and limestone internal architectures. Third, the Appendices for this thesis are included as hard copy in the accompanying volume, but numerical data (i.e., point-counting and geochemical data) are also reproduced in convenient form on a CD-ROM (CD1) contained in the back pocket.

Chapter 1 outlines the setting of the Plio-Pleistocene Te Aute limestones in southern Hawke's Bay, presents general descriptions of the different lithologic units, and describes and interprets the sedimentary facies distinguished within them. Six mixed carbonate-siliciclastic (petrographic) microfacies assemblages are defined. Results are used to propose two depositional models for the carbonates deposited in the eastern and western sectors of the former forearc basin, respectively.

Chapter 2 introduces and defines new concepts applicable for describing and interpreting the diagenetic evolution of cool-water carbonates. These concepts underpin both the stratigraphic analysis of the sedimentary successions presented in Chapter 4, and the high-resolution diagenetic stratigraphic approach used to decipher the nature of paleohydrologic systems that moved through the sediments over time (Chapter 5). Chapter 2 forms the basis of a manuscript that has already been submitted to the journal *Carbonates and Evaporites* for publication consideration, and is currently under peer review. Prof. C. S. Nelson appears as a co-author on that manuscript. While his editorial input and contribution to the discussion of scientific ideas and concepts have been significant, the data acquisition, presentation, and interpretations are those of V. Caron.

Chapter 3 provides detailed descriptions of the diagenetic features recognized within the many occurrences of Te Aute limestone units. Geochemical data are combined with more general microfacies properties to interpret diagenetic alteration and cementation products in terms of diagenetic environments. Patterns of pre-compaction diagenetic suites and sedimentary facies changes are correlated, and integrated into a predictive diagenetic model, constrained by sequence stratigraphic considerations.

Chapter 4 explores the facies stacking and diagenesis of the Te Aute carbonate deposits in relation to sedimentary unconformities, and highlights the complex internal architecture of the limestone units. Carbonate production and deposition are placed within a modern sequence stratigraphic context, and the influence and interplay of glacio-eustatic and tectonic forcing mechanisms are examined.

Chapter 5 shows that sequence stratigraphic concepts can be used to describe paragenetic relationships between cement generations that collectively build up the diagenetic history of cool-water carbonates. The "diagenetic sequence stratigraphy" approach applied to one limestone unit proves to be a powerful procedure by identifying

a suite of distinctive paleoaquifer systems that moved through the sediments over time. The diagenetic sequence stratigraphic concepts are defined and serve to model the diagenetic evolution of the Pliocene limestones related to regional paleohydrologic systems, tectonism, and sea-level variations.

Finally, an epilogue emphasizes some of the important conclusions drawn from this study, and outlines the perspectives and recommendations for future investigations.

During the course of this thesis research, the author has presented some preliminary results of various aspects of the study at a number of national and international conferences as oral or poster papers. These are referenced below, along with two manuscripts that have been submitted for publication and are currently in review, plus a fieldtrip guide report.

Caron, V. & Nelson, C. S. (in press) Developing concepts of high-resolution diagenetic stratigraphy for cool-water limestones: application to Pliocene Te Aute limestones, New Zealand, and their sequence stratigraphy. *Carbonates and Evaporites.*

Caron, V. & Nelson, C. S. (2001a) Cathodoluminescence sequences in the Early Pliocene cool-water Kairakau Limestone, Hawke's Bay, New Zealand. In: *Cathodoluminescence in geosciences: new insights from CL in combination with other techniques*, pp. 18. Technische Universitat Bergakademie Freiberg, Freiberg, University of Mining and Technology, Germany.

Caron, V. & Nelson, C. S. (2001b) Diagenetic and sedimentologic recognition of high-order (C. 150-20 ka) parasequences in cool-water carbonates: Plio-Pleistocene Te Aute limestones, New Zealand. In: *Advances in Geosciences, GSNZ Miscellaneous Publication Vol. 110A*, pp. 22., Geological Society of New Zealand, Hamilton, New Zealand.

Caron, V. & Nelson, C. S. (2000) Diagenetic patterns in early pre-compaction cements of Pliocene Te Aute limestones of Southern Hawke's Bay, New Zealand, and their possible sequence stratigraphic significance. In: *GSNZ/NZGS Joint Meeting, Miscellaneous Publication Vol. 108A*, pp. 22. Geological Society of New Zealand, Wellington, New Zealand.

Caron, V., Pallentin, A. & Nelson, C. S. (1999) Diagenetic stratigraphy of temperate carbonates: The Kairakau and Whakapunake Limestones (Opoitian, Early Pliocene), Hawke's Bay, New Zealand. In: *GSNZ Annual Conference, Vol. 107A*, pp. 24. Geological Society of New Zealand, Palmerston North, New Zealand.

Nelson, C. S., Kamp, P. J. J., Caron, V., Pallentin, A., Bland, K. J. & Graafhuis, R. B. (2001) Sedimentology, diagenesis, and sequence stratigraphy of Plio-Pleistocene mixed siliciclastic-carbonate forearc basin deposits, central Hawke's Bay, eastern North Island. In: *Fieldtrip Guides* (Ed. By R. T. Smith), Geol. Soc. of NZ Annual Conference "Advances in Geosciences", Univ. of Waikato, Hamilton. *GSNZ Miscellaneous Publication Vol. 110B,* FT8, pp. 45.

Nelson, C. S., Winefield, P. R., Hood, S. D., Caron, V., Pallentin, A. & Kamp, P. J. J. (in review) Pliocene Te Aute limestones, New Zealand: expanding notions for models of cool-water shelf carbonates. *New Zealand Journal of Geology and Geophysics.*

Ricketts, B. D., Nelson, C. S., Caron, V. & Pallentin, A. (2001) Pliocene to recent deformation of the East Coast forearc basin revealed by seismic sequences beneath Hawke Bay, New Zealand. In: *Advances in Geosciences, GSNZ Miscellaneous Publication Vol. 110A*, pp. 133. Geological Society of New Zealand, Hamilton, New Zealand.

References

Bathurst, R. G. C. (1975) *Carbonate Sediments and Their Diagenesis.* Elsevier, North Holland, pp. 658.

Beu, A. G. (1995) *Pliocene Limestones and Their Scallops.* Monograph 10, Institute of Geological & Nuclear Sciences Limited, Lower Hutt, New Zealand, 243 pp.

Haywick, D. W. (2000) Recognition and distinction of normal and forced regression in cyclothemic strata: a Plio-Pleistocene case study from eastern North Island, New Zealand. In: *Sedimentary Responses to Forced Regressions, Vol. 172* (Ed. by D. Hunt and R. L. Gawthorpe), pp. 193-215. Geological Society of London Special Publications, London.

Hood, S. & Nelson, C. S. (1996) Cementation scenarios for New Zealand non-tropical limestones. *New Zealand Journal of Geology and Geophysics*, **39**, p. 109-122.

James, N. P. & Clarke, J. A. D. Editors (1997) *Cool-Water Carbonates.* SEPM Special Publication, **56**, pp. 440.

Moore, C. H. (2001) *Carbonate Reservoirs - Porosity Evolution and Diagenesis in a Sequence Stratigraphic Framework.* Developments in Sedimentology, Elsevier, Amsterdam, **55**, pp. 444.

Nelson, C. S. Editor (1988) *Non-Tropical Shelf Carbonates: Modern and Ancient.* Sedimentary Geology, **60**, pp. 367.

Tucker, M. E. & Wright V. P. (1990) *Carbonate Sedimentology.* Blackwell, Oxford, pp. 482.

Chapter 1

STRATIGRAPHIC SEDIMENTOLOGY OF COOL-WATER PLIO-PLEISTOCENE LIMESTONES IN SOUTHERN HAWKE'S BAY, NEW ZEALAND

Abstract	1
1. Introduction	2
2. Geological and tectonic setting of the Plio-Pleistocene successions	5
3. Methods	7
4. Lithostratigraphy	11
5. Sedimentary facies	53
6. Skeletal and microfacies assemblages	69
7. The depositional model	77
8. Conclusions	81
References	85

Key Sections: 1, 2, 3.2, 4.1, 4.6, 4.10, 5, 6, 7, 8
Key Figures: 2, 4, 27, 29, 30
Key Tables: 1

Chapter 1

STRATIGRAPHIC SEDIMENTOLOGY OF COOL-WATER PLIO-PLEISTOCENE LIMESTONES IN SOUTHERN HAWKE'S BAY, NEW ZEALAND

ABSTRACT: Plio-Pleistocene cool-water carbonates in southern Hawke's Bay (eastern North Island, New Zealand), informally referred to as the Te Aute limestones, accumulated on and near the margins of a narrow forearc basin seaway that co-evolved with the convergent Pacific-Australian plate boundary located just east of North Island. The seaway became narrower and shallower over Pliocene times to eventually close during the Pleistocene. The active tectonic and varied paleogeographic depositional settings of the studied formations, in association with probable glacio-eustatic sea-level fluctuations, caused rapid lateral and vertical changes in sedimentary facies and thickness during Pliocene and Early Pleistocene times.

By contrast with previous studies of Plio-Pleistocene limestones in southern Hawke's Bay, this work, underpinned by detailed sedimentologic and stratigraphic descriptions, has enabled the recognition of recurring sedimentary facies within these formations, and the identification of shell concentrations and key surfaces separating the various facies or groups of facies in the stratigraphic columns, and defining a sequential architecture. The facies groups range from Bioclastic (B) to Siliciclastic (S) end-members via a Mixed (M) carbonate-siliciclastic group. These include a total of 14 different facies types that correspond to a large spectrum of depositional environments ranging from below storm-wave base, in outer shelf-type settings, to predominantly shallow-water shoreface-type conditions under the influence of tidal and wave currents.

Skeletal assemblages are diverse, but overall are dominated by epifaunal calcitic bivalves, bryozoans, and especially barnacles. The younger Pliocene and Early Pleistocene limestones that accumulated in the central part of the narrowed forearc basin are compositionally distinctive from their older easternmost and westernmost counterparts in having a lower terrigenous content, and more variable skeletal types, usually involving mixes of barnacles, bryozoans, epifaunal calcitic bivalves, benthic foraminifers, and especially endofaunal aragonitic bivalves. Such differences in skeletal associations, which translate in contrasting starting mineralogical compositions between pre- and syn-

Nukumaruan carbonates, are shown in the following chapters to influence the nature of diagenetic pathways.

The depositional system of the Pliocene carbonates in the eastern sector of the forearc basin can be characterized as neighbouring carbonate factories developed upon and about actively growing thrust-cored antiforms cut by a complicated network of channels that constrained tidal flows, and through which skeletons and skeletal fragments were transferred downslope via dunes, sand waves, or in avalanche flows. By way of contrast, the depositional setting for the western limestone occurrences is thought to correspond to continent attached-type carbonate platforms. Here, the shelf succession comprises alternating mixed terrigenous-skeletal (especially epifaunal bivalves and barnacles) limestones and siliciclastic sandstones and siltstones, overlain by conglomerates deposited in prograding fan-delta systems. Moderate to high contents of Mesozoic basement-derived siliciclastics indicate that carbonates probably formed and accumulated on a shelf regularly provided with terrigenous sediments, and influenced by strong tidal currents, which locally promoted barnacle growth.

1. Introduction

This chapter mainly concerns the results of fieldwork, supplemented by some summary laboratory data. It presents general descriptions of the many occurrences of Plio-Pleistocene limestones in southern Hawke's Bay, and the sedimentary facies distinguished within them. The construction of detailed stratigraphic columns through the deposits is considered a vital prerequisite for understanding the diagenetic evolution and sequence stratigraphy of the limestones, otherwise the prime focus of this study.

Outcrops were examined throughout southern Hawke's Bay (Figure 1) from the coastal Maraetotara Plateau and Kairakau Beach area westwards through the Kaokaoroa Range and Raukawa Range to Maraekakaho Valley (north) and Waipawa (south). In the far west of the study area, sections were logged from the southern end of the Maungaharuru Range southwards along the eastern side of the Kaweka Range and Ruahine Range to the western flanks of the Wakarara Range in the Ohara Depression (Figure 1).

This work builds upon the descriptions of the general stratigraphy and sedimentology made by Spörli and Pettinga (1980), Harmsen (1985), Kelsey *et al.* (1993), and Beu (1995) for the Pliocene limestones, and by Kelsey *et al.* (1993) and Beu

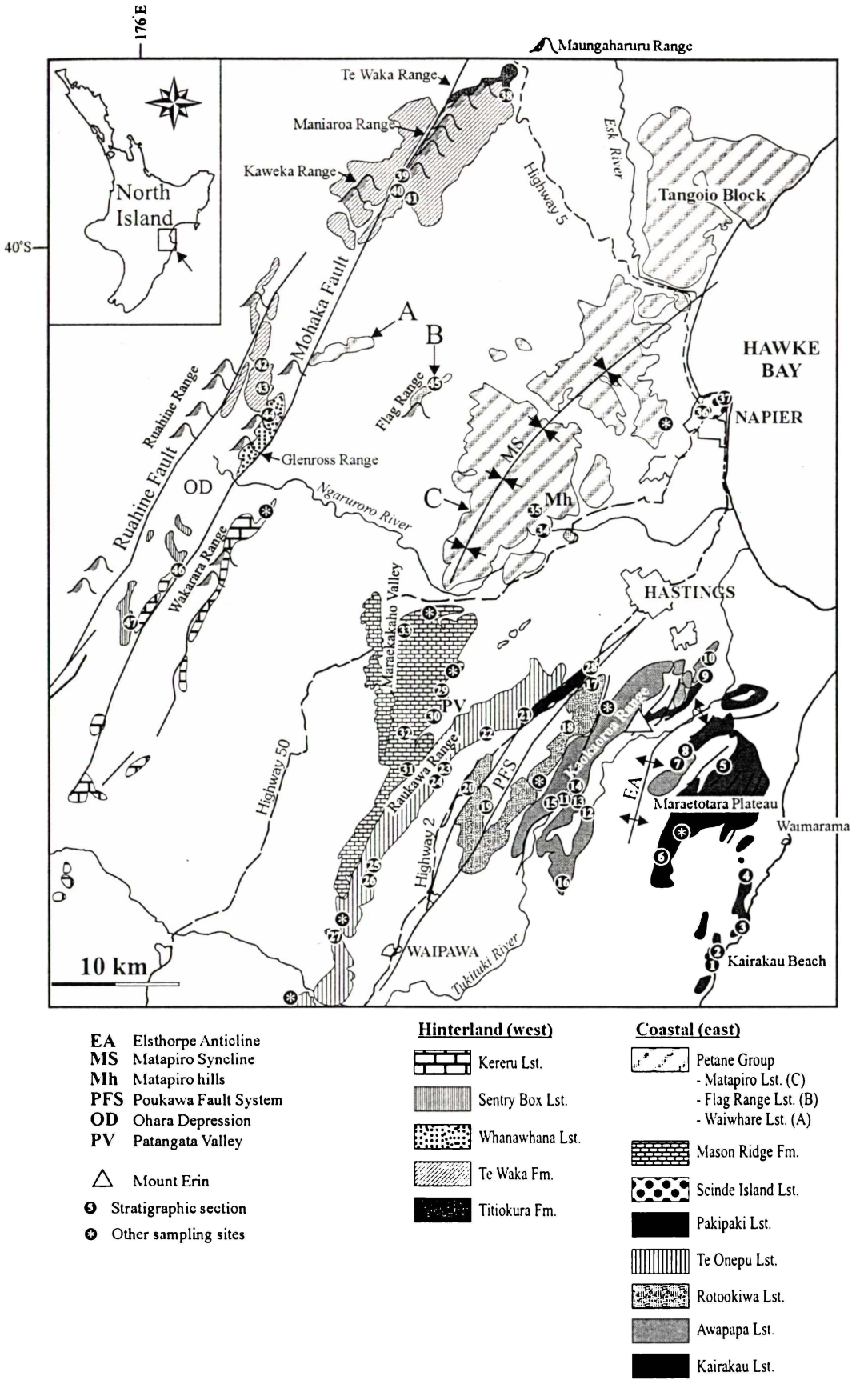

Figure 1- General distribution of the Plio-Pleistocene limestones in the study area, and location of logged sections and other sample sites (geological map from Beu, 1995). See Figure 2 for ages of the limestone units.

Figure 2- Regional stratigraphic relationships between the various Plio-Pleistocene limestone units in southern Hawke's Bay. The key with limestone names refers to the patterns on the inset geological map enlarged in Figure 1. Interbedded units, typically siliciclastic-dominated, are: (1) Mokopeka Sandstone; (2) Pukekura Calcarenite; (3) Waikareao Calcarenite; (4) Raukawa Mudstone; (5) Argyll Sandstone; (6) Makaretu Mudstone; (7) Willowford Mudstone; (8) Crownthorpe Mudstone; (9) Waitio Mudstone; (10) Pohue Formation (after Bland, 2001); (11) Ohara Mudstone.

(1995) for younger limestones, such as the Mason Ridge Formation (Figure 2). These authors provide ample references to previous work. New Zealand stage designations for the limestones are based on Beu's (1995) monograph and the mapping report of Kelsey *et al.* (1993), and are included in Figure 2.

The name "Te Aute" is used in this study for all the conspicuous limestone lithofacies within an otherwise predominantly siliciclastic basin-fill of Plio-Pleistocene strata. This differs from Kingma (1971) and Harmsen (1985) who employed the name Te Aute in the sense of a formal lithostratigraphic formation or group, and also from Beu (1995) who, while accepting more informal usage of the name, nevertheless restricted it to only barnacle-rich limestone of predominantly Pliocene age. Barnacle-rich lithofacies range in age from Opoitian to early Nukumaruan (Kairakau Limestone up to the lower limestone sheet of Mason Ridge Formation in the east of the basin, and Titiokura Formation up to the Sentry Box Limestone in the west; Figures 1, 2). Lateral changes of facies are common and rapid in these limestones. They exhibit a wide spectrum of internal sedimentary structures ranging from planar bedding to many different scales of cross-bedding whose most spectacular examples, though relatively uncommon, involve giant tabular sets up to 40 m thick (Kamp *et al.*, 1988).

In contrast, the younger Nukumaruan limestones are enriched in aragonitic bivalve skeletons and have locally rather higher terrigenous contents, and typically are thinner and more continuous laterally than their barnacle-rich Pliocene counterparts (Haywick, 1990; Beu, 1995).

2. Geological and tectonic setting of the Plio-Pleistocene successions

Eastern North Island Plio-Pleistocene sedimentary rocks represent the upper portion of a 5 km-thick Neogene forearc basin-fill sequence. The forearc basin is one of six tectono-geomorphic elements that formed in response to the evolution of the convergent Pacific-Australian plate boundary since the close of the Oligocene (Field *et al.*, 1997). The collisional system is bounded to the east by the Hikurangi Trough where the oceanic crust of the Pacific Plate is obliquely subducted beneath the continental lithosphere of North Island (Figure 3A). Abutting against the Hikurangi Trough is the subduction accretionary complex that consists of thrust fault-controlled anticlinal ridges and slope-parallel basins (Figure 3B). The forearc basin represents the major topographic and structural depression of the accretionary complex, and is bounded to the west by a structural ridge of Mesozoic

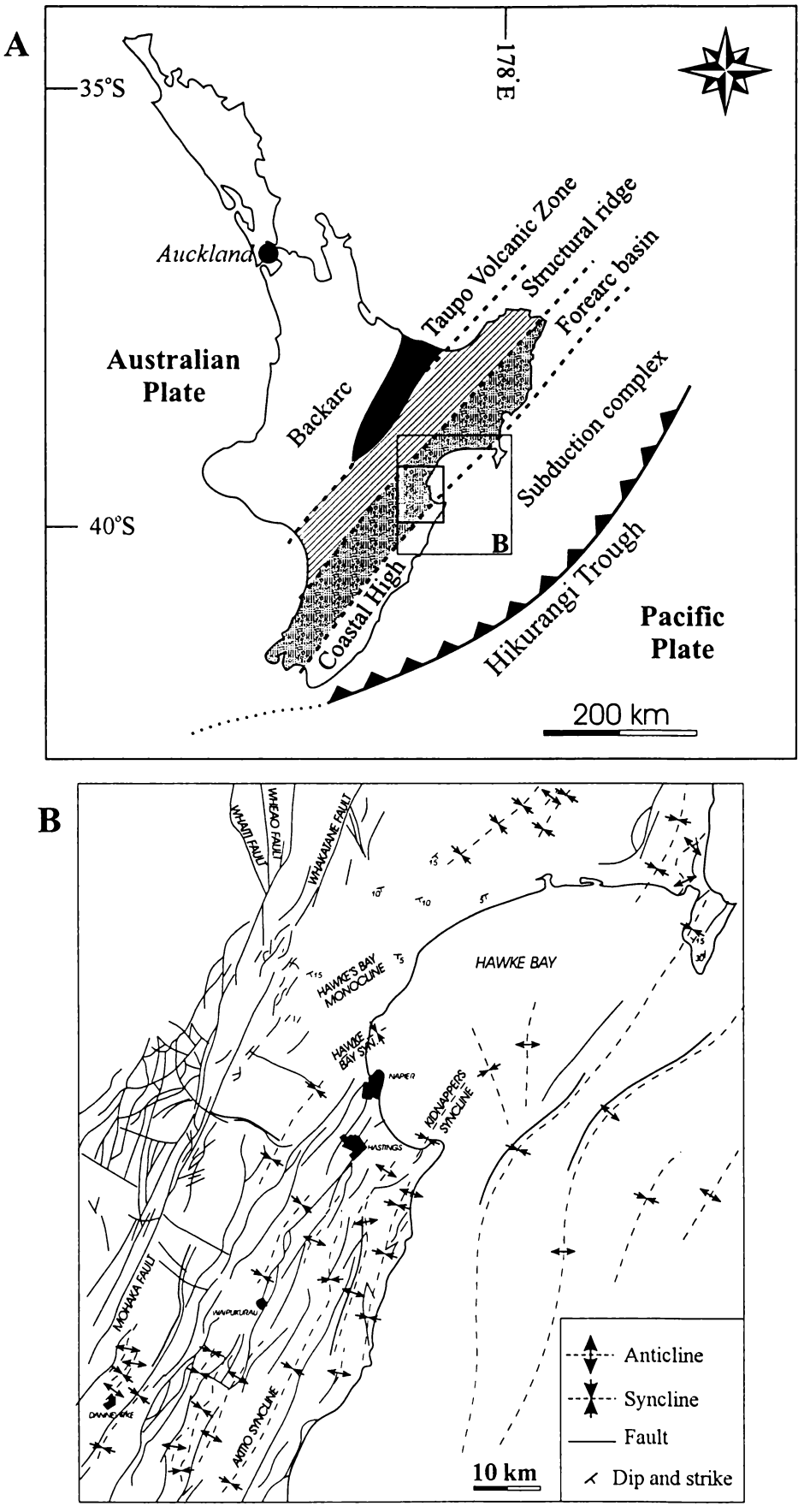

Figure 3- (A) Location of the study area (shaded) relative to the major tectonic features of eastern North Island, New Zealand (modified from Kamp *et al.*, 1988). (B) Structure map of southern Hawke's Bay region, emphasizing the NE-SW trending direction of faults and fold axes (modified from Bland, 2001).

basement (Torlesse terrane) rocks (Ruahine Range) separating the subduction complex from the Taupo Volcanic Zone and the backarc region (Figure 3A). In Early Pliocene time the structural ridge formed a central North Island highland surrounded by shelf-like shoal areas (Beu, 1995).

Although a minor component of the basin-infill Neogene stratigraphy, non-tropical limestones can locally be thick and quite extensive, exemplified best by the Te Aute Plio-Pleistocene limestones. Thus, Plio-Pleistocene limestones constitute a greater proportion of the stratigraphic record along the western and eastern margins of the forearc basin, grading basinward into siltstones and sandstones.

Kamp *et al.* (1988) and Kamp and Nelson (1987, 1988) suggested that the formation and evolution of the carbonate successions were closely related to the tectonic evolution of the forearc basin. As a result of subduction processes, differential uplift of the eastern margin (coastal high) of the forearc basin induced progressive narrowing and shallowing, which by mid-Pliocene times had constricted the basin into a NE-SW-trending seaway, the Ruataniwha Strait of Beu (1995). The outcrop pattern of the Early and mid-Pliocene occurrences, especially the more eastern ones adjacent to the inboard margin of the subduction complex, demonstrates that deposition migrated towards the centre of the basin over time, the younger sheets being present close to the forearc basin axis and at lower elevations compared to older Pliocene sheets located on the outer margins of the basin (Figure 1). By Late Pliocene, the coastal high had become emergent and as differential uplift persisted after the Pliocene, the Early Pleistocene limestones formed towards the axis of the basin (Field *et al.*, 1997).

The forearc seaway was situated near 40°S paleolatitude and was influenced by strong tidal flows involving mainly cool- to warm-temperate ocean currents (Kamp and Nelson, 1988; Beu, 1995). Many of the Plio-Pleistocene limestones are distinctive because of their high barnacle content (Te Aute lithofacies of Beu, 1995). These skeletal carbonates are subtidal deposits formed upon and about actively growing structural antiforms (submarine ridges) within the forearc to the east and at inner to middle shelf depths of the seaway throughout the Pliocene and Early Pleistocene (Kamp *et al.*, 1988).

3. Methods

The limestones of southern Hawke's Bay described in this chapter are generally moderately well to poorly exposed in cliffs along the eastern flanks of north-south

orientated parallel ranges, in quarries, and in road cuttings. The strata are typically relatively unconsolidated, but can be well cemented when related to a higher aragonitic content or to a longer burial history. 47 sections were measured and described, and limestones were sampled at these and 7 other localities (Figure 1A). All grid references given in this thesis relate to the 1:50 000 NZMS260 Topomap Series, and involve mainly sheets U21, V20, V21, and V22 (Appendix 10.4).

Over 750 samples were collected in the field, including rock samples, tephras, and macrofaunal samples (Appendix 2). Bivalves of the family Pectinidae were collected from the limestones and interbedded siliciclastic units as the scallops have been used as a practical field means of identifying the ages of the strata since the mid-sixties in New Zealand (Figure 4; Beu *et al.*, 1980; Beu, 1995).

Over 600 limestone samples were impregnated with epoxy resin to prevent the loss of any pore lining cement, and polished thin-sections were prepared and examined using both conventional and cathodoluminescent (CL) petrography. A few petrographic data are noted in this chapter, but are mainly the topic of subsequent chapters. The point-counting method developed by Chayes (1956) was first applied to determine the percentages by volume that the grains, interparticle matrix, intrinsic and extrinsic spar cements, and primary/secondary porosity make up in the samples (Appendices 3, 4; also on CD1). The point-counts were then also used to calculate the percentages of various grain types, including barnacles, bryozoans, bivalves, quartz, other siliciclasts, etc. The number of points needed to attain a certain reliability was controlled with the aid of charts (Galehouse, 1971) for a confidence interval of 95%. Thus, for each analysis, a minimum of two 200-point counts was performed on separate portions of 420 thin-sections to reduce errors linked to rock heterogeneity (Appendix 4; also on CD1). Standard deviation varies between 1% and 5%, depending on particle frequency. Data collected were used to determine skeletal assemblages following the classification scheme of Hayton *et al.* (1995).

A further step in the microfacies analysis was the clustering of point-counting data from 351 thin-sections (squared euclidean distances, complete linkage). This differed from the Hayton *et al.* (1995) analysis in that siliciclastic components were also taken into account (see Section 6).

X-ray diffraction (Appendix 8; also on CD1), microprobe (Appendix 6; also on CD1), and ICP-OES (Appendix 9; also on CD1) analyses were undertaken to recognize dominant minerals and for CaO, MgO, SrO, NaO, MnO, and FeO contents in both micro-

and bulk samples from all major limestone formations in southern Hawke's Bay (Appendices 8, 9; also on CD1).

3.1. Sedimentary nomenclature

Although siliciclastic contents are highly variable within the Plio-Pleistocene limestones in southern Hawke's Bay, their carbonate grain content is generally well above 50%, ranging on average between 60-80%. Consequently, the nomenclatural scheme developed by Dunham (1962) for carbonate rocks is used to describe the carbonate-rich lithologies in the study area. The classification scheme is illustrated in Appendix 10.4.

3.2. Geological age: Early Pliocene (Opoitian) to Early Pleistocene (late Nukumaruan)

In the eastern and central sectors of southern Hawke's Bay, the studied limestone formations range in age from late Opoitian (Kairakau Limestone) to Nukumaruan (Matapiro Limestone) on the basis of macropaleontology (Figures 2, 4). Kairakau Limestone has yielded one specimen of *Phialopecten marwicki* at Mt Kahuranaki section (V22/423515) and one specimen of *Towaipecten ongleyi* at Te Mata Peak section (V22/452597), taxa also reported by Beu (1995) in the Te Mata Peak area, and indicative of a late Opoitian age. Waitio and Moteo Mudstones, respectively underlying and overlying Matapiro Limestone, both contain specimens of the diagnostic Nukumaruan species *Pelicaria convexa* form *fossa* (Beu, 1995).

In the western portion of southern Hawke's Bay, the age of the limestone units has also been determined on the basis of macropaleontology. Bland (2001) reports specimens of both large *Phialopecten marwicki* and *Mesopeplum crawfordi* within the Titiokura Formation, suggesting a Waipipian age. However, he pointed out the absence of *Mesopeplum crawfordi* in the lower part of the formation and the presence of (?)Opoitian "gastropod fossils", and suggested that the Opoitian-Waipipian boundary may lie somewhere within the Titiokura Formation. Kereru Limestone, the uppermost limestone occurrence in the stratigraphy of studied formations, was assigned a late Nukumaruan age by Beu (1995) on the basis of several diagnostic molluscan taxa (including *Amalda mucronata* form *erica,* Olson; *Aeneator comptus,* Finlay; *Glaphyrina plicata*, Powell; *Cominella excoriata*, Finlay).

Southeastern Hawke's Bay

GROUP	FORMATION	MEMBER	EPOCH/NZ STAGE		FOSSIL
PETANE (Haywick *et al.*, 1991)	Matapiro Limestone (Beu, 1995)		PLIOCENE	1.57 Nukumaruan	*(Pelicaria convexa)*
	Flag Range Limestone (Beu, 1995)				
NAPIER (Beu, 1995)	Mason Ridge (Kelsey *et al.*, 1993)				*Phialopecten triphooki*
	Scinde Island Limestone (McKay, 1886a)				
	Pakipaki Limestone (Kelsey *et al.*, 1993)				*(Zygochlamys deliculata)*
HAWKE'S BAY (Beu, 1995)	Te Onepu Limestone (Harmsen, 1985)			2.28 Mangapanian	*Phialopecten thomsoni* *Towaipecten katieae*
	Rotookiwa Limestone (Kelsey *et al.*, 1993)			2.79 Waipipian	*Phialopecten marwicki* *Mesopeplum crawfordi*
	Awapapa Limestone (Harmsen, 1985)				*Phialopecten marwicki* *Mesopeplum crawfordi*
	Tuki Bell limestone (informal, this study)			3.6 Opoitian	*Phialopecten marwicki* *Towaipecten ongleyi*
	Kairakau Limestone (Harmsen, 1985)				*Phialopecten marwicki* *Towaipecten ongleyi*
				5.33 Ma	

Southwestern Hawke's Bay

GROUP	FORMATION	MEMBER	EPOCH/NZ STAGE		FOSSIL
POPORANGI (Beu, 1995)	Kereru Limestone (Erdman and Kelsey, 1992)		PLEIST.	Nukumaruan	
	Sentry Box Limestone (Erdman and Kelsey, 1992)		PLIOCENE		*(Zygochlamys deliculata)*
NAPIER (Beu, 1995)	Whanawhana Limestone (Beu, 1995)				*Phialopecten triphooki*
MAUNGAHARURU (Bland, 2001)	Te Waka (Beu, 1995)	Awhina (Bland, 2001)		Mangapanian	*(Phialopecten thomsoni)*
		Oakmere (Bland, 2001)			
	Titiokura (Beu, 1995)			Waipipian	*(Phialopecten marwicki* *Mesopeplum crawfordi)*

Figure 4- Summary of the stratigraphy of studied limestones in southern Hawke's Bay. The column "Fossil" refers to diagnostic specimens either collected during the present study, or reported by previous authors (those fossil names in brackets). Absolute ages for New Zealand stages from Beu (1995) and McIntyre (2002).

Figure 4 summarises the stratigraphic nomenclature employed in the present study. Beu (1995) proposed the name Hawke's Bay Group to contain Pliocene strata in southern Hawke's Bay, and to replace Te Aute Group of Harmsen (1985). The Group is overlain by Nukumaruan rocks of Napier Group (Figure 4). The Petane Group comprises formations partly equivalent to the upper units of the Napier Group, and formations significantly younger (late Nukumaruan). Most of these formations were defined by Haywick *et al.* (1991), and later completed and modified by Beu (1995). The Poporangi Group includes a succession of limestone and interbedded siliciclastic units occurring in the Ohara Depression (Figure 1), and ranging in age from Mangapanian to late Nukumaruan (Beu, 1995).

The lithostratigraphic schemes for the Plio-Pleistocene successions in eastern North Island have become increasingly complex over the years, with the constant addition of new formation names and members. This is primarily due to the lack of detailed mapping over large areas, in addition to the discontinuous nature of the limestone units. These are key problems that current studies at the University of Waikato are beginning to address (Bland, in prep.; Pallentin, in prep.).

4. Lithostratigraphy

Stratigraphic columns for all the localities identified in Figure 1 are presented in Appendix 1, which includes definition of all the symbols used on the columns. Only the key sections for each limestone formation are included within this chapter. Detailed discussion of the various sedimentary facies building the stratigraphy is delayed until Section 5, which includes a summary reference list in Table 1 defining the facies codes noted on the stratigraphic columns. For reader convenience, fold-out copies of Figures 1 and 2 are inserted in the pocket inside the back cover of the thesis.

4.1. Kairakau Limestone (Opoitian)

The name Kairakau Limestone is derived from Kairakau Beach (V22/457327). It was given to limestone units in this area and used informally by Beu *et al.* (1980). The Kairakau Limestone was also mapped by Spörli and Pettinga (1980) as the Maraetotara limestone in the Maraetotara Plateau area and north of Mount Kahuranaki, where it was subsequently formally defined as Kairakau Limestone by Harmsen (1985; Figures 5A,

Figure 5 – Late Opoitian and early Waipipian strata in southeastern Hawke's Bay

(A) Kairakau and Awapapa Limestones, north of Mt Kahuranaki on the western edge of Maraetotara Plateau, looking northeastwards (V22/420510). View showing bluffs of steeply dipping Kairakau Limestone on the eastern side of the Elsthorpe Anticline (see Figure 1). The central valley is occupied by the Mokopeka Sandstone, while Awapapa Limestone (15 m exposed) crops out along the upper eastern scarp edge of the valley.

(B) Northern cliff face of Kairakau Limestone at its type locality (see Appendix 1 – column 7; V22/423515), north of Mt Kahuranaki, where the Mangangarara Stream takes its rise. The cliff exposes about 40 m of Kairakau Limestone divided into four units based on the occurrence of sharp and erosional contacts. The lower unit underlies a sharp-based shell bed packed with oyster valves. Unit 2 overlies the shell bed and is bounded above by a sharp contact (surface a, white arrows), upon which overlying beds (unit 3) appear to onlap (arrowed). Tabular bed sets of unit 4 rest on an erosional surface (b, black arrow) truncating the underlying unit 3.

(C) Eastern scarp face of Te Mata Peak (looking southwards from V22/452599) exposing Kairakau Limestone at the foot of the cliff, the intermediate Tuki Bell limestone (informal) in the steep grassy slopes (underlain by the soft Mokopeka Sandstone), and the type section of Awapapa Limestone (see Figure 8). The total thickness is about 200 m.

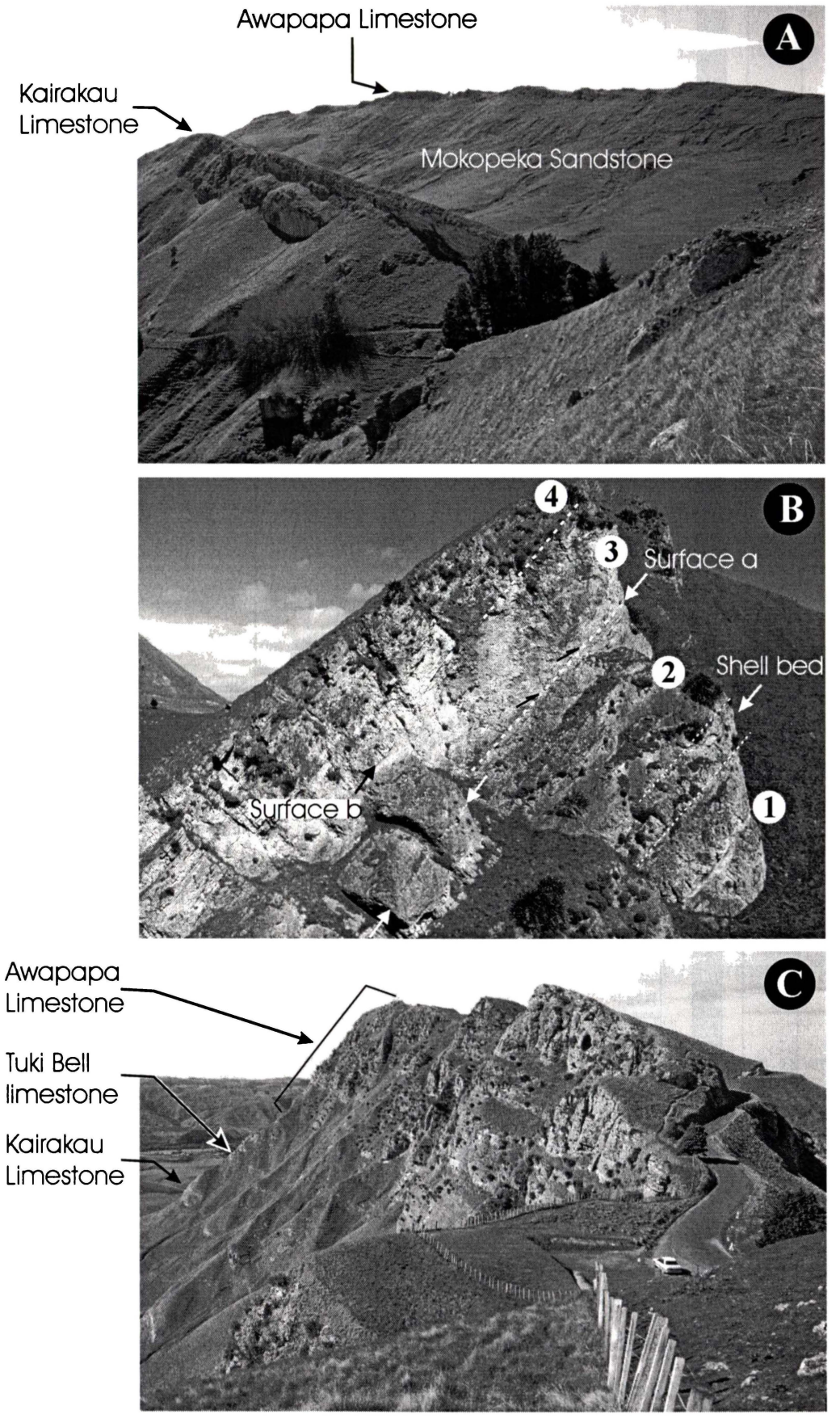
Awapapa Limestone
A
Kairakau
Limestone
Mokopeka Sandstone
B
4
3
Surface a
2
Shell bed
Surface b
1
Awapapa
Limestone
C
Tuki Bell
limestone
Kairakau
Limestone

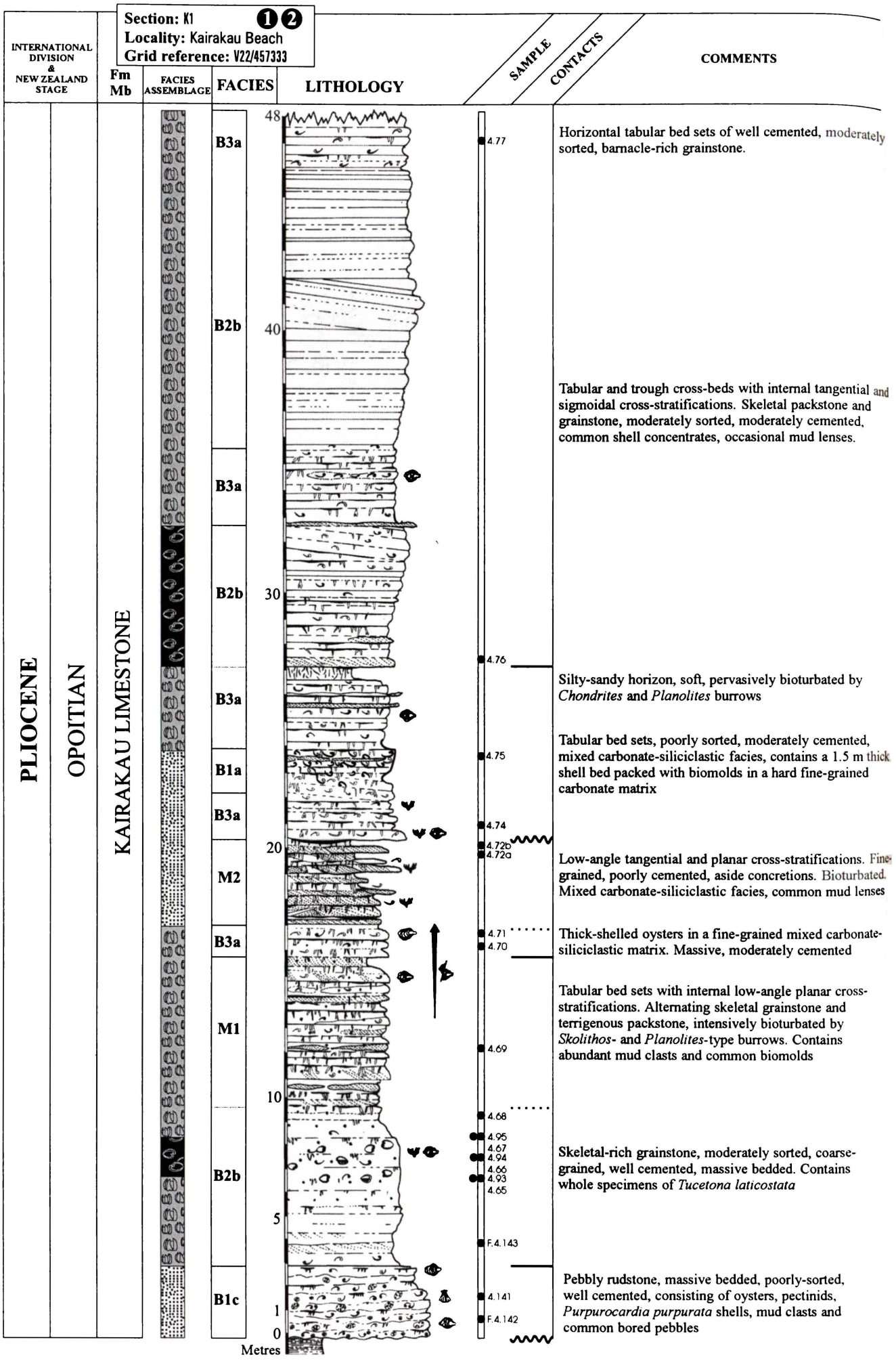

Figure 6- Section of the Kairakau Limestone exposed at Kairakau Beach (Key to patterns is given in Appendix 1 - p. A1-1).

5B). The limestone occurs on both sides of the Elsthorpe Valley, at the western edge of the Maraetotara Plateau, and within sea cliffs from south of Kairakau Beach northwards to Waimarama (Figure 1).

Kairakau Limestone is mainly characterized by mixed facies, transitional between barnacle-rich grainstone and terrigenous packstone, often bioturbated. Its thickness varies between 6 and 60 m.

Thirteen sections of Kairakau Limestone were examined and described (only ten are included in the thesis). 150 rock specimens were taken in the field, as well as 9 macrofaunal samples (Appendix 2).

Kairakau Beach section (Figure 6)

Location: Kairakau Limestone crops out along sea cliffs north of Kairakau Beach located at the end of Kairakau Road, about 10 km east of Elsthorpe. The section (column 1/2) is well exposed at V22/457333 (Figure 6). The basal unconformity is exposed in slumped blocks and in place within the cliff that borders the shoreline. One can access a good outcrop exposing the basal unconformity, located at V22/460339, from a car park along Te Apiti Road about 2km from its junction with Kairakau Road.

Lithology: Several sections are combined to provide an almost continuous profile of the Kairakau Limestone from its bottom disconformity with the underlying undifferentiated Miocene mudstone/siltstone (Figure 6).

The Kairakau Beach section (or close to it) was examined by Harmsen (1985) at her Mangakuri section, but she did not recognize its lower boundary.

Carbonate sediments of the Kairakau Limestone sit sharply across a ravinement surface on blue-grey Miocene mudstone. The base of the section consists of a 5 m-thick, well cemented, massive pebbly rudstone displaying occasional thin mud layers, and containing numerous mudstone clasts from the underlying mudstone formation, and abundant bored pebbles in places (see Figure 23D).

This bed is sharply overlain by moderately sorted, well cemented, medium-grained grainstone (6 m) that grades up into parallel laminated to low-angle cross-stratified, coarsening-upwards, interbedded skeletal-rich packstone and grainstone (7 m). Oyster and barnacle fragment content increases upwards and becomes dominant towards the top of this interval, while mud pebbles, numerous towards the base, become scarce up

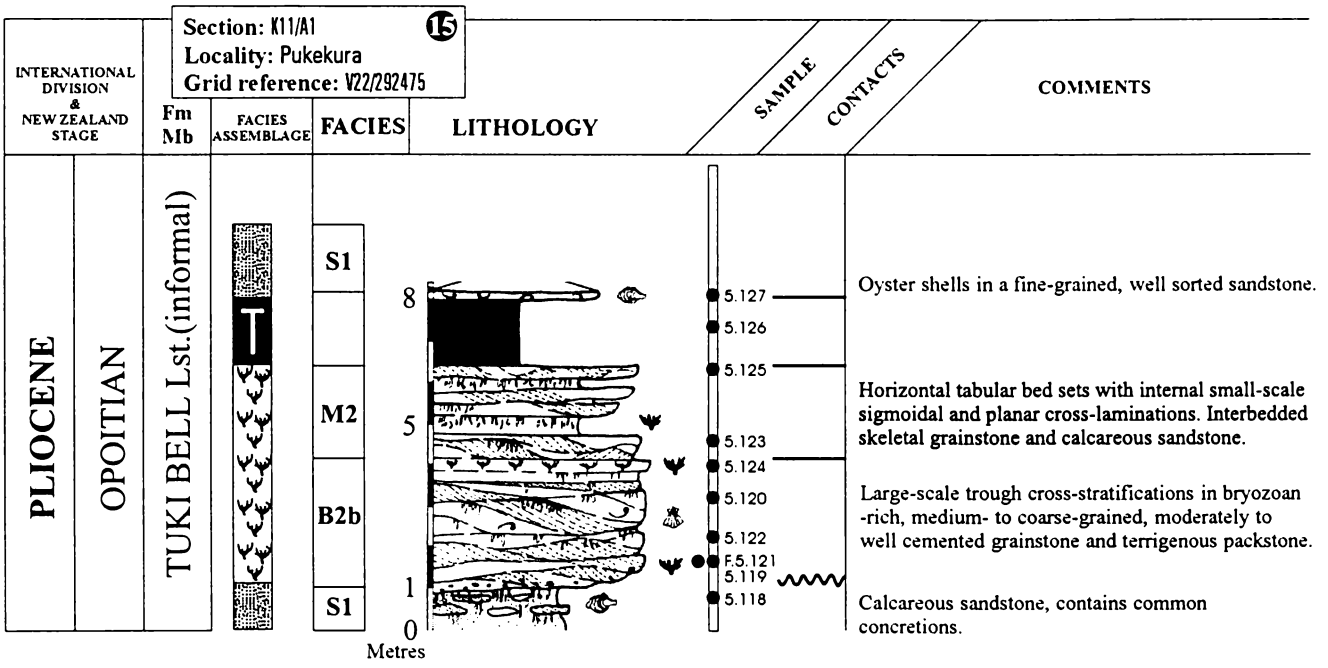

Figure 7- Reference section of the Tuki Bell limestone (informal) at Pukekura.

section. The upper boundary of this unit is poorly exposed, but appears to be sharp in places. From this surface, a lower massive, moderately cemented bed, containing whole specimens of thick-shelled oysters and common mud pebbles, grades upwards over 1 m into a low-angle planar bedded fine-grained siliciclastic unit (3.5 m) with interbedded mud lenses. This unit is bounded above by a sharp to erosional surface (see Figure 24I). Below the surface, vertical ichnofossils penetrate downwards, filled with coarser skeletal material from the overlying beds.

The next unit contains in its lower part, about 2.5 m above the previous contact, a 1.5 m-thick shell bed packed with calcitized articulated bivalves. Above the latter, the last interval (21 m) is characterized by planar bedded, alternating skeletal-rich packstones and grainstones with interbedded mud layers. It contains occasional oyster shell-rich lenses. The interval coarsens upwards and becomes a barnacle-rich grainstone in its upper part. The upper boundary is not exposed.

Thickness: 45 to 50 m.

4.2. Tuki Bell limestone (informal)

The informal name Tuki Bell limestone designates a thin discontinuous limestone sheet present between the Kairakau and Awapapa Limestones, within the undifferentiated Mokopeka Sandstone (Figure 5C). Harmsen (1984) refers to this limestone unit without naming it as "thin (up to 3 m) beds of well cemented, poorly sorted skeletal-rich grainstone" occurring within the Mokopeka Sandstone at Te Mata Peak. Recent examination of this outcrop indicates that it consists of a 4 m-thick coarse barnacle-rich grainstone containing *Phialopecten marwicki* and *Towaipecten ongleyi* towards its base. Its stratigraphic position and fossil content suggest a latest Opoitian age. Although discontinuous, grading laterally into calcareous sandstone, the limestone is present further south at Pukekura where a key section is proposed here (Figure 7). 9 rock samples were collected, plus 2 macrofossils and 1 tephra sample.

Pukekura section (Figure 7)

Location: Pukekura section (column 15) is located in the hillside a few hundred metres west of Middle Road alongside Tukituki River, across the paddock on Pukekura Station at V22/292475, and comprises exposures of both Kairakau and Awapapa Limestones below and above Tuki Bell limestone, respectively.

Lithology: The name Tuki Bell derives from the shape of the Tukituki River meander a few hundred metres east of the outcrop. The lower contact is sharp to erosional. The apparently massive limestone contains minor long-length wavy swells towards the base, and tangential to trough cross-stratifications above (Figure 7). It is moderately sorted, and moderately to well cemented. Bryozoan and barnacle fragments dominate the composition of the Tuki Bell limestone. It contains, about 3 m above the basal contact, a 0.20 m thick bryozoan-rich shell bed. This is in turn sharply overlain by alternating tabular bed sets of skeletal grainstone and packstone. A 2 m-thick tephra layer rests on the upper sharp surface, and is capped by calcareous sandstone with common *in situ* (?) oyster valves.

Thickness: the main limestone body is about 5 m.

4.3. Awapapa Limestone (Waipipian)

First introduced by Spörli and Pettinga (1980) for the upper limestone in the ridge north of Mount Kahuranaki (Figure 5A), the name Awapapa Member was extended to formation status as the Awapapa Limestone by Harmsen (1984, 1985) who defined the type section as the prominent limestone exposed in the eastern face of the Te Mata Peak (Figure 5C). The formation defined by Harmsen (1985) included both Awapapa Limestone *sensu stricto* as defined at its type section, and Rotookiwa Limestone established subsequently as a new formation by Kelsey *et al.* (1993).

The Awapapa Limestone is lithologically highly variable, ranging from interbedded terrigenous packstone and calcareous sandstone to pure bryozoan- and barnacle-rich grainstone. Despite this compositional heterogeneity, Awapapa Limestone has classically been referred to as a typical Te Aute lithofacies limestone (Harmsen, 1985; Kamp *et al.*, 1988; Beu, 1990b; Beu, 1995).

The Awapapa Limestone forms the prominent ridges of the eastern flank of the Elsthorpe Valley from Te Mata Peak southwards to the vicinity of Mount Erin, as well as cropping out discontinuously along the steep slopes of the Kaokaoroa Range (Figure 1A). Its thickness varies between 22 and 120 m.

Seven sections of Awapapa Limestone were examined and described (only six are included in the thesis). 118 rock samples were taken in the field and 32 macrofaunal samples (Appendix 2).

Te Mata Peak section (Figure 8)

Location: Best access is from the bottom of the cliff, climbing up along the northern face of the blocks in the steep grassed slopes. The key section (column 9) is located beneath the radio mast at V22/451602 (see Figure 10A).

Lithology: The Awapapa Limestone forms the eastern scarp face of the Te Mata Peak that Harmsen (1985) designated as the type section for this formation (Figures 5C, 8, 10A). Its lithology is vertically highly variable and consists broadly in the first 50 m of alternating calcareous sandstone and packstone (storm emplaced or turbidite-like deposits) overlain in turn by several packages of either alternating grainstone and packstone, or skeletal-rich grainstone with interbeds of either interbedded terrigenous packstone and calcareous sandstone, or interbedded grainstone and terrigenous packstone.

The following 60 m or so are dominated by the occurrence of four thick shell beds or shell concentrates packed with oyster and pectinid valves, with interbeds of alternating grainstone and terrigenous packstone. It is sharply overlain by a few metres of yellow sandstone cropping out just beneath the radio mast (see Figure 10A), probably equivalent to the Pukekura Calcarenite.

The base of the formation (11 m) consists of discontinuous, coarsening- and thickening-upwards grainy skeletal sheets inferred to have been emplaced either by storm-generated currents or debris flows (see later). Sheet tops are usually simple bedding planes whose underlying moderately to well consolidated nature may be related to firm grounds. Well-preserved delicate branching bryozoans in both fine-grained sandstones and coarser-grained sheets show evidence of reworking under low-energy conditions. The upper part of this interval contains coarse-grained, horizontally bedded, well sorted, poorly to moderately cemented sheets (up to 0.4 m thick).

The next 23 m-thick interval is bounded below by a sharp, strongly burrowed, surface. It consists of interbedded fine- to medium-grained packstone and medium- to coarse-grained grainstone sheets, with internal planar low-angle cross-stratifications, and trough and tangential cross-beddings, respectively. The interval is bounded above by an erosional surface, in turn overlain by a massive, poorly to moderately sorted, moderately to well cemented, bioclastic bed (2.5 m) containing scattered bored sandy and muddy pebbles (especially towards the base). This bed grades up section into planar-bedded mixed facies (23 m), with internal trough and tangential cross-stratifications, common well

rounded mud pebbles up to 6 cm across, shell concentrations (<0.5 m thick) packed with oyster valves, and occasional pectinid valve lineations. These lower 50 m of strata at the Te Mata Peak section are bounded above by a ravinement surface.

Above are four prominent fining-upwards intervals, each ranging in thickness from 8-20 m, which comprise towards their base 2-5 m-thick shell beds. Shell beds contain abundant oysters and pectinids, often bored and encrusted by bryozoans and serpulids, common mud clasts and mud pebbles, and scattered clumps of oysters. Random orientation of shells, common convex upwards-orientated shells together with slightly abraded and unabraded valves, and common whole shells suggest moderate post-mortem transportation. However, the abundance of randomly oriented shells in the middle part of the unit may reflect a mixed assemblage of *in situ* and variably transported populations. Shell beds can be traced laterally for hundreds of metres.

Thickness: 110 to 120 m.

4.4. Rotookiwa Limestone (Waipipian)

Rotookiwa Limestone was included in the Awapapa Limestone until Kelsey *et al.* (1993) established it as a new formation on the stratigraphic criteria that it overlies the Pukekura Calcarenite, while the Awapapa Limestone underlies the Pukekura Calcarenite (Figure 2).

Because the Rotookiwa Limestone is typically a pale yellow, coarse-grained, soft to poorly cemented barnacle-rich grainstone, good exposures are rare. There are a few good, but remote, sections exposed along the western flanks of the Kaokaoroa Range, and reasonable accessible outcrops occur along Highway 2 between Waikareao Road and Te Onepu Road, as mapped by Kelsey *et al.* (1993).

The following new information is provided by the present work on the Rotookiwa Limestone:

- Although incomplete, one specimen of *Phialopecten marwicki* has been collected from the type locality of Rotookiwa Limestone (V22/251451). Until now, only one other *Phialopecten* specimen was known from the main distribution area of Rotookiwa Limestone (Beu, 1995).
- The upper boundary of the unit has been identified. It consists of a 2 m-thick shell bed packed with oysters, pectinids, and brachiopods, conformably

Figure 8- Section of the Awapapa Limestone at Te Mata Peak.

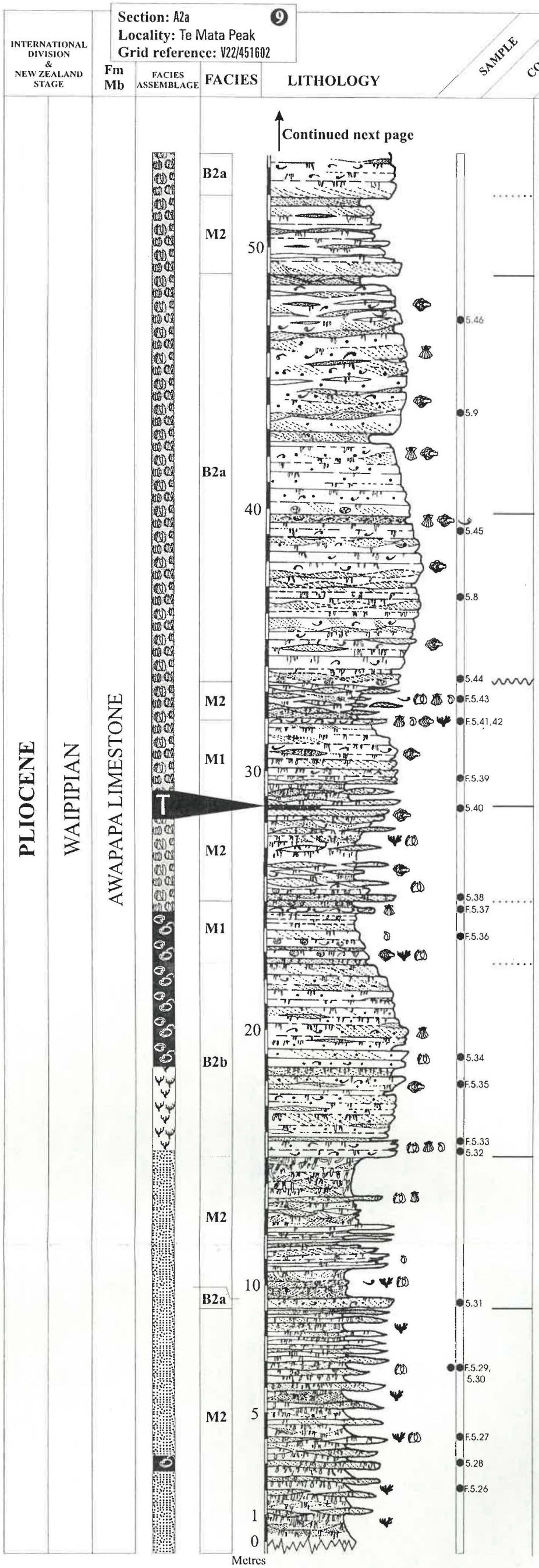

Figure 8 (continued)

Section: A2b ⑨
Locality: Te Mata Peak
Grid reference: V22/451602

INTERNATIONAL DIVISION & NEW ZEALAND STAGE	Fm Mb	FACIES ASSEMBLAGE	FACIES	LITHOLOGY	SAMPLE	CONTACTS	COMMENTS
PLIOCENE / WAIPIPIAN	AWAPAPA LIMESTONE		S1				
			B2b	115	5.146		
			M2				
			B2b		F5.143		Fining-upwards interbedded fossiliferous grainstone and terrigenous packstone. Contains numerous brachiopods and common oyster valves. Moderately sorted, moderately cemented.
				110	5.145		
					5.142		
			M3				
			B1a				Strongly burrowed surface (*Ophiomorpha?, Skolithos*).
					5.56		
					5.25		
			M2	100			Fining- then coarsening-upwards interval bounded below by a sharp contact, and above by an erosional surface. Moderately sorted, moderately cemented, interbedded skeletal packstone and grainstone. Common well rounded mud clasts and reworked tephra pebbles. Contains about half way between the bounding contacts a thin fine-grained, soft, terrigenous horizon.
			M3				
			M2		5.24		Fining-upwards interbedded grainstone and terrigenous packstone. Contains a thin pectinid shell lineation.
				90			
			B1a				Shell bed consisting of tabular bed sets up to 1 m thick. Poorly sorted, moderately cemented.
					5.55		
					F.5.54		
					5.21		
			M2				Fining-upwards interbedded grainstone and terrigenous packstone.
					5.20		
			B1a	80			Shell bed packed with oysters and pectinids, bounded below by a ravinement surface. Massive bedded, occasional sigmoidal cross-stratifications in mixed skeletal-terrigenous lenses.
					5.53		
					5.52		
			M2				Fining-upwards interbedded grainstone and terrigenous packstone.
			B3a				Planar bedded skeletal packstone containing scattered clumps of oysters, especially towards the base. Moderately sorted, moderately cemented.
					5.51		
			M1		F.5.50		Bioturbated interbedded grainstone and packstone.
				70			
			B1a		5.14		Common mud clasts and mud pebbles, scattered clumps of oysters often bored and encrusted by bryozoans and serpulids. Sparsely packed towards the base grades into densely packed shell bed. Random orientation of shells, common convex upwards-orientated shells together with slightly abraded and unabraded valves, common whole shells suggest moderate post-mortem transportation.
					5.48		
					5.49		
			M3				Tangential and planar cross-stratified, poorly cemented, interbedded fine-grained terrigenous packstone and medium-grained skeletal packstone. Coarsens upwards into fossiliferous bed sheets, consisting of pectinids, oysters, bryozoans and mud clasts.
				60	5.47		Shell concentration (<0.5 m) packed with oyster valves.
			M2		5.12		Fining-upwards interval bounded above by a sharp contact. Horizontal bedded, with uncommon tangential cross-stratifications, moderately sorted, moderately cemented, mixed carbonate-siliciclastic facies. Contains well rounded mud pebbles up to 6 cm across, oyster valves and branching bryozoan colonies towards the top.
				55			

Metres

- overlain in turn by a fine-grained shelly calcareous sandstone (Horse Shoe section, see below).
- The lower boundary of the formation might be the terrigenous packstone unit sharply overlying the Pukekura Calcarenite at Tainui (V22/285469; Appendix 1 – column 15).
- The Lonely Man section (Appendix 1 – column 20) differs from the almost constant lithofacies of Rotookiwa Limestone in the Kaokaoroa Range and at its type locality. It disconformably overlies calcareous sandstone/terrigenous packstone beds and sharply underlies a yellow-green fossiliferous calcareous sandstone that Kelsey *et al.* (1993) established as a new formation (Waikareao Calcarenite; Figure 2). Contrary to Kelsey *et al.* (1993), the upper contact of Rotookiwa Limestone with the overlying Waikareao Calcarenite appears to be exposed in Waitapuke Quarry at V22/224487.

The thickness of Rotookiwa Limestone measured sections varies between 20 and 42 m, but up to 50 m is exposed at the Horse Shoe locality (see later).

Five sections of the Rotookiwa Limestone were examined and described (only four are presented here). 58 rock samples, as well as 7 macrofaunal samples, were taken in the field (Appendix 2).

Horse Shoe section (Figure 9)

Location: From Mutiny Road, drive towards the residential area at V22/355590, and beyond the hill, across Wairunga block, follow the pathway at the foot of the western side of the hill along Poukawa Stream. The key section (column 17) is located at V22/345586.

Lithology: A moderately well exposed section occurs in the walls of a dry stream meander, here named Horse Shoe (Figure 9). Harmsen (1984, 1985) referred to the outcrop as the Poukawa Stream section and attributed the limestone to the Awapapa Formation. Kelsey *et al.* (1993) failed to recognize the upper boundary of the unit that consists of a 2-3 m-thick shell bed cropping out along Poukawa Stream and at the top of the western wall of the stream meander. The tabular nature of the shell bed, from the top of the hill down to the stream over a short distance, defines a steep homoclinal dip (up to 25°).

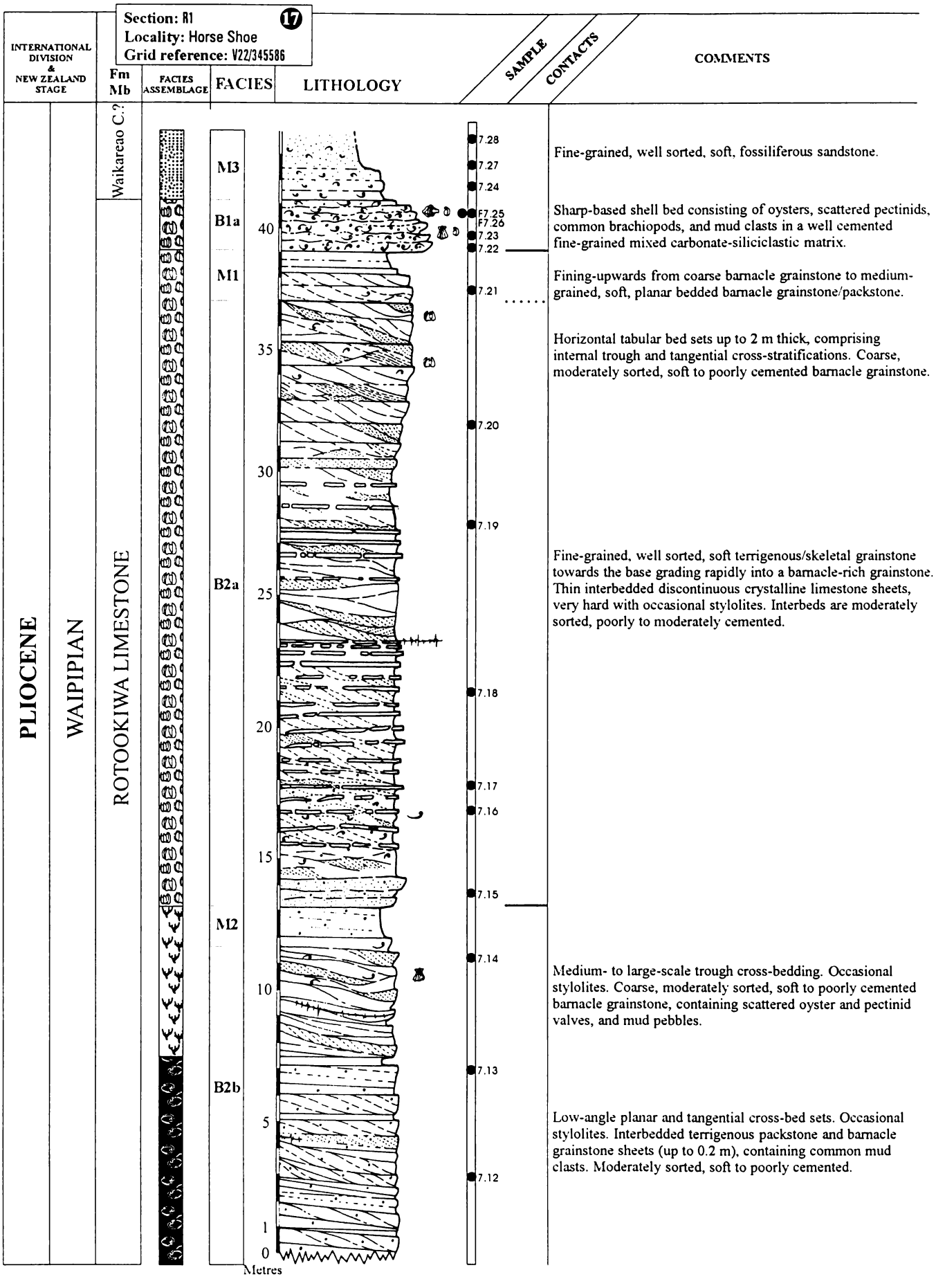

Figure 9- Section of the Rotookiwa Limestone at Horse Shoe.

At this locality, Rotookiwa Limestone is a poorly cemented, coarse-grained barnacle-rich grainstone, with interbedded, thin, discontinuous crystalline-like limestone sheets.

The lower part of the section (11 m) consists of massive to trough cross-bedded, moderately sorted, soft to poorly cemented, barnacle-rich grainstone that contains horizontally bedded terrigenous/skeletal packstone sheets (up to 0.2 m thick). This unit passes gradationally upwards into a 2 m-thick medium-grained, soft, massive interval sharply overlain by coarsening-upwards barnacle-rich grainstone (25 m). Occasional stylolites are present within thin, interbedded, discontinuous crystalline-like limestone sheets that are very hard due to preferential cementation. The upper part of this thick interval displays internal trough and tangential cross-bed sets (up to 1 m thick). A sharp surface places these beds in contact with a 2.5 m-thick shell bed packed with oysters, pectinids, and brachiopods in a well cemented muddy matrix. This in turn grades up into soft, green, shelly calcareous sandstone (numerous oysters and brachiopods, and occasional turritellid gastropods), of which only a few metres are exposed.

Thickness: 40 to 50 m.

4.5. Te Onepu Limestone (Mangapanian)

The Te Onepu Limestone was formally defined by Harmsen (1984, 1985). It was also the classical "Te Aute limestone" of early authors, and attracted the interest of geologists for it is characterized by very large-scale cross-bedded, coarse-grained barnacle-rich grainstone. Thus, several authors have described the unusual giant cross-bedding evident in the limestone in the faces of the Hatuma Lime Quarry (U23/043076; Harmsen 1984, 1985; Kamp *et al.*, 1988). It is also well known along the Raukawa Range (Figure 10B) because of its abundant *Crassostrea ingens* oyster shells, where the type section was designated in a small quarry along Te Onepu Road (V22/198493). This section (Figure 12A; Appendix 1 – column 23) was also formerly used as the type section for the "Te Aute limestone" (Kingma, 1971).

Several specimens of *Phialopecten thomsoni* were collected from different outcrops of Te Onepu Limestone, and one specimen of *Towaipecten katieae* from the section at Robottom Grave (Appendix 1 – column 26; Figure 10C), which are diagnostic taxa for the Mangapanian (Beu, 1995).

Figure 10– Waipipian and Mangapanian strata in southeastern Hawke's Bay

(A) Northern cliff face of Awapapa Limestone at V22/451602, showing the stratigraphic section presented in Figure 8 at Te Mata Peak. At this locality, Awapapa Limestone consists of two mega-units separated by an erosional surface (white dashed line). The lower mega-unit comprises interbedded packstones and grainstones organized in tabular bed sets (up to 1.5 m thick), while the upper mega-unit comprises several thick shell beds (arrowed) overlain by fining-upwards sediments. From bottom to top (at radio mast) the section is about 120 m thick.

(B) Almost continuous outcrop of Te Onepu Limestone in the eastern scarp of the Raukawa Range, looking northwards from the Robottom Grave section at V22/148422 (see below). Two distinct limestone sheets crop out in this area, separated by calcareous sandstone and terrigenous packstone beds. While the lower sheet is Mangapanian in age on the basis of the presence of *Phialopecten thomsoni* and *Towaipecten katieae*, the upper sheet consisting of two shell beds (see Kiwi Bush section in Appendix 1 – column 25) has yielded one specimen of *Phialopecten triphooki*, indicating an early Nukumaruan age.

(C) Northern scarp face of Te Onepu Limestone at Robottom Grave section at V22/148422 (see Appendix 1 – column 26). One specimen of both *Phialopecten thomsoni* and *Towaipecten katieae* were collected from this locality, indicating a Mangapanian age. The section is about 40 m thick (person gives scale; black arrow). The section is overall a coarsening-upwards succession of interbedded bryozoan packstone and grainstone towards the base grading into coarse barnacle grainstone up-section capped, across an erosional surface (dashed line), by a shell bed packed with *Crassostrea ingens* (white arrow). Note that the dipping to the right (east) of apparent foresets progressively changes up-section, suggesting syndepositional tectonic deformation on the margins of the forearc basin where the limestone formed (uplift).

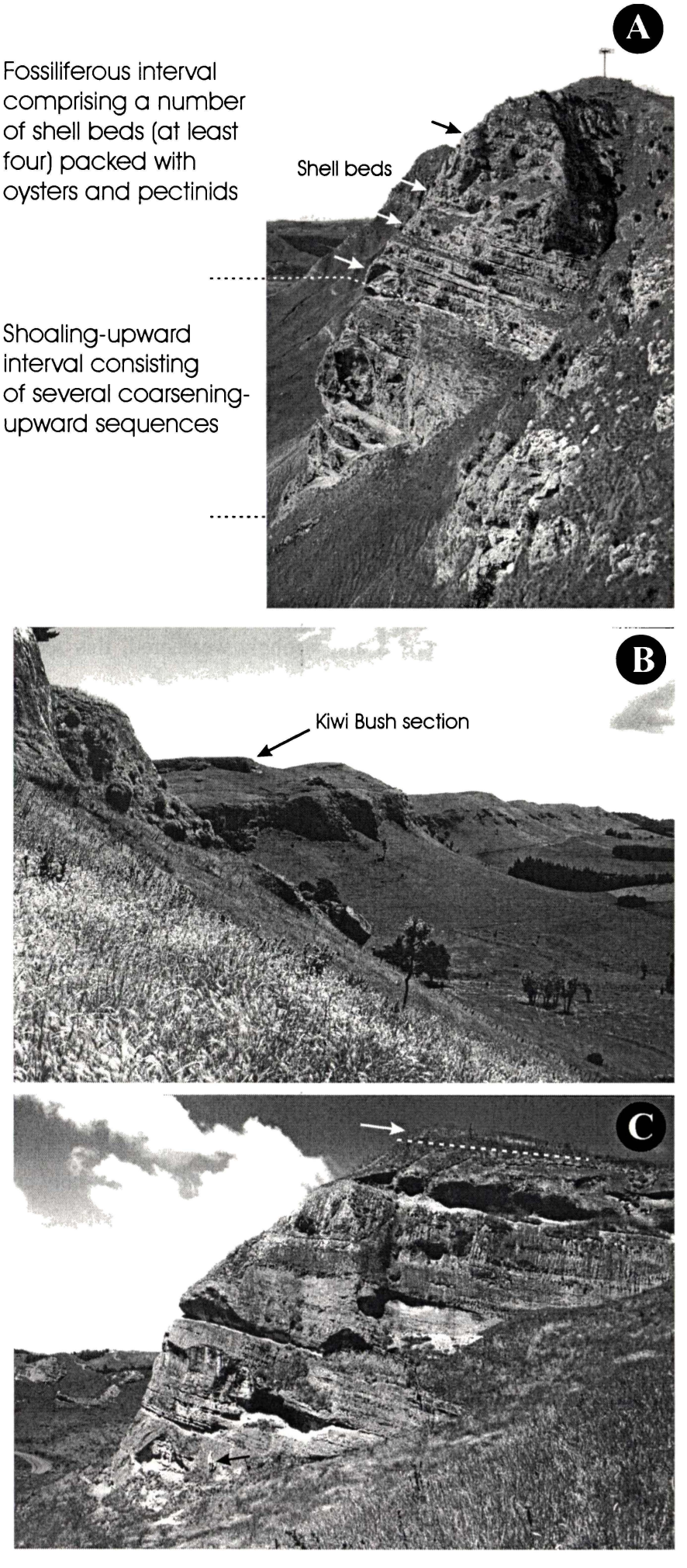
A
Fossiliferous interval comprising a number of shell beds (at least four) packed with oysters and pectinids
Shell beds
Shoaling-upward interval consisting of several coarsening-upward sequences
B
Kiwi Bush section
C

The Te Onepu Limestone forms the escarpment that bounds the Raukawa Range to the east (Figures 10B, 10C). At its type locality the Te Onepu Limestone lies sharply on the local Argyll Sandstone Member and in turn on the Raukawa Mudstone (Figure 2). Otherwise it directly lies on the Raukawa Mudstone and conformably underlies the Makaretu Mudstone (Figure 2). The thickness of measured sections varies between 27 and 60 m.

A total of 7 sections were examined and described. 106 samples were taken in the field, as well as 15 macrofaunal samples (Appendix 2).

Bee Swarm section (Figure 11)

Location: About 500 m southwest of Te Onepu Quarry, following the eastern crest of the Raukawa Range. The section (column 24) is located at V22/193484.

Lithology: Although poorly exposed and strongly weathered, this section of Te Onepu Limestone (Figure 11) helps complete the stratigraphic column provided by previous authors (e.g., Te Onepu Quarry section of Harmsen, 1984). A well indurated shell bed packed with oysters crops out about 15 m above the well-known *Crassostrea ingens* shell bed, from which it is separated by a fine-grained, poorly cemented terrigenous/skeletal packstone. Mixed carbonate-siliciclastic sands above this upper shell bed have yielded one specimen of *Phialopecten triphooki* (at Kiwi Bush section further south (Figure 9B); Appendix 1 – column 25), indicating that the Mangapanian-Nukumaruan boundary lies immediately on top of the capping shell bed. The complete stratigraphic column at the Bee Swarm section is described below (Figure 11).

About 1.5 m of well sorted, moderately cemented terrigenous packstone constitutes the base of the section, and probably represents the upper part of Argyll Sandstone (Figure 2). It is bounded above by a sharp surface (possibly erosional) overlain by a thin shell concentration with common mud clasts, which contains *Phialopecten thomsoni*. The shell layer forms the base of a coarsening-upwards interval (23 m), from skeletal packstone/grainstone to barnacle-rich grainstone. Selectively cemented horizons occur along large-scale cross-foresets (seen also at Te Onepu Quarry; Figure 12A), otherwise these are moderately sorted and poorly to moderately cemented. Occasional thin glauconitic and mud pebble-rich beds occur.

The upper boundary is a low relief erosional contact that places the underlying interval in contact with a 2 m-thick massive bed packed with mud pebbles and giant *in*

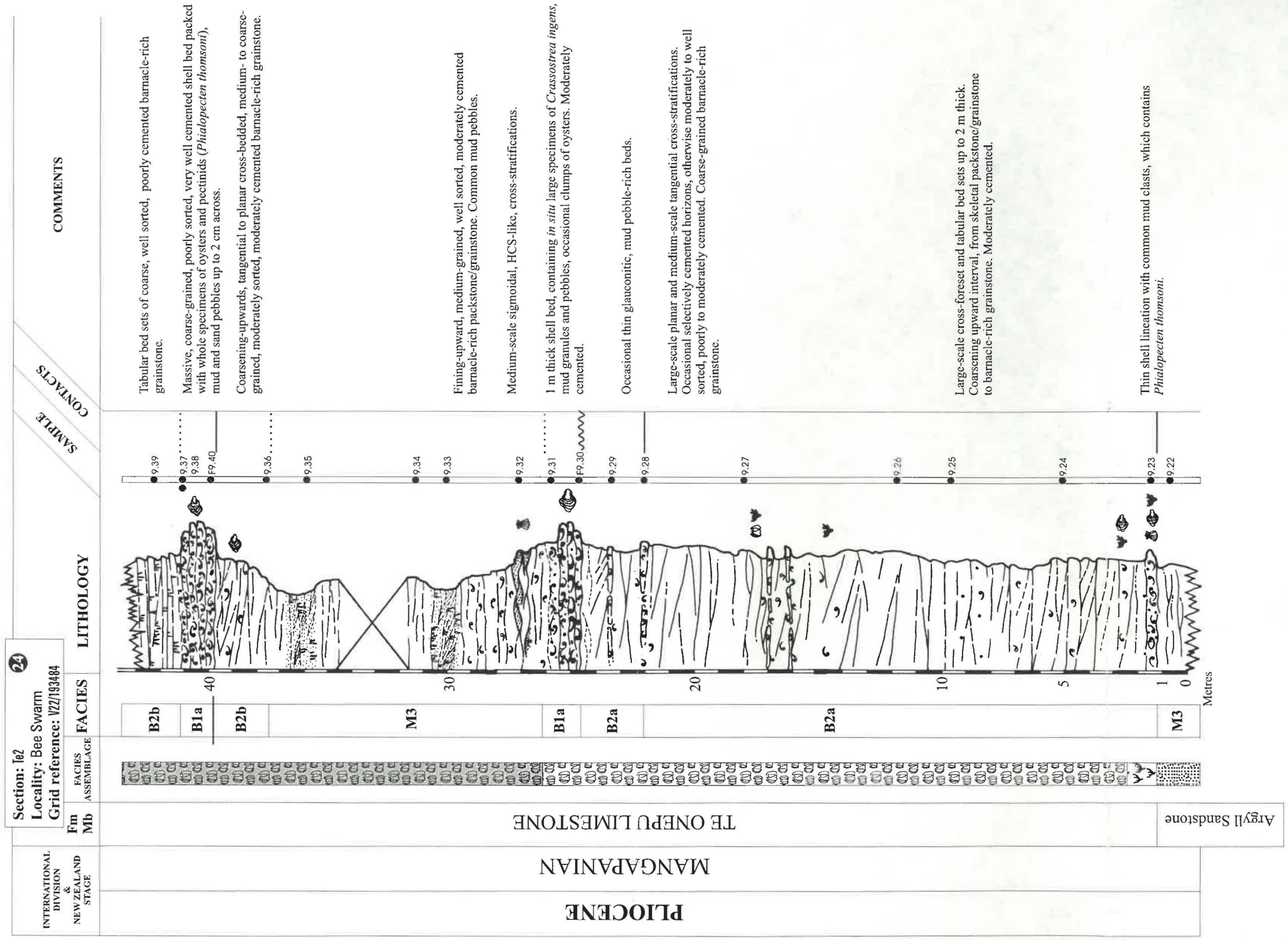

Figure 11- Section of the Te Onepu Limestone at Bee Swarm.

situ specimens of *Crassostrea ingens*. A fining-upwards trend exists above the shell bed, with minor HCS structures in a terrigenous/skeletal packstone (6 m). Common biomolds are present, and the deposits are moderately sorted and poorly to moderately cemented. Above a 2-3 m-thick covered interval, bioclastic sediments coarsen upwards once again into tangential to planar cross-bedded, moderately sorted, poorly to moderately cemented grainstone (5 m). This unit is sharply overlain by a very well cemented, 1.5 m-thick, shell bed packed with abundant oyster valves and scattered pectinids. It grades up section into horizontal-bedded grainstone, whose upper boundary is not exposed.

Thickness: 43 to 45 m.

4.6. Mason Ridge Formation (Nukumaruan)

Although hypothetically comprising Scinde Island Limestone, and for this reason included within the Napier Group (Beu, 1995; Figure 4), the name Mason Ridge Formation of Kelsey *et al.* (1993) is adopted here for several reasons:

- Its geographical distribution is important and well delimited.
- The limestone bodies (at least three) that form the Mason Ridge Formation are both vertically and laterally well developed and can easily be followed south of Ngaruroro River where the sections included in the present thesis were examined.
- Although several authors have correlated the lowest limestone sheet of Mason Ridge Formation to the Scinde Island Limestone on biostratigraphic and lithofacies arguments (Kingma, 1971; Kelsey *et al.*, 1993; Beu, 1995), correlation for the upper sheets with more geographically restricted limestones remains doubtful. Thus, a comprehensive study of the complete package is preferred that may help define in the future the stratigraphic position of isolated formations (e.g., Matapiro Limestone; see Chapter 4, Section 7.5.5).

Kelsey *et al.* (1993) proposed that the lowest limestone is early Nukumaruan based on the presence of *Phialopecten triphooki*, which might also suggest that this limestone is a lateral equivalent of Scinde Island and Pakipaki Limestones (Figure 2). Kelsey *et al.* (1993) proposed that the middle and upper beds of Mason Ridge Formation are middle to late Nukumaruan. However, one specimen of *Phialopecten triphooki* was collected from the shell bed capping the upper limestone at the Mangatai section

Figure 12– Mangapanian and Nukumaruan strata in southeastern Hawke's Bay

(A) Quarry within Te Onepu Limestone at its type locality (V22/198491). Sketch is superimposed on photograph to highlight some significant sedimentary characteristics of Te Onepu Limestone, including thin condensed shell lineation (black arrow), well cemented horizons (hardgrounds, white arrow) in otherwise poorly cemented coarse barnacle grainstone, and planar to tangential cross-foresets. A shell bed packed with giant *Crassostrea ingens* rests on an erosional surface on top of the section (see also Te Onepu Quarry section in Appendix 1 – column 23).

(B) Upper part of Mason Ridge Formation at Pakihirua section (V22/204564; Figure 13; column 30) showing basal horizontal planar bedded skeletal limestone overlain, across a sharp surface (dashed line), by a 4 m-thick shell bed.

(C) Sharp erosional surface (dashed line) within the Nukumaruan Matapiro Limestone on Ohiti Road (V21/300733; Figure 15; column 35), interpreted as a wave-cut surface of erosion formed after underlying beds had been tectonically tilted. Note that above the surface, bed sets are planar and almost horizontal, whereas below the surface bed sets are dipping towards right (20° N). Note also that the axis of water-escape structures (arrowed) makes a 20° angle from the vertical.

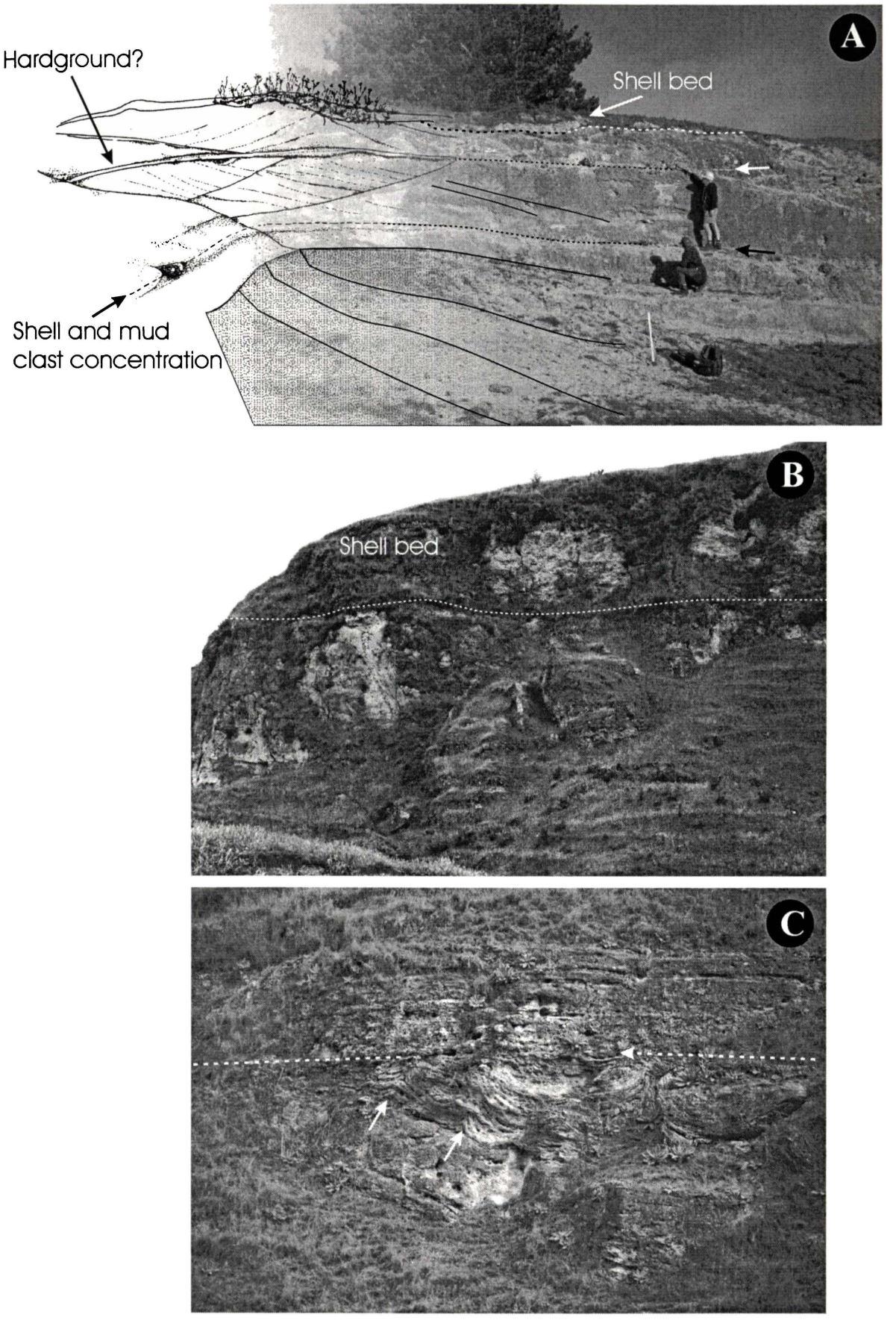
A
Hardground?
Shell bed
Shell and mud
clast concentration
B
Shell bed
C

(V22/163494; Appendix 1 – column 31), demonstrating that (1) *Phialopecten* survived beyond the earliest Nukumaruan time; and (2) Mason Ridge Formation is more likely to be early to middle Nukumaruan in age.

Beu (1995) suggested that the lowest limestone sheet of Mason Ridge Formation should be correlated to the Whanawhana Limestone (Section 4.11) by stratigraphic superposition and on the macrofaunal criterion that it also contains *Phialopecten triphooki*. However, once again the age of these limestone units is not constrained enough to allow high-resolution correlation, considering both the poor reliability of *Phialopecten triphooki* to assign a definite early Nukumaruan age (see above), and the discontinuous nature of the limestones deposited during this time interval (including Pakipaki and Scinde Island).

With this in mind, and because a prime interest here is to better understand the sequence stratigraphy of the Pliocene limestones, the present study has focused on the Mason Ridge Formation as providing a continuous stratigraphic record from the early to probably middle Nukumaruan, and does not discuss the limestones (Pakipaki and Scinde Island) inferred by others to be their lateral correlatives.

Although, as for older formations, fieldwork emphasized rapid lithological variations over short distances within each limestone sheet of the Mason Ridge Formation, these sheets are easily traceable along incised river valleys due to little variation in their lateral thickness and their low gradient, almost monoclinal, structure. The Mason Ridge Formation is cyclothemic in disposition, comprising thin mudstone/sandstone – limestone/shell bed (Figure 12B) formational couplets, remarkably similar to units within the upper part of the Petane Group within the Tangoio block in central Hawke's Bay (Figure 1; Haywick *et al.*, 1992; Haywick, 2000). Five sections of Mason Ridge Formation are included in this thesis. 91 rock samples were taken in the field, as well as 4 macrofaunal samples (Appendix 2).

Pakihirua section (Figure 13)

Location: The limestones crop out in the cliffs that dominate the Patangata Valley from V22/204564 to 188548, east of Raukawa-Te Onepu Road between its junctions with Whakapirau Road (north) and Paheke Road (south).

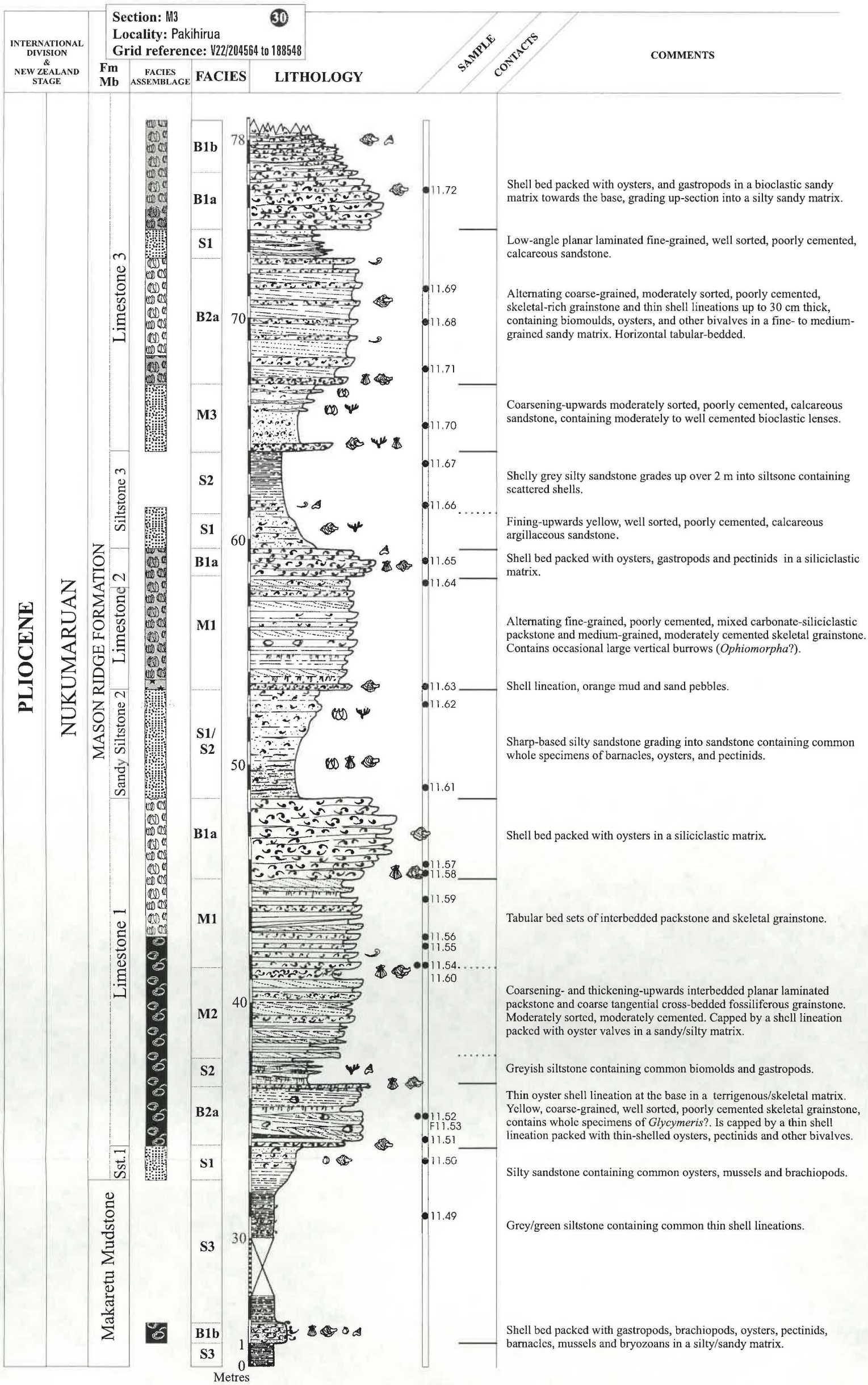

Figure 13- Section of the Mason Ridge Formation at Pakihirua.

Lithology: Three close sections along the western flank of the Pakihirua Stream and Patangata Stream valleys were measured, which in combination provide a continuous 75 m-thick profile (column 30; Figure 13). Sections were described at a decimetre-scale resolution where possible and sampled for petrography, carbonate content analysis, and biostratigraphy. These outcrops had never been described until now, though samples were taken for biostratigraphic study in correlative beds further south (V22/192526 and V22/174509; Beu, 1995).

The Pakihirua section involves three limestone sheets with interbedded mudstone/siltstone and sandstone that are well exposed and rather less weathered than their northern and southern equivalents (see Torran section and Mangatai sections; Appendix 1 – columns 29, 31). The vertical stratal pattern of each mudstone-sandstone/limestone formational couplet is remarkably similar, and more or less mirror one another (Figure 13).

About 30 m beneath the lower limestone sheet, Makaretu Mudstone (about 50 m exposed) contains a 1 m-thick shell bed packed with oysters, large gastropods, small pectinids, bryozoans (large robust branching), and other bivalves. Makaretu Mudstone grades, in the uppermost part of the formation, into fossiliferous silty sandstone. The upper contact is marked by a sharp surface and a thin shell lineation consisting of oysters and other bivalves in a medium-grained bioclastic matrix. Above is 2.5 m of low-angle planar bedded, skeletal grainstone containing articulated thick-shelled bivalves. The upper contact between this bioclastic limestone sheet and the overlying sandstone is sharp, and is marked by a 0.2 m-thick shell bed consisting of thin-shelled oysters, pectinids, and other unidentified bivalves. The fine-grained calcareous sandstone grades up over 2 m into coarsening-upwards alternating fossiliferous grainstone and packstone (8 m) in horizontal tabular bed sets, 0.3 m thick (see Figure 24B). This, in turn, is sharply overlain by a 4 m-thick shell bed, packed with oyster valves, that forms the base of the next couplet (see Figure 13 for details).

Figure 12B shows the upper part of the third formational couplet, which is sharply overlain by a 4-5 m-thick oyster shell bed.

Thickness: 50 to 55 m.

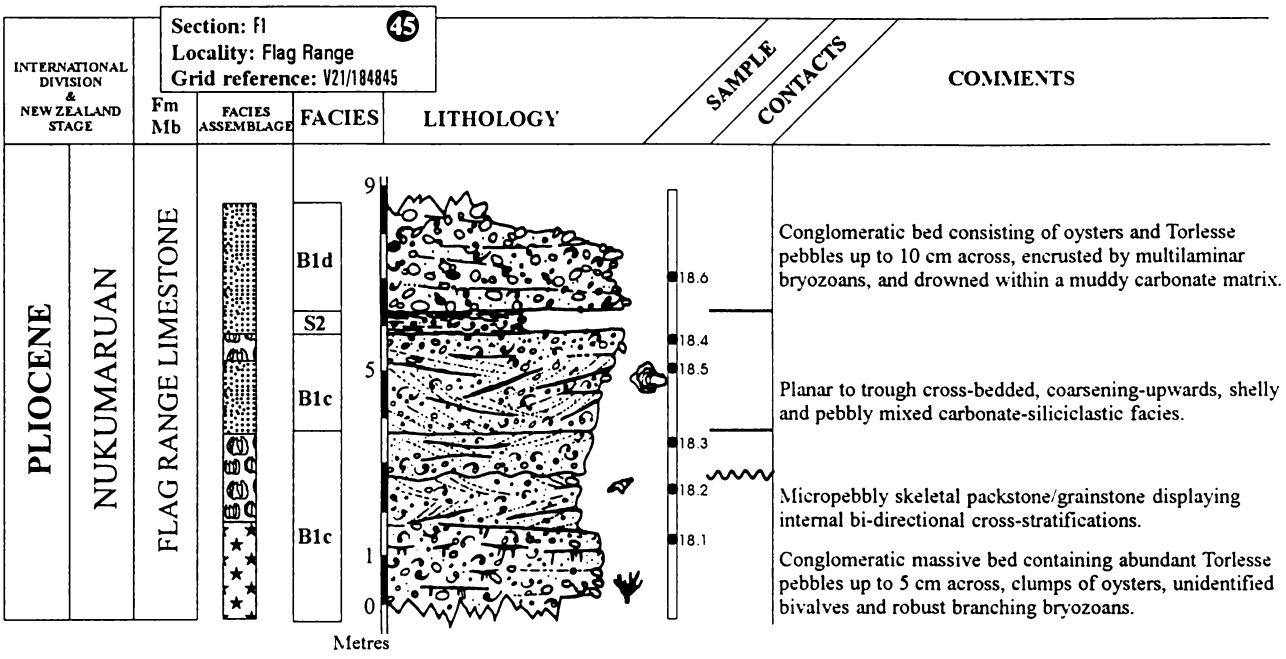

Figure 14- Reference section of the Flag Range Limestone on northwestern crest of the Flag Range.

4.7. Flag Range Limestone (Nukumaruan)

The Nukumaruan Flag Range Limestone was first investigated by Kingma (1971) who mapped it as part of the informal Sherenden greywacke gravels. Beu (1995) formally defined Flag Range Limestone as a new formation, and designated the type locality as 5 m-high bluffs along the northwestern edge of the crest of the Flag Range (Figures 1, 2). He suggested that Flag Range Limestone is a lateral equivalent of Tangoio Limestone, cropping out further east and north in Matapiro Syncline, which in turn has been proposed as a correlative to the lower limestone bed of Mason Ridge Formation (Beu, 1995). Flag Range Limestone contrasts with many previously described limestone formations by its high content of Mesozoic basement (Torlesse) granules and pebbles in a moderately to well cemented mixed carbonate-siliciclastic matrix. One stratigraphic column of Flag Range Limestone has been logged (Figure 14) from which 6 rock samples were collected.

Flag Range section (Figure 14)

Location: Flag Range Limestone crops out almost continuously on Flag Range Road about 2 km from its junction with the Napier-Taihape Road, in bluffs on the western crest of the Flag Range. The section (column 45) described below is located at V21/184845.

Lithology: The lower boundary of Flag Range Limestone is not exposed. The base of the measured section is a 2 m-thick conglomeratic massive bed that contains abundant Torlesse pebbles up to 5 cm across, clumps of oysters, and unidentified bivalves and robust branching bryozoans. It is overlain by 1 m of micropebbly skeletal packstone/grainstone displaying internal bi-directional cross-stratifications and thin mud layers. This interval is truncated above by an erosional wavy surface, upon which rest planar to trough cross-bedded, coarsening-upwards, shelly and pebbly mixed carbonate-siliciclastic facies (2.5 m). This is in turn overlain, across a thin muddy layer and a sharp surface successively, by a shelly conglomerate (2.5 m). The conglomeratic bed consists of oysters and Torlesse pebbles up to 10 cm across, encrusted by multilaminar bryozoans (celleporids), and drowned within a muddy carbonate matrix (trapped micrite). The upper boundary is not exposed.

Thickness: 8 to 9 m.

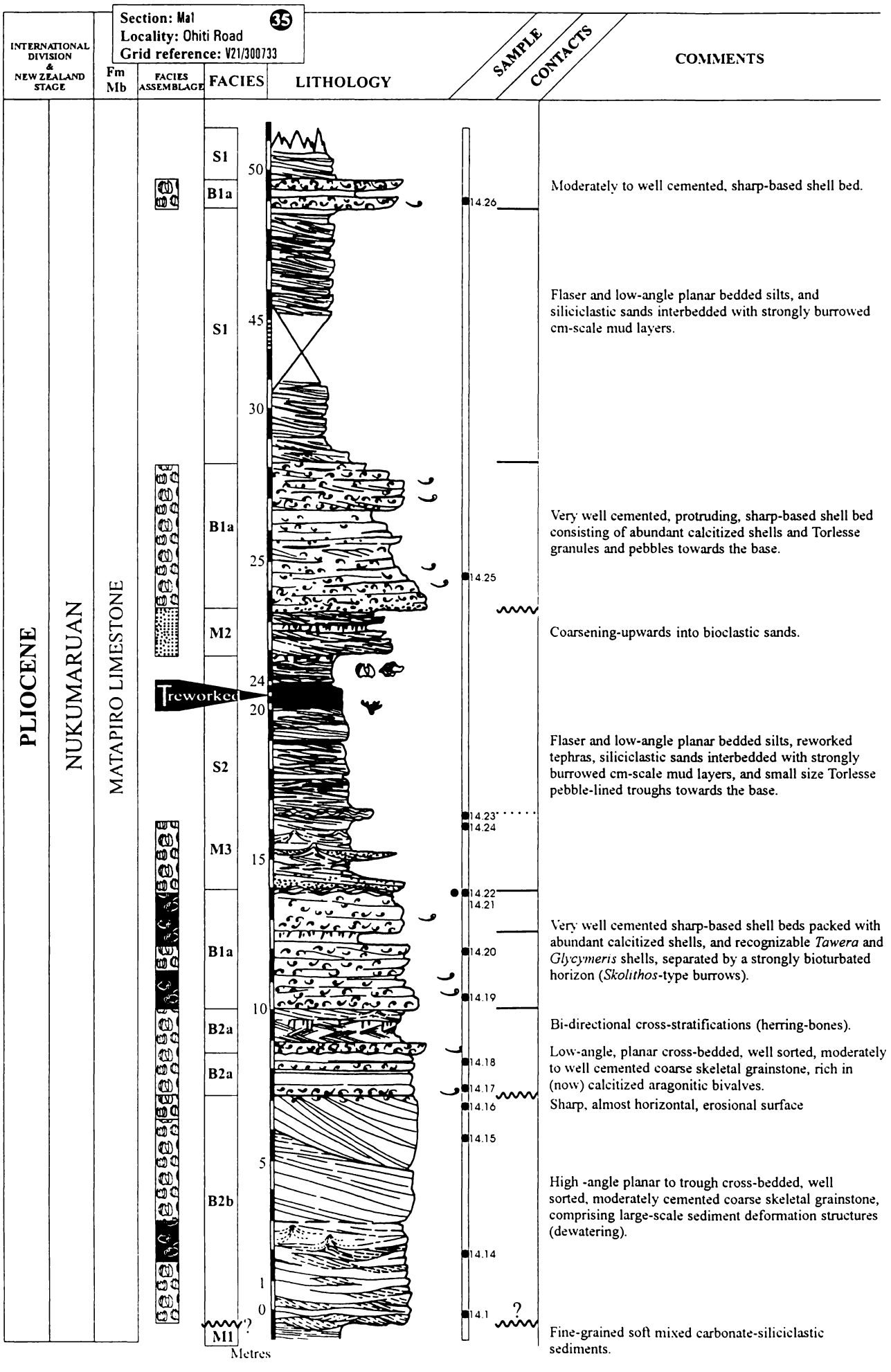

Figure 15- Reference section of the Matapiro Limestone on Ohiti Road.

4.8. Matapiro Limestone (Nukumaruan)

Previously correlated to the upper Scinde Island pebbly limestone at Napier (Kingma, 1971), the Nukumaruan Matapiro Limestone was formally described and named by Beu (1995) who considered it to be distinct from any limestone bed at Scinde Island. Matapiro Limestone is well exposed throughout the area of south central Matapiro Syncline, cropping out in the flanks of the Matapiro hills (Figure 1). It consists of three prominent well cemented shell beds containing common calcitic and aragonitic bivalves (*Tawera*, *Purpurocardia*, *Glycymeris*, etc), interbedded with planar laminated silts and siliciclastic sand intervals. The lower shell bed rests sharply on well sorted, soft to moderately cemented, cross-bedded skeletal-rich grainstone. Beu (1995) illustrated a sharp but uneven unconformable contact between Matapiro Limestone and the underlying Waitio Mudstone. 27 rock samples were collected from two stratigraphic sections.

Ohiti Road section (Figure 15)

Location: From SH 50 turn east (right) onto Napier-Taihape Road and soon south (left) into Ohiti Road, along which Matapiro Limestone is well exposed (V21/300733).

Lithology: This previously undescribed section (column 35) along Ohiti Road is a remarkably continuous outcrop of Matapiro Limestone and interbedded silt/siliciclastic sands (Figure 15).

The lowermost part of the exposure consists of fine-grained, soft, mixed carbonate-siliciclastic sediments overlain by 8 m of planar to trough cross-bedded, moderately cemented skeletal grainstone, which includes large-scale sediment deformation structures (dewatering). Both water-escape structures and cross-bed sets are truncated atop the foregoing interval by a sharp, almost horizontal, erosional surface (Figure 12C). In contrast, below the sharp surface, the axis of dewatering structures make a 20 to 25° angle with the vertical, suggesting that the lower interval was syndepositionally tectonically tilted, and that the truncation is a wave-planed surface or wave-cut surface of erosion.

This scenario is supported by the horizontal disposition of planar-bedded skeletal grainstone resting on the surface (Figure 12C). Horizontal bed sets (2 m) pass upwards into fine- to medium-grained poorly cemented skeletal grainstone (1.5 m) that exhibits bi-directional cross-stratifications (herring-bones; see Figures 16A, 23G).

Figure 16– Nukumaruan strata in southeastern Hawke's Bay, and Waipipian and Mangapanian strata in southwestern Hawke's Bay

(A) Lower part of Matapiro Limestone section along Ohiti Road (V21/300733; Figure 15) showing bi-directional cross-stratified skeletal beds (pointed by geologist; see Figure 23G) overlain by two distinct sharp-based shell beds separated by a strongly bioturbated fine-grained horizon (between the pair of upper dashed lines).

(B) Looking eastwards from the eastern slopes of the Maniaroa Range (Figure 1) showing shallow-dipping Waipipian to Mangapanian strata exposed in the southern flanks of the Waiiti Stream Valley at The Gorges section (V20/188007; Figure 18; column 40/41). Note the cyclothemic disposition of protruding limestone units and silt-sand interbeds. The lowermost limestone sheet is assumed to be a lateral equivalent of Titiokura Formation (Waipipian), though presently there are no data to constrain its age. The upper limestone succession (double arrow) consisting of several coarsening-upwards units belongs to the Te Waka Formation, Mangapanian in age as indicated by the common occurrence of *Phialopecten thomsoni*.

(C) Possible lateral equivalent of Titiokura Formation at the southern end of the Glenross Range (U21/032867; see Omahaki section in Appendix 1 – column 42). The bluff is about 20 m high. Note large-scale trough cross-beds (arrowed).

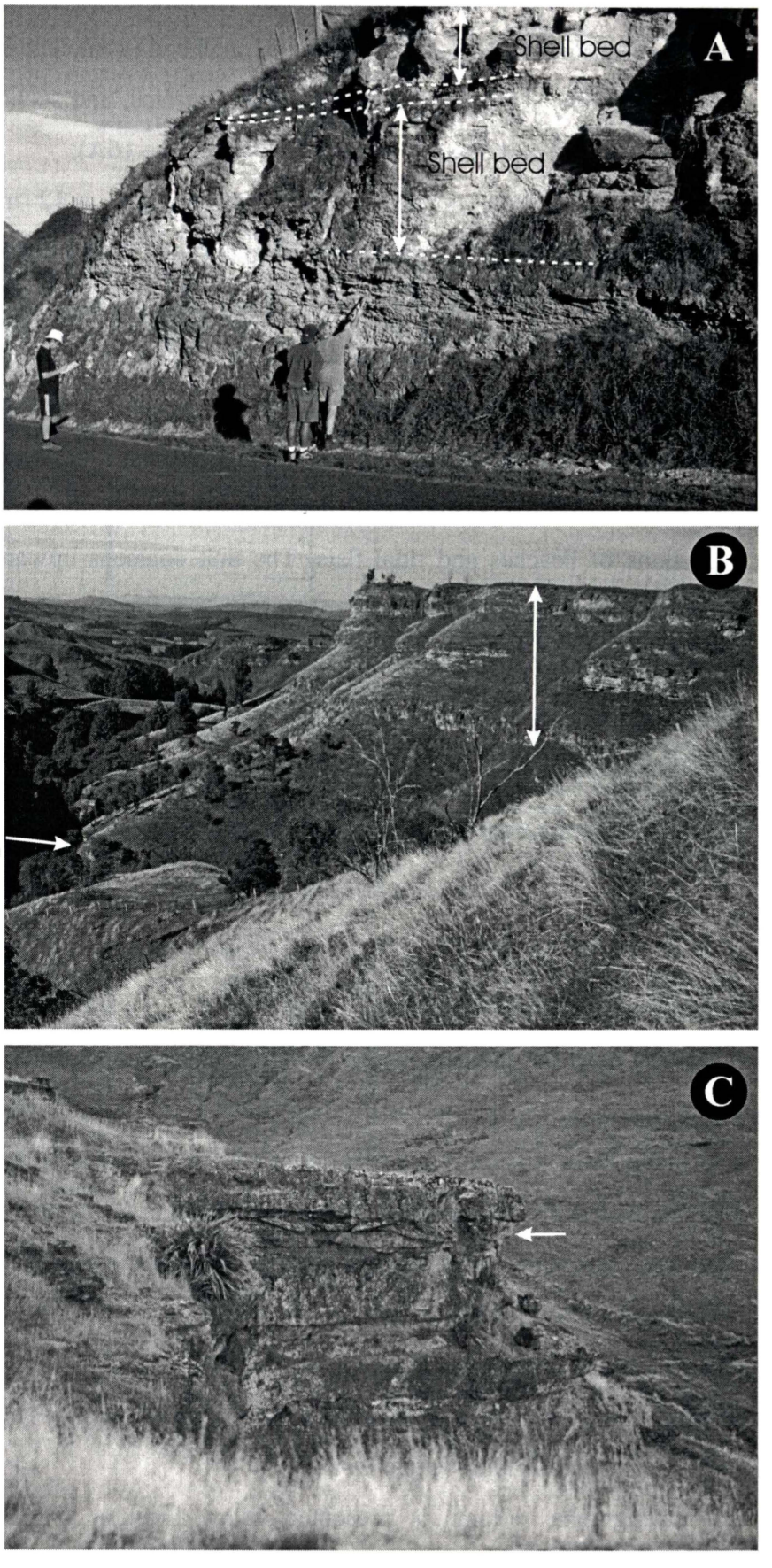
Shell bed
A
Shell bed
B
Titiokura
Formation?
C

Bioturbation is present in the form of individual *Skolithos*-type burrows, especially towards the top of this interval below a sharp-based shell bed (4 m). The latter comprises two fossiliferous members bounded below by a sharp surface, and separated by a thin, strongly burrowed, mixed carbonate-terrigenous layer (Figure 16A).

The upper fossiliferous member passes upward into a 12 m-thick interval characterized by silts, reworked tephras, siliciclastic sands interbedded with strongly burrowed cm-scale mud layers, and small size Torlesse pebble-lined troughs. Carbonate sand grains are generally subordinate to absent, and cementation is poor, although carbonate cemented concretionary mud nodules do occur. Sedimentary structures include flaser and lenticular beddings, low-angle planar cross-stratifications, and parallel laminations, which collectively suggest a flat depositional setting such as found on foreshore portions of beaches and tidal flats. The unit coarsens upwards and skeletal fragments become more evident again up section. A 5 m-thick, well cemented, sharp-based shell bed caps the preceding unit and is in turn overlain by 25 m of silt/siliciclastic facies similar to that described from lower in the section. The top of the section is marked by a well cemented shell bed (1.5 m) resting on a sharp contact with underlying beds.

Thickness: 55 to 60 m.

4.9. Titiokura Formation (Waipipian)

Beu *et al.* (1980) used the informal name Titiokura limestone to describe a Waipipian limestone unit exposed near the summit of the Napier-Taupo Road (Highway 5), which later was formally defined and given formation status by the same author (Beu, 1995). Bland (2001) extended the definition of Titiokura Formation to include a conglomeratic coquina bed and sandstone overlying the Titiokura Limestone of previous authors. Titiokura Formation rests unconformably on the Mokonui Formation and underlies the Mangapanian Te Waka Formation (Figure 2) across an erosional to laterally conformable contact (Bland, 2001). Titiokura Formation is well exposed along the crest of the Te Waka Range south of the Napier-Taupo Road.

One stratigraphic column is presented below (Figure 17). 8 samples were collected, mostly from the base and the middle part of the section.

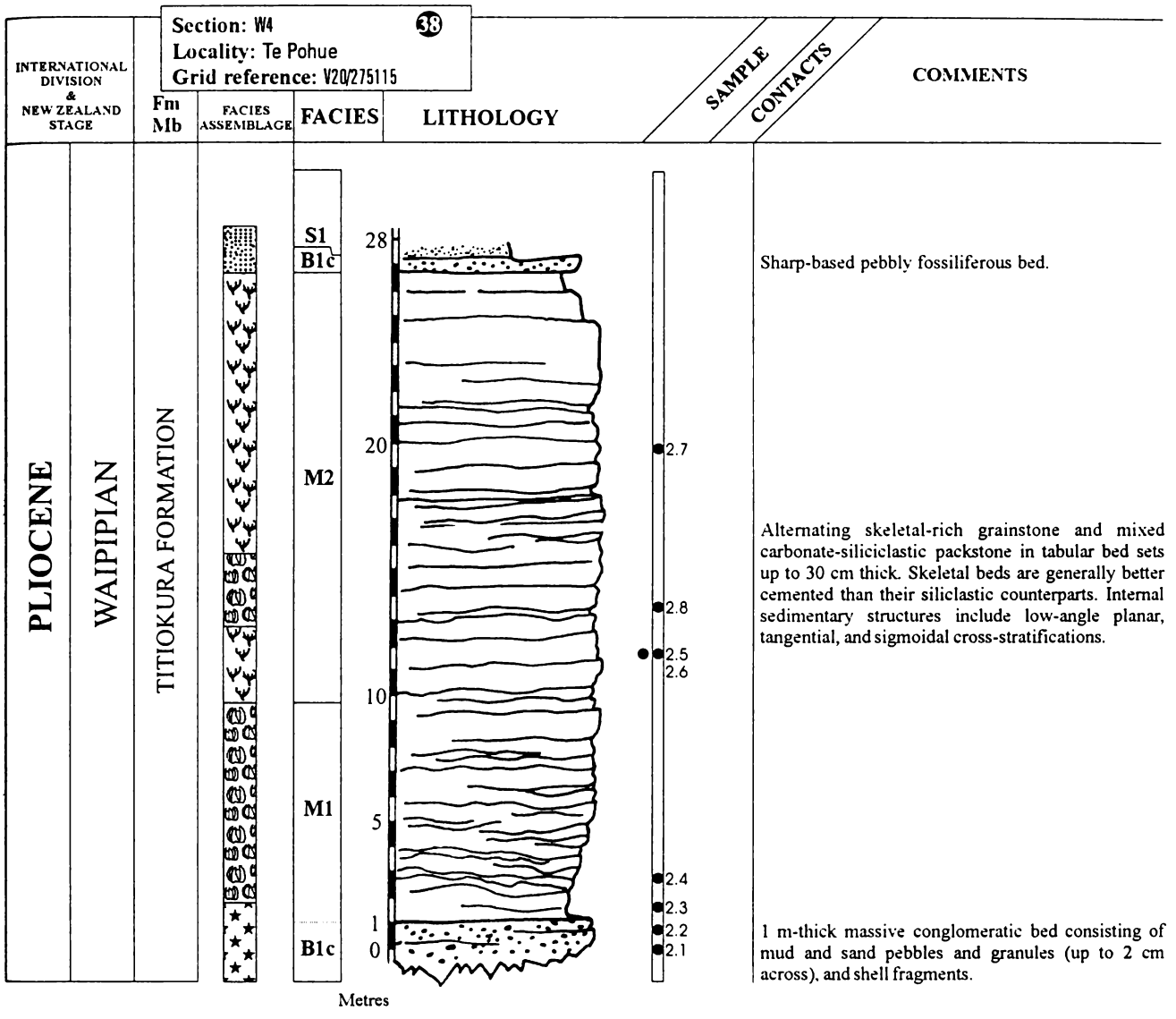

Figure 17- Section of the Titiokura Formation at Te Pohue.

Te Pohue section (Figure 17)

Location: The outcrop (column 38) occurs on Oakmere Station at V20/275115, and can be seen from the Napier-Taupo Road a few kilometres before entering Te Pohue in the grassy slopes beneath the prominent scarp faces of Te Waka Formation (see Section 4.10).

Lithology: The lower boundary is sharp to erosional, and is characterized by a 1.5 m-thick massive conglomeratic bed consisting of mud and sand pebbles and granules (up to 2 cm across), and shell fragments. This lower bed is sharply overlain by coarsening-upwards alternating skeletal-rich grainstone and mixed carbonate-siliciclastic packstone in tabular bed sets up to 30 cm thick. Skeletal beds are generally better cemented than their siliciclastic counterparts, although there is a strong modern meteoric overprint which tends to blur primary differential cementation. Internal sedimentary structures include low-angle planar, tangential, and sigmoidal cross-stratifications. The apparent flagginess of tabular cross-beds and horizontal beds originates in pressure-dissolution seams, which also enhance bedding in places. Shell fragments and barnacle plates dominate the composition of the limestone in its lower part, while in its middle and upper portions bryozoan fragments become more frequent. The upper boundary of the limestone unit of Titiokura Formation is marked by a sharp-based pebbly fossiliferous bed, in turn overlain by sandstone.

Thickness: 25 to 28 m.

4.10. Te Waka Formation (Mangapanian)

Beu *et al.* (1980) referred the Mangapanian limestone beds interlayered with silt-sandstone intervals cropping out along the eastern slopes of the axial Ruahine-Kaweka Ranges to the informal Te Waka limestone (Figures 1A, 2). Beu (1995) formally defined and gave formation status to Te Waka Limestone. He designated the northernmost outcrop of the formation, exposed on the north face of the Te Waka Trig, as the type section (V20/257131). Bland (2001) defined two new members (Awhina and Oakmere) in his new Te Waka Formation based on his recognition of two distinct, although laterally interdigitating, components that also crop out in the Te Waka Trig area. The Awhina Member consists of a lower sandstone overlying the Titiokura Formation, and an upper limestone composed of two separate beds. The Oakmere Member is the prominent

coquina limestone (50 m) cropping out on Oakmere and Te Waka Stations, and along Te Waka Road (V20/271106 to 248083). Bland (2001) assigned a latest Waipipian to earliest Mangapanian age to the Te Waka Formation, based on the co-occurrence of *Phialopecten marwicki* and *Mesopeplum crawfordi*, together with the presence of specimens of *Phialopecten marwicki/thomsoni* hybrids.

This study concentrated on outcrops south of the Te Waka Range, along the western crest of the Maniaroa Range and in river valleys incising its eastern slopes, and further south on the southern edges of the Glenross Range (Figures 1, 2). Five stratigraphic columns were logged, including one in the Te Waka Trig area (Appendix 1 – column 38), and 60 rock samples were collected.

The Gorges section (Figure 18)

Location: The name The Gorges derives from The Gorges Station on Puketitiri Road. Te Waka limestone beds form the bluffs bordering the northern and eastern flanks of the Waiiti Stream, and are better exposed (column 40/41) up stream at V20/188007.

Lithology: The section presented here includes limestone beds cropping out in the flanks of the Waiiti Stream valley, and is completed by the succession exposed in the slopes, and on top of Mount Romulus (V20/168027), north of Mount Hassal Station. The complete stratigraphic section at The Gorges is almost cyclothemic in disposition (Figures 16B, 18), and the seven main units comprising it can be grouped into siltstone-sandstone/limestone-conglomerate formational couplets.

The lower limestone (possibly a Titiokura equivalent; see below), whose basal contact with underlying beds is not exposed, consists of (at least) three coarsening-upwards, sharp-based units separated by thin (20-30 cm), fine-grained mixed carbonate-siliciclastic layers bioturbated by *Skolithos*-type burrows. The lower (5 m) and middle (5 m) units comprise alternating barnacle-rich grainstone and terrigenous packstone organized in horizontal tabular bed sets, 20-30 cm thick. Internal sedimentary structures include low-angle planar and tangential cross-stratifications. Both units are pervasively bioturbated. The upper unit (10 m) consists of four stacked bioclastic bodies, each 2-3 m thick.

Medium-scale trough and sigmoidal cross-stratifications occur within moderately cemented, coarse, barnacle-rich grainstones. Mud layers interbedded with small-scale sigmoidal cross-laminated skeletal beds are common up section. The top of the limestone

consists of planar-bedded, soft, fine-grained bioclastic sandstone sharply overlain by a thin (20 cm) shell concentration packed with oysters and pectinids.

This limestone grades up over 2 m of sandstone into 20 m of siltstone. The contact between the siltstone interval and the middle limestone (limestone 2 in Figure 18) is gradational. The vertical succession of facies within the middle limestone above the silty sandstone includes: (1) alternating, discontinuous, medium-grained skeletal lenses (probably tempestites) and interlayered, planar laminated, terrigenous packstone (2 m). Skeletal lenses become more continuous upwards and grade into (2) horizontal tabular bed sets of alternating grainstone and packstone (1.5 m); (3) these rapidly coarsen upwards and include up section coarse shell and barnacle fragments, and Torlesse granules (1.5 m). The middle limestone rapidly passes upwards, across a sharp surface, into poorly exposed soft silty sandstone (10 m).

The upper limestone (limestone 3 in Figure 18) corresponds to the limestone sheet that forms the scarp edge of the Maniaroa Range, and contains *Phialopecten thomsoni*. The limestone comprises three distinct components. The lower portion consists of pebbly and barnacle-rich grainstone, containing common, well rounded Torlesse pebbles and granules up to 1 cm across. The interval is organized in thickening-upwards tabular bed sets that exhibit internal low-angle planar and tangential cross-stratifications. A protruding, well cemented, massive, 0.5 m-thick shell bed with scattered Torlesse pebbles sits sharply on top of this lower limestone component. It contains rare *Phialopecten thomsoni* valves that are difficult to remove from the coarse skeletal matrix.

The upper contact between the shell bed and the next overlying limestone component is sharp. It is overlain by a sequence of coarsening-upwards facies from planar laminated terrigenous packstone to coarse pebbly barnacle grainstone, nodular in appearance. The uppermost component of the upper limestone at The Gorges mirrors the underlying one in its stratal architecture, even though its upper boundary is not exposed.

The overlying siltstone to sandstone interval (20-25 m) is sporadically exposed in the grassy slopes of Mount Romulus. A conspicuous ravinement surface places this soft succession in direct contact with a fossiliferous conglomerate (5 m) containing mud and Torlesse pebbles (up to 20 cm across), oysters, and various unidentified bivalves.

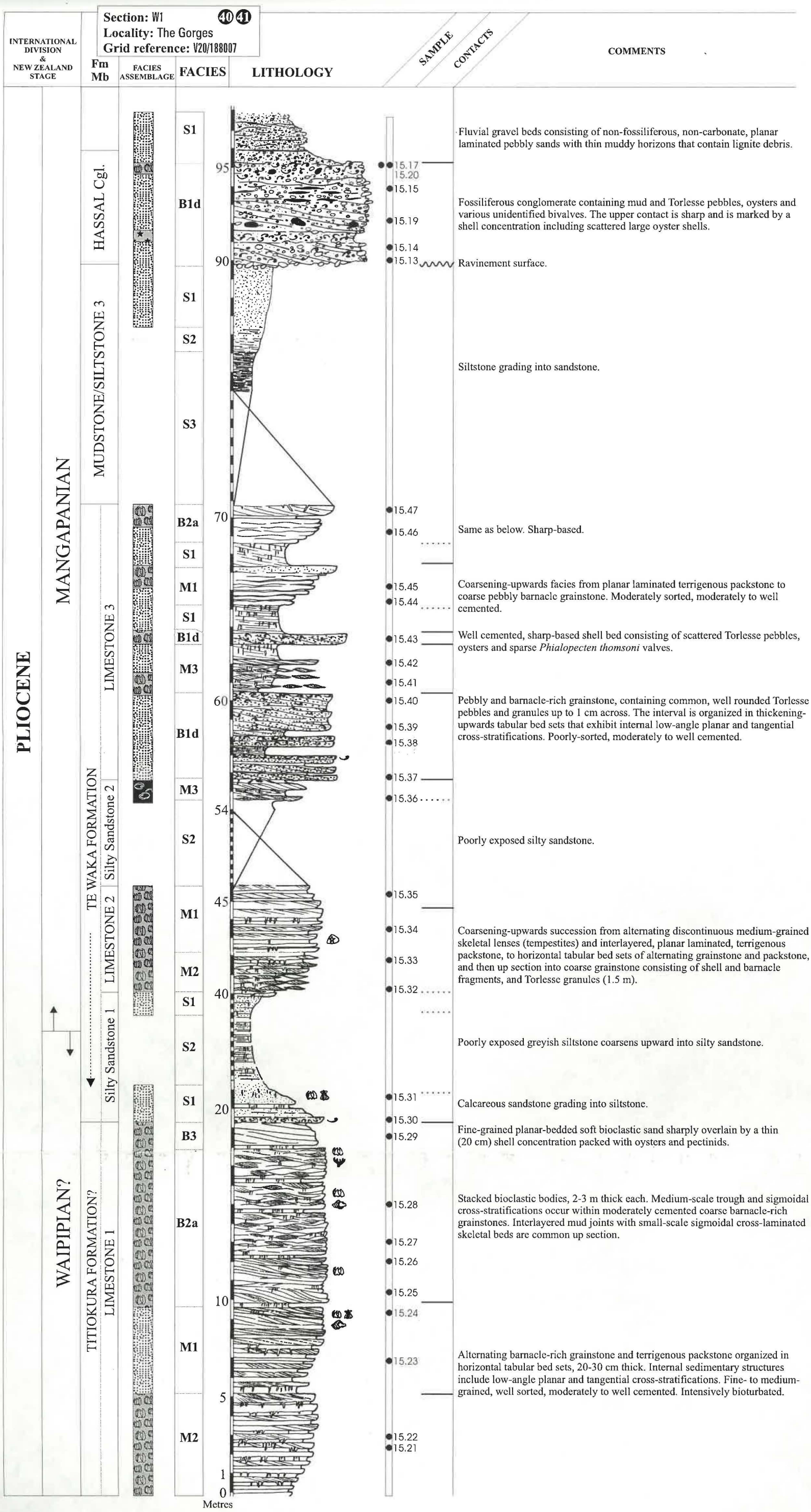

Figure 18- Section of the Te Waka Formation at The Gorges.

The upper contact is sharp and is marked by a shell concentration including scattered large oyster shells. This surface is overlain by fluvial gravel beds consisting of non-fossiliferous, non-carbonate, planar-laminated pebbly sandstones with thin muddy horizons that contain lignite debris.

Local correlation: Beu (1995) describes Te Waka Formation south and north of the Maniaroa Range area as two limestone members separated by 30 m of sandy mudstone. The description of his lower member cropping out on the edge of the Maniaroa Range conforms to the upper limestone unit at The Gorges (limestone 3; Figures 18, 19). Moore and Hatton (1985) reported a few km south of The Gorges section, two separate thin limestone bodies, which Beu (1995) inferred to represent his lower Te Waka Formation member, locally subdivided. These two thinner limestones obviously are correlative to our middle and upper limestone units (Figure 19). Beu (1995) records the upper Te Waka Formation member in road cuttings on the Puketitiri Road, otherwise not recognized at The Gorges section, but which could be, by superposition, a lateral equivalent of the fossiliferous conglomerate at Mount Romulus (Figure 19).

Neither Moore and Hatton (1985) nor Beu (1995) mention the 20 m-thick coquina limestone recognized at the base of The Gorges succession (Figures 18, 19). Although, there are no age data for this limestone, superposition indicates that it could be a lateral equivalent of Titiokura Formation present about 10 km further north in the Te Waka Trig area, and possibly present further south near the Napier-Taihape Road, as suggested by Beu (1995), and reported here (Omahaki section; Appendix 1 – column 42; U21/032867; see Figure 16C).

Thickness: 95 to 100 m, including Hassal Conglomerate and underlying mudstone/sandstone interval. Otherwise 70 m.

4.11. Whanawhana Limestone (Nukumaruan)

Beu (1995) first described and formally named the Nukumaruan age Whanawhana Limestone, cropping out at the southern end of the Glenross Range where it conformably overlies the Mangapanian Te Waka Formation. Beu (1995) reports *Phialopecten triphooki* and *Zygochlamys deliculata* within the formation, demonstrating an early Nukumaruan age. He designated a reference section for the Whanawhana Limestone on the western edge of the crest of the southern Glenross Range,

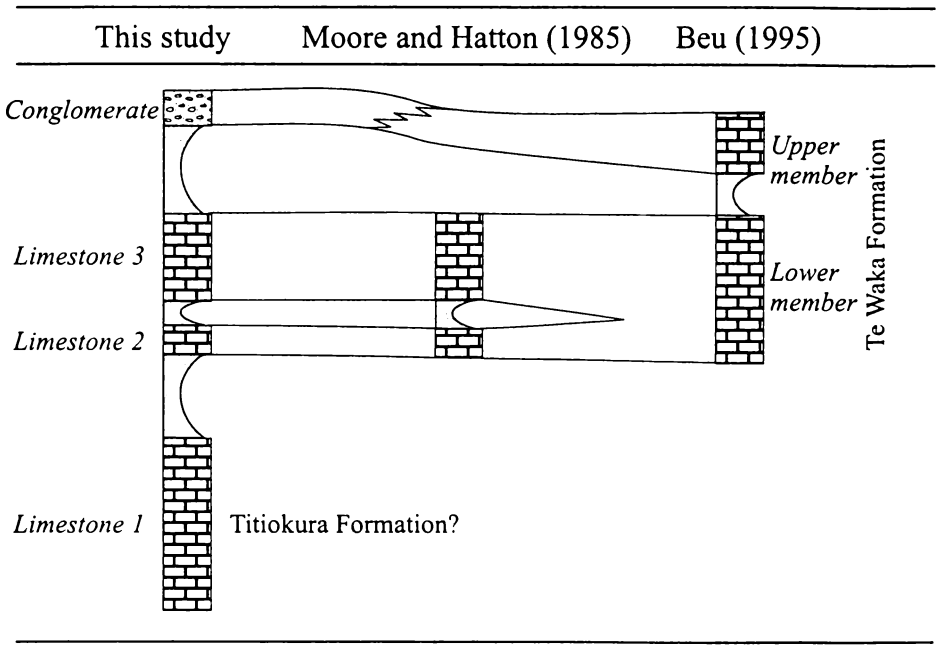

Figure 19- Summary comparison of the stratigraphy for the Te Waka Formation described by Moore and Hatton (1985) and Beu (1995) in the southern part of the Maniaroa Range (Figure 1), with the limestone successions identified in this study for The Gorges section (Figure 18). The correlation panel suggests, if correct, that the lower limestone unit at The Gorges section could be equivalent to the Titiokura Formation. See text for discussion.

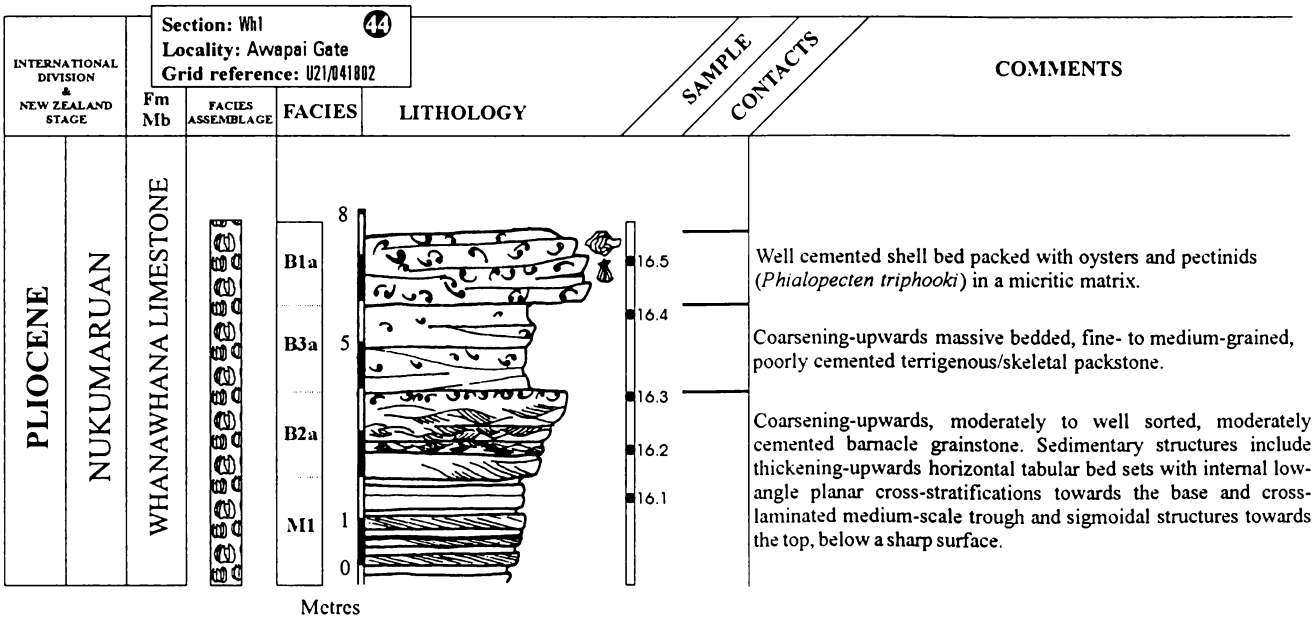

Figure 20- Reference section of the Whanawhana Limestone north of the Awapai Station gate on Whanawhana Road.

which is retained as a key section for this study (Figure 20), from which 5 samples were collected.

Awapai Gate section (Figure 20)

Location: A good exposure (column 44) is at U21/041802, about 200 m south of the Awapai Station gate on Whanawhana Road.

Lithology: Whanawhana Limestone comprises three separate components, which are from bottom to top: (1) Lower boundary not exposed, then 4 m of coarsening-upwards, moderately cemented barnacle grainstone. Sedimentary structures include thickening-upwards horizontal tabular bed sets with internal low-angle planar cross-stratifications towards the base and cross-laminated medium-scale trough and sigmoidal structures towards the top of the component. The contact between the lower and middle Whanawhana limestone components is sharp and is marked by a thin shell concentration; (2) coarsening-upwards massive bedded, fine- to medium-grained, poorly cemented terrigenous/skeletal packstone (2 m), containing common biomolds; and (3) a 2 m-thick, well cemented, shell bed packed with oysters and pectinids (*Phialopecten triphooki*) in a micritic matrix. The upper boundary is sharp.

Thickness: 8 m.

4.12. Sentry Box Limestone (Nukumaruan)

The Sentry Box Limestone was formally named and defined by Erdman and Kelsey (1992) and Kelsey *et al.* (1993) as a "pebbly barnacle grainstone to a fossiliferous mudstone-clast rudite with interbeds of massive mudstone and locally dominant granule to pebble conglomerate", containing common *Zygochlamys deliculata*. Sentry Box Limestone crops out in the central and southern Ohara Depression (Figures 1, 2). It conformably overlies complex siliciclastic beds of the Kaumatua Formation and grades upwards into the Ohara Mudstone. Beu (1995) pointed up the very unusual fossil content of both the Sentry Box Limestone and the overlying siliciclastic unit, containing deep- and cold-water fossils, and bathyal gastropod fauna, respectively. He argued that the Sentry Box Limestone was deposited during a glacial period, and that this contrasts with almost all other Nukumaruan limestones in eastern North Island thought to

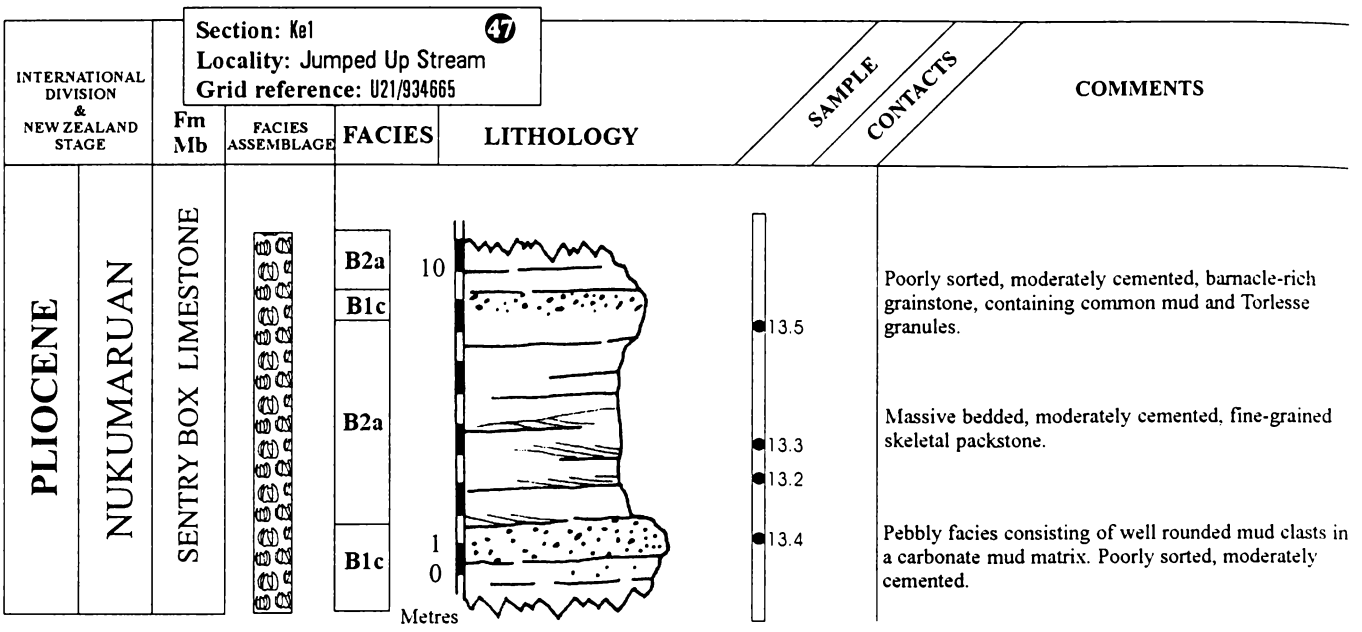

Figure 21- Reference section of the Sentry Box Limestone in the Jumped Up Stream Reserve.

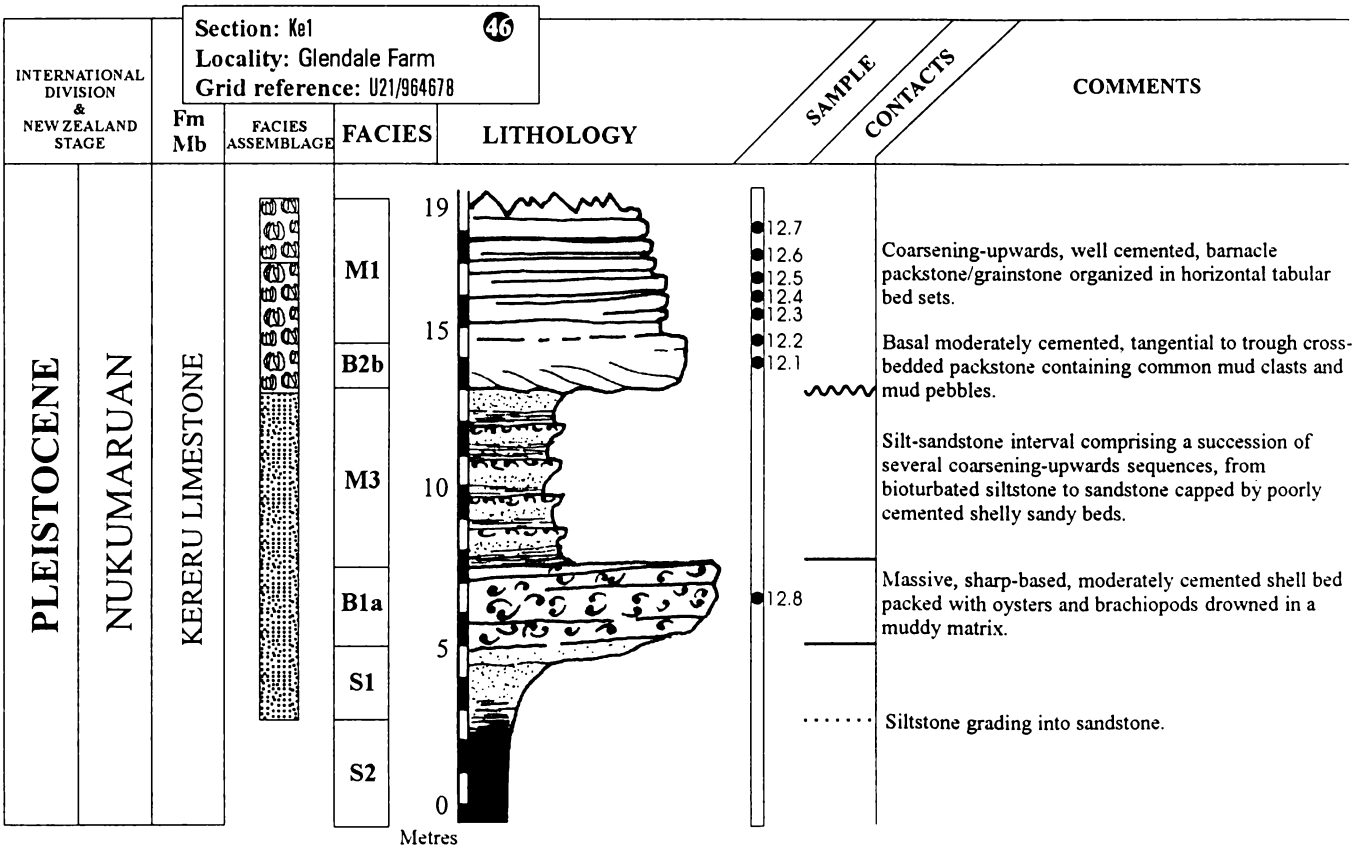

Figure 22- Reference section of the Kereru Limestone on Glendale Station..

have formed during interglacial periods (Beu, 1995).

The section visited is in a small quarry, about 200 m from the Jumped Up Stream (U21/934666) where Kelsey *et al.* (1993) designated the type section for Sentry Box Limestone. 5 samples were collected.

Jumped Up Stream section (column 47; Figure 21)

Location: A few hundred metres south of Mangleton Station, on the right side of Mangleton Road, beyond the bridge over Jumped Up Stream at U21/934665.

Lithology: The base of the measured section (Figure 21) contains numerous well rounded mud clasts in a carbonate mud matrix. The lower pebbly facies grades up over 2 m into massive bedded, fine-grained skeletal packstone (6-7 m). This interval coarsens towards its top into poorly sorted, moderately cemented, barnacle-rich grainstone, containing common mud and Torlesse granules. The upper boundary is not exposed at this locality.

Thickness: The measured section is 11 m thick.

4.13. Kereru Limestone (Nukumaruan)

Erdman and Kelsey (1992) formally defined the Kereru Limestone and restricted the name to the late Nukumaruan limestone cropping out along the eastern edge of the Wakarara Range, and as small platforms along the western edge of the same range (Figures 1, 2) where it forms the top of the Neogene stratigraphy in the Ohara Depression. At the locality visited in the course of this study, the Kereru Limestone sharply overlies calcareous sandstone probably forming the top of the Ohara Mudstone. 8 samples were taken from one stratigraphic section (Figure 22).

Glendale Farm section (Figure 22)

Location: Across Mangleton Road from Glendale Farm, along a farm pathway on a hill ascent at U21/967687 (column 46).

Lithology: Kereru Limestone consists of two distinct carbonate units separated by a 5-6 m-thick silt-sandstone interval comprising a succession of several coarsening-upward

sequences, from bioturbated siltstone to sandstone capped by poorly cemented shelly sandy beds (15-20 cm thick).

The lower carbonate bed is a 3-4 m-thick, massive, sharp-based, moderately cemented, shell bed packed with oysters and brachiopods drowned in a muddy matrix. Its upper boundary is sharp. The contact between the siltstone/sandstone interval and the overlying limestone unit is erosional. This limestone is 5-6 m thick, and consists of (1) a basal moderately cemented, tangential to trough cross-bedded, packstone (2 m) containing common mud clasts and mud pebbles from the underlying interval; and (2) an upper, coarsening-upwards, well cemented, barnacle packstone/grainstone (4 m exposed) organized in horizontal tabular bed sets (20-30 cm). The upper boundary is not exposed.

Thickness: The measured section is almost 20 m thick.

5. Sedimentary facies

During the course of fieldwork and section descriptions, an attempt was made to categorize the various deposits encountered into a finite number of sedimentary facies. In the end, 14 depositional facies have been erected for the Plio-Pleistocene bioclastic and siliciclastic rocks in southern Hawke's Bay, and these have been assigned facies codes for ease of reference on the stratigraphic columns (Appendices 1, 3) and elsewhere. It should be kept in mind that transitions between the various facies do occur. Three major facies assemblages have been established: Bioclastic, Mixed carbonate-siliciclastic, and Siliciclastic as follows:

- **Bioclastic facies (B1-3)** that include fossiliferous rudstone with a terrigenous/skeletal matrix (B1a); fossiliferous rudstone with a silty/muddy matrix (B1b); pebbly rudstone (B1c); conglomerates rich in Torlesse pebbles and fossiliferous in places (B1d); barnacle-rich grainstone (B2a); skeletal-rich grainstone (B2b); skeletal-rich packstone (B3a); and skeletal-rich packstone and wackestone (B3b).

- **Mixed carbonate-siliciclastic facies (M1-3)**, transitional between bioclastic facies and siliciclastic facies, include alternating grainstone and packstone (M1); interbedded grainstone and terrigenous packstone (M2); and interbedded terrigenous packstone and calcareous sandstone (M3).

- **Siliciclastic facies (S1-3)** include calcareous sandstone (S1); siltstone (S2); and mudstone (S3).

Table 1 summarizes the key attributes of the different sedimentary facies, including their constituents, physical structures, and ichnology. It also notes an interpreted depositional setting for each facies, elaborated upon in the following sections. An extra copy of Table 1 is contained in the thesis back cover pocket.

5.1. Bioclastic rudstone facies (B1a, B1b, B1c, B1d)

Molluscs, bryozoans, benthic foraminifers, and locally echinoderms dominate bioclastic rudstone facies. Other common components are bored pebbles, barnacles, glauconitic grains, and rounded intraformational mudstone and sandstone clasts. Accessory components include brachiopods and planktic foraminifers. Skeletal clasts are variably abraded, and generally skeletons are disarticulated and fragmented. Thickness of bioclastic rudstone facies ranges from 0.2 m up to 5.0 m.

Facies B1a - Fossiliferous rudstone: These mostly comprise uncommon *in situ* shell beds (up to 4 m thick) and frequent traction-emplaced or concentrated shell beds (up to 5 m thick) (Figure 23A). Their upper boundary is generally sharp or gradational, while their basal contact ranges from sharp to erosional with conspicuous medium-scale relief (up to 20 cm). B1a fossiliferous rudstones are massively bedded, but locally exhibit internal troughs up to 50 cm thick and 2 m across. Skeletons are dominated by ostreids and pectinids or scallops, but robust branching and encrusting cheilostome bryozoans are also common, within a mixed clast-mud supported matrix.

Scallops and thick-shelled oysters exhibit a wide spectrum of abrasion, bioerosion, and encrustation features. Scallops and oysters of *in situ* shell beds mostly are whole, but may be disarticulated, slightly abraded, encrusted by bryozoans and *Balanus* species (*Notobalanus vestitus, Austromegabalanus (Notomegabalanus) miodecorus, Fosterella tubulatus* – Harmsen, 1984; Kamp *et al.*, 1988; Beu, 1995), and commonly bored. In traction-emplaced shell beds, shells are moderately to well abraded, often disarticulated, extensively bored by endolithic algal and fungal borers (larger bores are also present due to ?crabs), and encrusted on the inside of valves.

Interpretation

Robust branching and encrusting cheilostome bryozoans are adapted to colonize stable shelly substrates in generally turbulent inner shelf settings (Nelson *et al.*, 1988a). Barnacles, as filter feeders, are inhabitants of sandy-gravelly sea floors where

Table 1- Summary of facies attributes and their interpretation for the Pliocene sedimentary deposits in southern Hawke's Bay.

Facies and constituents	Physical structures and geometries	Ichnology	Interpretation
Bioclastic Facies			
B1a Fossiliferous rudstone: terrigenous/skeletal matrix (<40% quartz); bivalves (especially oysters, pectinids, brachiopods, bryozoans (encrusting and robust branching), barnacles, rare echinoids, rare gastropods; mud pebbles and occasional bored pebbles	Massive bedding, local trough cross-bedding; medium to thick bedded (<0.5 m up to 4 m); continuous or lensoid	Bioturbation	Shallow water, high energy, intertidal to subtidal *in situ* oyster shell bank and traction emplaced shell beds
B1b Fossiliferous rudstone: silty/muddy matrix (<15% quartz); bivalves (especially oysters), brachiopods, turritellid gastropods, bryozoans (rigid and delicate branching)	Massive bedding, planar cross-bedding; sharp contact with underlying beds; thick bedded (up to 3 m), continuous	Bioturbation	Shallow water, low energy, sheltered subtidal environment oyster shell bank
B1c Pebbly rudstone (fossiliferous): terrigenous/skeletal matrix (<50% quartz) bivalves (especially oysters), pectinids, rare bryozoans (encrusting and robust branching); locally Torlesse pebbles, bored pebbles up to 15 cm in size, locally abundant mud and sand clasts	Massive bedding, flaggy bedding; erosional contact with underlying beds; thick bedded (up to 3 m), continuous or lensoid		Shallow water, high-energy, intertidal, possibly channel-fill deposits
B1d Conglomerate: terrigenous/skeletal matrix, Torlesse boulders and pebbles (average size 2 cm but up to 20 cm), fossiliferous in places	Massive bedding; thick bedded (up to 2 m), tangential and trough cross-bedding in the finer-grained beds	Bioturbation	Fan-delta channel-fill deposits fan delta front
B2a Barnacle-rich grainstone: (<20% quartz); coarse-grained debris; mostly barnacles, oysters, bryozoans and echinoids; locally whole specimens of pectinids and other bivalves; mud clasts in places	Planar cross-stratification, trough cross-bedding, sharp to erosional contact with underlying beds; medium to thick-bedded local mega and so-called giant foresets; continuous, up to 3 m thick sheet-like units	*Thallasinoides* *Skolithos*	Shallow, high energy setting, tidal currents swept sea floor, sand waves
B2b Bioclastic grainstone: (<25% quartz); medium to coarse-grained; barnacles, oysters, various bivalves, bryozoans (encrusting and rigid branching), brachiopods; sand and mud clasts	Planar and tangential cross-stratification, trough cross-bedding; often sharp base; medium-bedded (<1 m); continuous, though laterally discontinuous sheets in places	*Thallasinoides* *Skolithos*	Shallow, high energy setting, tidal or storm-driven currents swept sea floor; sand waves
B3a Bioclastic packstone: (<40% quartz); fine to medium-grained; barnacles, oysters, pectinids, brachiopods (common in places), bryozoans (rigid and delicate branching), rare echinoids; mud clasts	Trough and sigmoidal cross-bedding; ripple structures locally, planar and tangential cross-laminations; local coarse skeletal	Bioturbation *Ophiomorpha* *Planolites*	Moderate energy setting, below fair-weather and above storm wave base (equivalent to

		lenses and common interlayered mudstone sheet-like units (<0.5 m)		mid-shelf deposits)
B3b	Bioclastic packstone and wackestone: (<20% quartz); medium to coarse-grained; barnacles, oysters, pectinids, brachiopods, encrusting bryozoans, serpulids, echinoids, red algae, common benthic foraminifers; micritization	Planar and tangential cross-stratification, local small-scale trough and sigmoidal structures; common tabular bedding	Bioturbation *Skolithos*	Moderate energy, shallow water environment, close to fair-weather wave base; embayment
Mixed Facies				
M1	Alternating grainstone and packstone: (<30% quartz); fine to coarse-grained; especially barnacles and oysters, brachiopods, bryozoans (robust and delicate branching), rare echinoids, rare serpulids, pectinids; mud clasts	Trough cross-bedding, sigmoidal and convolute cross-laminations, minor HCS; skeletal lag lenses; sharp-based grainstone; mud layers; laterally discontinuous sheets; thin to medium-bedded (up to 0.25 m)	*Ophiomorpha* *Planolites* rare *Scolicia*	Contrasting conditions; between fair-weather and storm wave base sand dunes
M2	Interbedded grainstone and terrigenous packstone: (<40% quartz); fine to medium-grained; whole barnacles, oysters, brachiopods (abundant in places), bryozoans (delicate and rigid branching, local foliaceous), oysters, echinoids, pectinids, brachiopods; mud clasts	Planar and sigmoidal cross-laminations, HCS; laterally discontinuous, lensoid, sharp-based grainstone; tempestites, thin skeletal lag concentrates, interbedded mudstone lenses; horizontally-bedded sheet units	Dense bioturbation *Ophiomorpha* *Planolites* *Scolicia*	Between fair-weather and storm wave base sand dunes
M3	Interbedded terrigenous packstone and calcareous sandstone: (<50% quartz); lutite-sized debris; barnacles, bryozoans (delicate branching, foliaceous and fenestrate), oysters, echinoids, pectinids, brachiopods; mud clasts	Planar laminations, minor sigmoidal and convolute cross-laminations, ripple structures thin horizontally-bedded discontinuous sheets (5-15 cm); interbedded mudstone lenses	Dense bioturbation *Planolites* *Chondrites*	Moderate to low energy; close to lower storm wave base
Siliciclastic Facies				
S1	Calcareous sandstone: (<50% quartz); lutite-sized debris; bryozoans, Oysters, other bivalves including pectinids	Ripple and convolute structures, horizontal laminations, interbedded mudstone layers, massive to relict horizontally-bedded	Dense bioturbation *Chondrites* *Ophiomorpha*	Moderate to low energy; well-oxygenated; above storm wave base
S2	Siltstone: skeletal hash; rare bryozoans, oysters, pectinids, local Turritellid gastropods	Associated with thin mudstone lenses; medium-bedded (up to 1 m)	*Planolites* *Chondrites*	Quiet waters, more distal setting (equivalent outer shelf)
S3	Mudstone: yellow-grey to blue-grey; uncommon macrofauna (gastropods pectinids)	Lensoid to massive	*Chondrites*	Quiet waters (equivalent outer shelf)

persistently moderate- to high-energy tidal currents keep the bottom relatively free of terrigenous sediments (Beu *et al.*, 1980; Kamp *et al.*, 1988). *Notobalanus vestitus* and *Austromegabalanus (Notomegabalanus) miodecorus* are found mostly in the shallow subtidal zone attached to hard substrates (Beu, 1995). Furthermore, extensively bored shells, scarcity of mud-dominated lithologies, local presence of trough cross-bedding, fragmented and abraded constituent grains, and glauconite grains (up to 9% of constituents) suggest low to moderate sedimentation and active sediment movement on a shallow shelf. *In situ* shell beds, with common clumps of oysters, are interpreted to be oyster banks formed under conditions of high-energy swell, probably tide-dominated currents, similar to those found today in Foveaux Strait off the south coast of the South Island (Fleming, 1952; Harmsen, 1984).

Traction-emplaced shell beds are interpreted to have accumulated in intertidal to shallow subtidal settings where tidal currents or storm waves reworked shell debris and possibly concentrated them in migrating channels (Wilson, 1967; Harmsen, 1984; Kamp *et al.*, 1988).

Facies B1b - Fossiliferous rudstone with a mud-dominated matrix: These shell beds are uncommon in the studied successions (Figures 23B, 23C). In the few known examples, B1b facies shell beds exhibit a sharp contact with underlying beds and grade vertically into siltstones or mudstones (S2-3 facies). Thin-shelled oysters are the dominant component, and are usually fragmented and randomly oriented. They are drowned in a pale yellow-grey muddy matrix. Fossiliferous rudstones with a muddy matrix are internally planar-bedded, fining-upward deposits, the oyster shells getting thinner and smaller towards the top.

Interpretation

B1b facies is interpreted to have formed adjacent to oyster shell banks progressively buried by muddy sediments in possible association with either a rapid deepening of the depositional setting or an increase in silt-sized material input, or both.

Facies B1c - Pebbly rudstone: Conspicuous components of pebbly rudstones are locally bored pebbles up to 15 cm in size (Figure 23D), reworked, abraded, disarticulated, and fragmented oyster shells and scallops, and mudstone and sandstone clasts. These are enclosed in a terrigenous/skeletal grain-dominated matrix with local mud layers along

which pressure-dissolution features have preferentially developed to give a flaggy bedding in places. Pebbly rudstones are massive to planar cross-bedded and form continuous to lensoidal sheets up to 3 m thick. Their basal boundary is sharp to erosional with medium-scale relief up to 30 cm amplitude. Robust branching bryozoans and barnacles encrusting molluscan shells are present.

Bored pebbles occur in lag concentrations of clast-supported fossiliferous rudstones and conglomerates up to 1 m, but commonly less than 0.5 m, thick. The borings are developed preferentially in sandstone and mudstone clasts, in the lowermost part of any pebbly rudstone bed, though in places they occur throughout the latter. The clasts are abraded, well rounded, and bored on all surfaces by tear drop-shaped borings that are generally infilled with host rock-derived skeletal packstones or grainstones (Figure 23D). The borings are circular in cross-section, up to 30 mm deep and oriented perpendicular to the pebble surface, resembling pholad bores. They may be related to marine bivalve borings belonging to the ichnogenus *Gastrocoenolites* (Bromley, 1994).

Interpretation

Pebbly rudstones have characteristics intermediate between low- and high-energy deposits, including interbedded coarse-grained rudstones/packstones and thin discontinuous mud layers.

Pebbles have been bored in a high-energy marine setting, indicated by borings on all pebble surfaces, suggesting alternation of resting phases (allowing borers to settle) and reworking phases (when sediment supply to the area was low or null). Similar bored pebble lags have been reported in storm-generated gravel sheets, middle-upper shoreface bored-pebble pavements, and tidal current-dominated conglomerates that formed in shallow-marine shoreline areas (Radwanski, 1970).

The bored pebbles, together with reworked shells and a skeletal association comprising shallow-water high-energy organisms, suggest intertidal environmental settings. Shell debris, reworked mud clasts and bored pebbles were possibly concentrated in current-swept tidal channels where contrasting conditions prevailed. The abundance of abraded grains, encrustation, and multigeneration boring of pebbles also suggest frequent and active clast movement. Besides, the occurrence of authigenic glauconite and detrital glauconite (up to 11%) together with the common precipitation

Figure 23 – Sedimentological characteristics of the Bioclastic facies

(A) Fossiliferous rudstone of facies B1a, packed with oysters and pectinids. Note the internal planar bedding. Arrow indicates hammer, which is about 30 cm long. Awapapa Limestone at Te Mata Peak section (see Figure 8; about 80 m from the base).

(B) Fossiliferous rudstone of facies B1b, packed with thin-shelled oysters. Arrow indicates hammer. Mason Ridge Formation at Torran section (see Appendix 1 – column 29).

(C) Close-up of facies B1b in (B). Densely packed crushed oyster shells drowned within a silty matrix. Marker pen is about 10 cm long.

(D) Conspicuous components of facies B1c are bored pebbles. Note that soft clasts (sand or mud now eroded away) are well rounded and bored on all surfaces by tear drop-shaped borings (pholads) that are infilled with host rock-derived material. Base of Kairakau Limestone (0-3 m) at Kairakau Beach section (see Figure 6).

(E) Coarse-grained bioclastic grainstone of facies B2b overlies sharply burrowed mixed facies M2. Arrow lies at the contact and indicates trough cross-beds eroding through facies M2. Awapapa Limestone at Te Mata Peak section (see Figure 8; about 30 m from the base). Scale bar is 20 cm long.

(F) Barnacle and bryozoan-rich coarse-grained packstone of facies B3a. Note above camera cap (about 6 cm across) the closely packed colonies of branching bryozoans. Te Onepu Limestone at Robottom Grave section (see Appendix 1 – column 26 and Figure 9C).

(G) Bi-directional cross-stratifications within facies B2b. Matapiro Limestone at Ohiti section (see Figure 15).

(H) Coarse-grained pure coquina limestone of facies B1a. Barnacle plates are by far the dominant constituents. Note the internal deformation structure due to dewatering. Tahaenui Limestone (Waipipian) at Mahia Peninsula on the northern side of Hawke Bay.

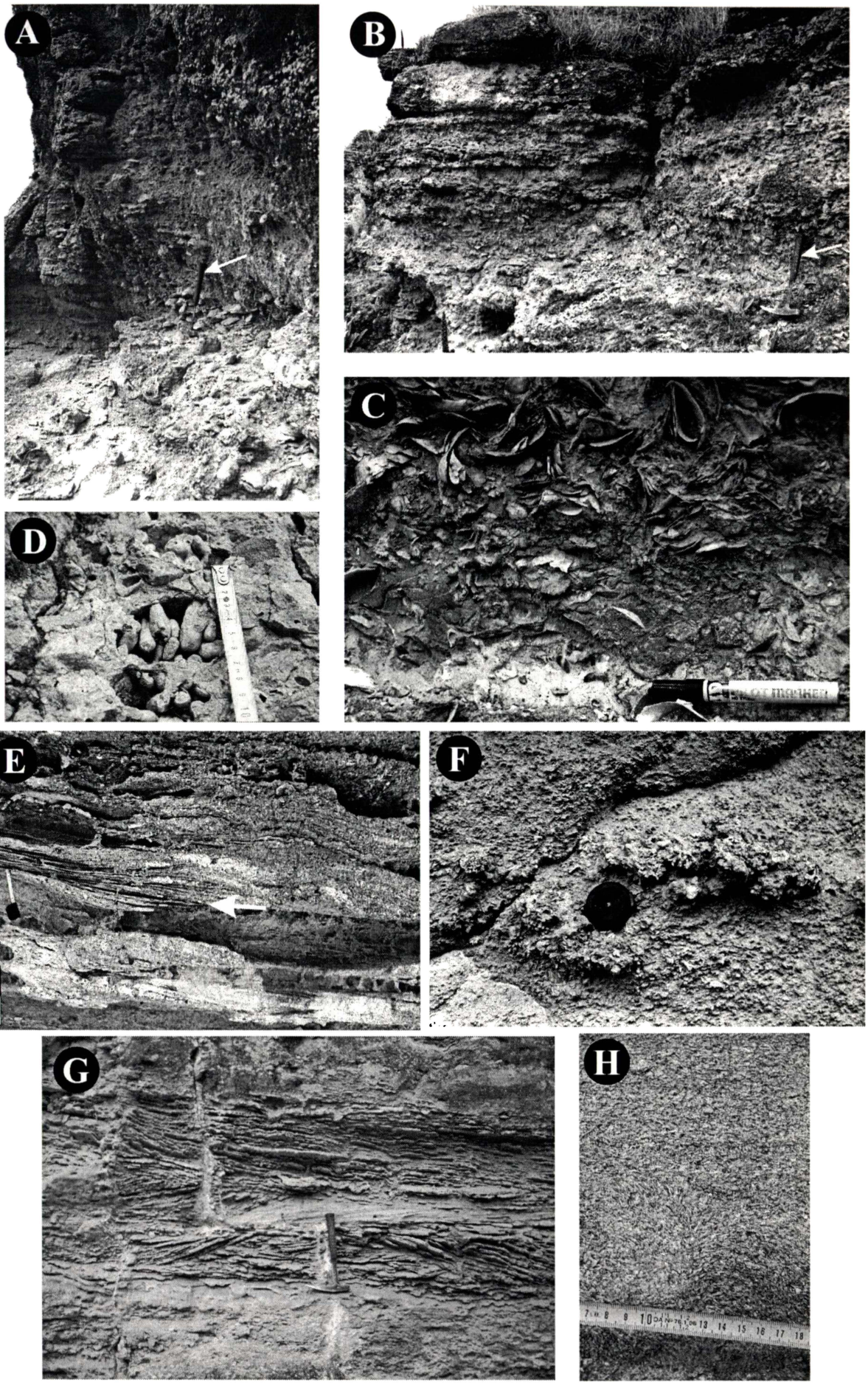
A
B
C
D
E
F
G
H

of marine acicular cements, give evidence for periods of arrested sedimentation.

Facies B1d - Bioclastic conglomerate: Conglomerate beds range from 1-6 m thick, and are dominated by pebbles up to 6 cm size but locally as large as 20 cm, all floating in a mixed skeletal/terrigenous sandy to microconglomeratic matrix. Some beds contain frequent bryozoan encrusters, oysters, other bivalves, and barnacles, locally concentrated into shell lags up to 20 cm thick. Sand-sized bioclasts are moderately to strongly abraded. With decreasing grain size of both pebbles and skeletal components, the abundance of bioclasts that make up the matrix increases, and planar to trough cross-stratifications become conspicuous.

Interpretation

Conglomerate beds mostly occur within Mangapanian and post-Mangapanian successions in the western and central parts of the study area, and clearly record the uplifting of the Torlesse basement that now forms the Ruahine Range bounding the forearc basin to the west. Thus, Torlesse basement-derived pebbles are the major lithoclastic component of the conglomerates, though mud pebbles up to 15 cm in size may be common in places. The local abundance of sand-sized bioclastic material, together with the occurrence of moderately fragmented specimens of oysters in skeletal lags and unilaminar bryozoans encrusting Torlesse pebbles, indicate that the deposits have been formed in a marine setting. The coarser conglomerate beds are interpreted as fan-delta deposits developed close to the western flanks of the basin, whereas finer-grained beds would represent a more distal setting in front of the fan-delta system. The high content of sand-sized bioclasts in the latter, in association with planar and trough cross-bedding, point towards a depositional environment frequently swept by currents, probably above fair-weather wave base and possibly under the influence of tidal currents.

5.2. Bioclastic grainstone facies: clast-supported facies B2a and B2b

Medium- to coarse-grained bioclastic-rich grainstones (Figures 23E, 23F, 23H) represent about 50% of the facies recognized within the studied carbonate deposits, and are commonly found overlying sediments of the shelly/pebbly facies of B1 described above. B2a and B2b have different skeletal compositions. B2a is a barnacle-rich grainstone, whereas B2b is dominated by bivalve clasts (barnamol and bimol

assemblages, respectively; Hayton *et al.*, 1995). Thickness of bioclastic grainstone facies ranges from 1-10 m.

Grainstones are medium- to thick-bedded (average 0.3-0.5 m, but up to 1 m), commonly exhibit internal planar (Figures 24F, 24G) to trough cross-stratifications (Figure 23E) made up of foreset laminae with tangential lower contacts and truncated upper contacts, and have a gradational to erosional contact with underlying beds (Figure 23E). Bi-directional cross-stratifications are locally present within facies B2b (Figure 23G). Major components are various molluscan fragments, barnacle plates, encrusting and rigid branching bryozoans, and benthic foraminifers (for example, common biserial agglutinates), all moderately to well abraded and poorly sorted. Such lithofacies typically show little internal facies variation, but cross-beds are coarser-grained near the base than higher beds (fining-upwards), contain common well rounded mud clasts, scattered whole specimens of oyster and pectinid valves encrusted by barnacles, and occasional bored pebbles. Bioturbation, involving *Skolithos* and *Thallasinoides*, tends to be more common towards the top of the facies and is associated with mud drapes.

Interpretation

Internal stratification, and repeated transport and abrasion of grains, of facies B2 are features shared with modern marine dune deposits and sand waves on the mid- to inner-shelf off southern Australia, New Zealand, and in the North Sea, at depths between 30 and 130 m (McCave, 1971; Collins, 1988; Nelson *et al.*, 1988b; Boreen *et al.*, 1993). Coarse-grained sediment, abraded shell debris, planar and trough cross-stratification, which internally show mud drapes and reactivation surfaces, mud clasts that suggest reworking of mud lenses or mud drapes, bored pebbles, and sparse planktic foraminifers, are all characteristics of migrating sand bodies deposited under the influence of tidal currents or semicontinuous storm-driven currents on the inner part of a paleoshelf, probably at less than 50 m water depths (Nelson *et al.*, 1988b; James *et al.*, 1992; Percival, 1992, Boreen and James, 1995).

Bimol assemblage is often associated with relatively turbid waters due to fine terrigenous material in suspension, while barnacles, being suspension-feeding organisms, are sensitive to the amount of terrigenous sediment supply. Thus, prerequisites for barnacle-dominated biofacies development are a low terrigenous, but high nutrient supply (Beu *et al.*, 1980). High-energy environmental conditions

promoting terrigenous material by-passing, such as tidal current-swept sea floors, are believed to provide such prerequisites for facies B2a.

5.3. Bioclastic packstone facies: mud-supported facies B3a and B3b

Facies B3a - Bioclastic-rich packstone: Facies B3a is characterized by high contents of siliciclastic material (<40%), even though skeletal material may be the major constituent locally (Figure 23F). It can be distinguished from facies B3b by its relatively lower content of bioclastic material (barnacles, bryozoans, echinoids, pectinids, oysters, brachiopods, foraminifers), its relatively higher content of lime mud, and a mixed assemblage of small benthic and planktic foraminifers. Fine- to medium-grained skeletal grains are moderately to well abraded, and commonly microbored, the bore holes being filled either by authigenic glauconite or by the host lime mud. Delicate branching bryozoans are common. Sedimentary structures comprise local trough cross-bedding, and planar and tangential cross-stratifications.

Interpretation

High mud and siliciclastic contents, a mixed planktic and benthic foraminiferal assemblage, delicate branching bryozoans, and the precipitation of authigenic glauconite, together with trough and planar cross-bedding structures, indicate quiet waters conditions only interrupted by storm-driven currents. Facies B3a sediments are therefore interpreted to represent mid to outer shelf deposits emplaced close to storm wave base.

Facies B3b - Bioclastic packstone and wackestone: Aside from comprising similar skeletal types to that of facies B3a, facies B3b is characterized by an unusually large content of benthic foraminifers (average 10%, but up to 30%), including unidentified troichoidal agglutinates and planispiral hyaline (*Elphidium, Notorotalia*), and other fauna and diagenetic fabrics that may indicate warm-temperate climatic conditions, such as red algae, and the infestation of skeletal grain margins by endolithic borers, the vacated holes of endoliths being filled by microcrystalline calcite. Although minor, red algae are a persistent component of the skeletal fraction.

The siliciclastic content is low compared to facies B3a (<15-20% quartz and other siliciclasts). Grains are generally moderately sorted and variably abraded. The content of lime mud is variable, from relatively low resulting in facies close to

grainstones in texture, to relatively high giving packstone and locally wackestone textures. Tabular bedding with internal tangential cross-stratifications is the dominant sedimentary structure, grading laterally into small-scale trough and sigmoidal stratifications with mud layers. Facies B3b is restricted in time to the early Nukumaruan Mason Ridge Formation.

Interpretation

Variable abrasion of grains, tangential to local trough cross-stratifications, and lateral variation in calcilutite mud content suggest contrasting low to moderate energy conditions. Pervasive infestation of skeletal grain margins and subsequent precipitation of microcrystalline calcite indicate that periodical exposures to turbulent conditions were separated by periods of rest at the sea floor, then favouring micritization processes (Kobluk and Risk, 1977). Although endolithic borers have wide depth tolerance (James and Choquette, 1990), the occurrence of some shallow-water indicators, such as phototroph calcareous algae commonly found encrusting shells and occasionally firmgrounds, and the abundance of benthic foraminifers suggest water depths within the photic zone, probably just below fair-weather wave base (Lukasik *et al.*, 2000). Facies B3b may therefore correspond to relatively protected, shallow mud-dominated settings such as marine embayments, which Beu (1995) infers to correspond to the depositional setting of some limestone occurrences during early Nukumaruan times in southern Hawke's Bay.

5.4. Mixed carbonate-siliciclastic facies: interbedded grainstones and packstones (M1), interbedded grainstones and terrigenous packstones (M2), and interbedded packstones and calcareous sandstones (M3)

Coarse-grained facies B1a to B2b pass up either gradationally or across a sharp contact into interbeds of often strongly burrowed, coarse-grained, poorly sorted, skeletal grainstones, commonly with erosive bases, and finer-grained moderately to well sorted packstones (Figures 24A, 24B). Thickness of mixed facies ranges from 3-8 m.

Burrows are mainly *Thallasinoides*, *Scolicia*, locally *Ophiomorpha* and *Planolites*, and rare coarse skeletal material-infilled fish-feeding structures. Burrows are conspicuous in the packstone beds where they are filled in their top third with coarse skeletal fragments from the overlying grainstones (Figure 24C), while their bottom part is filled with silt-size debris and mud. Mixed facies contain whole and fragmented

barnacles (locally dominant), bryozoans (mixed association of robust, erect rigid cheilostomes, and delicate branching cyclostomes), a diverse benthic and planktic foraminiferal assemblage, oysters, and brachiopods. Accessory components are echinoids, pectinids, serpulids, and mud clasts. Planar-tangential, sigmoidal, and ripple cross-laminations are common in packstones, while grainstones normally exhibit trough cross-beds (Figure 24A), and minor HCS, though they may show planar cross-laminations. Grainy beds occur as continuous to discontinuous sheets and lenses. Sheet tops usually are simple bedding planes. Spectacular sedimentary structures, amongst them water expulsion vents, convolution features, and slumping, are locally present (Figure 24D). Medium- to large-scale tabular cross-beds with subparallel bounding surfaces dominate in some limestone occurrences. Planar foresets, with tangential bases, have dips that seldom exceed 15°. Sets are less than 0.5 m thick and often show bi-polar cross-orientation with reactivation surfaces and mud drapes.

Often facies M1 and M2 grade laterally and upward into facies M3, characterized by fine-grained, well sorted mixed siliciclastic-skeletal hash material with common delicate branching and foliaceous bryozoans. Facies M3 often exhibits internal planar and tangential cross-laminations (Figure 24I), and convolute cross-laminae. Coarse, discontinuous lensoid skeletal lags are also a common feature in places.

Interpretation

Mixed lithofacies have characteristics intermediate between shallow-water inner shelf to deeper-water mid to outer shelf deposits, including coarse and fine grain sizes, and mixed planktic and benthic foraminiferal assemblages. The abundance of burrowing indicates well-oxygenated conditions. The sheet-like geometry of bedding, alternating grainstones and packstones, locally preserved hummocky cross-stratifications (Figure 24E), and ripple cross-laminations suggest alternating energy conditions that combine successive fair-weather and storm processes.

Local tabular bi-polar cross-beds of facies M1 (alternating grainstones and packstones), and the sheet-like geometry and decreasing flow conditions in these beds that favoured burrowing, are interpreted as migrating skeletal sand dunes produced by storms on the inner to mid shelf, with probable tidal current influence (Harmsen, 1984; Kamp *et al.*, 1988; Boreen and James, 1995).

Relict storm-deposited skeletal lag grainstone-terrigenous packstone couplets with common erosive bases, and simple bedding tops, of facies M2 (alternating

grainstones and terrigenous packstones) are viewed as transitional between inner-, mid- and outer-shelf facies, probably beneath the fair-weather wave base and above the storm wave base (Boreen *et al.*, 1993; Boreen and James, 1995).

This interpretation is consistent with the observed secondary sediment deformation structures, among them slumps and convoluted foresets, and the bryozoan assemblage with mixed erect rigid, robust, and delicate branching zoarial forms that also indicate mid- to outer-shelf environmental conditions (Nelson *et al.*, 1988; James *et al.*, 1992; Bone and James, 1993). When it overlies facies M1 and M2, facies M3 is believed to represent deeper-water settings under fair-weather wave base, close to storm wave base.

5.5. Siliciclastic facies: S1, S2, and S3 facies

Mixed facies pass gradationally, and vertically, into terrigenous packstone/wackestone, calcareous sandstone, and siltstone deposits. Lutite-sized debris in the siliciclastic-muddy deposits comprises fragments of molluscs, bryozoans, barnacles, and rare benthic but common planktic foraminifers. Locally, mudstone intraclasts also occur. Scattered, well-preserved pectinids encrusted by barnacles, and whole colonies of delicate branching bryozoans, are present. The deposits mostly are burrowed and bioturbated by *Planolites, Chondrites,* and *Ophiomorpha* (Figure 24E), and *Thalassinoides* burrows occur in places beneath unconformities (Figure 24H). Burrows are generally mud-infilled, but commonly under unconformities burrows are filled with coarse skeletal material of the overlying unit (Figure 24H).

Within siliciclastic and muddy facies, interbeds of skeletal hash form discontinuous graded packstone and grainstone thin sheets interpreted as distal tempestites derived from mid- to outer-shelf. Most beds are massive due to bioturbation, but when present, the main sedimentary structures are ripple and planar horizontal laminations.

Interpretation

Deposition in a low-energy well-oxygenated setting, only disturbed by storm-emplaced skeletal lags (Figure 24E), is indicated by the texture, sedimentary structures, and ichnofossils. Well preserved delicate bryozoan colonies also suggest deposition in

Figure 24 – Sedimentological characteristics of the Mixed facies

(A) Alternating grainstone and packstone of facies M1. Coarse-grained sediments exhibit tangential and sigmoidal cross-stratifications in sets 0.5 to 1.0 m thick, interpreted as prograding sand waves. Awapapa Limestone at Pukekura section (Appendix 1 – column 15).

(B) Interbedded grainstone and terrigenous packstone arranged in horizontal bed sets, 0.3 m thick (facies M2). Dashed line indicates sharp contact interpreted as a ravinement surface underlying a massive 2 to 3 m-thick shell bed at the Pakihirua section of Mason Ridge Formation (see Figure 13).

(C) Alternating coarse-grained skeletal-rich trough cross-beds and finer-grained terrigenous packstones forming facies M2. Burrows (arrowed) within terrigenous facies are filled with coarse material from overlying sharp-based grainstone. Scale = 14 cm. Awapapa Limestone at Te Mata Peak section (about 85 m from the base; see Figure 8).

(D) Dewatering structures in mixed carbonate-siliclastic sediments (facies M2). Hammer is about 30 cm long. Kairakau Limestone at Koanui section (Appendix 1 – column 5).

(E) Storm-driven wave currents are responsible for medium-scale hummocky cross-stratifications (black arrow) in otherwise quiet environments where planar-laminated calcareous sands accumulated (facies M3). Note *Ophiomorpha* burrows (white arrows) within fine-grained deposits. Te Waka Formation at The Gorges section (see Figure 18; about 62 m from the base).

(F) Horizontal and low-angle planar cross-stratifications in fine to medium-grained calcarenites (facies M3). Rotookiwa Limestone at Lonely Man section (Appendix 1 – column 20).

(G) Superposed tabular bed sets with internal planar cross-stratifications (facies M1). Kairakau Limestone at Kairakau Beach section (see Figure 6; about 18 m from the base).

(H) Ravinement surface (arrowed) places coarse-grained sediments of facies B2b in direct and erosive contact with siltstone of facies S2. Note that below and from the ravinement surface, ichnofossils (*?Thalassinoides*) penetrate downwards into siltstone. They are filled with carbonate sand from the overlying unit (dashed lines). Unconformity within Kairakau Limestone at Te Mata Peak section (Appendix 1 – column 9). Camera cap is about 6 cm across.

(I) Low-angle tangential cross-stratifications in facies M3 below unconformity (dashed line) within Kairakau Limestone at Kairakau Beach section (see Figure 6; about 20 m from the base). Scale at the leftside is 20 cm.

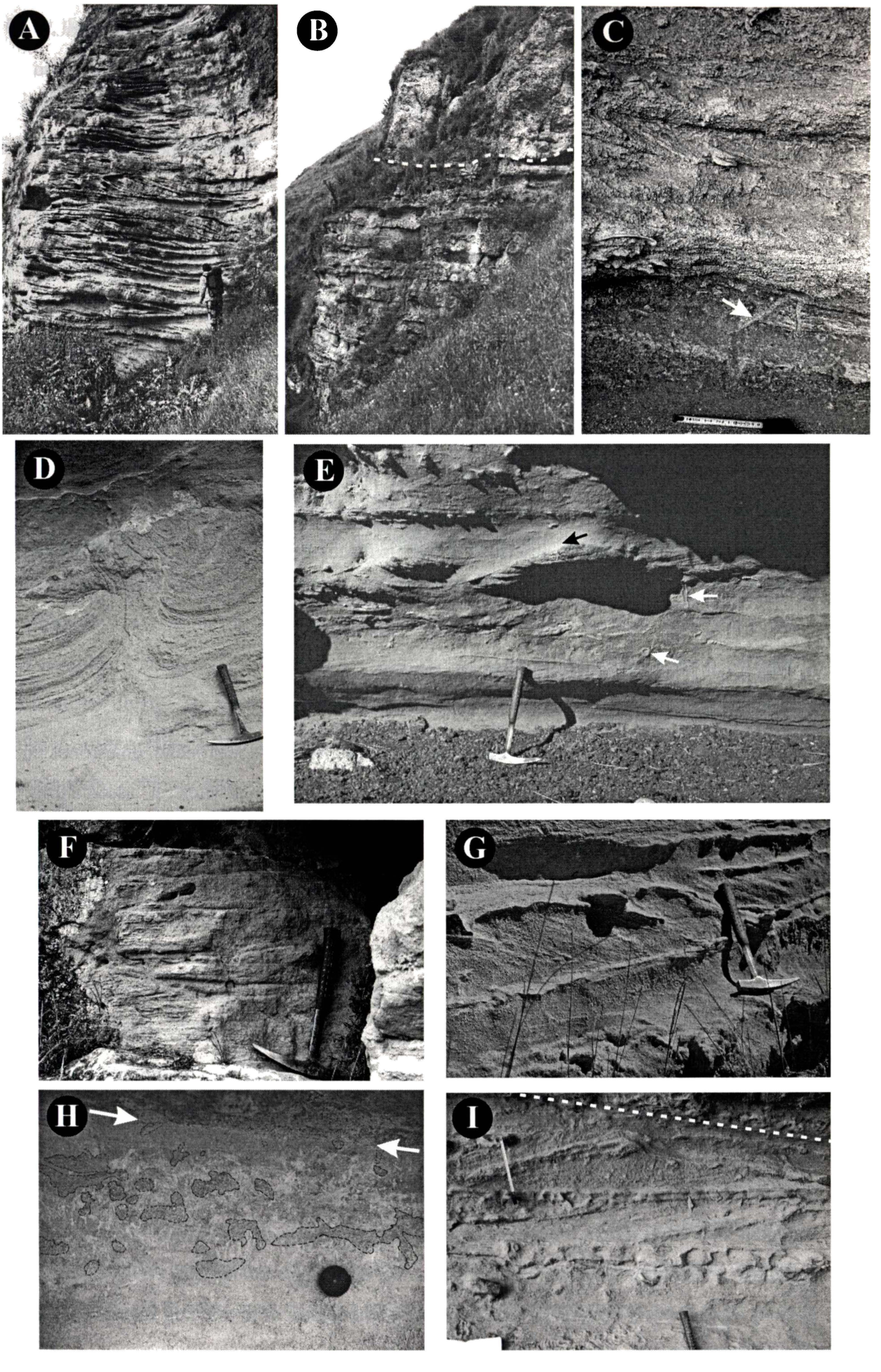
A
B
C
D
E
F
G
H
I

relatively quiet waters. Mud intraclasts probably were produced during storm events by reworking of suspension-deposited muds. Although *Planolites* and *Chondrites* have wide depth tolerances (Seilacher, 1967), they are indicative of marine, quiet water, and muddy substrates. Similar deposits are common on the outer shelf to upper slope of the modern southern Australian margin in environments deeper than 90 m (Boreen *et al.*, 1993), as well as in a deep setting on the New Zealand modern carbonate platform (Nelson *et al.*, 1988b). Nevertheless, sedimentary structures and the stacking pattern of the studied deposits, which shows S-type facies overlying mid- to outer-shelf facies (M1, M2, and M3) suggest that the former formed on the deeper ramp, close to storm wave base (Harmsen, 1984).

A depositional model, showing the relationships between environmental conditions about submarine antiforms, which are envisaged to be the most likely depositional setting for the Pliocene limestones in the eastern portion of southern Hawke's Bay, and the facies described above, is discussed in Section 7.1 and illustrated in Figure 29.

6. Skeletal and microfacies assemblages

6.1. Skeletal assemblages

Using the Hayton *et al.* (1995) classification scheme, Plio-Pleistocene limestones in southern Hawke's Bay fall into three major compositional skeletal associations: barnamol, dominated by barnacles and bivalve mollusc; bimol or bivalve-dominated carbonate sediments (infaunal and/or epifaunal molluscs); and bryomol or bryozoan-dominated carbonate sediments with various amounts of bivalve molluscs (Figure 25). Besides compositional differences related to the evolution of the forearc basin over time (progressive shallowing and narrowing; see Section 2), Pliocene limestones are in general characterized by a high content of barnacle plates and bivalve shell fragments, compared to cool-water carbonates in general, which are typically rich in bryozoan, echinoderm, and foraminiferal remains (Nelson, 1978b; Nelson *et al.*, 1988b; Boreen and James, 1995). Beu *et al.* (1980), Kamp *et al.* (1988), and Beu (1995) suggested that strong tidal flows over antiform ridges in the Pliocene seaway, and current by-passing of terrigenous sediment near the shores, maintained high nutrient levels that allowed barnacles and epifaunal bivalves to flourish. Furthermore, the dominance of barnacle over bryozoan growth was probably a result of the following combination of promoting factors: (1) the quick turnover of barnacles due to rapid replacement each year of a high

proportion of the barnacle population in high-energy tidal settings (Beu, 1995); (2) the lack of submarine rock outcrops to be colonized by bryozoans, but a coarse-grained seabed instead; and (3) favourable environmental conditions for epifaunal bivalves, which in turn provided a hard substrate for barnacle attachment.

6.2. Microfacies assemblages

The classification scheme of Hayton *et al.* (1995) was devised to determine easily the skeletal assemblage of any given temperate skeletal carbonate sample independently of its terrigenous content. As a consequence, samples referred to a barnamol association, for example, can have highly variable siliciclastic material contents related either to changes in external sediment inputs, or to transport and redeposition of skeletal clasts in terrigenous-dominated settings. Thus, Hayton *et al.* (1995) pointed out that skeletal assemblages should only be used with caution to evaluate paleoenvironmental conditions. In order to assess the possibility to differentiate microfacies and eventually to help discriminate depositional facies of the non-tropical Plio-Pleistocene carbonates, point-counting data, including terrigenous components, from 351 thin-sections were subjected to a complete linkage cluster analysis (Appendix 4.2). The following particles have been used in the cluster analysis: barnacles, bryozoans, bivalves, and siliciclastics (quartz, feldspar, other lithoclasts) as major components. Benthic and planktic foraminifers, brachiopods, echinoderms, red algae, and gastropods are typically minor components (total <15%), and have been grouped in a single class ("pot-pourri") so as not to distort the results.

The analysis distinguishes six clusters distributed between terrigenous-poor (15-20%) and terrigenous-rich (40-60%) end-members. The Hayton *et al.* (1995) classification terminology was followed for the relatively terrigenous-poor assemblages. The clusters have been given full names as well as contracted names that refer to their dominant components (Figure 26). The six microfacies assemblages, along with their mean skeletal composition are: (1) detrital (55-60% siliciclastics); (2) barbital = *bar*nacles (23%), *bi*valve molluscs (22%), and detri*tal* elements (37%); (3) bryotal = *bryo*zoans (33%) and detri*tal* elements (32%); (4) bimol = *bi*valve *mol*luscs (35%); mixed skeletal = "pot-pourri" (27%), bivalves (25%), bryozoan (14%); and (6) barnamol = *bar*nacles (39%) and bivalve *mol*luscs (26%). It is these microfacies categories that are included on all the stratigraphic columns for the Plio-Pleistocene strata.

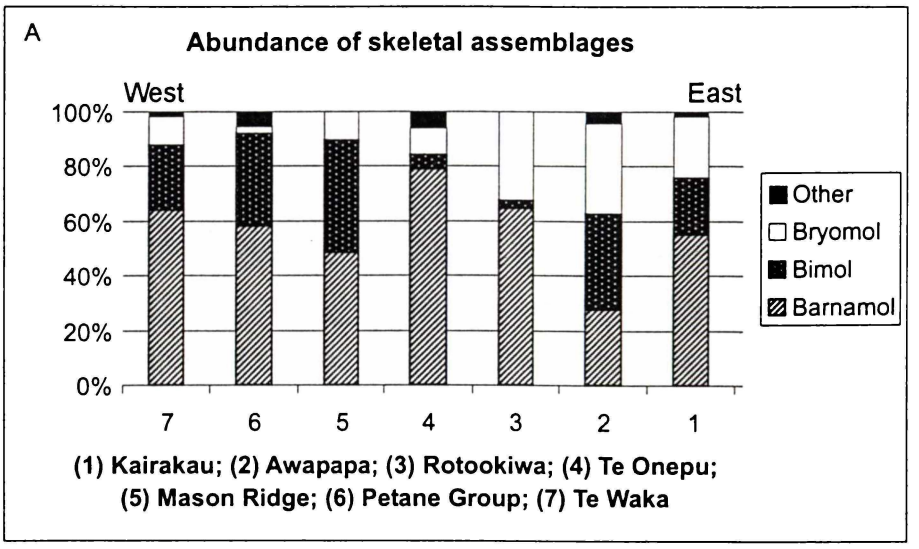

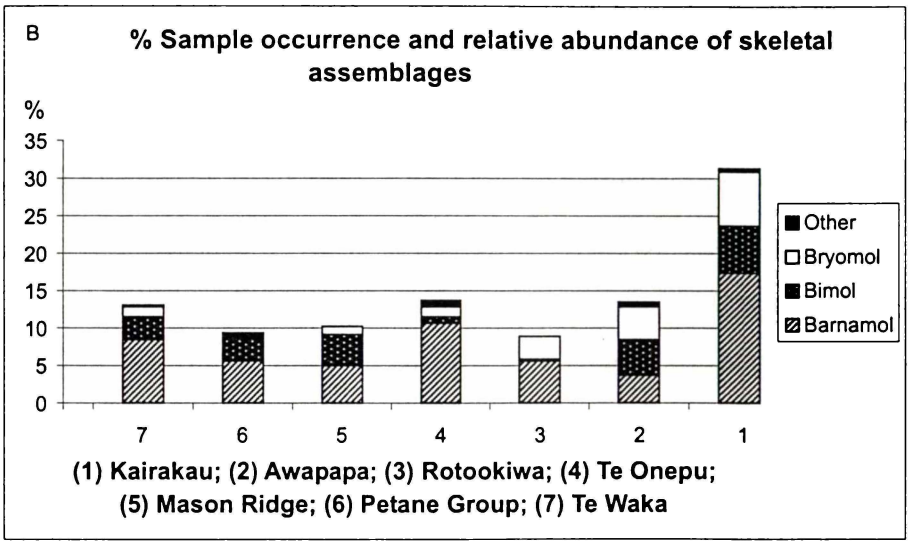

Figure 25- Petrographic histograms showing the abundance of the various skeletal assemblages accounting for the skeletal composition of the Plio-Pleistocene limestones in southern Hawke's Bay (based on point-counts for 382 thin-sections). The skeletal assemblage names are from Hayton *et al.* (1995).

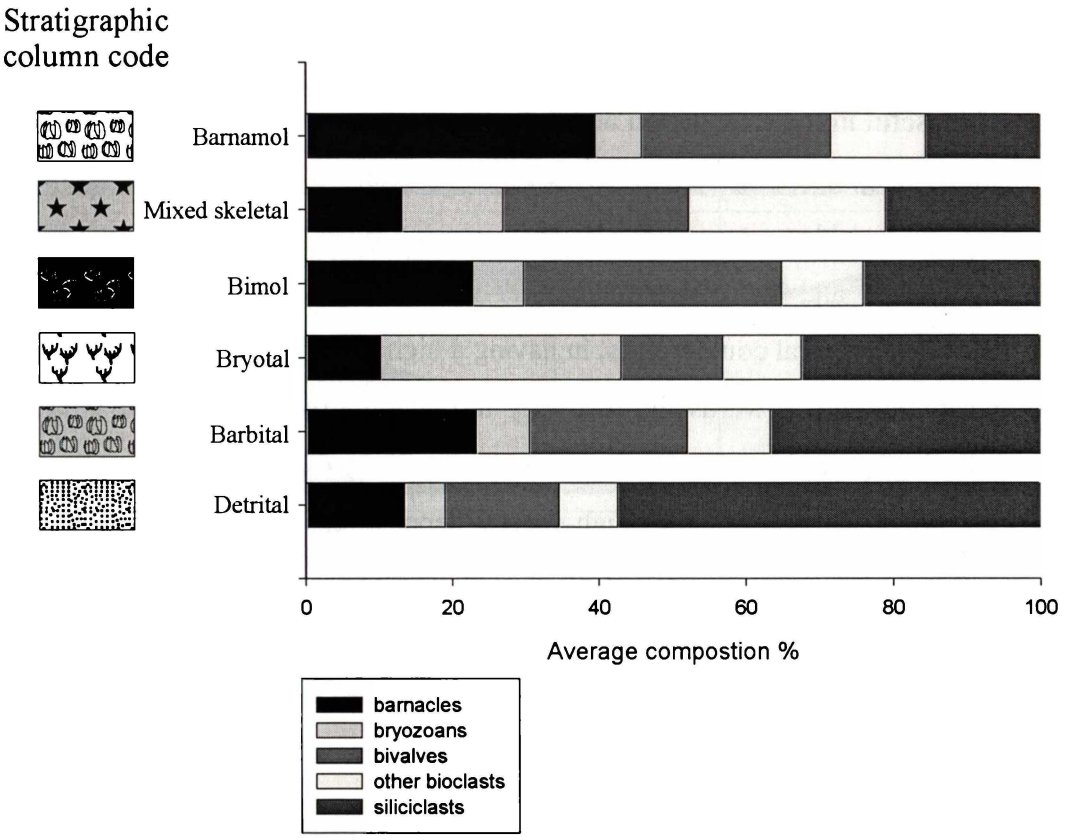

Figure 26- Mean skeletal and siliciclastic composition of the six microfacies assemblages identified in the Plio-Pleistocene limestone samples (n = 351) of southern Hawke's Bay. The codes at left define the microfacies on the stratigraphic columns (see Appendix 1, p.A1 – 1).

6.3. Evolution of microfacies contribution to the Plio-Pleistocene limestones with time

Figure 27 shows the relative contributions from each of the microfacies assemblages to the different limestone units in southern Hawke's Bay, from east to west, with reference to their age. Despite vertical and lateral variations within each limestone unit, that have proved to be useful in the recognition and definition of depositional cycles (see Chapter 4), this simple diagram points up the following characteristics of the Plio-Pleistocene successions: (1) older, easternmost and westernmost limestone occurrences (Kairakau/Awapapa and Te Waka, respectively) are compositionally distinctive from their younger more central counterparts, in having a higher terrigenous content; (2) there is a compositional shift towards the relatively terrigenous-free end-member over time from east to west, reaching its maximum with the Mangapanian "pure" coquina Te Onepu Limestone. This shows that high-energy depositional environments (structural highs and antiforms), cut off from external sediment input and promoting barnacle-dominated carbonate production, were to become more widespread from late Waipipian, following the progressive narrowing and shallowing of the forearc basin (Kamp *et al.*, 1988); (3) the overall terrigenous-dominated composition of Te Waka Formation (at least the middle and upper limestone sheets), the western time-equivalent of Te Onepu Limestone, reflects the uplift of the Torlesse basement along the axial ranges creating an eroding western source area that delivered siliciclastic sand and gravel to the carbonate-rich deposits, possibly through small fan-delta systems otherwise not directly observed because of post-depositional erosion. Increasing rates of uplift and relative sea-level fall at the end of the Mangapanian resulted in the development of a large fan-delta complex that is well preserved further north (Bland, 2001), of which only a few remnants have been observed directly overlying the Te Waka Formation (e.g., Hassal Conglomerate; Figures 2, 18).

From early Nukumaruan on, basement-derived sand and gravel constitute a persistent, though locally minor, component of the limestones in the western and central part of the studied area (Sentry Box, Kereru, and Petane Group).

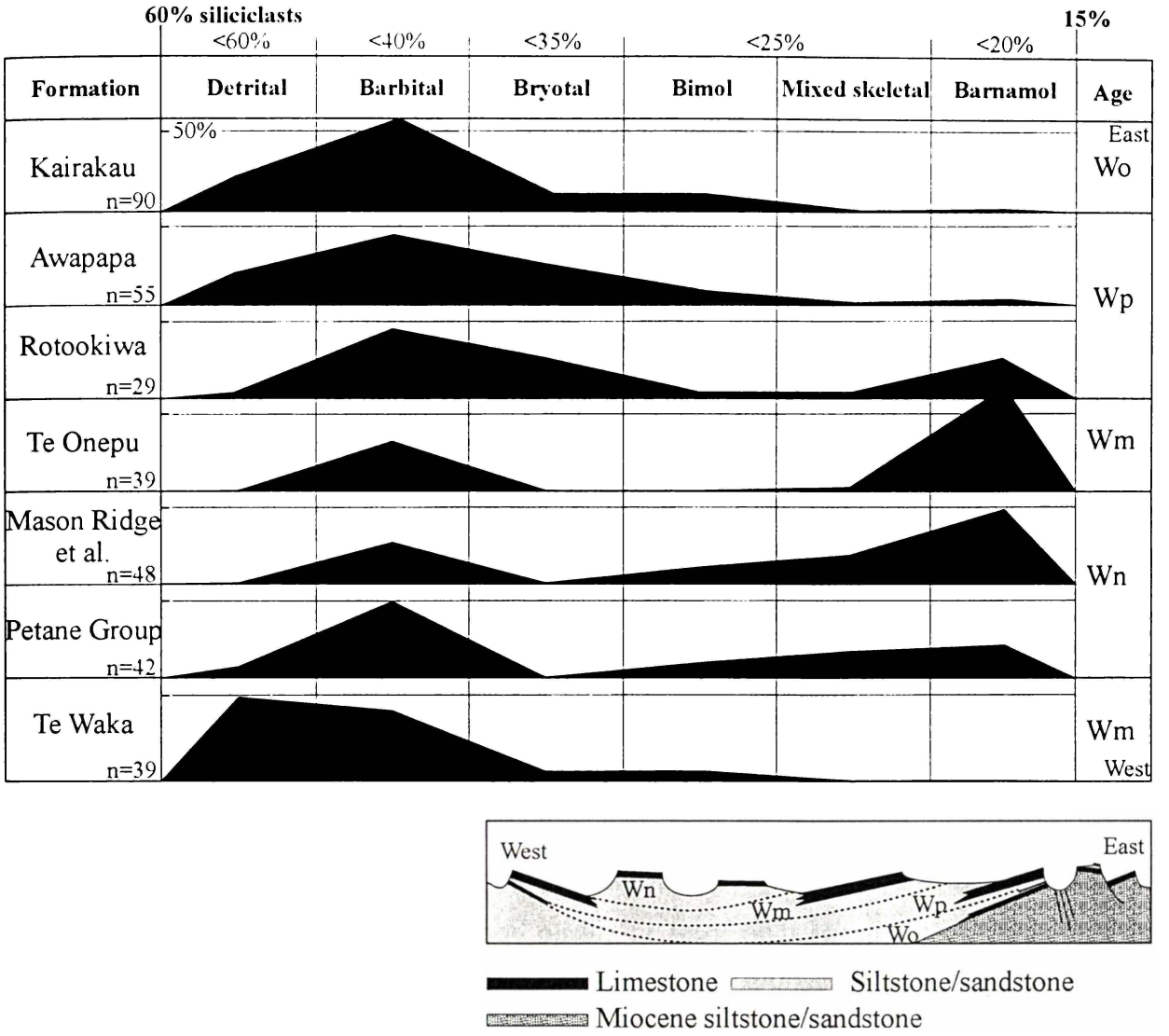

Figure 27- Relative contributions from each of the mixed carbonate-siliciclastic microfacies assemblages to the different Plio-Pleistocene limestone units in southern Hawke's Bay with reference to their age. See text for details and discussion. (Mason Ridge et al. includes samples from Mason Ridge Formation, Pakipaki Limestone, and Scinde Island Limestone).

6.4. XRD-ICPOES data for calcium carbonate and calcium content

X-ray diffractograms of whole samples from Plio-Pleistocene limestones show predominantly the occurrence of calcite with rare, if any, aragonite, the latter being most pronounced in the Pakipaki Limestone, Mason Ridge Formation, and Te Waka Formation (Table 2; Appendix 8; also on CD1). Limestones, ranging in age from Opoitian to Mangapanian, from the eastern sector of southern Hawke's Bay are dominated by low-Mg calcite mineralogies (Table 2), which indicate that less stable carbonate mineral phases, even though minor primary components, have been diagenetically altered (see the common occurrence of biomoulds in all limestones; Table 2) during post-depositional times in the marine, burial, and/or meteoric environments (see Chapter 3, Section 4.6). In contrast, XRD analyses of the Waipipian Te Waka Formation in the western part of the study area, and of most Nukumaruan limestones, indicate a wide spectrum of mineralogies, ranging from low-Mg to intermediate-Mg calcite, and aragonite. This suggests that either Nukumaruan and older western limestone occurrences were originally compositionally different from their eastern and older counterparts, or these limestones have been subjected to different diagenetic processes. The full implications of these observations are discussed in Chapters 3 and 5.

Qualitative estimation of calcite concentrations, by comparison of peak heights in diffractograms, shows minor differences in calcite content between limestones from Opoitian to Nukumaruan age. One possible explanation is that terrigenous-rich limestones, such as Kairakau, Awapapa, or Te Waka, for which lower calcite contents were expected, are better cemented than their younger counterparts, due to prolonged times of residence in the burial environment.

ICP-OES analysis provides the calcium content of whole samples in ppm. Results are plotted in Figure 28. Group means show that calcium content increases with time from Opoitian (Kairakau) to Nukumaruan (Mason Ridge to the east). The youngest limestones to the east and west of the forearc basin exhibit wider ranges of values than older limestones, which results in lowering the group means and increasing the standard deviation. Low values of Te Waka Formation are related to samples with high contents of siliciclasts (Torlesse pebbles). Magnesium contents conform to the XRD data (Table 2), and indicate higher values in the Te Waka and Nukumaruan limestones.

Table 2- The XRD analyses of bulk samples from limestones in southern Hawke's Bay indicate predominantly low-Mg (LMC) calcite mineralogies, especially within the older limestones located in the eastern part of the study area (see Figures 1, 2), and some intermediate-Mg calcite (IMC) and aragonite, especially within the younger Nukumaruan limestones (shadowed). The Mangapanian Te Waka Formation is the exception as shown in Figure 28. It retained both IMC and aragonite mineralogies of skeletal grains. The common (average 15% of skeletal grains) occurrence of biomoulds, either filled with secondary calcite or calcite-free, within all studied limestone units suggests that aragonitic molluscs have contributed to the skeletal composition of all the Pliocene limestones since the Opoitian.

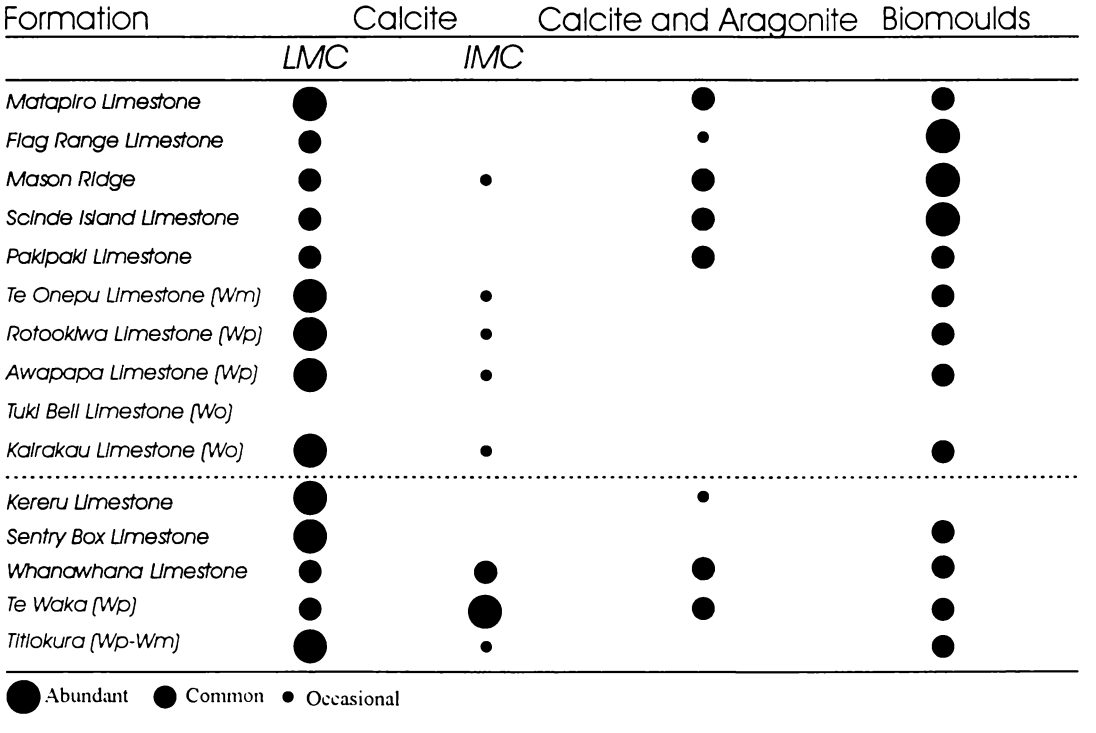

7. The depositional model

The study area represents about a third of the forearc basin exposed above sea level and as such provides a record of the differential emergence of the forearc basin margins and subsidence of its central part, the timing of successive carbonate deposition periods, and of uplift above sea level, spanning the interval from late Opoitian-early Waipipian to late Nukumaruan. The basin architecture bounded by thrust-controlled uplifted and folded coastal highs to the east, and structural ridges to the west (Figure 3), requires two different models to explain the facies distribution and highly evolving clastic composition of, respectively, the eastern limestone occurrences migrating westwards over time, and their more geographically-restricted western counterparts. Facies distribution and depositional models are schematically illustrated in Figures 29 and 30.

7.1. Eastern setting

The eastern part of the study area has been subjected to folding since at least the Early Pliocene, resulting in a number of anticlines and synclines generally trending NE-SW. Kamp *et al.* (1988), Beu (1995), and Nelson *et al.* (in review) inferred that the synsedimentary tectonic highs had been the major sites of carbonate formation during the Pliocene. The depositional system can be characterized as neighbouring carbonate factories developed upon and about actively growing thrust-cored antiforms cut by a complicated network of channels that constrained tidal flows, and through which skeletons and skeletal fragments were transferred downslope via dunes, sand waves, or in avalanche flows (Figure 29). Because sediments were poorly lithified at the sea floor, the rate of erosion must have been maximal on top of the antiforms once they had come under the influence of high-energy wave and tidal currents as a result of aggradation and progradation (see Chapter 3, Section 5.3). Thus, at the site of carbonate production, sediments were swept to the antiform flanks where they accumulated in the form of basinward-prograding sand waves and sand dunes. The minor early cement precipitation, together with a high rate of sediment supply, also resulted in highly unstable slopes as testified by common slumps, convolute bedding, and dewatering structures within the sand bodies (Figure 29).

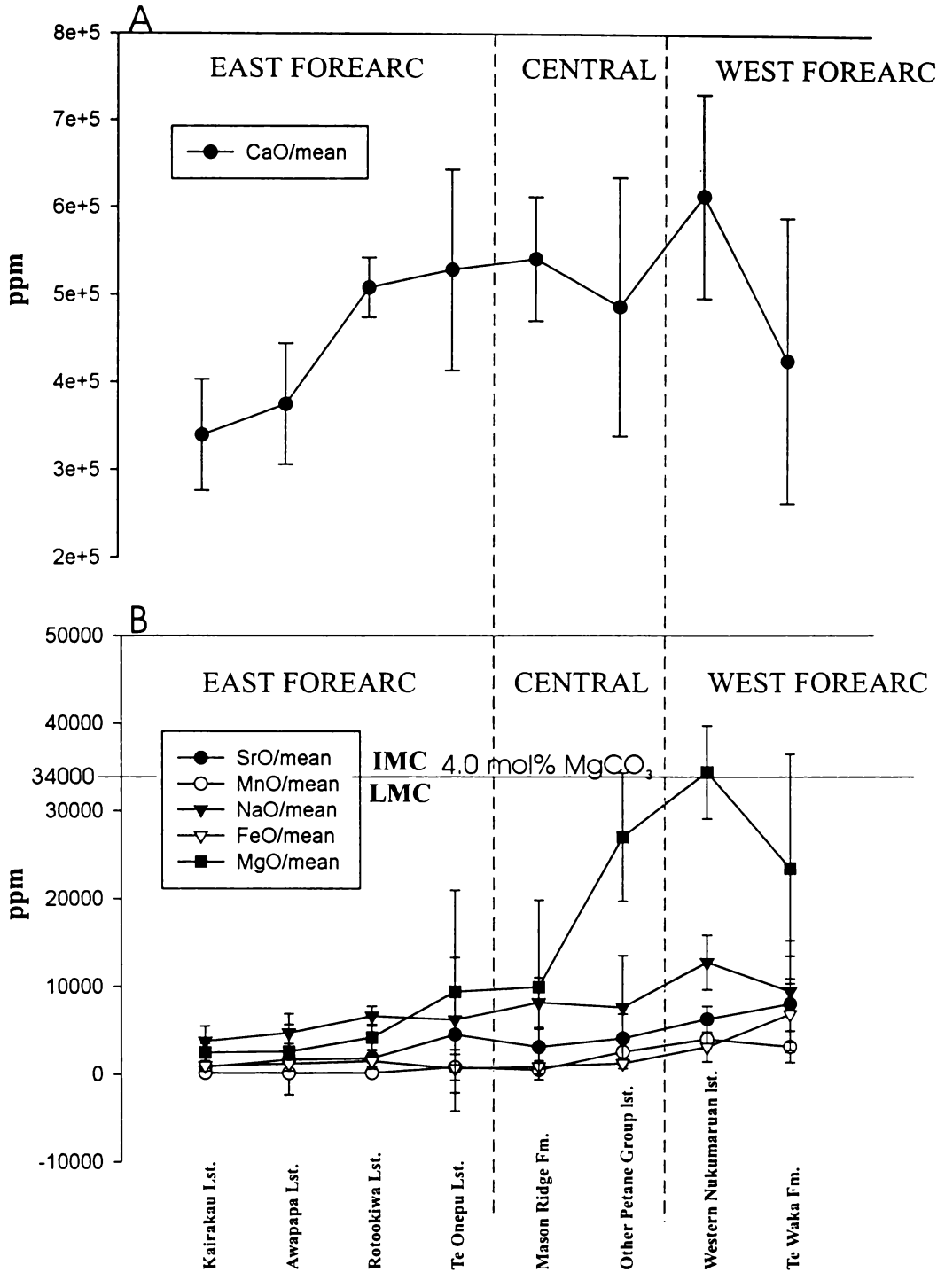

Figure 28- Trace element contents obtained from ICP-OES analysis of bulk samples of Pliocene limestones in southern Hawke's Bay with reference to their geographic location. The elemental weight is expressed in terms of microgram/gram or parts per million (ppm) of the respective element with regard to the particular sampled carbonate. Younger limestones are located in the central part of the former forearc basin. Note in (A) the increase in calcium content in limestones from eastern (older) to central areas (younger), probably associated with a decrease in terrigenous content. Note in (B) that the present carbonate mineralogy of most limestone samples is low-Mg calcite (LMC, <4 mol% $MgCO_3$). Only limestones from the central and western parts of the former forearc basin have slightly higher magnesium contents, and may be intermediate-Mg calcite (IMC, 4-12 mol %$MgCO_3$). These limestones are also the ones that retained aragonitic relict mineralogies (see Table 2). See text for comment. In (A), 6e+5ppm=600 000 ppm, etc.

The depositional model envisaged for the Pliocene carbonates shares many attributes with isolated structurally-controlled platforms that support major carbonate production, as documented in Southeast Asia (Emery and Myers, 1996). Characteristics of such isolated platforms are that they are generally siliciclastic free, best exemplified in the Hawke's Bay forearc basin by the Rotookiwa, Te Onepu, and Pakipaki Limestones, and lack the close interrelation with continent-derived sediments, as reported for continent-attached platforms, and exemplified in the Hawke's Bay setting by western Waipipian and Mangapanian limestones (Te Waka Formation; see below). Furthermore, this model contrasts with the low-gradient carbonate ramps suggested for many non-tropical carbonates, exemplified by the modern shelf of southern Australia, where the rate of erosion is too high to allow aggradation or progradation (shaved-shelf; James *et al.*, 1994). As a result, in these low-gradient carbonate ramp settings particles only accumulate on the mid- and outer-shelf where the prevailing current regime allows deposition. When the rate of sediment supply is higher than the rate of erosion, skeletal deposits aggrade to sea level in the form of variably extensive sheet-like or tabular bodies (Nelson, 1978; Boreen and James, 1995; Betzler *et al.*, 1997).

The depositional model proposed for the Pliocene limestones may not apply to the uppermost strata of the forearc basin sedimentary wedge in the study area (Mason Ridge Formation), whose lateral continuity, minor changes in thickness, and cyclothemic organization suggest that deposition occurred on a flattish shelf, with only subtle gradients, similar to that of the Tangoio Block (Figure 1) depositional model proposed by Haywick *et al.* (1992) and Haywick (2000) in central Hawke's Bay.

7.2. Western setting

By contrast with their eastern counterparts, the depositional system envisaged for the western mixed carbonate-siliciclastic accumulations is one of a narrow shelf swept by tidal and storm-driven currents periodically supplied with terrigenous sediments(continent-attached carbonate platform) in response to the timing of fault-controlled uplift of basement blocks to the west (Figure 30A). The continental shelf adjoining Otago Peninsula (eastern South Island, New Zealand) constitutes a satisfactory modern analogue of the depositional model proposed here, and was investigated by Andrews (1973). In this example, the relatively narrow (11 - 30 km in width)

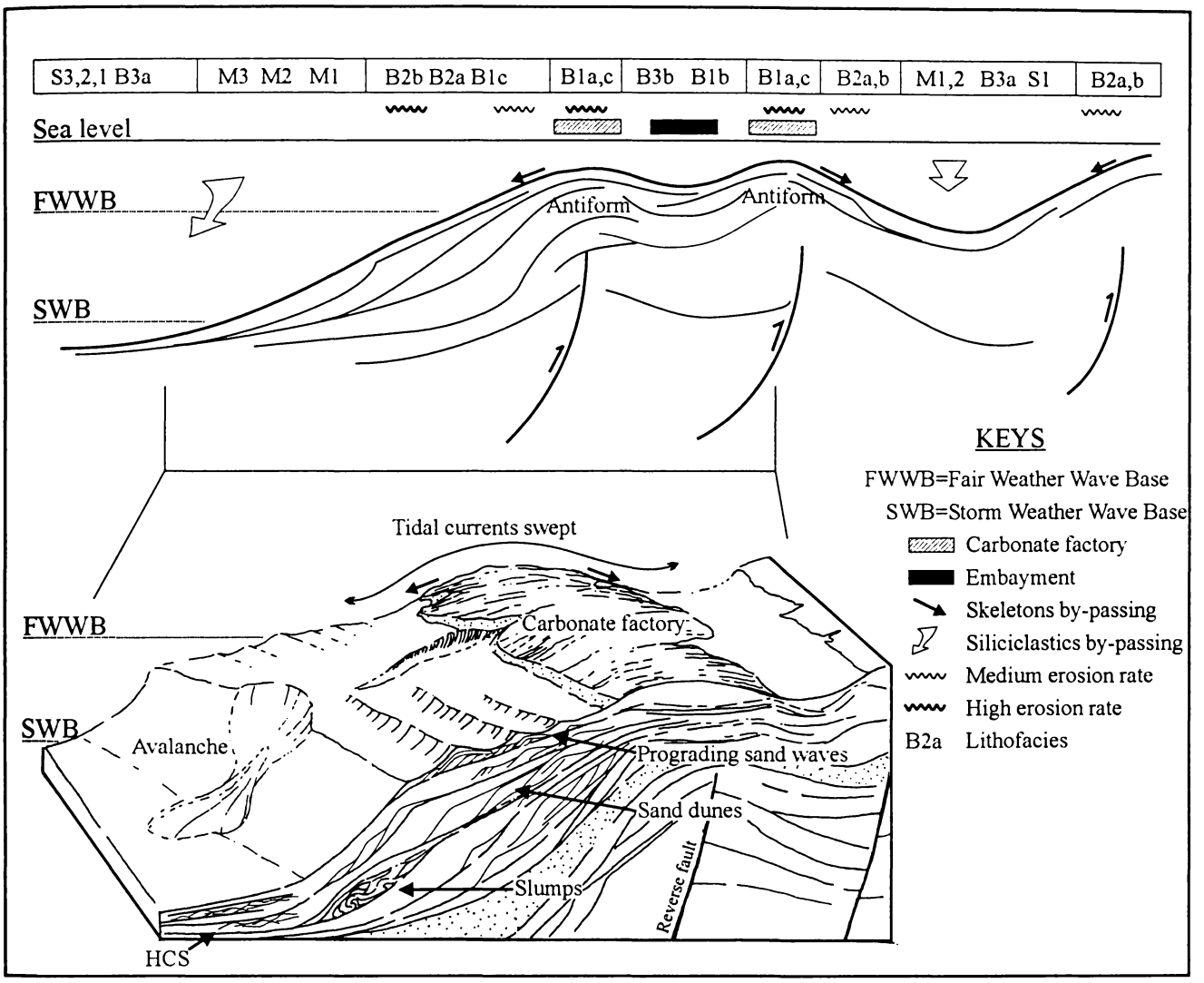

Figure 29- Depositional model proposed for Pliocene limestones in the eastern sector of southern Hawke's Bay showing relationships between carbonate sediment facies (see Table 1), hydrodynamic conditions, and sedimentary bedforms/structures in the vicinity of structural antiforms. See text for discussion.

shelf off the Peninsula abuts landward against basement schists that supply the detrital sand and pebble fraction deposited in inner- to mid-shelf settings. Seawards, gravelly sediments rich in skeletal debris cover the middle and outer shelf. By contrast with the Pliocene setting, whose skeletal fraction is dominated by barnacles and epifaunal bivalves, bryozoans comprise 60-90% of the coarse fraction of samples from the offshore shelf sediments off Otago Peninsula (Andrews, 1973; Probert *et al.*, 1979), suggesting that in Pliocene times shoal areas in mid- to outer-shelf positions in the Ruataniwha Strait promoted barnacle growth over bryozoans (Beu, 1995; Figure 30A), perhaps due to elevated nutrient supplies associated tidal flushing through the seaway.

During the Waipipian and early Mangapanian times, the western margin of the forearc basin was bounded by the North Island emerged land surrounded by shoal areas upon which barnacle-dominated limestones with moderate siliciclastic contents formed (Beu, 1995; Field *et al.*, 1997). The Mangapanian and Nukumaruan deposits in the northern part of the study area record the uplift of the Torlesse basement (Figure 30B). The succession comprises alternating mixed skeletal-siliciclastic limestones and siliciclastic sandstones and siltstones, overlain by conglomerates accumulated in platform and prograding fan-delta depositional systems, respectively (Erdman and Kelsey, 1992; Beu, 1995; Bland, 2001). In the south, during Nukumaruan times, sedimentation was strongly controlled by movements on strike-slip and reverse faults bounding downwarped and uplifted basement blocks, respectively. Thick mudstones and siltstones accumulated in structural troughs (Ohara Depression), whereas limestones formed in shallow waters on top of uplifted blocks (Sentry Box, Kereru Limestones; Cashman *et al.*, 1992; Erdman and Kelsey, 1992).

8. Conclusions

The construction of stratigraphic columns through the different Plio-Pleistocene limestone units in southern Hawke's Bay (Appendix 1) has emphasized the high variability of facies and skeletal composition, both lateral and vertical, within individual formations, and from one formation to another over time.

Rapid lateral facies changes and evolving facies characteristics over Pliocene and Early Pleistocene times are anticipated from the tectonic and paleogeographic setting of the studied formations. Limestones accumulated on the margins of a narrow forearc basin seaway that co-evolved with the convergent Pacific-Australian plate boundary to

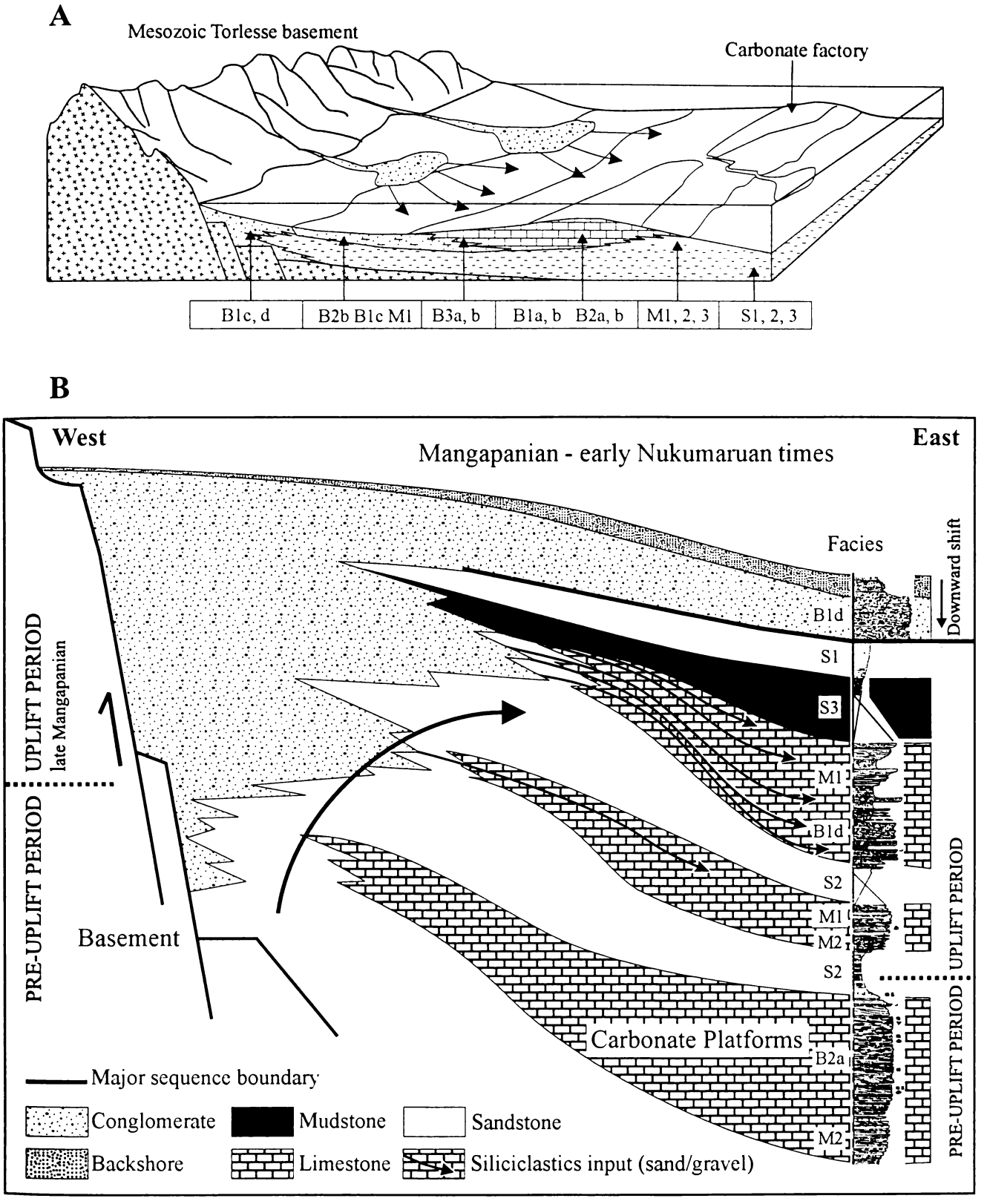

Figure 30- (A) Depositional model envisaged for limestones deposited on the western side of the forearc basin showing distribution of sedimentary facies (see Table 1). (B) Illustration showing the Torlesse basement-derived influx of siliciclastics in relation to the timing of uplift. Continent attached-type carbonate platform model illustrated at rightside by the Te Waka Formation and Titiokura Formation at The Gorges section (see Figure 18). See text for discussion.

the east of North Island. The seaway became narrower and shallower over Pliocene times to eventually close during the Pleistocene (Kamp and Nelson, 1987; Kamp *et al.*, 1988).

Three major facies groupings have been described and defined: Bioclastic (B); Mixed carbonate-siliciclastic (M); and Siliciclastic (S). These comprise a total of 14 different facies types that correspond to a large spectrum of depositional environments ranging from below storm-wave base, in outer shelf-type settings, to predominantly shallow-water shoreface-type environments under the influence of subtidal and tidal wave currents (Table 1).

By contrast with previous studies of Plio-Pleistocene limestones in southern Hawke's Bay (especially the ones that belong to the pre-Nukumaruan barnacle-rich facies), this work, underpinned by detailed sedimentologic and stratigraphic descriptions, has enabled the recognition of recurring sedimentary facies within these formations, and the identification of shell concentrations and key surfaces separating the various facies or groups of facies in the stratigraphic columns, a topic addressed in Chapter 4.

The clustering of petrographic point-counting data has enabled the definition of six mixed carbonate-siliciclastic microfacies between two end-members: terrigenous-rich and terrigenous-free dominated by skeletal fragments, especially barnacles (Figures 26, 27). Results support the hypotheses of previous authors regarding the non-tropical nature of Plio-Pleistocene limestones in southern Hawke's Bay, and the evolution (narrowing and shallowing) of the forearc basin in that: easternmost and westernmost (older) limestone occurrences are compositionally distinctive from their younger (up to earliest Nukumaruan times) more central counterparts, in having (1) a higher terrigenous content; and (2) more variable skeletal compositions, typically consisting of mixes of barnacles, bryozoans, epifaunal bivalves, and foraminifers, instead of being dominated by barnacles and to a lesser degree epifaunal bivalves.

Nukumaruan limestones differ from their pre-Nukumaruan counterparts as shown by a combination of: (1) the higher content of aragonitic infaunal molluscs; (2) the presence of carbonate mud as a rock framework in some Nukumaruan formations (Mason Ridge); and (3) the cyclothemic disposition of limestones and silt-sandstone interbeds.

The depositional setting for the cool-water Pliocene limestones in eastern Hawke's Bay is envisaged to be one of isolated, clastic-free, submarine antiforms and ridges that hosted carbonate factories (Figure 29). Around and about these submarine highs, which may have locally become emergent and formed either promontories or islands, tidal currents were accelerated and resulted in the development of sand dunes. Sand waves and sand dunes were deposited according to the diminishing energy of tidal currents, in a down-dip direction from the antiform tops, to form large sand banks on the antiform flanks. Thus it is inferred that the submarine topography caused the current regime to change from erosional to depositional, in a general down-slope direction.

In contrast, the depositional setting for the western limestone occurrences is thought to correspond to continent attached-type carbonate platforms (Figure 30A). Thus, the locally monoclinal and cyclothemic disposition of the Mangapanian successions in the western part of the study area, together with their moderate to high contents of Torlesse basement-derived siliciclastics, indicate that carbonates probably formed and accumulated on a shelf regularly provided with terrigenous sediments, and influenced by strong tidal currents, which locally promoted barnacle growth.

References

Andrews, P. B. (1973) Late Quaternary continental shelf sediments off Otago Peninsula, New Zealand. *New Zealand Journal of Geology and Geophysics*, **16**(4), 793-830.

Betzler, C., Brachert, T. C., Braga, J.-C. & Martin, J. M. (1997) Nearshore, temperate, carbonate depositional systems (lower Tortonian, Agua Amarga Basin, southern Spain): implications for carbonate sequence stratigraphy. *Sedimentary Geology*, **113**, 27-53.

Beu, A. G. (1990b) Field trip guide: Te Aute Limestone, *Vol. 50B*, pp. 203-227. Geological Society of New Zealand miscellaneous publication.

Beu, A. G. (1995) *Pliocene Limestones and Their Scallops*. Monograph 10, Institute of Geological & Nuclear Sciences Limited, Lower Hutt, New Zealand, 243 pp.

Beu, A. G., Grant-Taylor, T. L. & Hornibrook, N. d. B. (1980) The Te Aute limestone facies, Poverty Bay to northern Wairarapa, pp. 36. Dept. of Scientific and Industrial Research, Wellington.

Bland, K. (2001) Analysis of the Pliocene forearc basin succession - Esk river catchment, Hawke's Bay. Unpublished MsC Thesis, University of Waikato.

Bland, K. (in prep.) Analysis of Hawke's Bay basin, eastern North Island, New Zealand. PhD Thesis, University of Waikato.

Boreen, T., James, N. P., Heggie, D. & Wilson, C. (1993) Surficial cool-water carbonate sediments on the Otway continental margin, southeastern Australia. *Marine Geology*, **112**, 35-56.

Boreen, T. D. & James, N. P. (1995) Stratigraphic sedimentology of tertiary cool-water limestones, SE Australia. *Journal of Sedimentary Research*, **B65**(1), 142-159.

Bromley, R. G. (1994) The paleoecology of bioerosion. In: *The paleobiology of Trace Fossils* (Ed. by S. K. Donovan), pp. 134-154. Wiley, New York.

Cashman, S. M., Kelsey, H. M., Erdman, C. F., Cutten, H. N. C. & Berryman, K. R. (1992) Strain partitioning between structural domains in the forearc of the Hikurangi subduction zone, New Zealand. *Tectonics*, **11**(2), 242-257.

Chayes, F. (1956) *Petrographic Modal Analysis*. Wiley, New York, 113 pp.

Collins, L. (1988) Sediments and history of the Rottnest Shelf, southwest Australia: a swell-dominated, non-tropical carbonate margin. *Sedimentary Geology*, **60**, 15-49.

Dunham, R. J. (1962) Classification of carbonate rocks according to depositional texture. In: *Classification of Carbonate Rocks: A Symposium, Vol. 1* (Ed. by W. E. Ham), pp. 108-121. AAPG Memoir.

Emery, D. & Myers, K. (1996) *Sequence Stratigraphy*. Blackwell Science, Oxford, 297 pp.

Erdman, C. F. & Kelsey, H. M. (1992) pliocene and Pleistocene stratigraphy and tectonics, Ohara depression and Wakarara range, North Island, New Zealand. *New Zealand Journal of Geology and Geophysics*, **35**, 177-192.

Field, B. D., Uruski, C. I., *et al.* (1997) *Cretaceous-Cenozoic Geology and Petroleum Systems of the East Coast Region, New Zealand*. Monograph 19, Institute of Geological and Nuclear Sciences Limited, Lower Hutt, New Zealand, 301 pp.

Fleming, C. A. (1952) A Foveaux Strait oyster bed. *New Zealand Journal of Science and Technology*, **34**, 73-85.

Galehouse, J.S. (1971) Point-counting. In: *Procedures in Sedimentary Petrology* (Ed. By R.E. Carver), pp. 385-407. Wiley-Interscience, New York.

Harmsen, F. J. (1984) *Stratigraphic sections of the Pliocene Te Aute Group in Central and Southern Hawke's Bay, New Zealand.* Geology Department, Victoria University, Wellington, New Zealand, 109 pp.

Harmsen, F. J. (1985) Lithostratigraphy of Pliocene Strata, Central and Southern Hawke's Bay, New Zealand. *New Zealand Journal of Geology and Geophysics*, **28**, 413-433.

Hayton, S., Nelson, C. S. & Hood, S. D. (1995) A skeletal assemblage classification system for non-tropical carbonate deposits based on New Zealand Cenozoic limestones. *Sedimentary Geology*, **100**, 123-141.

Haywick, D. W. (2000) Recognition and distinction of normal and forced regression in cyclothemic strata: a Plio-Pleistocene case study from eastern North Island, New Zealand. In: *Sedimentary Responses to Forced Regressions, Vol. 172* (Ed. by D. Hunt and R. L. Gawthorpe), pp. 193-215. Geological Society of London Special Publications, London.

Haywick, D. W., Carter, R. M. & Henderson, R. A. (1992) Sedimentology of 40 000 year Milankovitch-controlled cyclothems from Central Hawke's Bay, New Zealand. *Sedimentology*, **39**, 675-696.

Haywick, D.W., Lowe, D.A., Beu, A.G., Henderson, R.A., & Carter, R.M. (1991) Pliocene-Pleistocene (Nukumaruan) lithostratigraphy of the Tangoio block, and origin of sedimentary cyclicity, central Hawke's Bay, New Zealand. *New Zealand Journal of Geology and Geophysics*, **34**, 213-225.

Haywick, D. W. N. (1990) Stratigraphy, sedimentology, paleoecology and diagenesis of the Petane Group (Pliocene-Pleistocene) in the Tangoio, central Hawke's Bay, New Zealand. Unpublished PhD Thesis, James Cook University of North Queensland, Australia.

Hornibrook, N. de B., Brazier, R.C. & Strong, C.P. (1989) Manual of New Zealand Permian to Pleistocene foraminiferal biostratigraphy. *New Zealand Geological Survey Paleontological Bulletin,* **56**, 175.

James, N. P., Bone, Y., Von Der Borch, C. C. & Gostin, V. A. (1992) Modern carbonate and terrigenous clastic sediments on a cool-water, high energy, mid-latitude shelf: Lacepede, southern Australia. *Sedimentology*, **39**, 877-903.

James, N. P., Boreen, T. D., Bone, Y. & Feary, D. A. (1994) Holocene carbonate sedimentation on the west Eucla Shelf, Great Australian Bight: A shaved shelf. *Sedimentary Geology*, **90**, 161-177.

James, N. P. & Choquette, P. W. (1990) Limestones - The sea-floor diagenetic environment. In: *Diagenesis, Vol. Reprint series 4* (Ed. by I. A. McIlreath and D.W. Morrow), pp. 13-34. Geoscience Canada.

Kamp, P. J. J., Harmsen, F. J., Nelson, C. S. & Boyle, S. F. (1988) Barnacle-dominated limestone with giant cross-beds in a non-tropical, tide swept, Pliocene forearc seaway, Hawke's Bay, New Zealand. *Sedimentary Geology*, **60**, 173-195.

Kamp, P. J. J. & Nelson, C. S. (1987) Tectonic and sea-level controls on non-tropical limestones in New Zealand. *Geology*, **15**, 610-613.

Kamp, P. J. J. & Nelson, C. S. (1988) Nature and occurrence of modern and Neogene active margin limestones in New Zealand. *New Zealand Journal of Geology and Geophysics*, **31**, 1-20.

Kelsey, H. M., Erdman, C. F. & Cashman, S. M. (1993) Geology of Southern Hawke's Bay from the Maraetotara Plateau and Waipawa westward to the Wakara Range and the Ohara depression, pp. 1-17. Institute of Geological & Nuclear Sciences, Lower Hutt, New Zealand.

Kingma, J. T. (1971) Geology of Te Aute Subdivision. *New Zealand Geological Survey Bulletin*, **70**, 173.

Kobluk, D. R. & Risk, M. J. (1977) Rate and nature of infestation of a carbonate substratum by a boring alga. *Journal of Experimental Marine Biology and Ecology*, **27**, 107-115.

Lukasik, J. J., James, N. P., McGowran, B. & Bone, Y. (2000) An epeiric ramp: low-energy, cool-water carbonate facies in a Tertiary inland sea, Murray Basin, south Australia. *Sedimentology*, **47**, 851-881.

McCave, I. N. (1971) Sand waves in the north sea off the coast of Holland. *Marine Geology*, **10**, 199-225.

McIntyre, A. (2002) Geology of Mangapanian (Late Pliocene) strata, Wanganui Basin: lithostratigraphy, paleontology, and sequence stratigraphy. Unpublished PhD Thesis, University of Waikato, 431p.

McKay, A. (1886a) Notes on the geology of Scinde Island and some parts of the northern district of Hawke's Bay. *Colonial Museum and Geological Survey of New Zealand. Reports of Geological Exploration during 1885*, **17**, 185-192.

Moore, P. R. & Hatton, B. A. (1985) Limestone resources of northern and central Hawke's Bay. *New Zealand Geological Survey Record*, **2**, 1-26.

Nelson, C. S. (1978) Temperate shelf carbonate sediments in the Cenozoic of New Zealand. *Sedimentology*, **25**, 737-771.

Nelson, C. S., Keane, S. L. & Head, P. S. (1988b) Non-tropical carbonate deposits on the modern New Zealand Shelf. *Sedimentary Geology*, **60**, 71-94.

Pallentin, A. (in prep.) Plio-Pleistocene geology of central and northern Hawke's Bay, New Zealand. PhD Thesis, University of Waikato.

Percival, C. J. (1992) The Harthope Ganister - A transgressive barrier Island to shallow marine sand ridge from the Namurian of Northern England. *Journal of Sedimentary Petrology*, **62**(3), 442-454.

Probert, P. K., Batham, E. J. & Wilson, J. B. (1979) Epibenthic macrofauna off southeastern New Zealand and mid-shelf bryozoan dominance. *New Zealand Journal of Marine & Freshwater Research,* **13**(3), 379-392.

Radwanski, A. (1970) Dependence of rock borers and burrowers on the environment conditions within the Tortonian littoral zone of Southern Poland. *Geological Journal,* **3**, 371-390.

Seilacher, A. (1967) Bathymetry of trace fossils. *Marine Geology*, **5**, 413-428.

Spörli, K. B. & Pettinga, J. R. (1980) Mount Kahuranaki, Hawkes Bay, New Zealand, a klippe emplaced by gravity sliding from the crest of the Nearby Elsthorpe anticline. *Journal of the Royal Society of New Zealand*, **10**(3), 287-307.

Wilson, J. B. (1967) Paleoecological studies on shell beds and associated sediments in the Solway Firth. *Scottish Journal of Geology*, **3**, 329-371.

Chapter 2

DEVELOPING CONCEPTS OF HIGH-RESOLUTION DIAGENETIC STRATIGRAPHY FOR COOL-WATER LIMESTONES: APPLICATION TO PLIOCENE TE AUTE LIMESTONES, NEW ZEALAND, AND THEIR SEQUENCE STRATIGRAPHY

Abstract 88
1. Introduction 89
2. Geological framework 90
3. Methods 96
4. Concept of diagenetic stratigraphy 96
5. Diagenetic stages: eogenesis-mesogenesis-telogenesis versus pre- and post-compaction terminology 102
    5.1. Early diagenesis – eogenesis 102
    5.2. Burial diagenesis – mesogenesis 103
    5.3. Late diagenesis – telogenesis 106
    5.4. Pre- and post-compaction diagenesis 107
6. Application of diagenetic stratigraphy concepts to Te Aute limestones 116
    6.1. Patterns of pre-compaction diagenesis 116
    6.2. Comment on post-compaction diagenesis 125
7. Conclusions 125
References 128

Key Sections: 1, 4, 5, 6, 7
Key Figures: 5, 6, 7, 9, 11
Key Tables: 1, 2

Chapter 2

DEVELOPING CONCEPTS OF HIGH-RESOLUTION DIAGENETIC STRATIGRAPHY FOR COOL-WATER LIMESTONES: APPLICATION TO PLIOCENE TE AUTE LIMESTONES, NEW ZEALAND, AND THEIR SEQUENCE STRATIGRAPHY

ABSTRACT: The diagenetic evolution of calcitic cool-water limestones can be markedly different from that for aragonite-dominated tropical carbonates. This petrographic study develops a "sequence stratigraphic" approach to cool-water carbonate diagenesis based on the chronological occurrence of all diagenetic features (i.e., a diagenetic rather than cement stratigraphy) within sedimentary successions, their vertical and lateral distribution, and their grouping into discontinuity-bounded (by dissolution surfaces, fractures, renucleation events) suites at a thin-section scale. The progression of diagenetic environments that moved through a succession is best explained when related to diagenetic discontinuities correlatable throughout the study area. In our limestones a critical discontinuity event to decipher is the first evidence of mechanically-induced skeletal fracturing, enabling the definition of pre-compaction and post-compaction diagenetic features. A comparison of pre-compaction diagenetic suites in samples from above and below significant outcrop disconformities enables isolation of the "specific diagenesis" of unconformity-bounded depositional units, which is that suite of diagenetic events associated with the evolution of the sedimentation realm of a unit, exclusive of diagenetic overprints shared with any overlying unit through an unconformity since these relate to some subsequent, different depositional stage. In this way it is possible for the specific diagenesis of a succession of depositional facies between consecutive unconformities to be interpreted within a sequence stratigraphic framework.

Sections of cool-water Pliocene skeletal limestones in eastern North Island, New Zealand, comprise deepening- and then sometimes shallowing-upwards, unconformity-bounded depositional packages, or sequences. We recognize ten different specific diagenetic signatures in these rocks that are correlatable to depositional lithofacies. The vertical distribution of specific diagenetic signatures within the sequences exhibits a trend from mainly constructive to mainly destructive diagenesis in the deepening-upwards member of the sequences, and constructive in their shallowing-upwards portion, that can be integrated in a sequence stratigraphic

framework. Constructive diagenesis occurs in the lower part of the transgressive system tract (TST) and in the upper part of the regressive system tract (RST), whereas destructive diagenesis is dominant in the upper part of the TST, the highstand system tract (HST), and the lower part of the RST.

1. Introduction

Most modern syntheses of carbonate diagenesis have focussed on the products and processes occurring in young marine carbonate deposits from warm-water or tropical settings, notably in surface or very shallow-burial marine and meteoric environments. The early (eogenesis) and burial to late diagenesis (meso- to telogenesis; Choquette and Pray, 1970) of many ancient limestones have also been widely documented, with comparisons frequently made to the Recent. Consequently, the diagenetic scenarios contained in an extensive literature on modern and ancient carbonates are inevitably pervaded by tropical perceptions (e.g., Bathurst, 1975; Longman, 1980; Heckel, 1983; Schroeder and Purser, 1986; Tucker and Wright, 1990).

Climate, seawater chemistry, depositional setting, skeletal assemblages, and sediment mineralogy are significant factors governing the type of diagenesis affecting carbonate sediments. In this regard there are several major differences between tropical and non-tropical carbonate sediments that are likely to have a major influence on their diagenetic behaviour and diagenetic patterns (Nelson 1988; Walker and James, 1992; Hood and Nelson, 1996; Nicolaides and Wallace, 1997a; Dodd and Nelson, 1998). These include the higher degree of saturation with respect to calcium carbonate of warm-tropical sea waters, the much greater abundance of aragonite in tropical sediments, the prevalence of a predominantly constructive diagenetic regime at the sea floor in warm waters but of an often rather destructive regime in cool-water settings, and the occurrence of photozoan (light dependent) grain associations in tropical settings versus heterozoan (light independent) grain assemblages in non-tropical shelf carbonates (James, 1997).

The degree of sea-water carbonate saturation, the hydrodynamic and fluid-flow regime, and the content of metastable carbonate minerals are factors of great importance to the timing of cement formation between grains and to the mineralogy and fabric of either marine or meteoric precipitates. In warm supersaturated sea water, thick coatings of marine cements may precipitate during the earliest stages of the diagenetic history of a carbonate sediment (James and Choquette, 1990).

Furthermore, the high diagenetic potential of tropical carbonate sediments due to their typically large content of aragonite may result in further early cement formation, either in the meteoric or very shallow burial environment. Such strongly armoured sediments develop resistance towards subsequent mechanical and chemical compaction. In contrast, a paucity of early cementation in cool-water aragonite-poor carbonates can result in extensive compaction effects occurring much earlier in their burial history than might otherwise be the case in their aragonite-rich tropical counterparts (Meyers, 1980; Nelson *et al.*, 1988; Nicolaides and Wallace, 1997b). These different diagenetic behaviours between cool-water aragonite-poor carbonates and tropical aragonite-rich carbonates are unlikely to result in the same timing and characteristics of alteration features as expounded by established carbonate diagenetic classification schemes, such as the early, burial, and late diagenetic categories of Choquette and Pray (1970).

Our wider study is concerned with the sedimentology and diagenesis of cool-water aragonite-poor Te Aute limestones of Pliocene age in eastern North Island, New Zealand. In this paper we focus first on some broad philosophical concepts and terminologies relating to carbonate diagenesis and their basis for interpreting diagenetic sequences in general. Into this discussion we weave microscopic observations from the non-tropical Pliocene limestones to develop a new petrographic approach for studying cool-water carbonate diagenesis, one potentially useful for relating diagenetic features to outcrop sequence stratigraphy. The method entails recording the high-resolution chronological (i.e., sequential) occurrence of all diagenetic features within samples, grouping these into discontinuity-bounded sequences at the thin-section scale, and noting their vertical and lateral distribution within sedimentary formations. We regard the recognition of pre- and post-compaction diagenetic features, and their timing, as central for helping better define the progression of diagenetic environments affecting cool-water carbonates. The paper concludes by applying more specifically the conceptual principles developed here for interpreting the diagenetic sequences in a section of Te Aute limestones.

2. Geological framework

The New Zealand Neogene is dominated by thick successions of terrigenous mudstone and sandstone formed in response to evolution of the convergent Pacific-

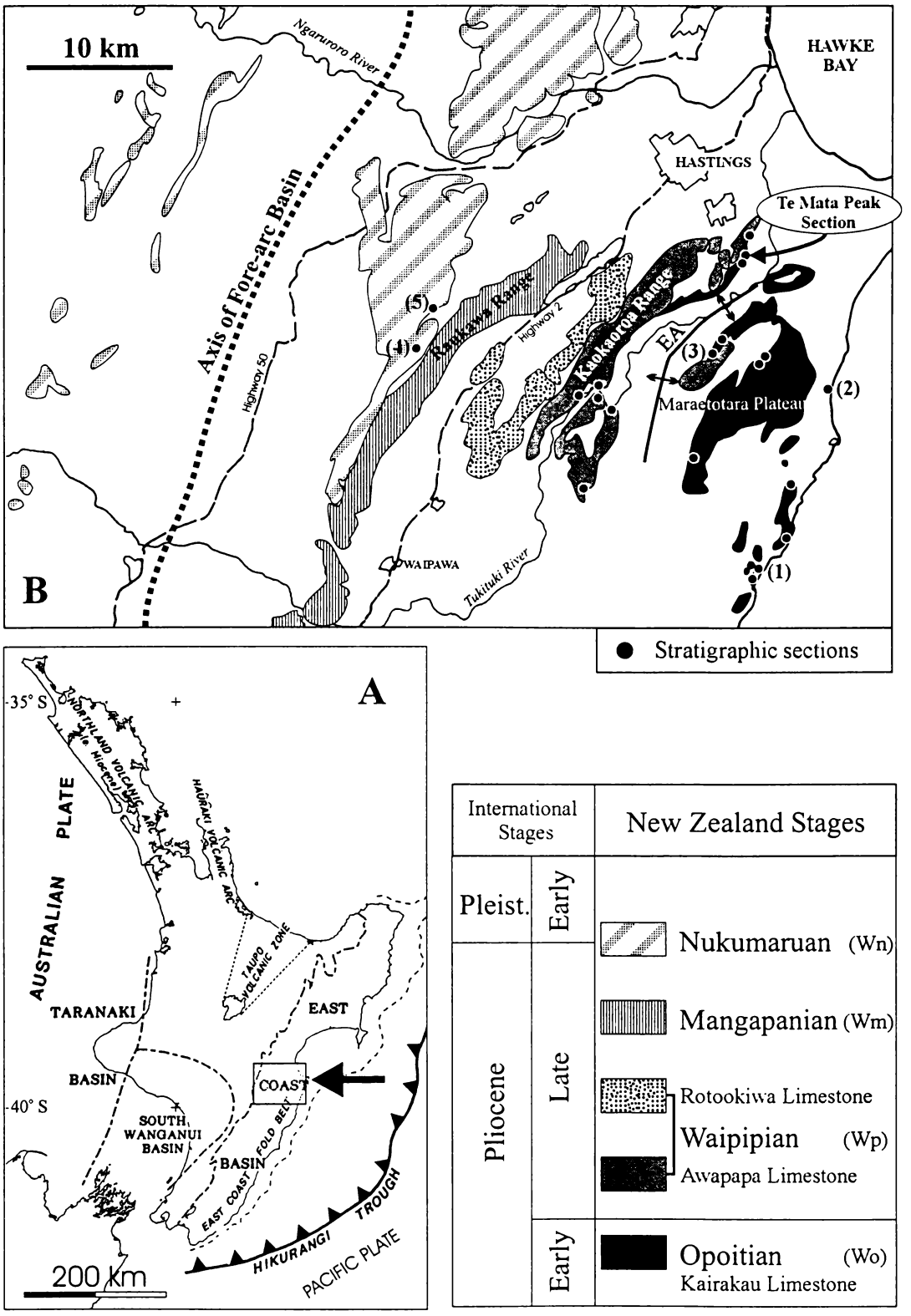

Figure 1- (A) Locality map outlining the tectonic setting of the East Coast Basin of North Island, New Zealand. (B) Simplified geologic map showing the outcrop pattern and ages (including New Zealand stages) of Pliocene Te Aute limestones in southern Hawke's Bay (after Beu, 1995), and locations of measured sections of the Kairakau and Awapapa Limestone sheets. EA: Elsthorpe Anticline. Other localities mentioned in this chapter: (1) Kairakau Beach; (2) Waimarama; (3) Mt Kahuranaki; (4) Mangatai; (5) Pakihirua.

Australian plate boundary through the subcontinent since the close of the Oligocene (Kamp, 1986). Non-tropical limestones comprise a minor but persistent component of this stratigraphy (Kamp and Nelson, 1987, 1988). Locally these limestones can be thick and quite extensive, exemplified best by the Te Aute limestones of Plio-Pleistocene age in the East Coast Basin of eastern North Island (Figure 1A; Beu, 1995; Field *et al.*, 1997). The Te Aute limestones were deposited in a progressively narrowed forearc basin seaway between an actively evolving subduction complex to the east and an uplifting structural ridge to the west (Kamp *et al.*, 1988; Nelson *et al.*, in review). The limestones are strung out along a NE-SW-trending belt and the outcrop pattern of the Early and Late Pliocene occurrences demonstrates that deposition migrated towards the centre of the basin over time, the younger sheets being present close to the forearc basin axis and at lower elevations compared to older Pliocene sheets located on the outer margins of the basin (Figure 1B). Differential uplift persisted after the Pliocene, and so the Early Pleistocene limestones formed in the axis of the basin.

The forearc seaway was situated near 40°S paleolatitude and was influenced by strong tidal flows involving mainly cool- to warm-temperate ocean currents (Kamp *et al.*, 1988; Hornibrook, 1992; Beu, 1995). Many of the Pliocene Te Aute limestones are distinctive because of their high barnacle content, although overall the skeletal assemblages typically involve variable mixtures of barnacles, bivalve molluscs, and bryozoans (Kamp *et al.*, 1988; Nelson *et al.*, in review). These skeletal carbonates are subtidal deposits formed upon and about actively growing structural antiforms (submarine ridges) within the forearc, and at inner and middle shelf depths of the seaway throughout the Pliocene and early Pleistocene (Kamp *et al.*, 1988).

Two of the Te Aute limestone units are the focus of this paper: the Early Pliocene (late Opoitian) Kairakau Limestone and the earliest Late Pliocene (early Waipipian) Awapapa Limestone (Figure 1B). They are well exposed in NE-trending parallel ranges that represent the eastern part of the exposed forearc in southern Hawke's Bay, south of Hastings (Figure 2A). The stratigraphic and structural framework of the Te Aute limestones are well described by Spörli and Pettinga (1980), Harmsen (1985), Kelsey et al. (1993), Beu (1995), and Field *et al.* (1997).

Figure 2- (A) Cliff outcrop, about 120 m high, in Awapapa Limestone at Te Mata Peak (Fig. 1B). (B) A discontinuity, interpreted as a transgressive surface of erosion (TSE), separating coarse-grained, oyster-bearing (black arrows) skeletal sediments from underlying fine-grained, planar laminated, densely *Ophiomorpha*-burrowed, mixed carbonate-siliciclastic sediments in Kairakau Limestone at Te Mata Peak. Note the relief along this mildly angular unconformable contact (white arrow). (C) Close view of discontinuity between underlying densely burrowed, medium-grained skeletal sediments and overlying very coarse-grained skeletal sediments containing abraded oyster shells (o) and whole specimens of barnacle (bc) in Kairakau Limestone at the Mt Kahuranaki section (locality 3 in Figure 1B).

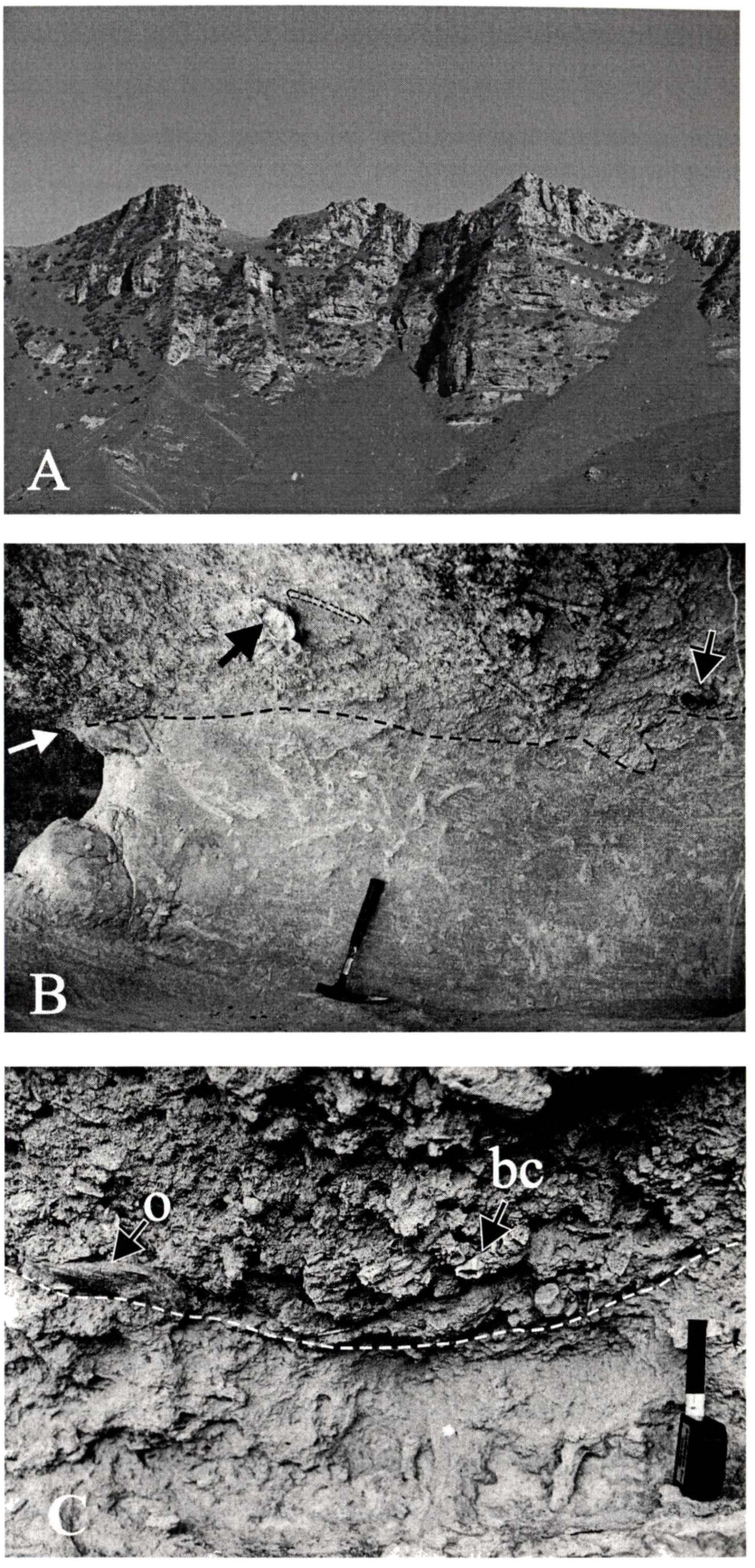
A
B
bc
o
C

Table 1- Some techniques applied at the thin-section scale and procedures followed during the diagenetic study of the Te Aute limestones.

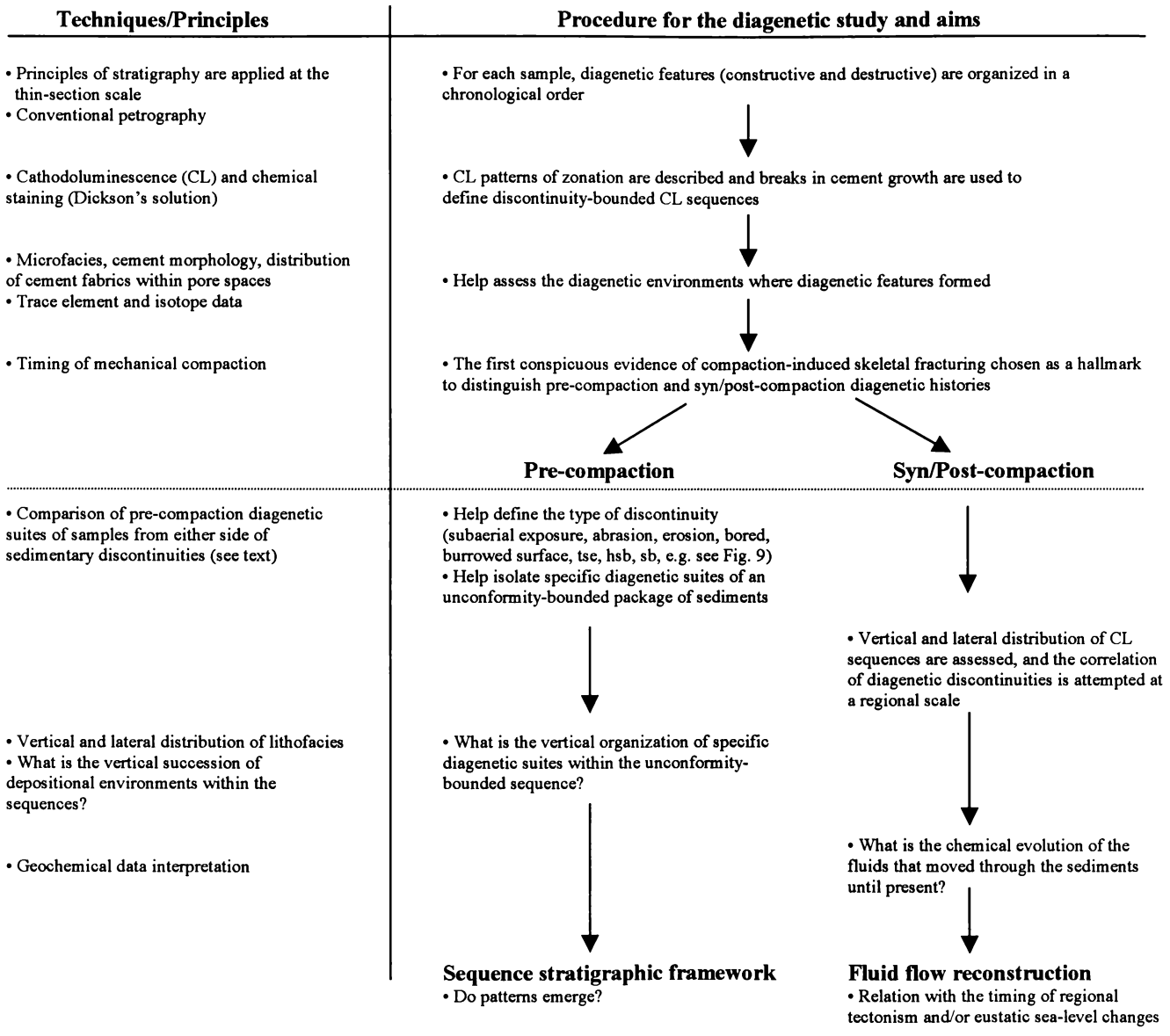

Kairakau Limestone is mainly characterized by mixed facies, transitional between bivalve- to barnacle-rich grainstone and terrigenous packstone, often bioturbated. Awapapa Limestone ranges from interbedded terrigenous packstone and calcareous sandstone to pure skeletal-rich grainstone, and is characteristically a bivalve- to locally barnacle plate-dominated limestone, and more rarely includes abundant bryozoan remains. In both limestones the stacked packages of different facies can be bounded by prominent discontinuity surfaces (Figures 2B, 2C), to which our diagenetic stratigraphies are related (see later).

3. Methods

About 300 samples were collected from ten sections of Kairakau Limestone and from eight sections of Awapapa Limestone in southern Hawke's Bay (Figure 1B). These samples were impregnated with epoxy resin to prevent the loss of any pore-lining cement, and polished thin-sections were prepared, examined, and point-counted using both conventional and cathodoluminescent petrography with a Technosyn 8200 MKII instrument (14-15 kv, 0.15 milliamps beam current). Selected samples were stained with Alizarin Red-S and potassium ferricyanide to help distinguish carbonate mineral phases (Dickson, 1965). Principles, procedures, and aims of our ongoing diagenetic study of the Te Aute limestones are summarized in Table 1, and full petrographic data are contained in Appendices 3, 4, and 5 (also on CD1).

4. Concept of diagenetic stratigraphy

Although based on the concept of "cement stratigraphy" (Meyers, 1974, 1978), a preferred term in the present work is "diagenetic stratigraphy" which takes into account not only the compositional zonation of carbonate cements revealed by chemical staining and cathodoluminescence, but also all paragenetic features related to either destructive (abrasion, bioerosion, maceration, chemical alteration) or constructive (cementation, encrustation) diagenetic processes. As noted earlier, the early sea-floor diagenesis of temperate carbonates has traditionally been regarded as predominantly destructive rather than constructive in nature (Alexandersson, 1978; Farrow and Fyfe, 1988; Nicolaides and Wallace, 1997a; Dodd and Nelson, 1998; Nelson and James, 2000), a diagenetic specificity that is approached in the present study from both quantitative (point-counting) and qualitative (relative abundance)

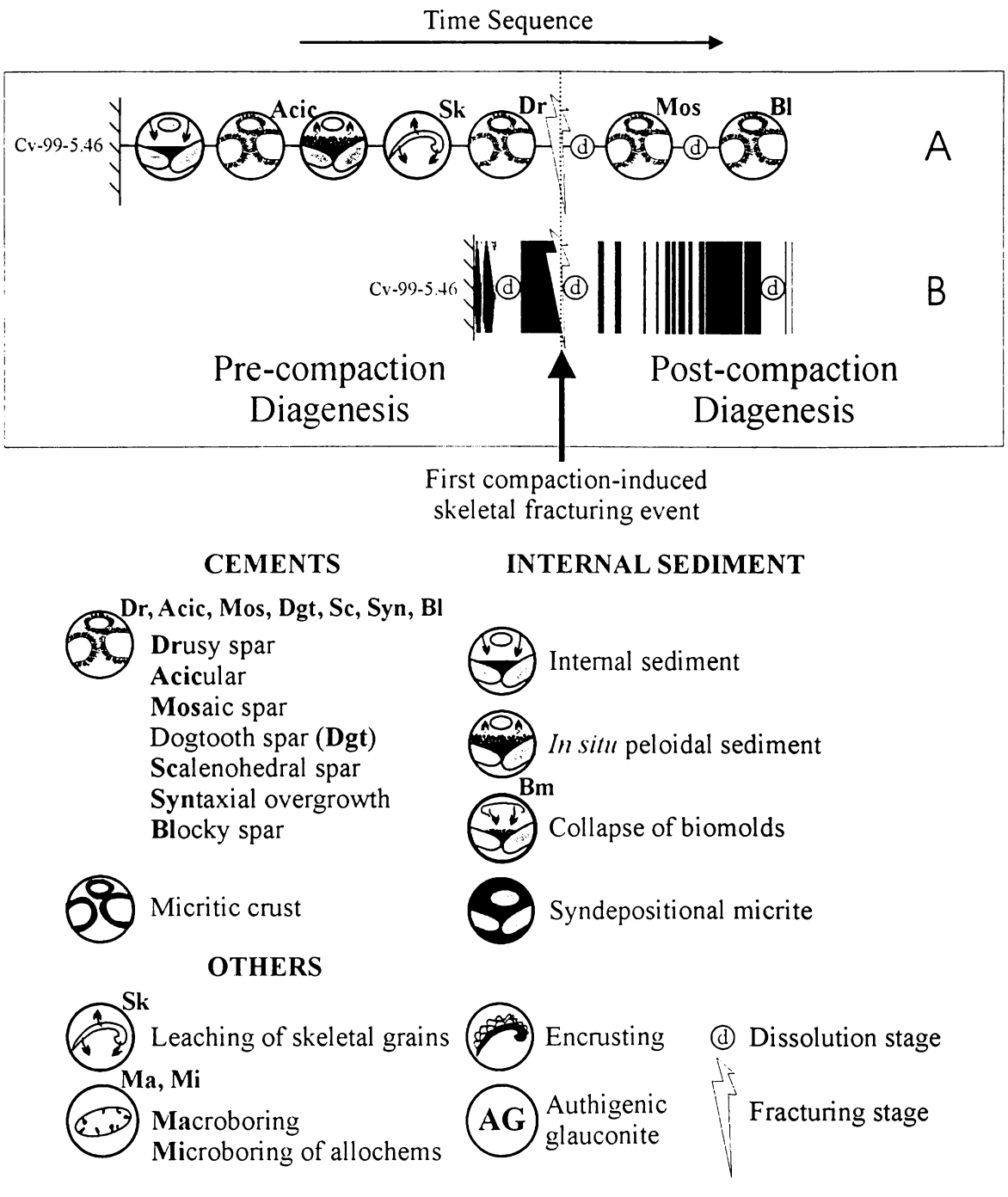

Figure 3- The "diagenetic sequence diagram" is a schematic representation of the chronological occurrence of diagenetic features, for which several logotypes have been created (some examples shown here). Diagenetic features are described in thin sections sequentially from grain surface to pore centre. The diagenetic sequence diagram combines observations made under plane polarized (A) and cathodoluminescent (B) light modes. The boundary between pre-compaction and post-compaction suites is the first occurrence of compaction-induced skeletal fracturing. Example here is sample Cv-99-5.46 from Awapapa Limestone (at 47 m in sequence D, Figure 9) at Te Mata Peak.

viewpoints.

4.1. The diagenetic sequence diagram

The intent to better understand diagenetic systems through synthetic representations has a long history, and several researchers over the past two decades have proposed schematic illustrations of diagenetic sequences. Examples include the petrogenetogram (Schroeder 1984, 1988), the diagenetic diagram (Loreau and Cros, 1988), the diagram of cement zones (Walkden, 1987; Goldstein, 1988; Kaufman *et al.*, 1988), and the diagenetic log (Durlet *et al.*, 1992; Durlet, 1996). These representations derive from observations made on ancient tropical carbonate successions. However, in our study of the non-tropical Te Aute limestones we have found the integration and application of the particular diagenetic pathways suggested by such schemes to seldom be straightforward, and to sometimes be problematical.

Thus, a different schematic representation of diagenetic data has been adopted here that takes into account all the significant diagenetic features interpretable in terms of possible diagenetic environments in a cool-water carbonate depositional realm. Named the "diagenetic sequence diagram" (Figure 3), the scheme is simply an attempt to reflect as completely as possible the diagenetic history of cool-water carbonate deposits. Therefore it integrates schematic representations of (1) the various diagenetic features evident in thin-section, organized in chronological sequence, and (2) the compositional zonation of the cements revealed by cathodoluminescence. Several logotypes have been devised to help record these data (Figure 3).

4.2. Cathodoluminescence (CL) zones and subzones

In carbonate rocks, CL petrography has found wide application for elucidating both the growth patterns of cement precipitates and the different stages of cementation, enabling construction of a cement stratigraphy (Meyers, 1974, 1978). CL zonations in clear spar cements are assumed to be due to changes in pore-fluid chemistry, so that each zone may represent a time-correlative discrete period of cementation. It appears that it is mainly variations in the contents (or ratio) of Fe and Mn that control calcite luminescence (Dorobek, 1987; Niemann and Read, 1988; Horbury and Adams, 1989; Meyers, 1989). Typically, Fe^{2+} inhibits luminescence, while Mn^{2+} activates it. Machel and Burton (1991) emphasized that even small concentrations of

Mn^{2+} in solid solution are sufficient to produce luminescence with or without Fe^{2+} present in solution (as little as 20 ppm Mn^{2+} for Fe^{2+} contents <150 ppm). CL colours that Mn^{2+} are responsible for range from yellow/orange-yellow to orange/red-orange. This range of colours represents either a chemical modification of calcite or a modification of the redox potential. CL colours that are related to the dominant inhibiting effect of Fe^{2+} range from dull brown to brown/black.

The shape and type of successive CL cement zones enable identification of such features as cementation stages and dissolution stages. Our definition of cement zones uses the concept of unconformity-bound depositional packages in sequence stratigraphy to group isochronous cementation episodes separated by either fracturing stages, which additionally provide a good control of the cross-cutting paragenetic relationships, or by dissolution surfaces, the corroded outer margins of successive generations of cement (Kaufman *et al.*, 1988; Braithwaite, 1993), or by both fracture and dissolution events. "Luminescent subzones" correspond to the thinnest divisions observed under CL light. Each subzone represents one stage of crystal growth during which physicochemical conditions supposedly remained more or less stable. The limit between two subzones can be sharp or progressive depending on the evolution of the pore-fluid chemistry (Meyers, 1974, 1978, 1989; Amieux, 1981; Walkden and Berry, 1984; Amieux *et al.*, 1989). "Luminescent zones" correspond to a relatively thick, homogeneous luminescent phase, or to a group of subzones. Because subzones are often complex, their description and analysis are sometimes better simplified. Thus very fine repetitions of the same basic couplet of subzones, such as thin bright yellow and black, are grouped into CL zones. The CL of the cements in the diagenetic sequence diagram is a schematic representation of the luminescent zones that may be broadly or complexly subzoned (Figure 3B).

4.3. CL sequences

Other studies have shown that the lateral distribution of cement zones may be continuous over several kilometres (Dorobek, 1987; Kaufman *et al.*, 1988; Niemann and Read, 1988) or discontinuous even over short distances (Machel and Burton, 1991). Also individual cement zones may not be isochronous throughout a particular area due to the progressive displacement of ground waters through strata (Frank *et al.*, 1995), or the repetition of the same diagenetic motif at different stratigraphic levels due to the

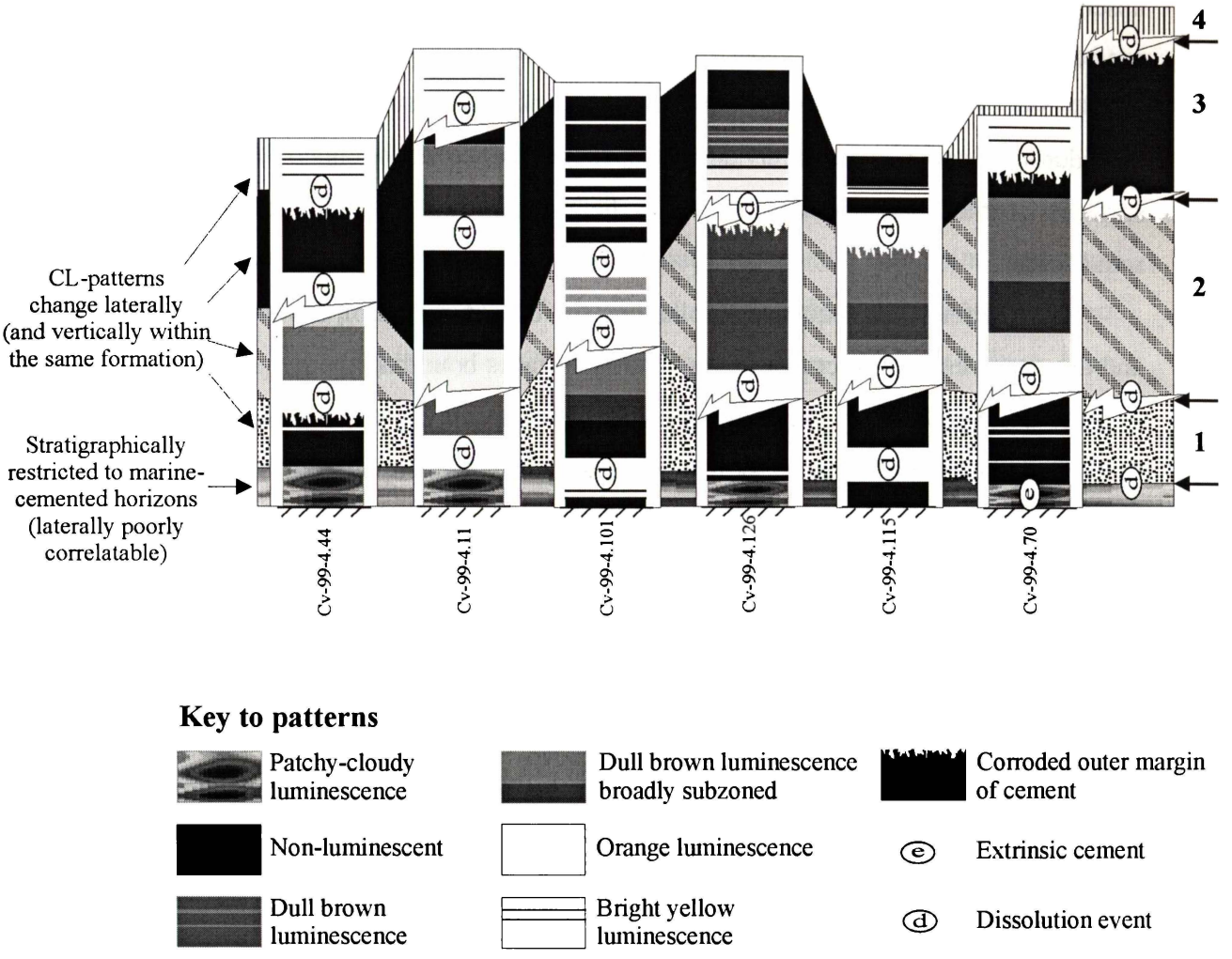

Figure 4- Samples from several localities of Kairakau Limestone exhibit cathodoluminescence (CL) patterns (a combination of successive zones and subzones) and breaks, or diagenetic discontinuities, within the cement growth successions as revealed by dissolution surfaces and corroded outer margin of cements (d and "corrosion" pattern) or fractures (zigzag logo). CL patterns vary laterally in thickness, intensity of luminescence, and internal zonation, whereas diagenetic discontinuities can often be correlated from one sample or one section to another. In order to better grasp the complexities of the diagenetic stratigraphy recorded at different localities, uncorrelatable CL patterns bounded by correlatable diagenetic discontinuities (horizontal black arrows) are used to define summary CL sequences 1 to 4 (at right). Samples: Cv-99-4.44, Te Mata Peak; 4.11, Mt Kahuranaki; 4.101, 126, 115, Maraetotara Plateau; 4.70, Kairakau Beach (see Fig. 1B).

occurrence within the succession of subaerial exposure surfaces and/or to the fluctuation of water tables (Walkden, 1987; Goldstein, 1988). Furthermore, cement zones may be absent in one area because the conditions that favoured their formation elsewhere were not regionally reproduced (Goldstein, 1988). Braithwaite (1993), following Kaufman *et al.* (1988), began to address these inconsistencies by suggesting that instead of considering cement zones individually, packages of zones bounded by discontinuity surfaces at the thin-section scale could help clarify the complexities of diagenetic sequences.

We define "CL sequences" following the determination of CL zonation patterns and the occurrence of fractures or dissolution surfaces bounding them that can be traced laterally and vertically within a sediment pile. Thus, each CL sequence is considered to be a genetically-related succession of cement zones limited by (correlative) physical diagenetic surfaces equivalent to discontinuities, which can be traced laterally and vertically within a sediment pile (Figure 4). In the Te Aute cement successions, dissolution along the outer margin of cement zones corrodes crystal surfaces and results in irregular, gulf-like crystal boundaries and terminations, and truncation of subzones. These dissolution features clearly document breaks during crystal growth that are likely to be related to waters undersaturated with respect to calcite. Again, although dissolution may not be synchronous at various stratigraphic levels, the ingress of aggressive pore fluids and the consequent interruption of crystal growth, even if not a time-correlative event, represents a significant spatial-correlative event.

Fractures are related either to compaction or regional tectonic processes, and as such represent good correlative discontinuities. Other minor discontinuities are also used for the definition of CL sequences, such as renucleation and internal sediments that seal a cement generation and are post-dated by another cementation phase having a different CL signature.

4.4. Diagenetic stratigraphy and sequence stratigraphy

Concepts of sequence stratigraphy, the subdivision of stratal successions into unconformity-bound sedimentary packages, have developed rapidly over the past two decades or so and have found widespread application for relating the origin of sedimentary units to eustatic sea-level changes (Vail, 1987; Posamentier *et al.*, 1988; Van Wagoner *et al.*, 1988). Braithwaite (1993) pointed out that diagenetic relationships and complex diagenetic sequences may be better explained by the application of such

concepts, showing that within the compositional zonation of cements conformable successions could be recognized bounded by breaks or time gaps, such as dissolution surfaces, analogous to disconformities (e.g., Figure 4).

From a sedimentary viewpoint, there have been relatively few attempts to integrate modern advances in recognizing and understanding the paths of carbonate diagenesis to patterns of relative sea-level changes, otherwise the underlying control on the formation of sedimentary sequences and their system tracts (Heckel, 1983; Tucker, 1993; Goldhammer *et al.*, 1994). From a carbonate diagenetic viewpoint, sequence stratigraphy concepts represent a powerful tool for understanding diagenesis in concert with the analysis of sedimentary processes, but again there appear to have been relatively few studies that have attempted to do this (e.g., Simo and Lehmann, 2000). Later we show that the *early* diagenetic patterns in our study sections of Te Aute cool-water carbonates can be intimately related to their depositional facies, and in turn to the stacking patterns of the sediments and their sequence stratigraphic framework.

5. Diagenetic stages: eogenesis-mesogenesis-telogenesis versus pre- and post-compaction terminology

5.1. Early diagenesis – eogenesis

Early diagenesis takes into account those early, near-surface-related processes that witness the evolution of the sedimentation realm. Thus terms like "early diagenesis", "eogenesis", "sea-floor diagenesis", or "syndepositional diagenesis" correspond to all the physicochemical events that occur during deposition of a sediment and following its stabilization, as long as the deposits are not separated from the sedimentation realm and its evolution (i.e., active chemical exchange is maintained between the interstitial pore solutions and the overlying water mass) (Choquette and Pray, 1970).

This definition belies the difficulty of specifying the eogenetic realm. While eogenesis begins at the time of sedimentation, what is its upper subsequent limit? On the one hand, breaks in sedimentation or several depositional events may occur within the sedimentation realm while interstitial solutions remain in communication with the water mass. Thus, sediments might record a continuum of similar diagenetic processes, such as cement crystallization without significant interruption to crystal growth, whereas the stratigraphic record registers a relatively unconformable succession. On the other hand, the communication of the same pile of sediments with the overlying water mass may be repeatedly sealed and unsealed, without burial diagenesis being triggered,

for example through deposition and erosion of impervious sediments, producing repeated "eogenetic records" separated by diagenetically unrecorded periods of time. In both cases, the diagenetic record that pre-dates burial diagenesis belongs to the eogenetic realm over a prolonged period of time that could possibly include changes in sea level or tectonic conditions.

Although it appears that defining early diagenesis is a key problem facing any diagenetic analysis, the term eogenesis appears not to meet the requirement for an integrated approach of sedimentary processes and contemporary diagenetic processes in a sequence stratigraphic framework. Such a requirement may best be fulfilled by attempting to relate the pattern of change of the pre-burial diagenetic record to the stacking pattern of the host sediments (see later).

5.2. Burial diagenesis – mesogenesis

Mesogenetic processes occur in a diagenetic realm independent from marine lithification and extensive meteoric diagenesis. Therefore, carbonate deposits spend most of their geological existence in the burial diagenetic environment and for those that have not been cemented during pre-burial diagenesis, it is the environment where major lithification and porosity loss occur (Bathurst, 1980; Scholle and Halley, 1985). It is inferred that sediments enter the mesogenetic realm when burial processes isolate interstitial solutions from the overlying water mass (Choquette and Pray, 1970). Thus, burial diagenesis may begin at depths of a few metres up to hundreds of metres beneath subaerial surfaces, and a metre or so to tens of metres beneath the sea floor. Again the transition between eogenesis and mesogenesis depends upon the inferred origin of cements and their precipitating fluids.

Burial diagenesis is commonly associated with compaction processes and products, defined as the sum of processes which result in a decrease in volume of the rock (Meyers, 1980; Bathurst, 1995). Compaction processes generally fall into two categories: mechanical and chemical.

5.2.1. Mechanical compaction

Mechanical compaction processes include dewatering, re-orientation or distortion of grains, and grain breakage (e.g., Nicolaides and Wallace, 1997b). Grain rotation and re-orientation can be difficult to identify except from incompatible directions of indurated geopetal fabrics. In the Te Aute limestone samples there is a wide spectrum of grain

breakage features, from minor to total collapse. Mechanical compaction principally affects bryozoan fragments, especially fenestrate forms, elongated grains such as bivalves, echinoderm spines, and sheet-like siliciclastic minerals; echinoderm plates generally show few compaction features.

As well as burial depth, the occurrence and timing of mechanical compaction depend on the sediment texture (Figure 5). Grain breakage is very common in fine- to medium-grained grainstones, but less evident in coarser-textured samples where poorly to moderately abraded thick skeletal clasts either prevented compaction or delayed its effect. Delay effects, also related to near-surface precipitation of marine cements or induration of micrite, may introduce an error in establishing the beginning of syn- or post-compaction diagenesis (Figure 5). Furthermore, in packstones and wackestones, purely mechanical compaction features can be difficult to identify because the bioclasts may not always appear to be in contact with one another. Therefore, compactional effects may be diachronous both laterally and vertically within a given limestone formation in response to lithofacies changes. Nevertheless, in our study the relationships of compaction features to spar cements are systematically investigated to determine the boundary between pre- and post-compaction.

From the above discussion, it appears that wherever mechanical compaction features cross-cut early diagenetic products, a delay or a no-time recording gap might separate the end of early diagenetic processes from the beginning of burial diagenesis. Thus, early diagenesis as defined previously is unlikely to end when burial diagenesis begins as revealed by physical criteria.

5.2.2. Chemical compaction

Pressure-dissolution features observed in the Te Aute limestones include interpenetrating grains with both planar and curved contacts, fitted fabrics, dissolution seams, microstylolites, and rare, if any, stylolites. Fitted fabric includes interpenetration of bioclasts but does not necessarily imply total destruction of interparticle pore space (Nicolaides and Wallace, 1997b). Dissolution seams are smooth, undulating surfaces or zones of dissolution, lacking sutures and fitting around bioclasts, which commonly show evidence of corrosion against the seam.

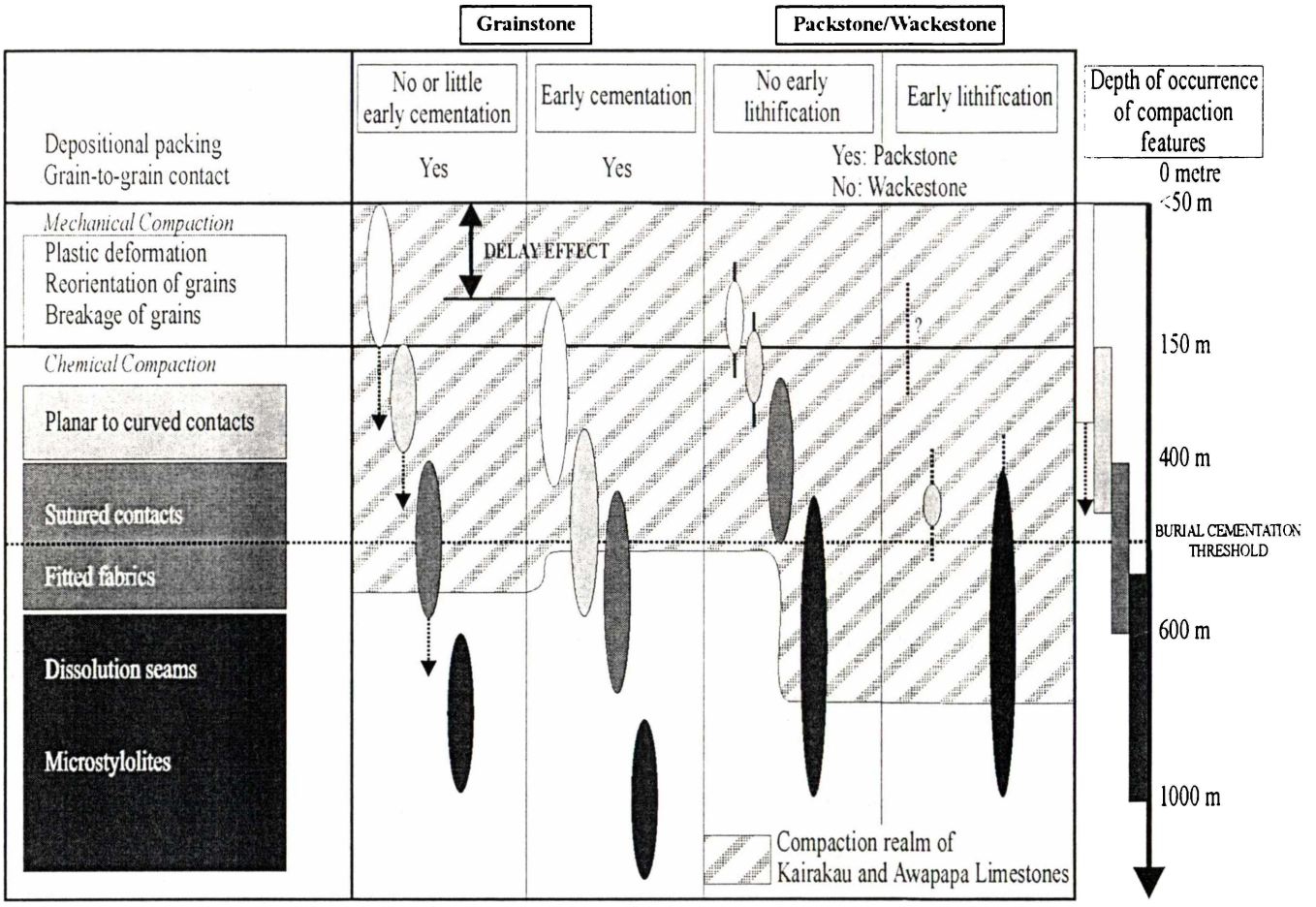

Figure 5- Schematic diagram showing that not only depth of burial, but also sediment texture and degree of early cementation, are significant factors in the timing of occurrence of compaction processes during progressive burial. For example, mechanical compaction occurs deeper in early-cemented limestones than in their non-cemented counterparts (delay effect). On the right side of the diagram is a compilation of the burial depths of occurrence of the various compaction features as reported by others (e.g., Meyers, 1980; Nelson *et al.*, 1988; Nicolaides and Wallace, 1997b).

Stylolites are serrated interfaces having sutured appearance with an amplitude greater than the diameter of the affected grains (Bathurst, 1980, 1995). They can cut indiscriminately through matrix, cement, and allochems. Microstylolites are fine stylolite-like features, discernible only under the microscope.

Factors that might promote chemical compaction processes include the mineralogy of allochems (calcitic rather than aragonite bioclasts could mean little early cementation, but on the other hand little mouldic porosity development), lithology, time of residence in the burial environment, pore-water composition, and especially its level of saturation with respect to $CaCO_3$. Thus, different combinations of these pressure-dissolution promoting factors could result in the development of similar compaction features at different burial depths (Figure 5), and possibly mainly at shallower depths for calcitic limestones than aragonite-rich ones.

5.2.3. Pressure-dissolution and cementation

Our Te Aute petrographic data suggest a possible correlation exists between extensive pressure-dissolution and pronounced cementation, a feature also of other calcitic limestones (Choquette and James, 1987; Nelson *et al.*, 1988; Hood and Nelson, 1996; Dodd and Nelson, 1998). In the southern Australian temperate limestones Nicolaides and Wallace (1997b) reported well developed sutured and fitted fabrics between 430 and 550 m burial depth, the same interval over which most of their core samples lost remaining porosity by calcite cementation, and in agreement with the threshold interval of burial cementation suggested by Nelson *et al.* (1988) for mid-Tertiary non-tropical limestones in New Zealand. In both the Australian and New Zealand limestones commonly as much as 75% of their primary depositional porosities of 40-50% had been lost prior to this main cementation phase, emphasizing that in these deposits compaction, and notably mechanical compaction, was a more important porosity-destroying process than was cementation (Hyden, 1979; Nelson *et al.*, 1988; Nicolaides and Wallace, 1997b).

5.3. Late diagenesis – telogenesis

The passage from the mesogenetic realm to the telogenetic realm is rather difficult to recognize from differences in cement fabrics and mineralogy. The passage is necessarily sought in the last diagenetic stages that are different from the products of burial diagenesis. These often are spar cements that post-date mesogenetic cements and can be

similar to clear spar cements precipitated during pre-compaction diagenesis. Telogenetic products often appear to have formed under the influence of meteoric solutions entering deposits following their uplift and the erosion of overlying younger strata (e.g., Fairbridge, 1967). Telogenetic cements are usually non-luminescent and stain pink with Alizarin Red-S and potassium ferricyanide solution (Dickson, 1965). In the Te Aute limestones, the equivalent of a telogenetic phase usually post-dates a late fracturing stage that cuts all previous diagenetic features and is preceded by the leaching of skeletal grains and the corrosion of crystal boundaries of previous cement generations (Figure 4).

5.4. Pre- and post-compaction diagenesis

Following determination of the mineralogical, textural, and CL attributes of the diagenetic processes and products, and their chronological occurrence within the studied successions, we divide any diagenetic sequence into a two-part history: pre-compaction and (syn- or) post-compaction diagenetic stages (Figure 3). We re-emphasize that pre-compaction diagenesis is not synonymous with early diagenesis in our view (see later).

Mechanical compaction begins soon after deposition, when sediments are still connected to the sedimentation realm, whereas chemical compaction mostly requires several hundred metres of burial (Meyers, 1980; Nelson *et al.*, 1988; Choquette and James, 1990; Tucker, 1993; Nicolaides and Wallace, 1997b). Thus, an important goal is to determine the timing of mechanical compaction events in the context of the overall history of the studied rocks.

Pre-compaction features pre-date any compaction-induced skeletal fractures. They comprise both destructive (mechanical abrasion, bioerosion, and dissolution fabrics) and constructive (internal micritic sediments and precipitates, inclusion-rich acicular to clear scalenohedral and blocky non-ferroan cement, authigenic glauconite, etc.) diagenetic features. Some petrographic properties of these pre-compaction diagenetic features in the Te Aute limestones are summarized in Table 2 and illustrated in Figure 6. Typically, pre-compaction cements comprise turbid acicular rinds and clear blocky to scalenohedral spars. The inclusion-rich cements and associated internal sediments and micrites have property and fabric relationships very similar to the marine cements documented for other Australasian non-tropical limestones by Nelson and James (2000). The staining (pink), fabric (blocky to scalenohedral), and CL signatures (non-luminescent) of the pre-compaction clear spar cements and dissolution of former

aragonitic skeletons are classically considered to be diagnostic of meteoric diagenesis (James and Choquette, 1990). However, such fabrics should be interpreted with caution as we document them (moldic porosity) in condensed lags formed at the sea floor (Maximum Flooding Surface; see later), and fabrics that mimic meteoric diagenesis have recently been documented in the mixing-zone diagenetic environment as well as in the marine burial environment (Melim *et al.*, in press).

The first generation of syn-/post-compaction diagenetic cements in the Te Aute limestones post-dates and infills compaction-induced skeletal fractures and spalled early cement rims. Associated features are dissolution fabrics, recrystallized allochems, and blocky to mosaic spar cements. The second generation of post-compaction clear spar cements post-dates a second fracturing stage related to telogenetic (uplift) processes. These cements are associated with micritic crusts, internal sediments, and turbid pendant cements. Cements that immediately post-date the first fracturing episode stain purple to blue, have brown to orange dull CL, and are broadly to faintly subzoned. They are interpreted as shallow burial cements. Later stage uplift-related cements stain pink, and are non-luminescent with bright yellow subzones. They are interpreted as meteoric in origin. The vertical distribution of syn/post-compaction cements in the Te Aute limestones is briefly mentioned at the end of this paper, but their nature and significance will be developed elsewhere.

5.4.1. Specific diagenesis and pre-compaction diagenesis

The terms "intrinsic diagenesis" (Durlet *et al.*, 1992; Durlet, 1996) and "specific diagenesis" (Caron *et al.*, 1998) have been proposed to help define the early diagenetic processes affecting sedimentary units through time. Their purpose is to trace the evolution of the pore-fluid chemistry responsible for complex diagenetic sequences in packages of sediments while these remain under the influence of the evolving sedimentation realm.

The concept of "intrinsic diagenetic sequence" specifically applies to lithified synsedimentary surfaces that show evidence of sea-floor exposure. Durlet *et al.* (1992) defined intrinsic diagenetic sequences as the sum of diagenetic products bounded by boring and abrasion processes. This concept might not be suitable in the case of most cool-water carbonate units where true hardgrounds are relatively uncommon or absent (James and Bone, 1992, 1994; Nelson and James, 2000).

Table 2- Classification of a range of constructive (CD) to destructive (DD) specific diagenetic suites based on petrographic properties of pre-compaction diagenetic features in Te Aute limestones.

Specific diagenetic suite	Facies	Chronological occurrence of diagenetic processes	Interpretation
CD^1 Constructive	Medium- to coarse-grained Clast-supported	- Skeletal grains are variably abraded - Macroboring of shells occurs occasionally; microboring is present to common, microbores penetrate deeply into bioclasts; micritization poor to moderate - Unilaminar encrusting bryozoans occasionally evident - Authigenic glauconite forms but is scattered, moderately evolved (pale green) - Dissolution of aragonite allochems predating marine cements occurs rarely - Internal sediments commonly pre-date and post-date acicular inclusion-rich isopachous cements (up to 100 µm thick). Internal sediments may be microbioclastic or micritic, are geopetally distributed in interparticle pores, but seldom laminated - *In* situ precipitated peloidal micrite (<50 µm in diameter, spherical, nucleus-free peloids)	Near sea floor, marine phreatic environment Marine waters undersaturated enough to dissolve aragonite near sea floor, marine phreatic environment Microbially induced, marine phreatic environment
M^1 Mixed	Medium- to coarse-grained Clast-supported	Same events as in CD^1, but followed by meteoric diagenesis. The capping surface of the sequence is subaerially exposed; neomorphism of metastable mineralogies is the dominant process - Dissolution of skeletal allochems (moldic voids and collapse of weakened shells), the outer margin of acicular cements may be corroded, and cements may be neomorphosed into scalenohedral crystal rims that exhibit internal ghosts of elongate inclusions - Drusy to mosaic clear spar	Phreatic meteoric environment undersaturated waters with respect to $CaCO_3$ percolate from the capping unconformity
M^2 Mixed	Medium- to coarse-grained Matrix-supported	Same events as in M^1, but clast-supported host of CD^1 becomes matrix-supported; clear spar cements are rare; micritic crust may form (iron stained or not); yellowish bioclast- to microquartz-rich homogenous to laminated micrite infiltrates	Phreatic and possibly vadose meteoric environment
CD^2 Constructive	Coarse- to very coarse-grained Matrix-supported	- Skeletal grains are poorly to moderately abraded - Macroboring is common to abundant; microboring is common - Common, well preserved encrusters such as red algae and uni- and multi-laminar bryozoans - Occasional thin isopachous acicular cements - Syndepositional homogenous micrite; *in situ* precipitated peloidal micrite - Matrix may be burrowed; burrows are filled with another generation of internal sediment - Induration of micrite may occur at this stage (seldom)	Near sea floor, marine environment
M^3 Mixed	Coarse- to very coarse-grained Matrix-supported	Same events as in CD^2, but followed by processes related to meteoric diagenesis - Occasional fracturing and micro-brecciation of host rock; rare mud cracks - Dissolution of skeletal allochems; micritic crust (iron-stained or not); yellowish bioclast- to microquartz-rich homogenous to laminated micrite infiltrates - Blocky to mosaic clear spar	Phreatic and possibly vadose meteoric environment

CD^3 Constructive	Medium-grained Clast- to matrix-supported	- Skeletal grains are moderately to well abraded; moderately preserved red algae and bryozoan encrusters - Homogenous syndepositional micrite pre-dated and post-dated by micritization (densely microbored and subsequently micritized margin of shell fragments is up to 200 μm thick) - Induration of micrite may occur at this stage	Near sea floor, marine phreatic environment
CD^4 Constructive	Medium- to coarse-grained Matrix-supported	- Moderately abraded grains - Moderately preserved encrusters (red algae, bryozoans); rare authigenic glauconite - Micritic crust possible; homogenous syndepositional micrite irregularly distributed in pore space (digitations toward pore centre and menisci) - Neomorphism of skeletal allochems may occur (relicts of microstructures common); precipitation of blocky to mosaic clear spar cement may also occur	Vadose marine (though phreatic marine possible) to vadose meteoric environment
DD^1 Destructive	Fine- to medium-grained Clast- to matrix-supported	- Strongly abraded skeletal grains (very well rounded); intensively microbored (multigeneration) - Evolved authigenic glauconite (deep green, brown) and iron oxides fill most intraparticle pores - Uncommon acicular inclusion-rich cement; dissolution of aragonitic shells may also occur - Common intrinsic homogenous micritic sediment seals the sequence	"Starved" sea floor, prolonged exposure of grains on the sea floor
DD^2 Destructive	Fine- to medium-grained Clast-supported	- Moderately to well abraded grains - Encrusting by uni- and multi-laminar bryozoans possible; common microboring - Common thin acicular isopachous extrinsic cement; rare to common authigenic glauconite	Marine phreatic environment
DD^3 Destructive	Fine- to medium-grained Matrix-supported	- Poorly to moderately abraded grains - Microboring is common; authigenic glauconite is common - Extrinsic thin (<50 μm) acicular cement is possible - Homogenous syndepositional micrite - Burrowing common; burrows are filled with clast-supported internal sediment (microquartz, planktic foraminifers, etc.)	Marine phreatic environment

Figure 6- Photomicrographs illustrating some of the **specific diagenetic suites** defined in this chapter (see also Table 2 and Figures 10, 11).

(A) CD^1 (Constructive diagenesis) - Geopetal internal sediment (white arrow) lies on top of grains, and predates marine acicular inclusion-rich cement (black arrow). Solution of probably aragonite shells and their encrusters (left) is a post-compaction event.

(B) M^1 (Mixed constructive/destructive) - Early marine acicular cement (c) is drowned in coarse detrital internal sediment (is). The latter fills in biomoulds (d) and as such post-dates meteoric-related solution of shells.

(C) CD^2 (Constructive diagenesis) - Macrobores in *Ostrea* shell host micritic internal sediments (white arrow) and inclusion-rich acicular cements (black arrow) from marine phreatic environment.

(D) CD^3 (Constructive when syndepositional micrite has been lithified prior to compaction) - Micritized margin of a barnacle plate (black arrow) from near sea-floor phreatic environment. Note that the walls of micrite-free intraparticle pores (white arrow) are not infested by endolithic borers (algae or fungi?). Spar cement is post-compaction cement.

(E) DD^1 (Destructive diagenesis) - Very well abraded and microbored (black arrow) bioclasts from a starved sea floor. Authigenic glauconite is abundant and fills in most intraparticle pores (foraminiferal chambers, white arrows).

(F) DD^2 (Destructive diagenesis) - Abrasion and microboring are the dominant diagenetic processes. Only a thin post-compaction dogtooth cement grew upon the outer surface of well abraded bioclasts.

(G) CD^4 (Constructive diagenesis) - Micritic cement projecting digitations towards pore centres (probably microbially induced), and bridges between grains (black arrow), from vadose or phreatic marine environment. There is no evidence that the micritic crust post-dates the dissolution or neomorphism of bioclasts.

(H) DD^3 (Destructive diagenesis) - Abraded and microbored bioclasts (white arrow) are drowned in a siliciclastic-rich matrix. No early cement formation.

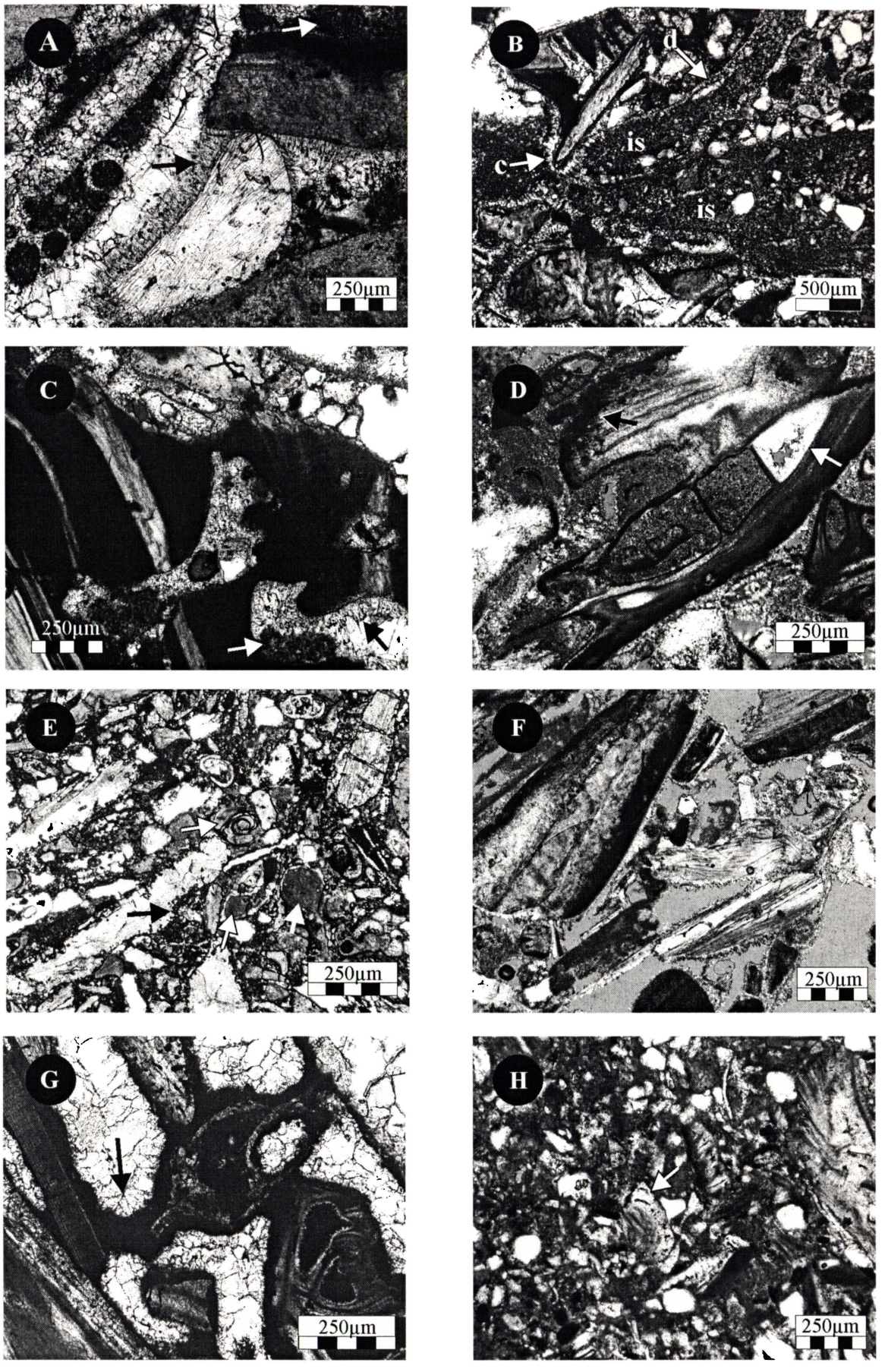
A
250µm
B
d
is
c
is
500µm
C
250µm
D
250µm
E
250µm
F
250µm
G
250µm
H
250µm

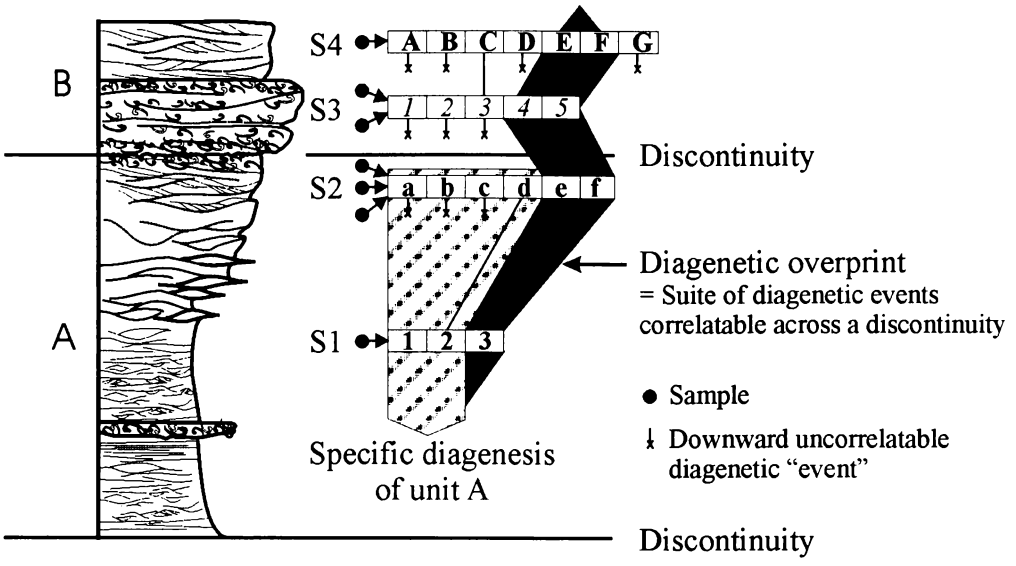

Figure 7- The specific diagenesis of an unconformity-bounded sedimentary unit derives from a comparison of diagenetic suites (microfacies and compositional zonation of cements, named after their position in the sequence) in samples collected from either side of its capping discontinuity. Here the diagenetic events that belong to overlying unit B (dark grey pattern), but that have been superimposed upon the diagenetic events within unit A, can be recognized, and the specific diagenesis isolated for the underlying unit A (diagonal hatch pattern). The shared diagenetic events amount to diagenetic overprint and do not relate to the true "early diagenesis", or the "specific diagenesis" of this study, following deposition of unit A only. Vertically within the same discontinuity-bounded unit there are variations in the characteristics of the specific diagenetic record. This observation has an important implication for the sequence stratigraphic interpretation of specific diagenetic suites (see text and Figures 8-10). Here, the specific diagenetic suite S1 (diagenetic features 1+2) is different from S2 (a to d), even though both share one diagenetic event (2 and d are the same).

In the studied Te Aute succession, sediments that underwent early marine cementation do not exhibit the attributes of consolidated sediments exposed at the sea floor, such as lithified capping surfaces where grains and cements are truncated, bored, or encrusted (James and Choquette, 1990). Instead, marine-cemented horizons without differentiated upper or lower boundaries are recognized often just above, and more rarely beneath, unconformities. Furthermore, marine-cemented levels are generally separated from one another by marine cement-free intervals of sediments, the next horizon being encountered through an unconformity surface. Thus, although marine-cemented horizons in the Te Aute limestones represent significant depositional events and a change in the depositional regime, they do not necessarily represent unconformity surfaces upon which intrinsic diagenetic sequences have been built, as envisaged by Durlet *et al.* (1992).

Instead, the concept of "specific diagenesis" is employed here that is based upon a comparison of the diagenetic attributes of sediments on either side of sedimentary discontinuity surfaces (Caron *et al.*, 1998). Specific diagenesis (Figure 7) only includes diagenetic features contemporary with sedimentation and with early post-sedimentation times, and excludes all the diagenetic events shared with any overlying sedimentary deposit, through a discontinuity surface, since they are related to subsequent and different depositional stages (see next section). Following Bates and Jackson (1987) and Clari *et al.* (1995), we regard a discontinuity surface as one which separates younger from older sedimentary rocks where evidence based on geometric, sedimentological, diagenetic, or biostratigraphic criteria can be used to infer a break in sedimentation of whatever length. Surfaces indicative of low or no deposition can be used to subdivide formations into depositional sequences in which specific diagenetic records are suspected. During episodes of starved deposition, a sedimentary unit beneath its capping surface may record a wide spectrum of diagenetic processes related to the evolution of the pore-fluid chemistry. Such a diagenetic time record follows the sedimentation-dominated time record and provides information that cannot normally be obtained from the conventional lithological description of strata.

In the Te Aute limestone successions, the recognition of discontinuity surfaces has been based on the following kinds of evidence: (1) Angular disconformities with erosional truncation of strata, so long as such angular relationships are not related to synsedimentary processes such as reactivation surfaces or sliding of unconsolidated sediments; (2) A sharp change in depositional conditions across the surface as revealed

by the direct superposition of contrasting facies or of contrasting skeletal assemblages (Figures 2B, 2C); (3) A contrast between compactional features of superposed strata due to either the underlying or overlying deposit including an early cementation phase (e.g., Figure 5); and (4) Marine-cemented limestone horizons overlying limestones lacking marine cements, typically across a sharp and burrowed surface or an erosional surface.

5.4.2. Specific diagenesis and diagenetic overprint

Diagenetic processes that take place during deposition of a sedimentary unit may also affect the underlying unit(s). This phenomenon is referred to as "diagenetic overprint" (Figure 7). The nature of diagenetic overprint principally depends upon the chemistry and the vertical and lateral distribution of the formative fluids. For example, meteoric waters that penetrate a sedimentary deposit from its capping surface may percolate deeply through several depositional units and be responsible for cementation or dissolution processes overprinting former diagenetic histories (see Figure 10). Marine diagenetic products are less likely to be involved in overprinting because the diagenetic potential of marine waters diminishes quickly below the sea floor (Longman, 1980; Aissaoui, 1988; James and Bone, 1992). Nevertheless, marine diagenetic overprints might occur in thin unconformity-bound packages of sediments, the diagenetic potential of marine waters remaining high enough through successive unconformities to favour cement formation.

Following the preceding discussion, we now define the "specific diagenesis" of a sedimentary unit bounded by discontinuity surfaces as corresponding to the suite of physicochemical events prior to any superposed diagenetic overprint associated with the sediments overlying the upper discontinuity surface. Inevitably the recognition of any specific diagenetic history is based on a comparison of diagenetic suites on either side of a discontinuity surface. Therefore, the specific diagenesis cannot be determined wherever the sedimentary unit from which the diagenetic overprint was derived has been eroded. In this case, the so-called specific diagenesis is in fact a "diagenetic polysuite" (Figure 8), defined as successive diagenetic suites including the "real" specific diagenesis and diagenetic events contemporaneous with the deposition of some now missing sedimentary unit or units. The erosion event(s) responsible for the missing sediments can be difficult to discern, and recognition mainly depends upon the characteristics of the surface that bounds the successive sediment packages (Figure 8).

By contrast with Choquette and Pray (1970), we restrict the definition of early

diagenesis to the specific diagenetic history, which is the time interval during which sediments remain under the influence of surficial processes that also drive the packaging of sediments and the generation of sedimentary surfaces bounding them. Thus, in the present study, pre-compaction diagenesis is not considered to be equivalent to early diagenesis, but to a combination of specific diagenetic histories. In other words, several "specific diagenetic suites" serve to build up the overall diagenetic pre-compaction history of a carbonate succession. Furthermore, specific diagenesis is related to depositional sequences limited by discontinuity surfaces. Such successions or packaging might be related to a hierarchical driving mechanism associated with tectonism and/or changes in relative sea level, so that specific diagenesis potentially has a direct application to sequence stratigraphy.

6. Application of diagenetic stratigraphy concepts to Te Aute limestones

Relatively few diagenetic fabrics are specific to a single diagenetic environment (Heckel, 1983; Longman, 1980). Most can form under a variety of physicochemical conditions, and/or may have suffered from the influence of an evolving pore-fluid chemistry that potentially modified their original texture, structure, and mineralogy. Consequently, only a combination of the criteria noted in Tables 1 and 2 are considered adequate to determine possible diagenetic settings of not only a particular fabric, but also successions of genetically-related fabrics, enabling construction of a sequence of diagenetic features bounded by diagenetic discontinuities. The application of these criteria has enabled the positive distinction of diagenetic patterns related to pre-compaction and post-compaction stages for the Te Aute limestones (Figures 9 to 11), the former of which is, in particular, illustrated here.

6.1. Patterns of pre-compaction diagenesis

6.1.1. Specific diagenetic patterns in metre-scale sequences

Detailed stratigraphic logs through the various sections of Kairakau and Awapapa Limestone sheets (Figure 1; columns in Appendix 1) reveal the systematic occurrence of packages of strata, or sequences, bounded by significant discontinuities, most being

Figure 8- The diagenetic history of the sedimentary unit A in cases 1 and 2 is a diagenetic polysuite that is different from its specific diagenesis but includes it and diagenetic suites of younger strata. Case 1: Poorly cemented sediment (typical of cool-water carbonates) – The capping surface of unit A, a burrowed surface, is a non-deposition-related surface. The time of no deposition may be recorded in the form of successive diagenetic events whose suite defines the specific diagenesis of unit A. The diagenetic history of overlying unit B may be partly or totally superimposed upon the previous specific diagenesis of unit A, producing a diagenetic overprint (*overprint 1*). After complete erosion of unit B and subsequent deposition of unit C, the comparison of the diagenetic suites on either side of the discontinuity may reveal an *overprint 2*, but not overprint 1. In this case the recognition of overprint 1 is dependent on the local preservation of unit B or the occurrence of lithoclasts of unit B within unit C. Case 2: Well-lithified sediment (typical of tropical carbonates) – Early lithification of unit A may favour the colonization of its capping surface by either encrusting organisms or boring organisms. Here the specific diagenesis of unit A is defined as the suite of diagenetic features that are truncated by borings. Overprints are then relatively easy to discern as they are post-dated by the first generation of borings. Diagenetic features contemporary with the deposition/lithification of unit B may also be truncated by a new generation of borings or by an abrasion/erosion surface prior to the deposition of unit C (see also Durlet et al., 1992). In both cases 1 and 2 the specific diagenetic suites witness the evolution of the sedimentation realm and therefore pre-date the conventional mesogenetic history revealed by other burial-related products, which nevertheless could constitute an *overprint 3* or more.

RECOGNITION OF DIAGENETIC POLYSUITES

CASE 1: POORLY CEMENTED SEDIMENT

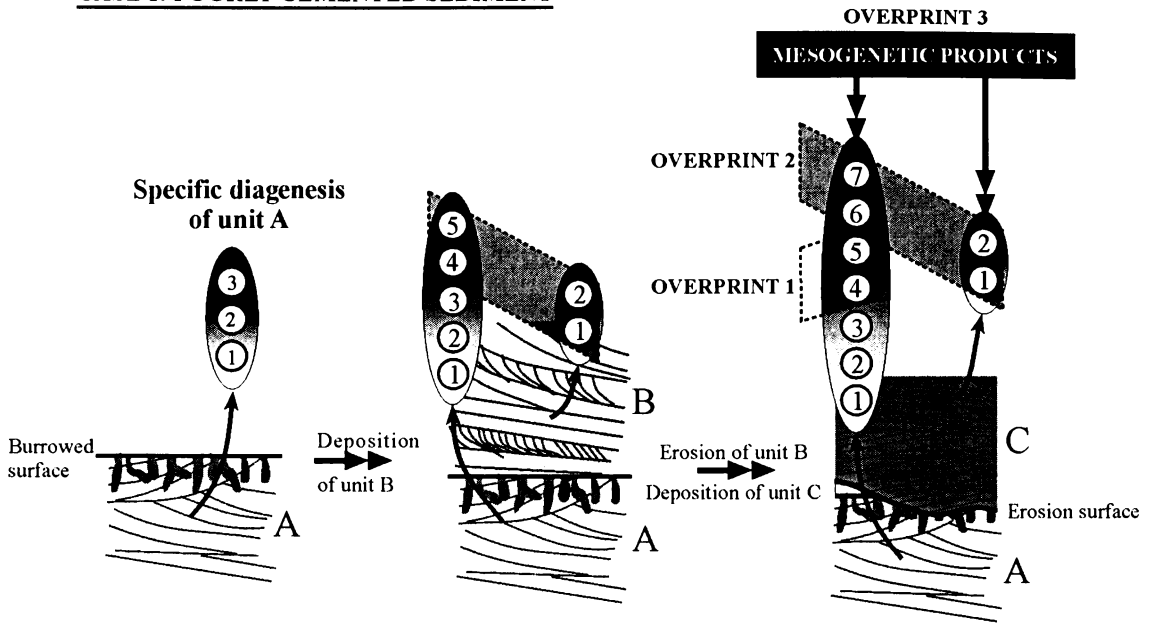

CASE 2: WELL-LITHIFIED SEDIMENT

(See Durlet et al. 1992)

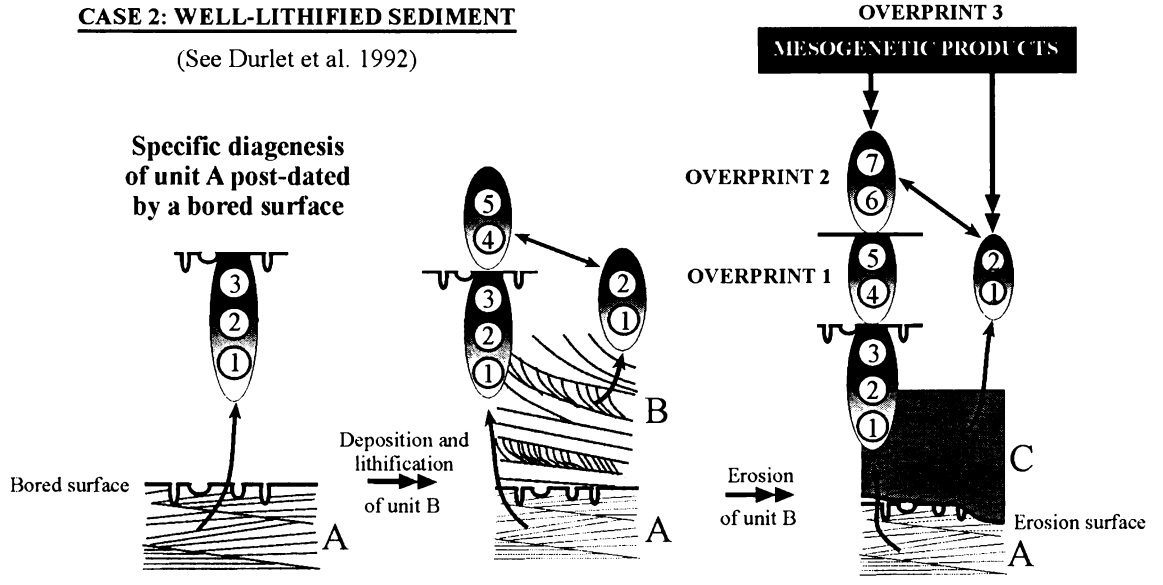

sharp and erosion surfaces (Figures 2B, 2C, 9). Both the textural and skeletal characteristics of the depositional facies within the discontinuity-bounded sediment packages mainly indicate a deepening-upward trend, and in places a deepening- then shallowing-upward trend (Figures 9, 10). In most cases, the surfaces bounding the sequences lack evidence of subaerial exposure and are sharp or erosional, often associated with strongly *Ophiomorpha*-burrowed sediment below (Figure 2B), and overlain by deepening-upward deposits, enriched at their base in reworked material. We interpret such surfaces as transgressive surfaces of erosion (TSE) that are coincident with high-frequency sequence boundaries (cf. Kidwell, 1991). We infer that various sequence boundary indicators may have been removed by the erosive ravinement accompanying the landward transfer of transgressive lags on otherwise poorly cemented sediments (Boreen and James, 1995; Naish and Kamp, 1997).

Typically (e.g., sequences F, G, and H in Figures 9, 10), basal fossiliferous and pebbly rudstones (facies B1a) interpreted as shallow-water, high energy, tide-influenced deposits, correspond to the lower member of transgressive systems tracts (TST) (the transgressive lags of Kidwell 1991). These pass upwards (deepening-upward trend) through interbedded skeletal grainstones and packstones (facies M1 and M2) into increasingly mixed siliciclastic-carbonate and muddy siliciclastic lithofacies (facies M3), interpreted as deeper water deposits (upper TST and high stand systems tracts - HST) that accumulated near storm-wave base, bounded above by the next TSE (e.g., sequences B1, B2, F, G, H, J and K in Figure 9). The upward change in depositional setting is usually accompanied by changing skeletal associations, typically from predominantly bimol to barnamol assemblages (Hayton *et al.*, 1995). Some sequences comprise in their upper part shallowing-upwards deposits (e.g., sequences A?, C, D, E, and I in Figure 9). In these cases, facies M3 usually exhibits a gradational upper contact, above which accumulated medium- to thick-bedded, planar to trough cross-stratified, medium- to coarse-grained skeletal- and barnacle-rich sediments interpreted as shallow-water prograding sandbars equivalent to regressive systems tract (RST) deposits. This sequence is terminated by the superjacent discontinuity (TSE), rarely coincident with a surface of subaerial exposure (e.g., sequences C and E in Figure 9). The TST-HST(-RST) stacking pattern of the Te Aute sequences is similar in style, but not in facies, to that described by Naish and Kamp (1997) for the shelly siliciclastic cyclothems comprising the thick Plio-Pleistocene succession in the nearby South Wanganui Basin

(Figure 1A).

One of the main observations of our study is that the attributes of the specific diagenesis of a sequence change vertically, and appear to be strongly correlated to its depositional facies. This provides a good sequence stratigraphic framework to assess the timing of diagenetic processes, and both their relation and contribution to the building-up of systems tracts. We have defined 10 type-specific diagenetic suites distributed on a scale from mainly constructive to mainly destructive diagenesis (Table 2; Figure 6). Considering the vertical distribution of the specific diagenetic suites, there exists a definite pattern of occurrence within the sequences (Figures 10, 11). Data compiled from many Te Aute limestone units indicate that marine constructive diagenesis (CD^1, CD^2, CD^3), characterized by turbid cements and interstratified internal sediments (Figure 6A), occurs most commonly close to the bounding-discontinuities, within the lower level of the sequences interpreted as TST deposits and in the upper level of RST deposits. These sediments equate to the highest energy facies, and include intertidal bored pebble horizons, oyster shell banks, and prominently cross-bedded coarse skeletal sediments. In contrast, such constructive diagenetic phases are usually rare or absent from the upper part of the TST, the HST, and the lower part of the RST, which are instead characterized by destructive marine diagenesis (DD^2, DD^3). Inferred maximum flooding surfaces (Mfs) are typified by starved sedimentation (authigenic glauconite-rich thin lags) and associated destructive diagenetic features, such as abrasion and multigeneration bioerosion (DD^1; Figures 6E, 11). The upper part of the RST is characterized by marine cementation overprinted by both constructive and destructive meteoric diagenesis (M^1, M^2, M^3), involving dissolution of former aragonite and even calcitic grains, and little spar cementation, when the top surface has been subaerially exposed (Table 2; Figures 6B, 11). The Te Aute sequences are mostly upward-deepening. Therefore, the vertical trend recorded by the specific diagenesis is one from mainly constructive in the lower TST to mainly destructive in the upper TST and HST (Figure 11).

Previous workers have documented constructive and destructive marine diagenetic features in temperate shallow-water carbonates, and commented on their possible sequence stratigraphic significance. Boreen and James (1995) found that

Figure 9- Stratigraphic log for the Awapapa Limestone at Te Mata Peak (Figures 1B, 2A) subdivided by disconformities, interpreted as transgressive surfaces of erosion (TSE) coincident with high-frequency sequence boundaries (hsb), into disconformity-bounded sedimentary packages A to K (e.g., Figure 2). The depositional trend of sedimentary sequences is either a deepening-upwards trend (for B1, B2, F, G, H, J, and K), or a deepening- then shallowing-upwards trend (for A?, C, D, E, and I). Note that within deepening-upwards units specific diagenesis is increasingly destructive towards the top of sequences, whereas within the deepening- then shallowing-upwards units specific diagenesis is increasingly constructive towards the top. SB = sequence boundary.

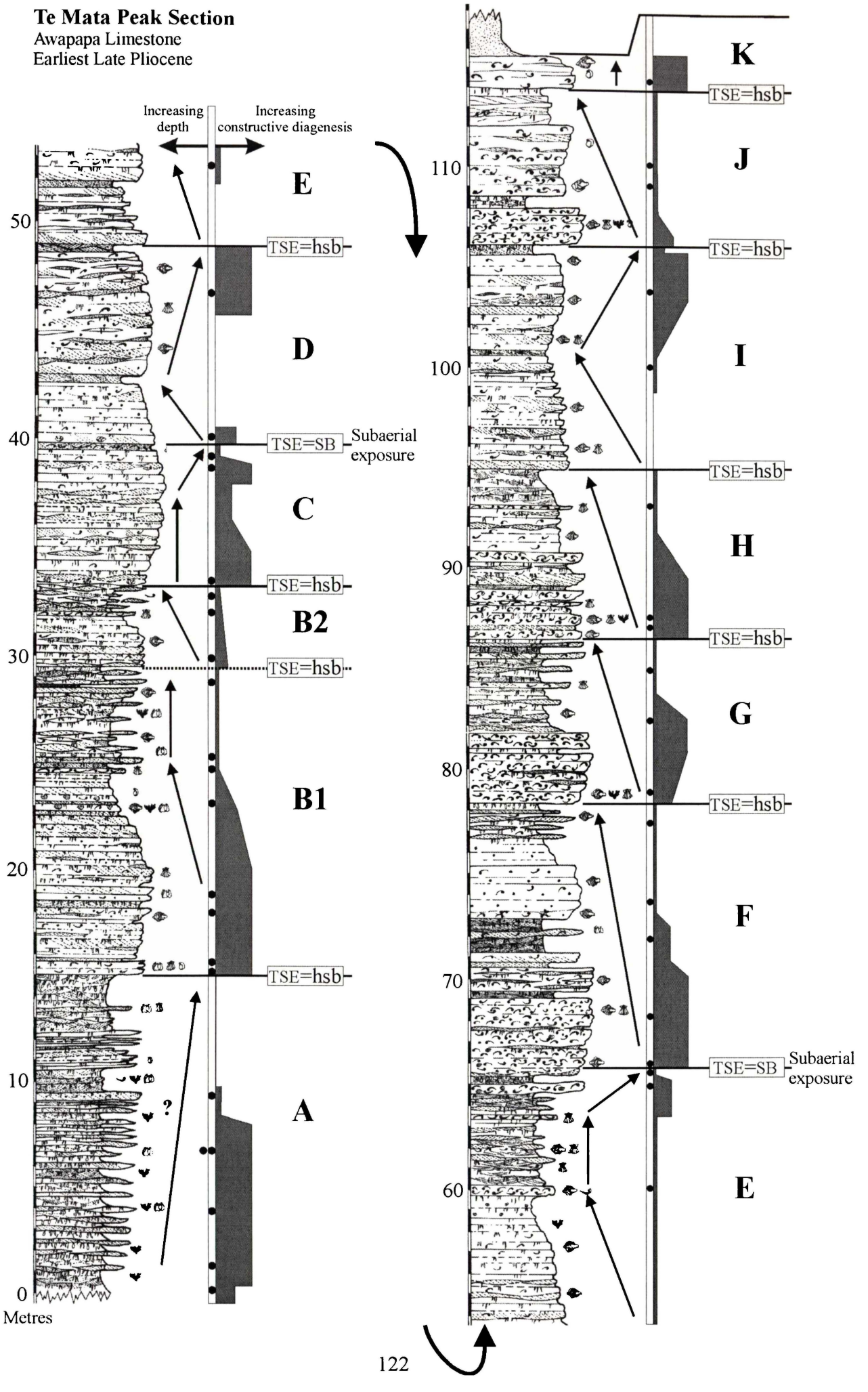
Te Mata Peak Section
Awapapa Limestone
Earliest Late Pliocene
Increasing depth
Increasing constructive diagenesis
E
D
C
B2
B1
A
K
J
I
H
G
F
E
TSE=hsb
TSE=SB
Subaerial exposure
?
0
10
20
30
40
50
60
70
80
90
100
110
Metres

marine hardgrounds mainly characterized by constructive diagenesis (micritic and turbid cements, internal sediments) were closely associated with sequence bounding surfaces such as flooding surfaces (our TSE) during periods of condensed sedimentation, whereas constructive diagenetic features were uncommon in late TST and HST. James (1997) pointed out that early diagenesis of temperate carbonates was characterized typically by abrasion and bioerosion. However he suggested that minor early cementation could occur on starved shelf sectors in the zone of wave abrasion during transgressions and regressions, and in the bounding hardgrounds of metre-scale cycles that developed as sequence boundaries during third-order highstands. Nelson and James (2000) reported that horizons dominated by constructive diagenesis (cementation, encrustation, internal micritic sediments) tended to recur in relatively high-energy environmental conditions and at specific stratigraphic positions, commonly below and above unconformities. They proposed that marine cementation developed principally during periods of stratigraphic condensation and lowered sea level. Tucker (1993) suggested that as sequences display vertical changes in facies, these are likely to be accompanied by systematic changes in the type and degree of diagenesis. He commented on the close relationship between movements of groundwater systems during sea-level changes and cementation, and suggested that marine cementation may be favoured at the sea floor within the lower part of the TST as a result of sea water being pumped through the shelf during the landward shift of marine groundwater zones. By contrast, sediments in the upper part of the TST and the HST become "drowned" in the stagnant marine zone (Longman, 1980) and marine cementation would likely be minimal. The Te Aute temperate carbonate successions generally conform to the foregoing observations and provide an opportunity to develop the application of carbonate diagenesis suggested in this paper to the sequence stratigraphy of cool-water carbonates more widely.

6.1.2. Diagenetic overprints cross sequence-bounding unconformities

Comparison of diagenetic suites on either side of discontinuities bounding the depositional sequences reveals that commonly pre-compaction meteoric diagenetic fabrics are not restricted to a single depositional unit, but can be superimposed upon the specific diagenesis of the latter (Figure 10). Throughout Awapapa Limestone successions, clear spar cement exhibits a first CL sequence (non-luminescent to dull orange) that post-dates a conspicuous dissolution stage (leaching of aragonite grains)

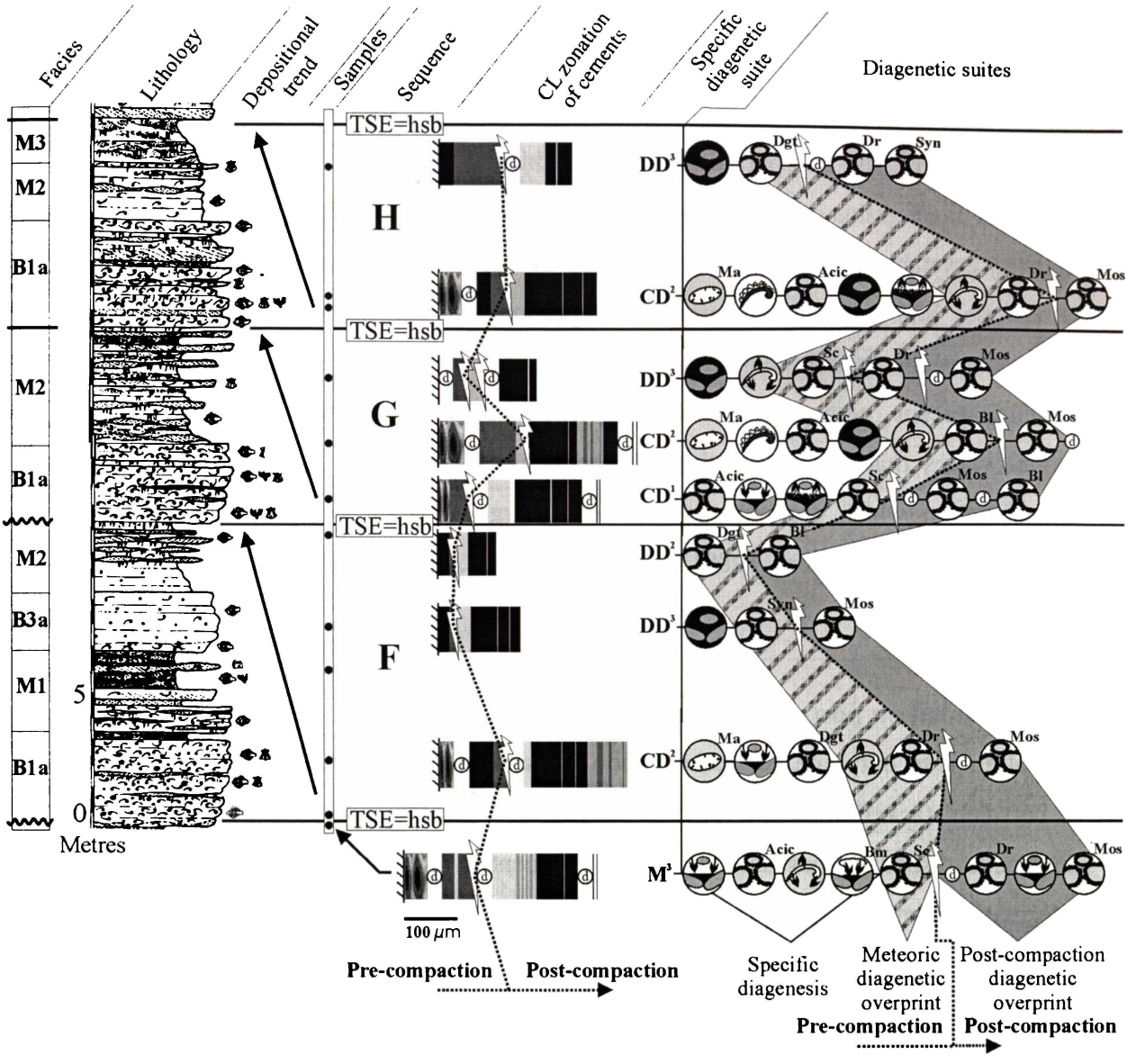

Figure 10- Succession of sedimentological properties (left side) typical of most disconformity-bounded limestone units within the Awapapa Limestone, exemplified here by units F, G, and H at the Te Mata Peak section (see Figure 9), and their interpretation as deepening-upwards sequences, in relation to a selection of corresponding, petrographically-determined diagenetic sequence diagrams (see Figure 3 for key to logotypes). Despite the complexity of diagenetic features the diagenetic suites are readily divisible into pre- and post-compaction stages based on the first occurrence of compaction-induced fracturing of skeletal material. Once recognized, the pre-compaction diagenetic records are compared on either side of the discontinuities and subsequently the specific diagenesis of each sequence is capable of being isolated (see Figure 7). Vertical changes in the specific diagenetic record define up to ten specific diagenetic suites, labelled constructive or destructive (Table 2, Figure 6), that can be correlated to the depositional pattern of the sequences (e.g., Figure 11). Note that meteoric diagenesis-related features (dissolution and cementation by spar cements = grey hash pattern) are associated with a diagenetic overprint probably due to the infiltration of fresh waters from an unconformity higher in the succession. Lithofacies codes: B1a, Fossiliferous rudstone packed with oysters and pectens, massive bedding to trough cross-bedding; M1, Alternating skeletal-rich grainstone and packstone, trough cross-bedding, minor hummocky cross-stratification; B3a, Bioclastic packstone; M2, Interbedded grainstone and terrigenous packstone, planar and sigmoidal cross-laminations; M3: Interbedded terrigenous packstone and calcareous sandstone, planar laminations and ripple structures. TSE = transgressive surface of erosion; hsb = high-frequency sequence boundary; SB = sequence boundary.

but pre-dates mechanical compaction-induced skeletal fracturing (Figure 10). This spar cement occurs in interparticle pores as bladed palisadic fringes and syntaxial overgrowth on grains or earlier marine cements, and in intraparticle pores as fine equant to drusy crystals. It is shared by all the depositional packages constructing the Awapapa Limestone, and as such represents a superimposed diagenetic suite, or diagenetic overprint, to the specific diagenetic suites of each disconformity-bounded package. The non-luminescent cement is likely to have formed from near-surface, oxidizing groundwaters that percolated through the entire succession from a capping regional unconformity, which probably acted as a recharge area (cf. Grover and Read, 1983; Dorobek, 1987; Goldstein, 1988; Niemann and Read, 1988; Horbury and Adams, 1989; Algeo *et al.*, 1992).

6.2. Comment on post-compaction diagenesis

The attempt to correlate post-compaction CL sequences within the same limestone unit or between stacked units at a regional scale is greatly enhanced by the traceability of the diagenetic discontinuities defining the CL sequences (e.g., Figure 10). Combined with information from trace element and stable isotope geochemistry (Table 1), this procedure provides a powerful tool to assess the chemical evolution of the fluids that moved through the sediments over time. Despite the already described highly variable pre-compaction cementation patterns within the Kairakau and Awapapa Limestones, both formations show generally similar post-compaction diagenetic features, typically involving a chronological suite of marine-modified burial ferroan calcite cements followed across a diagenetic discontinuity surface (fracture and dissolution) by uplift-related non-ferroan calcite meteoric cements. This comparability of post-compaction diagenetic events could be due to: (1) conditions that prevailed for formation of the post-compaction cements were repeated at different stratigraphic levels and at different times; or (2) precipitation of the majority of these mesogenetic/telogenetic cements from subsurface fluids was delayed until after deposition of the Late Pliocene Awapapa Limestone (Figure 1). More detailed discussion of the later diagenetic evolution of the Te Aute limestones is beyond the scope of this paper, and will be developed elsewhere.

7. Conclusions

We develop some petrographic concepts applicable for describing and interpreting the diagenetic evolution of cool-water limestones. The method involves (a) the

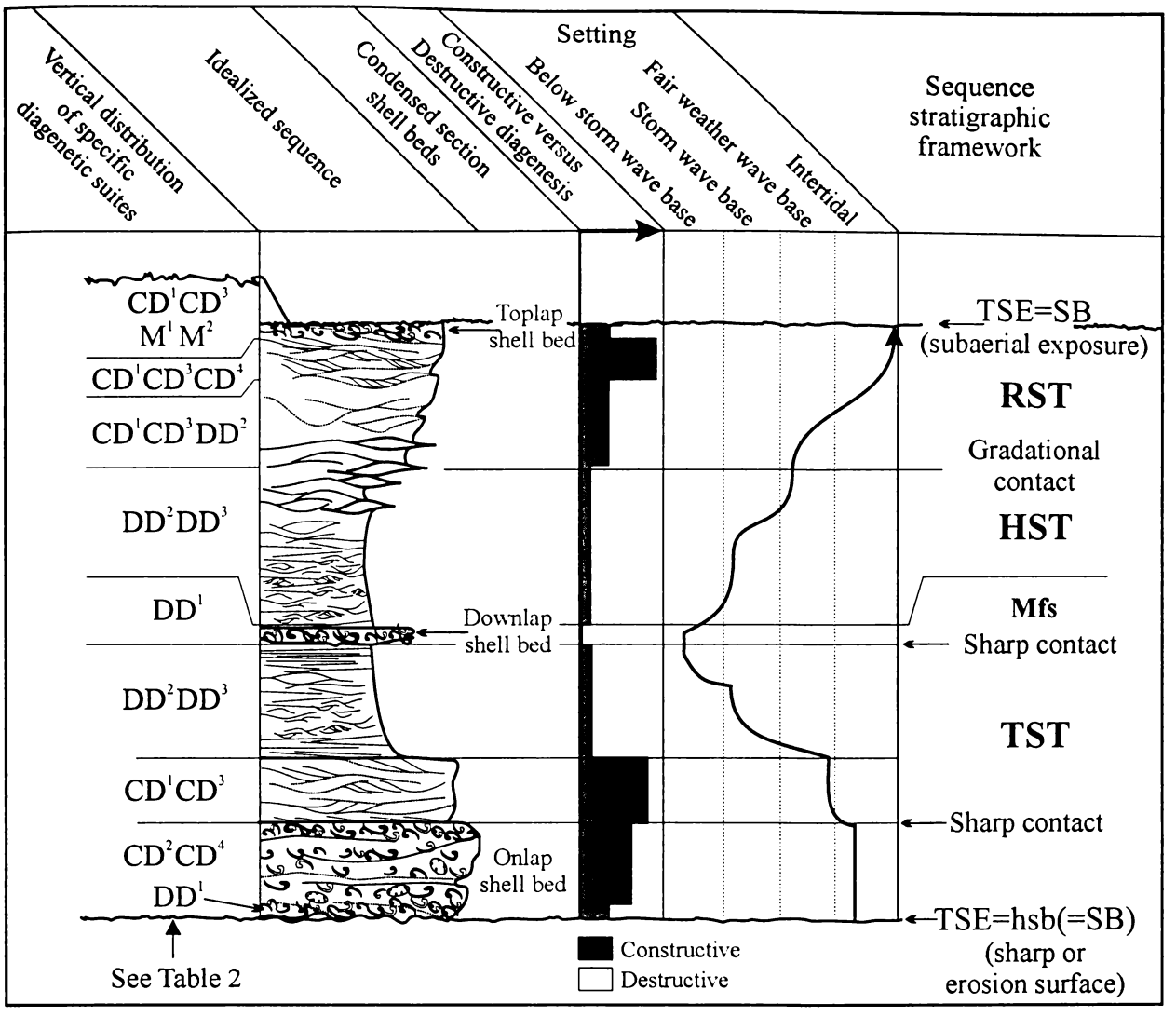

Figure 11- Model for the pattern of carbonate diagenesis in the Te Aute limestone sequences. The idealized sequence integrates the sedimentological, diagenetic, and inferred sequence stratigraphic attributes for the sequences recognized in 47 stratigraphic sections of Plio-Pleistocene Te Aute limestone (logged in Appendix 1). All sequences are bounded by TSEs (= hsb = high-frequency sequence boundary; locally a major sequence boundary = SB). The lower TSE lies at the base of the depositional sequence marked by condensed fossiliferous to pebbly transgressive lags, and the upper TSE is overlain by the basal transgressive lag of the next sequence. From the basal TST, sequences exhibit a deepening-upwards depositional trend (shallow-water transgressive lag to near storm-wave base mixed siliciclastic-carbonate sediments), and are characterized by increasingly destructive diagenesis ($CD^{1,2,3}$ to $DD^{1,2,3}$; see Table 2, Figure 6) towards the superjacent Mfs (maximum flooding surface). From this surface, the depositional trend is one of shoaling-upwards, and is bounded above by the TSE lying either in the RST, or is superimposed on the sequence boundary (SB). Specific diagenesis becomes more "constructive" ($CD^{1,3,4}$) compared to the underlying HST. Most Te Aute sequences fall into these types of sequences. The upper RST comprises thick marine cements, and as such is dominated by constructive diagenesis ($CD^{1,3,4}$). In some examples, the upper capping surface of the RST is a sequence boundary (SB) that shows discrete evidence of subaerial exposure (dissolution and little if any meteoric cementation). In these cases, due to meteoric influence, destructive diagenetic features dominate the specific diagenetic record beneath the SB ($M^{1,2}$).

chronological recording of *all* diagenetic features within rock units to provide a high-resolution diagenetic (not simply cement) stratigraphy, (b) noting the vertical and lateral distribution of these features, and (c) grouping them into discontinuity-bounded (by dissolution surfaces, fractures, renucleation events) suites at a thin-section scale. A critical discontinuity event to decipher is the first conspicuous evidence of compaction-induced skeletal fracturing, taken as the boundary between pre-compaction and post-compaction diagenetic stages. A comparison of *only* pre-compaction diagenetic suites in samples from either side of unconformities within outcrop sections enables isolation of the specific diagenesis for each of the unconformity-bounded depositional units, which in our case equate to high-frequency sequences. The specific diagenesis of a genetically-related succession of facies bounded by discontinuities is that which is free from any diagenetic overprinting associated with the diagenesis of overlying younger units, and as such is likely to record the evolution of the sedimentation realm forming the sequences during and between sedimentation breaks. In this manner the specific diagenetic attributes for a succession of depositional facies between consecutive discontinuities (sequence) may be interpreted within a sequence stratigraphic framework.

We illustrate the application of the approach to some cool-water limestones of Pliocene age from eastern North Island, New Zealand. Here several specific diagenetic signatures have been defined whose vertical distributions are related to the facies stacking within the stratal sequences (Figure 11), which are mainly deepening-upwards and sometimes deepening- then shallowing-upwards units bounded by transgressive surfaces of erosion coincident with high-frequency sequence boundaries (rarely subaerially exposed). In the deepening-upwards sequences constructive diagenesis characterizes their basal portions and destructive diagenesis their upper parts. Where shallowing-upwards caps are superposed their upper parts again include constructive diagenetic features, locally replaced by destructive meteoric diagenesis giving evidence of subaerial exposure at the top of some sequences. We propose that in the cool-water Te Aute limestones the constructive diagenetic suites are associated with the lower part of transgressive systems tracts (TST), and occur towards the top of regressive systems tracts (RST), whereas destructive diagenesis characterizes the upper part of the TST, the high stand systems tracts (HST), the lower part of the RST, and occasionally beneath the bounding surface of the RST in association with subaerial exposure (Figure 11).

References

Aissaoui, D.M., (1988) Magnesian calcite cements and their diagenesis: dissolution and dolomitization, Mururoa Atoll. *Sedimentology*, **35**, p. 821-841.

Alexandersson, E.T., (1978) Destructive diagenesis of carbonate sediments in the eastern Skagerrak, North Sea. *Geology*, **6**, p. 324-327.

Algeo, T.J., Wilkinson, B.H. and Lohman, K.C., (1992) Meteoric-burial diagenesis of Middle Pennsylvanian limestones in the Orogrande basin, New Mexico: Water/rock interactions and basin geothermics. *Journal of Sedimentary Petrology*, **62**, p. 652-670.

Amieux, P., (1981) La Cathodoluminescence dans les Roches Sédimentaires - Applications Sédimentologiques et Diagénétiques. Unpublished PhD Thesis, Université Claude Bernard Lyon1, Lyon, 212 p.

Amieux, P., Bernier, P., Dalongeville, R. and De Medwecki, V., (1989) Cathodolumiescence of carbonate-cemented Holocene beachrock from the Togo coastline (West Africa): An approach to early diagenesis. *Sedimentary Geology*, **65**, p. 261-272.

Bates, R.L. and Jackson, J.A., (1987) Glossary of Geology: American Geological Institute, Alexandria, 788 p.

Bathurst, R.G.C., (1975) Carbonate Sediments and their Diagenesis: Elsevier, Amsterdam, 658 p.

Bathurst, R.G.C., (1980) Deep crustal diagenesis in limestones. *Revista del Instituto de Investigaciones Geologicas Diputacion Provincial, Universidad de Barcelona*, **34**, p. 89-100.

Bathurst, R.G.C., (1995) Burial diagenesis of limestones under simple overburden. Stylolites, cementation and feedback. *Bulletin de la Société Géologique de France*, **166**, p. 181-192.

Beu, A.G., (1995) *Pliocene Limestones and Their Scallops*. Monograph 10, Institute of Geological and Nuclear Sciences Limited Monograph 10, Lower Hutt, New Zealand, 243 p.

Boreen, T.D. and James, N.P., (1995) Stratigraphic sedimentology of Tertiary cool-water limestones, SE Australia. *Journal of Sedimentary Research*, **B65**, p. 142-159.

Braithwaite, C.J.R., (1993) Cement sequence stratigraphy in carbonates: *Journal of Sedimentary Petrology*, **63**, p. 295-303.

Caron, V., Bernier, P., Keraudren, B. and Dalongeville, R., (1998) Les séquences diagénétiques des calcarénites littorales du Pléistocène récent de Crète septentrionale: une aide à la résolution de problèmes de correlation: *Bulletin de la Société Géologique de France*, **169**, p. 415-424.

Choquette, P.W. and James, N.P., (1987) Diagenesis 12. Diagenesis in limestones, 3. The deep burial environment: *Geoscience Canada*, v. 14, p. 3-35.

Choquette, P.W. and James, N.P., (1990) Limestones - The meteoric diagenetic environment. In: *Diagenesis* Ed. by McIlreath, I.A. and Morrow, D.W.), *Geoscience Canada Reprint*, v. 4, p. 35-73.

Choquette, P.W. and Pray, L.C., (1970) Geologic nomenclature and classification of porosity in sedimentary carbonates. *American Association of American Geologists Bulletin*, **54**, p. 207-250.

Clari, P.A., De La Pierre, F.D. and Martire, L., (1995) Discontinuities in carbonate successions: Identification, interpretation and classification of some Italian examples. *Sedimentary Geology*, **100**, p. 97-122.

Dickson, J.A.D., (1965) A modified staining technique for carbonates in thin-section. *Nature*, **205**, p. 587.

Dodd, J.R. and Nelson, C.S., (1998) Diagenetic comparisons between non-tropical Cenozoic limestones of New Zealand and tropical Mississippian limestones from Indiana, USA: Is the non-tropical model better than the tropical model? *Sedimentary Geology*, **121**, p. 1-21.

Dorobek, S.L., (1987) Petrography, geochemistry and origin of burial diagenetic facies, Siluro-Devonian Helderberg Group (Carbonate rocks), Central Appalachians. *American Association of Petroleum Geologists Bulletin*, **71**, p. 492-514.

Durlet, C., (1996) Apport de la Diagenèse des Discontinuités à l'Interprétation Paléoenvironnementale et Séquentielle d'une Plate-forme Carbonatée - Exemple des Calcaires Bajociens du Seuil de Bourgogne. Unpublished PhD Thesis, Université de Bourgogne, Dijon, 444 p.

Durlet, C., Loreau, J.P. and Pascal, A., (1992) Signature diagénétique des discontinuités et nouvelle représentation de la diagenèse. *Compte rendu de l'Académie des Sciences Paris*, **314**, p. 1507-1514.

Fairbridge, R.W., (1967) Phases of diagenesis and authigenesis. In: *Diagenesis in Sediments* (Ed. by Larsen, G. and Chilingar, G.V.), Elsevier, Amsterdam, p. 18-89.

Farrow, G.E. and Fyfe, J.A., (1988) Bioerosion and carbonate mud production on high-latitude shelves. *Sedimentary Geology*, **60**, p. 281-297.

Field, B. D., Uruski, C. I., *et al.* (1997) *Cretaceous-Cenozoic Geology and Petroleum Systems of the East Coast Region, New Zealand.* Monograph 19, Institute of Geological and Nuclear Sciences Limited, Lower Hutt, New Zealand, 301 pp.

Frank, T.D., Lohmann, K.C. and Meyers, W.J., (1995) Chronostratigraphic significance of cathodoluminescence zoning in syntaxial cement: Mississippian Lake Valley Formation, New Mexico. *Sedimentary Geology*, **105**, p. 29-50.

Goldhammer, R.K., Oswald, E.J. and Dunn, P.A., (1994) High-frequency, glacio-eustatic cyclicity in the Middle Pennsylvanian of the Paradox Basin: an evaluation of Milankovitch forcing. *International Association of Sedimentologists Special Publication*, **19**, p. 243-283.

Goldstein, R.H., (1988) Cement stratigraphy of Pennsylvanian Holder Formation, Sacramento Mountains, New Mexico. *American Association of Petroleum Geologists Bulletin*, **72**, p. 425-438.

Grover Jr, G. and Read, J.F., (1983) Paleoaquifer and deep burial related cements defined by regional cathodoluminescent patterns, Middle Ordovician carbonates, Virginia. *American Association of Petroleum Geologists Bulletin*, **67**, p. 1275-1303.

Harmsen, F.J., (1985) Lithostratigraphy of Pliocene strata, Central and Southern Hawke's Bay, New Zealand. *New Zealand Journal of Geology and Geophysics*, **28**, p. 413-433.

Hayton, S., Nelson, C.S. and Hood, S.D., (1995) A skeletal assemblage classification system for non-tropical carbonate deposits based on New Zealand Cenozoic limestones. *Sedimentary Geology,* **100**, p. 123-141.

Heckel, P.H., (1983) Diagenetic model for carbonate rocks in Midcontinent Pennsylvanian eustatic cyclothems. *Journal of Sedimentary Petrology*, **53**, p. 733-759.

Hood, S.D. and Nelson, C.S., (1996) Cementation scenarios for New Zealand non-tropical limestones. *New Zealand Journal of Geology and Geophysics*, **39**, p. 109-122.

Horbury, A.D. and Adams, A.E., (1989) Meteoric phreatic diagenesis in cyclic Late Dinantian carbonates,

northwest England. *Sedimentary Geology*, **65**, p. 319-344.

Hornibrook, N.deB., (1992) New Zealand paleoclimates: a review based on the distribution of some shallow water and terrestrial biota. In: *Pacific – Neogene Environment, Evolution, and Events* (Ed. by Tsuchi, R. and Ingle, Jr, J.C.), University of Tokyo, Tokyo, p. 83-106.

Hyden, F.M., (1979) Mid-Tertiary Temperate Shelf Bioclastic Limestones, Southland, New Zealand. Unpublished PhD Thesis, University of Otago, Dunedin, 487 p.

James, N.P., (1997) The cool-water carbonate depositional realm. In: *Cool-Water Carbonates* (Ed. by James, N.P. and Clarke, J.A.D), *SEPM Special Publ*ication, **56**, p. 1-20.

James, N.P. and Bone, Y., (1992) Synsedimentary cemented calcarenite layers in Oligo-Miocene cool water shelf limestones, Eucla Platform, Southern Australia. *Journal of Sedimentary Petrology*, **62**, p. 860-872.

James, N.P. and Bone, Y., (1994) Paleoecology of cool-water, subtidal cycles in mid-Cenozoic limestones, Eucla Platform, southern Australia. *Palaios*, **9**, p. 457-477.

James, N.P. and Choquette, P.W., (1990) Limestones - The sea floor diagenetic environment. In: *Diagenesis* (Ed. by McIlreath, I.A. and Morrow, D.W.), *Geoscience Canada Reprint*, v. 4, p. 13-34.

Kamp, P.J.J., (1986) The mid-Cenozoic Challenger Rift-System of western New Zealand and its implications for the age of Alpine fault inception. *Geological Society of America Bulletin*, **97**, p. 255-281.

Kamp, P.J.J., Harmsen, F.J., Nelson, C.S. and Boyle, S.F., (1988) Barnacle-dominated limestone with giant cross-beds in a non-tropical, tide swept, Pliocene forearc seaway, Hawke's Bay, New Zealand. *Sedimentary Geology*, **60**, p. 173-195.

Kamp, P.J.J. and Nelson, C.S., (1987) Tectonic and sea-level controls on non-tropical limestones in New Zealand. *Geology*, **15**, p. 610-613.

Kamp, P.J.J. and Nelson, C.S., 1988, Nature and occurrence of modern and Neogene active margin limestones in New Zealand. *New Zealand Journal of Geology and Geophysics*, **31**, p. 1-20.

Kaufman, J., Cander, H.S., Daniels, L.D. and Meyers, W.J., (1988) Calcite cement stratigraphy and cementation history of the Burlington-Keokuk Formation (Mississippian), Illinois and Missouri. *Journal of Sedimentary Petrology*, **58**, p. 312-326.

Kelsey, H.M., Erdman, C.F. and Cashman, S.M., (1993) Geology of Southern Hawkes Bay from the Maraetotara Plateau and Waipawa westward to the Wakara Range and the Ohara depression: Institute of Geological & Nuclear Sciences Report 93/2, Lower Hutt, New Zealand, p. 1-17.

Kidwell, S.M., (1991) Condensed deposits in siliciclastic sequences: expected and observed features. In: *Cycles and Events in Stratigraphy* (Ed. by Einsele, G., Ricken, W. and Seilacher, A.), Springer-Verlag, Heidelberg, p. 682-695.

Longman, M.K., (1980) Carbonate diagenetic textures from nearsurface diagenetic environments. *American Association of Petroleum Geologists Bulletin*, **64**, p. 461-487.

Loreau, J.P. and Cros, P., (1988) Limestone diagenesis and dolomitization of Tithonian carbonates at ODP site 639 (Atlantic Ocean West of Spain): *Proceedings of the Ocean Drilling Program Scientific Results*, **103**, p. 105-143.

Machel, H.G. and Burton, E.A., (1991) Factors governing cathodoluminescence in calcite and dolomite,

and their implications for studies of carbonate diagenesis. In: Luminescence Microscopy: Quantitative and Qualitative Aspects (Ed. by Barker, C.E. and Kopp, O.C.), *SEPM Short Course*, **25**, p. 37-57.

Melim, L.A., Westphal, H., Swart, P.K., Eberli, G.P. and Munnecke, A., in press, Questioning carbonate diagenetic paradigms: evidence from the Neogene of the Bahamas. *Marine Geology*.

Meyers, W.J., (1974) Carbonate cement stratigraphy of the Lake Valley Formation (Mississippian), Sacramento Mountains, New Mexico. *Journal of Sedimentary Petrology*, **44**, p. 837-861.

Meyers, W.J., (1978) Carbonate cements: Their regional distribution and interpretation in Mississippian limestones of Southwestern New Mexico. *Sedimentology*, **25**, p. 371-399.

Meyers, W.J., (1980) Compaction in Mississippian skeletal limestones, Southern New Mexico. *Journal of Sedimentary Petrology*, **50**, p. 457-474.

Meyers, W.J., (1989) Trace element and isotope geochemistry of zoned calcite cements, Lake Valley Formation (Mississippian, New Mexico): Insights from water-rock interaction modeling. *Sedimentary Geology*, **65**, p. 355-370.

Naish, T.R. and Kamp, P.J.J., (1997) High-resolution sequence stratigraphy of 6th order (41 ka) Plio-Pleistocene cyclothems, Wanganui Basin, New Zealand: A case for the regressive systems tract. *Geological Society of America Bulletin*, **109**, p. 978-999.

Nelson, C.S., (1988) An introductory perspective on non-tropical shelf carbonates. *Sedimentary Geology*, **60**, p. 3-12.

Nelson, C.S., Harris, G.J. and Young, H.R., (1988) Burial-dominated cementation in non-tropical carbonates of the Oligocene Te Kuiti Group, New Zealand. *Sedimentary Geology*, **60**, p. 233-250.

Nelson, C.S. and James, N.P., (2000) Marine cements in mid-Tertiary cool-water shelf limestones of New Zealand and southern Australia. *Sedimentology*, **47**, p. 609-629.

Nelson, C.S., Winefield, P.R., Hood, S.D., Caron, V., Pallentin, A. and Kamp, P.J.J., in review, Pliocene Te Aute limestones, New Zealand: expanding concepts for cool-water shelf carbonates. *New Zealand Journal of Geology and Geophysics*.

Nicolaides, S. and Wallace, M.W., (1997a) Submarine cementation and subaerial exposure in Oligo-Miocene temperate carbonates, Torquay Basin, Australia. *Journal of Sedimentary Research*, **67**, p. 397-410.

Nicolaides, S. and Wallace, M.W., (1997b) Pressure-dissolution and cementation in an Oligocene-Miocene non-tropical limestone (Clifton Formation), Otway basin, Australia. In: *Cool-Water Carbonates* (Ed. by James, N.P. and Clarke, J.A.D.), *SEPM Special Publication*, **56**, p. 127-140.

Niemann, J.C. and Read, J.F., (1988) Regional cementation from unconformity-recharged aquifer and burial fluids, Mississippian Neuman Limestone, Kentucky. *Journal of Sedimentary Petrology*, **58**, p. 688-705.

Posamentier, H.W., Jervey, M.T. and Vail, P.R., (1988) Eustatic controls on clastic deposition, part 1: Conceptual framework. In: *Sea Level Changes: An Integrated Approach* (Ed. by Wilgus, C.K., Hastings, B.S., Kendall, C.G.St.C., Posamentier, H.W., Ross, H.W. and Van Wagoner, J.C.), *SEPM Special Publication*, **42**, p. 125-154.

Scholle, P.A. and Halley, R.B., (1985) Burial diagenesis - out of sight, out of mind! In: *Carbonate*

Cements (Ed. by Schneidermann, N. and Harris, P.M.), *SEPM Special Publication*, **36**, p. 309-334.

Schroeder, J.H., (1984) The petrogenetogram of corals. Spatial variations in diagenetic sequences. *Palaeontographica Americana*, **54**, p. 261-271.

Schroeder, J.H., (1988) Spatial variations in the porosity development of carbonate sediments and rocks. *Facies*, **18**, p. 181-204.

Schroeder, J.H. and Purser, B.H., (1986) Reef Diagenesis, Springer-Verlag, New York, 455 p.

Simo, J.A. and Lehmann, P.J., (2000) Diagenetic history of Pipe Creek Jr. Reef, Silurian, North-Central Indiana, U.S.A. *Journal of Sedimentary Research*, **70**, p. 937-951.

Spörli, K.B. and Pettinga, J.R., (1980) Mount Kahuranaki, Hawke's Bay, New Zealand, a klippe emplaced by gravity sliding from the crest of the nearby Elsthorpe anticline: *Journal of the Royal Society of New Zealand*, **10**, p. 287-307.

Tucker, M.E., (1993) Carbonate diagenesis and sequence stratigraphy, *in* Wright, V.P., ed., Sedimentology Review, Volume 1, Blackwell Scientific, Oxford, p. 51-72.

Tucker, M.E. and Wright, V.P., (1990) Carbonate Sedimentology, Blackwell, Oxford, 482 p.

Vail, P., (1987) Seismic stratigraphy interpretation using sequence stratigraphy, Part 1: Seismic interpretation procedure. In: *Atlas of Seismic Stratigraphy* (Ed. by Bally, A.W.), *AAPG Special Publication*, **27**, p. 1-10.

Van Wagoner, J.C., Posamentier, H.W., Mitchum, R.M., Vail, P.R., Sarg, J.F., Loutit, T.S. and Hardenbol, J., (1988) An overview of sequence stratigraphy and key definitions. In: *Sea Level Changes: An Integrated Approach* (Ed. by Wilgus, C.K., Hastings, B.S., Kendall, C.G.St.C., Posamentier, H.W., Ross, H.W. and Van Wagoner, J.C.), *SEPM Special Publication*, **42**, p. 39-45.

Walkden, G.M., (1987) Sedimentary and diagenetic styles in Late Dinantian carbonates of Britain. In: *European Dinantian Environments* (Ed. by Miller, J., Adams, A.E. and Wright, V.P.), Wiley, New York, p. 131-155.

Walkden, G.M. and Berry, J.P., (1984) Syntaxial overgrowths in muddy crinoidal limestones: cathodoluminescence sheds new light on an old problem. *Sedimentology*, **31**, p. 251-267.

Walker, R.G. and James, N.P., (1992) Facies Models - Response to Sea Level Change, Geological Association of Canada, Ontario, 409 p.

Chapter 3

DIAGENESIS OF COOL-WATER PLIO-PLEISTOCENE LIMESTONES IN SOUTHERN HAWKE'S BAY, NEW ZEALAND

Abstract 133
1. Introduction 135
2. Analytical techniques 138
3. Times and environments of carbonate diagenesis 145
4. Diagenetic products and processes 148
    4.1. Early fine acicular precipitate 148
    4.2. Early inclusion-rich cement 149
    4.3. Clear spar cements 168
    4.4. Internal sediments 189
    4.5. Cryptocrystalline meniscus-type cements, irregular micrite bindings, and micrite envelopes 195
    4.6. Dissolution 196
    4.7. Bioactivity: biological alteration and encrustation 208
    4.8. Mechanical abrasion 212
    4.9. Non-carbonate cement: Glauconite and iron-oxides 213
    4.10. Compaction features 214
    4.11. Diagenetic sequence diagrams 219
5. Carbonate diagenesis and relative sea-level changes 219
    5.1. Sequence stratigraphic framework 221
    5.2. Depositional setting for the Te Aute carbonates (Opoitian to early Nukumaruan) 223
    5.3. Carbonate diagenesis on a high-frequency sequence scale 224
6. Conclusions 239
References 244

Key Sections: 1, 2.5.2, 3, 4.2, 4.3.5, 4.3.6, 4.6, 5, 6
Key Figures: 1, 6, 7, 17, 22, 23, 24, 25, 26, 27, 28
Key Tables: 1, 2

Chapter 3

DIAGENESIS OF COOL-WATER PLIO-PLEISTOCENE LIMESTONES IN SOUTHERN HAWKE'S BAY, NEW ZEALAND

ABSTRACT: This chapter is mainly concerned with the description of the wide variety of diagenetic products and fabrics recognized in the cool-water Plio-Pleistocene Te Aute limestone successions, and their interpretation in terms of diagenetic environment.

Among the pre-compaction diagenetic suites, marine diagenesis is mainly characterized by destructive processes (abrasion, bioerosion, dissolution), and occasionally by constructive features (rare sea-floor cementation, micritization, encrustation), while meteoric diagenesis produces little to moderate cementation (PrC = pre-compaction clear spar non-ferroan cement) and various neomorphic processes. In the post-compaction diagenetic suites, mesogenetic (burial) ferroan cements (PoFC = post-compaction ferroan cement) are subordinate to telogenetic (post-burial) non-ferroan cements (YnfC = youngest non-ferroan cement), and dissolution, partly associated with chemical compaction in the burial realm, and neomorphism are common during both diagenetic phases. There is a wide spectrum of compactional features due to the wide age range and variety of textures of the studied formations, which have been differentially buried before being differentially uplifted and exposed.

Constructive diagenetic products occur in all studied formations, but their attributes vary over time. Inclusion-rich fibrous cements constitute the main sea-floor constructive product in older, dominantly calcitic limestones (Kairakau, Awapapa), whereas micrite bindings, micrite cements, and micritization dominate in younger limestones with higher aragonitic contents (Mason Ridge Formation).

Neomorphic processes are also more diverse in younger limestones than in older ones. Alteration processes vary from total dissolution of aragonitic allochems (e.g., especially within Kairakau, Awapapa, Rotookiwa, Te Onepu Limestones, and Titiokura Formation) to retention of original mineralogy and microstructures, via little preservation of microstructures and loss of primary mineralogy (e.g., within Mason Ridge Formation, Matapiro and Scinde Island Limestones, and other Nukumaruan units). The water/rock

ratio and the nature of circulating pore fluids are considered to be critical factors to the degree of neomorphism and type of resulting neomorphic fabrics. Provided that the starting composition of interparticle fluids is undersaturated with respect to aragonite, the variety of aragonite shell alteration/preservation in relation to water/rock ratios, or water-rock interaction, can be summarized as follows: (1) high water/rock ratio systems (i.e., low water-rock interaction) are characterized by mouldic and intraskeletal porosity; (2) intermediate water/rock ratio systems are characterized by the partial retention of both the microstructures and the geochemical signature of the precursor aragonite; and (3) low water/rock ratio systems (i.e., high water-rock interaction) result in neomorphic fabrics that comprise pristine aragonite crystallites with retention of primary microstructures adjacent to, or entombed within, neomorphic calcite crystals.

A model is proposed to integrate the patterns of **pre-compaction** diagenesis into a scheme of sea-level changes. During sea-level rise (TST), landward transfer of the shoreline leads to active marine pore-fluid circulation promoting marine constructive diagenesis. The diagenetic suite recognized in Te Aute TST carbonate sediments comprises precipitation of inclusion-rich fibrous cements, the emplacement of geopetal sediments, *in situ* peloids, encrustation by uni- and multilaminar bryozoans, and bioerosion. At the inferred maximum flooding surface (Mfs), carbonate sedimentation appears to have been at its lowest. These conditions are reflected in thin condensed, locally shelly, lags enriched in both detrital and authigenic glauconite, and suffering intensive destructive diagenetic processes (i.e., abrasion and multigeneration microboring).

Once sea level begins to fall (HST), and if its rate equals or exceeds the rate of subsidence, then the rate of generation of new accommodation slows, and skeletal fragments start to accumulate and the main feature of sedimentation is aggradation. The depositional setting remains below the influence of strong storm and wave currents. Consequently, pre-compaction carbonate diagenesis continues to be predominantly destructive, including abrasion and bioerosion. As sea level continues to fall (RST), sediments come under the influence of high-energy wave and tidal currents, and they accumulate in the form of basinward-prograding sand waves and sand dunes. Under such conditions, siliciclastic sediments are by-passed into deeper environments. RST carbonate deposits that accumulated in the shallow-marine environment where the rates of accumulation are low, and where sea-water pumping through the sediments is

vigorous, are characterized by constructive diagenetic processes. Thick rinds of turbid fibrous cements line interparticle pores, micrite sediments percolate from the water-sediment interface, macroboring is common while microboring is moderate, and encrustation by uni- and multilaminar bryozoans is present. Dissolution of aragonite allochems may also occur in this setting.

The continuing loss of accommodation space, due to decreasing bathymetry associated with high rates of carbonate production and falling sea level, eventually causes sea level to reach the sea-bed elevation, and the depositional realm is exposed to subaerial processes. Diagenetic features attributable to meteoric influence comprise dissolution of aragonitic skeletal fragments, the subsequent collapse of insoluble constituents of shells and low-Mg calcite (LMC) micrite envelopes that form geopetal debris, the percolation of dark (in some examples iron-stained) microquartz-rich internal sediments, and minor blocky spar cementation. The transformation of intermediate- or high-Mg calcite inclusion-rich fibrous cements into LMC is likely active in this environment, although it may have started earlier in the marine phreatic realm.

1. Introduction

Most recent syntheses concerning advances in recognizing and understanding the products and processes of carbonate diagenetic environments have been based on modern and ancient tropical deposits (Longman, 1980; James and Choquette 1990a; Tucker and Wright, 1990; Moore, 1989, 2001). Nevertheless, over the past two decades, several researchers have recorded the widespread distribution of non-tropical or temperate-latitude carbonate sediments, especially on modern temperate shelves off New Zealand (e.g., Nelson *et al.*, 1988a), southern Australia (e.g., Nelson, 1978; Rao, 1981; James *et al.*, 1992, 2001), western Canada (e.g., Nelson and Bornhold, 1983; Carey *et al.*, 1995), and Europe (e.g., Henrich and Freiwald, 1995; Light and Wilson, 1998). Moreover, it has been emphasized that analogous carbonate facies are common in the Phanerozoic rock record (Rao, 1988; Lavoie and Bourque, 1993; Boreen and James, 1995; Hood and Nelson, 1996; Betzler *et al.*, 1997, 2000; James and Bone, 2000).

The diagenetic pathways of a few Cenozoic temperate limestone formations have recently been documented by Nelson *et al.* (1988c), Hood and Nelson (1996), and Nelson and James (2000) for New Zealand deposits, and by James and Bone (1989,

1992) and Nicolaides and Wallace (1997) for southern Australia examples. These rocks differ from tropical limestones in being mineralogically dominated by calcitic components. The greater abundance of aragonite in tropical sediments compared to their non-tropical counterparts has been shown to result in contrasting diagenetic behaviours, and principally in differences in the timing of interparticle cementation (Tucker and Wright, 1990; Hood and Nelson, 1996; Dodd and Nelson, 1998). Typically, in aragonite-rich sediments, carbonate cementation occurs in the early stages of their diagenetic history either on or just beneath the sea floor, or in the meteoric and shallow-burial environments (Bathurst, 1975; Longman, 1980). In contrast, aragonite-poor sediments may not be significantly cemented prior to being buried, and may subsequently suffer from both intensive mechanical and chemical compaction (Nelson *et al.*, 1988c; Nicolaides and Wallace, 1997). Thus, Nelson *et al.* (1988c), for the Oligocene Te Kuiti Group limestones in New Zealand, and James and Bone (1989) and Nicolaides and Wallace (1997) for Oligo-Miocene temperate limestones in southern Australia, envisaged cementation to originate principally from dissolved calcium carbonate released through chemical compaction processes that were actively triggered once a critical burial depth of ca. 500 m was reached.

Sea-floor diagenesis in cool-water carbonates is regarded as predominantly destructive (Alexandersson, 1978; Smith and Nelson, 1994), whereas carbonates formed in tropical settings are characterized by typically constructive sea-bed diagenetic processes (Nelson, 1988a; Nelson *et al.*, 1988b; James, 1997). Destructive diagenesis comprises all mechanical and chemical processes that reduce the potential for skeletal grain preservation, such as abrasion, bioerosion, and dissolution prior to burial history, and burial-related grain breakage and pressure-solution. These processes are greatly enhanced in non-tropical settings by the paucity of early cementation either at the sea floor or in the meteoric environment. Moreover, the Pliocene Te Aute carbonates of this study (Figure 1), like other Cenozoic limestones in New Zealand (Hood and Nelson, 1996) are primarily composed of solution-resistant low- to intermediate-Mg calcitic skeletal fragments that are unlikely to readily release calcium carbonate for early cementation. The higher CO_2 content of temperate waters, and consequently their lesser degree of carbonate saturation (James and Choquette, 1990a), also militates against

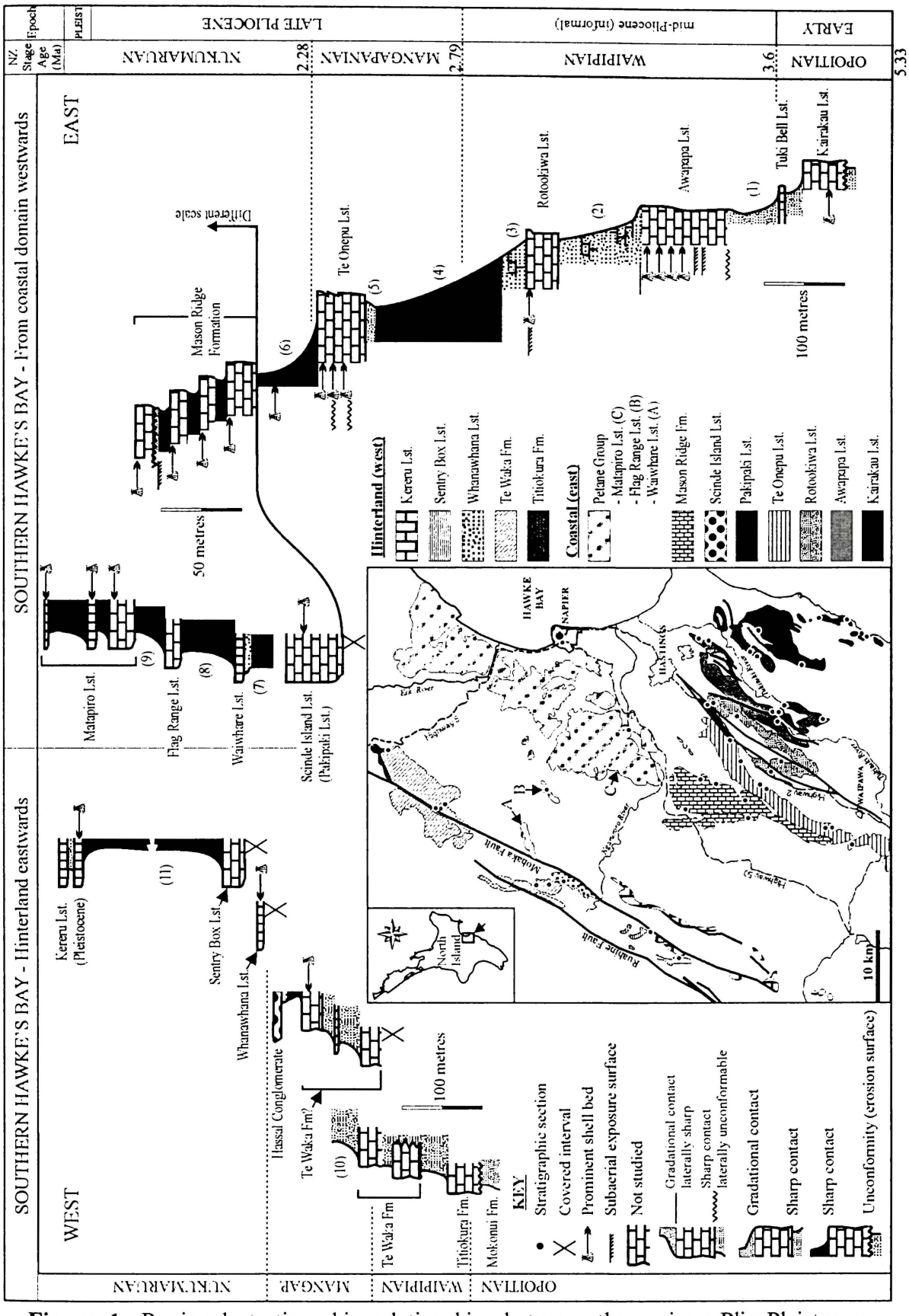

Figure 1- Regional stratigraphic relationships between the various Plio-Pleistocene limestone units in southern Hawke's Bay. The key with limestone names refers to the patterns on the inset geological map enlarged in Figure 1 of Chapter 1. Interbedded units, typically siliciclastic-dominated, are: (1) Mokopeka Sandstone; (2) Pukekura Calcarenite; (3) Waikareao Calcarenite; (4) Raukawa Mudstone; (5) Argyll Sandstone; (6) Makaretu Mudstone; (7) Willowford Mudstone; (8) Crownthorpe Mudstone; (9) Waitio Mudstone; (10) Pohue Formation (after Bland, 2001); (11) Ohara Mudstone.

intrinsic (interparticle) marine cementation that otherwise can be important in oversaturated warm waters (Nelson *et al.*, 1988c; Dodd and Nelson, 1998).

In contrast, constructive diagenesis involves armouring diagenetic processes, including early marine and/or meteoric spar cements, micritic crusts, indurated internal micrites, and encrustation of shells, all of which prevent grains from being frequently reworked and delay compaction-induced phenomena. These early diagenetic features are relatively uncommon in the Te Aute limestones where the bulk of the cements typically have burial and post-burial origins. Nonetheless they do recur at specific stratigraphic positions, commonly above and more rarely beneath discontinuities (see Chapter 2, Section 6.1).

Because of several fundamental differences in the facies attributes between non-tropical and tropical carbonates, as well as other properties such as the geochemistry of interstitial fluids, and sediment accumulation rates and climate, the consensus of a number of studies is that it is inappropriate to apply directly the diagenetic models for carbonate deposits originating from tropical settings to non-tropical carbonates (Nelson, 1988a; Hood and Nelson, 1996; James, 1997; Dodd and Nelson, 1998).

Developing diagenetic concepts and models applicable to non-tropical carbonates first requires detailed characterization of the products of diagenesis recognised in such occurrences. The diversity of Te Aute Plio-Pleistocene limestones in terms of depositional environments, sedimentary facies, and skeletal composition over time makes them particularly appropriate for assessing the nature and evolution of diagenetic pathways with respect to these controls. The purpose of this chapter is to document the diagenetic fabrics occurring in the Te Aute limestones in southern Hawke's Bay, and to interpret the diagenetic conditions and environments in which they originated.

2. Analytical techniques

The main objectives of this study necessitated detailed microfacies analyses and some supporting geochemical data of the various petrographic components in the limestones. Accordingly, the petrographic investigations combine: (1) the examination of microfacies and cements with a conventional polarizing microscope; (2) cathodoluminescence studies; (3) the determination of mineralogies by X-ray diffraction and chemical staining; (4) carbon and oxygen isotopic analysis of bulk samples and microsamples of cements;

and (5) the analysis of CaO, MgO, SrO, MnO, and FeO concentrations (ICPOES and microprobe) also performed on both bulk samples and successive cementation phases.

2.1. Sampling

About 600 samples, as unweathered as possible, were collected from 54 localities of the Te Aute successions in southern Hawke's Bay (Figure 1). Due to the poorly cemented and often friable nature of many of the Plio-Pleistocene limestones, the rock samples obtained in the field were routinely impregnated with epoxy resin prior to thin-sectioning. Several samples, especially the ones taken from limestones of late Opoitian and Nukumaruan age (Figure 1), were sufficiently cemented that impregnation was probably not necessary, but it was undertaken on all samples to ensure there was absolutely no loss of any delicate pore-lining carbonate cement or of poorly bound fine-grained material. Because all thin-sections were also examined under cathodoluminescent light, they were finished on a Buhler Metaserv Grinder Polisher so as to get a suitably prepared surface.

Geochemical analyses were performed on a variety of (crushed) samples that fall into three major categories: (1) bulk skeletal limestones; (2) microsamples of carbonate cements; and (3) microsamples of fossil skeletons (brachiopods and various bivalves).

Because sampling resolution increases with increasing crystal size, microsampling of cements focused on coarse skeletal grainstones and rudstones where the thickness of individual rinds of carbonate crystals (0.1 to 0.5 mm) was optimum. Microsamples were collected from polished slabs using a hook-shaped blade. The growth structure of cements was determined from cathodoluminescent (CL) zoning.

2.2. X-ray diffraction

Over 700 powders of bulk limestone samples were analysed using X-ray diffraction (XRD) to determine their carbonate mineralogy by Viviane Simard-Caron at the University of Waikato, Hamilton (Appendix 8; also on CD1). Analyses were performed on a Philips analytical X-ray diffractor with a PW 1729 X-ray generator, and a PW1840 diffractometer control on un-oriented powder mounts. Mounts were scanned between 18 to 34 °2θ at 0.02 °2θ/sec.

2.3. Chemical staining

Thin-sections were stained using Alizarin Red-S and potassium ferricyanide, following the procedure of Dickson (1965; see also Appendix 10.2).

Alizarin Red-S/potassium ferricyanide staining constitutes a preliminary approach to calcite cement stratigraphy: (1) it helps define the **diagenetic stratigraphy** - the record of successive diagenetic processes and products at the thin-section scale, and the diagenetic discontinuities bounding them (see Chapter 2, Section 4.1); and (2) it enables recognition of the major changes in the fluid chemistry from which cements precipitated over time through the amount of Fe incorporated in the carbonate crystal lattices.

The incorporation of ions such as Mn and Fe in the crystal lattice of calcite and dolomite occurs during the crystal growth and depends upon the chemical properties of the inter/intraparticle microenvironments. The incorporation is revealed by colour changes and zoning patterns in the crystals after chemical staining. It reflects changes in the interstitial fluid composition occurring as the crystals of calcite or dolomite grow. These changes can be related to temperature, redox potential (Eh), and the introduction of allochthonous ions inhibiting or activating the chemical reaction (Evamy, 1969).

The relationships between mineralogy and stain colour are as follows (e.g., Dickson, 1965, 1966; Evamy, 1969):

- All calcite crystals are stained red by Alizarin Red–S.
- Crystal lattices enriched with Fe are stained blue (Turnbull blue) by potassium ferricyanide.

Using a combination of the two reagents:

- Non-ferroan calcite is stained pink to red (<0.5% Fe^{2+})
- Slightly ferroan calcite is stained mauve (0.5-2.5% Fe^{2+})
- Ferroan calcite is stained purple-blue (>2.5% Fe^{2+})
- Non-ferroan dolomite is not stained, while ferroan dolomite stains deep blue.

2.4. Cathodoluminescence

2.4.1. Principles

The cathodoluminescence (CL) technique applied to sedimentary carbonates, and especially to carbonate cements, observes the radiation emitted by carbonate crystals after their excitation by an electron beam. As the carbonates emit a stable luminescence during the electron bombardment, the conditions of observation can be reproduced.

Cathodoluminescence can image polyphase growth since it is extremely sensitive to subtle changes in composition and structure of host minerals.

The colour and the intensity of luminescence are related to: (1) the mineralogy of the crystals; and (2) the geochemistry of the trace elements incorporated in the crystal lattice, either in interstitial or in substitution positions. Trace element incorporation and distribution into solids from aqueous solution are described either as homogeneous or heterogeneous (Machel and Burton, 1991). In the first case, the distribution of the trace ions is uniform throughout the whole growth zone, either because the trace/major ion ratios do not change during precipitation ("open system") or because the solid continuously recrystallizes during crystal growth. In the second case, the solid does not re-equilibrate with the solution, and the trace element amount in the solid changes with crystal growth ("closed system").

Chemical analyses made *in situ*, either with an electron microprobe or with an ion microprobe, have shown that the substitution of Ca^{2+} by Mn^{2+} typically gives rise to luminescence in calcite spar cements (Dorobek, 1987; Niemann and Read, 1988; Horbury and Adams, 1989; Meyers, 1989; Walkden and Williams, 1991). Further, variations in calcite luminescence appear *grosso modo* to be determined by variations of the iron to manganese ratio (Fe^{2+}/Mn^{2+}). Typically, Fe^{2+} inhibits luminescence while Mn^{2+} activates it.

2.4.2. Chemical considerations

Changes in redox-potential (Eh), the degree of openness of a system, element partitioning, organic matter content, and clay mineral transformations are all factors that determine the element concentrations in diagenetic fluids, and hence in precipitating carbonates (Horbury and Adams, 1989; Meyers, 1989; Machel and Burton, 1991). Other controls cited by Machel and Burton (1991) that govern CL include temperature, crystal surface structure, and the influence of some ions on the incorporation of Mn^{2+} and Fe^{2+}.

The alteration of organic matter and clay minerals may result in the release of many trace elements, including all known activators, sensitizers, and quenchers of CL in carbonates, and subsequently can lead to CL zonation in diagenetic carbonates. Indeed, release of trace elements commonly takes place sequentially, because the various minerals and organic components react over extended intervals of burial depth. Furthermore, cases have been reported where CL colour intensities, and corresponding

trace element contents, of carbonates are related to the proximity of a terrigenous influence (Nelson *et al.*, 1988c).

Most commonly, the incorporation of potential activators and inhibitors of CL is correlated to changes in Eh of the ambient environment. For example, $Mn^{4+}O_2$ is reduced at higher Eh than $Fe^{3+}OOH$. Thus, during a decrease in Eh, typically during progressive burial (Dorobek, 1987; Niemann and Read, 1988; and many others), first Mn^{2+} and then Fe^{2+} should increase in solution which could result in bright (high Mn^{2+}, low Fe^{2+}) and then dull or no CL in calcite (high Mn^{2+}, high Fe^{2+}). Consistently, as reported in many past studies (e.g. Walkden and Williams, 1991; Kaufman and Wendt, 2000), the transition from oxidising to reducing conditions translates into a typical CL motif: non-bright-dull.

Machel and Burton (1991) emphasized that even minor concentrations of Mn^{2+} in solution are sufficient to produce luminescence with or without Fe^{2+} present in solution (as little as 20 ppm Mn^{2+} for Fe^{2+} contents <150 ppm). Thus, non-luminescent calcite indicates an absence or exceptionally low concentration of Mn^{2+} rather than a high concentration of Fe^{2+}.

2.4.3. Use of cathodoluminescence in carbonate diagenetic studies

CL technology has been used by geologists since 1965 (Long and Agrell, 1965; Sippel and Glover, 1965; Weiblen, 1965). Its application expanded rapidly following the studies of Meyers (1974, 1978) on the petrography and stratigraphic distribution of CL cement zones in the Carboniferous (Mississippian) Lake Valley Formation (New Mexico, USA), who developed the concept of CL cement stratigraphy, and proposed regional and stratigraphic synchroneity for the precipitation of each cement zone in samples. Implicit in this concept was the acceptance that the CL character of individual zones is a unique discriminator for intercorrelation.

Since then, several studies have shown the temporal and spatial variability of the solution chemistry (saturation rates, precipitation rates, temperature, salinity, pH, and Eh) in many carbonate aquifers, and emphasized the inevitability of changes in the CL signatures of calcite cements over certain distances (Walkden, 1987; Goldstein, 1988; Machel and Burton, 1991; Braithwaite, 1993; Frank *et al.*, 1995). Clearly such conditions would render the use of CL cement zones for intercorrelation much more difficult and problematical.

In the present study (see Chapter 2, Section 4.3) complex cathodoluminescence patterns are grouped into CL sequences defined as genetically-related successions of CL cement zones limited by easily traceable (correlative) surfaces equivalent to discontinuities. Thus, diagenetic discontinuities are considered to be the principal discriminators for intercorrelation, not the CL cement zones.

CL microscopy was carried out using a Technosyn 8200 MK II instrument (cold cathode; 15kV gun potential, 0.35 milliamps beam current).

2.5. Isotopic analysis

2.5.1. Principles

The two most naturally abundant isotopes of oxygen (^{18}O and ^{16}O) and of carbon (^{13}C and ^{12}C) were used, variations in the $^{18}O/^{16}O$ and $^{13}C/^{12}C$ ratios between samples being measured by high-precision mass-spectrometry (Appendix 7). Isotopic ratios are given in per mil (= mg/g or $^{o}/_{oo}$) values relative to the international Pee Dee Belemnite (PDB) standard, and are expressed in the usual delta (δ) notation ($\delta^{18}O$ and $\delta^{13}C$).

The $\delta^{18}O$ value of a carbonate precipitated from water depends chiefly on the $\delta^{18}O$ composition and temperature of the water, while the $\delta^{13}C$ composition of precipitated carbonates primarily reflects the source of bicarbonate dissolved in the waters (Hudson, 1977). However, apart from water chemistry and precipitation temperature, other controls include water/host sediment ratios, mineral-water fractionation factors, biochemical reactions, degree of isotopic equilibrium, and the extent of post-formation isotopic exchanges, all potentially complicating interpretation.

Despite this, Nelson and Smith (1996) suggested that carbonates precipitated at or near isotopic equilibrium from natural waters tend to show a characteristic range of $\delta^{18}O$ and $\delta^{13}C$ isotopic values that reflect their genetic environment.

Samples were roasted under vacuum at 380°C for one hour to remove volatile contaminants, and then reacted at 80°C with anhydrous phosphoric acid to produce CO_2 for analysis. Analyses were carried out at three institutions: (1) by Dr Karyn Rogers at the Institute of Geological & Nuclear Sciences (Lower Hutt, New Zealand), where results were normalized to VPDB using GNS marble (internal standard), NBS-18 (international standard), and NBS-19 (international standard). Precision is $\pm$ 0.1$^{o}/_{oo}$ for $\delta^{18}O$ and $\delta^{13}C$ values; (2) by Helen Turner at the University of Waikato (Hamilton, New Zealand), where results were normalized using NBS-1959 and NBS-1960 (international

standards). Precision ranges from ± 0.004 to 0.06‰ for $\delta^{13}C$ values and from ± 0.008 to 0.08‰ for $\delta^{18}O$ values. Analyses were carried out using a CAPS carbonate device attached to a GEO-20 mass spectrometer; and (3) by Dr Helen Neil at the National Institute of Water and Atmospheric Research (Wellington, New Zealand). Internal precision of measurements is 0.02-0.06‰ for $\delta^{18}O$ and 0.01-0.03‰ for $\delta^{13}C$, external precision (between runs) is 0.05‰ $\delta^{18}O$ and 0.03‰ $\delta^{13}C$. Samples were reacted with three drops of H_3PO_4 at 75°C in an automated individual-carbonate reaction (Kiel) device coupled with a Finnigan MAT252 mass spectrometer.

2.5.2. Brachiopods and seawater composition

Ancient marine $\delta^{18}O$ signatures are routinely obtained from either marine cements (Gonzales and Lohmann, 1985) or brachiopods (Popp *et al.*, 1986). Typically, the primary low-Mg calcite mineralogy of brachiopods, less sensitive to diagenetic alteration than more metastable biogenic intermediate- and high-Mg calcite, is potentially retentive of the original isotopic composition of seawater (Wadleigh and Veizer, 1992). Eight texturally well preserved, relatively thick-shelled brachiopods collected at three different localities at various stratigraphic positions within the Awapapa Limestone (Waipipian) were microsampled for isotopic analysis. In thin-sections, brachiopod fragments from the same horizons are non-ferroan, non-luminescent to dull-orange, and lack evidence of dissolution features. The $\delta^{18}O$ values show a narrow range from –0.4 to +0.9‰PDB (mean = +0.25‰PDB) while $\delta^{13}C$ values range from +1 to 2.4‰ PDB (mean = +1.73‰PDB), well above values yielded by pre-compaction (including turbid fibrous) and post-compaction cements, and bulk limestone samples (see Table 1; Figure 6).

Non-luminescence and textural preservation of brachiopod shells have been shown in other studies to sometimes be unreliable criteria for lack of diagenetic alteration (Rush and Chafetz, 1990; Lavoie and Bourque, 1993). However, the relatively "heavy" $\delta^{18}O$ values of brachiopod shells, relative to presumably altered marine precipitates (turbid cements) and non-marine precipitates (pre- and post-compaction clear spar cements; see Section 4.3), are taken as the best approximation of the oxygen isotopic composition of the mid-Pliocene seawater in the Hawke's Bay forearc basin. When compared to published $\delta^{18}O$ marine values for temperate water carbonates that range in age from Oligocene to present (Rao and Nelson, 1992; Nelson and Smith, 1996), the Te Aute brachiopods plot in the fields of unaltered fully marine skeletons overlapping with,

and closely similar to, the field for modern marine skeletons which cluster at small positive values (0 to +3‰PDB) for both $\delta^{18}O$ and $\delta^{13}C$ (see Figure 6).

2.6. Trace elements

CaO, MgO, SrO, BaO, FeO, and MnO concentrations were determined on polished carbon-coated thin-sections by electron microprobe spot analysis along pre-defined transect lines, extending from grain margins porewards across one or more cement generations (Appendix 6; also on CD1). All microprobe analyses were conducted on a JEOL JXA 8900 RL microprobe with a beam current of 12 nA, a spot size of 5 μm, and an accelerating voltage of 15 kV for all elements. The instrument is housed at the University of Göttingen (Germany) and was operated by Arne Pallentin under the supervision of Dr Andreas Kronz.

Elemental concentrations (CaO, MgO, Sr, NaO, FeO, and MnO) were also determined at the University of Waikato by Franziska Schellenberg using inductively coupled plasma optical emission spectrometry (ICP-OES) on splits of powders from bulk samples of limestones ranging in age from Opoitian to Nukumaruan (Appendix 9; also on CD1).

3. Times and environments of carbonate diagenesis

3.1. Diagenetic environments

Common carbonate diagenetic environments and their products in tropical settings have been sufficiently documented to motivate the compilation of a number of syntheses over the last three decades (Choquette and Pray, 1970; Folk, 1974; Bathurst, 1975; Longman, 1980; McIlreath and Morrow, 1990; Tucker and Wright, 1990; Rao, 1997; Moore, 2001). Although temperate diagenetic environments differ from their tropical counterparts in the genetic processes and products responsible for porosity development and destruction, the same factors that are used to define diagenetic environments in tropical settings (Longman, 1980) apply to non-tropical ones.

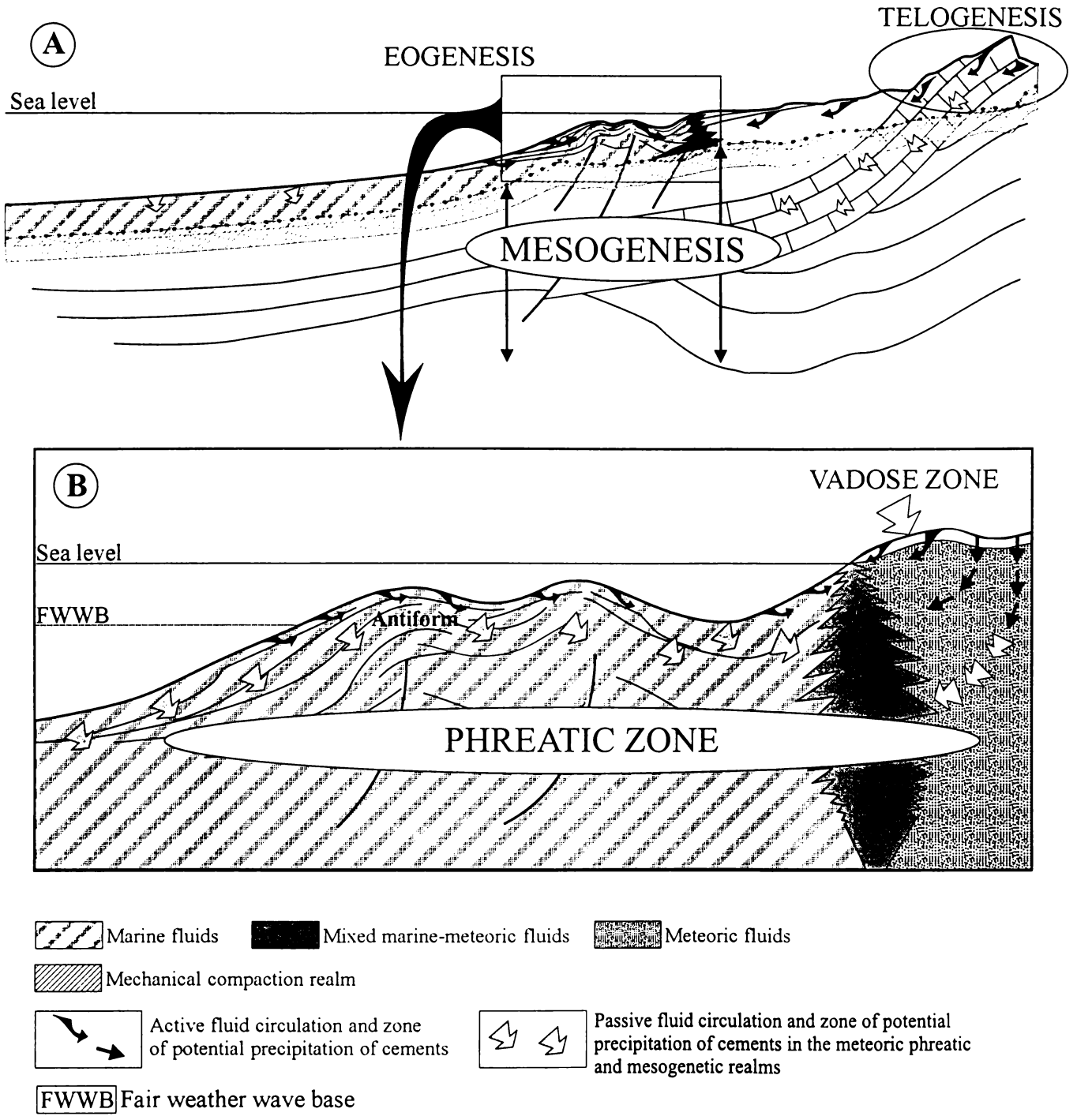

Figure 2- (A) Major time intervals in the diagenetic history of a carbonate system, and (B) common carbonate diagenetic environments in partly isolated carbonate antiforms, considered to be the most likely depositional setting for many Te Aute limestones. (Modified from Choquette and Pray, 1970; Longman, 1980).

Fundamentally, the fluid chemistry (marine, meteoric, burial brines) and the distribution of that fluid in the pore spaces (pores saturated or undersaturated with water) define the major diagenetic environments. In the shallow subsurface (tens of metres), pore fluids derive either from the sea, and are saline, or from the land (rainfall) and are fresh (meteoric). The combination of the foregoing factors, including the possible dilution of seawater by variable amounts of meteoric water, yields five basic diagenetic environments: (1) phreatic marine; (2) vadose marine; (3) a zone where marine and meteoric waters are mixed; (4) phreatic meteoric; and (5) vadose meteoric (Figure 2B). Additionally, flow rates, partial pCO_2, dominant skeletal mineralogy, and saturation with respect to calcium carbonate are other factors critical to porosity evolution (cementation versus dissolution), especially in non-tropical settings, that may result in further subdivisions of the diagenetic environments into constructive and destructive diagenetic zones.

In the deep subsurface (hundreds of metres), waters that become isolated from their source areas during burial are progressively chemically modified due to increasing temperature and pressure. There is a lack of exchanges with atmospheric oxygen and CO_2, and mixing with deeper burial waters can occur (Choquette and James, 1990). The burial environment comprises various domains defined on the basis of the degree of compaction, and resulting processes and products (see Figure 20).

3.2. Diagenetic stages

After final deposition, sediments typically pass through the above-mentioned diagenetic environments in a consistent sequence governed by relative sea-level changes and tectonic processes (phreatic marine to vadose meteoric). The time span over which loose carbonate sediments are transformed into limestones has been classically divided into three stages, named eogenesis, mesogenesis, and telogenesis by Choquette and Pray (1970) (Figure 2A).

The eogenetic stage relates to near-surface diagenesis that occurs prior to burial at depth where compactional processes are triggered. Following the discussion in the preceding Chapter (see Section 5), we divide the diagenetic history of carbonate sediments into discontinuity-bounded successions of diagenetic processes. Pre-compaction and post-compaction are deciphered on the basis of the first-generation of compaction-induced skeletal fracturing. The usual lack of early cementation in the non-

tropical Te Aute carbonates renders such a discontinuity surface readily traceable across a pile of sediments. Pre-compaction diagenesis includes eogenesis as defined by Choquette and Pray (1970) that we divide into successive specific diagenetic records. We define the "specific diagenesis" of a sedimentary unit bounded by discontinuity surfaces as corresponding to the sequence of physicochemical events prior to any superposed diagenetic overprint associated with the sediments overlying the upper discontinuity surface (see Chapter 2, Section 5.4.1). Thus, we restrict the definition of early diagenesis to the time interval during which sediments remained under the influence of surficial processes that also drove the packaging of sediments and the generation of the sedimentary surfaces bounding them.

The mesogenetic stage is the post-compaction time interval during which sediments are generally buried below the influence of surficial diagenetic processes (Figure 2A).

During the telogenetic stage, carbonate sediments that have been in the mesogenetic realm are tectonically uplifted to once again be influenced by shallow subsurface processes (Choquette and Pray, 1970).

4. Diagenetic products and processes

4.1. Early fine acicular precipitate

4.1.1. Description

These precipitates are quantitatively minor and are confined to intraskeletal cavities (Figures 3A, 3B). The term "precipitate" is adopted here to avoid confusion with the term "cement". Indeed, cements are regarded as precipitates binding grains, and are located between the grains (see Glossary in Appendix 10.1). Most commonly early fine acicular precipitate forms an isopachous fringe <50 μm thick, lining the internal openings of bryozoans and benthic foraminifera. Fine acicular spar is the only precipitate type that pre-dates the authigenesis of extrinsic glauconite (Figure 3B).

The acicular precipitate stains pink with Dickson's (1965) solution, and is generally non-luminescent, but occasionally shows a bright yellow CL. This minor phase of calcite precipitation seems to pre-date grain chemical alteration, but is coeval with mechanical alteration as revealed by the cross-cutting of fine acicular precipitates by grain abrasion surfaces. Neither isotopic nor elemental analyses were performed on this minor calcite precipitate.

4.1.2. Diagenetic environment

Fine acicular precipitate is interpreted to be a product of marine sea-floor diagenesis on the basis of the following evidence: (1) it is the first phase in the carbonate paragenetic suite; (2) fine acicular spar pre-dates authigenic glauconite, which forms in the early stages of sea-floor diagenesis in sediment-starved, slightly reducing environments (Amorosi, 1995); and (3) abrasion of both precipitates and host-grains indicate frequent reworking on the sea floor.

Synsedimentary intraparticle (extrinsic) thin acicular precipitates have been identified within ancient and modern temperate carbonate sediments (Rao, 1981, 1990; Harmsen, 1984; Nelson *et al.*, 1988c; James and Bone, 1989).

They have been shown to be locally the only sea-floor calcite precipitation phase. Presumably, certain intraskeletal chambers provided a suitable microenvironment where oversaturation with respect to $CaCO_3$, in conjunction with enhanced water circulation through the micropores, could lead to localized calcite precipitation (Illing, 1954; Rao, 1981).

4.2. Early inclusion-rich cement

4.2.1. Petrography of early turbid cements

Early rims of inclusion-rich (turbid) cements occur either in interparticle (intrinsic) or in intraparticle (extrinsic) pore spaces. In many Te Aute limestone samples, individual layers consist of isopachous rinds that range in thickness from 50-150 μm, but can be less than 30 μm (Figures 3C to 3H). Turbid cements grow selectively upon certain skeletal grains, including mainly bivalves, echinoderms, brachiopods, and barnacles (Figure 4B), and have never been found coating quartz or feldspar grains. Crystal habits are diverse and include: (1) bladed to scalenohedral crystals, commonly arranged in a palisade fashion; (2) acicular spar that consists of elongate, fibre- to needle-like crystals; (3) relatively large, individual host crystals of subequant to elongate habit, suggesting locally mosaic fabric; and (4) syntaxial overgrowths on echinoclasts, and more rarely upon molluscan and brachiopod fragments.

Staining (stain pink to pale mauve) and trace element analysis indicate that the turbid cements are now non- to slightly ferroan, low-Mg calcite (LMC).

Figure 3 – Photomicrographs of marine cements

(A) – (B) Early fine acicular cement – This intraparticle (bryozoan zooecia) pore-lining spar cement commonly predates a later stage of pore-filling authigenic glauconite (g). Plain light (PL): Sample 4.55 (Kairakau Limestone).

(C) Turbid fibrous cement – Note that the interior of the centre bivalve skeleton mould is filled by a discontinuous turbid fibrous and mosaic clear spar calcite cement sequence. Intra-mouldic (inferred) marine cement provides evidence of early dissolution at the sea floor. PL: Chemically stained sample 5.74 (Awapapa Limestone).

(D) Isopachous rind of elongate inclusion-rich cement about barnacle (top) and bivalve (bottom) grains is overgrown by scalenohedral clear calcite crystals (arrowed). PL: Sample 5.93 (Awapapa Limestone).

(E) Substrate selective inclusion-rich cement fringe about barnacle grains merges into scalenohedral spar crystals that comprise a thin generation of pale blue post-compactional cement (arrowed). The remaining pore space is occluded by non-ferroan (pale pink) mosaic telogenetic cement. Note that inclusion-rich cements have not grown upon moulds of aragonitic bioclasts (lower half of the photograph). PL: Chemically stained sample 5.61 (Awapapa Limestone).

(F) Inclusion-rich rinds of fibrous cement coat abraded calcitic skeletons (bivalves and barnacle plates). PL: Sample 5.87 (Awapapa Limestone).

(G) Thick isopachous rinds of dirty fibrous cement coat both preserved calcitic shells and moulds of (former aragonitic?) skeletons. Note the same cement suite as for sample 5.61 in E (post-compactional ferroan cement is arrowed). PL: Chemically stained sample 4.29 (Kairakau Limestone).

(H) Photomicrograph illustrating that fibrous cement typically grows upon a thin micritic crust (arrowed) that acted as a nucleating mat for fibrous crystals. PL: Sample 4.29 (Kairakau Limestone).

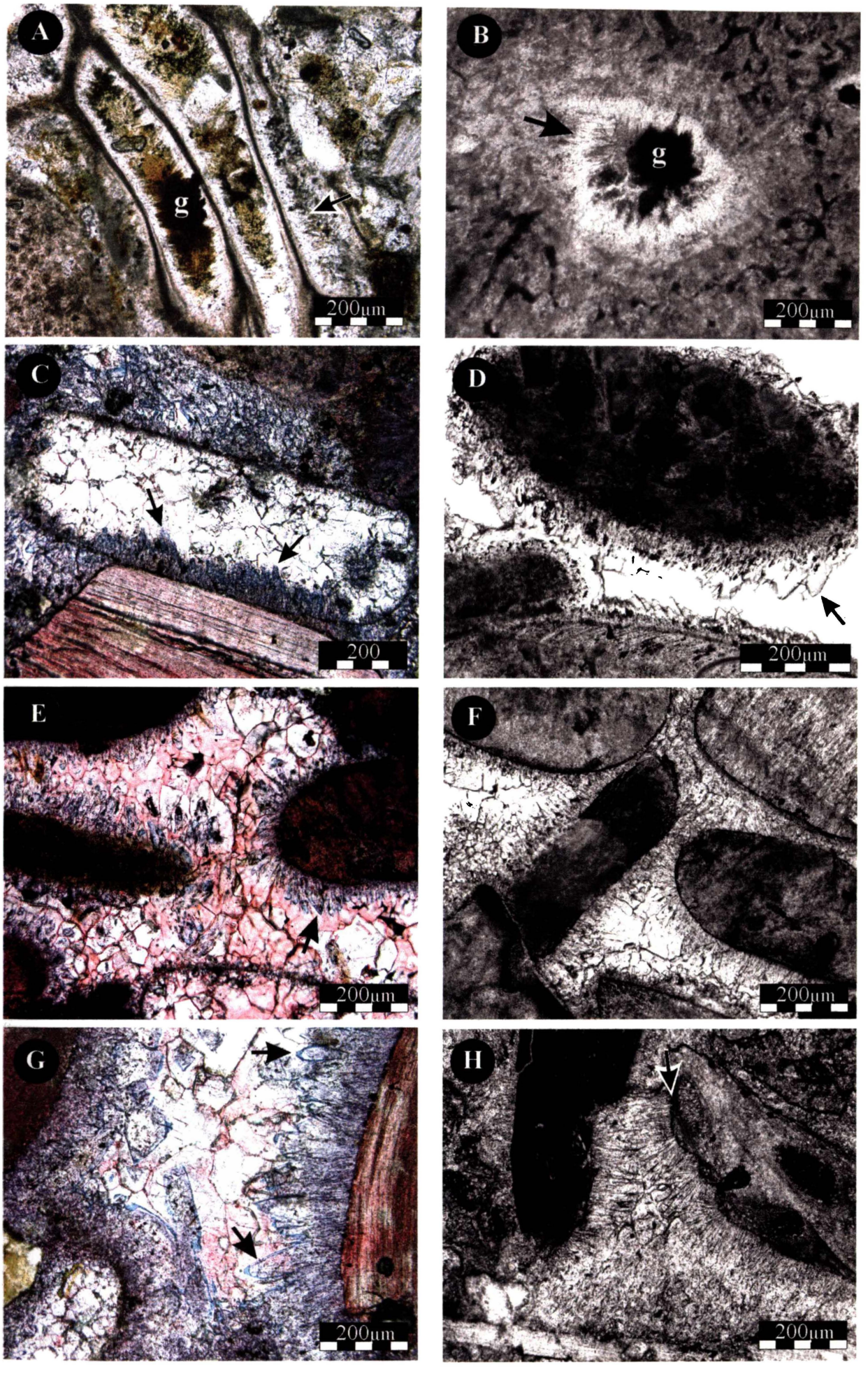
A
g
200µm
B
g
200µm
C
200
D
200µm
E
200µm
F
200µm
G
200µm
H
200µm

In the Te Aute limestones, the turbidity of early calcite cements is mostly a result of unidentifiable minute solid inclusions, up to a few microns in size, some perhaps of organic nature as suggested under fluorescent light (Figure 4G). In most cases, crystalline fabrics include various types of inclusions that may define precursor fibres instead of true relict fibre-shaped crystals. Commonly, inclusions surround and define the primary fibres within larger host crystals (Figures 3D, 3G). When enclosed within clear spar host crystals, the distinctive "primary fibres" behave optically as their host, and thus exhibit a uniform extinction. Otherwise, within palisade structures with all crystals parallel, individual crystals may behave optically independent from one another.

Where elongate crystals form bundles or fans, slightly undulose or straight cone-shaped extinction has sometimes been observed. However, even though subcrystals diverge away from their substrate, cements cannot be strictly referred to as radiaxial fibrous calcite (RFC) because: (1) optic axes do not converge away from the substrate; and (2) there is a lack of curved cleavage and twin lamellae (Kendall, 1985).

Terminations of individual crystals are generally poorly defined, ranging from flat to obtuse pyramidal or rhombohedral. Commonly, groups of primary fibres which define cone forms merge with younger translucent (inclusion-free) calcite spar overgrowths.

Typically, turbid cements exhibit a blotchy to cloudy luminescence that ranges from none to very dull brown, with internal moderately luminescent orange to bright yellow patches (Figures 4A, 4B, 4C, 4E). These underlie elongate inclusions and highlight the acicular morphology of the component crystals (Figures 4H, 8). The CL pattern within individual turbid rinds may be discontinuous laterally, especially across fractures that acted as barriers interrupting the normal course of neomorphosed fronts, and resulted in differing degrees of alteration and trace element incorporation on either side of the discontinuity (Figures 4B, 8).

4.2.2. Petrography of turbid syntaxial overgrowths

Syntaxial turbid calcite that grew in optical continuity with the host grain (echinoderm monocrystals in most cases) is rather an uncommon cement variety in the Te Aute carbonates, but has been recognized in many ancient carbonate settings (Lohmann and Meyers, 1977; Grover Jr and Read, 1983; Dorobek, 1987; Walker *et al.*, 1990).

Figure 4 – Photomicrographs illustrating the cathodoluminescence and fluorescence characteristics of inclusion-rich fibrous cements

(A) Cloudy orange luminescence of isopachous rinds of turbid cements (black arrow) coating bivalve and barnacle grains later followed by orange luminescent scalenohedral spar calcite cement of burial origin (white arrow), overgrown in turn by non-luminescent telogenetic/meteoric cement. Cathodoluminescent light (CL): Sample 5.95 (Awapapa Limestone).

(B) Neomorphism of turbid cement – The probable differential incorporation of Mn cations within the fibre-shaped crystals during neomorphism is responsible for contrasting luminescence (arrowed) of first generation isopachous dirty cement in adjacent intraskeletal pores (i.e., within barnacle plate). CL: Sample 16.5 (Whanawhana Limestone).

(C) Cathodoluminescence of pore-filling cement suite. Note the blotchy luminescence of early turbid cement (arrowed) about bivalve grains due to dissolution associated with post-compaction brightly luminescent cement. Dissolution is also outlined by the irregular aspect of the outer margin of turbid cements. CL: Sample 5.62 (Awapapa Limestone).

(D) Same field of view as in (C) under plain light. The black arrow with white background points at micritic crust and overlying turbid cement, both separated from the main body of the grain due to compaction. PL: Sample 5.62 (Awapapa Limestone).

(E) Patchy-cloudy luminescence of isopachous fibrous cement (arrowed) coating barnacle (bottom right) and bivalve (bottom left) grains. CL: Sample 4.5 (Kairakau Limestone).

(F) Same field of view as in (E) under plain light. Acicular turbid cement is arrowed. PL: Sample 4.5 (Kairakau Limestone).

(G) Fibres display a bright pale green fluorescence (white arrow) that may indicate the presence of some organic matter along elongate crystals within the turbid cement fringe. Fluorescent light: Sample 4.105 (Kairakau Limestone).

(H) The orange cathodoluminescence pattern outlines the acicular fabric of first generation turbid cement (white arrow). Note first compaction-induced fracturing stage (a) and later syn-uplift fracturing stage (b). CL: Sample 4.29 (Kairakau Limestone).

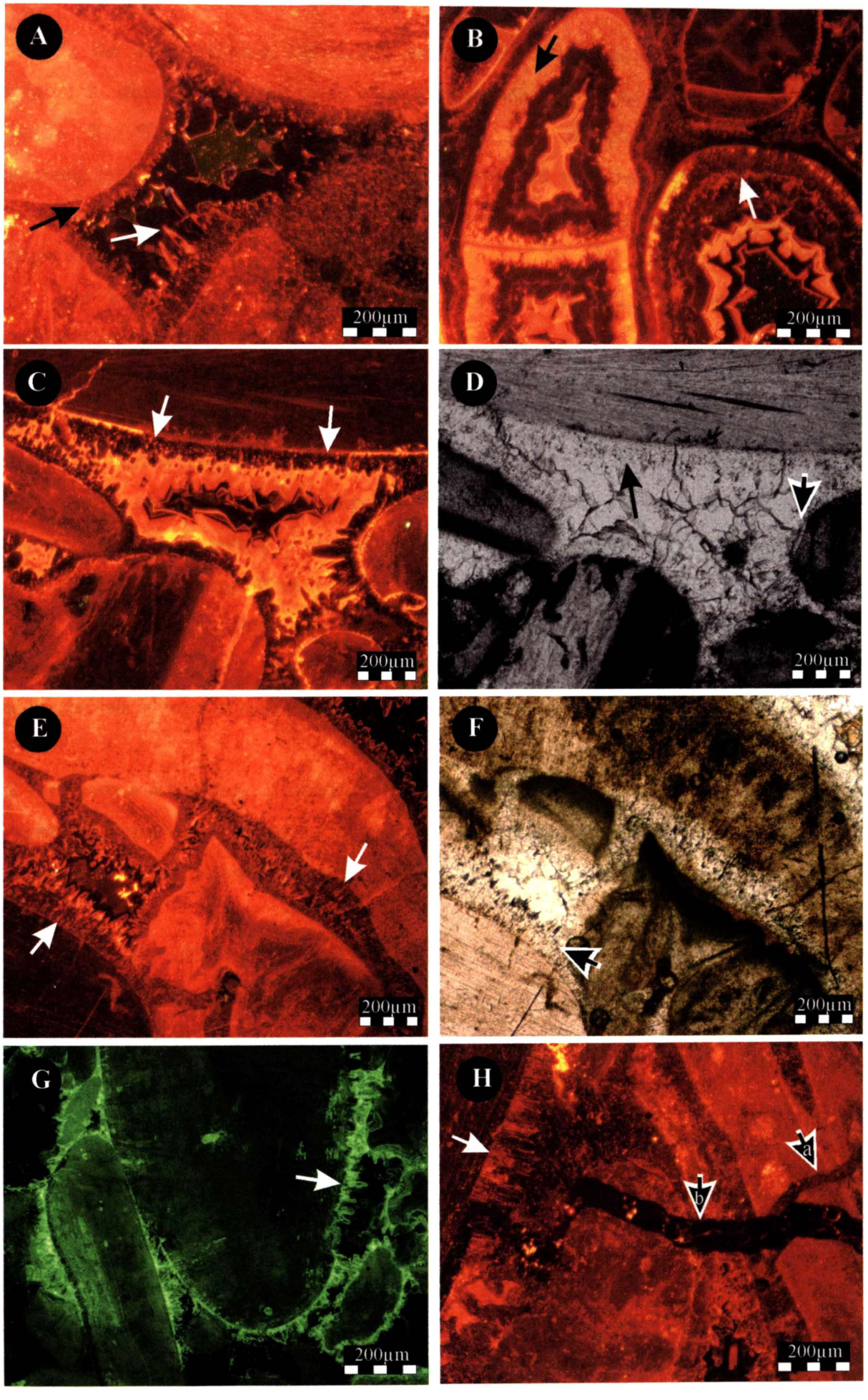
A
200µm
B
200µm
C
200µm
D
200µm
E
200µm
F
200µm
G
200µm
H
a
b
200µm

In the Te Aute case, the cloudy zone always occurs as the initial cement overgrowth, distinct from later clear enlargements, and can be as thick as 250 μm (Figures 5C, 5D, 5F). The cloudiness originates from elongate solid inclusions underlying precursor fibres whose long axes are coincident with the c-axis of the host echinoderm fragment. Consequently, turbid syntaxial overgrowths always display a straight extinction.

The luminescence of turbid syntaxial overgrowths is similar to that of their isopachous cement counterparts (Figure 5E).

4.2.3. Stratigraphic position of inclusion-rich cements

Turbid cements are uncommon in the Te Aute successions. The stratigraphic location of horizons including such cements turns out to be important when considering the sequence stratigraphic context of the studied deposits (see Chapters 2 and 4). Typically, turbid cements are found close to unconformities (above transgressive surfaces of erosion and below sequence boundaries *sensu stricto*), at stratigraphic positions associated with high-energy conditions (lower part of TSTs and upper part of RSTs), and in intervals inferred to have low or arrested sedimentation rates (close to Mfs).

4.2.4. Precursor mineralogy of inclusion-rich cements

A principal theme regarding the early diagenetic evolution of non-tropical sediments is the attempt to relate precursor mineralogy and habit with a corresponding replacement fabric.

The X-ray diffraction analyses of bulk samples indicate predominantly LMC mineralogies, with some intermediate-Mg calcite (IMC) ones. The calcite peak positions in slow-scan X-ray diffractograms range in D-spacing from 29.40 to 29.62°2Φ, indicating that the calcites contain from 2 to 7 mol% $MgCO_3$ (Chave, 1954). However, for more than 80% of analysed samples, concentrations fall in the interval 2 to 4 mol% $MgCO_3$.

$\delta^{18}O$ values for one microsample of turbid cement and for the bulk of pre-compaction cements, which include both turbid cements and later stage clear spar cements, range from –0.44 to –4.4‰PDB, while $\delta^{13}C$ values range from 1.17 to –2.4‰PDB (Table 1; Figure 6; see Appendix 7), compatible with a normal marine to mixed marine and meteoric signature (Nelson and Smith, 1996).

Figure 5 – Photomicrographs of isopachous inclusion-rich cement (continued) and turbid syntaxial overgrowths

(A) Elongate inclusion-rich cement (black arrow) that post-dates geopetal micrite sediment (i.s.), is overgrown by scalenohedral spar. The offset of the fibrous rim cement from its substrate (white arrow) is a result of mechanical compaction prior to precipitation of clear spar. Crossed nicols (CN): Sample 5.93 (Awapapa Limestone).

(B) Isopachous fibrous cement grows selectively upon the calcitic layer of bivalve shell at right. The margin of the previously aragonitic shell layer (now left as a spar-filled mould – M) is turbid cement-free. Black arrow points at the abrupt transition. PL: Sample 5.89 (Awapapa Limestone).

(C) Turbid syntaxial overgrowths (arrowed) upon echinoderm fragments (e). The inclusion-rich zone occurs as the initial cement overgrowth distinct from later clear enlargements. CN: Sample 5.75 (Awapapa Limestone).

(D) Initial inclusion-rich zone (black arrow) about echinoderm clast (e) predates mechanical compaction as shown by the offset of correlative isopachous turbid cement from its substrate (bivalve; white arrow). PL: Sample 4.6 (Kairakau Limestone).

(E) The blotchy luminescence of turbid syntaxial overgrowths (s.o.) upon echinoderm fragment (e) is similar to that of isopachous inclusion-rich cements (see Figure 4A, 4C). CL: Sample 5.65 (Awapapa Limestone).

(F) Same field of view as in E under plain light. PL: Sample 5.65 (Awapapa Limestone).

(G) - (H) Needle cement (n.c.; presumably of original aragonite with retention of microstructure and partial retention of mineralogy) is overgrown by two generations of isopachous turbid fringes (in H; black arrows) separated by an isopachous layer of clear spar cement (white arrow). Under CL light (G), turbid cement fringes are cloudy orange, while needle cement is non-luminescent with some internal orange patches and dissolution microcavities (white arrows) coeval with yellow luminescent pore-filling calcite mosaic spar. CL and PL: Sample 6.6 (Pakipaki Limestone).

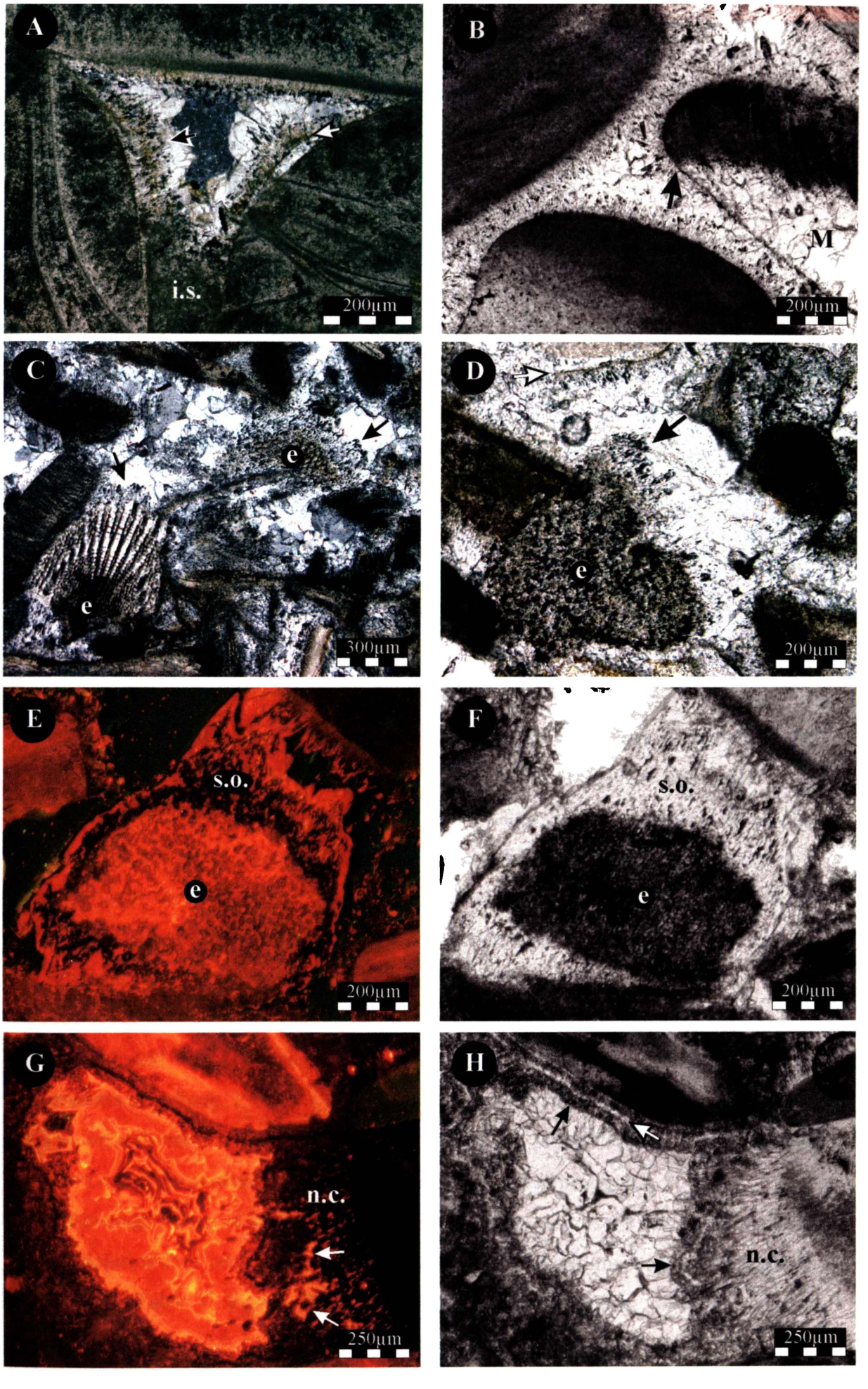
A
i.s.
200µm
B
M
200µm
C
e
e
300µm
D
e
200µm
E
s.o.
e
200µm
F
s.o.
e
200µm
G
n.c.
250µm
H
n.c.
250µm

Pore-lining inclusion-rich fibrous cements contain minor amounts of FeO (N = 26; 0 to 0.6 wt%, mean = 0.18 wt%), and virtually no MnO (0 to 0.05, mean = 0.02 wt%). SrO contents are low (0 to 0.5, mean = 0.09 wt%) and MgO is elevated compared to later stage cement varieties, ranging from 0.16 to 1.70 wt% (mean = 0.8 wt%; Table 1; Figures 7A, 8).

Previous studies have frequently addressed the problem of possible precursor mineralogies for early turbid cements (Lohmann and Meyers, 1977; Sandberg, 1985; Videtich, 1985; James and Choquette, 1990a; Mazzullo *et al.*, 1990; Nelson and James, 2000), and subsequently for their primary environmental origin. In tropical and non-tropical carbonate sediments, four major precursor mineralogies have been envisaged: (1) aragonite; (2) low-Mg calcite (0-4 mol% $MgCO_3$) = LMC; (3) intermediate-Mg calcite (4-12 mol% $MgCO_3$) = IMC; and (4) high-Mg calcite (>12 mol% $MgCO_3$) = HMC.

Precursor mineralogy = acicular to fibrous aragonite

There is no evidence for any aragonite precursor for turbid cements in the Te Aute non-tropical limestones, even though this model has been envisaged in some tropical early cement suites (Bathurst, 1975). Arguments are as follows:

(a) The primary mineralogy of skeletons in the Te Aute limestones is predominantly calcitic (LMC to IMC; Hood and Nelson, 1996). The aragonitic contributors have generally been dissolved in the early stages of diagenesis, by contrast with calcitic skeletons and turbid cements. Had turbid cements had an aragonite precursor, then it is difficult to envisage the likelihood of selective destruction by solution of the biogenic aragonite at the same time as non-destructive calcitization of primary aragonite turbid cements (e.g., Aissaoui *et al.*, 1986).

(b) Turbid cements in the Te Aute limestones neither display relicts of aragonitic fibres, nor botryoid morphologies, nor fine spar textures characterizing former aragonite cements (Sandberg, 1985).

(c) The orthorhombic crystal lattice of aragonite is not prone to syntaxial overgrowth upon echinoderm clasts, parallel to the c-axes of such monocrystals.

(d) The average values of SrO (0.09 wt%) for the turbid cements are low, similar to that of inclusion-free cements, particularly the (presumed non-marine) younger sparry calcites (Table 1; Figure 7B), and well below SrO contents of neomorphosed

Table 1- Some stable isotope and major and minor element compositions (mean and range values) of various cement phases and skeletons from Te Aute limestone samples (Kairakau, Awapapa, and Te Onepu).

	No.	**MgO** (wt%)	**SrO** (wt%)	**MnO** (wt%)	**FeO** (wt%)	No.	**$\delta^{18}O$** (PDB)	**$\delta^{13}C$** (PDB)
Turbid cement	26	0.8 (0.16-1.7)	0.09 (0-0.5)	0.02 (0-0.05)	0.18 (0-0.6)	1	-0.44	1.17
Pre-compaction clear spar cement (PrC)	41	0.57 (0.1-1.01)	0.16 (0-0.9)	0.016 (0-0.05)	0.16 (0-0.4)			
Post-compaction ferroan cement (PoFC)	20	0.4 (0.06-0.94)	0.4 (0-2.03)	0.04 (0-0.65)	0.3 (0-1.25)			
Youngest non-ferroan cement (YnfC)	113	0.2 (0-0.56)	0.04 (0-0.6)	0.01 (0-0.05)	0.05 (0-0.31)	7	-4.38 (-3.1 to -5.0)	-5.03 (-2.1 to -8.2)
Echinoderm	11	0.6 (0.07-1.03)	0.1 (0-0.25)	0.01 (0-0.03)	0.71 (0-1.56)			
Brachiopod						8	0.25 (-0.4 to 0.9)	1.73 (1 to 2.4)
Calcitic bivalve						2	0.1 (-1.3 to 1.5)	1.25 (1.2 to 1.3)

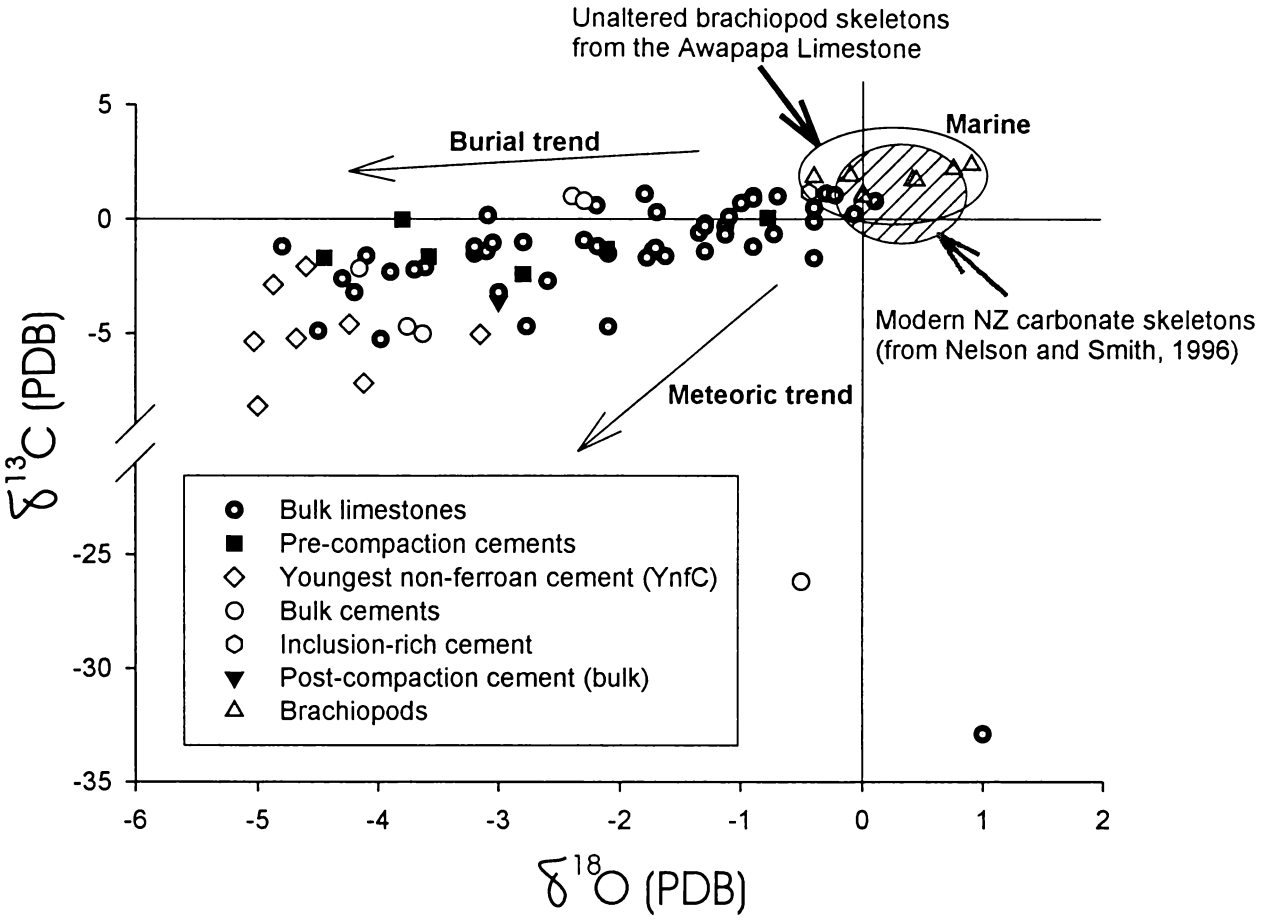

Figure 6- Stable isotope cross-plots for bulk samples of limestones, bulk samples of pre-compaction cements that contain (inferred) marine turbid cements, and various other samples including brachiopods from early Waipipian Awapapa Limestone. A variable degree of both burial and meteoric overprint characterizes most limestones.

aragonite cements and skeletal aragonites reported in previous studies (e.g., 0.1-0.34 wt% in Mazzullo, 1980; Sandberg and Hudson, 1983).

Precursor mineralogy = low-Mg calcite (LMC)

Sandberg (1985) and Saller (1986) have documented and interpreted radiaxial fibrous cements as primary LMC. By contrast, several attributes and properties of the turbid cements found in the Te Aute limestones indicate that their present mineralogy and habit correspond to a replacement fabric:

(a) The fabric of LMC cements recognized in modern marine sediments (Moore, 1989) is different from the ghost acicular or fibrous morphology of early turbid cements, which is underlain by elongate inclusions engulfed within larger spar crystals.

(b) Early inclusion-rich cements examined under cathodoluminescence exhibit a cloudy to patchy CL pattern (Figure 4), which is quite different from the homogeneous luminescence or concentric growth zones of younger clear LMC spar cements (see Figure 12). The distribution of CL activators and inhibitors in the former cements do not reflect the crystal growth stages, but rather a chemical reorganization through neomorphic transformation of former mineralogies during later diagenetic processes (Grover Jr and Read, 1983; Tucker and Wright, 1990; James and Bone, 1992; Kaufmann and Wendt, 2000).

(c) The cloudy luminescence of turbid cements is similar to that of former HMC skeletons, including echinoderms and some bryozoans, but differs from the homogeneous non- to orange luminescence of bioclasts that retain their primary LMC mineralogy, such as brachiopods and epifaunal bivalves (pectinids and ostreids).

Precursor mineralogy = intermediate- to high-Mg calcite (IMC and HMC)

The combination of microfacies, CL and geochemical evidence, indicates that the (now) LMC turbid cement in the Te Aute limestones corresponds to primary IMC to HMC:

(a) The patchy to cloudy CL of the inclusion-rich cements, similar to that of former HMC skeletons, supports the neomorphic stabilization of former IMC or HMC into LMC.

(b) The ghost fibrous fabric underlain by elongate inclusions, and palisadic crystals with scalenohedral terminations found in the Te Aute limestones, conform to the morphologic attributes of fibrous IMC and HMC cements described in modern carbonate settings (Rao, 1981; Videtich, 1985; Aissaoui *et al.*, 1986; Aissaoui, 1988).

(c) Early inclusion-rich cements whose primary mineralogy has been argued to be IMC or HMC have been documented in many ancient non-tropical and tropical carbonate deposits (Longman, 1980; Grover Jr and Read, 1983; Heckel, 1983; Dorobek, 1987; Kaufman *et al.*, 1988; James and Choquette, 1990a; James and Bone, 1992; Dodd and Nelson, 1998; Nelson and James, 2000).

So far, turbid cements in the Te Aute successions have not been seen to contain microdolomite inclusions, suggesting that they might originally have not been HMC (Lohmann and Meyers, 1977). Instead, a primary IMC mineralogy for the fibrous inclusion-rich cements would be consistent with the non-tropical Te Aute setting, as suggested by James and Bone (1992) for comparable fabrics in the cool-water Abrakurrie Limestone in southern Australia, using temperature-dependent relationships (Burton and Walter, 1987). This original IMC mineralogy of turbid cements is compatible with their present slightly elevated MgO contents compared to later cements, considering that part of the original magnesium was probably released during later stage neomorphism of the turbid generation (Figure 9).

4.2.5. Diagenetic environment

A literature review shows that early isopachous IMC and HMC cements have been interpreted as mostly of marine origin (e.g., Nelson and James, 2000). In contrast, turbid syntaxial overgrowths have been the subject of some controversial interpretations, some researchers suggesting that these enlargements originate exclusively in meteoric environments (Longman, 1980; Kaufman *et al.*, 1988), or can form in various environments, including marine. Undoubtedly, a major reason for the disagreement is that this type of cement can originate and continue to grow in all diagenetic environments. Among the proposed petrographic criteria for recognizing and interpreting the marine part of overgrowths, Walker *et al.* (1990) referred to the initial cloudy zone distinct from later more translucent zones, marine borings in overgrowth

Figure 7 – Electron microprobe analyses of (A) MgO and FeO, and (B) MnO and SrO variations in inclusion-rich fibrous cements, and both pre-compaction (PrC) and post-compaction (PoFC and YnfC) clear spar cements. Note in (A) the relatively high MgO content of pre-compaction cements compared to post-compaction ones (see text for discussion). Mean MgO concentrations decrease with each younger precipitate, from the (inferred) marine turbid cements to the telogenetic/meteoric cement (YnfC). Note also the relatively consistent increase of FeO associated with PoFC, interpreted to have formed from reducing burial fluids. Telogenetic cements (YnfC), interpreted to originate in the meteoric diagenetic environment, contrast with all previous phases in being mainly depleted in MgO, FeO, SrO, and MnO. Inclusion-rich cements typically have low Sr contents ruling out a possible aragonitic precursor for this early cement phase. Data gathered from 20 transects (12 thin-sections from Kairakau and Awapapa Limestones) starting at inclusion-rich cement and ending porewards either at PoFC or YnfC (see also Figure 8).

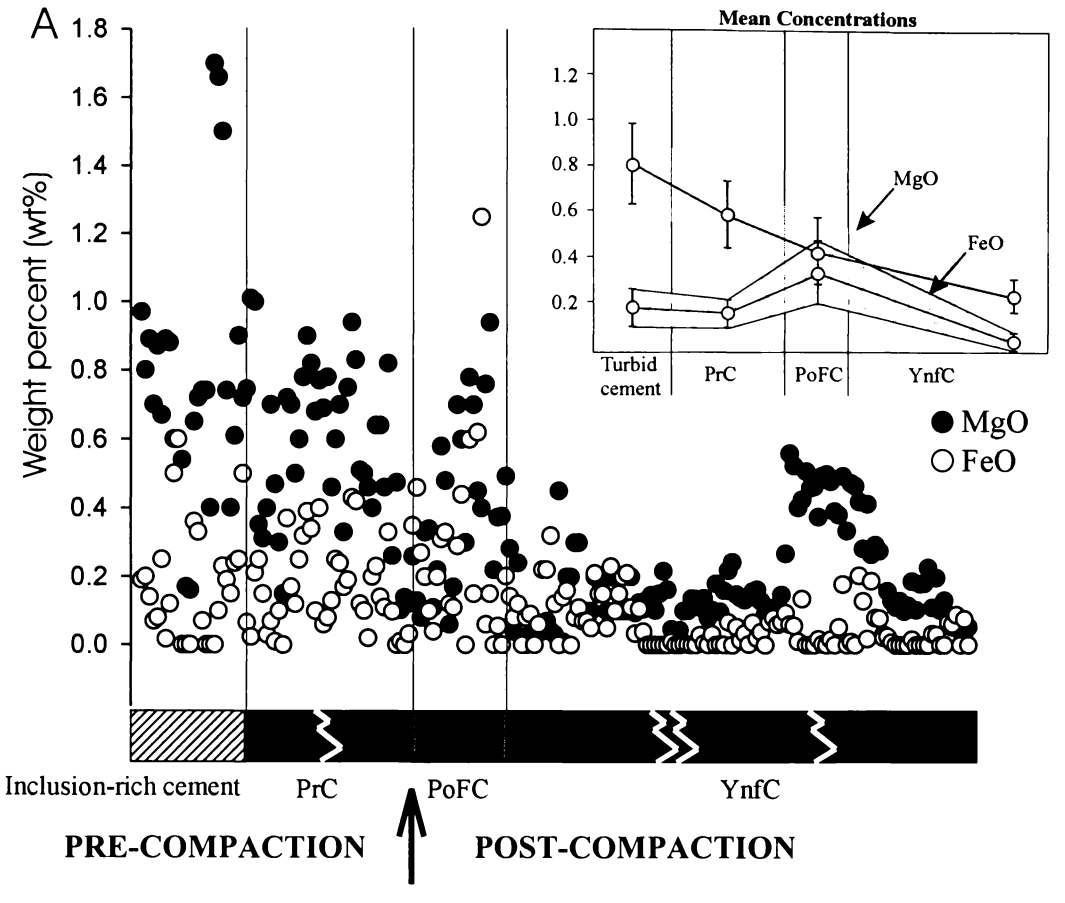
A
Weight percent (wt%)
1.8
1.6
1.4
1.2
1.0
0.8
0.6
0.4
0.2
0.0
Mean Concentrations
1.2
1.0
0.8
0.6
0.4
0.2
MgO
FeO
Turbid cement
PrC
PoFC
YnfC
MgO
FeO
Inclusion-rich cement
PrC
PoFC
YnfC
PRE-COMPACTION
POST-COMPACTION

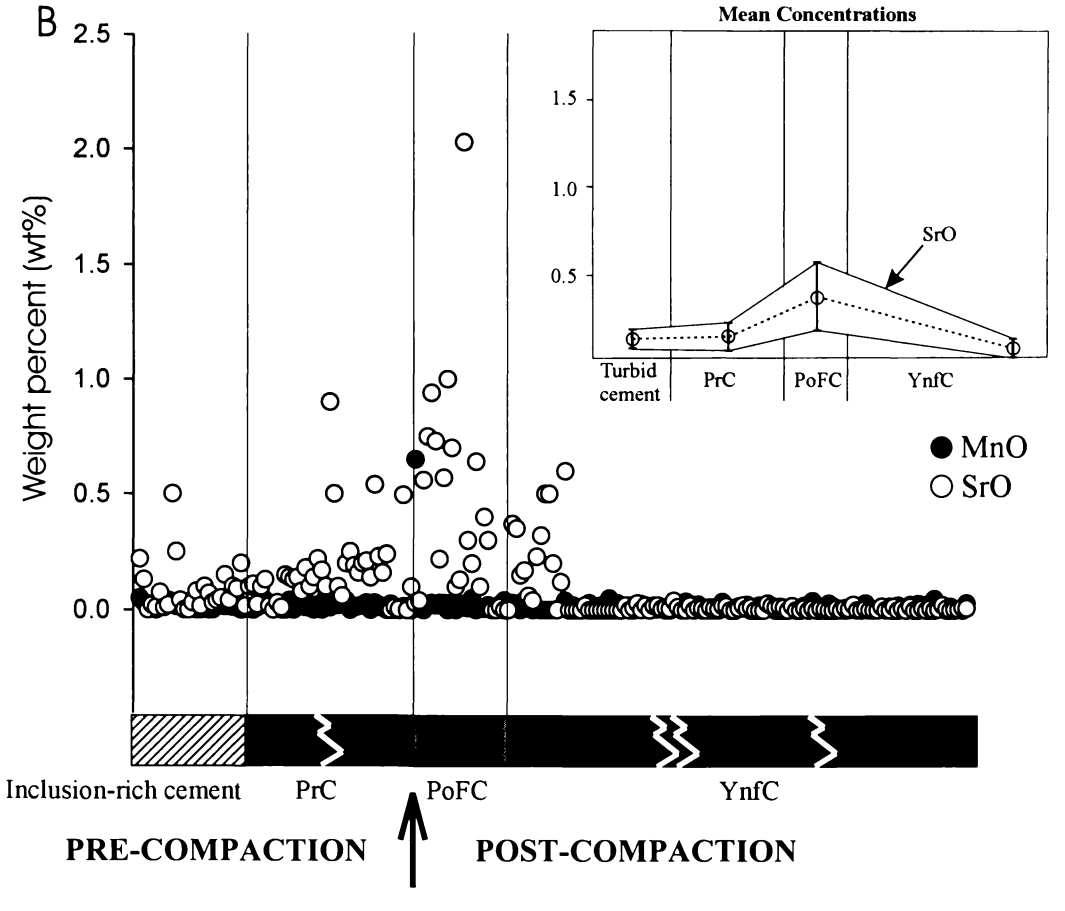
B
Weight percent (wt%)
2.5
2.0
1.5
1.0
0.5
0.0
Mean Concentrations
1.5
1.0
0.5
SrO
Turbid cement
PrC
PoFC
YnfC
MnO
SrO
Inclusion-rich cement
PrC
PoFC
YnfC
PRE-COMPACTION
POST-COMPACTION

Figure 8- MgO, FeO, SrO, and MnO distribution across intergranular pore space. L2 transect of microprobe spot measurements starts within calcitic bivalve fragment and ends within barnacle plate (b) fragment (white arrow gives the direction). The degree of neomorphism of inclusion-rich fibrous cement, as indicated by the differential incorporation of Mn and Fe (plots A and B), changes laterally depending, for instance, on fractures that interrupted the progression of the neomorphic front passing through the cement (black arrow). The incorporation of Mn in the crystal lattices translates in brightly luminescent fringes (see plot A). Note that the same generation of inclusion-rich cement across the pore is non-luminescent and has low MnO content. MgO concentrations are typically low within YnfC, while they are variable in inclusion-rich cement fringes. Thus, low MgO content correlates with a higher degree of alteration, suggested by the integration of Mn and Fe, while moderately elevated MgO content coincides with low MnO and FeO. SrO content is low in YnfC but increases in inclusion-rich cements and carbonate skeletons. Sample 5.28 (Awapapa Limestone).

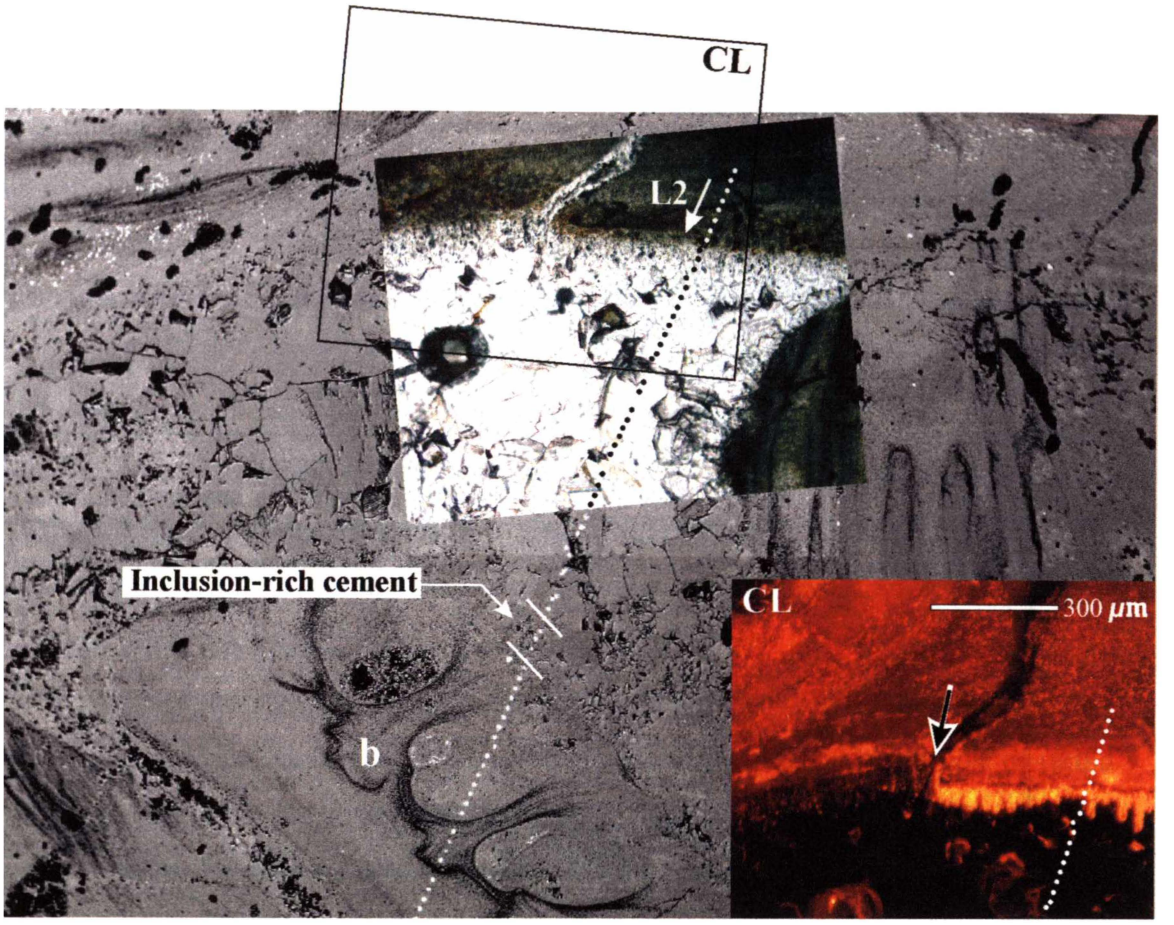
CL
L2
Inclusion-rich cement
b
CL
300 μm

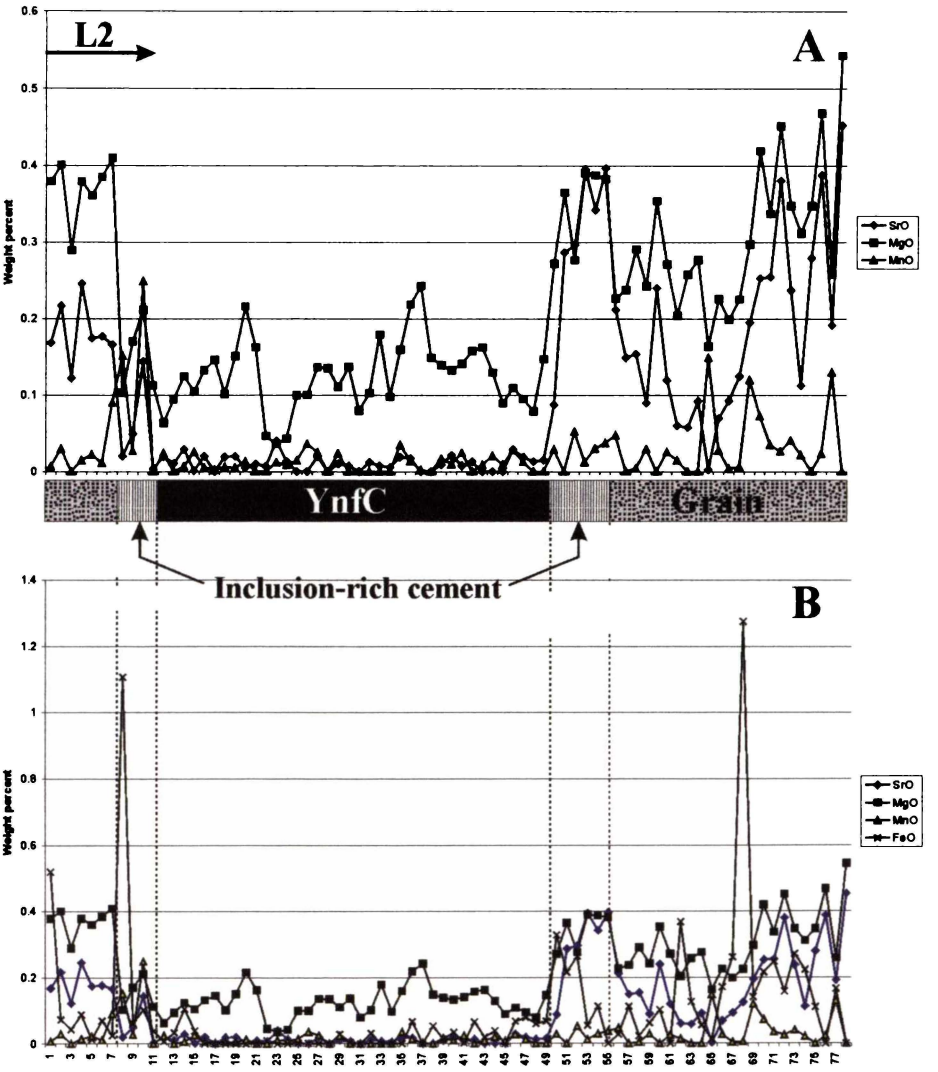
L2
A
Weight percent
SrO
MgO
MnO
YnfC
Grain
Inclusion-rich cement
B
Weight percent
SrO
MgO
MnO
FeO

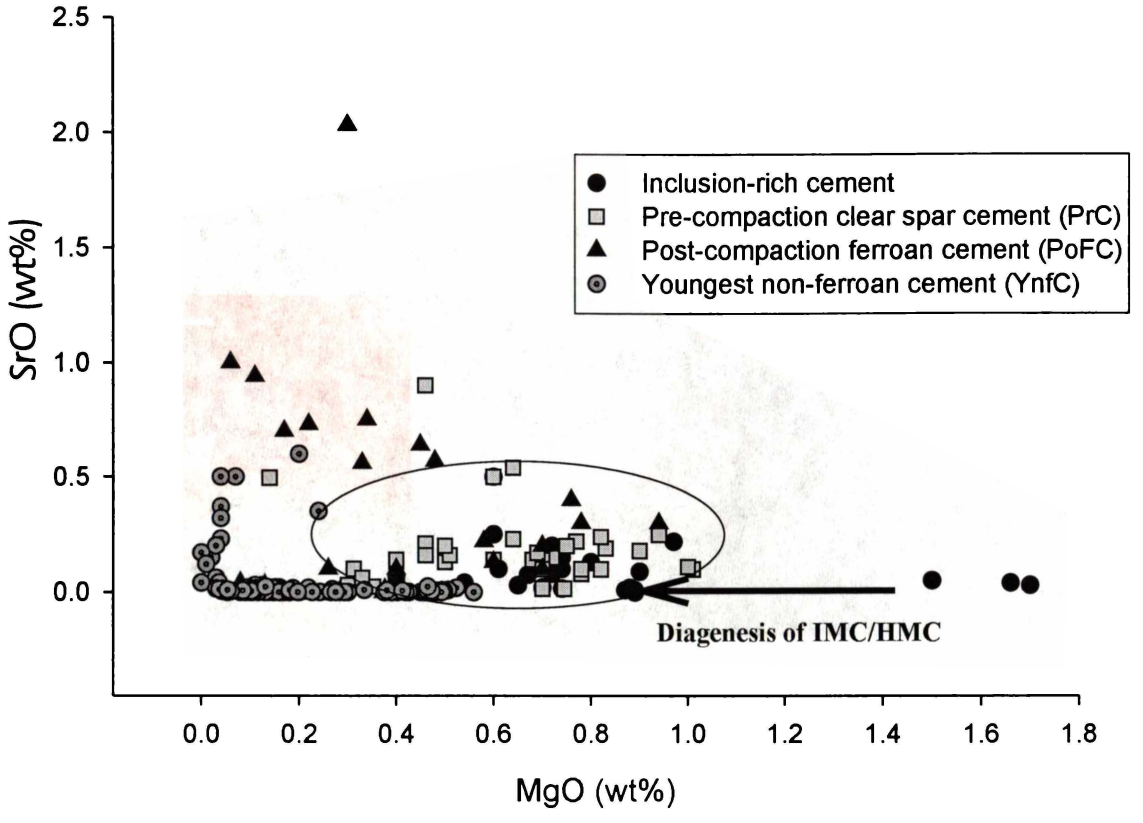

Figure 9- Cross-plot of the MgO and SrO contents of cement phases in the diagenetic suite from pre-compaction inclusion-rich fibrous cements to latest telogenetic YnfC. Inclusion-rich cements contain variable MgO concentrations (see Table 1). The decrease in MgO is attributed to increasing degree of neomorphism, and trends toward the MgO values held by primary LMC youngest non-ferroan cement (YnfC) interpreted to have formed in the meteoric environment. These data suggest that inclusion-rich cements were originally composed of IMC (possibly HMC) and were altered to LMC, probably during the precipitation of PrC cements. Indeed, the latter have intermediate MgO contents (circled) between the highest values associated with inclusion-rich cements and the lowest values yielded by meteoric YnfC. These data are consistent with petrographic observations that indicate that inclusion-rich rinds, when enclosed within larger PrC crystals, were stabilized during this cementation phase, interpreted to originate either in the meteoric environment or in the mixing zone.

cements, and micritic matrix surrounding overgrowths, all features recognized in the Te Aute carbonates (Figures 5C, 5D, 5F).

Besides their inferred IMC-HMC mineralogy, the following additional matters lend support for the interpretation of turbid cements as a product of marine diagenesis:

(a) The presence of solid (organic?) inclusions in these cements suggests turbid pore fluids, which is atypical of sub-surface mixing zone and meteoric environments, but typical of marine fluids replete with organic debris and other suspended debris.
(b) In the earliest stages of the chronological sequence of cementation, turbid cements always occur associated with marine internal sediments.
(c) Bulk samples and cement microsamples including inferred turbid IMC-HMC are the most enriched in ^{18}O. The heaviest value from one extracted microsample of turbid rind gives a $\delta^{18}O$ value of $-0.44‰$PDB that falls in the field of $\delta^{18}O$ values of unaltered brachiopod shells (Figure 6; Table 1).
(d) Their occurrence at stratigraphic locations within sediments deposited under high-energy conditions and low accumulation rates, suggesting strong marine water pumping through the sediments, and/or abundant water circulation, all factors that greatly favoured CO_2 degassing and enhanced pervasive cementation on or beneath the sea floor.

4.3. Clear spar cements

A dual approach has been taken for the description of clear spar cements: (1) textural - morphologic types of clear cements are recognized, and their paragenetic relationships to neighbouring microfabrics assessed; and (2) compositional - internal zonations of clear cements as revealed under cathodoluminescent light and through the use of artificial stains are grouped into discontinuity-bounded CL sequences tentatively mapped geographically (see Chapter 5, Section 4.2), and related to major stages of the host sediment diagenetic history.

4.3.1. Cement types

Calcite spar and microspar cements are the dominant interstitial crystalline components in the Te Aute carbonates. They can be meaningfully described in terms of their clarity, and crystal and zonal morphologies. Clear spar cements appear in a variety of crystal

forms whose development is controlled, among other factors, by the size of pore spaces: (1) microgranular spar >10 μm in size in the shape of small equant to subequant projecting crystals with subhedral forms termed blocky or "stubby" (see Glossary in Appendix 10); (2) coarse spar 0.1-1 mm in size having variable shapes, including scalenohedra or "dog-teeth" (Figures 10A, 10E, 10F), needles (Figures 11A-C), blades (Figure 10B), mosaics of interlocking crystals of various size (Figure 10C), and syntaxial cement rims about echinoderm particles (Figures 10D, 11E, 11F); and (3) poikilotopic cement sized between 0.1 and 2 mm that typically engulfs adjacent skeletal and non-skeletal grains.

Pre-compaction spar cements comprise scalenohedral, bladed palisadic, blocky to mosaic, and syntaxial crystal forms, while post-compaction cements are mostly characterized by syntaxial overgrowths, and blocky to mosaic and poikilotopic spars.

In the chronology of pre-compaction cement suites, scalenohedral cements (or dog-tooth cements) syntaxially overgrow the turbid acicular cements (Figure 3D). In the absence of early isopachous turbid rims, bladed epitaxial crystals arranged in a palisade fashion and blocky ("stubby") inclusion-free sparry calcites constitute fringes coating skeletal fragments.

Fine equant spar crystals and mosaic spar are substrate independent and nucleate upon: (1) internal sediments; (2) the exterior surface of older isopachous fringes (clear or turbid); and (3) the interior surface of biomoulds and fractures, forming in some cases a drusy fabric (Figure 10F). Typically, mosaic clear spar occludes the remainder of pore spaces (Figure 10C).

4.3.2. Compositional zoning of clear spar cements

By contrast with early turbid cements whose patchy luminescence reflects chemical alteration during later diagenetic processes (see Section 4.2.4), the homogeneous luminescence and compositional zonations of sparry calcite cements are assumed to be primary features. The zonations reflect the different stages of cement growth influenced by changes of the pore fluid chemistry (Dickson, 1965; Grover Jr and Read, 1983; Dorobek, 1987; Emery and Dickson, 1989; Meyers, 1991).

4.3.3. Chemical staining versus cathodoluminescence

The comparison of crystal zones recognized through the use of cathodoluminescence and artificial stains has shown that cathodoluminescence enables distinction of more and finer growth zones than does chemical staining. Thus, in many cases groups of subzones observed under cathodoluminescence are correlated to larger zones revealed by stains.

4.3.4. Growth patterns

Concentric banded growth stages of spar crystals correspond to discrete diagenetic changes, and can be hierarchically divided into luminescent zones and subzones.

Luminescent subzones correspond to the thinnest divisions observed under cathodoluminescence. Each subzone represents one stage of crystal growth in the course of which the physicochemical conditions supposedly remained more or less the same. The limit between two subzones can be sharp or progressive depending on the evolution of the pore-fluid chemistry (Meyers, 1978, 1989, 1991; Walkden and Berry, 1984).

Luminescent zones correspond to a group of subzones or to thick homogeneous luminescent stages. Because subzones are often complex, their description and analysis are sometimes better simplified. Indeed, subzones exhibit locally rhythmic features of luminescence corresponding to very fine repetitions of the same basic couplet of subzones, such as thin bright yellow and black. In such a case the rhythmites of luminescence are referred to as "zones".

Although each zone may potentially represent a time correlative discrete period of cementation, in the Te Aute rocks experience has shown that only bounding diagenetic discontinuities (including dissolution surfaces, fractures, and renucleation surfaces) have proved to be confidently traceable vertically within a measured section, and laterally between measured sections, so defining intervening CL sequences (see Chapter 2, Section 4.3).

4.3.5. Pre- and post-compaction clear spar cements: PrC, PoFC, and YnfC

Pre-compaction and post-compaction diagenetic histories of each Te Aute limestone, ranging from late Opoitian to Mangapanian (and possibly early Nukumaruan) in age, are generally characterized by three successive generations of calcite spar precipitates

Figure 10 – Photomicrographs of clear spar cements

(A) Dogtooth cement (arrowed) coating bivalve and barnacle grains. Note that this LMC cement did not form upon the partly altered aragonitic shell in the centre. PL: Sample 7.3 (Rotookiwa Limestone).

(B) Bladed palisadic cement (black arrow) about a molluscan valve fragment. Cement grew in optical continuity with oriented skeletal substrate. White arrow points at the undulose extinction front. CN: Sample 4.127 (Kairakau Limestone).

(C) Mosaic spar occludes enlarged pore after the remaining envelope of dissolved aragonitic shell fragment (dashed line) collapsed, accumulating debris (arrowed) that floors the former pore space. PL: Sample 7.17 (Rotookiwa Limestone).

(D) Syntaxial overgrowth (s.o.) about echinoderm grain (e) – Note that the pale blue overgrowth abuts against the ghost margin of former aragonitic shell, whereas the pale pink syntaxial phase partly fills the open mould. This suggests that dissolution probably pre-dates the pale pink zone. PL: Chemically stained sample 7.17 (Rotookiwa Limestone).

(E) Scalenohedral cement (black arrow) – This cement post-dates compaction-induced skeletal (bivalve) fracturing as indicated by tiny dark grey (blue stain) crystals covering the walls of the fracture (white arrow). PL: Sample 4.60 (Kairakau Limestone).

(F) Drusy spar about calcitic bivalve and coating the internal walls of dissolved former aragonitic grain – Note the crystal enlargement towards pore centre (black arrows), either outwards from grain substrates or from the interior walls of biomoulds. Intergranular drusy crystals exhibit a scalenohedral termination. PL: Sample 4.67 (Kairakau Limestone).

(G) Isopachous equant spar cement (arrowed) fringes barnacle grains, followed by homogeneous micrite and later dissolution of probably aragonite skeletons (top right corner). PL: Sample 11.22 (Mason Ridge Formation).

(H) Closely packed lozenge-shaped crystals (arrowed) form an isopachous fringe around calcitic bivalve fragments. CN: Sample 6.5 (Pakipaki Limestone).

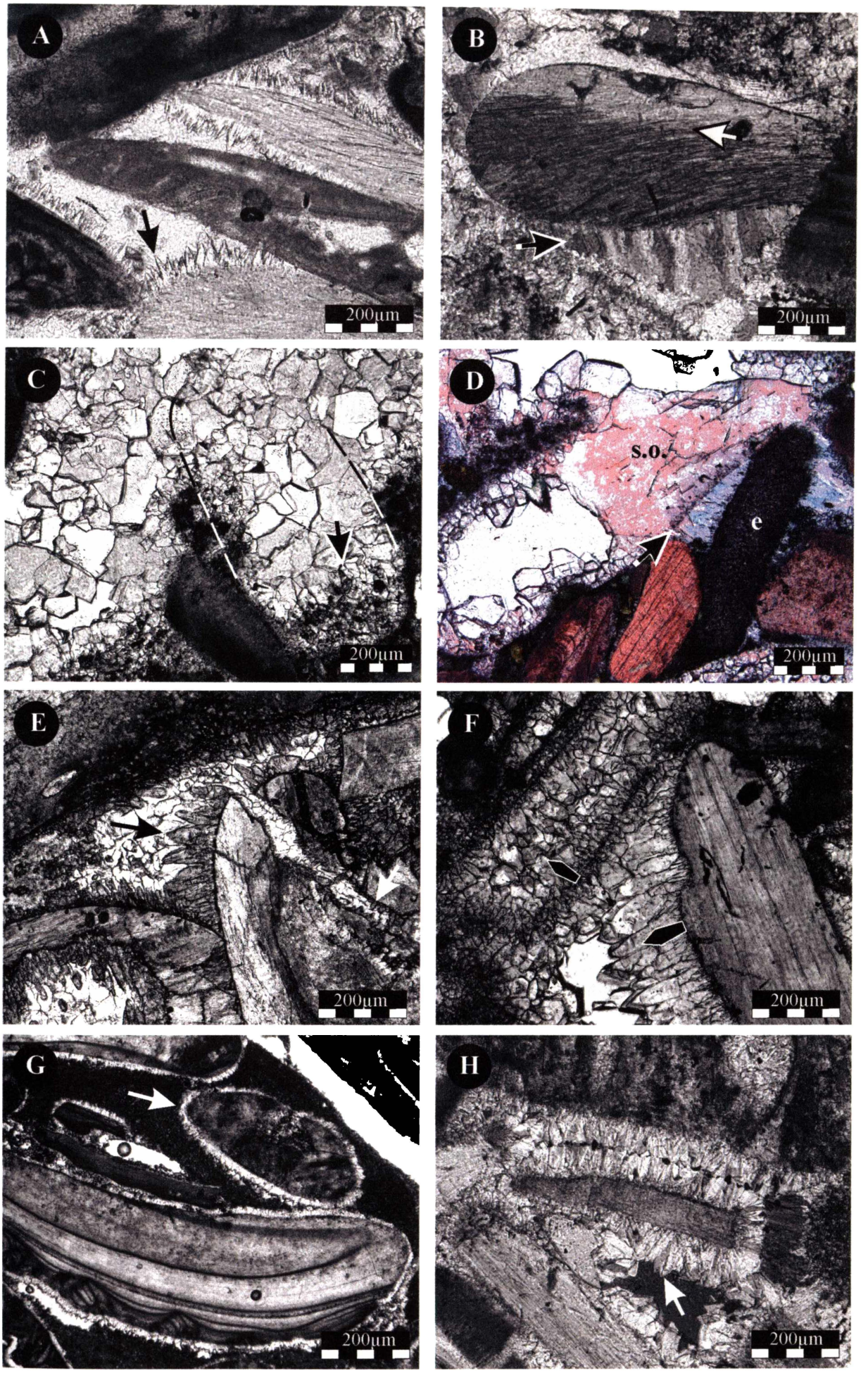
A
200µm
B
200µm
C
200µm
D
s.o.
e
200µm
E
200µm
F
200µm
G
200µm
H
200µm

having distinctive cathodoluminescence, chemical staining, and geochemical attributes, each generation being separated by correlative diagenetic discontinuities.

The first generation either constitutes the first cement in the pore space, or overgrows early turbid fringes, and systematically pre-dates compaction-induced skeletal fractures. First generation spar cements commonly coat walls of secondary pores (mouldic voids), and are represented by clear scalenohedral to mosaic calcite spar and syntaxial overgrowths. They are non- to slightly ferroan (N = 41; FeO = 0 to 0.43 wt%, mean = 0.16 wt%; stain pink to pale mauve) and are typically non-luminescent (e.g., their low MnO content; N = 41, 0 to 0.05 wt%, mean = 0.016 wt%), even though the spar may display orange and bright yellow internal subzones.

Generation 2 cements represent the first stage of post-compaction cementation, and consist of fine to coarsely crystalline (scalenohedral to drusy), faintly subzoned, brown to orange, moderately to dull luminescent spar. Generation 2 cements are generally ferroan, especially within the Kairakau Limestone (N = 20; FeO = 0 to 1.25 wt%, mean = 0.3 wt%; stain mauve, pale to deep blue), and fill compaction-induced skeletal fractures and spalled early cement rims.

This simple two-stage "cement stratigraphy" has been widely recognized in many ancient carbonates (Meyers, 1978; Grover Jr and Read, 1983; Niemann and Read, 1988; Tucker and Wright, 1990; Lavoie and Bourque, 1993; Hood and Nelson, 1996), and Meyers (1991) proposed to designate the two generations by the terms Older Banded Cements (OBC) and Younger Ferroan Cements (YFC), respectively. This cement terminology was not used in the present study because it does not adequately describe cement generations 1 and 2. The CL of generation 1 cements rarely displays CL bands or zones, but rather is usually homogeneous (Figure 12). Therefore, the term pre-compaction clear spar cement, abbreviated PrC, is proposed to designate this non- to (locally) slightly ferroan, non-luminescent cement generation.

According to Meyers (1991), YFC can pre-date compaction, even though they are more commonly fracture-hosted. To prevent this inconsistency, generation 2 cements are here referred to as post-compaction ferroan cements, abbreviated PoFC (Figures 12A-E).

The third generation of calcite spar may locally represent the volumetrically dominant cementation phase, occluding 50-80% of the total pore space (primary and secondary porosity). In most cases, this final void filling is usually clear, relatively

Figure 11 – Photomicrographs of clear spar cements (Continued)

(A) Isopachous rinds of lozenge spar cement (arrowed) coat calcitic (LMC) skeletons (Ba = barnacle; Bi = bivalve; Br = Bryozoan), whereas needle cement grows upon aragonitic substrates (top left corner). PL: Sample 6.5 (Pakipaki Limestone).

(B) Illustration of substrate selective fabrics – Note contrasting crystal morphology on either side of bivalve fragment (Bi). First-generation needle cement (aragonite? arrowed) is enclosed within second-generation LMC larger crystals. PL: Sample 6.5 (Pakipaki Limestone).

(C) Unaltered needle cement exhibits in places an undulose extinction reflected by the dark light cone-shaped appearance of the crystals (white arrow). Fibre relics that grew in optical continuity with, and normal to, their substrate show a uniform extinction. Note that calcite crystals of quite different extinction angles replace different segments of the length of needles (black arrows). CN: Sample 6.5 (Pakipaki Limestone).

(D) Non-ferroan (pale pink) pre-compaction blocky to scalenohedral cement (PrC) pre-dates post-compaction ferroan (pale blue) cement (PoFC). PoFC being the first cement generation that fills biomoulds (M), probably is contemporaneous with dissolution of skeletons. PL: Chemically stained sample 17.14 (Scinde Island Limestone).

(E) Syntaxial cement overgrowth upon echinoderm clast (e) has recorded a complex history of pore-fluid changes, ranging from marine (turbid cement = t.c.) to telogenetic/meteoric (YnfC), via meteoric or mixed marine-meteoric oxidizing (PrC), and reducing burial waters (PoFC). PL: Chemically stained sample 2.8 (Titiokura Formation).

(F) Similar diagenetic suite to that in (E), but without PrC. PL: Chemically stained sample 7.17 (Rotookiwa Limestone).

(G) Similar diagenetic suite to that in (F). Note that telogenetic YnfC is pre-dated by dissolution underlain by iron-stained silt at the boundary between PoFC and YnfC. PL: Chemically stained sample 5.74 (Awapapa Limestone).

(H) Pore-filling succession of cement phases records the transition (along the arrow) from Fe-enriched reducing fluids (deep blue) to more oxidizing waters (pale mauve) following probable progressive uplift. PL: Chemically stained sample 15.5b (Te Waka Formation).

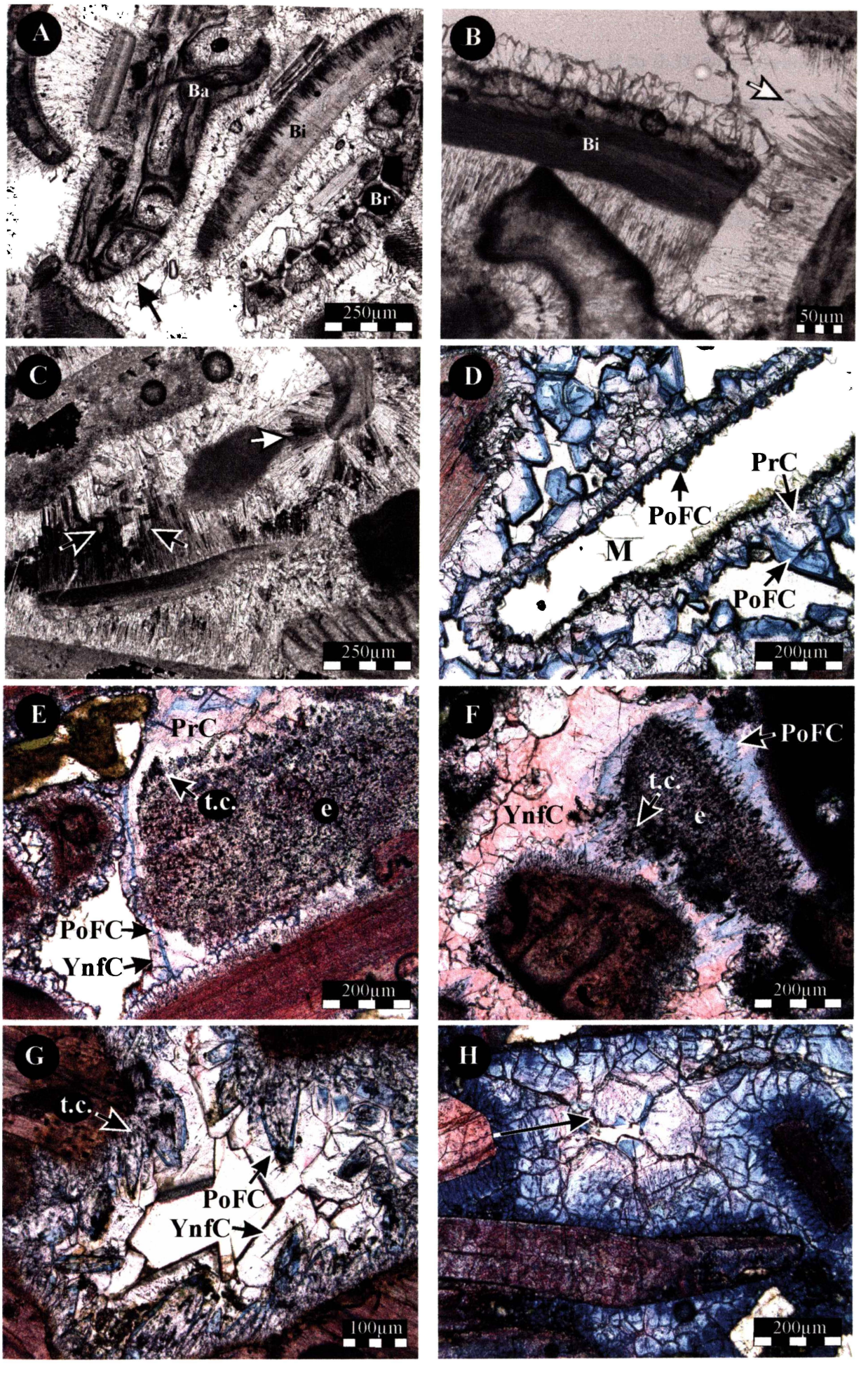
A
Ba
Bi
Br
250µm
B
Bi
50µm
C
250µm
D
PrC
PoFC
M
PoFC
200µm
E
PrC
t.c.
e
PoFC
YnfC
200µm
F
PoFC
t.c.
YnfC
e
200µm
G
t.c.
PoFC
YnfC
100µm
H
200µm

coarse, blocky to mosaic, non-ferroan calcite (N = 113; FeO = 0 to 0.31 wt%, mean = 0.05 wt%), which post-dates uplift-induced fractures and/or a correlative dissolution "event". Generation 3 cements have similar cathodoluminescence properties to those of PrC, and commonly start with a thin bright orange/yellow zone (up to 20 μm) that sharply passes into a thick non-luminescent zone further porewards (Figure 12B). In the present study, generation 3 cements are termed Youngest non-ferroan Cements (YnfC).

The traceability of the diagenetic discontinuities bounding PrC, PoFC, and YnfC indicate that these successive cement generations are widespread throughout a given formation, both vertically and laterally, even though some early building zones of PrC may be restricted to a few metres beneath subaerial discontinuities.

The cement generations are usually too thin to be confidently sampled individually, so that stable oxygen and carbon isotope values are available only for pre-compaction cements, including inferred marine turbid cements, and a few YnfC (Figure 6; Table 1). Bulk sample isotope analysis of pre-compaction cements (marine turbid cement and PrC) have yielded values (N = 6) ranging from $\delta^{18}O$ = –0.8 to –4.44‰PDB and $\delta^{13}C$ = 0.06 to –2.4‰PDB. Moderately depleted $\delta^{18}O$ composition (N = 7; -5.0 to –3.1‰PDB) of YnfC cements is coupled with also moderately depleted $\delta^{13}C$ values (–8.2 to -2.1‰PDB) (Table 1; Figure 6). Mineralogically, PrC, PoFC, and YnfC are low-Mg calcite.

4.3.6. Diagenetic environment for PrC, PoFC, and YnfC cements

PrC (pre-compaction clear spar cement)

The environment of precipitation of early non-luminescent cements that post-date inferred marine turbid cements remains controversial (e.g., Meyers, 1991), even though in the present study a burial environment at depth where compactional processes are triggered can be ruled out on the basis of the following evidence: (1) PrC are pre-compactional; (2) they pre-date pressure-dissolution; (3) their non- to low-ferroan mineralogy, and their occurrence early in the paragenetic suite, commonly post-dating the earliest dissolution fabrics, suggest that PrC formed from interstitial oxidizing waters with a starting composition undersaturated with respect to IMC, HMC, and aragonite; and (4) the few $\delta^{18}O$ and $\delta^{13}C$ data indicate that PrC did not precipitate from waters modified by burial. The Te Aute PrC most likely originated either in the shallow

Figure 12 – Cathodoluminescence of pre- and post-compaction clear spar cements

(A) Non-luminescent PrC is post-dated by compaction-induced fractures (white arrows) filled with orange luminescent ferroan cement (PoFC). Note that PrC is the first cement generation in biomoulds (black arrow). CL: Sample 4.65 (Kairakau Limestone).

(B) Same diagenetic suite as in (A), but post-compaction fracture-hosted (white arrows) PoFC is cross-cut by uplift-related fractures (black arrow) followed by thin orange subzone and latest non-luminescent, non-ferroan, banded YnfC. CL: Sample 4.127 (Kairakau Limestone).

(C) YnfC post-dates uplift-related fracturing (white arrow) and is the dominant cement phase occluding pore space after thin post-compaction PoFC (black arrow). CL: Sample 7.18 (Rotookiwa Limestone).

(D) Same suite as in (B). Note that latest YnfC exhibits a contrasting luminescence pattern (non-luminescent to bright yellow). CL: Sample 4.93 (Kairakau Limestone).

(E) Dissolution surface (black arrow) separating pre- and post-compactional (white arrows) calcite cements, PrC (black to dull brown luminescence) and PoFC (orange to bright yellow) respectively. Post-uplift cement (YnfC) is typically non-luminescent. CL: Sample 5.25 (Awapapa Limestone).

(F) Plain light photomicrograph of same field of view as in (E). Note compaction-induced fracture (arrowed). PL: Sample 5.25 (Awapapa Limestone).

(G) - (H) Abrasion and microbored surface (arrowed) within syntaxial overgrowth as seen under CL and plain light. Abraded cement is first generation PrC and is overgrown by post- (final) deposition PrC and post-compaction PoFC. CL/PL: Sample 4.70 (Kairakau Limestone).

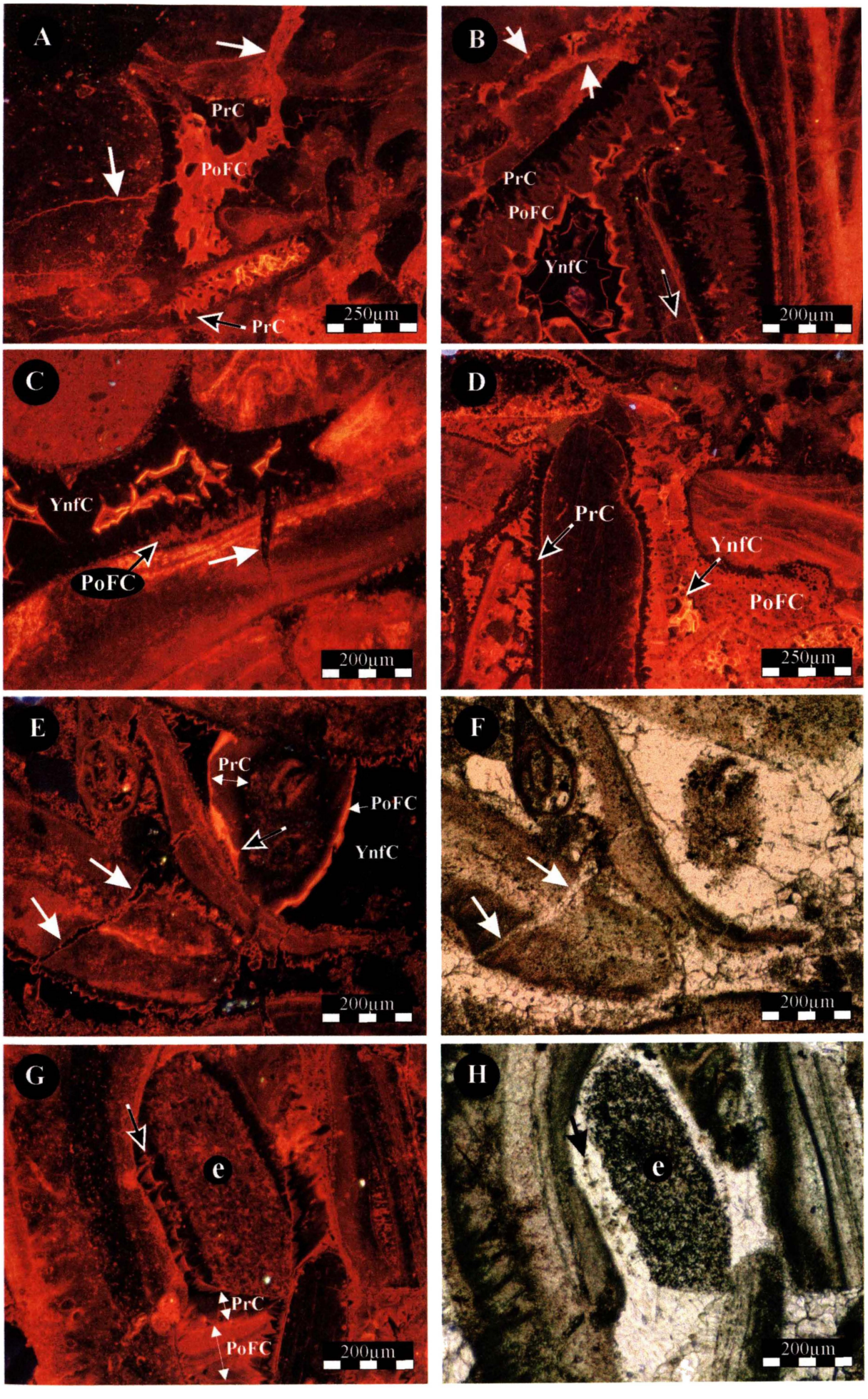
A
PrC
PoFC
PrC
250µm
B
PrC
PoFC
YnfC
200µm
C
YnfC
PoFC
200µm
D
PrC
YnfC
PoFC
250µm
E
PrC
PoFC
YnfC
200µm
F
200µm
G
e
PrC
PoFC
200µm
H
e
200µm

subsurface (tens of metres) marine or meteoric phreatic environments, origins that have commonly been invoked for these controversial precipitates.

Interpretation

Hypothesis 1: PrC = marine to shallow subsurface marine precipitates

A marine to shallow subsurface marine origin has previously been envisaged for early non-ferroan, non-luminescent, clear calcite cements on the basis of the presence of some microdolomite inclusions, and relatively high $\delta^{18}O$ and $\delta^{13}C$ values compared to later stage calcite precipitates (Wilkinson *et al.*, 1985; Kerans *et al.*, 1986; Lavoie and Bourque, 1993; Zempolich and Erba, 1999). In the Te Aute successions, low-Mg calcite PrC overlie inferred IMC-HMC marine cements (Figure 11E). They are not interstratified either with marine cements (with the single exception of one sample from the Pakipaki Limestone; Figures 5G, 5H) or with internal marine sediments that could otherwise argue for a marine origin. Further, it is difficult to envisage how marine waters would precipitate IMC-HMC marine cements in spatially restricted horizons (Section 4.2.5), but subsequently LMC cements distributed throughout formations and extending laterally over several kilometres (even though not necessarily synchronous; see Chapter 5, Section 4.2.2).

A shallow subsurface marine origin for the Te Aute PrC cements is partly supported by isotopic and trace element evidence. The heavy relatively enriched and narrow range of $\delta^{13}C$ values and the more depleted $\delta^{18}O$ values for bulk pre-compaction cements (including PrC) compared to the brachiopod shells (Figure 6) fall in the range of values determined from spar cements inferred to have precipitated from marine or mixed marine-meteoric fluids modified by burial (Nelson *et al.*, 1988c; Lavoie and Bourque, 1993; Group 1 cements of Nelson and Smith, 1996). Non-ferroan, non-luminescent cements contain relatively high amounts of MgO (N = 41, 0.1 to 1.01 wt%, mean = 0.57 wt%), slightly lower than early inclusion-rich cements, but much greater than later stage cement varieties (Table 1; Figure 7).

The relatively depleted $\delta^{18}O$ values could be explained by the progressive rise in temperature of pore waters during sediment burial. In the Te Kuiti limestones, Nelson *et al.* (1988c) demonstrated that variations in $\delta^{18}O$ were due to temperature-related fractionations associated with the geothermal gradient. However, precipitation of PrC, say 2.0‰ depleted from $\delta^{18}O$ marine (brachiopod) calcite, would require an increase in

burial temperature of 6-8 °C (Nelson *et al.*, 1988c; Meyers, 1991). Assuming a geothermal gradient of ca. 20 °C/km, this translates to subsurface depths between 250 m and 350 m. At this range of depths, poorly cemented skeletal sediments are likely to display extensive mechanical compaction features (Meyers, 1980; Nicolaides and Wallace, 1997b; Figure 19), incompatible with the pre-compactional nature of PrC.

Nonetheless, a shallow subsurface marine hypothesis cannot be totally ruled out because: (1) the relatively high MgO content of the clear spar calcite, consistently exceeding 0.25 wt%, is supportive of a non-meteoric origin (Meyers and Lohmann, 1985); and (2) the relatively heavy $\delta^{13}C$ values are more compatible with a shallow marine burial or mixed marine-meteoric signature than with a meteoric signature. Isotopic data at the cement scale for each limestone formation are so far insufficient to yield a satisfactory isotope-based interpretation for the early inclusion-free spar cements.

Hypothesis 2: PrC = meteoric phreatic precipitates

A meteoric phreatic origin is frequently invoked for PrC in modern (Major and Wilber, 1991) and ancient deposits (Niemann and Read, 1988; Horbury and Adams, 1989; Walkden and Williams, 1991). A similar origin could be envisaged here for the Te Aute PrC, and is compatible with the following evidence:

(a) The precipitation of PrC is both coeval with, and post-dates, dissolution fabrics of calcite and aragonite allochems (Figure 12A). Such fabrics in shallow-water facies frequently result from the percolation of meteoric waters undersaturated with respect to calcite and aragonite.
(b) PrC are pre-compactional cements.
(c) The depletion of $\delta^{18}O$ compared to the inferred marine signature could be the result of precipitation from isotopically depleted meteoric waters (Niemann and Read, 1988; Meyers, 1989; Saller and Moore Jr, 1991).
(d) The regional distribution of PrC, and their relatively increasing abundance up section in coarsening- and shallowing-upwards deposits, suggest that these non-luminescent cements could have formed from extensive meteoric aquifers beneath unconformities that developed during regional regression (see Chapter 5, Section 4.4).

This scenario is supported by the development, since late Opoitian - early Waipipian, of subaerially exposed (uplifted) coastal hills to the east of the forearc basin (Beu, 1995)

that could have acted as recharge areas for meteoric waters involved in early PrC formation (Chapter 5, Sections 4.1, 4.3.1).

Relatively high MgO values with respect to later diagenetic stages could result from an enrichment of pore waters in Mg cations released during degenerative neomorphism of former IMC-HMC skeletons and cements in contact with meteoric fluids (buffering). It can be envisaged that if the water/rock ratio during meteoric stabilization of IMC-HMC turbid cements is low then the Mg/Ca ratio of the diagenetic fluid can approach that of the dissolving phase (Figures 7A, 9). The MgO content of some PrC, overgrowing turbid cements, could imply formation of this phase under at least partially closed conditions during IMC-HMC stabilization. The same process has been envisaged to explain the high SrO content in clear blocky spars following aragonite stabilization (Tobin and Walker, 1998).

Relatively high $\delta^{13}C$ were measured on various microsamples, some including marine fibrous cements. The $\delta^{13}C$ values of PrC have probably been influenced by both the heavier $\delta^{13}C$ isotopic signature of neomorphosed marine cements and dissolved shell material in the sediments (Figure 6). It can be argued that as meteoric fluids penetrated the subsurface from a recharge area located somewhere eastward, and percolated through the sediments, increasing rock-interaction progressively enriched the $\delta^{13}C$-depleted meteoric pore water due to contributions from dissolution of carbonate clasts (Lohmann, 1988; South and Talbot, 2000). Precipitated cements would therefore inherit this isotopic signature. More investigation is needed so as to assess whether there exists a definite trend towards increasing $\delta^{13}C$ values from the eastern to the more basinward PrC in each formation deposited on the eastern margin of the forearc basin.

PoFC (post-compaction ferroan cement)

This variety of cement occurs mainly in the Opoitian, Waipipian, and Mangapanian limestone formations (Figure 1). To the east of the forearc basin, PoFC are generally thin (< 50 μm), even though they may locally be more prevalent than later YnfC in the oldest Kairakau Limestone (Opoitian) where they can totally occlude former interparticle porosity. To the west, PoFCs dominate in the Te Waka Formation (Waipipian-Mangapanian; Figure 11H), where they also commonly form the initial cement stage. PoFCs are poorly developed in the Nukumaruan limestones, and are locally absent in the upper limestone sheet of Mason Ridge Formation, and in the Matapiro Limestone.

Chemical staining identifies moderate to high concentrations of ferrous iron, which is partly supported by the few available electron microprobe spot analyses (Table 1; Figure 7A) that yielded FeO values ranging from 0 to 1.25 wt% (N = 20, mean = 0.3 wt%). These values are higher than both the older inclusion-rich and PrC, and the younger YnfC (Figure 7A). SrO concentrations are higher than that of pre-compaction cements (0 to 2.03 wt%, mean = 0.4 wt%; Figure 7B), but MgO is depleted (0.06 to 0.94 wt%, mean = 0.4 wt%) and MnO is slightly enriched (0 to 0.65 wt%, mean = 0.04 wt%) in comparison (Table 1). PoFC could not be isolated for isotopic analysis.

Former HMC skeletons (mainly echinoderms) showing evidence of chemical alteration have similar trace element geochemistry to that of PoFC, but higher FeO content (N = 11, mean = 0.7 wt%; Table 1), which could indicate that dissolution of some HMC grains was contemporaneous with precipitation of PoFC.

Interpretation

The interpretation of PoFCs, which include dull and moderately luminescent spar cements (Figure 12), is straightforward by comparison with non-ferroan PrCs. They conform to the attributes of mesogenetic products (Choquette and James, 1990), even though their FeO content is generally lower than has been reported from other studies of similar carbonate cements (Meyers, 1978; Haywick, 1990; Franck *et al.*, 1995). Their chemistry necessitates that they precipitated from pore fluids enriched in iron and dominantly reducing. Ferroan cements post-date compaction and fracturing, and commonly immediately follow in the cement suite a thin orange or bright yellow zone (Figures 12D, 12E), which is coeval with mechanical compaction. The succession from pre-compaction non-ferroan, non-luminescent cement (PrC) to post-compaction ferroan, dull-luminescent cement (PoFC) via an interlayered transitional brightly luminescent zone has been recognized in a number of cathodoluminescence studies (Grover Jr and Read, 1983; Niemann and Read, 1988; Moore, 1989; Meyers, 1991). The succession has been interpreted to record the transition from dominantly oxidizing meteoric or mixed marine-meteoric cementation to dominantly reducing burial cementation.

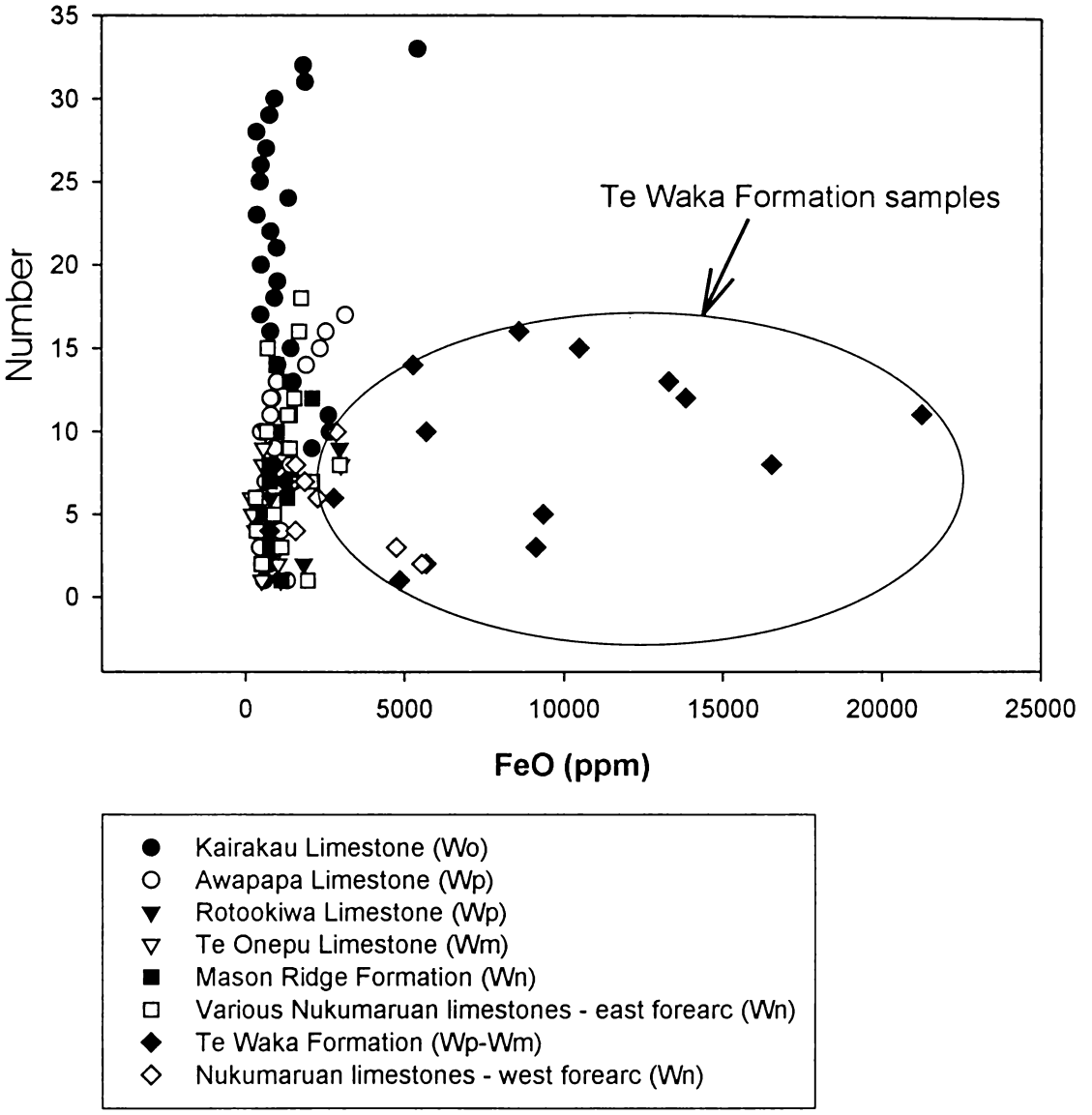

Figure 13- ICP-OES measurements of FeO contents in bulk samples of limestones ranging in age from Opoitian to Nukumaruan. The majority of samples have a FeO content <2500 ppm. The proximity of Te Waka Formation to a terrigenous source translates in a wide range of FeO values (2500 to 22000 ppm). See text for discussion.

Therefore, post-compactional ferroan cements are interpreted to have formed during burial when pore waters were shut off from recharge by oxidizing meteoric or mixed marine-meteoric waters. Not surprisingly, ferroan cements (PoFC) are better developed in the older limestones, which have experienced deeper burial than their younger counterparts which may even lack these precipitates. In the Te Waka Formation (Waipipian-Mangapanian) in the western part of the forearc basin, where there is a high content of terrigenous sediment, PoFC are the most enriched in iron and stain deep blue with Dickson's solution as a result (Figure 11H). ICP-OES analyses of bulk samples from Te Waka Formation confirm this observation and indicate very high iron concentrations, well above those from eastern Opoitian and Waipipian formations (Figure 13). In the latter, ferroan cements stain pale blue and mauve, indicative of relatively moderate iron contents as confirmed by microprobe measurements. Moderate FeO concentrations are not uncommon in burial cements. Nelson *et al.* (1988c) have documented comparable values in inclusion-free spar cements interpreted to be of burial origin, and related these low values to a greater isolation of the carbonate depositional setting from a terrigenous influence.

YnfC (youngest non-ferroan cement)

The youngest non-ferroan cements generally represent the dominant cementation phase in limestones ranging in age from Waipipian to Nukumaruan, locally accounting for up to 90% of the total cement within the youngest limestone formations. More usually, the YnfC comprise about 50-60% of the total cement.

YnfCs are generally non-luminescent (Figure 12), but may display in their early and latest growth stages orange and brightly yellow luminescent zones (Figures 12C, 12D). YnfCs post-date all previously described cements and in the Nukumaruan limestones may represent the first cement in the pore space having CL attributes otherwise like PrC. Typically, YnfCs are coeval with, and post-date, dissolution producing moulds and an irregular surface engulfed within older cements (when present), and fracturing. Further, the geochemistry of YnfCs contrasts significantly from older cements in being (1) more depleted with respect to $\delta^{13}C$ and $\delta^{18}O$ (Figure 6); and (2) strongly depleted relative to MgO, MnO, FeO, and SrO (Table 1; Figures 7, 8). This suggests that YnfCs have formed from near-surface, oxidizing groundwaters.

Interpretation

Therefore, YnfCs are interpreted as a meteoric phreatic phase of calcite cement precipitated in the time interval during which carbonate sediments that had been buried (mesogenetic zone producing PoFC) were tectonically exhumed (uplift) to once again be influenced by surficial processes (telogenesis). Uplift continued after these cements had developed to eventually expose the carbonate deposits (now transformed into limestones) to the most surficial diagenetic processes in the vadose meteoric environment. This latest stage is also pre-dated by fracturing and dissolution, and the remaining porosity is filled with pendant cements and geopetal sediments (see Figure 15A), which occur within the first few decimetres beneath exposed surfaces. The Te Aute YnfCs conform with the characteristics of many late (post-burial) meteoric diagenetic cements that have been described in ancient carbonate deposits and interpreted as telogenetic products (Grover Jr and Read, 1983; Meyers, 1991; Lavoie and Bourque, 1993; Hood and Nelson, 1996).

4.3.7. Pseudo-PrC: early blocky and "lozenge-shaped" isopachous sparry calcite

Two distinct varieties of non-ferroan inclusion-free spar cement are referred to here as pseudo-PrC (pseudo-pre-compaction clear spar cement):

(1) Blocky cement consists of a thin (<50 μm) isopachous rind that coats skeletal grains, and is non-luminescent under CL. Unlike PrC, this clear spar fringe pre-dates homogeneous and microbioclastic micrite, which are presumably marine (Figure 10G), and is not associated with dissolution features. Blocky isopachous pseudo-PrCs constitute the first cements in the pore space of some well-cemented horizons within the Nukumaruan Mason Ridge Formation, but were not unequivocally recognized within older formations.

(2) Lozenge-shaped isopachous sparry calcite (Figures 10H, 11A, 11B) is restricted to a single well-cemented horizon within the Pakipaki Limestone (early Nukumaruan). It occurs as a palisade of densely packed lozenge-shaped crystals, which are typically of equal length and are orientated perpendicular to the substrate. Crystal extinction may be straight or undulose. Lozenge cement precipitated simultaneously with elongate needle-like crystals of possible original aragonite mineralogy (Section 4.3.8).

Lozenge cement is substrate specific and grew upon LMC to HMC substrates, while needle cement only grew upon the primary aragonite layers of shell fragments.

Interpretation

Although no isotopic and trace element analyses were performed on these cements, their habit and chronological position in the diagenetic suite suggests that they probably originated in a marine phreatic environment. Cements similar to the isopachous blocky rinds, interpreted to be primary marine precipitates, have been documented in a number of Paleozoic to modern carbonate sequences (e.g., Aissaoui, 1988; Frank *et al.*, 1995; Zempolich and Erba, 1999).

4.3.8. Needle cement

Needle cement has only been recognized in the Pakipaki Limestone (early Nukumaruan). Clear needle cement is made up of nearly parallel needle-like crystals oriented in picket fence style perpendicular to the substrate (Figures 11A to 11C). Individual needles average 2 to 7 μm in width, while their length is highly variable, depending on the pore space available, and thus may reach up to 0.5 mm long. Crystal termination is flat. Needles commonly grow as optically syntaxial extensions of their substrate. Consequently, undulose as well as uniform extinction of the cement occurs on adjacent grains with different oriented shell microstructures (Figure 11C). Needles may exhibit small angular divergences from being perpendicular to the substrate, which results in undulose elongate cone-shaped extinction. In contrast, individual needles exhibit a uniform extinction. Needle cement is substrate specific, growing exclusively on aragonitic shells (gastropods and unidentifiable bivalves) and the aragonitic layer of shell fragments, which display variable alteration fabrics, ranging from dissolution microcavities to coarse neomorphic calcite with retention of microstructures underlain by insoluble inclusions along primary lamellae (see Section 4.6).

In the larger pores, needle cement is engulfed in later generation coarse crystalline LMC cement. Needle cement is typically non-luminescent under CL light, even though rare elongate orange patches have been observed (Figure 5G). In one example, needle cement is overgrown by two generations of (presumably marine) isopachous fibrous turbid cement (Figures 5G, 5H). The X-ray diffraction analyses of whole samples comprising needle cements indicate calcitic (IMC-LMC) and aragonitic

mineralogies. Pakipaki Limestone carbonates are compositionally very similar to those from other Nukumaruan limestone formations that lack needle cements, both in terms of skeletal content and degree of alteration. However, diffractograms from these carbonates do not reflect this apparent comparability, but reveal much higher aragonite contents in the Pakipaki Limestone samples containing needle cement than in the needle cement-free samples from their Nukumaruan counterparts (Figure 14). This suggests that the differing aragonite contents could be due to the contribution made by the intergranular cement to the chemical composition.

Interpretation

Similar fabrics to that of the needle cement occur as aragonitic precipitates in modern and ancient reefs (James *et al.*, 1976; Sandberg, 1985), and in submarine hardgrounds (Illing, 1954; Shinn, 1969; James *et al.*, 1976; Sandberg, 1985). Substrate control of cement habit and mineralogy also conform to observations as reported by previous authors (James *et al.*, 1976; Sandberg, 1985), and would support a primary aragonite mineralogy for the needle cement. The high aragonite content of bulk samples including needle cements provides further evidence about the mineralogy of these precipitate.

In a few thin-sections, needle cement is poorly to moderately altered compared to the adjacent aragonitic grains. It does not meet the criteria that may confirm that, if aragonite, needle cement has been calcitized (Sandberg, 1985): (1) it generally lacks replacement coarse calcite crystals that cross-cut the relics of the original structure as documented in calcitized cements and skeletons (Sandberg and Hudson, 1983; Sandberg, 1985); (2) there are no relics ("ghosts") of needle cement entombed in larger calcite crystals (Mazzullo, 1980); (3) needle cement is not pseudopleochroic as noted in calcitized botryoid aragonite (Sandberg, 1985); (4) by contrast with the segmented fabric of needles in calcitized aragonite relics, the Te Aute needles are generally entire and continuous to the substrate; and (5) needle cement lacks evidence of dissolution, aside from rare dissolution microcavities filled with secondary-stage sparry calcite (Figure 5G).

If the needle cement is interpreted as an aragonitic precipitate that has retained both its mineralogy and microstructure, then it is evident that diagenetic processes have selectively transformed the aragonitic skeletons but preserved the aragonitic cements. Furthermore, shallow-water marine aragonite cements are thought to be good indicators

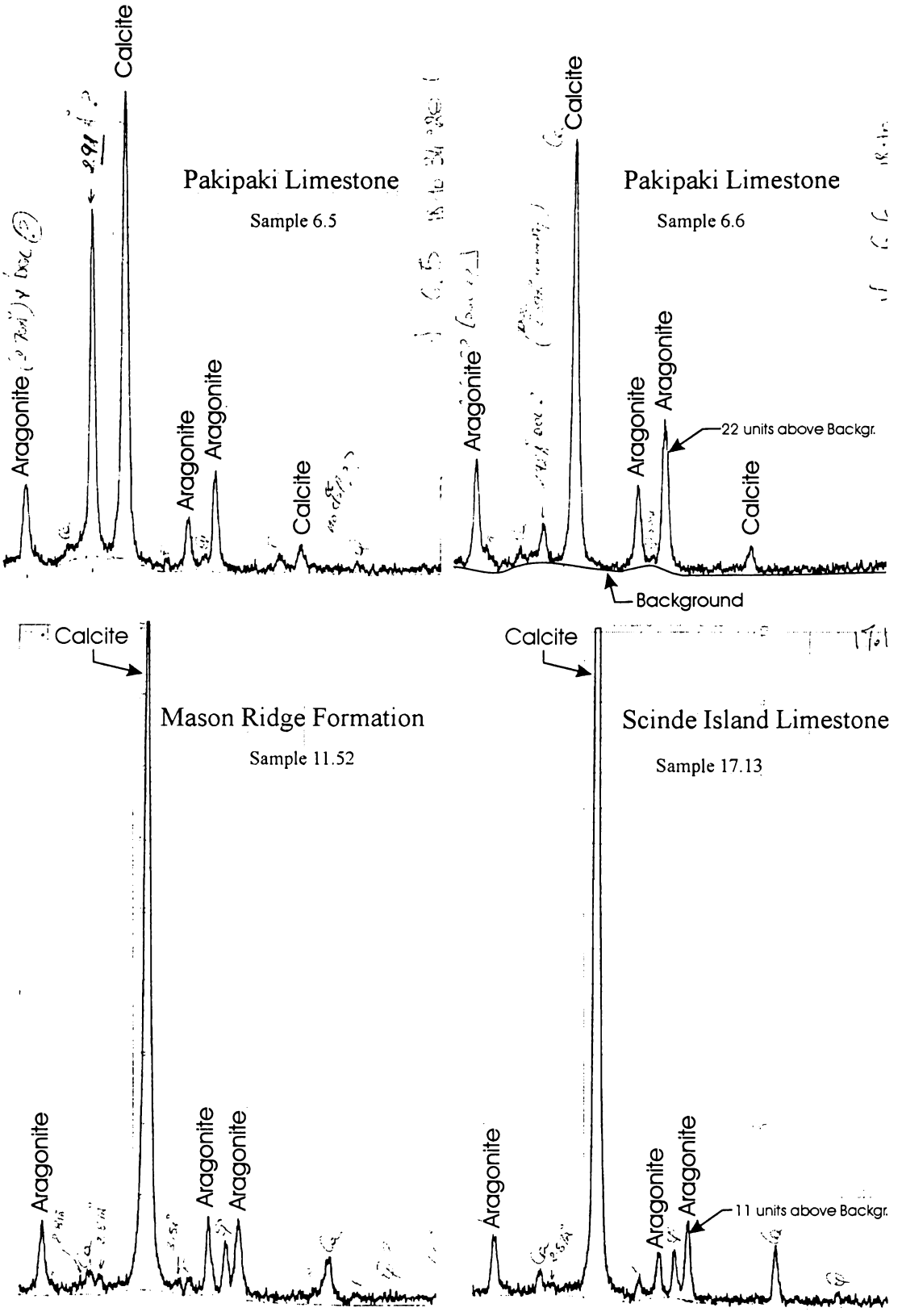

Figure 14- Differences in peak heights of aragonite between samples from Pakipaki Limestone and other Nukumaruan limestones are attributed to the cementing phase. Selected samples from Mason Ridge Formation and Scinde Limestone are texturally and compositionally (i.e., same amount of aragonite skeletons and same degree of alteration) similar to those from Pakipaki Limestone, but lack the intergranular needle cement that characterizes the latter. It is proposed that the needle cement is a former aragonitic cement that partly retained its original mineralogy.

of warm tropical waters oversaturated with respect to aragonite, which is seemingly incompatible with the cool-water depositional environment of Pakipaki Limestone. Indeed, Pakipaki Limestone has yielded several specimens of *Zygochlamys deliculata*, which is considered to be an excellent indicator of cold periods in New Zealand marine Late Pliocene and Early Pleistocene sediments (Beu, 1995).

However, preserved ancient aragonite cements have been reported in rocks that underwent later meteoric diagenesis (Shinn, 1969; Wendt, 1977; Sandberg, 1985). In these studies, unaltered first-generation needle fringe aragonite cement is encased in second-generation sparry calcite, and abuts against calcitized primary aragonitic skeletal substrates. The preservation of original mineralogy is a direct result of the engulfment of aragonite needles into stable calcite. Aragonite relics, once encased in larger low-Mg calcite crystals, can be isolated from diagenetic aggressive fluids and consequently can be retained barring remobilization of the surrounding spar (Mazzullo, 1980; Sandberg and Hudson, 1983).

For these reasons, and until further investigations (elemental analyses), it is proposed that needle cement is poorly altered first-generation aragonite cement that formed in shallow warm marine waters. Moreover, needle cement is in one case post-dated by marine turbid cement, which would argue for its marine phreatic origin. If confirmed, this interpretation would suggest that perhaps an especially warm interval of probable short duration has occurred during the overall cold early Nukumaruan stage during which Pakipaki sediments accumulated.

4.4. Internal sediments

4.4.1. Internal sediment types

Micritic and coarser detrital internal sediments are conspicuous features in the Te Aute limestones, frequently observed in horizons including inferred marine turbid cements. The term "internal sediment" refers to geopetally emplaced sediments and to sediments forming a geopetal fabric, whatever their allochthonous or autochthonous origin, that pre-date or post-date marine cements, and are distinguished from syndepositional micritic sediments occluding interparticle pore space.

Geopetal internal sediments examined in the present study can be grouped into six petrographically distinct microfacies, with all possible transitions (Figure 15): (1) homogeneous micrite, (2) microbioclastic micrite, (3) microquartz-rich micrite, (4)

matrix-free coarse detrital, (5) micropeloidal micrite, and (6) geopetal piles of broken micritic envelopes and so-called "vadose silts" (Dunham, 1969). These geopetal sediment types may co-occur within both primary (interparticle, skeletal cavities, internal chambers of bryozoan and foraminifers) and secondary voids (biomoulds and fractures).

Within such structures, consistent microstratigraphic successions include (1) coarsening-upward suites ranging from homogeneous micrite at the base grading into peloidal micrite and sparry overgrowth fabrics at the top (Figure 15C), and (2) fining-upward suites ranging from a lower layer rich in allochems that typically decrease in both size and abundance up-section (Figure 15D), and occasionally pass upwards into microbioclastic micrite and homogeneous micrite layers.

4.4.2. Origin and evolution of the geopetal microfabrics

The nature and abundance of skeletal and terrigenous components of internal sediments, the type of infilled voids, and the paragenetic relationships of such fabrics with inferred marine or diagenetic features were all used to constrain their early diagenetic environments.

Similarly, the timing of lithification of geopetal internal sediments is difficult to assess, but paragenetic relationships may provide useful indicators in this matter. For example, lithification is likely to originate from marine waters when inferred turbid cements overlie internal sediments (Figure 5A). Early lithification in either marine or meteoric diagenetic environments can be suspected when internal sediments post-date turbid marine cements and pre-date clear spar meteoric cements cut by compaction-induced fractures.

Three major processes are involved in the production of geopetal fabrics, summarized as follows:

Percolation of particles

Geopetally-emplaced internal sediments principally originate from particles in suspension that percolated downward within the host rock from the water-sediment (or air-sediment) interface. This suggests that active fluid exchange occurred between host inter- or intraparticle pores and the overlying water mass (or atmosphere). Particles filled in the bottom of pores or cavities under the influence of either gravity or interstitial fluid circulation (Kerans *et al.*, 1986).

In situ precipitates

Geopetal internal micrites may originate *in situ* due to early precipitation of calcite cryptocrystals, 4 μm or less in size, producing an unstructured or faintly laminated micritic interstitial material, which may serve as matrix and cement. Cryptocrystalline micrite generally grades up-section into coarsening-upward peloidal micrite, through clotted or vaguely peloidal fabrics (see below).

Such fabrics and initial homogeneous micrite, which are not necessarily associated with peloids, may produce laterally micritic envelopes, menisci, or protuberances (Figures 15F to 15H) towards empty pore spaces. These features have been widely recognized in the rock record, and have been interpreted to form through biogenically-induced calcification (Bathurst, 1966; Chafetz, 1986, 1992; Bernier and Dalongeville, 1988; Tucker and Wright, 1990; Hillgärtner *et al.*, 2001), and/or through various chemical processes (Shinn, 1969; Macintyre, 1984, 1985; Reid *et al.*, 1990; Wilber and Neumann, 1993; Nelson and James, 2000), either in the marine or meteoric diagenetic environments.

Diagenetic alteration of skeletons and carbonate cements

Early dissolution of metastable allochems by percolating waters undersaturated with respect to calcium carbonate can in some cases be associated with partial or total collapse of micritic envelopes which then accumulate at the bottom of pore spaces to produce geopetal fabrics with piles of lutite- to silt-sized debris (Figure 15E). In a few examples, iron-stained microspar crystals and mud fillings give a geopetal fabric comparable with "vadose silts", interpreted by Dunham (1969) to be meteoric vadose in origin. In either case, leaching and collapse took place prior to void filling by non-ferroan blocky to coarse mosaic clear spar that most likely relates to meteoric diagenetic processes (James and Choquette, 1990b).

4.4.3. Microclastic internal sediments

Microclastic internal sediments comprise microbioclastic micrites and microquartz-rich micrites (Figure 15D). Either fabric is a heterogeneous mix of a (now) LMC paste and silt- to clay-sized skeletal and non-skeletal detritus. Microbioclastic micrites mostly comprise unrecognizable detritus and some recognizable echinoderm, foraminifer, and

Figure 15 – Photomicrographs of internal sediments and micritic cements

(A) Meteoric (telogenetic) clotted micrite (c.m.) occludes much of the interparticle pore space, followed by non-ferroan mosaic spar (YnfC). PL: Sample 5.94 (Awapapa Limestone).

(B) Isopachous rinds of blocky clear spar cement are covered by homogeneous geopetal micrite (arrowed). CN: Sample 17.13 (Scinde Island Limestone).

(C) *In situ* peloidal micrite sediment. Note the typical texture exhibiting coarsening-upward (white arrow gives direction) micritic, interlocked spherical peloids that probably nucleated from fine crystalline micrite paste flooring intergranular pores. PL: Sample 4.76 (Kairakau Limestone).

(D) Detrital geopetal micrite (arrowed). PL: Sample 7.17 (Rotookiwa Limestone).

(E) Geopetal internal sediment that originated following the diagenetic alteration of aragonitic skeletons, in which debris from the partial collapse micrite envelopes accumulated at the bottom of pore spaces (arrowed). PL: Sample 7.17 (Rotookiwa Limestone).

(F) Irregularly shaped micritic crust fringes first-generation blocky to acicular spar coating calcitic bivalve grains, and produces protruding buttons and menisci (arrowed). This cement is contemporaneous with the percolation of micrite after exposure to surficial processes (vadose meteoric). PL: Sample 7.35 (Rotookiwa Limestone).

(G) - (H) Irregular micrite bindings locally project micrite bridges between adjacent grains (arrowed). This early diagenetic product, which is not coeval with dissolution, may originate either in the vadose or phreatic marine environment. PL: (G) Sample 11.84 (Mason Ridge Formation); (H) Sample 9.96 (Te Onepu Limestone).

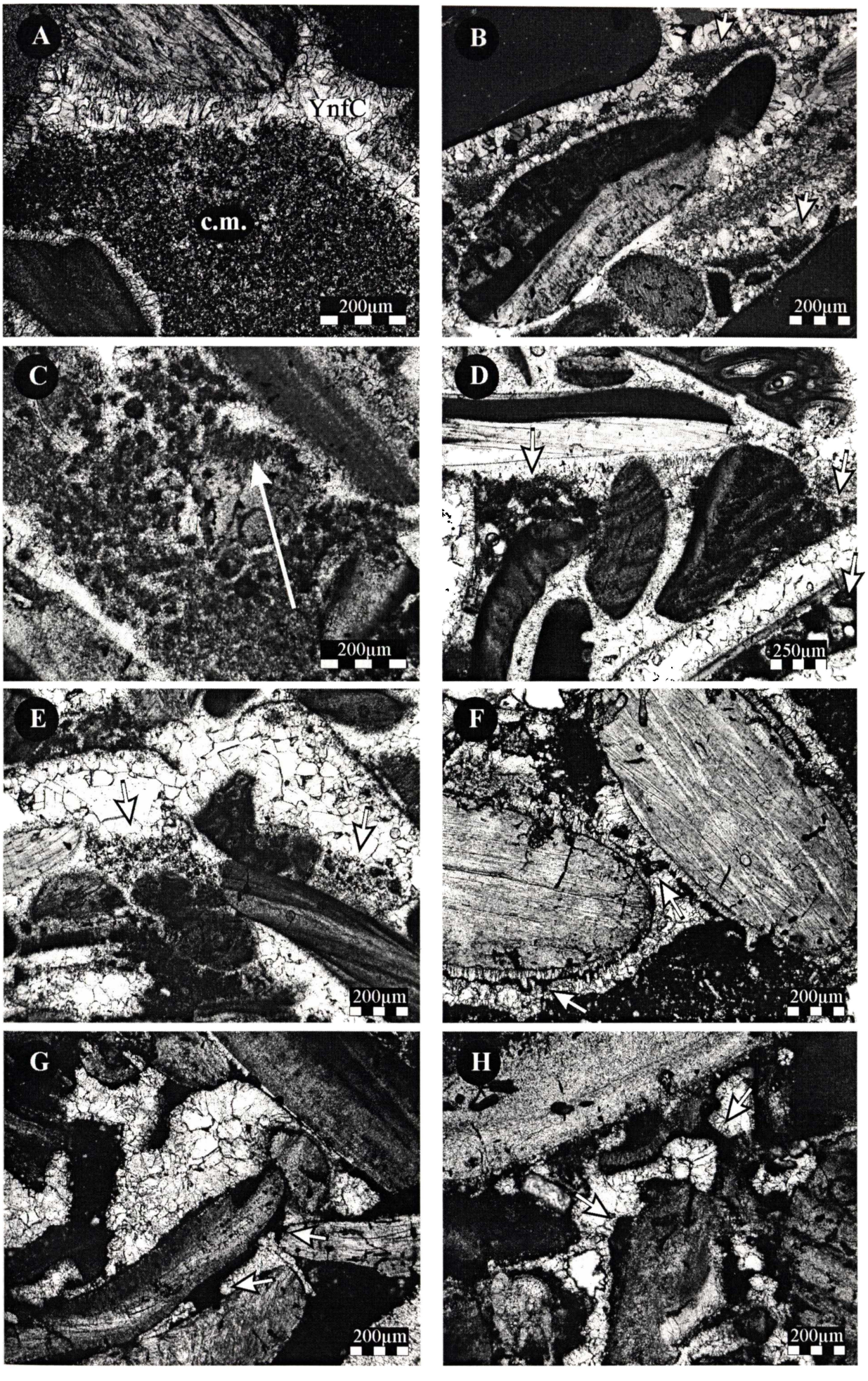
A
YnfC
c.m.
200μm
B
200μm
C
200μm
D
250μm
E
200μm
F
200μm
G
200μm
H
200μm

bivalve chips. Microquartz-rich and terrigenous micrites have various contents of angular to sub-rounded microquartz and occasional feldspars. Although both fabrics represent obvious internal sediments, paragenetic relationships indicate that they generally originate from different diagenetic environments. Typically, microbioclastic internal sediments are closely associated with marine diagenetic products, whereas terrigenous micrites occur beneath subaerially exposed surfaces and consist of laminated or graded dark brown to iron-stained mouldic void fillings (see Chapter 2, Figure 6B).

4.4.4. Micropeloidal internal sediment

Although uncommon, peloidal internal sediments are present within marine-cemented horizons, but are not restricted to them as they also occur in marine cement-free horizons. Diagenetic stratigraphy indicates that micropeloidal sediments always post-date homogeneous micritic paste and exhibit up-section epitaxial overgrowths or clear spar rim cements, and seldom pre-date inclusion-rich acicular cements.

Micropeloidal matrix consists of coarsening-upward micritic, nucleus-free, (sub)spherical peloids, 20 to 60 μm in diameter (Figure 15C). They differ from faecal pellets *sensu stricto*, which are generally larger and have ovoid shapes. Micropeloids are believed to represent a distinct diagenetic fabric that results from *in situ* precipitation of calcium carbonate through multiple nucleations of single crystals and subsequent crystal flocculation (Chafetz, 1986; Wilber and Neumann, 1993). Indeed, internal coarsening-upwards of such a fabric can hardly be explained by geopetal emplacement of peloids percolating from the water-sediment interface. Micropeloidal sediments have been described in various modern and ancient carbonate settings (e.g., tropical environment: Macintyre, 1985; Aissaoui, 1988; Wilber and Neumann, 1993; non-tropical environment: Reeckmann, 1988; James and Bone, 1992; Nelson and James, 2000), and despite much controversial research, a consensus seems to have been achieved concerning their biochemical origin (Chafetz, 1986; Kerans *et al.*, 1986; Aissaoui, 1988; Chafetz and Buczynski, 1992). Similarly, micropeloidal sediments that pre-date meteoric and burial diagenesis products in the Te Aute limestones are ascribed to bacterially-induced precipitation of calcite in the marine diagenetic environment.

4.5. Cryptocrystalline meniscus-type cements, irregular micrite bindings, and micrite envelopes

Initially restricted to calcite spar cements, the term meniscus designates grain-to-grain bridges with a double convex shape located preferentially near grain contacts. Literature review shows that meniscus cement fabrics are classically ascribed to vadose environments where their growth form is supposed to conform to the air-water interface of droplets held by capillarity in pores partly filled by air (Longman, 1980; Purser, 1980). Although the term meniscus has subsequently been extended to comparable structures of micro- to cryptocrystalline calcite precipitates, previous authors have emphasized that care should be taken when interpreting such fabrics in terms of diagenetic environment. For example, Bernier and Dalongeville (1988) and Hillgärtner *et al.* (2001) have reported micritic meniscus-type cements in subtidal environments.

In the Te Aute limestones, micritic meniscus-type cements could not be unequivocally interpreted as indicators of marine or meteoric vadose diagenesis, due to a lack of independent criteria such as the co-occurrence of sparitic menisci and pendant cements, dissolution features, and structures such as root traces or calcretes. In most samples presented here (Te Onepu Limestone and Mason Ridge Formation; Figures 15G, 15H), micritic menisci occur as the first cementation stage and commonly display a lateral transition to micritic envelopes of irregular thickness with small protuberances (Figure 15H). This suggests that the microfabric may have had a stabilizing effect on the sediments, with subsequent lithification at the water-sediment interface and a few centimetres below.

Two main varieties of micritic envelopes have been distinguished. One has a diffuse character and is associated with a destructive process at the outer rim of grains. Through a process of alteration–precipitation involving biochemical processes (Bernier, 1995; Hillgärtner *et al.*, 2001), successive generations of vacated microboring endoliths at grain margins are filled with cryptocrystalline cement, producing micritic envelopes (Bathurst, 1966), whose formation is often critical to grain preservation in later diagenetic environments (Figure 17E). This type of micritic envelope may evolve into the second variety, which results from accretion of crypto- to microcrystalline calcite on the surface of grains (Figure 15F). Previous studies have demonstrated that similar fabrics are the result of calcification of filaments of epilithic microorganisms (Calvet, 1982).

Micritic envelopes are not indicative of any particular diagenetic environment. They have been described from intertidal environments and beachrocks (Meyers, 1987; Bernier and Dalongeville, 1988), in subtidal firmgrounds and hardgrounds (Longman, 1980; Tucker and Wright, 1990; Hillgärtner *et al.*, 2001), and in supratidal to continental vadose environments (Calvet, 1982).

In the Te Aute examples, two frequent paragenetic relationships helped ascribe micritic envelopes (and cements) to specific diagenetic environments:

(a) Typically, fibrous and acicular turbid cements, inferred to be marine in origin, grow upon a micritic envelope < 25 μm thick (Figure 3H). This systematic co-occurrence (fibrous cements rarely form upon micritic mat-free surfaces) points at the possible triggering effect of micritic mats replete with microorganisms capable of initiating carbonate precipitation (Chafetz, 1992) and later calcite crystal nucleation (Bernier and Dalongeville, 1988). In this case, micritic envelopes are interpreted to have formed in the marine diagenetic environment.

(b) Irregularly-shaped, occasionally laminated, micritic crusts are also found lining solution voids that obviously relate to the ingress of meteoric waters undersaturated with respect to $CaCO_3$. Often displaying pendant structures, these micritic crusts are interpreted to result from meteoric diagenetic processes.

4.6. Dissolution

Dissolution is responsible for secondary porosity formation and may occur at any time after the death of skeleton-bearing organisms, and more generally after the deposition of sediments. Dissolution generally accompanies a significant change in the chemistry of the pore fluids, such as a change of salinity, temperature, or partial pCO_2. Such parameters influence the calcium carbonate saturation index of the fluids in the various diagenetic environments, and in turn the aggressiveness of the alteration reaction (James and Choquette, 1990b; Brand, 1994; Moore, 2001).

Modern shallow temperate carbonate sediments are composed of a polymineralic suite consisting of the metastable $CaCO_3$ minerals aragonite (gastropods) and HMC (echinoderms), and typically dominant stable LMC (brachiopods, bryozoans, barnacles, epifaunal bivalves; Rao, 1990; Hayton *et al.*, 1995). Both aragonite and HMC stability is achieved by the dissolution of the unstable phase and precipitation of the stable phase, which in most carbonate settings occurs under the influence of meteoric or mixed

marine-meteoric fluids undersaturated relative to the unstable phases (Smart *et al.*, 1988; James and Choquette, 1990b). However, undersaturation and alteration can also occur locally in shallow-marine temperate waters, with early dissolution occurring at, or just beneath, the sea floor (Alexandersson, 1978; Nelson, 1988a; Nelson *et al.*, 1988b; Freiwald, 1998; Kyser *et al.*, 1998; Nelson and James, 2000).

The abundance of aragonite and HMC skeletons is determinant to cementation as they may provide much of the calcite cement that armours sediments as they move through successive diagenetic environments to the mesogenetic realm (James and Choquette, 1990b; Hood and Nelson, 1996; Dodd and Nelson, 1998). HMC generally dissolves incongruently, releasing magnesium without the transport of significant $CaCO_3$, whereas aragonite, unstable in most diagenetic environments, but especially so in those dominated by meteoric fluids, dissolves resulting in significant transport of $CaCO_3$ (Moore, 1989; Haywick, 1990). Therefore, in temperate carbonates the abundance of metastable skeletons and their degree of alteration are likely to influence the chemistry of fluids circulating through the sediment pores, and consequently the nature of diagenetic pathways (Hood and Nelson, 1996).

In the Te Aute limestones, carbonate skeletons (and cements) display various degrees of chemical alteration, which constitute a continuous spectrum of transformation processes from pristine mineralogies to replacement fabric: (1) skeletons with preserved original mineralogy and microstructures; (2) skeletons with preserved original mineralogy and microstructures, but that include leaching cavities; (3) skeletons with original mineralogy relics (aragonite) either encased in, or adjacent to, larger neomorphic LMC crystals; (4) skeletons with aragonite (or HMC) neomorphically transformed into LMC, but with well-preserved relic shell microarchitectures; and (5) skeletons (in a few examples cements) dissolved away, with no visible relict microstructures, leaving a hole (mould) that may or may not be filled with calcite cement. Each of these aragonite alteration scenarios is described below.

4.6.1. Unaltered material

Pristine LMC skeletal grains are ubiquitous throughout most carbonate facies that range in age from Opoitian to early Nukumaruan, and they constitute the major biogenic components (barnacle plates, brachiopods, and bryozoans). LMC microstructures are also present in outer layers of pectinids and other epifaunal bivalves. Pristine LMC

biogenic carbonates stain pink with Dickson's solution and are non- to orange luminescent. Original LMC cements, including PrC, PoFC, and YnfC, do not seem to have undergone any significant alteration (growth stages, as shown under CL, are preserved, suggesting no chemical reorganization), even though dissolution surfaces are common at the boundary between contrasting CL patterns (e.g., Figure 12E). X-ray diffraction analyses reveal that aragonite is virtually absent in the limestones older than Nukumaruan (see Appendix 8). In a few Nukumaruan examples, X-ray diffraction reveals the presence of aragonite, and relatively unaltered aragonite shells with retention of microstructures have been observed in some thin-sections, frequently neighbouring variably altered ones. Pristine aragonite is weakly stained with Dickson's solution, and is usually non-luminescent. Pristine aragonite whole shells and fragments prevail in packstones and especially in poorly to moderately cemented coarse grainstones within the Matapiro and Scinde Island Limestones, and the Hassal Conglomerate (Figure 1).

4.6.2. Preserved mineralogy with evidence of chemical alteration

Partial dissolution of preserved metastable aragonite microstructures has been observed in bivalve shells within late Waipipian, Mangapanian, and Nukumaruan limestones from both the western and eastern sectors of the forearc basin. In these examples, leaching was not followed by, or did not take place simultaneously with, precipitation of calcite. At the thin-section scale dissolution appears either to have developed parallel to primary structural lamellae (Figure 16F), or to have left subcircular hollows producing a characteristic "Swiss-cheese" texture (Figures 16C, 16D). Shell microstuctures may be blurred by the density of microvoids, resulting in a dark clouded fabric replete with translucent hollows that range in size from 10 to 75 μm (Figure 16C). Partly altered aragonite fragments stain pale pink to mauve with Dickson's solution. The foregoing textures once again coexist with lower and higher degrees of shell alteration. At a macroscale, aragonite shells are typically white and powdery ("chalky" aragonite of Haywick, 1990). Partly leached aragonite is common in coarse, moderately to well cemented horizons within the Te Waka, Pakipaki, Matapiro, and Scinde Island Limestones.

Figure 16 – Photomicrographs illustrating dissolution/neomorphism fabrics

(A) Corrosion surface (white arrow) engulfed within rinds of turbid fibrous cement due to dissolution that resulted locally in total leaching at grain margin (black arrow). This dissolution surface is sealed by second-generation micrite geopetal sediment. PL: Sample 5.96 (Awapapa Limestone).

(B) Moulds of probable former aragonitic skeletons filled with drusy and mosaic spar. CN: Sample 4.95 (Kairakau Limestone).

(C) "Swiss-cheese" fabric – Subcircular hollows result from dissolution of aragonite shells with retention of their original mineralogy. PL: Chemically stained sample 17.10 (Scinde Island Limestone).

(D) "Swiss-cheese" fabric – Dissolution hollows are filled with non-ferroan clear calcite spar (black arrow). The aragonitic skeleton has partly retained its mineralogy and microarchitecture. PL: Chemically stained sample 17.10 (Scinde Island Limestone).

(E) Early sea-floor dissolution of probable aragonitic layer of bivalve skeleton (white arrow). Note that the interior of the mould is filled by coarsening-upward internal sediment upon which nucleated *in situ* peloids. CN: Sample 5.105 (Awapapa Limestone).

(F) Dissolution of aragonitic shell along first- and second-order lamellae, and calcite overgrowth of the same shell (N) with partial retention of microstructures. Note that replacement calcite did not nucleate at fracture sites suggesting that fractures were cemented prior to aragonite dissolution and neomorphism. CN: Sample 15.14 (Te Waka Formation).

(G) Photomicrograph showing that aragonite neomorphism is a multistage history. Replacement of aragonite by calcite started from the grain margin inward in oxidizing waters (pink to mauve stain of neomorphic calcite; white arrow). Nucleation sites of second-generation neomorphic calcite are preferentially located on first order lamellae (black arrow). Second-generation calcite stains deep blue indicative of reducing Fe-rich pore fluids, and overgrow first-generation neomorphic calcite. Neomorphism progressed from these nucleation sites along lamellae and from the grain margin inward while oxidizing waters percolated once again (last-generation pale pink neomorphic calcite). PL: Chemically stained sample 15.40 (Te Waka Formation).

(H) Photomicrograph illustrating various replacement fabrics of aragonite: (A) neomorphosed skeleton with poor retention of microstructures underlain by brownish colour; (B) preserved mineralogy with evidence of chemical alteration (dissolution was not followed by precipitation of calcite); (C) in this example, partial leaching of aragonitic skeleton was followed by precipitation of calcite that progressed from the grain margin inward (note the drusy fabric of replacement fabric). PL: Sample 17.13 (Scinde Island Limestone).

(I) Neomorphosed aragonitic shell that retained microstructures underlain by organic (?) inclusions along first- and second-order lamellae. PL: Sample 17.9 (Scinde Island Limestone).

(J) Original aragonite relics in neomorphic calcite appear dark and cloudy (black arrow). Note that coarse replacive calcite crystals cross-cut shell microstructures. PL: Chemically stained sample 17.10 (Scinde Island Limestone).

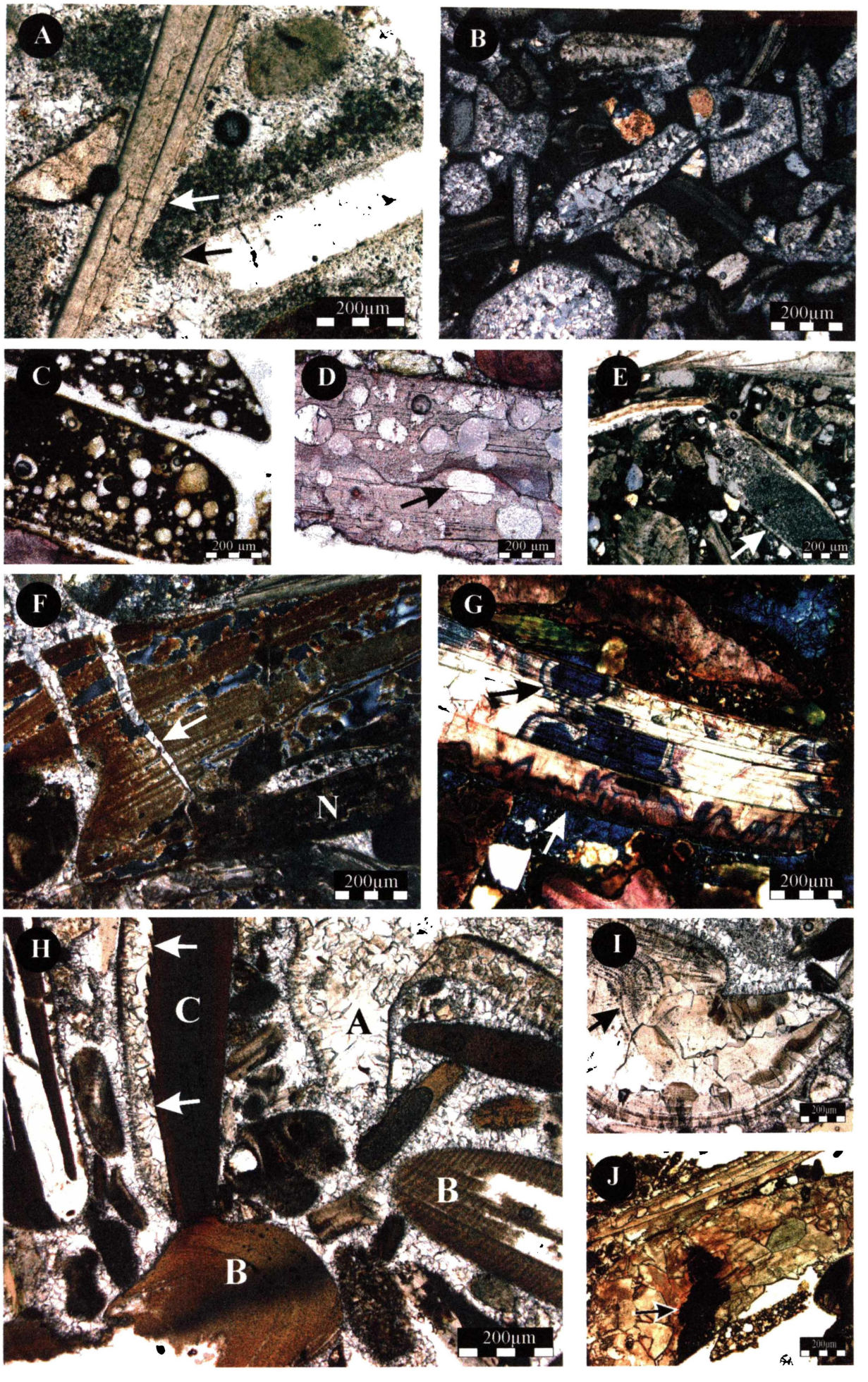
A
200µm
B
200µm
C
200 µm
D
200 µm
E
200 µm
F
N
200µm
G
200µm
H
C
A
B
B
200µm
I
200µm
J
200µm

4.6.3. Original mineralogy relics in neomorphic calcite

Original aragonite relics with partial preservation of microstructures may be retained as dark clouded patches in the calcite neomorphically replacing diverse aragonitic fossils (Figure 16J). In the few observed examples, the neomorphic replacement of pristine aragonite seems to progress from the grain margin inward along sharp and irregular fronts, and eventually has resulted in clear sparry calcite enclosing aragonite relics. Consequently, across the sharp neomorphic front, there is no optical continuity between replacement calcite crystals and aragonitic shell relics. In one example, the transition between neomorphic spar and aragonite relic appears gradational, and the extinction of calcite crystals seems to fade into the transitional zone.

4.6.4. Neomorphosed skeletons with the retention of microstructures

Early dissolution of skeletal aragonite may result in neomorphic calcite crystals having a partial void-filling origin. This is the case when calcite spar has filled in hollows of the "Swiss-cheese" texture (Figure 16D), and from these solution sites calcitization has extended to the shell with or without retention of microstuctures. However, the majority of neomorphic calcite crystals, as identified by the presence of ghosts of host microtextures, appear to have a replacement origin. The resulting texture is generally a mosaic of coarse low-Mg calcite (LMC) crystals which cross-cut original fabric outlined by brown insoluble organic and/or inorganic inclusions (Sandberg and Hudson, 1983) that display discernible cross-lamellar structures (Figures 16G to 16J). Replaced shells are usually preserved as pseudo-pleochroic spar. The extinction of the replacement crystals varies from uniform to undulose. The concentration of relics is often higher in areas of greater organic concentration, particularly near the outer surface of valves (Sandberg and Hudson, 1983; Maliva, 1998; Figure 16I). Neomorphosed shells stain pink to purple-blue, often in close relation with the interparticle spar cement. Staining may be homogeneous or patchy (Figure 16G), suggesting in the latter case that nucleation proceeded through several nucleation centres rather than progressively along dissolution-precipitation fronts as in the former (Sandberg and Hudson, 1983; Brand, 1994). Neomorphosed grains are generally non-luminescent. Examples of neomorphosed skeletons with retention of microstructures, in an order of increasing abundance, are recorded within limestone formations ranging in age from Opoitian to Nukumaruan in the eastern sector of the study area (see Figure 27).

The alteration of IMC or HMC marine fibrous cements into LMC, with the preservation of fabric details, has been discussed in Section 4.2.

4.6.5. Mouldic or "ghost" fabrics

Total leaching of unstable grains is widespread in all studied limestone formations (see Figures 27, 28). Although the original mineralogy of ghost fragments left as moulds outlined by thin micritic envelopes cannot be directly determined, the preservation (partial or total) of LMC and HMC (e.g., echinoderm plates and spines) allochems within the same horizons suggests that biomoulds were probably aragonite. Dissolution of shell fragments can be preceded by, or followed by, the precipitation of calcite cement. The timing of aragonite dissolution is highly variable within the same limestone formation, and from one formation to another. Aragonitic (and HMC) bioclasts may either: (a) have suffered from marine alteration at the sea floor; or (b) meteoric alteration after subaerial exposure; or (c) have survived these early processes and been dissolved by burial fluids; or (d) not even be significantly altered prior to being once again exposed to surficial processes after uplift. These options are elaborated upon below:

(a) In a few thin-sections, shells of probable original aragonite were totally leached away, and the internal walls of the moulds partly lined with isopachous inclusion-rich acicular cements contemporaneous with the first generation of intrinsic marine cement (Figure 3C). The presence of geopetal micritic sediments in aragonite skeletal moulds is another uncommon feature within mud-supported facies, also attributed to sea-floor diagenesis (Figure 16E).

(b) Mouldic voids may be filled with microquartz-rich geopetal sediments that percolated from the air-sediment interface, but generally pre-compaction equant (blocky) and drusy clear spar (PrC) follows dissolution. However, precipitation of calcite does not always accompany dissolution, and weakly armoured micritic envelopes may eventually collapse in the meteoric environment, accumulating debris at the bottom of enlarged pores (Figures 10C, 15E), until sealed by mesogenetic or telogenetic cements. CL and chemical staining reveal that pre-compaction precipitation of calcite has been limited, and rarely prevented biomoulds from being crushed during mechanical compaction, even in the older Opoitian limestones. Although the formation of a micritic envelope of IMC-HMC during marine diagenesis is often critical to mould preservation, moulds may also be underlain either by

insoluble (?)organic matter along shell lamellae, or by spar cements precipitated upon grains before their dissolution.

(c) In limestone formations of Opoitian to Mangapanian age, the first generation of cement that fills mouldic voids is commonly of burial origin (PoFC), suggesting that dissolution was either related to "aggressive" burial fluids, or dissolution occurred earlier in the marine and/or meteoric environment but cementation was delayed until after sediments were buried.

(d) A number of points indicate that in some Nukumaruan examples aragonitic grains survived pre-compaction and burial alteration, until they were exposed to surficial meteoric waters. For example, fracturing of aragonitic skeletons, which was most likely compaction-related, occurred before aragonite started to dissolve. Fractures are filled with clear sparry calcite while dissolution cavities within aragonite skeletons are spar-free (Figure 16F). Had fracturing occurred after or during dissolution of aragonite, newly developed intraskeletal porosity would have allowed the diffusion of diagenetic fluids from the fracture inward, thereby inducing neomorphism along its margins. Telogenetic dissolution is fabric non-selective. Dissolution surfaces cross-cut both cements and grains, commonly progressing from uplift-related fractures. Newly fractured aragonitic shells are leached away, and may or may not be filled with geopetal sediments, or vadose or phreatic meteoric cements, which in turn overgrow older burial or pre-compaction interparticle cements (see Figure 18A).

4.6.6. What controls the different modes of Mg-calcite (IMC-HMC) and aragonite neomorphism?

Diagenetic controls on carbonate alteration, and processes involved in the reaction, are multifarious and complex, rendering difficult the interpretation of their products in terms of diagenetic environment and original material (Brand, 1994; Maliva, 1998). The interpretative approach may be simplified by only considering the major controls on alteration as reported in previous studies, namely the relative solubility of both inorganic and organic minerals, the water/rock ratio, and the water chemistry.

Calcite with a low-Mg content, which by definition varies from 0-4 mol% $MgCO_3$ (Chave, 1954), is the most resistant to dissolution. This relative stability, however, may be greatly influenced by the particle size, surface ornamentation, and internal porosity of the carbonate grain or cement (Flessa and Brown, 1983). Solubility

of calcite increases exponentially with increasing Mg content. Consequently, of all the calcite species, HMC (>12 mol% $MgCO_3$) is the thermodynamically least stable of the group at Earth's surface conditions (Brand, 1994). Aragonite has a solubility that under ideal conditions overlaps with calcium carbonate of 9-15 mol% $MgCO_3$ (Brand, 1994).

In the Te Aute carbonates, most fossils and cements precipitated originally as LMC show well preserved macro- and microstructures. Only late meteoric processes have significantly altered LMC minerals. Indeed, uplift-related meteoric dissolution of LMC, being late in the suite of diagenetic processes recorded by the carbonate system, can easily be recognized and interpreted. Many skeletal grains and cements are fractured. Such fractures are commonly solution-enlarged producing voids developed across all previous fabrics (Figure 18A). In some cases fractures are filled with micrite geopetal sediment (iron stained or not). The walls of fractures and fossil moulds may also be covered by non-ferroan equant clear spar with no visible orientation, or by pendant dirty laminated cement, typically of vadose meteoric origin.

In contrast, inferred IMC-HMC marine cements and shells of this mineralogy show more variably preserved microfabrics and structures. Further, they have been altered to LMC as revealed by microprobe and X-ray diffraction analyses, and by their blotchy/cloudy luminescence. In the diagenetic suite, the alteration of IMC-HMC to LMC is clearly associated with a change of pore fluid chemistry, which is marked not only by dissolution processes, but also by the precipitation of distinct cement phases.

CL and chemical staining indicate that neomorphism of IMC-HMC mineralogies is a multiphase history. Although alteration may have started in the pre-compaction diagenetic history under the influence of marine waters (e.g., Kyser *et al.*, 1998), or with the ingress of meteoric or mixed marine-meteoric waters that precipitated PrC and induced dissolution (Figure 12A), it continued and significantly developed under the influence of post-compaction reducing waters. This is evident from: (1) the occasional enrichment of echinoderm plates and turbid cements in Fe and Mn (stain pink to mauve; Figure 3; Table 1); (2) the orange dull luminescence of patches within echinoderm plates and turbid cements mimics the CL pattern of PoFC (Figures 4, 5); and (3) occasional dissolution-related microcavities (1-2 μm) within the turbid cements are filled with a bright orange/yellow cement, which is in lateral continuity with the bright yellow/orange zone that in places is the first precipitate on the walls of compaction-induced fractures.

The variety of aragonite shell alteration/preservation has been shown by previous researchers to result from the complex interaction of internal controls, including surface area and morphology of the dissolving carbonate grain, thickness and integrity of individual organic envelopes, intraskeletal porosity, and external factors, including water/rock ratio and fluid chemistry (Sandberg and Hudson, 1983; Haywick, 1990; Brand, 1994; Maliva, 1998).

The water/rock ratio and the nature of interparticle fluids are especially critical to the degree and type of aragonite alteration (Figure 17). In addition, flow rates within the overall diagenetic system are of great importance to the timing of carbonate precipitation (Brand, 1994). At high flow rates, $CaCO_3$ released from aragonite dissolution will be transported outside the site of initial dissolution, and may be precipitated somewhere outside the system if carbonate saturation is achieved. It has been demonstrated that the complete dissolution and the neomorphism of aragonite to calcite proceed through or along intervening solution films adjacent to the surface layer of the original carbonate (James and Choquette, 1990b). The intensity of water/rock interaction determines the nature of geochemical reactions within the solution film and at neomorphic fronts (Brand, 1994; Maliva, 1998). High, intermediate, and low water/rock ratio systems (Brand, 1994) produce distinctive neomorphic fabrics that can readily be recognized within the Te Aute limestones, hence helping relate fabrics to possible diagenetic environments.

(a) High water/rock ratio systems (i.e., low water-rock interaction), provided that fluids are originally undersaturated with respect to aragonite, are characterized by the development of mouldic and intraskeletal porosity (Figure 17). Moulds may be filled with fine- to coarse-crystalline calcite, depending on flow rates and saturation levels. Shallow temperate marine waters can be mildly undersaturated with respect to aragonite allowing dissolution of the metastable mineral in the marine diagenetic environment, without implying exposure to meteoric diagenetic processes (Kyser *et al.*, 1998; Nelson and James, 2000). The emplacement of marine internal sediments and the precipitation of (inferred marine) turbid cements in skeletal aragonite moulds provide evidence of aragonite alteration on the sea floor in a high water/rock ratio regime (e.g., Figures 3C, 16E).

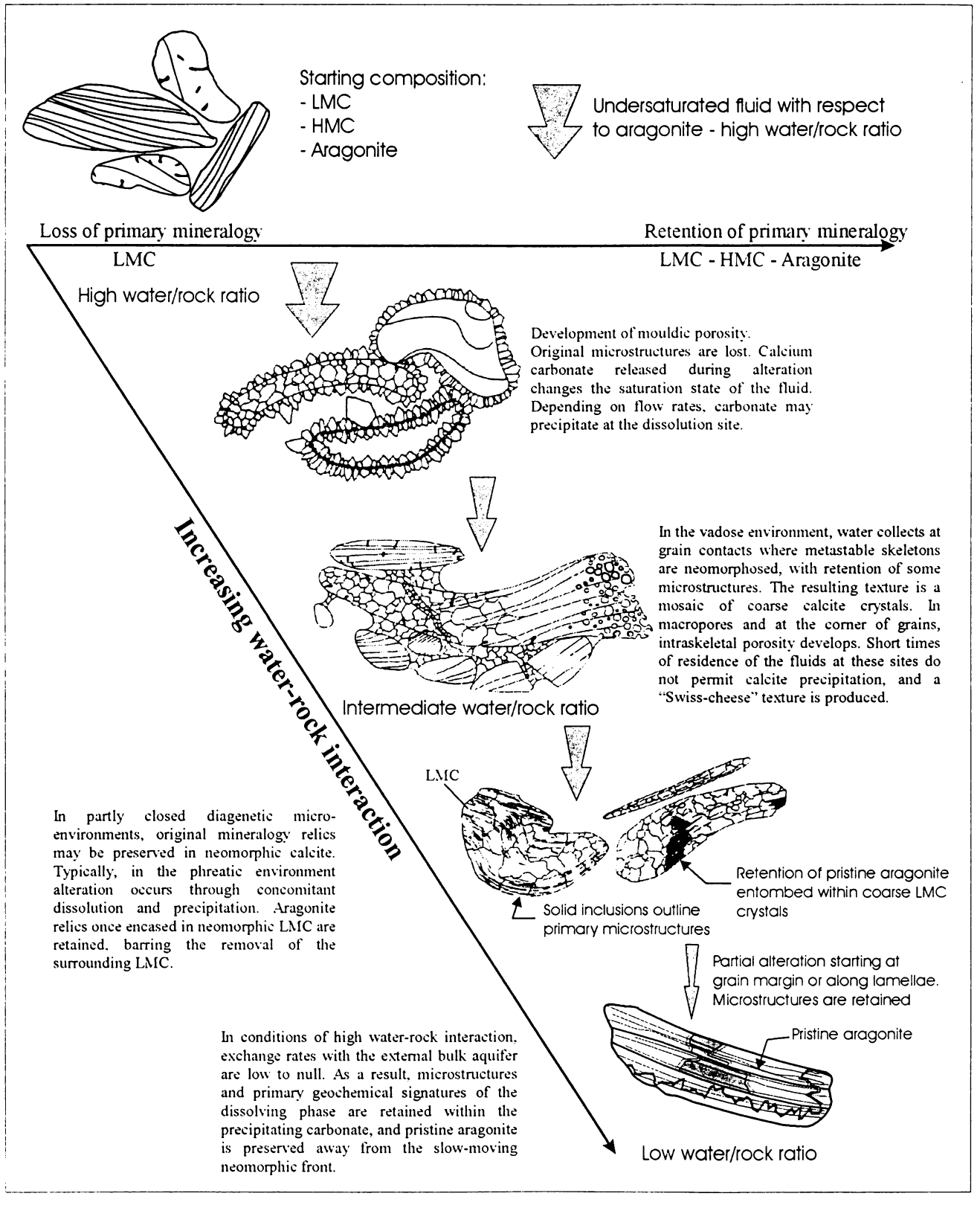

Figure 17- A model summarizing the various neomorphic fabrics of aragonite bioclasts in relation to inferred water/rock ratio systems. The starting composition of the ambient fluids is assumed to be the same in all systems. Although of probable great influence on the degree of alteration, and subsequent fabric development, the micro-architectures and geochemical signatures of pristine aragonitic skeletons, likely to differ from one taxum to another (Haywick, 1990), have not been integrated into this model. See text for discussion.

Fabric-selective dissolution that post-dates marine diagenesis and pre-dates mesogenesis is classically attributed either to the replacement of marine pore fluids by meteoric waters (James and Choquette, 1990b), or by the mixing of meteoric and marine waters (Smart *et al.*, 1988). Mouldic porosity, which is assumed to have originated in either of these environments, is present in all studied limestone formations. Differences lie in the degree of calcite precipitated within the moulds before the diagenetic system evolves in terms of hydrologic regime. Cementation varies from null to complete occlusion of moulds, but on average is poor in older limestones (Opoitian to Mangapanian) before burial and moderate in Nukumaruan limestones. Two scenarios can be envisaged to explain little or no cementation: (1) the dissolving solid did not change the saturation state to the point where calcite precipitation could commence - previous studies have demonstrated that sediments originally composed of calcitic components (LMC) could be exposed to meteoric influence for a prolonged period of time without being significantly cemented (James and Bone, 1989); (2) high flow rates through the system transported $CaCO_3$ away from the site of dissolution and thus prevented or slowed cementation.

(b) Intermediate water/rock ratio systems are characterized by the development of a chalky appearance in fossils (Brand, 1994). Carbonates formed in these systems retain part of the microstructures and geochemical signature of the precursor aragonite (Figure 17). Haywick (1990) suggested that the chalkification process compounds aragonite dissolution by increasing both the intraskeletal porosity and permeability. Alteration of aragonite across a chalky zone is thought to occur in the phreatic zone, and result, through concomitant dissolution and precipitation processes, in neomorphosed aragonite fabrics being poorly preserved (translucent brownish shells) in coarse cross-cutting mosaic calcite spars (James and Choquette, 1990b). The Matapiro Limestone (Nukumaruan) and the Te Waka Formation (Waipipian-Mangapanian) provide the best examples of aragonite replacement by coarse calcite crystals with little to moderate retention of original microstructures (Figures 16G to 16J). Horizons, where complete replacement occurred, are well cemented by coarse non-ferroan mosaic spar, which in turn provide evidence of a well-oxidized phreatic meteoric diagenetic environment. In mud-supported horizons and in moderately cemented horizons bearing evidence of residence in the vadose meteoric environment,

replacement may be incomplete. Typically, aragonite relics are either entombed in large calcite crystals, or are partly dissolved without displaying calcite cementation (Figures 16C, 16J). Aragonite relics once encased in neomorphic LMC are isolated from diagenetic solutions, and thus will be retained unless the surrounding LMC is remobilised (Sandberg and Hudson, 1983). All transitions either within the same thin-section or within single shells are common in those horizons, suggesting possible alternation of contrasting water flow and water/rock ratio conditions.

(c) In a diagenetic environment with relatively low water/rock ratio (i.e., high water-rock interaction in a closed system), neomorphosed aragonite grains retain their skeletal microarchitecture and primary geochemical signature (Figure 17) due to the isolation of solution films at the neomorphic front from the bulk interparticle waters (Brand, 1994; Maliva, 1998). The resulting fabrics comprise neomorphic calcites with small crystal sizes, and pristine aragonite crystallites adjacent to the latter (Haywick, 1990; Brand, 1994; Maliva, 1998). In the Te Aute carbonates, such fabrics accompany vadose diagenetic products, including pendant and meniscus spar cements. In the vadose zone, the average water/rock ratio is expected to be low due to the presence of air in the pores (Longman, 1980). Depending on the flow rates of meteoric waters through the sediments, and whether they reach the point of saturation, precipitation may or may not occur. Pristine aragonite with a "Swiss-cheese" texture, which is present in coarse-grained poorly-cemented horizons with calcite cements located at grains contacts or on the underside of grains, may originate from these conditions, though limited periods of exposure to undersaturated fluids could also produce such a fabric (Figure 17).

4.7. Bioactivity: biological alteration and encrustation

4.7.1. Bioerosion

Bioerosion of skeletal grains is a conspicuous diagenetic feature in cool-water carbonates, and may represent the main diagenetic process affecting sediments prior to entering the burial realm (Nelson *et al.*, 1988b; Young and Nelson, 1988). Bioalteration may be an important source of carbonate mud production, and as such is a factor of great importance to porosity loss in coarse skeletal sediments (Farrow and Fyfe, 1988). Bioerosion comprises a wide spectrum of processes, specific or indiscriminate, which occur on a wide variety of scales. On a microscale the mechanism involves infestation of

the carbonate host by endolithic algae, fungi, and bacteria. From petrographic data, endolith bores may be restricted to the outer margin of the infested grains, or penetrate grains at various levels, depending on the grain size and fabric, type of borers, and grain mineralogy. In some examples (e.g., Mason Ridge Formation), skeletal grains, which are densely microbored and/or micritized at their outer margin (Figure 18E), commonly bathe within homogeneous micrite. By contrast, walls of intraparticle pores free from infilling mud lack evidence of infestation by microborers (see Chapter 2, Figure 6D). This suggests that infestation started after sediments had been stabilized, and that pore-filling material hosted microborers. Thus, microboring and later stage micritization occurring in the early stages of diagenesis are most likely of marine origin.

Bores of endoliths may be filled with iron oxides, clays, authigenic glauconite (Figure 18C), and micritic sediment or micritic cement. The last named is related to environments where precipitation of cement occurs (see Section 4.5). Where precipitation of cement does not occur, endolithic bores weaken grains and enhance the potential for the dissolution of skeletons (Alexandersson, 1978; Smith *et al.*, 1992; Freiwald, 1998).

Macroborings on a thin-section scale (Figure 18D), mostly of molluscan skeletons (infaunal bivalves and oysters), involve gastropods, polychaetes, and clionids.

Bioalteration fabrics and attributes, including the occurrence of micro- and macroboring features, the number of grains affected, the intensity of host infestation (density of bores), and the thickness of micritic envelopes, were used in the course of the petrographic study in order to assess the degree of destructive diagenesis within samples at the thin-section scale. Fossiliferous and pebbly rudstones, and coarse skeletal-rich grainstones appear to be most prone to bioalteration, the former involving principally gastropod, polychaete, and clionid sponge macrobores, the latter mainly algal and fungal bores, and micritization features. Although present, bioalteration is typically only poorly to moderately developed in other facies, with the noticeable exception of mixed carbonate-siliciclastic packstones and grainstones located at stratigraphic positions indicative of condensation (e.g., Maximum flooding surface; see Figure 24C). This suggests the most favourable conditions for borer activity were associated with the relatively slower rates of sedimentation and prolonged exposure of skeletal grains on the sea floor.

Figure 18 – Photomicrographs of dissolution fabrics (continued) and bioactivity-induced diagenetic features

(A) Late fracturing stage (telogenetic) cross-cuts all previous fabrics (black arrows), and allows the percolation of vadose internal sediments (i.s.) once the limestone has been exposed to surficial meteoric processes. PL: Sample 12.5 (Kereru Limestone).

(B) Bioturbation within (now) moderately cemented mixed carbonate-siliciclastic sediment. Note that preferentially oriented skeletal grains outline the internal walls of the burrow (within circle), which is almost exclusively filled by terrigenous grains. PL: Sample 15.33 (Te Waka Formation).

(C) Microborings within calcitic bivalve shell, later filled by authigenic glauconite (arrowed). PL: Sample 5.81 (Awapapa Limestone).

(D) Anastomosed macrobores (arrowed) within oyster valve. PL: Sample 9.64 (Te Onepu Limestone).

(E) Densely microbored and micritized outer margins of calcitic bivalve skeletons (arrowed). PL: Sample 11.9 (Mason Ridge Formation).

(F) Multilaminar red algae (r.a.) encrusting multilaminar bryozoan encruster (arrowed). PL: Sample 11.11 (Mason Ridge Formation).

(G) Fenestrate barnacles encrusting bivalve shell. All barnacles within the sample are *in situ* and underwent sea-floor constructive diagenesis (see Figure 4.2) prior to being drowned within detrital matrix. PL: Sample 16.5 (Whanawhana Limestone).

(H) Well-preserved multilaminar bryozoan encrusting thin bivalve shell (Bi). Note that only the internal walls of zooecia in contact with micrite have been infested by microborers. PL: Sample 9.84 (Te Onepu Limestone).

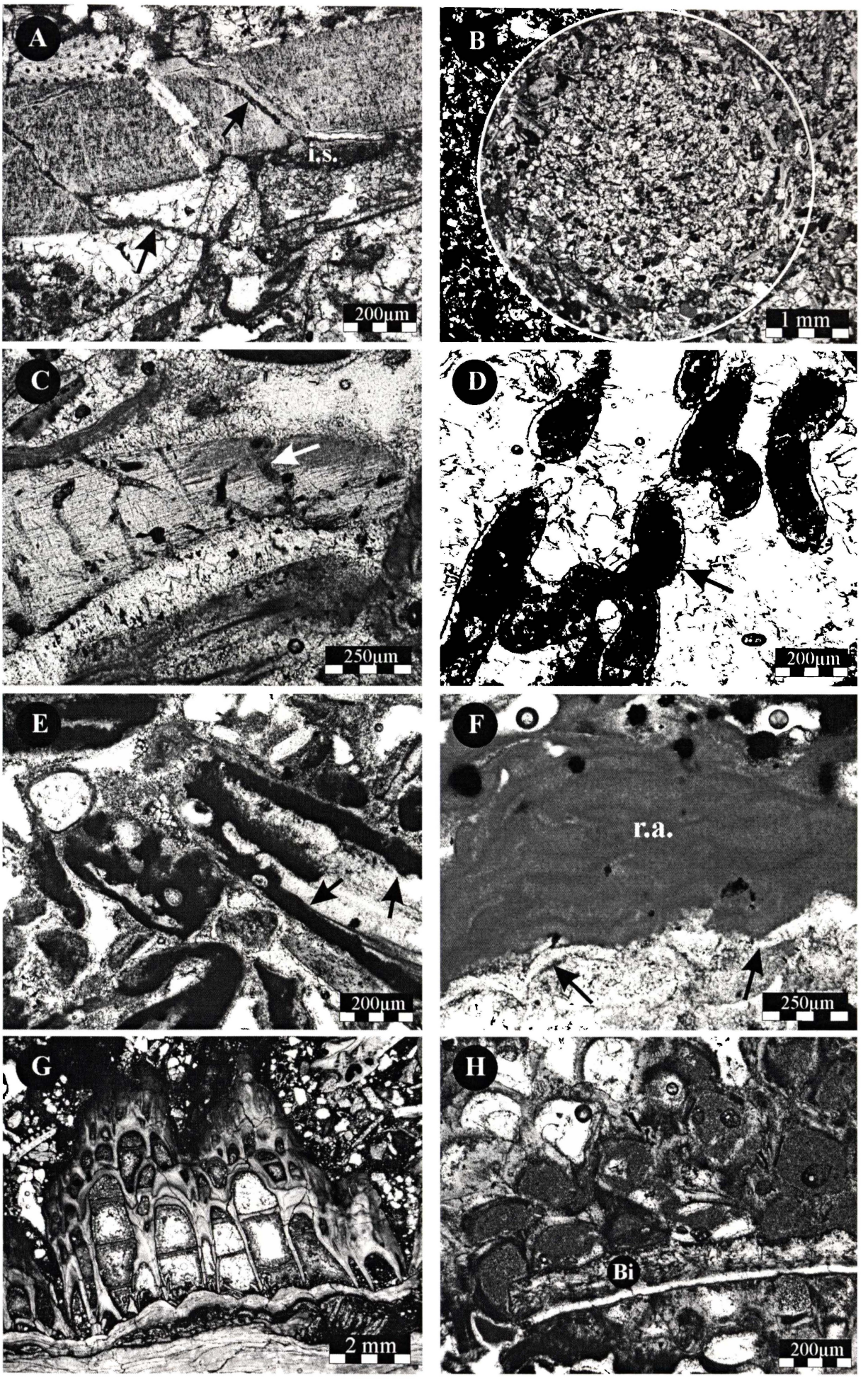
A
l.s.
200µm
B
1 mm
C
250µm
D
200µm
E
200µm
F
r.a.
250µm
G
2 mm
H
Bi
200µm

4.7.2. Encrustation

The calcified skeletons of encrusters, especially barnacles and to a lesser degree encrusting uni- and multilaminar bryozoans, are typically the dominant contributors to the Te Aute carbonate deposits (Harmsen, 1985; Beu, 1995; Hayton *et al.*, 1995). These skeletons have been subject at the sea floor to a variety of potentially destructive processes, including transport due to the influence of waves and currents, abrasion, and bioerosion. Both bryozoans and barnacles are not particularly resistant to breakage and dislocation of their constituent components (plates or chambers; Beu, 1995; Smith and Nelson, 1996), so that barnacles attached to their substrate (Figure 18G) and well preserved bryozoan encrusters are rarely observed both in macrosamples and at the thin-section scale. Thus, the preservation of encrusters may indirectly yield valuable information on environmental conditions, including current regime/velocity and sedimentation rate.

Uni- and multilaminar encrusting bryozoan encrusters in the Te Aute deposits that retained partly or totally their architecture are uncommon (Figures 18H, 27, 28). Being the least resistant to abrasion (Smith and Nelson, 1996), such well preserved growth forms are likely to have accumulated in low-energy environments and/or were rapidly buried. Well preserved unilaminar bryozoans occur in medium- to coarse-grained packstones, in rudstones commonly attached either to the underside of thick oyster shells or dwelling within sheltered macrobores, and more rarely in medium- to fine-grained grainstones. Well preserved multilaminar bryozoans occur mostly in mud-supported horizons, commonly associated with other encrusters, including unilaminar growth forms, barnacles, serpulids, and red algae (Figure 18F).

4.8. Mechanical abrasion

Shape and size of skeletal clasts are important indicators to assess sediment movement and reworking, and thus their time of residence on the sea floor. Amount of mechanical abrasion is seldom taken into account in diagenetic studies, though it is likely to influence the degree of any further diagenetic process. Indeed, shape and size of grains determine the amount of grain-fluid interactions, and thus their reactivity potential towards cementation or dissolution (Flessa and Brown, 1983; Meyers, 1989). Size of grains also determines their vulnerability to bioalteration processes, the smaller the grains, the faster their alteration, as suggested by Alexandersson (1978). Further, the

time of residence on the sea floor is also a critical parameter to grain abrasion. Frequent reworking by waves and currents combined with low accumulation rates (stratigraphic condensation) greatly accelerates mechanical processes of skeletal grain destruction.

The degree of mechanical abrasion, as revealed by the size and shape of grains, was used, in conjunction with other indicators of grain alteration (i.e., bioactivity) or preservation (i.e., cementation), to characterize the dominant destructive vs. constructive nature of the diagenesis undergone by carbonate sediments. This subsequently helped define the type-specific diagenetic suites (see Chapter 2, Section 5.4.1), whose properties are presented in Table 2.

4.9. Non-carbonate precipitate: Glauconite and iron-oxides

Glauconite and iron-oxides are non-carbonate precipitate types present in the Te Aute limestones. Both of these precipitates commonly fill intraparticle pores, such as foraminifers, zoarial chambers of bryozoans, and microbores (Figures 3A, 3B, 18C). Although present in all types of bioclasts, authigenic glauconite appears to be concentrated within bryozoan zooecia, barnacle plate pores, and benthic foraminifers, and commonly post-dates fine microcrystalline acicular extrinsic cements Figures 3A, 3B). Glauconitized grains are locally common and glauconite grains also occur in the form of reworked abraded to well-rounded siliciclasts. Glauconitization starts from a K-poor glauconitic smectite that progressively evolves toward an end member constituted by a K-rich glauconitic mica, namely glauconite (Amorosi, 1995). Glauconite is typically regarded as an indicator of low sedimentation rates in marine settings, and as diagnostic of transgressions, and in recent years has been used in sequence stratigraphic interpretations.

Sediment starvation determines the conditions most favourable for authigenesis and evolution of glauconite, especially in outer-shelf areas (Amorosi, 1995), resulting in the distinctive association between considerable concentrations and high maturity of glauconite (dark brown to dark green versus low maturity pale brown glauconite).

From point-counting data, the content of glauconite in the Te Aute rocks commonly is higher within rudstone and fine- to medium-grained grainstone facies (6-13%), than in mixed and siliciclastic lithofacies (2-8%). This is consistent with the former facies being preferentially associated with periods of low sedimentation (see Chapter 4, Section 5.4). Authigenic glauconite precipitated within intraskeletal pores

recurs at specific stratigraphic positions, such as maximum flooding surfaces, indicative of arrested to low sedimentation.

Brown red iron oxide is distributed both in intraparticle pores and along dissolution seams or at the interface between interpenetrating grains.

4.10. Compaction features

Burial (mesogenetic) diagenesis is commonly associated with compaction processes and products, defined as the sum of processes which result in a decrease in volume of the rock (Meyers, 1980; Bathurst, 1995). Compaction processes generally fall into two categories: mechanical and chemical.

4.10.1. Mechanical compaction

Mechanical compaction processes include dewatering, re-orientation or distortion of grains (Figure 19A), and grain breakage (Figure 19C; e.g., Nicolaides and Wallace, 1997b). Grain rotation and re-orientation can be difficult to identify except from incompatible directions of indurated geopetal fabrics. In the Te Aute limestone samples there is a wide spectrum of grain breakage features, from minor to total collapse. Mechanical compaction principally affects grains with intraskeletal cavities, including foraminifera (Figure 19A) and bryozoan fragments, especially fenestrate forms, elongated grains such as bivalves (Figure 19C), echinoderm spines, and sheet-like siliciclastic minerals; echinoderm plates generally show few compaction features.

As well as burial depth, the occurrence and timing of mechanical compaction depend on the sediment texture (Figure 20). Grain breakage is very common in fine- to medium-grained grainstones, but less evident in coarser-textured samples where poorly to moderately abraded thick skeletal clasts either prevented compaction or delayed its effect. Furthermore, in packstones and wackestones, purely mechanical compaction features can be difficult to identify because the bioclasts may not always appear to be in contact with one another. Therefore, compactional effects may be diachronous both laterally and vertically within a given limestone formation in response to lithofacies changes.

The burial depth of occurrence of mechanical compaction features (Figure 20) depends on the primary texture of the host rock, on the size, shape, and nature of the bioclastic components, whether they are fragmented or whole, on the abundance of

matrix, and on the extent of early dissolution and cementation processes (early development of mouldic porosity, sea-floor related cements, or very shallow meteoric cements). In cores of buried southern Australian cool-water skeletal carbonates, Nicolaides and Wallace (1997b) showed that mechanical compaction features began at depths of less than 160 m for bioclast fragments and about 430 m for intact bioclasts. Meyers (1980) suggested that mechanical compaction features could form under less than 30 m of overburden.

4.10.2. Chemical compaction

Pressure-dissolution features observed in the Te Aute limestones include interpenetrating grains with both planar and curved contacts (Figures 19B, 19D), fitted fabrics (Figure 19D), dissolution seams, microstylolites, and rare, if any, true stylolites. Fitted fabric includes interpenetration of bioclasts but does not necessarily imply total destruction of interparticle pore space (Nicolaides and Wallace, 1997b). Dissolution seams are smooth, undulating surfaces or zones of dissolution, lacking sutures and fitting around bioclasts, which commonly show evidence of corrosion against the seam. Stylolites are serrated interfaces having sutured appearance with an amplitude greater than the diameter of the affected grains (Bathurst, 1980b, 1995). They can cut indiscriminately through matrix, cement, and allochems. Microstylolites are fine stylolite-like features, discernible only under the microscope.

Thin-sections of Te Aute limestones show a relationship exists between lithology and pressure-dissolution features. While planar/curved contacts, sutured contacts, and fitted fabrics are recognized in grainstones and occasionally in packstones, dissolution seams preferentially occur in matrix-dominated packstone and wackestone lithologies (Figure 20). As noted by Meyers (1980), clay-bearing and matrix-dominated rocks seem to be more susceptible to intensive chemical compaction than clay-poor rocks. In packstone/wackestone facies where early marine constructive diagenesis has been suspected, compaction features range from sutured to uncommon dissolution seam fabrics, which suggests early lithification of the matrix, while dissolution seams and microstylolites are common in their non-lithified counterparts (Figure 20).

Due to differential growth of early cements, pressure-solution may preferentially be present at the top of grains rather than at their bottom. Mud and fine skeletal debris that accumulated on the tops of grains prevent cements from growing on these surfaces.

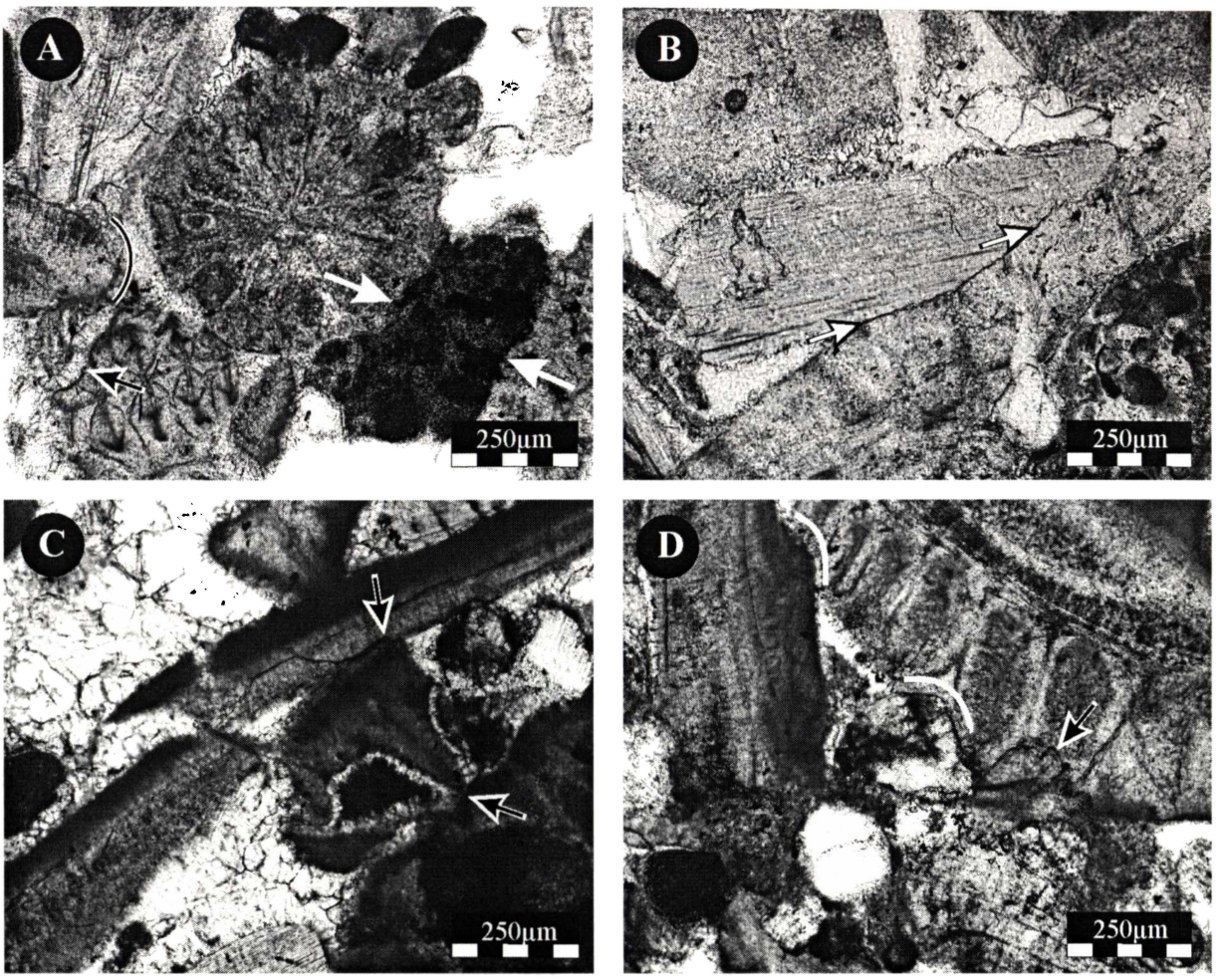

Figure 19- Plain light photomicrographs illustrating the various degrees of mechanical and chemical compaction, and their effects, within the Kairakau Limestone (Opoitian).

(A) Compactional plastic deformation (white arrows) and breakage of grains (black arrow). Note intergranular pressure-solution, underlain by the curved black line, between bivalve shell and crushed benthic foraminifer. PL: Sample 4.48.

(B) Planar to curved grain-to-grain contact (arrowed) associated with pressure-solution. PL: Sample 4.72.

(C) Compactional grain breakage and intergranular pressure-solution (arrowed). PL: Sample 4.76.

(D) Various chemical compaction features, including serrated contact (arrowed) and curved grain-to-grain contact (curved lines). PL: Sample 4.68.

Thus, during subsequent burial, pressure-dissolution will develop at the weaker grain tops mantled with uncemented sediments rather than on the sides and bottoms of grains that are armoured by cements.

The lithostatic pressure necessary to produce significant pressure-dissolution in carbonate deposits is poorly understood. The range of depths proposed by different authors suggests that the amount of overburden is not the only controlling factor. In southern Australian subsurface temperate limestones, Nicolaides and Wallace (1997b) record planar and concavo-convex contacts at relatively shallow depths (c. 160 m), and sutured contacts only at deeper levels (c. 430 m) where they are commonly associated with fitted fabrics. They observed fitted fabrics in deeper grainstone samples at about 550 m, whereas dissolution seams were noted in matrix-rich wackestones at depths shallower than 190 m. Microstylolites became evident in their deepest grainstone samples, at depths of approximately 550 m. Nelson *et al.* (1988c) estimated a critical pressure-dissolution threshold level of about 500 m burial in mid-Tertiary non-tropical limestones of the Te Kuiti Group in New Zealand, with the development of non-sutured seams and microstylolites (Figure 20).

As previously suggested, factors that might promote chemical compaction processes include the mineralogy of allochems (calcitic rather than aragonite bioclasts could mean little early cementation, but on the other hand little mouldic porosity development), time of residence in the burial environment, pore water composition, and especially its level of saturation with respect to $CaCO_3$. Thus, different combinations of these pressure-dissolution promoting factors could result in the development of similar compaction features at different burial depths, and possibly mainly at shallower depths for calcitic limestones than aragonite-rich ones.

4.10.3. Pressure-dissolution and cementation

The Te Aute petrographic data suggest a possible correlation exists between extensive pressure-dissolution and pronounced cementation, especially in the older Opoitian and Waipipian limestone formations, a feature also of other calcitic limestones (Nelson *et al.*, 1988c; James and Bone, 1989; Choquette and James, 1990; Hood and Nelson, 1996; Dodd and Nelson, 1998). Thus, in these Te Aute limestones (Kairakau, Awapapa, Rotookiwa, Titiokura, Te Waka) significant calcite precipitation only starts with the post-compaction PoFC generation. However, PoFCs commonly pre-date dissolution

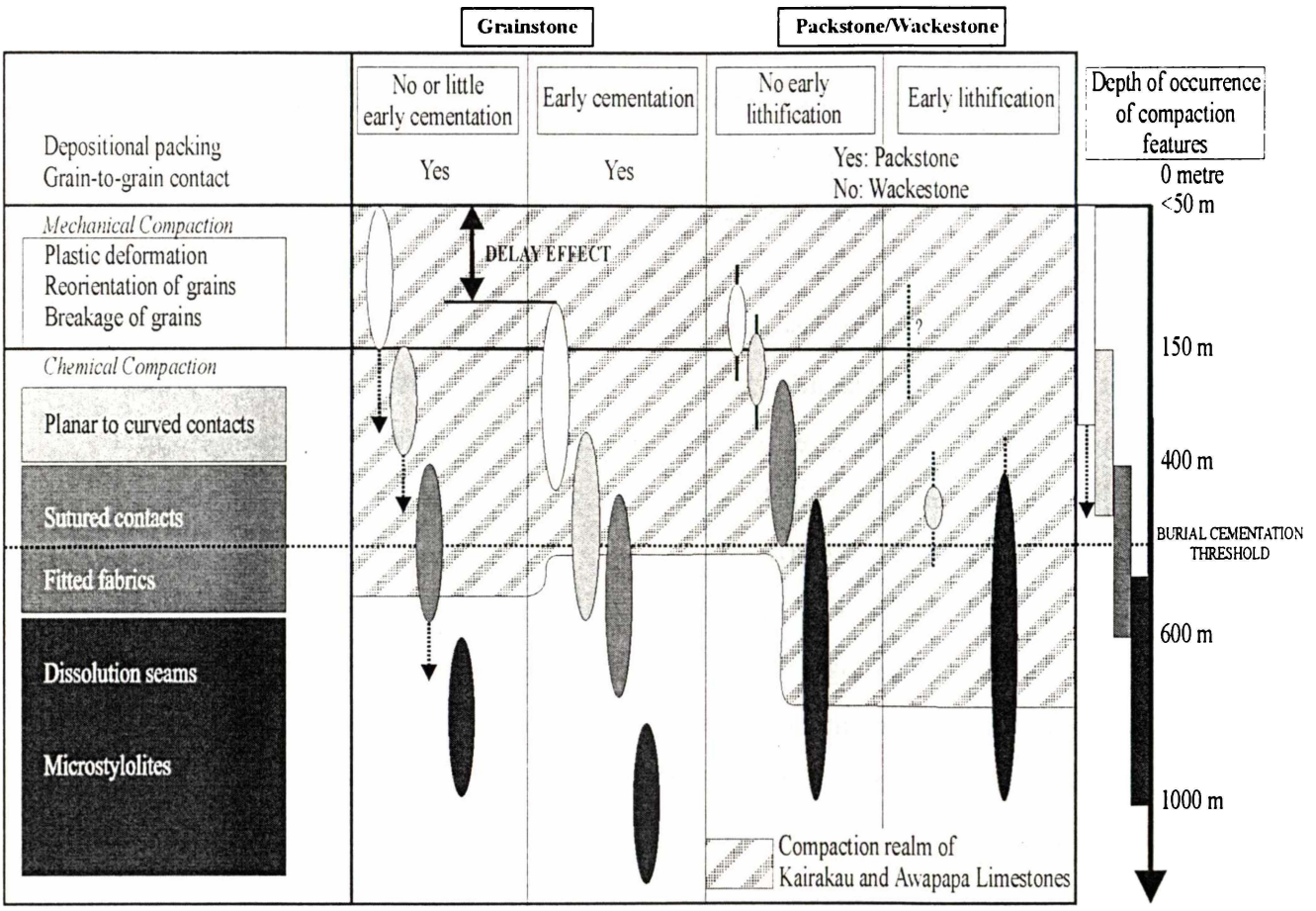

Figure 20- Schematic diagram showing that not only depth of burial but also sediment texture and degree of early cementation are significant factors in the timing of occurrence of compaction processes during progressive burial. For example, mechanical compaction occurs deeper in early-cemented limestones than in their non-early-cemented counterparts (delay effect). On the right side of the diagram is a compilation of the burial depths of occurrence of the various compaction features as reported by others (e.g., Meyers, 1980; Nelson *et al.*, 1988c; Nicolaides and Wallace, 1997b).

seams producing serrated contacts and microstylolites, which are essentially restricted to the base of the sediment pile (i.e., Kairakau and Awapapa Limestones), but pre-date and post-date grain-to-grain and curved-grain contacts. These relationships would indicate that carbonate derived from pressure-dissolution might have not been the major contributor to the cementing phase (see discussion in Chapter 5, Section 4.4).

In the southern Australian temperate limestones, Nicolaides and Wallace (1997b) reported well developed sutured and fitted fabrics between 430 and 550 m burial depth, the same interval over which most of their core samples lost remaining porosity by calcite cementation, and in agreement with the threshold interval of burial cementation suggested by Nelson *et al.* (1988c) for mid-Tertiary non-tropical limestones in New Zealand. In both the Australian and New Zealand limestones commonly as much as 75% of their primary depositional porosities of 40-50% had been lost prior to this main cementation phase, emphasizing that in these deposits compaction, and notably mechanical compaction, was a more important porosity-destroying process than was cementation (Nelson *et al.*, 1988c; Nicolaides and Wallace, 1997b).

4.11. Diagenetic sequence diagrams

Figure 21 illustrates the synthetic representation of diagenetic data, namely the diagenetic sequence diagram, which combines the chronological suite of both diagenetic fabrics evident in thin-sections and CL patterns of cements organized in discontinuity-bounded CL sequences (see Chapter 2, Section 4.3). The construction of diagenetic sequence diagrams like these for each collected sample (full data in Appendix 5) has proved determinant for understanding the diagenetic evolution of the Te Aute limestones in relation to both patterns of sea-level changes (see Chapter 4), and burial and tectonic processes (see Chapter 5).

5. Carbonate diagenesis and relative sea-level changes

In this section, a series of predictive stratigraphic-based diagenetic models is presented, constrained by sequence stratigraphic considerations. The discussion builds upon earlier works by Longman (1980), Heckel (1983), Tucker (1993), and the recent review by Moore (2001).

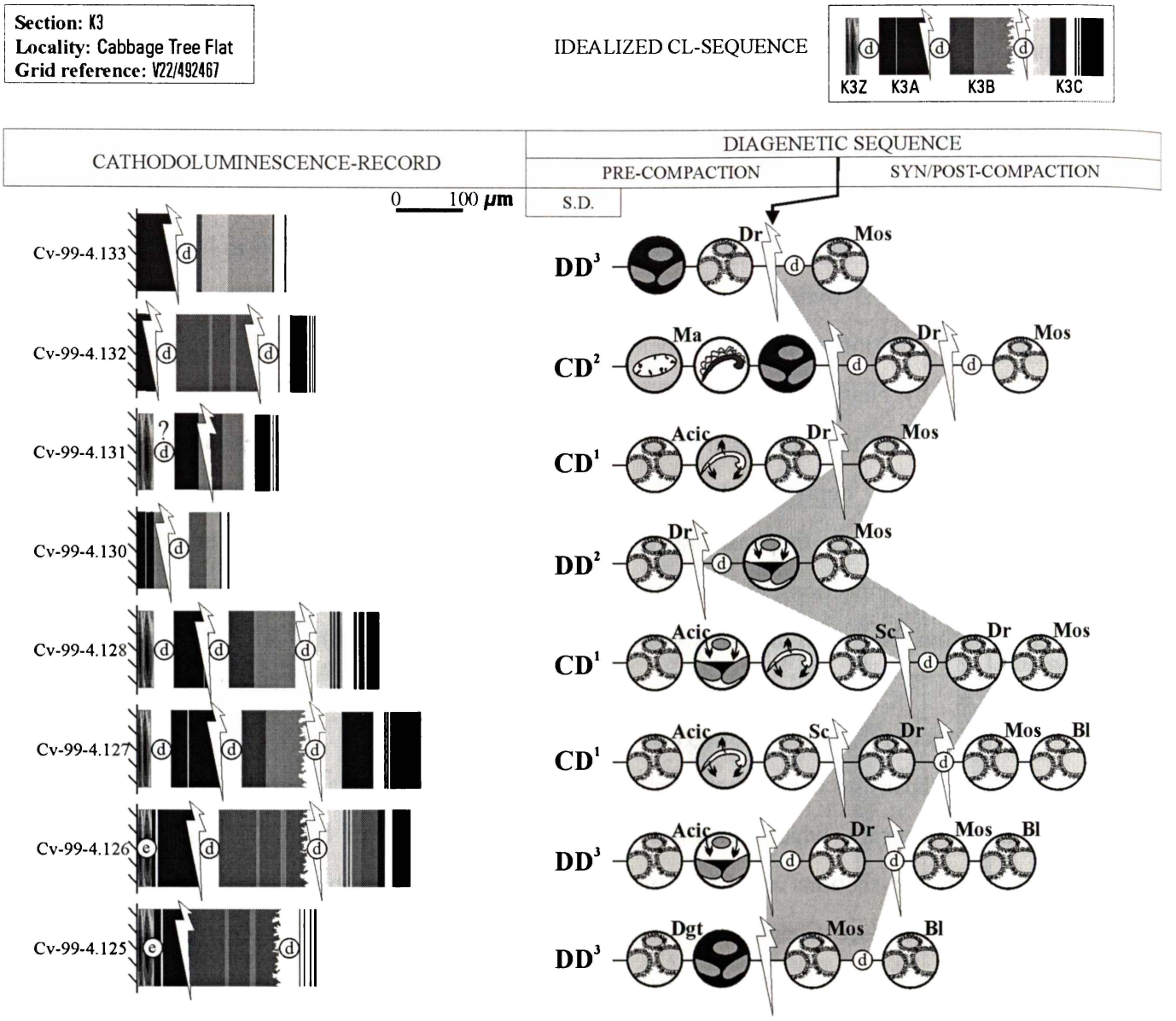

Figure 21- Diagenetic sequence diagrams of samples collected from one section of Kairakau Limestone. The diagenetic sequence diagram is a schematic representation of the chronological occurrence of diagenetic fabrics, for which several logotypes have been created (see Chapter 2 – Figure 3 for the petrographic logo scheme). Diagenetic features are described in thin-sections sequentially from grain surface to pore centre. The diagenetic sequence diagram combines observations made under plane polarized and cathodoluminescent light modes. Despite the complexity of diagenetic features, the diagenetic suites are readily divisible into pre- and post-compaction stages based on the first occurrence of compaction-induced skeletal fracturing. Sequence diagrams for all the Te Aute samples are presented in Appendix 5. The grey background relates to diagenetic phases attributed to the burial environment.

5.1. Sequence stratigraphic framework

Sedimentary successions bounded by unconformities, or sequences, are mostly produced by third- to sixth-order relative sea-level changes (Van Wagoner *et al.*, 1988; Vail *et al.*, 1991). Higher-frequency sequences typically constitute the building blocks of lower-frequency (longer term) sequences, and originate in climate changes forced by orbital perturbations (Milankovitch cyclicity) that subsequently drive changes in the volume of ice caps leading to glacio-eustasy.

Relative sea-level changes are affected by climate-driven eustasy and tectonism at the site of deposition, whose combined effects result in variations in terms of space available for sediments to accumulate, or accommodation space (Posamentier *et al.*, 1988). Typically, while tectonism is the major control on the creation of accommodation space, high-frequency glacio-eustasy determines the internal architecture of sedimentary sequences (Figure 22). Thus, the basic building packets of sedimentary sequences, referred to as systems tracts, stack in response to major inflections on the eustatic sea-level change curve divided into a rising (TST) and a falling limb (HST, RST and LST).

Sequence stratigraphy was first conceptualized in, and applied to, siliciclastic successions. Since then, researchers have shown such sequence stratigraphic concepts are applicable to the carbonate regimen, provided that potential modifications to the model are appreciated that take into account the specificities of carbonate systems (Sarg, 1988; Hardie *et al.*, 1991; Tucker, 1993; Goldhammer *et al.*, 1994; Zempolich and Erba, 1999).

In the case of the Te Aute temperate carbonates, such specificities include:

(a) Sensitivity to factors that specifically impact the rate of carbonate production, including terrigenous input and nutrient supply, especially in a filter feeder-dominated system (Kamp *et al.*, 1988; Beu, 1995). Therefore, temperate carbonate sedimentation develops in shallow-water depositional settings swept by strong currents that enhance terrigenous sediment by-passing. The importance of the water depth is that relative sea-level falls of moderate amplitude (>30 m) may result in exposure of carbonate factories to surface-related diagenesis.

(b) Temperate carbonate sediments also accumulate at slower rates than do tropical equivalents, typically on the order of 5 to 50 cm/1000 years, and often <10 cm/1000 years (Nelson *et al.*, 1988b; James, 1997; Figure 22). Because of these relatively slow

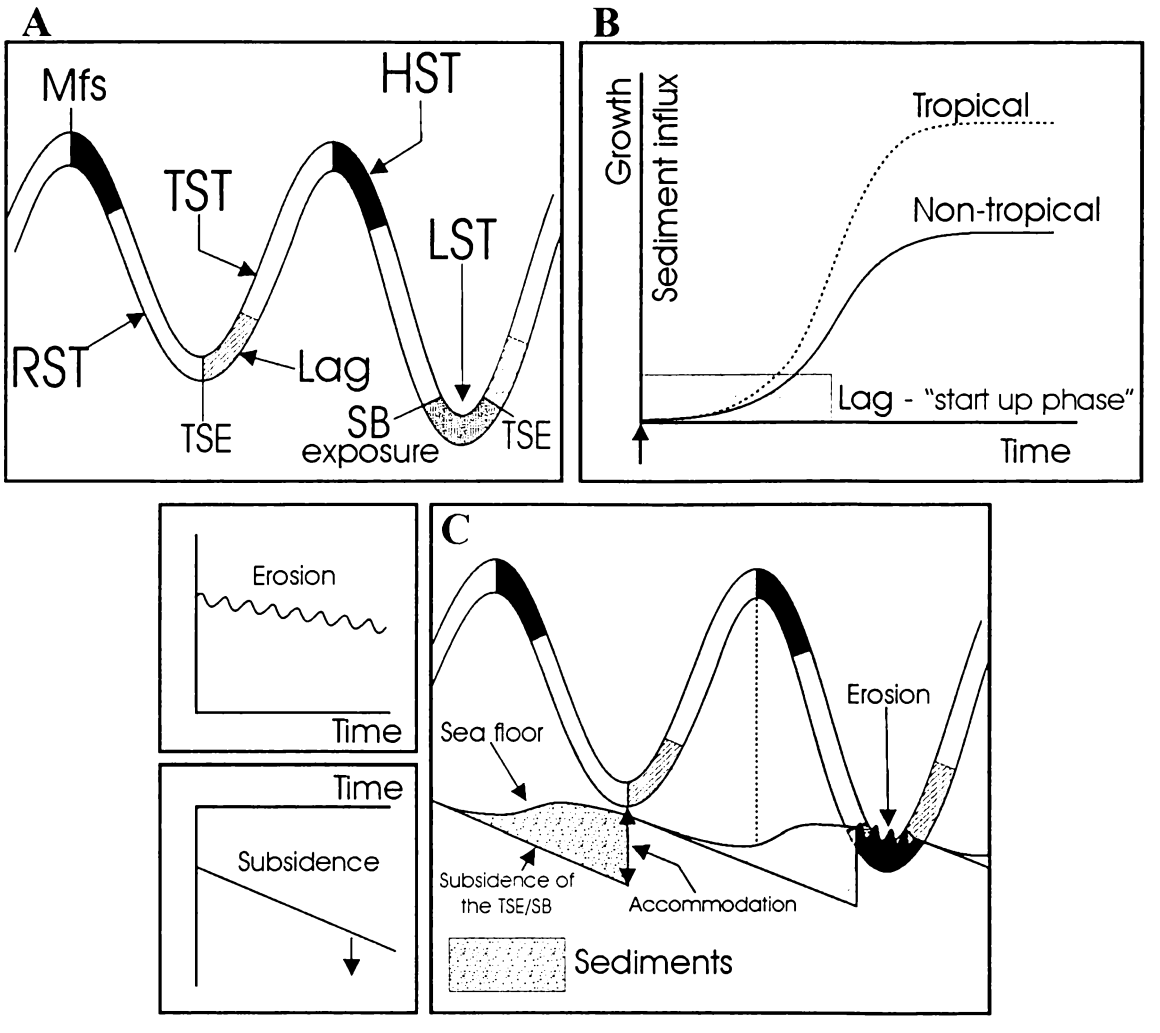

Figure 22- (A) Positions of systems tracts and significant bounding surfaces, including the transgressive surface of erosion (TSE), and the sequence boundary recording emergence (SB), during the course of one theoretical eustatic sea-level cycle (TSE – TST – Mfs – HST – RST – SB – LST). When the sea-level fall is strong, the antiform tops (see Chapter 1, Figure 29) are likely to be exposed (unless the rate of sea-level fall does not exceed the rate of subsidence minus the rate of sedimentation).

(B) Law of sigmoidal growth versus time for carbonate population after flooding (arrow) of carbonate factories (after Neumann and MacIntyre, 1985). The curve of population growth is assumed to mirror carbonate production. The curve applies to the flanks of the antiforms. Atop the antiforms, within the lag phase, carbonate factories partly rejuvenate and fossiliferous lags are deposited, before drowning, probably at the inflection point of the rising limb of the eustatic sea-level curve.

(C) Plot of the carbonate production curve against the eustatic sea-level. During the rising limb of the curve, carbonate production is low. During the HST, no more accommodation space is created, and carbonate populations start to grow. During the RST, the combination of falling eustatic sea-level and increasing sediment flux leads to the infilling of bathymetric space, and progradation on the flanks of the antiforms (see Figure 25). Eventually, carbonate production is maximized (top of sigmoid curve – see B), and if eustatic sea-level keeps falling and reaches the sea bed, a sequence boundary forms. The antiform tops are exposed and eroded, and LST sediments may accumulate at the foot of the antiform flanks (modified from Naish and Kamp, 1997).

TST – Transgressive Systems Tract; Mfs – Maximum flooding surface; HST – Highstand Systems Tract; RST – Regressive Systems Tract; LST – Lowstand Systems Tract.

(c) overall rates of accumulation, temperate carbonate systems are particularly sensitive to relative sea-level rises, and tend to be swamped by terrigenous sediments as current velocity decreases with increasing water depth. This contrasts with tropical carbonate systems where sedimentation rates are generally high enough to keep up and even exceed the rates of relative sea-level rise (Emery and Myers, 1996).

(d) The dominant LMC mineralogy for most Te Aute carbonates (from Opoitian to early Nukumaruan) is responsible for their low chemical reactivity, which translates into low dissolution potential of carbonate fragments and cements, and consequently poor cementation development. This contrast in mineral solubility with aragonite- and HMC-rich tropical deposits is particularly critical to the record of meteoric influence during exposure at sequence boundaries.

(e) The reduced saturation level with respect to calcium carbonate of temperate marine waters, and their high pCO_2 due to "cool" water temperatures compared to their tropical counterparts, do not favour sea-floor constructive diagenesis (James, 1997). Therefore, any evidence of marine cementation in these carbonates may be of great importance to their sequence stratigraphic interpretation. Indeed, cementation is not ubiquitous in marine temperate environments, but only occurs under certain favourable conditions, including high rates of fluid movements through the sediments, high sediment porosity and permeability, and low rates of sedimentation.

5.2. Depositional setting for the Te Aute carbonates (Opoitian to early Nukumaruan)

The eastern part of the studied area (Figure 1) has been subjected to folding since at least Early Pliocene resulting in a number of anticlines and synclines trending northeast-southwest, parallel to the subduction complex. Kamp *et al.* (1988), Beu (1995), and Nelson *et al.* (in review) inferred that sites of carbonate formation were located over the relict antiform topography associated with tectonically-emplaced structural elements such as thrust fault-bounded blocks (see Figure 24). Described as an archipelago of structural highs and neighbouring carbonate factories, the depositional setting for the Te Aute carbonates shares many attributes with isolated structurally-controlled platforms that support major carbonate production, as documented for example in Southeast Asia (Emery and Myers, 1996).

Characteristics of such isolated platforms are that they are generally siliciclastic free, best exemplified in the Hawke's Bay forearc basin by the Rotookiwa, Te Onepu, and Pakipaki Limestones (Figure 1), and lack the close interrelation with continent-derived sediments, as reported for continent-attached platforms, and exemplified in the Hawke's Bay setting by western Waipipian and Mangapanian limestones (Te Waka Formation; Figure 1).

The characteristics of the eastern and western depositional models for the Te Aute limestones were fully depicted in Chapter 1, Section 7 (Figures 29, 30).

5.3. Carbonate diagenesis on a high-frequency sequence scale

The following discussion is concerned with diagenesis at the level of discontinuity-bounded units produced by relative sea-level changes on a short time frame (mostly between 20 000 and 50 000 years). Although there is a great variation in the number of building sequences within the Te Aute limestones from one formation to another, or within the same formation, they generally consist of four to six metre-scale sequences (<20 m thick; see Chapter 4, Section 8). On the basis of stratigraphic and diagenetic criteria, discontinuity surfaces have been recognized within the limestone bodies that coincide with periods of erosion, or low and/or no sedimentation. The vertical stacking of sedimentary facies between consecutive key surfaces, and the comparison of diagenetic histories recorded on either side of key surfaces, have enabled the positive distinction of transgressive and transgressive-regressive depositional sequences, and of diagenetic patterns specific to the building of the systems tracts.

Figure 23 shows an idealized Te Aute carbonate sequence resulting from transgressive-regressive events (deepening- then shoaling-upwards depositional trend), that is bounded below by a transgressive surface of erosion (TSE) and above by a surface recording emergence (Sequence Boundary). Most Te Aute sequences differ from this idealized model by displaying a great variation in facies, thickness of building systems tracts and their attributes, the number of systems tracts (due to frequent erosion of the upper RST), and diagenesis (see Chapter 4, Section 8). Furthermore, by contrast with many tropical shallowing-upwards sequences (parasequences), the upper bounding surface of the Te Aute sequences appear rarely to have been subaerially exposed, barring any evidence for emergence that may have been removed by erosion. However, this idealized model amalgamates many field observations and constitutes the background

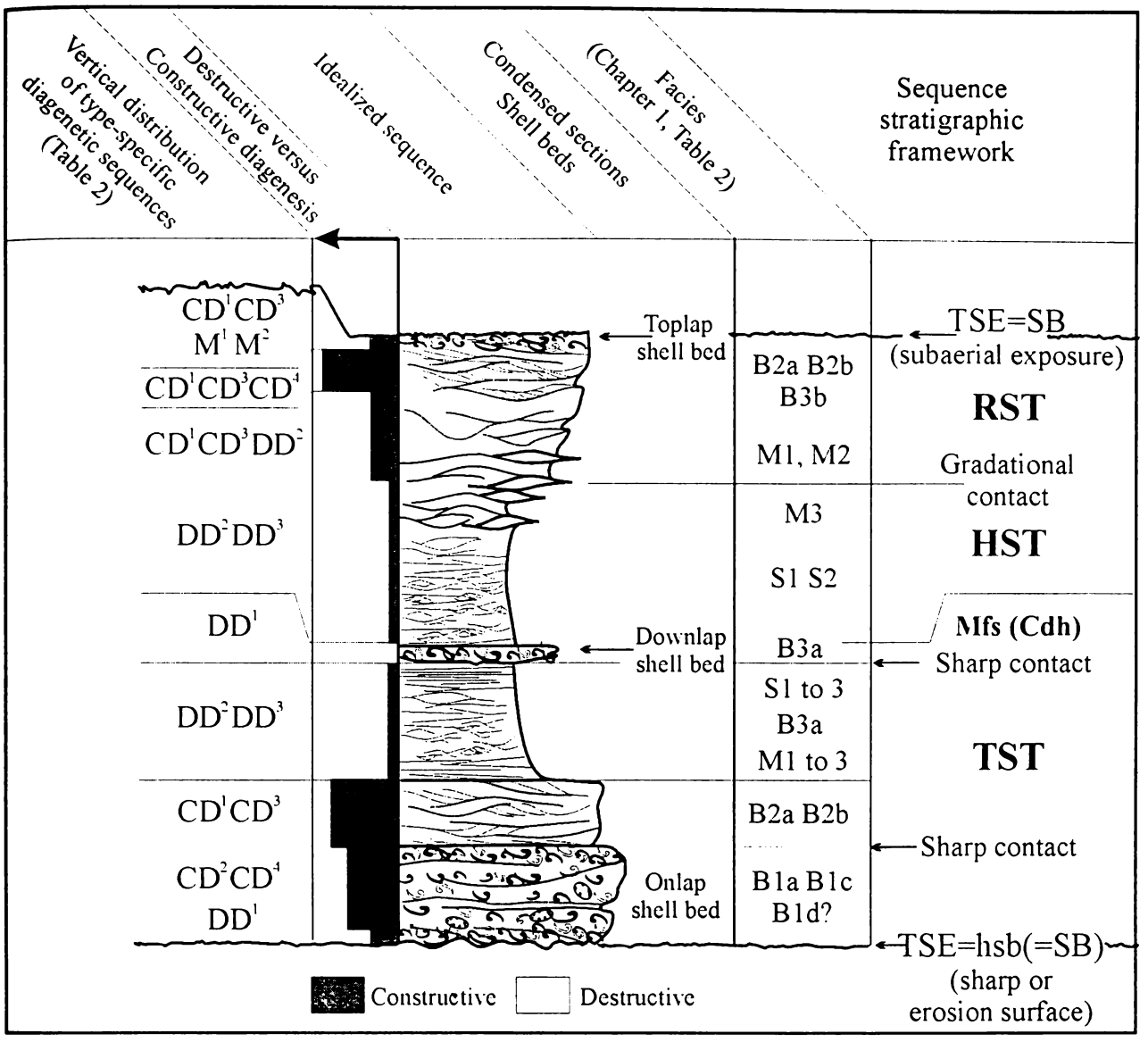

Figure 23- Model for the pattern of carbonate diagenesis in the Pliocene carbonat sequences. The idealized sequence integrates the sedimentological, diagenetic, an inferred sequence stratigraphic attributes for the sequences recognized in 47 stratigraphi sections of Plio-Pleistocene Te Aute limestone (see Appendix 1). All sequences ar bounded by TSEs (= hsb = high-frequency sequence boundary; locally a major sequenc boundary = SB). The lower TSE lies at the base of the depositional sequence marked b condensed fossiliferous to pebbly transgressive lags, and the upper TSE is overlain by th basal transgressive lag of the next sequence. From the basal TST, sequences exhibit deepening-upwards depositional trend (shallow-water transgressive lag to near storm wave base mixed siliciclastic-carbonate sediments), and are characterized by increasingl destructive early diagenesis ($CD^{1, 2, 3}$ to $DD^{1, 2, 3}$; see Table 2) towards the superjacer Mfs. From this surface, the depositional trend is one of shoaling-upwards, and is bounde above by the TSE lying in the RST. Most Te Aute sedimentary sequences comprise thi vertical stacking pattern. The upper RST comprises thick marine cements, and as such i dominated by constructive diagenesis ($CD^{1, 3, 4}$). In some examples, the upper cappin surface of the RST is a sequence boundary (SB) that shows discrete evidence of subaeri exposure (dissolution and little if any meteoric cementation). Thus, due to meteori influence, destructive diagenetic features dominate the specific diagenetic record beneat the SB ($M^{1, 2}$). Cdh = condensed diagenetic horizon (see Chapter 4, Section 5.3.3).

Table 2- Classification of a range of constructive (CD) to destructive (DD) specific diagenetic suites based on petrographic properties of pre-compaction diagenetic features in Te Aute limestones.

Specific diagenetic suite	Facies	Chronological occurrence of diagenetic processes	Interpretation
CD^1 Constructive	Medium- to coarse-grained Clast-supported	- Skeletal grains are variably abraded - Macroboring of shells occurs occasionally; microboring is present to common, microbores penetrate deeply into bioclasts; micritization poor to moderate - Unilaminar encrusting bryozoans occasionally evident - Authigenic glauconite forms but is scattered, moderately evolved (pale green) - Dissolution of aragonite allochems predating marine cements occurs rarely - Internal sediments commonly pre-date and post-date acicular inclusion-rich isopachous cements (up to 100 µm thick). Internal sediments may be microbioclastic or micritic, are geopetally distributed in interparticle pores, but seldom laminated - *In* situ precipitated peloidal micrite (<50 µm in diameter, spherical, nucleus-free peloids)	Near sea floor, marine phreatic environment Marine waters undersaturated enough to dissolve aragonite near sea floor, marine phreatic environment Microbially induced, marine phreatic environment
M^1 Mixed	Medium- to coarse-grained Clast-supported	Same events as in CD^1, but followed by meteoric diagenesis. The capping surface of the sequence is subaerially exposed; neomorphism of metastable mineralogies is the dominant process - Dissolution of skeletal allochems (moldic voids and collapse of weakened shells), the outer margin of acicular cements may be corroded, and cements may be neomorphosed into scalenohedral crystal rims that exhibit internal ghosts of elongate inclusions - Drusy to mosaic clear spar	Phreatic meteoric environment undersaturated waters with respect to $CaCO_3$ percolate from the capping unconformity
M^2 Mixed	Medium- to coarse-grained Matrix-supported	Same events as in M^1, but clast-supported host of CD^1 becomes matrix-supported; clear spar cements are rare; micritic crust may form (iron stained or not); yellowish bioclast- to microquartz-rich homogenous to laminated micrite infiltrates	Phreatic and possibly vadose meteoric environment
CD^2 Constructive	Coarse- to very coarse-grained Matrix-supported	- Skeletal grains are poorly to moderately abraded - Macroboring is common to abundant; microboring is common - Common, well preserved encrusters such as red algae and uni- and multi-laminar bryozoans - Occasional thin isopachous acicular cements - Syndepositional homogenous micrite; *in situ* precipitated peloidal micrite - Matrix may be burrowed; burrows are filled with another generation of internal sediment - Induration of micrite may occur at this stage (seldom)	Near sea floor, marine environment
M^3 Mixed	Coarse- to very coarse-grained Matrix-supported	Same events as in CD^2, but followed by processes related to meteoric diagenesis - Occasional fracturing and micro-brecciation of host rock; rare mud cracks - Dissolution of skeletal allochems; micritic crust (iron-stained or not); yellowish bioclast- to microquartz-rich homogenous to laminated micrite infiltrates - Blocky to mosaic clear spar	Phreatic and possibly vadose meteoric environment

CD^3 Constructive	Medium-grained Clast- to matrix-supported	- Skeletal grains are moderately to well abraded; moderately preserved red algae and bryozoan encrusters - Homogenous syndepositional micrite pre-dated and post-dated by micritization (densely microbored and subsequently micritized margin of shell fragments is up to 200 μm thick) - Induration of micrite may occur at this stage	Near sea floor, marine phreatic environment
CD^4 Constructive	Medium- to coarse-grained Matrix-supported	- Moderately abraded grains - Moderately preserved encrusters (red algae, bryozoans); rare authigenic glauconite - Micritic crust possible; homogenous syndepositional micrite irregularly distributed in pore space (digitations toward pore centre and menisci) - Neomorphism of skeletal allochems may occur (relicts of microstructures common); precipitation of blocky to mosaic clear spar cement may also occur	Vadose marine (though phreatic marine possible) to vadose meteoric environment
DD^1 Destructive	Fine- to medium-grained Clast- to matrix-supported	- Strongly abraded skeletal grains (very well rounded); intensively microbored (multigeneration) - Evolved authigenic glauconite (deep green, brown) and iron oxides fill most intraparticle pores - Uncommon acicular inclusion-rich cement; dissolution of aragonitic shells may also occur - Common intrinsic homogenous micritic sediment seals the sequence	"Starved" sea floor, prolonged exposure of grains on the sea floor
DD^2 Destructive	Fine- to medium-grained Clast-supported	- Moderately to well abraded grains - Encrusting by uni- and multi-laminar bryozoans possible; common microboring - Common thin acicular isopachous extrinsic cement; rare to common authigenic glauconite	Marine phreatic environment
DD^3 Destructive	Fine- to medium-grained Matrix-supported	- Poorly to moderately abraded grains - Microboring is common; authigenic glauconite is common - Extrinsic thin (<50 μm) acicular cement is possible - Homogenous syndepositional micrite - Burrowing common; burrows are filled with clast-supported internal sediment (microquartz, planktic foraminifers, etc.)	Marine phreatic environment

against which Te Aute sequences can be compared to emphasize minor to major differences from the model, which once recognized may be better explained.

The comparison of pre-compaction diagenetic suites in outcrop samples from above and below significant disconformities enables isolation of the "specific diagenesis" of unconformity-bounded depositional units (see Chapter 2, Section 5.4.1). One of the main observations of this study is that the attributes of the specific diagenesis of a sequence change vertically, and appear to be strongly correlated to depositional facies. This provides a good sequence stratigraphic framework to assess the timing of diagenetic processes, and both their relation and contribution to the building-up of systems tracts. Ten type-specific diagenetic suites have been defined, distributed on a scale from mainly constructive to mainly destructive diagenesis (Table 2). Considering the vertical distribution of the specific diagenetic suites, there exists a definite pattern of occurrence within the sequences which can tentatively be integrated into a scheme of relative sea-level changes.

5.3.1. Carbonate diagenesis model of isolated antiforms during relative sea-level rise: TST (Figure 24A-B)

Once marine flooding is initiated on the antecedent antiform topography (Figure 24A), water depth is expected to increase rapidly, because the rate of relative sea-level rise, being a function of eustasy and subsidence, can exceed the rate of eustatic rise, especially when the rate of sedimentation is low (Kamp and Naish, 1997). The rapid initial flooding of well developed carbonate factories (RST sediments of the previous sequence) causes carbonate production to slow, in some cases to be terminated, inducing a lag (Emery and Myers, 1996) until new populations of carbonate-secreting organisms are re-established on the antiform. This lag phase and progressive re-establishment of carbonate production is referred to as the "start-up" phase by Neumann and MacIntyre (1985; Figure 22).

In the Te Aute sequences, these initial conditions are sometimes reflected in thin condensed deposits (a few centimetres up to a few decimetres) overlying the transgressive surface of erosion (see discussion about bounding discontinuities in Chapter 4, Section 5.3.5). As the accumulation rate is low, there is a prolonged time of residence on the sea floor for the skeletal fragments, which consequently are potentially subject to frequent reworking and bioerosion processes. Therefore, carbonate diagenesis during the initial flooding is characterized by destructive processes. Sediments are fine-

grained, skeletal fragments are well abraded and intensively microbored, early thin acicular cement may form lining the walls of intraskeletal pores. Detrital, well rounded glauconite is also present in the lower TST, from erosion and reworking of older deposits, but also sediment starvation determines the conditions most favourable for authigenic glauconite to precipitate in intraskeletal pores (Amorosi, 1995). These attributes characterize the specific diagenetic suite DD^1 (Table 2; Figure 24A).

The stratal pattern of many Te Aute sequences indicates that before eustatic sea-level reaches its maximum (Maximum flooding), temporary carbonate factories form, probably atop the antiforms, characterized by distinct skeletal assemblages dominated by epifaunal bivalves (ostreids and pectinids) and bryozoans (see Chapter 4, Section 5.4.1). Coarse fossiliferous deposits are transferred along the TSE, and the previous condensed lag is reworked within the lower part of the coarse deposits. Transgressive fossiliferous deposits are typically coarse-grained, contain bored pebbles, well rounded mud pebbles, macrobored shells, and variable concentrations of detrital glauconite. Their diagenesis is characterized by constructive processes, including encrustation, precipitation of inclusion-rich fibrous cements, *in situ* precipitation of peloids, and percolation of micrite sediments, that collectively build up the specific diagenetic suite CD^2 (Table 2; Figures 23, 24B). Such sea-floor diagenetic fabrics suggest active circulation of marine waters within pore spaces. Tucker (1993) commented on the likelihood of marine cementation in TSTs as marine pore waters move landward during sea-level rise, pushing mixing zone and meteoric waters ahead (Figure 24). Marine constructive diagenesis in the lower part of TSTs has been reported by several researchers who also document decreases of constructive processes in the upper part of TSTs as sea-level continues to rise (James and Bone, 1992; Boreen and James, 1995; Nelson and James, 2000).

Eventually, the eustatic sea level reaches its highest point where bathymetry is also assumed to be greatest (Maximum flooding surface). These conditions cause current velocity to decrease to the point where marine pore waters become stagnant and cementation is no longer promoted. At this stage carbonate production is low due to partial drowning (Neumann and MacIntyre, 1985; Emery and Myers, 1996), and condensation occurs generating once again a suite of destructive diagenetic processes of type DD^1 above the TST (Figures 23, 24C).

Figure 24- Carbonate diagenesis model of isolated antiforms during sea-level rise: TST (A-B), and during sea-level highstand: HST (C-D).

(A) During the early stage of sea-level rise, the diagenetic suite of carbonate sediments on the flanks of the antiforms reflects conditions of destructive diagenesis, including abrasion, bioerosion, and minor dissolution, and conditions of sediment starvation with abundant detrital and authigenic glauconite (specific diagenetic suite DD^1).

(B) Atop the antiforms, carbonate factories are partly re-established. Sea-level rise leads to active marine pore-fluid circulation promoting marine constructive diagenesis. The diagenetic suite comprises precipitation of inclusion-rich fibrous cements, the emplacement of geopetal sediments, *in situ* peloids, encrustation by uni- and multilaminar bryozoans, and bioerosion (specific diagenetic suite CD^2).

(C) The maximum flooding surface (Mfs) marks the time interval during which carbonate sedimentation is at its lowest. These conditions are reflected in thin condensed lags suffering intensive destructive diagenetic processes (specific diagenetic suite DD^1).

(D) Once sea level starts to fall, and bathymetry is reduced, carbonate factories start to rejuvenate on the antiform tops. Skeletal fragments accumulate and the main feature of sedimentation is aggradation. The depositional setting remains below the influence of strong storm and wave currents. Consequently, carbonate diagenesis is one of a destructive type (DD^2), including abrasion and bioerosion but at a lesser degree than in periods A and C.

SL0 to SL2 is sequential sea-level change (continues in Figure 25).

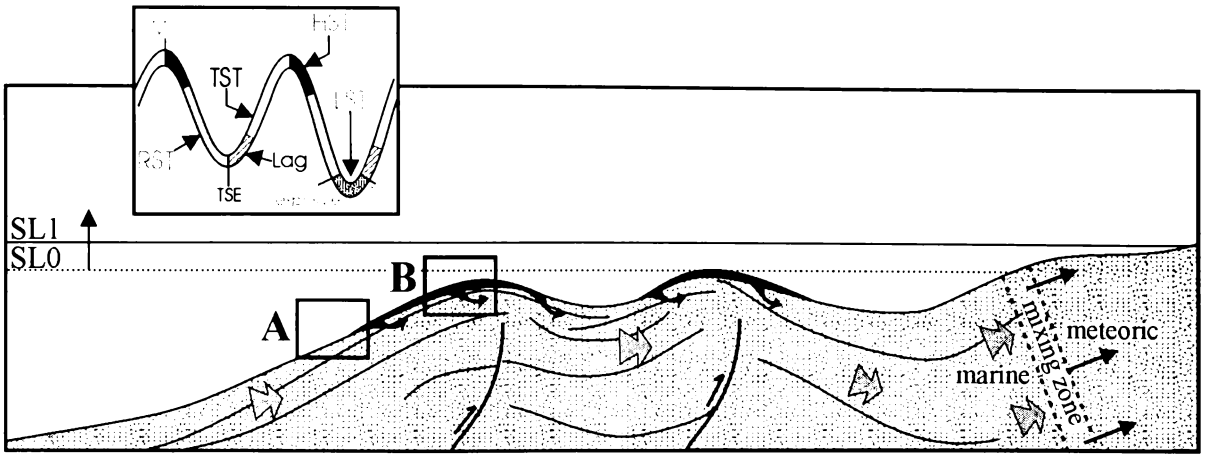

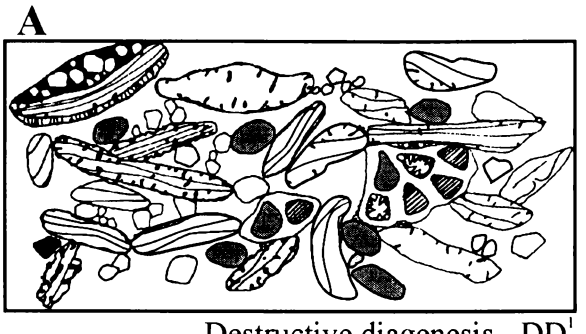

Destructive diagenesis - DD[1]

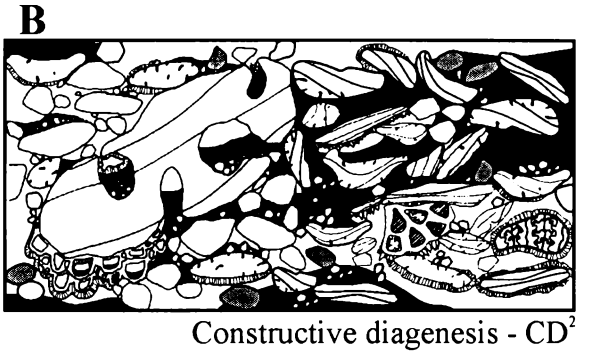

Constructive diagenesis - CD[2]

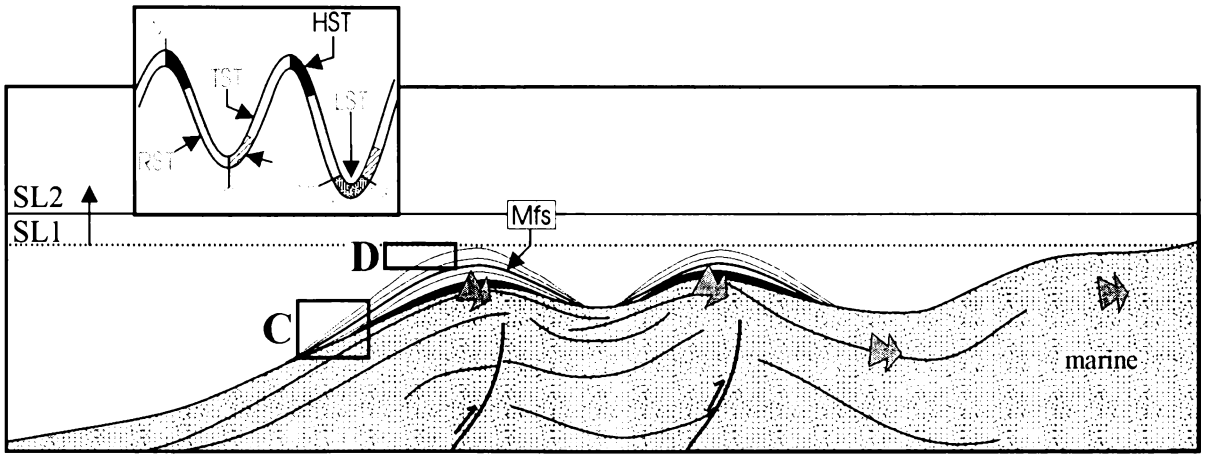

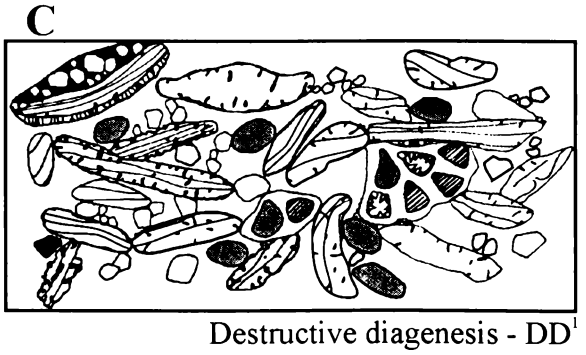

Destructive diagenesis - DD[1]

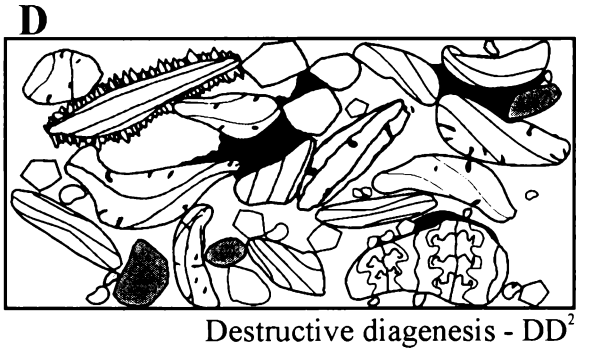

Destructive diagenesis - DD[2]

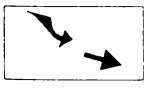

Active fluid circulation and zone of potential precipitation of cements

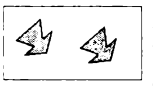

Passive fluid circulation and zone of potential precipitation of cements in the meteoric phreatic and mesogenetic realms

5.3.2. Carbonate diagenesis model of isolated antiforms during a sea-level highstand: HST (Figure 24D)

Beyond the inflection point on the sea-level curve, corresponding to the time of maximum flooding (Figures 22, 24), eustatic sea level starts to fall, and if its rate equals or exceeds the rate of subsidence, then the rate of generation of new accommodation space slows (Van Wagoner *et al.*, 1988; Vail *et al.*, 1991; Kamp and Naish, 1997). These conditions are reflected within planar-bedded deposits increasingly enriched in skeletal fragments, especially bivalves and barnacles, that overlie the previous condensed lag atop the TST. This suggests that the rate of carbonate production accelerates, and available accommodation space starts to be progressively filled (Figure 22). Thus, the main feature of carbonate sedimentation is expected to be aggradation (Emery and Myers, 1996).

HST sediments are fine- to medium-grained, and skeletal fragments are moderately to well abraded and become dominant over siliciclastic grains. Textures vary from medium-grained packstones to fine- to medium-grained grainstones. The specific diagenetic suite within the HST deposits records destructive processes (DD^2 and DD^3; Table 2; Figures 23, 24D), including abrasion, bioalteration (microboring), and rare dissolution of aragonitic allochems. Authigenic glauconite is common, while pore lining cementation is rare. This suggests that sediments remain below the influence of storm and wave currents, and consequently flow rates of marine waters through the sediments are low.

5.3.3. Carbonate diagenesis model of isolated antiforms during a sea-level fall: RST (Figure 25E)

Theoretically, the combination of maximized carbonate production in growing carbonate factories, and fast falling eustatic sea-level results eventually in a decrease of bathymetry (Figure 22) and causes available accommodation space to be filled, and the volume of excess carbonate sediments to be shed off the antiform tops into deeper water environments (Emery and Myers, 1996). Thus, as a result of aggradation and progradation, sediments come under the influence of high-energy wave and tidal currents, and are swept to the antiform flanks where they accumulate in the form of basinward-prograding sand waves and sand dunes (Figure 25). Under such conditions, siliciclastic sediments are by-passed into deeper environments, and barnacle-dominated

carbonate factories reach their maximum production rate (Kamp *et al.*, 1988; Beu, 1995; Nelson *et al.*, in review). As illustrated in Figure 25, in a regime of constant sediment flux the trough space (synforms) between neighbouring antiforms may be filled by prograding RST sediments derived from either bounding carbonate factories. This may lead to the coalescence of the neighbouring antiforms into continuous carbonate sheets, as appears to have been the case for the better-developed Te Aute limestones (e.g., Te Onepu Limestone).

Carbonate deposits consist of cross-stratified, coarse-grained pure-coquina sediments. At the site of carbonate production, and laterally but still atop the antiforms in shallow-water environments, active pore water circulation enhances CO_2 degassing and favours marine cementation. Therefore, RST carbonate deposits that accumulated in the shallow-marine environment where the rates of accumulation are low, and where sea-water pumping through the sediments is vigorous, are characterized by constructive diagenetic processes (specific diagenetic suite CD[1]; Table 2; Figures 23, 25E). Thick rinds of turbid fibrous cements line interparticle pores, micrite sediments percolate from the water-sediment interface, macroboring is common while microboring is moderate, and encrustation by unilaminar and multilaminar bryozoans is present, even though strong currents generally prevent them from being well preserved. Dissolution of aragonite allochems may also occur in this environment.

In contrast, on the flanks of the antiforms where accumulation rates are higher than on the antiform tops dominated by current sweeping, sediments are rapidly buried and consequently spend little time under the influence of high-energy surficial sea-waters. As a result, thick cross-bedded sand dunes, best exemplified by the Rotookiwa and Te Onepu Limestones with internal giant foresets (Kamp *et al.*, 1988), are typically non- to poorly cemented. The specific diagenetic record is one of a non-constructive to moderately destructive suite of processes comprising mechanical abrasion and bioerosion (DD[2]).

5.3.4. Carbonate diagenesis model of isolated antiforms during subaerial exposure: LST (Figure 25F)

The continuing loss of accommodation space, due to decreasing bathymetry associated with high rates of carbonate production and falling sea-level, eventually causes the

Figure 25- Carbonate diagenesis model of isolated antiforms during sea-level fall: RST (E), and during subaerial exposure: LST (F).

(E) During sea-level fall, the main features of sedimentation are aggradation and progradation. As a result, sediments come under the influence of high-energy wave and tidal currents, and are swept to the antiform flanks where they accumulate in the form of basinward-prograding sand waves and sand dunes. Under such conditions, siliciclastic sediments are by-passed into deeper environments, and barnacle-dominated carbonate factories reach their maximum production rate. RST deposits that accumulated in the shallow-marine environment where the rates of accumulation are low, and where sea-water pumping through the sediments is vigorous, are characterized by constructive diagenetic processes (specific diagenetic suite CD^1). Thick rinds of turbid fibrous cements line interparticle pores, micrite sediments percolate from the water-sediment interface, macroboring is common while microboring is moderate, and encrustation by uni- and multilaminar bryozoans is present. Dissolution of aragonite allochems may also occur in this environment.

(F) The continuing loss of accommodation space due to decreasing bathymetry associated with high rates of carbonate production and falling sea-level, causes eustatic sea-level to reach the sea-bed elevation, and the antiform tops are exposed to subaerial processes. Diagenetic features attributable to meteoric influence comprise dissolution of aragonitic skeletal fragments, the subsequent collapse of insoluble constituents of shells and LMC micrite envelopes that form geopetal debris, the percolation of dark (in some examples iron-stained) microquartz-rich internal sediments, and minor blocky spar cementation (specific diagenetic suite M^1). The transformation of IMC-HMC inclusion-rich fibrous cements into LMC is prominent in this environment.

SL2 to SL4 is sequential sea-level change (following from Figure 24).

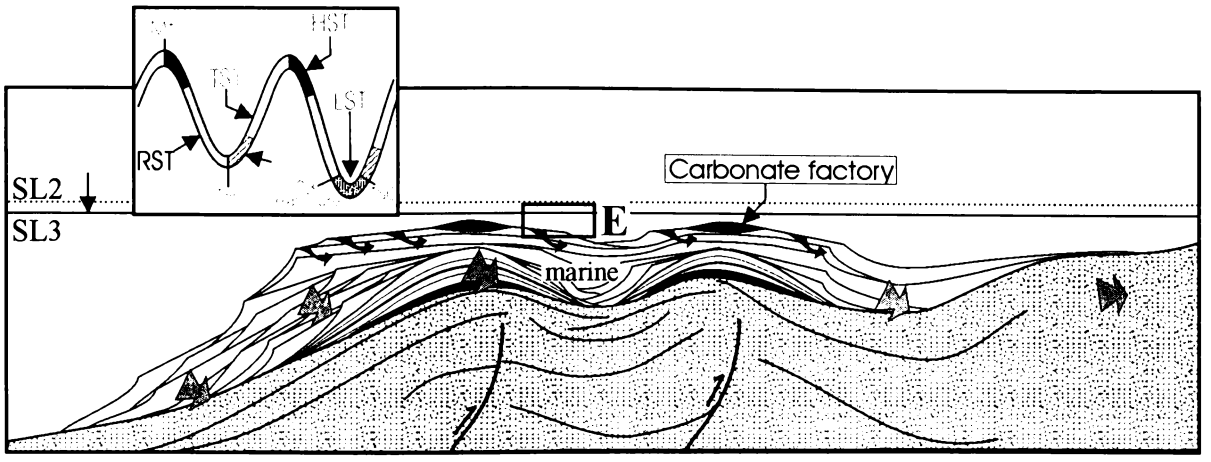

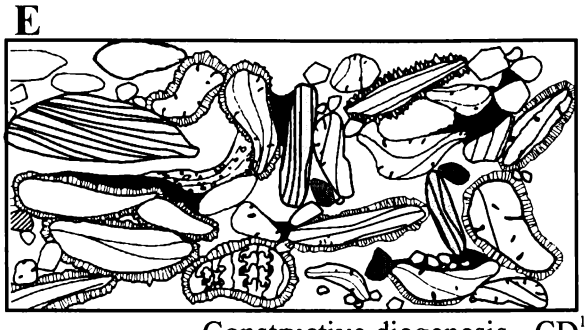

Constructive diagenesis - CD[1]

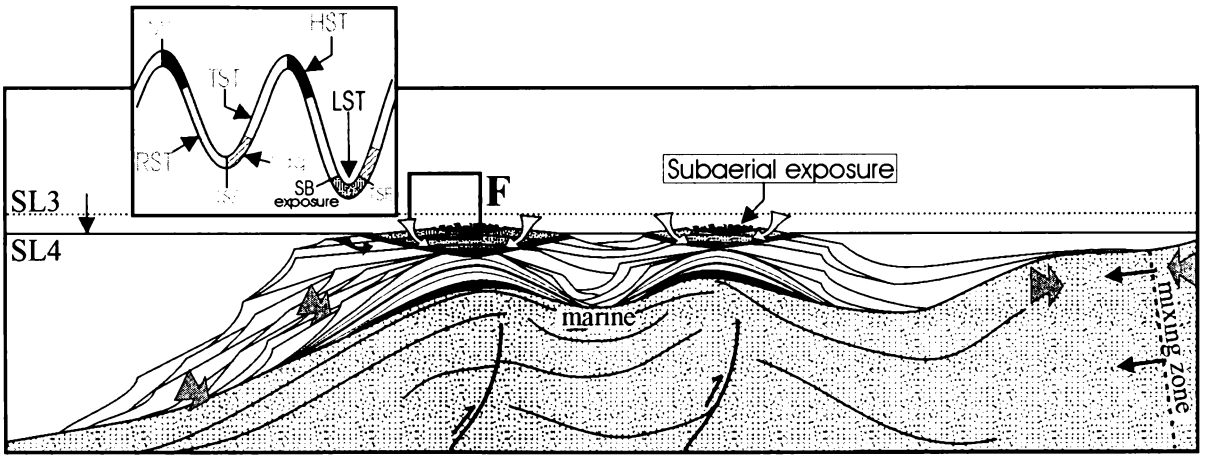

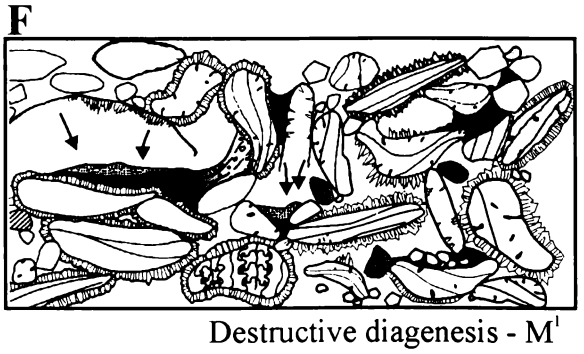

Destructive diagenesis - M[1]

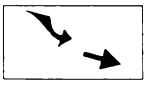

Active fluid circulation and zone of potential precipitation of cements

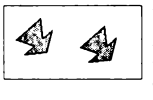

Passive fluid circulation and zone of potential precipitation of cements in the meteoric phreatic and mesogenetic realms

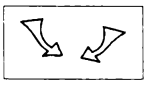

Rainfall - percolation of fresh water

Meteoric fluids

eustatic sea-level to reach the elevation of the sea floor, and the antiform tops become exposed to subaerial processes (Figure 22).

During the lowstand in carbonate platform systems, the meteoric groundwater zone migrates seawards and progressively moves through deposits that previously bathed in marine fluids (Tucker, 1993). Typically, under humid climate conditions, active pore-fluid circulations accompany the basinward shift of meteoric waters and mixed marine-meteoric fronts ahead, which lead to grain dissolution and pervasive cementation by calcite spar. By way of contrast, isolated carbonate antiforms are by definition at least partly disconnected from the continent, and subaerial exposure is responsible for the development of stagnant meteoric lenses floating on marine water beneath the antiform caps (Figure 25F).

Another expected difference between platform and isolated antiform settings during lowstand situations is that the latter remains siliciclastic free, whereas across the former there may be high rates of siliciclastic influxes that eventually will constitute mixed carbonate-siliciclastic lowstand deposits.

On carbonate platforms, subaerial unconformities are characterized by the development of karst surfaces and paleosols where the displacive and replacive introduction of calcium carbonate under fresh-water influence may result in the formation of calcrete profiles (Wright, 1982; Wright and Smart, 1994). Within the studied successions, subaerially exposed surfaces capping RST sediments are particularly discrete and in many cases could not be unequivocally determined. Diagenetic features referable to as calcrete formation are virtually absent. The uncommonness of aragonite and HMC mineralogies in the formations from Opoitian to Mangapanian in age probably reduced the potential for karst formation and subsequent calcite precipitation. Indeed, dissolution and precipitation of carbonate cements in the meteoric environment are mostly dependent upon the solubility of the dominant mineralogy of the host rock, temperature, and the degree of undersaturation with respect to calcium carbonate and CO_2 content of the percolating waters (James and Choquette, 1990b). In addition, considering both the low chemical reactivity of LMC mineralogies, and the low rate of fluid interaction upon carbonate grains, the time of exposure to meteoric water systems becomes critical to the development of mouldic porosity and calcite cementation.

When recognized, subaerial unconformity-related facies are poorly developed. Diagenetic features attributable to meteoric influence comprise dissolution of aragonitic skeletal fragments, the subsequent collapse of insoluble constituents of shells and LMC micrite envelopes that form geopetal debris, the percolation of dark (in some examples iron-stained) microquartz-rich internal sediments, and minor blocky spar cementation (specific diagenetic suite M^1; Table 2; Figures 23, 25F). Although potentially initiated earlier in the marine environment, the transformation of IMC-HMC inclusion-rich fibrous cements into LMC is likely active in this meteoric environment. It is one of a low water-rock interaction system, which translates in neomorphic scalenohedral meteoric crystals that enclose fibres of first-generation marine cements, and have partly inherited the isotopic and elemental signatures of the latter (see Section 4.3.6).

5.3.5. Drowning and termination of carbonate factories

Growth rates of tropical carbonate systems (>10 cm/ka) are typically significantly higher than rates of carbonate sediment production in temperate settings (<10 cm/ka), which are mainly reported to be low to moderate (Nelson, 1988a; James, 1997; Nelson *et al.*, in review). A first consequence of this difference is that carbonate production in cool-water settings may not be high enough to out-pace the rate of relative sea-level rise, resulting in drowning and covering of the carbonate factory by deeper-water sediments.

Steinhauff and Walker (1995) argued that a drowning unconformity forms when carbonate-producing environments pass below the euphotic zone, and carbonate production is greatly lowered or halted. In the Te Aute successions, the increase of water depth, which occurs in the early stages of rapid sea-level rise above barnacle-dominated carbonate factories, probably resulted in a decrease of current velocity, and subsequently in the decrease of nutrient supply and terrigenous sediment by-pass.

By contrast, in tropical environments, Schlager (1992) comparing growth rates of modern tropical carbonate producers to documented rates of relative sea-level rise, showed that in any situation carbonate production far outstrips positive rates of sea-level changes. This relationship implies that other factors must take place to generate a drowning unconformity in tropical environments, including changes of nutrient supply, siliciclastic input, or salinity variations (Moore, 2001). These are factors that could also account for ending carbonate production in temperate environments.

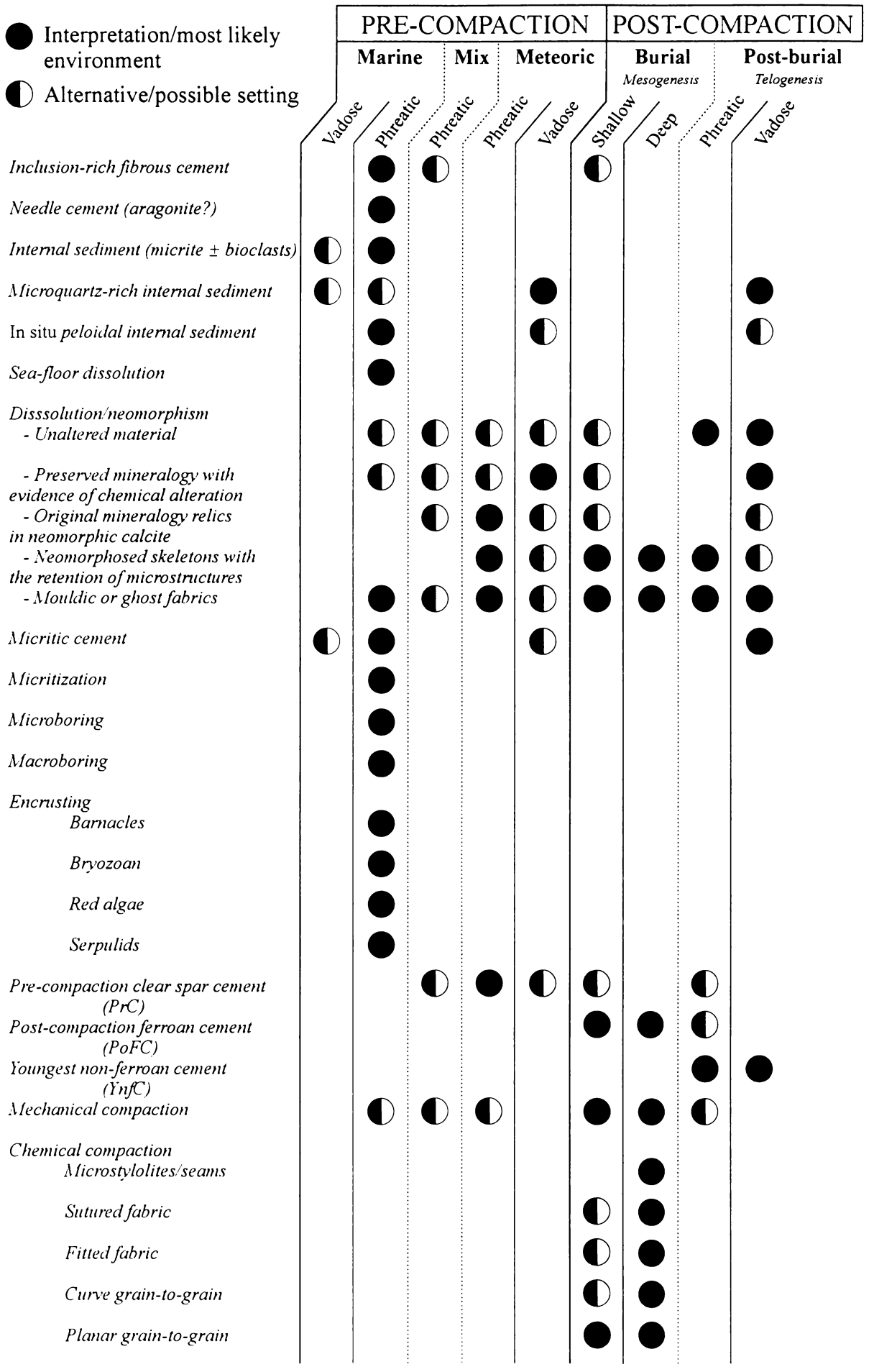

Figure 26- Interpretation of the major diagenetic features in the Te Aute carbonates in terms of diagenetic environment.

In the Te Aute successions, the termination of carbonate systems shows thick siltstone and sandstone units sitting sharply on top of shoaling-upwards carbonate deposits. This suggests drowning followed by high siliciclastic input. The transition between carbonate-dominated sedimentation and siliciclastic sedimentation occurs typically across either a sharp or erosion surface overlain or not by a fossiliferous lag. These relationships are best exemplified by the Kairakau Limestone at Mt Kahuranaki, where it is sharply overlain by Mokopeka Sandstone (see Chapter 1, Figures 5A, 5B), and by the Rotookiwa Limestone at Horse Shoe section capped by a 2 m-thick shell bed that is in turn overlain by Waikareao Calcarenite (see Chapter 1, Figure 10).

6. Conclusions

The diagenetic products and fabrics recognized in the Te Aute successions have been described and interpreted in terms of diagenetic environment (Figure 26).

Among the pre-compaction diagenetic suites, marine diagenesis is mainly characterized by destructive processes (abrasion, bioerosion, dissolution), and occasionally by constructive features (rare sea-floor cementation, micritization, encrustation), while meteoric diagenesis produces little to moderate cementation (PrC) and various neomorphic processes.

In the post-compaction diagenetic suites, telogenetic cements (YnfC) dominate over mesogenetic cements (PoFC), and dissolution and neomorphism are common during both diagenetic phases. There is a wide spectrum of compactional features due to the wide age range and variety of textures of the studied formations, which have been differentially buried before being exposed again.

Constructive diagenetic products occur in all studied formations, but their attributes vary over time (Figures 27, 28). Inclusion-rich fibrous cements constitute the main sea-floor constructive product in older, dominantly calcitic limestones (Kairakau, Awapapa), whereas micrite bindings, micrite cements, and micritization dominate in younger limestones with higher aragonitic contents (Mason Ridge Formation).

Neomorphic processes are also more diverse in younger limestones than in older ones. Alteration processes vary from total dissolution of aragonitic allochems (e.g., especially within Kairakau, Awapapa, Rotookiwa, Te Onepu, Titiokura) to retention of original mineralogy and microstructures, via little preservation of microstructures and loss of primary mineralogy (e.g., both neomorphic features being present within Mason

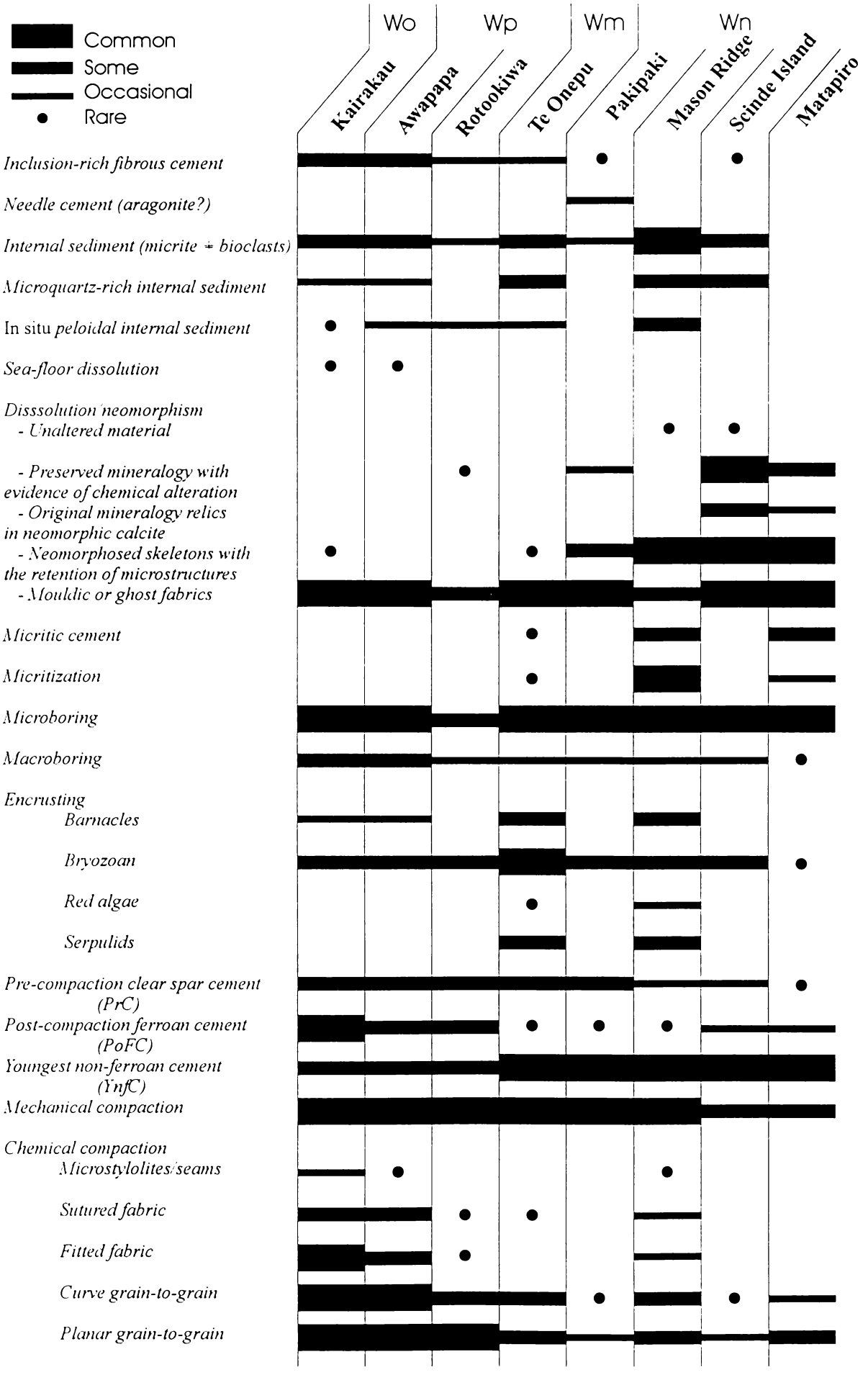

Figure 27- Distribution, characteristics, and fabrics of the diagenesis associated with the temperate Plio-Pleistocene carbonates, with reference to their age, in the eastern sector of southern Hawke's Bay. Wo: Opoitian; Wp: Waipipian; Wm: Mangapanian; Wn: Nukumaruan.

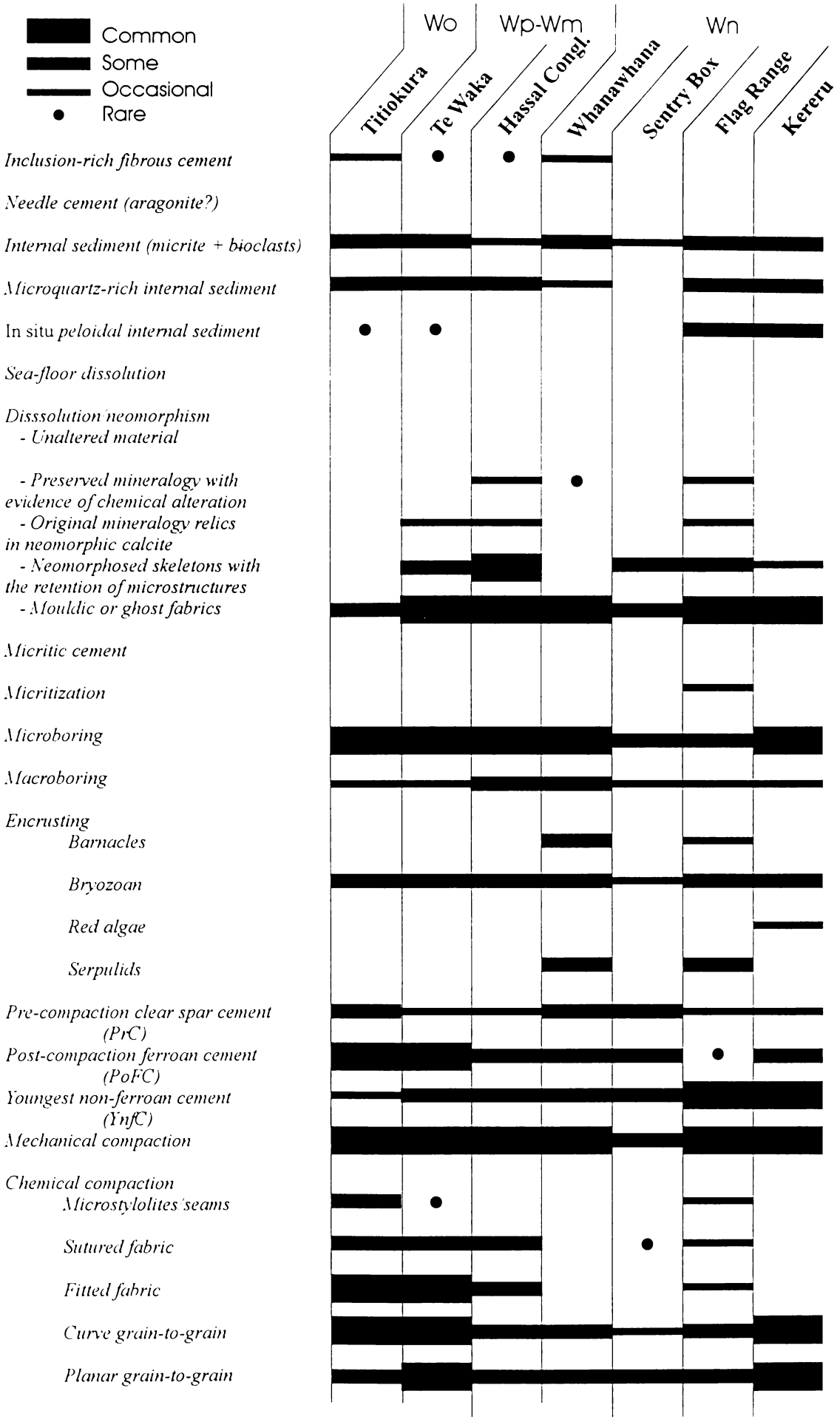

Figure 28- Distribution, characteristics, and fabrics of the diagenesis associated with the temperate Plio-Pleistocene carbonates, with reference to their age, in the western sector of southern Hawke's Bay. Wo: Opoitian; Wp: Waipipian; Wm: Mangapanian; Wn: Nukumaruan.

Ridge Formation, Matapiro and Scinde Island Limestones, and other Nukumaruan units). The water/rock ratio and the nature of circulating interparticle fluids are considered to be critical factors to the degree of neomorphism and type of resulting neomorphic fabrics. Provided that the starting composition of interparticle fluids is undersaturated with respect to aragonite, the variety of aragonite shell alteration/preservation in relation to water/rock ratios, or water-rock interaction, can be summarized as follows (Figure 17): (1) high water/rock ratio systems (i.e., low water-rock interaction) are characterized by mouldic and intraskeletal porosity; (2) intermediate water/rock ratio systems are characterized by the partial retention of the microstructures and geochemical signature of the precursor aragonite; and (3) low water/rock ratio systems (i.e., high water-rock interaction) result in neomorphic fabrics that comprise pristine aragonite crystallites with retention of primary microstructures adjacent to, or entombed within, neomorphic calcite crystals.

The degree of both mechanical and chemical compaction of the studied formations decreases over time. Not surprisingly, the amount of interparticle burial cementation follows the same trend, especially in the western limestones (Figure 28).

Pre-compaction diagenetic suites of eastern Te Aute limestones have been integrated into a sequence stratigraphic framework. The depositional setting for these limestones is envisaged to be one of isolated carbonate antiform type. One of the main conclusions of this study is that the attributes (Table 2) of the specific diagenesis of a sedimentary sequence change vertically, and appear to be strongly correlated to depositional facies (Figure 23). Data compiled from many Te Aute limestone units indicate that marine constructive diagenesis, characterized by turbid cements and interstratified internal sediments, occurs most commonly close to the bounding-discontinuities, within the lower level of the sequences interpreted as TST deposits, and in the upper level of RST deposits (Figures 23, 24B, 25E). These sediments equate to the highest energy facies located on antiform tops, where sedimentation rates are low, enabling frequent and strong marine-water pumping through the sediments. In contrast, such constructive diagenetic phases are usually rare or absent from the upper part of the TST, the HST, and the lower part of the RST (Figures 23, 24D), which are instead characterized by destructive marine diagenesis. Maximum flooding surfaces (Mfs) are typified by starved sedimentation (authigenic glauconite-rich thin lags) and associated destructive diagenetic features, such as abrasion and multigeneration bioerosion (Figures

23, 24C). The upper part of the RST is characterized by marine cementation overprinted by both constructive and destructive meteoric diagenesis, involving dissolution of former aragonite and even calcitic grains, and little spar cementation, when the top surface has been subaerially exposed (Figures 23, 25F).

References

Aissaoui, D. M. (1988) Magnesian calcite cements and their diagenesis: dissolution and dolomitization, Mururoa Atoll. *Sedimentology*, **35**, 821-841.

Aissaoui, D. M., Coniglio, M., James, N. P. & Purser, B. H. (1986) Diagenesis of a Miocene Reef-Platform: Jebel Abu Shaar, Gulf of Suez, Egypt. In: *Reef Diagenesis* (Ed. by J. H. Schroeder and B. H. Purser), pp. 112-131. Springer Verlag, Berlin Heidelberg.

Alexandersson, E. T. (1978) Destructive diagenesis of carbonate sediments in the eastern Skagerrak, North Sea. *Geology*, **6**, 324-327.

Amorosi, A. (1995) Glaucony and sequence stratigraphy: a conceptual framework of distribution in siliciclastic sequences. *Journal of Sedimentary Research*, **B65**(4), 419-425.

Bathurst, R. G. C. (1966) Boring algae, micrite envelopes and lithification of molluscan biosparites. *Geological Journal*, **5**, 15-32.

Bathurst, R. G. C. (1975) *Carbonate sediments and their diagenesis*. Elsevier, North Holland, 658 pp.

Bathurst, R. G. C. (1980b) Deep crustal diagenesis in limestones. *Revista del Instituto de Investigaciones Geologicas Diputacion Provincial, Universidad de Barcelona*, **34**, 89-100.

Bathurst, R. G. C. (1995) Burial diagenesis of limestones under simple overburden. Stylolites, cementation and feedback. *Bulletin de la Société Géologique de France*, **166**, 181-192.

Bernier, P. (1995) Lime mud production: Biological processes. In: *2nd International symposium on lithographic limestones* (Ed. by Universidad Autónoma de Madrid), pp. 35-38, Madrid.

Bernier, P. & Dalongeville, R. (1988) Incidence de l'activité biologique sur la cimentation des sédiments littoraux actuels. L'exemple des îles de Délos et de Rhénée (Cyclades, Grèce). *Compte rendu de l'Académie des Sciences*, **307**(Série 2), 1901-1907.

Betzler, C., Brachert, T. C., Braga, J. -C. & Martin, J. M. (1997) Nearshore, temperate, carbonate depositional systems (lower Tortonian, Agua Amarga Basin, southern Spain): implications for carbonate sequence stratigraphy. *Sedimentary Geology*, **113**, 27-53.

Betzler, C., Martin, J. M. & Braga, J. -C. (2000) Non-tropical carbonates related to rocky submarine cliffs (Miocene, Almeria, southern Spain). *Sedimentary Geology*, **131**, 51-65.

Beu, A. G. (1995) *Pliocene Limestones and Their Scallops*. Monograph 10, Institute of Geological & Nuclear Sciences Limited, Lower Hutt, New Zealand, 243 pp.

Bland, K. (2001) Analysis of the Pliocene forearc basin succession - Esk river catchment, Hawke's Bay. MsC, University of Waikato.

Boreen, T. D. & James, N. P. (1995) Stratigraphic sedimentology of tertiary cool-water limestones, SE Australia. *Journal of Sedimentary Research*, **B65**(1), 142-159.

Braithwaite, C. J. R. (1993) Cement sequence stratigraphy in carbonates. *Journal of Sedimentary Petrology*, **63**(2), 295-303.

Brand, U. (1994) Morphochemical and replacement diagenesis of biogenic carbonates. In: *Diagenesis, IV. Developments Sedimentology, Vol. 51* (Ed. by K. H. Wolf and G. V. Chilingarian), pp. 217-281. Elsevier Sc. B.V., Amsterdam.

Burton, E. A. & Walter, L. K. (1987) Relative precipitation of aragonite and Mg-calcite from seawater: temperature or carbonate ion control? *Geology*, **15**, 111-114.

Calvet, F. (1982) Constructive micrite envelopes developed in vadose continental environment in Pleistocene eolianites of Mallorca, Spain. *Acta Geologica Hispanica*, **17**, 169-178.

Carey, J.S., Moslow, T. F. & Barrie, J.V. (1995) Origin and distribution of Holocene temperate carbonates, Hecate Strait, western Canada continental shelf. *Journal of Sedimentary Research*, **A65**(1), 185-194.

Chafetz, H. S. (1986) Marine peloids: A product of bacterially induced precipitation of calcite. *Journal of Sedimentary Petrology*, **56**, 812-817.

Chafetz, H. S. (1992) Bacterially induced precipitates of Calcium carbonate and lithification of microbial mats. In: *Sediment stabilisation* (Ed. by V. Wachendorfer, W.E. Krumbein and H.J. Schelhnuber), pp. 149-163.

Chafetz, H. S. & Buczynski, C. (1992) Bacterially induced lithification of microbial mats. *Palaios*, **7**, 277-293.

Chave, K. E. (1954) Aspects of the biogeochemistry of magnesium, 1. Calcareous marine organisms. *Journal of Geology*, **62**, 266-283.

Choquette, P. W. & James, N. P. (1990) Limestones - The burial diagenetic environment. In: *Diagenesis* (Ed. by I. A. McIlreath and D. W. Morrow), pp. 75-112. Geoscience Canada Reprint Series 4.

Choquette, P. W. & Pray, L. C. (1970) Geologic nomenclature and classification of porosity in sedimentary carbonates. *American Association of Petroleum Geologists Bulletin*, **54**, 207-250.

Dickson, J. A. D. (1965) A modified staining technique for carbonates in thin-section. *Nature*, **205**, 587.

Dickson, J. A. D. (1966) Carbonate identification and genesis as revealed by staining. *Journal of Sedimentary Petrology*, **36**(2), 491-505.

Dodd, J. R. & Nelson, C. S. (1998) Diagenetic comparisons between non-tropical Cenozoic limestones of New Zealand and tropical Mississippian limestones from Indiana, USA: Is the non-tropical model better than the tropical model? *Sedimentary Geology*, **121**, 1-21.

Dorobek, S. L. (1987) Petrography, geochemistry and origin of burial diagenetic facies, Siluro-Devonian Helderberg Group (Carbonate rocks), Central Appalachians. *American Association of Petroleum Geologists Bulletin*, **71**(5), 492-514.

Dunham, R. J. (1969) Early vadose silt in Townsend mound (reef), New Mexico. In: *Depositional environments in carbonate rocks, Vol. 14* (Ed. by G. M. Friedman), pp. 139-181. SEPM Special Publication.

Emery, D. & Dickson, J. A. D. (1989) A syndepositional meteoric phreatic lens in the Middle Jurassic Lincolnshire Limestone, England, UK. *Sedimentary Geology*, **65**, 273-284.

Emery, D. & Myers, K. (1996) *Sequence Stratigraphy*. Blackwell Science, Oxford, 297 pp.

Evamy, B. D. (1969) The precipitational environment and correlation of some calcite cements deduced from artificial staining. *Journal of Sedimentary Petrology*, **39**(2), 787-821.

Farrow, G. E. & Fyfe, J. A. (1988) Bioerosion and carbonate mud production on high-latitude shelves. In: *Non-tropical Shelf Carbonates - Modern and Ancient, Vol. 60* (Ed. by C. S. Nelson), pp. 281-297. Sedimentary Geology.

Flessa, K. W. & Brown, T. J. (1983) Selective solution of macroinvertebrate calcareous hard parts: a laboratory study. *Lethaia*, **16**, 193-205.

Folk, R. L. (1974) The natural history of crystalline calcium carbonate: effect of magnesium content and salinity. *Journal of Sedimentary Petrology*, **44**, 40-53.

Frank, T. D., Lohmann, K. C. & Meyers, W. J. (1995) Chronostratigraphic significance of cathodoluminescence zoning in syntaxial cement: Mississippian Lake Valley Formation, New Mexico. *Sedimentary Geology*, **105**, 29-50.

Freiwald, A. (1998) Microbial maceration and carbonate dissolution on cold-temperate shelves. *Historical Biology*, **13**, 27-35.

Goldhammer, R. K., Oswald, E. J. & Dunn, P. A. (1994) High-frequency, glacio-eustatic cyclicity in the Middle Pennsylvanian of the Paradox Basin: an evaluation of Milankovitch forcing. *Spec. Publs Int. Ass. Sedim.*, **19**, 243-283.

Goldstein, R. H. (1988) Cement stratigraphy of Pennsylvanian Holder Formation, Sacramento Mountains, New Mexico. *American Association of Petroleum Geologists Bulletin*, **72**(4), 425-438.

Gonzales, L. A. & Lohmann, K. C. (1985) Carbon and oxygen isotopic composition of Holocene reefal carbonates. *Geology*, **13**, 811-814.

Grover Jr, G. & Read, J. F. (1983) Paleoaquifer and deep burial related cements defined by regional cathodoluminescent patterns, Middle Ordoviscian carbonates, Virginia. *American Association of Petroleum Geologists Bulletin*, **67**(8), 1275-1303.

Hardie, L. A., Dunn, P. A. & Goldhammer, R. K. (1991) Field and modelling studies of Cambrian carbonate cycles, Virginia Appalachians: a discussion. *Journal of Sedimentary Petrology*, **61**, 636-646.

Harmsen, F. J. (1984) *Stratigraphic Sections of the Pliocene Te Aute Group in Central and Southern Hawke's Bay, New Zealand.* Geology Department, Victoria University, Wellington, New Zealand, 109 pp.

Harmsen, F. J. (1985) Lithostratigraphy of Pliocene Strata, Central and Southern Hawke's Bay, New Zealand. *New Zealand Journal of Geology and Geophysics*, **28**, 413-433.

Hayton, S., Nelson, C. S. & Hood, S. D. (1995) A skeletal assemblage classification system for non-tropical carbonate deposits based on New Zealand Cenozoic limestones. *Sedimentary Geology*, **100**, 123-141.

Haywick, D. W. N. (1990) Stratigraphy, sedimentology, paleoecology and diagenesis of the Petane Group (Pliocene-Pleistocene) in the Tangoio, central Hawke's Bay, New Zealand. Unpublished PhD Thesis, James Cook University of North Queensland, Australia.

Heckel, P. H. (1983) Diagenetic model for carbonate rocks in Midcontinent Pennsylvanian eustatic cyclothems. *Journal of Sedimentary Petrology*, **53**(3), 733-759.

Henrich, R. & Freiwald A. (1995) Controls on modern carbonate sedimentation on warm-temperate to arctic coasts, shelves and seamounts in the northern hemisphere: implications for fossil counterparts. *Facies*, **32**, 71-108.

Hillgärtner, H., Dupraz, C. & Hug, W. (2001) Microbially induced cementation of carbonate sands: are micritic meniscus cements good indicators of vadose diagenesis? *Sedimentology*, **48**, 117-131.

Hood, S. D. & Nelson, C. S. (1996) Cementation scenarios for New Zealand non-tropical limestones. *New Zealand Journal of Geology and Geophysics*, **39**, 109-122.

Horbury, A. D. & Adams, A. E. (1989) Meteoric phreatic diagenesis in cyclic Late Dinantian carbonates, northwest England. *Sedimentary Geology*, **65**, 319-344.

Hudson, J.D. (1977) Stable isotopes and limestone lithification. *Journal of the Geological Society of London*, **133**, 637-660.

Illing, L. V. (1954) Bahaman calcareous sands. *American Association of Petroleum Geologists Bulletin*, **38**(1), 1-95.

James, N. P. (1997) The cool-water carbonate depositional realm. In: *Cool-Water Carbonates* (Ed. by N. P. James and J. A. D. Clarke), SEPM Special Publication, **56**, 1-22.

James, N. P. & Bone, Y. (1989) Petrogenesis of Cenozoic, temperate water calcarenites, South Australia: A model for meteoric/shallow burial diagenesis of shallow water calcite sediments. *Journal of Sedimentary Petrology*, **59**(2), 191-203.

James, N. P. & Bone, Y. (1992) Synsedimentary cemented calcarenite layers in Oligo-Miocene cool water shelf limestones, Eucla Platform, Southern Australia. *Journal of Sedimentary Petrology*, **62**(5), 860-872.

James, N. P. & Bone, Y. (2000) Eocene cool-water carbonate and biosiliceous sedimentation dynamics, St Vincent Basin, South Australia. *Sedimentology*, **47**, 761-786.

James, N. P., Bone, Y., Collins L. B. & Kyser, T. K. (2001) Surficial sediments of the Great Australian Bight: facies dynamics and oceanography on a vast cool-water carbonate shelf. *Journal of Sedimentary Research*, **71**(4), 549-567.

James, N. P., Bone, Y., Von Der Borch, C. C. & Gostin, V. A. (1992) Modern carbonate and terrigenous clastic sediments on a cool-water, high energy, mid-latitude shelf: Lacepede, southern Australia. *Sedimentology*, **39**, 877-903.

James, N. P. & Choquette, P. W. (1990a) Limestones - The sea-floor diagenetic environment. In: *Diagenesis* (Ed. by I. A. McIlreath and D.W. Morrow), pp. 13-34. Geoscience Canada Reprint Series 4.

James, N. P. & Choquette, P. W. (1990b) Limestones - The meteoric diagenetic environment. In: *Diagenesis* (Ed. by I. A. McIlreath and D.W. Morrow), pp. 35-74. Geoscience Canada Reprint Series 4.

James, N. P., Ginsburg, R. N., Marszalek, D. S. & Choquette, P. W. (1976) Facies and fabric specificity of early subsea cements in shallow Belize (British Honduras) reefs. *Journal of Sedimentary Petrology*, **46**(3), 523-544.

Kamp, P. J. J., Harmsen, F. J., Nelson, C. S. & Boyle, S. F. (1988) Barnacle-dominated limestone with giant cross-beds in a non-tropical, tide swept, Pliocene forearc seaway, Hawke's Bay, New Zealand. *Sedimentary Geology*, **60**, 173-195.

Kamp, P. J. J. & Naish, T. (1997) Forward modelling of the sequence stratigraphic architecture of shelf cyclothems: Application to Late Pliocene sequences, Wanganui basin (New Zealand). *Sedimentary Geology*, **00**, 1-24.

Kaufman, J., Cander, H. S., Daniels, L. D. & Meyers, W. J. (1988) Calcite cement stratigraphy and cementation history of the Burlington-Keokuk Formation (Mississippian), Illinois and Missouri. *Journal of Sedimentary Petrology*, **58**(2), 312-326.

Kaufmann, B. & Wendt, J. (2000) Calcite cement successions in middle Devonian (Givetian) carbonate mud buildups of the southern Ahnet basin (Algerian Sahara). *Carbonates and Evaporites*, **15**(2), 149-161.

Kendall, A. C. (1985) Radiaxial fibrous calcite: a reappraisal. In: *Carbonate Cements, Vol. 36* (Ed. by N. Schneidermann and P. M. Harris), pp. 59-77. SEPM Special Publication, Tulsa.

Kerans, C., Hurley, N. F. & Playford, P. E. (1986) Marine diagenesis in Devonian Reef Complexes of the Canning basin, Western Australia. In: *Reef Diagenesis* (Ed. by J. H. Schroeder and B. H. Purser), pp. 357-380. Springer Verlag, Berlin Heidelberg.

Kyser, T. K., James, N. P. & Bone, Y. (1998) Alteration of Cenozoic cool-water carbonates to low-Mg calcite in marine waters, Gambier embayment, South Australia. *Journal of Sedimentary Research*, **68**(5), 947-955.

Lavoie, D. & Bourque, P.-A. (1993) Marine, burial, and meteoric diagenesis of early Silurian carbonate ramps, Quebec Appalachians, Canada. *Journal of Sedimentary Petrology*, **63**(2), 233-247.

Light,J. M. & Wilson, J. B. (1998) Cool-water carbonate deposition on the West Shetland Shelf: a modern distally steepened ramp. In: *Carbonate Ramps* (Ed. By V. P. Wright and T. P. Burchette), pp. 73-105, Geological Society, London, Special Publication **149**.

Lohmann, K. C. (1988) Geochemical patterns of meteoric diagenetic systems and their application to studies of paleokarst. In: *Paleokarst* (Ed. by N. P. James and P. W. Choquette), pp. 58-80. Springer, Berlin.

Lohmann, K. C. & Meyers, W. J. (1977) Microdolomite inclusions in cloudy prismatic calcites: a proposed criterion for former high-magnesium calcites. *Journal of Sedimentary Petrology*, **47**, 1075-1088.

Long, J. V. P. & Agrell, S. O. (1965) The cathodoluminescence of minerals in thin-section. *Mineralogy Magazine*, **34**, 318-326.

Longman, M. K. (1980) Carbonate diagenetic textures from near surface diagenetic environments. *AAPG Bull.*, **64**, 461-487.

Machel, H. G. & Burton, E. A. (1991) Factors governing cathodoluminescence in calcite and dolomite, and their implications for studies of carbonate diagenesis. In: *Luminescence Microscopy: Quantitative and Qualitative aspects, Vol. 25* (Ed. by C. E. Barker and O. C. Kopp), pp. 37-57. SEPM Short Course.

Macintyre, I. G. (1984) Extensive submarine lithification in a cave in the Belize barrier reef. *Journal of Sedimentary Petrology*, **54**, 221-235.

Macintyre, I. G. (1985) Submarine cements - the peloidal question. In: *Carbonate cements, Vol. 36* (Ed. by N. Schneidermann and P. M. Harris), pp. 1098-1106. SEPM Special Publication.

Major, R. P. & Wilber, R. J. (1991) Crystal habit, geochemistry and cathodoluminescence of magnesian calcite marine cements from the lower slope of Little Bahama Bank. *Geological Society of America Bulletin*, **103**, 461-471.

Maliva, R. G. (1998) Skeletal aragonite neomorphism -Quantitative modelling of a two-water diagenetic system. *Sedimentary Geology*, **121**, 179-190.

Mazzullo, S. J. (1980) Calcite pseudospar replacive of marine acicular aragonite, and implications for aragonite cement diagenesis. *Journal of Sedimentary Petrology*, **50**(2), 409-422.

Mazzullo, S. L., Bischoff, W. D. & Lobitzer, H. (1990) Diagenesis of radiaxial fibrous calcites in a sbunconformity, shallow burial setting: Upper Triassic and Liassic, northern calcareous Alps, Austria. *Sedimentology*, **37**, 407-425.

McIlreath, I. A. & Morrow, D. W. (1990) *Diagenesis*. Geoscience Canada Reprint Series, 338 pp.

Meyers, J. M. (1987) Marine vadose beach-rock cementation by cryptocrystalline magnesian calcite. *Journal of Sedimentary Petrology*, **57**, 558-570.

Meyers, W. J. (1974) Carbonate cement stratigraphy of the Lake Valley Formation (Mississippian), Sacramento Mountains, New Mexico. *Journal of Sedimentary Petrology*, **44**, 837-861.

Meyers, W. J. (1978) Carbonate cements: Their regional distribution and interpretation in Mississippian limestones of Southwestern New Mexico. *Sedimentology*, **25**, 371-399.

Meyers, W. J. (1980) Compaction in Mississippian skeletal limestones, Southern New Mexico. *Journal of Sedimentary Petrology*, **50**(2), 457-474.

Meyers, W. J. (1989) Trace element and isotope geochemistry of zoned calcite cements, Lake Valley Formation (Mississippian, New Mexico): Insights from water-rock interaction modelling. *Sedimentary Geology*, **65**, 355-370.

Meyers, W. J. (1991) Calcite cement stratigraphy: an overview. In: *Luminescence Microscopy: Quantitative and Qualitative Aspects, Vol. 25* (Ed. by C. E. Baker and O. C. Kopp), pp. 133-147. SEPM Short Course.

Meyers, W. J. & Lohmann, K. C. (1985) Isotope geochemistry of regionally extensive calcite cement zones and marine components in Mississippian limestones, New Mexico. In: *Carbonate cements, Vol. 36* (Ed. by N. Schneidermann and P. M. Harris), pp. 223-240. SEPM Special Publication.

Moore, C. H. (1989) *Carbonate Diagenesis and Porosity*. Elsevier, Amsterdam.

Moore, C. H. (2001) *Carbonate Reservoirs - Porosity Evolution and Diagenesis in a Sequence Stratigraphic Framework*. Elsevier, Amsterdam, 444 pp.

Nelson, C. S. (1978) Temperate shelf carbonate sediments in the Cenozoic of New Zealand. *Sedimentology*, **25**, 737-771.

Nelson, C. S. (1988a) An Introductory perspective on non-tropical shelf carbonates. *Sedimentary Geology*, **60**, 3-12.

Nelson, C. S. & Bornhold, B. D. (1983) Temperate skeletal carbonates on Scott Shelf, northwestern Vancouver Island, Canada. *Marine Geology*, **52**, 241-266.

Nelson, C. S., Harris, G. J. & Young, H. R. (1988c) Burial-dominated cementation in non-tropical carbonates of the Oligocene Te Kuiti Group, New Zealand. *Sedimentary Geology*, **60**, 233-250.

Nelson, C. S. & James, N. P. (2000) Marine cements in mid-Tertiary cool-water shelf limestones of New Zealand and southern Australia. *Sedimentology*, **47**, 609-629.

Nelson, C. S., Keane, S. L. & Head, P. S. (1988b) Non-tropical carbonate deposits on the modern New Zealand Shelf. *Sedimentary Geology*, **60**, 71-94.

Nelson, C. S. & Smith, A. M. (1996) Stable oxygen and carbon isotope compositional fields for skeletal and diagenetic components in New Zealand Cenozoic non-tropical carbonate sediments and limestones: A synthesis and review. *New Zealand Journal of Geology and Geophysics*, **39**, 93-107.

Nelson, C. S., Winefield, P. R., Hood, S. D., Caron, V., Pallentin, A. & Kamp, P. J. J. (in review) Pliocene Te Aute limestones, New Zealand: expanding notions for models of cool-water shelf carbonates. .

Neumann, A. C. & MacIntyre, I. (1985) Reef response to sea-level rise: keep-up, catch-up or give-up. In: *Fifth International Coral Reef Congress, Vol. 3*, pp. 105-110, Tahiti.

Nicolaides, S. & Wallace, M. W. (1997) Pressure-dissolution and cementation in an Oligocene-Miocene non-tropical limestone (Clifton Formation), Otway basin, Australia. In: *Cool-water carbonates, Vol. 56* (Ed. by N. P. James and J. D. A. Clark), pp. 127-140. Society for Sedimentary Geologists (SEPM) Special Publication.

Niemann, J. C. & Read, J. F. (1988) Regional cementation from unconformity-recharged aquifer and burial fluids, Mississippian Neuman Limestone, Kentucky. *Journal of Sedimentary Petrology*, **58**(4), 688-705.

Popp, B. N., Anderson, T. F. & Sandberg, P. A. (1986) Brachiopods as indicators of original isotopic compositions in some Paleozoic limestones. *Geological. Society of America Memoir*, **97**, 1262-1269.

Posamentier, H. W., Jervey, M. T. & Vail, P. R. (1988) Eustatic controls on clastic deposition I - conceptual framework. In: *Sea-level changes: An Integrated Approach, Vol. 42* (Ed. by C. K. Wilgus, B. S. Hastings, C. G. S. C. Kendal, H. W. Posamentier, C. A. Ross and J. C. Van Wagoner), pp. 125-154. SEPM Special Publication.

Purser, B. H. (1980) *Sédimentation et diagenèse des carbonates néritiques récents*. Technip, Paris, 366 pp.

Rao, C. P. (1981) Cementation in cold-water bryozoan sand, Tasmania, Australia. *Marine Geology*, **40**, M23-M33.

Rao, C. P. (1988) Oxygen and carbon isotope composition of cold-water Berridale limestone (Lower Permian), Tasmania, Australia. *Sedimentary Geology*, **60**, 221-231.

Rao, C. P. (1990) Geochemical characteristics of cool-temperate carbonates, Tasmania, Australia. *Carbonates and Evaporites*, **5**, 209-221.

Rao, C.P. (1997) *Sedimentary Textures: Cold, Cool, Warm, Hot.* The University of Tasmania, 128 pp.

Rao, C. P. & Nelson, C. S. (1992) Oxygen and carbon isotope composition of cold shallow-marine carbonates of Tasmania, Australia. *Marine Geology*, **103**, 273-286.

Reeckmann, S. A. (1988) Diagenetic alterations in temperate shelf carbonates from Southeastern Australia. *Sedimentary Geology*, **60**, 209-219.

Reid, R. P., Macintyre, I. G. & James, N. P. (1990) Internal precipitation of microcrystalline carbonate: a fundamental problem for sedimentologists. *Sedimentary Geology*, **68**, 163-170.

Rush, P. F. & Chafetz, H. S. (1990) Fabric retentive non-luminescent brachiopods as indicators of original d13C and d18O composition: a test. *Journal of Sedimentary Petrology*, **60**, 968-981.

Saller, A. H. (1986) Radial calcite in Lower Miocene strata, subsurface Enewetak Atoll. *Journal of Sedimentary Petrology*, **56**, 743-762.

Saller, A. H. & Moore Jr, C. H. (1991) Geochemistry of meteoric calcite cements in some pleistocene limestones. *Sedimentology*, **38**, 601-621.

Sandberg, P. (1985) Aragonite cements and their occurrence in Ancient limestones. In: *Carbonate cements, Vol. 36* (Ed. by N. Schneidermann and P. M. Harris), pp. 33-57. SEPM Special Publication.

Sandberg, P. A. & Hudson, J. D. (1983) Aragonite relic preservation in Jurassic calcite-replaced bivalves. *Sedimentology*, **30**, 879-892.

Sarg, J. F. (1988) Carbonate sequence stratigraphy. In: *Sea-Level Changes: An Integrated Approach* (Ed. by C. K. Wilgus, H. Posamentier, C. A. Ross and C. G. St. C. Kendall), SEPM Special Publication, **42**, 155-181.

Schlager, W. (1992) *Sedimentology and sequence stratigraphy of reefs and carbonate platforms.* American Association of Petroleum Geologists, Tulsa, 71 pp.

Shinn, E.A. (1969) Submarine lithification of Holocene carbonate sediments in the Persian Gulf. *Sedimentology*, **12**, 109-144.

Sippel, R. F. & Glover, E. D. (1965) Structures in carbonate rocks made visible by luminescence petrography. *Science*, **150**, 1283-1287.

Smart, P. L., Dawans, J. M. & Whitaker, F. (1988) Carbonate dissolution in a modern mixing zone. *Nature*, **335**(6193), 811-813.

Smith, A. M. & Nelson, C. S. (1994) Selectivity in sea-floor processes: taphonomy of bryozoans. In: *Biology and Palaeobiology of Bryozoans* (Ed. By P. J. Hayward, J. S. Ryland and P. D. Taylor), pp. 177-180, Olsen & Olsen, Fredensborg, Denmark.

Smith, A. M. & Nelson, C. S. (1996) Differential abrasion of bryozoan skeletons: taphonomic implications for palaeoenvironmental interpretation. In: *Bryozoans in Space and Time. Proceedings of the 10th International Bryozoology Conference, Wellington, New Zealand.1995* (Ed. by D. P. Gordon, A. M. Smith and J. A. Grant-Mackie), pp. 305-313. National Institute of Water & Atmospheric Research Ltd, Wellington, New Zealand.

Smith, A. M. & Nelson, C. S. & Danaher, P.J. (1992) Dissolution behaviour of bryozoan sediments: taphonomic implications for non-tropical shelf carbonates. *Palaeogeography, Palaeoclimatology, Palaeoecology*, **93**, 213-226.

South, D. L. & Talbot, M. R. (2000) The sequence stratigraphic framework of carbonate diagenesis within transgressive fan-delta deposits: Sant Llorenç del Munt fan-delta complex, SE Ebro Basin, NE Spain. *Sedimentary Geology*, **138**, 179-198.

Steinhauff, D. M. & Walker, K. R. (1995) Recognizing exposure, drowning and missed beats. *Journal of Sedimentary Research*, **B65**(2), 183-207.

Tobin, K. J. & Walker, K. R. (1998) Diagenetic calcite from the Chazyan Group (Vermont): an example of aragonite alteration in a greenhouse ocean. *Sedimentary Geology*, **121**, 277-288.

Tucker, M. E. (1993) Carbonate diagenesis and sequence stratigraphy. In: *Sedimentology Review, Vol. 1* (Ed. by V. P. Wright), pp. 51-72. Blackwell scientific, Oxford.

Tucker, M. E. & Wright, V. P. (1990) *Carbonate sedimentology*. Blackwell, Oxford, 482 pp.

Vail, P. R., Audemard, F., Bowman, S. A., Eisner, P. N. & Perez-Cruz, C. (1991) The stratigraphic signatures of tectonics, eustasy and sedimentology - an overview. In: *Cycles and Events in Stratigraphy* (Ed. by G. Einsele, W. Ricken and A. Seilacher), pp. 617-659. Springer-Verlag, Berlin Heidelberg.

Van Wagoner, J. C., Posamentier, H. W., Mitchum, R. M. J., Vail, P. R., Sarg, J. F., Loutit, T. S. & Hardenbol, J. (1988) An overview of the fundamentals of sequence stratigraphy and key definitions. In: *Sea-Level Changes: An Integrated Approach, Vol. 42* (Ed. by C. K. Wilgus, B. S. Hastings, C. G. S. C. Kendall, H. W. Posamentier, C. A. Ross and J. C. Van Wagoner), pp. 39-45. SEPM Special Publication.

Videtich, P. E. (1985) Electron microprobe study of Mg distribution in recent Mg calcites and recrystallized equivalents from the Pleistocene and Tertiary. *Journal of Sedimentary Petrology*, **55**(3), 421-429.

Wadleigh, M. A. & Veizer, J. (1992) $^{18}O/^{16}O$ and $^{13}C/^{12}C$ in lower Paleozoic articulate brachiopods: implications for the isotopic composition of seawater. *Geochimica Cosmochimica Acta*, **56**, 431-443.

Walkden, G. M. (1987) Sedimentary and diagenetic styles in Late Dinantian carbonates of Britain. In: *European Dinantian Environments* (Ed. by J. Miller, A. E. Adams and V. P. Wright), pp. 131-155. Wiley, New York.

Walkden, G. M. & Berry, J. P. (1984) Syntaxial overgrowths in muddy crinoidal limestones: cathodoluminescence sheds new light on an old problem. *Sedimentology*, **38**, 643-670.

Walkden, G. M. & Williams, D. O. (1991) The diagenesis of late Dinantian Derbyshire-East Midland carbonate shelf, Central England. *Sedimentology*, **38**, 643-670.

Walker, K. R., Jernigan, D. G. & Weber, L. J. (1990) Petrographic criteria for the recognition of marine, syntaxial overgrowths, and their distribution in geologic time. *Carbonates and Evaporites*, **5**(2), 141-151.

Weiblen, P. (1965) Investigation of cathodoluminescence with the petrographic microscope. In: *Developments in applied spectroscopy, Vol. 4* (Ed. by E. N. Davis), pp. 245-251. Plenum, New York.

Wendt, J. (1977) Aragonite in Permian reefs. *Nature*, **267**(335-337).

Wilber, R. J. & Neumann, A. C. (1993) Effects of submarine cementation on microfabrics and physical properties of carbonate slope deposits, northern Bahamas. In: *Carbonate microfabrics* (Ed. by R. Rezak and D. L. Lavoie), pp. 79-94. Springer Verlag, New York.

Wilkinson, B. H., Owen, R. M. & Carrol, A. M. (1985) Submarine hydrothermal weathering, global eustasy, and carbonate polymorphism in Phanerozoic oolites. *Journal of Sedimentary Petrology*, **55**, 171-183.

Wright, V. P. (1982) The recognition and interpretation of paleokarsts: Two examples from the lower carboniferous of South Wales. *Journal of Sedimentary Petrology*, **52**(1), 83-94.

Wright, V. P. & Smart, P. L. (1994) Paleokarst (dissolution diagenesis): Its occurrence and hydrocarbon exploration significance. In: *Diagenesis, developments in sedimentology, Vol. 51* (Ed. by K. H. Wolf and G. V. Chilingarian), pp. 477-517. Elsevier Science BV, Amsterdam.

Young H. R. & Nelson C. S. (1988) Endolithic biodegradation of cool-water skeletal carbonates on Scott Shelf, northwestern Vancouver Island, Canada. *Sedimentary Geology*, **60**, 251-267.

Zempolich, W. G. & Erba, E. (1999) Sedimentologic and chemostratigraphic recognition of third-order sequences in resedimented carbonate: The middle Jurassic Vajont Limestone, Venetian Alps, Italy. In: *Advances in Carbonate Sequence Stratigraphy: Application to Reservoirs, Outcrops and Models*, pp. 335-370. SEPM Special Publication, **63**.

Chapter 4

INTERRELATIONSHIPS BETWEEN THE PETROGENESIS AND HIGH-RESOLUTION SEQUENCE STRATIGRAPHY OF THE PLIOCENE COOL-WATER LIMESTONES IN SOUTHERN HAWKE'S BAY, NEW ZEALAND

Abstract 254
1. Introduction 258
2. Geological and tectonic setting of the Pliocene successions 260
3. Diagenetic approach 261
4. Sequence stratigraphic approach 264
5. Facies architecture, diagenesis, and sequence stratigraphy of the Pliocene sequences 271
6. Hypothetical framework to account for the stacking of the Pliocene sequences 296
7. Sequences in the eastern limestone occurrences from late Opoitian to early Nukumaruan 300
    7.1. Kairakau Limestone (late Opoitian) 300
    7.2. Awapapa Limestone (early Waipipian) 308
    7.3. Rotookiwa Limestone (late Waipipian) 315
    7.4. Te Onepu Limestone (Mangapanian-early Nukumaruan) 320
    7.5. Mason Ridge Formation (Nukumaruan) 325
8. Te Aute sedimentary sequences periodicities 334
9. Sequence development and syndepositional tectonic overprint 335
10. Conclusions 337
References 342

Key Sections: 1, 3, 4, 5, 6, 7.1, 7.5, 8, 10
Key Figures: 1, 6, 9, 10, 11, 22, 23, 24

Chapter 4

INTERRELATIONSHIPS BETWEEN THE PETROGENESIS AND HIGH-RESOLUTION SEQUENCE STRATIGRAPHY OF THE PLIOCENE COOL-WATER LIMESTONES IN SOUTHERN HAWKE'S BAY, NEW ZEALAND

ABSTRACT: An integrated stratigraphic and diagenetic study of a Pliocene (late Opoitian to early Nukumaruan) cool-water mixed carbonate-siliciclastic succession in southern Hawke's Bay documents the previously unrecognized sequence stratigraphic architecture of limestone bodies of shallow-water, high-energy environmental origin. Each of the Pliocene limestones is subdivided into a number of sedimentary packages (between 4 to 12) on the basis of discontinuity surfaces bounding them, and of specific diagenetic patterns (part of their pre-compaction diagenetic history) restricted to portions of the building blocks.

Transgressive (deepening-upwards) and transgressive-regressive (deepening- then shallowing-upwards) sequences are identified, which are bounded by transgressive surfaces of erosion (TSE), locally coincident with either sequence boundaries (subaerially exposed surfaces) or regressive surfaces of erosion (wave-cut surfaces of erosion developed during early to late fall of sea level). Within the studied limestone bodies, the boundary between deepening-upwards and shallowing-upwards depositional trends typically corresponds to a thin (<1 m), locally sharp-based, mixed carbonate-siliciclastic condensed horizon consisting of fine-grained reworked shell fragments, detrital glauconite, and mud clasts, and characterized by highly destructive sea-floor marine diagenesis. Because no faunally-derived paleobathymetry is available to constrain its paleodepth, it is proposed to designate this condensed horizon, located at the turnaround between deepening- and shallowing-upwards depositional trends, by the term horizon of maximum diagenetic condensation (Cdh = condensed diagenetic horizon), rather than by the term maximum flooding surface (Mfs).

Vertical changes in thickness and depositional facies through the sedimentary sequences, in association with changes in the type and degree of diagenesis that outline vertical patterns of pre-compaction diagenetic suites, and fundamentally the position of bounding discontinuities, define four sedimentary sequence motifs, named Motifs 1-4.

All sedimentary motifs are bounded by TSEs that may locally coincide with major sequence boundaries (SB; i.e., subaerially exposed unconformities). The lower TSE lies at the base of the depositional sequence and is either overlain by condensed fossiliferous to pebbly transgressive lags, or condensed transgressive coarse-grained skeletal deposits. The upper contact generally also bears signs of marine ravinement produced during transgression (TSE), including a sharp or eroded surface, *Ophiomorpha* and/or *Skolithos* burrows, and is overlain by the basal transgressive lag of the next sequence.

(a) Sedimentary Motif 1 exhibits a deepening-upwards depositional trend from the basal shallow-water (intertidal to shoreface) transgressive lag to near storm-wave base mixed siliciclastic-carbonate sediments. Typically, the specific diagenetic attributes of Motif 1 record a vertical trend from constructive to increasingly destructive diagenesis towards the superjacent TSE. Sedimentary Motif 1 is interpreted to represent a transgressive systems tracts (TST), which is not bounded above by the horizon of maximum diagenetic condensation (Cdh), but instead is truncated by the next TSE.

(b) By contrast with Motif 1, the upper bounding discontinuity of Sedimentary Motif 2 lies above the Cdh, and within or at the top of the overlying highstand systems tract (HST). Motif 2 exhibits a predominantly constructive to destructive diagenetic vertical trend. Destructive diagenesis does not culminate immediately beneath the superjacent TSE, but within the Cdh.

(c) The upper part of Motif 3 exhibits a shallowing-upwards trend (coarsening- and thickening-upwards deposits), which corresponds to sediments emplaced during normal regression (i.e., regressive systems tract = RST). The RST deposits in Motif 3 are bounded below by a gradational contact, and above by a TSE not superposed to a subaerial unconformity. RSTs correspond to the time interval during which the destructive-to-constructive turnaround of the diagenetic regime occurs. Upward-coarsening of bioclasts, the lesser degree of microborer infestation, poorly mature authigenic glauconite (pale yellow to pale green), and fringes of intrinsic turbid cements are collectively indicative of increasing constructive processes compared to the underlying HST.

(d) Motif 4 indicates a deepening- (TST) then shallowing-upwards depositional trend (HST to RST). Intertidal to upper shoreface coarse skeletal sediments form

the upper part of the RST, and immediately at and beneath the capping surface record discrete evidence of subaerial exposure (dissolution, desiccation cracks, brecciation, and little, if any, meteoric cementation). Therefore, the discontinuity bounding the top of Motif 4 coincides with a major sequence boundary (SB). Characteristically, the upper part of the RSTs also comprises fabrics related to sea-floor constructive diagenesis, including thick isopachous turbid cements and micritic cements.

The sequence stratigraphic architecture of the Pliocene limestones in southern Hawke's Bay, defined by the stacking of sedimentary sequences assigned to Motifs 1-4, provides evidence of variations in carbonate production for the Te Aute limestones, which are inferred to be produced in response to a combination of Milankovitch-forced glacio-eustatic oscillations (precession) and tectonism.

Local thickness variations of sequences, and development of depocentres in the pre-Nukumaruan carbonate successions, which accumulated in the vicinity of structural highs and were dominated by epifaunal calcitic molluscs and barnacles, are considered to reflect tectonically-induced contrasting conditions of accommodation at a regional scale. As a result, the sequence architecture of individual formations is complex, and renders the traceability of discontinuity surfaces difficult, even over short distances.

In contrast, Nukumaruan limestone sheets and interbedded siltstones - sandstones are laterally more continuous, display only minor thickness variations, and comprise facies associations characterized by higher contents of infaunal aragonitic molluscs and muddier rock frameworks, which collectively indicate that by Late Pliocene the carbonate depositional environment had changed in southern Hawke's Bay from being related to localized structural ridges to more widespread marine embayments. The sequence architecture of Nukumaruan limestones, which is typically cyclothemic in southeastern and central Hawke's Bay, shows the influence of glacio-eustatically driven processes, including the Milankovitch obliquity periodicity. The sedimentary successions can be grouped into siltstone/sandstone - limestone formational couplets, which contain distinct systems tracts (TST, HST, RST, and possibly FRST) bounded by easily traceable surfaces (TSEs and local subaerial-exposure surfaces).

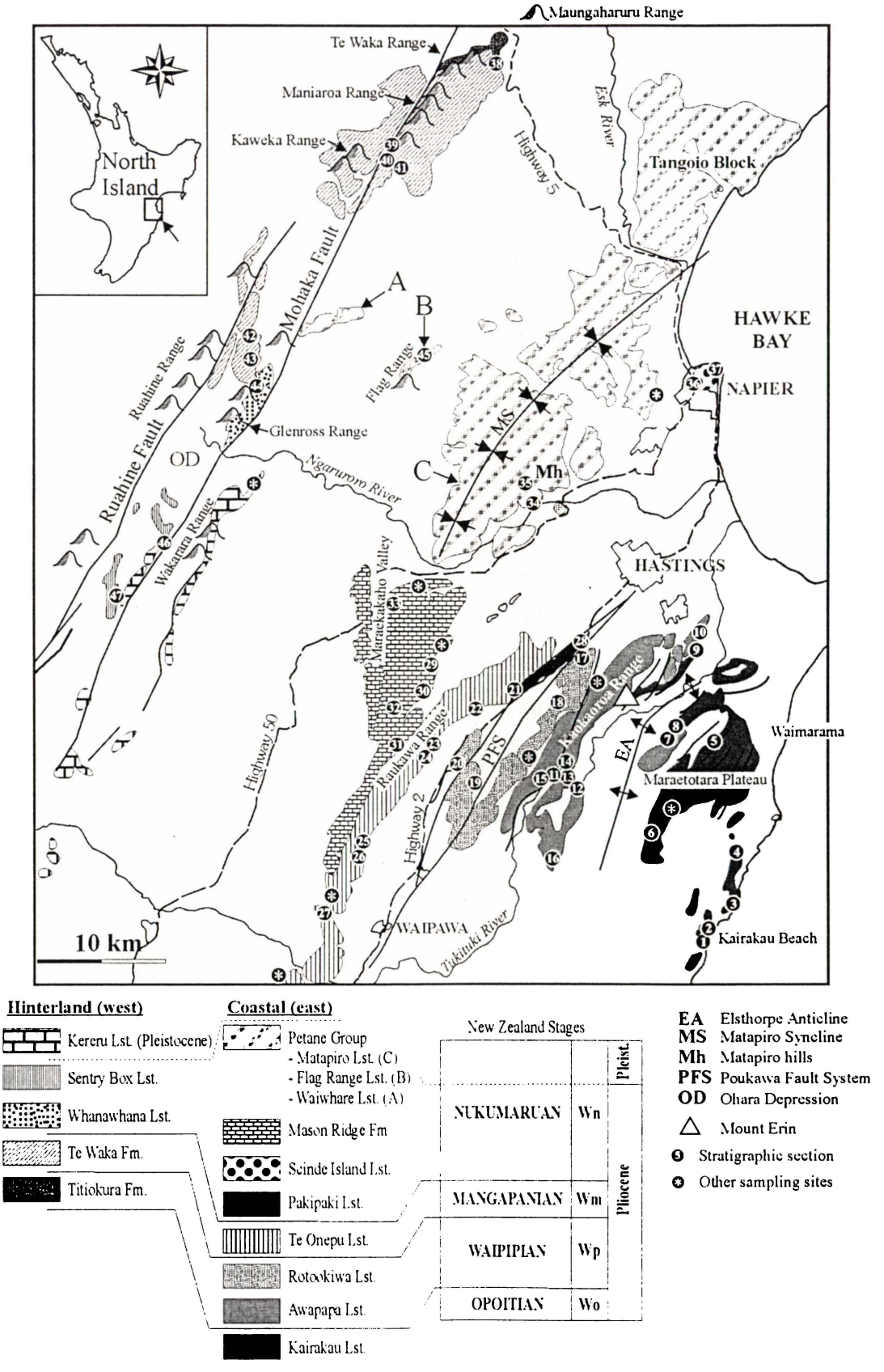

Figure 1- General distribution of the Plio-Pleistocene limestones in the study area, and location of logged sections and other sample sites (geological map from Beu, 1995).

1. Introduction

Pliocene to Pleistocene carbonates in southern Hawke's Bay are informally and collectively referred to here as the Te Aute limestones (see Chapter 1, Section 1). The Pliocene limestones of Opoitian to earliest Nukumaruan age (Figure 1) are characterized by an unusually high content of barnacle plates, and more generally by a typical cool-water skeletal association involving barnacles, epifaunal calcitic bivalves, and bryozoans (Kamp *et al.*, 1988; Beu, 1995; Hayton *et al.*, 1995). Cementation in the pre-Nukumaruan limestones, and to a varying but generally small degree (at least for the burial part) in some of the Nukumaruan limestones, has a predominantly burial and meteoric origin. Sea-floor cementation is rare overall, but occurs at specific stratigraphic horizons, typically in coarse shallow-water facies located either immediately above or below unconformities (see Chapter 3, Section 4.2). Internal sedimentary structures, ranging from planar/tangential to trough cross-stratifications, and faunal associations indicate that the barnacle-rich limestones formed in high-energy settings dominated by tidal and subtidal currents. Sediments accumulated in the form of sand waves and larger-scale sand dunes migrating basinwards from carbonate factories located upon upthrust ridges (see Chapter 1, Figure 29). Thus, lateral changes of facies are common and rapid in these limestones.

In contrast, the younger Pliocene to Early Pleistocene Nukumaruan limestones (Figure 1) are often enriched in aragonitic skeletons and have locally higher terrigenous contents, and typically are thinner and more continuous (Haywick, 1990; Beu, 1995). Further, Nukumaruan formations are more obviously cyclothemic in disposition, well exemplified by the Petane Group units in the Tangoio Block that comprise siltstone/sandstone - limestone formational couplets (Haywick *et al.*, 1992; Haywick, 2000). The cyclothemic nature of the Nukumaruan formations has been attributed to recurring sea-level fluctuations forced by inferred short-term (40 ka) orbital perturbations (Haywick *et al.*, 1992). This differs from the stratigraphic disposition of the pre-Nukumaruan Te Aute limestones that are interbedded with thick siltstones and sandstones, imparting the appearance of a low-order sedimentary cyclicity in the older Te Aute successions (see Chapter 1, Figure 2). Until now, pre-Nukumaruan limestones have been considered as parts of third-order relative sea-level cycles (Beu, 1995), but little attention has been given to their internal organization in terms of sedimentary stacking.

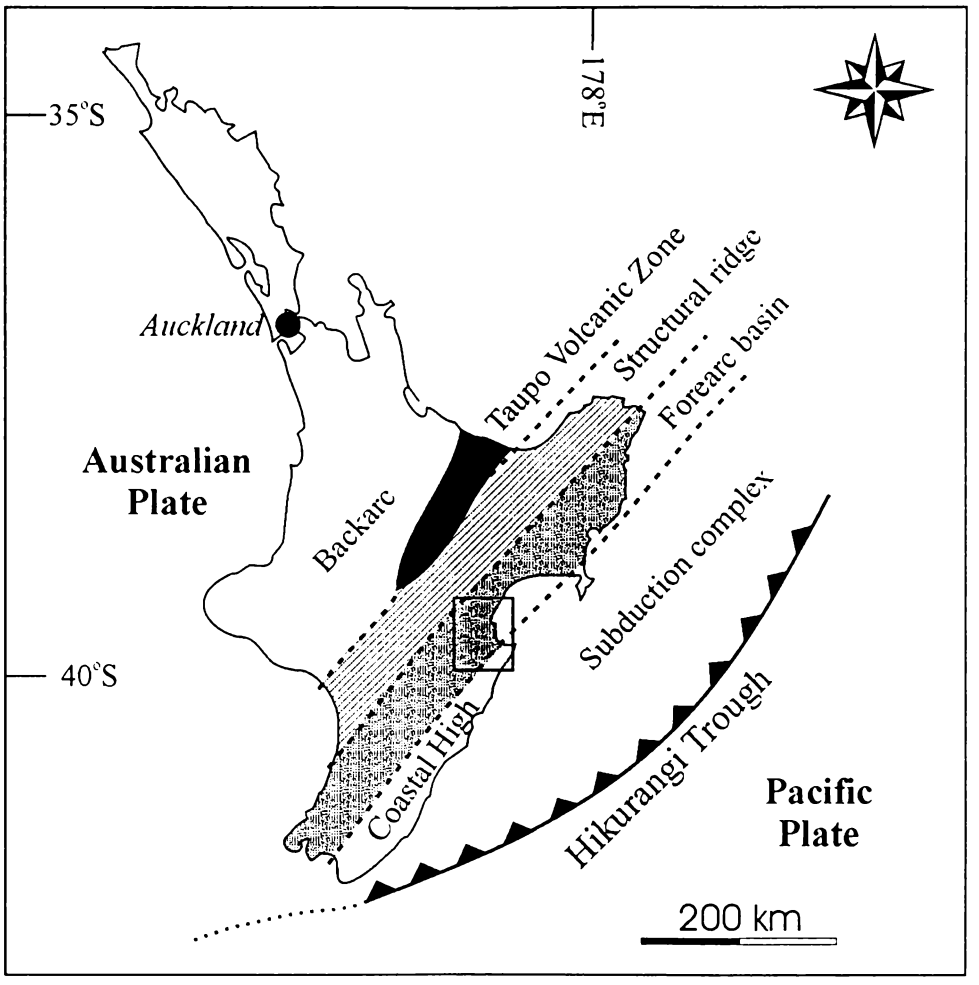

Figure 2- Location of the study area (outlined) relative to the major tectonic features of the eastern North Island, New Zealand (modified from Kamp *et al.*, 1988). See text for comment.

The construction of detailed stratigraphic columns through the different Pliocene units in southern Hawke's Bay (Appendix 1) has enabled the recognition of recurring sedimentary facies within these columns, and identification of key surfaces separating the various facies or groups of facies in the columns (i.e., systems tracts). The vertical stacking of sedimentary facies between consecutive key surfaces, and the comparison of diagenetic histories on either side of these key surfaces reveal distinct depositional sequences of transgressive and transgressive-regressive character (e.g., see Chapter 2, Figures 9 to 11).

The purpose of this chapter is to give insight into the complex diagenetic and sedimentological characters of sequences and their bounding surfaces, and to outline the interrelationship between diagenesis and the building of systems tracts. The approach aims at unravelling what may have been the role of tectonic and glacio-eustatic mechanisms, sediment type, and depositional setting on the stratal architecture of the Pliocene Te Aute limestone formations in southern Hawke's Bay.

2. Geological and tectonic setting of the Pliocene successions

Terrigenous-dominated marine Neogene successions accumulated in response to the evolution of the modern active Australia-Pacific plate boundary through New Zealand since the close of the Oligocene. Eastern North Island Plio-Pleistocene sedimentary rocks represent the upper portion of this Neogene stratigraphy, which consists of a 5 km-thick forearc basin fill of an overall Miocene-Pliocene regressive sequence. The forearc basin represents the major topographic and structural depression of the accretionary complex (Figure 2). It is bounded to the east by the subduction complex, and to the west by a structural ridge of Mesozoic basement rocks (locally the Ruahine Range, Figure 1) separating the subduction complex from a volcanic zone and the backarc region (Figure 2).

In the earlier forearc basin and subduction complex, Miocene limestones occur in the form of pods and lenses enclosed within massive mudstones or sandy siltstones, and are characterized by bivalve-foraminiferal-bryozoan skeletal associations. Kamp and Nelson (1988) interpreted these limestones as mainly outer shelf to upper slope channel fill-deposits. Production and accumulation of limestones increased during the

Pliocene as a result of narrowing and shallowing of the forearc basin caused by uplift on its margins, eventually constricting into a narrow northeast-southwest trending seaway named the Ruataniwha Strait by Beu (1995). With the tectonic shallowing of the basin through inner shelf depths and the progressive development of a narrow tide-dominated seaway, there is a corresponding change in the skeletal associations towards high-moderate energy and shallow-water barnacle-bivalve-dominated assemblages.

The outcrop pattern of the Early and mid-Pliocene limestone occurrences, especially the more eastern ones adjacent to the inboard margin of the subduction complex, demonstrates that deposition migrated towards the centre of the basin over time, the younger sheets being present close to the forearc basin axis and at lower elevations compared to older Pliocene sheets located on the outer margins of the basin (Figure 1) (Kamp *et al.*, 1988). By Late Pliocene, the coastal high had become emergent (Figure 2) and as differential uplift persisted after the Pliocene, the Early Pleistocene limestones formed towards the axis of the basin (Field *et al.*, 1997).

During deposition of the Te Aute limestones, sedimentation was influenced by strong tidal flows and waves, and to a varying degree by storm currents, involving mainly cool- to warm-temperate ocean waters (Kamp and Nelson, 1988; Beu, 1995).

3. Diagenetic approach

Because of differences in many facies attributes between warm- and cool-water carbonates, including shell mineral types, geochemistry, and accumulation rates, it is inappropriate to apply diagenetic models originating from warm-water settings directly to temperate-water carbonate deposits (Nelson, 1988a; James, 1997). The present study has developed some new concepts of high-resolution diagenetic stratigraphy that take into account the specificities of cool-water carbonates, especially the more destructive nature of their marine diagenesis in comparison to the predominantly constructive signature of marine diagenesis in tropical settings.

The diagenetic principles applied in this study have been described in detail in Chapters 2 and 3, and only a brief summary is provided here.

3.1. Destructive versus constructive diagenesis

Sea-floor diagenesis in cool-water carbonates is regarded as predominantly destructive (Alexandersson, 1978), whereas carbonates formed in tropical settings are characterized more by constructive sea-bed diagenetic processes (Nelson, 1988a; Nelson *et al.*, 1988b; James, 1997).

Destructive diagenesis comprises all mechanical and chemical processes that reduce the potential for skeletal grain preservation, such as abrasion, bioerosion, and dissolution prior to burial history, and burial-related grain breakage and pressure-solution, all processes greatly enhanced in non-tropical settings by the paucity of early cementation either at the sea floor or in the meteoric environment.

Diagenetic characterization of each thin-section between two end-members – destructive to constructive – was determined qualitatively from diagenetic features interpreted as pre-burial (Figure 3). Degrees of abrasion, bioerosion, encrustation and cementation are combined on the basis of specific attributes to characterize sample diagenesis in terms of highly constructive, an intermediate situation, and highly destructive. First devised as a practical petrographic means of describing thin-sections, the aforementioned criteria were later used to define the specific diagenetic suites CD/MD/DD (see below and Figure 4), whose diagnostic attributes are summarized in Chapter 2, Table 2.

3.2. Specific diagenesis

In Chapter 2 (Section 5.4.1), it has been emphasized that the progression of diagenetic environments that moved through a succession is best explained when related to diagenetic discontinuities correlatable throughout the study area. In the Pliocene limestones a critical discontinuity event to decipher is the first evidence of mechanically-induced skeletal fracturing, enabling the definition of pre-compaction and post-compaction diagenetic features. The comparison of pre-compaction diagenetic suites in outcrop samples from above and below significant disconformities enables isolation of the "specific diagenesis" (Caron *et al.*, 1998) of unconformity-bounded depositional units, which is that suite of physicochemical events prior to any superposed diagenetic overprint associated with the sediments overlying the upper discontinuity surface. Thus, specific diagenesis corresponds to the time interval during which

Index	Destructive			Constructive		Example
	Abrasion	Bioerosion	Dissolution	Encrustation	Cementation	
4	Angular to sub-rounded	Low to moderate density of microbores	No	Common, moderately to well preserved	Spar or micritic, intrinsic, thick (up to 200 μm)	Figs. 4A, 4C
2	Sub-rounded	Moderate to high	Seldom	Rare, poorly preserved	Seldom intrinsic, thin (<50 μm), common extrinsic	Figs. 4B, 4D, 4E, 4G, 4H
0	Well rounded	Intensive microboring	Present	Poorly preserved, if any	Seldom intrinsic, thin (<50 μm), seldom extrinsic	Fig. 4F

Figure 3- Degrees of abrasion, bioerosion, dissolution, encrustation, and cementation recognized in each thin section were assigned indices of low destructive/high constructive (4), moderate (2), and high destructive/low constructive diagenesis (0), based on specific characteristics. These criteria are used for diagenetic index characterization of samples between two end-members: highly constructive and highly destructive.

sediments remain under the influence of surficial processes that also drive the packaging of sediments and the generation of sedimentary surfaces bounding them.

In the course of unravelling the specific diagenetic histories of the Pliocene limestone samples in southern Hawke's Bay, 10 type-diagenetic suites have been recognized and defined, distributed on a scale from mainly constructive (CD types) to mainly destructive diagenesis (DD types) (see Chapter 2, Table 2). The diagenetic processes and products involved are described in Chapter 3, and some examples of the specific diagenetic suites are illustrated here in Figure 4. One of the main observations of this study is that the attributes (constructive versus destructive processes) of the specific diagenesis of a sequence change vertically, and appear to be strongly correlated to the succession of sedimentary facies that define the systems tracts, and as such may readily be explained within a sequence stratigraphic framework.

4. Sequence stratigraphic approach

4.1. Preamble

With the exception of the Sentry Box Limestone (Figure 1), interpreted as a lowstand systems tract (LST) deposit formed during a glacial period, Beu (1995) suggested that all Nukumaruan carbonate facies sitting sharply on offshore mudstones represent interglacial transgressive systems tracts (TST) of sixth-order, equivalent to type-A transgressive shell beds of Abbott and Carter (1994). In a recent study, Haywick (2000) pointed up the absence of such sharp contacts, interpreted as ravinement surfaces, at the base of carbonate facies in sections in the east of the Tangoio Block (Figure 1), otherwise present in the west. He argued that, in the east, carbonate facies upon correlative conformities developed during lowstand periods, and were LST deposits. Haywick (2000) also recognized some carbonate facies as being forced regressive systems tracts (FRST) because they were directly overlain by LST fluvial gravel beds across a sequence boundary (Hunt and Tucker, 1995).

Although there is little doubt that the cyclicity of the Nukumaruan formations in Hawke's Bay was generated through recurring sea-level changes (Kamp and Nelson, 1987; Beu, 1995; Haywick, 2000), the impact of such a controlling mechanism on the formation of the older Te Aute limestones is poorly understood, and has only been envisaged at lower order frequencies than for their Nukumaruan counterparts. Thus,

Figure 4- Photomicrographs illustrating some of the specific diagenetic suites defined in Table 2 in Chapter 2.

(A) CD^1 (Constructive diagenesis) - Geopetal internal sediment (g.s.) pre-dates isopachous marine acicular inclusion-rich cement (t.c.). Sample 5.93 (Awapapa Limestone; Appendix 5, p. A5-16).

(B) CD^2 (Constructive diagenesis) - Macrobores in pectinid valve host micropeloidal internal sediments (m.s.) from marine phreatic environment. Macrobores, encrusters, evidence of the proximity of the interface water-sediment, including geopetal internal sediment, *in situ* peloidal micrite and marine acicular cement, collectively define the specific diagenetic suite CD^2. Sample 5.86 (Awapapa Limestone; Appendix 5, p. A5-17).

(C) CD^4 (Constructive diagenesis) - Micritic cement projecting digitations towards pore centres, probably microbially induced (black arrows), and bridges between grains, from vadose or phreatic marine environment. There is no evidence that the micritic crust post-dates the dissolution or neomorphism of bioclasts. Sample 11.81 (Mason Ridge Formation; Appendix 5, p. A5-32).

(D) M1 (Mixed constructive/destructive) – Meniscus low-Mg calcite spar cements at grain contacts (black arrows) and neomorphism of aragonitic grains (Ar.), are testimony to both the uneven distribution of water in the pore spaces, and its undersaturation with respect to calcium carbonate. These attributes typically define the vadose diagenetic environment. Sample 17.10 (Scinde Island Limestone; Appendix 5, p. A5-36).

(E) M2 (Mixed constructive/destructive) – A suite of diagenetic fabrics, which are interpreted to have originated beneath a subaerial exposure surface: (a) dissolution of aragonitic shell fragments (between thick white arrows); (b) the percolation of dark detrital sediment (d.s.) through fissures and cracks; and (c) the precipitation of micritic crust (thin white arrows). Sample 6.7 (Pakipaki Limestone; Appendix 5, p. A5-38).

(F) DD^1 (Destructive diagenesis) - Very well abraded and microbored (black arrow) bioclasts from a starved sea floor. Authigenic glauconite is abundant and fills in most intraparticle pores (foraminifer chambers, white arrows). Sample 11.90 (Mason Ridge Formation; Appendix 5, p. A5-32).

(G) DD^2 (Destructive diagenesis) - Abrasion and microboring are the dominant diagenetic processes. Only a thin post-compaction dogtooth cement grew upon the outer surface of well abraded bioclasts. Sample 7.34 (Rotookiwa Limestone; Appendix 5, p. A5-20).

(H) DD^3 (Destructive diagenesis) - Abraded and moderately microbored bioclasts (black arrow) are drowned in a siliciclastic-rich matrix. No early cement formation. Sample 5.38 (Awapapa Limestone; Appendix 5, p. A5-14).

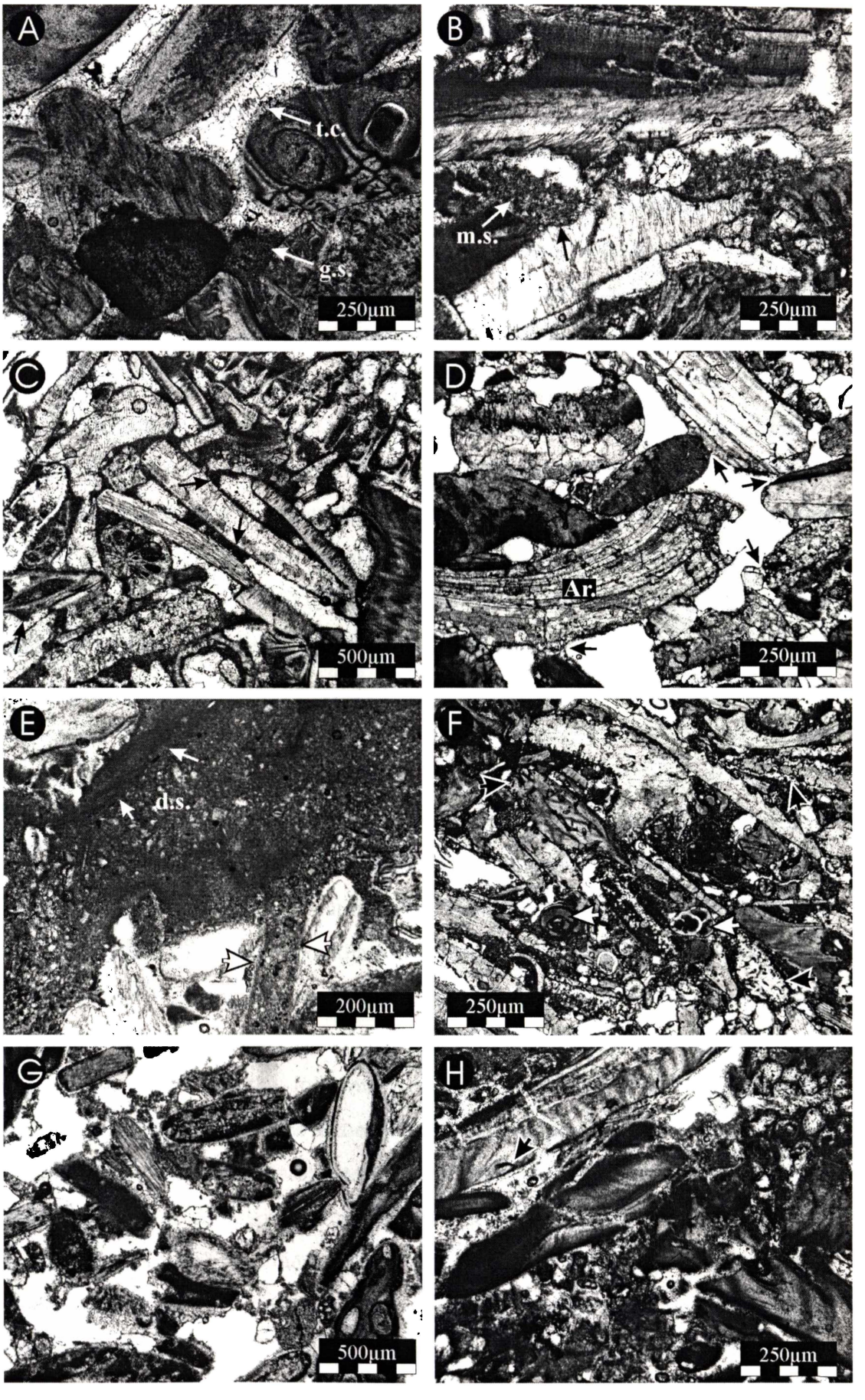
A
t.c.
g.s.
250µm
B
m.s.
250µm
C
500µm
D
Ar.
250µm
E
d.s.
200µm
F
250µm
G
500µm
H
250µm

using a global Plio-Pleistocene sequence scheme, derived from Gulf of Mexico sequences (Womardt and Vail, 1991) to help predict periods of limestone deposition, Beu (1995) assumed that each mid-Pliocene limestone started to form at a maximum flooding surface during third-order sea-level cycles. However, because of the lack of absolute ages available for the Pliocene Te Aute successions, the suggested correlations are rather poorly constrained and were not further envisaged in the present study.

Undoubtedly, tectonism also played a major role in the evolution and distribution of Plio-Pleistocene limestones in eastern North Island (see Section 2; Kamp and Nelson, 1987). Evidence of syndepositional tectonism in the Te Aute limestones has been reported in many past studies (Beu *et al.*, 1980; Harmsen, 1984; Kamp and Nelson, 1987, 1988; Kamp *et al.*, 1988; Beu, 1995), and Kamp and Nelson (1987) and Kamp *et al.* (1988) have emphasized the controlling effect of tectonism on the rate of terrigenous sediment influxes and subsequent development of carbonate sedimentation. Furthermore, tectonism, being the major control to the creation of accommodation space, has also the potential: (1) to force cyclicity; (2) to cause local thickness variations in the component systems tracts of glacio-eustatically forced sequences (see Section 7.2); and (3) to favour the record and preservation of glacio-eustatically forced sequences by locally creating accommodation space (see Section 6.2).

On the basis of stratigraphic and diagenetic criteria, discontinuity surfaces have been recognized within the Plio-Pleistocene limestone units that coincide with periods of erosion, or low and/or no sedimentation. The vertical stacking of sedimentary facies between consecutive key surfaces and the comparison of diagenetic histories recorded on either side of key surfaces has enabled the positive distinction of transgressive and transgressive-regressive depositional sequences, and of diagenetic patterns specific of the building systems tracts. In the following section, these metre-scale (1-15 m thick) fundamental building blocks of the Pliocene carbonate successions are described in far more detail than in the previous chapters. It is shown that the stratal pattern of the Pliocene limestones is complex and consists of unconformity-bounded sequences that define sixth and seventh-order intertidal and subtidal cycles. An attempt is also made to address the possible factors responsible for this stratal architecture (glacio-eustasy versus tectonism) and for local variations in the number and thickness of the component systems tracts.

4.2. Sequence stratigraphic concepts applied to the Te Aute carbonate successions

In their recent overview of sequence stratigraphic concepts, Carter *et al.* (1998), following Van Wagoner (1996), pointed out some inconsistencies of sequence stratigraphic studies that principally originate in the confusing usage of terms (for example Downlap Surface (DLS) and maximum flooding surface (Mfs)) that specifically apply either to seismic studies (DLS), or to outcrop studies (Mfs). In the former, systems tracts are treated as chronostratigraphic entities bounded by isochronous surfaces tied to specific positions on eustatic or relative sea-level curves, whereas in outcrop analyses systems tracts are considered to be lithologic packets of strata bounded by physical (observable) surfaces that may be diachronous across a basin.

At the high-resolution scale of the present study, the application of sequence stratigraphic concepts derived from conventional seismic profile analysis, including the definition of sequences, systems tracts, and bounding discontinuities, becomes problematical and even unrealistic for several reasons:

(a) The lack of a sound or detailed chronostratigraphic framework for the Pliocene successions in southern Hawke's Bay, especially at the scale of each individual limestone body that prevents any attempt of correlation to an independent sea-level record such as high-resolution oxygen isotope ice-volume records.

(b) In the absence of detailed geochemical and faunal studies of the Pliocene limestones, the traceability of surfaces across the study area can hardly be achieved, especially when the physical attributes of such surfaces change rapidly over short distances, as is often the case in the Te Aute carbonate strata. Consequently, such poorly time-constrained surfaces cannot be referred to as isochrons correlatable to inflection points on rising or falling limbs of sea-level curves, and the systems tracts that they bound cannot therefore be defined as time (chronostratigraphic) units.

(c) The change from a retrogradational to an aggradational reflector, classically taken as the boundary between TST and highstand systems tract (HST) in seismic studies (Van Wagoner *et al.*, 1988), is unlikely to be recognized in outcrops because in this interval the stratal geometry and facies of deposits from below and above the boundary can mirror one another.

Therefore, in the present study sequences and their building systems tracts are considered as lithologic units whose internal architecture is defined by either demonstrable sedimentologic discontinuities or discontinuities highlighted by diagenesis.

Detailed diagenetic analysis has become critical in the course of this study for completing field observations, and especially for the recognition of subaerial exposure and condensed horizons interpreted either as maximum flooding surfaces, marine flooding surfaces, or transgressive lags (see later), which were otherwise unrecognizable using a conventional sedimentologic approach because some do not correspond to well individualized surfaces or shell beds in the field.

Thus, it must be emphasized that studies aiming at unravelling the sequence stratigraphy of cool-water successions that comprise apparently monotonous limestone units should be accompanied by detailed diagenetic analysis to ascertain that no significant event has been missed, sealed within the diagenetic stratigraphy of the carbonate sediments.

4.3. Modelling of the diagenetic signature of carbonate facies: an attempt to predict the diagenesis of unsampled horizons

A large and directed sampling program has been the key to the present study. Coarse-grained facies (B1a-d, B2a-b, M1; Figure 5 and see Chapter 1, Table 1 for facies code definitions) were systematically sampled where possible, and when sufficiently cemented (even though loose coarse sediments were sampled and impregnated to assess the occurrence of pore-lining fine spar crystals). Only moderately to well cemented samples of packstones (B3a-b) and well cemented siliciclastic facies (S1, M2-3) were taken in the field. High-resolution sampling has been targeted, and therefore is not one of a "blind" type where samples would be taken at regular intervals regardless of the stratal architecture of the successions.

Thus, sampling concentrated in the vicinity of obvious or suspected discontinuities. As a result, there are gaps in the sample distribution within logged sections that are either motivated or forced by field constraints, and also by concerns regarding completion time of the thesis (detailed diagenetic analysis of thousands of samples would have been unrealistic in a three year project!). Consequently, a simple model was constructed to predict the diagenetic signature of the least sampled facies

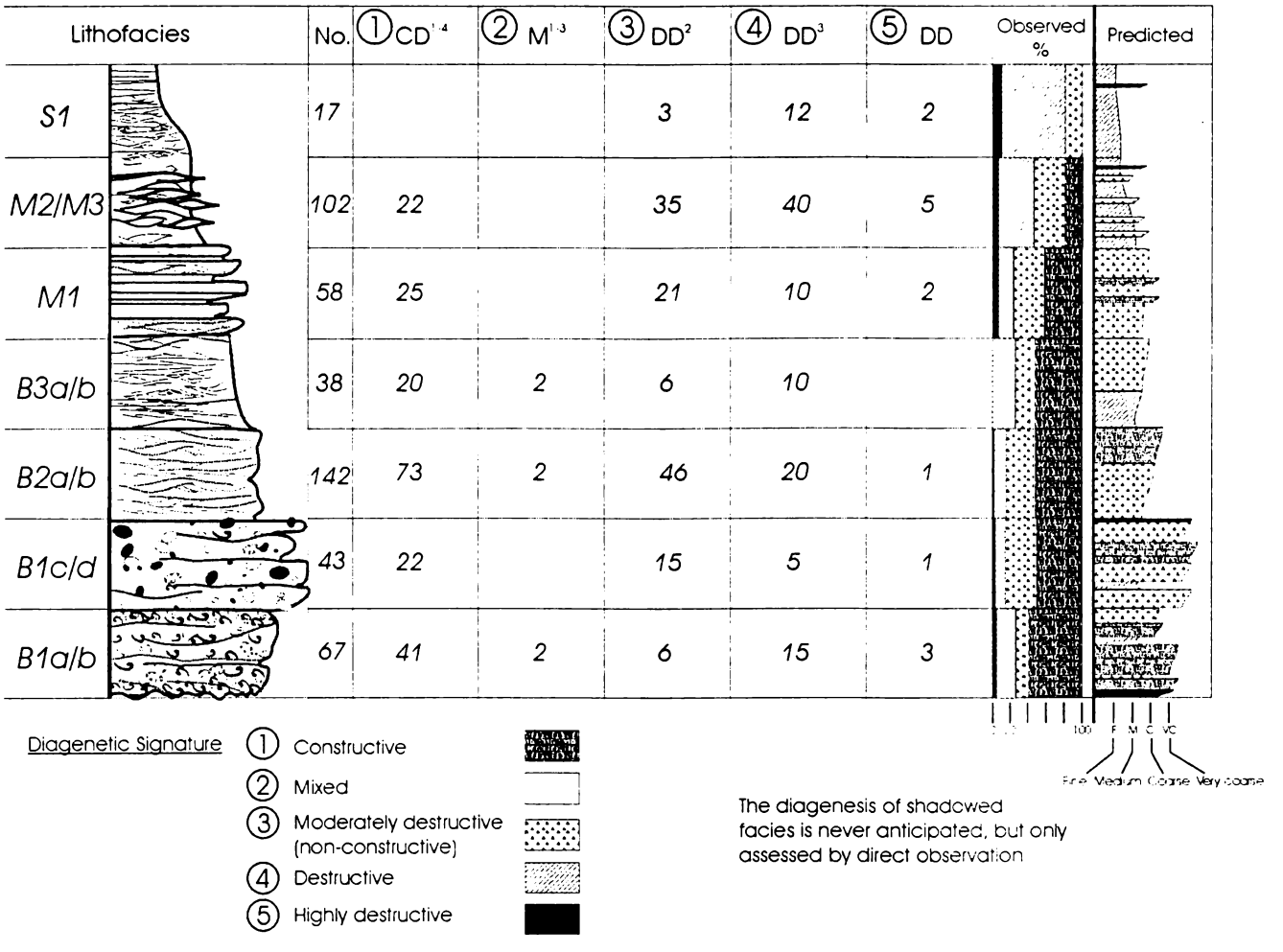

Figure 5- A specific diagenetic model for Pliocene mixed carbonate-siliciclastic (B3a/b, M2-3) and siliciclastic (S1) facies that integrates known specific diagenetic patterns (termed CD-type, M-type, and DD-type; see below) for these facies. Samples (column No.) collected from each facies type were categorized according to their pre-compaction paragenesis between two end-members, constructive (CD^{1-4}) and highly destructive (DD^{1}) diagenesis. The percentage taken by each category is displayed in the column "Observed %". Although known diagenetic patterns of coarse skeletal facies (shadowed) are displayed in the model, the specific diagenesis of their unsampled counterparts has never been anticipated during this study. Note that the predicted diagenesis for M2-3 and S1 facies is in close agreement with the observed diagenesis. In contrast, the predicted diagenesis for packstone facies (B3a/b) does not anticipate constructive features, as were observed. This is a consequence of the targeted sampling. Poorly cemented packstones were generally not sampled and their diagenesis is anticipated to include dominantly destructive features. Well cemented packstones were preferentially sampled and are in most cases the ones that comprise marine constructive features.

Summary definition of facies codes (see also Table 1 in Chapter 1): B1a/b = fossiliferous rudstone; B1c/d = Pebbly rudstone and conglomerate; B2a/b = skeletal grainstone; B3a/b = skeletal packstone; M1 = alternating grainstone and packstone; M2/M3 = alternating packstone and sandstone; S1 = Calcareous sandstone.

Summary definition of specific diagenetic codes (see also Table 2 in Chapter 2): CD^{1-4} = constructive diagenesis; M^{1-3} = constructive diagenesis overprinted by destructive diagenesis associated with subaerial exposure; DD^{2-3} = destructive diagenesis; DD^{1} = highly destructive diagenesis associated with condensed horizons.

(keeping in mind that these are also the least cemented in general) that integrates known diagenetic patterns for these facies (Figure 5).

5. Facies architecture, diagenesis, and sequence stratigraphy of the Pliocene sequences

5.1. Introduction

The vertical succession of lithofacies, tentatively interpreted in terms of depositional environments, together with the nature of surfaces/discontinuities and the vertical changes of specific diagenetic signatures between discontinuities enable the recognition of sedimentary sequences. The subdivision of sequences into systems tracts (i.e., recognition of depositional systems separated by key surfaces) results also from a combination of descriptive facies analysis, and of the specific diagenetic suites recorded by the successive packets of strata building up the sequences.

There have been 14 facies types identified and defined, and they are grouped into 3 major facies assemblages on the basis of sedimentological features, including sedimentary structures and ichnofossils. The facies assemblages are named Bioclastic (B), Mixed carbonate-siliciclastic (M), and Siliciclastic (S). Facies assemblages correspond to a range of depositional environments from shallow-water tide-dominated to mid-outer shelf. The diagnostic characteristics of each facies type are described in Chapter 1 (see Table 1; also contained inside the map pocket in the back cover of the thesis).

In the Pliocene limestone successions, surfaces of erosion and surfaces indicative of low or no deposition have been used to subdivide sedimentary packages into systems tracts and depositional sequences. The recognition of discontinuity surfaces is based on the following kinds of evidence: (1) Angular disconformities with erosional truncation of strata, so long as such angular relationships are not related to synsedimentary processes such as reactivation surfaces or sliding of unconsolidated sediments; (2) A sharp change in depositional conditions across the surface as revealed by the direct superposition of contrasting facies or of contrasting skeletal assemblages; (3) A change across a surface in the degree and type of bioturbation; (4) A contrast between compactional features of superposed strata due to either the underlying or overlying deposit including an early cementation phase; (5) Marine-cemented limestone horizons overlying limestones lacking

marine cements, typically across a sharp burrowed surface or an erosional surface; (6) Coarse pebbly skeletal lags or shell beds overlying sharp or erosional surfaces; (7) Diagenetic features that may indicate conditions of sediment starvation, including abundance and maturity of authigenic glauconite, frequency and intensity of shell infestation by boring and encrusting organisms, degree of skeletal grain abrasion and dissolution of shells on the sea floor; and (8) Diagenetic evidence of subaerial exposure.

5.2. Sequence architecture

The vertical occurrence of sedimentary facies in some characteristic sequences within various Te Aute limestone formations is illustrated in Figure 6. The interpretation of the depositional paleoenvironments for the stacked components of the sequences indicates that the depositional trend between consecutive bounding discontinuities varies from deepening-upwards (sequences 1-5, 9) to then sometimes shallowing-upwards (sequences 6, 7, 8, 10-14). Correspondingly, the vertical distribution of specific diagenetic signatures within the sequences exhibits a trend from mainly constructive to mainly destructive diagenesis in the deepening-upwards member of the sequences, and constructive in their shallowing-upwards portion.

Deepening-upwards sequences comprise the following facies, surfaces, and diagenetic signatures in ascending stratigraphic order: (1) a basal discontinuity coincident either with a sequence boundary (subaerial-exposure surface) or a transgressive surface of erosion (TSE); (2) a thin (<0.2 m) condensed lag, with abundant detrital glauconite and mud clasts, whose diagenetic signature is highly destructive (DD^{1}; see Chapter 3, Section 5.3.1); (3) a transgressive systems tract (3-12 m; TST) dominated by constructive diagenesis (CD^{1-2}), consisting of either fossiliferous and pebbly rudstone (B1a, c), or coarse skeletal-rich cross-bedded packstone and grainstone (B3a, B2a, b) at the base, overlain across a sharp surface by finer-grained mixed carbonate-siliciclastic facies (M1-3) or siltstone/sandstone (S1-3) characterized by moderately destructive to destructive diagenesis (DD^{2-3}); (4) in some examples these are bounded above by a condensed horizon referred to as the mid-sequence horizon of maximum diagenetic condensation (Cdh; see Section 6.3.3), including a highly

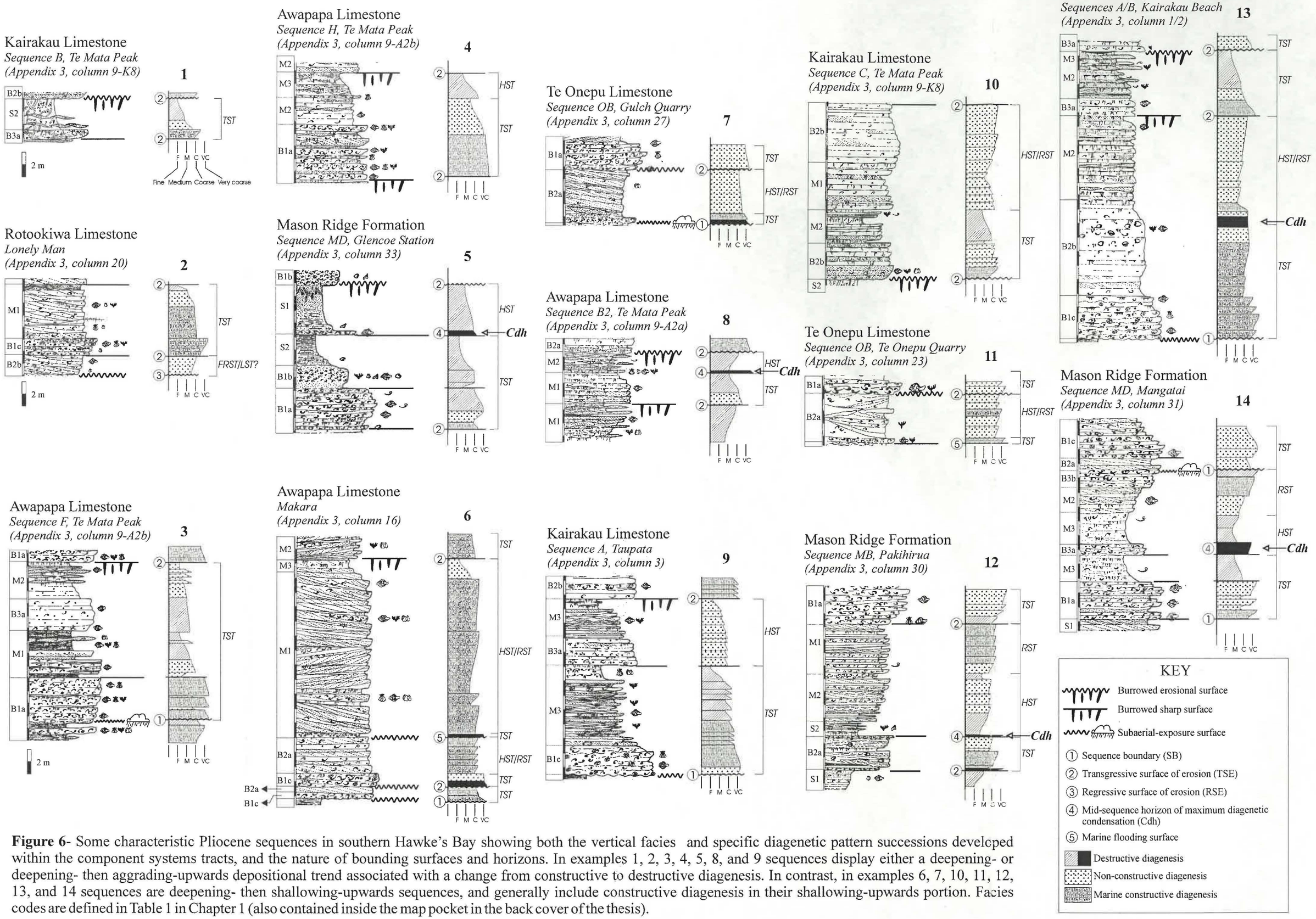

Figure 6- Some characteristic Pliocene sequences in southern Hawke's Bay showing both the vertical facies and specific diagenetic pattern successions developed within the component systems tracts, and the nature of bounding surfaces and horizons. In examples 1, 2, 3, 4, 5, 8, and 9 sequences display either a deepening- or deepening- then aggrading-upwards depositional trend associated with a change from constructive to destructive diagenesis. In contrast, in examples 6, 7, 10, 11, 12, 13, and 14 sequences are deepening- then shallowing-upwards sequences, and generally include constructive diagenesis in their shallowing-upwards portion. Facies codes are defined in Table 1 in Chapter 1 (also contained inside the map pocket in the back cover of the thesis).

destructive diagenetic suite (DD^1), in turn overlain by (5) the base of the HST that comprises siliciclastic facies (S1, M2-M3) and is bounded by a superjacent TSE.

The basal portion of deepening- then shallowing-upwards sequences is generally similar to that of their deepening-upwards counterparts, but may comprise instead of a thick TST, a thin TST (<1 m), which corresponds to a condensed fossiliferous to pebbly rudstone (B1c). From the mid-sequence horizon of maximum diagenetic condensation (see Section 6.3.3), the overlying HST includes destructive diagenetic features (DD^{2-3}) and comprises aggradational (planar- and tabular-bedded) mixed carbonate-siliciclastic facies (S1, M2-3) that grade into an interval referred to as the regressive systems tract (RST; Naish and Kamp, 1997). The RST commences at coarse mixed facies (M1-2) and passes up section into shallow-water cross-bedded skeletal facies (B1a, b) bounded above by either a TSE or a SB. The RST bears moderately destructive to constructive diagenetic attributes, overprinted by destructive meteoric diagenesis beneath the superjacent SB (when present).

By nature, the deepening-upwards sequences display an asymmetrical stratal architecture with respect to their deepening- then shallowing-upwards counterparts. In the latter, depending on the thickness of their basal TST, and on the level (related to the amount of material removed; see Figures 9, 23) where TSEs have truncated their shallowing-upwards member (RST), two styles of sequence architecture can be distinguished: (1) symmetrical when the thickness of the TST equates the thickness of both HST/RST (sequences 10, 13, 14); and (2) asymmetrical when the TST is thinner than the couplet HST/RST (sequences 7, 11, 12).

Naish and Kamp (1997) argued that asymmetrical (siliciclastic-dominated) cyclothems in the Wanganui Basin in southwestern North Island (see Chapter 2, Figure 1A) were a product of stratigraphic condensation in a more distal setting than their symmetrical counterparts. However, the depositional setting envisaged for the Pliocene limestones (at least the eastern ones) is not one of a continent-attached shelf, and therefore the Wanganui model is not applicable barring a few examples for Nukumaruan sequences. Instead, the anticipated irregular topography of neighbouring thrust ridges, combined with differing local conditions of subsidence and sediment supply, are thought to have either favoured preservation of "complete" sequences (in depressions) or to have resulted in erosion of the upper part of sequences during ensuing

transgression. Furthermore, high-frequency carbonate sequences are expected to be asymmetrical because of the initial lag in re-establishment of the carbonate factory induced by transgression (relatively slow initial carbonate production). Sedimentation rates, low during TST and HST, increase upwards into the RST with the regeneration of carbonate factories (see Chapter 3, Section 5.3.3) resulting in a rather thin TST/HST couplet compared to the overlying RST. Although, the asymmetry of sequences is in this case also a product of condensation, it is not driven by the same mechanism as in siliciclastic-dominated systems. The Wanganui model could probably apply for sequences located down-dip of the antiforms towards the forearc basin axis.

5.3. Key surfaces

5.3.1. Transgressive surface of erosion (TSE)

Transgressive surfaces of erosion develop when sea level rises and correspond to the process of erosional translation of the shoreface profile upwards and landwards (Nummedal and Swift, 1987). This process involves an intense reworking and winnowing of pre-existing deposits by the action of wave and storm currents.

The amount of erosion documented to occur during shoreface transgression ranges from a few centimetres up to 40 m (Nummedal and Swift, 1987; Walker, 1995; Bhattacharya and Willis, 2001). Consequently, TSEs may be responsible for the removal of previous RST sediments and surfaces developed upon them, including RSEs and surfaces of subaerial exposure. As such, TSEs may represent significant periods of time in which several metres of sediments could have been removed (analyze Figure 9). Thus, Haywick (2000) envisages that the combination of erosional processes during sea-level fall (RSE) and ensuing rise (TSE) could explain the absence of RST and forced regressive systems tracts (FRST) above HST deposits over much of the Tangoio area (Petane Group, Nukumaruan; Figure 1).

Transgressive surfaces of erosion are sharp or erosional with a relief up to 50 cm, and underlie deepening-upwards deposits that comprise either a basal, condensed, shallow-water transgressive lag packed with bored mud and sandstone pebbles, and variably disarticulated and abraded shells, or coarse bioclastic material grading into mixed facies (Figures 7A-D, 8). Below this ravinement surface, various ichnofossils (Figures 7E-G, 8D), including *Ophiomorpha, Skolithos,* and *Thalassinoides*, penetrate

downward into siltstone, calcareous sandstone, or packstone. They are filled by coarse material of the overlying TST, and are indicative of periods of low or arrested sedimentation, possibly upon firm substrates. TSEs have commonly been interpreted to form immediately after maximum regression of the shoreline (Embry, 1995; López-Blanco *et al.*, 2000; Bhattacharya and Willis, 2001), and as such are likely to be superimposed on, and erode previously developed subaerial unconformities and RSEs (Figure 9).

In the Pliocene limestones, transgressive surfaces of erosion are found overlying shallowing-upwards, aggrading, and deepening-upwards deposits. Even if ravinement is likely to have removed part of the sediments in the latter case, stacked deepening-upwards sediment packages, arranged in a landward-shingled series, can also be interpreted to represent successive transgressive impulses or drownings (Nummedal *et al.*, 1993; Naish and Kamp, 1997).

In conditions of continuous sea-level rise and high rates of carbonate production, space created for sediment accumulation may not be sufficient to accommodate part of the sediment supply. As a result, the excess of sediment, especially the shallowing-upward portion of the sedimentary sequence, is by-passed basinward by currents and a wave-cut erosion surface is generated upon which a condensed lag may form overlain by deepening- then shallowing-upwards deposits of the next sequence (Einsele and Bayer, 1991). The process of erosion of the shallowing-upward deposits being potentially repeated, the sedimentary section would show a succession of deepening-upwards sequences reflecting the rise of sea level, which are bounded by wave-cut surface unconformities generated during relative "regressive" conditions (by-passing of sediments produced in excess) and possibly overprinted by TSEs. In either case (preserved or overprinted), they are interpreted to be transgressive surfaces of erosion because they develop during a pulsating sea-level rise and bound thickening-upwards sequences.

This scenario is envisaged to explain the disposition of amalgamated shallow-water sequences (close to antiform tops), which are underlain by sharp surfaces marked by thin condensed lags (marine flooding surface) comprising detrital glauconite and mud pebbles. The deepening-upwards trend is indicated by rapid thickening-upwards of building sequences as more space becomes available to accommodate sediments (e.g., Makara section, Awapapa Limestone; example 6 in Figure 6).

Figure 7– Photographs of bounding unconformities

(A) Sharp to erosional contact (dashed line) with a low relief (less than 10 cm) between coarse bioclastic grainstone above (TST) and fine-grained terrigenous packstone below (upper TST of the underlying sequence). The contact is characterized by *Skolithos* burrows. Unconformity 3, interpreted as a TSE between sequences B and C of Kairakau Limestone at Mt Kahuranaki (Same succession as in Figures 7D and 7G below; Appendix 3, column 7). Scale is 50 cm.

(B) Ravinement surface representing a TSE (dashed line) between coarse bioclastic limestone (Gr), interpreted as a TST, and well sorted greenish sandstone (Sa; HST? of the previous sequence). Base of Kairakau Limestone at Pukekura section (Appendix 3, column 15). Person for scale at right.

(C) Sharp planar contact at the base of Kairakau Limestone between pebbly rudstone (TST) and Miocene mudstone at Kairakau Beach section (Appendix 3, column 1/2). Hammer (arrowed) is about 30 cm long.

(D) Surface of erosion (dashed line) with a low relief (less than 20 cm) between coarse bioclastic grainstone (Gr; base of TST) and interbedded fine-grained sandstone and terrigenous packstone (upper TST of the underlying sequence). Unconformity 3 within Kairakau Limestone at Kairakau Beach section (correlative of surface seen in A above; Appendix 3, column 1/2). Person for scale at left.

(E) Example of burrowed surface (arrow) interpreted as a TSE filled with shell hash from the overlying TST. Unconformity 6 within the Awapapa Limestone at Te Mata Peak section (Appendix 3, column 9-A2a). Scale length on tape measure is about 5 cm.

(F) Burrow (white arrow), below a sharp contact (dashed lined), interpreted as a TSE, is filled with bioclastic material from the overlying unit (TST) and penetrates into calcareous sandstone of the underlying unit (HST/RST?). Contact between Rotookiwa Limestone and Pukekura Calcarenite at Pukekura section (see also Figure 8A; Appendix 3, column 15). Scale length on tape measure is about 20 cm.

(G) A surface bioturbated by *Skolithos*-type burrows (black arrow) is interpreted as a TSE that marks the boundary between coarse bioclastic sediments above (base of TST) and dense homogenous siltstone below (upper TST of the underlying unit). Unconformity 3 within the Kairakau Limestone at Kairakau Beach section (see also A and D above; Appendix 3, column 1/2). Scale length on tape measure is about 5 cm.

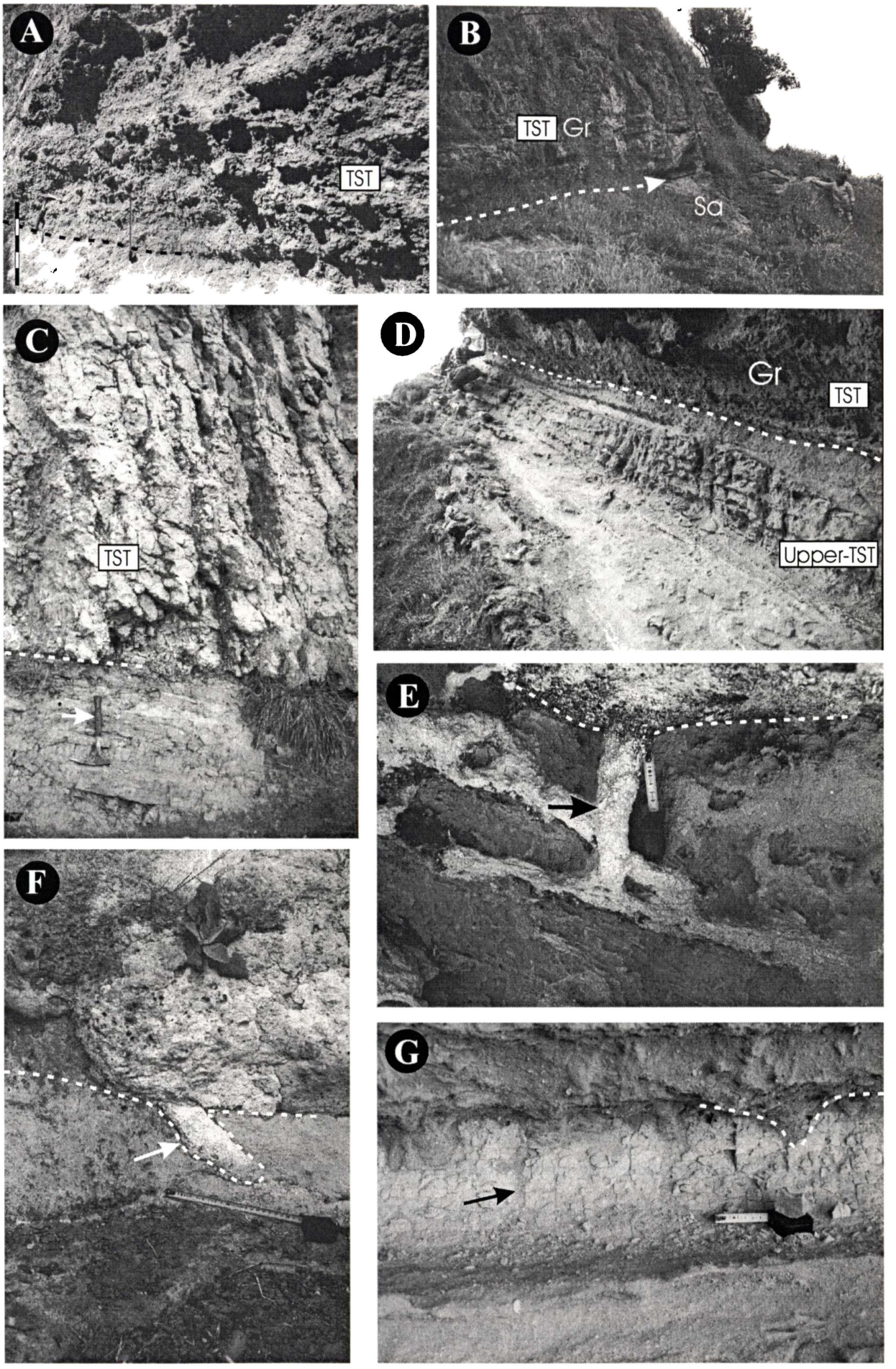
A
TST
B
TST Gr
Sa
C
TST
D
Gr
TST
Upper-TST
E
F
G

5.3.2. Maximum flooding surface (Mfs) versus horizon of maximum diagenetic condensation (Cdh)

Maximum flooding surfaces correspond to the time of change from transgressive to regressive trends (i.e., are located at the point of change from an increasing to a decreasing rate of sea-level rise), and as such bound the transgressive and highstand systems tracts (Vail *et al.*, 1991). Mfs represents the deepest paleodepth of water recorded in a succession of depositional facies and typically coincides with a period of starved sedimentation and condensed section development (Van Wagoner *et al.*, 1987, 1988). Starvation requires that clastic input be minimal relative to accommodation creation, either because sediments were trapped farther landward (i.e., the locus of terrigenous deposition is displaced in the nearshore environment) or the carbonate factories were partly drowned resulting in low carbonate production (Kidwell, 1991b).

Steinhauff and Walker (1995) argued that a drowning unconformity forms when tropical carbonate-producing environments pass below the euphotic zone, and carbonate production is greatly lowered or halted. In contrast, in the Te Aute cool-water successions, depth of light penetration is not a major deterrent to carbonate skeletal-bearing organisms. The increase of water depth above barnacle-dominated carbonate factories that might have developed in the early stages of rapid sea-level rise probably rather resulted in a decrease of current velocity, and subsequently in a decrease of nutrient supply and terrigenous sediment by-pass, responsible for lowering carbonate production.

Characteristics of condensed sections associated with marine flooding, as reported in previous studies, include marine hardgrounds and other evidence of omission surfaces (Boreen and James, 1995), shell beds (Kidwell, 1991b; Abbott and Carter, 1994; Naish and Kamp, 1997), authigenic glauconite (Amorosi, 1995; Clari *et al.*, 1995), and high organic matter (Heckel, 1986).

In the absence of detailed descriptive studies of the faunal content of Pliocene sequences that could have constrained the paleobathymetry of lithofacies formation, the surface or horizon that marks the maximum paleodepth cannot be unequivocally determined. Consequently, the use of the term Mfs may be inappropriate.

Abbott and Carter (1994) have shown that a mid-cycle shell bed (compounds the backlap and downlap shell beds of others) marks the major part of the condensed section encompassing both the top of the transgressive systems tract (TST) and the base of the

highstand systems tract (HST). Because the mid-cycle shell bed (MCS) is often bounded above and below by distinct surface, a local flooding surfaces and a downlap surface respectively, Carter *et al.* (1998) proposed to acknowledge a new systems tract, termed condensed section systems tract (CSST), which occurs between TST and HST.

Within the studied limestone bodies, the boundary between deepening-upwards and shallowing-upwards depositional trends typically corresponds to a thin (<1 m), locally sharp-based, mixed carbonate-siliciclastic condensed horizon consisting of fine-grained reworked shell fragments and mud clasts. The condensed horizon rarely corresponds to well-individualized shell beds bounded above by a downlap surface as defined by Kidwell, (1991a, b), and documented by Abbott and Carter (1994) and Naish and Kamp (1997) in the Wanganui Basin.

In contrast, the condensed horizon, identified in many of the Pliocene Te Aute sequences, is principally characterized by a diagenetic suite of highly destructive processes (specific diagenetic suite DD^1; Figure 4F) that record prolonged exposure on the sea floor and the termination, partial or total, of carbonate production. The destructive diagenetic suite includes: (1) bioclast destruction by bioerosion, and abrasion; (2) the abundance of both detrital glauconite and mature authigenic glauconite (dark brown to dark green); (3) occasional dissolution of aragonitic shell fragments; and (4) little extrinsic cementation. Because the condensed horizon is not systematically associated with a shell lag, and no faunally-derived paleobathymetry is available to constrain its paleodepth, it is proposed that the term horizon of maximum diagenetic condensation (Cdh= condensed diagenetic horizon) would therefore be appropriate to designate the condensed horizon located at the turnaround between a deepening- and shallowing-upwards depositional trend (TST and HST respectively).

By contrast with the CSST of Carter *et al.* (1998), the Te Aute horizon of maximum diagenetic condensation (Cdh) can hardly be elevated to systems tract status because it is generally not bounded above and below by physical surfaces (unless associated with shell lags). Instead, the Cdh has indistinguishable boundaries, and the transition between TST and HST is assumed to lie somewhere within the horizon at some indeterminate level (fuzzy boundary; Figure 10).

The recognition of the Cdh is based on sedimentologic and diagenetic evidence. Its traceability is generally poor, except when directly associated with easily correlatable shell beds located between mid- to outer-shelf siltstones and mudstones found above

transgressive lags, as is the case within the cyclothemic Mason Ridge Formation (see Figures 20, 21).

When the Cdh has unequivocally been recognized, it lies either within mixed facies a few metres above a basal transgressive lag (sequences 8, 13, 14 – Figure 6), or immediately on top of it outlining a sharp surface (sequence 12 – Figure 6). In this case, the TST consists exclusively of coarse-grained bioclastic material (the transgressive lag), locally packed with articulated and disarticulated shells (type-A shell bed of Abbott and Carter, 1994; compound shell bed of Naish and Kamp, 1997).

5.3.3. Regressive surface of erosion (RSE)

The abrupt occurrence of sharp-based anomalously coarser and more proximal shallowing-upwards deposits in a distal marine setting are the manifestation of a basinward and downward shift of the coastal environment, otherwise commonly interpreted as a forced regression, which occurs when the rate of relative sea-level fall exceeds the rate of subsidence of the host basin (Nummedal and Swift, 1987; Walker and Wiseman, 1995). Erosion of the sea floor is due to storm wave action, considering that with lowered relative sea level storm wave base would be lowered as well. Thus, forced regressive deposits are underlain by a wave-cut erosion surface equivalent to a regressive surface of marine erosion produced through wave planning during sea-level fall (Posamentier *et al.*, 1992), or a correlative conformity down-dip of the area where the erosional surface forms. The regressive deposits are detached from the previous highstand shoreline and the regressive surface of erosion (RSE) may be connected upward or landward to a surface of subaerial exposure. It would then coincide with a sequence boundary.

It is expected that during late sea-level fall, sediments of the previous sequence deposited during sea-level highstand (HST) or during an earlier phase of sea-level fall (RST) are partly or totally removed through wave planning that generates a ravinement surface (RSE), later overprinted by a transgressive surface of erosion (see below and Figure 9).

Within the Pliocene successions, only the erosion surface underlying the shallowing-upwards fan-delta Hassal Conglomerate (The Gorges section within Te Waka Formation; see Chapter 1, Section 4.10) can unequivocally be interpreted as a RSE coincident with a sequence boundary. The erosive basal contact of this proximal

Figure 8 – Photographs of bounding unconformities

(A) Contact interpreted as a transgressive surface of erosion (TSE) between Rotookiwa Limestone (TST) and Pukekura Calcarenite at Pukekura section (see close-up view of the contact in Figure 7F; Appendix 3, column 15). Hammer (arrowed) is about 30 cm long.

(B) Erosive basal contact (dashed line) of coarse bioclastic limestone (Ru) with underlying fine-grained well sorted calcarenite (Ca). Possibly represents a true sequence boundary (see text for discussion), separating HST sediments (below) from coarse LST sediments (above). Unconformity 10 or 12 within Rotookiwa Limestone at Lonely Man section (Appendix 3, column 20). Hammer is about 30 cm long.

(C) Northern cliff face of Kairakau Limestone at its type locality (see Appendix 3, column 7; V22/423515), north of Mt Kahuranaki, where the Mangangarara Stream takes its rise. The cliff exposes about 40 m of Kairakau Limestone divided into five sequences based on the occurrence of sharp and erosional contacts interpreted mostly as TSEs. Only the upper part of the lower sequence (sequence A1; see Section 7.1.2 for detail) is exposed. It is separated from the overlying sequence (sequence A2) by a TSE. Above is a deepening- (TST) then shallowing-upwards succession (HST/RST) of facies including a mid-sequence horizon of maximum diagenetic condensation (Cdh). The next sequence (sequence B) consists entirely of a TST that comprises a basal sharp-based (TSE 3) shell bed packed with oyster valves. This deepening-upwards sequence is bounded above by a sharp contact interpreted as a TSE (4), upon which the overlying shallowing-upwards sequence (C1) appears to onlap (black half-arrows). Tabular bed sets of the upper sequence (C2) rest on an erosional surface truncating the underlying unit. Above the surface sediments rapidly coarsen upwards and include thick sea floor cements. This carbonate facies is considered a FRST, and the surface on which it lays a RSE (5). This interpretation is based on the occurrence of meteoric cements overgrowing the previous marine diagenetic suite, which suggest that the superjacent surface atop the FRST has been subaerially exposed. The hypothesis of the RSE being in fact a TSE cannot be totally ruled out because the subaerial-exposure surface has not been physically recognized.

(D) Sharp contact (dashed line), interpreted as a transgressive surface of erosion, between silty sandstone (HST) and shell bed with a sandy matrix (TST). The silty sandstone below the surface is intensively burrowed by *Ophiomorpha*. Unconformity 24 within the Mason Ridge Formation at Glencoe Station (Appendix 3, column 33). Note book (24 cm high) for scale.

(E) Wavy erosional contact (dashed line) between fossiliferous pebbly rudstone (Ru) and bioclastic grainstone with internal bi-directional cross-stratifications (Gr). Surface of erosion (unconformity 22a) within Flag Range Limestone (Appendix 3, column 45). Hammer is about 30 cm long.

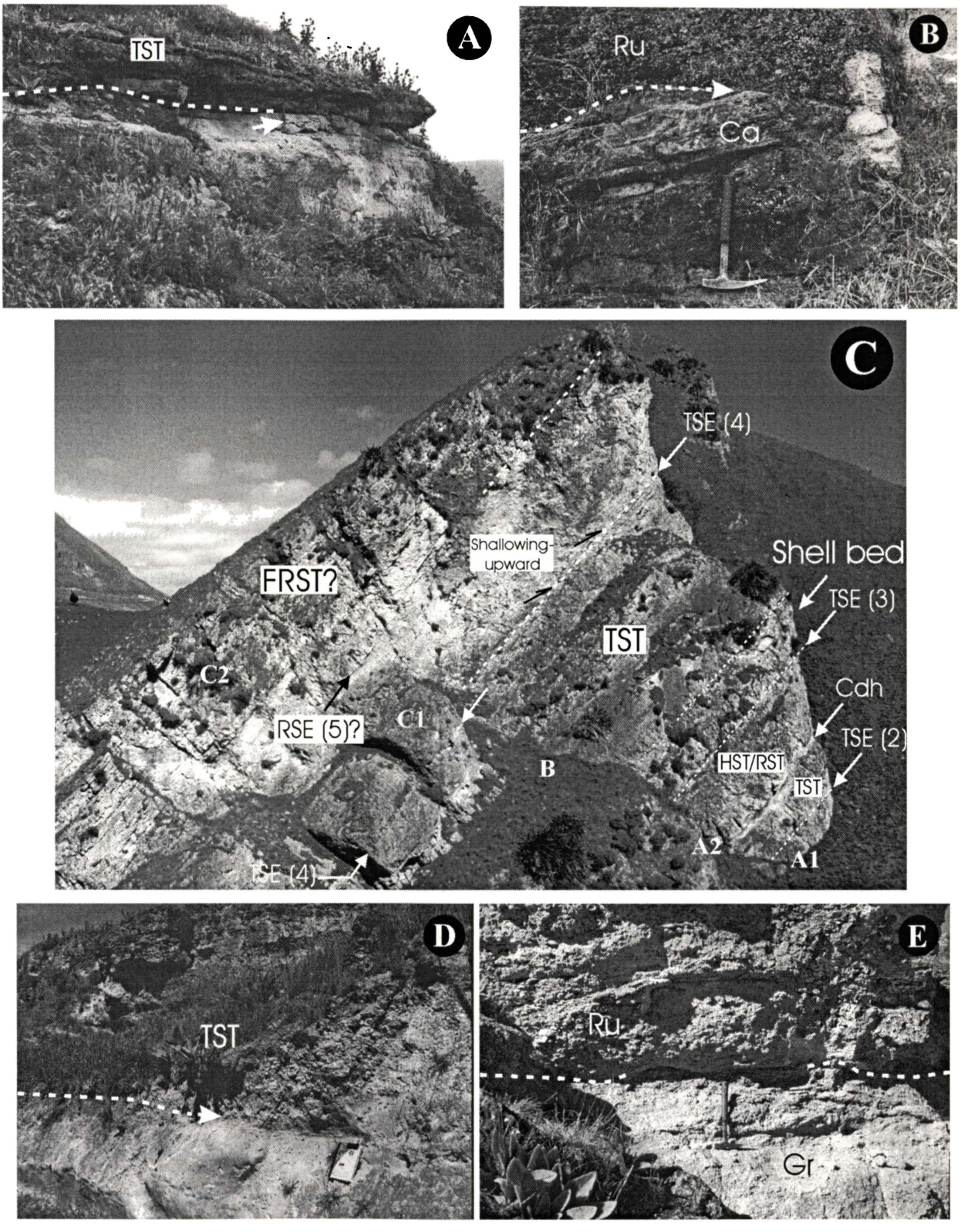
A
TST
B
Ru
Ca
C
TSE (4)
Shallowing-upward
FRST?
Shell bed
TSE (3)
TST
C2
Cdh
RSE (5)?
C1
TSE (2)
B
HST/RST
TST
A2
A1
TSE (4)
D
TST
E
Ru
Gr

facies (LST) with the underlying marine mid- to outer-shelf sandstone represents a sequence boundary. Thus, this lowstand conglomerate, overlain by braided plain deposits, probably developed down-dip of the area of the shelf undergoing subaerial exposure (cf.Van Wagoner *et al.*, 1988).

Another possible example of a RSE is illustrated in Figure 8C. At Mt Kahuranaki, tabular bed sets of the upper building sequence of Kairakau Limestone rest on an erosional surface truncating the underlying shallowing-upwards unit. Above the surface sediments rapidly coarsen up-section and include thick sea floor cements. This carbonate facies is considered a FRST and the surface on which it lies a RSE because meteoric cements overgrowing the previous marine diagenetic suite suggest that the superjacent surface atop the FRST has been subaerially exposed, and is therefore a genuine sequence boundary.

5.3.4. Subaerially exposed surfaces

Subaerial unconformities form in response to relative falls of sea level and typically occur at the top of the regressive systems tracts (Van Wagoner *et al.*, 1988).

On carbonate shelves, subaerial unconformities are characterized by erosion surfaces, incised valleys, and overall the development of karst surfaces and paleosols where the displacive and replacive introduction of calcium carbonate under fresh-water influence may result in the formation of calcrete profiles (Walls *et al.*, 1975; Wright, 1982; Vail *et al.*, 1991; Wright and Smart, 1994). Although not mutually exclusive, calcrete profiles are generally attributed to semi-arid climatic conditions, whereas surface karst facies can develop under all climates (James and Choquette, 1990).

Within the studied successions, subaerially exposed surfaces are particularly discrete and in many cases could not be unequivocally determined. Diagenetic features referable to possible calcrete formation were only observed in one example (Pakipaki Limestone), but their modern origin cannot be totally excluded because of the lack of criteria to confirm that the features are fossil (Wright, 1982).

Besides, karst surface facies are poorly developed and many of the diagenetic features attributable to meteoric influence, including mouldic voids, "vadose silts" (Bathurst, 1975), ferroxide stains, and uncommon non-ferroan blocky spar cements, were also found associated with mid-sequence horizons of maximum diagenetic condensation (Cdh). Furthermore, it is becoming better appreciated that there is a wide

range of other environments where fabrics traditionally considered to be diagnostic for meteoric diagenesis can also form, including the mixing-zone and marine-burial diagenetic environments (Melim *et al.*, in press).

Therefore, subaerial unconformities were only suspected in a few cases at the top of shallowing-upwards deposits, because this is the stratigraphic position where they are most likely to form. Never does a subaerial unconformity correspond to an actual physical surface. Thus, the recognition of subaerial exposure is always indirect, yielded by diagenetic evidence recorded beneath sharp to erosional surfaces interpreted as TSEs, which are assumed to have removed the actual direct physical evidence of any subaerial exposure surfaces (Figure 9).

The general lack of evidence for the existence of subaerially exposed surfaces could be explained as follows:

(a) Although some of the sequences might have been subaerially exposed at one time, the evidence has been removed during transgression, leaving only the coarse transgressive lag facies commonly found at the base of the unconformity-bounded units (Figure 6).

(b) The uncommonness of aragonite and high-Mg calcite mineralogies (HMC) in the formations from Opoitian to Mangapanian in age (Harmsen, 1984, 1985; Hood, 1993) probably reduced the potential for karst formation and subsequent calcite precipitation (James and Choquette, 1990). Indeed, dissolution and precipitation of carbonate cements in the meteoric environment are mostly dependent upon the solubility of the dominant mineralogy of the host rock, temperature, time of residence, the degree of undersaturation with respect to calcium carbonate, and the CO_2 content of the percolating waters (Esteban and Klappa, 1983). If present, poorly cemented sediments at subaerial unconformities were prone to removal and mobilization during the emplacement of the next transgressive deposits.

(c) The lack of calcrete profiles is certainly related to the temperate maritime climatic conditions that prevailed during the formation of the Pliocene limestones in eastern North Island (Hornibrook, 1992).

(d) The rate of subsidence along the basin margin might have been high enough to outpace the rate of falling eustatic sea level (López-Blanco *et al.*, 2000; Bhattacharya and Willis, 2001).

5.3.5. Discussion: Key surfaces and Sequence Boundary

Posamentier *et al.* (1992) and others have argued that sequence boundaries should be placed at the base of the deposits that formed during sea-level falls (LST), and correspond to regressive surfaces of erosion and to the subsequent subaerial unconformities generated landward. The shallowing-upwards deposits in the Te Aute limestones differ from this model in having gradational lower contacts, and as such would correspond to the RST defined by Naish and Kamp (1997). The lack of subaerial unconformities, only found in a few examples at the top of RSTs, does not make it possible to subdivide the Pliocene successions into depositional sequences *sensu stricto* (Van Wagoner *et al.*, 1988). In contrast, our transgressive surfaces of erosion, overlain by coarse, locally pebbly and shelly lags, are frequent and easily identifiable in the field, and suggest that in many cases underlying deposits were top-truncated during transgressions.

Nummedal and Swift (1987) argued that because of its genesis as a surface of sediment transfer during retrogradational shoreface retreat, the transgressive surface of erosion is diachronous, getting younger landward. Although the TSE may form a sharp, widespread lithologic boundary in the stratigraphic record, Demarest and Kraft (1987) showed that this surface should not be regarded as a hiatus between depositional sequences when it does not coincide with the regressive surface of erosion (RSE). The sharp and erosional surfaces that we recognize in the field overlain by deepening-upwards deposits indicate that, if RSE previously developed (at the top of the RST according to Naish & Kamp, 1997), they were not preserved but instead were modified into TSE.

If these erosion surfaces were misinterpreted as TSEs and instead represent sequence boundaries (Van Wagoner *et al.*, 1990), it might imply that the observed erosion associated with coarse-grained lags reflects valley incision and consequent by-pass of skeletal sands into the basin. Besides one example (Lonely Man Section of Rotookiwa Limestone; see Figure 17), there is no evidence for significant volumes of sediments by-passed basinward along the erosion surfaces.

Previous workers have suggested that the surface underlying transgressive deposits would be the most appropriate surface to bound the sequence. Arnott (1995), Hunt and Tucker (1995), and Naish and Kamp (1997) placed sequence boundaries

Figure 9 – Erosional processes that accompany the development of discontinuity surfaces are shown with respect to their timing in the course of one relative sea-level cycle. The amplitude of processes is exaggerated considering the stratal architecture of most Pliocene sequences. However, it explains the absence of RST, FRST, and subaerial exposure surfaces on top of some observed sequences (see Figure 6). Thus, the model emphasizes that an actual physical transgressive surface of erosion has potentially recorded many metres of erosion, and overprinted previous surfaces, including subaerial exposure surfaces and regressive surfaces of erosion, and may represent significant periods of time. The vertical distribution of specific diagenetic suites within the component systems tracts indicates that diagenesis may substitute for the missing sedimentary record of time, and therefore may contain evidence of the development of systems tracts and discontinuity surfaces, especially surfaces of subaerial exposure, otherwise not preserved because sea-level fall and ensuing rise have removed them.

(1) Submarine topography and bedforms change from depositional to erosional on the flanks of the antiforms, in accordance with the lowering of sea level and subsequent lowering of the high-energy wave base (tidal- and storm-generated). A regressive surface of erosion may be generated if the regression is not normal (see text for discussion), and FRST sediments are deposited (1A to 1B). If sea level keeps falling (1C), a subaerial-exposure surface forms and meteoric water percolates within the sediment pile (see 3). As sea level rises once again, and marine waters flow, the strong tidal energy removes the subaerial exposure surface on the antiform tops, and erodes the sea-bottom on their flanks. This process creates tidal bioclastic and oyster banks (TSTs) above the ravinement surface interpreted as a TSE (1D). During sea-level highstand, the increasing water depth above the antiforms results in tidal sedimentation being weakened, especially on the flanks of the antiforms where a condensed lag forms. On the antiform tops, increasing accommodation space contributes to the aggradation of mixed carbonate-siliclastic banks, poorly developed considering the low rate of carbonate production.

(2) Time-stratigraphic diagram illustrating the effect of successive erosional processes on the preservation of previously developed systems tracts. The original time gap on the antiform tops in the upper part of the RST (2B), due to erosion by strong tidal currents, increases as sediments are being removed in accordance with the formation of ravinement surfaces during relative sea-level fall and ensuing sea-level rise. In 2B and 2C, the sedimentary time gap, represented in the diagram by the interval between the surface on top of the previous deposits and the contemporary time line, pinches out basinwards in relation to the decreasing rate of erosion down-dip of the antiform tops and the diachronous nature of the surfaces (i.e., getting younger basinwards). In these cases, the sedimentary record of time, null on the antiform tops, is contained within the deposition of FRST and LST sediments. As sea level rises (1D, 1E), a TSE forms (i.e., getting younger upwards) and overprints previous surfaces. The time gap keeps increasing, as more sediments are being removed, until enough space has been created to accommodate them.

(3) The specific diagenetic history developed within the component systems tracts of the original sequence is altered during the processes described above in being both amputated by erosion of some specific diagenetic suites (constructive diagenesis in the upper RST), and overprinted by diagenetic processes associated with subaerial exposure (meteoric both destructive and constructive diagenesis). The schematic representation of both sedimentary and diagenetic time records points to the existence of unrecorded periods of time on the antiform tops (time interval represented by sediments removed by the SB and before the meteoric overprint associated with subaerial exposure), and of time intervals being only recorded by diagenesis (meteoric diagenetic features present several metres beneath the physical subaerial surface may be preserved during ensuing transgression and demonstrate exposure, whereas the surface itself has been removed).

Genesis of sedimentary unconformities in relation to sea-level changes

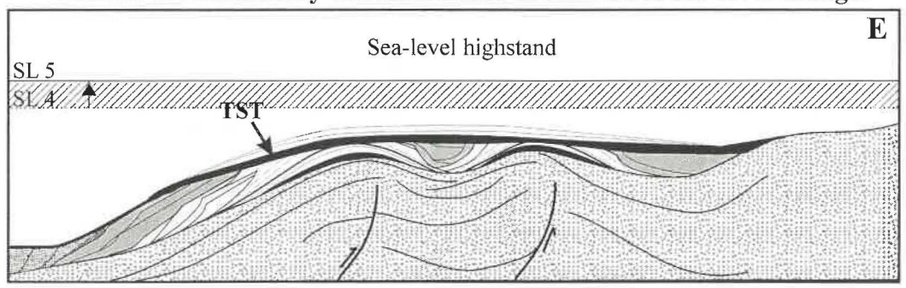

TST deposits are interpreted to form during the early and late rise of a relative sea-level cycle. During the early fall of sea level highstand sediments start to accumulate above the Cdh (capping the TST).

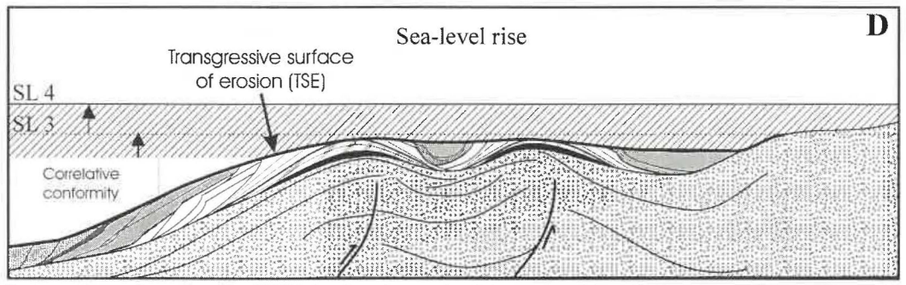

Transgressive surfaces of erosion (TSEs) develop when sea level rises and correspond to the process of erosional translation of the shoreface profile upward. This process involves an intense reworking and winnowing of pre-existing deposits by the action of wave and storm currents. Evidence of subaerial exposure may be removed during this time interval.

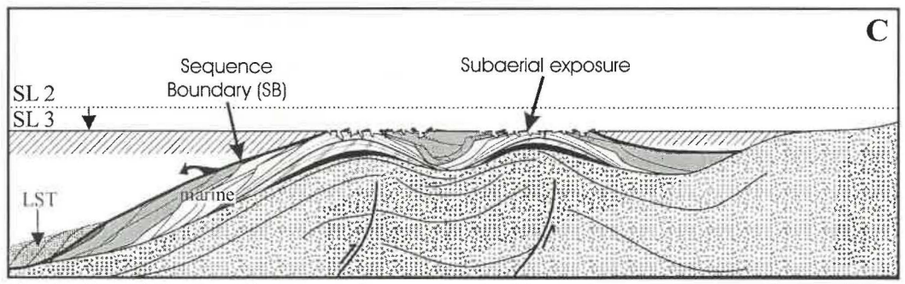

If sea level keeps falling, the antiform tops may be exposed to subaerial meteoric processes. A sequence boundary (SB) is generated, and sediments removed by wave action are transferred downslope where they accumulate in the form of a LST.

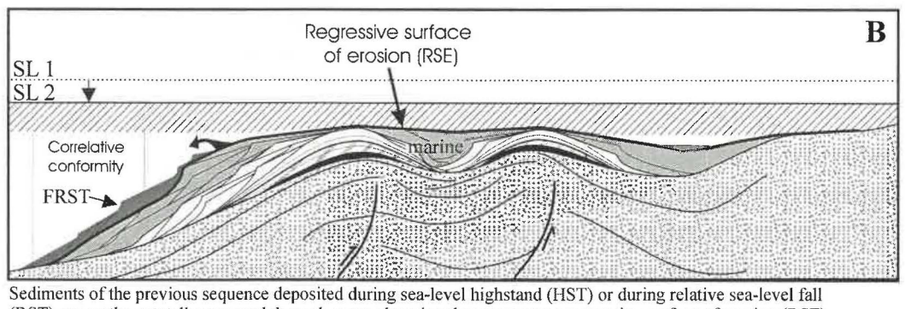

Sediments of the previous sequence deposited during sea-level highstand (HST) or during relative sea-level fall (RST) are partly or totally removed through wave planation that generates a regressive surface of erosion (RSE). Removed sediments accumulate on the flanks and at the foot of the antiforms, forming a FRST.

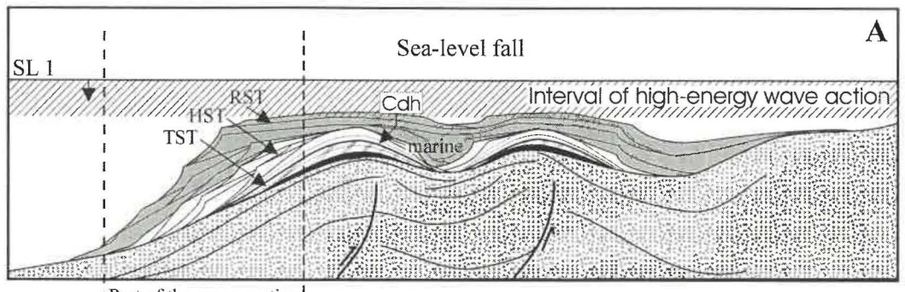

Relative sea-level fall causes fair-weather and storm wave base to be lowered
Cdh = horizon of maximum diagenetic condensation.

Time stratigraphic diagrams

Diagenetic history in the course of periods A-E

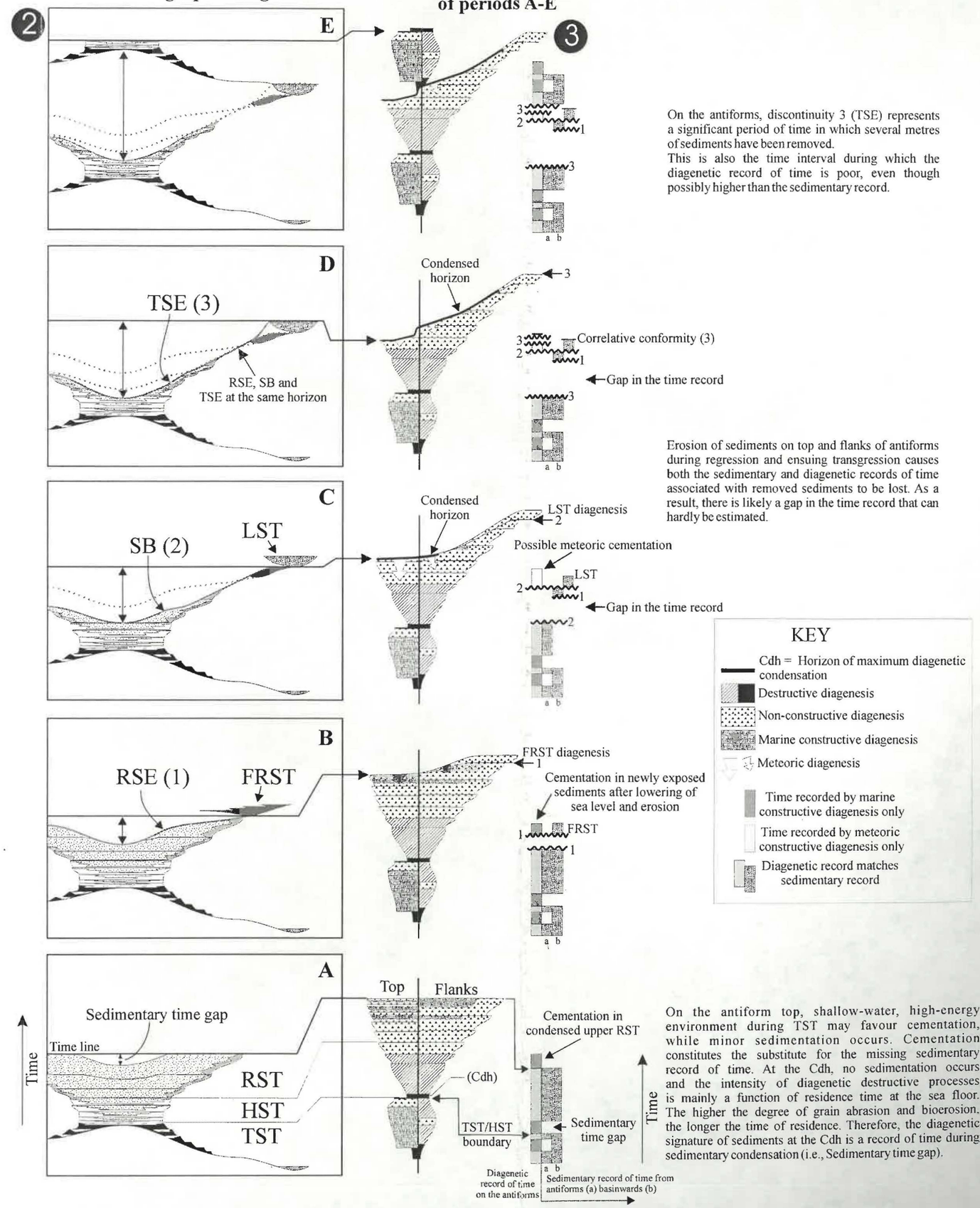

On the antiforms, discontinuity 3 (TSE) represents a significant period of time in which several metres of sediments have been removed.
This is also the time interval during which the diagenetic record of time is poor, even though possibly higher than the sedimentary record.

Erosion of sediments on top and flanks of antiforms during regression and ensuing transgression causes both the sedimentary and diagenetic records of time associated with removed sediments to be lost. As a result, there is likely a gap in the time record that can hardly be estimated.

On the antiform top, shallow-water, high-energy environment during TST may favour cementation, while minor sedimentation occurs. Cementation constitutes the substitute for the missing sedimentary record of time. At the Cdh, no sedimentation occurs and the intensity of diagenetic destructive processes is mainly a function of residence time at the sea floor. The higher the degree of grain abrasion and bioerosion, the longer the time of residence. Therefore, the diagenetic signature of sediments at the Cdh is a record of time during sedimentary condensation (i.e., Sedimentary time gap).

above regressive deposits (either forced or normal regressive systems tracts) and beneath transgressive deposits because the transgressive surface of erosion is typically extensive, readily identifiable in sections (cores or outcrops), and, by its very nature, usually preserved in the stratigraphic record (Figure 9). Walker (1995) emphasized that falling sea levels may not always be preserved in the geological record, and that instead many sequences might be bounded by unconformities developed during rising stages. Schlager (1999), with reference to Type 1 and Type 2 sequence boundaries defined by Vail *et al.* (1984), proposed to acknowledge the flooding surface between a HST and the overlying TST, without evidence of sea-level fall or lowstand deposits in between, as a third boundary considering its particular usefulness in carbonates.

The erosion/sharp surfaces interpreted to have formed by transgressive ravinement are chosen in this work to subdivide packages of sediments into sequences, and as such are inferred to be superposed on, or to have eroded through previous RSEs hierarchically not necessarily equivalent to SB *sensu* Van Wagoner *et al.* (1988). However, as previously mentioned, the Te Aute transgressive surfaces of erosion do not necessarily truncate regressive deposits. Although commonly there is an abrupt grain-size change across the TSE defined by a coarse-grained transgressive lag, TSEs do not always mark the boundary between underlying shallowing-upwards facies and overlying deepening-upwards facies (sequences 1-4 in Figure 6). Consequently the enclosed sequences are not strictly similar to the transgressive-regressive sequence of Embry (1995), as he also used transgressive ravinement surfaces as the main bounding discontinuity to define depositional units. In the cases that the TSE has eroded through a RST with preserved evidence of subaerial exposure, it then coincides with a sequence boundary (Van Wagoner *et al.*, 1988, 1990).

5.4. Systems tracts: TST, HST, RST, FRST, LST

The subdivision of the sequences into systems tracts is based on their internal stratal geometry and the interpretation of the stacking of depositional facies between key surfaces, which in most cases arose from condensation (TSE and Cdh). Characteristics of the fundamental building blocks given below for the barnacle-rich Te Aute limestones, and some aragonitic Nukumaruan limestones, are introductory and general. One must keep in mind that there are variations in the thickness and detailed facies characteristics of the component systems tracts (Figure 5) within contemporary formations, and

between formations of different ages that reflect the evolution of the forearc basin over time. Separate descriptions for each limestone formation given in Section 7 emphasize these differences.

5.4.1. Transgressive systems tracts (TST)

The transgressive part of the sequences corresponds to the deposits located above the transgressive surface of erosion and below the Cdh (Figure 9). That is, TST deposits are interpreted to form during the early to late rise of a relative sea-level cycle (Van Wagoner *et al.*, 1988; Vail *et al.*, 1991).

The lower segment of the TST overlying the TSE, coinciding or not with a sequence boundary, is characterized by either skeletal rudstones of facies B1a and B1c (intertidal-upper shoreface; B1b and B1d more rarely occur), or coarse trough and tangential cross-bedded skeletal grainstones of facies B2a and B2b (tidal-subtidal, shoreface; see Chapter 1, Table 1). Coarse transgressive lags are the product of the reworking of shoreface material bypassed along the ravinement surface and redeposited farther seaward upon the latter. However, sedimentary structures, near *in situ* shells in places, well-preserved encrusting bryozoans and constructive diagenesis (CD^1 and CD^2; Figures 4A, 4B) associated with B1-type facies collectively suggest transportation over short distances and redeposition in high-energy settings. Transgressive lags are 0.2 m up to 5 m thick. When absent, they are replaced by skeletal grainstones up to several metres thick underlain by a burrowed TSE (Figures 7E-G).

Typically, basal coarse transgressive deposits show a deepening-upwards trend passing either gradationally or sharply to mixed facies (M1 to M3; shoreface to mid-shelf) or siliciclastic facies (S1 to S3; mid- to outer-shelf), in turn capped by a condensed horizon (Cdh) interpreted to be located in the vicinity of the Mfs (Figures 6, 10).

Conspicuous features recognized in the depositional model described above are (1) a change in the depositional environment across its basal discontinuity surface, revealed by the direct superposition of contrasting microfacies; and (2) contrasting pre-compaction diagenetic scenarios above and below the lower boundary.

Terrigenous-dominated microfacies assemblages, Detrital and Bimol, commonly form the basal fossiliferous and pebbly rudstones (B1-type facies), while Bryotal, Bimol, and Barbital sediments form B2-type facies and overlying mixed facies (M-type facies)

grading in turn into siltstones below the Cdh (Figure 10). Diagenesis is characterized by an upwards constructive to destructive tendency, culminating within the Cdh.

5.4.2. Highstand systems tracts (HST)

Typically, HSTs comprise in ascending stratigraphic order aggradational siltstones (S2; mid- to outer-shelf), fine-grained, well sorted calcareous sandstones (S1; mid-shelf), terrigenous packstones (B3a; inner- to mid-shelf), and thin interbeds of storm-emplaced skeletal lags (M2 and M3 facies). These deposits represent the late rise, stillstand, and possibly early fall of a relative sea-level cycle. HSTs are bounded below by a thin condensed horizon corresponding to the Cdh and grade conformably into the overlying RST. Their upper boundary is therefore difficult to recognize and is referred to here as a fuzzy boundary within which the transition between HST and RST occurs at some indeterminate level (Figure 10). Commonly the upper boundary lies at the turnaround from S3-M3 (outer-, mid-shelf) facies to M2-M1 (inner-shelf, lower shoreface) facies, indicative of an increasing influence of storm and tidal currents in the early part of the regressive regime delivering coarser sediments and depositing thicker skeletal beds.

Destructive features dominate the diagenetic signature of HSTs. Nevertheless, by contrast with the underlying Cdh, the amount of authigenic minerals decreases as well as the degree of infestation of skeletal grains by microborers. This suggests that bioclasts were becoming more rapidly buried (Kidwell, 1991a), due to increasing sedimentation rate.

Again, terrigenous microfacies assemblages dominate HSTs. Characteristically, Detrital microfacies grade into Bimol and then in turn into Barbital microfacies (Figure 10).

5.4.3. Regressive systems tracts (RST)

The term RST (Naish and Kamp, 1997) is applied to strata that are thought to originate during the falling limb of a relative cycle of sea-level change, but are not assigned to forced regressive systems tracts (FRST). Thus, the lower gradational contact and the capping unconformity (TSE or SB) of the regressive (shallowing-upwards) part of the sequences distinguishes it from the sharp bases of FRSTs, and suggest that it represents sediments formed during normal regression (Posamentier *et al.*, 1992). However, in the

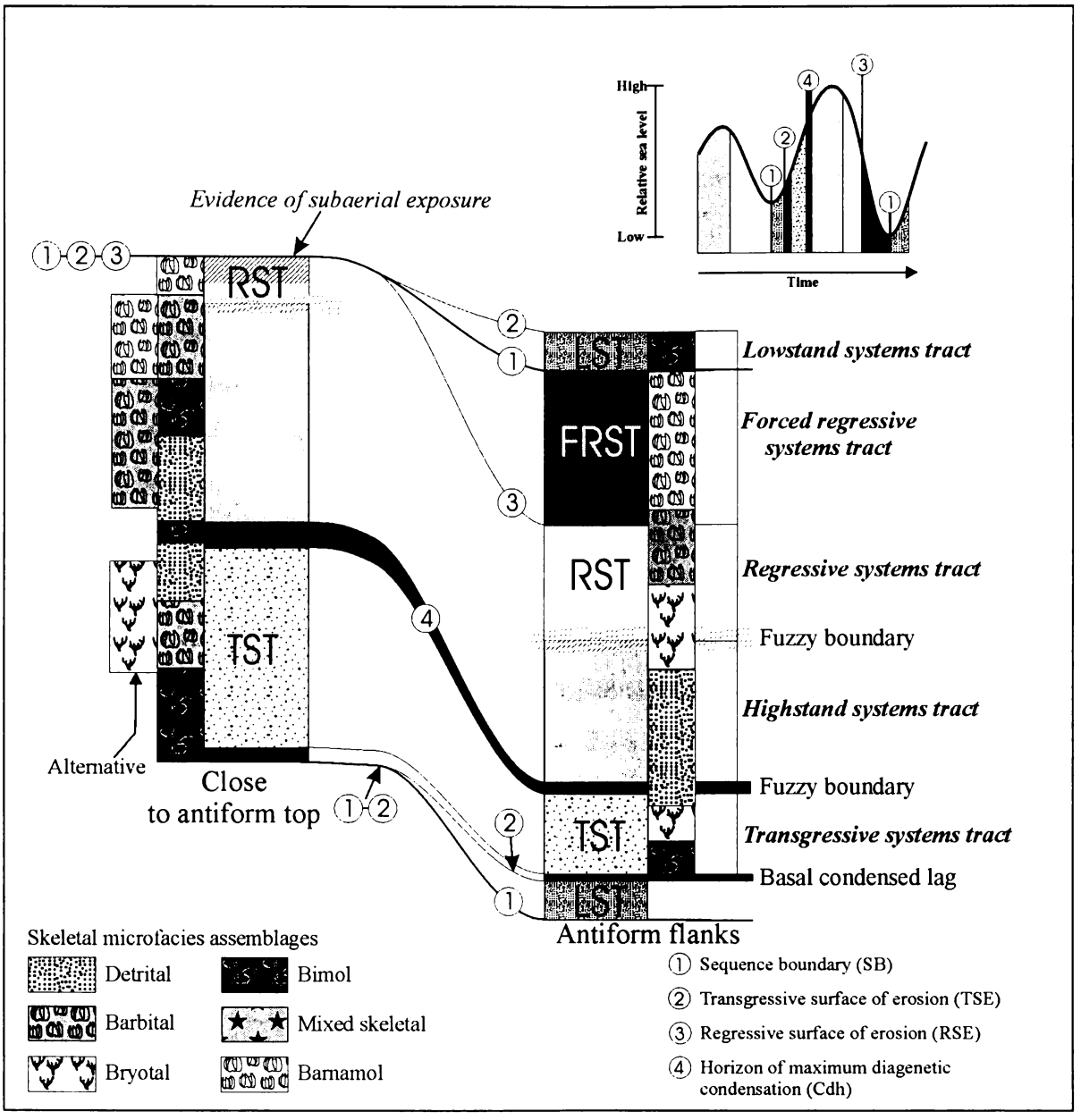

Figure 10- Stratigraphic architecture produced by hypothetical relative fluctuations in sea level, showing the vertical stacking of systems tracts and microfacies assemblages as observed in the Pliocene carbonate sequences of southern Hawke's Bay. The stratal succession shown on the antiform flanks is thought to develop during conditions of rapid sea-level fall, which favour the formation of a RST and late FRST/LST bounded below by a sequence boundary correlated upwards on the antiform tops to a subaerial exposure surface. The stratigraphic architecture showing a FRST sitting sharply on shallowing-upwards deposits interpreted as HST/RST has been observed at Mt Kahuranaki within the Kairakau Limestone (Figure 8C). LSTs are generally absent in the studied successions. Most Pliocene sequences comprise a basal TST passing upwards across a fuzzy boundary (Cdh) into a HST, in turn overlain by a RST bounded above by a TSE, rarely superposed on a subaerial exposure surface. (Relative sea-level curve modified from Naish and Kamp, 1997).

absence of isotope data to be tied to specific sectors of an oxygen isotope-derived sea-level curve, the Te Aute RSTs cannot unequivocally be shown to have formed during a period of continuously falling sea level. Consequently, the regressive part of the Pliocene sequences is at least equivalent to the regressive systems tracts of Embry and Johannessen (1992).

RSTs generally consist of basal mixed facies (M2, M1) grading vertically into skeletal grainstones (B2a and B2b). The transition between the highstand and the regressive systems tracts occurs across a fuzzy boundary above which coarsening- and thickening-upwards trends record the progressive vertical shallowing of the depositional environment (Figure 10).

Barbital and Barnamol microfacies assemblages dominate in the upper part of the RST, occasionally capped by a subaerial unconformity, but in most cases capped by the TSE of the next sequence that truncated the RST cap. Thick marine cements (up to 200 μm) and associated internal sediments characterize the diagenetic history in the upper part of the RST (marine constructive diagenesis; Figure 6).

5.4.4. Forced regressive systems tract (FRST)

The general texture of the FRST deposits is generally analogous to the regressive systems tracts. However, FRSTs are distinguished from RSTs exclusively on the stratigraphic criteria that FRSTs contain a basal regressive surface of erosion (Hunt and Tucker, 1995), while RSTs exhibit a conformable base (Naish and Kamp, 1997). The stratigraphic position of FRSTs is similar to that of RSTs, but differs in that FRSTs may overlie RSTs (Figures 8C, 10).

FRST deposits consist of rapidly shoaling-upwards successions from coarse mixed facies (M1) to shallow-water skeletal facies (B2a, b) that accumulated under the influence of strong subtidal and tidal currents. FRSTs include marine constructive diagenetic suites.

5.4.5. Lowstand systems tract (LST)

Theoretically, lowstand systems tracts comprise sediments deposited at and around the falling and lowstand segments of a eustatic cycle (Van Wagoner *et al.*, 1988). The lower boundary of the LST is, up-dip of the area where LST sediments accumulated (i.e., located landward of the lowstand shoreline), a subaerial-exposure surface. LST deposits

are particularly uncommon in the studied successions, unless they were not recognized due to the poor traceability of subaerial unconformities.

The abrupt superposition of marine fan-delta conglomerates upon inner-shelf sandstones, and the occurrence of fluvial deposits above, are considered diagnostic features to assign these conglomerates to LST deposits (exemplified by the Hassal Conglomerate on top of the Te Waka Formation; see Chapter 1, Section 4.10).

5.4.6. Microfacies stacking within the fundamental sequence

Although the different components of Barbital/Barnamol, Bimol, and Bryotal microfacies assemblages have wide depths and environmental tolerances, we follow here the general environmental interpretations provided by Beu *et al.* (1980, Barnamol), Nelson *et al.* (1988b, Bryomol), Kamp *et al.* (1988, Barnamol), Gillespie (1992, Bimol), Boreen *et al.* (1993, Bryomol), and Hayton *et al.* (1995, all associations). The depositional model developed by Hayton *et al.* (1995) is regarded as a basis to assist paleoenvironmental interpretations of possible interrelationships between microfacies assemblages.

The general vertical trend, Detrital/Bimol in B1-type facies and Barbital/Bryotal in B2-type facies of the TST, Detrital/Bimol/Barbital in the HST, and Barbital to Barnamol in the RST (Figure 10), is inferred to be related to evolving environmental conditions on the paleoshelf that progressively promoted barnacles. That is, increasing current velocity and terrigenous sediment by-passing recorded by the RST favoured barnacle-dominated carbonate factories over Bimol and Bryotal microfacies. Bryotal and Barbital microfacies occurrences in the lower part of TST (B2-type facies) reflect the prevailing high-energy conditions during transgression that probably suppressed the terrigenous input upon and about shoal areas.

5.5. Diagenetic and facies motifs in sedimentary sequences

Vertical changes in thickness and depositional facies through the fundamental building blocks recognized in many stratigraphic sections of the studied successions, in association with changes in the type and degree of diagenesis that outline vertical patterns of pre-compaction diagenetic sequences, and fundamentally the position of bounding discontinuities, define four sedimentary motifs referred to as Motif 1 to 4, and depicted in Figure 11.

All sedimentary motifs are bounded by transgressive surfaces of erosion (TSE) that may locally coincide with major sequence boundaries (SB; i.e., subaerially exposed unconformities). The lower TSE lies at the base of the depositional sequence and is either overlain by condensed fossiliferous to pebbly transgressive lags of facies B1a and B1c, or condensed transgressive coarse-grained skeletal deposits of facies B2a and B2b. The upper contact generally also bears signs of marine ravinement produced during transgression (TSE), including a sharp or eroded surface, *Ophiomorpha* and/or *Skolithos* burrows, and is overlain by the basal transgressive lag of the next sequence.

5.5.1. Motif 1

Sedimentary Motif 1 exhibits a deepening-upwards depositional trend from the basal shallow-water (intertidal to shoreface) transgressive lag to near storm-wave base mixed siliciclastic-carbonate sediments of M- to S-type facies (Figure 11A). Typically, the specific diagenetic attributes of Motif 1 record a vertical trend from constructive to increasingly destructive diagenesis (CD^{1-4} to DD^{2-3}; see Figures 5, 6, 11) towards the superjacent TSE. Sedimentary Motif 1 is interpreted to represent a transgressive systems tract, which is not bounded above by the mid-sequence horizon of maximum diagenetic condensation (Cdh), but instead is truncated by the next TSE.

5.5.2. Motif 2

By contrast with Motif 1, the upper bounding discontinuity of Sedimentary Motif 2 lies above the Cdh, and within or at the top of the overlying HST recognized through the attributes given above (Section 5.4). Motif 2 exhibits a predominantly constructive to destructive diagenetic vertical trend (Figure 11B). Destructive diagenesis does not culminate immediately beneath the superjacent TSE but within the Cdh marking the Mfs (specific diagenesis DD^{1}; Figure 4F).

5.5.3. Motif 3

The upper part of Motif 3 exhibits a shallowing-upwards trend (coarsening- and thickening-upwards deposits), which corresponds to sediments emplaced during normal regression (RST) (Figure 11C). The RST deposits in Motif 3 are bounded below by a gradational contact, and above by a TSE not superposed to a subaerial unconformity. RSTs correspond to the time interval during which the destructive-to-constructive

turnaround of the diagenetic regime occurs. Upward-coarsening of bioclasts, the lesser degree of microborer infestation, poorly mature authigenic glauconite (pale yellow to pale green), and fringes of intrinsic turbid cements are collectively indicative of increasing constructive processes compared to the underlying HST.

5.5.4. Motif 4

Motif 4 indicates a deepening- (TST) then shallowing-upwards depositional trend (HST to RST) (Figure 11D). Intertidal to upper shoreface coarse skeletal sediments of facies B2a and B2b form the upper part of the RST, and immediately at and beneath the capping surface record discrete evidence of subaerial exposure (dissolution, desiccation cracks, brecciation, and little, if any, meteoric cementation). Therefore, the discontinuity bounding the top of Motif 4 coincides with a major sequence boundary (SB). Characteristically, the upper part of the RSTs comprises fabrics related to sea-floor constructive diagenesis, including thick isopachous turbid cements and micritic cements (CD^1 and CD^4 specific diagenetic suites; Figure 4A, 4C), and micro-karst features interpreted to represent synsedimentary meteoric influence (M^{1-3} specific diagenetic suites; Figure 4D, 4E).

6. Hypothetical framework to account for the stacking of the Pliocene sequences

6.1. Multiple working hypotheses

From one sequence to another, both vertically and laterally, there are variations in the degree of diagenesis, and the thicknesses and facies characteristics of the component systems tracts. Changes in accommodation and sediment supply of differing amplitude and duration are critical factors controlling the style of depositional facies stacking, the genesis of key surfaces, stratal geometries, and at a higher hierarchical level the piling-up of sequences (Van Wagoner *et al.*, 1988; Vail *et al.*, 1991).

Factors governing changes in accommodation fall into three categories, glacio-eustatic, tectonic, and internal, while sediment supply typically is mainly governed by the climate and the tectono-geomorphic evolution of the forearc basin (see Section 2).

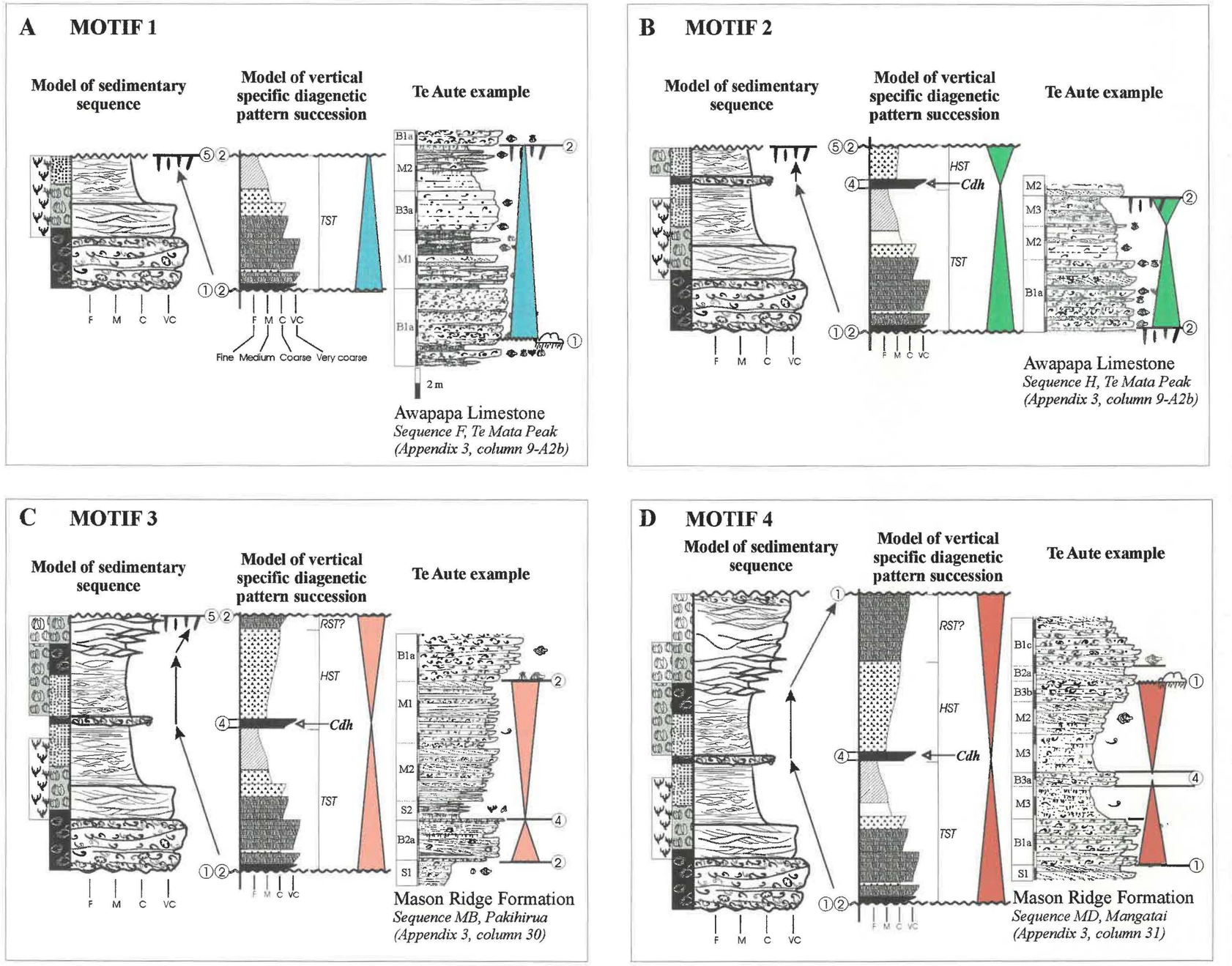

Figure 11- Sedimentary sequence Motifs 1-4 are defined on the basis of the vertical facies and specific diagenetic successions developed within the component systems tracts, and the nature of the bounding discontinuities. See text for details. Facies codes are defined in Table 1 in Chapter 1 (also contained inside the map pocket in the back cover of the thesis).

6.2. Tectonic forcing

Tectonic subsidence or uplift of structural basement blocks driven by faulting is a plausible mechanism for the creation of accommodation space and the generation of facies architectures recording shallowing- or deepening-upwards trends (Goldhammer *et al.*, 1994; López-Blanco *et al.*, 2000). The depositional trend mainly depends upon competing rates of sedimentation and tectonic forcing mechanisms. Step-wise, episodic subsidence, and alternate uplift and depression (yo-yo tectonics) driven by repeated tectonic pulses, have been proposed to induce the superposition of metre-scale sedimentary cycles in thick carbonate sequences (Hardie *et al.*, 1991).

Recent manifestations of co-seismic subsidence and uplift over variable areas associated with large earthquakes, such as the 1931 earthquake in Napier, suggest that similar tectonic movements have certainly occurred during Plio-Pleistocene times in Hawke's Bay situated at the convergent margin of the Pacific Plate (Kamp and Nelson, 1987). Portions of the Tangoio Block (Figure 1) experienced a vertical movement (uplift) that ranges from 0.5 m up to 2.5 m (Ishibashi, 1987), while in central Hawke's Bay neither uplift nor downwarping occurred. This suggests that earth movements are unlikely to have been uniform across the forearc basin during Pliocene times. Therefore, tectonism may be envisaged as a possible factor for the generation of local differences in the number of sequences and thicknesses in the Pliocene limestones (especially the eastern barnacle-rich occurrences), but this style of deformation can hardly generate large-scale cyclicity as observed in the Nukumaruan deposits of the Mason Ridge Formation and in the Tangoio Block (Haywick, 1990).

Furthermore, documented examples and data regarding amplitude of vertical movements and recurrence frequencies of such tectonic mechanisms are sparse, and generally refer to frequencies of 100 ka or more (Hardie *et al.*, 1991; Dickinson *et al.*, 1994).

6.3. Internal processes

The creation of accommodation space through the compaction of peat layers in clastic portions of cyclothems has been envisaged by Van Der Heide (1950) as a mechanism inducing repeated transgressions and cyclic deposition. Ginsburg (1971) proposed an autocyclic-driven model that accounts for metre-scale shallowing-upwards cycles, coupling continuous carbonate sedimentation and progradation of tidal flat complexes

across gently sloping carbonate platforms under conditions of constant subsidence and stationary sea level.

The geometry of the carbonate depositional systems envisaged for the eastern Te Aute limestone occurrences in southern Hawke's Bay is not one of a low dipping carbonate platform, regarded as a key parameter in Ginsburg's model formulation, but instead is one of an archipelago of submarine highs and possibly islands (Kamp *et al.*, 1988). By contrast with carbonate platforms where minor relative sea-level changes may expose or drown large areas, isolated submarine highs generate uneven sea floor topographies where evidence of any relative sea-level variations may only be recorded in quite restricted portions of the carbonate realm. Elsewhere, such evidence, and principally the genesis of key surfaces, may be more subtle or missing.

There is a lack of data regarding recurrent internal processes in the Pliocene successions that could account for the creation of accommodation space and the stacking of sequences. However, to take an example, stacked slumped deposits bounded by burrowed surfaces have been observed in the Kairakau and Awapapa Limestones. Besides tectonic pulses, such stacking could internally be controlled if a threshold stress is achieved to induce slope rupturing about the flanks of carbonate factories where sediments accumulate and are not stabilized by early cementation. In conditions of continuous carbonate production, the accommodation space created by avalanche would then be filled with sediments until the next threshold stress is achieved, leading to stacked avalanche deposits basinward (see Chapter, Figure 29).

6.4. Glacio-eustatic forcing

The Milankovitch theory has received increasing attention in New Zealand since high-frequency (5th- to 6th-order) cyclothemic architectures have been recognized in many Late Pliocene to Pleistocene deposits (Haywick, 1992, 2000; Abbott and Carter, 1994; Beu, 1995; Naish and Kamp, 1997), and high-resolution sea-level curves have become available in the form of oxygen isotope records for the corresponding time-period (e.g., Shackleton *et al.*, 1990; Chen *et al.*, 1995). Naish and Kamp (1995, 1997) successfully correlated 6th order (41 ka) cyclothems with the sea-level curve during isotope stages 100-58, and showed that their component systems tracts could be tied with specific parts of sea-level cycles. Lower in the hierarchy of high-frequency cycle periods, 4th-order (0.1-1.0 Ma) cycles of limestone accumulation in Hawke's Bay were tentatively

correlated with deep-sea oxygen isotope stratigraphies by Kamp *et al.* (1988), Kamp and Nelson (1988), and Beu (1995). Limestones were subsequently interpreted to have accumulated during segments of the longer-wavelength eustatic curve corresponding to regressive periods (pre-Nukumaruan limestones) or transgressive periods and high-stands periods (Nukumaruan aragonitic shell beds; e.g., Beu, 1995).

This study shows that the Pliocene limestones result from the stacking of metre-scale (1-15 m thick) sequences (from 3 up to 12 fundamental building-blocks) with recurring internal facies architectures and specific diagenetic patterns, suggesting that a high-frequency sea-level control (6th- to possibly 7th-order) should also be suspected during deposition of the Pliocene successions. However, there is strong evidence, including lateral variations in the thickness and number of cycles within the same formation, amalgamated sequences, key surfaces being laterally poorly traceable, and different degrees of diagenesis in laterally correlated sequences, to indicate that tectonic, glacio-eustatic, and at a lesser degree internal mechanisms may have operated in concert to build up the carbonate successions.

7. Sequences in the eastern limestone occurrences from late Opoitian to early Nukumaruan

In the following sections, references are made to outcrops and stratigraphic columns which are presented in Appendices 1 and 3, and were introduced in the field descriptions in Chapter 1.

7.1. Kairakau Limestone (late Opoitian)

7.1.1. Introduction

Kairakau Limestone is mainly characterized by mixed facies, transitional between barnacle-rich grainstone and terrigenous packstone, often bioturbated. The limestone occurs on both sides of the Elsthorpe Valley, at the western edge of the Maraetotara Plateau and within sea cliffs from south of Kairakau Beach northwards to Waimarama (Figure 1).

At Kairakau Beach, Kairakau Limestone unconformably overlies blue-grey siltstones of Miocene age. At Waimarama, Kairakau Limestone unconformably overlies undifferentiated pale green sandstones, which could be Opoitian in age (Beu, 1995).

Close to the Waimarama outcrop, the lower part of Kairakau Limestone (grainy terrigenous/skeletal packstone/grainstone with numerous mud clasts and mud pebbles towards the base) has recently been exposed in road cuttings along Waimarama Road (V21/464618). It rests unconformably on a thin glauconitic sandstone and in turn on a blue-grey siltstone/mudstone of Waiauan age (D. Francis, pers. comm., 2000). At Pukekura, both a lower limestone sheet, inferred to be Kairakau Limestone, and an upper one, the Tuki Bell limestone, unconformably overlie pale green-yellow sandstones.

At all other localities visited, the basal boundary of Kairakau Limestone is not exposed, though Harmsen (1984) mentioned a disconformity at the base of the Mt Kahuranaki section (her Morea section).

Vertical and lateral distributions of microfacies assemblages indicate a partition between southeast-central and northwest-southwest limestone occurrences (Figure 12). The latter are characterized by Detrital and to a lesser degree mixed Bryozoan-Barbital microfacies, whereas the former record two periods of skeletal-dominated carbonate deposition (mixed Barbital-Bimol) separated by one period of terrigenous sedimentation. This microfacies distribution suggests that the more western Kairakau carbonates were deposited in more distal environments compared to their eastern counterparts, which probably accumulated closer to the carbonate factories in higher-energy environments.

7.1.2. Description of the main subdivisions and their bounding surfaces

From the base of Kairakau Limestone to the top of Tuki Bell limestone, five fundamental building sequences and six discontinuities have been identified in the study area (Figure 13). These fundamental sequences are labelled A, B, C, D, and E, and the bounding discontinuities numbered from 1 to 6, from the oldest to the youngest. At Waimarama, the lower sandstone unconformably overlain by Kairakau Limestone may represent part of a previous Opoitian sequence, but there is presently no biostratigraphic data to assess this assumption. Nonetheless, the sandstone is referred to as sequence Z and temporarily attributed to the Opoitian.

Sequence A corresponds to a Motif 3 at Kairakau Beach where it reaches a thickness of 16 m (Figure 13). At this locality and further north at Taupata (see Appendix 1, column 3), a pebbly transgressive lag forms the base of the sequence. At

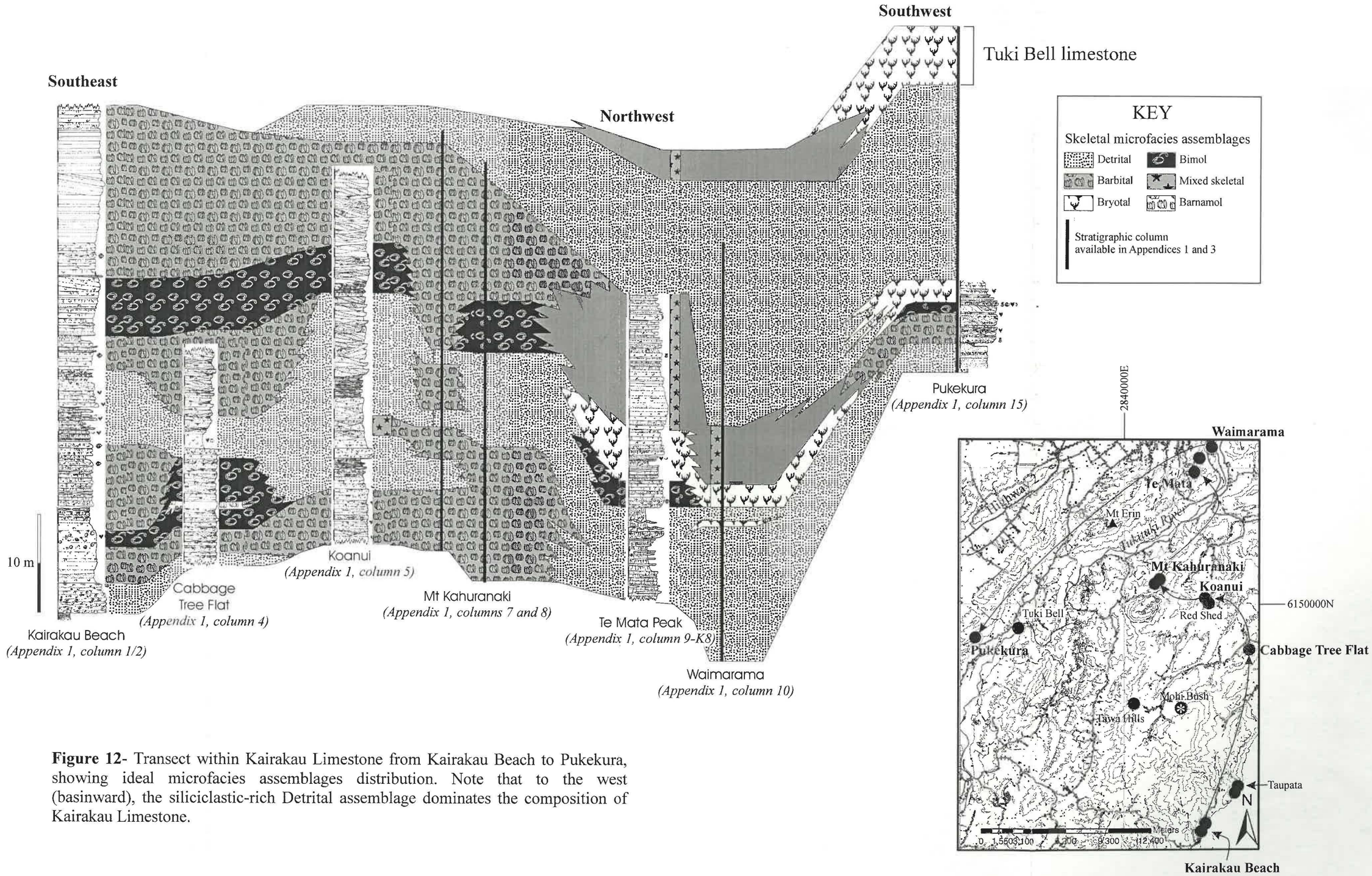

Figure 12- Transect within Kairakau Limestone from Kairakau Beach to Pukekura, showing ideal microfacies assemblages distribution. Note that to the west (basinward), the siliciclastic-rich Detrital assemblage dominates the composition of Kairakau Limestone.

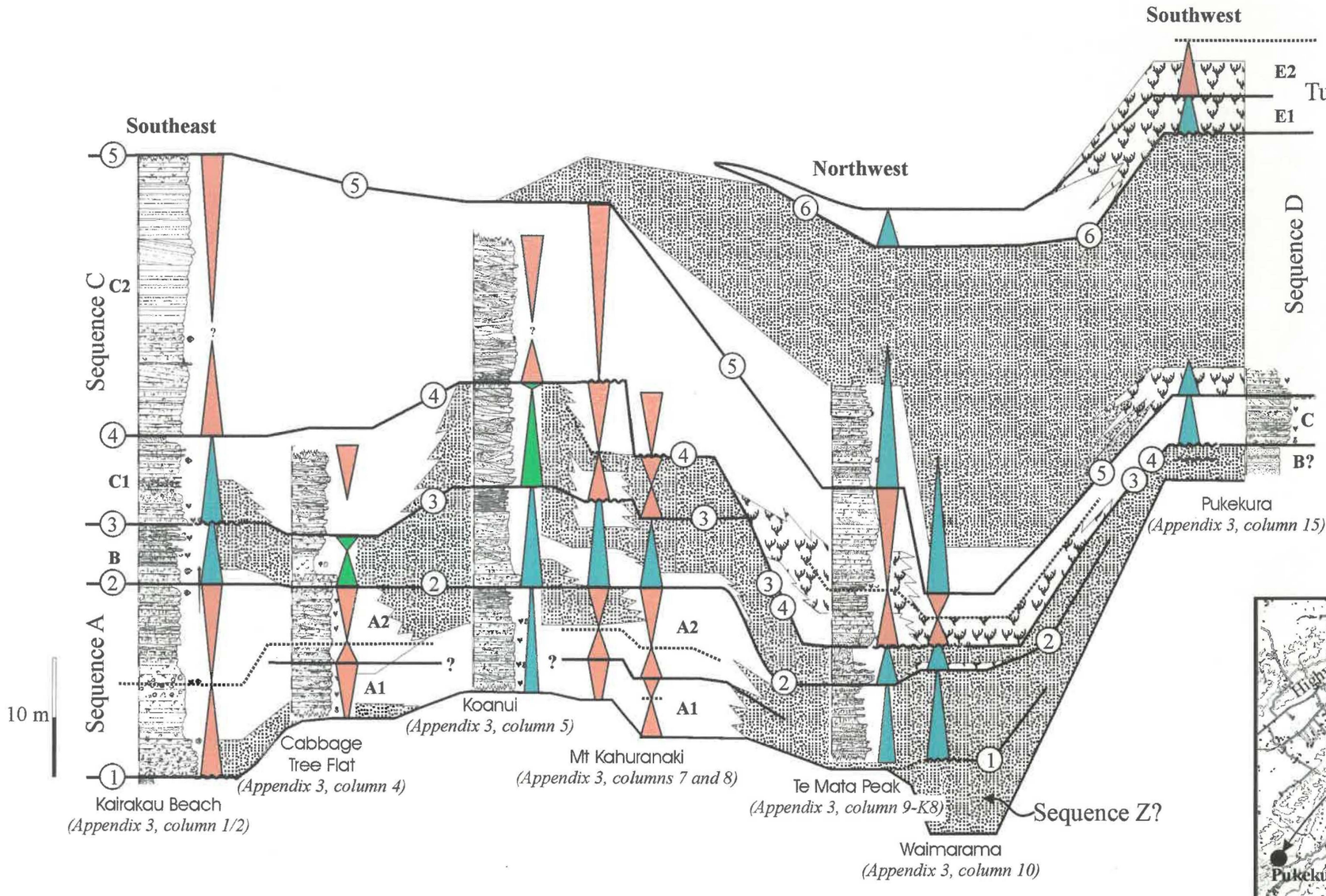

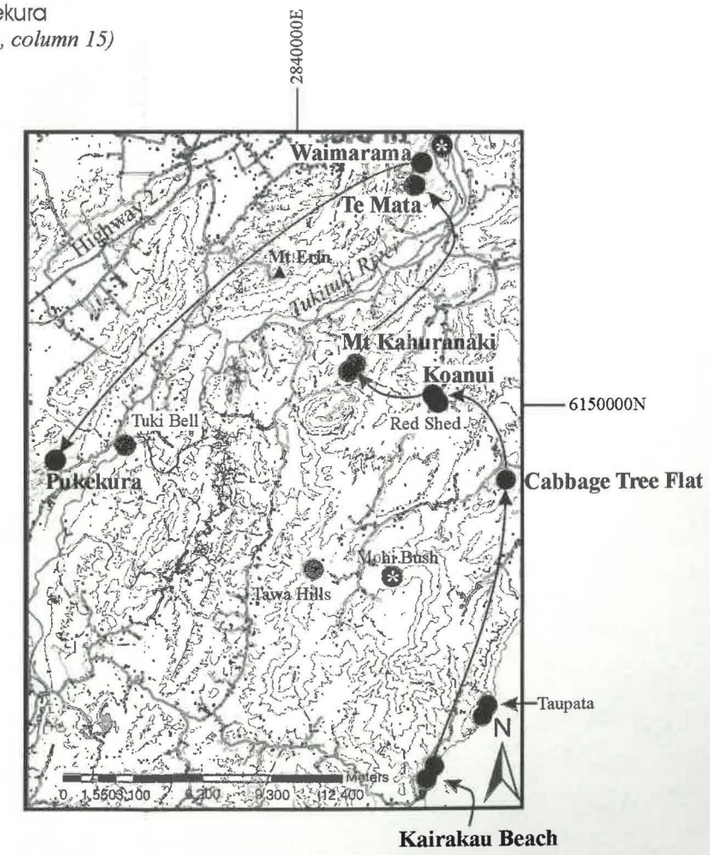

Figure 13- Correlation panel of eight stratigraphic columns within Kairakau Limestone, and including Tuki Bell limestone (at Te Mata Peak and Pukekura sections), from Kairakau Beach to Pukekura, showing the stacking of sedimentary sequences (corresponding Motifs 1-4 as defined in Figure 11; see text and Appendix 3, columns 1-10 and 15 for details) and discontinuity surfaces bounding them (labelled 1 to 6). See text for discussion.

Cabbage Tree Flat and in the Mt Kahuranaki area, sequence A (11 m and 14 m exposed, respectively) is subdivided into two Motifs 3, termed A1 and A2, separated by a sharp contact overlain by a thin shelly lag. Sequence A records the first stage of extensive carbonate production, represented by Barbital and Bimol microfacies, within the studied interval and the first major cut-off in the terrigenous input at these localities. Deepening-upwards Motif 1 (see Figure 11) characterized by high siliciclastic contents (Detrital and Barbital) builds up sequence A at Koanui and in the Te Mata Peak area (Figure 13). The lower boundary when exposed is erosional. Lower pale green-yellow sandstones at Pukekura are inferred to be, at least partly, lateral equivalents to sequence A.

At most localities, sequence B is a deepening-upwards Motif 1 bounded below by a sharp contact, and ranges from 3-8 m in thickness, thinning westwards. A 1 m-thick skeletal-rich rudstone (marker shell bed above surface 2; Figure 13) forms the base of the sequence, and passes upwards gradationally or across a sharp surface into fine-grained calcareous sandstones. At Pukekura, a 0.2 m-thick mud pebble (up to 5 cm across) lag is inferred to represent the lower boundary of sequence B characterized by pale green sandstones overlain by blue-grey mudstones. Detrital microfacies dominate throughout the study area, though locally Barbital and Bryotal microfacies constitute the lower part of sequence B.

Sequence C is the second and thickest stage (4-28 m thick) of carbonate production within the succession, and is represented by a skeletal-dominated unit over the entire area, lying on a sharp to erosional surface cutting through sequence B. Sequence C is overall a deepening- then shallowing-upwards sequence, comprising at Kairakau Beach, Mt Kahuranaki, and Koanui two sub-sequences, C1 and C2, deepening- and deepening- then shallowing-upwards, respectively. In the Mt Kahuranaki area, sequence B is bounded above by TSE 3, upon which the overlying shallowing-upwards sequence C1 onlaps (Figure 8C). Tabular bed sets of the sequence C2 rest on an erosional surface (surface 4), which truncates the underlying unit. Above the surface sediments rapidly coarsen upward and include thick sea-floor cements. This carbonate facies is considered a FRST and the surface on which it lies a RSE based on the occurrence of meteoric cements overgrowing the previous marine diagenetic suite, which suggests that the superjacent surface (surface 5) atop the FRST has been subaerially exposed (see below). The hypothesis of the RSE being in fact a TSE cannot

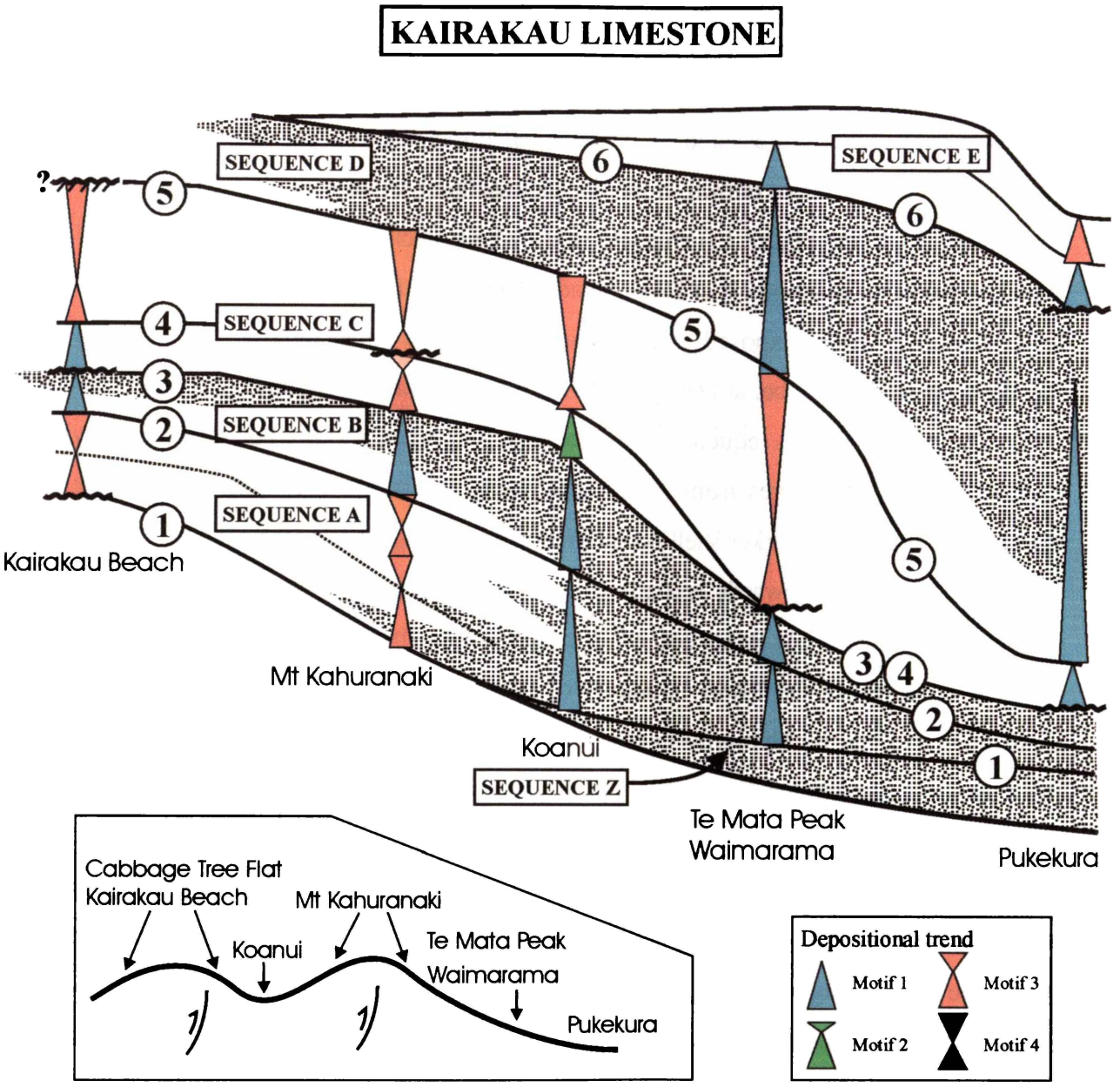

Figure 14- Summary of bounding surfaces (1 to 6) and vertical succession of sedimentary sequences (as shown in Figure 13 and detailed in Appendix 3, columns 1-10 and 15) in the Kairakau Limestone, showing in the inset possible location of deposition upon antiforms for each section (see Figure 13 for location of sections in the study area). Kairakau Limestone records two periods of carbonate production (between surfaces 1 and 2, and 3 and 5, respectively) separated by one period of partial suppression of carbonate sedimentation (dominated by siliciclastics; between surfaces 2 and 3). Surfaces 1, 2, 3, 5, and 6 are interpreted as TSEs coincident or not with a SB, while surface 4 is assigned to a RSE. See text for discussion.

be totally ruled out because the subaerial-exposure surface has not been physically recognized. At Pukekura, sequence C consists of a 4 m-thick Sedimentary Motif 1. Barbital microfacies dominate in the upper part of sequence C together with marine constructive diagenetic features, including turbid cements. Pre-compaction, non-ferroan, non-luminescent, clear spar cements (scalenohedral and blocky) are found coating biomouldic cavities and overgrowing upon previous turbid cements throughout the vertical sections of Kairakau Limestone at Kairakau Beach, Cabbage Tree Flat, and Mt Kahuranaki, and are interpreted to be meteoric in origin. If so, meteoric cements might have formed from meteoric waters that percolated from a subaerially exposed surface somewhere above sequence C that would then correspond to an overall Motif 4. At Koanui and in the Te Mata Peak area, such meteoric cements are absent, and sequence C is inferred to define a Motif 3.

To the north- and southwest, sequence D sharply overlies surface 5, and comprises mixed carbonate-siliciclastic deposits grading into calcareous sandstones referred to as Mokopeka Sandstone by Harmsen (1985). Sequence D represents a Motif 1 or Motif 2 and corresponds to the termination of Kairakau Limestone carbonate factories.

Only present in the Te Mata Peak area and at Pukekura, sequence E, subdivided into two sub-sequences, E1 and E2 (corresponding to Motifs 1 and 2, respectively), is bounded below by a sharp to erosional surface (TSE 6) and corresponds to the informal Tuki Bell bryozoan limestone (up to 6 m thick).

7.1.3. Carbonate production development within a sequence stratigraphic framework

The stacking pattern of fundamental sequences records fluctuations in the development of carbonate production that comprise three periods of carbonate accumulation (i.e., sequences A, C, and E) and two periods of terrigenous input (i.e., sequences B and D), which partly or totally suppressed the former (Figure 14). Conditions of intermittent sea-level rise during the overall long-term regressive trend that brought the sea floor into high-energy settings, are indicated in the deeper terrigenous-dominated environments in mid- to outer-shelf position represented by the Te Mata Peak area (Figures 13, 14; see Appendix 3, columns 9 and 10).

Lateral variations in the attributes of sequence A indicate the existence of simultaneous transgressive (Motif 1) and transgressive-regressive (Motif 3) deposits, the latter being locally decomposed into transgressive-regressive sub-sequences. Such lateral changes are interpreted to correspond to different depositional settings under variable influence (sediment supply) of newly developed carbonate factories.

Early relative sea-level rise created favourable conditions (accommodation) for barnacle-dominated factories to develop and grow upon structural highs in their infancy compared to their future development from Waipipian onward. At Kairakau Beach, the aggradational stratal pattern of skeletal deposits above the TST (see sequence 13, Figure 6) is interpreted as a "keeping-up" phase during the rise and early fall in relative sea-level (HST), while the following coarsening-upwards trend (HST/RST) may correspond to the "catch-up" phase during normal regression. Stacked transgressive-regressive sequences at Cabbage Tree Flat and Mt Kahuranaki may represent either the carbonate factory response to successive transgressive pulses (Monstad, 2000), of eustatic or tectonic origin, or a percentage of the sediment supply being not accommodated upon the antiforms where wave-cut erosion is generated and sediments are by-passed. In the latter case a new sequence forms when enough accommodation space is created for sediments to accumulate (Einsele and Bayer, 1991).

Sequence B records partial suppression or decrease of carbonate production due to an increase in siliciclastic influx. Sequence B indicates a deepening-upwards trend over the entire area and as such is interpreted to represent drowning of the depositional realm during transgression.

The transition from sequences B to C is one from fine-grained siliciclastic to coarse-grained mixed carbonate-siliclastic deposits across a sharp to erosional surface. This abrupt superposition would classically be referred to as a basinward shift of shallow-water deposits into more distal settings (Posamentier *et al.*, 1992; Van Wagoner *et al.*, 1988). Nonetheless, the surface bounding below sequence C, though possibly superposed on a regressive or wave-cut surface of erosion (see Section 5.3.2), is interpreted as a TSE, and the overlying deposits as part of a transgressive-to-regressive sequence different from a FRST or LST, for the following reasons: (1) there is no evidence of valley incision, channel development, or subaerial exposure corresponding to boundary 3 in the studied area; (2) boundary 3 is immediately overlain by deepening-

upwards deposits, in the base of which is incorporated a pebbly to shelly lag at Te Mata Peak and Pukekura that bears all characteristics of a transgressive lag; and (3) sequence C1 is not bounded above by a subaerial-exposure surface that could assign it to a FRST, but by a RSE.

The shallowing-upwards trend recorded throughout the studied area (but at Pukekura in more distal position), accompanied by increasing skeletal contents (barnacles) towards the top of sequence C, local slumps and dewatering structures (Koanui) indicative of increasing rates of carbonate production, probably eventually led to subaerial exposure atop the better developed antiforms (Figure 14). The well-developed ravinement surface (surface 4) at the base of sequence C2 in the Mt Kahuranaki area is interpreted as a RSE produced through wave planation during sea-level fall. Because sequence C2 contains a RSE at its base and a probable SB (surface 5) at its top, the shoaling-upwards carbonate facies is considered a FRST (Hunt and Tucker, 1995).

Sequence D terminates the carbonate production due to an increase in siliciclastic input triggered by decreasing current velocity relative to sea-level rise. This suggests that surface 5 is a TSE superposed on a SB (i.e., compound surface).

Sequence E corresponds to the discontinuous Tuki Bell limestone. Sequence E is interpreted to represent transgressive carbonate deposits on the criteria that this carbonate facies is in sharp to erosional contact with outer shelf sandstone facies (Harmsen, 1985), and is in turn overlain by comparable deeper-water sandstones.

7.2. Awapapa Limestone (early Waipipian)

7.2.1. Introduction

The Awapapa Limestone is lithologically highly variable, ranging from interbedded terrigenous packstone and calcareous sandstone to barnacle-rich grainstone. It forms the prominent ridges of the eastern flank of the Elsthorpe Valley from Te Mata Peak southwards to the vicinity of Mount Erin, and crops out discontinuously along the steep slopes of the Kaokaoroa Range (Figures 1, 15).

Three depositional areas can be distinguished on the basis of lateral and vertical distribution of microfacies assemblages, which still indicate a strong terrigenous influence (see Appendix 3, columns 9, 12-16): (1) Makara area (southeast) dominated by Barbital; (2) Pukekura area (southwest) which comprises Pukekura section where

Awapapa Limestone mainly consists of bryozoan skeletons (Bryotal), and Hawea/Rowe Road sections where Bryotal and Barbital assemblages constitute the base and the top of Awapapa successions, respectively; and (3) Te Mata Peak area where Barbital microfacies alternates with Detrital microfacies.

7.2.2. Description of the main subdivisions and their bounding surfaces

The Awapapa Limestone successions are constructed of metre-scale sequences, which range in thickness from 1-17 m. From one locality to another, the number of building sequences is highly variable, ranging from four at Pukekura to up to twelve at Te Mata Peak, where the limestone reaches its maximum thickness (120 m). The limited number of studied sections, the generally poor exposures and rapid lateral facies changes, the limited traceability of sequence-bounding surfaces, and the laterally variable number of sequences all render correlation extremely difficult, which therefore has not been attempted at a high-resolution scale (Figure 15).

At Pukekura, TSEs can hardly be deciphered. Common reactivation surfaces, slumps, and convolute structures indicate a highly unstable depositional environment probably on the flanks or at the foot of antiforms, where key surfaces are likely to have been removed. Nonetheless, preserved strongly bioturbated silty-sandy layers that represent significant breaks of sedimentation were used to subdivide the shoaling-upwards succession into sequences (see Appendix 3, column 15; Figure 15).

Three transgressive surfaces of erosion have been tentatively correlated over the study region and, following on from the underlying Kairakau TSEs (1 to 6, Figure 14), are numbered from 7 to 10 in ascending order through the Awapapa Limestone Figure 15).

TSE 7 coincides with the angular unconformity at the base of Awapapa Limestone at Makara and Hawea, while at Te Mata Peak it marks the siliciclastic-to-skeletal turnaround of the sedimentation regime.

TSE 8 is sharp and possibly underlies shelly-pebbly lags both at Makara and Hawea capping sedimentary Motifs 1/3, whereas at Te Mata Peak it is superimposed on a discrete subaerial unconformity capping a Motif 4.

TSE 9 corresponds to a time of transgressive/regressive-to-transgressive turnaround of sequence stacking pattern.

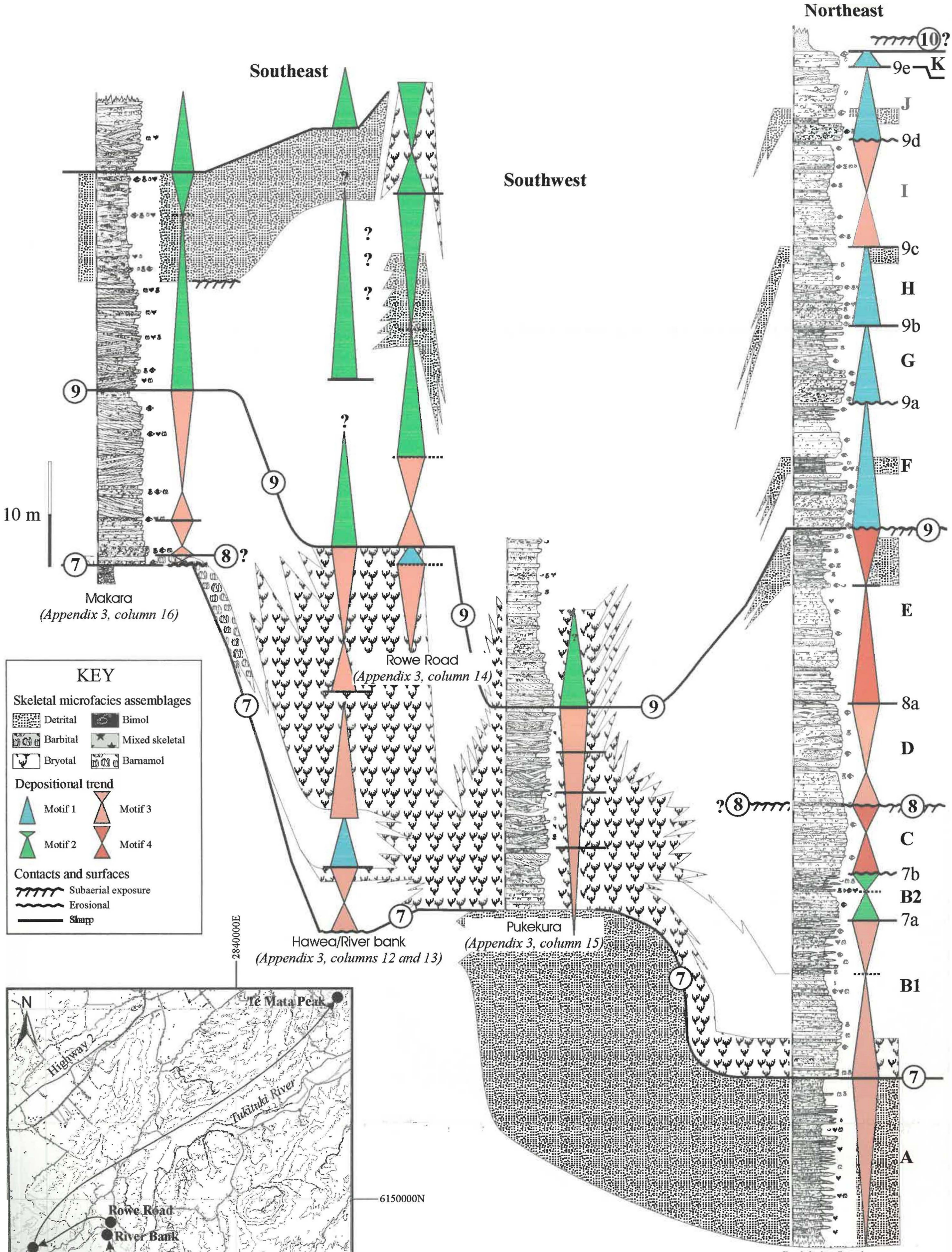

Figure 15- Correlation panel of five stratigraphic columns within Awapapa Limestone, from Makara to Pukekura, showing the stacking of sedimentary sequences (corresponding Motifs 1-4 are described in text and presented in Appendix 3, columns 9 and 12-16) and discontinuity surfaces bounding them (labelled 7 to 10). Note the local thickness variations of the building sequences, and differences in their number from one locality to another, which emphasize the complex stratal architecture of the Awapapa Limestone, rendering correlation difficult. See text for discussion.

TSE 10 sits on top of Awapapa Limestone and is assumed to coincide with a subaerial exposure surface that developed in some sectors of the Awapapa Limestone's regional distribution (see Section 7.2.3 for discussion).

Below TSE 9 at Te Mata Peak, the analysis of vertical facies successions within the shallowing-upwards sequences combined with the stacking pattern analysis of sequences enable the recognition of: (1) sequences bounded either by marine flooding surfaces or subaerial exposure surfaces; and (2) the progressive shoaling-upwards depositional trend of the complete lower member of Awapapa Limestone, which makes up a low-frequency regressive sequence that contains evidence of subaerial exposure towards the superjacent surface TSE 9. Thus, TSE 9 is coincident with a sequence boundary (SB).

Both at Te Mata Peak and in the Hawea-Rowe Road area, TSE 9 separates lithologies consisting below of medium-grained mixed carbonate-siliciclastics facies (occurrence of Bryotal and Bimol microfacies), from lithologies dominated above by coarse material involving shell beds or shell concentrates packed with oysters, brachiopods, and pectinid valves, with interbeds of alternating grainstone and terrigenous packstone (Barbital microfacies).

At Makara, TSE 9 presumably coincides with the boundary between a lower 16 m-thick limestone body, which characteristically consists of stacked cross-bedded sand waves separated by flooding surfaces and with internal marine-cemented horizons, and an upper 12 m-thick limestone body, which comprises alternating skeletal grainstone and terrigenous packstone, with marine cements present towards the base of the unit.

At Pukekura, no indisputable evidence exists for locating the position of TSE 9. It might coincide with a sharp surface resting on a silty-sandy shell-rich bioturbated horizon, above which Awapapa Limestone grades into Pukekura Calcarenite (Figure 15). Such a scenario would suggest that Pukekura Calcarenite is merely a lateral equivalent of the upper fossiliferous member at Te Mata Peak section.

7.2.3. Carbonate production development within a sequence stratigraphic framework

Lateral changes in thickness of Awapapa Limestone, and subsequent changes in the number of fundamental building sequences from one locality to another, are interpreted to represent local differences in sediment supply and in accommodation space created over time and available for sediments to accumulate. The former is a function of the rate

of carbonate production at the carbonate factory level and also of the distance from this source area, while the latter depends on inherited and evolving geomorphic parameters (highs and depressions, slopes), rates of subsidence, and amplitude of relative sea-level changes.

Besides, changes in sedimentologic attributes (microfacies) and types of sequence patterns on either sides of surface 9 suggest differential rates of creation of accommodation space, possibly higher above surface 9 interpreted as a drowning unconformity.

The depositional model for Awapapa Limestone is envisaged to be very similar to that for Kairakau Limestone (Figure 14). Makara and Pukekura are amalgamated sedimentary sequences, or incomplete successions with respect to the number of sequences recognized at Te Mata Peak, positioned in proximal (close to structural antiforms or more classically landward) and distal locations (basinward), respectively. Both have comparable thicknesses (between 25 and 30 m), comprise less than six building cycles but differ markedly in their diagenetic attributes, microfacies, internal sedimentary structures, and stratigraphic signatures of sequence-bounding discontinuities. Makara section consists of barnacle-rich migrating planar-bedded sand bodies, containing common marine-cemented horizons and stacked discontinuities (three in less than 5 m towards the base of the section; see example 6 in Figure 6) overlain by condensed pebbly lags. Conversely, Pukekura section consists of bryozoan-rich trough cross-bedded sand waves disrupted by slumps and dewatering structures, with rare early marine cements, and bounded by sharp burrowed surfaces.

If one introduces the assumption that Te Mata Peak sediments accumulated in an intermediate position (probably closer to the carbonate source than Pukekura) between the two end-members described above, then a likely oversimplified model for Awapapa Limestone deposition can be proposed. This is described in the following paragraph.

As mentioned earlier, a differential interplay between the creation of accommodation space and sediment supply is assumed to control the distribution of sediments on a proximal-to-distal transect. Close or atop antiforms (Makara), in shallow-water environments, starved sedimentation conditions and high carbonate production must have prevailed. Due to limited creation of accommodation space together with a high hydrodynamic regime dominated by tidal and storm waves, the excess in sediment supply was swept and by-passed further seaward, and erosional or sharp discontinuities

were generated overprinted by ensuing minor flooding surface. Both strong currents pumping though the sediments and low sedimentation favoured sea-floor constructive diagenetic processes and the genesis of condensed lags (comprising detrital glauconite and mud pebbles). However, the thickening-upwards of the amalgamated shallow-water sequences suggests that more space becomes available to accommodate sediments, and that deposition occurred in conditions of overall relative sea-level rise.

The Te Mata Peak section indicates that sediments delivered from neighbouring local factories could be accommodated either in tectonic depressions or on gently dipping slopes of structural highs. The complex stacking pattern of sequences and the occurrence of subaerial unconformities suggest that tectonic processes and sea-level changes combined their effects to produce a high-frequency cyclicity whose locally restricted components also reflect probable internal (autocyclic) mechanisms.

Further seaward, but still above storm wave base, the depositional environment was characterized by an overall low sedimentation rate (sediment-starved conditions) that generated amalgamated sequences. At Pukekura, sediments which by-passed the previous environments or were transported through episodic slope rupturing, up-dip of the area of deposition, formed stacked sequences separated by silty-sandy strongly burrowed layers reflecting low or arrested sedimentation. Carbonate diagenesis was dominantly destructive.

Stacked sedimentary Motifs 1 and 2 above TSE 9 at Te Mata Peak probably reflect conditions of increasing rate of relative sea-level rise.

This interpretation that infers that Awapapa sediments remained in the marine environment until the deposition of overlying beds (Pukekura Calcarenite?) is apparently inconsistent with the occurrence throughout the limestone, at Te Mata Peak, Makara, and in the Hawea/Rowe Road area, of pre-compaction clear spar cements that are interpreted to have precipitated from meteoric waters. This spar cement is shared by all the depositional packages constructing the Awapapa Limestone, and has not been recognized in the fine-grained Pukekura Calcarenite.

The meteoric cement is likely to have formed from near-surface, oxidizing groundwaters that percolated through the entire succession from a capping regional unconformity (surface 10) somewhere above Awapapa successions, which probably acted as a recharge area (Grover Jr and Read, 1983; Dorobek, 1987; Goldstein, 1988;

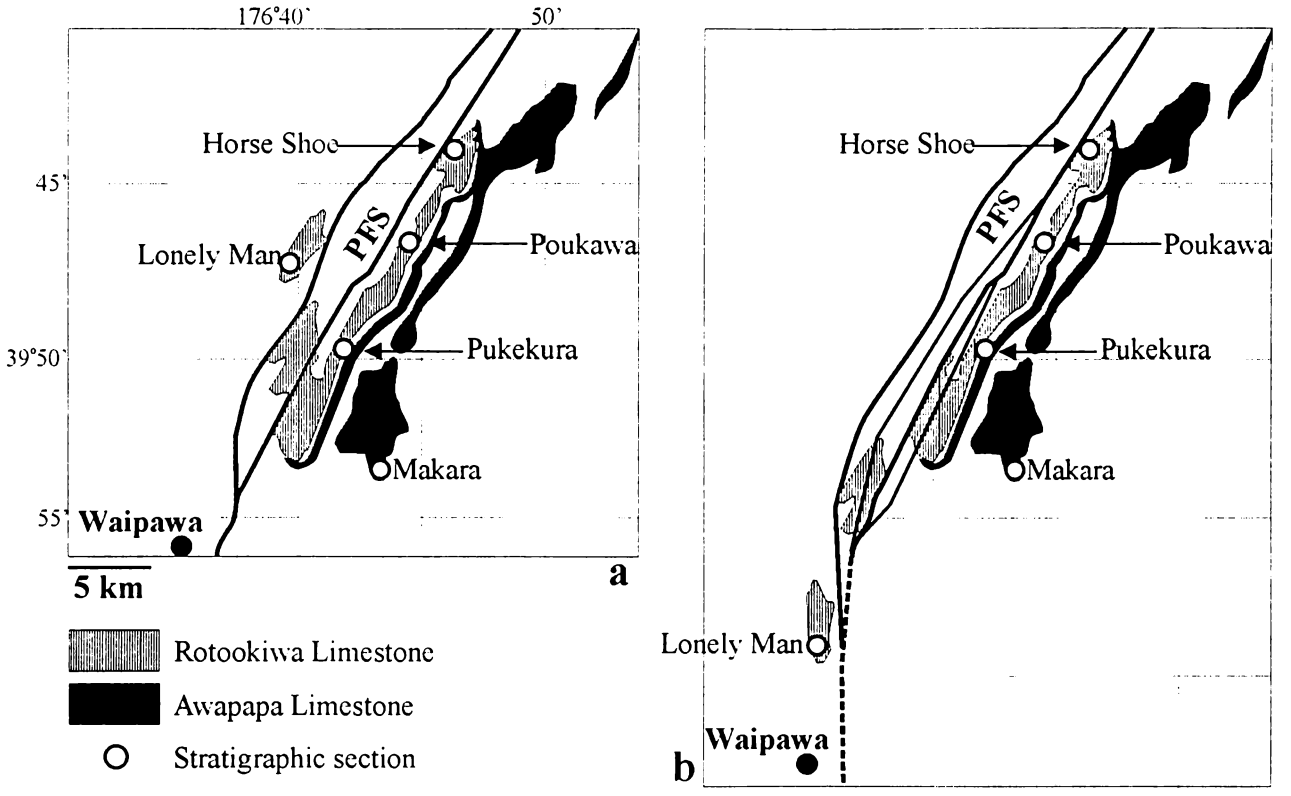

Figure 16- Outcrop distribution maps of the Rotookiwa Limestone, and a part of the Awapapa Limestone, showing location of Rotookiwa sections, and (a) present outcrop distribution due to dextral offset along the Poukawa Fault System (PFS); and (b) outcrop distribution after restoring the limestones to their presumably original configuration (c. 2.4 Ma). (Modified from Cashman *et al.*, 1992).

Niemann and Read, 1988). Consequently, a relative fall of sea level could be envisaged to explain the ingress of meteoric waters into the system that would correspond in the course of an overall sea-level rise trend to a forced regression *sensu* Posamentier *et al.* (1992) and Walker and Wiseman (1995), though such an unconformity was not observed in the field at the top of the studied sections. Instead, the contact between Awapapa Limestone and the overlying Pukekura Calcarenite (if the two formations are effectively distinct; see above) is gradational at Pukekura, Makara, and possibly in the Hawea/Rowe Road area.

7.3. Rotookiwa Limestone (late Waipipian)

7.3.1. Introduction

Kelsey *et al.* (1993) referred to the lower contact of Rotookiwa Limestone with the underlying Pukekura Calcarenite as being gradational, though in places it appears to be sharp (Pukekura section, column 15 in Appendix 3; see Figures 7F, 8A), and possibly erosional (Lonely Man section, column 20 in Appendix 3; see Figure 8B). The upper contact of Rotookiwa Limestone with the overlying Waikareao Calcarenite is gradational in its exposure in Waitapuke Quarry (Figure 17).

Because the Rotookiwa Limestone is typically a pale-yellow, coarse-grained, soft to poorly cemented barnacle-rich grainstone, good exposures are rare and are mostly found in a region of localised downwarped basins and uplifted folded hills collectively referred to as the Poukawa Fault System (Cashman *et al.*, 1992) (Figures 1, 16). Few good sections are exposed in the western flanks of the Kaokaoroa Range together with outcrops along Highway 2 between Waikareao Road and Te Onepu Road (Figure 17) as mapped by Kelsey *et al.* (1993). The Poukawa Fault System cuts through Rotookiwa Limestone and trends obliquely through it, dextrally displacing the limestone bank whose original outcrop pattern once restored shows a linear configuration (Figure 16; cf. Cashman *et al.*, 1992).

The vertical distribution of facies assemblages is remarkably similar to that of Awapapa Limestone. Bryotal, Bimol, and locally Barbital constitute the lower part of the successions, whereas Barbital and Barnamol are found in their upper part (see columns 17, 18, 20 in Appendix 3).

7.3.2. Description of the main subdivisions and their bounding surfaces

At Pukekura and Makara (Figure 17), between 7 and 14 m of trough cross-bedded, medium-grained barnacle- to bryozoan-rich grainstones and packstones sharply overlie fine-grained, well sorted calcarenites referred to as Pukekura Calcarenite, and are assumed to represent the base of Rotookiwa Limestone. The sharp burrowed contact that bounds below Rotookiwa Limestone (Figure 7F) is interpreted to be a TSE, labelled surface 11, and the overlying deposits are inferred to correspond to the transgressive part of the sequence. At Horse Shoe and Poukawa (Figure 17), the succession is divided into three major sequences. Although not exposed, it is inferred that the lower transgressive-to-regressive Motif 3 at Horse Shoe section is bounded below by TSE 11, and its lower deepening-upwards member is equivalent to those at Makara and Pukekura on the basis of sedimentologic and diagenetic similarities. The upper part of the lower sequence is characterized by an upwards increasing number of very hard discontinuous layers in beds up to 15 cm thick that comprise marine turbid cements. An abrupt change underlain by superposed stylolites, from well-cemented skeletal grainstones to soft coarse skeletal sands, is chosen as the upper bounding surface labelled TSE 12. The latter is directly overlain by coarsening-upwards and shallowing-upwards barnacle-rich grainstones of the intermediate sequence whose uppermost 2 m, which are sharply overlain by a 2 m-thick shell bed, exhibit a deepening-upwards trend. These last 2 m may represent a Motif 1 sub-sequence capped by the next discontinuity labelled TSE 13. The occurrence of pre-compaction meteoric cements throughout Horse Shoe and Poukawa successions, and solution fabrics towards the surface bounding below the upper sequence (TSE 13), suggest that the intermediate sedimentary package has been subaerially exposed. Nonetheless, solution fabrics found in the lower part of the capping shell bed close to TSE 13 may also be of marine origin as the latter and the overlying green marine sands bear the hallmark of condensed deposits (DD^1-type diagenesis). Consequently, solution fabrics in the condensed transgressive lag might not be related to the ingress of meteoric waters from which clear spar cements were precipitated.

The shell bed above TSE 13 might represent the uppermost member of Rotookiwa Limestone and the overlying siliciclastic sands the base of Waikareao Calcarenite (Appendix 3, column 17). If so, Rotookiwa Limestone probably does not exceed 80-100 m in thickness, which contradicts the estimation of Kelsey *et al.* (1993) of 285 m for Rotookiwa Limestone. If such a thickness is to be confirmed then the lower

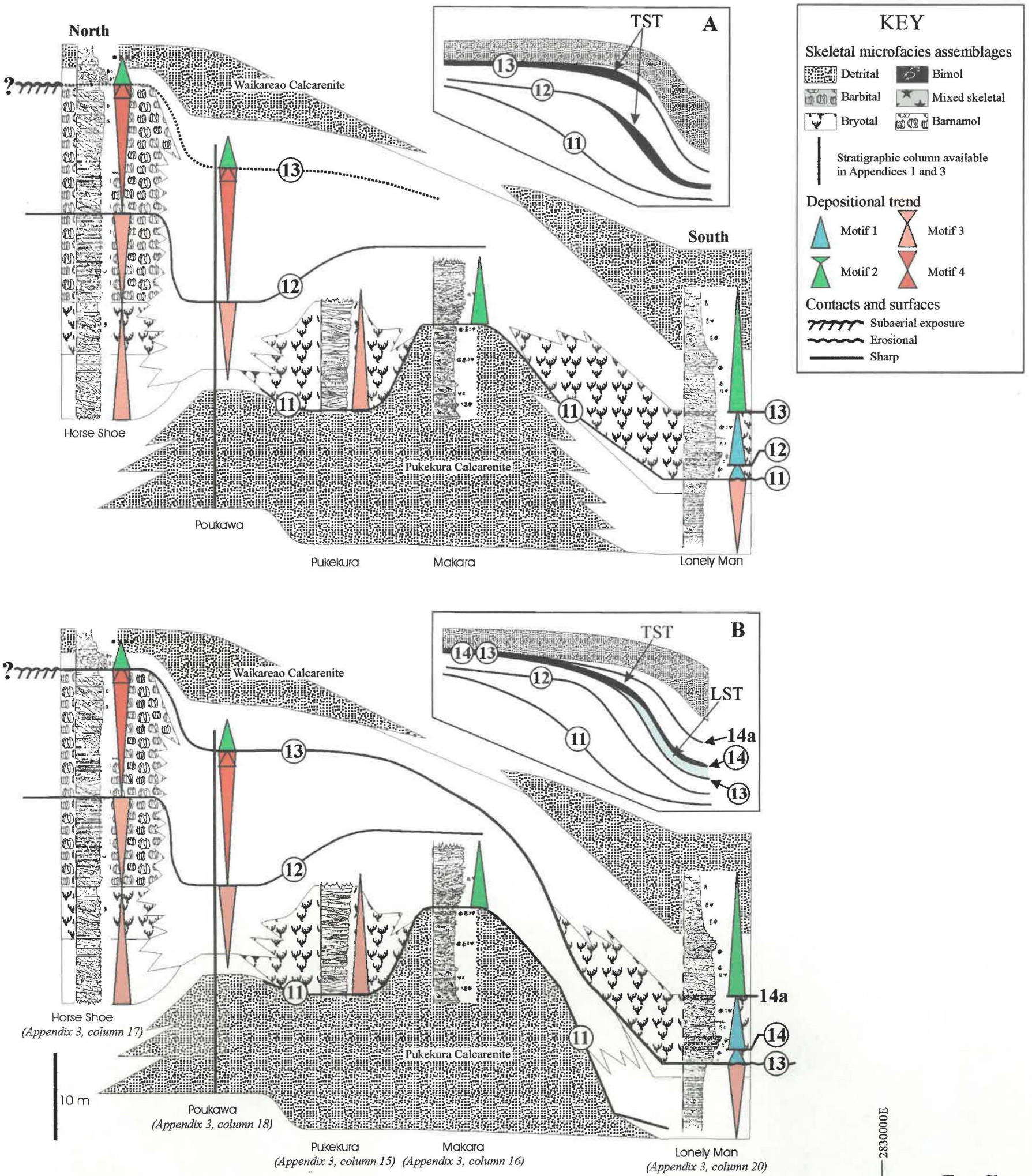

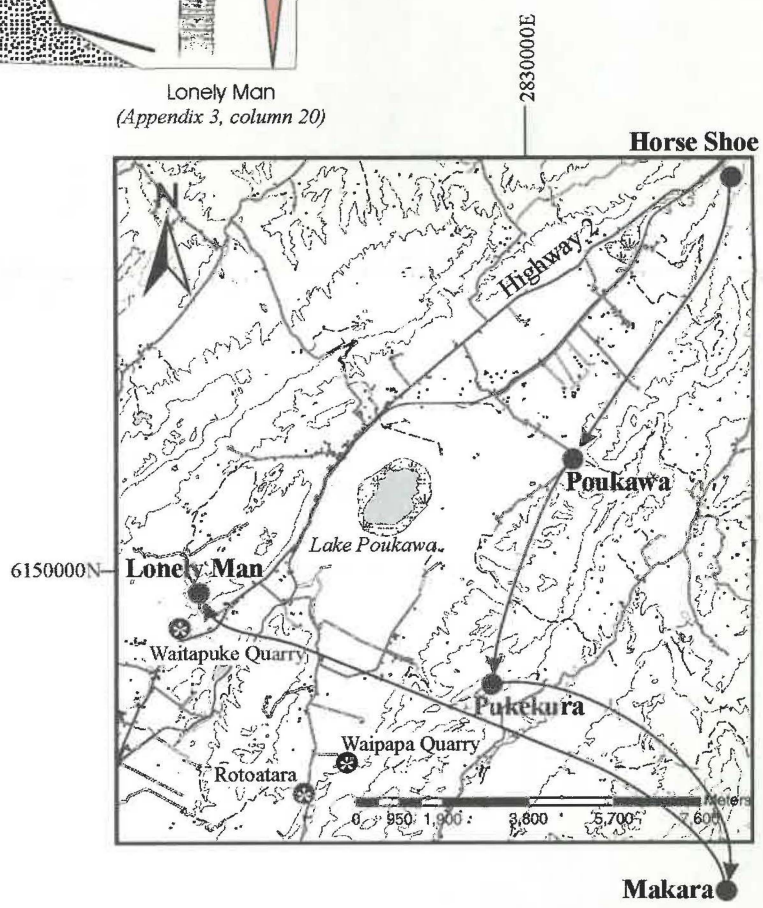

Figure 17- Correlation panels of five stratigraphic columns within Rotookiwa Limestone. Two models are proposed to link northern and southern outcrops. In model A, the sharp surface (TSE 11) underlying Rotookiwa Limestone at Makara and Pukekura is correlated to the erosional surface cutting through the lower skeletal calcarenite at Lonely Man, which is consequently assumed to be laterally equivalent to the Pukekura Calcarenite. In model B, the lower sequence at Lonely Man section overlies TSE 11, and as such is part of the Rotookiwa Limestone and constitutes its distal expression.TSE 13 is coincident with a sequence boundary *sensu stricto*, and the sequence bounded by surfaces 13 and 14 at Lonely Man section is assigned to a LST or FRST.
See text for discussion.

sequence at Horse Shoe can probably not be correlated with the basal deposits at Makara and Pukekura.

The Lonely Man section differs from the almost constant stratigraphic pattern and lithofacies of Rotookiwa Limestone in the Kaokaoroa Range. It disconformably overlies (Figure 8B) shallowing-upwards skeletal calcarenite/sandstone beds (Motif 3), comprises an internal pebbly transgressive lag, and conformably underlies a yellow-green fossiliferous calcareous sandstone that Kelsey *et al.* (1993) established as the Waikareao Calcarenite. Lonely Man section has been subdivided into four sequences: (1) a lower Motif 3 whose top is truncated by an erosional surface (Figure 8B); (2) and then three deepening-upwards Motifs 1 to 2 bounded by sharp surfaces interpreted to be TSEs.

The paleogeographic distribution of Rotookiwa Limestone (Figure 16b) indicates that Lonely Man section was probably situated about 25 km and 60 km south of Makara and Horse Shoe, respectively. The lack of good sections between Lonely Man section and the other localities renders correlation difficult. Two models are proposed to link northern and southern outcrops that are equally satisfactory (see below; Figures 17A, 17B), though it is emphasized that more field investigation should be undertaken to assess their respective validity.

7.3.3. Carbonate production development within a sequence stratigraphic framework

The discontinuity surfaces that bound the building sequences of the northern and southern successions can be linked in several ways, schematically shown by Figures 17A and 17B.

In model A, the sharp surface (TSE 11) underlying Rotookiwa Limestone at Makara and Pukekura is correlated to the erosional surface cutting through the lower skeletal calcarenite at Lonely Man, which is consequently assumed to be laterally equivalent to the Pukekura Calcarenite.

The discrete sharp conformable TSE 12 at Horse Shoe is correlated to a sharp surface at Lonely Man section that caps 2 m of bryozoan-rich grainstones deposited above TSE 11, and is overlain by a 2 m-thick shelly/pebbly coarse-grained bed, which is interpreted to have been transgressively emplaced. The latter is in turn overlain by bryozoan grainstones with internal tangential cross-beds capped by HCS structures. The overall deepening-upwards trend above TSE 12 at Lonely Man section is interrupted by

a sharp surface, supposedly equivalent to TSE 13, covered by planar-bedded barnacle-rich deposits, which exhibit the same depositional trend as the sequence below, but gradationally pass upwards into the Waikareao Calcarenite. By contrast, northwards (Horse Shoe and Poukawa sections), TSE 13 is overlain by transgressive shell lag deposits, and in turn by siliciclastic condensed beds at the base of Waikareao Calcarenite. Transgressive sequences of Lonely Man section are correlated northwards (Horse Shoe) to, in ascending order, transgressive-regressive, regressive, and transgressive sequences. Considering the distribution of transgressive lag deposits and the nature of sequences on a south-north transect, the Rotookiwa Limestone sequence, beneath TSE 13, shows a slightly shallowing-upwards pattern (i.e., progradational), recording an overall sea-level fall and shoreline advance. This scenario conforms to the depositional history envisaged for the older Kairakau and Awapapa Limestones. Limestones accumulated during a long-term (4th- or 5th- order) shallowing-upwards megasequence (regressive) that records transgressive-regressive pulses on a shorter sequential time-scale (6th- to 7th- order), and are overlain by transgressive and highstand deposits of the next megasequence represented by sandstones or calcarenites.

In model B, the lower sequence at Lonely Man section overlies TSE 11, and as such is part of the Rotookiwa Limestone and constitutes its distal expression. Neither TSE 11 nor TSE 12 is exposed at this locality. The erosional TSE 13 represents the surface of basinward transfer of sediments eroded northward, and of basinward shift of shallow-water environments. TSE 13 coincides, up-dip of Lonely Man section area, at Poukawa and Horse Shoe, with a surface of subaerial exposure, and the subsequent development of fresh-water paleoaquifers. TSE 13 is therefore coincident with a sequence boundary *sensu stricto*, and the sequence bounded by surfaces 13 and 14 at Lonely Man section is assigned to a LST or FRST. These sediments were deposited during relative sea-level fall, and they are overlain by a transgressive surface of erosion (TSE 14; but possibly TSE 14a), accompanied by transgressive lags, which probably removed the previous subaerial unconformity at Poukawa and Horse Shoe. In the latter localities TSE 14 is superimposed upon TSE 13. Continuing sea-level rise eventually led to the deposition of Waikareao Calcarenite.

7.4. Te Onepu Limestone (Mangapanian-early Nukumaruan)

7.4.1. Introduction

The Te Onepu Limestone forms the escarpment that bounds the Raukawa Range to the east (Figure 1). At its type locality the Te Onepu Limestone lies sharply on the local Argyll Sandstone Member, which in turn overlies the Raukawa Mudstone. Otherwise the Te Onepu Limestone directly lies on the Raukawa Mudstone and conformably underlies the Makaretu Mudstone (see Chapter 1, Figure 2).

Figure 18 shows the lateral and vertical facies variability of Te Onepu successions in a north-south transect parallel to the forearc basin axis. While Bryotal deposits occur locally towards the base of the units, Te Onepu Limestone is overall characterized by a high content of barnacle skeletons. Typically, Barnamol assemblage builds up the base of the succession, while Barbital assemblage in the upper part indicates an increase in terrigenous input (Figure 18), which probably anticipates the drowning of Te Onepu carbonate factories by the overlying Makaretu Mudstone.

7.4.2. Description of the main subdivisions and their bounding surfaces

Five main depositional sequences are identified in the Te Onepu Limestone, termed in ascending order OA to OE (Figure 19), within a framework of sharp surfaces and laterally extensive marker shell beds. Sequences OA to OE consist of thin transgressive and thicker regressive metre-scale members (Motifs 3 and 4) that are locally subdivided into higher-frequency sub-units, though the latter cannot be traced across the north-south trending belt between several kilometre-spaced localities. Consequently, sequences OA to OE highlight stratal architectures in which the individual components stack into minor transgressive and major regressive sets.

Sequence OA is gradationally based at Robottom Grave section, and sharply based at Te Onepu Quarry, Bee Swarm, and Burma Road sections where condensed shelly lags, from 0.3-0.5 m thick, define boundary 15.

Sequence OA consists of a basal, coarsening-upwards, facies succession capped by a condensed shelly deposit (0.2-0.5 m thick) across a sharp surface labelled TSE 16, which at Gulch Quarry is erosional with a relief up to 0.2 m, and contains evidence of subaerial exposure (dissolution and vadose silts).

The depositional trend of sequence OB above TSE 16 is unclear, though in general upward-increasing grain size, tide-influenced sedimentary structures, and marine-cemented horizons towards the top indicate higher energy and shallower environments than in the basal deposits (see example 11 in Figure 6).

At most localities, generally poorly defined TSE 17 underlies a 1-2 m-thick marker shell bed packed with near *in situ Crassostrea ingens*, which constitutes the base of sequence OC. At Horanui and Gulch Quarry sections, TSE 17 is better defined and consists of sharp and erosional surfaces, respectively, also overlain by shell beds interpreted to be transgressive lags with abundant reworked scallops and oyster shells. TSE 18 on top of sequence OC is sharp to erosional in the southern successions where it underlies 1-2 m-thick transgressive lags packed with abundant bivalves. TSE 18 cannot be confidently traced northwards. However, at Horanui, the surface which underlies channelized shelly/pebbly deposits, incised within the underlying coarse skeletal sands of sequence OC, is assumed to be the lateral equivalent to the southern TSE 18. Throughout the study area, sequence OC shows a transgressive-to-regressive succession of facies (Motif 3).

At Robottom Grave, sequence OD is bounded below by TSE 18 and above by a sharp discontinuity surface (TSE 19), which may correspond to a conformable, possibly gradational contact at Horanui between coarse-grained barnacle-rich grainstones and rudstones packed with whole specimens of bivalves (see Appendices 1 and 3, column 21). Sequence OD shows a sharp transition from a basal shelly packstone with common clumps of oysters to fine-grained calcareous sandstones, in turn grading into coarse-grained barnacle-rich grainstones, indicative of a shallowing-upwards upper segment. At Robottom Grave, one specimen of *Phialopecten triphooki* was collected from the calcareous sandstone overlying the basal shell bed, which indicates that the Mangapanian-Nukumaruan boundary lies within the upper part of Te Onepu Limestone.

Only at Robottom Grave section does the base of sequence OE occur. It consists of coarse-grained barnacle-rich deposits packed with common clumps of oysters, interpreted as shallow subtidal facies and assigned to a TST.

7.4.3. Carbonate production development within a sequence stratigraphic framework

Similarly to that of its older counterparts, Te Onepu Limestone started to accumulate while the forearc basin was probably experiencing tectonically-driven shallowing.

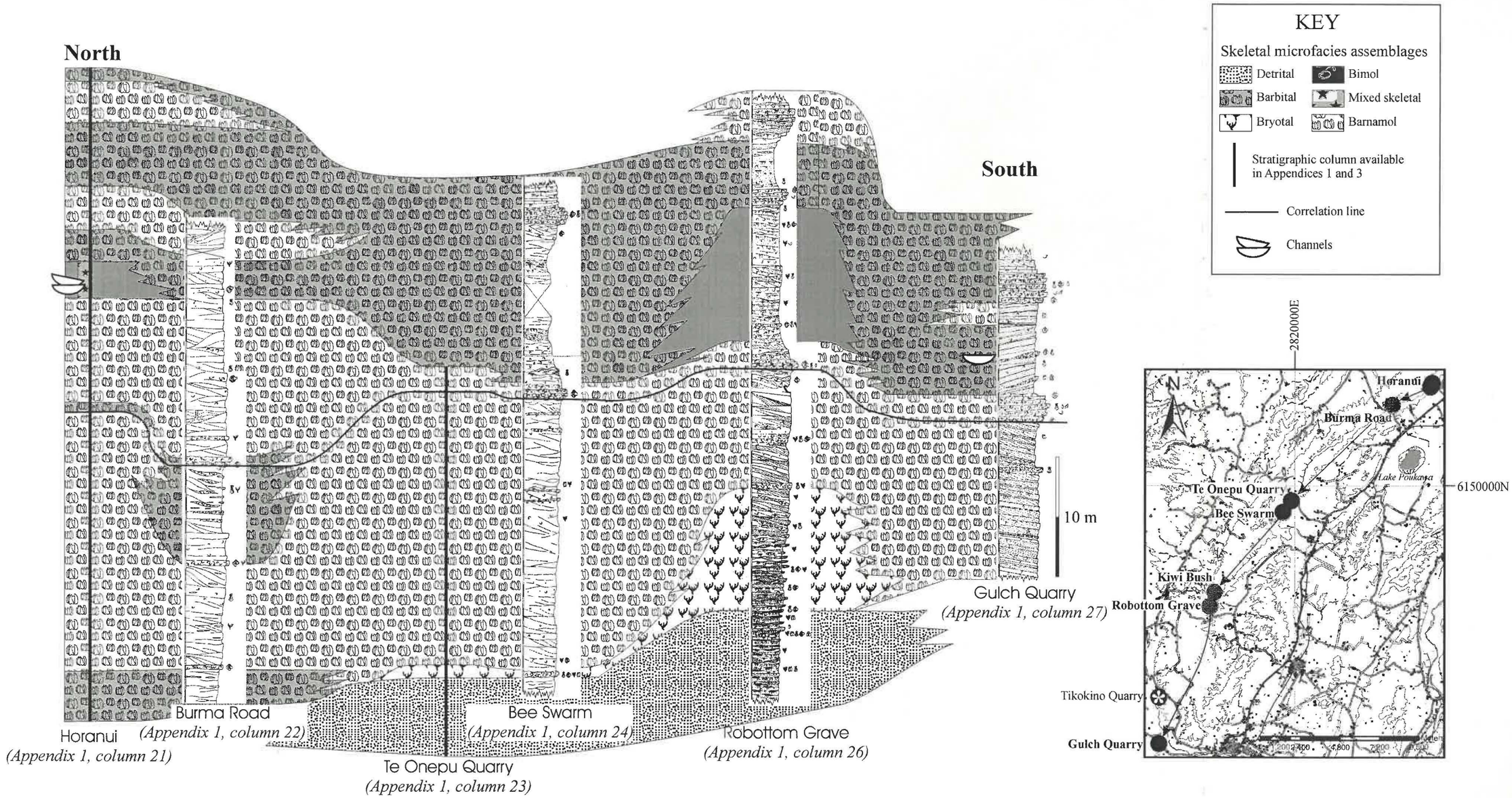

Figure 18- Transect within Te Onepu Limestone from Horanui to Gulch Quarry, showing ideal microfacies assemblages distribution. Note that Barnamol assemblage builds up the base of the succession, while Barbital assemblage in the upper part indicates an increase in terrigenous input, which probably anticipates the drowning of Te Onepu carbonate factories by the overlying Makaretu Mudstone.

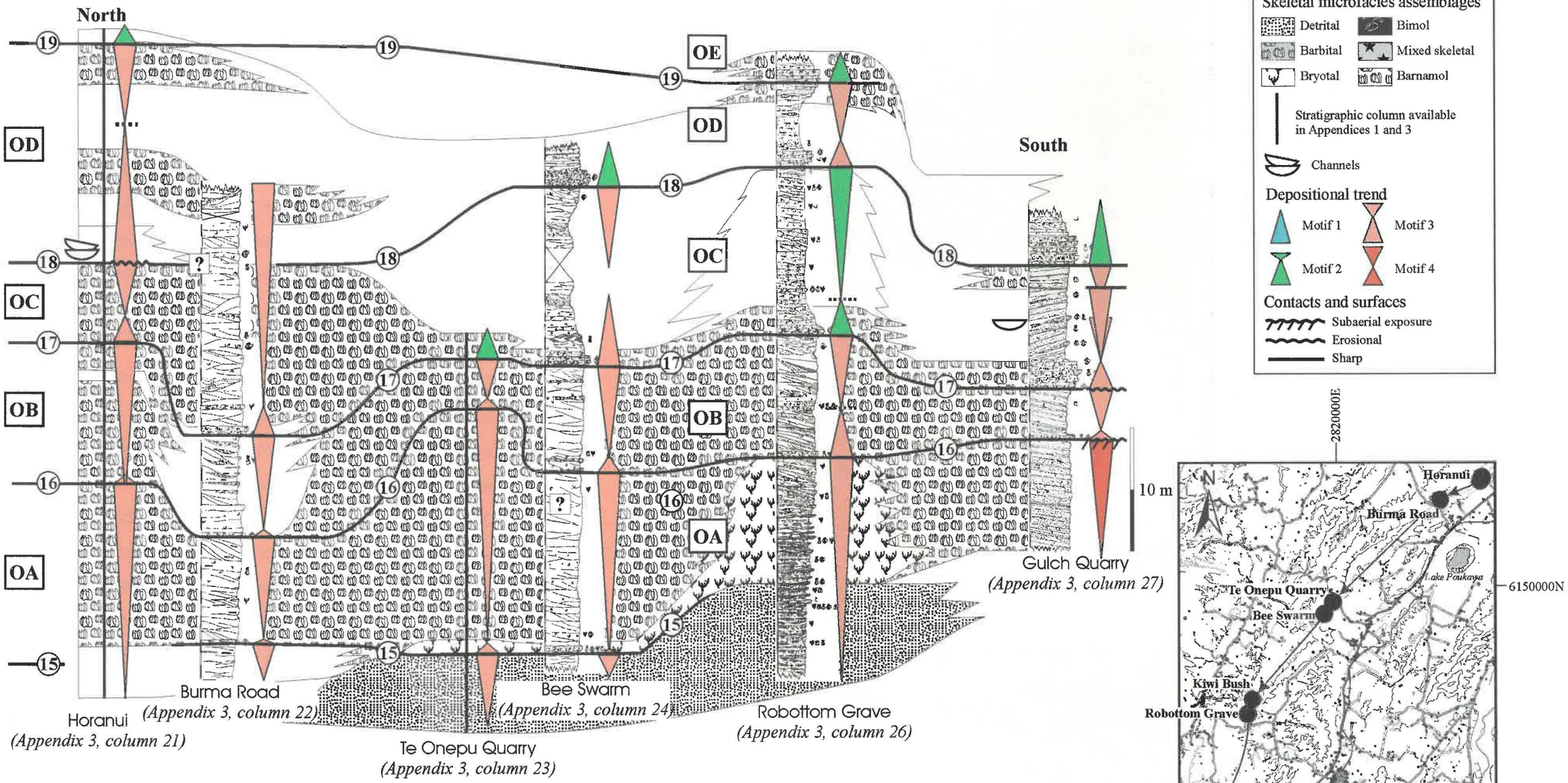

Figure 19- Correlation panel of six stratigraphic columns within Te Onepu Limestone, from Horanui to Gulch Quarry, showing the stacking of sedimentary sequences (corresponding Motifs 1-4 are described in text and presented in Apendix 3, columns 21-27) and discontinuity surfaces bounding them (labelled 15 to 19). See text for discussion.

Regional shallowing was rapidly accompanied by carbonate production and accumulation free from terrigenous pollution as indicated by the lateral extent of pure coquina barnamol facies in the lower portion of sequence OA (Figure 18), and their local abrupt occurrence upon underlying sandstones.

Condensed shelly lags associated with TSE 16 indicate a break of sedimentation probably associated with transgressive drowning of the depositional environments and subsequent condensation, after subaerial exposure in some areas (Gulch Quarry).

The deepening- then shallowing-upwards trend observed in the deposits above TSE 16 in most localities, together with the overall upward-coarsening, shallowing, and internal prograding architecture (so-called giant foresets) within sequence OB, suggest that the succession of facies may have only been driven by sediment supply during stable or slowly rising relative sea-level so that carbonate production could be accommodated.

TSE 17 marks the time of Barnamol-to-Barbital turnaround of facies, that is, a change in the rate of terrigenous influx into the system. Nonetheless, in the neighbourhood of carbonate factories coarse skeletal sands kept accumulating in the form of tabular sand bodies, as at Gulch Quarry, or prograding cross-bedded barnacle-rich sand bars with common dewatering structures, as at Horanui and Burma Road.

Sequence OD consists of a basal transgressive shell bed (the onlap shell bed of Kidwell, 1991b), which at Horanui fills in troughs, up to 2 m deep and 10 m across, interpreted to be intertidal channels. Such channel incision followed by transgressively emplaced deepening-upwards deposit may indicate that TSE 18 was superimposed on a previous regressive surface of erosion, which formed at the top of the regressive segment of sequence OC during significant lowering of relative sea-level.

Sequence OE is poorly exposed in the study area. Above the shallowing-upwards segment of sequence OD at Robottom Grave, deepening-upwards deposits on top of surface 19, which eventually pass upwards into the mid- to outer-shelf Makaretu Mudstone, record the drowning and shutting off of Te Onepu carbonate factories. Between sequences OD and OE, a flooding surface must therefore exist, though this surface is difficult to pinpoint in the field. At Robottom Grave, sharp surfaces could be identified both within the shell-rich bed capping sequence OD and immediately at its top.

Nonetheless, a TSE superimposed on a RSE might correspond to the uppermost sharp surface as pre-compaction cement fabrics of samples from beneath the latter bear characteristics of meteoric water-derived cement, indicative of possible meteoric paleoaquifer development from otherwise unrecognized emerged antiforms.

However, one must keep in mind that similar fabrics are produced by a number of different diagenetic environments, amongst them mixed marine-meteoric environments (Melim *et al.*, in press), which in turn could explain the lack of subaerial unconformities. It is re-emphasized here that more specific fieldwork should be undertaken to assess some of the above assumptions.

7.5. Mason Ridge Formation (Nukumaruan)

7.5.1. Introduction

By contrast with older Te Aute limestones, limestone sheets of the Mason Ridge Formation are characterized by a high content of carbonate muds, infaunal aragonitic bivalves, and indicators of possibly warm-temperate shallow-water environmental conditions, including micritization, micritic microbial coatings, abundant benthic foraminifers and red algal skeletons, though barnacles, bivalves, and bryozoans remain persistent skeletal components (Figure 20). The abundance of aragonitic components within this formation (especially within the upper limestone sheets), compared to older barnacle-epifaunal calcitic mollusc-dominated Te Aute limestones, indicates that the conditions that prevailed during Early to mid-Pliocene times evolved with respects to environmental factors, including water depth, substrate, and current velocity. Such factors are believed to have favoured colonization of the sea floor by increased quantities of aragonitic bivalves by the Late Pliocene (Haywick, 1990; Beu, 1995).

Limestone units of the Mason Ridge Formation are interpreted to have formed in less open marine environments than their older counterparts, possibly in shallow marine flat embayments as suggested by Beu (1995).

Although, as for older formations, fieldwork has emphasized rapid lithological variations over short distances between each of the correlative limestone sheets, they are easily traceable along incised river valleys due to little variation in their lateral thicknesses and their low gradient, almost monoclinal structure. The Mason Ridge Formation is cyclothemic in disposition, comprising thin mudstone/sandstone - limestone (i.e., fine – coarse) formational couplets, remarkably similar to those forming

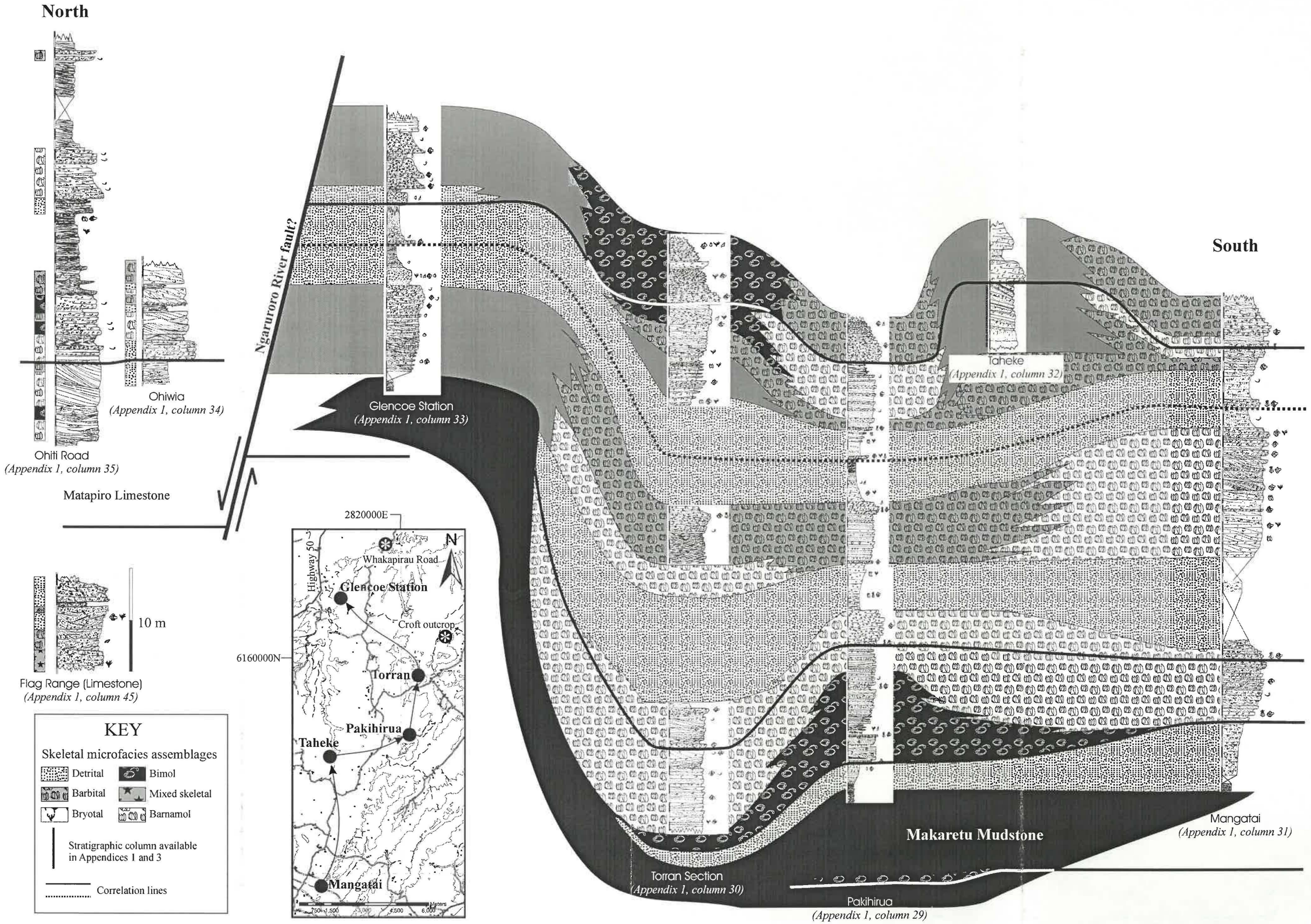

Figure 20- Transect within Mason Ridge Formation from Mangatai to Glencoe Station, showing ideal microfacies assemblages distribution. Note the cyclothemic disposition of Mason Ridge strata, which can be grouped into skeletal (Barnamol, Barbital, Bimol)/Detrital assemblage couplets. Marker shell beds are used as practical field means of correlation between outcrops. See Figure 1 for the location of Ohiti, Ohiwia, and Flag Range sections with reference to column numbers.

the upper part of the Petane Group within the Tangoio Block in central Hawke's Bay (Figure 1; Haywick *et al.*, 1992; Haywick, 2000).

7.5.2. Description of the main subdivisions and their bounding surfaces

South of Ngaruroro River (Figure 1), Mason Ridge Formation is divided into four mixed carbonate-siliciclastic sequences informally termed MB to ME bounded by flooding surfaces (transgressive surfaces of erosion and their correlative surfaces) chronologically labelled 21 to 24 (Figure 21). Most sequences in the study interval can easily be traced, though northward the sequences MB and MC seem to onlap upon the underlying Makaretu Mudstone, which abuts against the Ngaruroro normal fault and has been uplifted in relation to formations north of the fault (Beu, 1995). As a result, only sequences MD and ME are wholly represented close to Ngaruroro River.

Besides shell beds, which characteristically sit on top of each sequence, two regional markers were used to organize the studied successions into a comprehensive stratigraphic scheme: (1) the condensed shell bed associated with a mid-sequence horizon of maximum diagenetic condensation (Cdh) within sequence MD, traceable over more than 15 km; and (2) the prominent discontinuity 24, which consists of a subaerial unconformity at Mangatai, an erosional surface at Taheke, Torran, and Glencoe Station, and a sharp contact at Pakihirua (Figures 20, 21).

The siliciclastic-dominated sequence MA is bounded at the base by discontinuity 20, and at the top by discontinuity 21. It includes a 1 m-thick basal shell bed overlain by 35 m of siltstone, and in turn by 2 m of sandstone. Laterally, at Mangatai, the contact between sequences MA and MB is conformable.

Individual facies in Mason Ridge Formation stack into deepening- then shoaling-upward sequences (Motif 2 and Motifs 3/4), c. 15 m thick on average (from 7-20 m). Subaerial-exposure surfaces are present only at the top of sequences MB and MD at Mangatai.

Typical sequences consist, from base to top, of: (1) a discontinuity and its lateral conformity interpreted to be a TSE, which may or may not be superimposed on a RSE; (2) a TST either only composed of a shell bed up to 7 m thick (onlap shell bed of Kidwell, 1991b; Naish and Kamp, 1997; type-A shell bed of Abbott and Carter, 1994), locally subdivided into fining-upwards higher-frequency sequences, or consisting of a basal shell bed (up to 3 m thick) overlain by calcareous sandstones grading into

siltstones; (3) a thin (up to 1 m thick) glauconite-rich, in places biomould-rich, condensed shell bed, which corresponds to the Cdh; and (4) a HST that consists of a basal calcareous sandstone, sharply lying on the Cdh, that grades into (5) an upward-coarsening carbonate unit. Because of the typical lack of development of a physical surface within these coarsening-upwards strata, which instead exhibit a conformable base, they are attributed to a regressive systems tract (RST; Naish and Kamp, 1997).

The stratal architecture within the mixed carbonate-siliciclastic Mason Ridge sequences is remarkably similar to that of the cyclic repetition of mudstone and limestone in Pukenui Limestone (Vella, 1963) of Wairarapa area in southeastern North Island, to the cyclothems of the Tangoio Block of central Hawke's Bay (Haywick *et al.*, 1991, 1992; Haywick, 2000), and to the even more widespread thick siliciclastic sequences described by Abbott and Carter (1990, 1994), Naish and Kamp (1995, 1997), and Kamp and Naish (1997) in the Wanganui Basin, all Nukumaruan in age. All previous authors have attributed the cyclic pattern of Nukumaruan successions to high-frequency glacio-eustatic oscillations forced by Milankovitch climatic rhythms.

7.5.3. Summary of attributes identifying systems tracts in the Mason Ridge Formation

High-frequency sequences of the Mason Ridge Formation can be interpreted in terms of high-frequency relative changes in sea level, which are indicated by the repetition of transgressive-to-regressive stacking patterns of facies bounded by transgressive surfaces of erosion, locally superimposed on subaerial unconformities.

Transgressive systems tract (TST)

The majority of the TSTs in each sequence consists of a basal shell bed packed with oysters and articulated bivalves (e.g., *Glycymeris* sp.) in a micritic matrix. The coarse fossiliferous facies is in sharp contact with sediments of the previous sequence composed either of coarse skeletal-rich grainstones, or silty sandstones bioturbated by *Ophiomorpha* and/or *Skolithos* burrows (Figure 8D).

The upper contact between shell bed and overlying deeper-water sandstone/siltstone deposits is generally sharp.

At Pakihirua and Torran sections, the shell beds at the base of sequence ME, and atop the bioclastic limestone of the previous sequence MD, consist of various bivalves in a fining-upwards matrix, from fine-grained mixed carbonate-siliciclastic to siltstone.

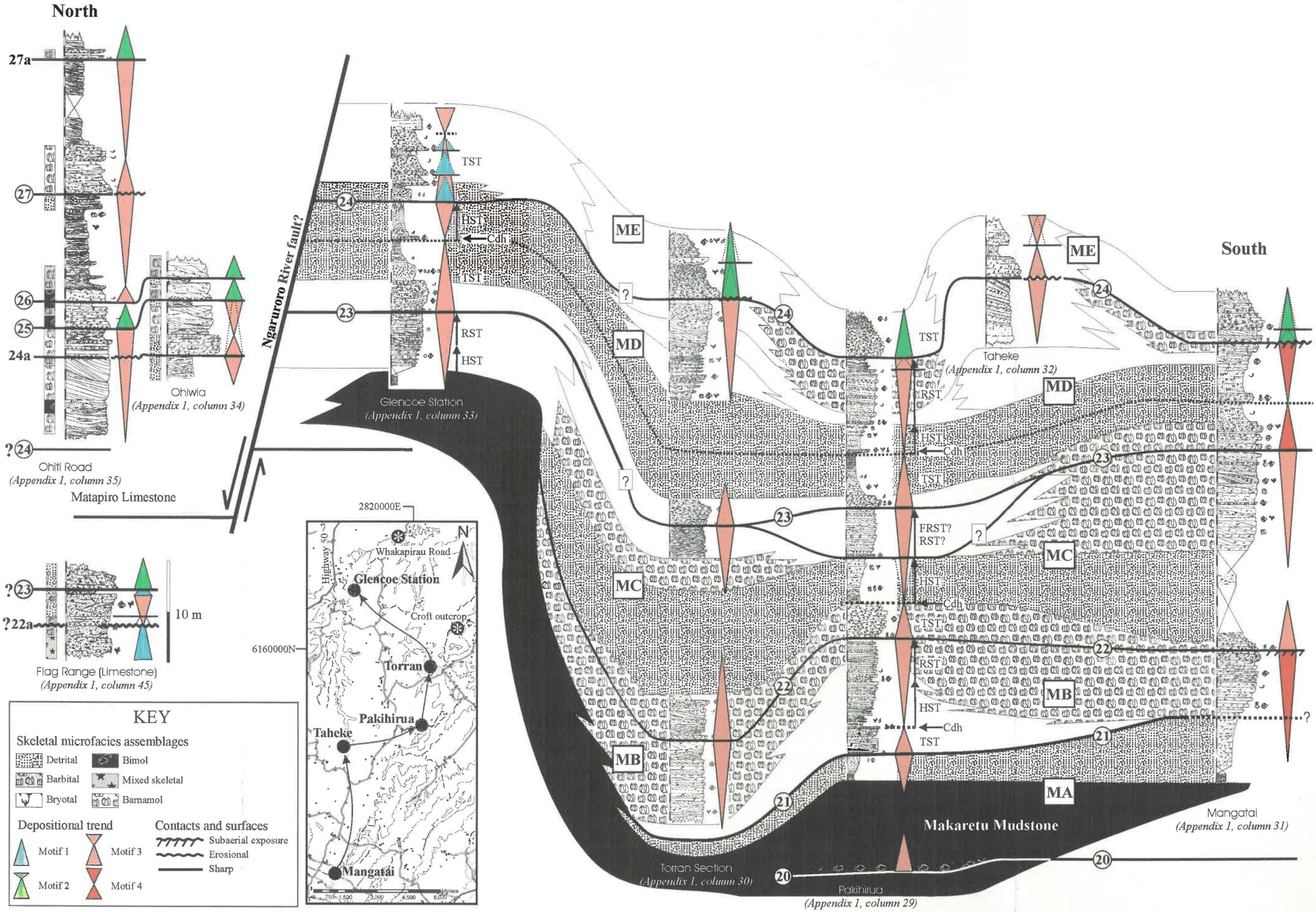

Figure 21- Correlation panel of five stratigraphic columns within Mason Ridge Formation from Mangatai to Glencoe Station, showing sedimentary sequences (corresponding Motifs 1-4 are described in text and presented in Appendix 3, columns 29-35 and 45) and their bounding surfaces (labelled 20 to 24). A sequence stratigraphic interpretation is proposed for the mixed carbonate-siliciclastic sequences MB to ME, showing the vertical succession of the component systems tracts at Pakihirua and Glencoe Station. The attempt to correlate unconformities 23 and 24 across the Ngaruroro River fault with unconformities recognized within the presumably time-equivalent Flag Range and Matapiro Limestones is discussed in text.

The shell beds are interpreted as TSTs, deposited above a flooding surface (TSE) during rapid sea-level rise.

Horizon of maximum diagenetic condensation (Cdh)

The horizon of maximum diagenetic condensation is either located in a mid-sequence position, associated with a thin condensed shell bed (e.g., within sequence MD at all localities), or coincident with the sharp surface on top of the basal shell bed. In the former case, TSTs consist of a basal shell bed overlain by fining-upwards siliciclastics, and in the latter the shell bed represents the entire TST (e.g., sequence MC at Pakihirua and Torran section).

Highstand systems tract (HST)/Regressive systems tract (RST)

Gradational contacts between HSTs, composed of silty sandstones and terrigenous packstones, and overlying alternating packstones and grainstones assigned to RSTs, indicate uninterrupted deposition during late rise and falling sea level. Thus, the boundary between the HST and RST is somewhat arbitrarily determined, and is referred to as a fuzzy boundary (see Section 6.3.3).

RSTs are made of the carbonate end-member of the mixed carbonate-siliciclastic spectrum composing the Mason Ridge successions. Only at Pakihirua, within sequence MC, the transition from HST sandstone to RST bioclastic limestone is abrupt, and underlain by a thin shell lineation (Figure 21). This exception, which could neither be traced to the south nor to the north, may indicate that the carbonate facies is a FRST, and the contact on which it rests a wave-cut surface of erosion (RSE) produced during sea-level fall.

Detailed mapping of bounding discontinuities is needed to assess this assumption.

7.5.4. Carbonate production development within a sequence stratigraphic framework

The basal part of each high-frequency sequence (with the exception of sequence MB at Mangatai) consists of a shell bed interpreted to be a transgressive bed deposited under moderate- to high-energy conditions. The vertical facies succession above indicates a decrease of current velocity enabling sandstone to siltstone deposition. From the condensed lag, interpreted as a Cdh, which caps the preceding deposits, the upwards

facies transition from fine-grained sandstones to coarse skeletal packstones/grainstones records a shallowing-upwards trend from lower-energy (or deeper-water) deposition to higher-energy (or relatively shallow-water) deposition. The occurrence of subaerial exposure atop shallowing-upwards segments of sequences at Mangatai suggests that not only sediment influx was responsible for accommodation space reduction, but also that the latter was probably accompanied by eustatically-forced shoreline retreat. Consequently, the carbonate deposits and the subaerial-exposure surfaces are interpreted to represent either the late part of the relative stillstand to the early part of the relative fall in sea level, or the late part of the relative fall in sea level.

The lateral poor-traceability or absence of subaerial-exposure surfaces indicates that either (1) in the case of sediment influx-driven shallowing-upwards mechanisms, accommodation space was locally not filled during deposition of the sequences; or (2) the amplitude of eustatic fall was not great enough to expose large areas of the carbonate realm; or (3) the subsequent emplacement of transgressive deposits locally removed the evidence of subaerial exposure.

The remarkable consistency of thickness of both sequences and their internal systems tracts suggests an aggradational stacking pattern (Vail *et al.*, 1991; Goldhammer *et al.*, 1994;) for the Mason Ridge Formation, which makes it difficult to decipher the longer-term depositional trend (shallowing- or deepening-upwards). Nonetheless, the successive drownings that initiated the building of each sequence suggest that deposition occurred during an overall rise of sea level, which enhanced the aggradation potential of carbonate production across the study area (Meyer, 1989), as it probably did for older limestone formations (see for example Sections 7.1.3, 7.2.3, and 7.4.3). In this case, the general lack of subaerial exposure atop the carbonate-dominated RSTs of each sequence probably reflects that sea-level fluctuation maintained carbonate production at rates sufficient to keep-up, but not exceed, the available accommodation space of the depositional realm (see Chapter 3, Section 5.3.3).

7.5.5. Correlation across Ngaruroro River

Beu (1995) commented on the abrupt termination of Matapiro Syncline at the Ngaruroro River (Figure 1), and the lack of match of stratigraphy from north and south of the river. He attributed the poor traceability of Mason Ridge limestone sheets across the river to a vertical offset of rocks south of the normal Ngaruroro River fault in relation to their

northern counterparts. This implies that the lower sequence MB should be underlying the central part of Matapiro Syncline, as suggested by Beu (1995) who correlated it, following Kingma (1971), to Scinde Island Limestone (see Chapter 1, Section 4.6).

The shell bed which overlies discontinuity 24 south of Ngaruroro River, forms a prominent ridge bordering Patanga Stream Valley, easily traceable from Mangatai section northwards to Glencoe Station (Figure 21). This shell bed implies that within the succession underlying discontinuity 24 at Glencoe Station, one sequence is missing (unless the underlying siltstone was not correctly mapped as the Makaretu Mudstone, but is merely a member of sequence MC), which is likely to be sequence MB (i.e., correlated to Scinde Island Limestone). As suggested before, and on the basis of this stratigraphic criterion, it is proposed that sequence MB onlaps the structural high formed by the uplifted block along the southern boundary of Ngaruroro fault, somewhere between the Torran section and Glencoe Station area (Figure 21). This does not contradict the possibility of sequence MB being present further north (across the fault), but points out the probable discontinuous nature of the corresponding limestone sheet in relation to the structural high.

There is little argument to constrain correlation between upper limestones at Glencoe Station and Matapiro Limestone north of Ngaruroro River. However, there are strong similarities in the attributes of interparticle cements within limestones on either side of the river, which consist of thick non-luminescent meteoric cements, different from the CL patterns of cements within limestone occurrences further south (compare CL sequence diagrams in Appendix 5, pages A5 – 30-36). This suggests that limestones at Glencoe Station and further north at Ohiti were subjected to the same fluid systems, though this does not preclude the timing of meteoric water ingress, in other words that limestones were deposited at different times but came under the influence of contemporaneous meteoric fluids.

With this reservation in mind, it is proposed that discontinuity 23 lies at the base of Matapiro Limestone. The nature of surfaces bounding Matapiro Limestone has been presented in Chapter 1 (Section 4.8). A simple sequence stratigraphic interpretation is proposed in the upper left side of Figure 21 that needs more detailed work to be assessed. The sharp contact underlying each prominent shell bed is interpreted as a TSE (discontinuities 25, 26, 27, and 27a).

TIME FRAME FOR PLIOCENE LIMESTONES AND THEIR BUILDING SEQUENCES

New Zealand Stage	Formation			Sedimentary sequences	
	Duration (Ma)		Duration (ka)	Minimum no. of sequences	Duration (ka)
Nukumaruan 2.28-1.57	0.71	Mason Ridge (including the basal Scinde Island Limestone)	<250	4-6	62.5-41.7
Mangapanian 2.79-2.28	0.51	Te Onepu (east)	>175	5	35
		Te Waka (west)	>250?	5-8?	50-31.2
Waipipian 3.6-2.79	0.81	Rotookiwa (east)	100	4	25
		Awapapa (east)	>150	4-12	35-12.5
		Base of Te Waka (west)??	?	?	?
		Titiokura (west)	>200	?	?
Opoitian 5.33-3.6	1.73	Kairakau (east)	<100	4-5	25-20
		+ Tuki Bell limestone	>150	7-8	21.4-19

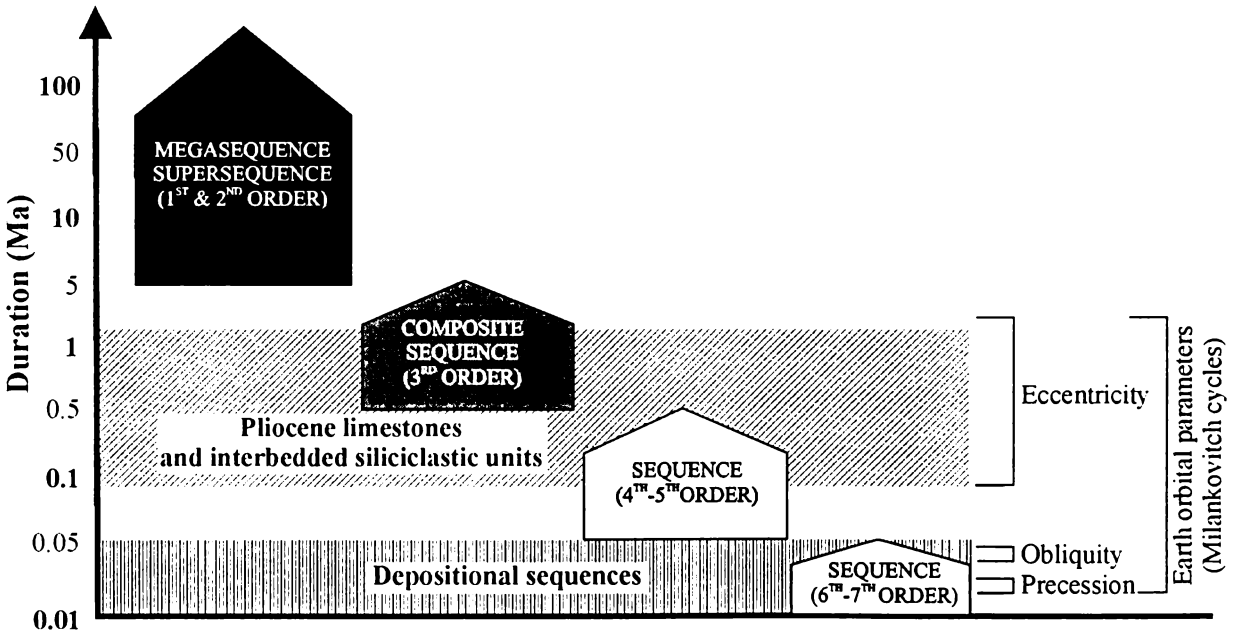

Figure 22- Estimated durations for the deposition of some Pliocene limestones, and duration estimates of their component sequences. If one assumes that all high-frequency sequences were eustatically forced, then their minimum periodicities include the Milankovitch precession and obliquity bands. Pre-Nukumaruan Te Aute limestones and interbedded sandstones and siltstones probably make up a lower order cyclicity, including Milankovitch eccentricity periodicities (3rd- to 4th-order). Mason Ridge Formation includes siltstone-sandstone/limestone formational couplets. Absolute ages for New Zealand Stages from Beu (1995, 2001) and McIntyre (2002). Estimates of Pliocene Te Aute limestones duration from Harmsen (1985), Kamp *et al.* (1988), Beu (1995), and Field *et al.* (1997).

8. Te Aute sedimentary sequences periodicities

8.1. Periodicity approximates

Sequence periodicities are impossible to estimate with any confidence because of an absence of radiometric ages for the Pliocene successions in southern Hawke's Bay. Compounding the inaccuracy of the time interval represented by each limestone formation is the even more untestable possibility that their successive high-frequency building sequences are not of equal duration.

Average durations of the Pliocene limestones and component sequences were estimated on the basis of data from several sources (Harmsen, 1985; Kamp *et al.*, 1988; Beu, 1995; Field *et al.*, 1997), and are summarized in Figure 22. The duration estimates range from 0.1-0.25 Ma for the Pliocene limestones. Minimum duration of the average number of the higher-frequency sequences within the limestones is estimated to range from 20 ka to 60 ka, and thus would include Milankovitch precession and obliquity periodicities if one assumes that the transgressive and transgressive-regressive sequences were eustatically forced.

8.2. Pliocene climate variability from the isotopic record

It is now widely accepted that fluctuations in the extent of polar ice sheets in response to astronomically-driven climatic changes are responsible for high-frequency sea-level oscillations, thereby forcing cyclic stratigraphic and facies depositional architectures in sedimentary basins.

The development of the East and West Antarctic ice sheets to near permanent state in the Middle and Late Miocene, respectively (e.g., Flower and Kennett, 1993; Kennett, 1995), is indicated by an increase in ice-rafted detritus and turbidite sequences deposited on the continental margins near East and West Antarctica, and especially by the stable oxygen-isotope records (i.e., an increase of absolute values of planktic and benthic foraminiferal $\delta^{18}O$). Although there is much evidence away from Antarctica for a significant warming during the Early Pliocene (5-3 Ma; e.g., Dowsett *et al.*, 1992), controversy still exists as to whether this impacted significantly the Antarctic ice sheets and polar climate (Kennett, 1995). A distinct increase in $\delta^{18}O$ in deep-sea sediments during the Late Pliocene between 3 and 2.5 Ma suggests that a major cooling occurred, associated with further ice accumulation on Antarctica that is coincident with the

extensive development of the continental Northern Hemisphere ice sheet (Chen *et al.*, 1995; Shackleton, 1995). From 2.5 Ma onwards, $\delta^{18}O$ fluctuations in deep-water sediments are interpreted to result mostly from the sequential ice volume increase of major ice sheets in the Northern Hemisphere. This implies, at least from mid-Pliocene onwards, the existence of a bipolar "icehouse"-climate system (Head and Nelson, 1994; Kennett, 1995) favouring the development of both high-frequency (e.g., 40 ka) and high-amplitude (e.g., up to 120 m in the Late Quaternary) glacio-eustatic sea-level changes.

High-resolution oxygen-isotope records from the East Pacific (Mix *et al.*, 1995) and the Tasman Sea (Head and Nelson, 1994) show Early Pliocene planktic and benthic foraminifer $\delta^{18}O$ values lighter than for the Late Pliocene-Recent interval, indicative of warmer conditions and/or less ice. Although the oxygen-isotope curves are also characterized by frequencies of around 40 to 50 ka for the time interval 4 Ma (late Opoitian) to 2.5 Ma (latest Mangapanian), they show that the amplitude of variations during the same period was lower than that from the Nukumaruan (post-2.3 Ma) to the Late Quaternary. An expected consequence of such variations is to produce less well-individualized high-frequency (6th- to 7th-order cyclicity) glacio-eustatically-forced sedimentary sequences in the Pliocene than those described in the Pleistocene record.

The Te Aute Pliocene successions appear to conform to this model, with pre-Nukumaruan (pre-2.3 Ma) high-frequency sequences amalgamated, for example, within thick limestone units, while post-Nukumaruan high-frequency sequences consisting of well-individualized siltstone/sandstone – limestone formational couplets.

9. Sequence development and syndepositional tectonic overprint

The possible impact of tectonism on the stratal architecture of the Pliocene successions has been mentioned in Section 6.2. Areas of both anomalously thin and anomalously thick sequences and their component systems tracts are present in the Te Aute successions (e.g., Makara and Te Mata Peak sections of Awapapa Limestone). Changes in the thickness of correlatable sequences, and in the number of component sequences within limestones over their area of distribution, are considered to originate in tectonically-induced changes in accommodation during deposition, which translate through differential uplift/subsidence to produce both local arches and depressions. Formation of local depocentres of increased marine accommodation (Figure 23), in

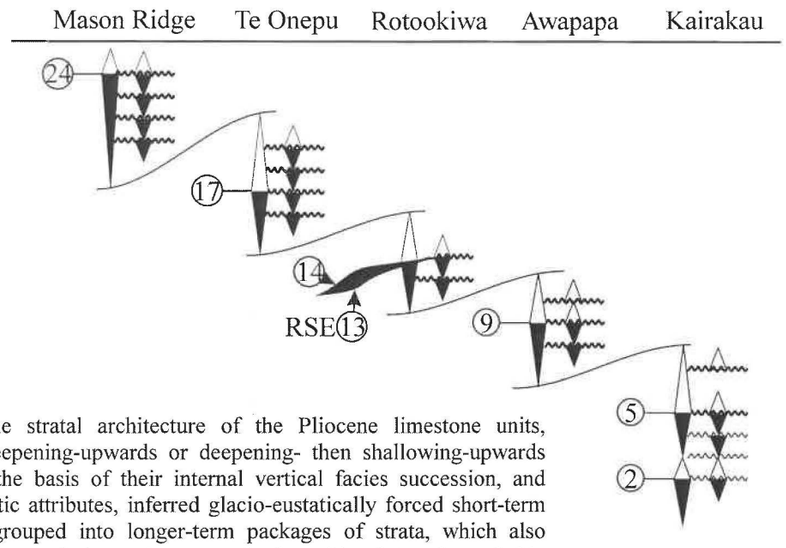

Summary of the stratal architecture of the Pliocene limestone units, consisting of deepening-upwards or deepening- then shallowing-upwards sequences. On the basis of their internal vertical facies succession, and specific diagenetic attributes, inferred glacio-eustatically forced short-term sequences are grouped into longer-term packages of strata, which also define shallowing- and deepening-upwards depositional trends probably driven by a combination of glacio-eustatic and tectonic mechanisms.

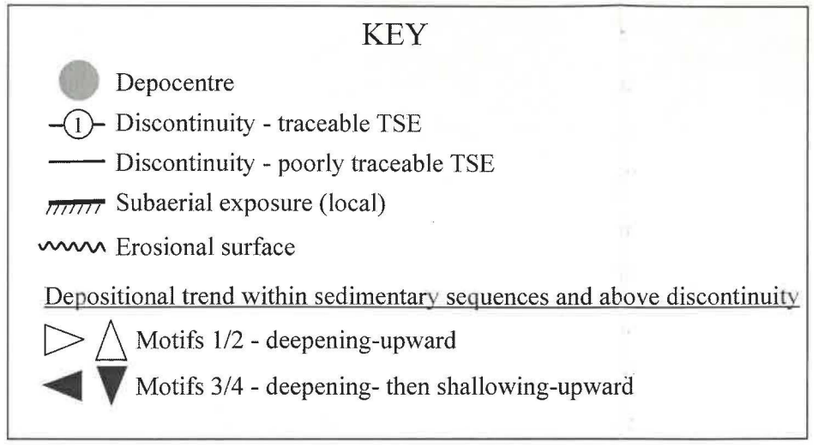

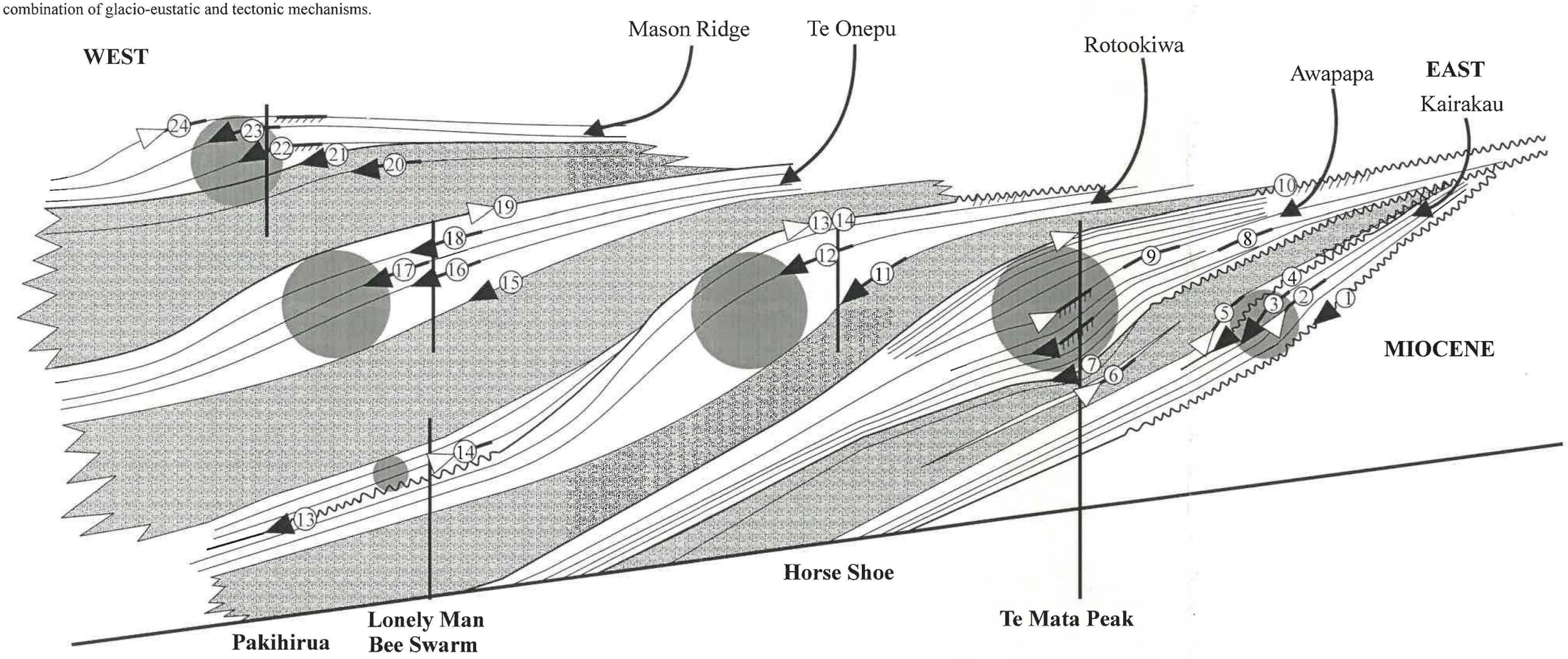

Figure 23- Interpretative E-W cross-section of the development of the various Pliocene limestone units in southern Hawke's Bay as discontinuity-bounded sedimentary sequences. Each limestone unit is constructed of metre-scale (high-frequency) deepening-upwards and/or deepening- then shallowing-upwards sequences that collectively define a lower-order cyclicity. Limestone formation commences as the basin experiences progressive shallowing, and carbonate production terminates after drowning of the depositional realm. See text for details.

which systems tracts maintain their shallow-water depositional aspects (locally showing subaerial exposure), is particularly evident in the Te Mata Peak area.

Although tectonism was apparently coincident with deposition (see Section 4.1), there is no evidence that it recurred with a pulsating or episodic nature with intensities to overlap, and even mimic, that of glacio-eustasy. Previous studies have documented presumable tectonic pulses that operated at a quasi-periodicity of 10^4-10^6 years (Dickinson *et al.*, 1994), which is well above the average duration of the Pliocene sequences (Figure 22). This supports the previous assumption that the major mechanism forcing the stacking of the high-frequency unconformity-bounded sequences has been glacio-eustatically driven.

However, tectonism probably had major effects on the development of the successions by causing local thickness variations, and differential preservation of sequences that resulted in the architectural complexity observed within some of the Te Aute limestone formations.

10. Conclusions

The sequence stratigraphic approach used to subdivide packages of Pliocene carbonate sediments is based on the recognition of discontinuity surfaces bounding them, and of specific diagenetic patterns (part of their pre-compaction diagenetic history) restricted to portions of the building systems tracts.

Transgressive and transgressive-regressive sequences are identified (Figure 23), which are enveloped by transgressive surfaces of erosion, locally coincident with either sequence boundaries (subaerially exposed surfaces) or regressive surfaces of erosion (wave-cut surfaces of erosion developed during early to late fall of sea level). Vertical changes in thickness and depositional facies through the sedimentary sequences, in association with changes in the type and degree of diagenesis that outline vertical patterns of pre-compaction diagenetic suites, and fundamentally the position of bounding discontinuities, define four sedimentary sequence motifs, named Motif 1-4 (Figure 11).

Figure 24 is a schematic representation of an idealized relation between sea level and subsidence that could possibly explain the vertical stacking of depositional facies in each Sedimentary Motif. The absence of RST sediments on top of some sequences, and

Figure 24- Schematic representation of an idealized relation between sea level and subsidence that could possibly explain the vertical stacking of depositional facies in each sedimentary Motif 1-4 (see Figure 11). It is proposed that the sedimentary sequence architecture defining Motifs 1-4 is a function of the combined effects of the relative sea-level amplitude, the duration of a eustatic cycle, the carbonate production rate, tectonics, and the amount of material removed during erosional processes associated with regression and ensuing transgression. The model infers that the rate of sediment influx is not uniform through a cycle, but reflects conditions of carbonate production under the law of sigmoidal growth (see Chapter 3, Figure 22; Neumann and MacIntyre, 1985). The rate of subsidence is assumed to be uniform. Another main assumption of the model is that the internal facies architecture results from changes in accommodation created through differences between the rate of eustatic sea-level fall (or rise) and the rate of subsidence. The position of inflection points on the sea-level curve determines the stratigraphic position of the sequence-bounding discontinuities and systems tracts boundaries. Specifically, a transgressive surface of erosion (probably preceded by a regressive surface of erosion) develops when sea level rises, and corresponds to the process of erosional translation of the shoreface profile upward and landward. The absence of RST sediments on top of some sequences, and the uncommonness of FRST deposits, is inferred to originate in the erosional process that accompanies sea-level fall and the ensuing transgression (Figure 9). The erosion recorded by TSEs, represented by the time gap between the deposition of the last sediments beneath the TSE and the first sediments on top of it, is assumed to comprise erosional processes that occurred during the preceding regression, if the latter was not normal. Thus, transgressive surfaces of erosion on top of Motif 1, Motif 2, and possibly Motif 3, are likely to overprint earlier regressive surfaces of erosion (RSE), and therefore record many metres of erosion. See conclusions for comment.

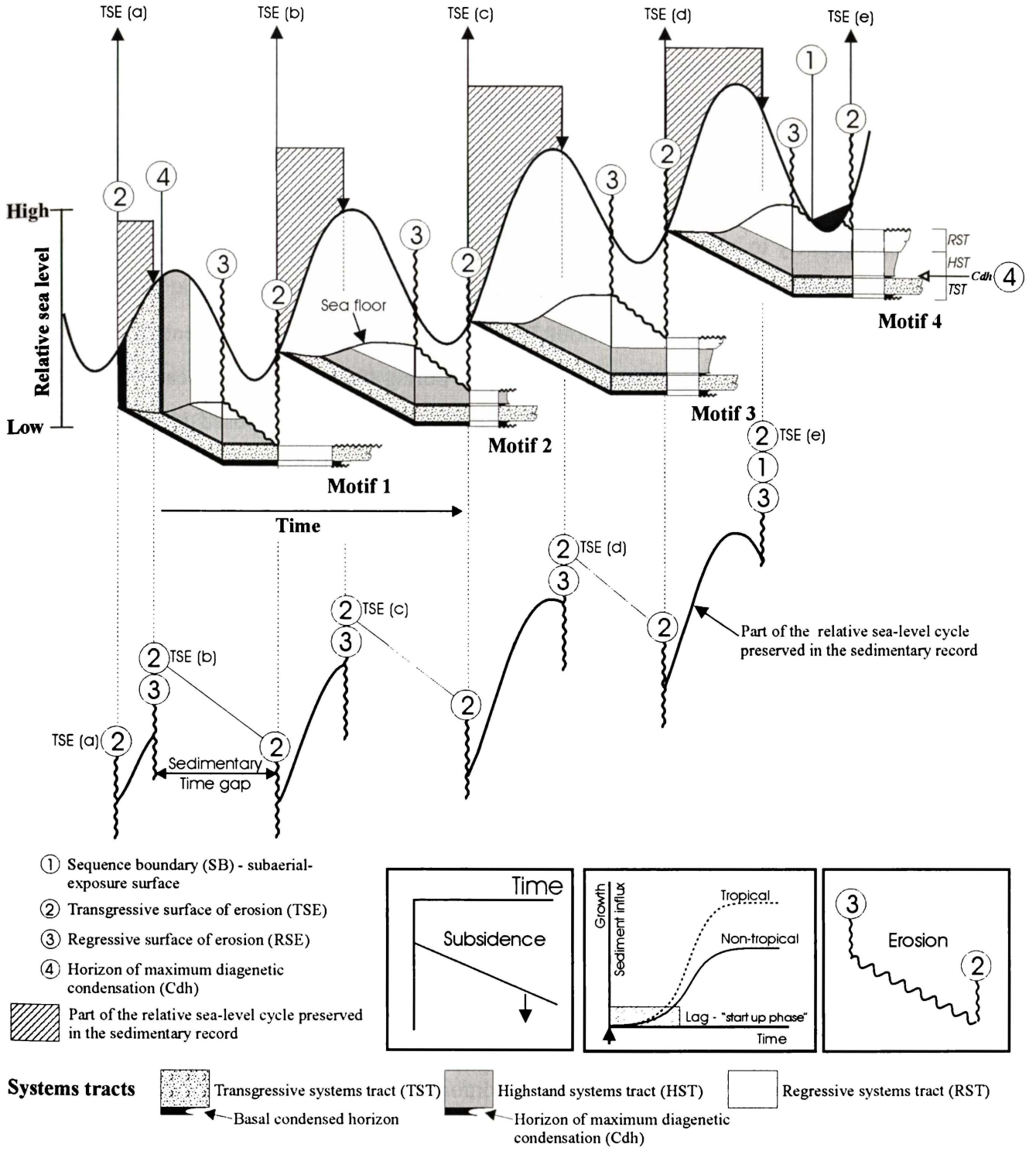
TSE (a)
TSE (b)
TSE (c)
TSE (d)
TSE (e)
High
Relative sea level
Low
Sea floor
RST
HST
TST
Cdh
Motif 1
Motif 2
Motif 3
Motif 4
Time
Sedimentary
Time gap
Part of the relative sea-level cycle
preserved in the sedimentary record
① Sequence boundary (SB) - subaerial-exposure surface
② Transgressive surface of erosion (TSE)
③ Regressive surface of erosion (RSE)
④ Horizon of maximum diagenetic condensation (Cdh)
Part of the relative sea-level cycle preserved in the sedimentary record
Time
Subsidence
Growth
Sediment influx
Tropical
Non-tropical
Lag - "start up phase"
Time
Erosion
Systems tracts
Transgressive systems tract (TST)
Basal condensed horizon
Highstand systems tract (HST)
Horizon of maximum diagenetic condensation (Cdh)
Regressive systems tract (RST)

the uncommonness of FRST deposits, is inferred to originate in the erosional process that accompanies sea-level fall and the ensuing transgression (Figures 9, 24).

The stratal architectures of Sedimentary Motifs are considered in this model to be proxies for the erosion that occurred prior to the final generation of the upper bounding physical surface interpreted as a TSE. Motifs 1 to 4 represent increasingly preserved portions of the relative sea-level record (i.e., longer segments), which translates in the superjacent TSE to representing decreasing amounts of sediment having been removed by erosion (likely to coincide with shorter time gaps). If the drowning event, following regression, apparently occurs during the rising segment of the sea-level curve, a Motif 1 is generated, whereas Motif 2 and Motif 3 are generated when drowning events seem to interrupt the course of the normal sea-level cycle during the late-rising and early-falling segment of the relative sea-level curve. The capping subaerially exposed surface that defines Motif 4 forms when the rate of sea-level fall exceeds the rate of subsidence, and where the sea level intersects the sea-floor elevation. Any superimposed transgressive surface of erosion would develop after the formation of a subaerial unconformity has been initiated.

This oversimplified model is regarded as a basic depositional scheme whose main interests are that: (1) it does not preclude the origin of sea-level changes during the deposition of each sedimentary sequence. The driving-mechanism could be glacio-eustatic, tectonic, or internal (see below). The linear interpolation for the rate of subsidence would then correspond to a background-subsidence upon which the former processes are superimposed; (2) it does not preclude the origin of the stacking pattern of sequences, which could also be tectonic, glacio-eustatic, or driven by internal (autocyclic) processes; and (3) the comparison of the model with observed field data is most likely to highlight significant differences, which subsequently may be better explained.

The time span represented by the unconformity-bounded sequences ranges from c. 20 to 60 ka. These sequences are interpreted to record fluctuations in the rate of carbonate production, which for the pre-Nukumaruan limestones occurred in the vicinity of structural highs where high-energy currents, in a cool-water seaway, favoured terrigenous sediments by-passing, and promoted filter feeding skeletal associations.

Variations in carbonate production for the Te Aute limestones are thought to be produced in response to a combination of glacio-eustatically forced Milankovitch oscillations (precession) and tectonism.

Local thickness variations of sequences, and development of depocentres in the pre-Nukumaruan carbonate successions, are considered to reflect tectonically-induced contrasting conditions of accommodation at a regional scale (Figure 23). As a result, the stratal architecture of individual formations is complex, and renders the traceability of discontinuity surfaces difficult, even over short distances.

In contrast, Nukumaruan limestone sheets and interbedded siltstones - sandstones are laterally continuous, display minor thickness variations, and comprise facies associations characterized by higher contents of infaunal aragonitic molluscs and muddier rock frameworks, which collectively indicate that by Late Pliocene the depositional environment had changed in southern Hawke's Bay. Previous authors have suggested that continuing shallowing and narrowing of the forearc basin eventually led to the development of flat embayments and platform-type margins in the Late Pliocene (Kamp and Nelson, 1988; Haywick, 1990; Beu, 1995; Field *et al.*, 1997).

The stratal architecture of Nukumaruan limestones (Mason Ridge and Matapiro), which is typically cyclothemic in southeastern and central Hawke's Bay, shows the influence of glacio-eustatically driven processes, including the Milankovitch precession and obliquity periodicities. The sedimentary successions can be grouped into siltstone/sandstone - limestone formational couplets (i.e., sequences), which contain distinct systems tracts (TST, HST, RST, and possibly FRST) bounded by easily traceable surfaces (TSEs and local subaerial-exposure surfaces).

References

Abbott, S. T. & Carter, R. M. (1990) *Seismic sequence analysis of Plio-Pleistocene cyclothems, Wanganui Basin, New Zealand. A field workshop for the Basin Studies Group of the Geological Survey of New Zealand.* Marine Geophysical Laboratory, James Cook University, Townsville, 113 pp.

Abbott, S. T. & Carter, R. M. (1994) The sequence architecture of Mid-Pleistocene (c.1.1-0.4Ma) cyclothems from New-Zealand: Facies development during a period of orbital control on sea-level cyclicity. In: *Orbital forcing and cyclic sequences, Vol. 19* (Ed. by P. L. de Boer and D.G. Smith), pp. 367-394. Spec. Publ. of the International Association of Sedimentologists.

Alexandersson, E. T. (1978) Destructive diagenesis of carbonate sediments in the eastern Skagerrak, North Sea. *Geology*, **6**, 324-327.

Amorosi, A. (1995) Glaucony and sequence stratigraphy: a conceptual framework of distribution in siliciclastic sequences. *Journal of Sedimentary Research*, **B65**(4), 419-425.

Arnott, R. W. C. (1995) The parasequence definition - Are transgressive deposits inadequately addressed? *Journal of Sedimentary Research*, **B65**(1), 1-6.

Bathurst, R. G. C. (1975) *Carbonate sediments and their diagenesis.* Elsevier, North Holland, 658 pp.

Beu, A. G. (1995) *Pliocene Limestones and Their Scallops.* Monograph 10, Institute of Geological & Nuclear Sciences Limited, Lower Hutt, New Zealand, 243 pp.

Beu, A. G. (2001) Local stages to be used for the Wanganui series (Pliocene-Pleistocene) and their means of definition. *New Zealand Journal of Geology and Geophysics*, **44**, 113-125.

Beu, A. G., Grant-Taylor, T. L. & Hornibrook, N. d. B. (1980) The Te Aute limestone facies, Poverty Bay to northern Wairarapa, pp. 36. Dept. of Scientific and Industrial Research, Wellington.

Bhattacharya, J. P. & Willis, B. J. (2001) Lowstand deltas in the Frontier Formation, Powder River basin, Wyoming: implications for sequence stratigraphic models. *American Association of Petroleum Geologists Bulletin*, **85**(2), 261-294.

Boreen, T., James, N. P., Heggie, D. & Wilson, C. (1993) Surficial cool-water carbonate sediments on the Otway continental margin, southeastern Australia. *Marine Geology*, **112**, 35-56.

Boreen, T. D. & James, N. P. (1995) Stratigraphic sedimentology of tertiary cool-water limestones, SE Australia. *Journal of Sedimentary Research*, **B65**(1), 142-159.

Caron, V., Bernier, P., Keraudren, B. & Dalongeville, R. (1998) Les séquences diagénétiques des calcarénites littorales du Pléistocène récent de Crète septentrionale: une aide à la résolution de problèmes de corrélation. *Bulletin de la Société Géologique de France*, **169**(3), 415-424.

Carter, R. M., Fulthorpe, C. S. & Naish, T. R. (1998) Sequence concepts at seismic and outcrop scale: the distinction between physical and conceptual stratigraphic surfaces. *Sedimentary Geology*, **122**, 165-179.

Cashman, S. M., Kelsey, H. M., Erdman, C. F., Cutten, H. N. C. & Berryman, K. R. (1992) Strain partitioning between structural domains in the forearc of the Hikurangi subduction zone, New Zealand. *Tectonics*, **11**(2), 242-257.

Chen, J., Farrell, J. W., Murray, D. W. & Prell, W. L. (1995) Timescale and paleoceanographic implications of a 3.6 m.y. oxygen isotope record from the northeast Indian Ocean (Ocean Drilling Program site 758). *Paleoceanograhy*, **10**(1), 21-47.

Clari, P. A., Dela Pierre, F. D. & Martire, L. (1995) Discontinuities in carbonate successions: Identification, interpretation and classification of some italian examples. *Sedimentary Geology*, **100**, 97-122.

Demarest, J. M. & Kraft, J. C. (1987) Stratigraphic record of Quaternary sea levels: implications for more recent strata. In: *Sea-level Fluctuation and Coastal Evolution, Vol. 41* (Ed. by D. Nummedal), pp. 223-240. SEPM Spec. Publ.

Dickinson, W. R., Soreghan, G. S. & Giles, K. A. (1994) Glacio-eustatic origin of Permo-Carboniferous stratigraphic cycles: evidence from the southern Cordilleran foreland region. In: *Tectonic and Eustatic Controls on Sedimentary Cycles, Vol. 4* (Ed. by J. M. Dennison and F. R. Ettensohn), pp. 25-34. SEPM, Tulsa. *Concepts in Sedimentology and Paleontology.*

Dickson, J. A. D. (1965) A modified staining technique for carbonates in thin-section. *Nature*, **205**, 587.

Dorobek, S. L. (1987) Petrography, geochemistry and origin of burial diagenetic facies, Siluro-Devonian Helderberg Group (Carbonate rocks), Central Appalachians. *American Association of Petroleum Geologists Bulletin*, **71**(5), 492-514.

Dowsett, H. J., Cronin, T. M., Poore, R. Z., Thompson, R. S., Whatley, R. C. & Wood, A. M. (1992) Micropaleontological evidence for increased meridional heat transport in the North Atlantic during the Pliocene. *Science*, **258**, 1133-1135.

Embry, A. F. (1995) Sequence boundaries and sequence hierarchies: problems and proposals. In: *Sequence Stratigraphy: Advances and Applications for Exploration and Production in Northwest Europe* (Ed. by V. L. F. R. J. Steel, E. P. Johannesen and C. Mathieu), pp. 1-11.

Embry, A. F. & Johannessen, E. P. (1992) T-R sequence stratigraphy, facies analysis and reservoir distribution in the uppermost Triassic-Lower Jurassic succession, western Sverdup Basin, Arctic. In: *Arctic Geology and Petroleum Potential, Vol. 2* (Ed. by T. O. Vorren, E. Bergsager, O. A. Dahl-Stamnes, E. Holter, B. Johansen, E. Lie and T. B. Lund), pp. 121-146. NPF Special Publication.

Esteban, M. & Klappa, C. F. (1983) Subaerial exposure environment. In: *Carbonate Depositional Environments, Vol. 33* (Ed. by P. A. Scholle, B. G. Bebout and C. H. Moore), pp. 1-54. American Association of Petroleum Geologists Memoir.

Field, B. D., Uruski, C. I., *et al.* (1997) *Cretaceous-Cenozoic Geology and Petroleum Systems of the East Coast Region, New Zealand.* Monograph 19, Institute of Geological and Nuclear Sciences Limited, Lower Hutt, New Zealand, 301 pp.

Flower, B. P. & Kennett, J. P. (1993) Middle Miocene ocean/climate transition: high-resolution oxygen and carbon isotopic records from DSDP Site 588A, southwest Pacific. *Paleoceanography*, **8**(6), 811-843.

Gillespie, J. L. (1992) Late Quaternary Carbonate-Clastic Sedimentation on a Temperate Shelf, Offshore Wanganui, New Zealand. M. Sc. Unpublished, Waikato.

Ginsburg, R. N. (1971) Landward movement of carbonate mud: new model for regressive cycles in carbonates. *American Association of Petroleum Geologists Bulletin*, **55**, 340-340.

Goldhammer, R. K., Oswald, E. J. & Dunn, P. A. (1994) High-frequency, glacio-eustatic cyclicity in the Middle Pennsylvanian of the Paradox Basin: an evaluation of Milankovitch forcing. *International Association of Sedimentologists Special Publication*, **19**, 243-283.

Goldstein, R. H. (1988) Cement stratigraphy of Pennsylvanian Holder Formation, Sacramento Mountains, New Mexico. *American Association of Petroleum Geologists Bulletin*, **72**(4), 425-438.

Grover Jr, G. & Read, J. F. (1983) Paleoaquifer and deep burial related cements defined by regional cathodoluminescent patterns, Middle Ordoviscian carbonates, Virginia. *American Association of Petroleum Geologists Bulletin*, **67**(8), 1275-1303.

Hardie, L. A., Dunn, P. A. & Goldhammer, R. K. (1991) Field and modelling studies of Cambrian carbonate cycles, Virginia Appalachians: a discussion. *Journal of Sedimentary Petrology*, **61**, 636-646.

Harmsen, F. J. (1984) *Stratigraphic sections of the Pliocene Te Aute Group in Central and Southern Hawke's Bay, New Zealand.* Geology Department, Victoria University, Wellington, New Zealand, 109 pp.

Harmsen, F. J. (1985) Lithostratigraphy of Pliocene Strata, Central and Southern Hawke's Bay, New Zealand. *New Zealand Journal of Geology and Geophysics*, **28**, 413-433.

Hayton, S., Nelson, C. S. & Hood, S. D. (1995) A skeletal assemblage classification system for non-tropical carbonate deposits based on New Zealand Cenozoic limestones. *Sedimentary Geology*, **100**, 123-141.

Haywick, D. W. (2000) Recognition and distinction of normal and forced regression in cyclothemic strata: a Plio-Pleistocene case study from eastern North Island, New Zealand. In: *Sedimentary Responses to Forced Regressions, Vol. 172* (Ed. by D. Hunt and R. L. Gawthorpe), pp. 193-215. Geological Society of London Special Publications, London.

Haywick, D. W., Carter, R. M. & Henderson, R. A. (1992) Sedimentology of 40 000 year Milankovitch-controlled cyclothems from Central Hawke's Bay, New Zealand. *Sedimentology*, **39**, 675-696.

Haywick, D. W., Lowe, D. A., Beu, A. G., Henderson, R. A. & Carter, R. M. (1991) Pliocene-Pleistocene (Nukumaruan) lithostratigraphy of the Tangoio block, and origin of sedimentary cyclicity, central Hawke's Bay, New Zealand. *New Zealand Journal of Geology and Geophysics*, **34**, 213-225.

Haywick, D. W. N. (1990) Stratigraphy, sedimentology, paleoecology and diagenesis of the Petane Group (Pliocene-Pleistocene) in the Tangoio, central Hawke's Bay, New Zealand. Unpublished PhD Thesis, James Cook University of North Queensland, Australia.

Heckel, P. H. (1986) Sea-level curve for Pennsylvanian eustatic marine transgressive-regressive depositional cycles along Midcontinent outcrop belt. *Geology*, **14**, 330-334.

Head, H. S. & Nelson, C. S. (1994) A high-resolution oxygen isotope record for the past 6.4 million years at DSDP Site 593, Challenger Plateau, southern Tasman Sea. In: *Evolution of the Tasman Sea Basin* (Ed. by G. J. Van Der Lingen, K. M. Swanson & R. J. Muir), A.A. Balkema, pp. 159-179.

Hood, S. D. (1993) Skeletal and diagenetic petrofacies of temperate-latitude limestones, North Island, New Zealand. Unpublished MsC Thesis, University of Waikato.

Hornibrook, N. d. (1992) New Zealand paleoclimates: a review based on the distribution of some shallow water and terrestrial biota. In: *Pacific: Neogene Environment, Evolution and Events* (Ed. by R. Tsuchi and J. C. Ingle Jr), pp. 83-106. University of Tokyo, Tokyo.

Hunt, D. & Tucker, M. E. (1995) Stranded parasequences and the forced regressive wedge systems tract: deposition during base level fall - reply. *Sedimentary Geology*, **95**, 147-160.

Ishibashi, K. (1987) Faulting of the Hawke's Bay earthquake and its implications in subduction tectonics in the Hikurangi Margin, North Island, New Zealand (Preliminaries). In: *Holocene Coastal Tectonics of Eastern North Island, New Zealand* (Ed. by Y. Ota), pp. 97-99.

James, N. P. (1997) The cool-water carbonate depositional realm. In: *Cool-Water Carbonates* (Ed. by N. P. James and J. A. D. Clarke), SEPM Special Publication, **56**, 1-22.

James, N. P. & Choquette, P. W. (1990) Limestones - The meteoric diagenetic environment. In: *Diagenesis, Vol. Reprint series 4* (Ed. by I. A. McIlreath and D.W. Morrow), pp. 35-74. Geoscience Canada.

Kamp, P. J. J., Harmsen, F. J., Nelson, C. S. & Boyle, S. F. (1988) Barnacle-dominated limestone with giant cross-beds in a non-tropical, tide swept, Pliocene forearc seaway, Hawke's Bay, New Zealand. *Sedimentary Geology*, **60**, 173-195.

Kamp, P. J. J. & Naish, T. (1997) Forward modelling of the sequence stratigraphic architecture of shelf cyclothems: Application to Late Pliocene sequences, Wanganui basin (New Zealand). *Sedimentary Geology*, **00**, 1-24.

Kamp, P. J. J. & Nelson, C. S. (1987) Tectonic and sea-level controls on non-tropical limestones in New Zealand. *Geology*, **15**, 610-613.

Kamp, P. J. J. & Nelson, C. S. (1988) Nature and occurrence of modern and Neogene active margin limestones in New Zealand. *New Zealand Journal of Geology and Geophysics*, **31**, 1-20.

Kelsey, H. M., Erdman, C. F. & Cashman, S. M. (1993) Geology of Southern Hawke's Bay from the Maraetotara Plateau and Waipawa westward to the Wakara Range and the Ohara depression, pp. 1-17. Institute of Geological & Nuclear Sciences, Lower Hutt, New Zealand.

Kennett, J. P. (1995) A review of polar climatic evolution during the Neogene, based on the marine sediment record. In: *Paleoclimate and Evolution, with Emphasis on Human Origins* (Ed. By E. S. Urba, G. H. Denton, T. C. Partridge & L. H. Burckle), Yale University, pp. 49-64.

Kidwell, S. M. (1991a) Taphonomic feedback (live/dead interactions) in the genesis of bioclastic beds: keys to reconstructing sedimentary dynamics. In: *Cycles and events in Stratigraphy* (Ed. by G. Einsele, W. Ricken and A. Seilacher), pp. 268-282. Springer-Verlag, Heidelberg, Germany.

Kidwell, S. M. (1991b) Condensed deposits in siliciclastic sequences: expected and observed features. In: *Cycles and events in Stratigraphy* (Ed. by G. Einsele, W. Ricken and A. Seilacher), pp. 682-695. Springer-Verlag, Heidelberg, Germany.

Kingma, J. T. (1971) Geology of Te Aute Subdivision. *New Zealand Geological Survey Bulletin*, **70**, 173.

López-Blanco, M., Marzo, M. & Piña, J. (2000) Transgressive-regressive sequence hierarchy of foreland, fan-delta clastic wedges (Montserrat and Sant Llorenç del Munt, Middle Eocene, Ebro Basin, NE Spain). *Sedimentary Geology*, **138**, 41-69.

McIntyre, A. (2002) Geology of Mangapanian (Late Pliocene) strata, Wanganui Basin: lithostratigraphy, paleontology, and sequence stratigraphy. Unpublished PhD Thesis, University of Waikato, 431p.

Melim, L. A., Westphal, H., Swart, P. K., Eberli, G. P. & Munnecke, A. (in press) Questioning carbonate diagenetic paradigms: evidence from the Neogene of the Bahamas. *Marine Geology*.

Meyer, F. O. (1989) Siliciclastic influence on Mesozoic platform development: Baltimore canyon trough, Western Atlantic. In: *Controls on Carbonate Platform and Basin Development, Vol. 44* (Ed. by P. D. Crevello, J. L. Wilson, J. F. Sarg and J. F. Read), pp. 213-232. SEPM Special Publication, Tulsa, USA.

Mix, A. C., Pisias, N. G., Rugh, W., Wilson, J., Morey, A. & Hagelberg, T. K. (1995) Benthic foraminifer stable isotope record from site 849 (0-5 Ma): local and global isotope changes. In: *Proceedings of the Ocean Drilling Program, Scientific Results* (Ed. by N. G. Pisias, L. A. Mayer, T. R. Janacek, A. Palmer-Julson & T. H. van Handel), **138**, 371-390.

Monstad, S. (2000) Carbonate sedimentation on inactive fan-delta lobes: response to sea-level changes, Sant Llorenç del Munt fan-delta complex, NE Spain. *Sedimentary Geology*, **138**, 99-124.

Naish, T. & Kamp, P. J. J. (1997) Sequence stratigraphy of sixth-order (41 k.y.) Pliocene-Pleistocene cyclothems, Wanganui basin, New Zealand: A case for the regressive systems tract. *Geological Society of America Bulletin*, **109**(8), 978-999.

Naish, T. R. & Kamp, P. J. J. (1995) Pliocene-Pleistocene marine cyclothems, Wanganui basin, New Zealand: a lithostratigraphic framework. *New Zealand Journal of Geology and Geophysics*, **38**, 223-243.

Nelson, C. S. (1988a) An Introductory perspective on non-tropical shelf carbonates. *Sedimentary Geology*, **60**, 3-12.

Nelson, C. S., Keane, S. L. & Head, P. S. (1988b) Non-tropical carbonate deposits on the modern New Zealand Shelf. *Sedimentary Geology*, **60**, 71-94.

Neumann, A. C. & MacIntyre, I. (1985) Reef response to sea-level rise: keep-up, catch-up or give-up. In: *Fifth International Coral Reef Congress, Vol. 3*, pp. 105-110, Tahiti.

Niemann, J. C. & Read, J. F. (1988) Regional cementation from unconformity-recharged aquifer and burial fluids, Mississippian Neuman Limestone, Kentucky. *Journal of Sedimentary Petrology*, **58**(4), 688-705.

Nummedal, D., Riley, G. W. & Templet, P. L. (1993) High-resolution sequence architecture: a chronostratigraphic model based on equilibrium profile studies. In: *Sequence Stratigraphy and Facies Association, Vol. 18* (Ed. by H. Posamentier, C. P. Summerhayes, B. U. Haq and C. P. Allen), pp. 55-68. SEPM Special Publication.

Nummedal, D. & Swift, D. J. P. (1987) Transgressive stratigraphy at sequence-bounding unconformities: Some principles derived from Holocene And Cretaceous examples. In: *Sea-level Fluctuation and*

Coastal Evolution, Vol. 41 (Ed. by D. Nummedal, O. H. Pilkey and H. J.D.), pp. 241-260. SEPM Special Publication, Tulsa, USA.

Posamentier, H. W., Allen, G. P., James, D. P. & Tesson, M. (1992) Forced regressions in a sequence stratigraphic framework: concepts, examples, and exploration significance. *American Association of Petroleum Geologists Bulletin*, **76**(11), 1687-1709.

Schlager, W. (1999) Type 3 sequence boundary. In: *Advances in Carbonate Sequence Stratigraphy: Application to Reservoirs, Outcrops and Models, Vol. 63* (Ed. by P. M. Harris, A. H. Saller and J. A. Simo), pp. 35-45. SEPM Special Publication, Tulsa, USA.

Shackleton, N. J., Berger, A. & Peltier, W. R. (1990) An alternative astronomical calibration of the lower Pleistocene time scale based on ODP site 677. *Transactions of the Royal Society of Edinburgh*, **81**, 251-261.

Shackleton, N. J. (1995) New data on the evolution of Pliocene climatic variability. In: *Paleoclimate and Evolution, with Emphasis on Human Origins* (Ed. By E. S. Urba, G. H. Denton, T. C. Partridge & L. H. Burckle), Yale University, pp. 242-248.

Steinhauff, D. M. & Walker, K. R. (1995) Recognizing exposure, drowning and missed beats. *Journal of Sedimentary Research*, **B65**(2), 183-207.

Vail, P. R., Audemard, F., Bowman, S. A., Eisner, P. N. & Perez-Cruz, C. (1991) The stratigraphic signatures of tectonics, eustasy and sedimentology - an overview. In: *Cycles and Events in Stratigraphy* (Ed. by G. Einsele, W. Ricken and A. Seilacher), pp. 617-659. Springer-Verlag, Berlin Heidelberg.

Vail, P. R., Hardenbol, J. & Todd, R. G. (1984) Jurassic unconformities, chronostratigraphy, and sea level changes from seismic stratigraphy and biostratigraphy. In: *Interregional Unconformities and Hydrocarbon Accumulation, Vol. 36* (Ed. by J. S. Schlee), pp. 129-144. *American Association of Petroleum Geologists* Memoir, Tulsa, USA.

Van Der Heide, S. (1950) Compaction as a possible factor in Upper Carboniferous rhythmic sedimentation. *Report of the 18th International Geologic Congress*, **4**, 38-45.

Van Wagoner, J. C. (1996) Overview of sequence stratigraphy of foreland basin deposits: terminology, summary of papers, and glossary of sequence stratigraphy. *American Association of Petroleum Geologists Memoir*, **64**, ix-xxi.

Van Wagoner, J. C., Mitchum, R. M. J., Campion, K. M. & Rahmanian, V. D. (1990) *Siliciclastic sequence stratigraphy in well logs, cores and outcrop*, 55 pp.

Van Wagoner, J. C., Mitchum, R. M. J., Posamentier, H. W. & Vail, P. R. (1987) Seismic stratigraphy interpretation using sequence stratigraphy. Part 2: key definitions of sequence stratigraphy. In: *Atlas of Seismic Stratigraphy, Vol. 27* (Ed. by A. W. Bally), pp. 11-14. American Association of Petroleum Geologists Bulletin - Studies in Geology.

Van Wagoner, J. C., Posamentier, H. W., Mitchum, R. M. J., Vail, P. R., Sarg, J. F., Loutit, T. S. & Hardenbol, J. (1988) An overview of the fundamentals of sequence stratigraphy and key definitions. In: *Sea-Level Changes: An Integrated Approach, Vol. 42* (Ed. by C. K. Wilgus, B. S.

Hastings, C. G. St. C. Kendall, H. W. Posamentier, C. A. Ross and J. C. Van Wagoner), pp. 39-45. SEPM Special Publication.

Vella, P. (1963) Plio-Pleistocene cyclothems, Wairarapa, New Zealand. *Transactions of the Royal Society of New Zealand*, **2**(2), 15-50.

Walker, R. G. (1995) Sedimentary and tectonic origin of a transgressive surface of erosion: Viking Formation, Alberta, Canada. *Jounal of Sedimentary Research*, **B65**(2), 209-221.

Walker, R. G. & Wiseman, T. R. (1995) Lowstand shorefaces, transgressive incised shorefaces, and forced regressions: examples from the Viking Formation, Joarcam area, Alberta. *Journal of Sedimentary Research*, **B65**(1), 132-141.

Walls, R. A., Harris, W. B. & Nunan, W. E. (1975) Calcareous crust (caliche) profiles and early subaerial exposure of carboniferous carbonates, Noertheastern Kentucky. *Sedimentology*, **22**, 417-440.

Womardt, W. W. & Vail, P. R. (1991) Tentative revision of the global Plio-Pleistocene sequences based on the sequence stratigraphy in the Gulf of Mexico. *American Association of Petroleum Geologists Bulletin*, **75**, 1425 (abstract).

Wright, V. P. (1982) The recognition and interpretation of paleokarsts: Two examples from the lower carboniferous of South Wales. *Journal of Sedimentary Petrology*, **52**(1), 83-94.

Wright, V. P. & Smart, P. L. (1994) Paleokarst (dissolution diagenesis): Its occurrence and hydrocarbon exploration significance. In: *Diagenesis, developments in sedimentology, Vol. 51* (Ed. by K. H. Wolf and G. V. Chilingarian), pp. 477-517. Elsevier Science BV, Amsterdam.

Chapter 5

DIAGENETIC SEQUENCE STRATIGRAPHY OF CALCITE CEMENT SUCCESSIONS IN PLIOCENE TE AUTE COOL-WATER LIMESTONES, SOUTHERN HAWKE'S BAY, NEW ZEALAND

Abstract 349
1. Introduction 351
2. Analytical methods 354
3. Concept of CL sequence stratigraphy 357
4. Application of the concept of CL sequence to the Te Aute limestones 365
5. Sequence stratigraphic approach to cool-water carbonate diagenesis of the Te Aute Pliocene limestones 410
6. Conclusions 430
References 434

Key Sections: 1, 3, 4.1, 4.2, 4.4, 4.5, 4.6, 5, 6
Key Figures: 1, 2, 5, 7, 8, 10, 11, 14, 15, 18

Chapter 5

DIAGENETIC SEQUENCE STRATIGRAPHY OF CALCITE CEMENT SUCCESSIONS IN PLIOCENE TE AUTE COOL-WATER LIMESTONES, SOUTHERN HAWKE'S BAY, NEW ZEALAND

ABSTRACT: Concepts that classically underpin the sequence stratigraphic analysis of sedimentary successions have been used to group zoned cement successions of the Pliocene (Opoitian to Nukumaruan) Te Aute limestones, revealed under cathodoluminescent (CL) light, into diagenetic discontinuity-bounded CL sequences. A CL sequence is a genetically-related succession of cement zones bounded by correlative diagenetic discontinuities, including dissolution surfaces, renucleation surfaces, and/or fractures, which are traceable vertically over several tens of metres, and laterally over several kilometres.

In the Early Pliocene (Opoitian) Kairakau Limestone, the procedure identifies a distinct succession of five CL sequences, termed KZ and KA to KD, and referred to collectively as the *Kairakau motif*. CL sequence KZ locally consists of marine turbid cements (now low-Mg calcite, originally probably intermediate-Mg calcite) growing upon the abraded surface of skeletons and bounded above by a dissolution surface at the base of the next CL sequence KA. The KZ cements are poorly correlatable, and are only found associated with shallow-water facies from above and below marine ravinement surfaces. CL sequence KA is enveloped by a dissolution surface at the base and by a fracturing surface at the top. Clear spar cements within CL sequence KA stain pink, are non-luminescent, and mainly formed from oxidizing, meteoric waters in a regional aquifer that formed during a likely localized emergent event associated with a relative sea-level drop in the late Opoitian. CL sequence KB comprises the first generation of post-compaction fracture-hosted cements. The low-Mg calcite cement stains blue, shows a brown to orange dull luminescent zonation, and its percentage volume is highest in the southeast of the study region, which is proposed as the probable recharge area for an extended confined aquifer system of meteoric or mixed marine-meteoric origin. CL sequence KC is bounded by dissolution surfaces superposed to uplift-related fractures. It consists of pink, non-luminescent, low-Mg calcite cements, which constitute the volumetrically dominant carbonate precipitates, especially along a north-south trending

line coincident with the axis of the former forearc basin on the eastern margin of which the Kairakau sediments accumulated. The abundance of this telogenetic cement within the Kairakau Limestone diminishes eastwards and southwards, assumed to represent the gravity-driven flow direction of the cementing aquifer. CL sequence KD is the least abundant cementing phase. The cement suite consists of a bright-luminescent zone overgrown by non-luminescent cement. Both CL sequences KC and KD are interpreted as tectonic-related cementing phases that formed from meteoric, dominantly oxidizing, waters.

The same *Kairakau motif* is present in the younger Waipipian-age Awapapa and Rotookiwa, and the Mangapanian-age Te Onepu Limestones. On the basis of geochemical data, and paleogeographic and tectonic considerations, it is proposed that pre-compaction non-ferroan clear spar CL sequences within Kairakau, Awapapa, and Rotookiwa (and possibly Te Onepu) Limestones were associated with the establishment of a new meteoric, or mixed marine-meteoric water aquifer, during each emergent event that is inferred to have occurred at the end of each limestone deposition in some restricted portions of their geographic distribution. In contrast, it is assumed that the post-compaction ferroan (burial) CL sequence is shared by all the pre-Nukumaruan formations, and formed from a single aquifer, whose probable recharge area was located to the east of the study region. This assumption implies that recharge of the system was delayed until after deposition of the late Waipipian Rotookiwa Limestone, and possibly after deposition of the Mangapanian Te Onepu Limestone. The remaining late telogenetic/meteoric non-ferroan CL sequence probably formed during (?early) Nukumaruan times, during regional uplift of the central part of the study area, as suggested by the apparent west-to-east-trending flow direction.

The *Kairakau motif* has also been recognized within early-Nukumaruan limestones, but it is hypothesized that the mesogenetic (burial) – telogenetic (uplift) suites from within the pre- and syn-Nukumaruan limestones are unrelated.

A further step in the present diagenetic study has been to fully describe the paragenesis of the cool-water Te Aute limestones in terms of sequence stratigraphic relationships, implicitly by recognizing diagenetic sequence boundaries, transgressive and regressive precipitational trends, onlap and downlap behaviours, cycles, and different orders of cyclicity. It is shown that the vertical succession of CL sequences within a sediment pile can hierarchically be grouped within a framework that takes into account the type of bounding diagenetic discontinuity, the relation of CL sequences to the

patterns of syndepositional sea-level changes, and the relation of CL sequences to diagenetic processes dominantly driven by compactional and tectonic mechanisms.

An idealized pre-compaction transgressive-regressive diagenetic suite mimics the evolution of the depositional environment, and is forced by relative sea-level changes. The transgressive CL sequence records the evolution of the marine phreatic environment (marine diagenesis) between consecutive marine ravinement surfaces, while the regressive CL sequence (meteoric diagenesis) records the local subaerial exposure of shoaling-upwards sedimentary sequences.

An idealized post-compaction transgressive-regressive diagenetic suite is forced by subsidence and tectonic mechanisms. The transgressive CL sequence forms when the combined effects of subsidence and tectonics bury the host sediments to depths where significant compaction-induced fracturing occurs, and confinement modifies the ambient fluids towards reducing conditions (burial diagenesis). The post-compaction regressive sequence records the reducing-oxidizing turnaround of the chemical environment, due to exhumation of the sediments by tectonic-induced uplift (renewed meteoric diagenesis).

1. Introduction

The understanding of the physicochemical processes responsible for the transformation of loose carbonate sediments into hard rocks is an on-going and still intriguing problem for sedimentologists. It is now widely recognized that interparticle precipitation of aragonite, dolomite, and especially calcite crystals is the main transformational process involved in porosity destruction and cementation of limestones.

Since coarse skeletal carbonate deposits potentially constitute hydrocarbon reservoirs, their diagenesis, which encompasses all processes capable of modifying porosity, has long attracted the attention of petroleum geologists (see review by Moore, 2001).

The type and timing of diagenesis depend primarily upon the mineralogy of the carbonate phase, with which fluids moving through pore spaces will interact (Choquette and James, 1990a). Both the starting composition and the evolution of the ambient fluids are a function of the chemical environment, which can be marine, meteoric, or burial (Choquette and Pray, 1970). The transition from one environment to another is controlled by relative sea-level changes and tectonics (Tucker, 1993).

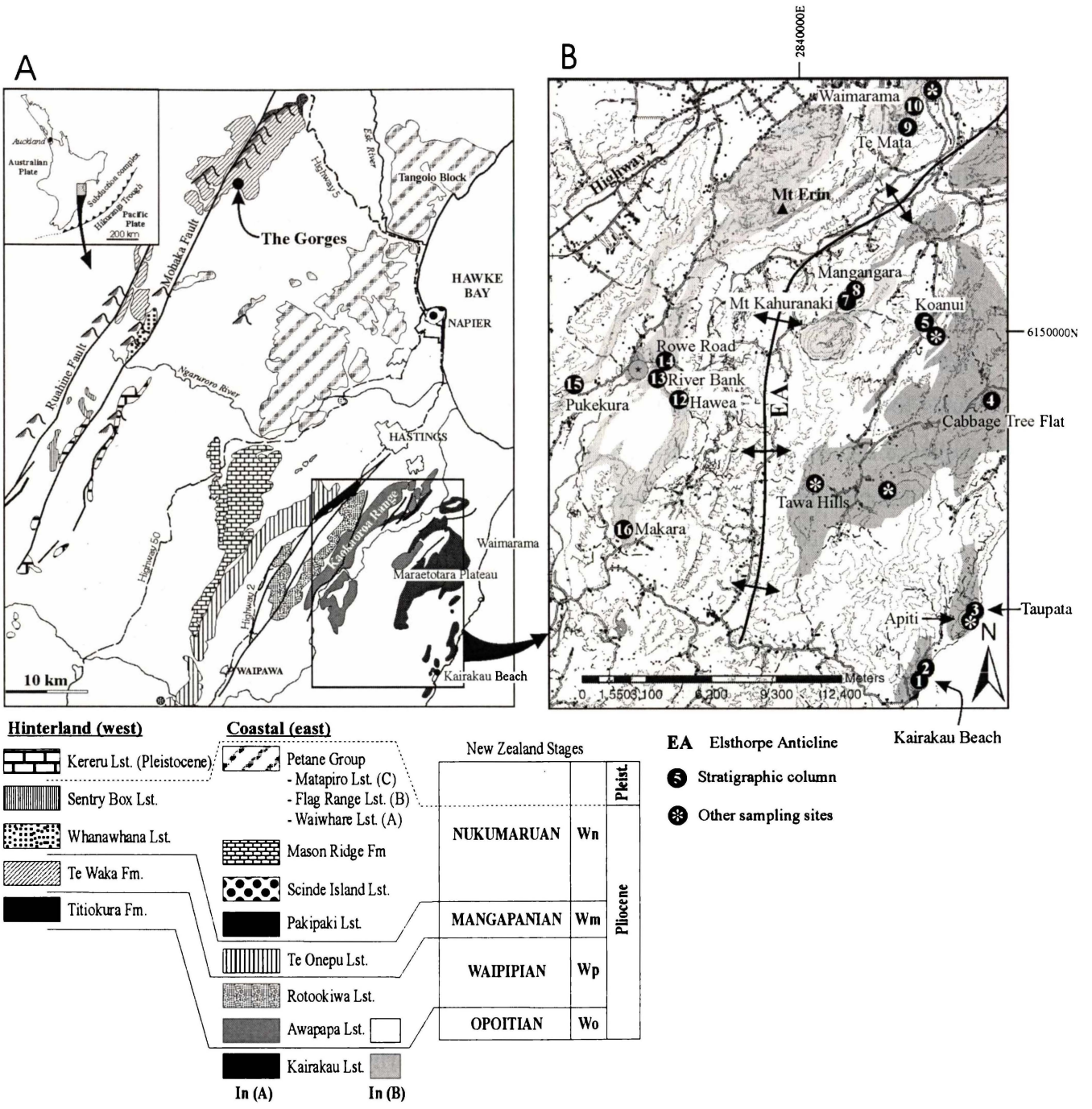

Figure 1- (A) General distribution of the Plio-Pleistocene limestones in the study area, and (B) location of logged sections (running column numbers as in Appendices 3 and 5) and other sample sites of Kairakau (dark grey) and Awapapa Limestones (light grey) (geological maps from Beu, 1995, and Kelsey *et al.*, 1993).

In tropical, predominantly aragonitic, carbonate settings, the essentials of porosity evolution within host sediments occur typically in surficial environments, prior to burial (Longman, 1980). In contrast, in cool-water, predominantly calcitic, carbonate settings, porosity modification may be delayed until after burial at depths where mechanical compaction and pressure-dissolution are triggered (Nelson *et al.*, 1988).

Cathodoluminescence, in combination with information from trace element and stable isotope geochemistry, has proved to be a powerful tool to assess the chemical evolution of the fluids that moved through carbonate sediments over time (e.g., Meyers, 1978; Kaufman *et al.*, 1988; Lavoie and Bourque, 1993; Frank and Lohmann, 1995). Not only does the analytical procedure help infer settings and processes of diagenetic imprint, but it also permits a certain degree of prediction since the reproducibility of diagenetic mechanisms, in relation to cyclic environmental changes, has been demonstrated (Niemann and Read, 1988; Braithwaite, 1993; Tucker, 1993). As a result, several researchers have pointed out that diagenetic pathways could be better understood by putting the patterns of porosity alteration into a sequence stratigraphic framework (Braithwaite, 1993; Moore, 2001). These advances in approaches to carbonate diagenesis, however, mainly derive from, and apply to, tropical carbonates, and there has been little attempt to produce diagenetic models that integrate the unique aspects of cool-water carbonates.

A few studies in New Zealand have used cathodoluminescence, in conjunction with geochemical analyses, to interpret the origin of calcite cements in cool-water carbonate deposits (Nelson *et al.*, 1988; Hood and Nelson, 1996), but so far no attempt has been made to regionally map cathodoluminescence (CL) cement zones as practical means for reconstructing fluid flow patterns.

The Pliocene Te Aute cool-water limestones of southeastern Hawke's Bay (Figure 1) are variably cemented. Typically, the older limestone occurrences, which spent longer periods of time in the burial environment than their younger counterparts, are best cemented by complex calcite overgrowths. This study focuses on variations between successive generations of these crystal overgrowths, which are separated by diagenetic discontinuities that equate to breaks in cement growth, and represent unrecorded periods of time of whatever length. Thus, conformable successions of cement CL zones, interrupted by diagenetic unconformities, are grouped into pre- and post-compaction CL sequences.

Within the Opoitian-age Kairakau Limestone and the Waipipian-age Awapapa Limestone (Figure 1), the regional distribution of CL patterns and chemistry of CL sequences are used to constrain the nature and scale of the fluid systems involved in cementation, their likely sources, and flow directions. Because the motif of cementation recognized within the Kairakau Limestone was found to be repeated within overlying limestone units, both the timing of cementation, and of establishment of the cementing aquifers within each individual formation are assessed.

Finally, the successive emplacement of cementing aquifers, which produced temporally and spatially distinct CL sequences, is shown to be best explained when modelled using a sequence stratigraphic conceptual approach that integrates the specificities of the cool-water Te Aute carbonates.

2. Analytical methods

2.1. Chemical staining

Thin-sections were stained using Alizarin Red-S and potassium ferricyanide. As Alizarin Red-S and potassium ferricyanide act upon the carbonates independently and do not interfere with each other, a solution of the two reagents was used according to Dickson (1965; see also Appendix 10.2 for the procedure).

Alizarin Red-S/potassium ferricyanide staining constitutes a preliminary approach to calcite cement stratigraphy, and enables recognition of the major changes in the fluid chemistry from which cements precipitated over time based principally on the content of Mn and Fe incorporated in the carbonate crystal lattices.

The incorporation of Mn and Fe is revealed by colour changes and zoning patterns in the crystals after chemical staining with Dickson's solution. These changes can be related to temperature, redox potential (Eh), or the introduction of allochthonous ions inhibiting or activating the chemical reaction.

2.2. Cathodoluminescence (CL)

Principles of cathodoluminescence (CL) and chemical considerations regarding the origin of calcite luminescence have been presented in Chapter 3 (Section 2.4). They can be summarized as follows: CL petrography exploits heterogeneities in the luminescence behaviour of minerals associated with changes in the chemistry of circulating interparticle

fluids that produce (non-) luminescent zones organized in conformable successions and/or bounded by diagenetic discontinuities.

Over 600 thin-sections were cut and polished for cathodoluminescence analysis. CL petrography employed a Technosyn 8200 MK II system (cold cathode) operating at 15kV gun potential and 0.35 milliamps beam current. Cathodoluminescence sequence diagrams, which integrate schematic representations of the compositional zonation of the cements and of their bounding discontinuities (see Chapter 2, Section 4.1), were established for each thin-section and are displayed in Appendix 5. The procedure uses an average of four images considered representative of each thin-section, and captured with a Nikon digital still camera DXM 1200 mounted on an Olympus AX70 microscope system. Over 1800 photomicrographs were transferred onto CD-ROMS (a total of 45) and constitute the first database of this kind to document the cathodoluminescence of cool-water carbonates in New Zealand. The images are held by the Department of Earth Sciences, University of Waikato, and are available for future investigations.

The study presented in this chapter concentrates on about 300 thin-sections of samples collected from a total of 20 stratigraphic sections of the Kairakau and Awapapa Limestones, of Opoitian and Waipipian age, respectively. For each stratigraphic column, between 4 and 25 thin-sections were analysed, depending on the quality of exposure and accessibility.

2.3. Trace elements

MgO, SrO, FeO, and MnO concentrations were determined on polished carbon-coated thin-sections by electron microprobe spot analysis along pre-defined transect lines, extending from grain margins porewards across one or more cement generations, (Appendix 6; also on CD1). All microprobe analyses were conducted on a JEOL JXA 8900 RL housed at the University of Göttingen (Germany). This instrument permits accurate discrimination of major cement zones as specimens can be viewed simultaneously in cathodoluminescence mode instrument was operated at an accelerating voltage of 15 kV for all elements, using a beam current of 12 nA, and a spot size of 5 μm. A total of 145 spot analyses from 9 selected samples are included in this chapter. Results and microprobe transects not reported here are presented in Appendix 6.

Elemental concentrations (CaO, MgO, SrO, NaO, FeO and MnO) were also determined by inductively coupled plasma optical emission spectrometry (ICP-OES) on

splits of powders from bulk samples of limestones ranging in age from Opoitian to Nukumaruan (Appendix9; also on CD1)

2.4. Isotopic analysis

This study includes 38 stable isotope analyses, 18 from Kairakau and 12 from Awapapa cements and whole-rocks, and 8 from texturally well preserved, relatively thick-shelled brachiopods collected from three different localities at various stratigraphic positions within the Awapapa Limestone. In thin-sections, brachiopod fragments from the same horizons are non-ferroan, non-luminescent to dull-orange, and lack evidence of dissolution features.

Isotope ratios are given in per mil (= mg/g or ‰) values relative to the international Pee Dee Belemnite (PDB) standard, and are expressed in the usual delta (δ) notation ($\delta^{18}O$ and $\delta^{13}C$).

Microsamples were scratched from polished slabs under a binocular microscope using a hook-shaped scalpel. This technical limitation, together with the typical thinness of most cement generations in the cool-water Te Aute limestones, made the sampling not fully satisfactory in all but in a few samples. For this reason, many microsampled cements are referred to as whole cements, or even whole rocks, to avoid misinterpretation.

Samples were roasted under vacuum at 380°C for one hour to remove volatile contaminants, and then reacted at 80°C with anhydrous phosphoric acid to produce CO_2 for analysis. Analyses were carried out at three institutions: (1) by Dr Karyn Rogers at the Institute of Geological & Nuclear Sciences (Lower Hutt, New Zealand), where results were normalized to VPDB using GNS marble (internal standard), NBS-18 (international standard), and NBS-19 (international standard). Precision is ± 0.1 ‰ for $\delta^{18}O$ and $\delta^{13}C$ values; (2) by Helen Turner at the University of Waikato (Hamilton, New Zealand), where results were normalized using NBS-1959 and NBS-1960 (international standards). Precision ranges from ± 0.004 to 0.06 ‰ for $\delta^{13}C$ values and from ± 0.008 to 0.08 ‰ for $\delta^{18}O$ values. Analyses were carried out using a CAPS carbonate device attached to a GEO-20 mass spectrometer; and (3) by Dr Helen Neil at the National Institute of Water and Atmospheric Research (Wellington, New Zealand). Internal precision of measurements is 0.02-0.06 ‰ for $\delta^{18}O$ and 0.01-0.03 ‰ for $\delta^{13}C$, external precision (between runs) is 0.05 ‰ $\delta^{18}O$ and 0.03 ‰ $\delta^{13}C$. Samples were reacted with

three drops of H_3PO_4 at 75°C in an automated individual-carbonate reaction (Kiel) device coupled with a Finnigan MAT252 mass spectrometer.

3. Concept of CL sequence stratigraphy

3.1. Introduction

CL technology has found wide application in carbonate cement studies since Meyers (1974, 1978), on the basis of the petrographic characteristics and stratigraphic distribution of CL cement zones in the Lake Valley Formation (New Mexico, USA), developed the concept of CL cement stratigraphy. Implicit in the usage of the phrase "cement stratigraphy" is the acceptance that the principles and the terminology, which classically define the physical relationships of sedimentary strata (e.g., superposition, inclusion, cross-cutting, etc), are suitable to describe paragenetic relationships in thin-section.

The attributes (colour, intensity, internal zonation) of successive CL cement zones, and the nature of the contact between them (conformable versus unconformable), enable identification of such features as cementation stages and breaks in crystal growth. CL zonations in clear spar cements are assumed to form in response to temporal changes in the chemistry of the ambient fluids, so that each zone may theoretically represent a time-correlative period of cementation. Thus Meyers (1978), in his pioneer study, inferred that each individual cement zone is synchronously precipitated across a basin, and can serve as a practical petrographic means of intercorrelation between cements from distant localities, and subsequently can help recognize the extension of cementing aquifers. Since then, parent studies have also convincingly demonstrated the lateral continuity of cement zones over several kilometres (Dorobek, 1987; Kaufman *et al.*, 1988; Niemann and Read, 1988). However, other researchers have pointed out that identical cement zones may not be isochronous throughout a particular area due to the progressive displacement of groundwaters through strata (Machel and Burton, 1991; Frank and Lohmann, 1995), and the possible reproducibility (i.e., both in time and space) of diagenetic motifs from within aquifers beneath stratigraphically distinct subaerial unconformities (Goldstein, 1988; Horbury and Adams, 1989; Walkden and Williams, 1991). Also cement zones and CL patterns may be absent or different in distant portions of the same groundwater system because conditions that favoured their formation elsewhere were not regionally reproduced.

Thus, the temporal and spatial variability of both the solution chemistry (saturation rates, precipitation rates, temperature, salinity, pH, and Eh) in many carbonate aquifers, and the permeability of the host-rock, are likely to induce changes in the CL signatures of calcite cements over certain distances (Machel and Burton, 1991; Braithwaite, 1993; Frank *et al.*, 1995) that render the use of CL cement zones for intercorrelation difficult.

3.2. CL sequences

Braithwaite (1993), following Kaufman *et al.* (1988), began to address the foregoing inconsistencies by suggesting that instead of considering cement zones individually, packages of zones bounded by discontinuity surfaces at the thin-section scale could help clarify the complexities of diagenetic suites.

Conformable and unconformable successions of calcite crystal growth zones, as revealed by chemical staining and cathodoluminescence, are common within the Te Aute limestones. Although these zonations are believed to reflect chemical modifications of the diagenetic environment, they are laterally poorly correlatable, even over short distances, and have a vertical continuity of generally no more than a few tens of metres (Figure 2). Thus, the occurrence of different cements, with respect to their concentric zonal pattern, in laterally equivalent strata, appears to be the rule in the Te Aute successions, and spatial continuity of cement zones, the exception.

Diagenetic discontinuities, including fractures and dissolution surfaces, which interrupt the normal succession of cement zones, are widespread in the studied carbonates. By contrast with CL patterns, diagenetic discontinuities can be traced laterally over several kilometres, and vertically, depending on their eustatic or tectonic origin (see later), over tens to a few hundreds of metres. It follows that the concept of unconformity-bound depositional packages of sediments in sequence stratigraphy (i.e., sequences) can readily be applied to CL cement successions, by using correlatable unconformities bounding uncorrelatable CL patterns, to define CL sequences (Braithwaite, 1993).

A CL sequence is a relatively conformable succession of genetically-related CL cement zones limited by (correlative) physical diagenetic surfaces equivalent to discontinuities, which can be traced laterally and vertically within a sediment pile (Figure

2). Thus, diagenetic discontinuity surfaces are considered to be the principal discriminator for intercorrelation, not the "inter-discontinuity" CL cement zones.

Typically in the Te Aute CL sequences, diagenetic suites from above and below a diagenetic discontinuity show an abrupt change in the chemical properties of the diagenetic environment, which translate into contrasting CL patterns and chemical stains, and differing geochemical signatures across the unconformable surface.

3.3. Diagenetic discontinuities (Figure 3)

Diagenetic discontinuities fall into three major categories, namely fractures, dissolution surfaces, and renucleation surfaces. A number of minor discontinuity surfaces are also used for the definition of CL sequences, such as abrasion surfaces (Figure 3A) and internal sediments, but they are generally of limited spatial extent.

3.3.1. Fractures

Fractures and fissures are present in almost all limestone samples ranging in age from Opoitian to Nukumaruan. The majority of these fractures cut across already cemented rocks (Figures 3B, 3C), and are generally related to mechanical compaction and tectonic processes. However, fissures which only affect skeletal fragments and pre-date any cementation phase are also common in the examined thin-sections. They are interpreted, when they are not associated with compaction-induced repacking of grains, as a product of syndepositional mechanical processes that occur during transport of grains under the influence of strong wave currents. Compaction- and tectonic-induced fractures have shown to be good correlative discontinuities between samples from within the same measured section, and between measured sections. Fractures further provide a good control of the cross-cutting paragenetic relationships.

As well as burial depth, compactional effects are closely dependent upon both the texture and the degree of early cementation of the host sediments (see Chapter 2, Figure 5). Differences in lithofacies attributes within a given limestone formation may therefore cause a fracturing "event" to be both laterally and vertically diachronous. Furthermore, within previously well cemented sediments, compaction- (and uplift-) related fractures may be transformed into correlative conformities, which can only be identified by comparison of CL-patterns from within and out of the cemented horizon.

Figure 2- Stacking panel of cathodoluminescence (CL) sequence diagrams for the Kairakau Limestone at Kairakau Beach (column 1/2, Figure 1). The panel highlights conformable successions of cement zones, or CL patterns, limited by diagenetic discontinuities, including dissolution surfaces (d and "corrosion pattern") and fractures (zigzag logo). The paragenetic relationships are schematically represented on the right. The paragenetic scheme shows that unconformity-bounded cements vary vertically in thickness, pinching out in places (indicated by triangles), and CL pattern (indicated by chevron logo). Although diagenetic discontinuities may apparently merge (d3 and d4) or change into a conformable contact from one sample to another (dashed line), they can easily be correlated throughout the stratigraphic section. The complex diagenetic stratigraphy is best explained when conformable successions of cement zones are grouped into unconformity-bounded diagenetic suites, termed CL sequences. Such a procedure here identifies five summary or idealized CL sequences, termed KZ to KD, limited by four correlative discontinuities, labeled d1 to d4. When tentatively traced laterally, CL patterns of cements prove to change rapidly and are uncorrelatable on this basis, whereas the same suite of discontinuities can be correlated over tens of kilometers.

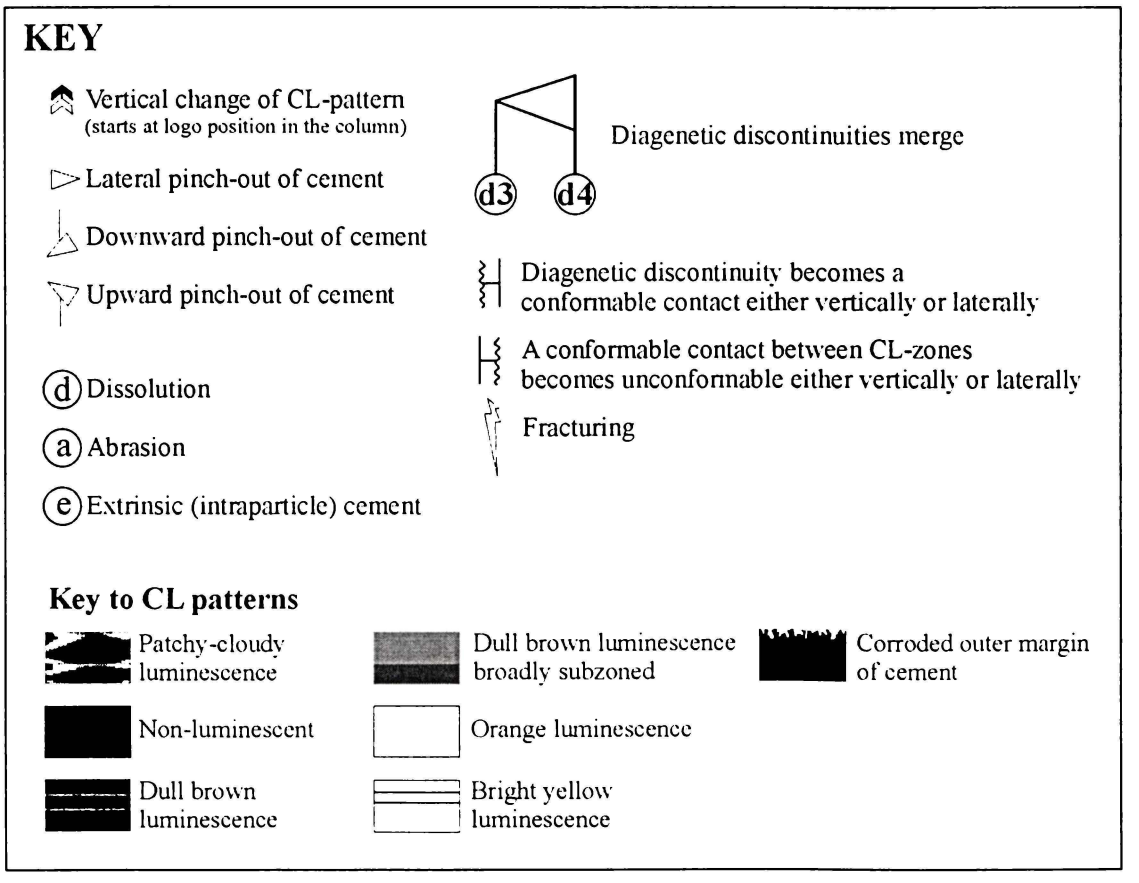

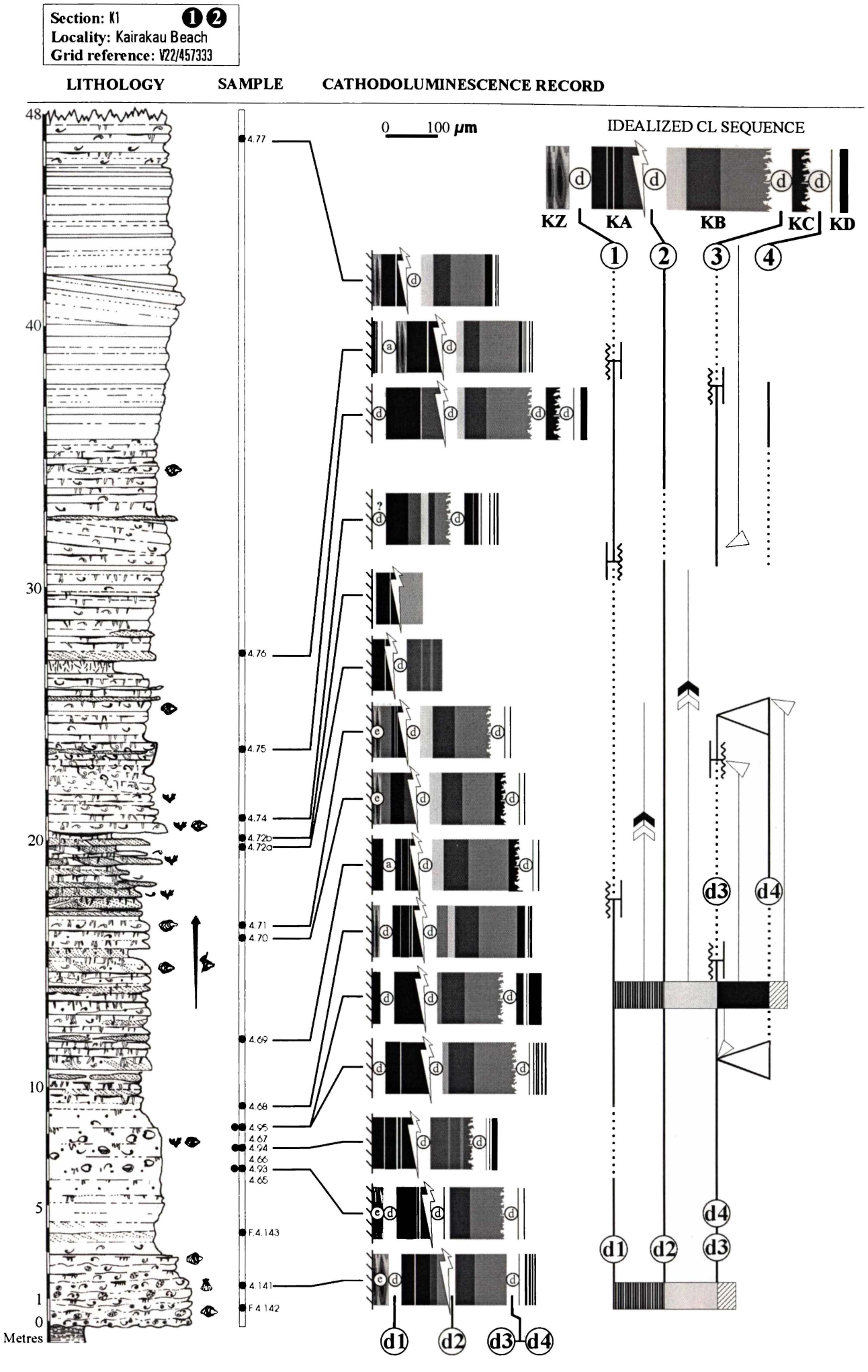
Section: K1 1 2
Locality: Kairakau Beach
Grid reference: V22/457333
LITHOLOGY
SAMPLE
CATHODOLUMINESCENCE RECORD
0 100 μm
IDEALIZED CL SEQUENCE
KZ
KA
KB
KC
KD
48
40
30
20
10
5
1
0
Metres
4.77
4.76
4.75
4.74
4.72b
4.72a
4.71
4.70
4.69
4.68
4.95
4.67
4.94
4.66
4.93
4.65
F.4.143
4.141
F.4.142
d1
d2
d3
d4

Figure 3 – Cathodoluminescence photomicrographs of diagenetic discontinuities.

(A) An abrasion and microbored surface (black arrow) separates two generations of pre-compaction non-luminescent calcite overgrowth (referred to as PrC in Chapter 3, Section 4.3.5). Subzoned PrC is apparently conformably overlain by orange, moderately luminescent, faintly subzoned cement (referred to as PoFC in Chapter 3, Section 4.3.5). The three cement generations syntaxially overgrow an echinoid plate fragment (e). Sample 4.69 from Kairakau Beach section of Kairakau Limestone (see Appendix 1 – column 1/2).

(B) Fracture-hosted (white arrows), orange/brownish, moderately luminescent PoFC unconformably overgrows non-luminescent PrC. Banded YnfC (= Youngest non-ferroan cement; see Chapter 3, Section 4.3.5) completes the cement suite. A dissolution surface that post-dates YnfC is also engulfed within PoFC (black arrow) and is outlined by brightly luminescent cement. Sample 4.75 from same locality as (A).

(C) Illustration of contrasting paragenetic relationships between successive cement generations. Sharp, but apparently conformable contact (white arrow) between two generations of syntaxial overgrowth about an echinoid plate (e), appears to be unconformable only a short distance away (black arrows point at the unconformable contact). There is no difficulty in interpretation here but this also illustrates how problems can come about when the paragenetic relationships are not as straightforward as in this example. Sample 12.4 from Glendale Farm section of Kereru Limestone (see Appendix 1 – column 46).

(D) A dissolution surface along the outer margin of non-luminescent cement produces an irregular corroded crystal boundary (white arrows). Sample 4.24 from Mt Kahuranaki section of Kairakau Limestone (see Appendix 1 – column 7).

(E) Brightly luminescent yellow cement lies on a dissolution surface that cross-cuts cathodoluminescence zones of the previous cement generation. Sample 2.2 from Te Pohue section of Titiokura Formation (see Appendix 1 - column 38).

(F) White arrows point at temporally distinct dissolution surfaces within YnfC. Sample 4.75 from Kairakau Beach section (see Appendix 1 – column 1/2).

(G) Renucleation (R) in calcite. Note that early brownish crystals are overgrown across a discontinuity surface (arrowed) by crystals of differing shape and CL pattern. Sample 2.2 from Te Pohue section of Titiokura Formation (see Appendix 1 - column 38).

(H) A dissolution surface (black arrow) provides substrate for renucleated large calcite crystals (R). Note the irregular dissolution surface (white arrow) within renucleated intraparticle crystal that underlies a new generation of cement overgrowth. Sample 12.7 from Glendale Farm section of Kereru Limestone (see Appendix 1 – column 46).

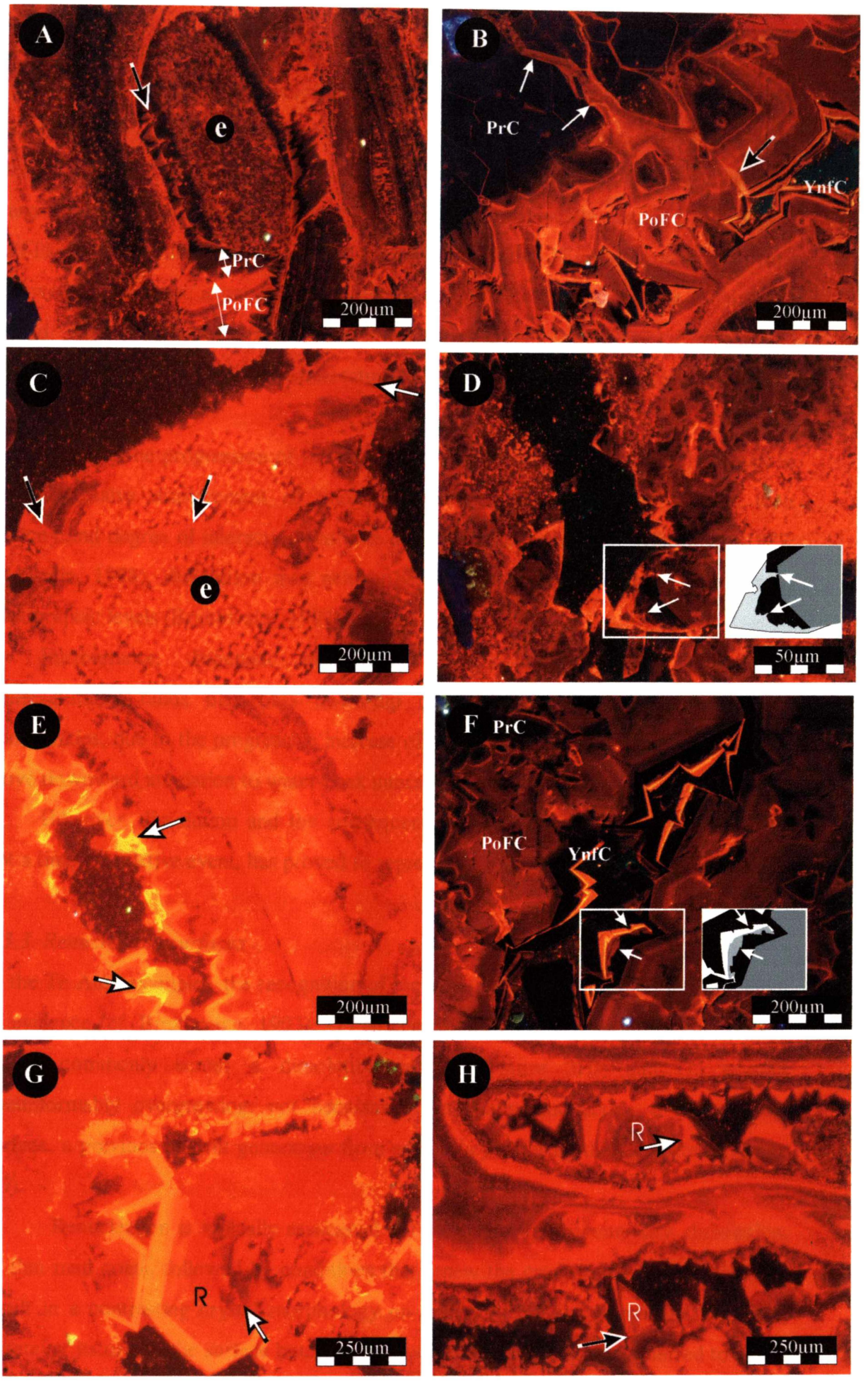
A
e
PrC
PoFC
200µm
B
PrC
YnfC
PoFC
200µm
C
e
200µm
D
50µm
E
200µm
F
PrC
PoFC
YnfC
200µm
G
R
250µm
H
R
R
250µm

3.3.2. Dissolution surfaces

The chemical evolution observed across a diagenetic discontinuity is commonly accompanied by dissolution of cements of the previous CL sequence, and/or metastable carbonate skeletal fragments. Thus, dissolution is commonly indicated by corroded outer margins of crystal surfaces and biomoulds. Dissolution, typically resulting in irregular, gulf-like crystal boundaries and terminations (Figures 3D to 3F), and truncation or total removal of CL zones, is comparable in its effects to erosion surfaces in the sedimentary record. These dissolution features clearly document breaks during crystal growth that attest to the influence of waters undersaturated with respect to calcium carbonate (Simo and Lehmann, 2000).

Because the progression of the diagenetic dissolution front is intimately related to the progressive displacement of undersaturated groundwaters, together with their velocity and degree of interaction with the host metastable carbonates (Dorobek, 1987; Goldstein, 1988), dissolution may neither be synchronous nor continuous at various stratigraphic levels (Braithwaite, 1993).

Furthermore, diagenetic discontinuities associated with the ingress of undersaturated fluids may pass down-dip of the recharge area into correlative conformities, due to the progressive increase of saturation level of groundwaters as they move downward in relation to water-rock interaction.

However, dissolution and the consequent interruption of crystal growth, even if not a time-correlative event, has proved to represent a good spatial-correlative event.

3.3.3. Renucleation surfaces

In the Te Aute examples, the recognition of renucleation is based on the following kinds of evidence (cf. Braithwaite, 1993): (1) an abrupt change in crystal size within cement suites, commonly across a dissolution surface (Figure 3H); and (2) crystals unconformably overgrowing, not necessarily syntaxially, and across a discontinuity surface, a previous cement generation from which they differ by the CL pattern (Figure 3G).

Renucleation is typically associated with a diagenetic discontinuity, dissolution, or thin mud coats, followed by conditions that renew the crystal growth potential, and result in a contrasting crystal morphology on either side of the discontinuity surface. Whatever its origin, the surface bounding below renucleated crystals is referred to as the

renucleation surface. Aside the transition from marine acicular cement to scalenohedral or mosaic later stage calcite that Braithwaite (1993) attributes to renucleation, renucleation is difficult to identify and can only be unequivocally designated in limestones from the western sector of the study area (Titiokura Formation, Te Waka Formation, and Kereru Limestone; see Figure 1).

3.3.4. Summary of general attributes of diagenetic discontinuity surfaces

A diagenetic discontinuity surface represents a period of time during which there is no evidence of cement being precipitated above the previous cement suite and beneath the one above, at the regional scale where the discontinuity was recognized.

This does not preclude the possibility for consecutive diagenetic discontinuities to locally merge, due to lateral pinch-out of cements, or cements above the older discontinuity surface having been totally removed during the genesis of the younger unconformity, or cements not being precipitated at all between discontinuity surfaces (Figure 2).

Diagenetic discontinuities and their correlative conformities are probably diachronous across the distribution of a given limestone body, or stacked limestone sheets.

Diagenetic discontinuities and their correlative conformities mark an abrupt change in the chemical environment.

4. Application of the concept of CL sequence to the Te Aute limestones

A major aim of the petrographic study described here has been to develop a CL sequence stratigraphic approach to cool-water carbonate diagenesis that is formally conceptualised later in Section 5. The procedure is based on the chronological occurrence of diagenetic features within sedimentary successions, their vertical and lateral distribution, and their grouping into discontinuity-bounded sequences at the thin-section scale (Figure 2). It is shown that the chemical evolution of the diagenetic environment of the studied carbonate sediments is best explained when related to correlative diagenetic discontinuities that mark the transition between surface-related processes to processes reflecting confined conditions, and conversely (Caron and Nelson, 2001).

The Early Pliocene (late Opoitian) Kairakau Limestone, and in lesser details the earliest Late Pliocene (early Waipipian) Awapapa Limestone were chosen to illustrate this study because: (1) they are the oldest Pliocene limestone occurrences in the study area, and as such represent the early stages of the forearc basin seaway development (see Chapter 1, Section 2); (2) they are the best documented limestones in terms of the number of logged stratigraphic sections (13 and 7, respectively), samples (about 150 thin-sections each), stable isotope data (a total of 38), and microprobe spot analyses (145); and (3) they are composed of similar dominant microfacies associations (see Chapter 1, Section 6.2), which translates into comparable original mineralogies, so that geochemical data of bulk samples from either formation can be graphed together and compared.

4.1. Setting

Kairakau and Awapapa Limestones are well exposed in NE-trending parallel ranges that represent the eastern part of the exposed forearc basin in southern Hawke's Bay (Figure 1). The stratigraphic and structural framework of the Te Aute limestones are presented in the previous chapters, and follow the descriptions of previous authors (Spörli and Pettinga, 1980; Harmsen, 1985; Kelsey *et al.*, 1993; Beu, 1995; Field *et al.*, 1997).

Kairakau Limestone, the focus of this chapter, occurs on both sides of the Elsthorpe Valley, at the western edge of the Maraetotara Plateau, and within sea cliffs from south of Kairakau Beach northwards to Waimarama (Figure 1). Kairakau Limestone is mainly characterized by mixed facies, transitional between barnacle-rich grainstone and terrigenous packstone, often bioturbated, and consists of four major sedimentary sequences bounded by unconformities interpreted either as transgressive surfaces of erosion (TSE), or regressive surfaces of erosion (RSE) (see Chapter 4, Section 7.1). Its thickness varies between 6 m in the Kaokaoroa Range and 60 m in the Maraetotara Plateau area (Figure 1). It rests unconformably either on Miocene mudstones or green sandstones, probably of Opoitian age.

Awapapa Limestone crops out principally along the eastern flanks of the Kaokaoroa Range (Figure 1). The Awapapa Limestone successions are constructed of metre-scale sequences, which range in thickness from 1-17 m. From one locality to another, the number of building sequences is highly variable, ranging from four at Pukekura (total 25 m) to up to twelve at Te Mata Peak, where the limestone reaches its

maximum thickness (120 m). The limited number of studied sections, the generally poor exposures and rapid lateral facies changes, the limited traceability of sequence-bounding surfaces, and the laterally variable number of sequences all render correlation highly difficult, which has therefore not been attempted at a high-resolution scale (see Chapter 4, Section 7.2). The contact between Awapapa Limestone and the underlying siliciclastic strata (Mokopeka Sandstone) is unconformable to the east and apparently gradational to the west (Harmsen, 1985).

Early Pliocene and earliest Late Pliocene skeletal limestones pinch out gradually to the west in the subsurface (Field *et al.*, 1997). Data recovered from subsurface cores in the central part of the study region only contain predominantly siliciclastic lithologies for this time interval, including successions of massive grey, soft to firm, mudstones and silty mudstones (Mason Ridge-1 well; Leslie, 1971a), with occasional limestone and sandstone beds, especially to the south (Ongaonga-1 well; Leslie, 1971b). These drilling sites help reconstitute the subsurface configuration of the early Te Aute carbonates. The scarcity or absence of limestone sheets in the wells suggests either that skeletal facies change basinward into mixed carbonate-siliciclastic facies and siliciclastics, or that the limestones were eroded or faulted (Leslie, 1971a). This also points out the absence of physical continuity between time equivalent limestones that were deposited on both sides of the former forearc basin (Croft Exploration Ltd., 1992; Beu, 1995; Nelson *et al.*, in review). Further, in the study area limestones sheets are interbedded with thick silty or sandy units that grade westwards into muddy facies.

The fine-grained strata, in the central part of the depositional trough, constitute potential aquitards, which may have prevented or slowed the circulation of groundwaters both basinward from recharge areas located in tectonic highs (to the east or to the west), and downwards from syndepositional subaerial unconformities, between successive limestone sheets.

4.2. CL sequences in the Early Pliocene cool-water Kairakau Limestone

Photomicrographs of thin-sections under CL light were used to build up detailed diagenetic CL sequence diagrams (Figure 2 and Appendix 5). CL sequence correlations, and the recognition of spatial pattern variations between consecutive diagenetic discontinuities, were made by comparing closely adjacent samples with respect to their stratigraphic position within each individual column (Figure 2). And then laterally, from

one locality to another, diagenetic sequence diagrams were compared from samples located within intervals bounded by correlative sedimentary unconformities (Figure 5). Calcite cements in the Kairakau Limestone are grouped into four major CL sequences, termed in ascending order KA to KD, limited by four diagenetic surfaces, chronologically labelled d1 to d4 (Figures 2, 4), and are tentatively correlated over tens of kilometres (Figure 5). CL sequences appear to change vertically, at any one locality, in thickness and slightly in their zonal pattern. In particular, CL patterns of cement zones are variable from one locality to another, and appear to be geographically controlled. CL sequence KA is preceded by a poorly traceable marine CL sequence, termed KZ (Figure 2).

Thus, individual or successive cement zones, between consecutive diagenetic discontinuities, are usually discontinuous, even over short distances, and CL sequences may locally be absent (Caron and Nelson, 2001). Because of discontinuity, together with the typical thinness of CL sequences, only the origin of spatial variations in thickness, CL patterns, and geochemical signatures of whole CL sequences is addressed in the present study.

However, the reconnaissance nature of this CL study of cool-water limestones in New Zealand is emphasized, and in particular it will be important in the future to obtain more stable isotope and minor element data from individual cement generations so as to better attempt to establish the source of cementing waters. For this reason, the present study mainly concentrates on physical relationships between CL sequences, and both their lateral and vertical distribution, so highlighting the spatial geometry of the cementing aquifers.

4.2.1. Pre-d1 CL sequence (KZ)

Description

Pre-d1 cements consist of rims of (now) low-Mg calcite, inclusion-rich (turbid), acicular cements, occurring either in interparticle or in intraparticle pore spaces (see Figure 6). In many Kairakau samples, individual layers consist of isopachous rinds that range in thickness from 50 to 150 μm, but can be less than 30 μm. Turbid cements selectively grow upon skeletal grains (bivalves, echinoids, and brachiopods principally), and have never been found coating quartz or feldspars. Turbid cements also occur as syntaxial

overgrowths upon echinoid plates and spine fragments. Marine geopetal sediments commonly overlie fringes of acicular inclusion-rich cement.

Turbid cements stain pale pink to pale mauve with Dickson's solution (1965), and are non-luminescent or show a typical patchy orange to bright yellow CL (Figure 4E). Patchy cathodoluminescence demonstrates that pre-d1 cements have undergone diagenetic alteration since precipitation (Grover Jr and Read, 1983; Meyers and Lohmann, 1985; Kaufmann and Wendt, 2000).

The eroded outer margin of skeletal fragments, which results from mechanical abrasion and/or the activity of microborers, is regarded as the basal bounding-discontinuity surface of CL sequence KZ. The upper bounding discontinuity is a dissolution surface (d1) either engulfed within previous cements or marked by biomoulds lined with cements of the next CL sequence (Figure 4A). When acicular cements are absent, the basal discontinuity surface and discontinuity d1 become superposed, and CL sequence KZ consists of a compound diagenetic discontinuity.

$\delta^{18}O$ values for one microsample of turbid cement and for the bulk of pre-compaction cements, which include both turbid cements and later stage clear spar cements, range from –0.44 to –4.4 $^{o}/_{oo}$PDB, while $\delta^{13}C$ values range from 1.17 to –1.7 $^{o}/_{oo}$PDB (see Figure 10).

Pore-lining inclusion-rich fibrous cements contain minor amounts of FeO (N = 26; 0 to 0.6 wt%, mean = 0.18 wt%), and virtually no MnO (0 to 0.05, mean = 0.02 wt%). SrO contents are low (0 to 0.5, mean = 0.09 wt%) and MgO is abundant compared to later stage cement varieties, ranging from 0.16 to 1.70 wt% (mean = 0.8 wt%; see Figure 9A).

Inclusion-rich acicular cements are interpreted as a product of marine (near) sea-floor diagenesis. Their primary mineralogy is envisaged to be intermediate-Mg calcite (IMC). The diagenetic attributes of this early cementation stage are described and interpreted in detail in Chapter 3, Section 4.2.

Distribution

Pre-d1 cements are the least abundant cement variety in the Kairakau Limestone. They are restricted to specific portions of sedimentary sequences, typically immediately above and below unconformities, within carbonate sediments that accumulated in shallow-water high-energy settings, including intertidal bored pebble horizons, oyster shell

banks, or prominently cross-bedded coarse skeletal facies (Caron and Nelson, 2000). As a result, turbid cements are discontinuous, and cannot confidently be correlated over more than a few metres laterally, and a few decimetres vertically.

4.2.2. Post-d1/Pre-d2 CL sequence (KA)

Description

CL sequence KA cements comprise clear spar (i.e., inclusion-free) scalenohedral, bladed palisadic, blocky, and syntaxial crystal forms. Their present (and probable original) mineralogy is low-Mg calcite (LMC). CL sequence KA either constitutes the first cement in the pore space, or overgrows early turbid fringes, and systematically pre-dates compaction-induced skeletal fractures referred to as discontinuity d2 (Figure 4). CL sequence KA is bounded below by dissolution surface d1 and, as a result, spar cements of CL sequence KA are commonly found coating walls of mouldic voids (Figure 4A).

Fine equant spar crystals and clear spar crystals arranged in picket fence fashion with scalenohedral terminations appear to be substrate dependent, and nucleate upon: (1) internal carbonate sediments; (2) the exterior surface of older isopachous fringes (clear or turbid); and (3) directly upon the outer margin of carbonate skeletal fragments (Figures 4A to 4D).

These pre-compaction cements stain pink in the southeast sector of the study area, but become pale mauve to pale blue towards the north.

CL sequence KA cements (referred to as PrC or pre-compaction clear spar cement in Chapter 3) are typically non-luminescent (Figures 4A to 4D), with occasional moderately to bright orange luminescent zones (see Figure 3A). The homogeneous luminescence of these sparry calcite cements and the preservation of compositional zoning are assumed to indicate no alteration since precipitation (e.g., Dickson, 1965; Emery and Dickson, 1989).

Post-d1/pre-d2 cements are non- to slightly ferroan (N= 36; FeO = 0.01 to 0.4 wt%, mean = 0.2 wt%). They have moderate SrO (0 to 0.9 wt%, mean = 0.17 wt%) and low MnO (0 to 0.05 wt%, mean = 0.017 wt%) concentrations. MgO concentrations are variable (Figure 6), but generally moderate (0.15 to 1.01 wt%, mean = 0.6 wt%), slightly lower than that of early inclusion-rich cements, but much higher compared to later stage cement varieties (see Figure 9A).

Figure 4 – Cathodoluminescence sequence stratigraphy of the Kairakau Limestone. In the upper left corner is a schematic representation of the characteristic paragenesis identified throughout the distribution of Kairakau carbonates in the study area, and referred to as the *Kairakau motif* in text. In ascending order the diagenetic discontinuities coincide with a dissolution surface (d1), and fractures overprinted by dissolution (d2, d3, and d4). CL sequence KZ (blotchy pattern) consists of marine acicular turbid cements outgrown by an unconformable succession of clear spar cements: pre-compaction CL sequence KA (non-ferroan), post-compaction CL sequences KB (ferroan), KC (non-ferroan), and KD (slightly- to non-ferroan).

(A) Non-luminescent cement of CL sequence KA is post-dated by compaction-induced fractures (d2) filled with orange luminescent ferroan cement of CL sequence KB. Note that dissolution surface d1 is coincident with the inner wall of a biomould and provides substrate for the non-luminescent cement generation. Sample 4.65 from Kairakau Beach section (see Appendix 5 – sequence diagram K1).

(B) Same suite of CL sequences as in above sample 4.65. Note that spalling of scalenohedral non-luminescent crystals provides substrate for growth of orange cement of CL sequence KB, and accompanies compaction-induced skeletal fracturing. Sample 4.90 from Apiti section (see Appendix 5 – sequence diagram K10).

(C) The photomicrograph illustrates the suite of cements KA to KC, which collectively almost totally occlude the interparticle pore space. Sample 4.127 from Cabbage Tree Flat section (see Appendix 5 – sequence diagram K3).

(D) Note the change in CL pattern of CL sequence KA, compared to previous samples. This first cement generation in the pore space consists of an early non-luminescent growth stage conformably followed by a late brownish calcite overgrowth. Sample 4.120 from Tawa Hills section (see Appendix 5 – sequence diagram K12).

(E) Paragenetic relationships of pre- and post-compaction cements. The youngest fracture (d3) cross-cuts both fracture-hosted CL sequence KB and early patchy acicular cement from CL sequence KZ. Note that CL sequence KA is absent. Late dissolution event d4 produces irregular intracrystalline pores filled with brightly luminescent cement of CL sequence KD. Sample 4.29 from Mt Kahuranaki (see Appendix 5 – sequence diagram K5b).

(F) Collapse of biomould envelope indicates that dissolution occurred prior to mechanical compaction and probably equates to d1. This dissolution event was not followed by cement KA, but instead by cement KB, suggesting that cementation was coeval or delayed until after fracturing. In this case, discontinuity d2 is superposed to d1. However, in other portions of the same thin-section, CL sequence KB is bounded above and below by fractures, and overgrows poorly developed CL sequence KA. Sample 4.40 from Mangangara section (see Appendix 5 – sequence diagram K6).

(G) Orange moderately luminescent cement of CL sequence KB fills compaction-induced fractures, and is not preceded by non-luminescent calcite overgrowth. Sample 4.46 from Waimarama 1 section (see Appendix 5 – sequence diagram K7).

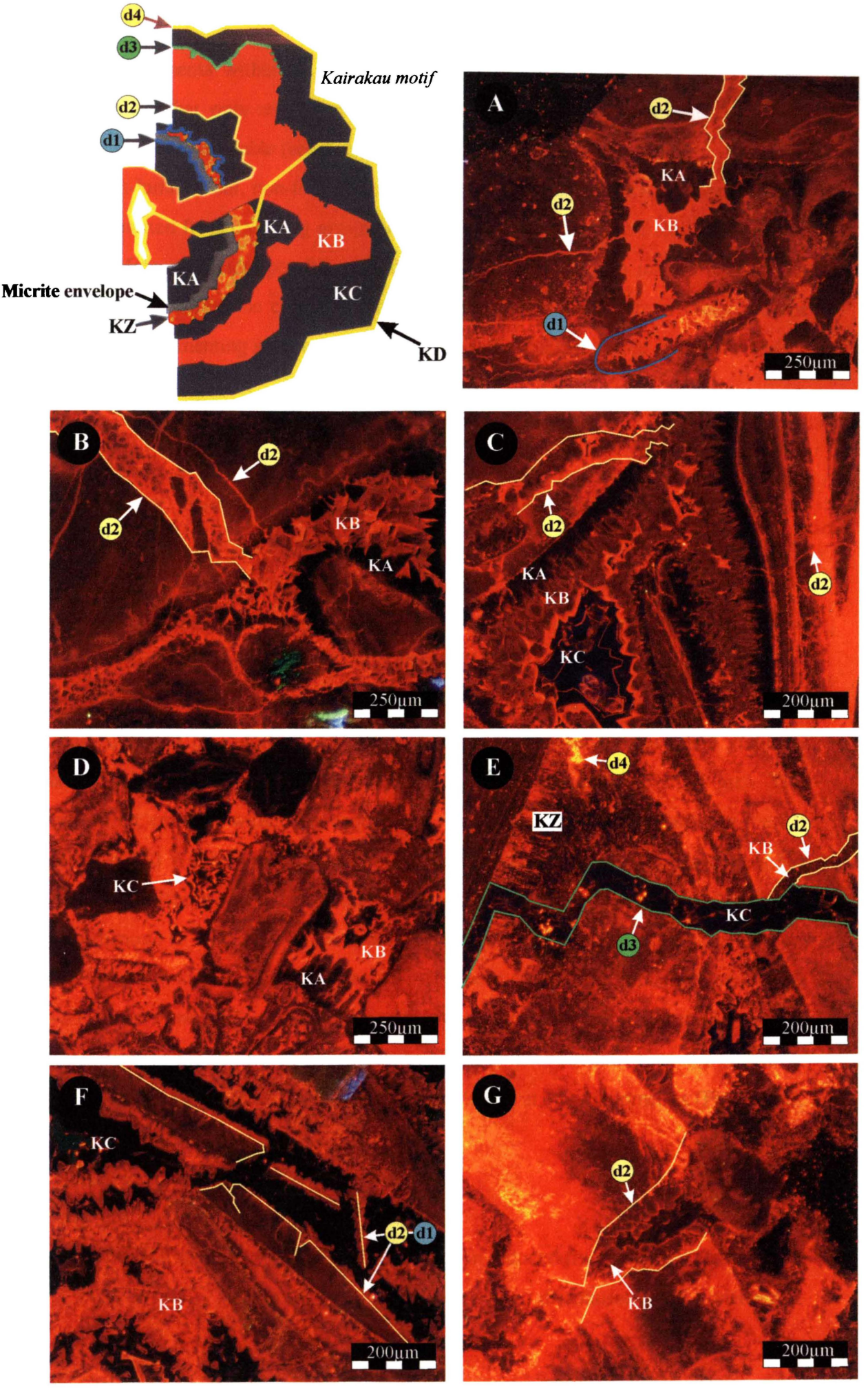
d4
d3
d2
d1
Kairakau motif
KA
KB
KA
KC
Micrite envelope
KZ
KD
A
d2
KA
d2
KB
d1
250µm
B
d2
d2
KB
KA
250µm
C
d2
KA
KB
KC
d2
200µm
D
KC
KB
KA
250µm
E
d4
KZ
d2
KB
KC
d3
200µm
F
KC
d2
d1
KB
200µm
G
d2
KB
200µm

Spar cements within CL sequence KA are too thin to be confidently sampled individually so that only stable isotope values for pre-compaction cements, including turbid cements, are available (see Section 4.3.3).

Non-luminescent, non-ferroan cements within CL sequence KA are interpreted to have precipitated from oxidising groundwaters whose chemical nature still remains to be assessed. Meteoric fluids, possibly mixed in various portions with marine waters, that interacted with metastable carbonates of the local host sediment are envisaged as the most plausible cementing source for the pre-compaction inclusion-free spar cements (see Chapter 3, Section 4.3.6).

Distribution

The percentage abundance of each post-d1 CL sequence, including KA, has been calculated from its average thickness in the interparticle pore spaces, using a minimum of from 8 to 25 samples at each locality. This allows the CL sequences to be mapped petrographically. Data are inferred to be proxies for the regional volumetric abundance of each CL sequence, and are displayed in Figures 5A, 5B, and 5C.

The pre-compaction non-luminescent cement (KA) is common throughout the southern outcrops of Kairakau Limestone, but from this sector northwards it gradually thins and is eventually absent from the northernmost portion of the study area. This suggests that cements within CL sequence KA pinch out somewhere between the Mt Kahuranaki and Waimarama sections (Figure 5). Vertical pinch-outs of CL sequence KA occur in the northern sections of Kairakau Limestone at various stratigraphic levels, and may correspond to digitations of the cementing fluid system.

The total amount of CL sequence KA is about 40% of the cement volume in the Tawa Hills area and at the western edge of the Maraetotara Plateau, decreasing gradually to about 30% to the southeast, but rapidly to below 25% to the northeast and northwest of the "ridge" of high values, from where it drops to 0% in a few kilometres (Figure 5A).

4.2.3. Post-d2/Pre-d3 CL sequence (KB)

Description

CL sequence KB cements develop upon compaction-induced fractures (i.e., discontinuity d2; Figure 4), commonly accompanied by dissolution of metastable

Figure 5- Stratigraphic distribution and relative abundance of CL sequences KA to KD, in relation to sedimentary surfaces (labelled 1 to 4) dividing Kairakau Limestone into four sedimentary sequences (see Chapter 4, Section 7.1). The regional distribution of CL sequences is shown along a south-north cross-section (from Kairakau Beach to Waimarama). Note that CL sequence KA is absent from Waimarama section, the abundance of CL sequence KB decreases northwards, whereas CL sequence KC varies inversely and is more abundant in the north. See text for discussion.

The major CL sequences, namely KA, KB, and KC, have been petrographically mapped, using the average of their percentage abundance at each locality, calculated from 8 to 25 samples. Each data point is used to draw contours of iso-abundance, and the result is illustrated in top Figures (A) to (C). In the Mt Kahuranaki/Mangangara area, only the highest percentage of each CL sequence, yielded by either section, is displayed. In (A), percentages of CL sequence KA define a southwest-northeast trending ridge of values above 35%. From the head of this "ridge", located near Koanui, percentage values must decrease rapidly to explain the absence of CL sequence KA at Waimarama section. In (B), percentage of CL sequence KB is highest to the east, reflecting probable recharge of waters into the confined aquifer from this direction. In (C), percentage of CL sequence KC is highest to the northwest, partly overlapping the axis of the Elsthorpe Anticline, and decreases southwards. See text for discussion.

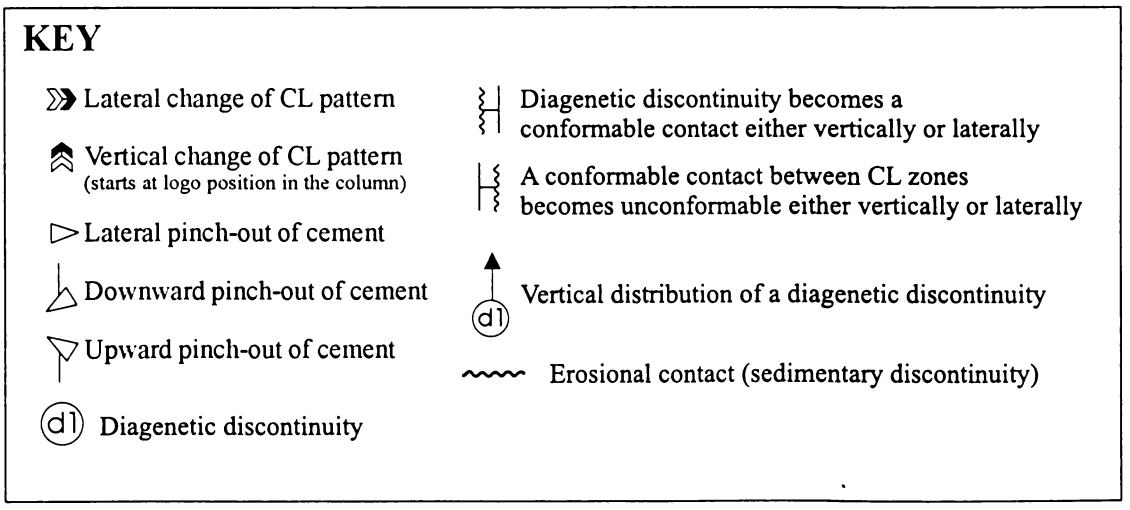

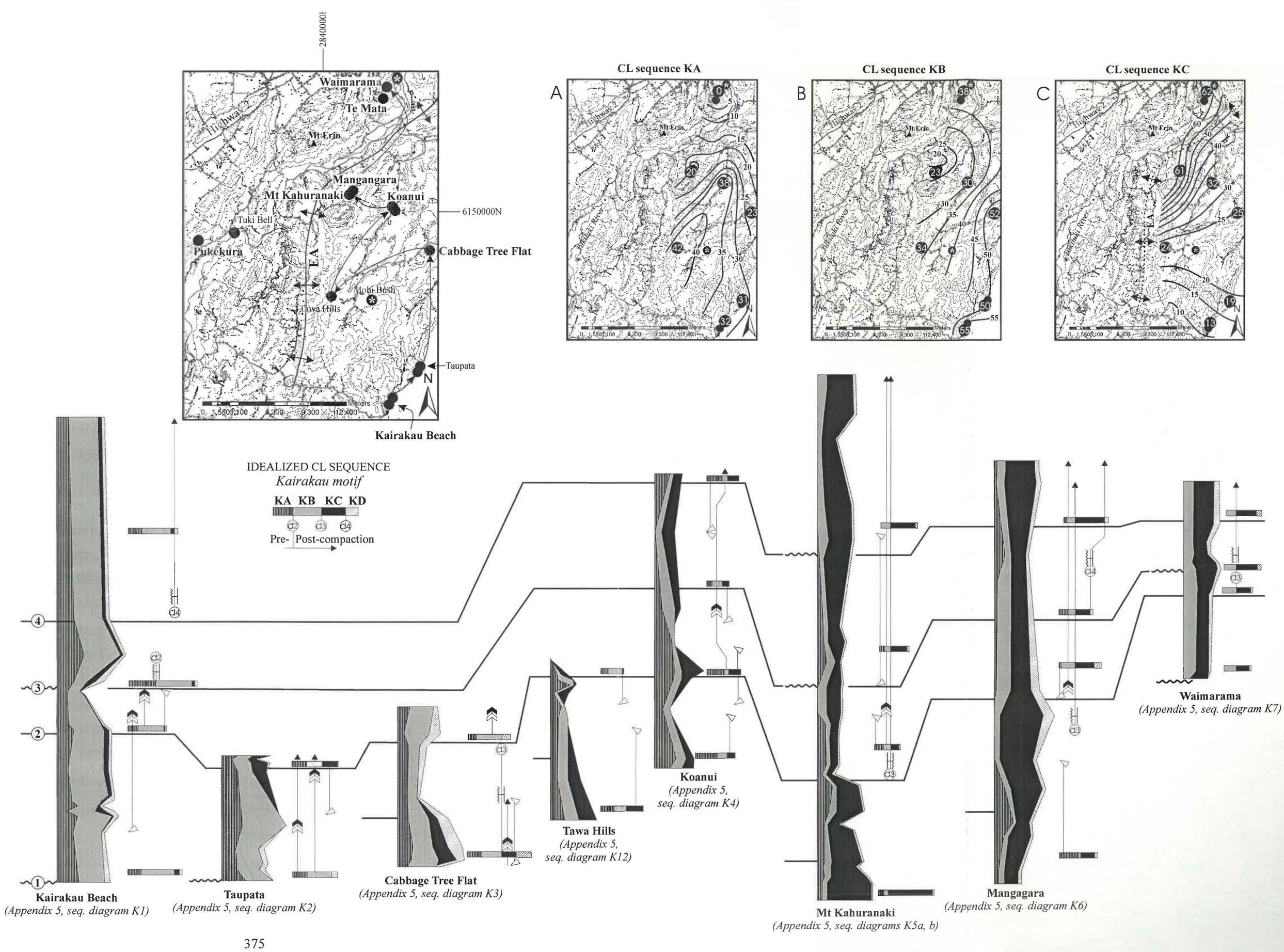
2840000E
Waimarama
Te Mata
Mt Erin
Highway 2
Mangangara
Mt Kahuranaki
Koanui
6150000N
Tuki Bell
Pukekura
EA
Cabbage Tree Flat
Mohi Bush
Tawa Hills
Taupata
N
Meters
0 1,550 3,100 6,200 9,300 12,400
Kairakau Beach
CL sequence KA
CL sequence KB
CL sequence KC
A
B
C
Parkituki River
IDEALIZED CL SEQUENCE
Kairakau motif
KA KB KC KD
d2 d3 d4
Pre- Post-compaction
4
3
2
1
Kairakau Beach
(Appendix 5, seq. diagram K1)
Taupata
(Appendix 5, seq. diagram K2)
Cabbage Tree Flat
(Appendix 5, seq. diagram K3)
Tawa Hills
(Appendix 5, seq. diagram K12)
Koanui
(Appendix 5, seq. diagram K4)
Mt Kahuranaki
(Appendix 5, seq. diagrams K5a, b)
Mangagara
(Appendix 5, seq. diagram K6)
Waimarama
(Appendix 5, seq. diagram K7)

skeletal carbonates and cements, and terminate with another fracturing stage, which is characteristically post-dated by dissolution (i.e., discontinuity d3; Figure 4E). The relation of these ferroan cements to pressure-dissolution features is not clear (i.e., they post-date and pre-date curved grain-to-grain contacts), but in most pre-cemented grainstone facies they appear to be truncated by dissolution seams (see Figure 17G). This suggests that CL sequence KB cements pre-date burial to pressure-dissolution depths producing serrated contacts.

Cements within CL sequence KB are mostly characterized by bladed epitaxial crystals arranged in a palisade fashion, syntaxial overgrowths, and blocky to mosaic clear LMC spar. They are substrate independent and typically nucleate on siliciclastic grains, carbonate grains, and cements, and the interior surface of biomoulds and fractures giving in some cases a drusy fabric.

Chemical staining identifies moderate to high concentrations of ferrous iron (pale to deep blue, respectively), which are partly supported by the few electron microprobe spot analyses (Figures 6, 9) that yielded FeO values ranging from 0 to 1.25 wt% (N= 20; mean = 0.3 wt%). These values are higher than that of older inclusion-rich and CL sequence KA cements, as well as younger CL sequence KC cements (see below).

Post-d2/pre-d3 cements consist of homogeneous to faintly zoned orange moderately luminescent to orange/brown dull calcite (Figures 4A to 4G).

SrO concentrations are significantly higher than that of pre-compaction cements (0.1 to 2.03 wt%, mean = 0.5 wt%; Figure 9A), but MgO is depleted (0.06 to 0.94 wt%, mean = 0.44 wt%). MnO concentration is low (0 to 0.03 wt%, mean = 0.016 wt%). Cements from CL sequence KB could not be extracted for isotopic analysis.

Post-compaction ferroan calcite cements (referred to as PoFC in Chapter 3), which include dull and moderately luminescent cements, conform to the attributes of mesogenetic products (Choquette and James, 1990b), even though their FeO content is generally lower than has been reported from other studies of similar carbonate cements (Meyers, 1978; Dorobek, 1987; Nelson and Read, 1990; Walkden and Williams, 1991). Their chemistry necessitates that they precipitated from pore-fluids enriched in iron and dominantly reducing. Their burial origin is fully discussed in Chapter 3, Section 4.3.6.

Figure 6- Electron microprobe analysis of MgO, FeO, MnO, and SrO variations in inclusion-rich fibrous cements (CL sequence KZ), and both pre-compaction (CL sequence KA) and post-compaction (CL sequence KB) clear spar cements. Although present, no spot measurement was performed on CL sequence KC.
In (A), a schematic representation of the succession of CL sequences is superposed on the SEM photomicrograph. Note the thinness of CL sequence KB compared to well-developed scalenohedral crystals of CL sequence KA overgrowing the turbid acicular fringe of CL sequence KZ seen in (B).
Note in (C) that the MgO content is highly variable across the microprobe transect, but typically increases within pre-compaction CL sequences KZ and KA, and decreases within CL sequence KB. Note also the variability of FeO concentrations. Although on average, higher in "KB" cements, FeO contents may also be relatively high in "KZ" cements, suggesting that this cement generation was partly altered during burial diagenesis. The scenario is partly supported by the variable MnO contents in "KZ" cements, the highest values coinciding with bright patchy luminescence.

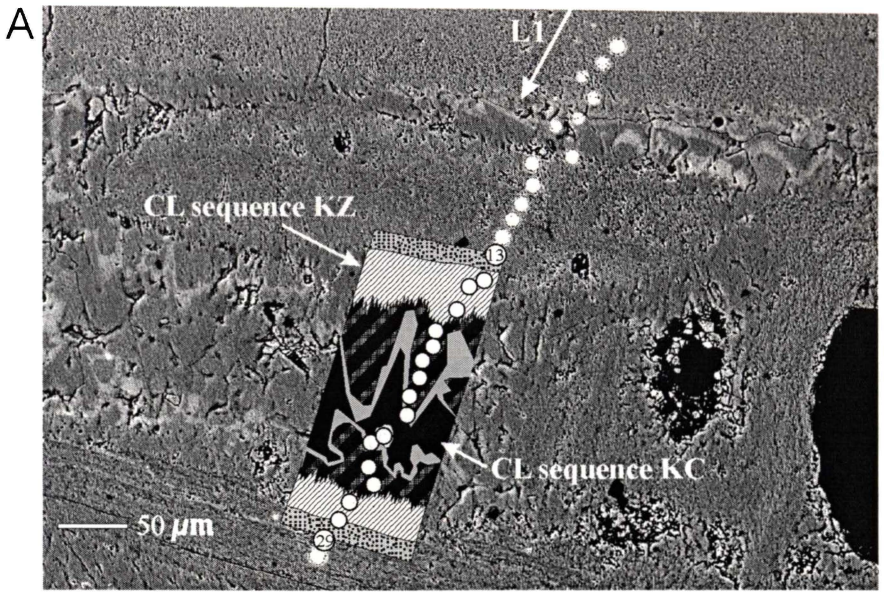

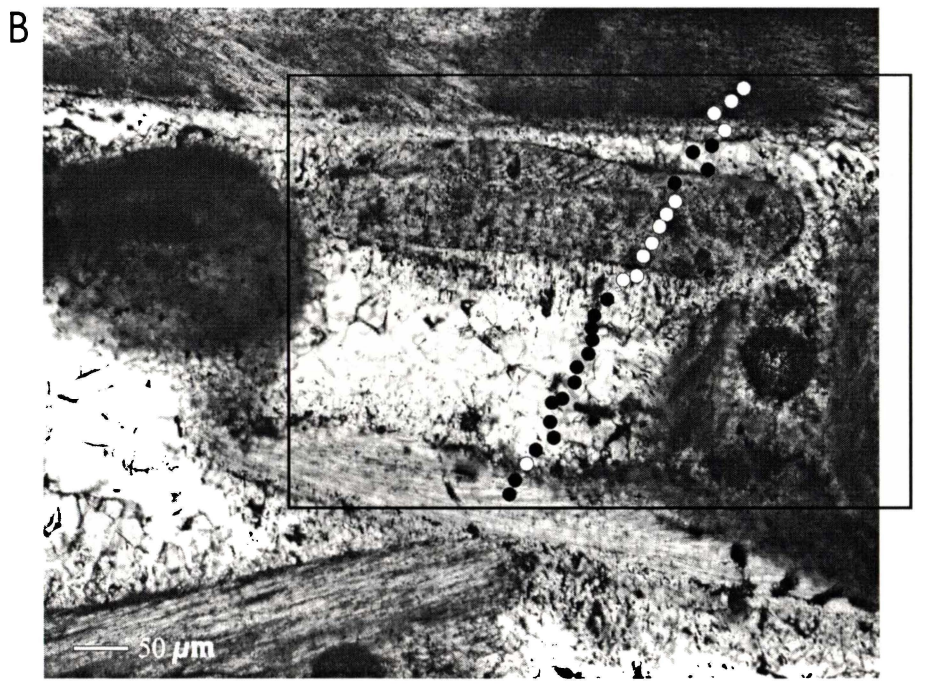

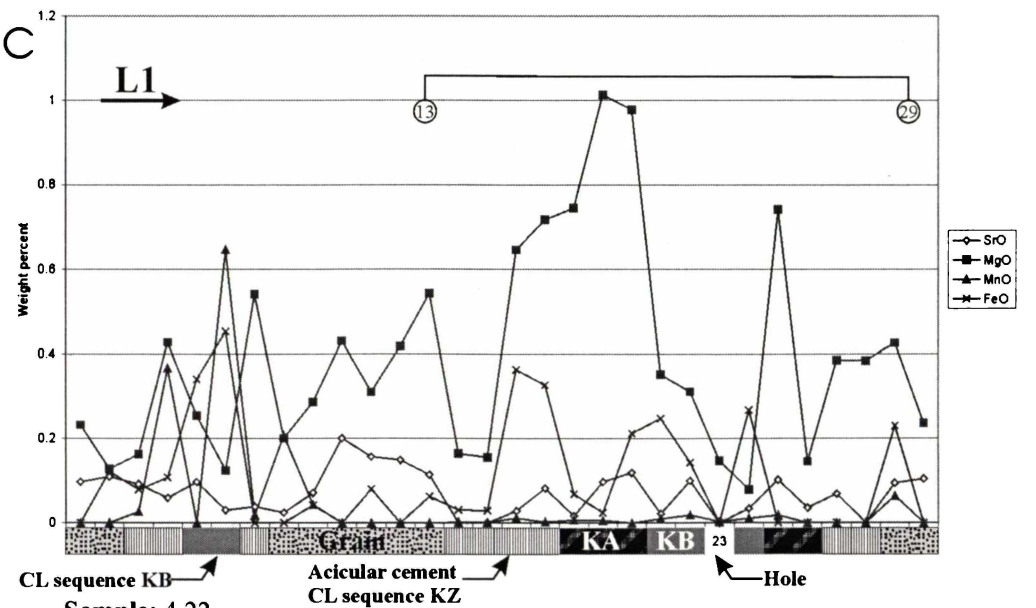

Sample: 4.22
Location: Mount Kahuranaki
Stratigraphy: Sequence B of Kairakau Limestone
Age: Opoitian

Distribution

CL sequence KB occurs throughout Kairakau Limestone, and by contrast with previous CL sequence KA extends as far north as the Waimarama section (Figure 5). However, post-compaction ferroan cements are best developed in the Kairakau sections located in the southeastern part of the study area where they are more prevalent than any other cement generation, even totally occluding the interparticle porosity in some samples, prior to uplift-related fracturing (discontinuity d3). Typically, they tend to thin in a south-northwestern trending direction.

The total amount of post-compaction ferroan cements represents more than 50% of the cement volume in sections parallel to the axis of the forearc basin from Kairakau Beach northwards to Cabbage Tree Flat, and regionally decreases westwards defining a "trough" of values below 25% in the Mt Kahuranaki area (Figure 5B).

4.2.4. Post-d3/Pre-d4 CL sequence (KC)

Description

Typically CL sequence KC cements start with discontinuity 3, which consists of uplift-induced fractures (Figure 4E) and/or correlative dissolution underlain by moulds, especially in the upper part of the Kairakau sections, and an irregular surface engulfed within older cements (when present). Discontinuity 4 terminates CL sequence KC, and tends to be outlined by dissolution, even though fractures occur.

In most cases, CL sequence KC cement represents the final void filling, and is typically clear, relatively coarse (blocky to mosaic), non-ferroan (N = 31; FeO = 0 to 0.3 wt%; mean = 0.12 wt%; stain pink with Dickson's solution) low-Mg calcite (MgO = 0 to 0.6 wt%, mean = 0.2 wt%).

It is generally non-luminescent, but may display in its early and latest growth stage orange and brightly yellow luminescent zones (Figures 4C, 4F). Further, the geochemistry of this late non-luminescent cement contrasts significantly from older CL sequences in being (1) more depleted with respect to $\delta^{18}O$ and $\delta^{13}C$ (see Section 4.3.3); and (2) strongly depleted relative to MnO (0 to 0.05 wt%; mean = 0.014 wt%), and SrO (0 to 0.6 wt%; mean = 0.06 wt%)(see Figure 9A).

CL sequence KC cements (referred to as YnfC in Chapter 3) are interpreted as a meteoric phreatic phase of calcite cement precipitated in the time interval during which carbonate sediments that had been buried (mesogenetic zone producing CL sequence

KB) were tectonically exhumed (uplift) to once again be influenced by surficial processes (see Chapter 3; Section 4.3.6). Uplift continued after these cements had developed to eventually expose the carbonate deposits to the most surficial diagenetic processes either in the phreatic or vadose meteoric environment. This latest stage is also pre-dated by fracturing and dissolution (i.e., diagenetic discontinuity d4).

The non-luminescent, non-ferroan cements within CL sequence KC conform with many late (telogenetic) meteoric diagenetic cements that have been described in ancient carbonate deposits and interpreted to have formed from oxidising fluids (e.g., Meyers, 1991; Lavoie and Bourque, 1993).

Distribution

The third generation of calcite spar may locally represent the volumetrically dominant cementation phase, exceeding 60% of the cement volume. Percentages of CL sequence KC vary inversely to that of CL sequence KA, in being higher in the north and west of the study region, decreasing to below 30% in the central part of the Maraetotara Plateau, eventually not representing more than 15% at Kairakau Beach (Figure 5C).

This regional distribution may either be a consequence of CL sequence KC occupying the remaining pore space after precipitation of cements within previous CL sequences, or the source area for CL sequence KC being different than for its older counterparts. The first scenario is partly supported by the local volumetric abundance of both CL sequences KA and KB that could have not permitted further cementation if porosity creation processes had not immediately pre-dated CL sequence KC (i.e., dissolution and fracturing). Therefore, pore space was available to accommodate calcite precipitates in the better-cemented carbonate facies at the time of the late non-luminescent cement development.

Moreover, petrographic analysis demonstrates that available accommodation pore space was not fulfilled by CL sequence KC in the southern part of its distribution (see also Figures 3B, 3F), suggesting that there exists a definite decreasing gradient of cementation in a north-south trending direction.

CL sequence KC pinches out within the silty calcareous sandstone of sedimentary sequence B in the southern Kairakau sections (Figure 5). This is probably related to the loss of permeability of this fine-grained facies after interparticle occlusion by previous cements.

4.2.5. Post-d4 CL sequence (KD)

Description

Post-d4 cement consists typically of a thin bright yellow zone that fills fractures cross-cutting all previous CL sequences (Figure 4). These fractures coincide with a very young tectonic event as they occur and can be correlated within most of the Pliocene limestones above the Kairakau unit. They connect with the same pore-lining bright cement revealing dissolutional gulf-like crystal boundaries (see also Figures 3D, 3F). The thin bright luminescent zone is followed across a sharp to erosional surface (i.e., etching once again) by non-luminescent cements.

The starting cementation stage stains pale blue to pale pink, while the latest non-luminescent stage stains pink. CL sequence KD is not found in sufficient quantities for isotopic analysis, and no microprobe spot analysis was performed on this cement generation.

The thin bright yellow zone is probably associated with slowed cementation, compared to the previous pre-d4 cementation stage, in partly reducing conditions, which suggest that the zone probably formed in a period of low carbonate supply after the system had been cut off from its source of well-oxygenated waters (Walkden and Berry, 1984; Walkden and Williams, 1991). Fracture-fed bright cement is believed to be related to the sealing of the sediment pile after a regional tectonic event, and is followed by the ingress of cementing oxidised meteoric waters probably indicative of the reopening of the system.

Distribution

CL sequence KD is sparsely developed throughout Kairakau Limestone and, on average, does not represent more than 5-10% of the total cement volume (Figure 5). It is absent from the central part of the Maraetotara Plateau, and poorly represented elsewhere, except in the lower part of the Cabbage Tree Flat section where it exceeds 20% of the cement volume.

4.3. Discussion and interpretation

4.3.1. Regional distribution of CL sequences

Petrographic mapping of cement zones has extensively been used by past researchers as a practical means of reconstituting the geometry of cementing paleoaquifer systems, and

for recognizing recharge areas and fluid flow directions (Meyers, 1978; Goldstein, 1988; Kaufman *et al.*, 1988; Niemann and Read, 1988).

The traceability of the diagenetic discontinuities bounding the three major CL sequences (KA, KB, KC) that collectively build up the diagenetic history of Kairakau Limestone, indicate that these successive cement generations are widespread throughout the formation, both vertically and laterally, but vary in their patterns of zonation and ferroan content (Figures 7A, 7B).

Spatial pinch-outs of cements enable determination of the geometry of CL sequences, and of their respective cementing aquifers at the regional scale, even though more detailed work is needed to assess the cements distribution in an east-west direction.

Upward pinch-out of CL sequences may either be caused by the impermeability of strata above, acting as aquitards, or be related to the surface from which fluids percolated (e.g., subaerial exposure surface; Goldstein, 1988), or simply highlight the uppermost limit of extension of some groundwater lenses, provided that their thickness is also determined by the volume of fluids allowed to be driven down-dip from the recharge area.

Downward pinch-out of CL sequences may also be related to the impermeability of strata stratigraphically located below (Simo and Lehmann, 2000), or may result from the downward limit of percolation of groundwaters, saturated enough with respect to calcium carbonate to cause cementation (Goldstein, 1988; Niemann and Read, 1988). Further, lateral facies changes and fluid flow levels are likely to determine the geographic distribution of cements (e.g., Niemann and Read, 1988; Meyers, 1991).

In all cases, the occurrence of cements within the CL sequences is dependent upon the saturation level of the groundwaters, whose evolution may also determine pinch-out geometries. Goldstein (1988) and Durlet (1996) report that the progressive increase of saturation level of primarily undersaturated meteoric waters beneath subaerial exposure surfaces, due to the release of $CaCO_3$ during water/rock interaction, eventually leads to cementation producing an upward pinch-out. The pinch-out corresponds to the interval where fluids were not yet saturated enough to favour calcite precipitation.

Figure 7- (A) Correlation panel of summary diagenetic suites for the Kairakau Limestone from Kairakau Beach in the south to Waimarama section in the north. Note that CL patterns within each CL sequence vary laterally in thickness, intensity of luminescence, and internal zonation, whereas diagenetic discontinuities and their correlative conformities can be traced from one locality to another. (B) Colour scheme of calcite cements stained with a solution of Alizarine-Red S/potassium ferricyanide (Dickson, 1965), and lateral variations. Note that in some portions of the overall oxidizing cementing aquifer (cements stain pink), involved in the formation of CL sequence KA, reducing conditions developed (blue stain). Calcite cement of CL sequence KB differs from its younger and older counterparts in staining blue, instead of pink, suggesting that it incorporated ferrous iron during precipitation under reducing conditions. (C) Hypothetical fluid flow directions envisaged for the successive paleohydrological systems that produced CL sequences KA to KD. Note that the flow direction is reversed for telogenetic CL sequence KC with respect to CL sequences KA and KB. See text for discussion.

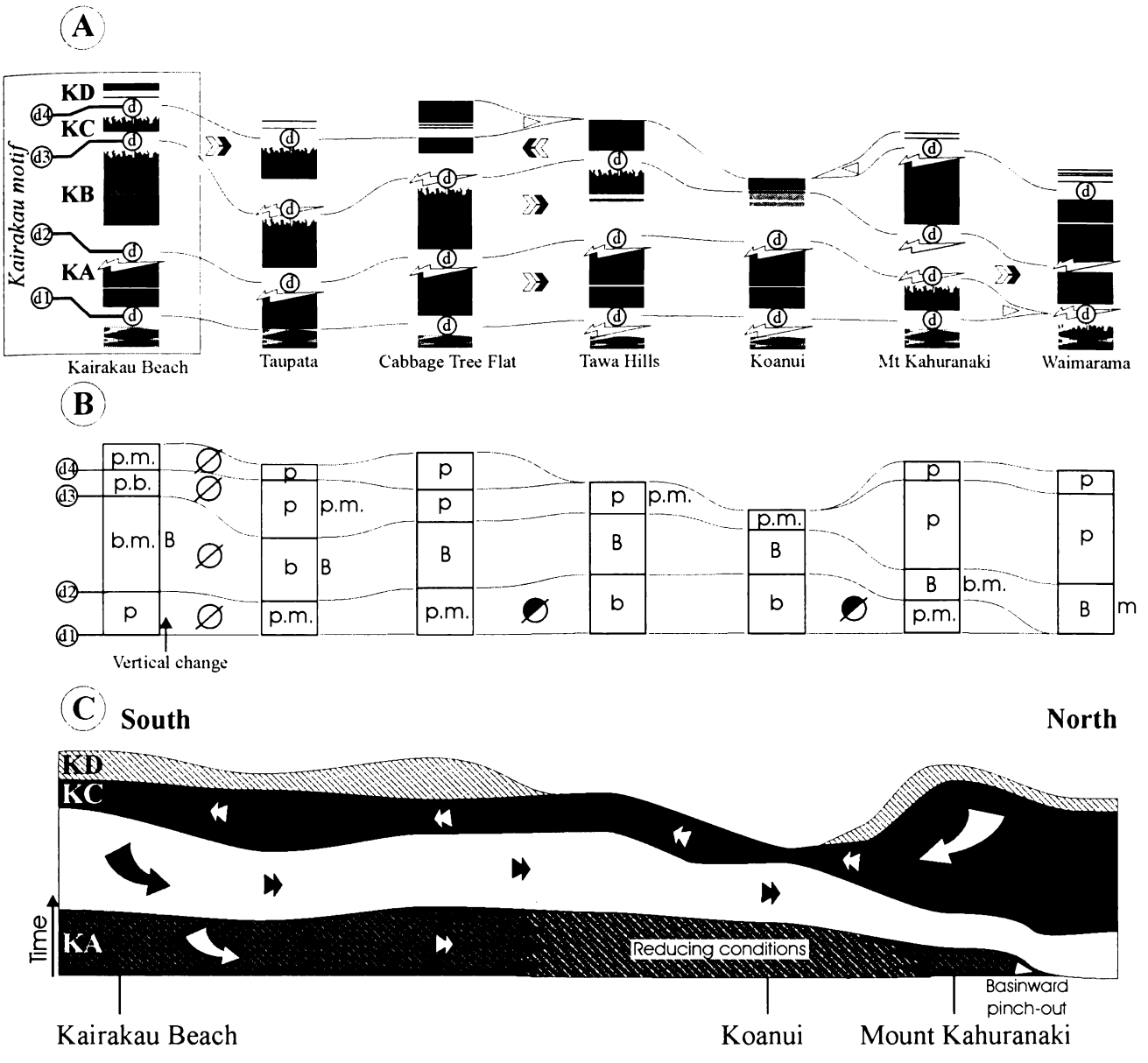

KEY

- Lateral change of CL pattern
- Lateral pinch-out of cement
- Downward pinch-out of cement
- Upward pinch-out of cement
- (d) Dissolution
- Fracturing
- Laterally or vertically uncorrelatable CL pattern
- Minor change of stain colour
- Major change of stain colour
- Diagenetic discontinuity becomes a conformable contact either vertically or laterally
- A conformable contact between CL zones becomes unconformable either vertically or laterally

Codes for chemical stains

p - Pink	B - Deep blue	p.m. - Pink/mauve
m - Mauve	b - Pale blue	b.m. - Pale-blue/mauve
		p.b. - Pink/pale-blue

CL sequence KA

The regional distribution of the pre-compaction non-luminescent cement, which extends throughout much of the Kairakau Limestone, conforms to the one expected for cements precipitated from extensive meteoric aquifer systems, and associated with subaerial exposure surfaces (Grover Jr and Read, 1983; Goldstein, 1988; Horbury and Adams, 1989).

The average percentages of non-luminescent cement volumes suggest that the recharge area for the meteoric fluids would be either located along the ridge of high percentage values (Tawa Hills – Koanui axis), or to the southeast in the Kairakau Beach area (Figure 5A). The latter scenario is supported by the progressive decreasing volume of CL sequence KA northwards, together with changes in its CL patterns and chemical stains, indicating that fluids involved in cementation were becoming more reducing in the same trending direction (Figures 7B, 7C). Identical diagenetic patterns, along gravity driven flows from recharge areas located on highlands, have been documented by Dorobek (1987) and Grover Jr and Read (1983).

The shallowing-upwards depositional trend of the upper sedimentary sequence of Kairakau Limestone argues in favour of subaerial exposure in some portions of the carbonate system (i.e., the top of antiform ridges; see Chapter 4, Section 5.3.4), allowing percolation of meteoric fluids. However, the relative low reactivity of the Kairakau carbonates dominated by LMC mineralogies, with some aragonite, is apparently not compatible with much cementation associated with primarily undersaturated meteoric waters moving downwards from an unconformity which, as pointed out in the previous chapters, if present, has not been unequivocally recognized. An attempt is made to address these inconsistencies in the light of geochemical data in the next section (Section 4.3.2).

CL sequence KB

A burial origin is suggested for dull moderate ferroan cements because they post-date non-ferroan cements and the onset of significant compaction-induced grain fracturing. They precipitated from an extended paleohydrological system, below the reach of well-oxygenated waters. Again the volumetric abundance of dull cements to the southeast, compared to the north, may reflect the dominant fluid flow trending direction (Figures 5B, 7C). The timing of establishment of this cementing aquifer system is discussed in

detail in Sections 4.4 and 4.5. Briefly, the comparability of post-compaction diagenetic suites, and the traceability of discontinuity 2 within Waipipian (Awapapa and Rotookiwa) and possibly Mangapanian formations (Te Onepu), suggest that precipitation of the majority of burial cements was delayed until after deposition of the Rotookiwa Limestone, unless conditions that prevailed for formation of post-compaction cements have no chronostratigraphic significance (i.e., repetition of the same post-compaction diagenetic motif).

CL sequence KC

Non-ferroan, non-luminescent, fracture-hosted cements were precipitated from oxidising meteoric waters. The regional percentage distribution of these cements reflects recharge of meteoric water into a fresh water aquifer from a north-south trending line (Figure 7C), which is superposed to the axis of the Elsthorpe Anticline (Figure 5C). Pettinga (1982) and Cashman *et al.* (1992) proposed that the Elsthorpe Anticline formed in Nukumaruan times (Late Pliocene), which may relate to the age of CL sequence KC, unless the relationship between the distribution of these telogenetic cements and the anticline is purely coincidental.

Upward and downward pinch-out of CL sequence KC (and KD) within the pre-cemented, fine-grained, siliciclastic sedimentary sequence B of Kairakau Limestone (between sedimentary unconformities 2 and 3; Figure 5) in the south, provide evidence that this horizon slowed penetration of cementing waters, and probably forced them to be stratified. In contrast, in the north, the sedimentary sequence B did not act as an aquitard, hence enabling recharge for the units below and reappearance of CL sequence KC.

4.3.2. Trace elements

Whole-rock compositions (Figure 8)

Because there are no major differences in the chemistry of carbonate constituents of Kairakau Limestone throughout its eastern distribution, observed contrasting trace element compositions between samples are assumed to be either due to differing degrees of (syn-) post-depositional alteration or to the interparticle cementing phase (Veizer, 1983a, b).

Figure 8- Element versus element plots of whole-rock samples from two sections of Kairakau Limestone to illustrate that there exists a significant departure between the two populations. The difference is attributed to the dominant cementing phase, which is CL sequence KB (post-compaction burial), and to a lesser degree CL sequence KA (pre-compaction meteoric), in Kairakau Beach samples, but is CL sequence KC (post-compaction telogenetic/meteoric) in Mt Kahuranaki samples. Diagenetic trends point to differing degrees of post-depositional alteration and chemical environments. See text for discussion.

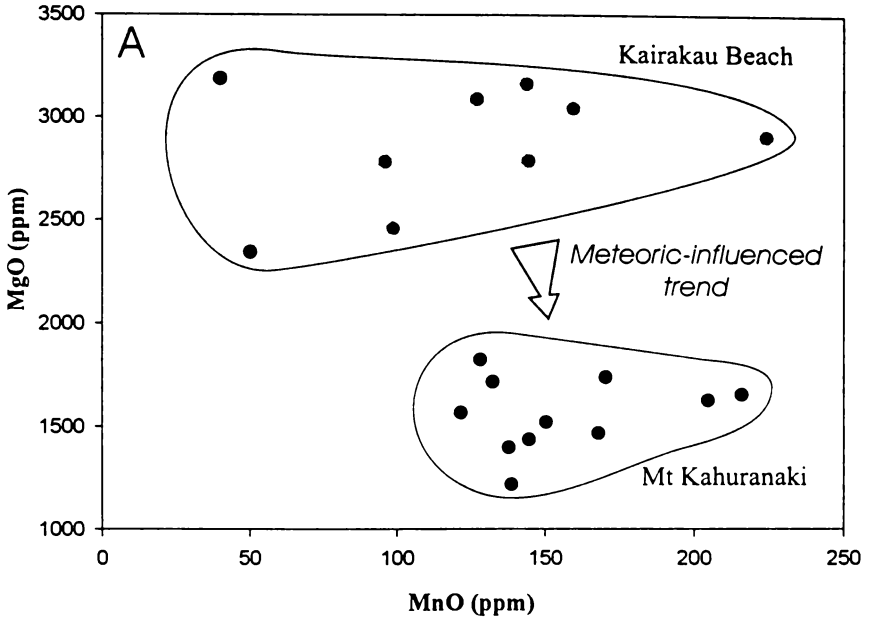
A
Kairakau Beach
Meteoric-influenced trend
Mt Kahuranaki
MgO (ppm)
MnO (ppm)
3500
3000
2500
2000
1500
1000
0
50
100
150
200
250

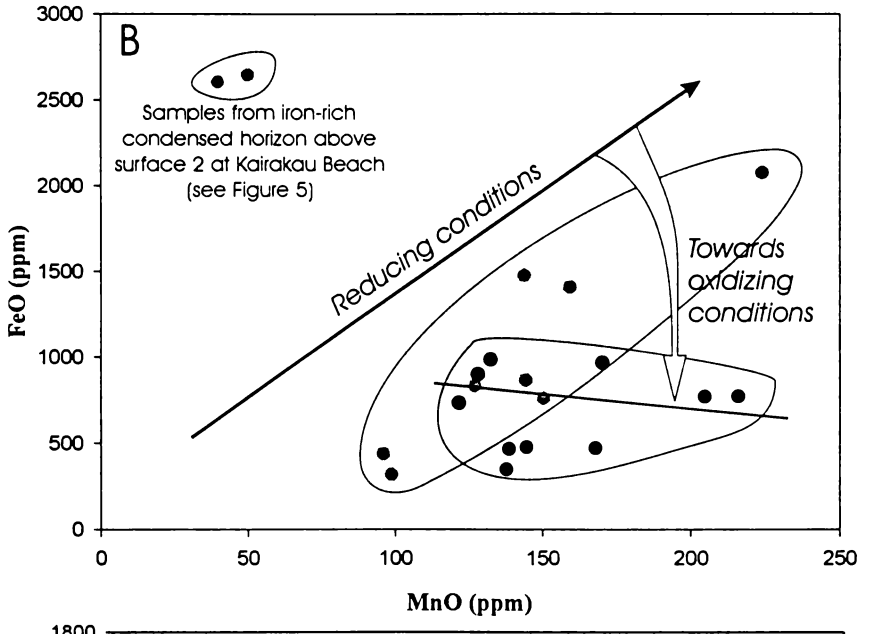
B
Samples from iron-rich condensed horizon above surface 2 at Kairakau Beach (see Figure 5)
Reducing conditions
Towards oxidizing conditions
FeO (ppm)
MnO (ppm)
3000
2500
2000
1500
1000
500
0
0
50
100
150
200
250

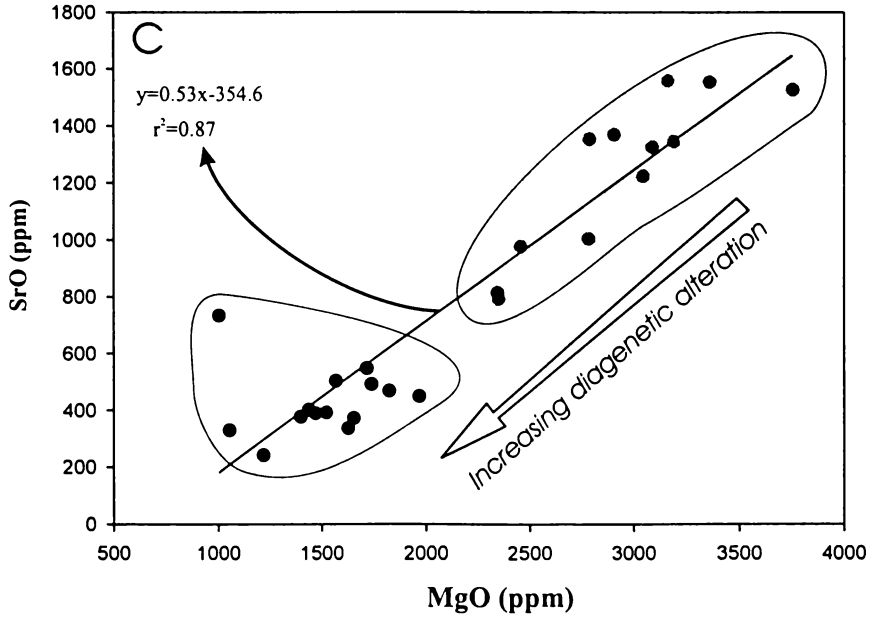
C
y=0.53x-354.6
r²=0.87
Increasing diagenetic alteration
SrO (ppm)
MgO (ppm)
1800
1600
1400
1200
1000
800
600
400
200
0
500
1000
1500
2000
2500
3000
3500
4000

MgO, SrO, MnO, and FeO cross-plots of whole-rock samples from the distinctive Kairakau Beach and Mt Kahuranaki areas, in terms of the contribution of the different CL sequences to their cement composition, is presented in Figure 8. The pool of values for both areas show a significant departure away from one another that can readily be interpreted as a result of differing meteoric diagenetic influence. Mt Kahuranaki samples show both a higher degree of meteoric alteration, and a greater contribution of meteoric cements to their composition than their Kairakau Beach counterparts.

Support for this interpretation includes: (1) the decrease in MgO and the higher mean of MnO concentrations in Mt Kahuranaki samples defining a meteoric-influenced trend (Figure 8A; Brand and Veizer, 1980; Veizer, 1983a); (2) the two populations of samples show contrasting diagenetic trends in FeO/MnO cross plots (Figure 8B). FeO and MnO values for Kairakau Beach samples define a positive trend suggesting the overprint of reducing conditions (Brand and Veizer, 1980; Winefield, 1995), while Mt Kahuranaki values lie along a trending line with a low gradient negative slope suggesting the influence of more oxidizing conditions; and (3) plotted MgO and SrO concentrations from both populations define a strong linear covariant diagenetic trend (Figure 8C), with the lowest values associated with Mt Kahuranaki samples, suggesting once again a higher degree of meteoric alteration (Brand and Veizer, 1980; Winefield, 1995).

These observations agree well with the aforementioned volumetrically dominant overprint by cements formed from meteoric oxidizing fluids on the Mt Kahuranaki carbonates (CL sequence KC). In contrast, Kairakau Beach carbonates were not as much diagenetically altered, and show the contribution of CL sequence KB cements precipitated from reducing fluids.

Relatively low SrO and variable, though moderate, MgO concentrations within both populations are consistent with a primary LMC mineralogy for the host-rock, with little aragonite (Rao, 1990).

CL sequences

The main aim of the geochemical analysis is to determine whether the diagenetic trends observed in the cements reflect post-depositional alteration of an original carbonate phase and/or record changes in the composition of the ambient fluid between each

cement generation. In other words, is the carbonate supply to the cementing fluids derived from the host-rock or from an external source?

Figure 9 presents MgO, SrO, MnO, and FeO cross-plots of CL sequences KA, KB, and KC. Average compositions plotted in Figure 9A shows a progressive decrease in MgO concentrations from the (inferred) marine original intermediate-Mg calcite (IMC) turbid cements (KZ) to the telogenetic cements of CL sequence KC.

Among the post-KZ cements, CL sequence KA contains the highest average level of MgO. This falls in the range of values comparable to those for the probable starting composition of the main marine components. Indeed, the Mg content of the initial rock is assumed to be 2-4 mol% $MgCO_3$, corresponding to the dominant primary LMC mineralogy of skeletons in a cool-water carbonate system (Nelson, 1988; Rao, 1990; Hood and Nelson, 1996).

The composition of CL sequence KB departs significantly from its older and younger counterparts, in having relatively high concentrations of both FeO and SrO (Figures 9A to 9D).

In element versus element cross-plots, each cement generation typically defines overlapping fields (Figures 9B to 9E). Both CL sequences KA and KB have a wide range of MgO, but differ in their FeO content. CL sequence KA has a narrow and low range of FeO, while CL sequence KB contains a broad range of values. In contrast, CL sequence KC has low concentrations of both MgO and FeO (Figure 9D).

All cement generations have broad fields of MnO, within an overall range of low values (Figure 9E).

Relatively high MgO values with respect to later diagenetic stages in CL sequence KA could result from an enrichment of pore waters in Mg cations released during degenerative neomorphism of IMC and high-Mg calcite (HMC) skeletons and cements in contact with undersaturated fluids. It can be envisaged that if the water/rock ratio during stabilization of these metastable carbonate phases was low, then the Mg/Ca ratio of the diagenetic fluid can approach that of the dissolving phase (Brand and Veizer, 1980; Meyers, 1989).

Carbonate released during dissolution of aragonite allochems and alteration of IMC-HMC allochems could account for the volume of cements (c. 5 % on average of the total rock volume) precipitated during CL sequence KA. Consistently, these non-luminescent cements post-date the (moderate) development of mouldic porosity (see

Figure 9- Plots of trace element concentrations obtained by microprobe spot analysis performed on the successive cement generations that make up the Kairakau Limestone diagenetic history. (A) Mean MgO, FeO, SrO, and MnO concentrations for CL sequences KZ to KC. MgO concentration decreases with each younger precipitate, from the (inferred) marine turbid cements of CL sequence KZ to the telogenetic/meteoric cement of CL sequence KC. FeO and SrO contents of CL sequence KB depart from those of its counterparts. This is interpreted to be a result of precipitation under low water/rock ratio and reducing conditions. (B) to (E) Compared element versus element cross-plots of CL sequences KA to KC. Non-linear covariant trends defined by the fields of MgO-SrO, FeO-MgO, and MnO-MgO for CL sequences KA and KB are hypothetically attributed to result from solubility-driven water-rock exchange. "L-shaped" covariant trend of FeO-MnO in (C), from CL sequence KA to KB, is consistent with the predicted model invoking water-rock interaction and decreasing Eh changes in diagenetic fluids (Meyers, 1989). Low MgO, SrO, FeO, and MnO concentrations point to probable high water/rock ratio, well oxygenated, and meteoric cementing fluids for CL sequence KC (in plots B and D, note that the fields where the majority of CL sequence KC samples plot are shaded). See discussion in text.

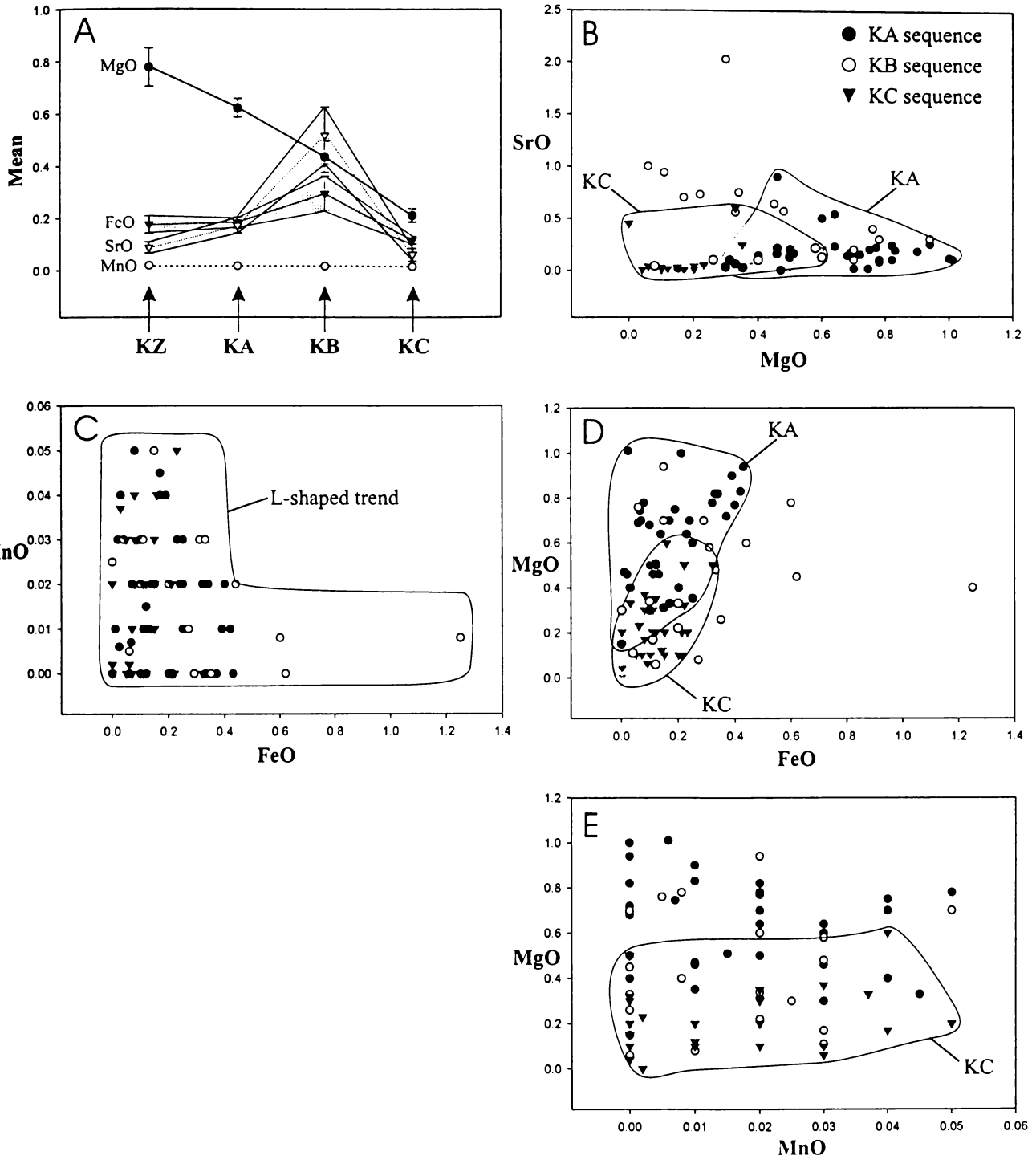
A
MgO
FeO
SrO
MnO
Mean
KZ
KA
KB
KC
B
KA sequence
KB sequence
KC sequence
SrO
MgO
KC
KA
C
L-shaped trend
MnO
FeO
D
KA
KC
MgO
FeO
E
KC
MgO
MnO

Figure 4A), are coeval with neomorphism of aragonite (see Figures 17C, 17D), and overgrow neomorphosed turbid acicular crystals (see Figures 6, 17B).

Non-linear covariant patterns defined by FeO vs. MgO and MnO vs. MgO concentrations for ferroan cements of CL sequence KB (Figures 9D, 9E) are compatible with the L-shaped patterns of the evolution curves used by Meyers (1989) to predict trends of evolving rock during interaction of carbonate phases with Mn/Fe-bearing fluids. Also the water/rock interaction model predicts that SrO concentrations should increase as dissolution of the metastable carbonate phase supplies Sr to the cementing fluids. In addition, the FeO vs. MnO plot should define a straight linear covariant trend with a positive slope (Lohmann, 1988; Meyers, 1989).

Moderately higher SrO contents in CL sequence KB cements than in the previous and following phases partly conform to the predicted model. In contrast, the L-shaped pattern of the FeO vs. MnO cross-plot contradicts the expected trend. Meyers (1989) reported similar inconsistencies, and explained the non-linear Fe/Mn covariance as resulting from an interplay between redox variations and water/rock interaction.

Thus, it is proposed that dull cements of CL sequence KB result from interaction between Fe-bearing fluids and host carbonate sediments in reducing conditions, allowing both Fe and Mn to be incorporated in the calcite precipitate. These cements post-date dissolution that promoted new porosity creation either by enlarging previously developed mouldic porosity, or etching unaltered skeletons.

Low MgO concentrations, and relatively low narrow ranges of FeO-MnO contents of CL sequence KC, suggest low water/rock interaction and oxidizing conditions during precipitation (Lohmann, 1988). Although dissolution once again accompanies the precipitation of the telogenetic cements, trace element data do not permit determination of the source of carbonate supply. However, the non-linear covariant pattern of the FeO vs. MnO plot does not rule out the possibility of water interaction upon Mg-depleted carbonate phases (Meyers, 1989).

4.3.3. Stable isotope data (Figure 10)

One must re-emphasize that the scant database of stable isotope measurements on individual cement generations calls for caution, and consequently does not allow the origin and nature of the precipitating fluids to be confidently deciphered. More isotope

data are needed to address the speculations made regarding the origin of the CL sequences, and which are presented below.

Whole-rock and CL sequences data

The major non-biogenic contributors to the composition of the Kairakau samples, namely CL sequences KB and KC, and at a lesser degree CL sequence KA, are expected to cause significant departures from the original isotopic composition of marine waters, whose best estimate is assumed to be the one yielded by Waipipian brachiopods (N = 8; -0.4< $\delta^{18}O$<+0.9, mean = +0.25 ‰PDB; +1.0<$\delta^{13}C$<+2.4, mean = +1.73 ‰PDB). The contribution of CL sequences KZ and KD is considered insignificant.

Consistently, Kairakau carbon-oxygen isotope values define two fields, presumably reflecting the proportions of CL sequences KB and KC included in the samples. Samples (N = 5) with high proportions of CL sequences KA and KB have a narrow range of both $\delta^{18}O$ and $\delta^{13}C$ values, between –1.0 and –0.4 ‰PDB, and between –0.1 and +1.13 ‰PDB, respectively. These values plot close to the field of inferred marine carbonates (brachiopods and CL sequence KZ; Figure 10). In contrast, samples (N = 4) with high proportions of CL sequence KC are depleted in both $\delta^{18}O$ and $\delta^{13}C$, with values ranging between –3.98 and –1.78 ‰PDB, and between –5.25 and –1.0 ‰PDB, respectively. Values plot between the fields defined by marine carbonates and cements from CL sequence KC, partly overlapping the latter (Figure 10).

The carbon-oxygen isotope cross-plot of the bulk of pre-compaction cements defines a plateau of narrow ranging $\delta^{13}C$ values (between +0.06 and –1.7 ‰PDB) and broadly ranging $\delta^{18}O$ values (between –4.45 and –0.8 ‰PDB) (Figure 10).
Samples from CL sequence KC are the most depleted in both $\delta^{18}O$ and $\delta^{13}C$. Their $\delta^{18}O$ values (N = 5) range between -3.1 and –4.9 ‰PDB, and $\delta^{13}C$ values between -2.1 and –5.3 ‰PDB.

Discussion

The pattern of nearly constant $\delta^{13}C$ and variable $\delta^{18}O$ values defined by pre-compaction cements compares with the high water/rock interaction model predicted for undersaturated fluids interacting with marine carbonates (Meyers and Lohmann, 1985; Lohmann, 1988), and would support the interpretation based on trace element data for CL sequence KA.

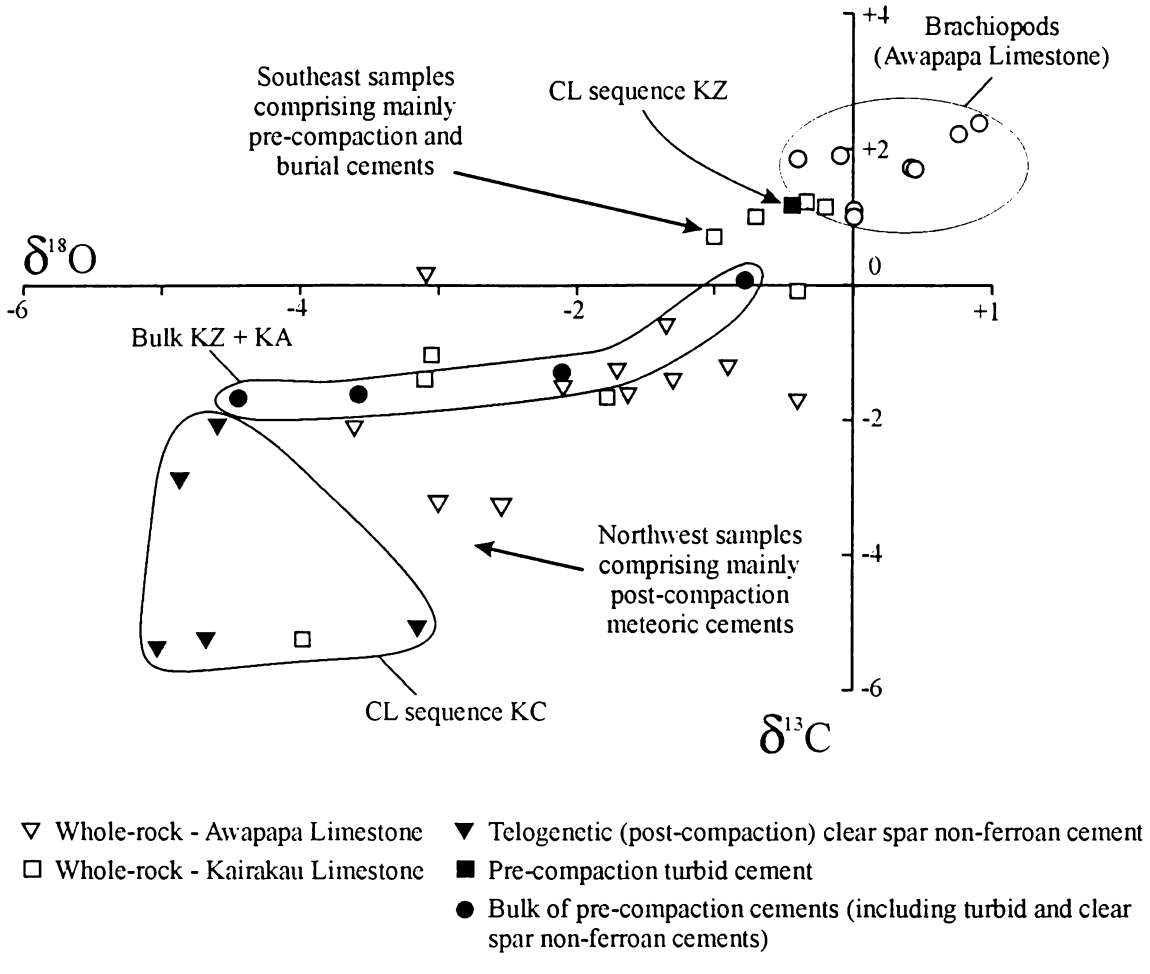

Figure 10- Carbon and oxygen isotope compositions of cements within CL sequences KZ to KC, brachiopods from Awapapa Limestone sections, and whole-rock samples from Kairakau and Awapapa Limestones. The cross-plot identifies two fields of values (shaded) for Kairakau samples that reflect differing contributions from the component CL sequences. See text for details. Note that telogenetic/meteoric cement of CL sequence KC is the most depleted in $\delta^{13}C$, suggesting an allochthonous carbon source. The covariation for data from the bulk of CL sequences KZ and KA defines a plateau-shaped trend that is consistent with the water/rock interaction model (Lohmann, 1988). See text for discussion.

Although no isotope data are available for CL sequence KB, the proximity of samples with high proportions of both CL sequences KA and KB to the field of marine carbon-oxygen values, also supports the water/rock interaction model (low water/rock ratio) as envisaged before (Section 4.3.2), but also suggests that the cements from CL sequence KA may have formed during marine-meteoric fluid mixing, and cements from CL sequence KB in marine fluids modified by burial and possibly mixed with meteoric waters (Frank and Lohmann, 1995; Frank *et al.*, 1995). The potential for not only dissolution, but also for precipitation of mixed marine-meteoric waters is well documented from experimental simulations (Runnels, 1969), and mixed fluids have been envisaged as the major cementing source of aragonite cements (Kimbell and Humphrey, 1994), and especially of pre-compaction non-luminescent banded cements (Frank *et al.*, 1995). However, the mixing model first requires that at least one of the two end-members is carbonate-saturated. The saturation level of the mixture is then determined by the percentage of either waters in the diagenetic fluid, besides temperature and pCO_2 considerations (Runnels, 1969).

The principal requirement is apparently incompatible with the inferred relatively low-saturation level of cool Pliocene sea waters, unless meteoric waters constituted the supersaturated fluids. In this case, either $CaCO_3$ is intrinsically sourced and water/interaction is the main process, or the carbonate source is external and then dissolution that pre-dates CL sequences KA and KB becomes problematical. Furthermore, the comparability of $\delta^{13}C$ values from both whole-rock samples and bulk pre-compaction cements suggests that the rock body is the most likely source for carbon, arguing again in favour of the water/rock interaction model.

The $\delta^{13}C$-depleted compositions of telogenetic cements distinguish them from other cement generations and whole-rock samples. Their relatively light $\delta^{13}C$ values compare with the range of values from meteorically altered cool-water carbonates (Nelson and Smith, 1996), and can possibly be attributed to the effects of soil-derived CO_2 (Lohmann, 1988). Because $\delta^{13}C$ values of CL sequence KC depart significantly from those of whole-rock samples, it is indeed assumed that at least part of the carbon incorporated in the cements is allochthonous (Walkden and Williams, 1991), and was transported with new fluids from a source located somewhere to the west (see Section 4.3.1).

4.4. Cementation history of Kairakau Limestone and origin of CL sequences

The diagenetic history of Kairakau Limestone combines a chronological suite of cementation and non-cementation stages, which define five CL sequences, namely KZ, KA, KB, KC, and KD, with distinct CL patterns, ferroan contents, and geochemical signatures. The unconformable succession, here named the *Kairakau motif* (Figures 4, 5, 7A, 11, 15D), builds upon conformable suites of cements bounded by correlative diagenetic discontinuities, and records the transition between surface-related processes (i.e., CL sequences KZ and KA) to processes reflecting a confined evolution of the pore fluids (i.e., CL sequence KB), and once again to surficial processes after tectonic uplift of the sediment pile (i.e., CL sequences KC and KD).

CL sequence KZ corresponds to syndepositional marine cementation.

CL sequence KA is pre-compacted, post-dates dissolution fabrics, and comprises non-ferroan, non-luminescent cements. It is proposed that the cements formed from near-surface, oxidizing meteoric groundwaters that percolated from a syndepositional unconformity on top of Kairakau Limestone, and were possibly mixed, in unknown portions, with marine fluids. A water/rock interaction model is proposed here to account for the carbonate supply to the originally undersaturated fluids. Implicit in this interpretation is the assumption that $CaCO_3$ is autochthonous, and derives from dissolving metastable carbonate phases, namely aragonite and IMC/HMC present in the host-rock. The few geochemical data do not rule out the possibility that supersaturation was attained during mixture of carbonate-rich marine and meteoric fluids, but in either scenario point to a definite degree of meteoric influence, which remains to be assessed.

CL sequence KB post-dates compaction-induced fractures and dissolution fabrics, and comprises moderately ferroan to highly ferroan (from chemical stain), dull luminescent cements. The cements precipitated from an extended paleohydrological aquifer that passed through the sediments from a recharge area located somewhere to the east of the study area, and became progressively buried below the influence of well-oxygenated waters. Ferroan contents and dull luminescence indicate that reducing conditions prevailed during cementation. CL sequence KB pre-dates dissolution seams producing serrated contacts and microstylolites, but pre-dates and post-dates grain-to-grain and curved-grain contacts. These would indicate that carbonate derived from pressure-dissolution is not the major contributor to the cementing phase. However, it is suggested that solubility-driven exchange with autochthonous carbonates, and to a lesser

degree pressure-dissolution, are the dominant processes that added $CaCO_3$ to the ambient fluids. These became supersaturated, and were enriched with host carbonate-derived elements, such as SrO. One can argue that a prolonged time of residence in the burial environment resulted in low water/rock ratios, thereby allowing a high degree of water/rock interaction to be attained, as suggested by Walkden and Williams (1991). The timing of establishment of the confined aquifer is discussed below.

CL sequence KC is fracture-hosted and is associated with dissolution. It comprises non-ferroan, non-luminescent cements that formed from oxidizing meteoric groundwaters that entered the previously sealed carbonate system, while the Kairakau Limestone was being tectonically exhumed. The probable source area for the cementing fluids was located in the central part of the study region.

CL sequence KD also post-dates a fracturing event and appears to be the latest stage in the paragenetic suite. It is mostly represented by non-ferroan, non-luminescent, meteoric fluid-derived cements, though the early cement growth stage (bright yellow, pale blue to pink) suggests partial closure of the system.

4.5. Comparability of diagenetic pathways for the Kairakau and Awapapa Limestones

4.5.1. Cementation within the Kairakau and Awapapa units

Awapapa Limestone occurs above Kairakau Limestone, from which it is separated by the silty Mokopeka Sandstone. The construction of detailed CL sequence diagrams through both units enables recognition of similar patterns of cementation (compare Kairakau and Awapapa sequence diagrams in Appendix 5). Thus, Awapapa Limestone contains the full suite of diagenetic components that collectively build up the *Kairakau motif* previously described (Figure 11).

Typically, in ascending order the diagenetic suite involves: (1) marine turbid acicular cements growing upon the eroded outer margin of carbonate grains, and restricted to specific stratigraphic horizons; (2) a dissolution surface; (3) clear, non-ferroan, non-luminescent, substrate-selective cements; (3) compaction-induced fractures associated with dissolution fabrics; (4) thin, ferroan, dull orange luminescent, substrate-independent cements; (5) fractures and locally well-developed mouldic porosity; (6) non-ferroan, non-luminescent, mosaic spar; (7) fractures and corrosion of the outer

Figure 11- Suggested correlation of cement suites through the Kairakau and Awapapa limestones at Te Mata Peak. Unconformity-bounded depositional units in the limestone succession are lettered from ka to kd and from A to K, respectively. Each patterned rectangle represents one cathodoluminescence (CL) sequence bounded by discontinuities at the thin-section scale, which can be traced vertically and laterally. CL characteristics of samples within each limestone are synthesized and converted into an "idealized" CL sequence, built as a sum of CL sequences, that represents the broad CL signature of a limestone at a given location. Such idealized CL sequences are given for the Awapapa (note that the sequence is given for the middle part of the succession where CL sequence a^1 is missing) and the Kairakau Limestone. The CL log represents vertical variations in thickness of CL sequences. Not all samples are represented. Thin vertical arrows follow the vertical distribution of correlated CL sequences. For the Awapapa Limestone, pre-compaction cements correspond to the vertically restricted marine-cemented horizons (AZ not represented), and to CL sequences a^1 and a^2 (part of AA) precipitated from meteoric waters that probably originated from some regional unconformity surface(s). Note that CL sequence a^1 pinches out within depositional unit H (arrowed), whereas CL sequence a^2 that post-dates a^1 in the diagenetic suite, persists downward through the entire succession, except for the base of unit A (arrowed). Note that this vertical pinch-out also occurs at Hawea/River Bank and Pukekura sections (see Figure 1). Pre-compaction meteoric cements overprint the specific diagenetic suites involving marine destructive and constructive diagenetic features in all units. The post-compaction suites of discontinuities and cements in the Kairakau and Awapapa Limestones are similar. Besides differences in their CL patterns, sequences AB and KB that are both ferroan cements could correspond to the same diagenetic event, and likewise it is inferred that CL sequences AC-AD correlate to CL sequences KC-KD (non-ferroan telogenetic/meteoric cements). This would suggest that either the same post-compaction pattern was repeated at different times or that the cements originated from the same post-compaction waters sometime after deposition of the Awapapa Limestone.

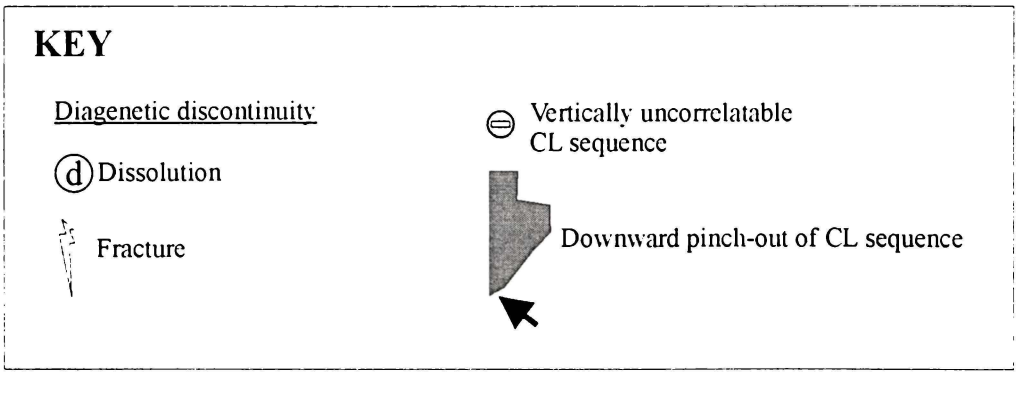

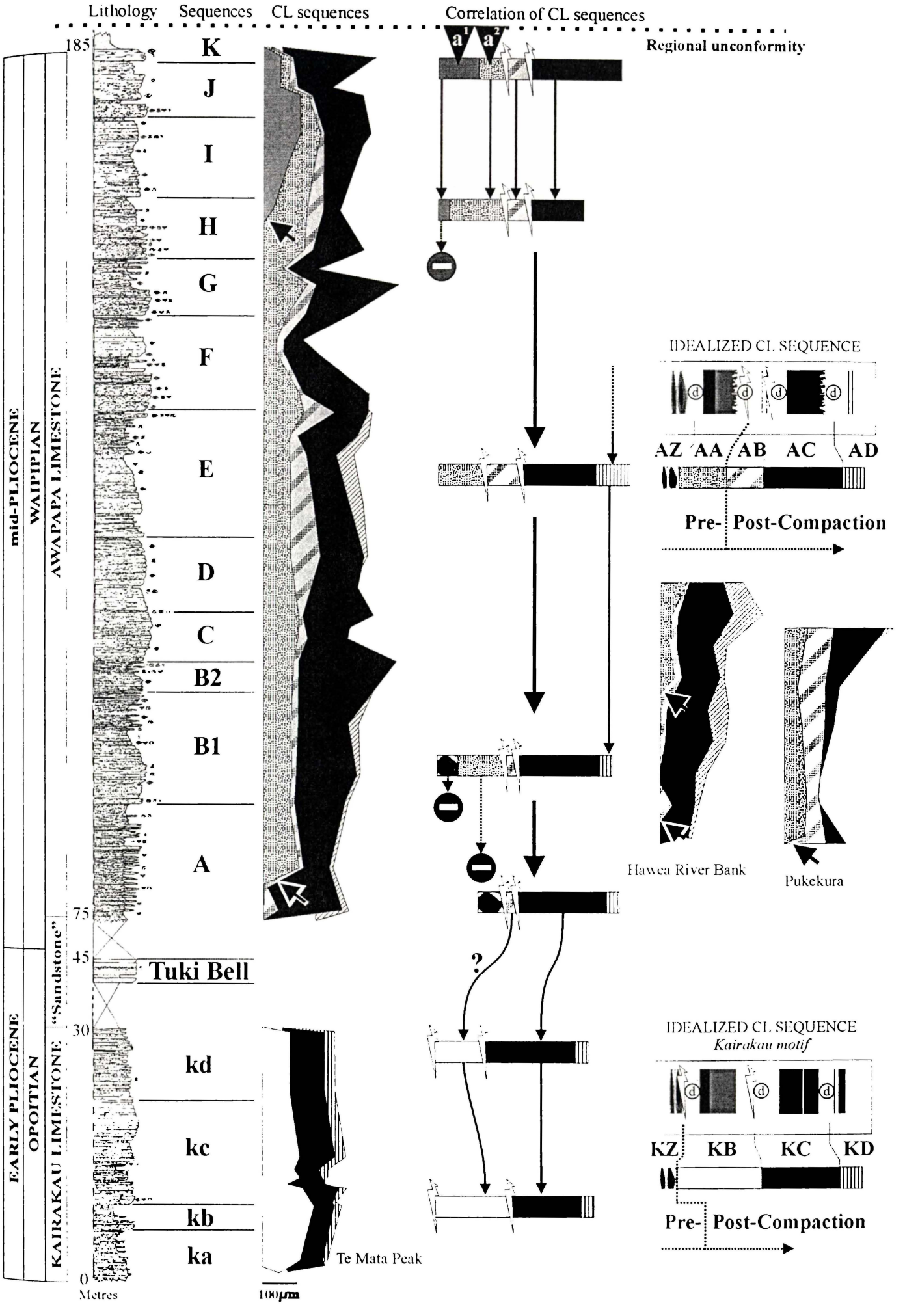
Lithology
Sequences
CL sequences
Correlation of CL sequences
Regional unconformity
mid-PLIOCENE
WAIPIPIAN
AWAPAPA LIMESTONE
EARLY PLIOCENE
OPOITIAN
"Sandstone"
KAIRAKAU LIMESTONE
185
75
45
30
0
Metres
K
J
I
H
G
F
E
D
C
B2
B1
A
Tuki Bell
kd
kc
kb
ka
Te Mata Peak
100 µm
IDEALIZED CL SEQUENCE
AZ AA AB AC AD
Pre- Post-Compaction
Hawea River Bank
Pukekura
IDEALIZED CL SEQUENCE
Kairakau motif
KZ KB KC KD
Pre- Post-Compaction

margin of calcite crystals; and (8) a suite of yellow brightly luminescent and non-luminescent cement.

Clear spar cements are generally widespread throughout the Awapapa Limestone. The traceability of diagenetic discontinuities, bounding the successive cementation stages, greatly facilitates regional correlation and highlights lateral changes of CL patterns and ferroan contents. For example, the pre-compaction clear spar cement is typically non-luminescent at Te Mata Peak and as far south as the Hawea/River Bank area, but is orange moderately luminescent at Pukekura (Figure 11 and Appendix 5, sections K11/A1 and A2-A6).

The repetition of the same diagenetic motif within limestone units from above and below a silty sandstone that may potentially act as an aquitard points out the question of the chronostratigraphic significance of the observed component CL sequences. In other words, does the comparability of diagenetic suites result from the repeated development of precipitating fluid systems at different stratigraphic levels and at different times? Or, does the diagenetic motif result from the passage of successive fluid systems through the sediment pile, each precipitating one CL sequence, thereby becoming correlatable between the limestone units?

The latter assumption is partly supported by the strong overlap of Awapapa whole-rock trace elemental signatures with those of Kairakau Limestone (Figure 12). Considering the comparable skeletal compositions of Awapapa and Kairakau carbonates, this suggests that the majority of cements within both limestones were precipitated from compositionally similar fluids.

4.5.2. Timing of formation of CL sequences

Pre-compaction clear spar CL sequence

It is proposed that non-luminescent cements that pre-date compaction-induced skeletal fracturing, and are found in both Kairakau and Awapapa Limestones, formed from temporally distinct aquifer systems. Despite the lack of geochemical data, the following kinds of evidence argues in favour of this proposition: (1) the spar cement is shared by all the depositional packages constructing the Awapapa Limestone, and has not been recognized in the overlying, fine-grained, Pukekura Calcarenite. This suggests that the pre-compaction cement is likely to have formed from near-surface, oxidizing groundwaters that percolated through the entire succession from a capping regional

unconformity somewhere above Awapapa successions, which probably acted as a recharge area; and (2) throughout its distribution, the pre-compaction cement characteristically pinches out downward (Figure 11), suggesting either that the underlying silty sandstone prevented downward flow, or the vertical extent of the cementing lens was locally limited due to insufficient recharge (cf. Goldstein, 1988).

Post-compaction CL sequences

Post-compaction fracture-hosted cements are proposed to be shared by both Kairakau and Awapapa Limestones, on the basis of the following evidence: (1) in addition to assuming that fractures (compactional and tectonic) represent distinct chronostratigraphic events (e.g., Zeeh *et al.*, 1997), one can argue that if the post-compaction diagenetic suites are temporally and spatially distinct, then one must admit that the same suite of fracturing events was repeated in time at different stratigraphic levels, and diagenetic overprints should be expected. There is no evidence that the compaction-induced fracturing events observed in both units, and filled with similar cements, are distinct, because no cross-cutting relationship distinguishes them; (2) the range of trace element data for Awapapa post-compaction ferroan cements overlaps with the fields defined by Kairakau data. The same diagenetic trends are recognized, even though Awapapa samples have lower SrO contents that may relate to lower water/rock interaction during precipitation (Figure 13); and (3) the burial CL sequence (equivalent to CL sequence KB) is always unconformably overlain by the same fracture-hosted meteoric/telogenetic CL sequence (KC), which provides a useful hallmark for correlation (Figure 11).

The same *Kairakau motif* is present in the younger Rotookiwa (and possibly Te Onepu) Limestone (Figure 14), suggesting that burial and later telogenetic cements precipitated from basin-wide aquifers whose base was located within the Kairakau Limestone.

4.5.3. Configuration of the burial CL sequence

The volumetric abundance of this cementation stage is highest in the Kairakau Limestone, and diminishes upwards within the Awapapa and Rotookiwa Limestones. This contrast does not originate in differences in pore space available to accommodate

Figure 12- Element versus element plots of whole-rock samples from Kairakau and Awapapa Limestones to illustrate that there exists no significant difference between the two pools of data. Awapapa samples from Te Mata Peak section have similar skeletal compositions to their Kairakau counterparts. The strong overlap suggests that both limestones are also compositionally similar with respect to their respective cementing phases. Samples from Pukekura section (shaded) of Awapapa Limestone depart significantly from both Awapapa at Te Mata Peak and Kairakau data. By contrast with Awapapa carbonate sediments at Te Mata Peak, mostly composed of barnacles and bivalves, Pukekura carbonates are dominated by bryozoan skeletons and were probably deposited down-dip from the Te Mata Peak area. Within their post-depositional cement suite, CL sequences AA (pre-compaction meteoric) and AD (post-compaction burial) are the volumetrically dominant phases, whereas CL sequence AC (post-compaction meteoric) dominates the paragenetic suite of Awapapa Limestone at Te Mata Peak (see Figure 11). The combined effects of both differing skeletal composition and contribution of each cement phase may explain the departure observed between Pukekura and Te Mata Peak data.

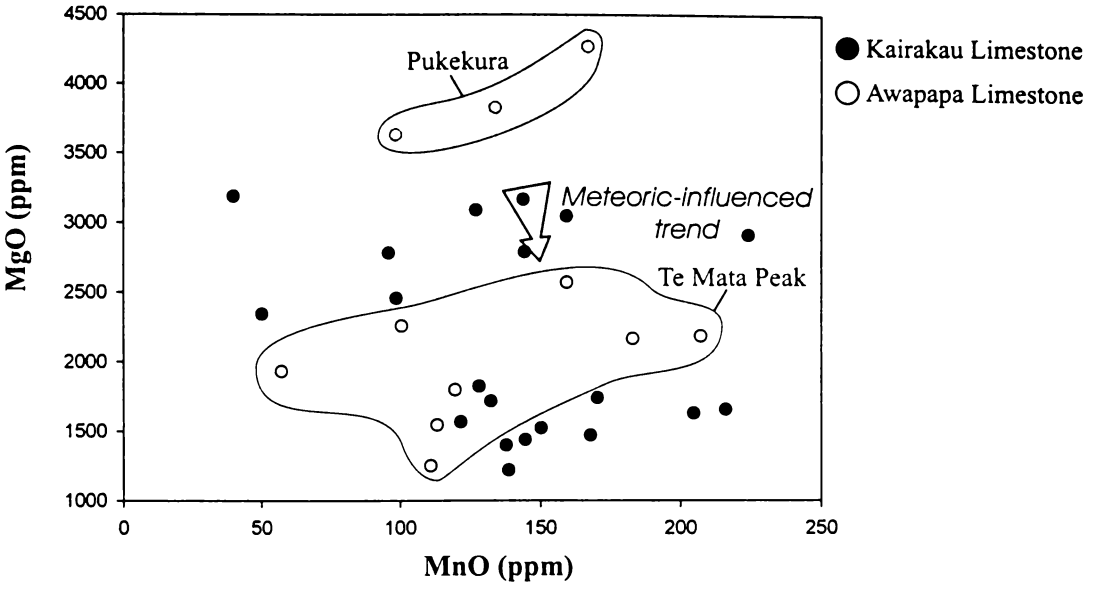
Kairakau Limestone
Awapapa Limestone
Pukekura
Meteoric-influenced trend
Te Mata Peak
MgO (ppm)
MnO (ppm)
4500
4000
3500
3000
2500
2000
1500
1000
0
50
100
150
200
250

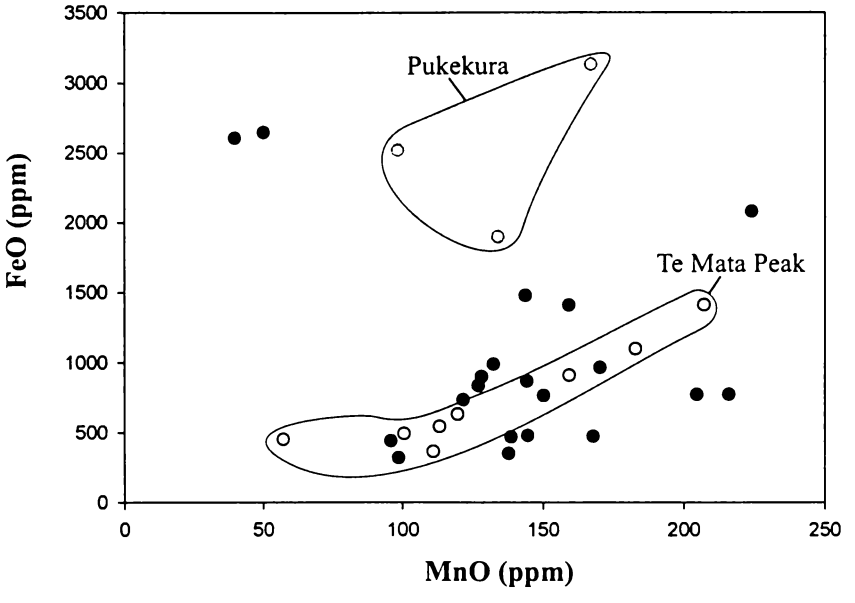
Pukekura
Te Mata Peak
FeO (ppm)
MnO (ppm)
3500
3000
2500
2000
1500
1000
500
0
0
50
100
150
200
250

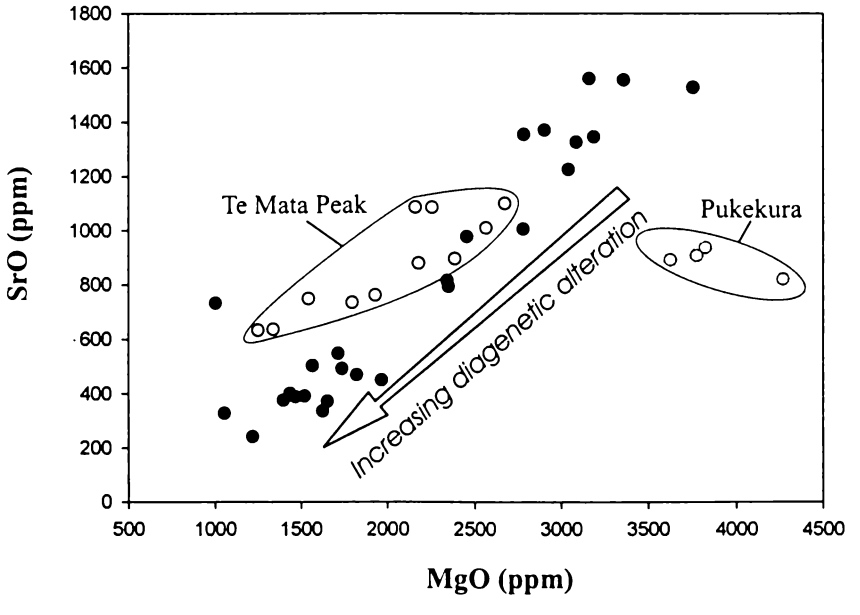
Te Mata Peak
Pukekura
Increasing diagenetic alteration
SrO (ppm)
MgO (ppm)
1800
1600
1400
1200
1000
800
600
400
200
0
500
1000
1500
2000
2500
3000
3500
4000
4500

Figure 13- Trace element plots for post-compaction burial cements of CL sequences KB and AB of Kairakau and Awapapa Limestones, respectively, are compared to assess compositional similarities. Although the two pools of data overlap each other, and exhibit similar MnO-MgO and FeO-MnO covariation diagenetic trends, SrO contents of Awapapa samples are lower than those of Kairakau Limestone on average. It is suggested that Awapapa "AB" cements formed under higher water/rock ratios than "KB" cements. This is consistent with the hypothesis that burial cements in Awapapa and Kairakau Limestones precipitated within the same aquifer, but in spatially distinct portions of its ground-distribution. It is proposed that burial cements from the Awapapa Limestone formed in the upper part of a confined aquifer where high water/rock ratios and less reducing conditions prevailed, compared to the same cement generation from Kairakau Limestone precipitated in deeper portions of the aquifer under low water/rock ratios and more reducing conditions. See text for comment.

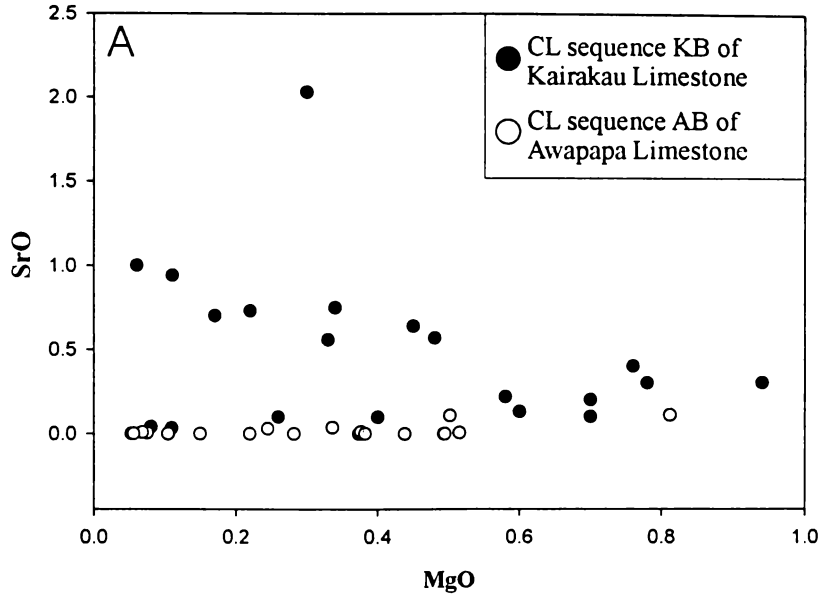
A
CL sequence KB of Kairakau Limestone
CL sequence AB of Awapapa Limestone
SrO
MgO
2.5
2.0
1.5
1.0
0.5
0.0
0.0
0.2
0.4
0.6
0.8
1.0

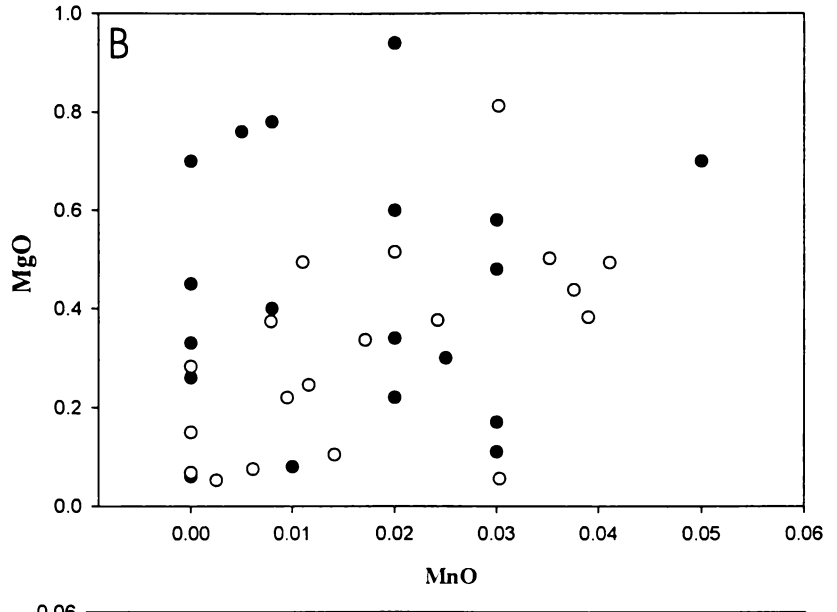
B
MgO
MnO
1.0
0.8
0.6
0.4
0.2
0.0
0.00
0.01
0.02
0.03
0.04
0.05
0.06

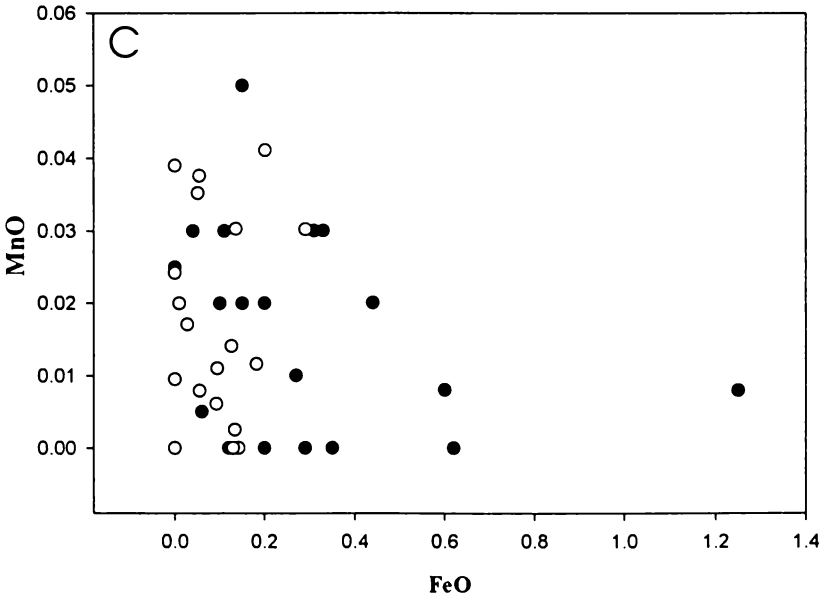
C
MnO
FeO
0.06
0.05
0.04
0.03
0.02
0.01
0.00
0.0
0.2
0.4
0.6
0.8
1.0
1.2
1.4

the ferroan cements at the time of its development. Indeed, little to moderate pre-compaction cementation within the various medium- to coarse-grained units suggests that the strata retained high porosity and permeability levels, later enhanced by mechanical fracturing, allowing facile fluid circulation both within limestones and between them through the interbedded siliciclastic units.

As previously mentioned, the velocity of groundwater flows, the dominant mineralogy of the host sediments, and the degree of saturation with respect to $CaCO_3$, are critical factors to cementation development in cool-water carbonates, either in the phreatic marine and meteoric environments (Choquette and James, 1990a; Nelson and James, 2000), or in the burial realm (Nicolaides and Wallace, 1997).

With these considerations in mind, two scenarios can be envisaged to explain the observed post-compaction CL sequence configuration: differences in groundwater flow velocity or in the degree of fluid saturation.

Groundwater flow velocity

Higher flow rates within the lower, high-porosity, Kairakau strata than within the units above, could have favoured cementation near the base of the paleoaquifer system. Conversely, lower flow velocity towards the top of the paleoaquifer system may have slowed or even delayed cementation until the progressively decreasing permeability of the lower strata, due to cementation, would result in relatively higher water flow rates in the overlying strata, hence becoming capable of inducing calcite precipitation. This process was envisaged by Goldstein (1988) and Haywick (1990) to explain similar asymmetrical cement configurations in interbedded limestone and mudstone units. Implicit in this scenario is the diachroneity of the cements making up the burial CL sequence that become younger up-section. The scenario is apparently compatible with the low SrO contents of burial cements in Awapapa Limestone, suggesting high water/rock ratios, but does not agree with the relatively high SrO content of CL sequence KB in the Kairakau Limestone, indicative instead of low water/rock ratios (high water-rock interaction).

Degree of fluid saturation

Kairakau and Awapapa Limestones are characterized by similar cool-water LMC-dominated microfacies compositions, while Rotookiwa Limestone differs from its older

counterparts by lower contents of siliciclastics (see Chapter 1, Section 6.3). Biomoulds, which originated from dissolution of aragonitic skeletons, are relatively common in the three formations, suggesting comparable primary aragonitic contents. If one assumes that burial waters had the same starting composition throughout the sediment pile, and interacted similarly with the host sediments (i.e., same water/rock ratio), then they could not become differentially saturated, and would have precipitated comparable volumes of calcite. Therefore, the saturation level must have differentially evolved over time, becoming higher towards the base than towards the top of the confined aquifer. One can tentatively interpret that undersaturated fluids, first present in the upper Awapapa and Rotookiwa strata, could have progressively become supersaturated as they penetrated downwards into the Kairakau strata where they were capable of promoting pervasive cementation. Once again, this scenario implies that the component cements of the burial CL sequence do not represent synchronous episodes of cementation.

4.5.4. Configuration of the telogenetic CL sequence

The cement succession in all stratigraphic units up to at least the lower limestone sheet of Mason Ridge Formation (Nukumaruan), includes a late, non-ferroan, non-luminescent, fracture-hosted cement generation that cross-cuts all previous diagenetic features, and is interpreted as a telogenetic product (Figure 14). The diagenetic attributes of the CL sequence (equivalent to CL sequence KC) are remarkably reproduced throughout its regional distribution, suggesting that it formed from a single fluid system, Nukumaruan in age.

4.5.5. Diagenetic and fluid flow pathways

The precipitational model envisaged for pre-compaction CL sequences within Kairakau, Awapapa, and Rotookiwa (and possibly Te Onepu) Limestones involves establishment of a new meteoric, or mixed marine-meteoric water aquifer, during each emergent event that is inferred to have occurred at the end of each limestone deposition in some restricted portions of their geographic distribution (see later in Section 5, Figure 15).

For the fluids involved in the formation of the burial CL sequence, an east-west orientated gravity-driven fluid flow is suggested (Figure 7C). The assumption that the majority of burial cements precipitated from a single aquifer implies that recharge of the system was delayed until after deposition of the late Waipipian Rotookiwa Limestone.

The paleogeographic reconstruction proposed by Beu (1995) for the Waipipian and Mangapanian times in southeastern Hawke's Bay suggests that active tectonics at the plate boundary led to some parts of the carbonate bodies becoming buried by thick siliciclastic units, while others were uplifted at the eastern margin of the forearc basin ("East Coast Highlands"). As the central part of the carbonate system subsided, the eastern portion became emergent, creating a potential recharge area for meteoric aquifer systems. Subsequently, meteoric water could flow down-dip and serve as a potential source for burial waters, later reduced as a result of redox reactions. More geochemical data are needed to decipher between marine-modified fluids and meteoric-derived burial fluids as the principal source for post-compaction ferroan cements.

The carbonate system must have been, at least intermittently, in contact with the East Coast Highlands for fluid recharge, as this SW-NE trending belt became more extended with the progressive closure of the forearc basin over Nukumaruan times (Kamp and Nelson, 1987; Beu, 1995; Field *et al.*, 1997).

The remaining late telogenetic CL sequence probably formed during (? early) Nukumaruan times, during regional uplift of the central part of the study area, as suggested by the apparent west-east trending flow direction.

4.6. Comment on the CL attributes of the Waipipian-Mangapanian limestones on the western margin of the forearc basin

The general characteristics of CL sequences within limestone units exposed at The Gorges section are presented in Figure 14, and detailed CL sequence diagrams are grouped in Appendix 5 (sections labelled W1-5, pp. A5-39 to A5-45). Lithostratigraphic units exposed at this locality include, in ascending order, the Titiokura and Te Waka Formations, and the Hassal Conglomerate, separated from one another by siliciclastic interbeds (see Chapter 1, Figure 2).

The CL successions differ markedly from the Kairakau motif in consisting of only post-compaction mesogenetic and telogenetic LMC cement phases. In the Titiokura and Te Waka Formations, the fracture-hosted mesogenetic CL sequence comprises thick, deep blue (suggesting high ferroan contents), moderately orange/brownish luminescent cements, overlain by an unconformable succession of moderately (pale blue to mauve) to non-ferroan (pink), orange- to non-luminescent cements filling in fractures, upon which dissolution surfaces are superposed. High ferroan contents did not totally

quench luminescence, suggesting that mesogenetic cements precipitated from Fe/Mn-bearing fluids in reducing conditions (Machel and Burton, 1991). FeO concentrations of whole-rock samples from Te Waka Formation depart significantly from values measured on eastern limestone samples (see Figure 16), suggesting the proximity of a terrigenous source (Nelson *et al.*, 1988).

Fracture-hosted blue to mauve, orange luminescent cements, post-dating the deep blue mesogenetic sequence are believed to be transitional between (?) deep burial conditions to shallow burial/surficial conditions, the latter producing the last pink, non-luminescent cement generation.

Titiokura and Te Waka Formations deposited about the western margin of the forearc basin abutted against emerged lands of Mesozoic basement rocks in the west (Beu, 1995), and were not connected to their eastern time-equivalent counterparts (the Awapapa, Rotookiwa, and Te Onepu Limestones). This, together with geochemical and petrographic constraints, suggest that mesogenetic, and possibly telogenetic, cementing aquifers in the west and in the east were spatially unrelated, and compositionally distinct.

5. Sequence stratigraphic approach to cool-water carbonate diagenesis of the Te Aute Pliocene limestones

5.1. Introduction

Braithwaite (1993) pointed out that the concepts of sequence stratigraphy, the subdivision of stratal successions into unconformity-bound sedimentary packages (Van Wagoner *et al.*, 1988), could help clarify complex diagenetic suites within carbonate sediments, showing that within the compositional zonation of cements conformable successions could be recognized bounded by breaks or time gaps, such as dissolution surfaces, analogue to disconformities. The previous discussion has emphasized that one general advantage of applying the concept of "sequence" to explain and simplify paragenetic relationships, is that it allows more accurate correlations by using diagenetic discontinuities as the main interregional tracers.

Because diagenesis determines the porosity evolution of a carbonate system, attempts have been made to predict diagenetic pathways by relating their products to patterns of sea-level changes (Heckel, 1983, 1986; Sarg, 1988; Tucker, 1993; Moore, 2001). In most recent studies, meteoric diagenetic products associated with subaerial

Figure 14- Detailed cathodoluminescence (CL) sequence diagrams or CL "logs" from limestones, ranging in age from Opoitian (Kairakau Limestone) to Nukumaruan (Mason Ridge Formation), showing the chronological succession of CL cement zones, bounding discontinuities, and information relative to both lateral and vertical CL pattern changes, and chemical stains. Note that the Kairakau Limestone CL "log", referred to as the *Kairakau motif* in text, is repeated within younger limestone units, up to Sequence MC of Mason Ridge Formation, even though the component CL sequences vary in thickness, CL patterns, and ferroan content. The full implication of the reproducibility of the Kairakau motif within successive limestone bodies, separated from one another by siliciclastic interbeds, is commented in text.

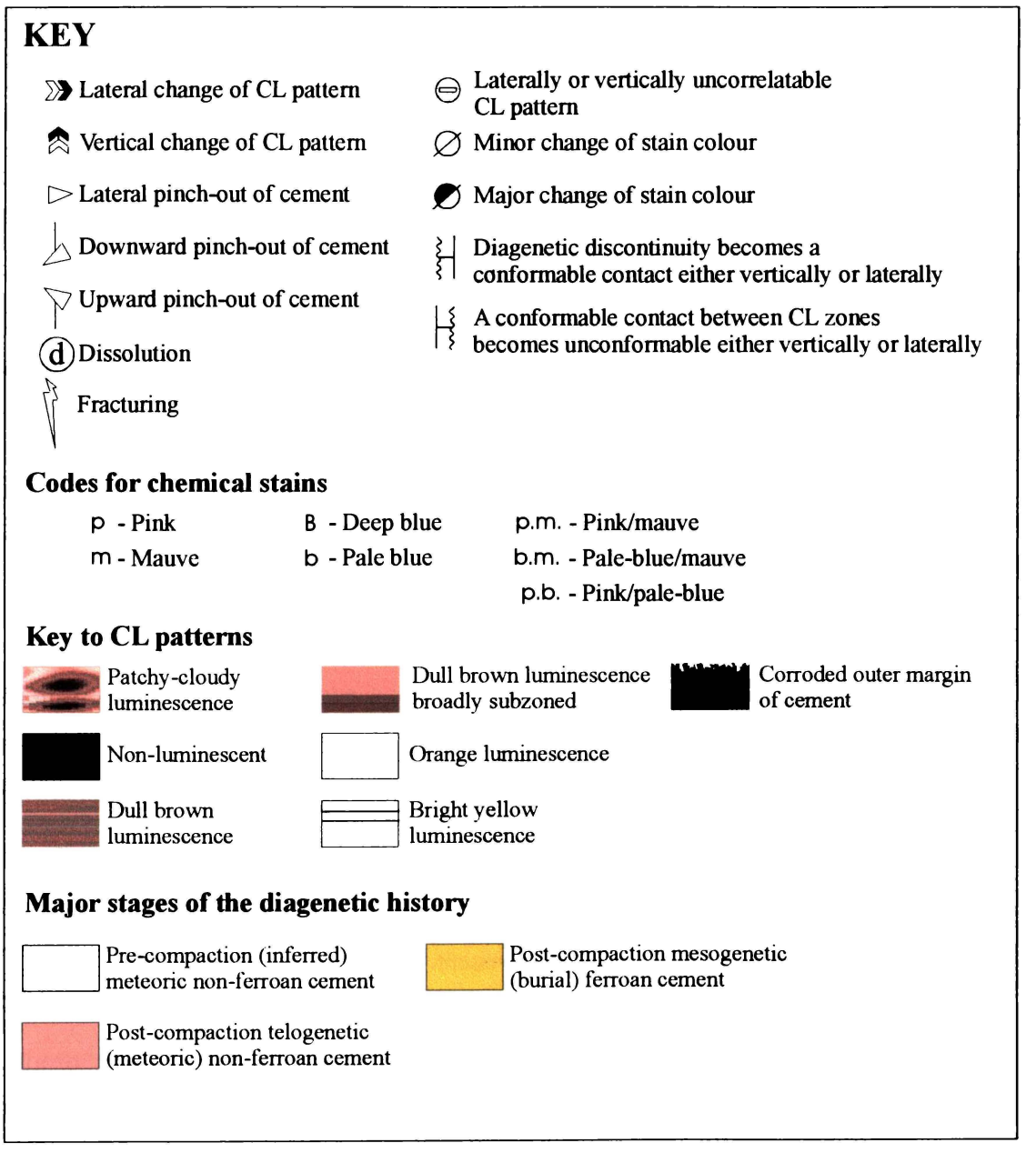

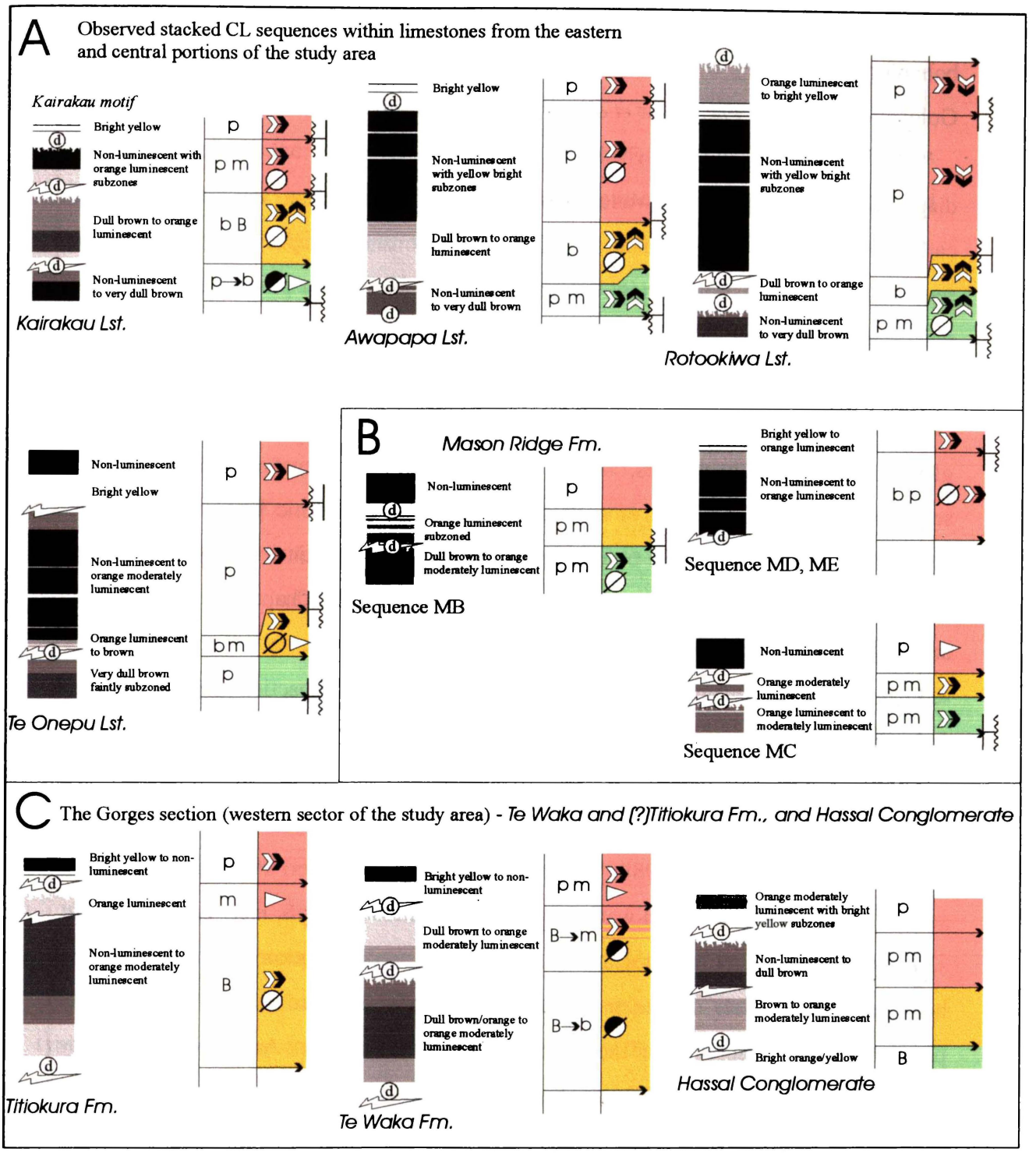
A
Observed stacked CL sequences within limestones from the eastern and central portions of the study area
Kairakau motif
Bright yellow
Non-luminescent with orange luminescent subzones
Dull brown to orange luminescent
Non-luminescent to very dull brown
p
p m
b B
p→b
Kairakau Lst.
Bright yellow
Non-luminescent with yellow bright subzones
Dull brown to orange luminescent
Non-luminescent to very dull brown
p
p
b
p m
Awapapa Lst.
Orange luminescent to bright yellow
Non-luminescent with yellow bright subzones
Dull brown to orange luminescent
Non-luminescent to very dull brown
p
p
b
p m
Rotookiwa Lst.
Non-luminescent
Bright yellow
Non-luminescent to orange moderately luminescent
Orange luminescent to brown
Very dull brown faintly subzoned
p
p
bm
p
Te Onepu Lst.
B
Mason Ridge Fm.
Non-luminescent
Orange luminescent subzoned
Dull brown to orange moderately luminescent
p
p m
p m
Sequence MB
Bright yellow to orange luminescent
Non-luminescent to orange luminescent
b p
Sequence MD, ME
Non-luminescent
Orange moderately luminescent
Orange luminescent to moderately luminescent
p
p m
p m
Sequence MC
C
The Gorges section (western sector of the study area) - Te Waka and (?)Titiokura Fm., and Hassal Conglomerate
Bright yellow to non-luminescent
Orange luminescent
Non-luminescent to orange moderately luminescent
p
m
B
Titiokura Fm.
Bright yellow to non-luminescent
Dull brown to orange moderately luminescent
Dull brown/orange to orange moderately luminescent
p m
B→m
B→b
Te Waka Fm.
Orange moderately luminescent with bright yellow subzones
Non-luminescent to dull brown
Brown to orange moderately luminescent
Bright orange/yellow
p
p m
p m
B
Hassal Conglomerate

exposure surfaces, and the degree of porosity destruction considered as a proxy for the time of residence in the meteoric environment, are the main diagenetic features to be integrated into a sequence stratigraphic framework as they help determine the nature of bounding sedimentary discontinuities and the recognition sequence boundaries (e.g., Goldhammer *et al.*, 1994; Saller *et al.*, 1994; Rankey *et al.*, 1999).

The next logical step, which was proposed as a perspective to future carbonate diagenetic studies by Braithwaite (1993), is to fully describe the paragenesis of carbonates in terms of sequence stratigraphic relationships, implicitly by recognizing sequences, sequence boundaries, transgressive and regressive precipitational trends, onlap and downlap behaviours, cycles, and different orders of cyclicity.

The main justification for modelling the sequence stratigraphic evolution of carbonate paragenesis lies in the potential of carbonate systems to translate regional and global environmental changes, which also control the formation of sedimentary sequences of different orders of cyclicity, into distinct diagenetic patterns. Thus, this study has shown that: (1) pre-compaction specific diagenetic suites relate intimately to the patterns of high-frequency relative sea-level changes (see Chapter 2, Section 6.1); and (2) tectonic/subsidence, which is the main driving force in defining low-order sedimentary megasequences, also produces motifs of post-compaction diagenetic suites (e.g., the post-compactional diagenetic suite of the *Kairakau motif*; see Figure 5).

The diagenetic sequence stratigraphic model presented below adopts the conceptual framework that underpins sedimentary sequence analysis (Posamentier *et al.*, 1988; Van Wagoner *et al.*, 1988; Vail *et al.*, 1991; Van Wagoner, 1996), and integrates several unique aspects of cool-water carbonate diagenetic systems, including: (1) low *in situ* carbonate production rates and subsequent low sedimentation rates that result in high maturation levels on the sea floor; (2) uncommonness of metastable carbonate phases and low reactivity of the dominant LMC mineralogy. As a result, porosity distribution in cool-water carbonates may not be significantly altered, especially in terms of porosity destruction, during subaerial exposure and meteoric diagenesis; and (3) lithification may be delayed until burial.

The following section is an attempt to synthesize both the observations and concepts developed in the course of the present study, and should be regarded only as a preliminary step towards the development of a comprehensive sequence diagenetic stratigraphy of cool-water carbonates. CL patterns and CL sequences observed in the

Pliocene limestones from the eastern portion of the study area serve to illustrate the sequence stratigraphical concepts (Figure 15).

5.2. CL sequence geometries

5.2.1. CL sequences within Pliocene limestones

Figure 14 illustrates the characteristics of the typical successions of CL sequences recognized within the limestone formations of southeastern (Figures 14A, 14B) and southwestern (Figure 14C) Hawke's Bay, and ranging in age from Opoitian (Kairakau Limestone) to Nukumaruan (e.g., Mason Ridge Formation).

The pattern of CL sequences in each individual limestone unit up to sedimentary sequence MC of Mason Ridge Formation compares remarkably well with the *Kairakau motif* (Figures 14A, 15D), and consists of: (1) a pre-compaction CL sequence (CL sequence KA in the *Kairakau motif*), which post-dates locally marine cements (CL sequence KZ in the *Kairakau motif* not represented on Figure 14A); (2) a first post-compaction mesogenetic CL sequence (CL sequence KB in the *Kairakau motif*); and (3) a second post-compaction telogenetic CL sequence (CL sequence KC in the *Kairakau motif*); commonly followed (4) by a late CL sequence that equates to CL sequence KD in the *Kairakau motif*.

In contrast, the CL sequence patterns within the upper limestone sheets of Mason Ridge Formation (sedimentary sequences MD and ME) lack the mesogenetic part of the *Kairakau motif*, and consist only of a thick CL sequence of non-luminescent, non- to slightly ferroan cements (Figure 14B).

The volumetric abundance of the mesogenetic CL sequence is less in the Rotookiwa and Te Onepu diagenetic suites than in their older and younger counterparts (Figures 14, 14B). In contrast, the telogenetic CL sequence varies inversely, and typically constitutes the dominant cementing phase within the Awapapa, Rotookiwa, and Te Onepu diagenetic suites. In sedimentary sequences MB and MC of Mason Ridge Formation, the total cement volume is distributed equally between the pre-compaction, mesogenetic, and telogenetic CL sequences (Figure 14B).

5.2.2. Architecture of the Pliocene CL sequences

Figure 15 presents two variants of the precipitational model proposed for the pattern of CL sequences in the Te Aute successions in the eastern and central sectors of southern

Figure 15- Two variants of a CL sequence stratigraphy precipitational model showing in (A) the chronological repetition of two mega-CL sequences, each of which involves a set of pre-compaction meteoric CL sequences (KA, AA, RA, TeA for the first megasequence; M1A, M2A, and M3A for the second), partly or totally overlapped by post-compaction burial CL sequences (B1 and B2), followed by telogenetic/meteoric CL sequences (C1 and C2); and in (B) a single burial CL sequence unconformably overlies successive pre-compaction CL sequences, hypothetically related to temporally and spatially distinct cementing aquifers.
Figure (C) illustrates the relationships between diagenetic discontinuity surfaces and the precipitational suites, whose combination defines successive CL sequences. Cross cutting physical relationships allow recognizing the vertical (both sedimentary and diagenetic) stratigraphic extent of discontinuity surfaces, and subsequent cement overprints. Discontinuity surfaces provide substrate for growth of cement. They either behave like onlap or downlap surfaces, depending on the dynamic process involved in their formation. The downward percolation of fluids associated with pre-compaction meteoric CL sequences and post-compaction telogenetic/meteoric CL sequences generates downward-younging dissolution surfaces, which equate to downlap surfaces in terms of physical relationship to substrate. In contrast, compactional processes are theoretically triggered by depth, and consequently associated features, such as fractures, are younger in the upper part of a sediment pile than in the lower part, hence defining an upward-younging or onlap relationship to substrate.
(D) The *Kairakau motif*, which records the transition between shallow marine – meteoric – mesogenetic (burial) – telogenetic/meteoric diagenetic environments, illustrates the precipitational architecture of CL sequences for Te Aute Pliocene limestones in the eastern portion of southern Hawke's Bay.

Cements above an onlap surface are referred to as transgressive (T), while cements above a downlap surface are referred to as regressive (R). Diagenetic surfaces have been hierarchically divided into Diagenetic Sequence Boundaries (DSB) and Diagenetic discontinuities (Dd). DSBs record dramatic change in the chemical environment, such as the transition from telogenesis to marine eogenesis (Type-A DSB) or eogenesis to mesogenesis (Type-B DSB). Dds record the transition from either marine to meteoric diagenesis in the eogenetic realm (type-b Dd), or mesogenesis to telogenesis (type-c Dd).

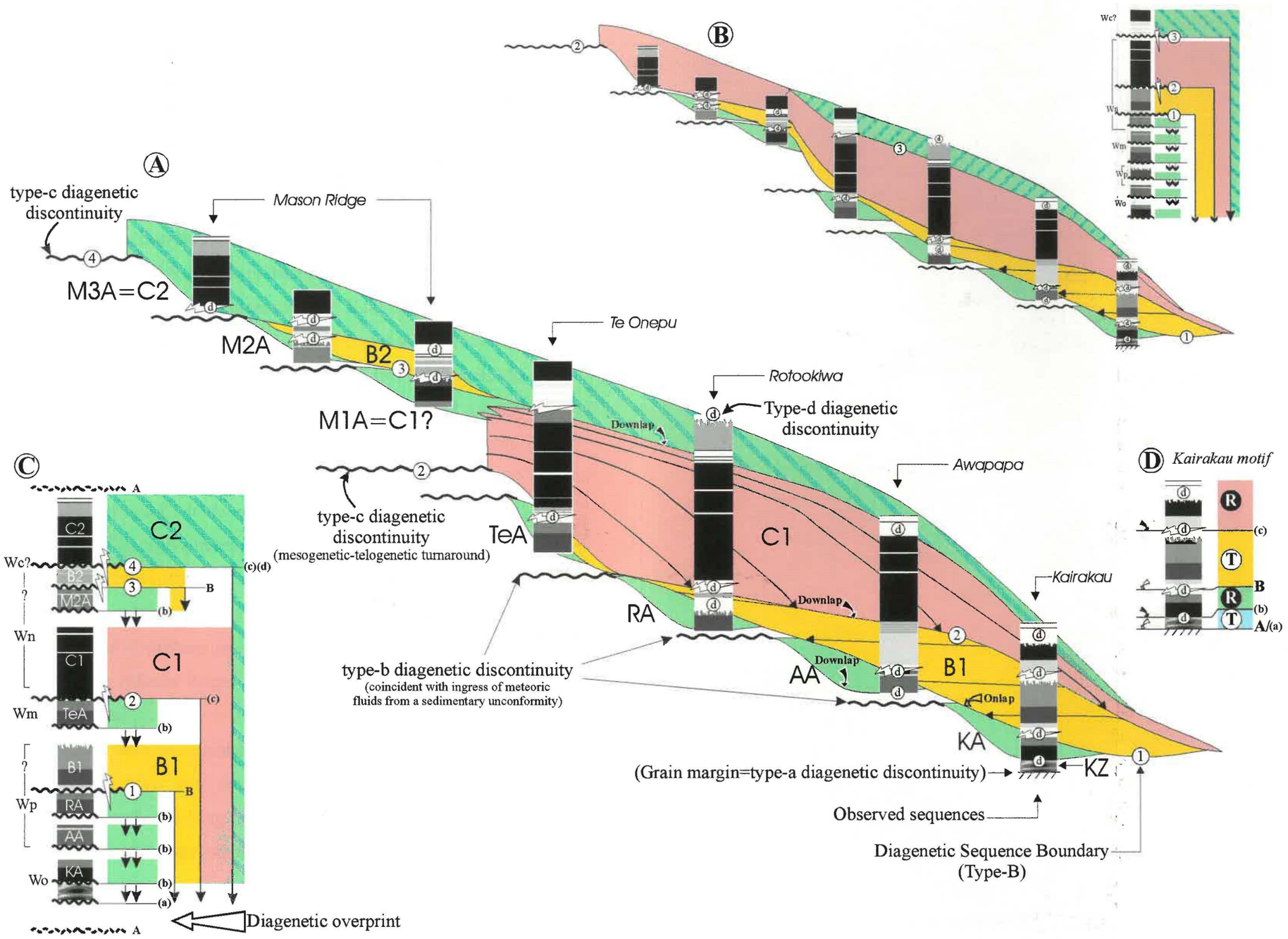

KEY

Key to CL patterns

- Patchy-cloudy luminescence
- Non-luminescent
- Dull brown luminescence
- Dull brown luminescence broadly subzoned
- Orange luminescence
- Bright yellow luminescence
- Corroded outer margin of cement

Major stages of the diagenetic history

- Marine cements
- Post-compaction (uplift) meteoric aquifer and cements
- Pre-compaction meteoric aquifer and cements
- Burial aquifer and cements

- (d) Dissolution
- Fracturing
- (T) Transgressive CL sequence
- (R) Regressive CL sequence
- Downlap
- Onlap

Hawke's Bay. The hypothetical model integrates the volumetric abundance of the successive CL sequences within each limestone unit to determine the idealized geometries of the cementing aquifers, and infers that pre-compaction cements precipitated from either temporally distinct (CL sequences KA, AA, RA, and TeA) or stratified (M1A, M2A, and M3A) aquifers. Each cementing lens was established during an emergent event that is inferred to have exposed the top of each limestone unit in some restricted portions of their geographic distribution.

In (preferred) model A (Figure 15A), it is hypothesized that the post-compaction mesogenetic CL sequences within the pre-Nukumaruan and Nukumaruan units are separate, and originated from temporally and spatially distinct groundwater systems (CL sequences B1 and B2). This assumption forces the recognition of two telogenetic CL sequences, namely C1 and C2. CL sequence C1 overlaps CL sequence B1, and possibly correlates to the pre-compaction CL sequence M1A recognized within the lower limestone sheet of Mason Ridge Formation. CL sequence C2 overlaps CL sequences B2 in the central part of the study area and C1 in the east, where it coincides with the "D" member of the *Kairakau motif*. The non-luminescent cement of CL sequence C2 is assumed to have been precipitated beneath an unconformity capping the upper limestone sheet of Mason Ridge Formation, within which it makes up the dominant cementing phase (CL sequence M3A). Model A explains the differing abundance of mesogenetic cements from within Nukumaruan (Mason Ridge) and late Waipipian (Rotookiwa) to Mangapanian (Te Onepu) limestones.

Model A is supported by both geochemical data and tectonic considerations. Although, Nukumaruan limestones differ from their pre-Nukumaruan counterparts by their microfacies composition, typically involving higher contents of variably preserved aragonitic skeletons, red algae, and echinoids, within a marine mud framework, this does not fully explain their trace element composition. SrO, MnO, NaO, MgO, and at a lesser degree CaO and FeO concentrations of bulk samples from Mason Ridge Formation, and other correlative limestones in central southern Hawke's Bay, depart significantly from their pre-Nukumaruan counterparts (Figure 16). High SrO and MgO contents certainly relate to the common occurrence of relict aragonite and HMC mineralogies in the Nukumaruan limestones (see Chapter 3, Section 4.6), but also probably involve interactions between pore fluids and the host-rock (low water/rock ratios) (Meyers, 1989; Tobin and Walker, 1998). Past studies have shown that MnO

Figure 16- Plot of SrO, MnO, NaO, MgO, FeO, and CaO contents (ppm) in whole-rock samples from Te Aute limestones in southeastern Hawke's Bay. Note the significant departure of Nukumaruan SrO, MnO, NaO, and MgO values (e.g., Mason Ridge, Matapiro et al., Flag Range et al. Limestones from the central and western sectors of the study region) from those of pre-Nukumaruan limestones in the eastern sector of the study area (e.g., Kairakau, Awapapa, Rotookiwa, Te Onepu Limestones). The observed contrast is attributed to differing starting skeletal compositions, and compositionally and temporally different cementing phases. See text for discussion. In CaO plot, 1e+5 = 10 000 ppm, etc.

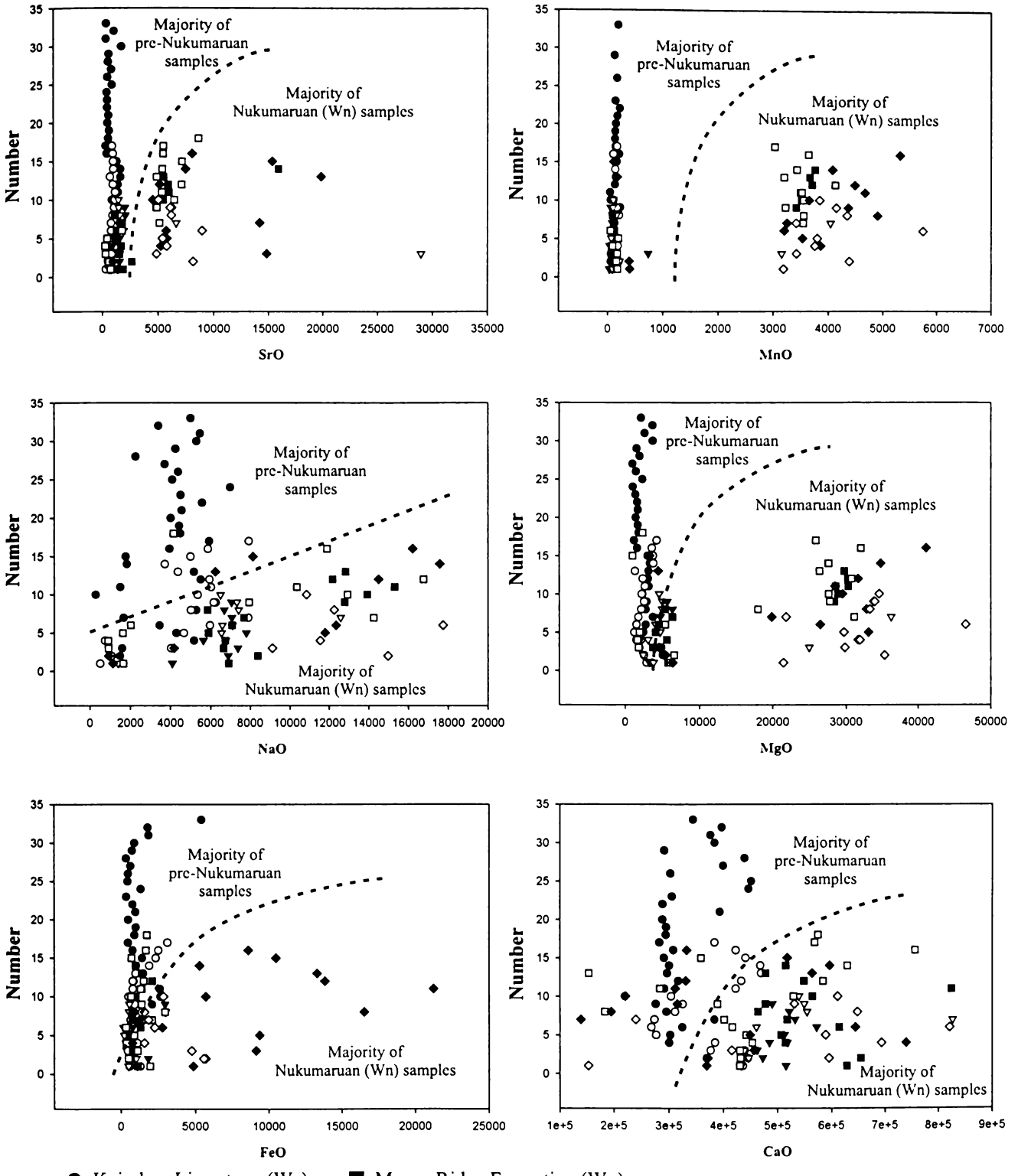
Majority of pre-Nukumaruan samples
Majority of Nukumaruan (Wn) samples
Number
SrO
MnO
NaO
MgO
FeO
CaO
Kairakau Limestone (Wo)
Awapapa Limestone (Wp)
Rotookiwa Limestone (Wp)
Te Onepu Limestone (Wm)
Mason Ridge Formation (Wn)
Matapiro and upper members of Scinde Island Limestones (Wn)
Flag Range, Kereru and Sentry Box Limestones (Wn)
Te Waka Formation (Wp-Wm)

increases with increasing aragonite content (Rao and Adabi, 1992). However, this does not compare with the 2000 ppm difference between the MnO-rich Nukumaruan and the MnO-poor pre-Nukumaruan samples. This difference is attributed to a cementing phase, likely the meteoric CL sequence C2. High MnO concentrations are thought to demonstrate the contribution of Mn-bearing cementing fluids to the composition of Nukumaruan limestones. Low water/rock ratio and partial confinement of the aquifer allowing reducing conditions to develop, could explain high MnO contents. The development of reducing conditions is supported by the blue stain observed in the early growth stages of CL sequence C2 (= KD in *the Kairakau motif*; see Section 4.4) throughout the study area.

The hypothetical occurrence of two confined aquifers in model A, producing two temporally distinct fracture-hosted burial cements, implies the repeated development of compactional fractures. In this case, one should expect the Nukumaruan compactional fractures to cross-cut the complete suite of diagenetic CL sequences within the pre-Nukumaruan limestones. This cross-cutting relationship has not been observed. However, differential uplift of pre-Nukumaruan limestones in the eastern portion of the forearc basin, and subsidence towards the axis in Nukumaruan times is a plausible scenario to account for this discrepancy, considering the evolution of the forearc basin (Kamp and Nelson, 1987, 1988; Beu, 1995; Field *et al.*, 1997). Thus, while non- to poorly cemented Nukumaruan limestones in the west were being buried, their moderately cemented pre-Nukumaruan counterparts in the east were being exhumed, hence not suffering this compactional process but instead experiencing uplift-related fracturing. Implicit in this hypothetical scenario is the possibility that the emergent eastern region was a potential source for the burial fluids in the central region (?)interdigitation of C1, M1A, and B2; Figure 15A).

Model B (Figure 15B) is derived from the comparability of diagenetic suites from one unit to another. The compactional fracturing event is assumed to be traceable throughout the Pliocene successions, and subsequently the mesogenetic then telogenetic CL sequences can be correlated between the Nukumaruan and the Opoitian limestones. The synchroneity of both discontinuity and cement developments can hardly be envisaged and needs to be addressed. For example, what is the timing of the single confined aquifer development? One can also argue that the differential burial history of the Pliocene limestones from the east to the west allows compactional fractures to be

diachronous (see later), that is older in the more deeply buried units and younger in the upper units.

The two variants illustrate possible scenarios, only envisaged here as working hypotheses to account for the CL sequence geometries. Model A is preferred here because it agrees well with geochemical data and the paleogeographic evolution of the east coast region. However, many assumptions are poorly supported, for example the occurrence of a single aquifer (i.e., B1) to precipitate the mesogenetic cements of Kairakau, Awapapa, and Rotookiwa units, and emphasize the need for more detailed investigations.

5.3. Modelling the diagenetic sequence stratigraphy of the Te Aute Pliocene carbonates: principles and definitions

5.3.1. Definition of diagenetic (CL) sequences

CL sequences are defined and identified by the physical relationships of their component diagenetic stages, including the lateral and vertical continuity of the diagenetic surfaces bounding conformable successions of cement zones. CL sequences and their components are interpreted to form in response to the interaction between:

(a) the mineralogical composition of the host-sediment, considered to be critical as a potential source of carbonate to be mobilized for interparticle cementation;

(b) external processes, including eustasy and tectonism, that determine the timing of ingress and nature of fluids within pore spaces;

(c) the permeability of the host-rock, and the volume of inter-/intraparticle pore space available for cements to precipitate in;

(d) the starting composition of the groundwaters, namely their degree of saturation, and the rate of fluid flow, whose combined effects determine the degree of interaction between fluids and sediments, and the chemical evolution of the diagenetic environment;

(e) burial depth of the aquifer that influences the ambient temperature, pCO_2, and redox potential, and subsequently the distribution of trace elements and stable isotopes incorporated in the cementing phase.

A CL sequence is considered to be a genetically-related conformable succession of cement zones bounded by physical diagenetic discontinuities that are commonly diachronous across a basin, and mark an abrupt change of chemical environment.

The nature of the chemical transition across the diagenetic unconformity enables to hierarchically differentiate diagenetic sequence boundaries, termed **T**ype-A and **T**ype-B with reference to the sequence stratigraphical terms defined by Van Wagoner *et al.* (1987), and diagenetic discontinuities, termed **t**ype-a to **t**ype-d. Figure 18 summarizes the physical relationships between discontinuities and cements, and provides a description of the general characteristics of the various CL sequences.

5.3.2. Type-A diagenetic sequence boundary

A Type-A diagenetic sequence boundary (DSB) is characterized by the overprint of marine diagenesis upon a mesogenetic or meteoric/telogenetic CL sequence (Figure 17A). Therefore, in the rock record, a Type-A DSB is contemporaneous with the formation of a major flooding surface upon consolidated sediments that experienced telogenesis. It may be associated with sea-floor constructive diagenesis a few decimetres above and beneath the physical flooding surface, but more likely with reworking of clasts from the underlying rocks that can become incorporated in the deposits above the surface, and that will show truncation of cement zones from the telogenetic sequence by marine abrasion and bioerosion.

Thus, a Type-A DSB corresponds to a marine erosive surface on the outer margin of rock clasts that had previously been subjected to telogenetic processes (Figure 18).

5.3.3. Type-B diagenetic sequence boundary

A Type-B DSB separates pre-compaction and post-compaction CL sequences, and is marked by compaction-induced fractures, commonly accompanied by dissolution. It generally corresponds to a chemical turnaround from oxidizing to reducing conditions, due to the burial modification of interparticle fluids that have been cut off from their up-dip oxidized source (Figures 17C to 17E, 17G).

Therefore, a Type-B DSB typically separates older CL sequences, characterized by either marine turbid, patchy luminescent cement (CL sequence KZ in the *Kairakau motif*), and/or meteoric inclusion-free, non-ferroan, non-luminescent cements (CL sequence KA; Figure 15A), from a younger CL sequence (CL sequence B1; Figure 15A), characterized by clear spar, ferroan, and dull luminescent, faintly subzoned cements (Figure 18).

5.3.4. Pre-compaction type-a and type-b diagenetic discontinuities

Within the pre-compaction diagenetic history (pre-Type-B DSB), two diagenetic discontinuities are recognized, type-a and type-b, which are located at the base of marine and meteoric CL sequences, respectively.

The formation of type-a and type-b diagenetic discontinuities (Dd) is fundamentally tied to the development of physical sedimentary surfaces. A type-a Dd is marine in origin, follows the development of marine ravinement surfaces formed during transgression or forced regression (e.g., TSE and RSE), and consequently can be developed in the overlying marine sediments (e.g., within TSTs to RSTs, and FRSTs). It may or may not be overlain by marine constructive diagenetic products which, if present, are bounded above by a type-b Dd.

Typically, a type-a Dd is marked by either an erosion surface, the carbonate grain margin (Figure 17E), which originated from mechanical abrasion and bioerosion at the sea floor, or a dissolution surface formed in the marine environment, such as the internal walls of aragonitic biomoulds, or both (Figure 18).

A type-b Dd is marked by a dissolution surface (rarely by fissures) along the outer margin of cements from the previous CL sequence, and the inner walls of leached metastable carbonate skeletons. It coincides with the percolation through the sediment pile of undersaturated meteoric fluids (possibly mixed with marine waters) from a subaerial exposure surface (Figures 15A, 15C). Type-b Dds clearly document breaks both in the sedimentary and diagenetic records, and are typically overlain by non-ferroan, non-luminescent cements (CL sequence KA in the *Kairakau motif*), which are also testimony to a new change of chemical environment (i.e., now supersaturated) (Figure 18).

5.3.5. Post-compaction type-c and type-d diagenetic discontinuities

Within the post-compaction diagenetic history of the Te Aute sediments (post-Type-B DSB), type-c and type-d Dds are differentiated.

A type-c Dd is marked by fractures (Figure 17C) that cross-cut all previous CL sequences and their bounding discontinuities, and is typically followed by dissolution, resulting in irregular, gulf-like crystal boundaries and terminations, and truncation of cement zones. Type-c Dds mark the mesogenetic-telogenetic turnaround of the diagenetic history of the sediment pile (Figure 15A). The diagenetic suites commonly

Figure 17 – Diagenetic sequence stratigraphic relationships between cementation stages and bounding discontinuities (thin-sections are stained with Dickson's solution, 1965). See text for details.

(A) A Type-A Diagenetic Sequence Boundary (DSB) consists of a marine erosion surface (abrasion and bioerosion) along the outer margin of lithoclasts derived from limestones that experienced mesogenesis (burial). In this example, a limestone unit that had buried and cemented by ferroan calcite, was later exhumed and exposed to marine erosion. The Type-A DSB was then produced, that provided substrate for later stage meteoric clear spar cements. This suite of diagenetic fabrics necessitates that a type-b Dd (see below and text) is superposed on a Type-A DSB. Sample 14.7 from Ohiwia section of Matapiro Limestone (see Appendix 3 – column 34).

(B) Illustration of the *Kairakau motif* (see Figures 14A, 15D) in thin-section, and its sequence stratigraphic precipitational architecture. The pre-compaction transgressive (T) - regressive (R) diagenetic suite consists of marine turbid cements (T), lying on an onlap surface (the grain margin), and overgrown by meteoric clear scalenohedral calcite crystals (R). The post-compaction T-R diagenetic suite consists of thin ferroan (stains blue) burial cement (T) followed by telogenetic/meteoric non-ferroan (stains pink) mosaic spar (R). Sample 5.93 from Makara section of Awapapa Limestone (see Appendix 3 – column 16).

(C) Former aragonitic skeletons experienced meteoric neomorphism prior to compaction (pink outer margin), then burial diagenesis (blue crystals), and eventually were cut by uplift-derived fractures referred to as type-c diagenetic discontinuities (Dd), which are filled with pale pink telogenetic/meteoric spar. Sample 4.75 from Kairakau Beach section of Kairakau Limestone (see Appendix 3 – column 46).

(D) Same sample as in (C) illustrating that a compaction-induced fracturing event, referred to as Type-B DSB, pre-dates precipitation of ferroan cement (blue).

(E) A type-a Dd (marine abrasion surface) provides substrate for growth of non-ferroan (pink) acicular to scalenohedral calcite (transgressive component of the *Kairakau motif*; see Figure 15D). Follows the same suite of post-compaction cements as in (B). The outer margin of pre-compaction acicular crystals is onlapped by post-compaction burial overgrowths (blue zone). This cement phase is overgrown, across a downlap surface, by later stage telogenetic/meteoric mosaic spar (pink). Note that the cement suite lacks the pre-compaction regressive component of the *Kairakau motif*. Sample 4.50 from Waimarama section of Kairakau Limestone (see Appendix 3 – column 10).

(F) Illustration of post-compaction transgressive (T) – regressive (R) sequence and physical relationships between cementation stages and their bounding surfaces. Sample 16.5 from Awapai Gate section of Whanawhana Limestone (see Appendix 3 – column 44).

(G) Illustration of the *Kairakau motif*. See (B) and (E) for comments. Note that the burial cementing phase (blue zone) is wedged within a serrated contact between pre-compaction pink cement and the echinoid plate (thin white arrow). This suggests that the burial cements pre-date significant pressure-dissolution processes. Sample 2.8 from Te Pohue section of Titiokura Formation (see Appendix 3 – column 38).

(H) Transgressive (T) – regressive (R) diagenetic suite in sample that only experienced post-compaction cementation. Note the gradational change from reducing (pale blue) to oxidizing (pale mauve) conditions recorded by the regressive component of the sequence. This is interpreted as a result of progressive uplift. Sample 15.5b from Hawkston section of Te Waka Formation (see Appendix 3 – column 39).

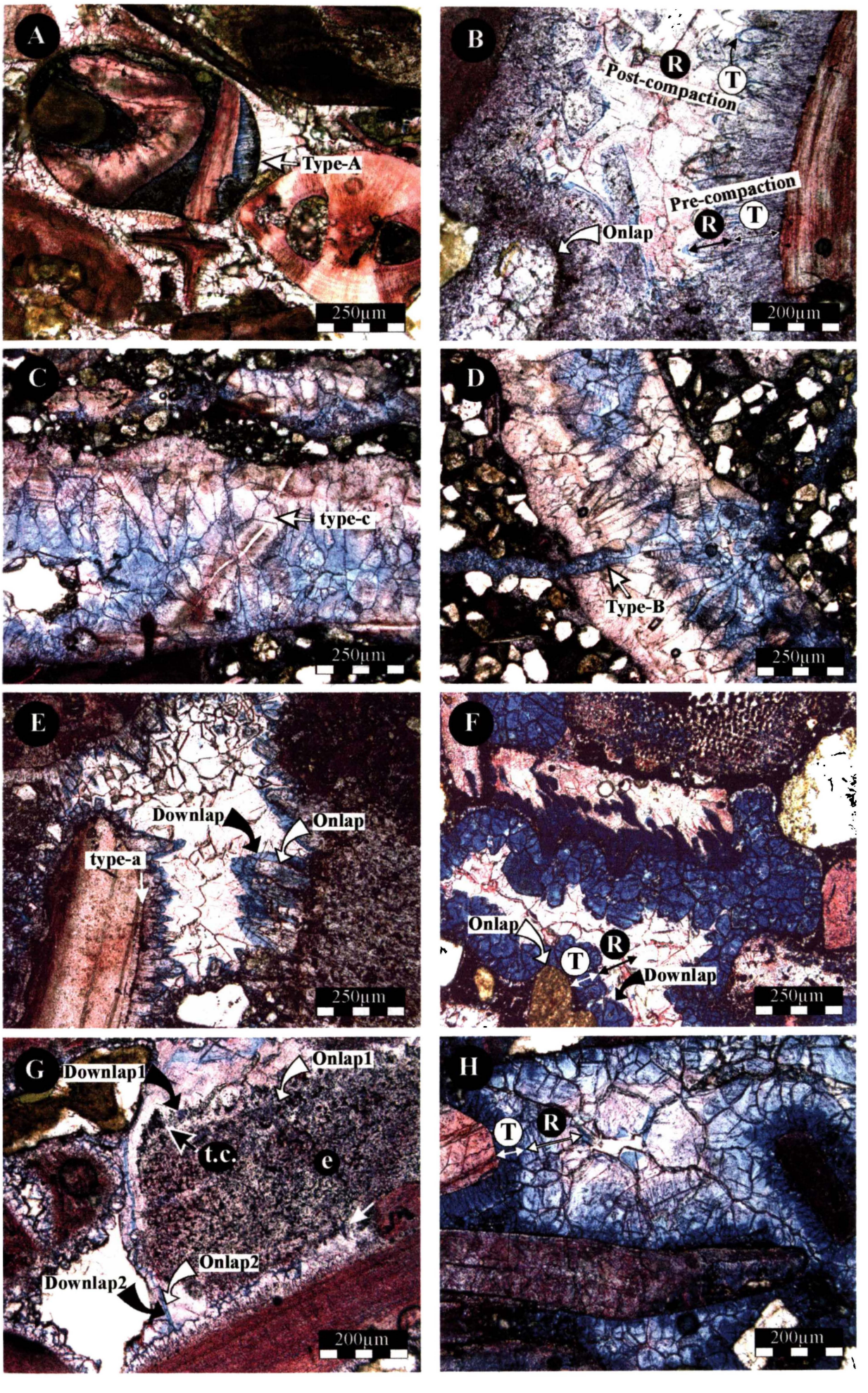
A
Type-A
250μm
B
R
T
Post-compaction
Pre-compaction
R
T
Onlap
200μm
C
type-c
250μm
D
Type-B
250μm
E
Downlap
Onlap
type-a
250μm
F
Onlap
R
T
Downlap
250μm
G
Downlap1
Onlap1
t.c.
e
Onlap2
Downlap2
200μm
H
T
R
200μm

show ferroan, brown/orange dull luminescent cements overlain, across type-c discontinuity surfaces, by thin brightly yellow zones followed by non-ferroan, non-luminescent cement zones (CL sequence KC in the *Kairakau motif*) (Figure 18). This diagenetic suite records the transition from reducing to oxidizing conditions, hence the renewed exposure of the carbonate sediments to surficial processes after tectonic uplift.
A type-d Dd is characterized by dissolution and fractures, and cross-cuts the older type-c Dd (Figure 15C). Type-d Dds represent the latest influence of meteoric fluids within the host-rock prior to possibly eventually being once again exposed to marine processes (Type-A DSB).

5.4. Transgressive-regressive CL megasequences

The vertical succession of CL sequences within a sediment pile can hierarchically be grouped within a framework that takes into account the type of bounding diagenetic discontinuity, the relation of CL sequences to the patterns of syndepositional sea-level changes, and integrates this period of time during which diagenetic processes become dominantly driven by compactional and tectonic mechanisms.

Type-B DSBs are treated as key surfaces, which divide any diagenetic suite into pre-compaction CL sequences that stack in response to eustatic changes and include specific diagenetic suites (see Chapter 2, Section 5.4), and post-compaction CL sequences, whose stacking pattern reflects burial and post-burial processes.

5.4.1. Pre-compaction transgressive-regressive CL sequence

An idealized pre-compaction CL sequence is bounded below by a Type-A DSB and above by a Type-B DSB, and consists of one major transgressive-regressive formational couplet ("megasequence") of CL sequences (equivalent to systems tracts) separated by a type-b Dd (Figure 18).

The initiation of the marine transgressive CL sequence coincides with the formation of the transgressive surface of erosion at the base of the sediment pile, and its termination is indicated by a type-b Dd associated with the percolation of meteoric waters from a subaerial-exposure surface.

Theoretically, marine diagenesis becomes younger up-section as sediments are progressively buried, and removed from the influence of sea-floor processes. Consequently, a Type-A DSB is more likely to be restricted to the base of a sediment

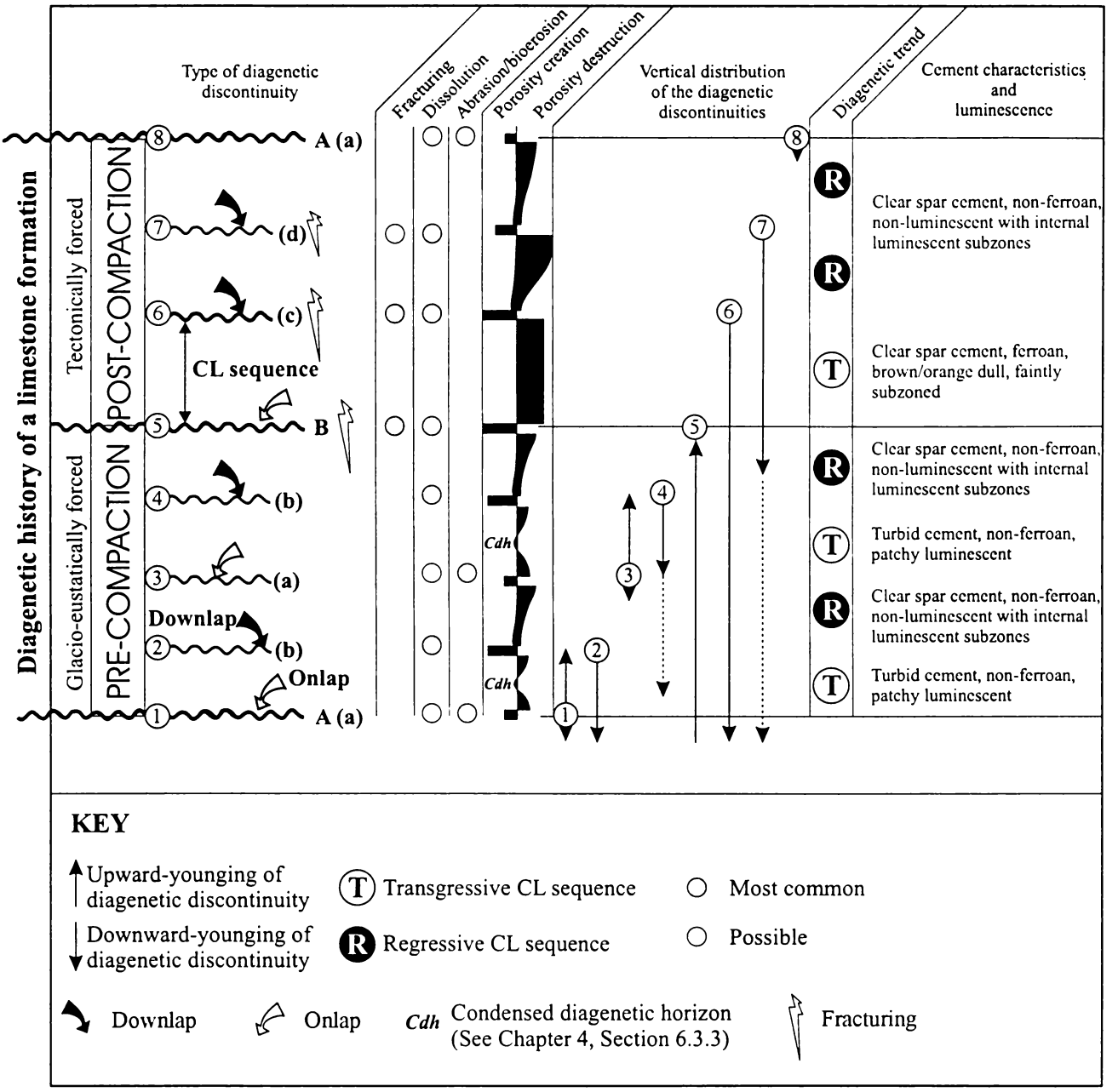

Figure 18- Summary characteristics of pre- and post-compaction transgressive (T) - regressive (R) CL sequences, showing the type and hierarchy of bounding discontinuities (A, B, and a, b, c, and d), periods of porosity alteration, and a brief description of the cement components of CL sequences. Note that within the cool-water carbonates, porosity destruction occurs principally during the post-compaction diagenetic history. The pre-compaction diagenetic history of a sediment pile may consist of more than one T-R CL sequence depending on the number of building sedimentary cycles. While the building CL sequence of a pre-compaction megasequence, bounded by Diagenetic Sequence Boundaries (DSB; Type-A and Type-B), may be associated with periodic climatic changes that cause high-frequency cyclicity (fifth- and higher-order), the post-compaction megasequence, also bounded by DSBs coincides with landward and basinward oscillation of lower-order cyclicity (second- to fourth-order). This oscillation is produced by changes in the rate of tectonic subsidence and uplift, caused by changes in rates of plate motion for example. See text for details.

pile, close to the basal TSE, and be converted into an upward-younging type-a Dd, which as such behaves like an onlap surface upon which marine cements may precipitate (Figures 15A, 15D, 17B, 17G). In particular, a given type-a Dd should only be defined for the specific diagenetic suite of a sedimentary sequence.

In contrast, the type-b Dd, which bounds the top of the initial transgressive CL sequence, behaves like a downlap surface because it forms in association with the downward penetration of meteoric waters, hence becoming younger down-dip from a subaerial exposure surface (Braithwaite, 1993) (Figures 15A, 15D, 18). Consequently, a type-b Dd may cross several sedimentary surfaces and overprint successive specific diagenetic suites and type-a Dds.

In model A, illustrated in Figure 15A, the regressive part of the pre-compaction "CL megasequence" consists in fact of three stacked regressive CL sequences, namely KA, AA, and RA, overlapped by CL sequence B1, which constitutes the transgressive part of the post-compaction CL megasequence (see below). This points at the delay in triggering compactional processes, and subsequent penetration of confined groundwaters (see below).

5.4.2. Post-compaction transgressive-regressive CL sequence

An idealized post-compaction CL sequence is bounded below by a Type-B DSB and above by a Type-A DSB above (Figure 18), and consists also of a transgressive-regressive formational couplet of component CL sequences separated by a type-c Dd.

As discussed in previous chapters, not only compactional effects can be diachronous, both laterally and vertically, within a given limestone unit in response to lithofacies changes (e.g., Meyers, 1980), but also the depth of burial is a critical factor in the timing of triggering compactional processes during progressive burial. Theoretically, mechanical compaction effects, including fracturing and dissolution, occur first in the rock bodies that first enter the compaction realm, and consequently become younger up-section (Nicolaides and Wallace, 1997), determining an onlap relationship between host-rock and compactional discontinuity surface, namely the Type-B DSB (Figures 15D, 18).

Post-Type-B DSB diagenetic features typically involve a chronological suite of burial ferroan calcite cements (i.e., the "transgressive" CL sequence B1; Figures 15A, 17F to 17H) unconformably followed by uplift-related non-ferroan cements (i.e., the

"regressive" CL sequence C1; Figure 15A). These cements are unequivocally interpreted as meteoric in origin. They precipitated when the basin was tectonically uplifted, enabling the percolation of undersaturated groundwaters, which produced a downward-younging discontinuity (downlap) surface (i.e., type-c Dd; Figures 15C, 15C, 15D), and became supersaturated with time as they interacted with the host sediments.

5.5. Variations in the attributes of CL sequences across their distribution area

Although CL sequences are proposed to contain conformable suites of cement zones, dissolution surfaces of limited spatial extent may accompany their development, especially in association with microenvironment-type conditions, which also promote concentration of trace elements. Therefore, the definition of CL sequences calls for caution, and the traceability of discontinuities and their potential status as correlation surfaces can only be assessed when supported by a large sampling programme.

Because of the uncommonness of marine precipitates within the Te Aute successions, the pre-compaction transgressive CL sequence is typically restricted to its basal Type-A/type-a discontinuity, to which the younger type-b Dd is superposed (Figure 17A), or even the next Type-B DSB (Figure 17H), when no meteoric influence has been recognized (e.g., the absence of CL sequence KA at Waimarama section; Figure 5).

When present, marine precipitates are found in specific horizons, typically in coarse-grained, shallow-water sediments at the base of TSTs, and towards the top of RSTs. Thus, in the cool-water Te Aute setting, rapidly down-dip from the antiform tops, which is the most likely environment where cementation may occur, the transgressive CL sequence is constricted to a compound diagenetic discontinuity: type-b Dds superposed to type-a Dds.

Lateral changes of the thickness and pinch-out of the pre-compaction regressive CL sequence highlight the geometry of the cementing aquifer system which, in combination with lateral changes of CL patterns, help determine the source area and flow direction of the groundwaters. Typically, while in up-dip areas, close to the source, cements within the regressive CL sequence precipitate from oxidizing waters, in down-dip regions, confinement of the aquifer leads to the development of reducing conditions, and the precipitation of increasingly ferroan cements. This down-flow chemical scheme has been documented in many past studies (e.g., Dorobek, 1987), and Machel and

Burton (1991) emphasized the unlikelihood of groundwaters remaining oxygenated for more than 100 km down-dip from their recharge area.

Chemical staining enables qualitative determination the ferroan content of cement phases (Dickson, 1966). The unconformity-bounded cements of CL sequence B1 (Figures 15A, 18) stain from pale to deep blue, respectively from the top to the base of the confined paleoaquifer system, pointing to differential redox conditions with increasing depth of burial.

6. Conclusions

Conformable successions of calcite cement growth stages in the Pliocene Te Aute limestone units are commonly interrupted by discontinuities at the thin-section scale, including dissolution and renucleation surfaces, and fractures (Figure 3). The complex chronological suite of diagenetic fabrics reflects the evolution of the chemical environment from conditions promoting cementation, to conditions inducing prolonged periods of non-deposition and alteration of calcite crystals.

In order to better explain the probable progression of diagenetic environments that moved through the cool-water carbonate deposits, concepts that classically underpin the sequence stratigraphic analysis of sedimentary successions have been used to group cement zones, revealed under cathodoluminescent (CL) light, into diagenetic discontinuity-bounded CL sequences (Figure 2).

A CL sequence is a genetically-related succession of cement zones enveloped by correlative diagenetic discontinuities, which are traceable vertically over several tens of metres, and laterally over several kilometres.

In the Early Pliocene (Opoitian) Kairakau Limestone, the procedure identifies a distinct succession of five CL sequences, termed KZ and KA to KD (Figures 2, 4, and 5), which can be summarised as follows:

(a) CL sequence KZ locally consists of marine turbid cements (now low-Mg calcite, originally probably intermediate-Mg calcite) growing upon the abraded surface of skeletons and bounded above by the dissolution surface at the base of the next CL sequence KA. These cements are poorly correlatable, and are only found associated with shallow-water facies from above and below marine ravinement surfaces.

(b) CL sequence KA is enveloped by a dissolution surface at the base and by a fracturing surface at the top. Clear spar cements within CL sequence KA stain pink, are non-

luminescent, and formed from oxidizing waters that interacted with metastable carbonate phases to reach saturation levels within a meteoric aquifer system. This pre-compaction low-Mg calcite cement is common throughout the southern outcrops of Kairakau Limestone, but from this sector northwards, it gradually thins and eventually pinches out towards the northernmost portion of the study area. The meteoric aquifer is interpreted to have formed during a likely localized emergent event associated with a relative sea-level drop.

(c) CL sequence KB comprises the first generation of post-compaction fracture-hosted cements. The low-Mg calcite cement stains blue, show a brown to orange dull luminescent zonation, and its percentage volume is highest in the southeast of the study region, which is proposed as the probable recharge area for an extended confined aquifer system. In the north, cements within CL sequence KB stain deep blue and show an orange moderately to bright luminescent zonation. It is proposed that carbonates present in the ambient reducing fluids were intrinsically sourced and derived from solubility-driven mechanisms under conditions of low water/rock ratios.

(d) CL sequence KC is bounded by dissolution surfaces superposed to uplift-related fractures. It consists of pink, non-luminescent, low-Mg calcite cements, which constitute the volumetrically dominant carbonate precipitates, especially along a north-south trending line coinciding with the axis of the forearc basin. The abundance of this telogenetic cement within the Kairakau Limestone diminishes eastwards and southwards, assumed to represent the gravity-driven flow direction of the cementing aquifer. The low $\delta^{13}C$ values of the non-luminescent cement, compared to whole-rock data, are interpreted to demonstrate an allochthonous carbon source, possibly involving soil organic matter.

(e) CL sequence KD is the least abundant cementing phase. The cement suite consists of a bright-luminescent zone overgrown by non-luminescent cement. It is interpreted as a late tectonic-related cementing phase that formed from meteoric, dominantly oxidizing, waters.

The overall CL sequence pattern is referred to as the *Kairakau motif*, and is a reflection of a suite of processes from marine to meteoric forced by sea-level changes, to burial to telogenetic/meteoric forced by subsidence and tectonics.

The identification of the *Kairakau motif* within the limestone units overlying Kairakau Limestone, with the exception of the youngest "mid"-Nukumaruan ones where the motif is incomplete, is the basis for modelling the diagenetic sequence stratigraphic architecture of the cool-water Pliocene carbonates (Figures 14, 15). The construction of a sequence stratigraphic model for cementation and diagenetic discontinuity successions aims at unravelling the chronostratigraphic significance of the CL sequences making up the *Kairakau motif*, which is fundamentally dependent upon the traceability of the bounding diagenetic discontinuity surfaces.

In limestones ranging in age from Opoitian to Waipipian (and possibly Mangapanian), located in the eastern region of southern Hawke's Bay, the mesogenetic (CL sequence KB in the *Kairakau motif*) and telogenetic (KC and KD) diagenetic suites are proposed to be common to all units, and are interpreted to have formed from three fluid systems, each precipitating one cement generation. In contrast, the post-depositional pre-compaction cements from one limestone body to another are proposed to be genetically unrelated, and are assumed to derive from temporally and spatially distinct meteoric or possibly mixed marine-meteoric systems.

The repetition of the *Kairakau motif* within the early-Nukumaruan limestones from the central part of the study area is hypothesized on the basis of geochemical and tectonic considerations. Implicit in this statement is the acceptance that the mesogenetic-telogenetic suites from within the pre- and syn-Nukumaruan limestones are unrelated. The tectonic evolution of the forearc basin suggests that the central region could have experienced subsidence, hence burying limestone sheets and producing a new mesogenetic CL sequence, while the eastern region was being uplifted, hence bringing out the previously developed "older" mesogenetic CL sequence into the telogenetic realm (Figure 15A).

The application of sequence stratigraphic concepts enables recognition of transgressive-regressive CL sequences in the pre- and post-compaction diagenetic suites of the studied carbonates.

An idealized pre-compaction transgressive-regressive diagenetic suite mimics the evolution of the depositional environment, and is forced by relative sea-level changes. The transgressive CL sequence records the evolution of the marine phreatic environment between consecutive marine ravinement surfaces, while the regressive CL sequence records the subaerial exposure of shoaling-upwards sedimentary sequences.

An idealized post-compaction transgressive-regressive diagenetic suite is forced by subsidence and tectonic mechanisms. The transgressive CL sequence forms when the combined effects of subsidence and tectonics bury the host sediments to depths where significant compaction-induced fracturing occurs, and confinement modifies the ambient fluids towards reducing conditions. The post-compaction regressive sequence records the reducing-oxidizing turnaround of the chemical environment, due to exhumation of the sediments by tectonic-induced uplift (Figure 18).

CL studies of cool-water Pliocene limestones in New Zealand are in their infancy. However, the present study has shown that diagenetic pathways are complex, but can be intimately related to the patterns of regional and global paleogeographic changes. What is needed are further high-resolution petrographic studies which, by combining more detailed isotopic, elemental, and stratigraphic information, will undoubtedly bring out more accurate interpretations.

References

Beu, A. G. (1995) *Pliocene Limestones and Their Scallops*. Monograph 10, Institute of Geological & Nuclear Sciences Limited, Lower Hutt, New Zealand, 243 pp.

Braithwaite, C. J. R. (1993) Cement sequence stratigraphy in carbonates. *Journal of Sedimentary Petrology*, **63**(2), 295-303.

Brand, U. & Veizer, J. (1980) Chemical diagenesis of a multicomponent carbonate system 1: trace elements. *Journal of Sedimentary Petrology*, **51**, 987-997.

Caron, V. & Nelson, C. S. (2001) Cathodoluminescence sequences in the Early Pliocene cool-water Kairakau Limestone, Hawke's Bay, New Zealand. In: *Cathodoluminescence in geosciences: new insights from CL in combination with other techniques*, pp. 18. Technische Universitat Bergakademie Freiberg, Freiberg, University of Mining and Technology, Germany.

Cashman, S. M., Kelsey, H. M., Erdman, C. F., Cutten, H. N. C. & Berryman, K. R. (1992) Strain partitioning between structural domains in the forearc of the Hikurangi subduction zone, New Zealand. *Tectonics*, **11**(2), 242-257.

Choquette, P. W. & James, N. P. (1990a) Limestones - The meteoric diagenetic environment. In: *Diagenesis, Vol. 4* (Ed. by I. A. McIlreath and D. W. Morrow), pp. 35-73. Geoscience Canada Reprint Series 4.

Choquette, P. W. & James, N. P. (1990b) Limestones - The burial diagenetic environment. In: *Diagenesis* (Ed. by I. A. McIlreath and D. W. Morrow), pp. 75-112. Geoscience Canada Reprint Series 4.

Choquette, P. W. & Pray, L. C. (1970) Geologic nomenclature and classification of porosity in sedimentary carbonates. *American Association of Petroleum Geologists Bulletin*, **54**, 207-250.

Croft Exploration Ltd. (1992) Petroleum prospecting licence PPL38320, onshore New Zealand. Information brochure. *Ministry of Economic Development New Zealand*, Unpublished Petroleum Report PR1837.

Dickson, J. A. D. (1965) A modified staining technique for carbonates in thin-section. *Nature*, **205**, 587.

Dickson, J. A. D. (1966) Carbonate identification and genesis as revealed by staining. *Journal of Sedimentary Petrology*, **36**(2), 491-505.

Dorobek, S. L. (1987) Petrography, geochemistry and origin of burial diagenetic facies, Siluro-Devonian Helderberg Group (Carbonate rocks), Central Appalachians. *American Association of Petroleum Geologists Bulletin*, **71**(5), 492-514.

Durlet, C. (1996) Apport de la diagenèse des discontinuités à l'interprétation paléoenvironnementale et séquentielle d'une plate-forme carbonatée - Exemple des calcaires bajociens du Seuil de Bourgogne. Unpublished PhD Thesis, Université de Bourgogne, France.

Emery, D. & Dickson, J. A. D. (1989) A syndepositional meteoric phreatic lens in the Middle Jurassic Lincolnshire Limestone, England, UK. *Sedimentary Geology*, **65**, 273-284.

Field, B. D., Uruski, C. I., *et al.* (1997) *Cretaceous-Cenozoic Geology and Petroleum Systems of the East Coast Region, New Zealand.* Monograph 19, Institute of Geological and Nuclear Sciences Limited, Lower Hutt, New Zealand, 301 pp.

Frank, T. D. & Lohmann, K. (1995) Early cementation during marine-meteoric fluid mixing: Mississippian Lake Valley Formation, New Mexico. *Journal of Sedimentary Research*, **A65**(2), 263-273.

Frank, T. D., Lohmann, K. C. & Meyers, W. J. (1995) Chronostratigraphic significance of cathodoluminescence zoning in syntaxial cement: Mississippian Lake Valley Formation, New Mexico. *Sedimentary Geology*, **105**, 29-50.

Goldhammer, R. K., Oswald, E. J. & Dunn, P. A. (1994) High-frequency, glacio-eustatic cyclicity in the Middle Pennsylvanian of the Paradox Basin: an evaluation of Milankovitch forcing. *International Association of Sedimentologists Special Publication*, **19**, 243-283.

Goldstein, R. H. (1988) Cement stratigraphy of Pennsylvanian Holder Formation, Sacramento Mountains, New Mexico. *American Association of Petroleum Geologists Bulletin*, **72**(4), 425-438.

Grover Jr, G. & Read, J. F. (1983) Paleoaquifer and deep burial related cements defined by regional cathodoluminescent patterns, Middle Ordoviscian carbonates, Virginia. *American Association of Petroleum Geologists Bulletin*, **67**(8), 1275-1303.

Harmsen, F. J. (1985) Lithostratigraphy of Pliocene Strata, Central and Southern Hawke's Bay, New Zealand. *New Zealand Journal of Geology and Geophysics*, **28**, 413-433.

Haywick, D. W. N. (1990) Stratigraphy, sedimentology, paleoecology and diagenesis of the Petane Group (Pliocene-Pleistocene) in the Tangoio, central Hawke's Bay, New Zealand. Unpublished PhD Thesis, James Cook University of North Queensland, Australia.

Heckel, P. H. (1983) Diagenetic model for carbonate rocks in Midcontinent Pennsylvanian eustatic cyclothems. *Journal of Sedimentary Petrology*, **53**(3), 733-759.

Heckel, P. H. (1986) Sea-level curve for Pennsylvanian eustatic marine transgressive-regressive depositional cycles along Midcontinent outcrop belt. *Geology*, **14**, 330-334.

Hood, S. D. & Nelson, C. S. (1996) Cementation scenarios for New Zealand non-tropical limestones. *New Zealand Journal of Geology and Geophysics*, **39**, 109-122.

Horbury, A. D. & Adams, A. E. (1989) Meteoric phreatic diagenesis in cyclic Late Dinantian carbonates, northwest England. *Sedimentary Geology*, **65**, 319-344.

Kamp, P. J. J. & Nelson, C. S. (1987) Tectonic and sea-level controls on non-tropical limestones in New Zealand. *Geology*, **15**, 610-613.

Kamp, P. J. J. & Nelson, C. S. (1988) Nature and occurrence of modern and Neogene active margin limestones in New Zealand. *New Zealand Journal of Geology and Geophysics*, **31**, 1-20.

Kaufman, J., Cander, H. S., Daniels, L. D. & Meyers, W. J. (1988) Calcite cement stratigraphy and cementation history of the Burlington-Keokuk Formation (Mississippian), Illinois and Missouri. *Journal of Sedimentary Petrology*, **58**(2), 312-326.

Kaufmann, B. & Wendt, J. (2000) Calcite cement successions in middle Devonian (Givetian) carbonate mud buildups of the southern Ahnet basin (Algerian Sahara). *Carbonates and Evaporites*, **15**(2), 149-161.

Kelsey, H. M., Erdman, C. F. & Cashman, S. M. (1993) Geology of Southern Hawke's Bay from the Maraetotara Plateau and Waipawa westward to the Wakara Range and the Ohara depression, pp. 1-17. Institute of Geological & Nuclear Sciences, Lower Hutt, New Zealand.

Kimbell, T. N. & Humphrey, J. D. (1994) Geochemistry and crystal morphology of aragonite cements of mixing-zone origin, Barbados, West Indies. *Journal of Sedimentary Research*, **A64**, 604-614.

Lavoie, D. & Bourque, P.-A. (1993) Marine, burial, and meteoric diagenesis of early Silurian carbonate ramps, Quebec Appalachians, Canada. *Journal of Sedimentary Petrology*, **63**(2), 233-247.

Leslie, W. C. (1971a) Mason Ridge No.1 - well completion report, pp. 16. Beaver Exploration New Zealand Limited - Longreach Oil Limited.

Leslie, W. C. (1971b) Ongaonga No.1 - well completion report, pp. 20. Beaver Exploration New Zealand Limited - Longreach Oil Limited.

Lohmann, K. C. (1988) Geochemical patterns of meteoric diagenetic systems and their application to studies of paleokarst. In: *Paleokarst* (Ed. by N. P. James and P. W. Choquette), pp. 58-80. Springer, Berlin.

Longman, M. K. (1980) Carbonate diagenetic textures from nearsurface diagenetic environments. *American Association of Petroleum Geologists Bulletin*, **64**, 461-487.

Machel, H. G. & Burton, E. A. (1991) Factors governing cathodoluminescence in calcite and dolomite, and their implications for studies of carbonate diagenesis. In: *Luminescence Microscopy: Quantitative and Qualitative aspects, Vol. 25* (Ed. by C. E. Barker and O. C. Kopp), pp. 37-57. SEPM Short Course.

Meyers, W. J. (1974) Carbonate cement stratigraphy of the Lake Valley Formation (Mississippian), Sacramento Mountains, New Mexico. *Journal of Sedimentary Petrology*, **44**, 837-861.

Meyers, W. J. (1978) Carbonate cements: Their regional distribution and interpretation in Mississippian limestones of Southwestern New Mexico. *Sedimentology*, **25**, 371-399.

Meyers, W. J. (1980) Compaction in Mississippian skeletal limestones, Southern New Mexico. *Journal of Sedimentary Petrology*, **50**(2), 457-474.

Meyers, W. J. (1989) Trace element and isotope geochemistry of zoned calcite cements, Lake Valley Formation (Mississippian, New Mexico): Insights from water-rock interaction modelling. *Sedimentary Geology*, **65**, 355-370.

Meyers, W. J. (1991) Calcite cement stratigraphy: an overview. In: *Luminescence Microscopy: Quantitative and Qualitative Aspects, Vol. 25* (Ed. by C. E. Baker and O. C. Kopp), pp. 133-147. SEPM Short Course.

Meyers, W. J. & Lohmann, K. C. (1985) Isotope geochemistry of regionally extensive calcite cement zones and marine components in Mississippian limestones, New Mexico. In: *Carbonate cements, Vol. 36* (Ed. by N. Schneidermann and P. M. Harris), pp. 223-240. SEPM Special Publication

Moore, C. H. (2001) *Carbonate Reservoirs - Porosity Evolution and Diagenesis in a Sequence Stratigraphic Framework*. Elsevier, Amsterdam, 444 pp.

Nelson, C. S. (1988) An Introductory perspective on non-tropical shelf carbonates. *Sedimentary Geology*, **60**, 3-12.

Nelson, C. S., Harris, G. J. & Young, H. R. (1988) Burial-dominated cementation in non-tropical carbonates of the Oligocene Te Kuiti Group, New Zealand. *Sedimentary Geology*, **60**, 233-250.

Nelson, C. S. & James, N. P. (2000) Marine cements in mid-Tertiary cool-water shelf limestones of New Zealand and southern Australia. *Sedimentology*, **47**, 609-629.

Nelson, C. S. & Smith, A. M. (1996) Stable oxygen and carbon isotope compositional fields for skeletal and diagenetic components in New Zealand Cenozoic non-tropical carbonate sediments and limestones: A synthesis and review. *New Zealand Journal of Geology and Geophysics*, **39**, 93-107.

Nelson, C. S., Winefield, P. R., Hood, S. D., Caron, V., Pallentin, A. & Kamp, P. J. J. (in review) Pliocene Te Aute limestones, New Zealand: expanding notions for models of cool-water shelf carbonates.

Nelson, W. A. & Read, J. F. (1990) Updip to downdip cementation and dolomitization patterns in a Mississippian aquifer, Appalachians. *Journal of Sedimentary Petrology*, **60**(3), 379-396.

Nicolaides, S. & Wallace, M. W. (1997) Pressure-dissolution and cementation in an Oligocene-Miocene non-tropical limestone (Clifton Formation), Otway basin, Australia. In: *Cool-water carbonates, Vol. 56* (Ed. by N. P. James and J. D. A. Clark), pp. 127-140. SEPM Special Publication.

Niemann, J. C. & Read, J. F. (1988) Regional cementation from unconformity-recharged aquifer and burial fluids, Mississippian Neuman Limestone, Kentucky. *Journal of Sedimentary Petrology*, **58**(4), 688-705.

Pettinga, J. R. (1982) Upper Cenozoic structural history, coastal southern Hawke's Bay, New Zealand. *New Zealand Journal of Geology and Geophysics*, **25**, 149-191.

Posamentier, H. W., Jervey, M. T. & Vail, P. R. (1988) Eustatic controls on clastic deposition I - conceptual framework. In: *Sea-level changes: An Integrated Approach, Vol. 42* (Ed. by C. K. Wilgus, B. S. Hastings, C. G. S. C. Kendal, H. W. Posamentier, C. A. Ross and J. C. Van Wagoner), pp. 125-154. SEPM Special Publication.

Rankey, E. C., Bachtel, S. L. & Kaufman, J. (1999) Controls on stratigraphic architecture of icehouse mixed carbonate-siliciclastic systems: a case study from the Holder Formation (Pennsylvanian, Virgilian), Sacramento Mountains, New Mexico. In: *Advances in Carbonate Sequence Stratigraphy: Application to Reservoirs, Outcrops, and Models, Vol. 63* (Ed. by P. M. Harris, A. H. Saller and J. A. Simo), pp. 127-150. SEPM Special Publication, Tulsa.

Rao, C. P. (1990) Geochemical characteristics of cool-temperate carbonates, Tasmania, Australia. *Carbonates Evaporites*, **5**, 209-221.

Rao, C. P. & Adabi, M. (1992) Carbonate minerals, major and minor elements, and oxygen and carbon isotopes, and their variation with water depth in cool, temperate carbonates, western Tasmania, Australia. *Marine Geology*, **103**, 249-272.

Runnels, D. D. (1969) Diagenesis, chemical sediments, and the mixing of natural waters. *Journal of Sedimentary Petrology*, **39**, 1188-1201.

Saller, A. H., Dickson, J. A. D. & Boyd, S. A. (1994) Cycle stratigraphy and porosity in Pennsylvanian and Lower Permian shelf limestones, eastern Central Basin platform. *American Association of Petroleum Geologists Bulletin*, **78**, 1820-1842.

Sarg, J. F. (1988) Carbonate sequence stratigraphy. In: *Sea-Level Changes: An Integrated Approach, Vol. 42* (Ed. by C. K. Wilgus, H. Posamentier, C. A. Ross and C. G. St. C. Kendall), pp. 155-181. SEPM Special Publication, Tulsa.

Simo, J. A. & Lehmann, P. J. (2000) Diagenetic history of Pipe Creek Jr. Reef, Silurian, North-Central Indiana, U.S.A. *Journal of Sedimentary Research*, **70**(4), 937-951.

Spörli, K. B. & Pettinga, J. R. (1980) Mount Kahuranaki, Hawke's Bay, New Zealand, a klippe emplaced by gravity sliding from the crest of the Nearby Elsthorpe anticline. *Journal of the Royal Society of New Zealand*, **10**(3), 287-307.

Tobin, K. J. & Walker, K. R. (1998) Diagenetic calcite from the Chazyan Group (Vermont): an example of aragonite alteration in a greenhouse ocean. *Sedimentary Geology*, **121**, 277-288.

Tucker, M. E. (1993) Carbonate diagenesis and sequence stratigraphy. In: *Sedimentology Review, Vol. 1* (Ed. by V. P. Wright), pp. 51-72. Blackwell scientific, Oxford.

Vail, P. R., Audemard, F., Bowman, S. A., Eisner, P. N. & Perez-Cruz, C. (1991) The stratigraphic signatures of tectonics, eustasy and sedimentology - an overview. In: *Cycles and Events in Stratigraphy* (Ed. by G. Einsele, W. Ricken and A. Seilacher), pp. 617-659. Springer-Verlag, Berlin Heidelberg.

Van Wagoner, J. C. (1996) Overview of sequence stratigraphy of foreland basin deposits: terminology, summary of papers, and glossary of sequence stratigraphy. *American Association of Petroleum Geologists Memoir*, **64**, ix-xxi.

Van Wagoner, J. C., Mitchum, R. M. J., Posamentier, H. W. & Vail, P. R. (1987) Seismic stratigraphy interpretation using sequence stratigraphy. Part 2: key definitions of sequence stratigraphy. In: *Atlas of Seismic Stratigraphy, Vol. 27* (Ed. by A. W. Bally), pp. 11-14. American Association of Petroleum Geologists – Studies in Geology.

Van Wagoner, J. C., Posamentier, H. W., Mitchum, R. M. J., Vail, P. R., Sarg, J. F., Loutit, T. S. & Hardenbol, J. (1988) An overview of the fundamentals of sequence stratigraphy and key definitions. In: *Sea-Level Changes: An Integrated Approach, Vol. 42* (Ed. by C. K. Wilgus, B. S. Hastings, C. G. S. C. Kendall, H. W. Posamentier, C. A. Ross and J. C. Van Wagoner), pp. 39-45. SEPM Special Publication.

Veizer, J. (1983a) Chemical diagenesis of carbonates: theory and application of trace element techniques. In: *Stable Isotopes in Sedimentary Geology, Vol. 10*, pp. 3.1-3.100. SEPM Short Course.

Veizer, J. (1983b) Trace elements and isotopes in sedimentary carbonates. *Reviews in Mineralogy*, **11**, 265-299.

Walkden, G. M. & Berry, J. P. (1984) Syntaxial overgrowths in muddy crinoidal limestones: cathodoluminescence sheds new light on an old problem. *Sedimentology*, **31**, 251-267.

Walkden, G. M. & Williams, D. O. (1991) The diagenesis of late Dinantian Derbyshire-East Midland carbonate shelf, central England. *Sedimentology*, **38**, 643-670.

Winefield, P. R. (1995) Elemental geochemistry of non-tropical Cenozoic limestones in New Zealand. Unpublished MsC Thesis, University of Waikato, New Zealand.

Zeeh, S., Walter, U., Kuhlemann, J., Keppens, E. & Bechstadt, T. (1997) Carbonate cements as a tool for fluid flow reconstruction : a study in parts of the eastern Alps (Austria, Germany, Slovenia). *SEPM Special Publication*, **57**, 167-181.

EPILOGUE

This thesis describes the sedimentologic and diagenetic stratigraphy of the Plio-Pleistocene cool-water Te Aute limestones in southern Hawke's Bay, eastern North Island, New Zealand. The study is mainly concerned with the analysis of diagenetic processes in non-tropical carbonates, a topic that relatively few studies have so far addressed in much detail. Four principal objectives were examined and the main conclusions and perspectives are noted below.

The non-tropical Te Aute limestones, which are coarse-grained skeletal hashes dominated by barnacle, epifaunal bivalve, and bryozoan remains, developed under the influence of strong tidal flows and probable storm-associated currents in shoal areas on continent-attached shelves to the west of the study region, and about actively growing upthrust-cored antiforms to the east, along the margins of an actively deforming and uplifting forearc basin or seaway, adjacent to the Pacific-Australian Plate boundary off eastern North Island.

The study is underpinned by detailed sedimentologic and stratigraphic analyses, which are regarded as critical for the comprehension of the role that sediment composition and depositional facies have exerted over diagenetic pathways. Rapid lateral and vertical facies changes are ubiquitous in the carbonate successions. Nevertheless, it has been possible to recognize a number of recurring sedimentary facies, and importantly the occurrence of shell concentrations sitting immediately above or below a variety of sedimentary surfaces, including sharp and erosional contacts. Three major facies groupings have been described and defined that comprise a total of 14 different facies types. Associated depositional environments are interpreted to range from below storm wave base to shallow-water shoreface-type influenced by high-energy currents.

While the older (Early- to mid-Pliocene) limestone occurrences from the eastern and western margins of the forearc basin punctuate thick siliciclastic deposits and consist of calcite-dominated mineralogies, their younger (Late Pliocene) and more basin central counterparts alternate with sandstone/siltstone over relatively thin stratigraphic intervals giving a pronounced cyclothemic architecture, and comprise well individualized shell beds packed with aragonitic bivalves.

The Te Aute cool-water limestones bear a remarkable array of diagenetic features that have been described and tentatively assigned to a wide spectrum of environments involving marine, meteoric, and burial influences. While in tropical, predominantly aragonitic, carbonate settings, the essentials of porosity evolution within host sediments occur typically in surficial environments, prior to burial, in cool-water, predominantly calcitic, carbonate settings, porosity modification may be delayed until after burial at depths where mechanical compaction and pressure-dissolution are triggered. In order to decipher what diagenetic features reflect the evolution of the depositional realm while under the influence of surficial processes prior to burial, new concepts have been developed that provide a unique potential to integrate the diagenetic evolution of the limestones into inferred patterns of relative sea-level changes. These concepts integrate several of the specificities of non-tropical carbonates and environments, especially their low reactive primary stable mineralogy, and the typically destructive nature of sea-floor diagenesis (e.g., grain attrition, boring, dissolution) as a consequence of relatively slow rates of sedimentation in cool-sea water. Therefore, the proposed diagenetic approach can potentially be applied to cool-water carbonate facies elsewhere.

In the Pliocene Te Aute limestone units, conformable successions of calcite cement growth stages, as revealed by chemical staining and cathodoluminescence, are commonly interrupted by discontinuities at the thin-section scale, including dissolution and renucleation surfaces, and fractures. A critical discontinuity event to decipher is the first evidence of mechanically-induced skeletal fracturing, enabling the definition of pre-compaction and post-compaction diagenetic features. A comparison of pre-compaction diagenetic suites in samples from above and below significant outcrop disconformities enables isolation of the "specific diagenesis" of unconformity-bounded depositional units, which is that suite of diagenetic events associated with the evolution of the sedimentation realm of a unit or a given horizon within a unit, exclusive of diagenetic overprints shared with any overlying unit through an unconformity since these relate to some subsequent, different depositional stage. In this way it is possible for the specific diagenesis of a succession of depositional facies between consecutive unconformities to be interpreted within a sequence stratigraphic framework.

For the Te Aute limestones several specific diagenetic suites have been defined, which are characteristically dominated either by marine and meteoric destructive (abrasion, dissolution, bioerosion) or constructive (cementation, encrustation) processes. Their vertical distributions are related to the facies stacking within deepening- or deepening- then shallowing-upwards sedimentary sequences bounded by discontinuity surfaces. It is proposed that the constructive diagenetic suites are associated with the lower part of transgressive systems tracts (TST), and occur towards the top of regressive systems tracts (RST). Thus, sea-floor cements are restricted to high-energy depositional facies, immediately above or below unconformities associated, for example, with marine condensation. In comparison, destructive diagenesis characterizes the upper part of the TST, the highstand systems tract (HST), the lower part of the RST, and occasionally beneath the bounding surface of the RST in association with subaerial exposure.

The integrated sedimentologic and diagenetic approach developed in the course of this study, by also revealing condensed horizons and key surfaces otherwise unrecognized in the field, has helped unlock the cryptic sedimentary architecture within many of the Te Aute limestone formations. Thus, the analytical procedure demonstrates that studies aiming at unravelling the sequence stratigraphy of cool-water successions that comprise apparently monotonous limestone units should be accompanied by detailed diagenetic analysis to ascertain that no significant event has been missed, sealed within the diagenetic stratigraphy of the carbonate sediments.

The Te Aute cool-water deposits are constructed of metre-scale (1-15 m) sequences bounded by mainly transgressive surfaces of erosion (TSEs) locally superimposed on wave-cut surfaces of erosion formed during normal regression (RSE) or subaerial exposure surfaces (i.e., sequences boundaries). The internal architectural styles within the Te Aute successions have been integrated into a sequence stratigraphic scheme, emphasizing that not only the production and deposition, but also the diagenesis of carbonate sediments were forced by glacio-eustatically and tectonically-driven processes.

Although common in the Te Aute limestones, conformable and unconformable successions of calcite crystal growth zones under cathodoluminescent (CL) light are

typically laterally poorly correlatable, even over short distances, and have a vertical continuity of generally no more than a few tens of metres. Therefore cement zones, being poorly traceable across a given area, can hardly serve as petrographic means of intercorrelation between cements from distant localities, and consequently cannot help discriminate and recognize the extension of paleohydrologic systems, marine, meteoric, or burial in origin. In order to address these inconsistencies, the concept of cathodoluminescence (CL) sequence, which derives from the concept of "sequence" in traditional sequence stratigraphy, has been applied to the cement suites recognized in the various Te Aute limestones. A CL sequence is a conformable succession of cement zones bounded by diagenetic discontinuities that equate to breaks in cement growth. This concept, which has received little attention from carbonate sedimentologists so far, has proved a powerful tool to explain the diagenetic evolution of the cool-water Te Aute limestones, and enabled the identification of correlative diagenetic discontinuities marking the transition between surface-related processes to processes reflecting confined conditions, and conversely. In most Pliocene limestones, the procedure, in combination with geochemical data, has: (1) identified recurring and correlative motifs of pre- and post-compaction CL sequence stratigraphies; (2) enabled regional mapping of CL sequences; (3) highlighted the spatial geometry and timing of emplacement of cementing aquifers; and (4) led to the construction of paleohydrologic models, invoking location of recharge areas and fluid-flow directions.

An attempt has been made to fully describe the paragenetic relationships of the Te Aute carbonates applying sequence stratigraphic concepts, implicitly by recognizing, besides CL sequences, sequence boundaries, transgressive and regressive precipitational trends, onlap and downlap behaviours between successive cement generations, diagenetic cycles, and different orders of cyclicity. The main justification for modelling the sequence stratigraphic evolution of carbonate paragenesis lies in the potential of carbonate systems to translate regional and global environmental changes, which also control the formation of sedimentary sequences of different orders of cyclicity, into distinct diagenetic patterns. Thus, this study has shown that: (1) pre-compaction specific diagenetic suites relate intimately to the patterns of high-frequency relative sea-level changes; and (2) tectonic subsidence, which is the main driving force in defining low-order sedimentary megasequences, also produces motifs of post-compaction diagenetic suites, namely burial- and uplift-related.

Thus, a diagenetic motif has been found to be repeated in almost all studied formations, except in the youngest ones (latest Pliocene) which have not experienced significant burial. The motif includes a local pre-compaction marine CL sequence, a more persistent pre-compaction CL sequence of meteoric or mixed marine-meteoric origin, a post-compaction burial CL sequence, and finally a post-compaction uplift-related CL sequence, meteoric in origin. CL sequences vary volumetrically from one formation to another, and typically the burial CL sequence decreases in abundance in ascending stratigraphic order. The pre-compaction CL sequence represents a minor cementing phase in all limestones, while the post-compaction uplift-related CL sequence constitutes the dominant cement generation.

An important difference between the mechanisms for cementation proposed in this study for pre-compaction, post-compaction burial, and uplift cements lies in the inferred sources of the $CaCO_3$. For the pre-compaction sequences and post-compaction burial CL sequences it is suggested that $CaCO_3$ is intrinsically sourced, and cements precipitated from meteoric or mixed marine-meteoric waters (oxidized for the pre-compaction phase and reduced for the burial phase) modified compositionally during solubility-driven exchange with the least stable carbonate phases in the host rock. The calcite-dominated nature of most of the cool-water Te Aute carbonates imposes a lesser degree of diagenetic potential than in aragonite-dominated tropical carbonates, and so the time of residence within diagenetic environments becomes critical to the nature of cementation. This explains the observed minor amounts of pre-compaction cements, and the decreasing amounts of burial cements with decreasing age since younger limestones spent less time in the burial environment than their older, more deeply buried, counterparts. In contrast, it is proposed that $CaCO_3$ for the post-compaction uplift-related cements are extrinsically sourced from supersaturated diagenetic fluids, and that the amount of material derived from dissolving metastable phases present in the host rock is not significant. $CaCO_3$ may have been sourced from the dissolution of aragonite skeletons present in the youngest latest Pliocene units, and transported in the underlying units via percolating meteoric fluids during uplift.

The full spectrum of diagenetic features and processes for the Te Aute limestones have been integrated into a comprehensive model of diagenetic evolution in

which paragenetic relationships are expressed following sequence stratigraphic concepts. Not only does the analytical procedure help infer settings and processes of diagenetic imprint, but it also permits a certain degree of prediction since the reproducibility of diagenetic mechanisms, in relation to the patterns of regional (i.e., tectonic) and global (i.e., glacio-eustatic) paleogeographic changes, has been demonstrated.

Perspectives and recommendations for further research

By integrating high-resolution sedimentologic and diagenetic considerations, and in an attempt to decipher the interplay between sedimentary, skeletal, and mineralogical facies, and the nature and activity upon host sediments of interparticle fluids, this study has emphasized that diagenetic pathways are more diverse in cool-water carbonates than most existing sedimentary models advocate.

The development of some new concepts has become imperious in the course of this research to take into account the specificities of cool-water carbonates and environments, and their application has provided new perspectives for correctly assessing and predicting pathways and timing of carbonate diagenesis in non-tropical carbonates in relation to patterns of sea-level changes and regional tectonics.

The proposed diagenetic approach has demonstrated that within the often cryptic sedimentary architecture building cool-water limestones a complex suite of both constructive and destructive diagenetic processes was encoded that records the evolution of the environmental conditions. As such, the analytical procedure should prove to be a powerful tool to assist unravelling both the sequence stratigraphy and fluid-flow history of other cool-water carbonate occurrences in New Zealand and abroad. In doing so, it is anticipated that the spectrum of other cool-water carbonate facies encountered, encompassing different depositional settings, environmental temperatures, dynamic conditions, and skeletal compositions, should serve to enrich and advance the models developed for the Te Aute limestones. In this way the diagenetic sequence stratigraphic concepts can ultimately be built into an ideal diagenetic model applicable to cool-water carbonate facies in general.

In New Zealand, future investigations should first concentrate on individual formations so as to fully document the interrelationships between facies stacking, facies lateral changes, and diagenetic signatures basinwide. Such investigations should also aim at providing a solid chronostratigraphic framework, especially for the Pliocene successions in southern Hawke's Bay, by integrating detailed geochemical and faunal studies as a basis for correlation with recognized patterns of relative sea-level changes in the region.

The small number of elemental and isotopic analyses at the cement scale due to technical limitations, including the unavailability of both a high-resolution microsampler and of a microprobe spot analyser at the University of Waikato, did not permit the chemistry of cement generations to be fully appreciated in this study, and therefore calls for further investigations. These should also concentrate on single limestone formations so as to give a better insight into the nature and extent of paleohydrologic systems that caused porosity alteration over time, and to serve as a basis for comparison between the successive Pliocene carbonate units comprising the Te Aute deposits.

Petrogenesis of Pliocene limestones in southern Hawke's Bay, New Zealand: a contribution to unravelling the sequence stratigraphy and diagenetic pathways of cool-water shelf carbonate facies

Vincent Caron



The University of Waikato
Te Whare Wānanga o Waikato

APPENDICES

THE UNIVERSITY OF WAIKATO
HAMILTON, NEW ZEALAND
2002

Petrogenesis of Pliocene limestones in southern Hawke's Bay, New Zealand: a contribution to unravelling the sequence stratigraphy and diagenetic pathways of cool-water shelf carbonate facies

Vincent Caron



The University of Waikato
Te Whare Wānanga o Waikato

APPENDICES

THE UNIVERSITY OF WAIKATO
HAMILTON, NEW ZEALAND
2002

CONTENTS

Appendix 1 – Stratigraphic columns	A1-1 to A1-44
Appendix 2 .1 - Sample list	A2-1 to A2-13
.2 – Macrofauna	A2-14 to A2-17
Appendix 3 – Sedimentary motifs	A3-1 to A3-44
Appendix 4 .1 - Point-counting data	A4.1-1 to A4.1-11
.2 – Cluster analysis	A4.2-1 to A4.2-9
Appendix 5 – Sequence diagrams	A5-1 to A5-48
Appendix 6 – Microprobe spot analysis	A6-1 to A6-10
Appendix 7 – Stable isotopes	A7-1 to A7-2
Appendix 8 – XRD analysis and data	A8-1 to A8-10
Appendix 9 – ICPOES analysis and data	A9-1 to A9-12
Appendix 10 .1 – Glossary	A10.1-1 to A10.1-3
.2 – Chemical staining	A10.2-1
.3 – Topomap Series 1/50 000	A10.3-1
.4 – Dunham's classification scheme	A10.4-1

CD1 – (.xls) ICPOES data
(.xls) XRD data
(.xls) Point-counting data
(.xls) Stable isotope data
(.xls) Microprobe data and transects
(.cdr) Photomicrographs:
- Figure 3, Chapter 3 (p.151)
- Figure 5, Chapter 3 (p.157)
- Figure 11, Chapter 3 (p.175)
- Figure 16, Chapter 3 (p.200)
- Figure 4, Chapter 4 (p.266)

APPENDIX 1

STRATIGRAPHIC COLUMNS

APPENDIX 1 - STRATIGRAPHIC COLUMNS

KEYS TO STRATIGRAPHIC SECTIONS

Where possible, all sedimentary structures have been represented as they were observed at outcrop. For features such as burrows, dewatering structures, convolute bedding, and slump structures, the scale of representation is exaggerated.

6 Running column numbers refer to localities on location map page A1-2

CONTACTS

Erosional surface

Sharp surface

Gradational

MICROFACIES ASSEMBLAGE

 Detrital

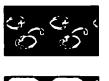 Bimol

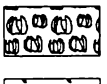 Barbital

 Mixed skeletal

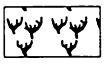 Bryotal

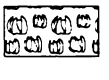 Barnamol

MACROFAUNA

 Oysters

 Biomoulds

 Bivalves

 Barnacles

 Echinoids

 Scallops

 Bryozoans

 Brachiopods

 Gastropods

SAMPLES

● 5.36 Rock sample ● F.5.32 Macrofauna sample

Te = Tephra layer

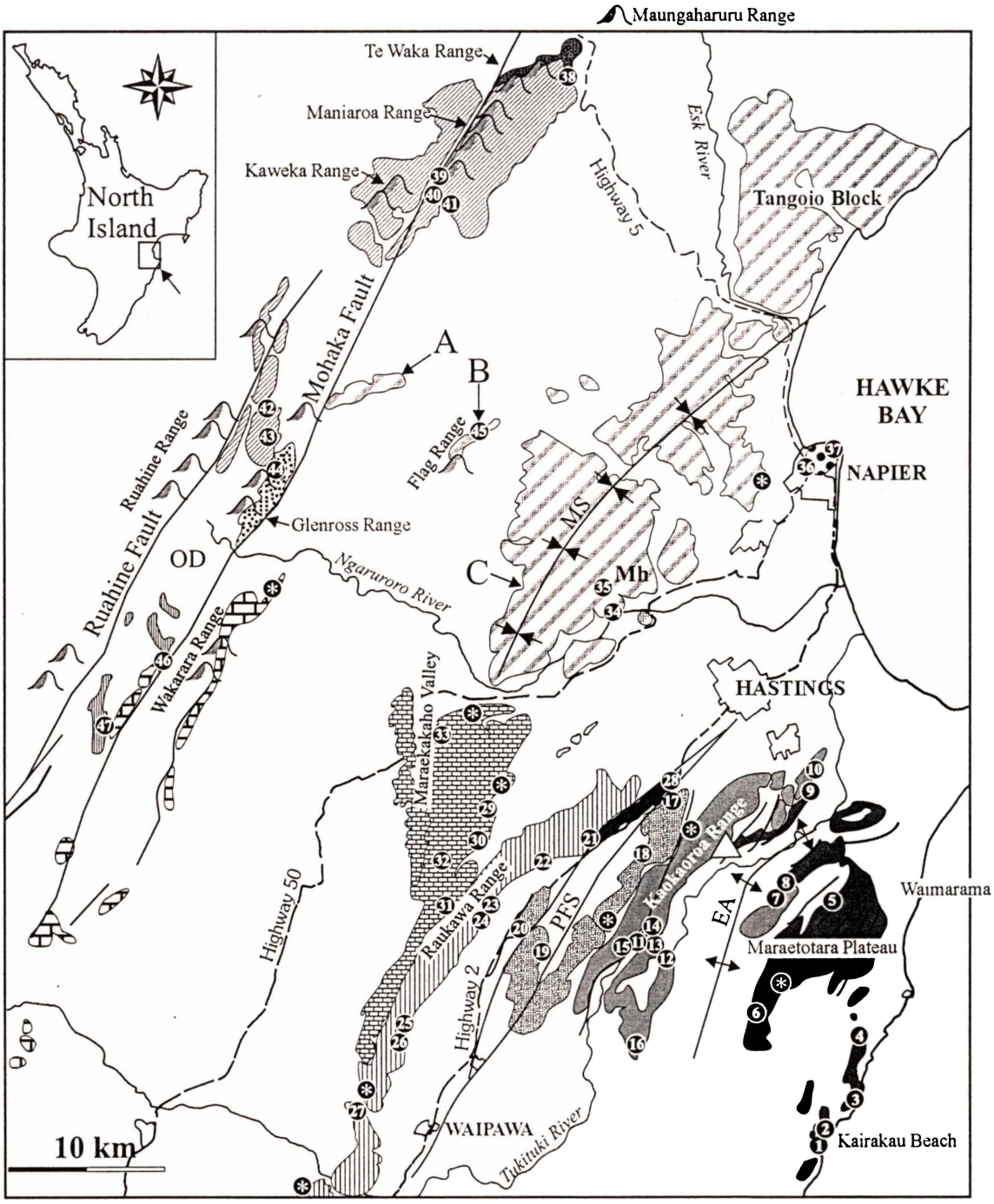

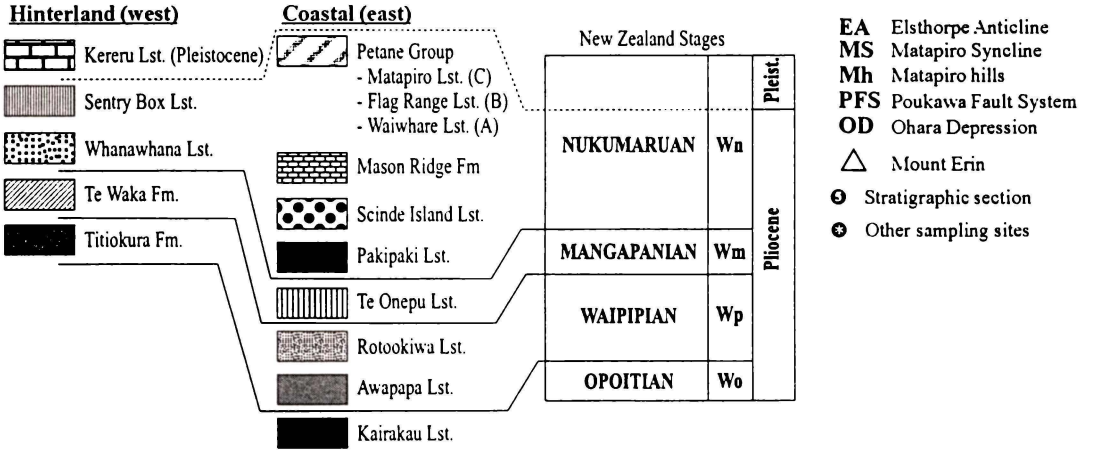

General distribution of the Plio-Pleistocene limestones in the study area, and location of logged sections and other sample sites (geological map from Beu, 1995).

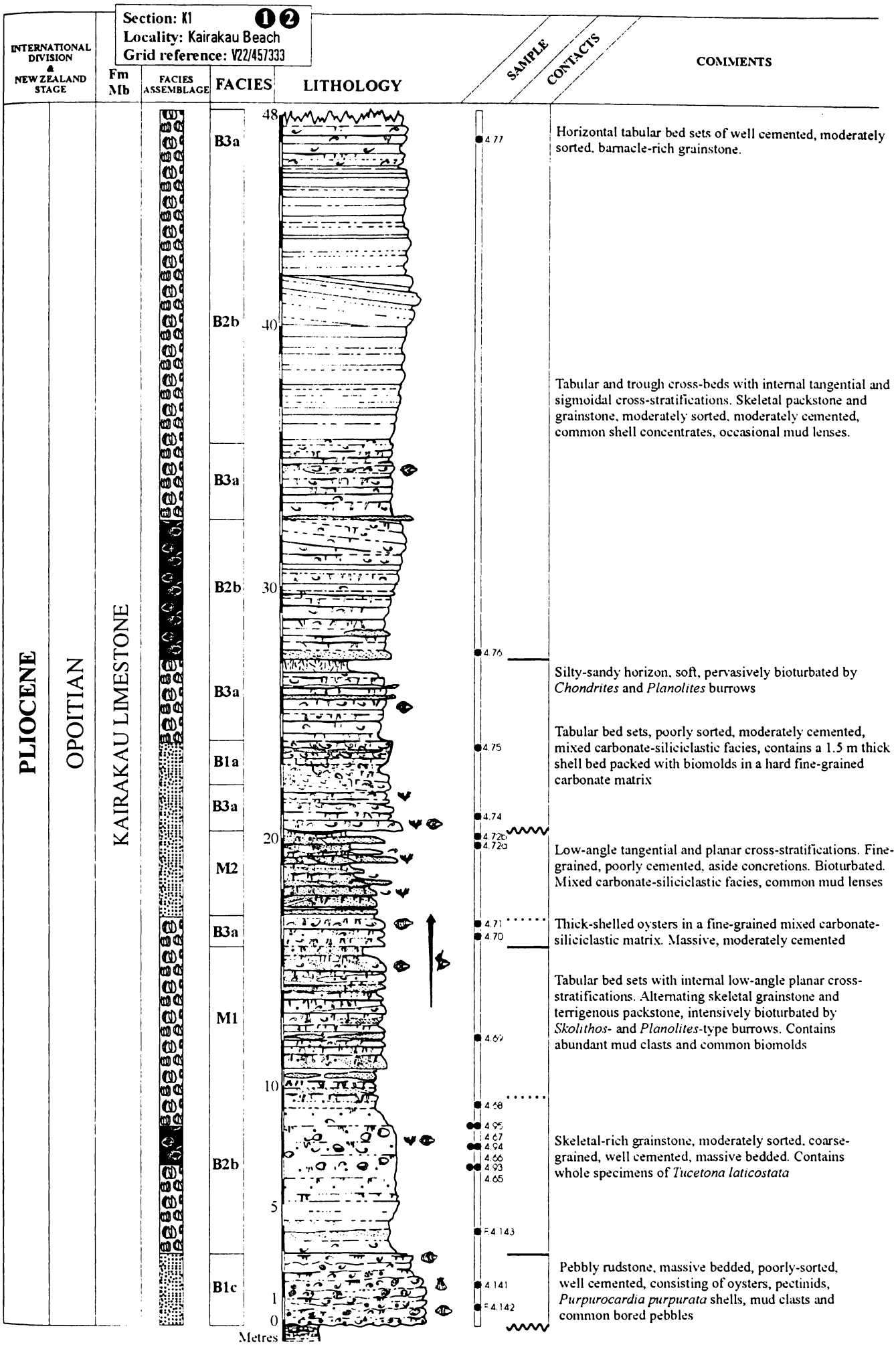
Section: K1 1 2
Locality: Kairakau Beach
Grid reference: V22/457333
INTERNATIONAL DIVISION & NEW ZEALAND STAGE
Fm Mb
FACIES ASSEMBLAGE
FACIES
LITHOLOGY
SAMPLE
CONTACTS
COMMENTS
PLIOCENE
OPOITIAN
KAIRAKAU LIMESTONE
B3a
B2b
B3a
B2b
B3a
B1a
B3a
M2
B3a
M1
B2b
B1c
48
40
30
20
10
5
1
0
Metres
4.77
4.76
4.75
4.74
4.72b
4.72a
4.71
4.70
4.69
4.68
4.95
4.67
4.94
4.66
4.93
4.65
F.4.143
4.141
F.4.142
Horizontal tabular bed sets of well cemented, moderately sorted, barnacle-rich grainstone.
Tabular and trough cross-beds with internal tangential and sigmoidal cross-stratifications. Skeletal packstone and grainstone, moderately sorted, moderately cemented, common shell concentrates, occasional mud lenses.
Silty-sandy horizon, soft, pervasively bioturbated by *Chondrites* and *Planolites* burrows
Tabular bed sets, poorly sorted, moderately cemented, mixed carbonate-siliciclastic facies, contains a 1.5 m thick shell bed packed with biomolds in a hard fine-grained carbonate matrix
Low-angle tangential and planar cross-stratifications. Fine-grained, poorly cemented, aside concretions. Bioturbated. Mixed carbonate-siliciclastic facies, common mud lenses
Thick-shelled oysters in a fine-grained mixed carbonate-siliciclastic matrix. Massive, moderately cemented
Tabular bed sets with internal low-angle planar cross-stratifications. Alternating skeletal grainstone and terrigenous packstone, intensively bioturbated by *Skolithos*- and *Planolites*-type burrows. Contains abundant mud clasts and common biomolds
Skeletal-rich grainstone, moderately sorted, coarse-grained, well cemented, massive bedded. Contains whole specimens of *Tucetona laticostata*
Pebbly rudstone, massive bedded, poorly-sorted, well cemented, consisting of oysters, pectinids, *Purpurocardia purpurata* shells, mud clasts and common bored pebbles

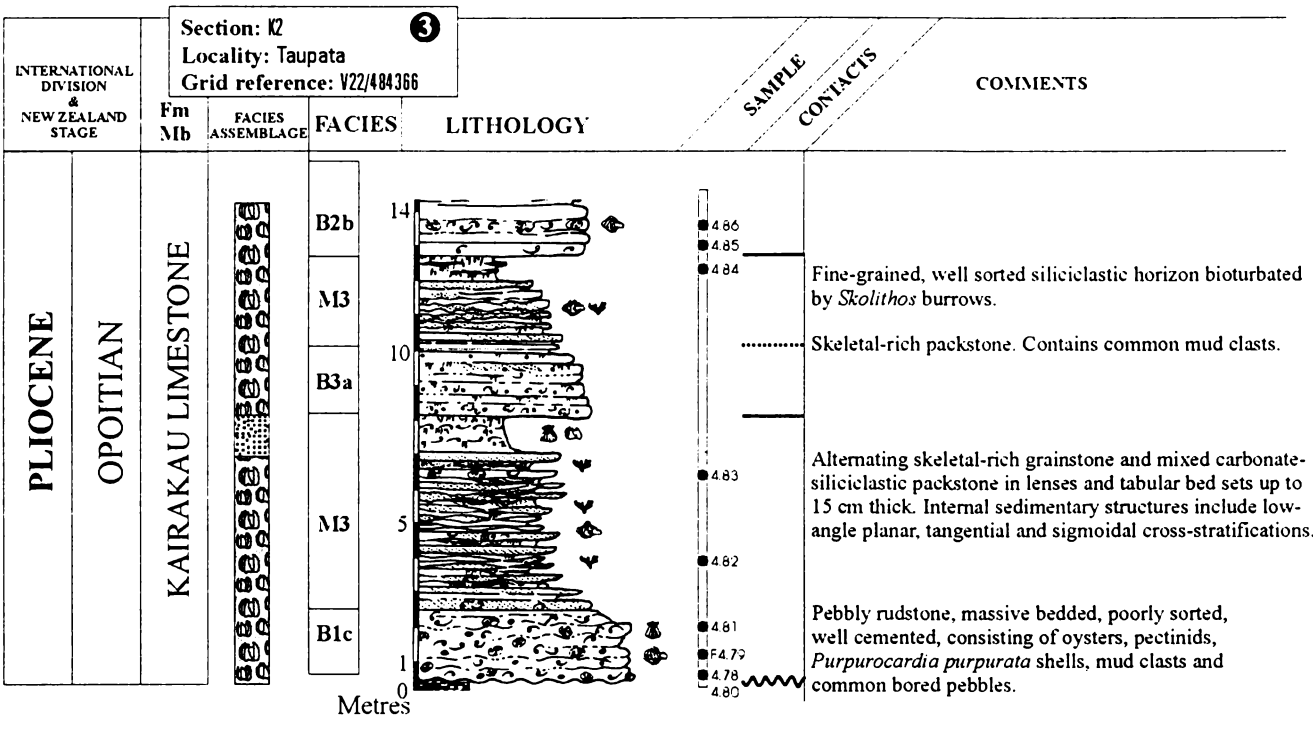
Section: K2
Locality: Taupata
Grid reference: V22/484366
3
INTERNATIONAL DIVISION & NEW ZEALAND STAGE
PLIOCENE
OPOITIAN
Fm
Mb
KAIRAKAU LIMESTONE
FACIES ASSEMBLAGE
FACIES
B2b
M3
B3a
M3
B1c
LITHOLOGY
14
10
5
1
0
Metres
SAMPLE
CONTACTS
4.86
4.85
4.84
4.83
4.82
4.81
F4.79
4.78
4.80
COMMENTS
Fine-grained, well sorted siliciclastic horizon bioturbated by *Skolithos* burrows.
Skeletal-rich packstone. Contains common mud clasts.
Alternating skeletal-rich grainstone and mixed carbonate-siliciclastic packstone in lenses and tabular bed sets up to 15 cm thick. Internal sedimentary structures include low-angle planar, tangential and sigmoidal cross-stratifications.
Pebbly rudstone, massive bedded, poorly sorted, well cemented, consisting of oysters, pectinids, *Purpurocardia purpurata* shells, mud clasts and common bored pebbles.

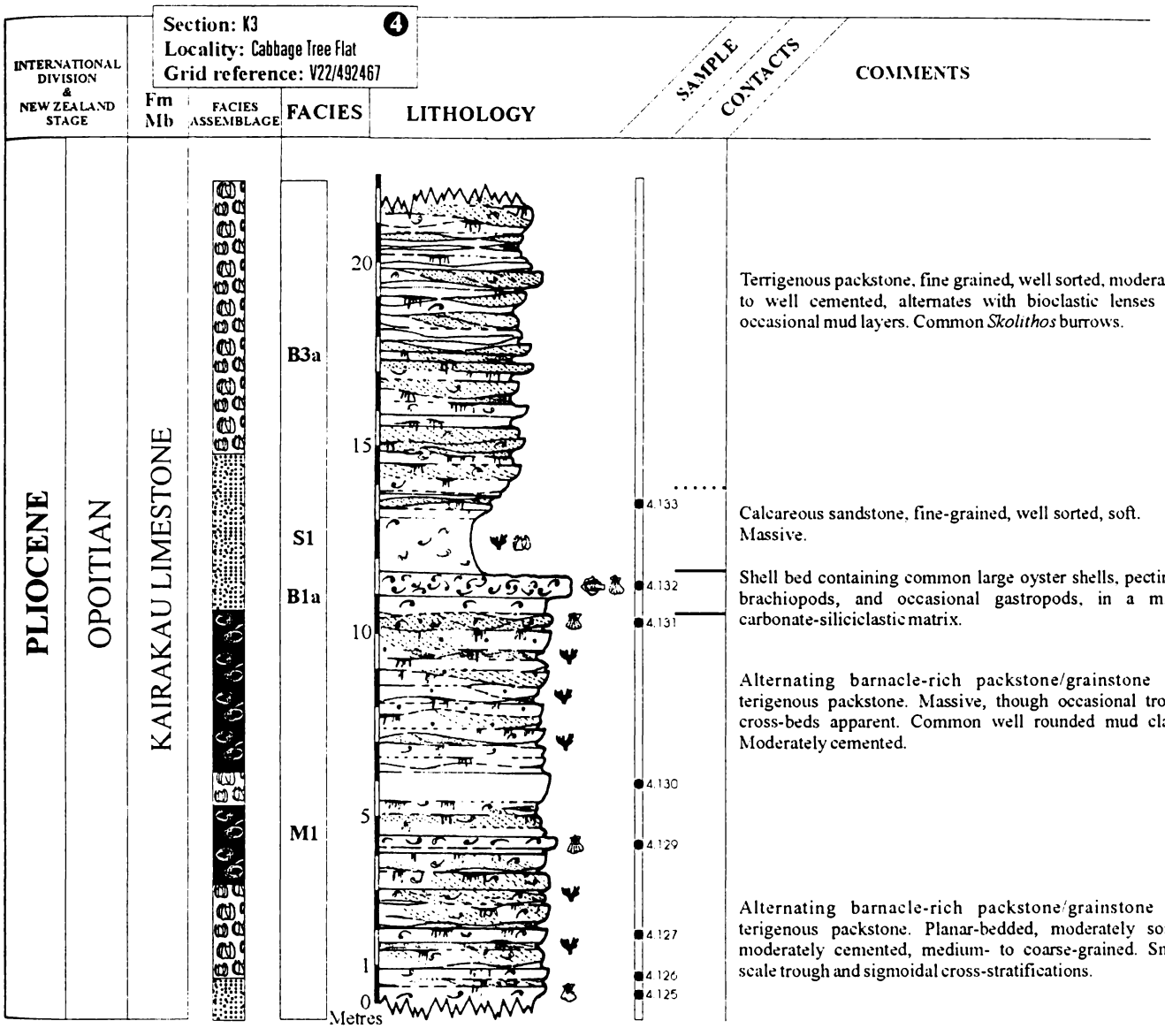
Section: K3
Locality: Cabbage Tree Flat
Grid reference: V22/492467
4
INTERNATIONAL DIVISION & NEW ZEALAND STAGE
Fm
Mb
FACIES ASSEMBLAGE
FACIES
LITHOLOGY
SAMPLE
CONTACTS
COMMENTS
PLIOCENE
OPOITIAN
KAIRAKAU LIMESTONE
B3a
S1
B1a
M1
20
15
10
5
1
0
Metres
4.133
4.132
4.131
4.130
4.129
4.127
4.126
4.125
Terrigenous packstone, fine grained, well sorted, moderately to well cemented, alternates with bioclastic lenses and occasional mud layers. Common *Skolithos* burrows.
Calcareous sandstone, fine-grained, well sorted, soft. Massive.
Shell bed containing common large oyster shells, pectinids, brachiopods, and occasional gastropods, in a mixed carbonate-siliciclastic matrix.
Alternating barnacle-rich packstone/grainstone and terigenous packstone. Massive, though occasional trough cross-beds apparent. Common well rounded mud clasts. Moderately cemented.
Alternating barnacle-rich packstone/grainstone and terigenous packstone. Planar-bedded, moderately sorted, moderately cemented, medium- to coarse-grained. Small-scale trough and sigmoidal cross-stratifications.

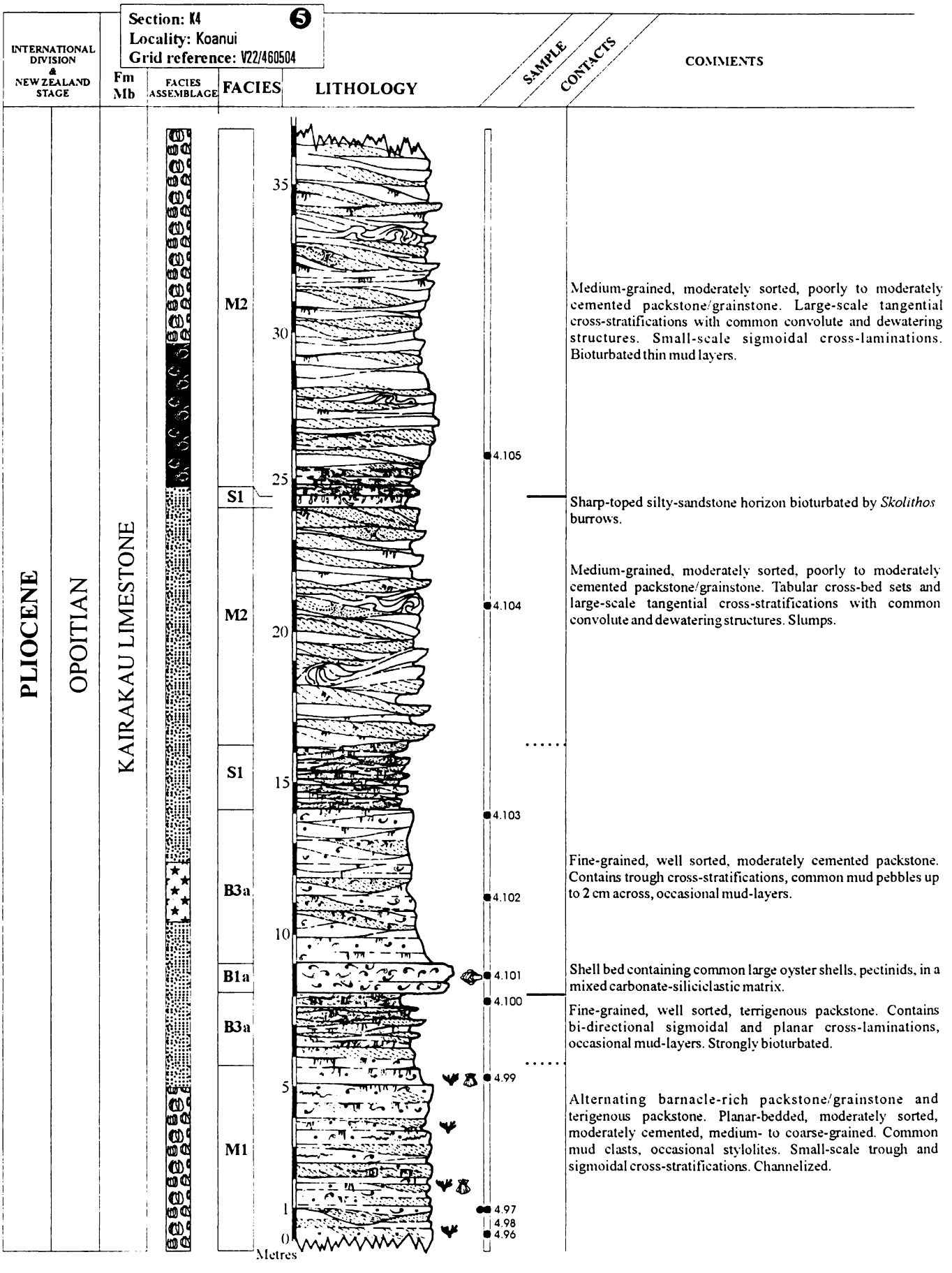
Section: K4
5
Locality: Koanui
Grid reference: V22/460504
INTERNATIONAL DIVISION & NEW ZEALAND STAGE
Fm Mb
FACIES ASSEMBLAGE
FACIES
LITHOLOGY
SAMPLE
CONTACTS
COMMENTS
PLIOCENE
OPOITIAN
KAIRAKAU LIMESTONE
M2
S1
M2
S1
B3a
B1a
B3a
M1
35
30
25
20
15
10
5
1
0
Metres
4.105
4.104
4.103
4.102
4.101
4.100
4.99
4.97
4.98
4.96
Medium-grained, moderately sorted, poorly to moderately cemented packstone/grainstone. Large-scale tangential cross-stratifications with common convolute and dewatering structures. Small-scale sigmoidal cross-laminations. Bioturbated thin mud layers.
Sharp-toped silty-sandstone horizon bioturbated by *Skolithos* burrows.
Medium-grained, moderately sorted, poorly to moderately cemented packstone/grainstone. Tabular cross-bed sets and large-scale tangential cross-stratifications with common convolute and dewatering structures. Slumps.
Fine-grained, well sorted, moderately cemented packstone. Contains trough cross-stratifications, common mud pebbles up to 2 cm across, occasional mud-layers.
Shell bed containing common large oyster shells, pectinids, in a mixed carbonate-siliciclastic matrix.
Fine-grained, well sorted, terrigenous packstone. Contains bi-directional sigmoidal and planar cross-laminations, occasional mud-layers. Strongly bioturbated.
Alternating barnacle-rich packstone/grainstone and terigenous packstone. Planar-bedded, moderately sorted, moderately cemented, medium- to coarse-grained. Common mud clasts, occasional stylolites. Small-scale trough and sigmoidal cross-stratifications. Channelized.

Section: K5 ❼
Locality: Mont Kahuranaki
Grid reference: V22/423515

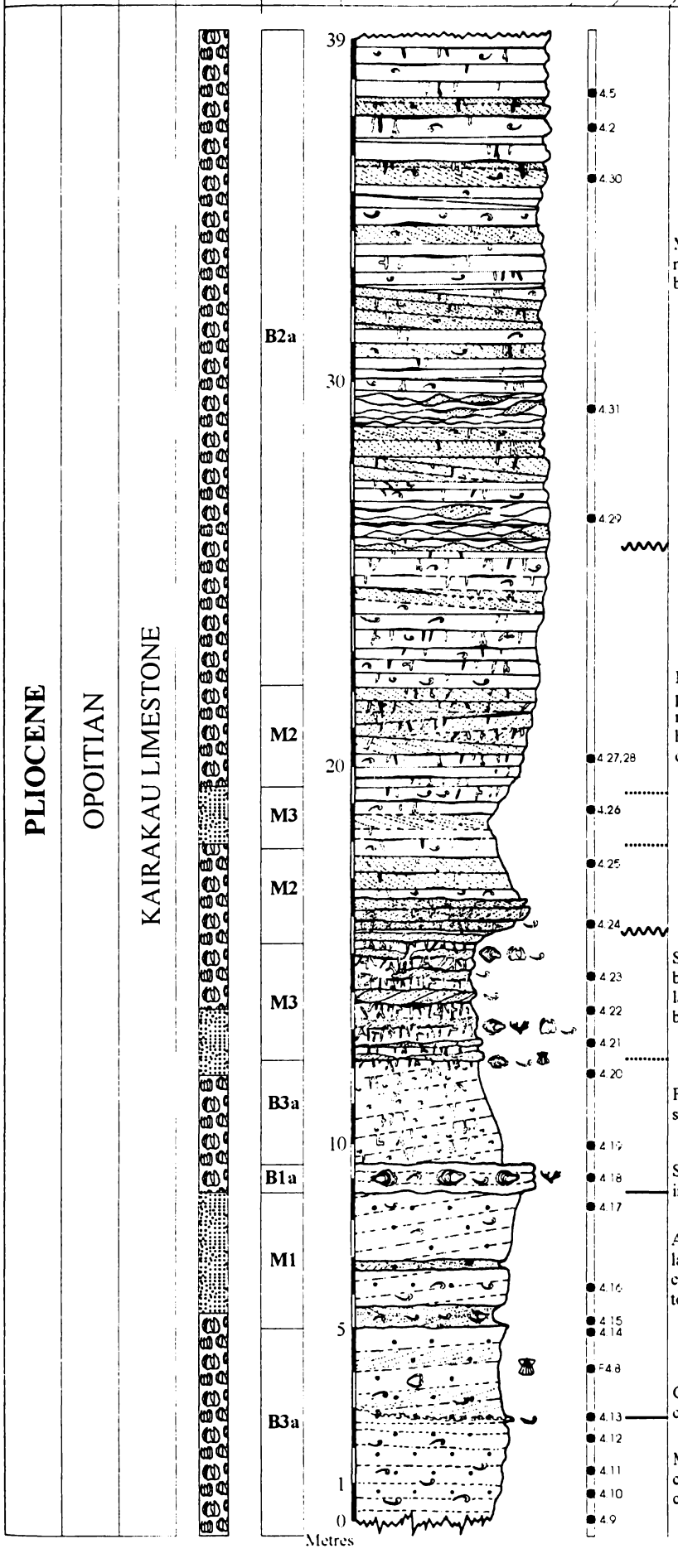

Medium- to coarse-grained, poorly to moderately sorted, moderately cemented grainstone. Large-scale tabular cross-bed sets that display internal trough cross-stratifications.

Medium-grained, moderately sorted, moderately cemented packstone alternates with coarse-grained, poorly sorted, moderately to well cemented grainstone. Oblique and horizontal tabular bed sets that display internal tangential cross-stratifications.

Same facies as below that alternates with medium-grained bioclastic lenses. Smale-scale sigmoidal and planar cross-laminations. Strongly bioturbated towards the top by *Skolithos* burrows.

Fine-grained, well sorted, poorly cemented calcareous sandstone, strongly bioturbated.

Shell bed containing common large oyster shells, pectinids, in a mixed carbonate-siliciclastic matrix.

Alternating fine-grained, well sorted, planar cross-laminated layers, and medium-grained, moderately sorted, moderately cemented packstone/grainstone in tabular cross-bed sets up to 0.4 m thick.

Condensed shell lineation consisting of oyster shell, mud clasts and detrital glauconite grains.

Medium-grained, moderately sorted, moderately to well cemented skeletal-rich grainstone. Massive. Contains mud clasts and scattered shells.

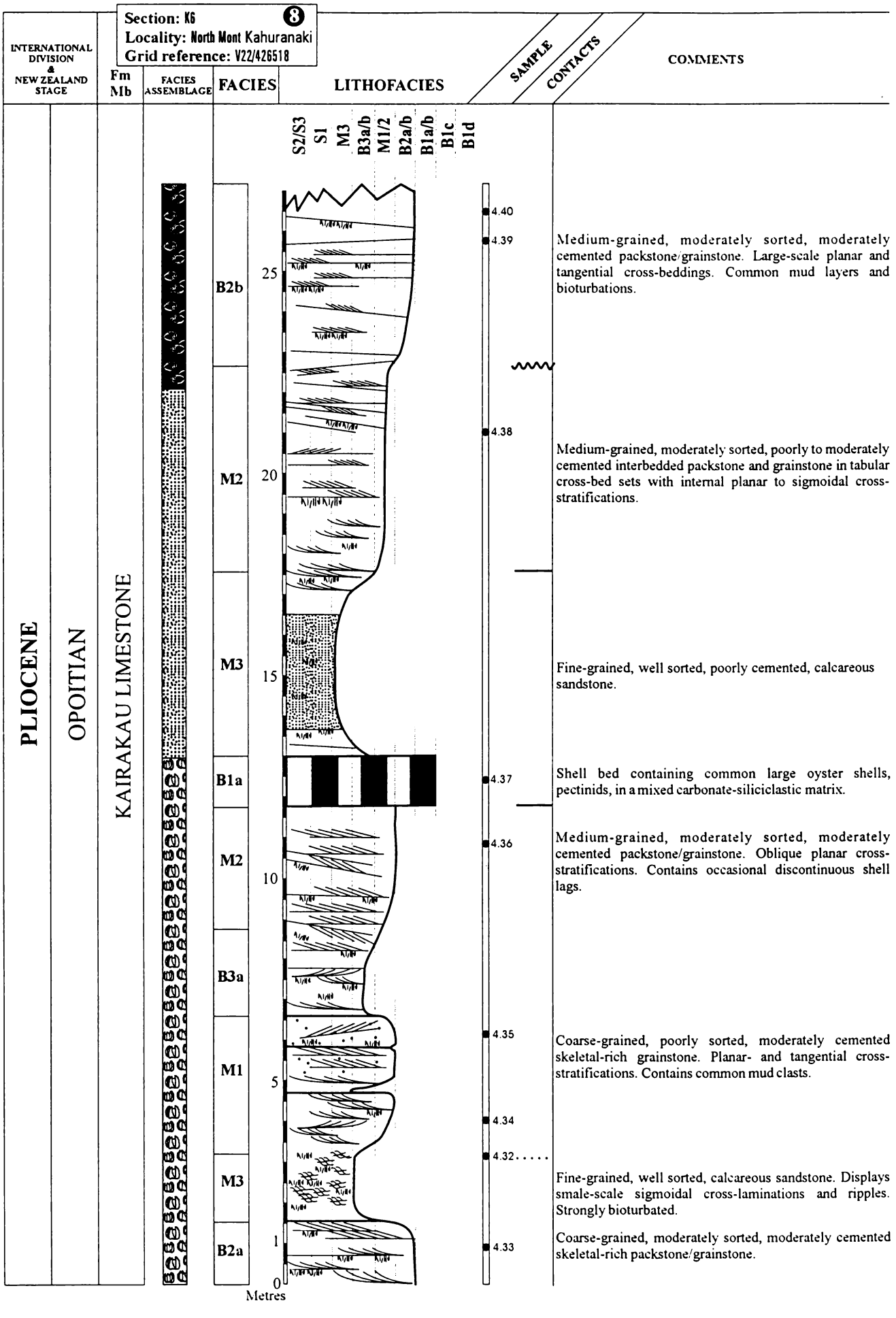
Section: K6
8
Locality: North Mont Kahuranaki
Grid reference: V22/426518
INTERNATIONAL DIVISION & NEW ZEALAND STAGE
Fm Mb
FACIES ASSEMBLAGE
FACIES
LITHOFACIES
SAMPLE
CONTACTS
COMMENTS
S2/S3
S1
M3
B3a/b
M1/2
B2a/b
B1a/b
B1c
B1d
PLIOCENE
OPOITIAN
KAIRAKAU LIMESTONE
B2b
M2
M3
B1a
M2
B3a
M1
M3
B2a
25
20
15
10
5
1
0
Metres
4.40
4.39
4.38
4.37
4.36
4.35
4.34
4.32
4.33
Medium-grained, moderately sorted, moderately cemented packstone/grainstone. Large-scale planar and tangential cross-beddings. Common mud layers and bioturbations.
Medium-grained, moderately sorted, poorly to moderately cemented interbedded packstone and grainstone in tabular cross-bed sets with internal planar to sigmoidal cross-stratifications.
Fine-grained, well sorted, poorly cemented, calcareous sandstone.
Shell bed containing common large oyster shells, pectinids, in a mixed carbonate-siliciclastic matrix.
Medium-grained, moderately sorted, moderately cemented packstone/grainstone. Oblique planar cross-stratifications. Contains occasional discontinuous shell lags.
Coarse-grained, poorly sorted, moderately cemented skeletal-rich grainstone. Planar- and tangential cross-stratifications. Contains common mud clasts.
Fine-grained, well sorted, calcareous sandstone. Displays smale-scale sigmoidal cross-laminations and ripples. Strongly bioturbated.
Coarse-grained, moderately sorted, moderately cemented skeletal-rich packstone/grainstone.

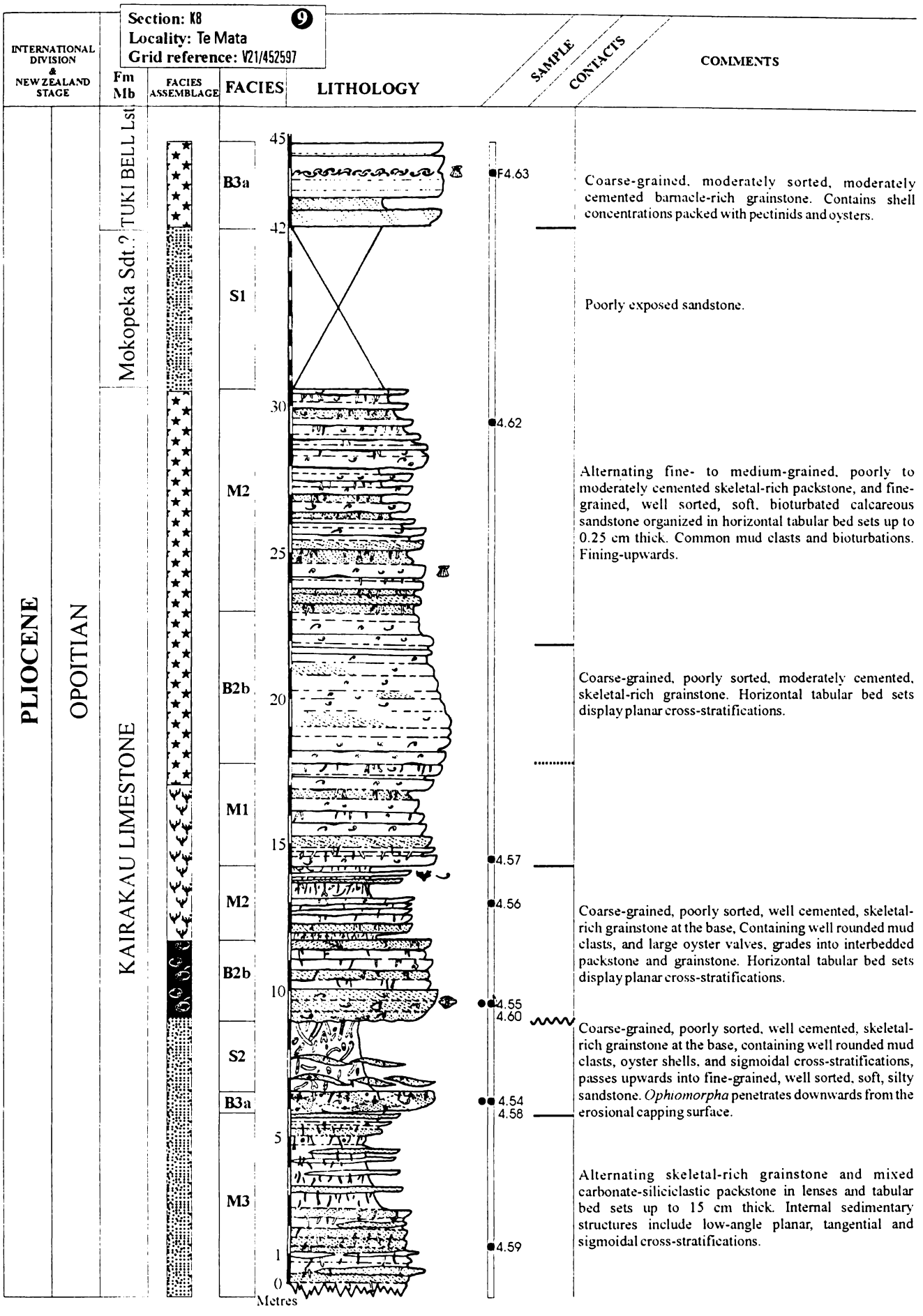
Section: K8
Locality: Te Mata
Grid reference: V21/452597
9
INTERNATIONAL DIVISION & NEW ZEALAND STAGE
PLIOCENE
OPOITIAN
Fm Mb
TUKI BELL Lst
Mokopeka Sdt. ?
KAIRAKAU LIMESTONE
FACIES ASSEMBLAGE
FACIES
LITHOLOGY
SAMPLE
CONTACTS
COMMENTS
B3a
S1
M2
B2b
M1
M2
B2b
S2
B3a
M3
45
42
30
25
20
15
10
5
1
0
Metres
F4.63
4.62
4.57
4.56
4.55
4.60
4.54
4.58
4.59
Coarse-grained, moderately sorted, moderately cemented barnacle-rich grainstone. Contains shell concentrations packed with pectinids and oysters.
Poorly exposed sandstone.
Alternating fine- to medium-grained, poorly to moderately cemented skeletal-rich packstone, and fine-grained, well sorted, soft, bioturbated calcareous sandstone organized in horizontal tabular bed sets up to 0.25 cm thick. Common mud clasts and bioturbations. Fining-upwards.
Coarse-grained, poorly sorted, moderately cemented, skeletal-rich grainstone. Horizontal tabular bed sets display planar cross-stratifications.
Coarse-grained, poorly sorted, well cemented, skeletal-rich grainstone at the base, Containing well rounded mud clasts, and large oyster valves, grades into interbedded packstone and grainstone. Horizontal tabular bed sets display planar cross-stratifications.
Coarse-grained, poorly sorted, well cemented, skeletal-rich grainstone at the base, containing well rounded mud clasts, oyster shells, and sigmoidal cross-stratifications, passes upwards into fine-grained, well sorted, soft, silty sandstone. *Ophiomorpha* penetrates downwards from the erosional capping surface.
Alternating skeletal-rich grainstone and mixed carbonate-siliciclastic packstone in lenses and tabular bed sets up to 15 cm thick. Internal sedimentary structures include low-angle planar, tangential and sigmoidal cross-stratifications.

Section: A2a ⑨
Locality: Te Mata Peak
Grid reference: V22/451602

INTERNATIONAL DIVISION & NEW ZEALAND STAGE	Fm Mb	FACIES ASSEMBLAGE	FACIES	LITHOLOGY	SAMPLE	CONTACTS	COMMENTS
PLIOCENE / WAIPIPIAN / AWAPAPA LIMESTONE				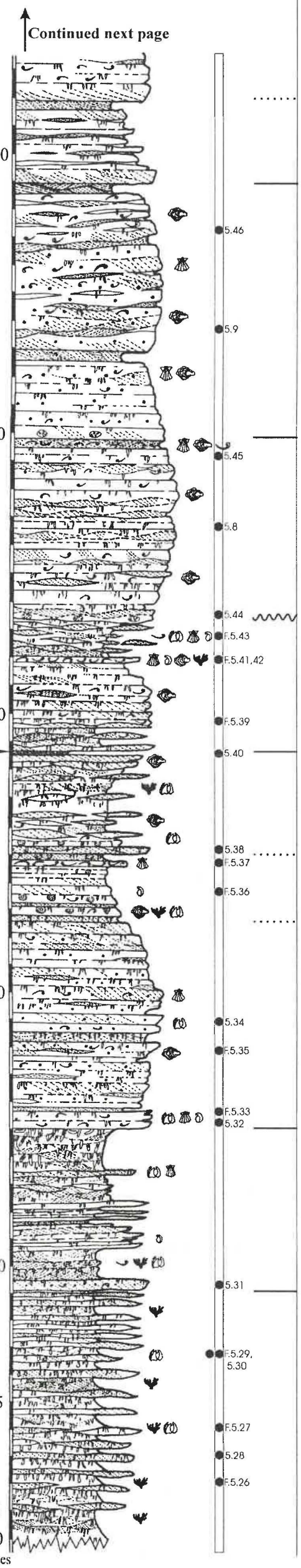			

Common soft terrigenous lenses. Sigmoidal and HCS-type sedimentary structures. Scattered macrofossils, common mud clasts.

Fining-upward from planar bedded, moderately to well cemented skeletal grainstone containing scattered bored pebbles, into moderately sorted, moderately cemented packstone.

Thin, 0.4 m thick, cross-laminated, poorly to moderately sorted, moderately to well cemented packstone.

Scattered sandy and muddy bored pebbles, towards the base. Horizontal tabular bed sets with internal trough and tangential cross-stratifications. Skeletal grainstone, moderately-sorted, moderately cemented.

Fining- then coarsening-upwards interval bounded below by a sharp contact, and above by an erosional surface. Moderately sorted, moderately cemented, interbedded skeletal packstone and grainstone. Contains about half way between the bounding contacts a thin shell lineation with oysters, pectinids (*Phialopecten marwicki*), brachiopods and bryozoans.

Coarsening-upwards, interbedded skeletal lenses and planar laminated terrigenous packstone. Moderately sorted, poorly to moderately cemented. Contains a thin tephra layer (10 cm), strongly bioturbated below a sharp surface.

Thin shell lineation packed with pectinid valves (*Phialopecten marwicki*) encrusted by barnacles.

Coarse skeletal material fills fish-feeding structures. Fining-upwards, well to moderately sorted, poorly to moderately cemented.

Horizontal continuous tabular bed sets consisting of planar to tangential cross-stratified, moderately sorted, moderately cemented, skeletal grainstone that contains common mud clasts, oyster and pectinid valves, common discontinuous terrigenous lenses, and *Skolithos*-type burrows.

Ophiomorpha burrows penetrate downwards into mixed carbonate-siliciclastic facies from a sharp surface.

Stacked coarsening- and thickening-upwards sequences comprising from bottom to top: (1) fine-grained, poorly cemented, intensively bioturbated, planar laminated calcareous sandstone; (2) interbedded mixed carbonate-siliciclastic, poorly cemented, planar and tangential cross-laminated packstone, and coarse-grained, moderately cemented, skeletal grainstone lenses; and (3) coarse-grained, well sorted, poorly to moderately cemented, horizontally-bedded sheets (up to 0.4m).

Sheet tops are usually simple bedding planes whose moderately consolidated nature may be related to firm grounds. Well-preserved delicate branching bryozoans in both fine-grained sandstones and coarser-grained sheets show evidence of reworking under low-energy conditions.

Section: A2b ⑨
Locality: Te Mata Peak
Grid reference: V22/451602

INTERNATIONAL DIVISION & NEW ZEALAND STAGE	Fm Mb	FACIES ASSEMBLAGE	FACIES	LITHOLOGY	SAMPLE	CONTACTS	COMMENTS
PLIOCENE / WAIPIPIAN / AWAPAPA LIMESTONE			S1				
			B2b	115	5.146		
			M2				Fining-upwards interbedded fossiliferous grainstone and terrigenous packstone. Contains numerous brachiopods and common oyster valves. Moderately sorted, moderately cemented.
			B2b		F5.143		
				110	5.145		
					5.142		
			M3				
			B1a				Strongly burrowed surface (*Ophiomorpha?*, *Skolithos*).
					5.56		
					5.25		Fining- then coarsening-upwards interval bounded below by a sharp contact, and above by an erosional surface. Moderately sorted, moderately cemented, interbedded skeletal packstone and grainstone. Common well rounded mud clasts and reworked tephra pebbles. Contains about half way between the bounding contacts a thin fine-grained, soft, terrigenous horizon.
			M2	100			
			M3		5.24		Fining-upwards interbedded grainstone and terrigenous packstone. Contains a thin pectinid shell lineation.
			M2				
			B1a	90			Shell bed consisting of tabular bed sets up to 1 m thick. Poorly sorted, moderately cemented.
					5.55		
					F.5.54		
			M2		5.21		Fining-upwards interbedded grainstone and terrigenous packstone.
					5.20		
			B1a	80			Shell bed packed with oysters and pectinids, bounded below by a ravinement surface. Massive bedded, occasional sigmoidal cross-stratifications in mixed skeletal-terrigenous lenses.
					5.53		
			M2		5.52		Fining-upwards interbedded grainstone and terrigenous packstone.
			B3a		5.51		Planar bedded skeletal packstone containing scattered clumps of oysters, especially towards the base. Moderately sorted, moderately cemented.
			M1		F.5.50		Bioturbated interbedded grainstone and packstone.
				70			
			B1a		5.14		Common mud clasts and mud pebbles, scattered clumps of oysters often bored and encrusted by bryozoans and serpulids. Sparsely packed towards the base grades into densely packed shell bed. Random orientation of shells, common convex upwards-orientated shells together with slightly abraded and unabraded valves, common whole shells suggest moderate post-mortem transportation.
					5.48		
					5.49		
			M3				Tangential and planar cross-stratified, poorly cemented, interbedded fine-grained terrigenous packstone and medium-grained skeletal packstone. Coarsens upwards into fossiliferous bed sheets, consisting of pectinids, oysters, bryozoans and mud clasts.
				60	5.47		Shell concentration (<0.5 m) packed with oyster valves.
			M2		5.12		Fining-upwards interval bounded above by a sharp contact. Horizontal bedded, with uncommon tangential cross-stratifications, moderately sorted, moderately cemented, mixed carbonate-siliciclastic facies. Contains well rounded mud pebbles up to 6 cm across, oyster valves and branching bryozoan colonies towards the top.
				55			

Metres

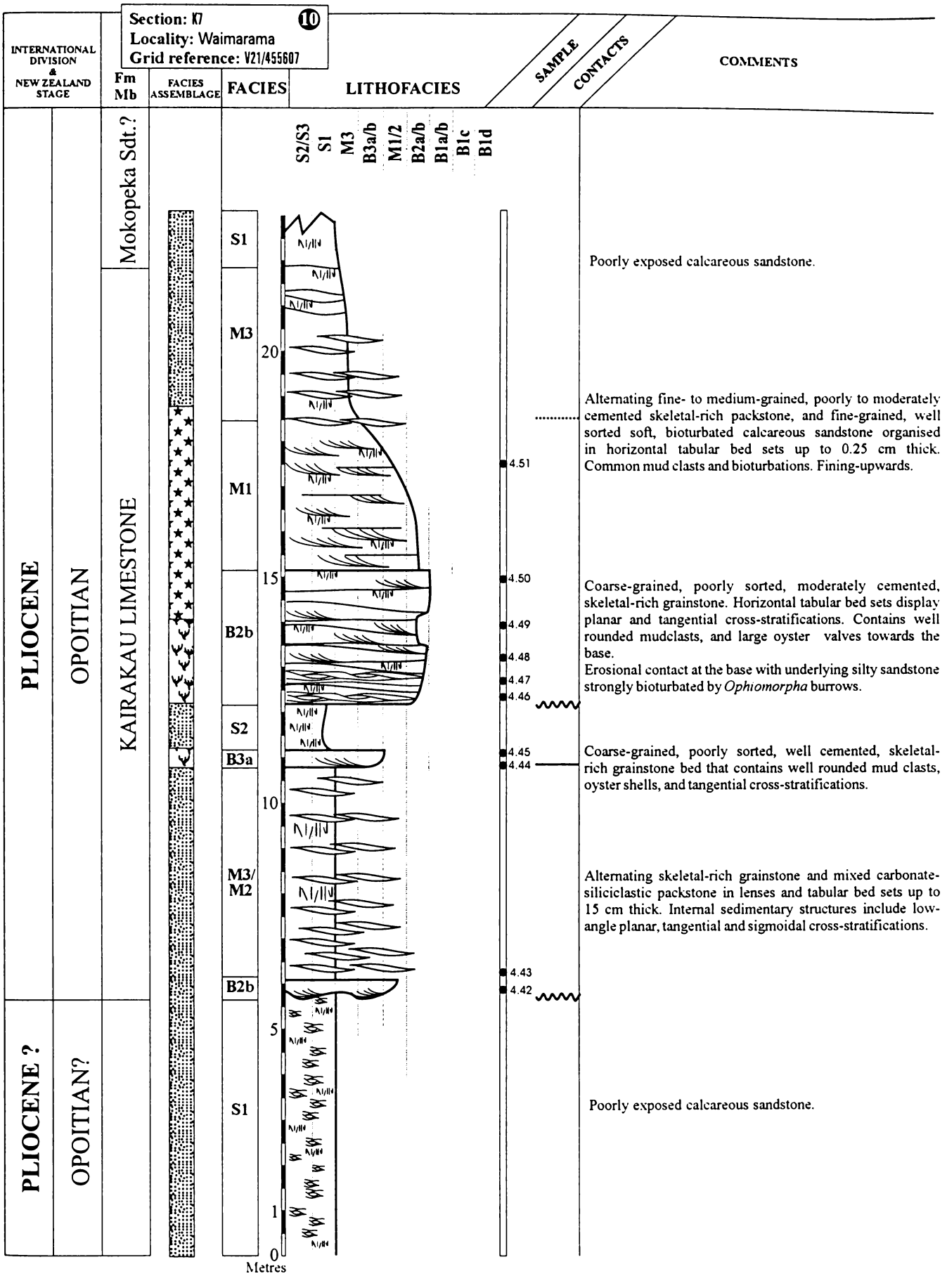
Section: K7
10
Locality: Waimarama
Grid reference: V21/455607
INTERNATIONAL DIVISION & NEW ZEALAND STAGE
Fm Mb
FACIES ASSEMBLAGE
FACIES
LITHOFACIES
SAMPLE
CONTACTS
COMMENTS
S2/S3
S1
M3
B3a/b
M1/2
B2a/b
B1a/b
B1c
B1d
PLIOCENE
OPOITIAN
Mokopeka Sdt.?
KAIRAKAU LIMESTONE
PLIOCENE ?
OPOITIAN?
S1
M3
M1
B2b
S2
B3a
M3/ M2
B2b
S1
20
15
10
5
1
0
Metres
4.51
4.50
4.49
4.48
4.47
4.46
4.45
4.44
4.43
4.42
Poorly exposed calcareous sandstone.
Alternating fine- to medium-grained, poorly to moderately cemented skeletal-rich packstone, and fine-grained, well sorted soft, bioturbated calcareous sandstone organised in horizontal tabular bed sets up to 0.25 cm thick. Common mud clasts and bioturbations. Fining-upwards.
Coarse-grained, poorly sorted, moderately cemented, skeletal-rich grainstone. Horizontal tabular bed sets display planar and tangential cross-stratifications. Contains well rounded mudclasts, and large oyster valves towards the base.
Erosional contact at the base with underlying silty sandstone strongly bioturbated by *Ophiomorpha* burrows.
Coarse-grained, poorly sorted, well cemented, skeletal-rich grainstone bed that contains well rounded mud clasts, oyster shells, and tangential cross-stratifications.
Alternating skeletal-rich grainstone and mixed carbonate-siliciclastic packstone in lenses and tabular bed sets up to 15 cm thick. Internal sedimentary structures include low-angle planar, tangential and sigmoidal cross-stratifications.
Poorly exposed calcareous sandstone.

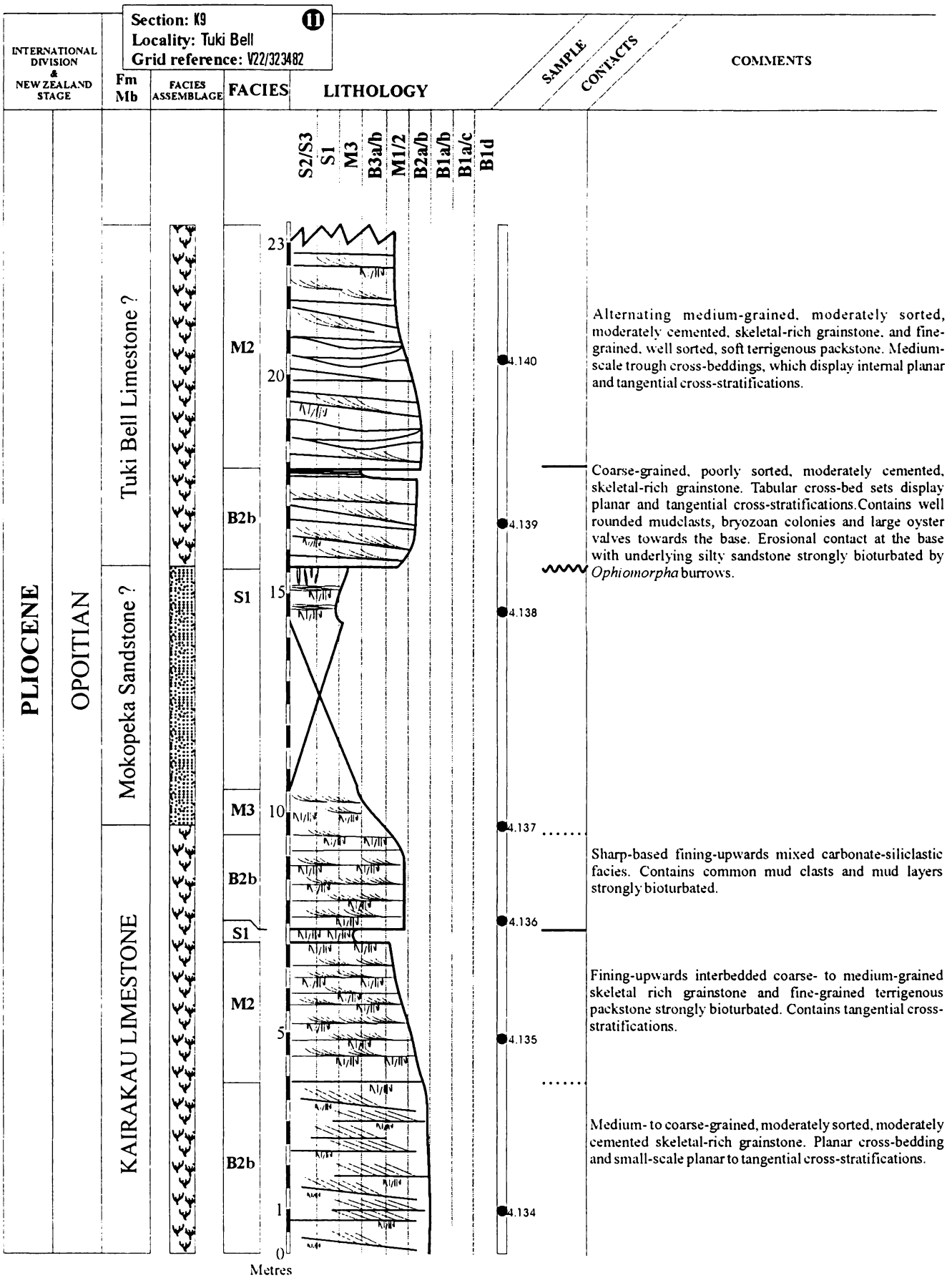
Section: K9
Locality: Tuki Bell
Grid reference: V22/323482
INTERNATIONAL DIVISION & NEW ZEALAND STAGE
Fm Mb
FACIES ASSEMBLAGE
FACIES
LITHOLOGY
SAMPLE
CONTACTS
COMMENTS
S2/S3
S1
M3
B3a/b
M1/2
B2a/b
B1a/b
B1a/c
B1d
PLIOCENE
OPOITIAN
Tuki Bell Limestone ?
Mokopeka Sandstone ?
KAIRAKAU LIMESTONE
M2
B2b
S1
M3
B2b
S1
M2
B2b
23
20
15
10
5
1
0
Metres
4.140
4.139
4.138
4.137
4.136
4.135
4.134
Alternating medium-grained, moderately sorted, moderately cemented, skeletal-rich grainstone, and fine-grained, well sorted, soft terrigenous packstone. Medium-scale trough cross-beddings, which display internal planar and tangential cross-stratifications.
Coarse-grained, poorly sorted, moderately cemented, skeletal-rich grainstone. Tabular cross-bed sets display planar and tangential cross-stratifications.Contains well rounded mudclasts, bryozoan colonies and large oyster valves towards the base. Erosional contact at the base with underlying silty sandstone strongly bioturbated by *Ophiomorpha* burrows.
Sharp-based fining-upwards mixed carbonate-siliclastic facies. Contains common mud clasts and mud layers strongly bioturbated.
Fining-upwards interbedded coarse- to medium-grained skeletal rich grainstone and fine-grained terrigenous packstone strongly bioturbated. Contains tangential cross-stratifications.
Medium- to coarse-grained, moderately sorted, moderately cemented skeletal-rich grainstone. Planar cross-bedding and small-scale planar to tangential cross-stratifications.

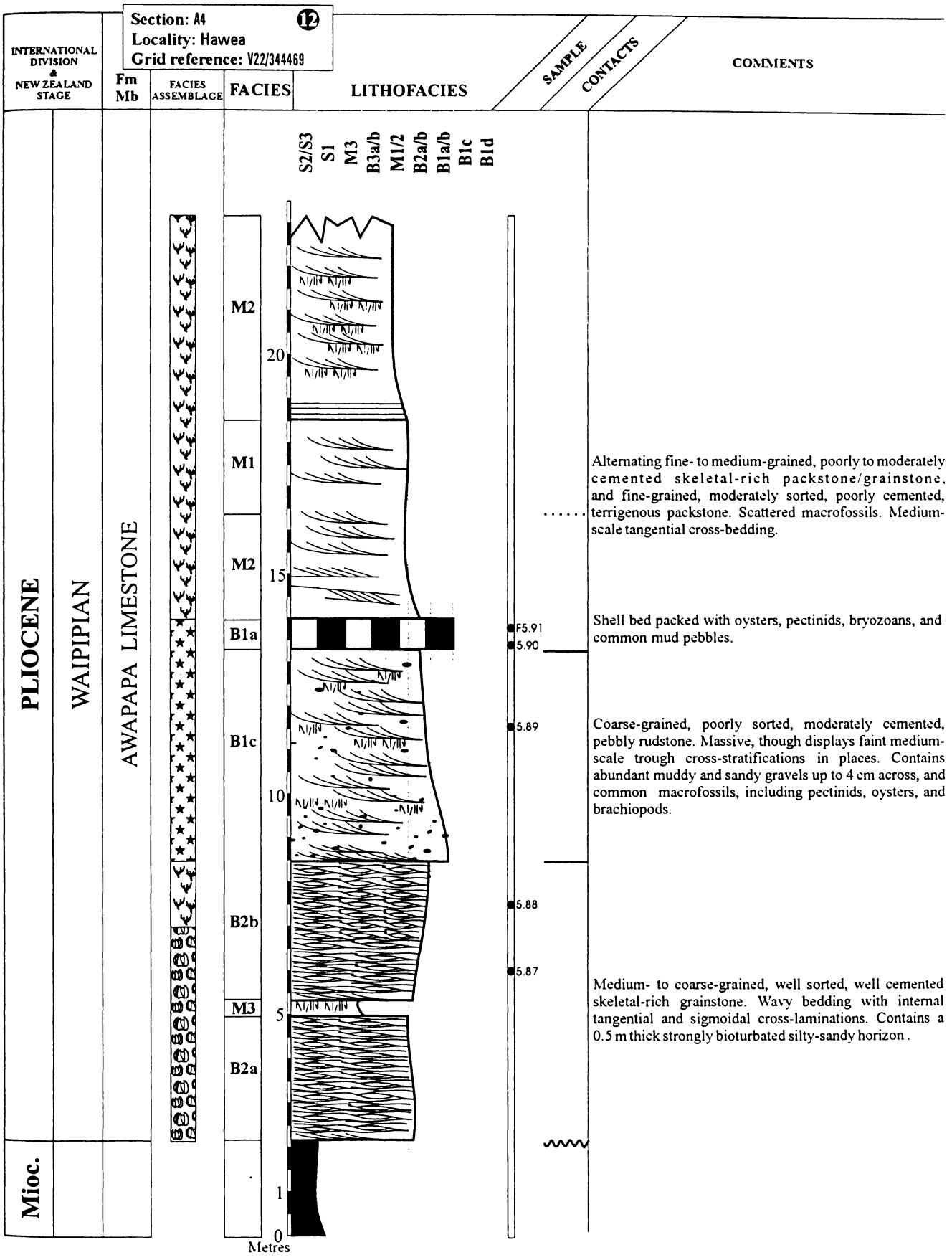
Section: A4
Locality: Hawea
Grid reference: V22/344469
INTERNATIONAL DIVISION & NEW ZEALAND STAGE
Fm Mb
FACIES ASSEMBLAGE
FACIES
LITHOFACIES
SAMPLE
CONTACTS
COMMENTS
S2/S3
S1
M3
B3a/b
M1/2
B2a/b
B1a/b
B1c
B1d
PLIOCENE
WAIPIPIAN
AWAPAPA LIMESTONE
Mioc.
M2
M1
M2
B1a
B1c
B2b
M3
B2a
20
15
10
5
1
0
Metres
F5.91
5.90
5.89
5.88
5.87
Alternating fine- to medium-grained, poorly to moderately cemented skeletal-rich packstone/grainstone, and fine-grained, moderately sorted, poorly cemented, terrigenous packstone. Scattered macrofossils. Medium-scale tangential cross-bedding.
Shell bed packed with oysters, pectinids, bryozoans, and common mud pebbles.
Coarse-grained, poorly sorted, moderately cemented, pebbly rudstone. Massive, though displays faint medium-scale trough cross-stratifications in places. Contains abundant muddy and sandy gravels up to 4 cm across, and common macrofossils, including pectinids, oysters, and brachiopods.
Medium- to coarse-grained, well sorted, well cemented skeletal-rich grainstone. Wavy bedding with internal tangential and sigmoidal cross-laminations. Contains a 0.5 m thick strongly bioturbated silty-sandy horizon.

Section: A5 (13)
Locality: River Bank
Grid reference: V22/332482

INTERNATIONAL DIVISION & NEW ZEALAND STAGE	Fm / Mb	FACIES ASSEMBLAGE	FACIES	SAMPLE	CONTACTS	COMMENTS
PLIOCENE	WAIPIPIAN	AWAPAPA LIMESTONE	M3			Alternating fine- to medium-grained, poorly to moderately cemented skeletal-rich packstone, and fine-grained, well sorted soft, bioturbated calcareous sandstone. Tangential cross-stratifications. Common bioturbations. Fining-upwards.
			B1a		?	
			S1			Poorly exposed calcareous sandstone.
			M3			Interbedded terrigenous packstone and bioclastic lenses. Fining-upwards trend. Moderately to poorly cemented. Strongly bioturbated.
			M1	5.84		
			B1a	F5.85 5.86 5.83		Alternating coarse-grained, poorly sorted, moderately to well cemented skeletal-rich rudstone and medium-grained, moderately sorted, moderately cemented skeletal packstone/ grainstone. Sedimentary structures include medium- to large-scale low-angle planar, tangential and sigmoidal cross-stratifications. Shelly beds contain abundant reworked shell material (well abraded and polished oyster valves) and mud clasts.
			M1	5.81 F5.82 F5.80		Shelly lags commonly concentrate into up to 10 m large channels.
			B1a	5.79a 5.79b F.5.78		Skeletal and pebbly rudstone, poorly sorted, moderately to well cemented. Displays large-scale tangential cross-stratifications, and common dewatering structures.
			B3a	F.5.77 5.76		Alternating medium- to coarse-grained, moderately sorted. Moderately cemented bioclastic lenses, and fine-grained, well sorted, poorly cemented terrigenous packstone containing common mud layers, strongly bioturbated.
			B3a	5.74		
			M3	F5.73		Fining-upwards mixed carbonate-siliciclastic facies, medium grained, moderately cemented. Exhibits medium-scale tangential cross-stratifications.
			M2	5.75		

S2/S3 S1 M3 B3a/b M1/2 B2a/b B1a/b B1c B1d

70 60 50 40 30 20 10 5 1 0

Metres

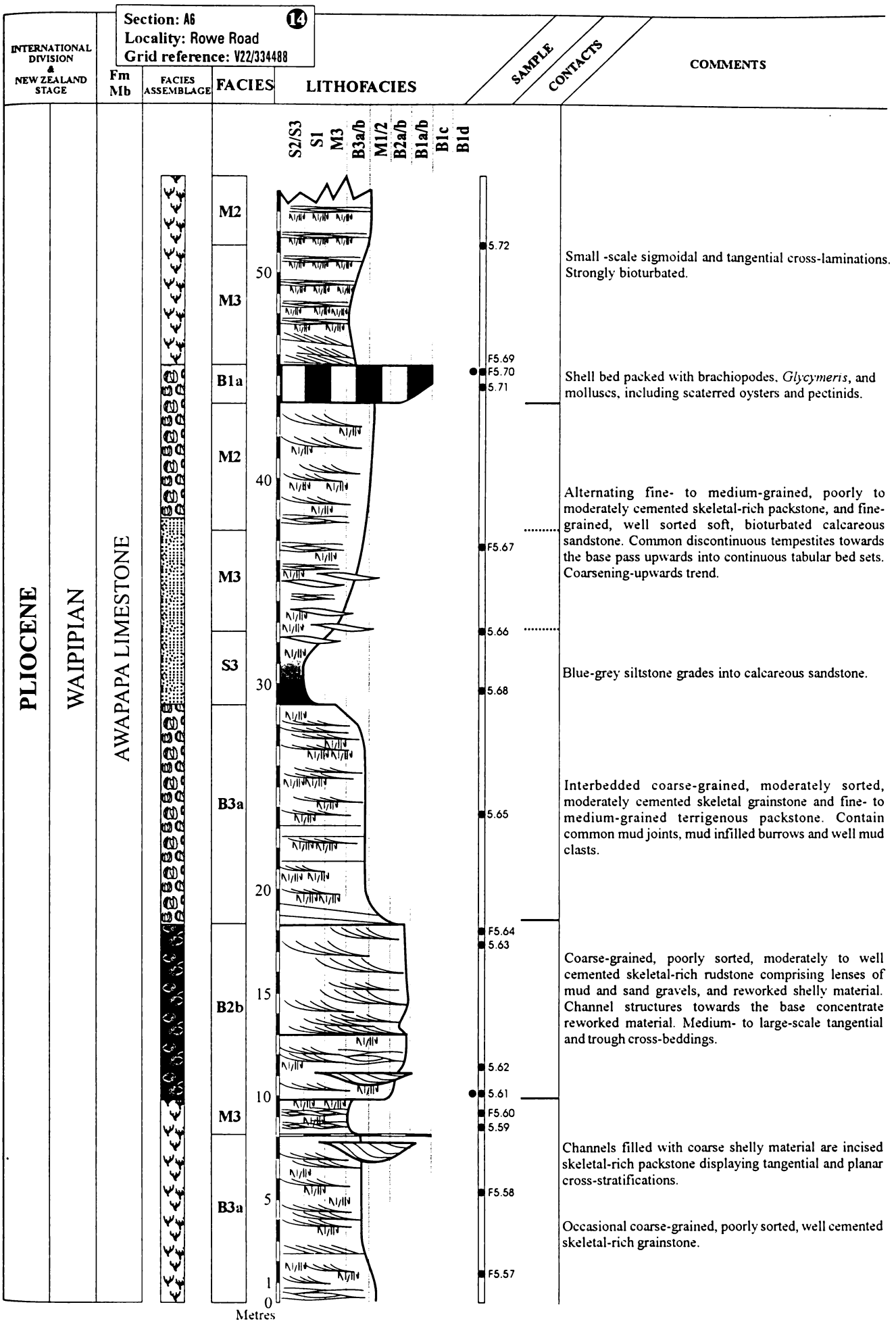
Section: A6
Locality: Rowe Road
Grid reference: V22/334488
14
INTERNATIONAL DIVISION & NEW ZEALAND STAGE
Fm Mb
FACIES ASSEMBLAGE
FACIES
LITHOFACIES
SAMPLE
CONTACTS
COMMENTS
S2/S3
S1
M3
B3a/b
M1/2
B2a/b
B1a/b
B1c
B1d
PLIOCENE
WAIPIPIAN
AWAPAPA LIMESTONE
M2
M3
B1a
M2
M3
S3
B3a
B2b
M3
B3a
50
40
30
20
15
10
5
1
0
Metres
F5.72
F5.69
F5.70
F5.71
F5.67
5.66
5.68
5.65
F5.64
5.63
5.62
5.61
F5.60
5.59
F5.58
F5.57
Small -scale sigmoidal and tangential cross-laminations. Strongly bioturbated.
Shell bed packed with brachiopodes, *Glycymeris*, and molluscs, including scaterred oysters and pectinids.
Alternating fine- to medium-grained, poorly to moderately cemented skeletal-rich packstone, and fine-grained, well sorted soft, bioturbated calcareous sandstone. Common discontinuous tempestites towards the base pass upwards into continuous tabular bed sets. Coarsening-upwards trend.
Blue-grey siltstone grades into calcareous sandstone.
Interbedded coarse-grained, moderately sorted, moderately cemented skeletal grainstone and fine- to medium-grained terrigenous packstone. Contain common mud joints, mud infilled burrows and well mud clasts.
Coarse-grained, poorly sorted, moderately to well cemented skeletal-rich rudstone comprising lenses of mud and sand gravels, and reworked shelly material. Channel structures towards the base concentrate reworked material. Medium- to large-scale tangential and trough cross-beddings.
Channels filled with coarse shelly material are incised skeletal-rich packstone displaying tangential and planar cross-stratifications.
Occasional coarse-grained, poorly sorted, well cemented skeletal-rich grainstone.

Section: K11/A1 (15)
Locality: Pukekura
Grid reference: V22/292475

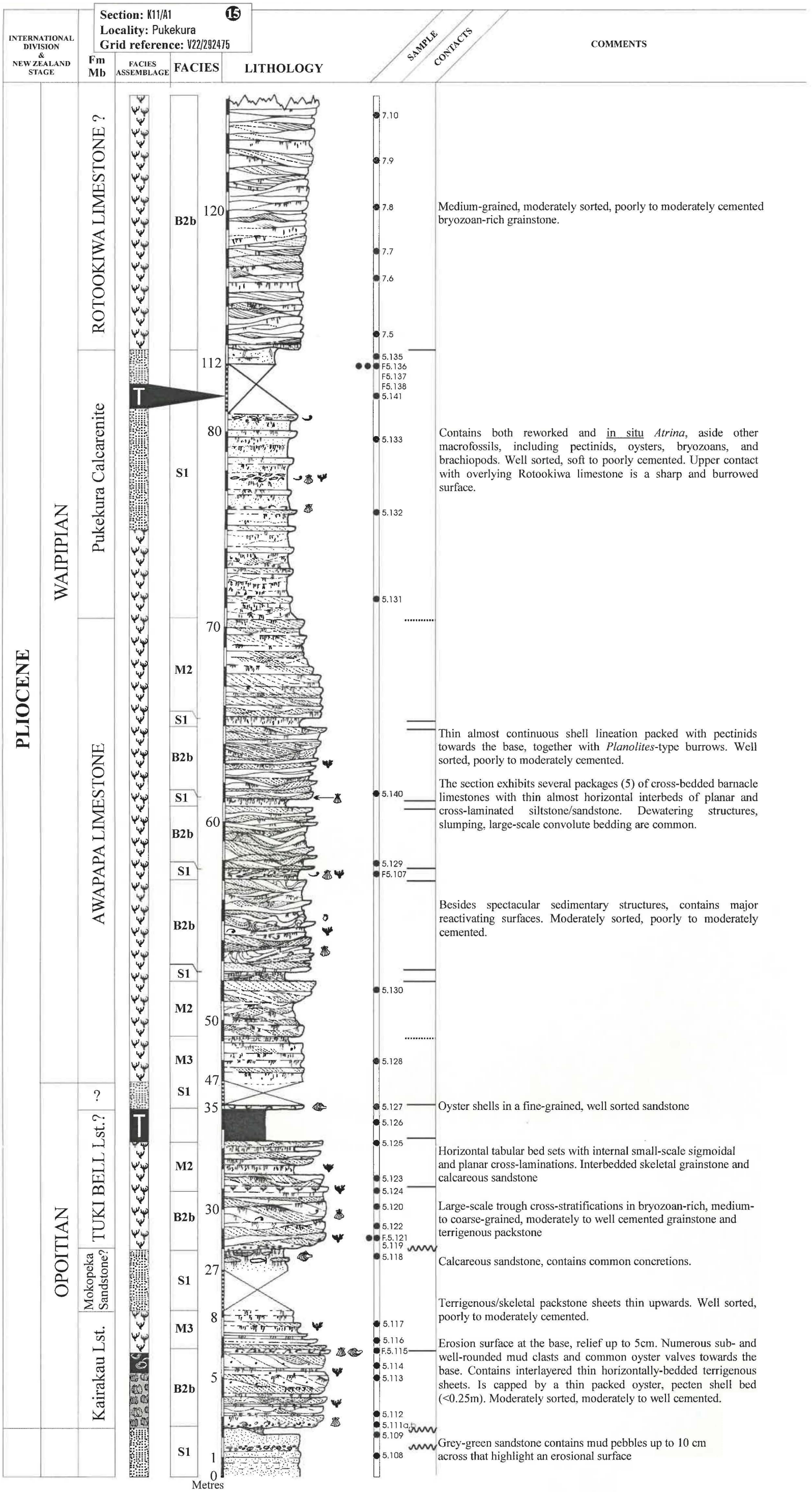

Section: A3 (16)
Locality: Makara
Grid reference: V22/318405

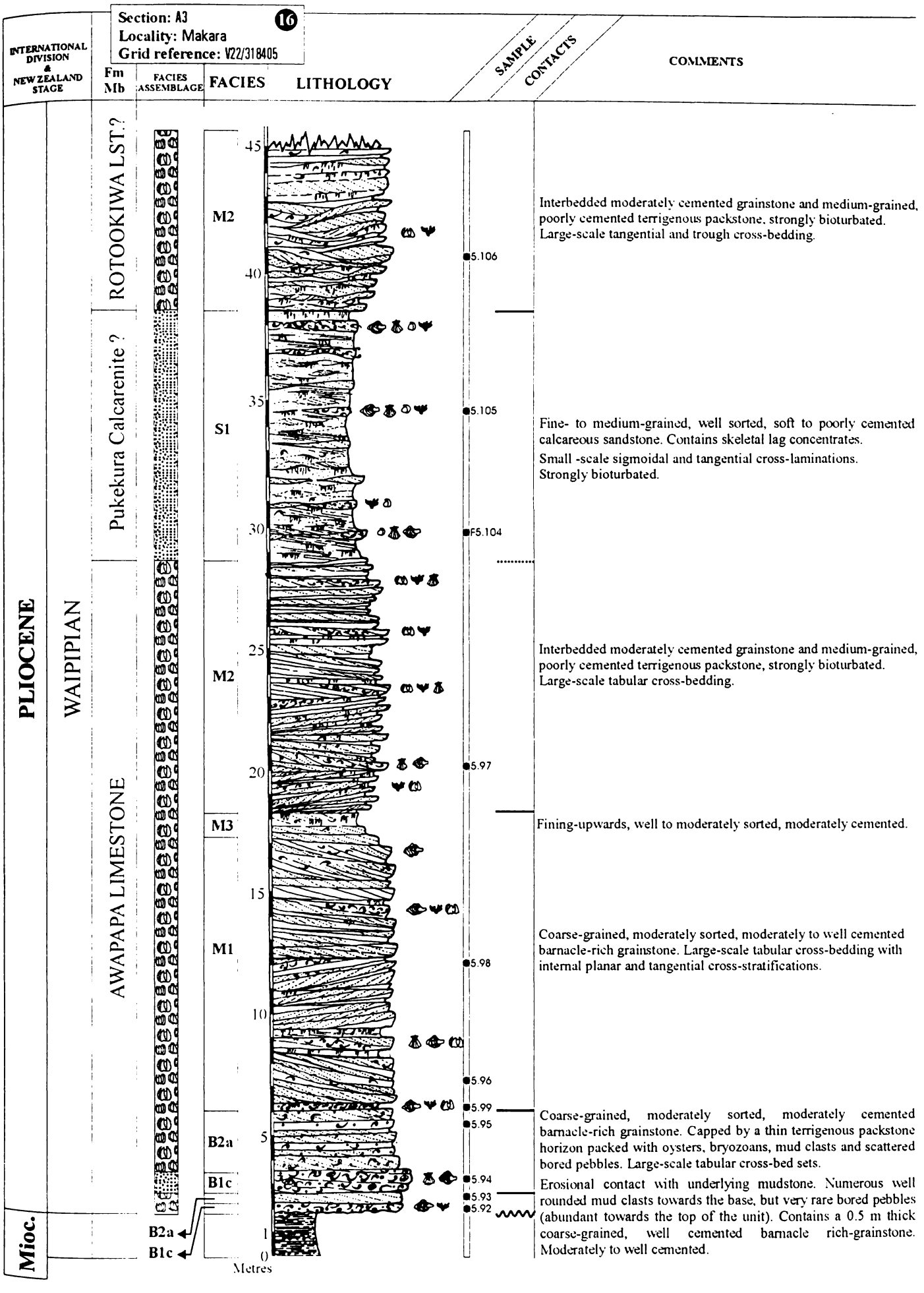

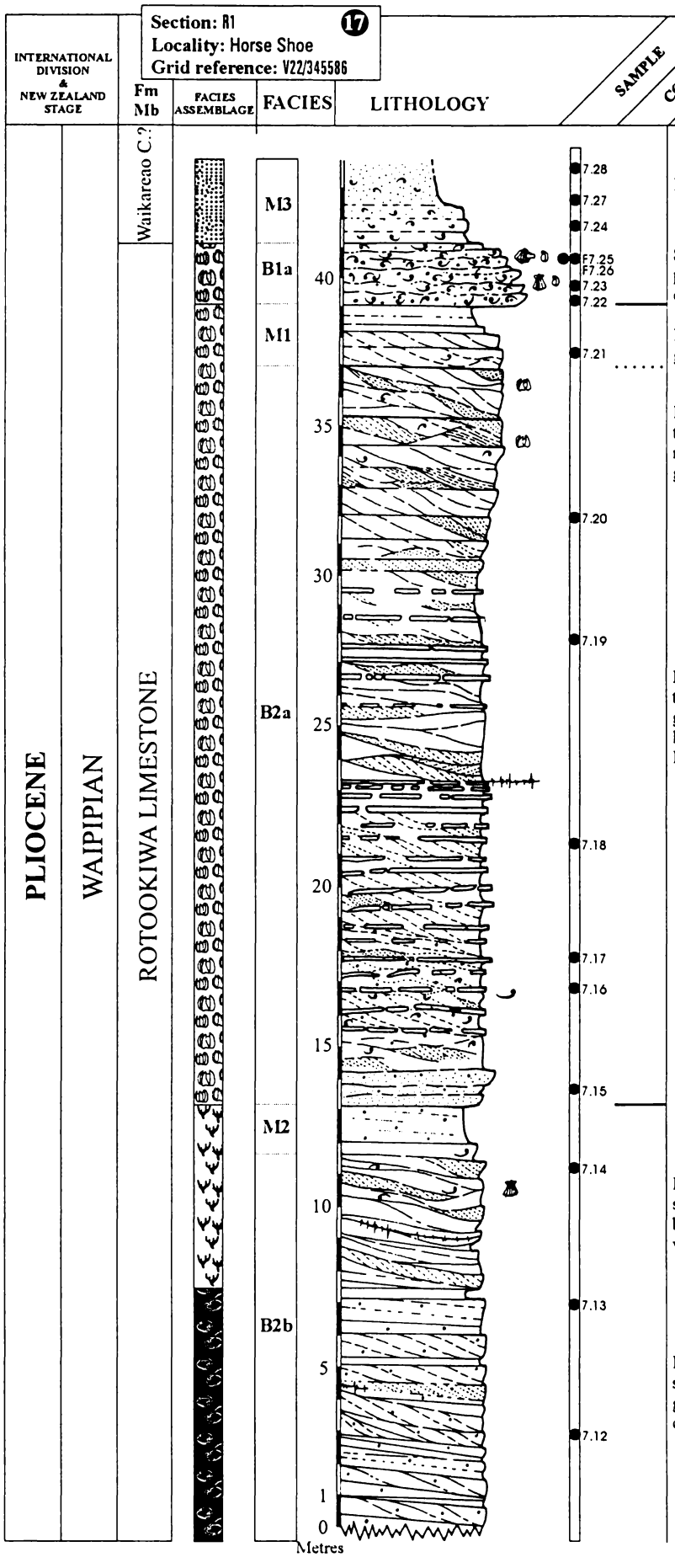
Section: R1
Locality: Horse Shoe
Grid reference: V22/345586
17
INTERNATIONAL DIVISION & NEW ZEALAND STAGE
Fm
Mb
FACIES ASSEMBLAGE
FACIES
LITHOLOGY
SAMPLE
CONTACTS
COMMENTS
PLIOCENE
WAIPIPIAN
Waikareao C.?
ROTOOKIWA LIMESTONE
M3
B1a
M1
B2a
M2
B2b
40
35
30
25
20
15
10
5
1
0
Metres
7.28
7.27
7.24
F7.25
F7.26
7.23
7.22
7.21
7.20
7.19
7.18
7.17
7.16
7.15
7.14
7.13
7.12
Fine-grained, well sorted, soft, fossiliferous sandstone.
Sharp-based shell bed consisting of oysters, scattered pectinids, common brachiopods, and mud clasts in a well cemented fine-grained mixed carbonate-siliciclastic matrix.
Fining-upwards from coarse barnacle grainstone to medium-grained, soft, planar bedded barnacle grainstone/packstone.
Horizontal tabular bed sets up to 2 m thick, comprising internal trough and tangential cross-stratifications. Coarse, moderately sorted, soft to poorly cemented barnacle grainstone.
Fine-grained, well sorted, soft terrigenous/skeletal grainstone towards the base grading rapidly into a barnacle-rich grainstone. Thin interbedded discontinuous crystalline limestone sheets, very hard with occasional stylolites. Interbeds are moderately sorted, poorly to moderately
Medium- to large-scale trough cross-bedding. Occasional stylolites. Coarse, moderately sorted, soft to poorly cemented barnacle grainstone, containing scattered oyster and pectinid valves, and mud pebbles.
Low-angle planar and tangential cross-bed sets. Occasional stylolites. Interbedded terrigenous packstone and barnacle grainstone sheets (up to 0.2 m), containing common mud clasts. Moderately sorted, soft to poorly cemented.

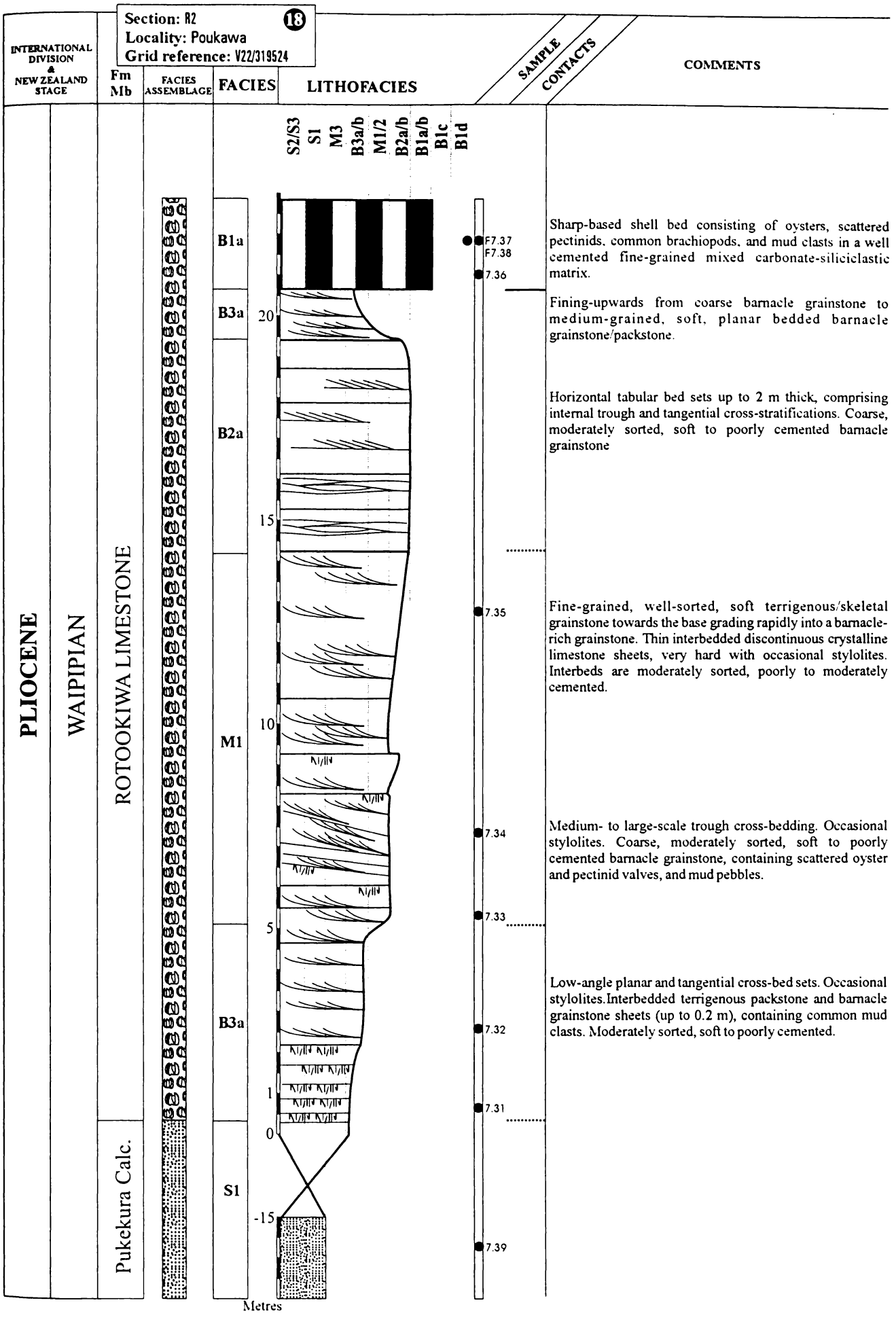
Section: R2
Locality: Poukawa
Grid reference: V22/319524
18
INTERNATIONAL DIVISION & NEW ZEALAND STAGE
Fm Mb
FACIES ASSEMBLAGE
FACIES
LITHOFACIES
SAMPLE
CONTACTS
COMMENTS
S2/S3
S1
M3
B3a/b
M1/2
B2a/b
B1a/b
B1c
B1d
PLIOCENE
WAIPIPIAN
ROTOOKIWA LIMESTONE
Pukekura Calc.
B1a
B3a
B2a
M1
B3a
S1
20
15
10
5
1
0
-15
Metres
F7.37
F7.38
7.36
7.35
7.34
7.33
7.32
7.31
7.39
Sharp-based shell bed consisting of oysters, scattered pectinids, common brachiopods, and mud clasts in a well cemented fine-grained mixed carbonate-siliciclastic matrix.
Fining-upwards from coarse barnacle grainstone to medium-grained, soft, planar bedded barnacle grainstone/packstone.
Horizontal tabular bed sets up to 2 m thick, comprising internal trough and tangential cross-stratifications. Coarse, moderately sorted, soft to poorly cemented barnacle grainstone
Fine-grained, well-sorted, soft terrigenous/skeletal grainstone towards the base grading rapidly into a barnacle-rich grainstone. Thin interbedded discontinuous crystalline limestone sheets, very hard with occasional stylolites. Interbeds are moderately sorted, poorly to moderately cemented.
Medium- to large-scale trough cross-bedding. Occasional stylolites. Coarse, moderately sorted, soft to poorly cemented barnacle grainstone, containing scattered oyster and pectinid valves, and mud pebbles.
Low-angle planar and tangential cross-bed sets. Occasional stylolites. Interbedded terrigenous packstone and barnacle grainstone sheets (up to 0.2 m), containing common mud clasts. Moderately sorted, soft to poorly cemented.

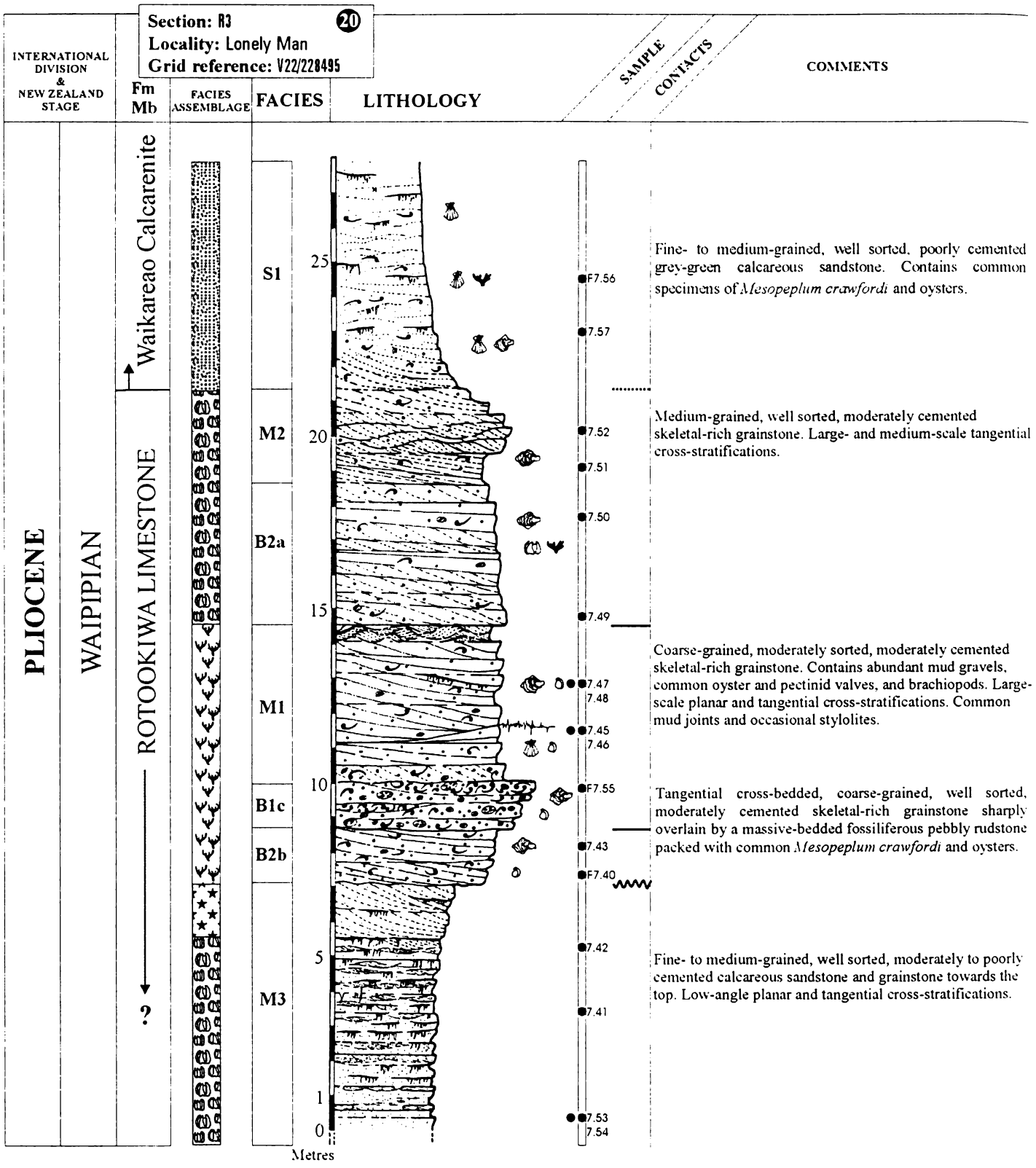
Section: R3
20
Locality: Lonely Man
Grid reference: V22/228495
INTERNATIONAL DIVISION & NEW ZEALAND STAGE
Fm Mb
FACIES ASSEMBLAGE
FACIES
LITHOLOGY
SAMPLE
CONTACTS
COMMENTS
PLIOCENE
WAIPIPIAN
Waikareao Calcarenite
ROTOOKIWA LIMESTONE
?
S1
M2
B2a
M1
B1c
B2b
M3
25
20
15
10
5
1
0
Metres
F7.56
7.57
7.52
7.51
7.50
7.49
7.47
7.48
7.45
7.46
F7.55
7.43
F7.40
7.42
7.41
7.53
7.54
Fine- to medium-grained, well sorted, poorly cemented grey-green calcareous sandstone. Contains common specimens of *Mesopeplum crawfordi* and oysters.
Medium-grained, well sorted, moderately cemented skeletal-rich grainstone. Large- and medium-scale tangential cross-stratifications.
Coarse-grained, moderately sorted, moderately cemented skeletal-rich grainstone. Contains abundant mud gravels, common oyster and pectinid valves, and brachiopods. Large-scale planar and tangential cross-stratifications. Common mud joints and occasional stylolites.
Tangential cross-bedded, coarse-grained, well sorted, moderately cemented skeletal-rich grainstone sharply overlain by a massive-bedded fossiliferous pebbly rudstone packed with common *Mesopeplum crawfordi* and oysters.
Fine- to medium-grained, well sorted, moderately to poorly cemented calcareous sandstone and grainstone towards the top. Low-angle planar and tangential cross-stratifications.

Section: Te6 (21)
Locality: Horanui
Grid reference: V22/283562

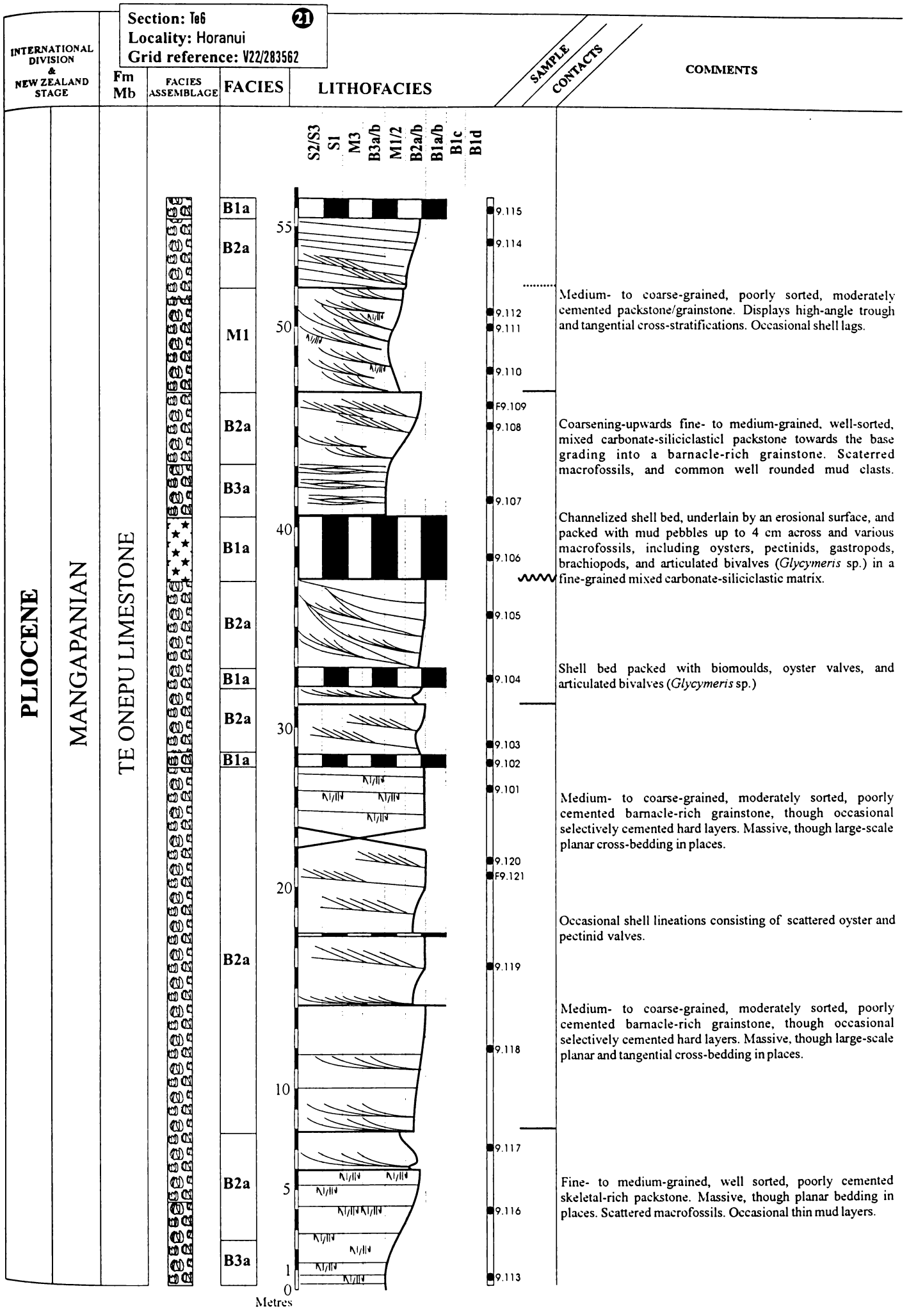

Medium- to coarse-grained, poorly sorted, moderately cemented packstone/grainstone. Displays high-angle trough and tangential cross-stratifications. Occasional shell lags.

Coarsening-upwards fine- to medium-grained, well-sorted, mixed carbonate-siliciclastic packstone towards the base grading into a barnacle-rich grainstone. Scaterred macrofossils, and common well rounded mud clasts.

Channelized shell bed, underlain by an erosional surface, and packed with mud pebbles up to 4 cm across and various macrofossils, including oysters, pectinids, gastropods, brachiopods, and articulated bivalves (*Glycymeris* sp.) in a fine-grained mixed carbonate-siliciclastic matrix.

Shell bed packed with biomoulds, oyster valves, and articulated bivalves (*Glycymeris* sp.)

Medium- to coarse-grained, moderately sorted, poorly cemented barnacle-rich grainstone, though occasional selectively cemented hard layers. Massive, though large-scale planar cross-bedding in places.

Occasional shell lineations consisting of scattered oyster and pectinid valves.

Medium- to coarse-grained, moderately sorted, poorly cemented barnacle-rich grainstone, though occasional selectively cemented hard layers. Massive, though large-scale planar and tangential cross-bedding in places.

Fine- to medium-grained, well sorted, poorly cemented skeletal-rich packstone. Massive, though planar bedding in places. Scattered macrofossils. Occasional thin mud layers.

Section: Is5 (22)
Locality: Burma Road
Grid reference: V22/259549

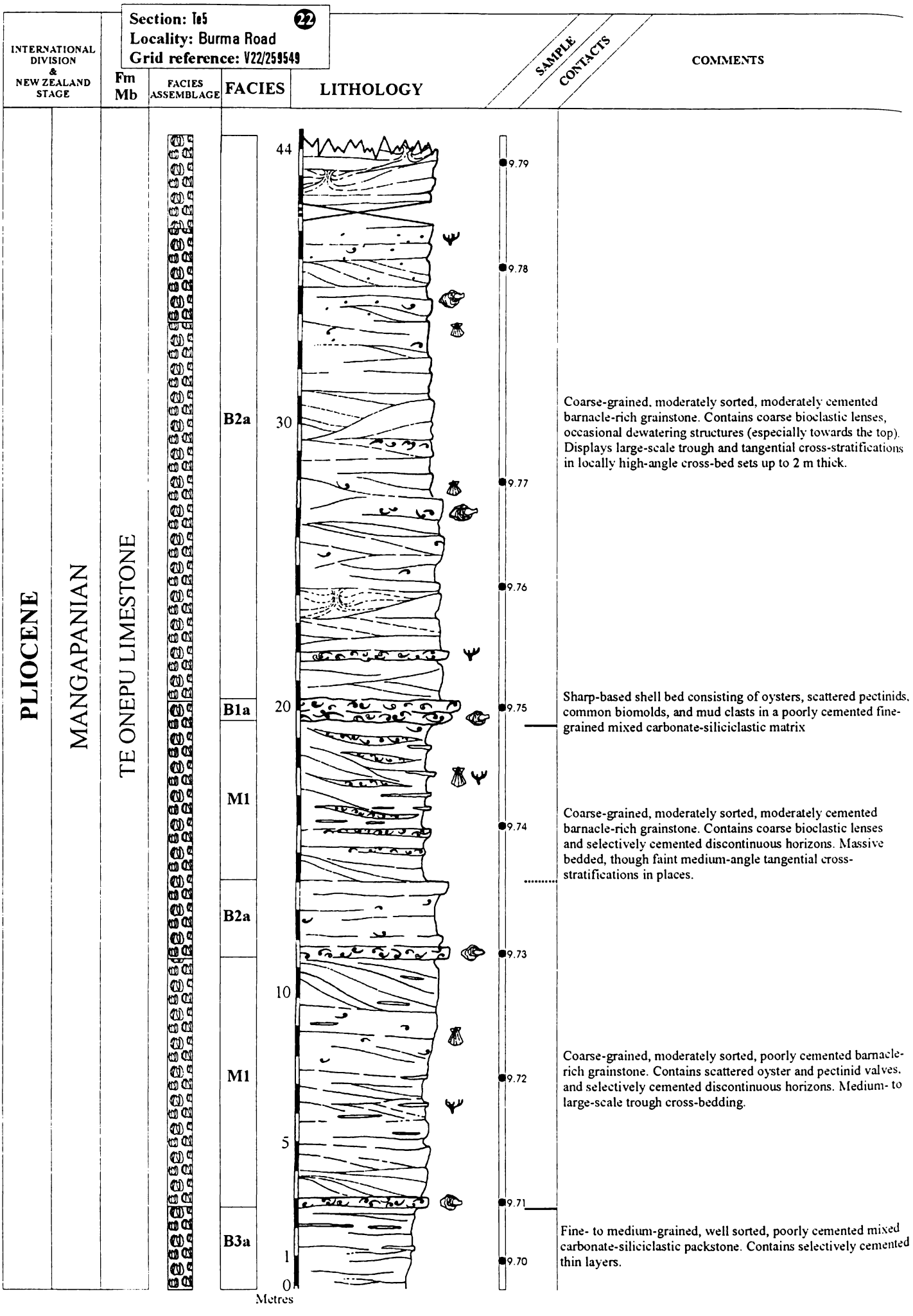

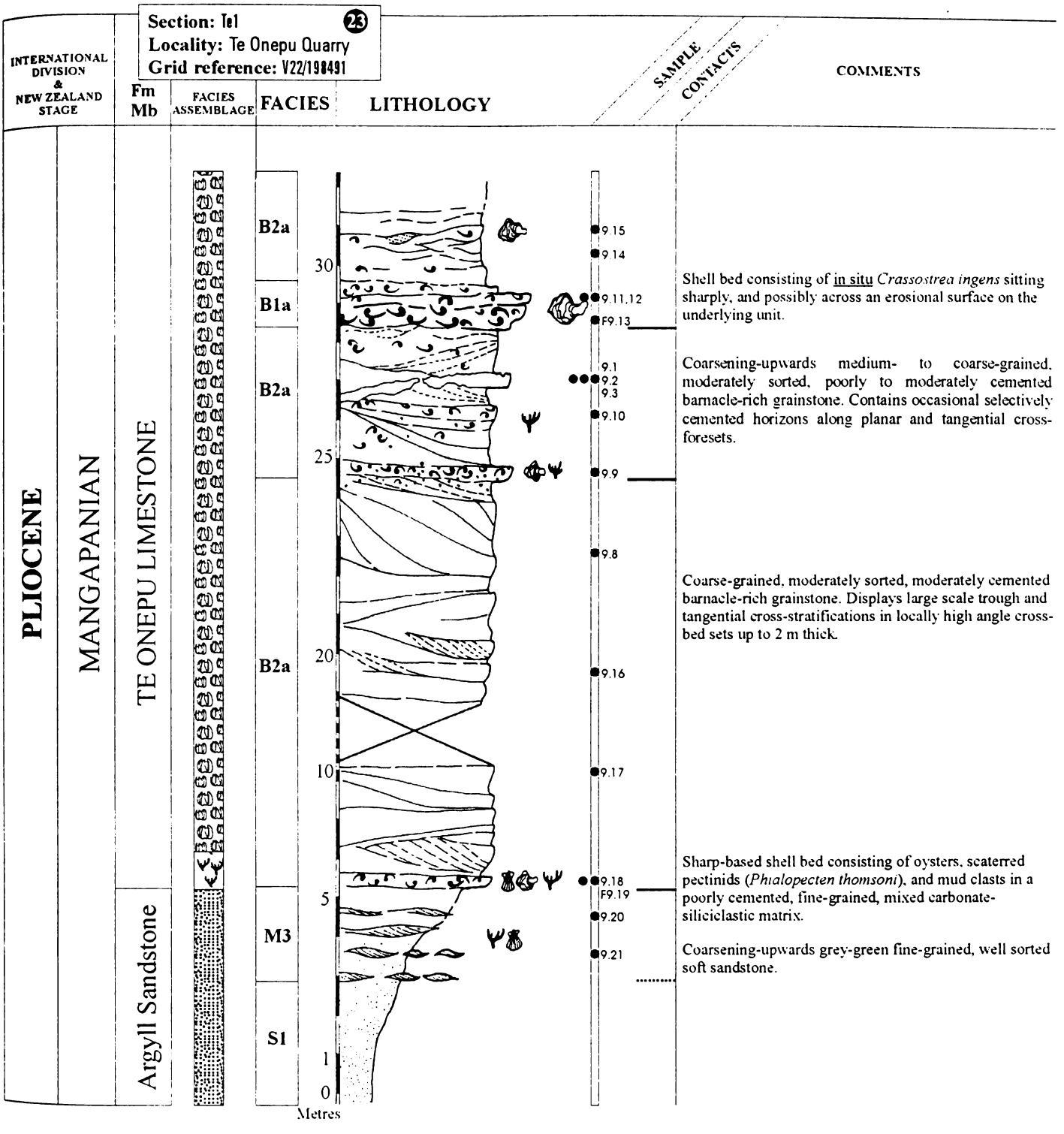
Section: Tel
Locality: Te Onepu Quarry
Grid reference: V22/198491
INTERNATIONAL DIVISION & NEW ZEALAND STAGE
Fm Mb
FACIES ASSEMBLAGE
FACIES
LITHOLOGY
SAMPLE
CONTACTS
COMMENTS
PLIOCENE
MANGAPANIAN
TE ONEPU LIMESTONE
Argyll Sandstone
B2a
B1a
B2a
B2a
M3
S1
30
25
20
10
5
1
0
Metres
9.15
9.14
9.11,12
F9.13
9.1
9.2
9.3
9.10
9.9
9.8
9.16
9.17
9.18
F9.19
9.20
9.21
Shell bed consisting of in situ Crassostrea ingens sitting sharply, and possibly across an erosional surface on the underlying unit.
Coarsening-upwards medium- to coarse-grained, moderately sorted, poorly to moderately cemented barnacle-rich grainstone. Contains occasional selectively cemented horizons along planar and tangential cross-foresets.
Coarse-grained, moderately sorted, moderately cemented barnacle-rich grainstone. Displays large scale trough and tangential cross-stratifications in locally high angle cross-bed sets up to 2 m thick.
Sharp-based shell bed consisting of oysters, scaterred pectinids (Phialopecten thomsoni), and mud clasts in a poorly cemented, fine-grained, mixed carbonate-siliciclastic matrix.
Coarsening-upwards grey-green fine-grained, well sorted soft sandstone.

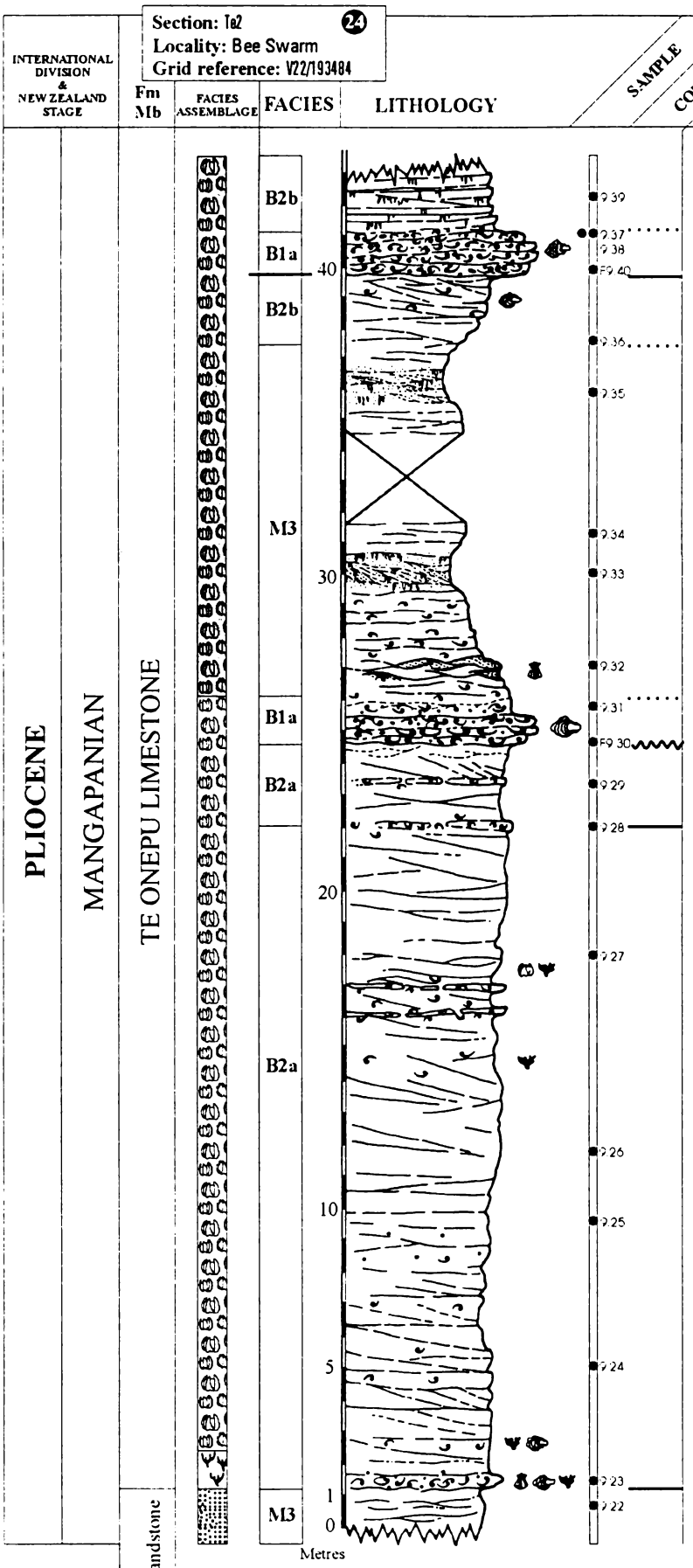

Tabular bed sets of coarse, well sorted, poorly cemented barnacle-rich grainstone

Massive, coarse-grained, poorly sorted, very well cemented shell bed packed with whole specimens of oysters and pectinids (*Phialopecten thomsoni*), mud and sand pebbles up to 2 cm across.

Coarsening-upwards, tangential to planar cross-bedded, medium- to coarse-grained, moderately sorted, moderately cemented barnacle-rich grainstone

Fining-upward, medium-grained, well sorted, moderately cemented barnacle-rich packstone/grainstone. Common mud pebbles.

Medium-scale sigmoidal, HCS-like, cross-stratifications.

1 m thick shell bed, containing *in situ* large specimens of *Crassostrea ingens*, mud granules and pebbles, occasional clumps of oysters. Moderately cemented.

Occasional thin glauconitic, mud pebble-rich beds.

Large-scale planar and medium-scale tangential cross-stratifications. Occasional selectively cemented horizons, otherwise moderately to well sorted, poorly to moderately cemented. Coarse-grained barnacle-rich grainstone.

Large-scale cross-foreset and tabular bed sets up to 2 m thick. Coarsening upward interval, from skeletal packstone/grainstone to barnacle-rich grainstone. Moderately cemented.

Thin shell lineation with common mud clasts, which contains *Phialopecten thomsoni*.

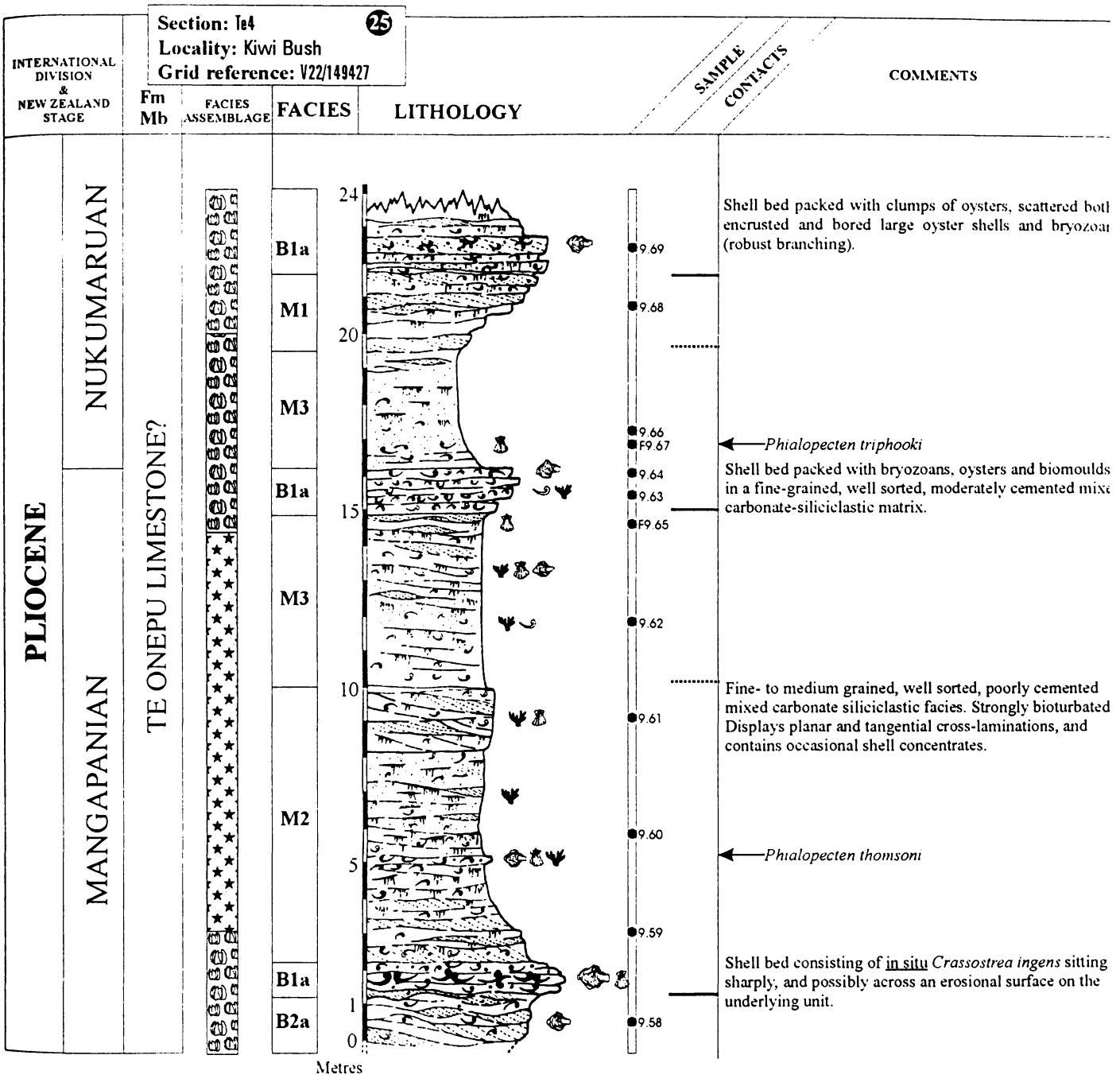
Section: Te4
25
Locality: Kiwi Bush
Grid reference: V22/149427
INTERNATIONAL DIVISION & NEW ZEALAND STAGE
Fm
Mb
FACIES ASSEMBLAGE
FACIES
LITHOLOGY
SAMPLE
CONTACTS
COMMENTS
PLIOCENE
NUKUMARUAN
MANGAPANIAN
TE ONEPU LIMESTONE?
B1a
M1
M3
B1a
M3
M2
B1a
B2a
24
20
15
10
5
1
0
Metres
9.69
9.68
9.66
F9.67
9.64
9.63
F9.65
9.62
9.61
9.60
9.59
9.58
Shell bed packed with clumps of oysters, scattered bot encrusted and bored large oyster shells and bryozoa (robust branching).
Phialopecten triphooki
Shell bed packed with bryozoans, oysters and biomoulds in a fine-grained, well sorted, moderately cemented mix carbonate-siliciclastic matrix.
Fine- to medium grained, well sorted, poorly cemented mixed carbonate siliciclastic facies. Strongly bioturbated Displays planar and tangential cross-laminations, and contains occasional shell concentrates.
Phialopecten thomsoni
Shell bed consisting of in situ Crassostrea ingens sitting sharply, and possibly across an erosional surface on the underlying unit.

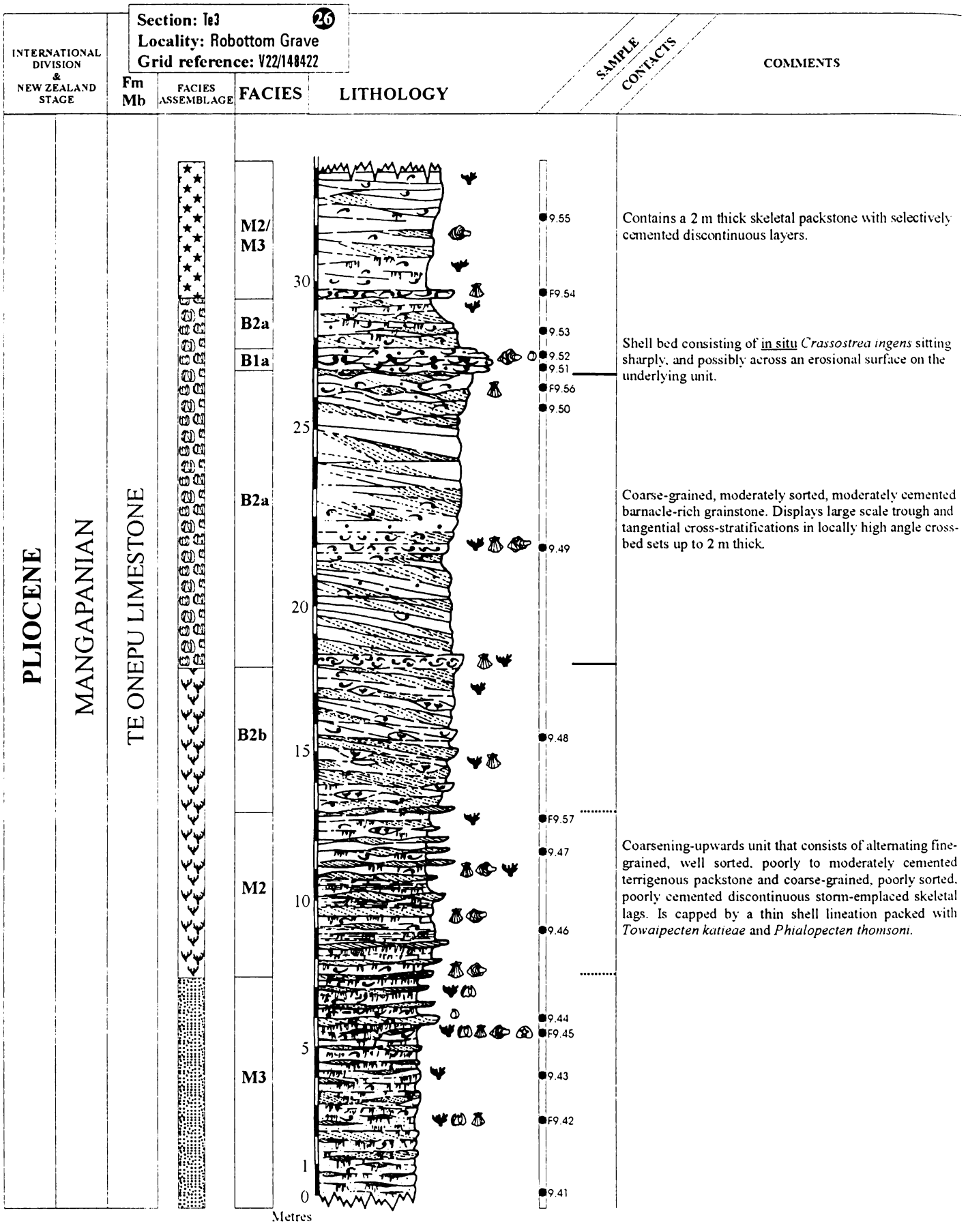
Section: Te3
26
Locality: Robottom Grave
Grid reference: V22/148422
INTERNATIONAL DIVISION & NEW ZEALAND STAGE
Fm Mb
FACIES ASSEMBLAGE
FACIES
LITHOLOGY
SAMPLE
CONTACTS
COMMENTS
PLIOCENE
MANGAPANIAN
TE ONEPU LIMESTONE
M2/ M3
B2a
B1a
B2a
B2b
M2
M3
30
25
20
15
10
5
1
0
Metres
F9.55
F9.54
F9.53
F9.52
F9.51
F9.56
F9.50
F9.49
F9.48
F9.57
F9.47
F9.46
F9.44
F9.45
F9.43
F9.42
F9.41
Contains a 2 m thick skeletal packstone with selectively cemented discontinuous layers.
Shell bed consisting of in situ Crassostrea ingens sitting sharply, and possibly across an erosional surface on the underlying unit.
Coarse-grained, moderately sorted, moderately cemented barnacle-rich grainstone. Displays large scale trough and tangential cross-stratifications in locally high angle cross-bed sets up to 2 m thick.
Coarsening-upwards unit that consists of alternating fine-grained, well sorted, poorly to moderately cemented terrigenous packstone and coarse-grained, poorly sorted, poorly cemented discontinuous storm-emplaced skeletal lags. Is capped by a thin shell lineation packed with Towaipecten katieae and Phialopecten thomsoni.

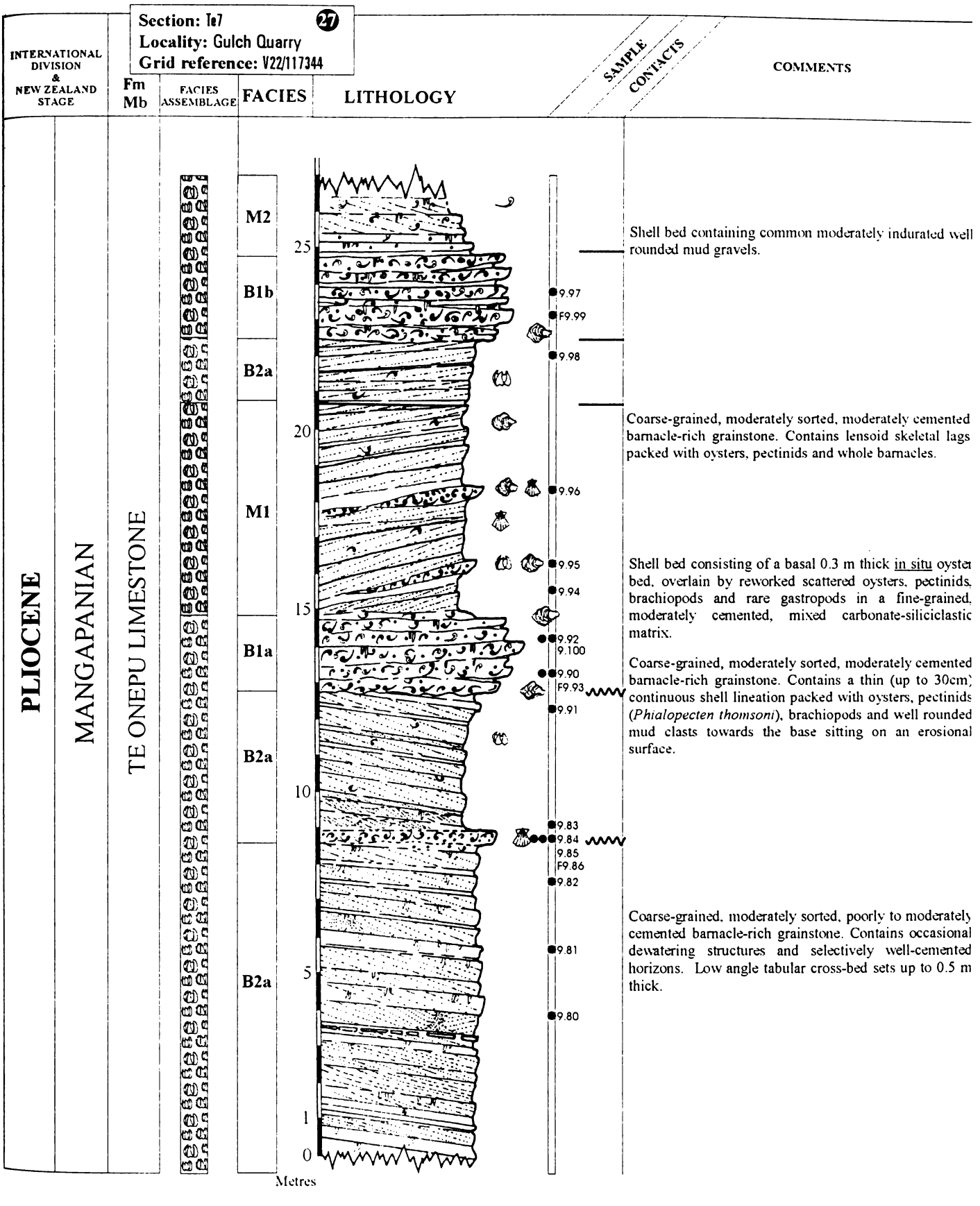
Section: Te7
27
Locality: Gulch Quarry
Grid reference: V22/117344
INTERNATIONAL DIVISION & NEW ZEALAND STAGE
Fm Mb
FACIES ASSEMBLAGE
FACIES
LITHOLOGY
SAMPLE
CONTACTS
COMMENTS
PLIOCENE
MANGAPANIAN
TE ONEPU LIMESTONE
M2
B1b
B2a
M1
B1a
B2a
B2a
25
20
15
10
5
1
0
Metres
9.97
F9.99
9.98
9.96
9.95
9.94
9.92
9.100
9.90
F9.93
9.91
9.83
9.84
9.85
F9.86
9.82
9.81
9.80
Shell bed containing common moderately indurated well rounded mud gravels.
Coarse-grained, moderately sorted, moderately cemented barnacle-rich grainstone. Contains lensoid skeletal lags packed with oysters, pectinids and whole barnacles.
Shell bed consisting of a basal 0.3 m thick in situ oyster bed, overlain by reworked scattered oysters, pectinids, brachiopods and rare gastropods in a fine-grained, moderately cemented, mixed carbonate-siliciclastic matrix.
Coarse-grained, moderately sorted, moderately cemented barnacle-rich grainstone. Contains a thin (up to 30cm) continuous shell lineation packed with oysters, pectinids (*Phialopecten thomsoni*), brachiopods and well rounded mud clasts towards the base sitting on an erosional surface.
Coarse-grained, moderately sorted, poorly to moderately cemented barnacle-rich grainstone. Contains occasional dewatering structures and selectively well-cemented horizons. Low angle tabular cross-bed sets up to 0.5 m thick.

Section: M2 (29)
Locality: Torran
Grid reference: V22/208592 to 213593

INTERNATIONAL DIVISION & NEW ZEALAND STAGE	Fm / Mb	FACIES ASSEMBLAGE	FACIES	LITHOLOGY	SAMPLE	CONTACTS	COMMENTS
PLIOCENE	NUKUMARUAN	MASON RIDGE FORMATION	Limestone 3	B1b	11.45		Shell bed consisting of various bivalves in a fining-upwards matrix, from fine-grained mixed carbonate-siliciclastic to siltstone. Contains a 0.5 m thick skeletal-rich grainstone tabular bed.
				B3b	11.44		
				B1b	11.43		
					11.42		
				B3b	11.41		Coarse-grained, moderately sorted, moderately cemented, skeletal-rich packstone. Displays low-angle planar cross-stratifications, and contains scattered macrofossils, including oysters, gastropods and bryozoan colonies.
					11.40		
				M3			Alternating fine-grained, well sorted, soft, silty calcareous sandstone, and coarser-grained bioclastic discontinuous lags. Contains scattered articulate bivalves *(Glycymeris* sp). Strongly bioturbated.
				M3	11.39		
				S2	11.38		
				B1a	11.37		Fining-upwards, from basal coarse-grained, well sorted, well cemented skeletal-rich grainstone with common mud drapes. Sedimentary structures include, from base to top, medium-scale wavy and sigmoidal cross-beddings (HCS-like structures) to flaser bedding structures and rippled cross-laminations outlined by thin mud layers, strongly bioturbated.
				B2a	11.36		
					11.35		
					11.34		
					11.33		
				S2	11.32		
					F.11.31		
					11.30		
				B1a	11.29		Coarse-grained, moderately to well cemented skeletal-rich unit bounded above and below by 0.5-1 m thick shell beds. Medium-scale planar to tangential cross-stratifications.
				M1	11.28		
					11.27		Small- and medium-scale tangential to trough cross-stratifications within a well cemented, skeletal-rich grainstone.
			Limestone 2				
		Sandstone 3		M1	11.26		Medium-grained, moderately to well sorted, moderately cemented barnacle-rich grainstone, interbedded with mixed carbonate-siliciclastic packstone. Low-angle planar cross-stratifications. Scattered macrofossils.
					11.25		
		Sandstone/Siltstone 2	Limestone 1				

Metres: 55, 50, 45, 30, 25, 20, 15, 10, 5, 1, 0

Section: M3 (30)
Locality: Pakihirua
Grid reference: V22/204564 to 188548

INTERNATIONAL DIVISION & NEW ZEALAND STAGE	Fm / Mb	FACIES ASSEMBLAGE	FACIES	LITHOLOGY	SAMPLE	CONTACTS	COMMENTS
PLIOCENE / NUKUMARUAN	MASON RIDGE FORMATION — Limestone 3		B1b	78	11.72		Shell bed packed with oysters, and gastropods in a bioclastic sandy matrix towards the base, grading up-section into a silty sandy matrix.
			B1a				
			S1				Low-angle planar laminated fine-grained, well sorted, poorly cemented, calcareous sandstone.
			B2a	70	11.69 11.68		Alternating coarse-grained, moderately sorted, poorly cemented, skeletal-rich grainstone and thin shell lineations up to 30 cm thick, containing biomoulds, oysters, and other bivalves in a fine- to medium-grained sandy matrix. Horizontal tabular-bedded.
			M3		11.71 11.70		Coarsening-upwards moderately sorted, poorly cemented, calcareous sandstone, containing moderately to well cemented bioclastic lenses.
	Siltstone 3		S2		11.67		Shelly grey silty sandstone grades up over 2 m into siltsone containing scattered shells.
	Limestone 2		S1	60	11.66		Fining-upwards yellow, well sorted, poorly cemented, calcareous argillaceous sandstone.
			B1a		11.65 11.64		Shell bed packed with oysters, gastropods and pectinids in a siliciclastic matrix.
			M1				Alternating fine-grained, poorly cemented, mixed carbonate-siliciclastic packstone and medium-grained, moderately cemented skeletal grainstone. Contains occasional large vertical burrows (*Ophiomorpha*?).
	Sandy Siltstone 2		S1/ S2	50	11.63 11.62 11.61		Shell lineation, orange mud and sand pebbles. Sharp-based silty sandstone grading into sandstone containing common whole specimens of barnacles, oysters, and pectinids.
	Limestone 1		B1a		11.57 11.58		Shell bed packed with oysters in a siliciclastic matrix.
			M1		11.59 11.56 11.55		Tabular bed sets of interbedded packstone and skeletal grainstone.
			M2	40	11.54 11.60		Coarsening- and thickening-upwards interbedded planar laminated packstone and coarse tangential cross-bedded fossiliferous grainstone. Moderately sorted, moderately cemented. Capped by a shell lineation packed with oyster valves in a sandy/silty matrix.
			S2				Greyish siltstone containing common biomolds and gastropods.
			B2a		11.52 F11.53 11.51		Thin oyster shell lineation at the base in a terrigenous/skeletal matrix. Yellow, coarse-grained, well sorted, poorly cemented skeletal grainstone, contains whole specimens of *Glycymeris*?. Is capped by a thin shell lineation packed with thin-shelled oysters, pectinids and other bivalves.
	Sst.1		S1		11.50		Silty sandstone containing common oysters, mussels and brachiopods.
	Makaretu Mudstone		S3	30	11.49		Grey/green siltstone containing common thin shell lineations.
			B1b	1			Shell bed packed with gastropods, brachiopods, oysters, pectinids, barnacles, mussels and bryozoans in a silty/sandy matrix.
			S3	0			

Metres

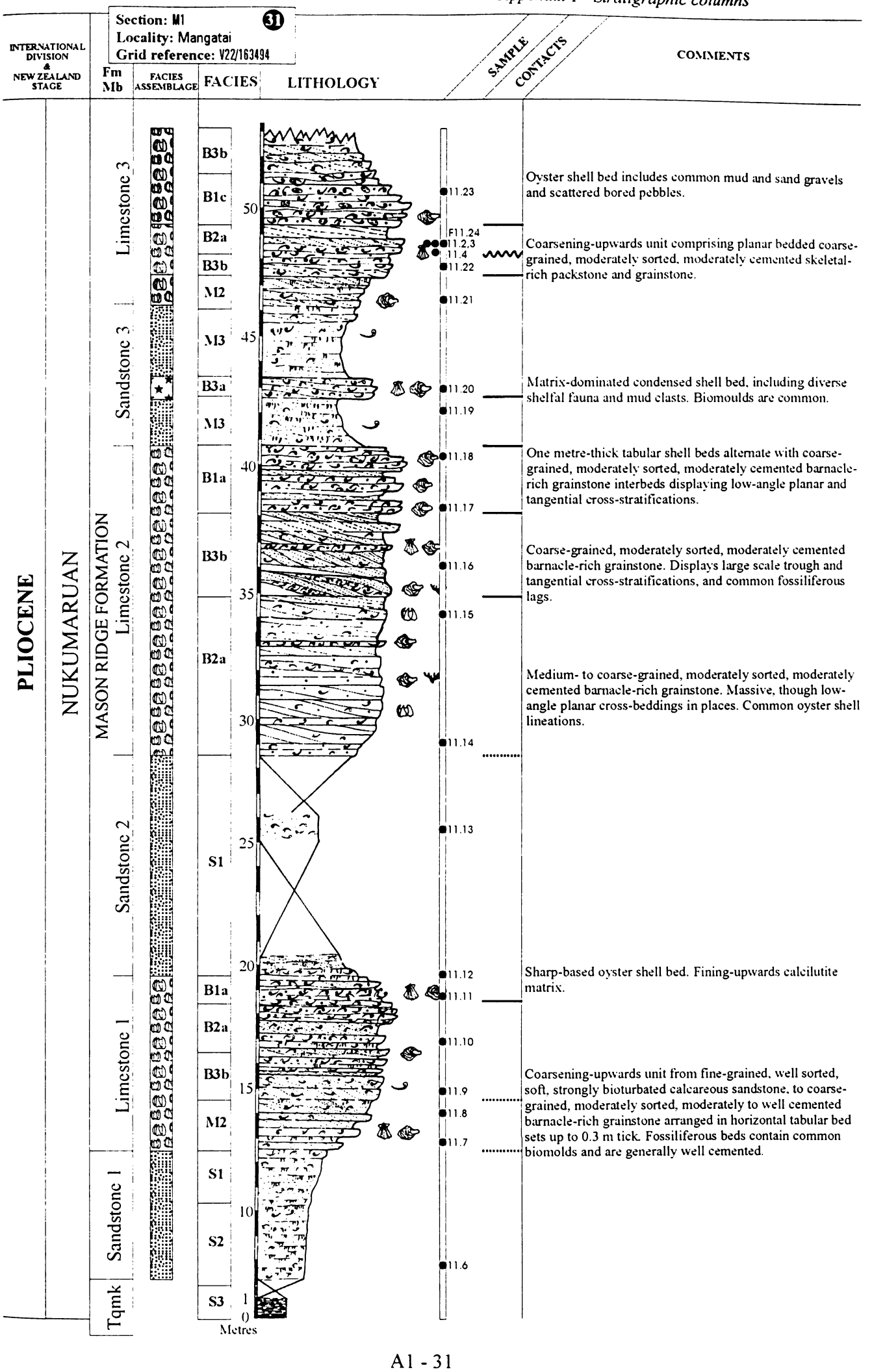
Section: M1
31
Locality: Mangatai
Grid reference: V22/163494
INTERNATIONAL DIVISION & NEW ZEALAND STAGE
Fm Mb
FACIES ASSEMBLAGE
FACIES
LITHOLOGY
SAMPLE
CONTACTS
COMMENTS
PLIOCENE
NUKUMARUAN
MASON RIDGE FORMATION
Limestone 3
Sandstone 3
Limestone 2
Sandstone 2
Limestone 1
Sandstone 1
Tqmk
B3b
B1c
B2a
B3b
M2
M3
B3a
M3
B1a
B3b
B2a
S1
B1a
B2a
B3b
M2
S1
S2
S3
50
45
40
35
30
25
20
15
10
1
0
Metres
11.23
F11.24
11.2,3
11.4
11.22
11.21
11.20
11.19
11.18
11.17
11.16
11.15
11.14
11.13
11.12
11.11
11.10
11.9
11.8
11.7
11.6
Oyster shell bed includes common mud and sand gravels and scattered bored pebbles.
Coarsening-upwards unit comprising planar bedded coarse-grained, moderately sorted, moderately cemented skeletal-rich packstone and grainstone.
Matrix-dominated condensed shell bed, including diverse shelfal fauna and mud clasts. Biomoulds are common.
One metre-thick tabular shell beds alternate with coarse-grained, moderately sorted, moderately cemented barnacle-rich grainstone interbeds displaying low-angle planar and tangential cross-stratifications.
Coarse-grained, moderately sorted, moderately cemented barnacle-rich grainstone. Displays large scale trough and tangential cross-stratifications, and common fossiliferous lags.
Medium- to coarse-grained, moderately sorted, moderately cemented barnacle-rich grainstone. Massive, though low-angle planar cross-beddings in places. Common oyster shell lineations.
Sharp-based oyster shell bed. Fining-upwards calcilutite matrix.
Coarsening-upwards unit from fine-grained, well sorted, soft, strongly bioturbated calcareous sandstone, to coarse-grained, moderately sorted, moderately to well cemented barnacle-rich grainstone arranged in horizontal tabular bed sets up to 0.3 m tick. Fossiliferous beds contain common biomolds and are generally well cemented.

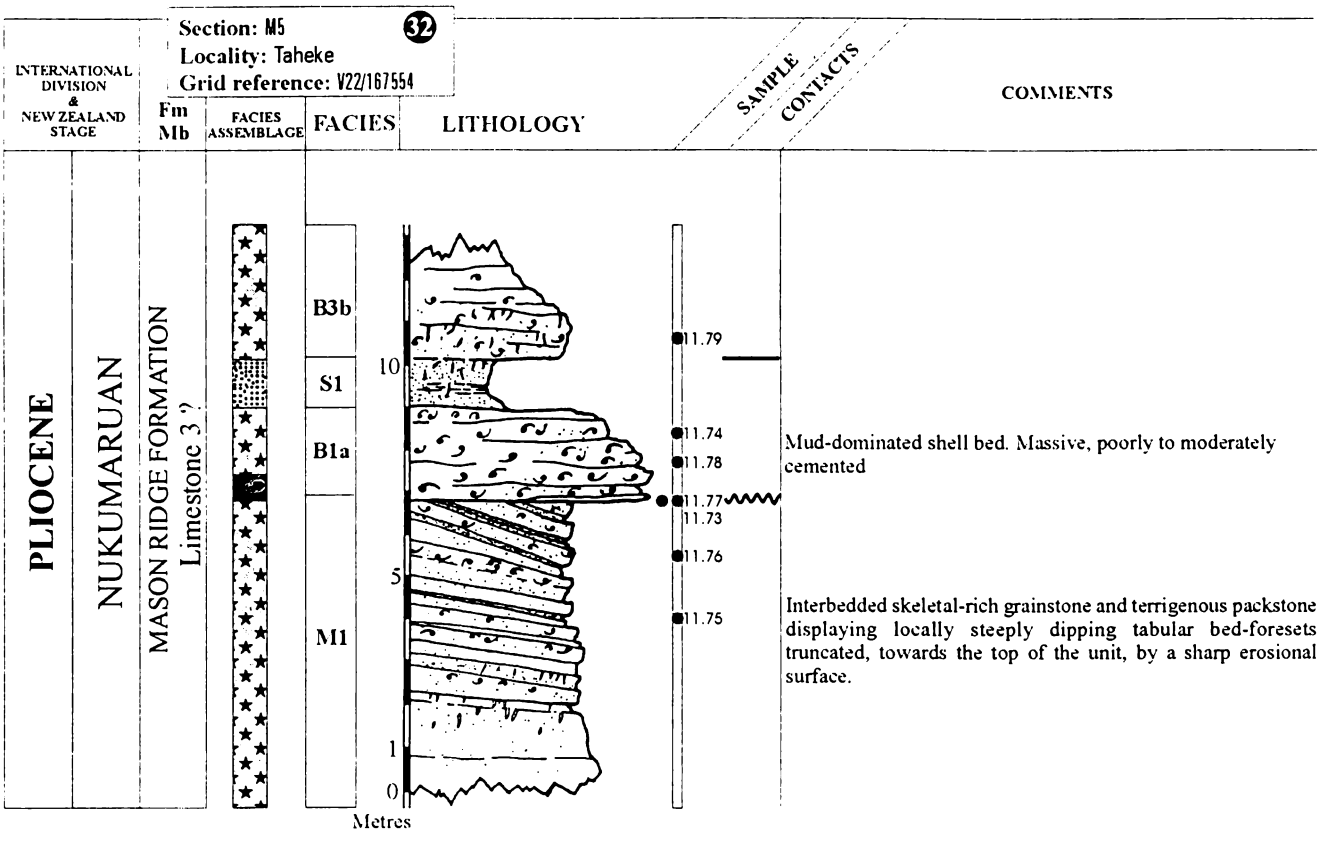
Section: M5
32
Locality: Taheke
Grid reference: V22/167554
INTERNATIONAL DIVISION & NEW ZEALAND STAGE
Fm Mb
FACIES ASSEMBLAGE
FACIES
LITHOLOGY
SAMPLE
CONTACTS
COMMENTS
PLIOCENE
NUKUMARUAN
MASON RIDGE FORMATION
Limestone 3 ?
B3b
S1
B1a
M1
10
5
1
0
Metres
11.79
11.74
11.78
11.77
11.73
11.76
11.75
Mud-dominated shell bed. Massive, poorly to moderately cemented
Interbedded skeletal-rich grainstone and terrigenous packstone displaying locally steeply dipping tabular bed-foresets truncated, towards the top of the unit, by a sharp erosional surface.

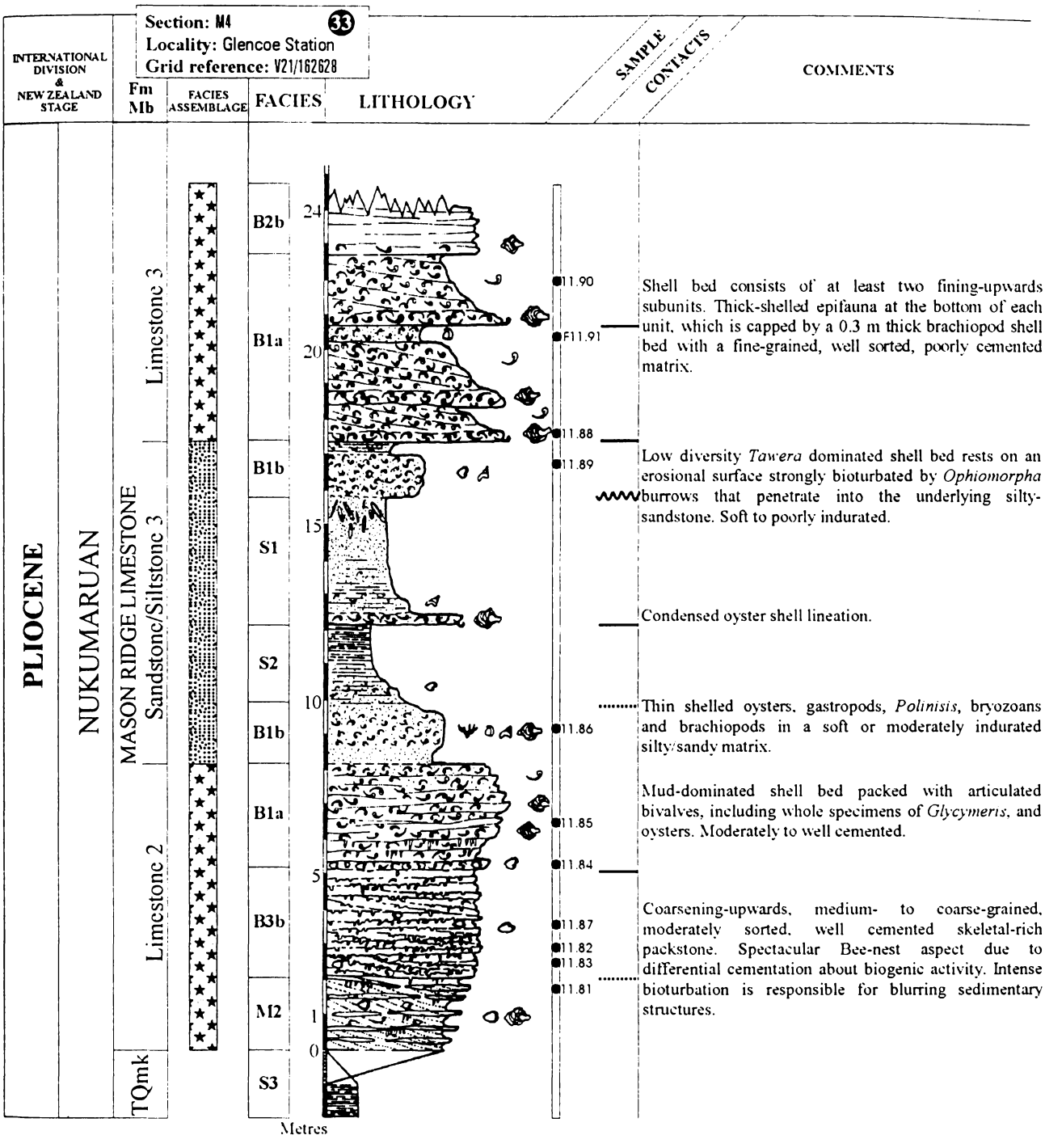
Section: M4
33
Locality: Glencoe Station
Grid reference: V21/162628
INTERNATIONAL DIVISION & NEW ZEALAND STAGE
Fm Mb
FACIES ASSEMBLAGE
FACIES
LITHOLOGY
SAMPLE
CONTACTS
COMMENTS
PLIOCENE
NUKUMARUAN
MASON RIDGE LIMESTONE
Limestone 3
Sandstone/Siltstone 3
Limestone 2
TQmk
B2b
B1a
B1b
S1
S2
B1b
B1a
B3b
M2
S3
24
20
15
10
5
1
0
Metres
11.90
F11.91
11.88
11.89
11.86
11.85
11.84
11.87
11.82
11.83
11.81
Shell bed consists of at least two fining-upwards subunits. Thick-shelled epifauna at the bottom of each unit, which is capped by a 0.3 m thick brachiopod shell bed with a fine-grained, well sorted, poorly cemented matrix.
Low diversity *Tawera* dominated shell bed rests on an erosional surface strongly bioturbated by *Ophiomorpha* burrows that penetrate into the underlying silty-sandstone. Soft to poorly indurated.
Condensed oyster shell lineation.
Thin shelled oysters, gastropods, *Polinisis*, bryozoans and brachiopods in a soft or moderately indurated silty/sandy matrix.
Mud-dominated shell bed packed with articulated bivalves, including whole specimens of *Glycymeris*, and oysters. Moderately to well cemented.
Coarsening-upwards, medium- to coarse-grained, moderately sorted, well cemented skeletal-rich packstone. Spectacular Bee-nest aspect due to differential cementation about biogenic activity. Intense bioturbation is responsible for blurring sedimentary structures.

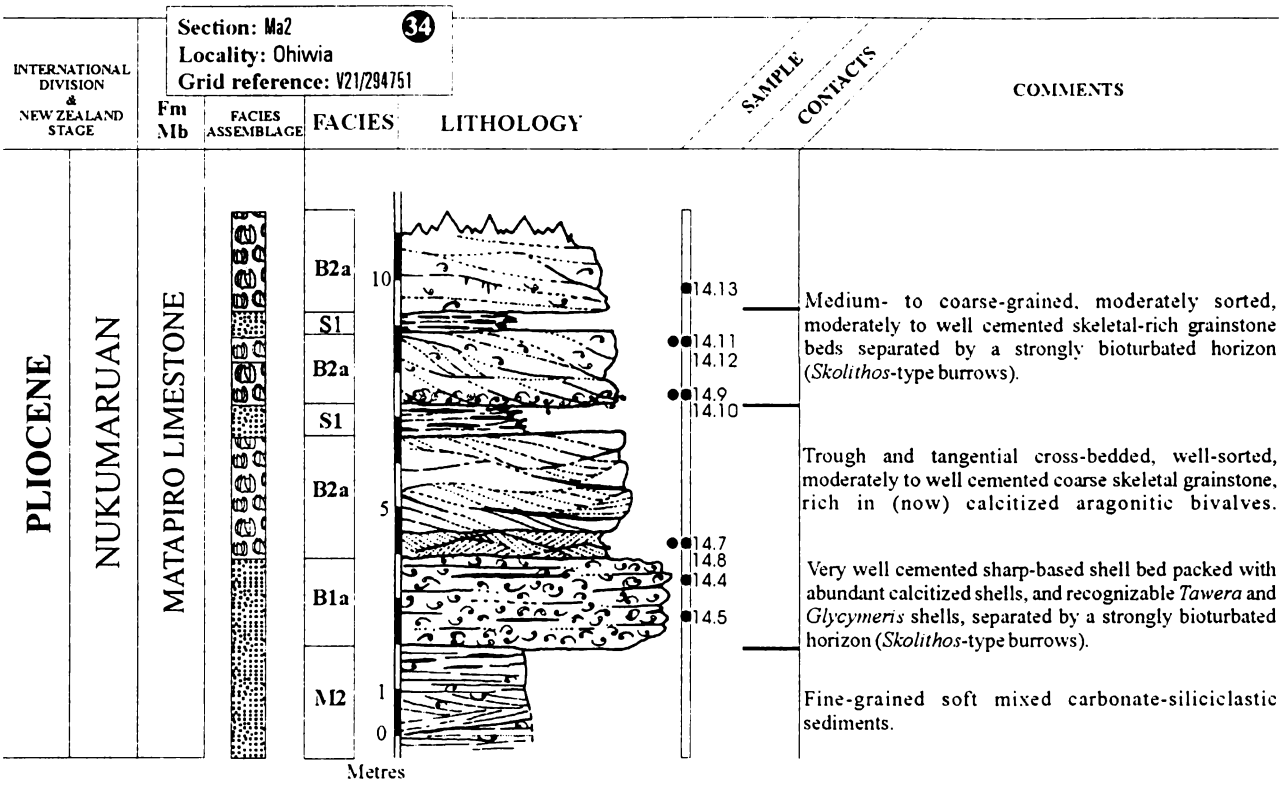
Section: Ma2
34
Locality: Ohiwia
Grid reference: V21/294751
INTERNATIONAL DIVISION & NEW ZEALAND STAGE
Fm
Mb
FACIES ASSEMBLAGE
FACIES
LITHOLOGY
SAMPLE
CONTACTS
COMMENTS
PLIOCENE
NUKUMARUAN
MATAPIRO LIMESTONE
B2a
S1
B2a
S1
B2a
B1a
M2
10
5
1
0
Metres
14.13
14.11
14.12
14.9
14.10
14.7
14.8
14.4
14.5
Medium- to coarse-grained, moderately sorted, moderately to well cemented skeletal-rich grainstone beds separated by a strongly bioturbated horizon (*Skolithos*-type burrows).
Trough and tangential cross-bedded, well-sorted, moderately to well cemented coarse skeletal grainstone, rich in (now) calcitized aragonitic bivalves.
Very well cemented sharp-based shell bed packed with abundant calcitized shells, and recognizable *Tawera* and *Glycymeris* shells, separated by a strongly bioturbated horizon (*Skolithos*-type burrows).
Fine-grained soft mixed carbonate-siliciclastic sediments.

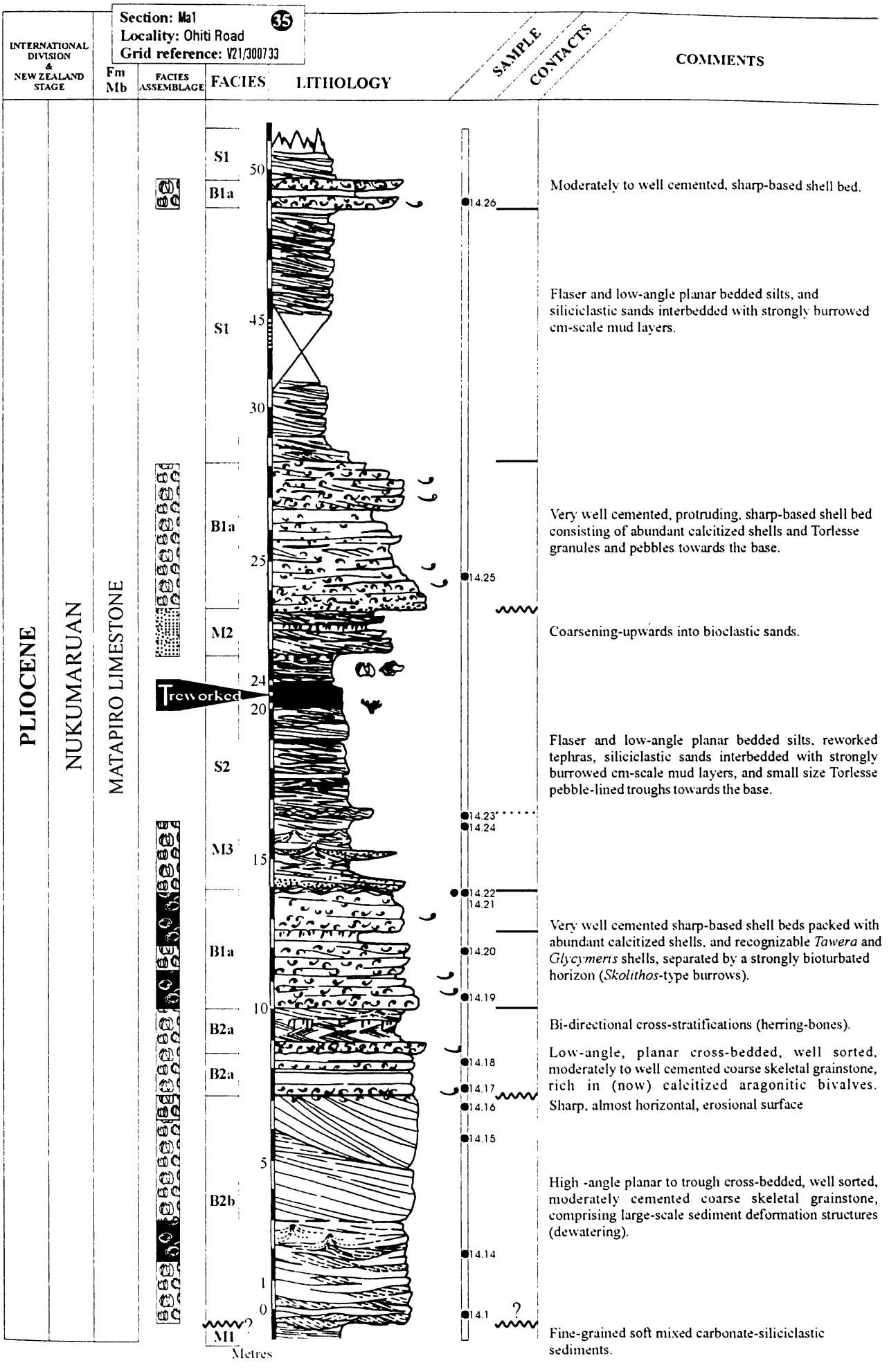
Section: Ma1
35
Locality: Ohiti Road
Grid reference: V21/300733
INTERNATIONAL DIVISION & NEW ZEALAND STAGE
Fm Mb
FACIES ASSEMBLAGE
FACIES
LITHOLOGY
SAMPLE
CONTACTS
COMMENTS
PLIOCENE
NUKUMARUAN
MATAPIRO LIMESTONE
S1
B1a
S1
B1a
M2
Reworked
S2
M3
B1a
B2a
B2a
B2b
M1
50
45
30
25
24
20
15
10
5
1
0
Metres
14.26
14.25
14.23
14.24
14.22
14.21
14.20
14.19
14.18
14.17
14.16
14.15
14.14
14.1
Moderately to well cemented, sharp-based shell bed.
Flaser and low-angle planar bedded silts, and siliciclastic sands interbedded with strongly burrowed cm-scale mud layers.
Very well cemented, protruding, sharp-based shell bed consisting of abundant calcitized shells and Torlesse granules and pebbles towards the base.
Coarsening-upwards into bioclastic sands.
Flaser and low-angle planar bedded silts, reworked tephras, siliciclastic sands interbedded with strongly burrowed cm-scale mud layers, and small size Torlesse pebble-lined troughs towards the base.
Very well cemented sharp-based shell beds packed with abundant calcitized shells, and recognizable *Tawera* and *Glycymeris* shells, separated by a strongly bioturbated horizon (*Skolithos*-type burrows).
Bi-directional cross-stratifications (herring-bones).
Low-angle, planar cross-bedded, well sorted, moderately to well cemented coarse skeletal grainstone, rich in (now) calcitized aragonitic bivalves.
Sharp, almost horizontal, erosional surface
High -angle planar to trough cross-bedded, well sorted, moderately cemented coarse skeletal grainstone, comprising large-scale sediment deformation structures (dewatering).
Fine-grained soft mixed carbonate-siliciclastic sediments.

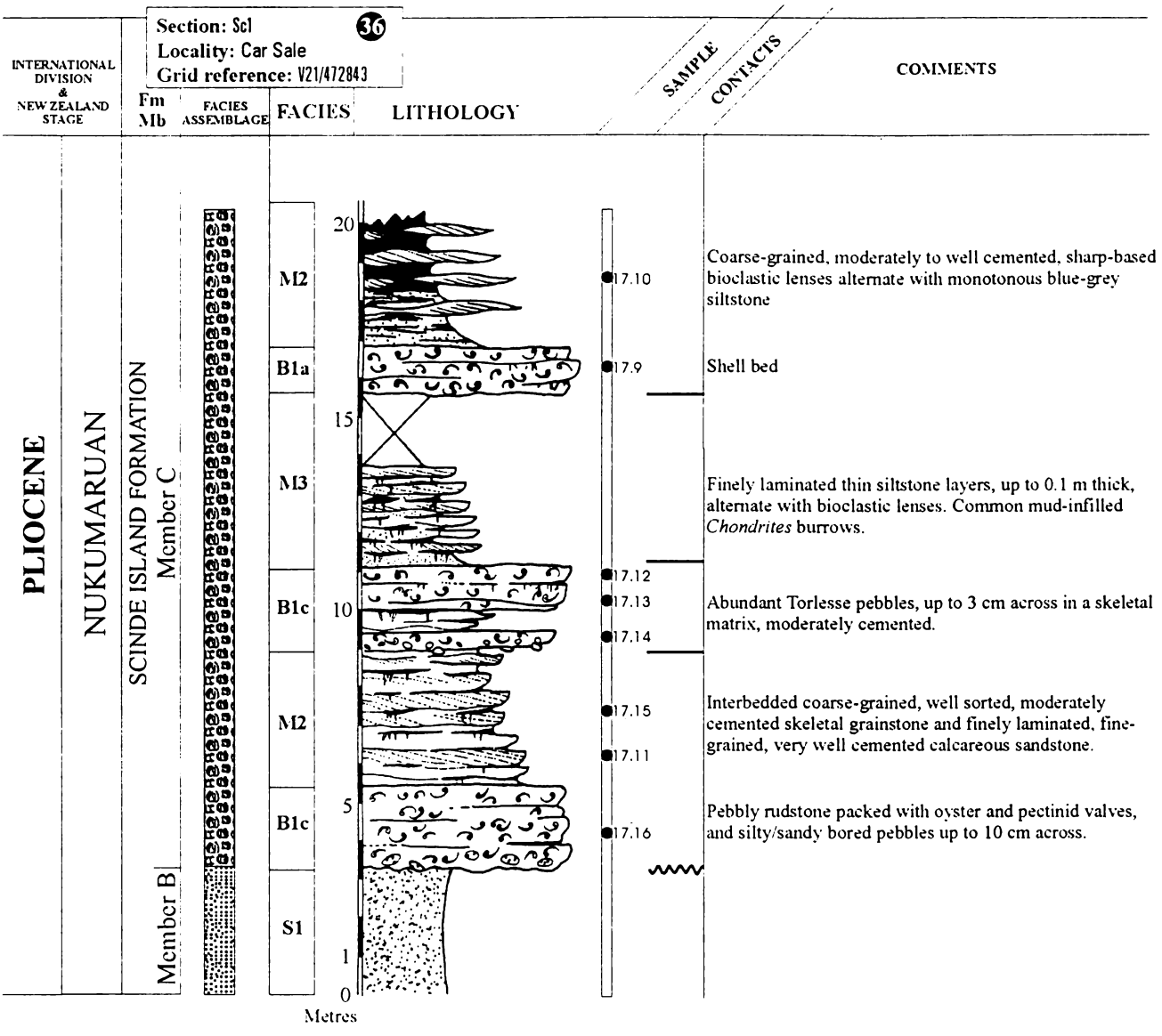
Section: Scl
36
Locality: Car Sale
Grid reference: V21/472843
INTERNATIONAL DIVISION & NEW ZEALAND STAGE
Fm Mb
FACIES ASSEMBLAGE
FACIES
LITHOLOGY
SAMPLE
CONTACTS
COMMENTS
PLIOCENE
NUKUMARUAN
SCINDE ISLAND FORMATION
Member C
Member B
M2
B1a
M3
B1c
M2
B1c
S1
20
15
10
5
1
0
Metres
17.10
17.9
17.12
17.13
17.14
17.15
17.11
17.16
Coarse-grained, moderately to well cemented, sharp-based bioclastic lenses alternate with monotonous blue-grey siltstone
Shell bed
Finely laminated thin siltstone layers, up to 0.1 m thick, alternate with bioclastic lenses. Common mud-infilled *Chondrites* burrows.
Abundant Torlesse pebbles, up to 3 cm across in a skeletal matrix, moderately cemented.
Interbedded coarse-grained, well sorted, moderately cemented skeletal grainstone and finely laminated, fine-grained, very well cemented calcareous sandstone.
Pebbly rudstone packed with oyster and pectinid valves, and silty/sandy bored pebbles up to 10 cm across.

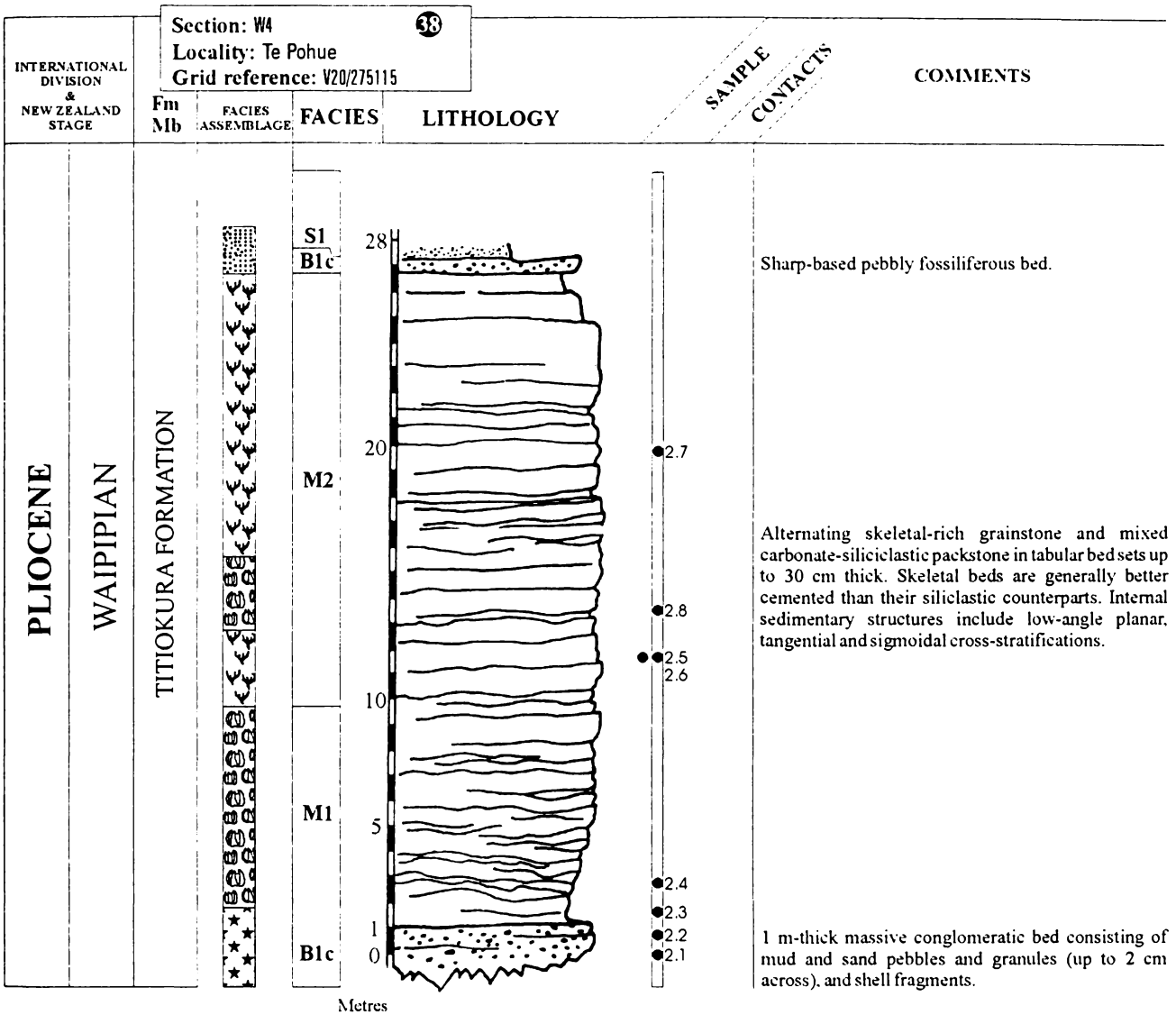
Section: W4
38
Locality: Te Pohue
Grid reference: V20/275115
INTERNATIONAL DIVISION & NEW ZEALAND STAGE
Fm Mb
FACIES ASSEMBLAGE
FACIES
LITHOLOGY
SAMPLE
CONTACTS
COMMENTS
PLIOCENE
WAIPIPIAN
TITIOKURA FORMATION
S1
B1c
M2
M1
B1c
28
20
10
5
1
0
2.7
2.8
2.5
2.6
2.4
2.3
2.2
2.1
Sharp-based pebbly fossiliferous bed.
Alternating skeletal-rich grainstone and mixed carbonate-siliciclastic packstone in tabular bed sets up to 30 cm thick. Skeletal beds are generally better cemented than their siliclastic counterparts. Internal sedimentary structures include low-angle planar, tangential and sigmoidal cross-stratifications.
1 m-thick massive conglomeratic bed consisting of mud and sand pebbles and granules (up to 2 cm across), and shell fragments.
Metres

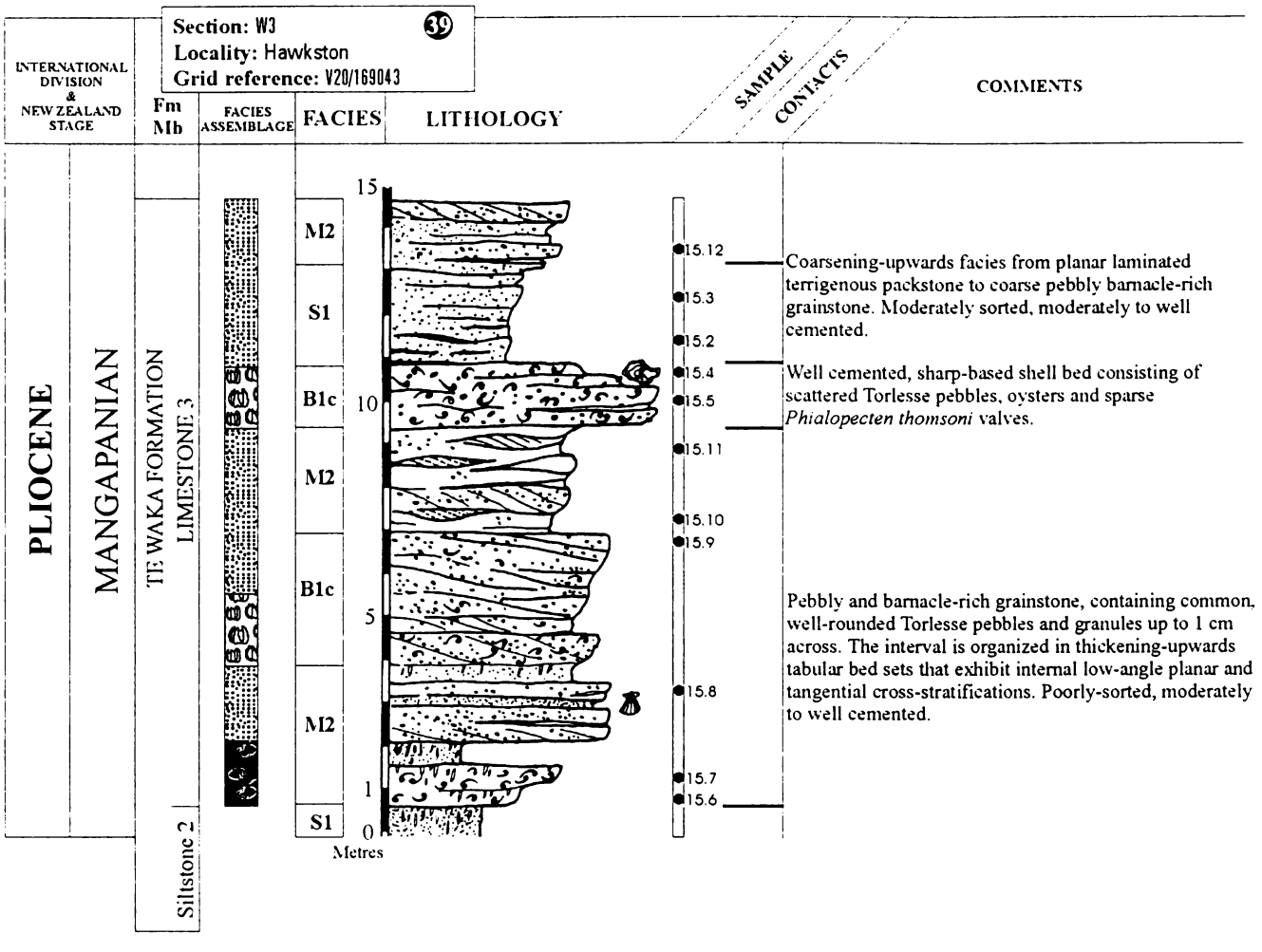
Section: W3
39
Locality: Hawkston
Grid reference: V20/169043
INTERNATIONAL DIVISION & NEW ZEALAND STAGE
Fm Mb
FACIES ASSEMBLAGE
FACIES
LITHOLOGY
SAMPLE
CONTACTS
COMMENTS
PLIOCENE
MANGAPANIAN
TE WAKA FORMATION
LIMESTONE 3
Siltstone 2
M2
S1
B1c
M2
B1c
M2
S1
15
10
5
1
0
Metres
15.12
15.3
15.2
15.4
15.5
15.11
15.10
15.9
15.8
15.7
15.6
Coarsening-upwards facies from planar laminated terrigenous packstone to coarse pebbly barnacle-rich grainstone. Moderately sorted, moderately to well cemented.
Well cemented, sharp-based shell bed consisting of scattered Torlesse pebbles, oysters and sparse *Phialopecten thomsoni* valves.
Pebbly and barnacle-rich grainstone, containing common, well-rounded Torlesse pebbles and granules up to 1 cm across. The interval is organized in thickening-upwards tabular bed sets that exhibit internal low-angle planar and tangential cross-stratifications. Poorly-sorted, moderately to well cemented.

Section: W1 (40 41)
Locality: The Gorges
Grid reference: V20/188007

INTERNATIONAL DIVISION & NEW ZEALAND STAGE	Fm Mb	FACIES ASSEMBLAGE	FACIES	SAMPLE	CONTACTS	COMMENTS
	HASSAL Cgl.		S1	15.17		Fluvial gravel beds consisting of non-fossiliferous, non-carbonate, planar laminated pebbly sands with thin muddy horizons that contain lignite debris.
				15.20		
			B1d	15.15		Fossiliferous conglomerate containing mud and Torlesse pebbles, oysters and various unidentified bivalves. The upper contact is sharp and is marked by a shell concentration including scattered large oyster shells.
				15.19		
				15.14		
				15.13		Ravinement surface.
	MUDSTONE/SILTSTONE 3		S1			
			S2			Siltstone grading into sandstone.
			S3			
			B2a	15.47		
				15.46		Same as below. Sharp-based.
			S1			
			M1	15.45		Coarsening-upwards facies from planar laminated terrigenous packstone to coarse pebbly barnacle grainstone. Moderately sorted, moderately to well cemented.
				15.44		
			S1			
			B1d	15.43		Well cemented, sharp-based shell bed consisting of scattered Torlesse pebbles, oysters and sparse *Phialopecten thomsoni* valves.
			M3	15.42		
				15.41		
			B1d	15.40		Pebbly and barnacle-rich grainstone, containing common, well rounded Torlesse pebbles and granules up to 1 cm across. The interval is organized in thickening-upwards tabular bed sets that exhibit internal low-angle planar and tangential cross-stratifications. Poorly-sorted, moderately to well cemented.
				15.39		
				15.38		
			M3	15.37		
				15.36		
			S2			Poorly exposed silty sandstone.
			M1	15.35		
				15.34		Coarsening-upwards succession from alternating discontinuous medium-grained skeletal lenses (tempestites) and interlayered, planar laminated, terrigenous packstone, to horizontal tabular bed sets of alternating grainstone and packstone, and then up section into coarse grainstone consisting of shell and barnacle fragments, and Torlesse granules (1.5 m).
			M2	15.33		
				15.32		
			S1			
			S2			Poorly exposed greyish siltstone coarsens upward into silty sandstone.
			S1	15.31		Calcareous sandstone grading into siltstone.
				15.30		
			B3	15.29		Fine-grained planar-bedded soft bioclastic sand sharply overlain by a thin (20 cm) shell concentration packed with oysters and pectinids.
			B2a	15.28		Stacked bioclastic bodies, 2-3 m thick each. Medium-scale trough and sigmoidal cross-stratifications occur within moderately cemented coarse barnacle-rich grainstones. Interlayered mud joints with small-scale sigmoidal cross-laminated skeletal beds are common up section.
				15.27		
				15.26		
				15.25		
				15.24		
			M1	15.23		Alternating barnacle-rich grainstone and terrigenous packstone organized in horizontal tabular bed sets, 20-30 cm thick. Internal sedimentary structures include low-angle planar and tangential cross-stratifications. Fine- to medium-grained, well sorted, moderately to well cemented. Intensively bioturbated.
			M2	15.22		
				15.21		

PLIOCENE
MANGAPANIAN
WAIPIPIAN?
TE WAKA FORMATION
LIMESTONE 3
Silty Sandstone 2
LIMESTONE 2
Silty Sandstone 1
TITIOKURA FORMATION?
LIMESTONE 1

Metres: 95, 90, 70, 60, 54, 45, 40, 20, 10, 5, 1, 0

Section: W2 (42)
Locality: Omahaki
Grid reference: U21/032867 to 035878

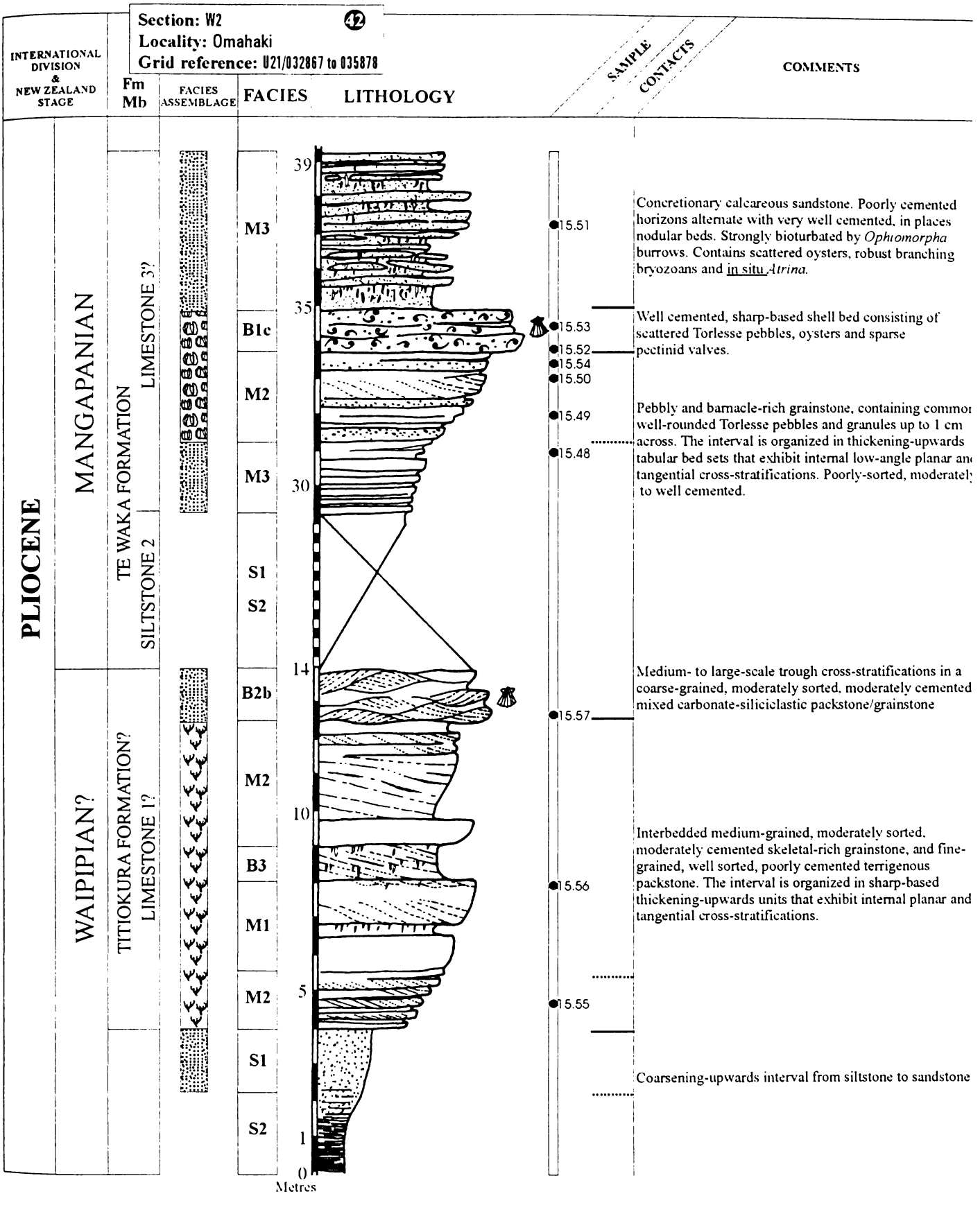

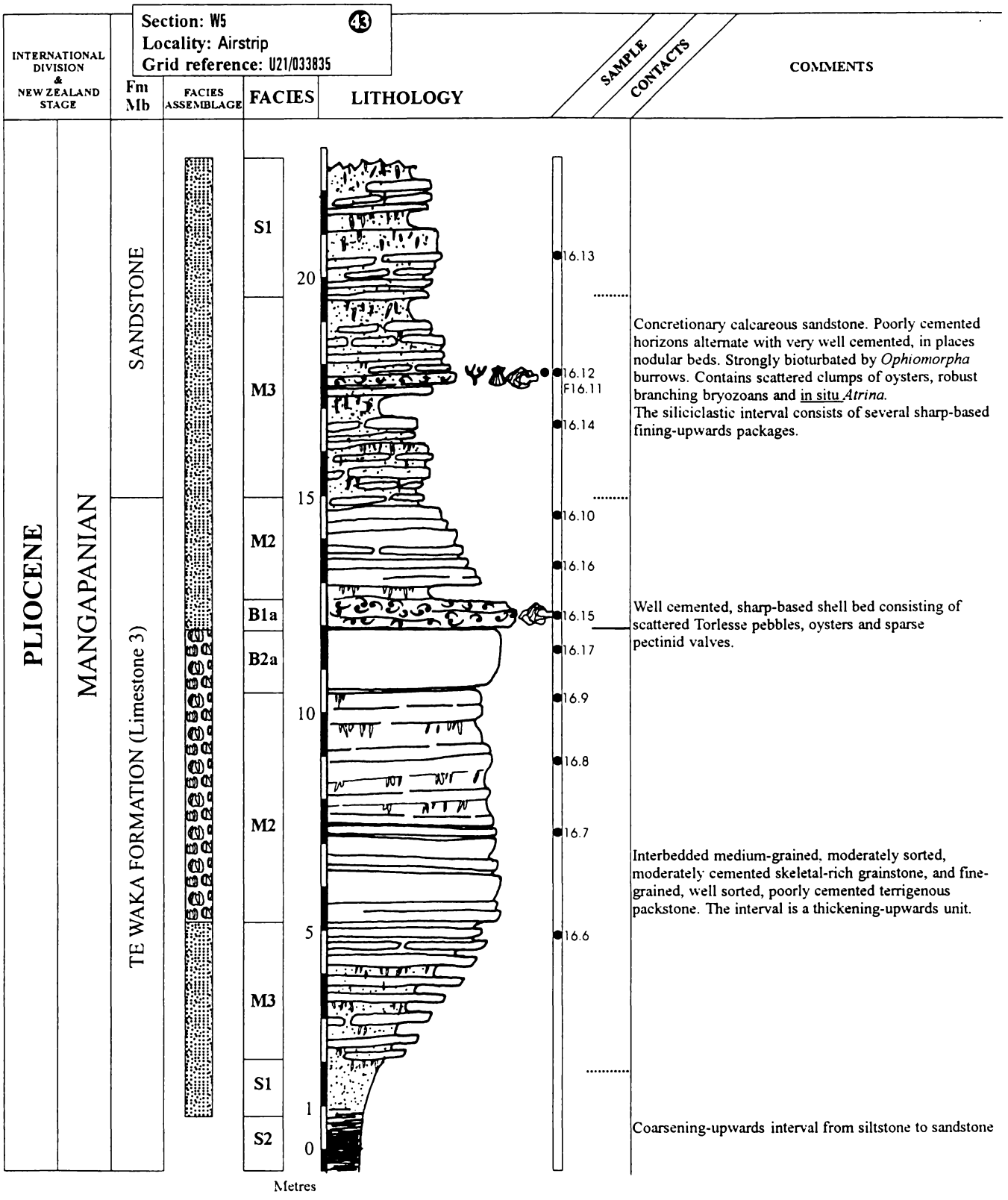
Section: W5
Locality: Airstrip
Grid reference: U21/033835
INTERNATIONAL DIVISION & NEW ZEALAND STAGE
Fm Mb
FACIES ASSEMBLAGE
FACIES
LITHOLOGY
SAMPLE
CONTACTS
COMMENTS
PLIOCENE
MANGAPANIAN
SANDSTONE
TE WAKA FORMATION (Limestone 3)
S1
M3
M2
B1a
B2a
M2
M3
S1
S2
20
15
10
5
1
0
Metres
16.13
16.12
F16.11
16.14
16.10
16.16
16.15
16.17
16.9
16.8
16.7
16.6
Concretionary calcareous sandstone. Poorly cemented horizons alternate with very well cemented, in places nodular beds. Strongly bioturbated by *Ophiomorpha* burrows. Contains scattered clumps of oysters, robust branching bryozoans and in situ *Atrina*.
The siliciclastic interval consists of several sharp-based fining-upwards packages.
Well cemented, sharp-based shell bed consisting of scattered Torlesse pebbles, oysters and sparse pectinid valves.
Interbedded medium-grained, moderately sorted, moderately cemented skeletal-rich grainstone, and fine-grained, well sorted, poorly cemented terrigenous packstone. The interval is a thickening-upwards unit.
Coarsening-upwards interval from siltstone to sandstone

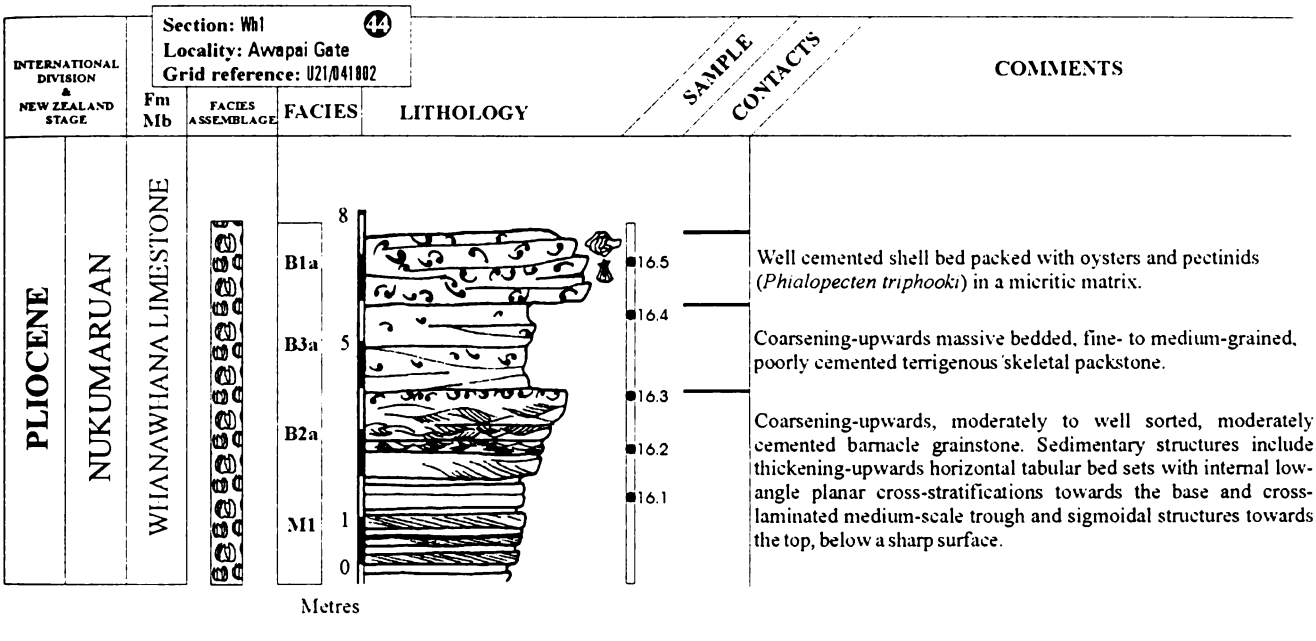
Section: Wh1
Locality: Awapai Gate
Grid reference: U21/041802
44
INTERNATIONAL DIVISION
NEW ZEALAND STAGE
Fm
Mb
FACIES ASSEMBLAGE
FACIES
LITHOLOGY
SAMPLE
CONTACTS
COMMENTS
PLIOCENE
NUKUMARUAN
WHANAWHANA LIMESTONE
B1a
B3a
B2a
M1
8
5
1
0
16.5
16.4
16.3
16.2
16.1
Well cemented shell bed packed with oysters and pectinids (*Phialopecten triphooki*) in a micritic matrix.
Coarsening-upwards massive bedded, fine- to medium-grained, poorly cemented terrigenous skeletal packstone.
Coarsening-upwards, moderately to well sorted, moderately cemented barnacle grainstone. Sedimentary structures include thickening-upwards horizontal tabular bed sets with internal low-angle planar cross-stratifications towards the base and cross-laminated medium-scale trough and sigmoidal structures towards the top, below a sharp surface.
Metres

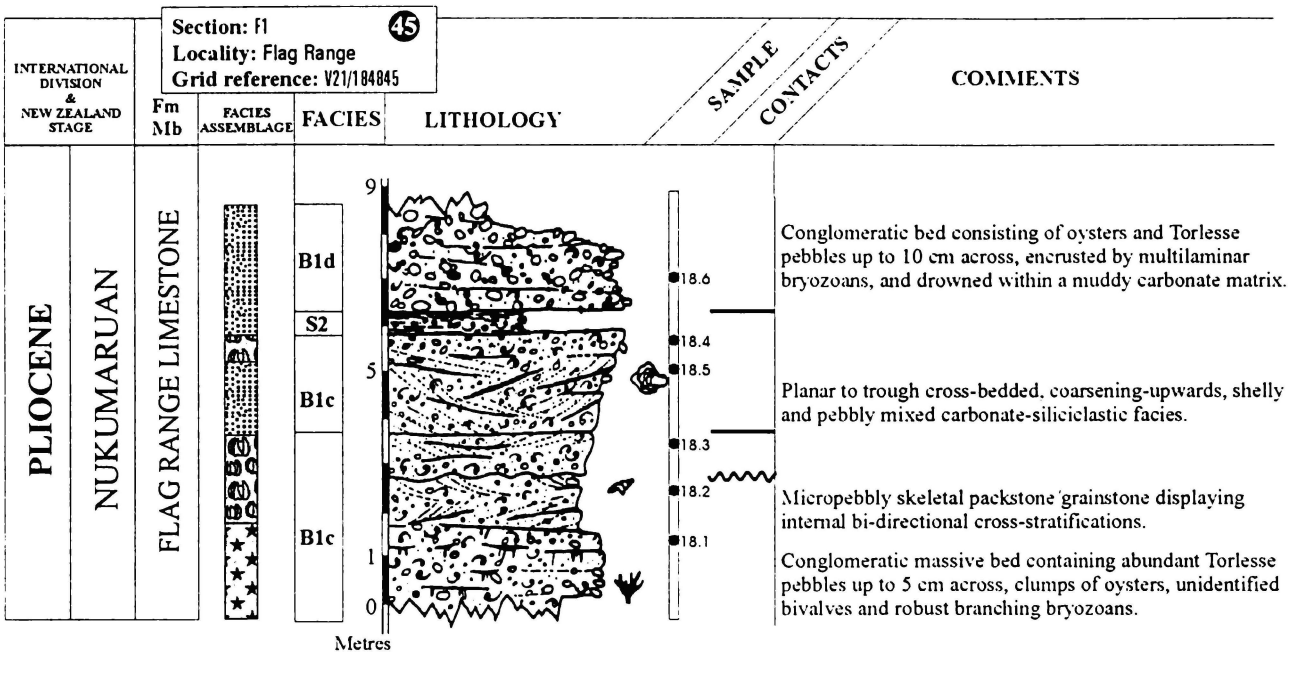
Section: f1
45
Locality: Flag Range
Grid reference: V21/184845
INTERNATIONAL DIVISION & NEW ZEALAND STAGE
Fm Mb
FACIES ASSEMBLAGE
FACIES
LITHOLOGY
SAMPLE
CONTACTS
COMMENTS
PLIOCENE
NUKUMARUAN
FLAG RANGE LIMESTONE
B1d
S2
B1c
B1c
9
5
1
0
Metres
18.6
18.4
18.5
18.3
18.2
18.1
Conglomeratic bed consisting of oysters and Torlesse pebbles up to 10 cm across, encrusted by multilaminar bryozoans, and drowned within a muddy carbonate matrix.
Planar to trough cross-bedded, coarsening-upwards, shelly and pebbly mixed carbonate-siliciclastic facies.
Micropebbly skeletal packstone/grainstone displaying internal bi-directional cross-stratifications.
Conglomeratic massive bed containing abundant Torlesse pebbles up to 5 cm across, clumps of oysters, unidentified bivalves and robust branching bryozoans.

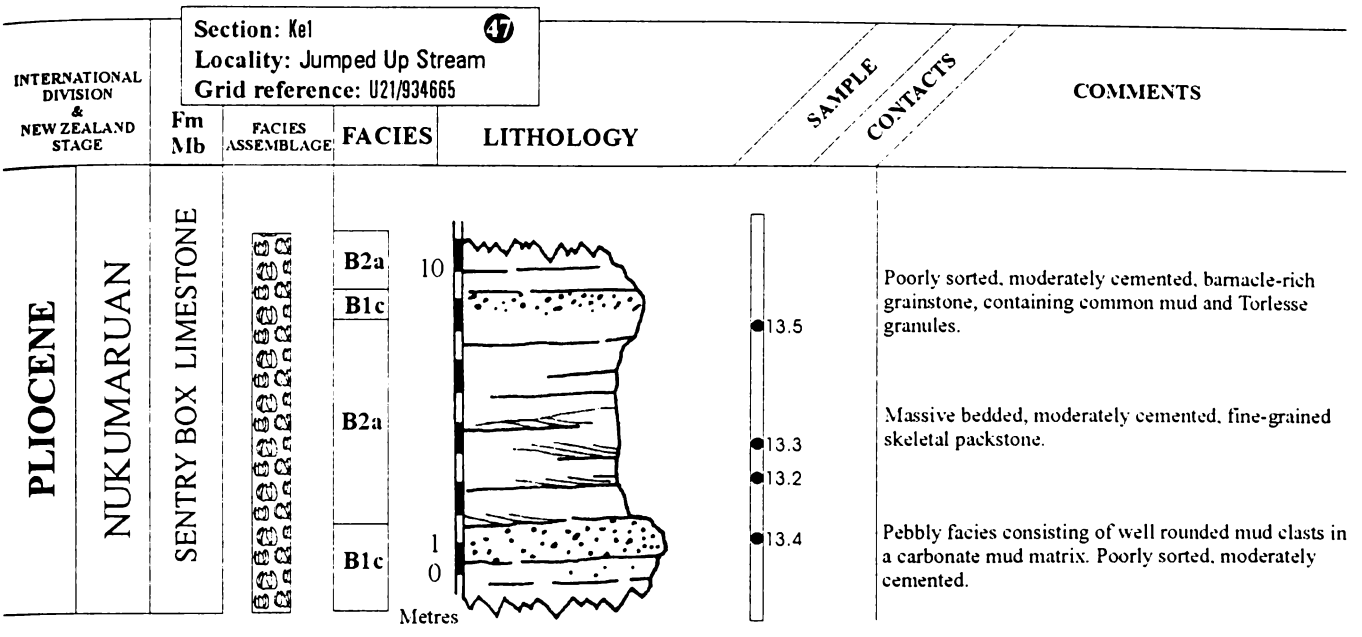
Section: Kel
47
Locality: Jumped Up Stream
Grid reference: U21/934665
INTERNATIONAL DIVISION & NEW ZEALAND STAGE
Fm Mb
FACIES ASSEMBLAGE
FACIES
LITHOLOGY
SAMPLE
CONTACTS
COMMENTS
PLIOCENE
NUKUMARUAN
SENTRY BOX LIMESTONE
B2a
B1c
B2a
B1c
10
1
0
Metres
13.5
13.3
13.2
13.4
Poorly sorted, moderately cemented, barnacle-rich grainstone, containing common mud and Torlesse granules.
Massive bedded, moderately cemented, fine-grained skeletal packstone.
Pebbly facies consisting of well rounded mud clasts in a carbonate mud matrix. Poorly sorted, moderately cemented.

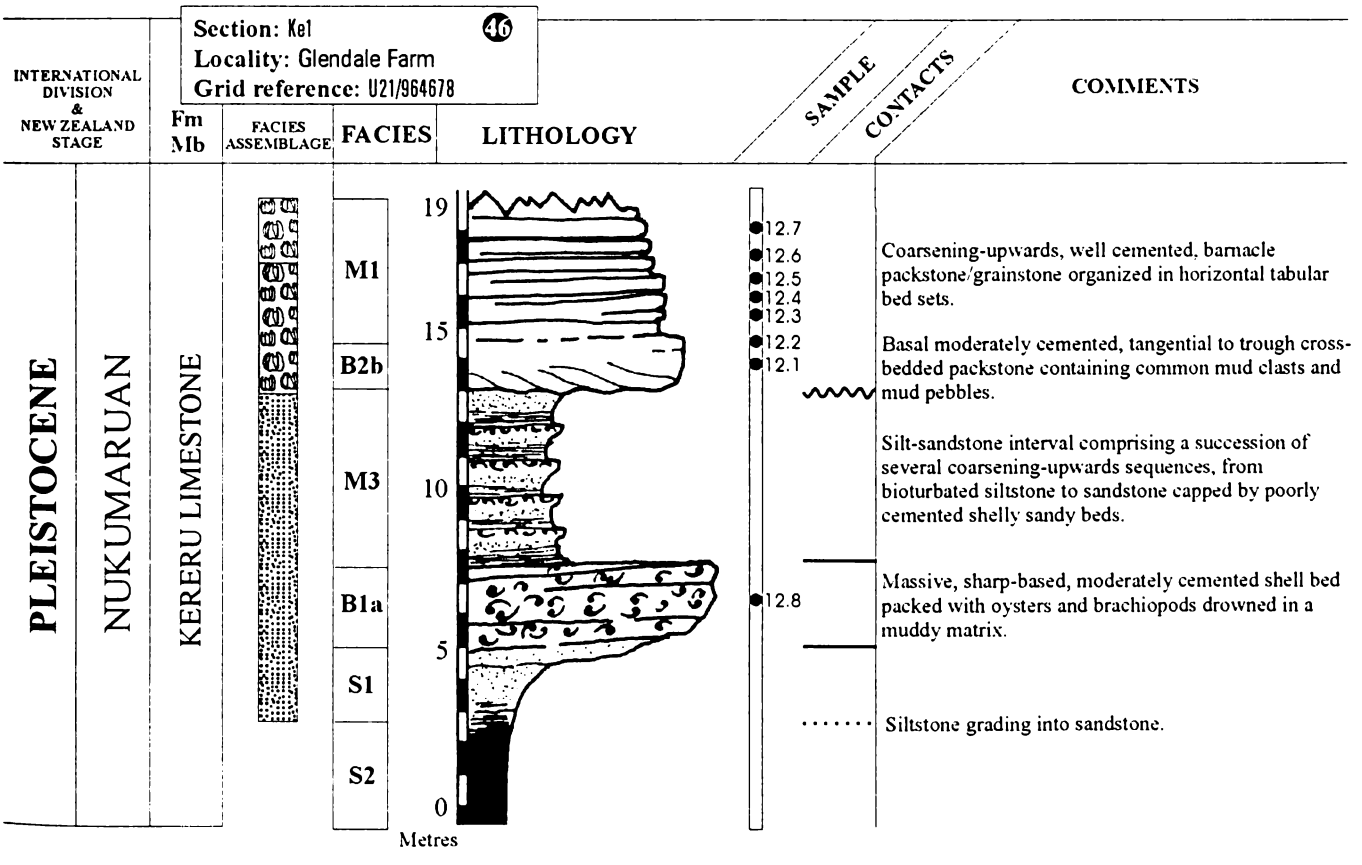
Section: Kel
46
Locality: Glendale Farm
Grid reference: U21/964678
INTERNATIONAL DIVISION & NEW ZEALAND STAGE
Fm Mb
FACIES ASSEMBLAGE
FACIES
LITHOLOGY
SAMPLE
CONTACTS
COMMENTS
PLEISTOCENE
NUKUMARUAN
KERERU LIMESTONE
M1
B2b
M3
B1a
S1
S2
19
15
10
5
0
Metres
12.7
12.6
12.5
12.4
12.3
12.2
12.1
12.8
Coarsening-upwards, well cemented, barnacle packstone/grainstone organized in horizontal tabular bed sets.
Basal moderately cemented, tangential to trough cross-bedded packstone containing common mud clasts and mud pebbles.
Silt-sandstone interval comprising a succession of several coarsening-upwards sequences, from bioturbated siltstone to sandstone capped by poorly cemented shelly sandy beds.
Massive, sharp-based, moderately cemented shell bed packed with oysters and brachiopods drowned in a muddy matrix.
Siltstone grading into sandstone.

APPENDIX 2

SAMPLE LIST
MACROFAUNA

APPENDIX 2 - SAMPLE LIST

Waikato no.	Field no.	Thin section no.	Section/locality	Column	Grid reference		Formation	Stage
					East	North		
w02-0001	1.1	cv-99-1.1	Te Pohue	38	2827500	6211500	Te Waka Fm.	Wm
w02-0002	1.2	cv-99-1.2	Te Pohue	38	2827500	6211500	Te Waka Fm.	Wm
w02-0003	1.3	cv-99-1.3	Te Pohue	38	2827500	6211500	Te Waka Fm.	Wm
w02-0004	1.4	cv-99-1.4	Te Pohue	38	2827500	6211500	Te Waka Fm.	Wm
w02-0005	1.5	cv-99-1.5	Te Pohue	38	2827500	6211500	Te Waka Fm.	Wm
w02-0006	2.1	cv-99-2.1	Te Pohue	38	2827500	6211500	Titiokura Fm.	Wp
w02-0007	2.2	cv-99-2.2	Te Pohue	38	2827500	6211500	Titiokura Fm.	Wp
w02-0008	2.3	cv-99-2.3	Te Pohue	38	2827500	6211500	Titiokura Fm.	Wp
w02-0009	2.4	cv-99-2.4	Te Pohue	38	2827500	6211500	Titiokura Fm.	Wp
w02-0010	2.5	cv-99-2.5	Te Pohue	38	2827500	6211500	Titiokura Fm.	Wp
w02-0011	2.6	cv-99-2.6	Te Pohue	38	2827500	6211500	Titiokura Fm.	Wp
w02-0012	2.7	cv-99-2.7	Te Pohue	38	2827500	6211500	Titiokura Fm.	Wp
w02-0013	2.8	cv-99-2.8	Te Pohue	38	2827500	6211500	Titiokura Fm.	Wp
w02-0014	3.1	cv-99-3.1	Kahuranaki		2842200	6150700	Awapapa Lst.	Wp
w02-0015	3.2	cv-99-3.2	Kahuranaki		2842200	6150700	Awapapa Lst.	Wp
w02-0016	4.1	cv-99-4.1	North Mt Kahuranaki	7	2841800	6150900	Kairakau Lst.	Wo
w02-0017	4.2	cv-99-4.2	North Mt Kahuranaki	7	2841800	6150900	Kairakau Lst.	Wo
w02-0018	4.3	cv-99-4.3	North Mt Kahuranaki	7	2841800	6150900	Kairakau Lst.	Wo
w02-0019	4.4	cv-99-4.4	North Mt Kahuranaki	7	2841800	6150900	Kairakau Lst.	Wo
w02-0020	4.5	cv-99-4.5	North Mt Kahuranaki	7	2841800	6150900	Kairakau Lst.	Wo
w02-0021	4.6	cv-99-4.6	North Mt Kahuranaki	7	2841800	6150900	Kairakau Lst.	Wo
w02-0022	4.7	cv-99-4.7	North Mt Kahuranaki	7	2841800	6150900	Kairakau Lst.	Wo
w02-0023	4.8		North Mt Kahuranaki	7	2841800	6150900	Kairakau Lst.	Wo
w02-0024	4.9	cv-99-4.9	North Mt Kahuranaki	7	2842300	6151500	Kairakau Lst.	Wo
w02-0025	4.10.	cv-99-4.10	North Mt Kahuranaki	7	2842300	6151500	Kairakau Lst.	Wo
w02-0026	4.11	cv-99-4.11	North Mt Kahuranaki	7	2842300	6151500	Kairakau Lst.	Wo
w02-0027	4.12	cv-99-4.12	North Mt Kahuranaki	7	2842300	6151500	Kairakau Lst.	Wo
w02-0028	4.13	cv-99-4.13	North Mt Kahuranaki	7	2842300	6151500	Kairakau Lst.	Wo
w02-0029	4.14	cv-99-4.14	North Mt Kahuranaki	7	2842300	6151500	Kairakau Lst.	Wo
w02-0030	4.15	cv-99-4.15	North Mt Kahuranaki	7	2842300	6151500	Kairakau Lst.	Wo
w02-0031	4.16	cv-99-4.16	North Mt Kahuranaki	7	2842300	6151500	Kairakau Lst.	Wo
w02-0032	4.17	cv-99-4.17	North Mt Kahuranaki	7	2842300	6151500	Kairakau Lst.	Wo
w02-0033	4.18	cv-99-4.18	North Mt Kahuranaki	7	2842300	6151500	Kairakau Lst.	Wo
w02-0034	4.19	cv-99-4.19	North Mt Kahuranaki	7	2842300	6151500	Kairakau Lst.	Wo
w02-0035	4.20.	cv-99-4.20	North Mt Kahuranaki	7	2842300	6151500	Kairakau Lst.	Wo
w02-0036	4.21	cv-99-4.21	North Mt Kahuranaki	7	2842300	6151500	Kairakau Lst.	Wo
w02-0037	4.22	cv-99-4.22	North Mt Kahuranaki	7	2842300	6151500	Kairakau Lst.	Wo
w02-0038	4.24	cv-99-4.24	North Mt Kahuranaki	7	2842300	6151500	Kairakau Lst.	Wo
w02-0039	4.25	cv-99-4.25	North Mt Kahuranaki	7	2842300	6151500	Kairakau Lst.	Wo
w02-0040	4.26	cv-99-4.26	North Mt Kahuranaki	7	2842300	6151500	Kairakau Lst.	Wo
w02-0041	4.27	cv-99-4.27	North Mt Kahuranaki	7	2842300	6151500	Kairakau Lst.	Wo
w02-0042	4.28	cv-99-4.28	North Mt Kahuranaki	7	2842300	6151500	Kairakau Lst.	Wo
w02-0043	4.29	cv-99-4.29	North Mt Kahuranaki	7	2842300	6151500	Kairakau Lst.	Wo
w02-0044	4.30.	cv-99-4.30	North Mt Kahuranaki	7	2842300	6151500	Kairakau Lst.	Wo
w02-0045	4.31	cv-99-4.31	North Mt Kahuranaki	7	2842300	6151500	Kairakau Lst.	Wo
w02-0046	4.32	cv-99-4.32	Mangangara	8	2842600	6155800	Kairakau Lst.	Wo
w02-0047	4.33	cv-99-4.33	Mangangara	8	2842600	6155800	Kairakau Lst.	Wo
w02-0048	4.34	cv-99-4.34	Mangangara	8	2842600	6155800	Kairakau Lst.	Wo
w02-0049	4.35	cv-99-4.35	Mangangara	8	2842600	6155800	Kairakau Lst.	Wo
w02-0050	4.36	cv-99-4.36	Mangangara	8	2842600	6155800	Kairakau Lst.	Wo
w02-0051	4.37	cv-99-4.37	Mangangara	8	2842600	6155800	Kairakau Lst.	Wo
w02-0052	4.38	cv-99-4.38	Mangangara	8	2842600	6155800	Kairakau Lst.	Wo
w02-0053	4.39	cv-99-4.39	Mangangara	8	2842600	6155800	Kairakau Lst.	Wo
w02-0054	4.40.	cv-99-4.40	Mangangara	8	2842600	6155800	Kairakau Lst.	Wo
w02-0055	4.41	cv-99-4.41	Waimaramal	10	2846300	6161500	Kairakau Lst.	Wo
w02-0056	4.42	cv-99-4.42	Waimaramal	10	2846300	6161500	Kairakau Lst.	Wo
w02-0057	4.43	cv-99-4.43	Waimaramal	10	2846300	6161500	Kairakau Lst.	Wo
w02-0058	4.44	cv-99-4.44	Waimaramal	10	2846300	6161500	Kairakau Lst.?	Wo
w02-0059	4.45	cv-99-4.45	Waimaramal	10	2846300	6161500	Kairakau Lst.?	Wo
w02-0060	4.46	cv-99-4.46	Waimaramal	10	2846300	6161500	Kairakau Lst.?	Wo
w02-0061	4.47	cv-99-4.47	Waimaramal	10	2846300	6161500	Kairakau Lst.?	Wo
w02-0062	4.48	cv-99-4.48	Waimaramal	10	2846300	6161500	Kairakau Lst.?	Wo
w02-0063	4.49	cv-99-4.49	Waimaramal	10	2846300	6161500	Kairakau Lst.?	Wo

APPENDIX 2 - SAMPLE LIST

Waikato no.	Field no.	Thin section no.	Section/locality	Column	Grid reference		Formation	Stage
					East	North		
w02-0064	4.50.	cv-99-4.50	Waimarama1	10	2846300	6161500	Kairakau Lst.?	Wo
w02-0065	4.51	cv-99-4.51	Waimarama1	10	2846300	6161500	Kairakau Lst.?	Wo
w02-0066	4.52	cv-99-4.52	Waimarama2		2845500	6160700	Kairakau Lst.	Wo
w02-0067	4.53	cv-99-4.53	Waimarama2		2845500	6160700	Kairakau Lst.	Wo
w02-0068	4.54	cv-99-4.54	Waimarama2		2845500	6160700	Kairakau Lst.	Wo
w02-0069	4.55	cv-99-4.55	Waimarama2		2845500	6160700	Kairakau Lst.	Wo
w02-0070	4.56	cv-99-4.56	Waimarama2		2845500	6160700	Kairakau Lst.	Wo
w02-0071	4.57	cv-99-4.57	Waimarama2		2845500	6160700	Kairakau Lst.	Wo
w02-0072	4.58	cv-99-4.58	Te Mata Peak	9	2845200	6159700	Kairakau Lst.	Wo
w02-0073	4.59	cv-99-4.59	Te Mata Peak	9	2845200	6159700	Kairakau Lst.	Wo
w02-0074	4.60.	cv-99-4.60	Te Mata Peak	9	2845200	6159700	Kairakau Lst.	Wo
w02-0075	4.61	cv-99-4.61	Te Mata Peak	9	2845200	6159700	Kairakau Lst.	Wo
w02-0076	4.62	cv-99-4.62	Te Mata Peak	9	2845200	6159700	Kairakau Lst.	Wo
w02-0077	4.63		Te Mata Peak	9	2845200	6159700	Kairakau Lst.	Wo
w02-0078	4.64	cv-99-4.64	Te Mata Peak	9	2845200	6159700	Kairakau Lst.	Wo
w02-0079	4.65	cv-99-4.65	Kairakau Beach	1	2845700	6133300	Kairakau Lst.	Wo
w02-0080	4.66	cv-99-4.66	Kairakau Beach	1	2845700	6133300	Kairakau Lst.	Wo
w02-0081	4.67	cv-99-4.67	Kairakau Beach	1	2845700	6133300	Kairakau Lst.	Wo
w02-0082	4.68	cv-99-4.68	Kairakau Beach	1	2845700	6133300	Kairakau Lst.	Wo
w02-0083	4.69	cv-99-4.69	Kairakau Beach	1	2845700	6133300	Kairakau Lst.	Wo
w02-0084	4.70.	cv-99-4.70	Kairakau Beach	1	2845700	6133300	Kairakau Lst.	Wo
w02-0085	4.71	cv-99-4.71	Kairakau Beach	1	2845700	6133300	Kairakau Lst.	Wo
w02-0086	4.72a	cv-99-4.72a	Kairakau Beach	1	2845700	6133300	Kairakau Lst.	Wo
w02-0087	4.72b	cv-99-4.72	Kairakau Beach	1	2845700	6133300	Kairakau Lst.	Wo
w02-0088	4.72c	cv-99-4.72c	Kairakau Beach	1	2845700	6133300	Kairakau Lst.	Wo
w02-0089	4.73		Kairakau Beach	1	2845700	6133300	Kairakau Lst.	Wo
w02-0090	4.74	cv-99-4.74	Kairakau Beach	1	2845700	6133300	Kairakau Lst.	Wo
w02-0091	4.75	cv-99-4.75	Kairakau Beach	1	2845700	6133300	Kairakau Lst.	Wo
w02-0092	4.76	cv-99-4.76	Kairakau Beach	1	2845700	6133300	Kairakau Lst.	Wo
w02-0093	4.77	cv-99-4.77	Kairakau Beach	1	2845700	6133300	Kairakau Lst.	Wo
w02-0094	4.78	cv-99-4.78	Taupata	3	2848400	6136600	Kairakau Lst.	Wo
w02-0095	4.79		Taupata	3	2848400	6136600	Kairakau Lst.	Wo
w02-0096	4.80.	cv-99-4.80	Taupata	3	2848400	6136600	Kairakau Lst.	Wo
w02-0097	4.81a	cv-99-4.81a	Taupata	3	2848400	6136600	Kairakau Lst.	Wo
w02-0098	4.81b	cv-99-4.81b	Taupata	3	2848400	6136600	Kairakau Lst.	Wo
w02-0099	4.82	cv-99-4.82	Taupata	3	2848400	6136600	Kairakau Lst.	Wo
w02-0100	4.83	cv-99-4.83	Taupata	3	2848400	6136600	Kairakau Lst.	Wo
w02-0101	4.84	cv-99-4.84	Taupata	3	2848400	6136600	Kairakau Lst.	Wo
w02-0102	4.85	cv-99-4.85	Taupata	3	2848400	6136600	Kairakau Lst.	Wo
w02-0103	4.86a	cv-99-4.86a	Taupata	3	2848400	6136600	Kairakau Lst.	Wo
w02-0104	4.86b	cv-99-4.86b	Taupata	3	2848400	6136600	Kairakau Lst.	Wo
w02-0105	4.87		Taupata	3	2848400	6136600	Kairakau Lst.	Wo
w02-0106	4.88	cv-99-4.88	Apiti		2848100	6136200	Kairakau Lst.	Wo
w02-0107	4.89	cv-99-4.89	Apiti		2848100	6136200	Kairakau Lst.	Wo
w02-0108	4.90a	cv-99-4.90a	Apiti		2848100	6136200	Kairakau Lst.	Wo
w02-0109	4.90b	cv-99-4.90b	Apiti		2848100	6136200	Kairakau Lst.	Wo
w02-0110	4.91	cv-99-4.91	Apiti		2848100	6136200	Kairakau Lst.	Wo
w02-0111	4.92	cv-99-4.92	Apiti		2848100	6136200	Kairakau Lst.	Wo
w02-0112	4.93	cv-99-4.93	Waimoana	2	2846000	6133900	Kairakau Lst.	Wo
w02-0113	4.94	cv-99-4.94	Waimoana	2	2846000	6133900	Kairakau Lst.	Wo
w02-0114	4.95	cv-99-4.95	Waimoana	2	2846000	6133900	Kairakau Lst.	Wo
w02-0115	4.96	cv-99-4.96	Koanui	5	2846000	6150400	Kairakau Lst.	Wo
w02-0116	4.97	cv-99-4.97	Koanui	5	2846000	6150400	Kairakau Lst.	Wo
w02-0117	4.98	cv-99-4.98	Koanui	5	2846000	6150400	Kairakau Lst.	Wo
w02-0118	4.99	cv-99-4.99	Koanui	5	2846000	6150400	Kairakau Lst.	Wo
w02-0118	4.100.	cv-99-4.100	Koanui	5	2846000	6150400	Kairakau Lst.	Wo
w02-0119	4.101	cv-99-4.101	Koanui	5	2846000	6150400	Kairakau Lst.	Wo
w02-0120	4.102	cv-99-4.102	Koanui	5	2846000	6150400	Kairakau Lst.	Wo
w02-0121	4.103	cv-99-4.103	Koanui	5	2846000	6150400	Kairakau Lst.	Wo
w02-0122	4.104	cv-99-4.104	Koanui	5	2846000	6150400	Kairakau Lst.	Wo
w02-0123	4.105	cv-99-4.105	Koanui	5	2846000	6150400	Kairakau Lst.	Wo
w02-0124	4.106	cv-99-4.106	Red Shed		2846200	6150100	Kairakau Lst.	Wo

APPENDIX 2 - SAMPLE LIST

Waikato no.	Field no.	Thin section no.	Section/locality	Column	Grid reference		Formation	Stage
					East	North		
w02-0125	4.107a	cv-99-4.107a	Red Shed		2846200	6150100	Kairakau Lst.	Wo
w02-0126	4.107b	cv-99-4.107b	Red Shed		2846200	6150100	Kairakau Lst.	Wo
w02-0127	4.108	cv-99-4.108	Red Shed		2846200	6150100	Kairakau Lst.	Wo
w02-0128	4.109	cv-99-4.109	Red Shed		2846200	6150100	Kairakau Lst.	Wo
w02-0129	4.110.	cv-99-4.110	Red Shed		2846200	6150100	Kairakau Lst.	Wo
w02-0130	4.111	cv-99-4.111	Red Shed		2846200	6150100	Kairakau Lst.	Wo
w02-0131	4.112	cv-99-4.112	Red Shed		2846200	6150100	Kairakau Lst.	Wo
w02-0132	4.113	cv-99-4.113	Red Shed		2846200	6150100	Kairakau Lst.	Wo
w02-0133	4.114	cv-99-4.114	Tawa Hills		2840700	6142700	Kairakau Lst.	Wo
w02-0134	4.115	cv-99-4.115	Tawa Hills		2840700	6142700	Kairakau Lst.	Wo
w02-0135	4.116		Tawa Hills		2840700	6142700	Kairakau Lst.	Wo
w02-0136	4.117	cv-99-4.117	Tawa Hills		2840700	6142700	Kairakau Lst.	Wo
w02-0137	4.118	cv-99-4.118	Tawa Hills		2840700	6142700	Kairakau Lst.	Wo
w02-0138	4.119	cv-99-4.119	Tawa Hills		2840700	6142700	Kairakau Lst.	Wo
w02-0139	4.120.	cv-99-4.120	Tawa Hills		2840700	6142700	Kairakau Lst.	Wo
w02-0140	4.121	cv-99-4.121	Tawa Hills		2840700	6142700	Kairakau Lst.	Wo
w02-0141	4.122	cv-99-4.122	Tawa Hills		2840700	6142700	Kairakau Lst.	Wo
w02-0142	4.123	cv-99-4.123	Tawa Hills		2840700	6142700	Kairakau Lst.	Wo
w02-0143	4.124	cv-99-4.124	Mohi Reserve		2844200	6142400	Kairakau Lst.	Wo
w02-0144	4.125	cv-99-4.125	Cabbage Tree Flat	4	2849200	6146700	Kairakau Lst.	Wo
w02-0145	4.126	cv-99-4.126	Cabbage Tree Flat	4	2849200	6146700	Kairakau Lst.	Wo
w02-0146	4.127	cv-99-4.127	Cabbage Tree Flat	4	2849200	6146700	Kairakau Lst.	Wo
w02-0147	4.128	cv-99-4.128	Cabbage Tree Flat	4	2849200	6146700	Kairakau Lst.	Wo
w02-0148	4.129	cv-99-4.129	Cabbage Tree Flat	4	2849200	6146700	Kairakau Lst.	Wo
w02-0149	4.130.	cv-99-4.130	Cabbage Tree Flat	4	2849200	6146700	Kairakau Lst.	Wo
w02-0150	4.131	cv-99-4.131	Cabbage Tree Flat	4	2849200	6146700	Kairakau Lst.	Wo
w02-0151	4.132	cv-99-4.132	Cabbage Tree Flat	4	2849200	6146700	Kairakau Lst.	Wo
w02-0152	4.133	cv-99-4.133	Cabbage Tree Flat	4	2849200	6146700	Kairakau Lst.	Wo
w02-0153	4.134	cv-99-4.134	Tuki Bell	11	2832300	6148200	Kairakau Lst.	Wo
w02-0154	4.135	cv-99-4.135	Tuki Bell	11	2832300	6148200	Kairakau Lst.	Wo
w02-0155	4.136	cv-99-4.136	Tuki Bell	11	2832300	6148200	Kairakau Lst.	Wo
w02-0156	4.137	cv-99-4.137	Tuki Bell	11	2832300	6148200	Kairakau Lst.	Wo
w02-0157	4.138	cv-99-4.138	Tuki Bell	11	2832300	6148200	Kairakau Lst.	Wo
w02-0158	4.139	cv-99-4.139	Tuki Bell	11	2832300	6148200	Kairakau Lst.	Wo
w02-0159	4.140.	cv-99-4.140	Tuki Bell	11	2832300	6148200	Kairakau Lst.	Wo
w02-0160	4.141	cv-99-4.141	Waimoana	2	2846000	6133900	Kairakau Lst.	Wo
w02-0161	4.142		Waimoana	2	2846000	6133900	Kairakau Lst.	Wo
w02-0162	4.143		Waimoana	2	2846000	6133900	Kairakau Lst.	Wo
w02-0163	4.144		Waimarama Road		2846400	6161500	Kairakau Lst.	Wo
w02-0164	4.145	cv-99-4.145	Waimarama Road		2846400	6161500	Kairakau Lst.	Wo
w02-0165	4.146		Waimarama Road		2846400	6161500	Kairakau Lst.	Wo
w02-0166	4.147		Waimarama Road		2846400	6161500	Kairakau Lst.	Wo
w02-0167	5.1	cv-99-5.1	Webster's Quarry		2838500	6158800	Awapapa Lst.	Wp
w02-0168	5.2	cv-99-5.2	Webster's Quarry		2838500	6158800	Awapapa Lst.	Wp
w02-0169	5.3	cv-99-5.3	Webster's Quarry		2838500	6158800	Awapapa Lst.	Wp
w02-0170	5.4	cv-99-5.4	Webster's Quarry		2838500	6158800	Awapapa Lst.	Wp
w02-0171	5.5	cv-99-5.5	Te Mata Peak1	9	2845300	6160600	Awapapa Lst.	Wp
w02-0172	5.6	cv-99-5.6	Te Mata Peak1	9	2845300	6160600	Awapapa Lst.	Wp
w02-0173	5.7	cv-99-5.7	Te Mata Peak1	9	2845300	6160600	Awapapa Lst.	Wp
w02-0174	5.8	cv-99-5.8	Te Mata Peak1	9	2845300	6160600	Awapapa Lst.	Wp
w02-0175	5.9	cv-99-5.9	Te Mata Peak1	9	2845300	6160600	Awapapa Lst.	Wp
w02-0176	5.10.	cv-99-5.10	Te Mata Peak1	9	2845300	6160600	Awapapa Lst.	Wp
w02-0177	5.11		Te Mata Peak2	9	2845300	6160600	Awapapa Lst.	Wp
w02-0178	5.12	cv-99-5.12	Te Mata Peak1	9	2845300	6160600	Awapapa Lst.	Wp
w02-0179	5.13		Te Mata Peak1	9	2845300	6160600	Awapapa Lst.	Wp
w02-0180	5.14	cv-99-5.14	Te Mata Peak2	9	2845300	6160600	Awapapa Lst.	Wp
w02-0181	5.15		Te Mata Peak1	9	2845300	6160600	Awapapa Lst.	Wp
w02-0182	5.16	cv-99-5.16	Te Mata Peak1	9	2845300	6160600	Awapapa Lst.	Wp
w02-0183	5.17	cv-99-5.17	Te Mata Peak1	9	2845300	6160600	Awapapa Lst.	Wp
w02-0184	5.18	cv-99-5.18	Te Mata Peak1	9	2845300	6160600	Awapapa Lst.	Wp
w02-0185	5.19	cv-99-5.19	Te Mata Peak1	9	2845300	6160600	Awapapa Lst.	Wp
w02-0186	5.20.	cv-99-5.20	Te Mata Peak1	9	2845300	6160600	Awapapa Lst.	Wp

APPENDIX 2 - SAMPLE LIST

Waikato no.	Field no.	Thin section no.	Section/locality	Column	Grid reference		Formation	Stage
					East	North		
w02-0187	5.21	cv-99-5.21	Te Mata Peak1	9	2845300	6160600	Awapapa Lst.	Wp
w02-0188	5.22	cv-99-5.22	Te Mata Peak1	9	2845300	6160600	Awapapa Lst.	Wp
w02-0189	5.23	cv-99-5.23	Te Mata Peak1	9	2845300	6160600	Awapapa Lst.	Wp
w02-0190	5.24	cv-99-5.24	Te Mata Peak1	9	2845300	6160600	Awapapa Lst.	Wp
w02-0191	5.25	cv-99-5.25	Te Mata Peak1	9	2845300	6160600	Awapapa Lst.	Wp
w02-0192	5.26		Te Mata Peak2	9	2845300	6160600	Awapapa Lst.	Wp
w02-0193	5.27		Te Mata Peak2	9	2845300	6160600	Awapapa Lst.	Wp
w02-0194	5.28	cv-99-5.28	Te Mata Peak2	9	2845100	6160200	Awapapa Lst.	Wp
w02-0195	5.29		Te Mata Peak2	9	2845100	6160200	Awapapa Lst.	Wp
w02-0196	5.30.	cv-99-5.30	Te Mata Peak2	9	2845100	6160200	Awapapa Lst.	Wp
w02-0197	5.31	cv-99-5.31	Te Mata Peak2	9	2845100	6160200	Awapapa Lst.	Wp
w02-0198	5.32a	cv-99-5.32a	Te Mata Peak2	9	2845100	6160200	Awapapa Lst.	Wp
w02-0199	5.32b	cv-99-5.32b	Te Mata Peak2	9	2845100	6160200	Awapapa Lst.	Wp
w02-0200	5.32c	cv-99-5.32c	Te Mata Peak2	9	2845100	6160200	Awapapa Lst.	Wp
w02-0201	5.33		Te Mata Peak2	9	2845100	6160200	Awapapa Lst.	Wp
w02-0202	5.34	cv-99-5.34	Te Mata Peak2	9	2845100	6160200	Awapapa Lst.	Wp
w02-0203	5.35		Te Mata Peak2	9	2845100	6160200	Awapapa Lst.	Wp
w02-0204	5.36		Te Mata Peak2	9	2845100	6160200	Awapapa Lst.	Wp
w02-0205	5.37		Te Mata Peak2	9	2845100	6160200	Awapapa Lst.	Wp
w02-0206	5.38	cv-99-5.38	Te Mata Peak2	9	2845100	6160200	Awapapa Lst.	Wp
w02-0207	5.39		Te Mata Peak2	9	2845100	6160200	Awapapa Lst.	Wp
w02-0208	5.40.		Te Mata Peak2	9	2845100	6160200	Awapapa Lst.	Wp
w02-0209	5.41		Te Mata Peak2	9	2845100	6160200	Awapapa Lst.	Wp
w02-0210	5.42		Te Mata Peak2	9	2845100	6160200	Awapapa Lst.	Wp
w02-0211	5.43		Te Mata Peak2	9	2845100	6160200	Awapapa Lst.	Wp
w02-0212	5.44	cv-99-5.44	Te Mata Peak2	9	2845100	6160200	Awapapa Lst.	Wp
w02-0213	5.45a	cv-99-5.45a	Te Mata Peak2	9	2845100	6160200	Awapapa Lst.	Wp
w02-0214	5.45b	cv-99-5.45b	Te Mata Peak2	9	2845100	6160200	Awapapa Lst.	Wp
w02-0215	5.46a	cv-99-5.46a	Te Mata Peak2	9	2845100	6160200	Awapapa Lst.	Wp
w02-0216	5.46b	cv-99-5.46b	Te Mata Peak2	9	2845100	6160200	Awapapa Lst.	Wp
w02-0217	5.47	cv-99-5.47	Te Mata Peak2	9	2845100	6160200	Awapapa Lst.	Wp
w02-0218	5.48	cv-99-5.48	Te Mata Peak2	9	2845100	6160200	Awapapa Lst.	Wp
w02-0219	5.49	cv-99-5.49	Te Mata Peak2	9	2845100	6160200	Awapapa Lst.	Wp
w02-0220	5.50.		Te Mata Peak2	9	2845100	6160200	Awapapa Lst.	Wp
w02-0221	5.51	cv-99-5.51	Te Mata Peak2	9	2845100	6160200	Awapapa Lst.	Wp
w02-0222	5.52	cv-99-5.52	Te Mata Peak2	9	2845100	6160200	Awapapa Lst.	Wp
w02-0223	5.53	cv-99-5.53	Te Mata Peak2	9	2845100	6160200	Awapapa Lst.	Wp
w02-0224	5.54	cv-99-5.54	Te Mata Peak2	9	2845100	6160200	Awapapa Lst.	Wp
w02-0225	5.55	cv-99-5.55	Rowe Road	14	2833400	6148800	Awapapa Lst.	Wp
w02-0226	5.56	cv-99-5.56	Rowe Road	14	2833400	6148800	Awapapa Lst.	Wp
w02-0227	5.57		Rowe Road	14	2833400	6148800	Awapapa Lst.	Wp
w02-0228	5.58		Rowe Road	14	2833400	6148800	Awapapa Lst.	Wp
w02-0229	5.59	cv-99-5.59	Rowe Road	14	2833400	6148800	Awapapa Lst.	Wp
w02-0230	5.60.		Rowe Road	14	2833400	6148800	Awapapa Lst.	Wp
w02-0231	5.61a	cv-99-5.61a	Rowe Road	14	2833400	6148800	Awapapa Lst.	Wp
w02-0232	5.61b	cv-99-5.61b	Rowe Road	14	2833400	6148800	Awapapa Lst.	Wp
w02-0233	5.62	cv-99-5.62	Rowe Road	14	2833400	6148800	Awapapa Lst.	Wp
w02-0234	5.63	cv-99-5.63	Rowe Road	14	2833400	6148800	Awapapa Lst.	Wp
w02-0235	5.64		Rowe Road	14	2833400	6148800	Awapapa Lst.	Wp
w02-0236	5.65	cv-99-5.65	Rowe Road	14	2833400	6148800	Awapapa Lst.	Wp
w02-0237	5.66	cv-99-5.66	Rowe Road	14	2833400	6148800	Awapapa Lst.	Wp
w02-0238	5.67		Rowe Road	14	2833400	6148800	Awapapa Lst.	Wp
w02-0239	5.68	cv-99-5.68	Rowe Road	14	2833400	6148800	Awapapa Lst.	Wp
w02-0240	5.69		Rowe Road	14	2833400	6148800	Awapapa Lst.	Wp
w02-0241	5.70.		Rowe Road	14	2833400	6148800	Awapapa Lst.	Wp
w02-0242	5.71a	cv-99-5.71a	Rowe Road	14	2833400	6148800	Awapapa Lst.	Wp
w02-0243	5.71b	cv-99-5.71b	Rowe Road	14	2833400	6148800	Awapapa Lst.	Wp
w02-0244	5.72	cv-99-5.72	Rowe Road	14	2833400	6148800	Awapapa Lst.	Wp
w02-0245	5.73	cv-99-5.73	River Bank	13	2833200	6148200	Awapapa Lst.	Wp
w02-0246	5.74	cv-99-5.74	River Bank	13	2833200	6148200	Awapapa Lst.	Wp
w02-0247	5.75	cv-99-5.75	River Bank	13	2833200	6148200	Awapapa Lst.	Wp
w02-0248	5.76	cv-99-5.76	River Bank	13	2833200	6148200	Awapapa Lst.	Wp

APPENDIX 2 - SAMPLE LIST

Waikato no.	Field no.	Thin section no.	Section/locality	Column	Grid reference		Formation	Stage
					East	North		
w02-0249	5.77	cv-99-5.77	River Bank	13	2833200	6148200	Awapapa Lst.	Wp
w02-0250	5.78	cv-99-5.78	River Bank	13	2833200	6148200	Awapapa Lst.	Wp
w02-0251	5.79a	cv-99-5.79a	River Bank	13	2833200	6148200	Awapapa Lst.	Wp
w02-0252	5.79b	cv-99-5.79b	River Bank	13	2833200	6148200	Awapapa Lst.	Wp
w02-0253	5.80.		River Bank	13	2833200	6148200	Awapapa Lst.	Wp
w02-0254	5.81	cv-99-5.81	River Bank	13	2833200	6148200	Awapapa Lst.	Wp
w02-0255	5.82	cv-99-5.82	River Bank	13	2833200	6148200	Awapapa Lst.	Wp
w02-0256	5.83	cv-99-5.83	River Bank	13	2833200	6148200	Awapapa Lst.	Wp
w02-0257	5.84	cv-99-5.84	River Bank	13	2833200	6148200	Awapapa Lst.	Wp
w02-0258	5.85	cv-99-5.85	River Bank	13	2833200	6148200	Awapapa Lst.	Wp
w02-0259	5.86	cv-99-5.86	River Bank	13	2833200	6148200	Awapapa Lst.	Wp
w02-0260	5.87	cv-99-5.87	Hawea	12	2834400	6146900	Awapapa Lst.	Wp
w02-0261	5.88	cv-99-5.88	Hawea	12	2834400	6146900	Awapapa Lst.	Wp
w02-0262	5.89	cv-99-5.89	Hawea	12	2834400	6146900	Awapapa Lst.	Wp
w02-0263	5.90.	cv-99-5.90	Hawea	12	2834400	6146900	Awapapa Lst.	Wp
w02-0264	5.91		Makara	16	2831800	6140500	Awapapa Lst.	Wp
w02-0265	5.92	cv-99-5.92	Makara	16	2831800	6140500	Awapapa Lst.	Wp
w02-0266	5.93	cv-99-5.93	Makara	16	2831800	6140500	Awapapa Lst.	Wp
w02-0267	5.94	cv-99-5.94	Makara	16	2831800	6140500	Awapapa Lst.	Wp
w02-0268	5.95	cv-99-5.95	Makara	16	2831800	6140500	Awapapa Lst.	Wp
w02-0269	5.96	cv-99-5.96	Makara	16	2831800	6140500	Awapapa Lst.	Wp
w02-0270	5.97	cv-99-5.97	Makara	16	2831800	6140500	Awapapa Lst.	Wp
w02-0271	5.98	cv-99-5.98	Makara	16	2831800	6140500	Awapapa Lst.	Wp
w02-0272	5.99	cv-99-5.99	Makara	16	2831800	6140500	Awapapa Lst.	Wp
w02-0273	5.100.	cv-99-5.100	Makara	16	2831800	6140500	Awapapa Lst.	Wp
w02-0274	5.101	cv-99-5.101	Makara	16	2831800	6140500	Awapapa Lst.	Wp
w02-0275	5.102	cv-99-5.102	Makara	16	2831800	6140500	Awapapa Lst.	Wp
w02-0276	5.103	cv-99-5.103	Makara	16	2831800	6140500	Awapapa Lst.	Wp
w02-0277	5.104		Makara	16	2831800	6140500	Awapapa Lst.	Wp
w02-0278	5.105	cv-99-5.105	Makara	16	2831800	6140500	Awapapa Lst.	Wp
w02-0279	5.106	cv-99-5.106	Makara	16	2831800	6140500	Awapapa Lst.	Wp
w02-0280	5.107		Pukekura	15	2829200	6147500	Kairakau Lst.?	Wo?
w02-0281	5.108		Pukekura	15	2829200	6147500	Kairakau Lst.?	Wo?
w02-0282	5.109		Pukekura	15	2829200	6147500	Kairakau Lst.?	Wo?
w02-0283	5.110.		Pukekura	15	2829200	6147500	Kairakau Lst.?	Wo?
w02-0284	5.111a	cv-99-5.111a	Pukekura	15	2829200	6147500	Kairakau Lst.?	Wo?
w02-0285	5.111b	cv-99-5.111b	Pukekura	15	2829200	6147500	Kairakau Lst.?	Wo?
w02-0286	5.112	cv-99-5.112	Pukekura	15	2829200	6147500	Kairakau Lst.?	Wo?
w02-0287	5.113	cv-99-5.113	Pukekura	15	2829200	6147500	Kairakau Lst.?	Wo?
w02-0288	5.114	cv-99-5.114	Pukekura	15	2829200	6147500	Kairakau Lst.?	Wo?
w02-0289	5.115		Pukekura	15	2829200	6147500	Kairakau Lst.?	Wo?
w02-0290	5.116	cv-99-5.116	Pukekura	15	2829200	6147500	Kairakau Lst.?	Wo?
w02-0291	5.117	cv-99-5.117	Pukekura	15	2829200	6147500	Kairakau Lst.?	Wo?
w02-0292	5.118	cv-99-5.118	Pukekura	15	2829200	6147500	Kairakau Lst.?	Wo?
w02-0293	5.119	cv-99-5.119	Pukekura	15	2829200	6147500	Kairakau Lst.?	Wo?
w02-0294	5.120.	cv-99-5.120	Pukekura	15	2829200	6147500	Kairakau Lst.?	Wo?
w02-0295	5.121		Pukekura	15	2829200	6147500	Kairakau Lst.?	Wo?
w02-0296	5.122	cv-99-5.122	Pukekura	15	2829200	6147500	Kairakau Lst.?	Wo?
w02-0297	5.123	cv-99-5.123	Pukekura	15	2829200	6147500	Kairakau Lst.?	Wo?
w02-0298	5.124	cv-99-5.124	Pukekura	15	2829200	6147500	Kairakau Lst.?	Wo?
w02-0299	5.125	cv-99-5.125	Pukekura	15	2829200	6147500	Kairakau Lst.?	Wo?
w02-0300	5.126		Pukekura	15	2829200	6147500	Kairakau Lst.?	Wo?
w02-0301	5.127	cv-99-5.127	Pukekura	15	2829200	6147500	Kairakau Lst.?	Wo?
w02-0302	5.128	cv-99-5.128	Pukekura	15	2829200	6147500	Awapapa Lst.	Wp
w02-0303	5.129	cv-99-5.129	Pukekura	15	2829200	6147500	Awapapa Lst.	Wp
w02-0304	5.130.	cv-99-5.130	Pukekura	15	2829200	6147500	Awapapa Lst.	Wp
w02-0305	5.131	cv-99-5.131	Pukekura	15	2829200	6147500	Awapapa Lst.	Wp
w02-0306	5.132	cv-99-5.132	Pukekura	15	2829200	6147500	Pukekura Calcarenite	Wp
w02-0307	5.133		Pukekura	15	2829200	6147500	Pukekura Calcarenite	Wp
w02-0308	5.134	cv-99-5.134	Tainui		2828500	6146900	Pukekura Calcarenite	Wp
w02-0309	5.135	cv-99-5.135	Tainui		2828500	6146900	Pukekura Calcarenite	Wp
w02-0310	5.136		Tainui		2828500	6146900	Pukekura Calcarenite	Wp

APPENDIX 2 - SAMPLE LIST

Waikato no.	Field no.	Thin section no.	Section/locality	Column	Grid reference		Formation	Stage
					East	North		
w02-0311	5.137		Tainui		2828500	6146900	Pukekura Calcarenite	Wp
w02-0312	5.138		Tainui		2828500	6146900	Pukekura Calcarenite	Wp
w02-0313	5.139	cv-99-5.139	Tainui		2828500	6146900	Rotookiwa Lst.?	Wp
w02-0314	5.140.	cv-99-5.140	Pukekura	15	2829200	6147500	Awapapa Lst.	Wp
w02-0315	5.141		Pukekura	15	2829200	6147500	Awapapa Lst.	Wp
w02-0316	5.142	cv-00-5.142	Te Mata Peak2	9	2845100	6160200	Awapapa Lst.	Wp
w02-0317	5.143		Te Mata Peak2	9	2845100	6160200	Awapapa Lst.	Wp
w02-0318	5.144	cv-00-5.144	Te Mata Peak2	9	2845100	6160200	Awapapa Lst.	Wp
w02-0319	5.145a	cv-00-5.145a	Te Mata Peak2	9	2845100	6160200	Awapapa Lst.	Wp
w02-0320	5.145b	cv-00-5.145b	Te Mata Peak2	9	2845100	6160200	Awapapa Lst.	Wp
w02-0321	5.146	cv-00-5.146	Te Mata Peak2	9	2845100	6160200	Awapapa Lst.	Wp
w02-0322	6.1	cv-99-6.1	Pakipaki Quarry		2834900	6160200	Pakipaki Lst.	Wn
w02-0323	6.2	cv-99-6.2	Pakipaki Quarry		2834900	6160200	Pakipaki Lst.	Wn
w02-0324	6.3a	cv-99-6.3a	Pakipaki Quarry		2834900	6160200	Pakipaki Lst.	Wn
w02-0325	6.3b	cv-99-6.3b	Pakipaki Quarry		2834900	6160200	Pakipaki Lst.	Wn
w02-0326	6.4	cv-99-6.4	Pakipaki Quarry		2834900	6160200	Pakipaki Lst.	Wn
w02-0327	6.5	cv-99-6.5	Pakipaki Quarry		2834900	6160200	Pakipaki Lst.	Wn
w02-0328	6.6	cv-99-6.6	Pakipaki Quarry		2834900	6160200	Pakipaki Lst.	Wn
w02-0329	6.7	cv-99-6.7	Pakipaki Quarry		2834900	6160200	Pakipaki Lst.	Wn
w02-0330	6.8	cv-99-6.8	Pakipaki Quarry		2834900	6160200	Pakipaki Lst.	Wn
w02-0331	7.1	cv-99-7.1	Rotoatara		2825100	6145100	Rotookiwa Lst.	Wp
w02-0332	7.2		Rotoatara		2825100	6145100	Rotookiwa Lst.	Wp
w02-0333	7.3		Rotoatara		2825100	6145100	Rotookiwa Lst.	Wp
w02-0334	7.4	cv-99-7.4	Rotoatara		2825100	6145100	Rotookiwa Lst.	Wp
w02-0335	7.5	cv-99-7.5	Pukekura	15	2829200	6147500	Rotookiwa Lst.	Wp
w02-0336	7.6	cv-99-7.6	Pukekura	15	2829200	6147500	Rotookiwa Lst.	Wp
w02-0337	7.7		Pukekura	15	2829200	6147500	Rotookiwa Lst.	Wp
w02-0338	7.8	cv-99-7.8	Pukekura	15	2829200	6147500	Rotookiwa Lst.	Wp
w02-0339	7.9	cv-99-7.9	Pukekura	15	2829200	6147500	Rotookiwa Lst.	Wp
w02-0340	7.10.	cv-99-7.10	Pukekura	15	2829200	6147500	Rotookiwa Lst.	Wp
w02-0341	7.11		Horse Shoe	17	2834500	6158600	Rotookiwa Lst.	Wp
w02-0342	7.12	cv-99-7.12	Horse Shoe	17	2834500	6158600	Rotookiwa Lst.	Wp
w02-0343	7.13		Horse Shoe	17	2834500	6158600	Rotookiwa Lst.	Wp
w02-0344	7.14	cv-99-7.14	Horse Shoe	17	2834500	6158600	Rotookiwa Lst.	Wp
w02-0345	7.15	cv-99-7.15	Horse Shoe	17	2834500	6158600	Rotookiwa Lst.	Wp
w02-0346	7.16	cv-99-7.16	Horse Shoe	17	2834500	6158600	Rotookiwa Lst.	Wp
w02-0347	7.17	cv-99-7.17	Horse Shoe	17	2834500	6158600	Rotookiwa Lst.	Wp
w02-0348	7.18	cv-99-7.18	Horse Shoe	17	2834500	6158600	Rotookiwa Lst.	Wp
w02-0349	7.19	cv-99-7.19	Horse Shoe	17	2834500	6158600	Rotookiwa Lst.	Wp
w02-0350	7.20.	cv-99-7.20	Horse Shoe	17	2834500	6158600	Rotookiwa Lst.	Wp
w02-0351	7.21	cv-99-7.21	Horse Shoe	17	2834500	6158600	Rotookiwa Lst.	Wp
w02-0352	7.22	cv-99-7.22	Horse Shoe	17	2834500	6158600	Rotookiwa Lst.	Wp
w02-0353	7.23	cv-99-7.23	Horse Shoe	17	2834500	6158600	Rotookiwa Lst.	Wp
w02-0354	7.24		Horse Shoe	17	2834500	6158600	Sandstone n.f.?	Wp
w02-0355	7.25		Horse Shoe	17	2834500	6158600	Sandstone n.f.?	Wp
w02-0356	7.26		Horse Shoe	17	2834500	6158600	Sandstone n.f.?	Wp
w02-0357	7.27	cv-99-7.27	Horse Shoe	17	2834500	6158600	Sandstone n.f.?	Wp
w02-0358	7.28	cv-99-7.28	Horse Shoe	17	2834500	6158600	Sandstone n.f.?	Wp
w02-0359	7.29		Poukawa	18	2831000	6152400	Rotookiwa Lst.	Wp
w02-0360	7.30.		Poukawa	18	2831000	6152400	Rotookiwa Lst.	Wp
w02-0361	7.31	cv-99-7.31	Poukawa	18	2831000	6152400	Rotookiwa Lst.	Wp
w02-0362	7.32	cv-99-7.32	Poukawa	18	2831000	6152400	Rotookiwa Lst.	Wp
w02-0363	7.33	cv-99-7.33	Poukawa	18	2831000	6152400	Rotookiwa Lst.	Wp
w02-0364	7.34	cv-99-7.34	Poukawa	18	2831000	6152400	Rotookiwa Lst.	Wp
w02-0365	7.35	cv-99-7.35	Poukawa	18	2831000	6152400	Rotookiwa Lst.	Wp
w02-0366	7.36	cv-99-7.36	Poukawa	18	2831000	6152400	Rotookiwa Lst.	Wp
w02-0367	7.37		Poukawa	18	2831000	6152400	Rotookiwa Lst.	Wp
w02-0368	7.38		Poukawa	18	2831000	6152400	Rotookiwa Lst.	Wp
w02-0369	7.39		Poukawa	18	2831000	6152400	Pukekura Calcarenite?	Wp
w02-0370	7.40.	cv-99-7.40	Lonely Man	20	2822800	6149500	Rotookiwa Lst.	Wp
w02-0371	7.41	cv-99-7.41	Lonely Man	20	2822800	6149500	Sandstone n.f.?	Wp
w02-0372	7.42	cv-99-7.42	Lonely Man	20	2822800	6149500	Sandstone n.f.?	Wp

APPENDIX 2 - SAMPLE LIST

Waikato no.	Field no.	Thin section no.	Section/locality	Column	Grid reference		Formation	Stage
					East	North		
w02-0373	7.43	cv-99-7.43	Lonely Man	20	2822800	6149500	Rotookiwa Lst.	Wp
w02-0374	7.45	cv-99-7.45	Lonely Man	20	2822800	6149500	Rotookiwa Lst.	Wp
w02-0375	7.46	cv-99-7.46	Lonely Man	20	2822800	6149500	Rotookiwa Lst.	Wp
w02-0376	7.47	cv-99-7.47	Lonely Man	20	2822800	6149500	Rotookiwa Lst.	Wp
w02-0377	7.48	cv-99-7.48	Lonely Man	20	2822800	6149500	Rotookiwa Lst.	Wp
w02-0378	7.49	cv-99-7.49	Lonely Man	20	2822800	6149500	Rotookiwa Lst.	Wp
w02-0379	7.50.	cv-99-7.50	Lonely Man	20	2822800	6149500	Rotookiwa Lst.	Wp
w02-0380	7.51		Lonely Man	20	2822800	6149500	Rotookiwa Lst.	Wp
w02-0381	7.52	cv-99-7.52	Lonely Man	20	2822800	6149500	Rotookiwa Lst.	Wp
w02-0382	7.53	cv-99-7.53	Lonely Man	20	2822800	6149500	Sandstone n.f.?	Wp
w02-0383	7.54	cv-99-7.54	Lonely Man	20	2822800	6149500	Sandstone n.f.?	Wp
w02-0384	7.55		Waitapuke Quarry		2822400	6148700	Waikaraeo Calcarenite	Wp
w02-0385	7.56		Waitapuke Quarry		2822400	6148700	Waikaraeo Calcarenite	Wp
w02-0386	7.57		Waitapuke Quarry		2822400	6148700	Waikaraeo Calcarenite	Wp
w02-0387	8.1	cv-99-8.1	Waitapuke Quarry		2825800	6145700	Rotookiwa Lst.	Wp
w02-0388	8.2	cv-99-8.2	Waitapuke Quarry		2825800	6145700	Rotookiwa Lst.	Wp
w02-0389	9.1	cv-99-9.1	Te Onepu Quarry	23	2819800	6149100	Te Onepu Lst.	Wm
w02-0390	9.2	cv-99-9.2	Te Onepu Quarry	23	2819800	6149100	Te Onepu Lst.	Wm
w02-0391	9.3	cv-99-9.3	Te Onepu Quarry	23	2819800	6149100	Te Onepu Lst.	Wm
w02-0392	9.4	cv-99-9.4	Te Onepu Quarry	23	2819800	6149100	Te Onepu Lst.	Wm
w02-0393	9.5	cv-99-9.5	Te Onepu Quarry	23	2819800	6149100	Te Onepu Lst.	Wm
w02-0394	9.8	cv-99-9.8	Te Onepu Quarry	23	2819800	6149100	Te Onepu Lst.	Wm
w02-0395	9.9	cv-99-9.9	Te Onepu Quarry	23	2819800	6149100	Te Onepu Lst.	Wm
w02-0396	9.10.	cv-99-9.10	Te Onepu Quarry	23	2819800	6149100	Te Onepu Lst.	Wm
w02-0397	9.11	cv-99-9.11	Te Onepu Quarry	23	2819800	6149100	Te Onepu Lst.	Wm
w02-0398	9.12	cv-99-9.12	Te Onepu Quarry	23	2819800	6149100	Te Onepu Lst.	Wm
w02-0399	9.13		Te Onepu Quarry	23	2819800	6149100	Te Onepu Lst.	Wm
w02-0400	9.14		Te Onepu Quarry	23	2819800	6149100	Te Onepu Lst.	Wm
w02-0401	9.15	cv-99-9.15	Te Onepu Quarry	23	2819800	6149100	Te Onepu Lst.	Wm
w02-0402	9.16	cv-99-9.16	Te Onepu Quarry	23	2819800	6149100	Te Onepu Lst.	Wm
w02-0403	9.17	cv-99-9.17	Te Onepu Quarry	23	2819800	6149100	Te Onepu Lst.	Wm
w02-0404	9.18	cv-99-9.18	Te Onepu Quarry	23	2819800	6149100	Te Onepu Lst.	Wm
w02-0405	9.19		Te Onepu Quarry	23	2819800	6149100	Te Onepu Lst.	Wm
w02-0406	9.20.	cv-99-9.20	Te Onepu Quarry	23	2819800	6149100	Te Onepu Lst.	Wm
w02-0407	9.21		Te Onepu Quarry	23	2819800	6149100	Te Onepu Lst.	Wm
w02-0408	9.22		Bee Swarm	24	2819300	6148400	Te Onepu Lst.	Wm
w02-0409	9.23	cv-99-9.23	Bee Swarm	24	2819300	6148400	Te Onepu Lst.	Wm
w02-0410	9.24		Bee Swarm	24	2819300	6148400	Te Onepu Lst.	Wm
w02-0411	9.25		Bee Swarm	24	2819300	6148400	Te Onepu Lst.	Wm
w02-0412	9.26		Bee Swarm	24	2819300	6148400	Te Onepu Lst.	Wm
w02-0413	9.27		Bee Swarm	24	2819300	6148400	Te Onepu Lst.	Wm
w02-0414	9.28	cv-99-9.28	Bee swarm	24	2819300	6148400	Te Onepu Lst.	Wm
w02-0415	9.29	cv-99-9.29	Bee swarm	24	2819300	6148400	Te Onepu Lst.	Wm
w02-0416	9.30.		Bee swarm	24	2819300	6148400	Te Onepu Lst.	Wm
w02-0417	9.31		Bee swarm	24	2819300	6148400	Te Onepu Lst.	Wm
w02-0418	9.32	cv-99-9.32	Bee swarm	24	2819300	6148400	Te Onepu Lst.	Wm
w02-0419	9.33		Bee swarm	24	2819300	6148400	Te Onepu Lst.	Wm
w02-0420	9.34	cv-99-9.34	Bee swarm	24	2819300	6148400	Te Onepu Lst.	Wm
w02-0421	9.35		Bee swarm	24	2819300	6148400	Te Onepu Lst.	Wm
w02-0422	9.36		Bee swarm	24	2819300	6148400	Te Onepu Lst.	Wm
w02-0423	9.37	cv-99-9.37	Bee swarm	24	2819300	6148400	Te Onepu Lst.	Wm
w02-0424	9.38	cv-99-9.38	Bee swarm	24	2819300	6148400	Te Onepu Lst.	Wm
w02-0425	9.39		Bee swarm	24	2819300	6148400	Te Onepu Lst.	Wm
w02-0426	9.40.		Robottom Grave	26	2814800	6142200	Te Onepu Lst.	Wm
w02-0427	9.41		Robottom Grave	26	2814800	6142200	Te Onepu Lst.	Wm
w02-0428	9.42	cv-99-9.42	Robottom Grave	26	2814800	6142200	Te Onepu Lst.	Wm
w02-0429	9.43		Robottom Grave	26	2814800	6142200	Te Onepu Lst.	Wm
w02-0430	9.44	cv-99-9.44	Robottom Grave	26	2814800	6142200	Te Onepu Lst.	Wm
w02-0431	9.45		Robottom Grave	26	2814800	6142200	Te Onepu Lst.	Wm
w02-0432	9.46		Robottom Grave	26	2814800	6142200	Te Onepu Lst.	Wm
w02-0433	9.47		Robottom Grave	26	2814800	6142200	Te Onepu Lst.	Wm
w02-0434	9.48		Robottom Grave	26	2814800	6142200	Te Onepu Lst.	Wm

APPENDIX 2 - SAMPLE LIST

Waikato no.	Field no.	Thin section no.	Section/locality	Column	Grid reference		Formation	Stage
					East	North		
w02-0435	9.49		Robottom Grave	26	2814800	6142200	Te Onepu Lst.	Wm
w02-0436	9.50.	cv-99-9.50	Robottom Grave	26	2814800	6142200	Te Onepu Lst.	Wm
w02-0437	9.51	cv-99-9.51	Robottom Grave	26	2814800	6142200	Te Onepu Lst.	Wm
w02-0438	9.52	cv-99-9.52	Robottom Grave	26	2814800	6142200	Te Onepu Lst.	Wm
w02-0439	9.53	cv-99-9.53	Robottom Grave	26	2814800	6142200	Te Onepu Lst.	Wm
w02-0440	9.54a		Robottom Grave	26	2814800	6142200	Te Onepu Lst.	Wm
w02-0441	9.54b		Robottom Grave	26	2814800	6142200	Te Onepu Lst.	Wm
w02-0442	9.55		Robottom Grave	26	2814800	6142200	Te Onepu Lst.	Wm
w02-0443	9.56		Robottom Grave	26	2814800	6142200	Te Onepu Lst.	Wm
w02-0444	9.57	cv-99-9.57	Robottom Grave	26	2814800	6142200	Te Onepu Lst.	Wm
w02-0445	9.58		Kiwi Bush	25	2814900	6142700	Te Onepu Lst.?	Wm
w02-0446	9.59		Kiwi Bush	25	2814900	6142700	Te Onepu Lst.?	Wm
w02-0447	9.60.	cv-99-9.60	Kiwi Bush	25	2814900	6142700	Te Onepu Lst.?	Wm
w02-0448	9.61	cv-99-9.61	Kiwi Bush	25	2814900	6142700	Te Onepu Lst.?	Wm
w02-0449	9.62		Kiwi Bush	25	2814900	6142700	Te Onepu Lst.?	Wm
w02-0450	9.63	cv-99-9.63	Kiwi Bush	25	2814900	6142700	Te Onepu Lst.?	Wm
w02-0451	9.64	cv-99-9.64	Kiwi Bush	25	2814900	6142700	Te Onepu Lst.?	Wm
w02-0452	9.65		Kiwi Bush	25	2814900	6142700	Te Onepu Lst.?	Wm
w02-0453	9.66		Kiwi Bush	25	2814900	6142700	Te Onepu Lst.?	Wm
w02-0454	9.67		Kiwi Bush	25	2814900	6142700	Te Onepu Lst.?	Wm
w02-0455	9.68		Kiwi Bush	25	2814900	6142700	Te Onepu Lst.?	Wm
w02-0456	9.69		Kiwi Bush	25	2814900	6142700	Te Onepu Lst.?	Wm
w02-0457	9.70.		Burma Road	22	2825900	6154900	Te Onepu Lst.?	Wm
w02-0458	9.71	cv-99-9.71	Burma Road	22	2825900	6154900	Te Onepu Lst.?	Wm
w02-0459	9.72	cv-99-9.72	Burma Road	22	2825900	6154900	Te Onepu Lst.?	Wm
w02-0460	9.73	cv-99-9.73	Burma Road	22	2825900	6154900	Te Onepu Lst.?	Wm
w02-0461	9.74	cv-99-9.74	Burma Road	22	2825900	6154900	Te Onepu Lst.?	Wm
w02-0462	9.75	cv-99-9.75	Burma Road	22	2825900	6154900	Te Onepu Lst.?	Wm
w02-0463	9.76	cv-99-9.76	Burma Road	22	2825900	6154900	Te Onepu Lst.?	Wm
w02-0464	9.77		Burma Road	22	2825900	6154900	Te Onepu Lst.?	Wm
w02-0465	9.78	cv-99-9.78	Burma Road	22	2825900	6154900	Te Onepu Lst.?	Wm
w02-0466	9.79	cv-99-9.79	Burma Road	22	2825900	6154900	Te Onepu Lst.?	Wm
w02-0467	9.80.	cv-99-9.80	Gulch Quarry	27	2811800	6134400	Te Onepu Lst.	Wm
w02-0468	9.81	cv-99-9.81	Gulch Quarry	27	2811800	6134400	Te Onepu Lst.	Wm
w02-0469	9.82	cv-99-9.82	Gulch Quarry	27	2811800	6134400	Te Onepu Lst.	Wm
w02-0470	9.83	cv-99-9.83	Gulch Quarry	27	2811800	6134400	Te Onepu Lst.	Wm
w02-0471	9.84	cv-99-9.84	Gulch Quarry	27	2811800	6134400	Te Onepu Lst.	Wm
w02-0472	9.85	cv-99-9.85	Gulch Quarry	27	2811800	6134400	Te Onepu Lst.	Wm
w02-0473	9.86		Gulch Quarry	27	2811800	6134400	Te Onepu Lst.	Wm
w02-0474	9.87		Gulch Quarry	27	2811800	6134400	Te Onepu Lst.	Wm
w02-0475	9.88		Gulch Quarry	27	2811800	6134400	Te Onepu Lst.	Wm
w02-0476	9.89		Gulch Quarry	27	2811800	6134400	Te Onepu Lst.	Wm
w02-0477	9.90.	cv-99-9.90	Gulch Quarry	27	2811800	6134400	Te Onepu Lst.	Wm
w02-0478	9.91	cv-99-9.91	Gulch Quarry	27	2811800	6134400	Te Onepu Lst.	Wm
w02-0479	9.92	cv-99-9.92	Gulch Quarry	27	2811800	6134400	Te Onepu Lst.	Wm
w02-0480	9.93		Gulch Quarry	27	2811800	6134400	Te Onepu Lst.	Wm
w02-0481	9.94	cv-99-9.94	Gulch Quarry	27	2811800	6134400	Te Onepu Lst.	Wm
w02-0482	9.95	cv-99-9.95	Gulch Quarry	27	2811800	6134400	Te Onepu Lst.	Wm
w02-0483	9.96	cv-99-9.96	Gulch Quarry	27	2811800	6134400	Te Onepu Lst.	Wm
w02-0484	9.97	cv-99-9.97	Gulch Quarry	27	2811800	6134400	Te Onepu Lst.	Wm
w02-0485	9.98		Gulch Quarry	27	2811800	6134400	Te Onepu Lst.	Wm
w02-0486	9.99		Gulch Quarry	27	2811800	6134400	Te Onepu Lst.	Wm
w02-0487	9.100.	cv-99-9.100	Gulch Quarry	27	2811800	6134400	Te Onepu Lst.	Wm
w02-0488	9.101	cv-99-9.101	Horanui l	21	2828300	6156200	Te Onepu Lst.	Wm
w02-0489	9.102	cv-99-9.102	Horanui l	21	2828300	6156200	Te Onepu Lst.	Wm
w02-0490	9.103	cv-99-9.103	Horanui l	21	2828300	6156200	Te Onepu Lst.	Wm
w02-0491	9.104	cv-99-9.104	Horanui l	21	2828300	6156200	Te Onepu Lst.	Wm
w02-0492	9.105	cv-99-9.105	Horanui l	21	2828300	6156200	Te Onepu Lst.	Wm
w02-0493	9.106	cv-99-9.106	Horanui l	21	2828300	6156200	Te Onepu Lst.	Wm
w02-0494	9.107		Horanui l	21	2828300	6156200	Te Onepu Lst.	Wm
w02-0495	9.108		Horanui l	21	2828300	6156200	Te Onepu Lst.	Wm
w02-0496	9.109		Horanui l	21	2828300	6156200	Te Onepu Lst.	Wm

APPENDIX 2 - SAMPLE LIST

Waikato no.	Field no.	Thin section no.	Section/locality	Column	Grid reference		Formation	Stage
					East	North		
w02-0497	9.110.		Horanui1	21	2828300	6156200	Te Onepu Lst.	Wm
w02-0498	9.111	cv-99-9.111	Horanui1	21	2828300	6156200	Te Onepu Lst.	Wm
w02-0499	9.112	cv-99-9.112	Horanui1	21	2828300	6156200	Te Onepu Lst.	Wm
w02-0500	9.113	cv-99-9.113	Horanui2	21	2828200	6156000	Te Onepu Lst.	Wm
w02-0501	9.114	cv-99-9.114	Horanui1	21	2828300	6156200	Te Onepu Lst.	Wm
w02-0502	9.115	cv-99-9.115	Horanui1	21	2828300	6156200	Te Onepu Lst.	Wm
w02-0503	9.116		Horanui2	21	2828200	6156000	Te Onepu Lst.	Wm
w02-0504	9.117		Horanui2	21	2828200	6156000	Te Onepu Lst.	Wm
w02-0505	9.118		Horanui2	21	2828200	6156000	Te Onepu Lst.	Wm
w02-0506	9.119	cv-99-9.119	Horanui2	21	2828200	6156000	Te Onepu Lst.	Wm
w02-0507	9.120.		Horanui2	21	2828200	6156000	Te Onepu Lst.	Wm
w02-0508	9.121		Tikokino Quarry		2811800	6137200	Te Onepu Lst.	Wm
w02-0509	9.122	cv-99-9.122	Tikokino Quarry		2811800	6137200	Te Onepu Lst.	Wm
w02-0510	9.123		Tikokino Quarry		2811800	6137200	Te Onepu Lst.	Wm
w02-0511	9.124	cv-99-9.124	Tikokino Quarry		2811800	6137200	Te Onepu Lst.	Wm
w02-0512	9.125		Tikokino Quarry		2811800	6137200	Te Onepu Lst.	Wm
w02-0513	9.126	cv-99-9.126	Tikokino Quarry		2811800	6137200	Te Onepu Lst.	Wm
w02-0514	9.127	cv-99-9.127	Tikokino Quarry		2811800	6137200	Te Onepu Lst.	Wm
w02-0515	9.128	cv-00-9.128	Pukeora				Pukeora Oyster Bed	Wn
w02-0516	11.1	cv-99-11.1	Tirohia		2816900	6150200	Mason Ridge Fm.	Wn
w02-0517	11.2	cv-99-11.2	Tirohia		2816900	6150200	Mason Ridge Fm.	Wn
w02-0518	11.3	cv-99-11.3	Tirohia		2816900	6150200	Mason Ridge Fm.	Wn
w02-0519	11.4	cv-99-11.4	Tirohia		2816900	6150200	Mason Ridge Fm.	Wn
w02-0520	11.5		Tirohia		2816900	6150200	Mason Ridge Fm.	Wn
w02-0521	11.6		Mangatai	31	2816300	6149400	Mason Ridge Fm.	Wn
w02-0522	11.7	cv-99-11.7	Mangatai	31	2816300	6149400	Mason Ridge Fm.	Wn
w02-0523	11.8	cv-99-11.8	Mangatai	31	2816300	6149400	Mason Ridge Fm.	Wn
w02-0524	11.9	cv-99-11.9	Mangatai	31	2816300	6149400	Mason Ridge Fm.	Wn
w02-0525	11.10.	cv-99-11.10	Mangatai	31	2816300	6149400	Mason Ridge Fm.	Wn
w02-0526	11.11	cv-99-11.11	Mangatai	31	2816300	6149400	Mason Ridge Fm.	Wn
w02-0527	11.12	cv-99-11.12	Mangatai	31	2816300	6149400	Mason Ridge Fm.	Wn
w02-0528	11.13		Mangatai	31	2816300	6149400	Mason Ridge Fm.	Wn
w02-0529	11.14		Mangatai	31	2816300	6149400	Mason Ridge Fm.	Wn
w02-0530	11.15	cv-99-11.15	Mangatai	31	2816300	6149400	Mason Ridge Fm.	Wn
w02-0531	11.16	cv-99-11.16	Mangatai	31	2816300	6149400	Mason Ridge Fm.	Wn
w02-0532	11.17	cv-99-11.17	Mangatai	31	2816300	6149400	Mason Ridge Fm.	Wn
w02-0533	11.18	cv-99-11.18	Mangatai	31	2816300	6149400	Mason Ridge Fm.	Wn
w02-0534	11.19		Mangatai	31	2816300	6149400	Mason Ridge Fm.	Wn
w02-0535	11.20.	cv-99-11.20	Mangatai	31	2816300	6149400	Mason Ridge Fm.	Wn
w02-0536	11.21	cv-99-11.21	Mangatai	31	2816300	6149400	Mason Ridge Fm.	Wn
w02-0537	11.22	cv-99-11.22	Mangatai	31	2816300	6149400	Mason Ridge Fm.	Wn
w02-0538	11.23	cv-99-11.23	Mangatai	31	2816300	6149400	Mason Ridge Fm.	Wn
w02-0539	11.24		Mangatai	31	2816300	6149400	Mason Ridge Fm.	Wn
w02-0540	11.25	cv-00-11.25	Torran	29	2820800	6159200	Mason Ridge Fm.	Wn
w02-0541	11.26	cv-00-11.26	Torran	29	2820800	6159200	Mason Ridge Fm.	Wn
w02-0542	11.27	cv-00-11.27	Torran	29	2820800	6159200	Mason Ridge Fm.	Wn
w02-0543	11.28	cv-00-11.28	Torran	29	2820800	6159200	Mason Ridge Fm.	Wn
w02-0544	11.29	cv-00-11.29	Torran	29	2820800	6159200	Mason Ridge Fm.	Wn
w02-0545	11.30.		Torran	29	2820800	6159200	Mason Ridge Fm.	Wn
w02-0546	11.31		Torran	29	2820800	6159200	Mason Ridge Fm.	Wn
w02-0547	11.32		Torran	29	2820800	6159200	Mason Ridge Fm.	Wn
w02-0548	11.33	cv-00-11.33	Torran	29	2820800	6159200	Mason Ridge Fm.	Wn
w02-0549	11.34	cv-00-11.34	Torran	29	2820800	6159200	Mason Ridge Fm.	Wn
w02-0550	11.35	cv-00-11.35	Torran	29	2820800	6159200	Mason Ridge Fm.	Wn
w02-0551	11.36	cv-00-11.36	Torran	29	2820800	6159200	Mason Ridge Fm.	Wn
w02-0552	11.37	cv-00-11.37	Torran	29	2820800	6159200	Mason Ridge Fm.	Wn
w02-0553	11.38		Torran	29	2820800	6159200	Mason Ridge Fm.	Wn
w02-0554	11.39	cv-00-11.39	Torran	29	2820800	6159200	Mason Ridge Fm.	Wn
w02-0555	11.40.	cv-00-11.40	Torran	29	2820800	6159200	Mason Ridge Fm.	Wn
w02-0556	11.41	cv-00-11.41	Torran	29	2820800	6159200	Mason Ridge Fm.	Wn
w02-0557	11.42	cv-00-11.42	Torran	29	2820800	6159200	Mason Ridge Fm.	Wn
w02-0558	11.43		Torran	29	2820800	6159200	Mason Ridge Fm.	Wn

APPENDIX 2 - SAMPLE LIST

Waikato no.	Field no.	Thin section no.	Section/locality	Column	Grid reference		Formation	Stage
					East	North		
w02-0559	11.44	cv-00-11.44	Torran	29	2820800	6159200	Mason Ridge Fm.	Wn
w02-0560	11.45		Torran	29	2820800	6159200	Mason Ridge Fm.	Wn
w02-0561	11.46	cv-00-11.46	Croft Outcrop		2822100	6161000	Mason Ridge Fm.	Wn
w02-0562	11.47		Croft Outcrop		2822100	6161000	Mason Ridge Fm.	Wn
w02-0563	11.48		Croft Outcrop		2822100	6161000	Mason Ridge Fm.	Wn
w02-0564	11.49		Pakihirua	30	2820400	6156400	Mason Ridge Fm.	Wn
w02-0565	11.50.		Pakihirua	30	2820400	6156400	Mason Ridge Fm.	Wn
w02-0566	11.51	cv-00-11.51	Pakihirua	30	2820400	6156400	Mason Ridge Fm.	Wn
w02-0567	11.52		Pakihirua	30	2820400	6156400	Mason Ridge Fm.	Wn
w02-0568	11.53		Pakihirua	30	2820400	6156400	Mason Ridge Fm.	Wn
w02-0569	11.54	cv-00-11.54	Pakihirua	30	2820400	6156400	Mason Ridge Fm.	Wn
w02-0570	11.55	cv-00-11.55	Pakihirua	30	2820400	6156400	Mason Ridge Fm.	Wn
w02-0571	11.56	cv-00-11.56	Pakihirua	30	2820400	6156400	Mason Ridge Fm.	Wn
w02-0572	11.57	cv-00-11.57	Pakihirua	30	2820400	6156400	Mason Ridge Fm.	Wn
w02-0573	11.58	cv-00-11.58	Pakihirua	30	2820400	6156400	Mason Ridge Fm.	Wn
w02-0574	11.59	cv-00-11.59	Pakihirua	30	2820400	6156400	Mason Ridge Fm.	Wn
w02-0575	11.6	cv-00-11.60	Pakihirua	30	2820400	6156400	Mason Ridge Fm.	Wn
w02-0576	11.61		Pakihirua	30	2820400	6156400	Mason Ridge Fm.	Wn
w02-0577	11.62	cv-00-11.62	Pakihirua	30	2820400	6156400	Mason Ridge Fm.	Wn
w02-0578	11.63	cv-00-11.63	Pakihirua	30	2820400	6156400	Mason Ridge Fm.	Wn
w02-0579	11.64	cv-00-11.64	Pakihirua	30	2820400	6156400	Mason Ridge Fm.	Wn
w02-0580	11.65		Pakihirua	30	2820400	6156400	Mason Ridge Fm.	Wn
w02-0581	11.67		Pakihirua	30	2820400	6156400	Mason Ridge Fm.	Wn
w02-0582	11.68	cv-00-11.68	Pakihirua	30	2820400	6156400	Mason Ridge Fm.	Wn
w02-0583	11.69	cv-00-11.69	Pakihirua	30	2820400	6156400	Mason Ridge Fm.	Wn
w02-0584	11.70.		Pakihirua	30	2820400	6156400	Mason Ridge Fm.	Wn
w02-0585	11.71	cv-00-11.71	Pakihirua	30	2820400	6156400	Mason Ridge Fm.	Wn
w02-0586	11.72		Pakihirua	30	2820400	6156400	Mason Ridge Fm.	Wn
w02-0587	11.73	cv-00-11.73	Taheke	32	2816700	6155400	Mason Ridge Fm.	Wn
w02-0588	11.74	cv-00-11.74	Taheke	32	2816700	6155400	Mason Ridge Fm.	Wn
w02-0589	11.75	cv-00-11.75	Taheke	32	2816700	6155400	Mason Ridge Fm.	Wn
w02-0590	11.76	cv-00-11.76	Taheke	32	2816700	6155400	Mason Ridge Fm.	Wn
w02-0591	11.77	cv-00-11.77	Taheke	32	2816700	6155400	Mason Ridge Fm.	Wn
w02-0592	11.78	cv-00-11.78	Taheke	32	2816700	6155400	Mason Ridge Fm.	Wn
w02-0593	11.79	cv-00-11.79	Taheke	32	2816700	6155400	Mason Ridge Fm.	Wn
w02-0594	11.80.	cv-00-11.80	Whakapirau Road		2819300	6165300	Mason Ridge Fm.	Wn
w02-0595	11.81	cv-00-11.81	Glencoe Station	33	2817200	6162800	Mason Ridge Fm.	Wn
w02-0596	11.82	cv-00-11.82	Glencoe Station	33	2817200	6162800	Mason Ridge Fm.	Wn
w02-0597	11.83	cv-00-11.83	Glencoe Station	33	2817200	6162800	Mason Ridge Fm.	Wn
w02-0598	11.84	cv-00-11.84	Glencoe Station	33	2817200	6162800	Mason Ridge Fm.	Wn
w02-0599	11.85	cv-00-11.85	Glencoe Station	33	2817200	6162800	Mason Ridge Fm.	Wn
w02-0600	11.86	cv-00-11.86	Glencoe Station	33	2817200	6162800	Mason Ridge Fm.	Wn
w02-0601	11.87	cv-00-11.87	Glencoe Station	33	2817200	6162800	Mason Ridge Fm.	Wn
w02-0602	11.88	cv-00-11.88	Glencoe Station	33	2817200	6162800	Mason Ridge Fm.	Wn
w02-0603	11.89	cv-00-11.89	Glencoe Station	33	2817200	6162800	Mason Ridge Fm.	Wn
w02-0604	11.90.	cv-00-11.90	Glencoe Station	33	2817200	6162800	Mason Ridge Fm.	Wn
w02-0605	11.91		Glencoe Station	33	2817200	6162800	Mason Ridge Fm.	Wn
w02-0606	12.1	cv-99-12.1	Glendale Farm	46	2896600	6168500	Kereru Lst.	Wn
w02-0607	12.2	cv-99-12.2	Glendale Farm	46	2896600	6168500	Kereru Lst.	Wn
w02-0608	12.3	cv-99-12.3	Glendale Farm	46	2896600	6168500	Kereru Lst.	Wn
w02-0609	12.4	cv-99-12.4	Glendale Farm	46	2896600	6168500	Kereru Lst.	Wn
w02-0610	12.5	cv-99-12.5	Glendale Farm	46	2896600	6168500	Kereru Lst.	Wn
w02-0611	12.6	cv-99-12.6	Glendale Farm	46	2896600	6168500	Kereru Lst.	Wn
w02-0612	12.7	cv-99-12.7	Glendale Farm	46	2896600	6168500	Kereru Lst.	Wn
w02-0613	12.8	cv-99-12.8	Glendale Farm	46	2896600	6168500	Kereru Lst.	Wn
w02-0614	13.1	cv-99-13.1	Jumped Up Stream	47	2893400	6166500	Sentry Box Lst.	Wn
w02-0615	13.2	cv-99-13.2	Jumped Up Stream	47	2893400	6166500	Sentry Box Lst.	Wn
w02-0616	13.3	cv-99-13.3	Jumped Up Stream	47	2893400	6166500	Sentry Box Lst.	Wn
w02-0617	13.4	cv-99-13.4	Jumped Up Stream	47	2893400	6166500	Sentry Box Lst.	Wn
w02-0618	14.1	cv-99-14.1	Ohiti Road	35	2830000	6173400	Matapiro Lst.	Wn
w02-0619	14.2	cv-99-14.2	Ohiti Road	35	2830000	6173400	Matapiro Lst.	Wn
w02-0620	14.3	cv-00-14.3	Ohiti Road	35	2830000	6173400	Matapiro Lst.	Wn

APPENDIX 2 - SAMPLE LIST

Waikato no.	Field no.	Thin section no.	Section/locality	Column	Grid reference		Formation	Stage
					East	North		
w02-0621	14.4	cv-00-14.4	Ohiwia	34	2829400	6175100	Matapiro Lst.	Wn
w02-0622	14.5	cv-00-14.5	Ohiwia	34	2829400	6175100	Matapiro Lst.	Wn
w02-0623	14.6	cv-00-14.6	Ohiwia	34	2829400	6175100	Matapiro Lst.	Wn
w02-0624	14.7	cv-00-14.7	Ohiwia	34	2829400	6175100	Matapiro Lst.	Wn
w02-0625	14.8	cv-00-14.8	Ohiwia	34	2829400	6175100	Matapiro Lst.	Wn
w02-0626	14.9	cv-00-14.9	Ohiwia	34	2829400	6175100	Matapiro Lst.	Wn
w02-0627	14.10.	cv-00-14.10	Ohiwia	34	2829400	6175100	Matapiro Lst.	Wn
w02-0628	14.11	cv-00-14.11	Ohiwia	34	2829400	6175100	Matapiro Lst.	Wn
w02-0629	14.12	cv-00-14.12	Ohiwia	34	2829400	6175100	Matapiro Lst.	Wn
w02-0630	14.13	cv-00-14.13	Ohiwia	34	2829400	6175100	Matapiro Lst.	Wn
w02-0631	14.14	cv-00-14.14	Ohiti Road	35	2830000	6173400	Matapiro Lst.	Wn
w02-0632	14.15	cv-00-14.15	Ohiti Road	35	2830000	6173400	Matapiro Lst.	Wn
w02-0633	14.16	cv-00-14.16	Ohiti Road	35	2830000	6173400	Matapiro Lst.	Wn
w02-0634	14.17	cv-00-14.17	Ohiti Road	35	2830000	6173400	Matapiro Lst.	Wn
w02-0635	14.18	cv-00-14.18	Ohiti Road	35	2830000	6173400	Matapiro Lst.	Wn
w02-0636	14.19	cv-00-14.19	Ohiti Road	35	2830000	6173400	Matapiro Lst.	Wn
w02-0637	14.20.	cv-00-14.20	Ohiti Road	35	2830000	6173400	Matapiro Lst.	Wn
w02-0638	14.21	cv-00-14.21	Ohiti Road	35	2830000	6173400	Matapiro Lst.	Wn
w02-0639	14.22	cv-00-14.22	Ohiti Road	35	2830000	6173400	Matapiro Lst.	Wn
w02-0640	14.23	cv-00-14.23	Ohiti Road	35	2830000	6173400	Matapiro Lst.	Wn
w02-0641	14.24	cv-00-14.24	Ohiti Road	35	2830000	6173400	Matapiro Lst.	Wn
w02-0642	14.25	cv-00-14.25	Ohiti Road	35	2830000	6173400	Matapiro Lst.	Wn
w02-0643	14.26	cv-00-14.26	Ohiti Road	35	2830000	6173400	Matapiro Lst.	Wn
w02-0644	14.27	cv-00-14.27	Ohiti Road	35	2830000	6173400	Matapiro Lst.	Wn
w02-0645	15.1	cv-00-15.1	Hawkston	39	2816900	6204300	Te Waka Fm.	Wm
w02-0646	15.2	cv-00-15.2	Hawkston	39	2816900	6204300	Te Waka Fm.	Wm
w02-0647	15.3	cv-00-15.3	Hawkston	39	2816900	6204300	Te Waka Fm.	Wm
w02-0648	15.4a	cv-00-15.4a	Hawkston	39	2816900	6204300	Te Waka Fm.	Wm
w02-0649	15.4b	cv-00-15.4b	Hawkston	39	2816900	6204300	Te Waka Fm.	Wm
w02-0650	15.5a	cv-00-15.5a	Hawkston	39	2816900	6204300	Te Waka Fm.	Wm
w02-0651	15.5b	cv-00-15.5b	Hawkston	39	2816900	6204300	Te Waka Fm.	Wm
w02-0652	15.6	cv-00-15.6	Hawkston	39	2816900	6204300	Te Waka Fm.	Wm
w02-0653	15.7	cv-00-15.7	Hawkston	39	2816900	6204300	Te Waka Fm.	Wm
w02-0654	15.8	cv-00-15.8	Hawkston	39	2816900	6204300	Te Waka Fm.	Wm
w02-0655	15.9	cv-00-15.9	Hawkston	39	2816900	6204300	Te Waka Fm.	Wm
w02-0656	15.10.	cv-00-15.10	Hawkston	39	2816900	6204300	Te Waka Fm.	Wm
w02-0657	15.11	cv-00-15.11	Hawkston	39	2816900	6204300	Te Waka Fm.	Wm
w02-0658	15.12	cv-00-15.12	Hawkston	39	2816900	6204300	Te Waka Fm.	Wm
w02-0659	15.13	cv-00-15.13	Mount Romulus	41	2816800	6202600	Te Waka Fm.?	Wm?
w02-0660	15.14	cv-00-15.14	Mount Romulus	41	2816800	6202600	Te Waka Fm.?	Wm?
w02-0661	15.15	cv-00-15.15	Mount Romulus	41	2816800	6202600	Te Waka Fm.?	Wm?
w02-0662	15.16	cv-00-15.16	Mount Romulus	41	2816800	6202600	Te Waka Fm.?	Wm?
w02-0663	15.17	cv-00-15.17	Mount Romulus	41	2816800	6202600	Te Waka Fm.?	Wm?
w02-0664	15.18	cv-00-15.18	Mount Romulus	41	2816800	6202600	Te Waka Fm.?	Wm?
w02-0665	15.19	cv-00-15.19	Mount Romulus	41	2816800	6202600	Te Waka Fm.?	Wm?
w02-0666	15.20.	cv-00-15.20	Mount Romulus	41	2816800	6202600	Te Waka Fm.?	Wm?
w02-0667	15.21	cv-00-15.21	The Gorges	40	2818800	6200700	Te Waka Fm.	Wm
w02-0668	15.22	cv-00-15.22	The Gorges	40	2818800	6200700	Te Waka Fm.	Wm
w02-0669	15.23	cv-00-15.23	The Gorges	40	2818800	6200700	Te Waka Fm.	Wm
w02-0670	15.24	cv-00-15.24	The Gorges	40	2818800	6200700	Te Waka Fm.	Wm
w02-0671	15.25	cv-00-15.25	The Gorges	40	2818800	6200700	Te Waka Fm.	Wm
w02-0672	15.26	cv-00-15.26	The Gorges	40	2818800	6200700	Te Waka Fm.	Wm
w02-0673	15.27	cv-00-15.27	The Gorges	40	2818800	6200700	Te Waka Fm.	Wm
w02-0674	15.28	cv-00-15.28	The Gorges	40	2818800	6200700	Te Waka Fm.	Wm
w02-0675	15.29	cv-00-15.29	The Gorges	40	2818800	6200700	Te Waka Fm.	Wm
w02-0676	15.30.	cv-00-15.30	The Gorges	40	2818800	6200700	Te Waka Fm.	Wm
w02-0677	15.31	cv-00-15.31	The Gorges	40	2818800	6200700	Te Waka Fm.	Wm
w02-0678	15.32	cv-00-15.32	The Gorges	40	2818800	6200700	Te Waka Fm.	Wm
w02-0679	15.33	cv-00-15.33	The Gorges	40	2818800	6200700	Te Waka Fm.	Wm
w02-0680	15.34	cv-00-15.34	The Gorges	40	2818800	6200700	Te Waka Fm.	Wm
w02-0681	15.35	cv-00-15.35	The Gorges	40	2818800	6200700	Te Waka Fm.	Wm
w02-0682	15.36	cv-00-15.36	The Gorges	40	2818800	6200700	Te Waka Fm.	Wm

APPENDIX 2 - SAMPLE LIST

Waikato no.	Field no.	Thin section no.	Section/locality	Column	Grid reference		Formation	Stage
					East	North		
w02-0683	15.37	cv-00-15.37	The Gorges	40	2818800	6200700	Te Waka Fm.	Wm
w02-0684	15.38	cv-00-15.38	The Gorges	40	2818800	6200700	Te Waka Fm.	Wm
w02-0685	15.39	cv-00-15.39	The Gorges	40	2818800	6200700	Te Waka Fm.	Wm
w02-0686	15.40.	cv-00-15.40	The Gorges	40	2818800	6200700	Te Waka Fm.	Wm
w02-0687	15.41	cv-00-15.41	The Gorges	40	2818800	6200700	Te Waka Fm.	Wm
w02-0688	15.42	cv-00-15.42	The Gorges	40	2818800	6200700	Te Waka Fm.	Wm
w02-0689	15.43	cv-00-15.43	The Gorges	40	2818800	6200700	Te Waka Fm.	Wm
w02-0690	15.44	cv-00-15.44	The Gorges	40	2818800	6200700	Te Waka Fm.	Wm
w02-0691	15.45	cv-00-15.45	The Gorges	40	2818800	6200700	Te Waka Fm.	Wm
w02-0692	15.46	cv-00-15.46	The Gorges	40	2818800	6200700	Te Waka Fm.	Wm
w02-0693	15.47	cv-00-15.47	The Gorges	40	2818800	6200700	Te Waka Fm.	Wm
w02-0694	15.48	cv-00-15.48	Omahaki	42	2803200	6186700	Te Waka Fm.	Wm
w02-0695	15.49	cv-00-15.49	Omahaki	42	2803200	6186700	Te Waka Fm.	Wm
w02-0696	15.50.	cv-00-15.50	Omahaki	42	2803200	6186700	Te Waka Fm.	Wm
w02-0697	15.51	cv-00-15.51	Omahaki	42	2803200	6186700	Te Waka Fm.	Wm
w02-0698	15.52	cv-00-15.52	Omahaki	42	2803200	6186700	Te Waka Fm.	Wm
w02-0699	15.53	cv-00-15.53	Omahaki	42	2803200	6186700	Te Waka Fm.	Wm
w02-0700	15.54	cv-00-15.54	Omahaki	42	2803200	6186700	Te Waka Fm.	Wm
w02-0701	15.55	cv-00-15.55	Omahaki	42	2803200	6186700	Te Waka Fm.	Wm
w02-0702	15.56	cv-00-15.56	Omahaki	42	2803200	6186700	Te Waka Fm.	Wm
w02-0703	15.57	cv-00-15.57	Omahaki	42	2803200	6186700	Te Waka Fm.	Wm
w02-0704	15.58	cv-00-15.58	Gentle Annie				Te Waka Fm.	Wm
w02-0705	16.1	cv-00-16.1	Awapai	44	2804100	6180200	Whanawhana Lst.	Wn
w02-0706	16.2	cv-00-16.2	Awapai	44	2804100	6180200	Whanawhana Lst.	Wn
w02-0707	16.3	cv-00-16.3	Awapai	44	2804100	6180200	Whanawhana Lst.	Wn
w02-0708	16.4	cv-00-16.4	Awapai	44	2804100	6180200	Whanawhana Lst.	Wn
w02-0709	16.5	cv-00-16.5	Awapai	44	2804100	6180200	Whanawhana Lst.	Wn
w02-0710	16.6	cv-00-16.6	Airstrip	43	2803300	6183500	Te Waka Fm.	Wm
w02-0711	16.7	cv-00-16.7	Airstrip	43	2803300	6183500	Te Waka Fm.	Wm
w02-0712	16.8	cv-00-16.8	Airstrip	43	2803300	6183500	Te Waka Fm.	Wm
w02-0713	16.9	cv-00-16.9	Airstrip	43	2803300	6183500	Te Waka Fm.	Wm
w02-0714	16.10.	cv-00-16.10	Airstrip	43	2803300	6183500	Te Waka Fm.	Wm
w02-0715	16.11		Airstrip	43	2803300	6183500	Te Waka Fm.	Wm
w02-0716	16.12	cv-00-16.12	Airstrip	43	2803300	6183500	Te Waka Fm.	Wm
w02-0717	16.13	cv-00-16.13	Airstrip	43	2803300	6183500	Te Waka Fm.	Wm
w02-0718	16.14	cv-00-16.14	Airstrip	43	2803300	6183500	Te Waka Fm.	Wm
w02-0719	16.15	cv-00-16.15	Airstrip	43	2803300	6183500	Te Waka Fm.	Wm
w02-0720	16.16	cv-00-16.16	Airstrip	43	2803300	6183500	Te Waka Fm.	Wm
w02-0721	16.17	cv-00-16.17	Airstrip	43	2803300	6183500	Te Waka Fm.	Wm
w02-0722	17.1	cv-00-17.1	Battery Point		2844800	6183400	Scinde Island Fm. (Mc)	Wn
w02-0723	17.2	cv-00-17.2	Battery Point		2844800	6183400	Scinde Island Fm. (Mc)	Wn
w02-0724	17.3	cv-00-17.3	Milton Road		2844800	6183400	Scinde Island Fm. (Mc)	Wn
w02-0725	17.4	cv-00-17.4	Milton Road		2844800	6183400	Scinde Island Fm. (Mc)	Wn
w02-0726	17.5	cv-00-17.5	Milton Road		2844800	6183400	Scinde Island Fm. (Mc)	Wn
w02-0727	17.6	cv-00-17.6	Bluff Hill		2847200	6184300	Scinde Island Fm. (Ma)	Wn
w02-0728	17.7	cv-00-17.7	Bluff Hill		2847200	6184300	Scinde Island Fm. (Ma)	Wn
w02-0729	17.8	cv-00-17.8	Bluff Hill		2847200	6184300	Scinde Island Fm. (Ma)	Wn
w02-0730	17.9	cv-00-17.9	Car Sale	36	2847200	6184300	Scinde Island Fm. (Me)	Wn
w02-0731	17.10.	cv-00-17.10	Car Sale	36	2847200	6184300	Scinde Island Fm. (Me)	Wn
w02-0732	17.11	cv-00-17.11	Car Sale	36	2847200	6184300	Scinde Island Fm. (Me)	Wn
w02-0733	17.12	cv-00-17.12	Car Sale	36	2847200	6184300	Scinde Island Fm. (Me)	Wn
w02-0734	17.13	cv-00-17.13	Car Sale	36	2847200	6184300	Scinde Island Fm. (Me)	Wn
w02-0735	17.14	cv-00-17.14	Car Sale	36	2847200	6184300	Scinde Island Fm. (Me)	Wn
w02-0736	17.15	cv-00-17.15	Car Sale	36	2847200	6184300	Scinde Island Fm. (Me)	Wn
w02-0737	17.16	cv-00-17.16	Car Sale	36	2847200	6184300	Scinde Island Fm. (Me)	Wn
w02-0738	17.17	cv-00-17.17	Faraday Winery		2845600	6182900	Scinde Island Fm. (Ma)	Wn
w02-0739	18.1	cv-00-18.1	Flag Range	45	2818400	6184500	Flag Range Lst.	Wn
w02-0740	18.2	cv-00-18.2	Flag Range	45	2818400	6184500	Flag Range Lst.	Wn
w02-0741	18.3	cv-00-18.3	Flag Range	45	2818400	6184500	Flag Range Lst.	Wn
w02-0742	18.4	cv-00-18.4	Flag Range	45	2818400	6184500	Flag Range Lst.	Wn
w02-0743	18.5	cv-00-18.5	Flag Range	45	2818400	6184500	Flag Range Lst.	Wn
w02-0744	18.6	cv-00-18.6	Flag Range	45	2818400	6184500	Flag Range Lst.	Wn

APPENDIX 2 - SAMPLE LIST

Waikato no.	Field no.	Thin section no.	Section/locality	Column	Grid reference		Formation	Stage
					East	North		
w02-0745		cv-611	North Mt Kahuranaki		2842300	6151500	Kairakau Lst.	Wo
w02-0746		cv-613	North Mt Kahuranaki		2842300	6151500	Kairakau Lst.	Wo
w02-0747		cv-618	Otanui		2845800	6150800	Kairakau Lst.	Wo
w02-0748		cv-621	Otanui		2845800	6150800	Kairakau Lst.	Wo
w02-0749		cv-637	Wairunga		2845000	6143400	Kairakau Lst.	Wo
w02-0750		cv-638	Wairunga		2845000	6143400	Kairakau Lst.	Wo
w02-0751		cv-639	Wairunga		2845000	6143400	Kairakau Lst.	Wo
w02-0752		cv-647	Kairakau		2844100	6130900	Kairakau Lst.	Wo
w02-0753		cv-650	Kairakau		2844100	6130900	Kairakau Lst.	Wo
w02-0754		cv-653	Kairakau		2844100	6130900	Kairakau Lst.	Wo
w02-0755		cv-654	Kairakau		2844100	6130900	Kairakau Lst.	Wo
w02-0756		cv-655	Ongaonga/core3		2801000	6140800	Rotookiwa Lst.	Wp
w02-0757		cv-656	Ongaonga/core3		2801000	6140800	Rotookiwa Lst.	Wp
w02-0758		cv-657	Takapau/core6		2892500	6131500	Awpapa Lst.	Wp
w02-0759		cv-658	Takapau/core6		2892500	6131500	Awpapa Lst.	Wp

APPENDIX 2 - MACROFAUNA

Sample: 4.8 **Waikato no.:** w02-0023
Location: North Mount Kahuranaki, V22/423 515 **Column:** 7
Stratigraphy: Sequence A, base of Kairakau Limestone
Age: Opoitian (inferred) **Range:** Wo - Wp
Fauna: *Phialopecten marwicki*

Sample: 4.63 **Waikato no.:** w02-0077
Location: Te Mata Peak, V22/452 597 **Column:** 9
Stratigraphy: Base of Tuki Bell limestone (informal)
Age: Opoitian **Range:** Wo
Fauna: *Phialopecten ongleyi*

Sample: 4.79 **Waikato no.:** w02-0095
Location: Taupata, V22/484 366 **Column:** 3
Stratigraphy: Shell bed at the base of sequence A of Kairakau Limestone
Age: Opoitian (inferred) **Range:** Wo -Wn
Fauna: *Ovicardium rossi*

Sample: 4.142 **Waikato no.:** w02-0161
Location: Kairakau Beach, V22/457 333 **Column:** 1/2
Stratigraphy: Shell bed at the base of sequence A of Kairakau Limestone
Age: Opoitian (inferred) **Range:** Wo - Wn
Fauna: *Purpurocardia purpurata*

Sample: 4.143 **Waikato no.:** w02-0162
Location: Kairakau Beach, V22/457 333 **Column:** 1/2
Stratigraphy: Sequence A of Kairakau Limestone
Age: Opoitian (inferred) **Range:** Wo - Wn
Fauna: *Tucetona laticostata*

Sample: 5.37 **Waikato no.:** w02-0205
Location: Te Mata Peak, V22/451 602 **Column:** 9-A2a
Stratigraphy: Shell lineation in sequence B1 of Awapapa Limestone
Age: Waipipian (inferred) **Range:** Wo - Wp
Fauna: *Phialopecten marwicki*

Sample: 5.41 **Waikato no.:** w02-0209
Location: Te Mata Peak, V22/ 451 602 **Column:** 9-A2a
Stratigraphy: Shell lineation in sequence B2 of Awapapa Limestone
Age: Waipipian (inferred) **Range:** Wo - Wp
Fauna: *Phialopecten marwicki*

Sample: 5.43 **Waikato no.:** w02-0211
Location: Te Mata Peak, V22/451 602 **Column:** 9-A2a
Stratigraphy: Upper part of sequence B2 of Awapapa Limestone
Age: Waipipian (inferred) **Range:** Wo - Wp
Fauna: *Phialopecten marwicki*

Sample: 5.50 **Waikato no.:** w02-0220
Location: Te Mata Peak, V22/451 602 **Column:** 9-A2b
Stratigraphy: Sequence F of Awapapa Limestone
Age: Waipipian (inferred) **Range:** Wo - Wp
Fauna: *Phialopecten marwicki*

Sample: 5.80 **Waikato no.:** w02-0253
Location: River Bank, V22/332 482 **Column:** 13
Stratigraphy: Awapapa Limestone
Age: Waipipian (inferred) **Range:** Wp -Wn
Fauna: *Mesopeplum convexum*

Sample: 5.136 **Waikato no.:** w02-0310
Location: Tainui, V22/285 469 **Column:** 15
Stratigraphy: Upper part of Pukekura Calcarenite
Age: Waipipian (inferred) **Range:** Wo - Wp
Fauna: *Mesopeplum crawfordi*

Sample: 5.137 **Waikato no.:** w02-0311
Location: Tainui, V22/285 469 **Column:** 15
Stratigraphy: Upper part of Pukekura Calcarenite
Age: Waipipian (inferred) **Range:** Wo - Wp
Fauna: *Phialopecten marwicki*

Sample: 5.138 **Waikato no.:** w02-0312
Location: Tainui, V22/285 469 **Column:** 15
Stratigraphy: Upper part of Pukekura Calcarenite
Age: Waipipian (inferred) **Range:** Wo - Wp
Fauna: *Mesopeplum crawfordi*

Sample: 7.2 **Waikato no.:** w02-0332
Location: Rotoatara, V22/251 451 **Column:** sample site
Stratigraphy: Rotookiwa Limestone
Age: Waipipian (inferred) **Range:** Wo - Wp
Fauna: *Phialopecten marwicki*

Sample: 9.19 **Waikato no.:** w02-0405
Location: Te Onepu Quarry, V22/198 491 **Column:** 23
Stratigraphy: Basal shell concentration in contact with underlying Argyll Sandstone
Age: Mangapanian **Range:** Wm
Fauna: *Phialopecten thomsoni*

Sample: 9.40 **Waikato no.:** w02-0426
Location: Bee Swarm, V22/193 484 **Column:** 24
Stratigraphy: Upper shell bed (base of sequence OD), Te Onepu Limestone
Age: Mangapanian **Range:** Wm
Fauna: *Phialopecten thomsoni*

Sample: 9.45 **Waikato no.:** w02-0431
Location: Robottom Grave, V22/148 422 **Column:** 26
Stratigraphy: Lower part of Te Onepu Limestone
Age: Mangapanian **Range:** Wm
Fauna: *Phialopecten thomsoni*

Sample: 9.54 **Waikato no.:** w02-0440
Location: Robottom Grave, V22/148 422 **Column:** 26
Stratigraphy: Shell lineation within sequence OC of Te Onepu Limestone
Age: Mangapanian **Range:** Wm
Faunal List: *Phialopecten thomsoni*
Towaipecten katieae

Sample: 9.65 **Waikato no.:** w02-0452
Location: Kiwi Bush, V22/149 427 **Column:** 25
Stratigraphy: Upper part of sequence OC of Te Onepu Limestone
Age: Mangapanian **Range:** Wm
Fauna: *Phialopecten thomsoni*

Sample: 9.67 **Waikato no.:** w02-0454
Location: Kiwi Bush, V22/149 427 **Column:** 25
Stratigraphy: Base of sequence OD of Te Onepu Limestone
Age: Nukumaruan **Range:** early Wn
Fauna: *Phialopecten triphooki*

Sample: 9.86 **Waikato no.:** w02-0473
Location: Gulch Quarry, V22/118 344 **Column:** 27
Stratigraphy: Condensed shell lineation at the base of sequence OB of Te Onepu Limestone
Age: Mangapanian **Range:** Wm
Fauna: *Phialopecten thomsoni*

Sample: 9.121 **Waikato no.:** w02-0508
Location: Tikokino Quarry, V22/118 372 **Column:** sample site
Stratigraphy: Te Onepu Limestone
Age: Mangapanian **Range:** Wm
Fauna: *Phialopecten thomsoni*

Sample: 11.24 **Waikato no.:** w02-0539
Location: Mangatai, V22/163 494 **Column:** 31
Stratigraphy: Upper part of sequence MD of Mason Ridge Formation
Age: Nukumaruan **Range:** early Wn
Fauna: *Phialopecten triphooki*

Sample: 11.48
Location: Croft Station, V21/221 610 **Column:** sample site
Stratigraphy: Above sequence MD of Mason Ridge Formation
Age: Nukumaruan **Range:** Wn

Faunal List:		**UWC:**
	Chlamys gemmulata	3031
	Patro undatus	3032
	Ostrea chiliensis	
	Gonomyrtea concinna	3082
	Felaniella (Zemysia) zelandica	3073
	Pleuromeris hectori	3093
	Purpurocardia purpurata	3035
	Volupicuna sp. indet.	3077
	Talabrica sp. indet.	3080
	Leptomya retiaria	3094
	Dosina zelandica	
	Tawera sp. indet.	3097
	Bivalvia gen. indet.	
	Tugali suteri	3095
	Maoricolpus roseus	3037
	Stiracolpus sp. indet.	3075
	Taxonia suteri	3088
	Crepidula costata	3081
	Sigapatella novaezelandiae	3089
	Trichosirius inornatus	3079
	Taniella planisuturalis	3038
	Cirsostrema cf. *zelebori*	3034
	Austrofusus sp. indet.	3037
	Iredalula venusta	3086
	Penion sp. indet.	3091
	Xymene plebius	

Neoguraleus sp. indet.	3090
Gastropoda gen. indet.	3076
Antalis nana	3085
Waltonia cf. *iconspicua*	3033
Echinoida ge. indet.	3087
Balanidae gen. indet.	3096
Cirripedia gen. indet.	
Decapoda gen. indet.	3083

APPENDIX 3

SEDIMENTARY MOTIFS

APPENDIX 3 - SEDIMENTARY MOTIFS

KEYS TO STRATIGRAPHIC SECTIONS

Where possible, all sedimentary structures have been represented as they were observed at outcrop. For features such as burrows, dewatering structures, convolute bedding, and slump structures, the scale of representation is exaggerated.

6 Running column numbers refer to localities on location map page A1-2 (Appendix 1)

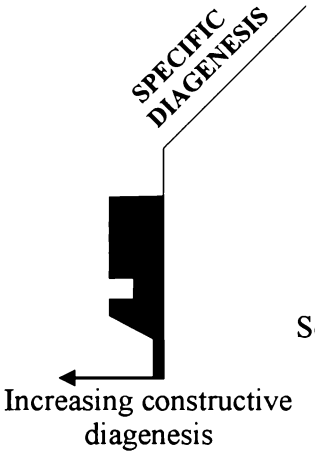

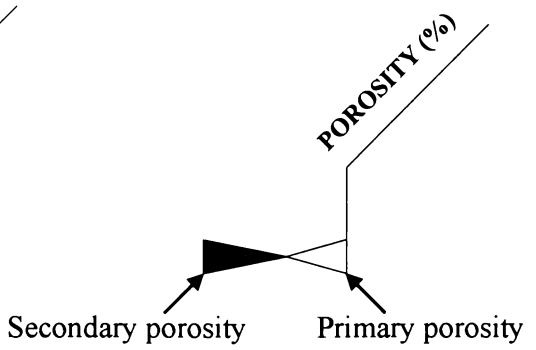

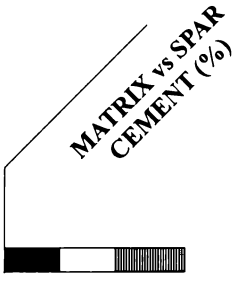

Matrix - Carbonate mud

Interparticle spar cement

Intraparticle spar cement

SEDIMENTARY SEQUENCE MOTIF: **M1, M2, M3, and M4**

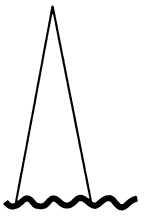

Deepening-upward

Erosional surface



Turnaround between deepening- and shallowing-upward trends, coincident with the condensed diagenetic horizon (Cdh)

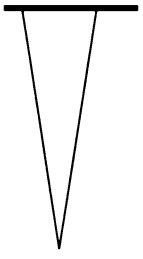

Sharp surface

Shallowing-upward

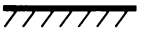

Subaerial unconformity

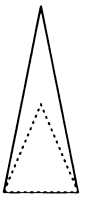

Lower-frequency sequence or alternative

MICROFACIES ASSEMBLAGE



Detrital



Bimol

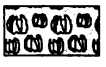

Barbital



Mixed skeletal

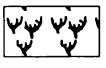

Bryotal

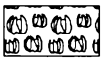

Barnamol

MACROFAUNA



Oysters



Biomoulds



Bivalves



Barnacles



Echinoids



Scallops



Bryozoans



Brachiopods



Gastropods

SAMPLES

●5.36 Rock sample ●F.5.32 Macrofauna sample

Te = Tephra layer

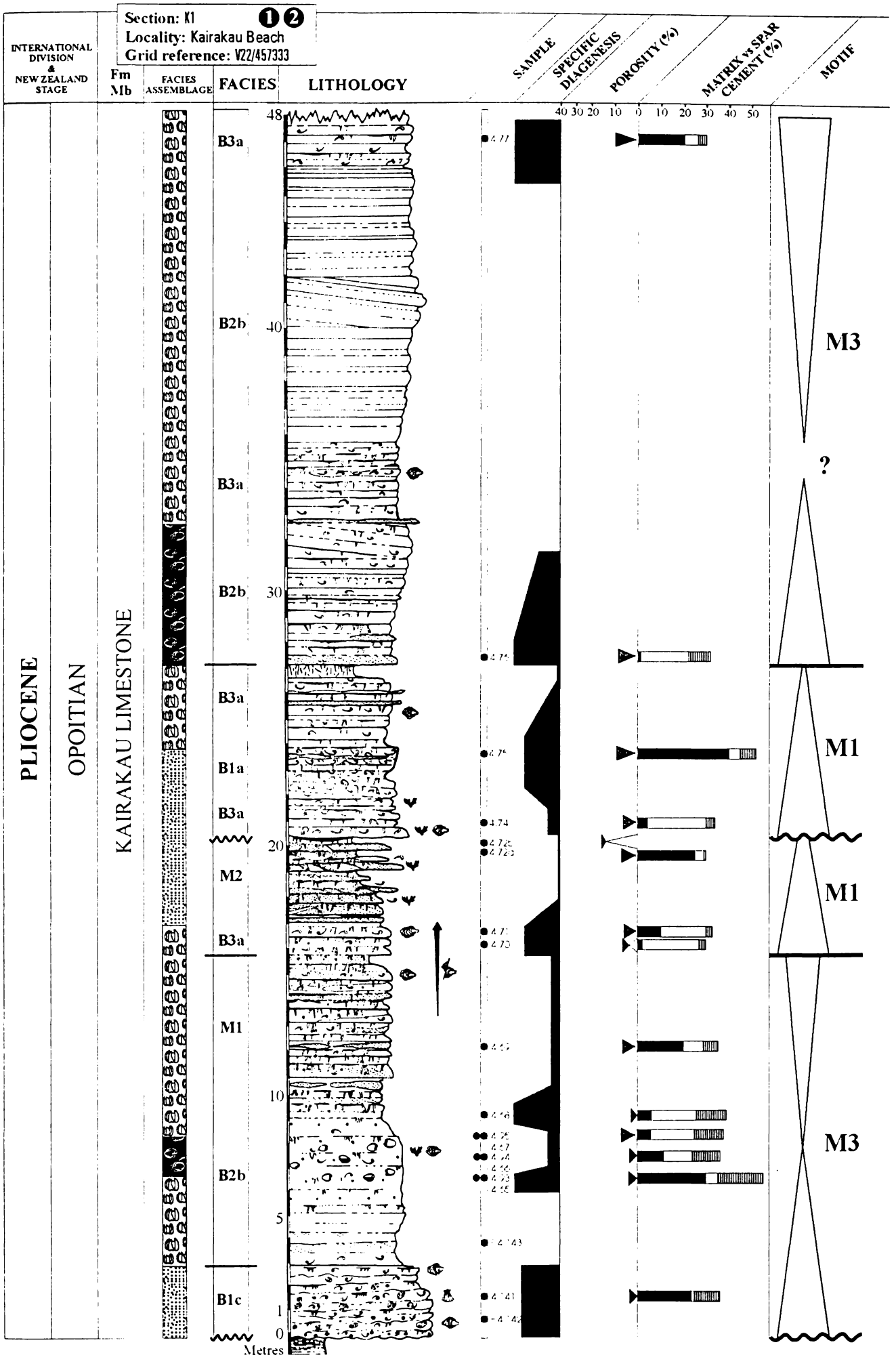
Section: K1
Locality: Kairakau Beach
Grid reference: V22/457333
INTERNATIONAL DIVISION & NEW ZEALAND STAGE
Fm Mb
FACIES ASSEMBLAGE
FACIES
LITHOLOGY
SAMPLE
SPECIFIC DIAGENESIS
POROSITY (%)
MATRIX vs SPAR CEMENT (%)
MOTIF
PLIOCENE
OPOITIAN
KAIRAKAU LIMESTONE
B3a
B2b
B3a
B2b
B3a
B1a
B3a
M2
B3a
M1
B2b
B1c
Metres
M3
?
M1
M1
M3

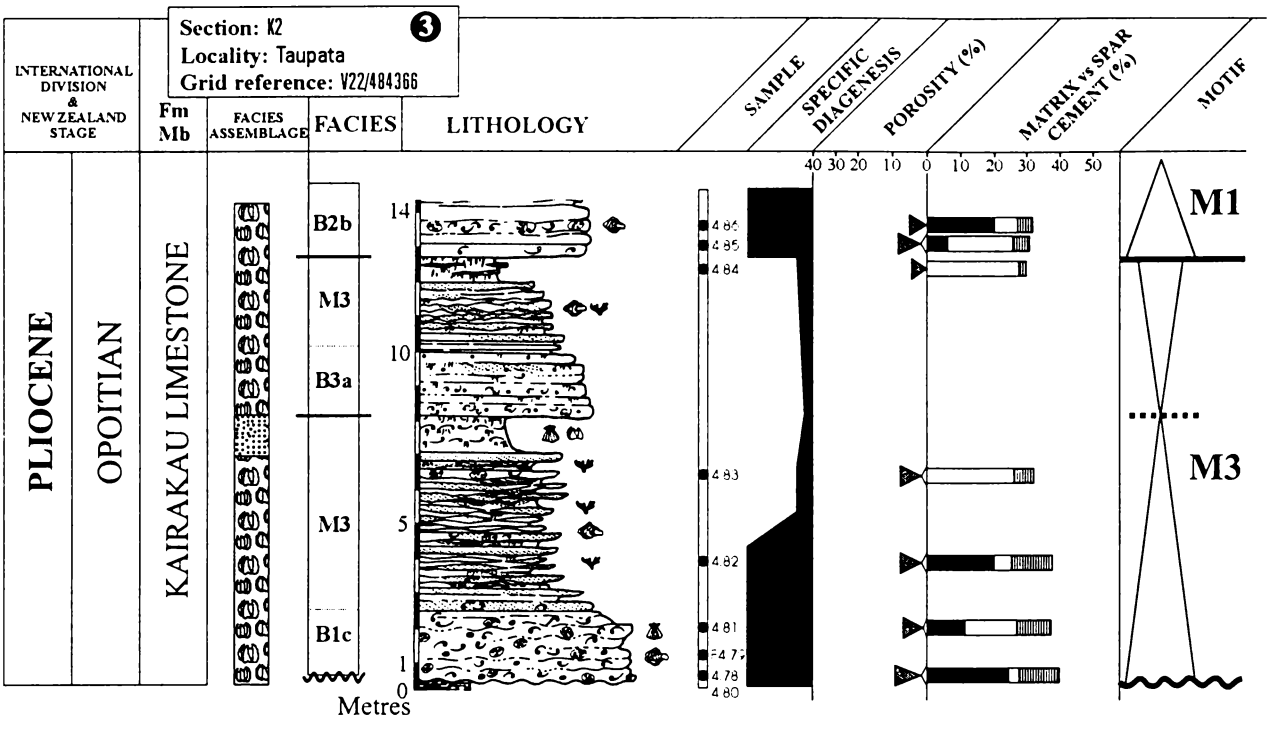
Section: K2
Locality: Taupata
Grid reference: V22/484366
3
INTERNATIONAL DIVISION & NEW ZEALAND STAGE
Fm Mb
FACIES ASSEMBLAGE
FACIES
LITHOLOGY
SAMPLE
SPECIFIC DIAGENESIS
POROSITY (%)
MATRIX vs SPAR CEMENT (%)
MOTIF
PLIOCENE
OPOITIAN
KAIRAKAU LIMESTONE
B2b
M3
B3a
M3
B1c
14
10
5
1
0
Metres
4 86
4 85
4 84
4 83
4 82
4 81
4 78
4 80
40 30 20 10 0 10 20 30 40 50
M1
M3

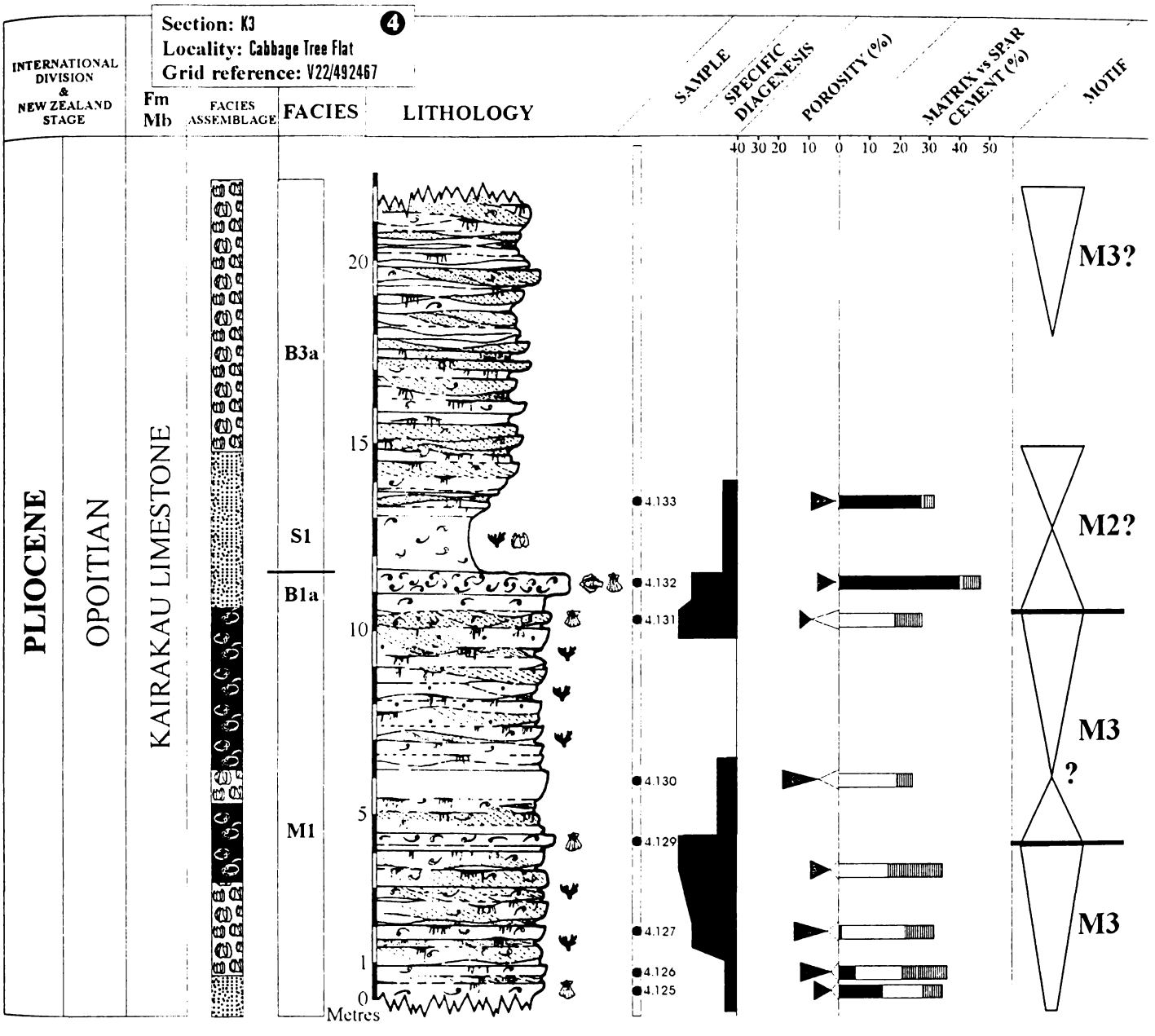
Section: K3
Locality: Cabbage Tree Flat
Grid reference: V22/492467
4
INTERNATIONAL DIVISION & NEW ZEALAND STAGE
Fm Mb
FACIES ASSEMBLAGE
FACIES
LITHOLOGY
SAMPLE
SPECIFIC DIAGENESIS
POROSITY (%)
MATRIX vs SPAR CEMENT (%)
MOTIF
PLIOCENE
OPOITIAN
KAIRAKAU LIMESTONE
B3a
S1
B1a
M1
20
15
10
5
1
0
Metres
4.133
4.132
4.131
4.130
4.129
4.127
4.126
4.125
40 30 20 10 0 10 20 30 40 50
M3?
M2?
M3
?
M3

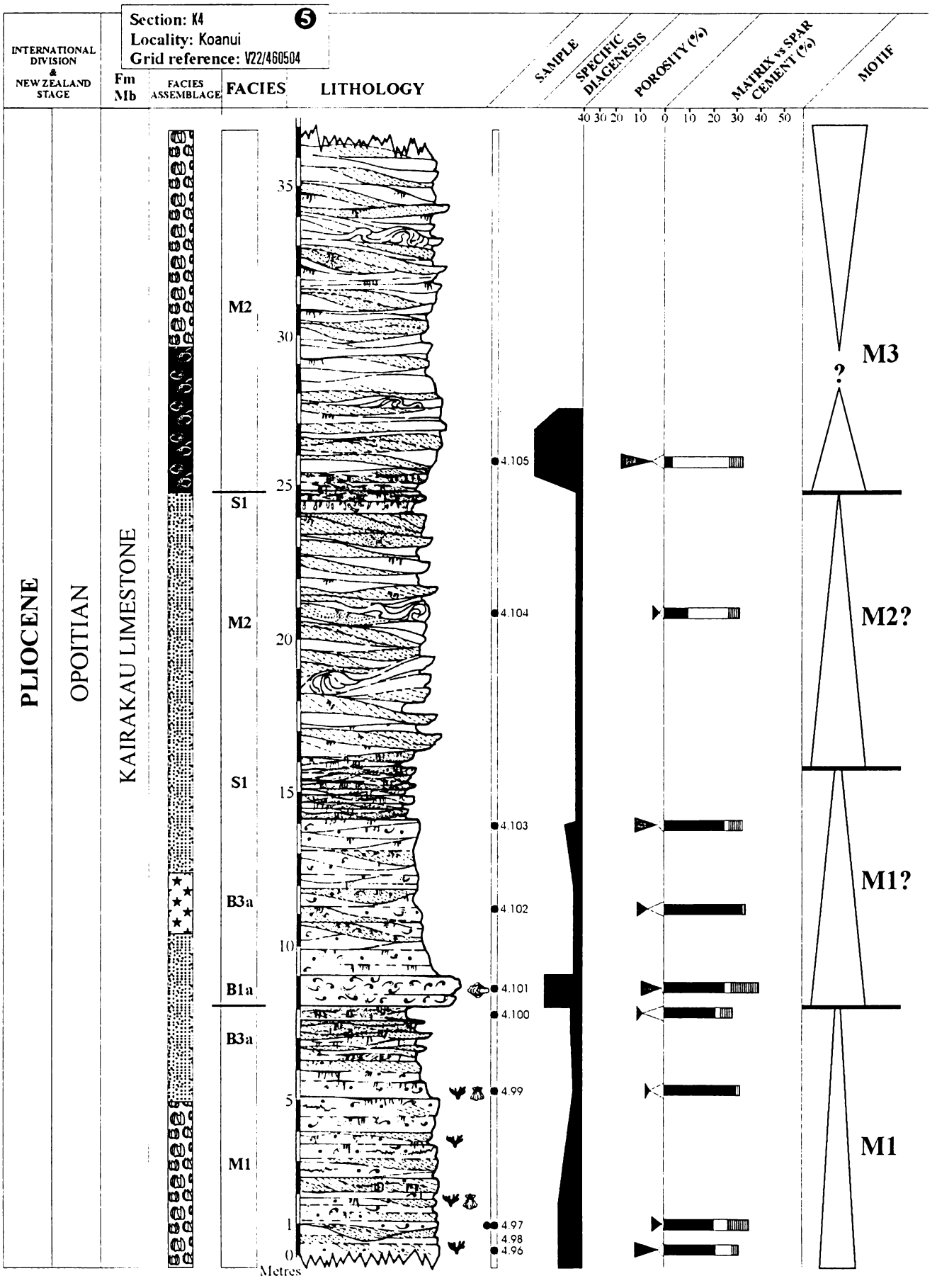
Section: K4
Locality: Koanui
Grid reference: V22/460504
INTERNATIONAL DIVISION & NEW ZEALAND STAGE
Fm
Mb
FACIES ASSEMBLAGE
FACIES
LITHOLOGY
SAMPLE
SPECIFIC DIAGENESIS
POROSITY (%)
MATRIX vs SPAR CEMENT (%)
MOTIF
40 30 20 10 0 10 20 30 40 50
PLIOCENE
OPOITIAN
KAIRAKAU LIMESTONE
M2
S1
M2
S1
B3a
B1a
B3a
M1
35
30
25
20
15
10
5
1
0
Metres
4.105
4.104
4.103
4.102
4.101
4.100
4.99
4.97
4.98
4.96
M3
?
M2?
M1?
M1

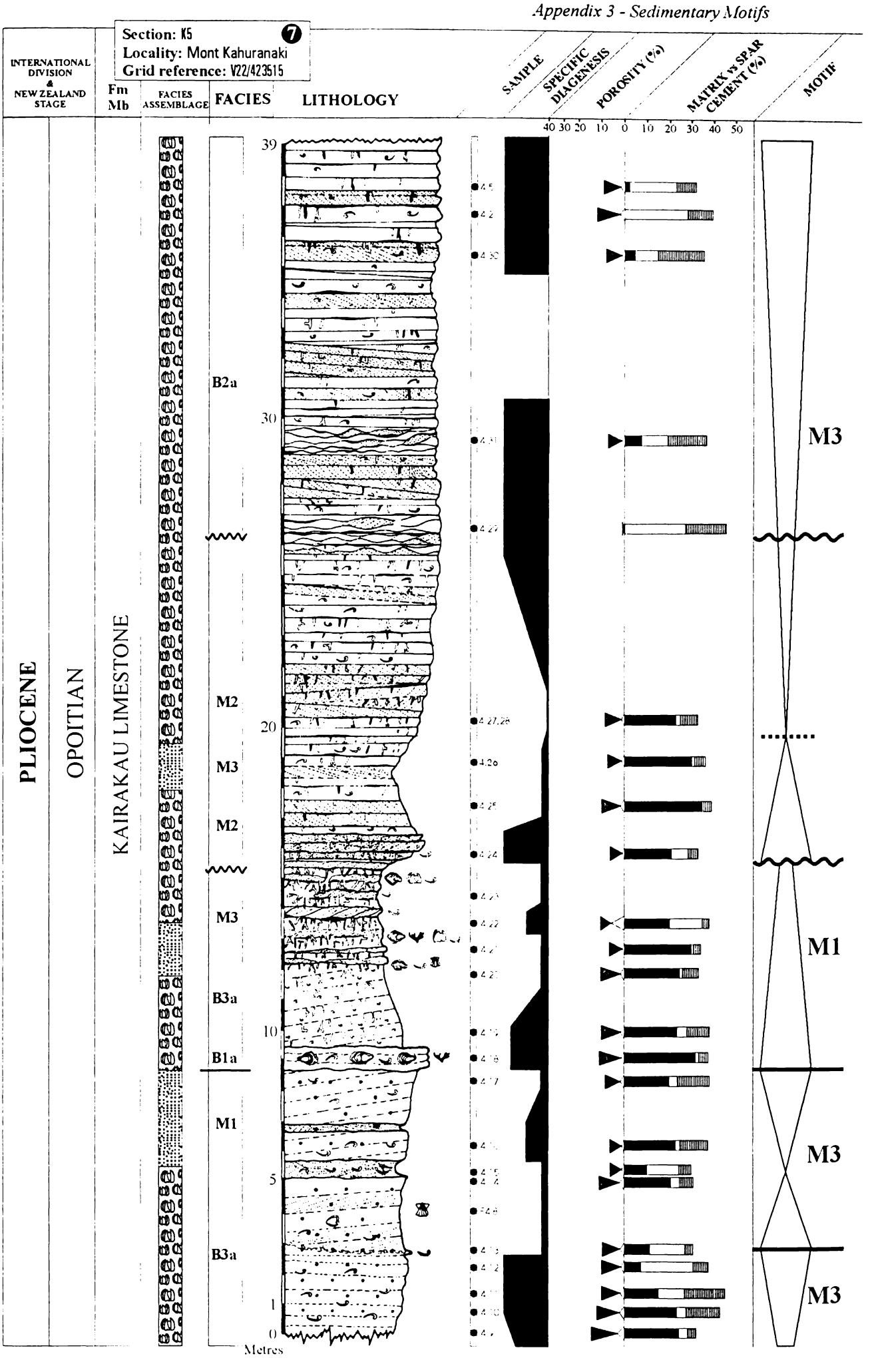
Section: K5
Locality: Mont Kahuranaki
Grid reference: V22/423515
INTERNATIONAL DIVISION & NEW ZEALAND STAGE
Fm
Mb
FACIES ASSEMBLAGE
FACIES
LITHOLOGY
SAMPLE
SPECIFIC DIAGENESIS
POROSITY (%)
MATRIX vs SPAR CEMENT (%)
MOTIF
40 30 20 10 0 10 20 30 40 50
PLIOCENE
OPOITIAN
KAIRAKAU LIMESTONE
B2a
M2
M3
M2
M3
B3a
B1a
M1
B3a
39
30
20
10
5
1
0
Metres
M3
M1
M3
M3

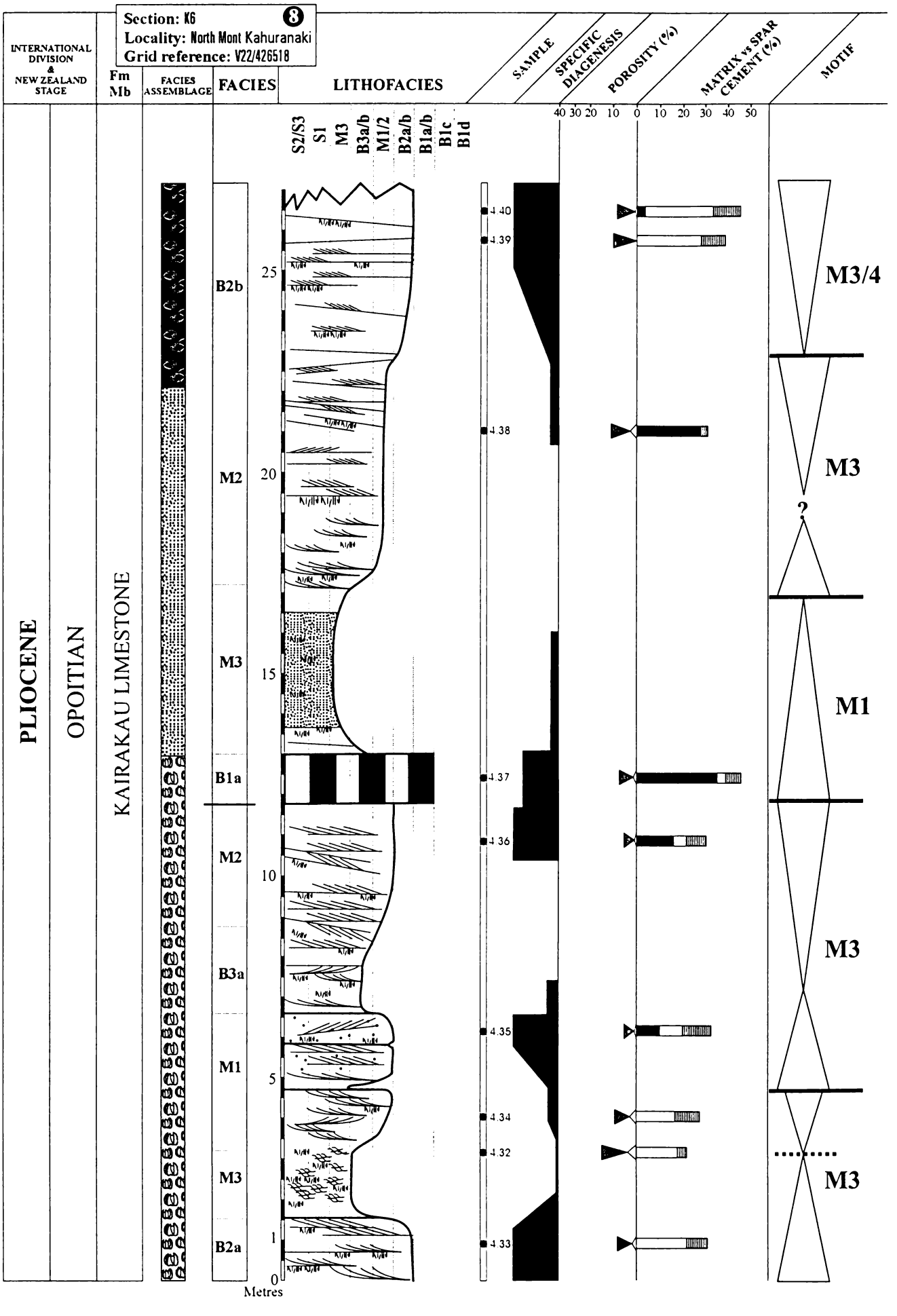
Section: K6
8
Locality: North Mont Kahuranaki
Grid reference: V22/426518
INTERNATIONAL DIVISION & NEW ZEALAND STAGE
Fm Mb
FACIES ASSEMBLAGE
FACIES
LITHOFACIES
SAMPLE
SPECIFIC DIAGENESIS
POROSITY (%)
MATRIX vs SPAR CEMENT (%)
MOTIF
PLIOCENE
OPOITIAN
KAIRAKAU LIMESTONE
S2/S3
S1
M3
B3a/b
M1/2
B2a/b
B1a/b
B1c
B1d
40 30 20 10 0 10 20 30 40 50
B2b
M2
M3
B1a
M2
B3a
M1
M3
B2a
25
20
15
10
5
1
0
Metres
4.40
4.39
4.38
4.37
4.36
4.35
4.34
4.32
4.33
M3/4
M3
?
M1
M3
M3

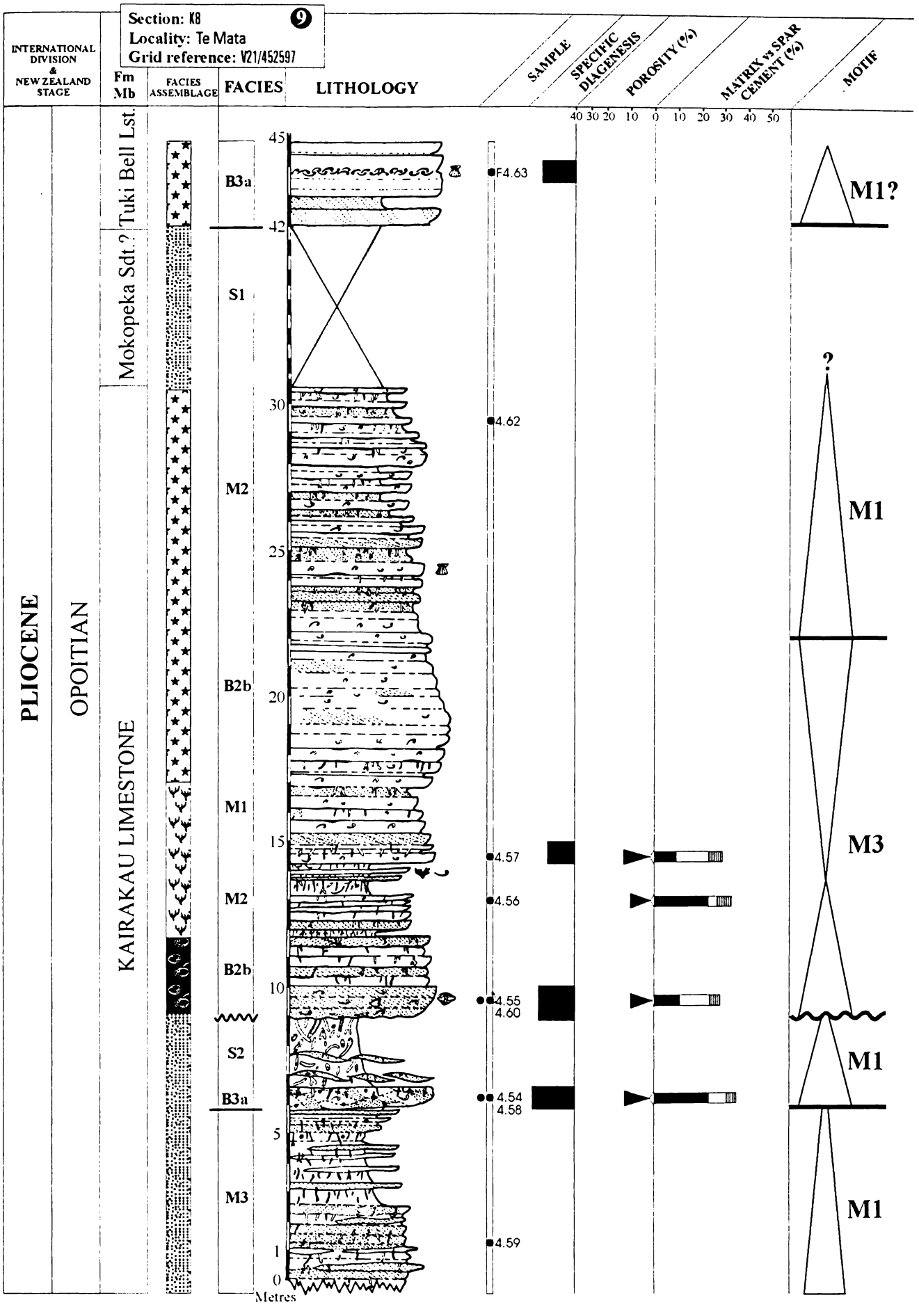
Section: K8
9
Locality: Te Mata
Grid reference: V21/452597
INTERNATIONAL DIVISION & NEW ZEALAND STAGE
PLIOCENE
OPOITIAN
Fm Mb
Tuki Bell Lst.
Mokopeka Sdt.?
KAIRAKAU LIMESTONE
FACIES ASSEMBLAGE
FACIES
LITHOLOGY
B3a
S1
M2
B2b
M1
M2
B2b
S2
B3a
M3
45
42
30
25
20
15
10
5
1
0
Metres
SAMPLE
F4.63
4.62
4.57
4.56
4.55
4.60
4.54
4.58
4.59
SPECIFIC DIAGENESIS
POROSITY (%)
40 30 20 10 0 10 20 30 40 50
MATRIX vs SPAR CEMENT (%)
MOTIF
M1?
?
M1
M3
M1
M1

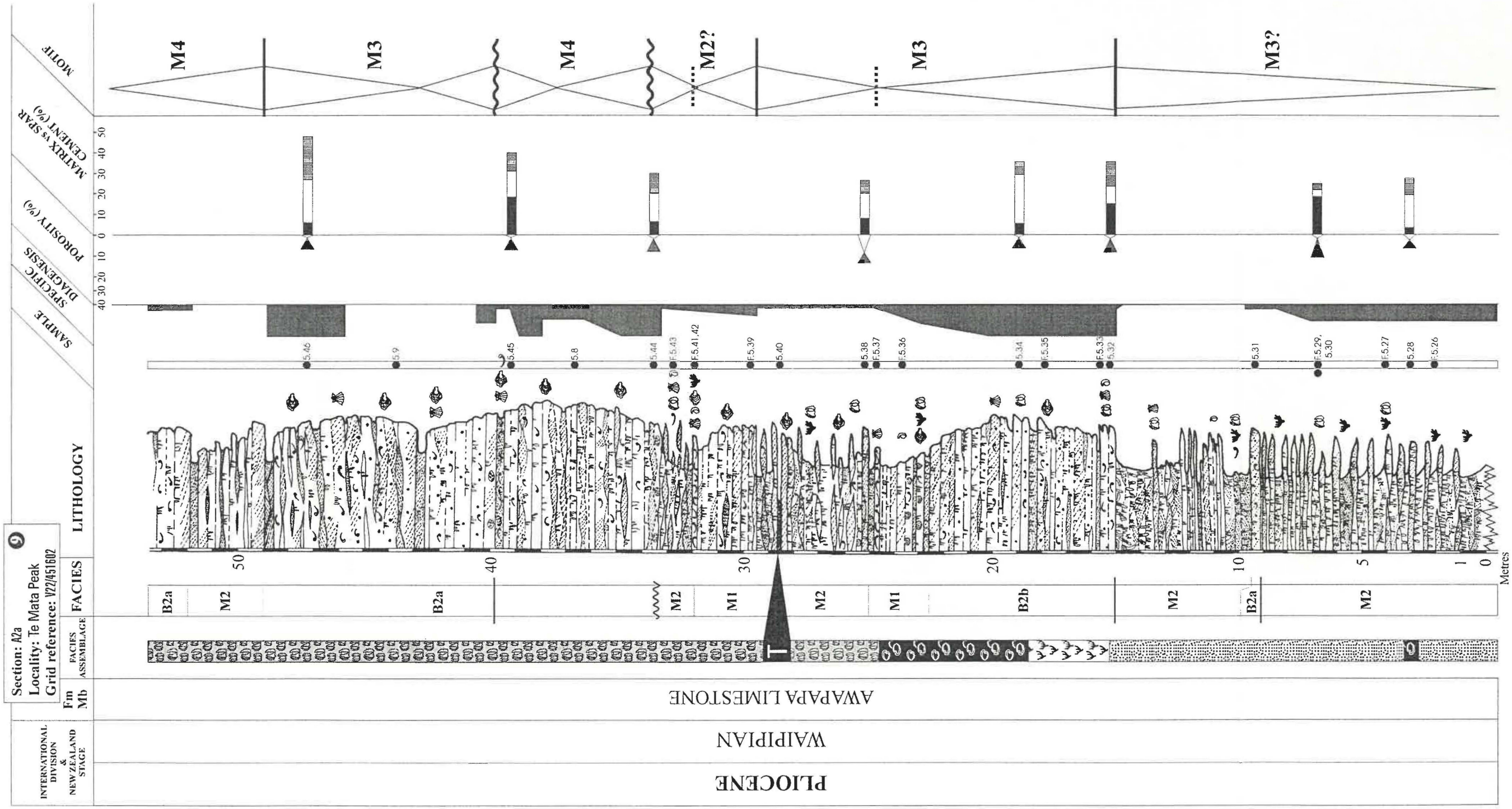
Section: A2a
Locality: Te Mata Peak
Grid reference: V22/451602
INTERNATIONAL DIVISION & NEW ZEALAND STAGE
PLIOCENE
WAIPIPIAN
AWAPAPA LIMESTONE
Fm Mb
FACIES ASSEMBLAGE
FACIES
LITHOLOGY
SAMPLE
SPECIFIC DIAGENESIS
POROSITY (%)
MATRIX vs SPAR CEMENT (%)
MOTIF
M4
M3
M4
M2?
M3
M3?
B2a
M2
B2a
M2
M1
M2
M1
B2b
M2
B2a
M2
Metres

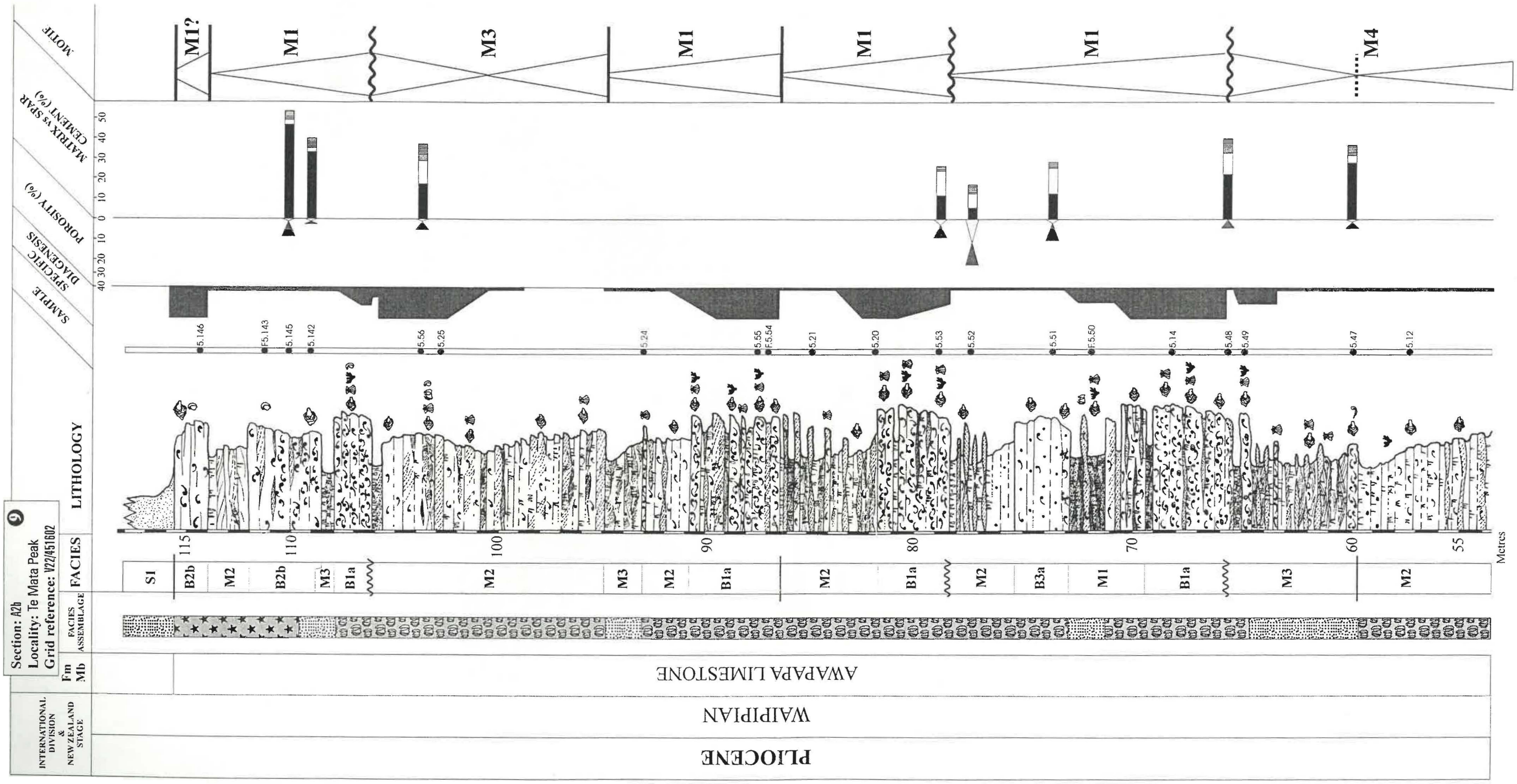
Section: A2b
Locality: Te Mata Peak
Grid reference: V22/451602
INTERNATIONAL DIVISION & NEW ZEALAND STAGE
PLIOCENE
WAIPIPIAN
Fm
Mb
AWAPAPA LIMESTONE
FACIES ASSEMBLAGE
FACIES
LITHOLOGY
SAMPLE
SPECIFIC DIAGENESIS
POROSITY (%)
MATRIX vs SPAR CEMENT (%)
MOTIF
M1?
M1
M3
M1
M1
M1
M4
S1
B2b
M2
B2b
M3
B1a
M2
M3
M2
B1a
M2
B1a
M2
B3a
M1
B1a
M3
M2
115
110
100
90
80
70
60
55
Metres

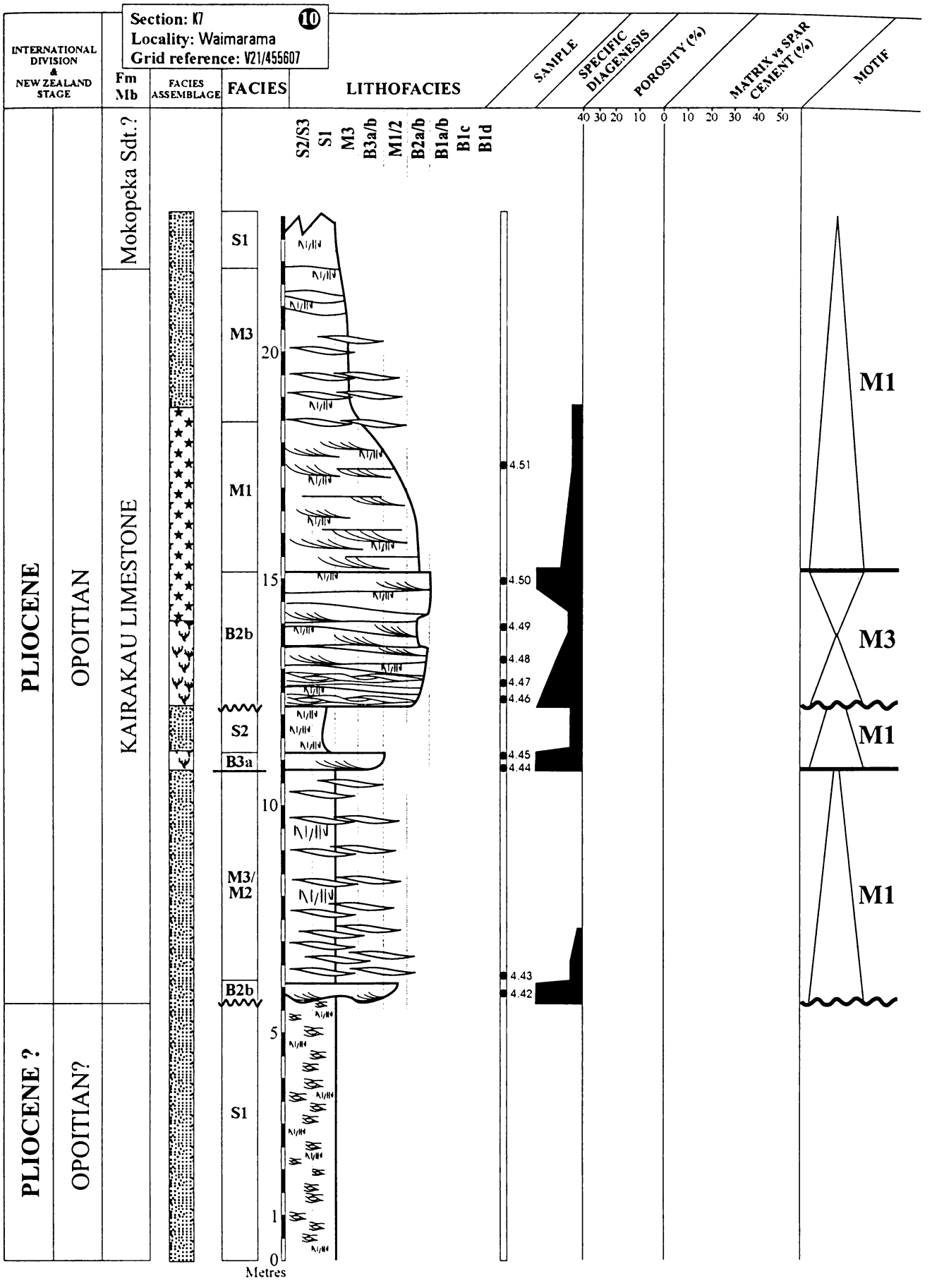
Section: K7
Locality: Waimarama
Grid reference: V21/455607
10
INTERNATIONAL DIVISION & NEW ZEALAND STAGE
Fm Mb
FACIES ASSEMBLAGE
FACIES
LITHOFACIES
SAMPLE
SPECIFIC DIAGENESIS
POROSITY (%)
MATRIX vs SPAR CEMENT (%)
MOTIF
S2/S3
S1
M3
B3a/b
M1/2
B2a/b
B1a/b
B1c
B1d
40 30 20 10 0 10 20 30 40 50
PLIOCENE
OPOITIAN
Mokopeka Sdt.?
KAIRAKAU LIMESTONE
PLIOCENE ?
OPOITIAN?
S1
M3
M1
B2b
S2
B3a
M3/ M2
B2b
S1
20
15
10
5
1
0
Metres
4.51
4.50
4.49
4.48
4.47
4.46
4.45
4.44
4.43
4.42
M1
M3
M1
M1

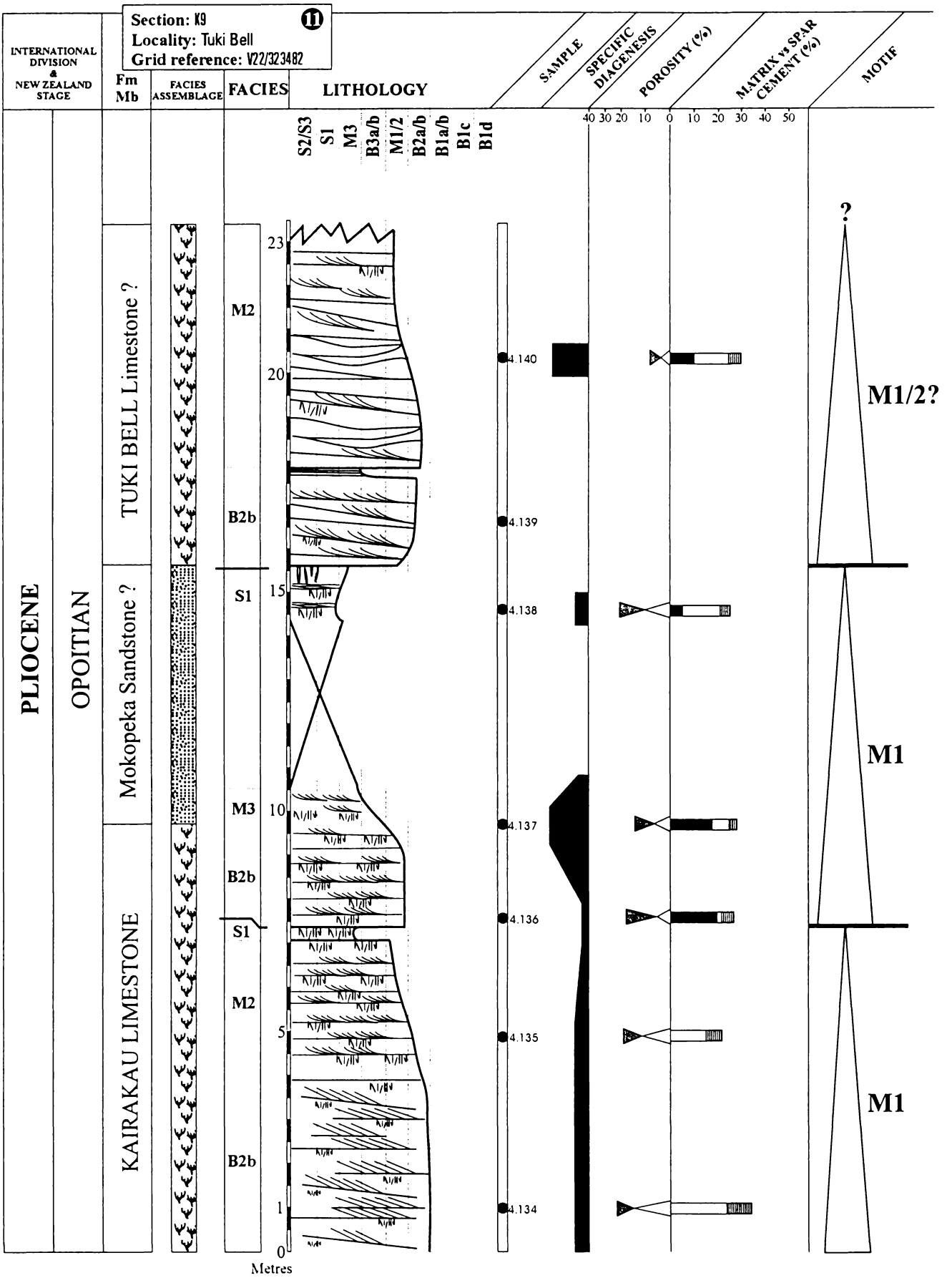
Section: K9
Locality: Tuki Bell
Grid reference: V22/323482
INTERNATIONAL DIVISION & NEW ZEALAND STAGE
Fm Mb
FACIES ASSEMBLAGE
FACIES
LITHOLOGY
SAMPLE
SPECIFIC DIAGENESIS
POROSITY (%)
MATRIX vs SPAR CEMENT (%)
MOTIF
S2/S3
S1
M3
B3a/b
M1/2
B2a/b
B1a/b
B1c
B1d
40 30 20 10 0 10 20 30 40 50
PLIOCENE
OPOITIAN
TUKI BELL Limestone ?
Mokopeka Sandstone ?
KAIRAKAU LIMESTONE
M2
B2b
S1
M3
B2b
S1
M2
B2b
23
20
15
10
5
1
0
4.140
4.139
4.138
4.137
4.136
4.135
4.134
?
M1/2?
M1
M1
Metres

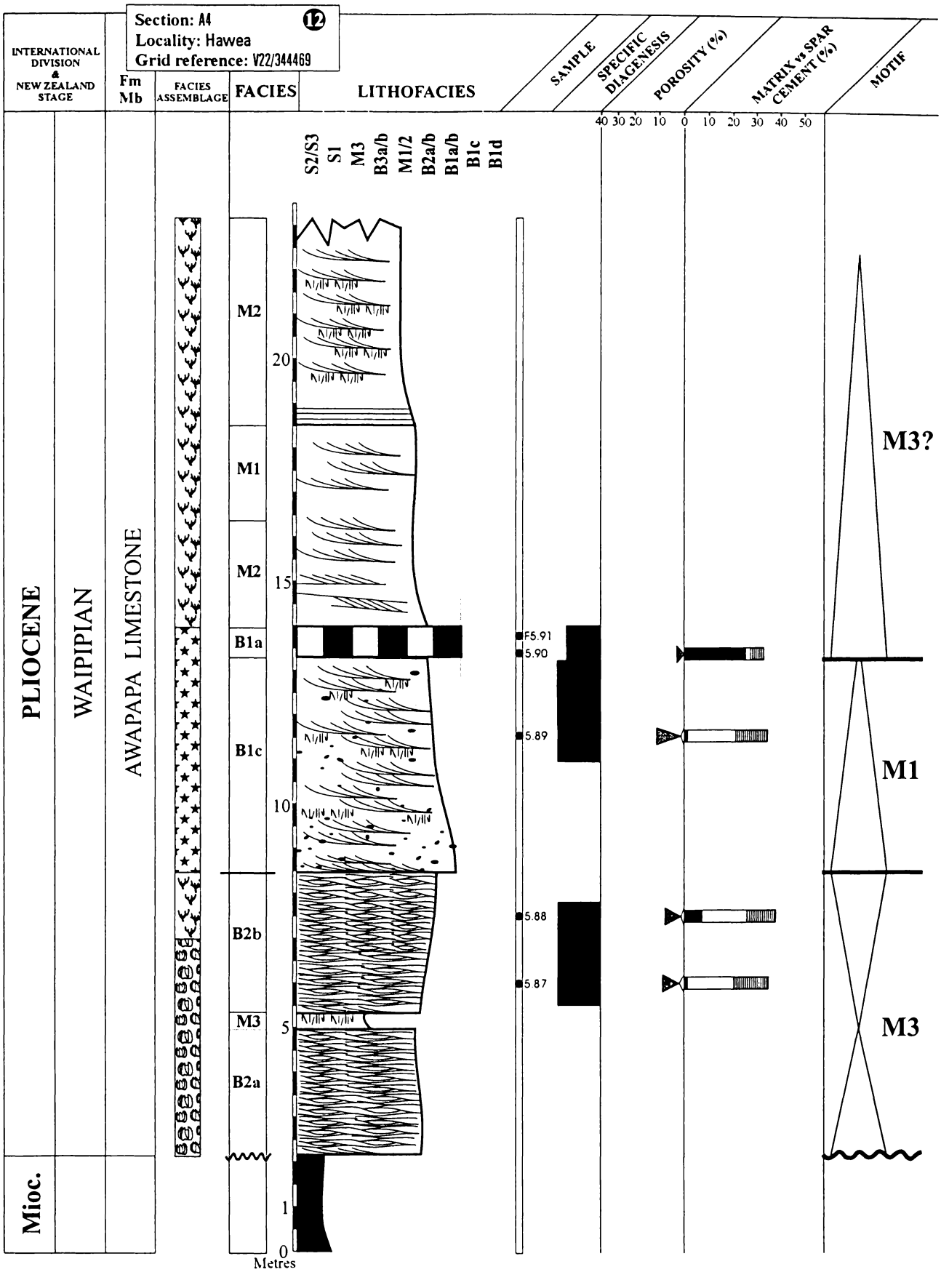
Section: A4
Locality: Hawea
Grid reference: V22/344469
INTERNATIONAL DIVISION & NEW ZEALAND STAGE
Fm Mb
FACIES ASSEMBLAGE
FACIES
LITHOFACIES
SAMPLE
SPECIFIC DIAGENESIS
POROSITY (%)
MATRIX vs SPAR CEMENT (%)
MOTIF
S2/S3 S1 M3 B3a/b M1/2 B2a/b B1a/b B1c B1d
40 30 20 10 0 10 20 30 40 50
PLIOCENE
WAIPIPIAN
AWAPAPA LIMESTONE
Mioc.
M2
M1
M2
B1a
B1c
B2b
M3
B2a
20
15
10
5
1
0
Metres
F5.91
5.90
5.89
5.88
5.87
M3?
M1
M3

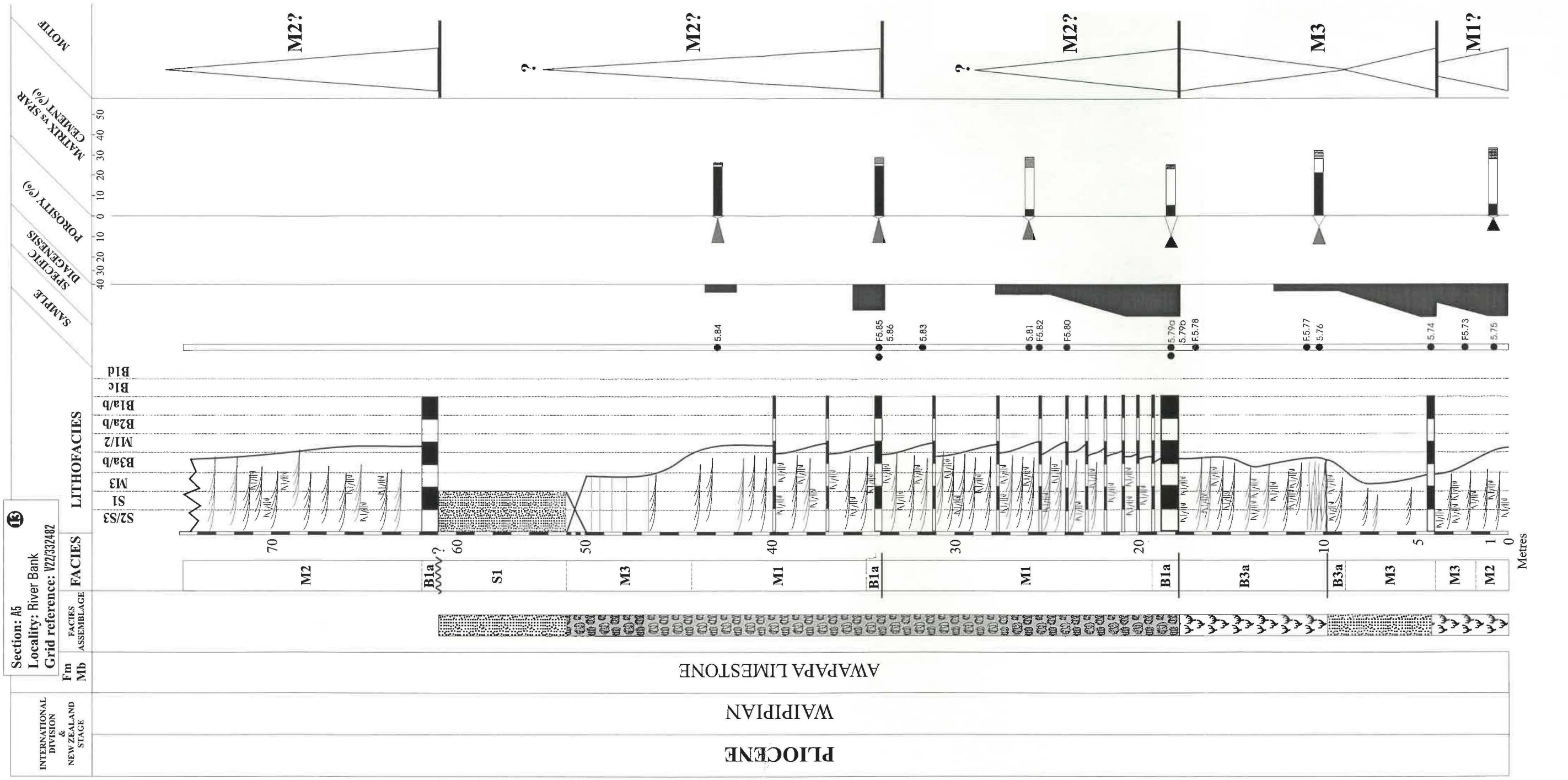
MOTIF
M2?
?
M2?
?
M2?
M3
M1?
MATRIX VS SPAR CEMENT (%)
POROSITY (%)
SPECIFIC DIAGENESIS
SAMPLE
5.84
F5.85
5.86
5.83
5.81
F5.82
F5.80
5.79a
5.79b
F.5.78
F.5.77
5.76
5.74
F5.73
5.75
B1d
B1c
B1a/b
B2a/b
M1/2
B3a/b
M3
S1
S2/S3
LITHOFACIES
FACIES
FACIES ASSEMBLAGE
Fm
Mb
INTERNATIONAL DIVISION & NEW ZEALAND STAGE
Section: A5
Locality: River Bank
Grid reference: V22/332482
M2
B1a
?
S1
M3
M1
B1a
M1
B1a
B3a
B3a
M3
M3
M2
70
60
50
40
30
20
10
5
1
0
Metres
AWAPAPA LIMESTONE
WAIPIPIAN
PLIOCENE

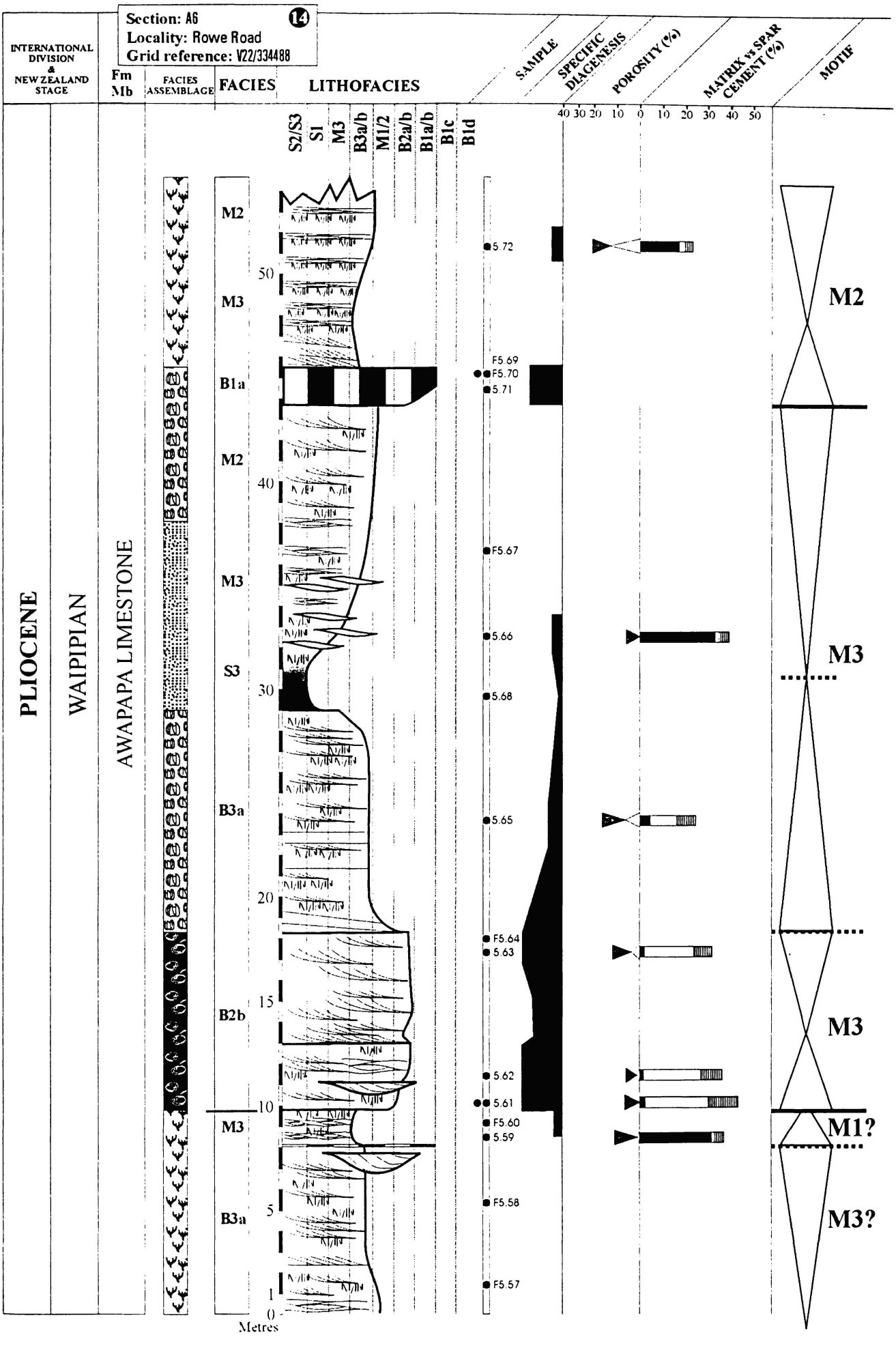
Section: A6
Locality: Rowe Road
Grid reference: V22/334488
INTERNATIONAL DIVISION & NEW ZEALAND STAGE
Fm Mb
FACIES ASSEMBLAGE
FACIES
LITHOFACIES
SAMPLE
SPECIFIC DIAGENESIS
POROSITY (%)
MATRIX vs SPAR CEMENT (%)
MOTIF
S2/S3
S1
M3
B3a/b
M1/2
B2a/b
B1a/b
B1c
B1d
40 30 20 10 0 10 20 30 40 50
PLIOCENE
WAIPIPIAN
AWAPAPA LIMESTONE
M2
M3
B1a
M2
M3
S3
B3a
B2b
M3
B3a
50
40
30
20
15
10
5
1
0
Metres
5.72
F5.69
F5.70
5.71
F5.67
5.66
5.68
5.65
F5.64
5.63
5.62
5.61
F5.60
5.59
F5.58
F5.57
M2
M3
M3
M1?
M3?

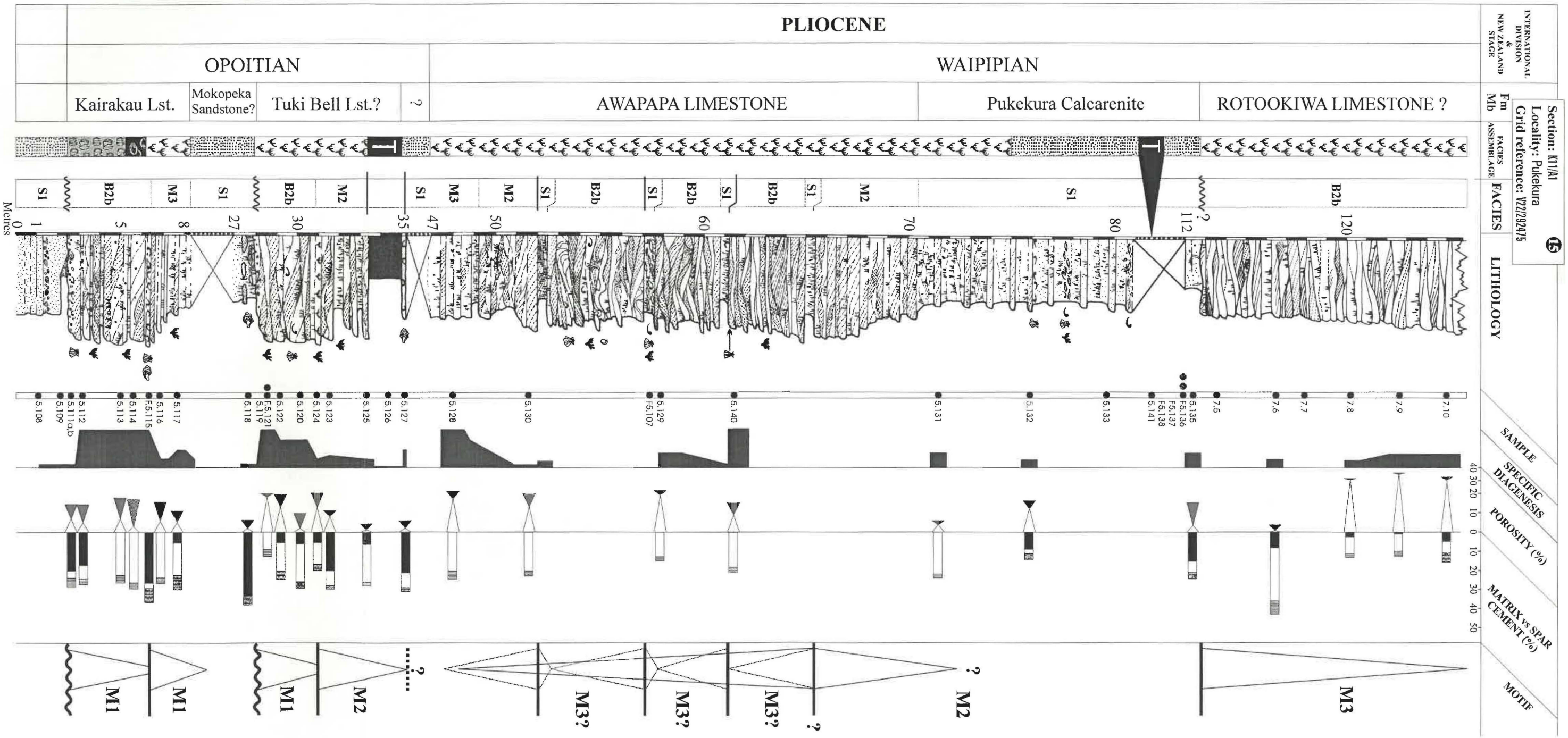

Appendix 3 - Sedimentary Motifs

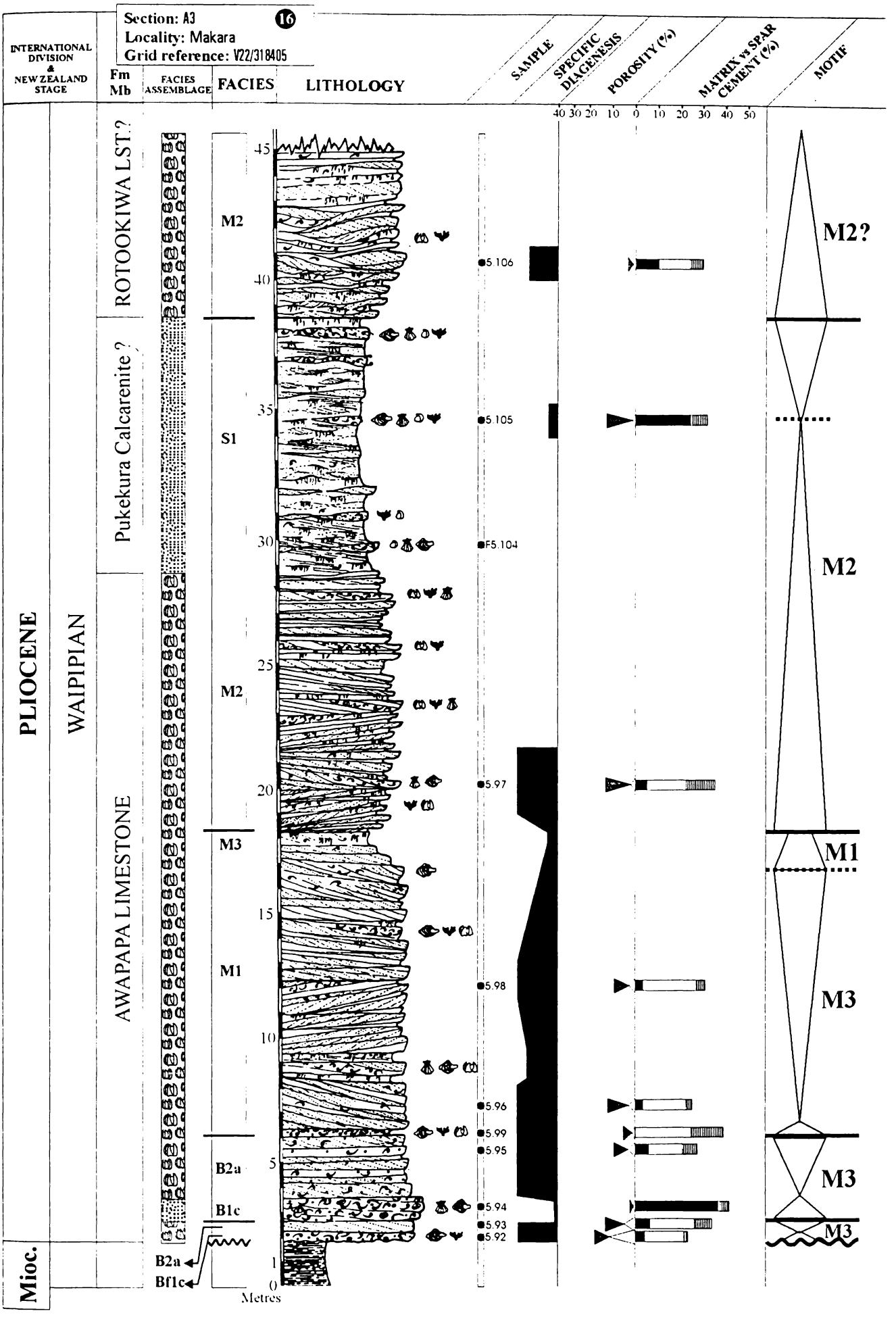
Section: A3
Locality: Makara
Grid reference: V22/318405
INTERNATIONAL DIVISION & NEW ZEALAND STAGE
Fm Mb
FACIES ASSEMBLAGE
FACIES
LITHOLOGY
SAMPLE
SPECIFIC DIAGENESIS
POROSITY (%)
MATRIX vs SPAR CEMENT (%)
MOTIF
40 30 20 10 0 10 20 30 40 50
PLIOCENE
WAIPIPIAN
Mioc.
ROTOOKIWA LST ?
Pukekura Calcarenite ?
AWAPAPA LIMESTONE
M2
S1
M2
M3
M1
B2a
B1c
B2a
Bf1c
45
40
35
30
25
20
15
10
5
1
0
Metres
5.106
5.105
F5.104
5.97
5.98
5.96
5.99
5.95
5.94
5.93
5.92
M2?
M2
M1
M3
M3
M3

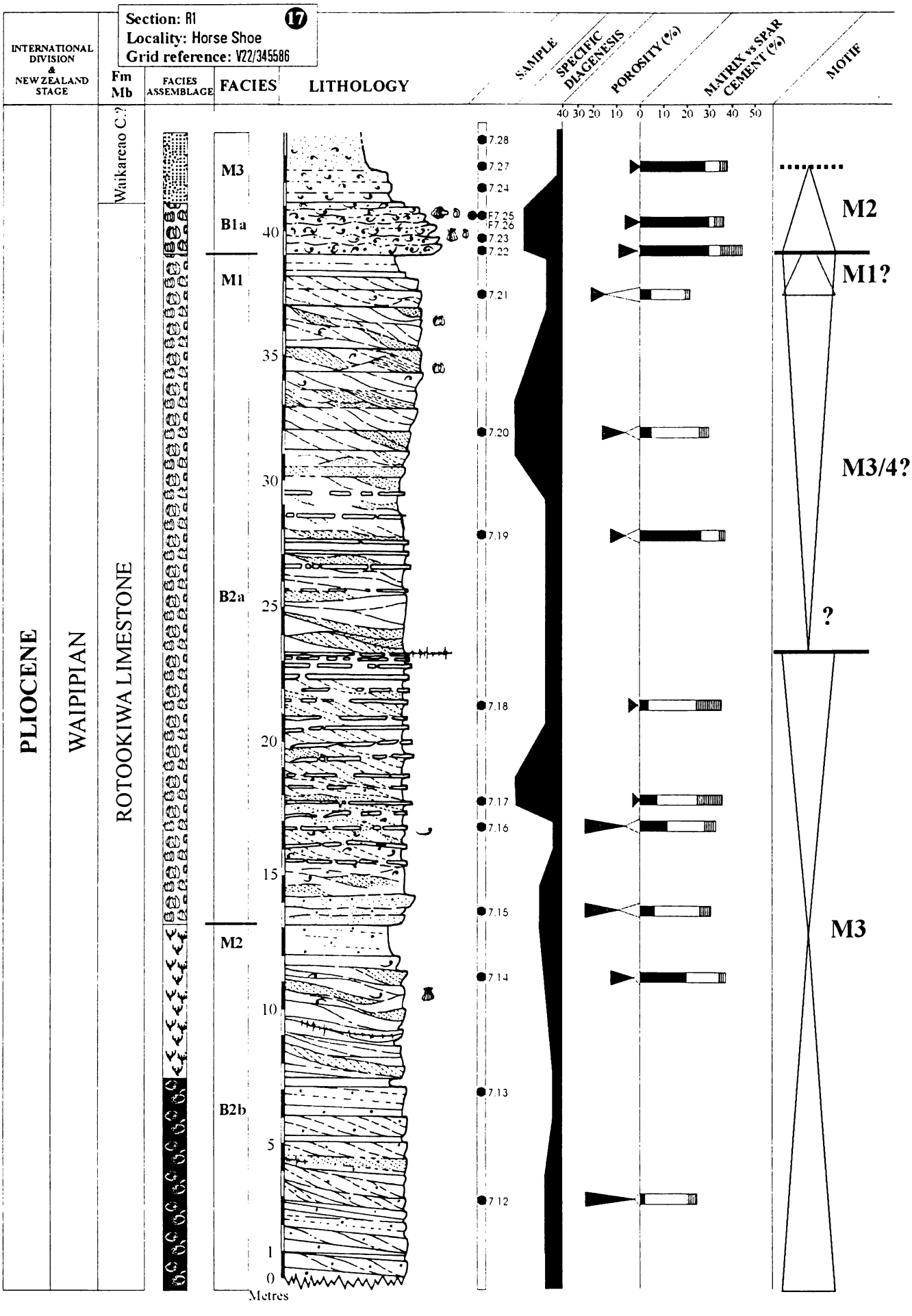
Section: A1
Locality: Horse Shoe
Grid reference: V22/345586
INTERNATIONAL DIVISION & NEW ZEALAND STAGE
Fm Mb
FACIES ASSEMBLAGE
FACIES
LITHOLOGY
SAMPLE
SPECIFIC DIAGENESIS
POROSITY (%)
MATRIX vs SPAR CEMENT (%)
MOTIF
PLIOCENE
WAIPIPIAN
ROTOOKIWA LIMESTONE
Waikareao C.?
M3
B1a
M1
B2a
M2
B2b
Metres
M2
M1?
M3/4?
?
M3

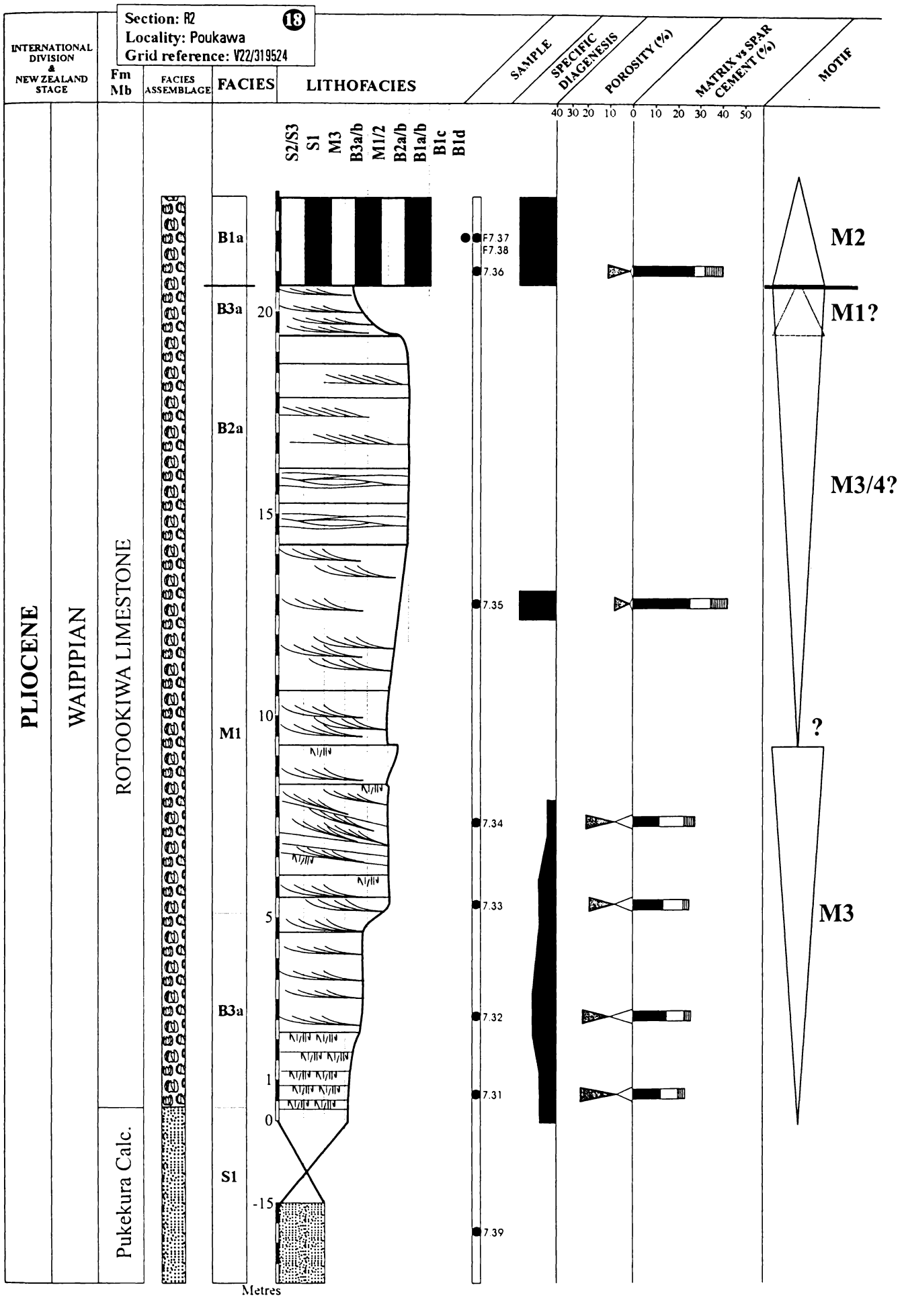
Section: R2
Locality: Poukawa
Grid reference: V22/319524
18
INTERNATIONAL DIVISION & NEW ZEALAND STAGE
Fm Mb
FACIES ASSEMBLAGE
FACIES
LITHOFACIES
SAMPLE
SPECIFIC DIAGENESIS
POROSITY (%)
MATRIX vs SPAR CEMENT (%)
MOTIF
PLIOCENE
WAIPIPIAN
ROTOOKIWA LIMESTONE
Pukekura Calc.
S2/S3
S1
M3
B3a/b
M1/2
B2a/b
B1a/b
B1c
B1d
B1a
B3a
B2a
M1
B3a
S1
20
15
10
5
1
0
-15
Metres
F7.37
F7.38
7.36
7.35
7.34
7.33
7.32
7.31
7.39
40 30 20 10 0 10 20 30 40 50
M2
M1?
M3/4?
?
M3

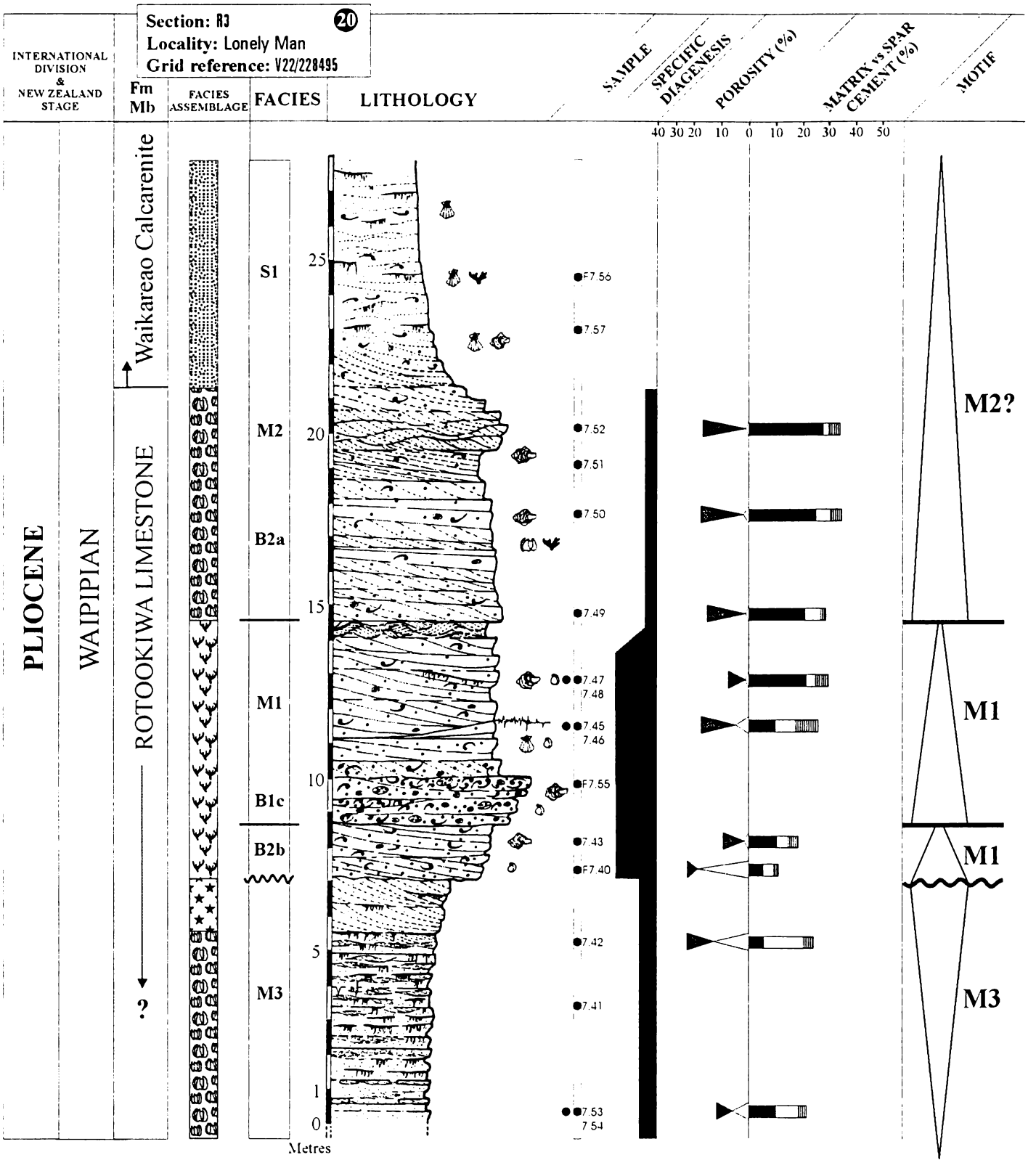
Section: R3
20
Locality: Lonely Man
Grid reference: V22/228495
INTERNATIONAL DIVISION & NEW ZEALAND STAGE
Fm Mb
FACIES ASSEMBLAGE
FACIES
LITHOLOGY
SAMPLE
SPECIFIC DIAGENESIS
POROSITY (%)
MATRIX vs SPAR CEMENT (%)
MOTIF
40 30 20 10 0 10 20 30 40 50
PLIOCENE
WAIPIPIAN
ROTOOKIWA LIMESTONE
Waikareao Calcarenite
?
S1
M2
B2a
M1
B1c
B2b
M3
25
20
15
10
5
1
0
Metres
F7.56
7.57
7.52
7.51
7.50
7.49
7.47
7.48
7.45
7.46
F7.55
7.43
F7.40
7.42
7.41
7.53
7.54
M2?
M1
M1
M3

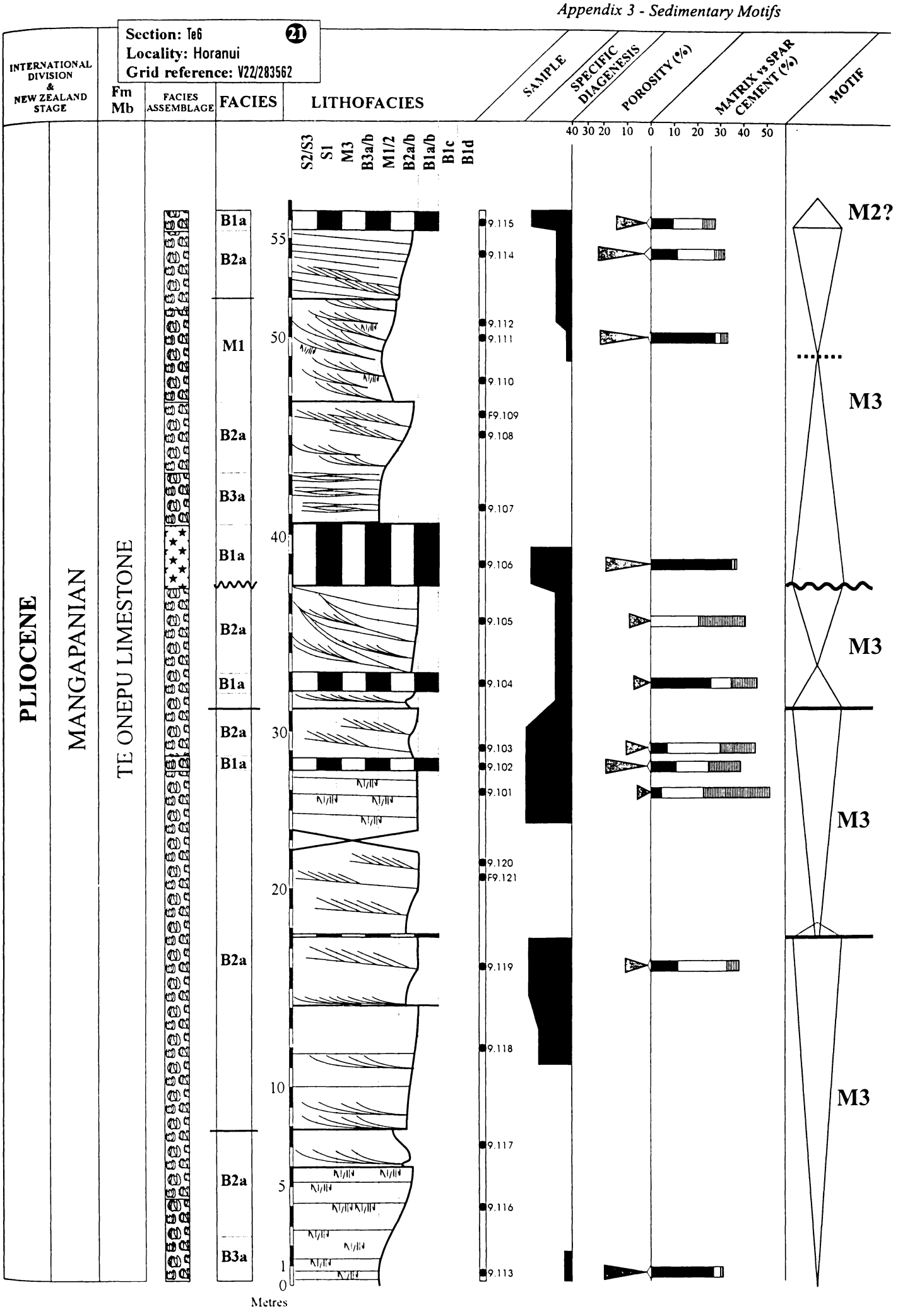
Section: Te6
21
Locality: Horanui
Grid reference: V22/283562
INTERNATIONAL DIVISION & NEW ZEALAND STAGE
Fm
Mb
FACIES ASSEMBLAGE
FACIES
LITHOFACIES
SAMPLE
SPECIFIC DIAGENESIS
POROSITY (%)
MATRIX vs SPAR CEMENT (%)
MOTIF
S2/S3
S1
M3
B3a/b
M1/2
B2a/b
B1a/b
B1c
B1d
40 30 20 10 0 10 20 30 40 50
PLIOCENE
MANGAPANIAN
TE ONEPU LIMESTONE
B1a
B2a
M1
B2a
B3a
B1a
B2a
B1a
B2a
B2a
B3a
55
50
40
30
20
10
5
1
0
Metres
9.115
9.114
9.112
9.111
9.110
F9.109
9.108
9.107
9.106
9.105
9.104
9.103
9.102
9.101
9.120
F9.121
9.119
9.118
9.117
9.116
9.113
M2?
M3
M3
M3
M3

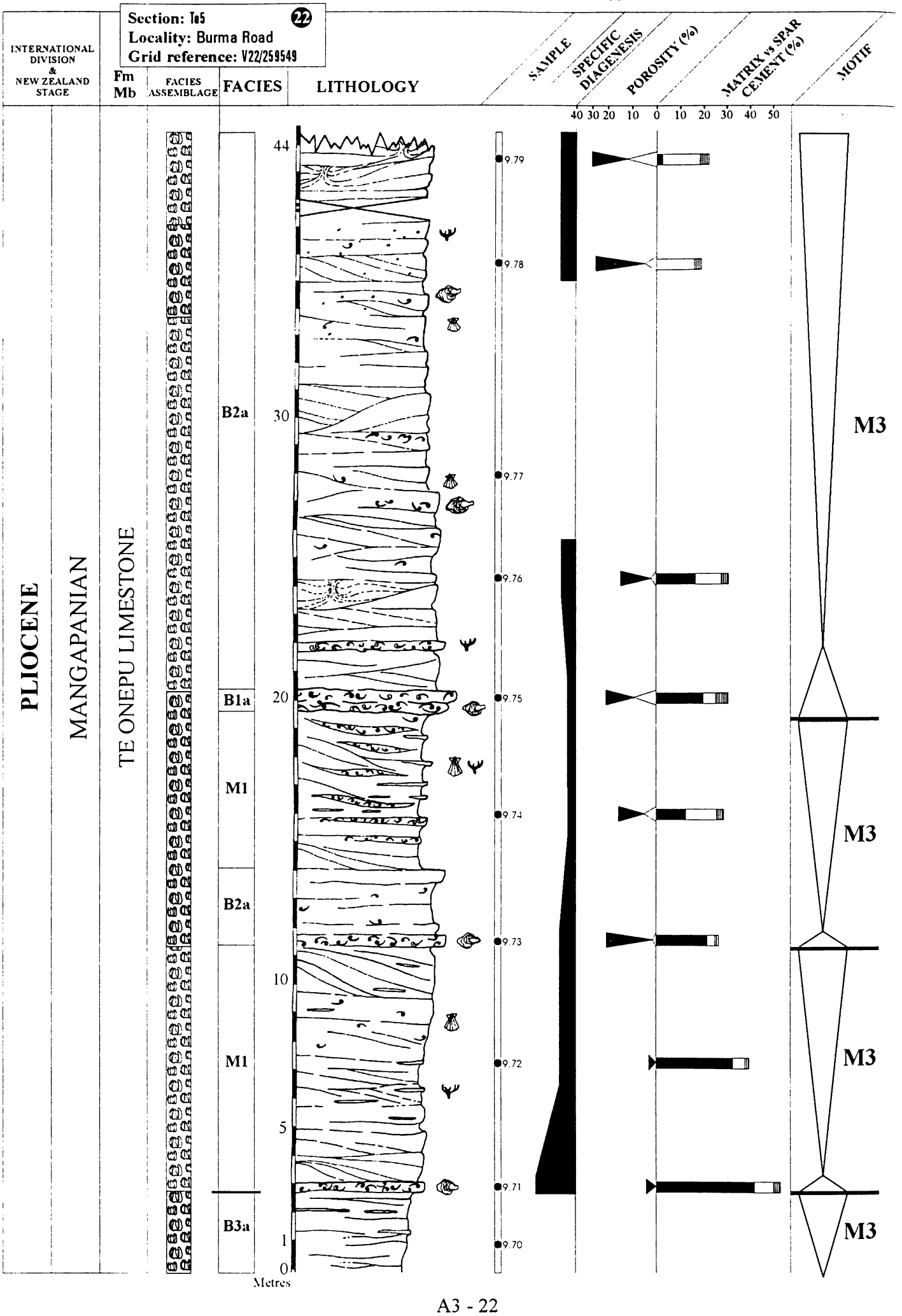
Section: Te5
Locality: Burma Road
Grid reference: V22/259549
22
INTERNATIONAL DIVISION & NEW ZEALAND STAGE
Fm
Mb
FACIES ASSEMBLAGE
FACIES
LITHOLOGY
SAMPLE
SPECIFIC DIAGENESIS
POROSITY (%)
MATRIX vs SPAR CEMENT (%)
MOTIF
40 30 20 10 0 10 20 30 40 50
PLIOCENE
MANGAPANIAN
TE ONEPU LIMESTONE
B2a
B1a
M1
B2a
M1
B3a
44
30
20
10
5
1
0
Metres
9.79
9.78
9.77
9.76
9.75
9.74
9.73
9.72
9.71
9.70
M3
M3
M3
M3

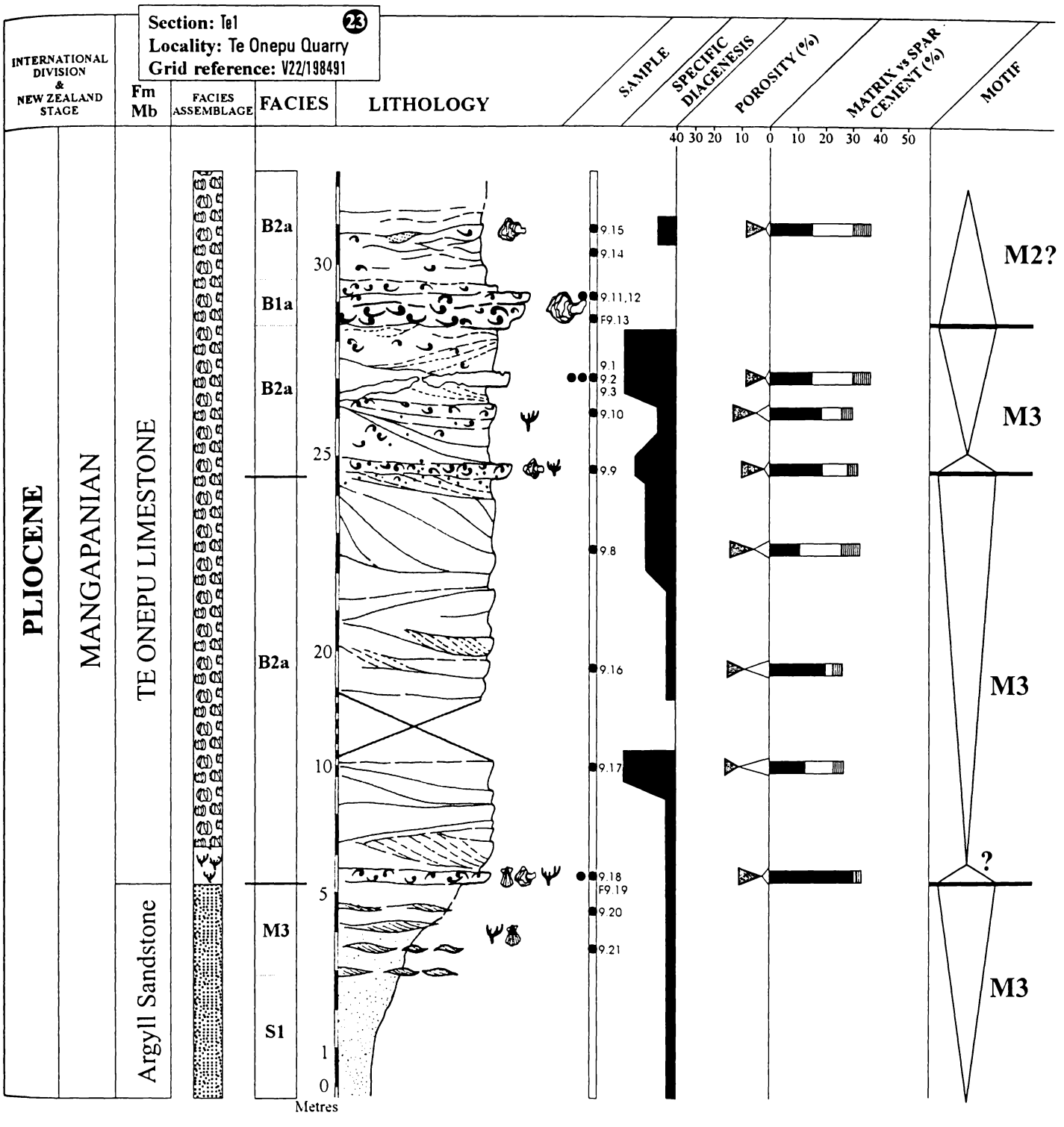
Section: Te1
23
Locality: Te Onepu Quarry
Grid reference: V22/198491
INTERNATIONAL DIVISION & NEW ZEALAND STAGE
Fm Mb
FACIES ASSEMBLAGE
FACIES
LITHOLOGY
SAMPLE
SPECIFIC DIAGENESIS
POROSITY (%)
MATRIX vs SPAR CEMENT (%)
MOTIF
PLIOCENE
MANGAPANIAN
TE ONEPU LIMESTONE
Argyll Sandstone
B2a
B1a
B2a
B2a
M3
S1
30
25
20
10
5
1
0
Metres
9.15
9.14
9.11,12
F9.13
9.1
9.2
9.3
9.10
9.9
9.8
9.16
9.17
9.18
F9.19
9.20
9.21
40 30 20 10 0 10 20 30 40 50
M2?
M3
M3
?
M3

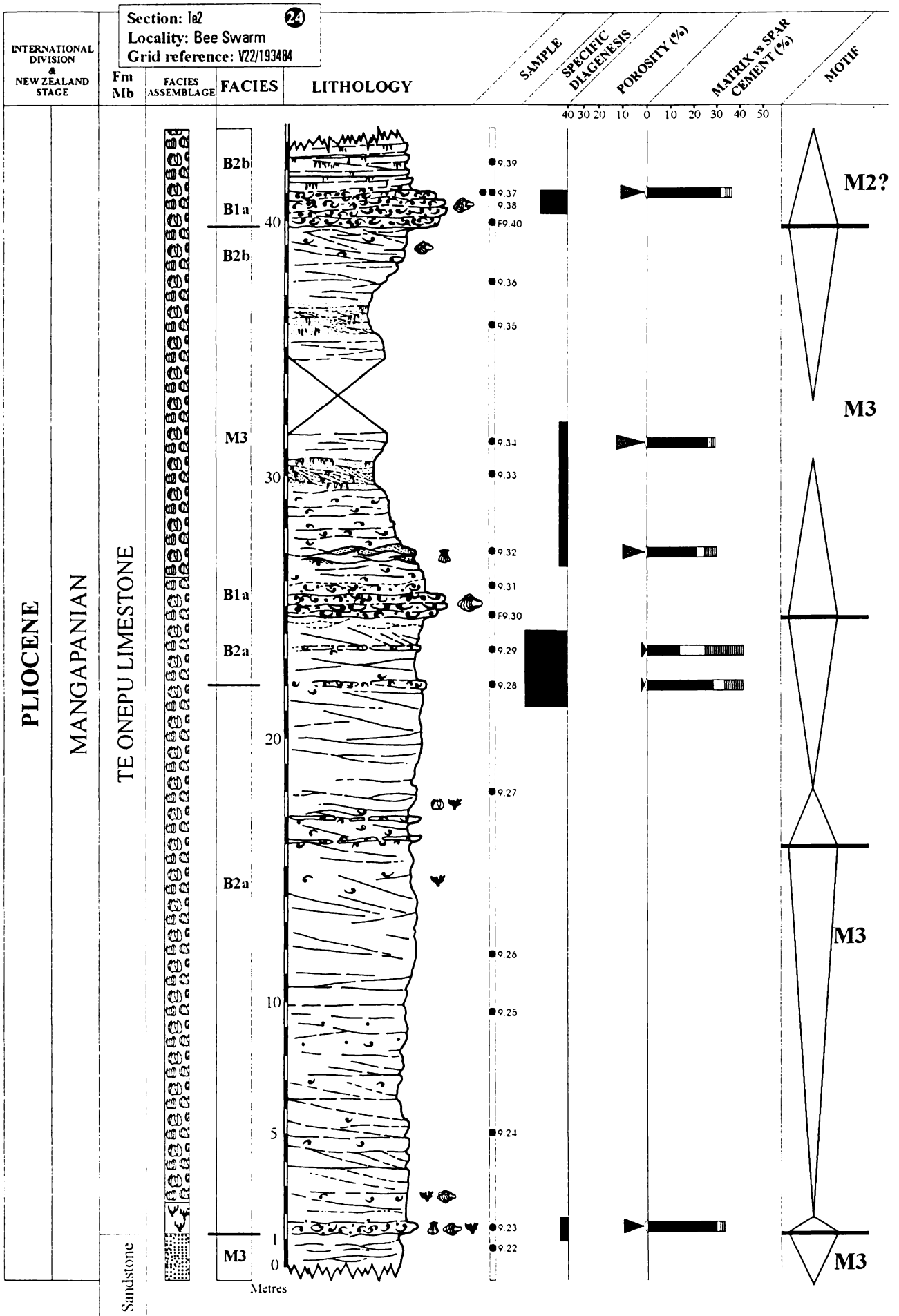
Section: Ie2
24
Locality: Bee Swarm
Grid reference: V22/193484
INTERNATIONAL DIVISION & NEW ZEALAND STAGE
Fm
Mb
FACIES ASSEMBLAGE
FACIES
LITHOLOGY
SAMPLE
SPECIFIC DIAGENESIS
POROSITY (%)
MATRIX vs SPAR CEMENT (%)
MOTIF
40 30 20 10 0 10 20 30 40 50
PLIOCENE
MANGAPANIAN
TE ONEPU LIMESTONE
Argyll Sandstone
B2b
B1a
B2b
M3
B1a
B2a
B2a
M3
40
30
20
10
5
1
0
Metres
9.39
9.37
9.38
F9.40
9.36
9.35
9.34
9.33
9.32
9.31
F9.30
9.29
9.28
9.27
9.26
9.25
9.24
9.23
9.22
M2?
M3
M3
M3

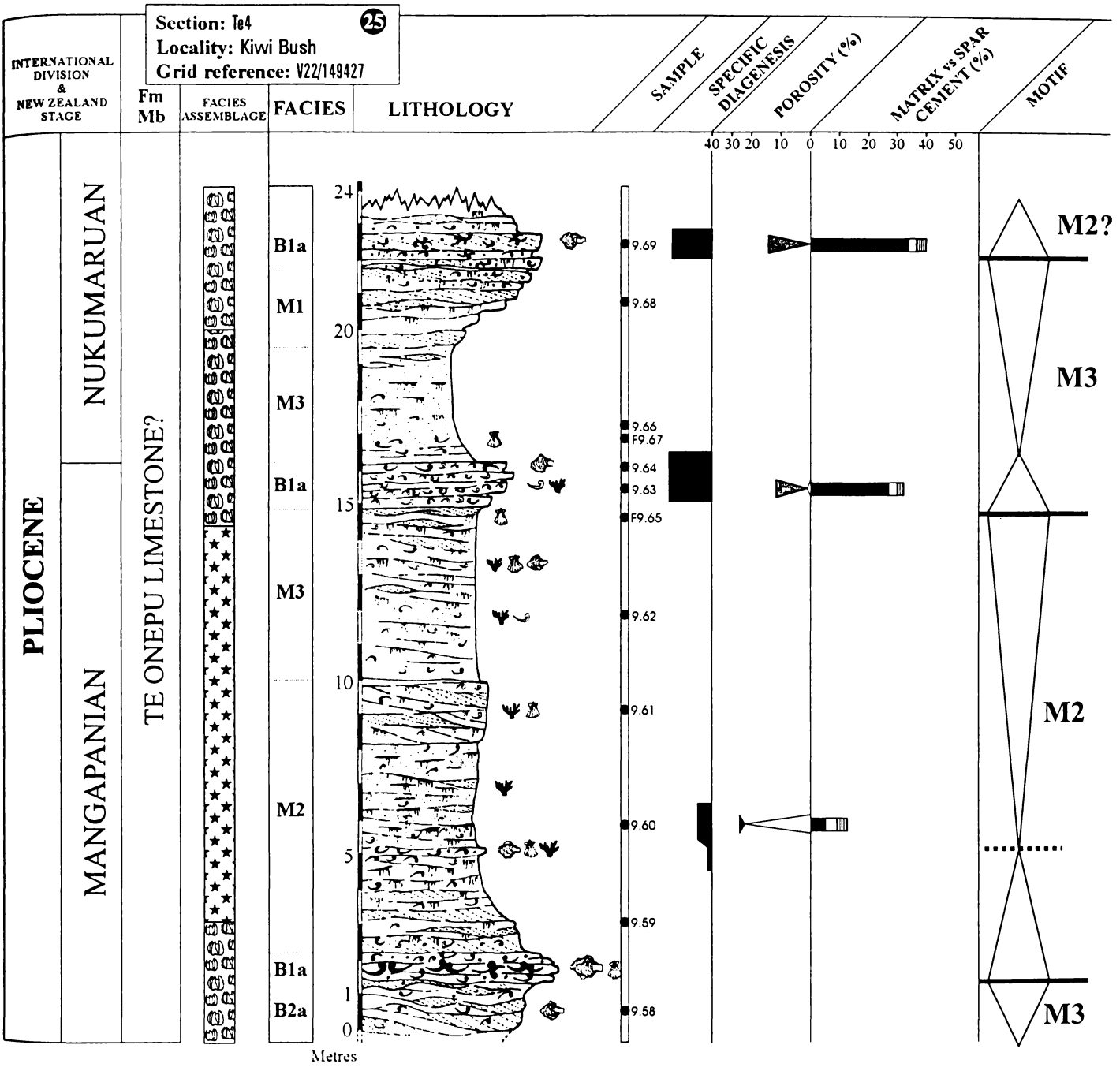
Section: Te4
25
Locality: Kiwi Bush
Grid reference: V22/149427
INTERNATIONAL DIVISION & NEW ZEALAND STAGE
Fm Mb
FACIES ASSEMBLAGE
FACIES
LITHOLOGY
SAMPLE
SPECIFIC DIAGENESIS
POROSITY (%)
MATRIX vs SPAR CEMENT (%)
MOTIF
PLIOCENE
NUKUMARUAN
MANGAPANIAN
TE ONEPU LIMESTONE?
B1a
M1
M3
B1a
M3
M2
B1a
B2a
24
20
15
10
5
1
0
Metres
9.69
9.68
9.66
F9.67
9.64
9.63
F9.65
9.62
9.61
9.60
9.59
9.58
40 30 20 10 0 10 20 30 40 50
M2?
M3
M2
M3

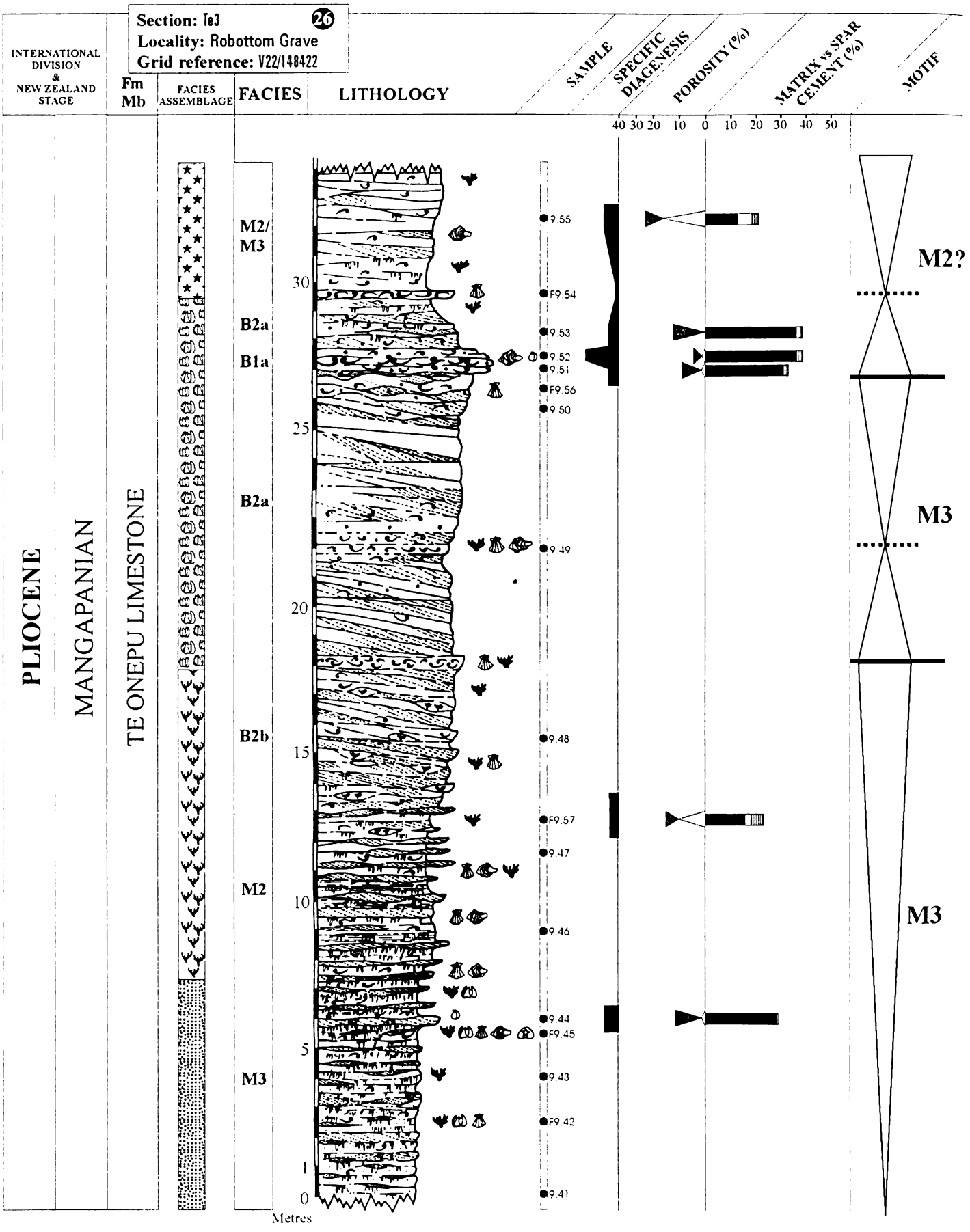
Section: Te3
26
Locality: Robottom Grave
Grid reference: V22/148422
INTERNATIONAL DIVISION & NEW ZEALAND STAGE
Fm Mb
FACIES ASSEMBLAGE
FACIES
LITHOLOGY
SAMPLE
SPECIFIC DIAGENESIS
POROSITY (%)
MATRIX vs SPAR CEMENT (%)
MOTIF
40 30 20 10 0 10 20 30 40 50
PLIOCENE
MANGAPANIAN
TE ONEPU LIMESTONE
M2/ M3
B2a
B1a
B2a
B2b
M2
M3
30
25
20
15
10
5
1
0
Metres
F9.55
F9.54
F9.53
F9.52
F9.51
F9.56
F9.50
F9.49
F9.48
F9.57
F9.47
F9.46
F9.44
F9.45
F9.43
F9.42
F9.41
M2?
M3
M3

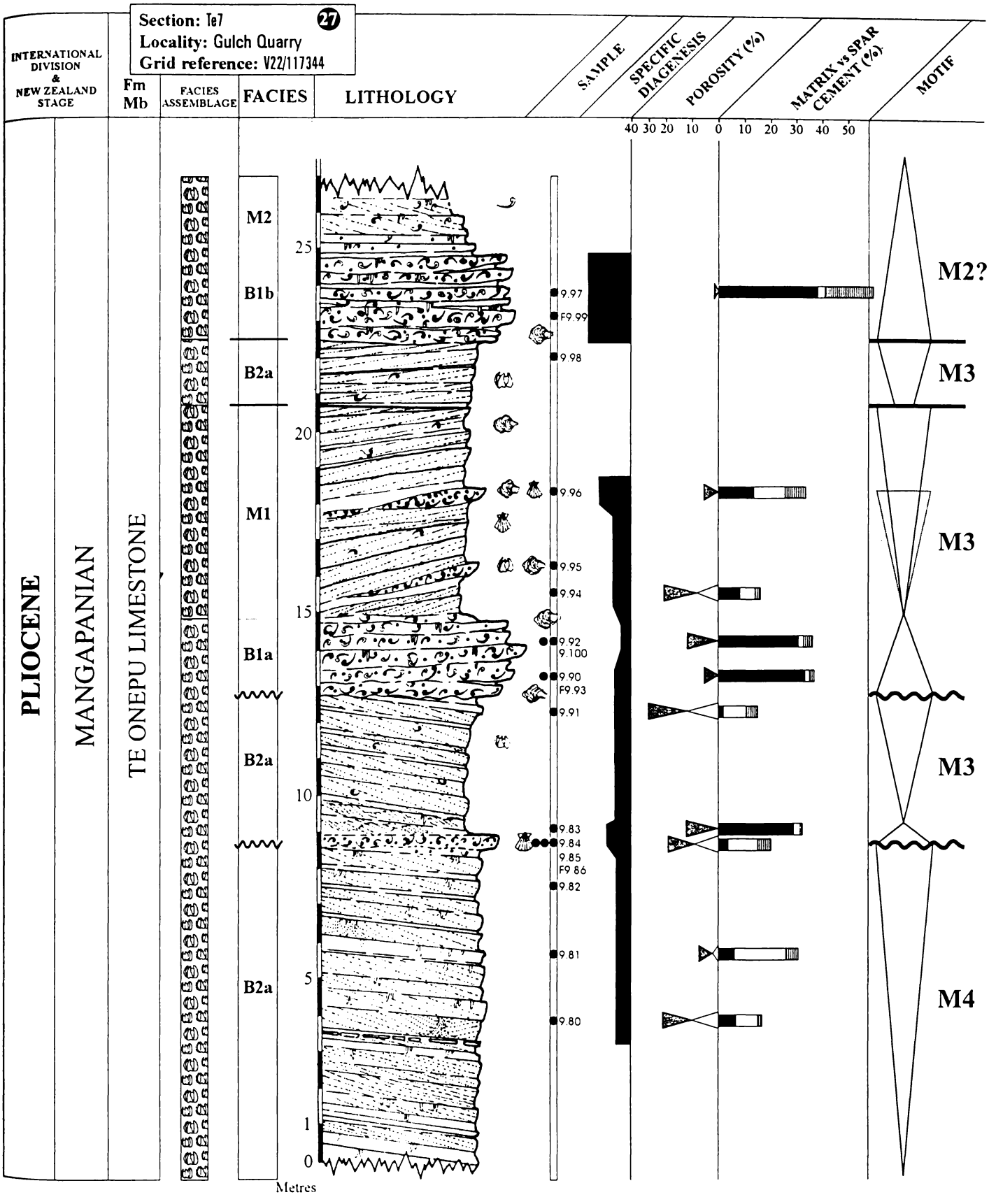
Section: Te7
27
Locality: Gulch Quarry
Grid reference: V22/117344
INTERNATIONAL DIVISION & NEW ZEALAND STAGE
Fm Mb
FACIES ASSEMBLAGE
FACIES
LITHOLOGY
SAMPLE
SPECIFIC DIAGENESIS
POROSITY (%)
MATRIX vs SPAR CEMENT (%)
MOTIF
40 30 20 10 0 10 20 30 40 50
PLIOCENE
MANGAPANIAN
TE ONEPU LIMESTONE
M2
B1b
B2a
M1
B1a
B2a
B2a
25
20
15
10
5
1
0
Metres
9.97
F9.99
9.98
9.96
9.95
9.94
9.92
9.100
9.90
F9.93
9.91
9.83
9.84
9.85
F9.86
9.82
9.81
9.80
M2?
M3
M3
M3
M4

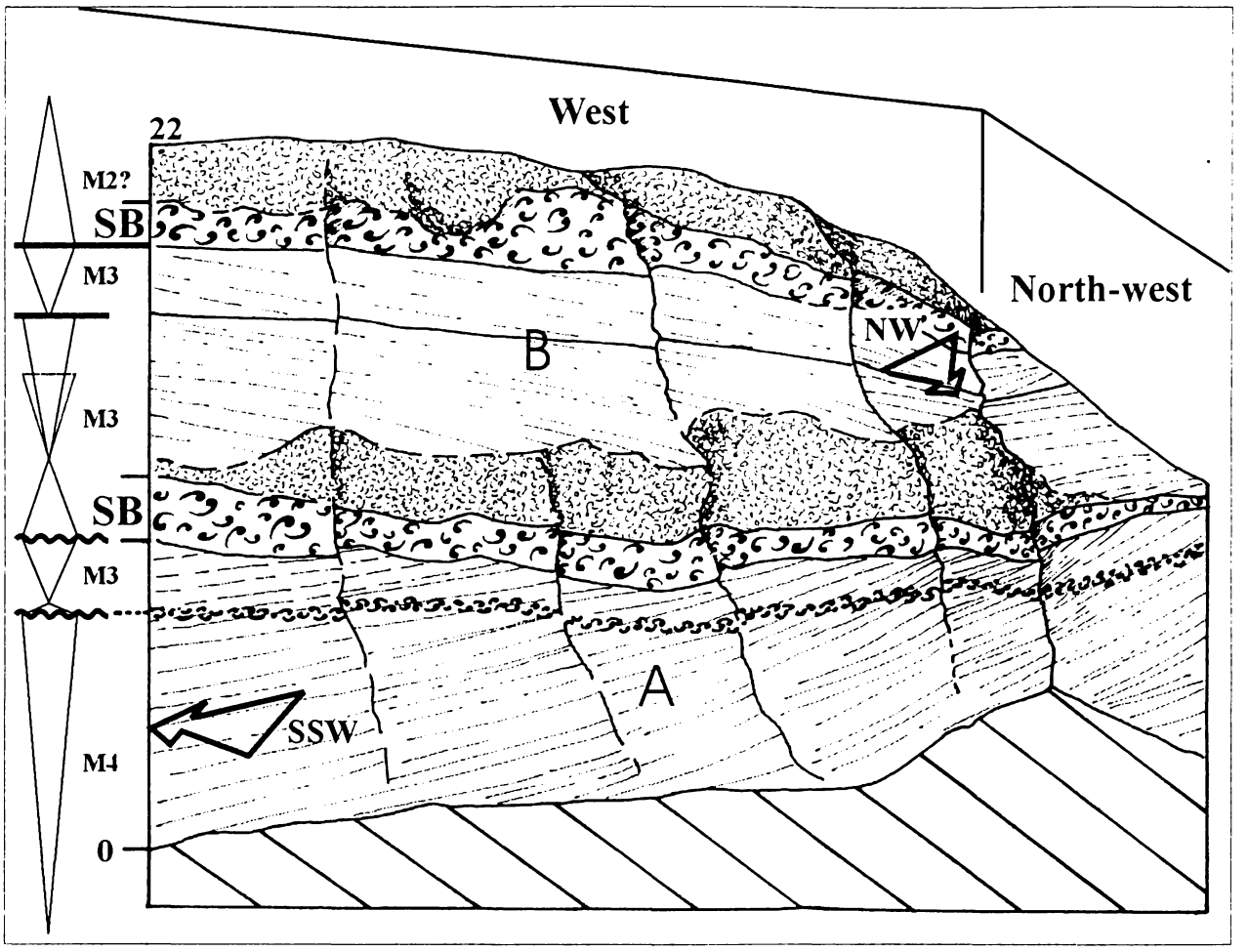

The Te Onepu limestone in the Gulch Quarry consists of two limestone bodies disconformably capped by ostreid-pectinid-brachiopod shell beds (SB). Units A and B exhibit large-scale planar and trough cross-bedded structures, and form thick sand bodies migrating in opposite directions.

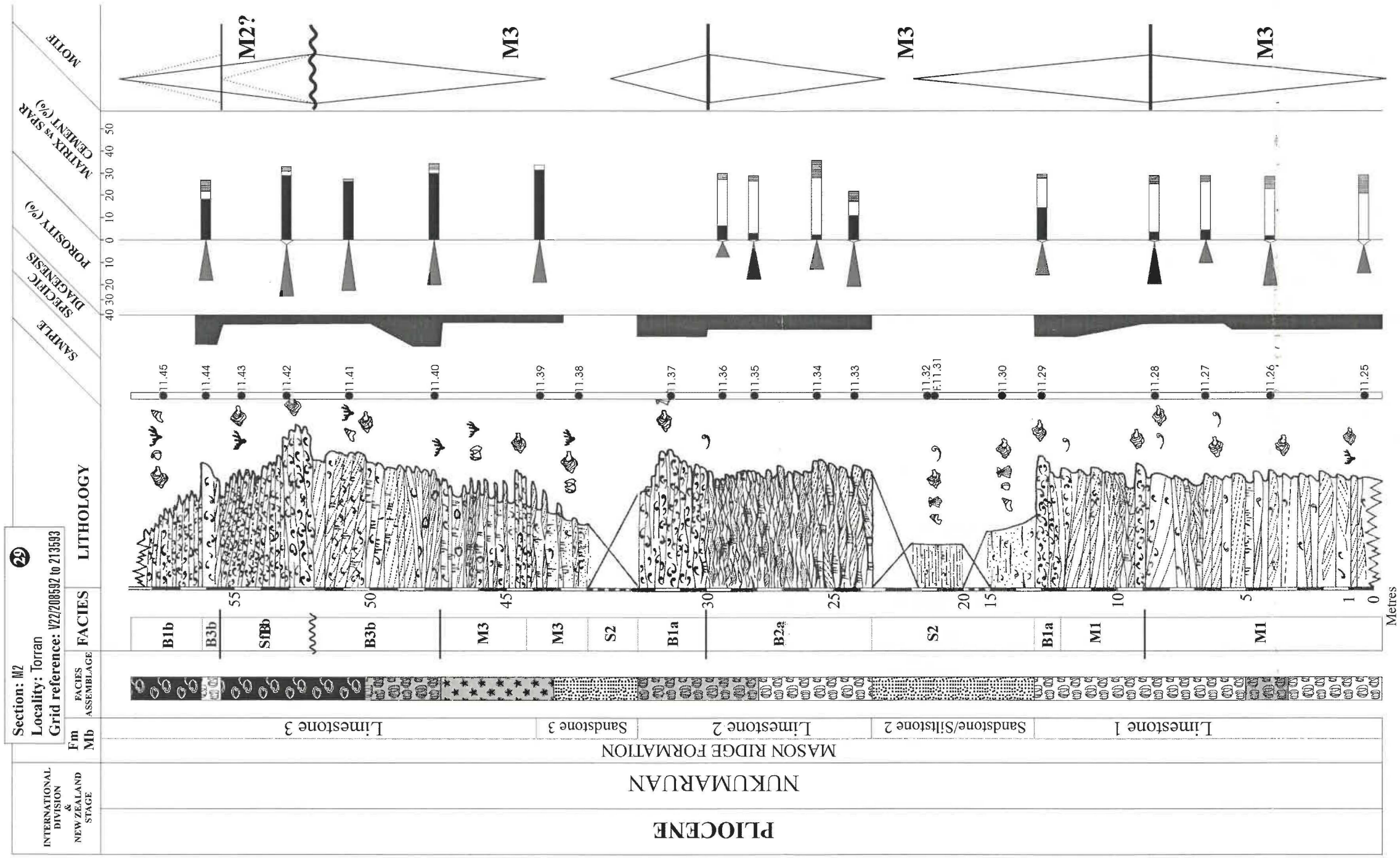
Section: M2
Locality: Torran
Grid reference: V22/2088592 to 213593
INTERNATIONAL DIVISION & NEW ZEALAND STAGE
PLIOCENE
NUKUMARUAN
MASON RIDGE FORMATION
Fm Mb
Limestone 3
Sandstone 3
Limestone 2
Sandstone/Siltstone 2
Limestone 1
FACIES ASSEMBLAGE
FACIES
LITHOLOGY
Metres
SAMPLE
SPECIFIC DIAGENESIS
POROSITY (%)
MATRIX VS SPAR CEMENT (%)
MOTIF
M2?
M3
M3
M3

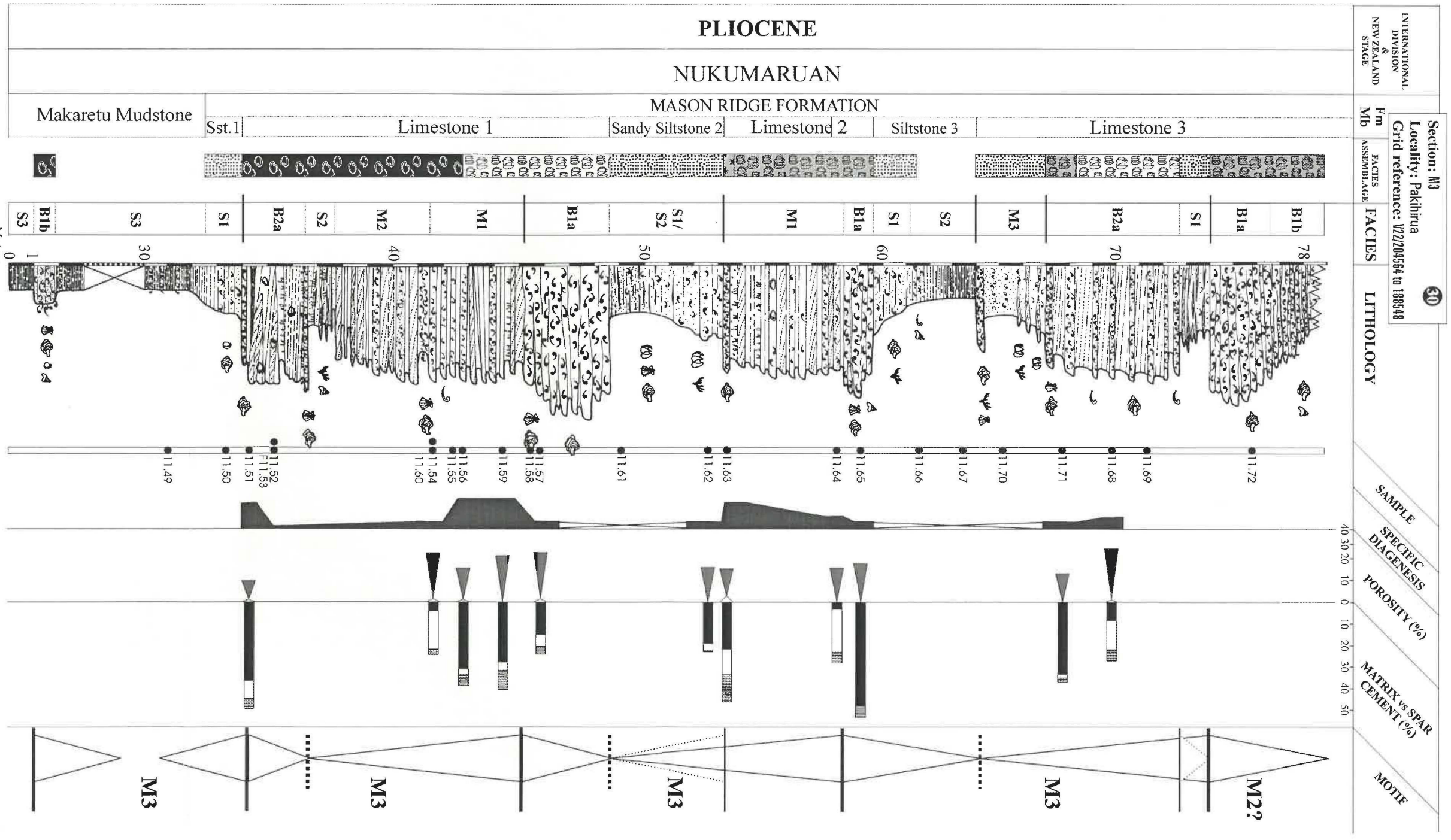

Appendix 3 - Sedimentary Motifs

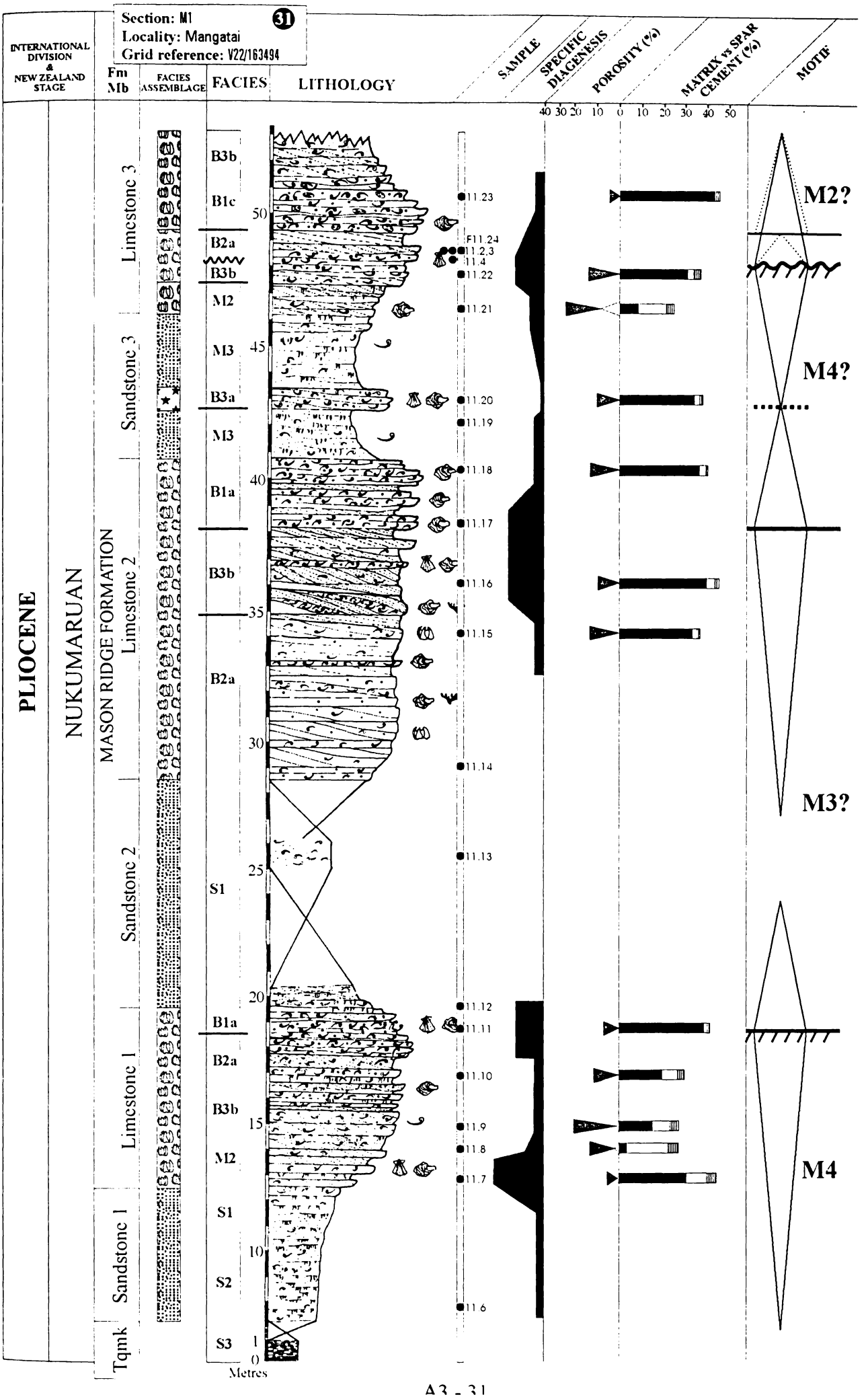
Section: M1
31
Locality: Mangatai
Grid reference: V22/163494
INTERNATIONAL DIVISION & NEW ZEALAND STAGE
Fm Mb
FACIES ASSEMBLAGE
FACIES
LITHOLOGY
SAMPLE
SPECIFIC DIAGENESIS
POROSITY (%)
MATRIX vs SPAR CEMENT (%)
MOTIF
40 30 20 10 0 10 20 30 40 50
PLIOCENE
NUKUMARUAN
MASON RIDGE FORMATION
Limestone 3
Sandstone 3
Limestone 2
Sandstone 2
Limestone 1
Sandstone 1
Tqmk
B3b
B1c
B2a
B3b
M2
M3
B3a
M3
B1a
B3b
B2a
S1
B1a
B2a
B3b
M2
S1
S2
S3
50
45
40
35
30
25
20
15
10
1
0
Metres
F11.24
11.23
11.2,3
11.4
11.22
11.21
11.20
11.19
11.18
11.17
11.16
11.15
11.14
11.13
11.12
11.11
11.10
11.9
11.8
11.7
11.6
M2?
M4?
M3?
M4

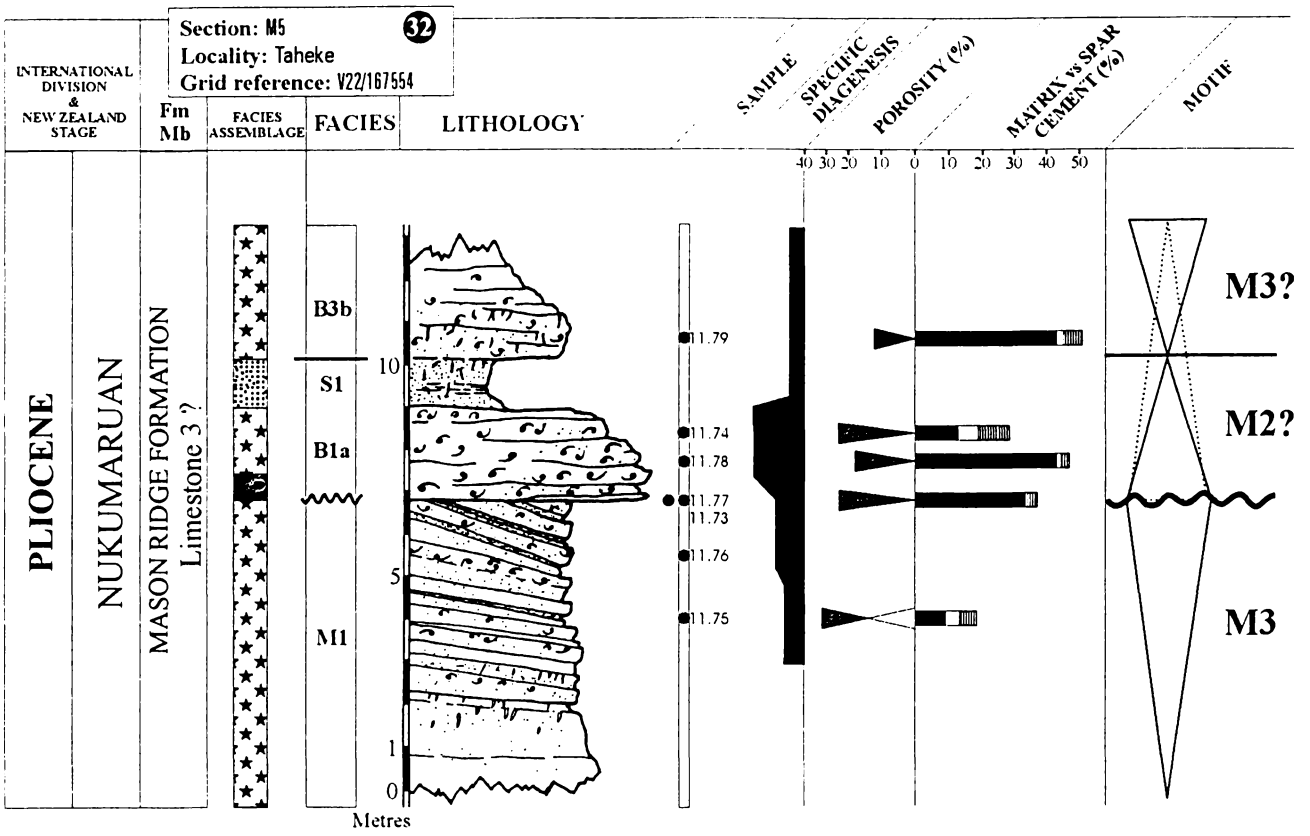
Section: M5
32
Locality: Taheke
Grid reference: V22/167554
INTERNATIONAL DIVISION & NEW ZEALAND STAGE
Fm Mb
FACIES ASSEMBLAGE
FACIES
LITHOLOGY
SAMPLE
SPECIFIC DIAGENESIS
POROSITY (%)
MATRIX vs SPAR CEMENT (%)
MOTIF
40 30 20 10 0 10 20 30 40 50
PLIOCENE
NUKUMARUAN
MASON RIDGE FORMATION
Limestone 3 ?
B3b
S1
B1a
M1
10
5
1
0
Metres
11.79
11.74
11.78
11.77
11.73
11.76
11.75
M3?
M2?
M3

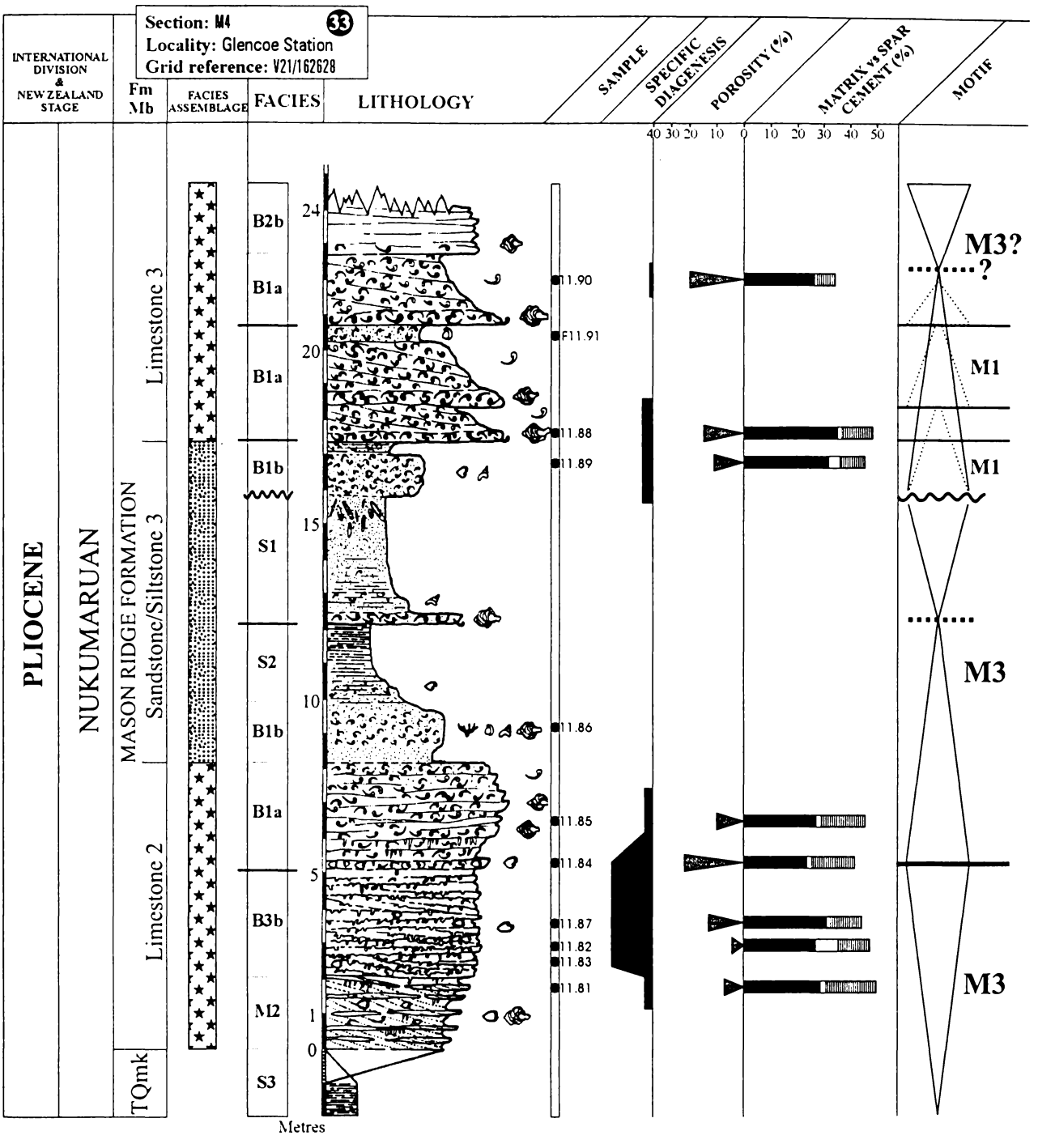
Section: M4
Locality: Glencoe Station
Grid reference: V21/162628
INTERNATIONAL DIVISION & NEW ZEALAND STAGE
Fm Mb
FACIES ASSEMBLAGE
FACIES
LITHOLOGY
SAMPLE
SPECIFIC DIAGENESIS
POROSITY (%)
MATRIX vs SPAR CEMENT (%)
MOTIF
PLIOCENE
NUKUMARUAN
MASON RIDGE FORMATION
Limestone 3
Sandstone/Siltstone 3
Limestone 2
TQmk
B2b
B1a
B1a
B1b
S1
S2
B1b
B1a
B3b
M2
S3
24
20
15
10
5
1
0
Metres
11.90
F11.91
11.88
11.89
11.86
11.85
11.84
11.87
11.82
11.83
11.81
40 30 20 10 0 10 20 30 40 50
M3?
?
M1
M1
M3
M3

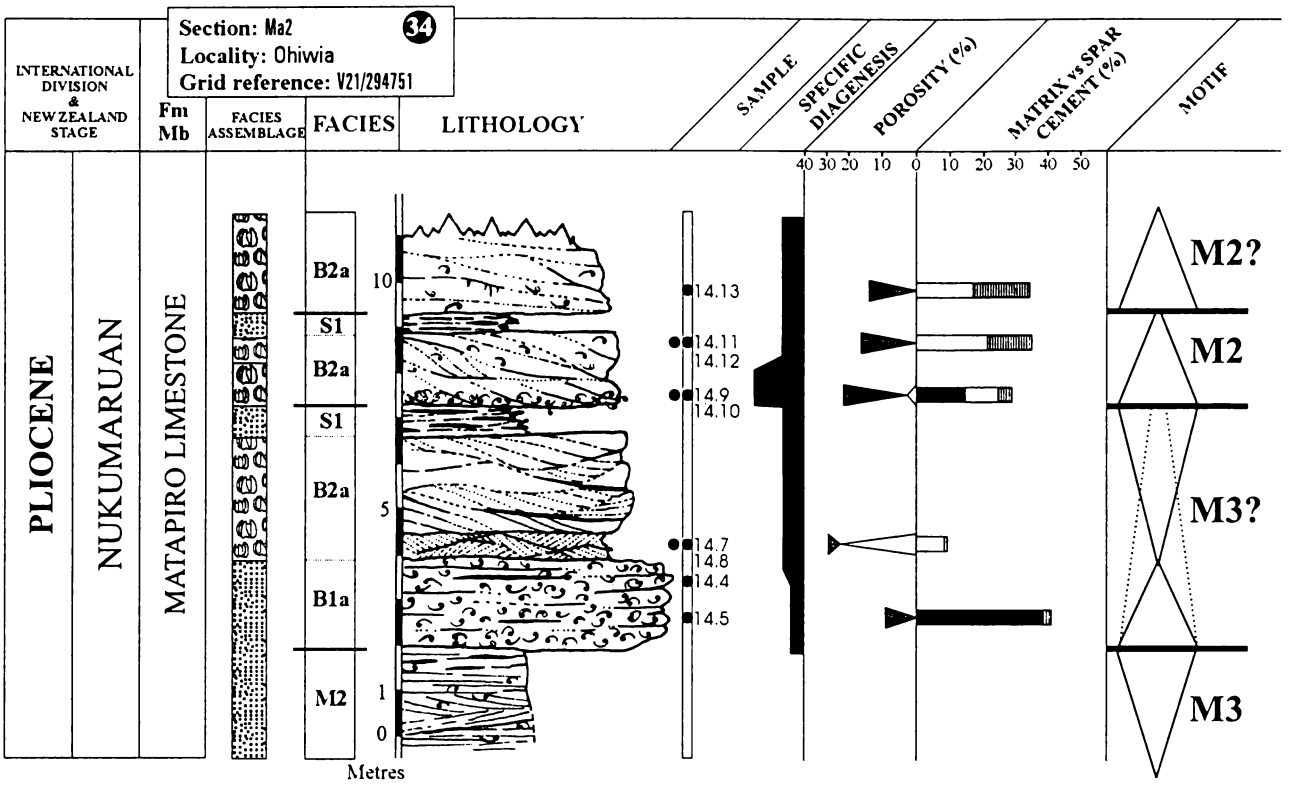
Section: Ma2
34
Locality: Ohiwia
Grid reference: V21/294751
INTERNATIONAL DIVISION & NEW ZEALAND STAGE
PLIOCENE
NUKUMARUAN
Fm Mb
MATAPIRO LIMESTONE
FACIES ASSEMBLAGE
FACIES
LITHOLOGY
B2a
S1
B2a
S1
B2a
B1a
M2
10
5
1
0
Metres
SAMPLE
SPECIFIC DIAGENESIS
POROSITY (%)
MATRIX vs SPAR CEMENT (%)
MOTIF
40 30 20 10 0 10 20 30 40 50
14.13
14.11
14.12
14.9
14.10
14.7
14.8
14.4
14.5
M2?
M2
M3?
M3

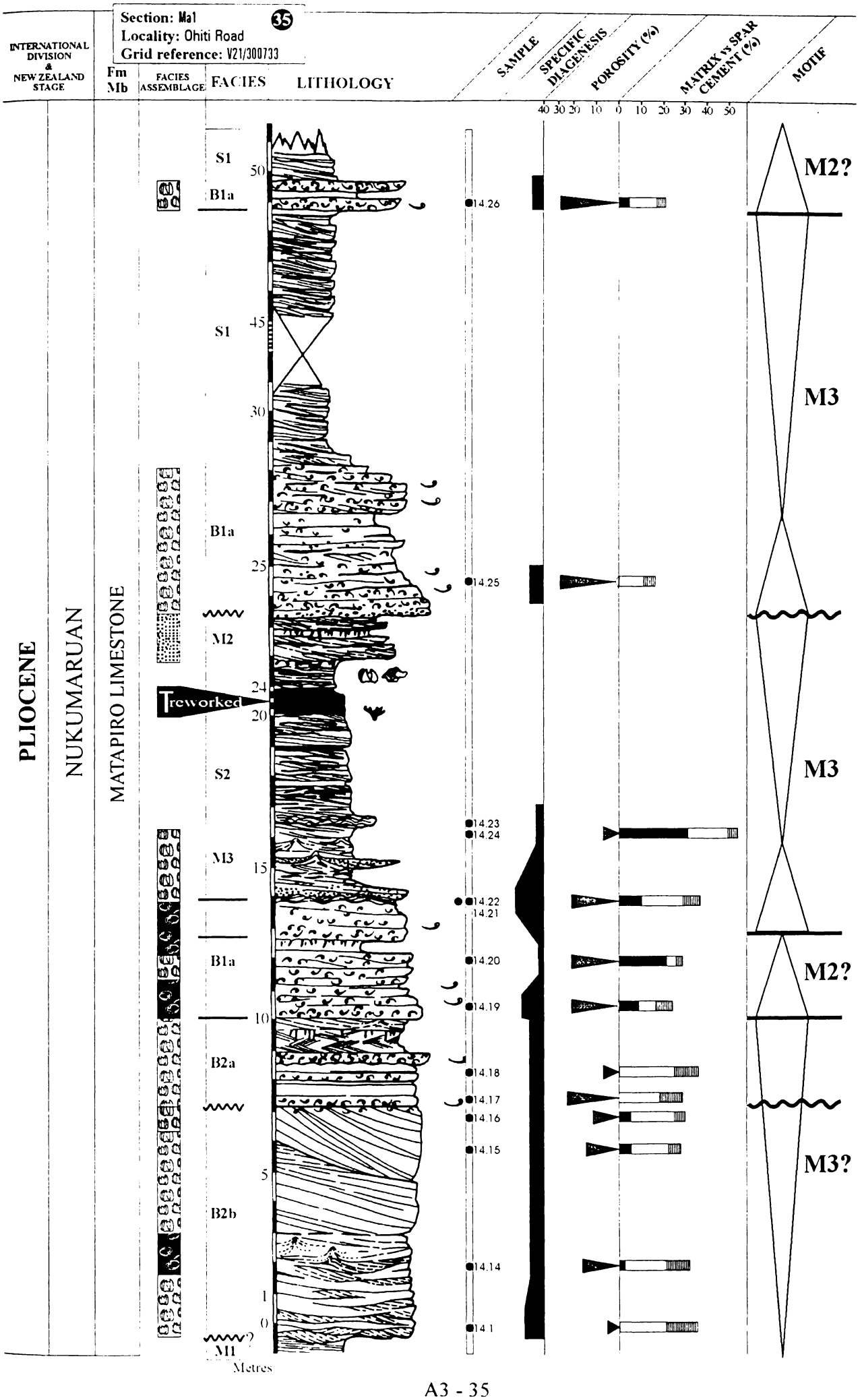
Section: Ma1
35
Locality: Ohiti Road
Grid reference: V21/300733
INTERNATIONAL DIVISION & NEW ZEALAND STAGE
Fm
Mb
FACIES ASSEMBLAGE
FACIES
LITHOLOGY
SAMPLE
SPECIFIC DIAGENESIS
POROSITY (%)
MATRIX vs SPAR CEMENT (%)
MOTIF
40 30 20 10 0 10 20 30 40 50
PLIOCENE
NUKUMARUAN
MATAPIRO LIMESTONE
S1
B1a
S1
B1a
M2
Treworked
S2
M3
B1a
B2a
B2b
M1
50
45
30
25
24
20
15
10
5
1
0
Metres
14.26
14.25
14.23
14.24
14.22
14.21
14.20
14.19
14.18
14.17
14.16
14.15
14.14
14.1
M2?
M3
M3
M2?
M3?

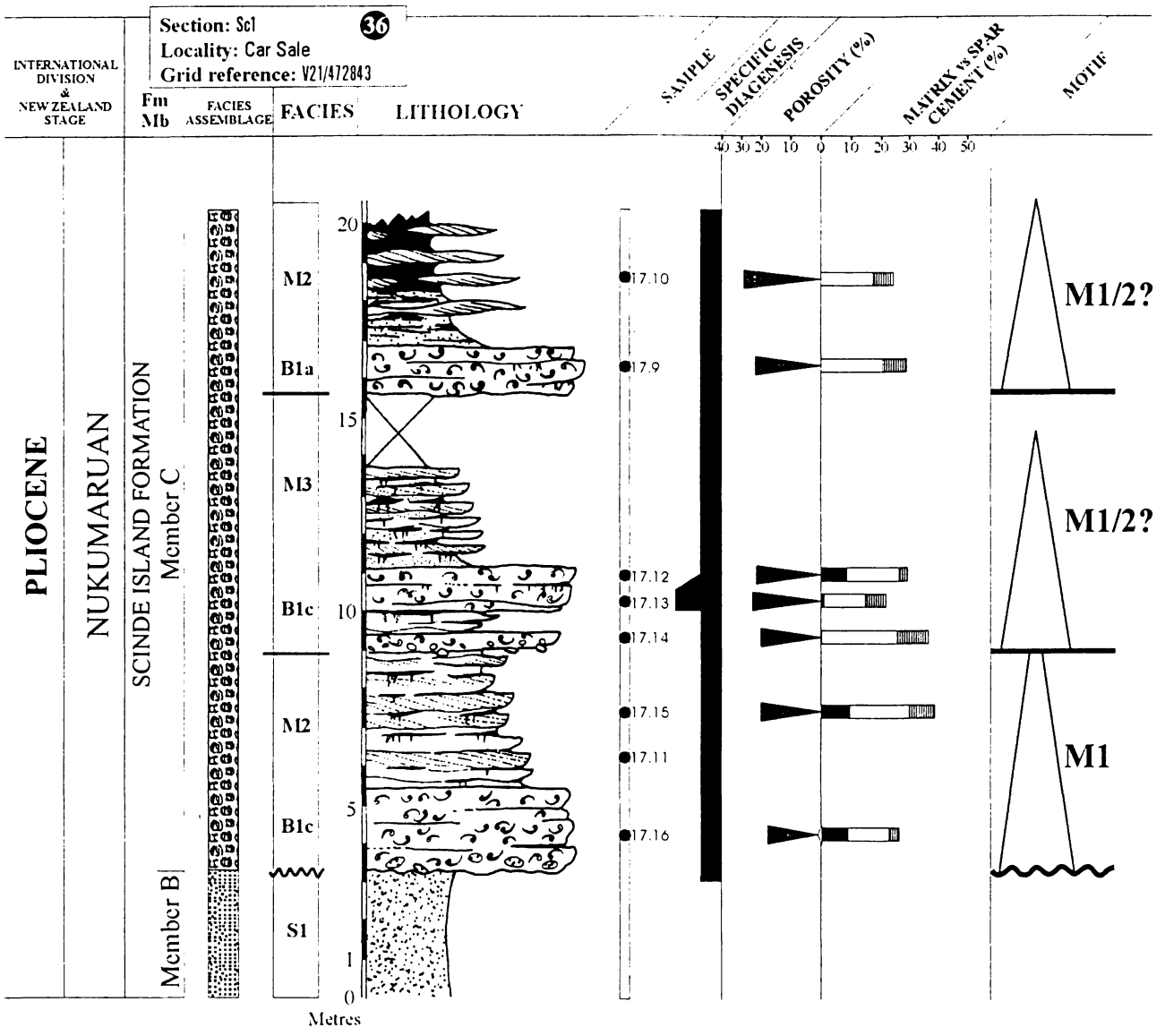
Section: Scl
Locality: Car Sale
Grid reference: V21/472843
36
INTERNATIONAL DIVISION & NEW ZEALAND STAGE
Fm
Mb
FACIES ASSEMBLAGE
FACIES
LITHOLOGY
SAMPLE
SPECIFIC DIAGENESIS
POROSITY (%)
MATRIX vs SPAR CEMENT (%)
MOTIF
40 30 20 10 0 10 20 30 40 50
PLIOCENE
NUKUMARUAN
SCINDE ISLAND FORMATION
Member C
Member B
M2
B1a
M3
B1c
M2
B1c
S1
20
15
10
5
1
0
Metres
17.10
17.9
17.12
17.13
17.14
17.15
17.11
17.16
M1/2?
M1/2?
M1

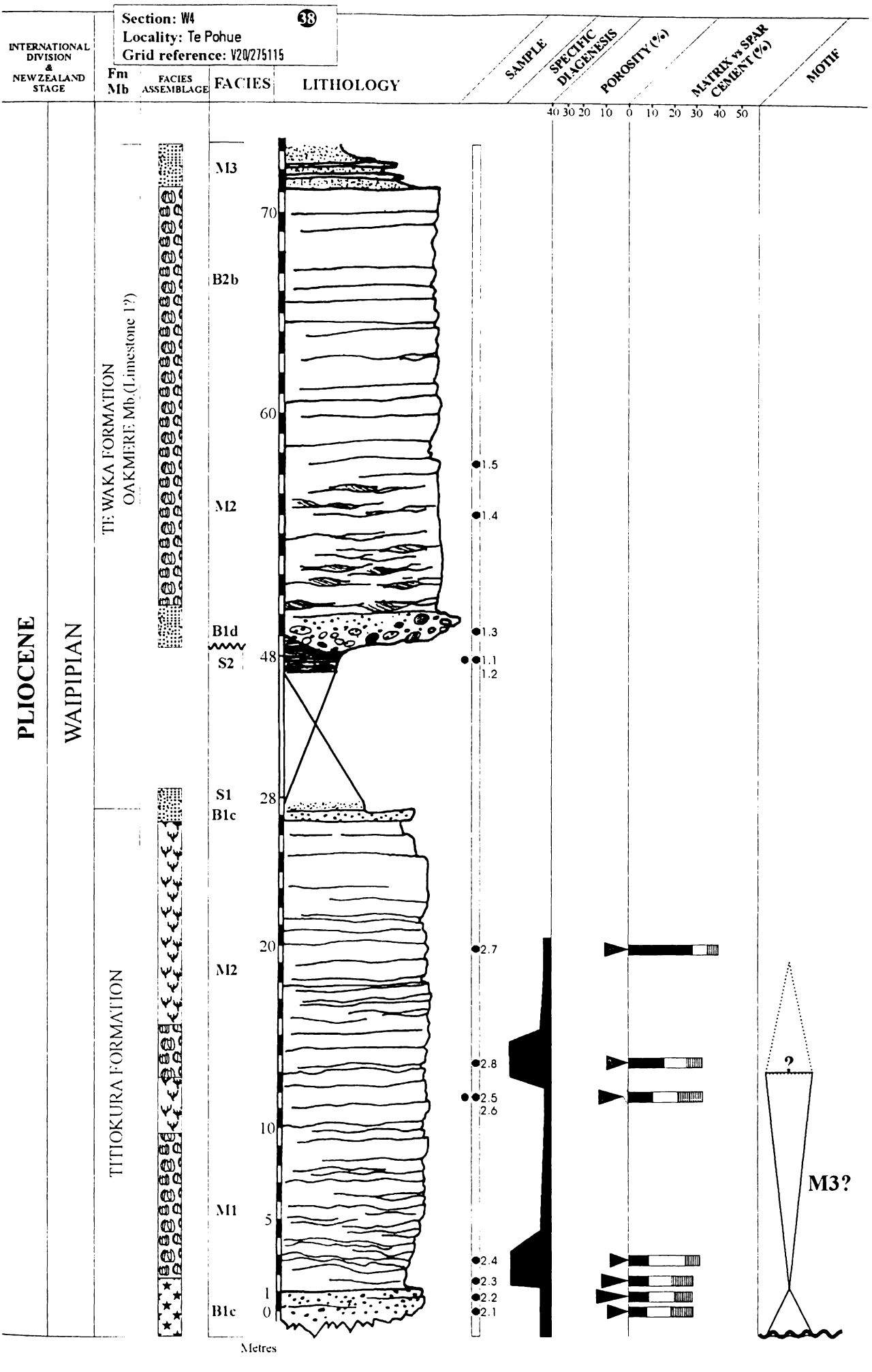
Section: W4
38
Locality: Te Pohue
Grid reference: V20/275115
INTERNATIONAL DIVISION & NEW ZEALAND STAGE
Fm
Mb
FACIES ASSEMBLAGE
FACIES
LITHOLOGY
SAMPLE
SPECIFIC DIAGENESIS
POROSITY (%)
MATRIX vs SPAR CEMENT (%)
MOTIF
40 30 20 10 0 10 20 30 40 50
PLIOCENE
WAIPIPIAN
TE WAKA FORMATION
OAKMERE Mb.(Limestone ?)
TITIOKURA FORMATION
M3
B2b
M2
B1d
S2
S1
B1c
M2
M1
B1c
70
60
48
28
20
10
5
1
0
1.5
1.4
1.3
1.1
1.2
2.7
2.8
2.5
2.6
2.4
2.3
2.2
2.1
?
M3?
Metres

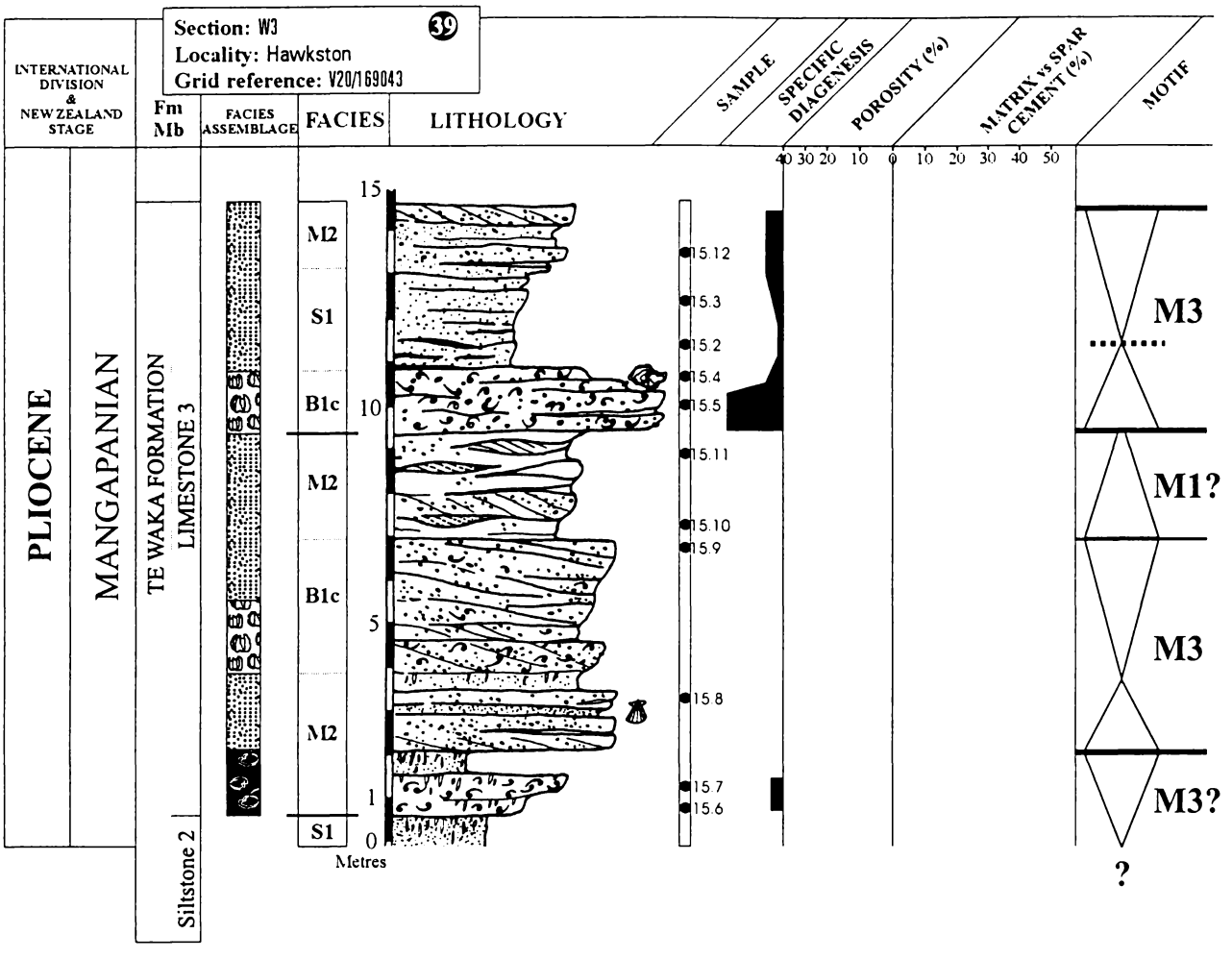
Section: W3
Locality: Hawkston
Grid reference: V20/169043
39
INTERNATIONAL DIVISION & NEW ZEALAND STAGE
Fm Mb
FACIES ASSEMBLAGE
FACIES
LITHOLOGY
SAMPLE
SPECIFIC DIAGENESIS
POROSITY (%)
MATRIX vs SPAR CEMENT (%)
MOTIF
40 30 20 10 0 10 20 30 40 50
PLIOCENE
MANGAPANIAN
TE WAKA FORMATION
LIMESTONE 3
Siltstone 2
M2
S1
B1c
M2
B1c
M2
S1
15
10
5
1
0
Metres
15.12
15.3
15.2
15.4
15.5
15.11
15.10
15.9
15.8
15.7
15.6
M3
M1?
M3
M3?
?

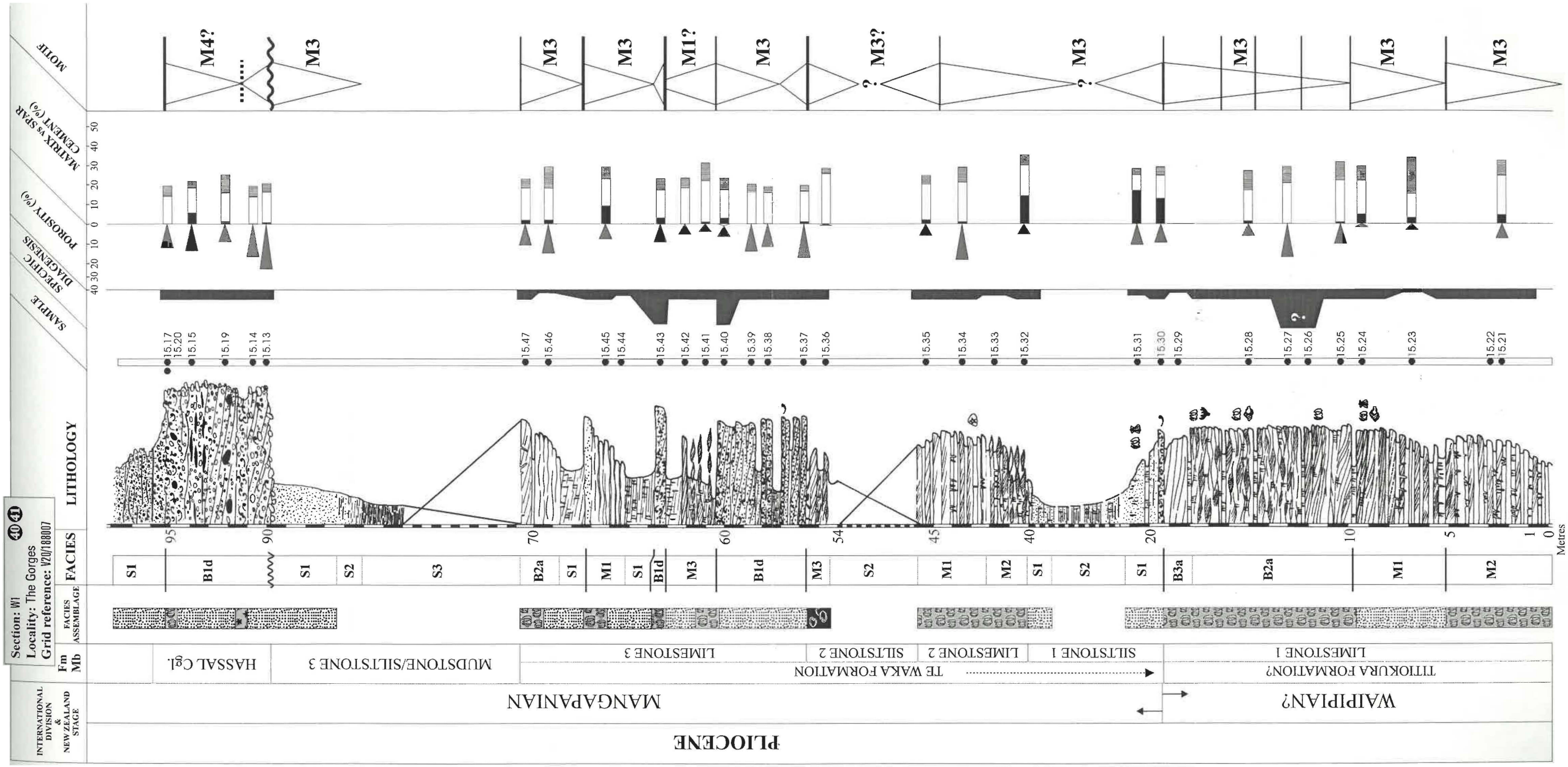
Section: W1
Locality: The Gorges
Grid reference: V20/188007
INTERNATIONAL DIVISION & NEW ZEALAND STAGE
PLIOCENE
MANGAPANIAN
WAIPIPIAN?
Fm
Mb
TE WAKA FORMATION
TITIOKURA FORMATION?
LIMESTONE 1
SILTSTONE 1
LIMESTONE 2
SILTSTONE 2
LIMESTONE 3
MUDSTONE/SILTSTONE 3
HASSAL Cgl.
FACIES ASSEMBLAGE
FACIES
S1 B1d S1 S2 S3 B2a S1 M1 S1 B1d M3 B1d M3 S2 M1 M2 S1 S2 S1 B3a B2a M1 M2
LITHOLOGY
Metres
95 90 70 60 54 45 40 20 10 5 1 0
SAMPLE
SPECIFIC DIAGENESIS
POROSITY (%)
MATRIX vs SPAR CEMENT (%)
MOTIF
M4? M3 M3 M3 M1? M3 ? M3? ? M3 M3 M3 M3
15.17 15.20 15.15 15.19 15.14 15.13 15.47 15.46 15.45 15.44 15.43 15.42 15.41 15.40 15.39 15.38 15.37 15.36 15.35 15.34 15.33 15.32 15.31 15.30 15.29 15.28 15.27 15.26 15.25 15.24 15.23 15.22 15.21

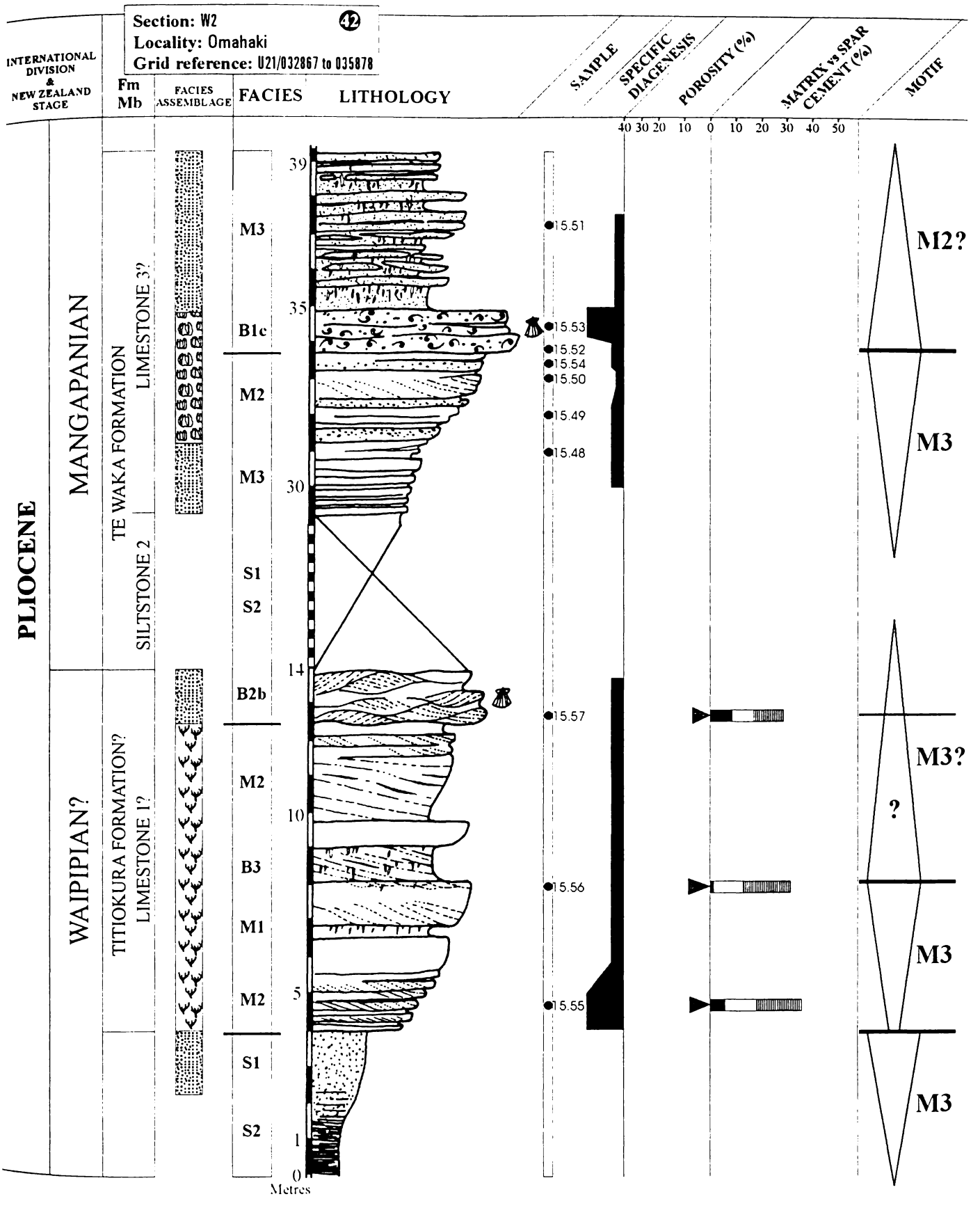
Section: W2
42
Locality: Omahaki
Grid reference: U21/032867 to 035878
INTERNATIONAL DIVISION & NEW ZEALAND STAGE
Fm
Mb
FACIES ASSEMBLAGE
FACIES
LITHOLOGY
SAMPLE
SPECIFIC DIAGENESIS
POROSITY (%)
MATRIX vs SPAR CEMENT (%)
MOTIF
40 30 20 10 0 10 20 30 40 50
PLIOCENE
MANGAPANIAN
WAIPIPIAN?
TE WAKA FORMATION
LIMESTONE 3?
SILTSTONE 2
TITIOKURA FORMATION?
LIMESTONE 1?
M3
B1c
M2
M3
S1
S2
B2b
M2
B3
M1
M2
S1
S2
39
35
30
14
10
5
1
0
Metres
15.51
15.53
15.52
15.54
15.50
15.49
15.48
15.57
15.56
15.55
M2?
M3
M3?
?
M3
M3

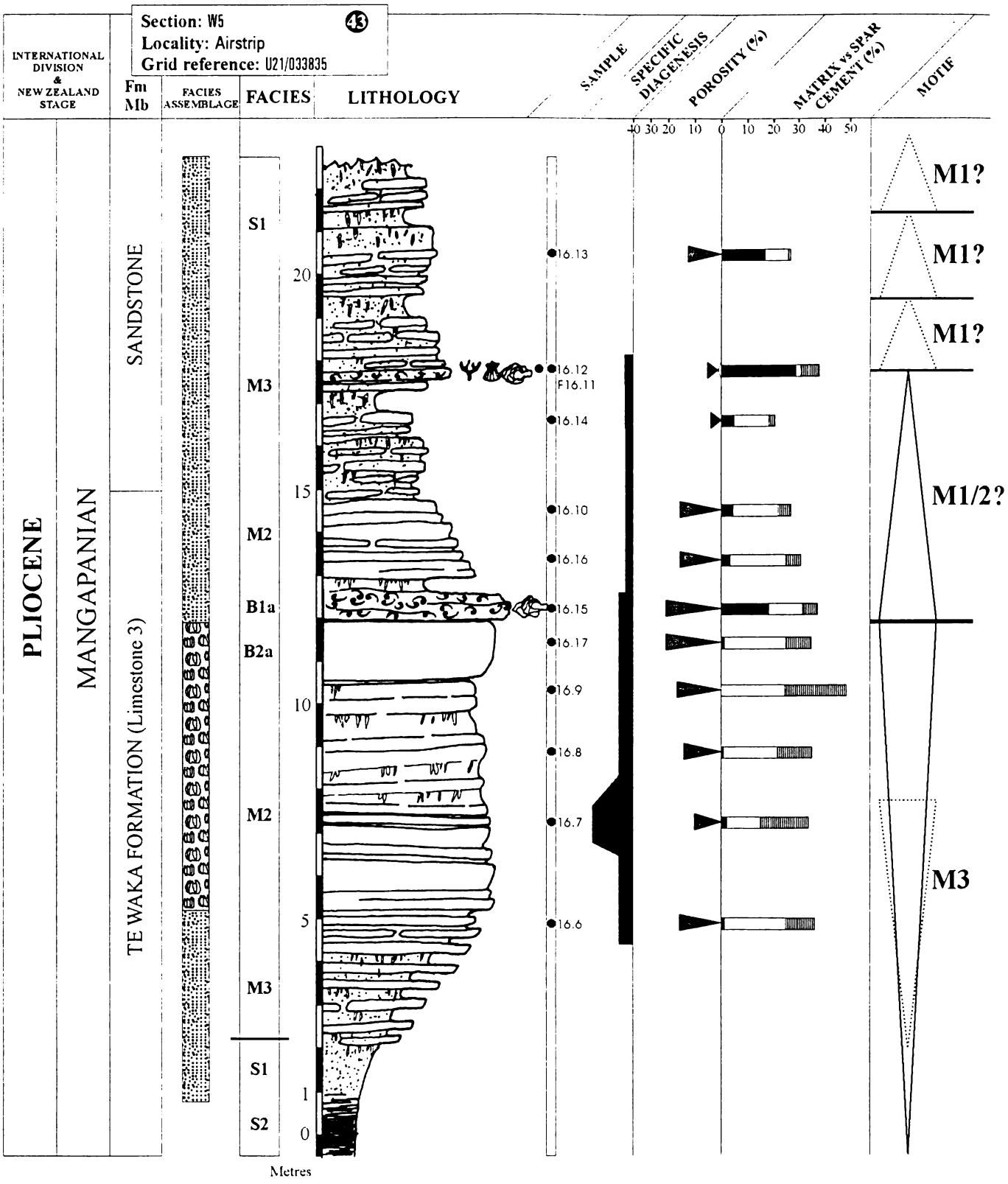
Section: W5
Locality: Airstrip
Grid reference: U21/033835
INTERNATIONAL DIVISION & NEW ZEALAND STAGE
Fm Mb
FACIES ASSEMBLAGE
FACIES
LITHOLOGY
SAMPLE
SPECIFIC DIAGENESIS
POROSITY (%)
MATRIX vs SPAR CEMENT (%)
MOTIF
PLIOCENE
MANGAPANIAN
SANDSTONE
TE WAKA FORMATION (Limestone 3)
S1
M3
M2
B1a
B2a
M2
M3
S1
S2
16.13
16.12
F16.11
16.14
16.10
16.16
16.15
16.17
16.9
16.8
16.7
16.6
M1?
M1?
M1?
M1/2?
M3
Metres

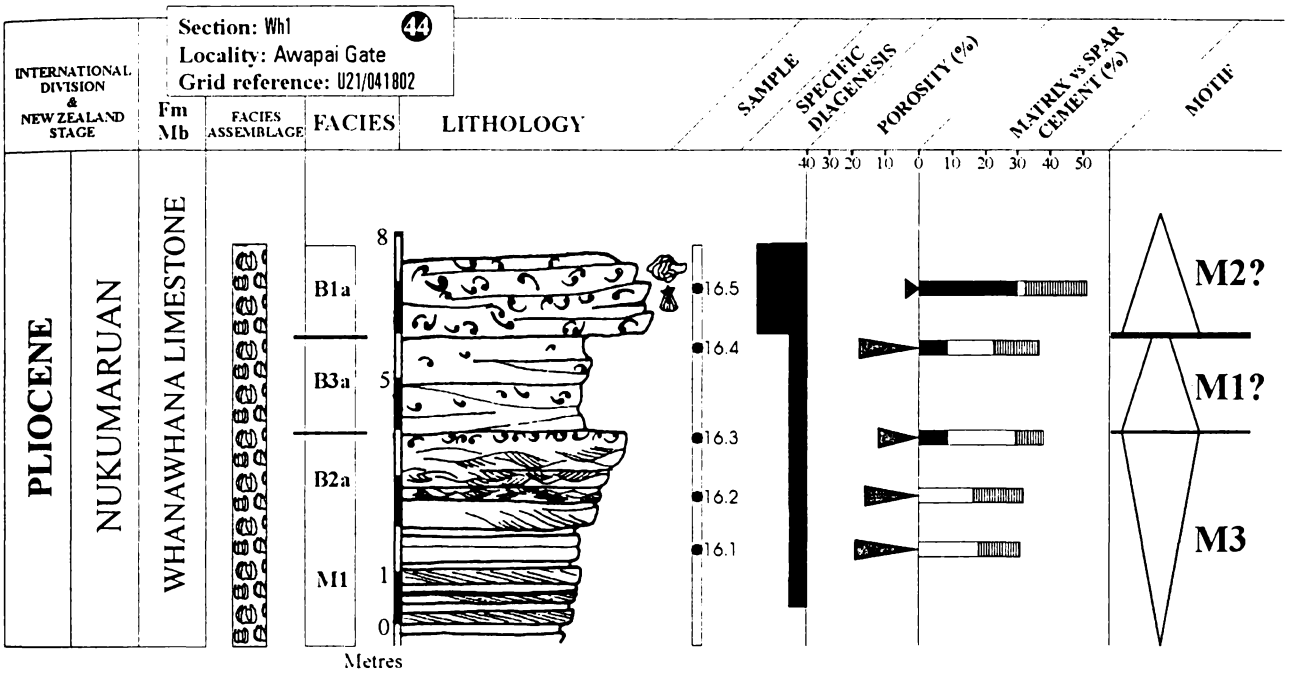
Section: Wh1
44
Locality: Awapai Gate
Grid reference: U21/041802
INTERNATIONAL DIVISION & NEW ZEALAND STAGE
Fm Mb
FACIES ASSEMBLAGE
FACIES
LITHOLOGY
SAMPLE
SPECIFIC DIAGENESIS
POROSITY (%)
MATRIX vs SPAR CEMENT (%)
MOTIF
40 30 20 10 0 10 20 30 40 50
PLIOCENE
NUKUMARUAN
WHANAWHANA LIMESTONE
B1a
B3a
B2a
M1
8
5
1
0
Metres
16.5
16.4
16.3
16.2
16.1
M2?
M1?
M3

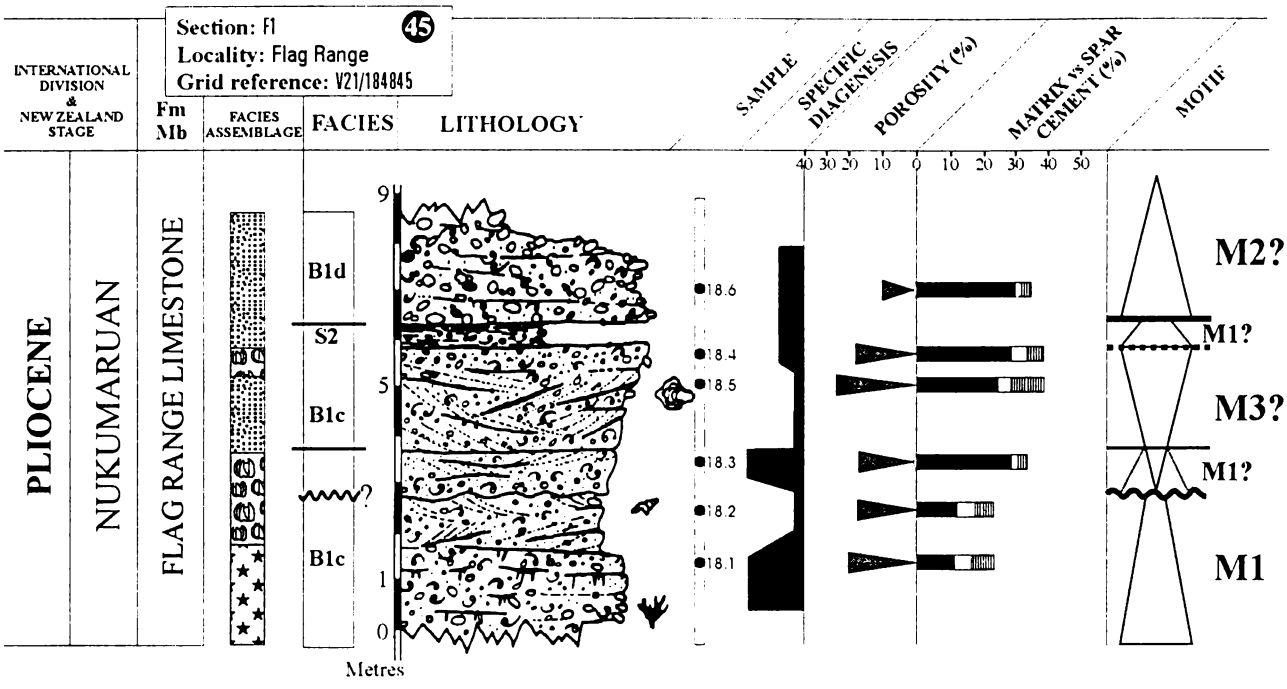
Section: F1
45
Locality: Flag Range
Grid reference: V21/184845
INTERNATIONAL DIVISION & NEW ZEALAND STAGE
Fm Mb
FACIES ASSEMBLAGE
FACIES
LITHOLOGY
SAMPLE
SPECIFIC DIAGENESIS
POROSITY (%)
MATRIX vs SPAR CEMENT (%)
MOTIF
PLIOCENE
NUKUMARUAN
FLAG RANGE LIMESTONE
B1d
S2
B1c
B1c
9
5
1
0
Metres
18.6
18.4
18.5
18.3
18.2
18.1
40 30 20 10 0 10 20 30 40 50
M2?
M1?
M3?
M1?
M1

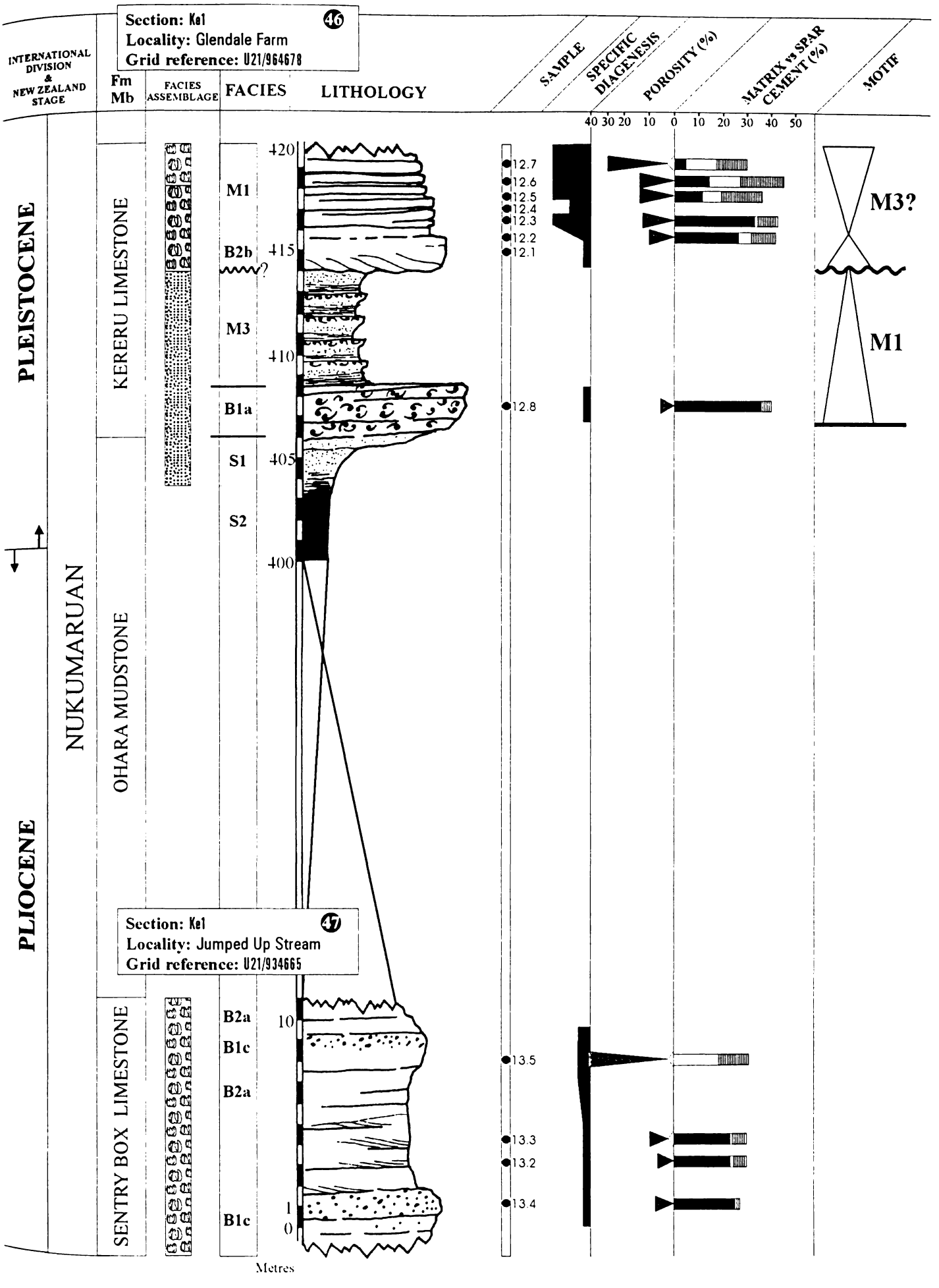
Section: Kel 46
Locality: Glendale Farm
Grid reference: U21/964678
INTERNATIONAL DIVISION & NEW ZEALAND STAGE
Fm Mb
FACIES ASSEMBLAGE
FACIES
LITHOLOGY
SAMPLE
SPECIFIC DIAGENESIS
POROSITY (%)
MATRIX vs SPAR CEMENT (%)
MOTIF
40 30 20 10 0 10 20 30 40 50
PLEISTOCENE
PLIOCENE
NUKUMARUAN
KERERU LIMESTONE
OHARA MUDSTONE
SENTRY BOX LIMESTONE
M1
B2b
M3
B1a
S1
S2
B2a
B1c
B2a
B1c
420
415
410
405
400
10
1
0
?
12.7
12.6
12.5
12.4
12.3
12.2
12.1
12.8
13.5
13.3
13.2
13.4
M3?
M1
Section: Kel 47
Locality: Jumped Up Stream
Grid reference: U21/934665
Metres

APPENDIX 4

POINT-COUNTING DATA
CLUSTER ANALYSIS

APPENDIX 4.1 - POINT-COUNTING

KEY

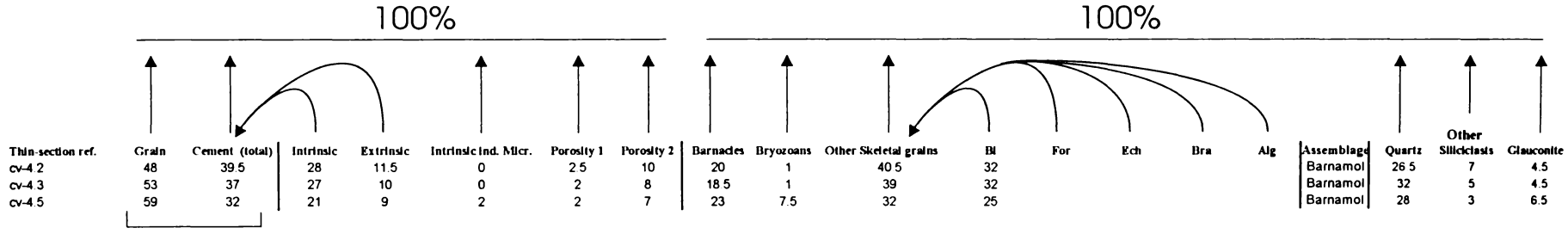

Thin-section ref.	Grain	Cement (total)	Intrinsic	Extrinsic	Intrinsic ind. Micr.	Porosity 1	Porosity 2	Barnacles	Bryozoans	Other Skeletal grains	Bi	For	Ech	Bra	Alg	Assemblage	Quartz	Other Siliciclasts	Glauconite
cv-4.2	48	39.5	28	11.5	0	2.5	10	20	1	40.5	32					Barnamol	26.5	7	4.5
cv-4.3	53	37	27	10	0	2	8	18.5	1	39	32					Barnamol	32	5	4.5
cv-4.5	59	32	21	9	2	2	7	23	7.5	32	25					Barnamol	28	3	6.5

Not shown on spread sheet
but available in Appendix CD1

Intrinsic	Intrinsic (interparticle) cement
Extrinsic	Extrinsic (intraparticle) cement
Intrinsic ind. Micr.	Intrinsic indurated micrite
Porosity 1	Primary porosity
Porosity 2	Secondary porosity
Bi	Bivalves
For	Foraminifers
Ech	Echinoderms
Bra	Brachiopods
Alg	Red algae
Assemblage	After Hayton *et al.* (1995)

Thin-section ref.	Intrinsic	Extrinsic	Intrinsic ind. Micr.	Porosity 1	Porosity 2	Barnacles	Bryozoans	Other Skeletal gr	Bi	For	Ech	Bra	Alg	Assemblage	Quartz	Siliciclasts	Glauconite
cv-4.2	28	11.5	0	2.5	10	20	1	40.5	32					Barnamol	26.5	7	4.5
cv-4.3	27	10	0	2	8	18.5	1	39	32					Barnamol	32	5	4.5
cv-4.5	21	9	2	2	7	23	7.5	32	25					Barnamol	28	3	6.5
cv-4.6	30	11.5	0	3	8.5	22.5	7	42.5	34					Barnamol	21	2	5
cv-4.7	28	8	0	2	10	19	5.5	33	26					Barnamol	34.5	2	6
cv-99-4.9	4	4	24	3	12	16	6.5	32.5	26	4				Bimol	32.5	1	11.5
cv-99-4.10	4	16	23	2	10	15	10	29	23	3.5				Bryomol	37	1	8
cv-99-4.11	12	18	15	2	8	15	6	32.5	25		3.5			Bimol	38	2	6.5
cv-99-4.12	24	6	7	1.5	8.5	15	6	36	28		4			Bimol	35	2	6
cv-99-4.13	16	4	11.5	2	7.5	17	10	28.5	23					Bimol	39.5	1	4
cv-99-4.14	3	7	21	2	9	15.5	5.5	33	25	4				Bimol	37.5	1	7.5
cv-99-4.15	14	6	10	1	6	16	8.5	30	21	6				Barnamol	37	2	6.5
cv-99-4.16	1.5	13.5	22.5	1	6	14	6	26	18	5				Barnamol	44	2.5	7.5
cv-99-4.17	3.5	14.5	20	1.5	6.5	13.5	4.5	28	23		3		2	Bimol	43	3.5	7.5
cv-99-4.18	1	4.5	32	1	10	20	9	24	14		3			Barnamol	37.5	3.5	6
cv-99-4.19	4.5	10.5	23	1.5	8.5	20	9	23.5	14		8			Barnamol	39	2.5	6
cv-99-4.20	1	7	24.5	1.5	9	21	7	25.5	13		8			Barnamol	35.5	4	7
cv-99-4.21	0.5	3.5	30	1	6	21	4	23.5	12		6			Barnamol	40	3.5	8
cv-99-4.22	14.5	3.5	20	6	4.5	26	6	27	15		8			Barnamol	29	5	7
cv-99-4.24	7	5.5	21	2	8.5	28	5.5	23	18					Barnamol	36	4.5	3
cv-99-4.25	0	5	34	2	8	26	5	23	18					Barnamol	36	1	9
cv-99-4.26	1	5	30	1	6	24	4	20.5	16					Barnamol	42	3	6.5
cv-99-4.27	2	8	23	1	8	24	8.5	23.5	18					Barnamol	36	2	6
cv-99-4.29	27	18.5	0	0	1	29	6	28	22					Barnamol	29	3	5
cv-99-4.31	12	18	7	1	6	22	10	30	24					Barnamol	27	4	7
cv-99-4.30	10	22	4	1	7	24	2	31	25					Barnamol	31	4	8
cv-99-4.65	5	20	30	0	4	27	7.5	34.5	25	5				Barnamol	25.5	4	1.5
cv-99-4.66	28	12	11.5	0	3.5	28.5	5	39	32	4				Bimol	22	4.5	1
cv-99-4.67	24	8.5	5	1	6.5	17.5	5	29	24	4				Bimol	36	9	3.5
cv-99-4.68	26	8	5	0	3	29	5	24	15	5				Barnamol	32	5	5
cv-99-4.69	9	6	20	1.5	6	27	5	28.5	20	5				Barnamol	32.5	3	4
cv-99-4.70	27	3	0	3	4	34	6	26.5	21	3				Barnamol	25	6	2.5
cv-99-4.71	20	3	10	0.5	4.5	19	5.5	26.5	19	6				Bimol	40	6	3
cv-99-4.72a	4	1	25	3.5	0.5	13	2	27	16	8				Bimol	48	7	3
cv-99-4.72b	8	1	5	14	2	23.5	5	29.5	15	12				Barnamol	34.5	5	2.5
cv-99-4.72c	28	3	0	2	4	8	1	28	23	4				Bimol	51.7	7	4.5
cv-99-4.74	31	3	0	6		7	1	28	21	6				Bimol	55	7	2
cv-99-4.75	5	7	40	1	8	8	2	35	21	10				Bimol	46	4	5
cv-99-4.76	23	10	0	1	7	40	10	28	20	6				Barnamol	17	2	3
cv-99-4.77	6	4	20	1	9	23	2.5	28	21	4				Barnamol	39	3	4.5
cv-99-4.78	3	12	24.5	2	7.5	17	5	31	22	6				Bimol	42	3	2
cv-99-4.81a	15	10	12	1	6	16	10	27	16	4	4			Barnamol	38	5	4
cv-99-4.81b	2	6	19	2	6	19.5	12	22	13	3	5			Barnamol	38.5	5	3
cv-99-4.82	3	15	20	2	6	20	15	25	17		6			Bryomol	31	3	6

Thin-section ref.	Intrinsic	Extrinsic	Intrinsic ind. Micr.	Porosity 1	Porosity 2	Barnacles	Bryozoans	Other Skeletal gr	Bi	For	Ech	Bra	Alg	Assemblage	Quartz	Other siliciclasts	Glauconite
cv-99-4.83	26	6	0	2	7	20.5	2.5	31	18		10			Barnamol	36.5	6.5	3
cv-99-4.84	28	2	0	0	4	22	4	27	16	3	5			Barnamol	36	7	4
cv-99-4.85	20	5	6	2	6.5	24	2	28	21		4			Barnamol	36	6	4
cv-99-4.86a	7	5	20	0	5	38	2	22	15	4				Barnamol	27	6	5
cv-99-4.96	7	3	21.5	2.5	9	14	4	26.5	20	4				Bimol	43	6	6.5
cv-99-4.97	6	9	20.5	1	4	13	10	33	13	6	10			Bryomol	35	1.5	7.5
cv-99-4.99	0	2	30	6	2	15	2	23	14	5				Barnamol	51	3	6
cv-99-4.100	2	6	21	9	2	14	4	26	9	8	5			Barnamol	46	4	6
cv-99-4.101	3	12	25	1	8.5	11	5	28	16	6				Barnamol	46	5	5
cv-99-4.102	0	2	33	7	4	14	8	36	18	5	11			Bramol	34	2	6
cv-99-4.103	2	6	25	3	9	14	6	29	17	5	5			Barnamol	44	3	4
cv-99-4.104	17	5	10	2	3	12	4	24	12	6	5			Barnamol	54	1	5
cv-99-4.105	24	6	3	5	13	23	6	34	27					Barnamol	26	7	4
cv-99-4.33	22	9	0	2	6	23	18.5	25	15		6			Bryomol	26	4.5	3
cv-99-4.32	18	4	0	4	11	23.5	4	27	21					Barnamol	34	4	7.5
cv-99-4.34	17	11	0	3	6	26	4	27	16	4	4			Barnamol	34	4	5
cv-99-4.35	10	13	10	0.5	4.5	22	4	26	13	5	5			Barnamol	41	6	1
cv-99-4.36	5	9	16.5	1	4.5	23.5	2	29.5	21	5				Barnamol	39	4	2
cv-99-4.37	4	7	35	1	6	21	5	27	14	8				Barnamol	37	4.5	5.5
cv-99-4.38	0	3	28	4	7	16	6	21	9	8				Barnamol	38	4	15
cv-99-4.39	28	11	0	0	10	28.5	3	41	41					Barnamol	19	2.5	6
cv-99-4.40	30	12	3.5	0.5	7.5	30	1	46	46					Barnamol	14	3	6
cv-99-4.114	21	9	0	3.5	10	23	16	25	15		5			Bryomol	29	3	4
cv-99-4.115	14	6	9	3	6	18	3	25	17	5				Barnamol	49	2	3
cv-99-4.117	14	3.5	0	20	4.5	21	8	29	21		5			Barnamol	35	3.5	3.5
cv-99-4.118	6	4	17	5	8	14.5	18	26	13		8			Bryomol	32	2	7.5
cv-99-4.119	22	10	0	7	3	17	10.5	37	19	11				Barnamol	29	1.5	5
cv-99-4.120	7	3	20	4	7	25	4.5	28	20	6				Barnamol	35	1.5	6
cv-99-4.121	1	5	25	2	8	15	5	26	18	5				Barnamol	45	4	5
cv-99-4.122	4	1	23	10	5	13	5	23	13	7				Barnamol	48	5	6
cv-99-4.123	1	3	24	6	5	23	4	23	14	7				Barnamol	41	1	8
cv-99-4.125	14	6	14	3	5	12	4	24.5	13	5	5			Barnamol	45	9.5	5
cv-99-4.126	16	15	5	3	10	20	6	32	22		5			Barnamol	34	2	6
cv-99-4.127	21	10	0	4	11	30	3	31	24	3				Barnamol	28	5	3
cv-99-4.128	17	17	0	3	6	28	4	42	34					Barnamol	19	3	4
cv-99-4.129	17	17	0	3	6	28	4	42	34					Barnamol	19	3	4
cv-99-4.130	19	5	0	7	12	28	14	42	34					Barnamol	11	2	3
cv-99-4.131	18	9	0	9	4	21	11	40	32	4				Bimol	23	1	4
cv-99-4.132	1	6	40	1	5	11	5	24	16	6				Bimol	53	4	3
cv-99-4.133	1	4	27	1	8	12	5	26	26					Bimol	51	3.5	2.5
cv-99-4.108				10.5		25.5	8	30	30					Barnamol	29	3	4.5
cv-99-4.109				6		17	7.5	22.5	22.5					Barnamol	44	6	3
cv-99-4.106				6		16	6	28.5	28.5					Barnamol	41.5	4	4

Thin-section ref.	Intrinsic	Extrinsic	Intrinsic ind. Micr.	Porosity 1	Porosity 2	Barnacles	Bryozoans	Other Skeletal gr	Bi	For	Ech	Bra	Alg	Assemblage	Quartz	Other siliciclasts	Glauconite
cv-99-4.107a				7		18	6	25	25					Barnamol	42	6	3
cv-99-4.110				8		12	4	25	25					Bimol	46	7	6
cv-99-4.111				8		24.5	5	38	38					Barnamol	25	5	2.5
cv-99-4.113				6		7.5	3.5	20	20					Bimol	62	3	4
cv-99-4.112				9		16.5	6	27.5	27.5					Barnamol	41	3	6
cv-99-4.141			24	0	3	12	8	29	23						41	5	5
cv-99-4.93	4	16	28	0	7	23	5	41	21	8	8			Barnamol	25	1	5
cv-99-4.95	6	24	27	0	4	28	4	43	34	6				Bimol	19	2.5	3.5
cv-99-4.52	12	5	5	6.5	4.5	10.5	3.5	32	22		6			Bimol	40	7	7
cv-99-4.53	22	6	0	2	8	19.5	4	35	24		7			Barnamol	31.5	2	8
cv-99-4.54	18	7	10	3	10	14.5	7.5	30	21		6			Bimol	39	3.5	5.5
cv-99-4.55	13	5	11	1	9	15	8.5	28	20		6			Bryomol	35	8.5	5
cv-99-4.56	4	6	23	2	8	10.5	16.5	23	14	3	5			Bryomol	36.5	3.5	10
cv-99-4.57	14	6	9	3	10	17	18.5	31.5	19	6	4			Bryomol	22.5	2	8.5
cv-99-4.134	19	5	0	15	8	10	40	15	12					Bryomol	20	6	9
cv-99-4.135	17	4	0	11	8	12	41	25	20					Bryomol	15	2	5
cv-99-4.136	3	4	20	6	12	8	28	23	14		5			Bryomol	31	2	8
cv-99-4.137	6	4	18	7	7	16.5	20.5	30	18	6				Bryomol	24	4	
cv-99-4.138	16	4	5	10	11	12	28	29.5	15	3	8			Bryomol	22	4	4.5
cv-99-4.140	14	6	10	4	4	13	23.5	28	20		5			Bryomol	24.5	4	8
cv-99-5.111b	3.5	5	20	7	7	16	7.5	37.5	32					Bimol	23	8	8
cv-99-5.112	7	3	17	5	9	21	23	36	29					Bryomol	16	1.5	2.5
cv-99-5.113	22	4	0	7	11	22	21	38	30					Bryomol	13	1.5	4.5
cv-99-5.114	26	3.5	0	3	14	19.5	10.5	43	34					Bimol	20	2	5
cv-99-5.116	23	3	0	6	10	9	33	22	16					Bryomol	23	3	10
cv-99-5.117	17	8	5	5.5	5.5	6	31	24.5	19					Bryomol	25	8.5	5
cv-99-5.118	0	5	33	2	4	5	14	20	16					Bryomol	51	3	7
cv-99-5.119	9	4	0	18	2	8.5	54	16.5	13					Bryomol	15	0	6
cv-99-5.122	15	4.5	5	12.5	7	11	39	23	18					Bryomol	19	0	8
cv-99-5.120	20	3.5	6	2	7.5	9	38	17	17					Bryomol	24	0	12
cv-99-5.124	12	3	5	12.5	8	3	54	11	10					Bryomol	20	1	11
cv-99-5.123	8	2	20	8	3	7	47	15	8	6				Bryomol	21	1	9
cv-99-5.125	20	2	6	1	3	6.5	25	20	12	6				Bryomol	34	3.5	11
cv-99-5.127	8	2	21	2	4	5	20	14	8	5				Bryomol	38	10	13
cv-99-5.128	20	4.5	0	17	4	3	43	31	12		10			Bryomol	13.5	0	9.5
cv-99-5.130	20	2.5	0	12.5	6	8	43.5	23.5	12		8			Bryomol	14	1	10
cv-99-5.129	13	2	0	19	3	7	37	24	10		11			Bryomol	20	3	9
cv-99-5.140b	18	3	0	8.5	6.5	8	38	30	10		15			Bryomol	13	2	9
cv-99-5.131	22	2	0	4	2	8.5	30	28	5	15	8			Bryomol	20.5	6	7
cv-99-5.132	2	3	9	12	4	2	23	15	12					Bryomol	44	11	5
cv-99-5.135	6	3	15	3.5	12	17	33	19	9		6			Bryomol	18	8	5
cv-99-7.6	28	7	8	0.5	3	12	34.5	36	13	6	15			Bryomol	10.5	5	2
cv-99-7.8	9	2	2.5	30.5	1.5	12	28.5	24.5	11		6			Bryomol	20	12	3

Thin-section ref.	Intrinsic	Extrinsic	Intrinsic ind. Micr.	Porosity 1	Porosity 2	Barnacles	Bryozoans	Other Skeletal gr	Bi	For	Ech	Bra	Alg	Assemblage	Quartz	Other siliciclasts	Glauconite
cv-99-7.9	9	3	1	35	1	18	34	25	10		11			Bryomol	11	7	5
cv-99-7.10	6	5	5	30	3	13	44.5	21.5	11		9			Bryomol	10	8.5	2.5
cv-99-5.92	18	2	3.5	11.5	6	37	4	21	17					Barnamol	27	1	10
cv-99-5.93	18	10	6	4	9	48	4	22	17					Barnamol	14	6	6
cv-99-5.94	0.5	5	36.5	0.5	1.5	12	12.5	19.5	16					Bryomol	43	3	10
cv-99-5.95	16	5	6	3.5	5.5	31	14	26	21					Barnamol	17.5	2	9.5
cv-99-5.99	30	9	0	1	4	22	11	31.5	24					Barnamol	19	4	12.5
cv-99-5.96	22	3	0	3	9	25	23	24	19					Barnamol	18	2	8
cv-99-5.98	24	7	0	3	6	28	23	28	24					Barnamol	11	3	7
cv-99-5.97	21	9	5	2	11	22	23	22	17					Bryomol	23	2	8
cv-99-5.105	1	7	24	1	12	9	8	27	21						42	5	9
cv-99-5.106	18	4	8	1	2	21	9	23	17					Barnamol	30	6	11
cv-99-5.102			0	2	3	40	7	35	28					Barnamol	10	5	3
cv-99-5.103			2.5	1	6	31	11	32	25					Barnamol	13	4	9
cv-99-5.87	20	13	1.5	1.5	7	23	10	38.5	31					Bimol	15.5	6.5	6.5
cv-99-5.88	20	10	7	1	7	19	24	35.5	27		4			Bryomol	16	3	2.5
cv-99-5.89	19	14	1	1	10	18	12.5	38	24	6				Barnamol	11	15.5	5
cv-99-5.90	2	6.5	25.5	0	3	12	20	25	19	3				Bryomol	27	9	7
cv-99-5.59	1	4	32	1	10	9	22	32	22	5				Bryomol	25	8	4
cv-99-5.61a	28	13	2.5	0	6	24	3	52	41			7		Bimol	11.5	8	1.5
cv-99-5.62	25	9.5	2	1	5	20	13	48	38			5		Bimol	12	5	2
cv-99-5.63	22	8	2	4	8	20	10	48	38		3	3		Bimol	13	7	2
cv-99-5.65	13	9	4	7	10	12	18	44	32		8			Bimol	15	5	6
cv-99-5.66	2	4	33	0	6	2	6	25	15	8				Bimol	53	7	7
cv-99-5.72	3	3	17	14	7	6	32	32	19		6			Bryomol	22	5	3
cv-99-5.75	23	5.5	4.5	1	6	16	20.5	38	26		8			Bryomol	10	11.5	4
cv-99-5.76	7	4	21	6	8	10	17.5	19	13		3			Bryomol	34	12	7.5
cv-99-5.79a	16	4	5	9	6.5	24	10	44	27		8	8		Barnamol	10	8.5	3.5
cv-99-5.81	21	5.5	3	2	9.5	14	9.5	36	25	4	4			Bimol	28	5.5	7
cv-99-5.86	1	3	25	1	12	10	13	37	26		6			Bimol	28	9	3
cv-99-5.84	0	2	24	1	12	16	20	41	33		6			Bimol	14	3	6
cv-99-5.28	16	8.5	3	2.5	4	16	11	42	33		4			Bimol	20	6	5
cv-99-5.30	3	3	18.5	2	9	7.5	11.5	31	21	6				Bimol	36	7	7
cv-99-5.32c	8	12	15.5	2	6	8	27	33	18	8				Bryomol	21	5	6
cv-99-5.34	24	6	5.5	1	5	18	12	40	32	6				Bimol	18	4	8
cv-99-5.38	12	6	8	8	5	13	13	32.5	25	4				Bimol	27	6	8.5
cv-99-5.44	14	10	6	2	6	15	12.5	38.5	27	6				Bimol	23	2	9
cv-99-5.45a	13	9	18	1	7	12.5	11	36	25	7				Bimol	28.5	5	7
cv-99-5.46a	21	21	6	1	5	16	9	41.5	29	9				Bimol	24	4	5.5
cv-99-5.47	4	5	28	1	3	4	6	22	15		3			Bimol	50	10	8
cv-99-5.48	11	7	22	0	4	17	8	35	28	3.5				Bimol	25	6	9
cv-99-5.51	12	3	13	2	8	18	9	39	24		8			Barnamol	23	5	6
cv-99-5.52	8	4	5	11	13	20	6	44	28	9				Barnamol	25	3	2

Thin-section ref.	Intrinsic	Extrinsic	Intrinsic ind. Micr.	Porosity 1	Porosity 2	Barnacles	Bryozoans	Other Skeletal gr	Bi	For	Ech	Bra	Alg	Assemblage	Quartz	Other siliciclasts	Glauconite
cv-99-5.53	12	2.5	12	2.5	6	18	4	36.5	22	6	6			Barnamol	30	4	7.5
cv-99-5.56	12	8	17	1	4	12	15	36	21	8				Bryomol	26	6	5
cv-00-5.142	2	4.5	33.5	1	1	11	3	34	17			10		Bramol	34	7	11
cv-00-5.145a	2	4	47	1	7	9	14	39	16		11			Bryomol	26	7	5
cv-99-7.12	18	5	2	2.5	23	16	7	63	48		7			Bimol	6.5	2	2.5
cv-99-7.14	13	3	21	3	10	16	22	31	22	5				Bryomol	25	3.5	2.5
cv-99-7.15	20	5	6	9	17	27	14	43	34		4			Barnamol	12	2	2
cv-99-7.16	17	4	12	7	19	27.5	14.5	41.5	25		11			Barnamol	12	2	2.5
cv-99-7.17	18	11	7	0	3	34	9	46.5	35		3.5			Barnamol	8.5	1.5	0.5
cv-99-7.18	22	10	3.5	0.5	4	43	7.5	42	36		2	2		Barnamol	4.5	2	1
cv-99-7.19	7	3	27	7	6	31	8	45	32		6			Barnamol	13	1	2
cv-99-7.20	21	5	4	7	10	37	7	40	24		8	4		Barnamol	10	4	2
cv-99-7.21	14	3	4.5	15	6.5	37.5	4	42	32	4	4			Barnamol	11	3.5	2
cv-99-7.22	4	10	30	1	8	29	4	29	16	5	4			Barnamol	28	4	6
cv-99-7.23	2	4	30	0	6	29	6.5	23	14	7				Barnamol	30	4.5	7
cv-99-7.27	6	4	28	0	4	18.5	4	22	13	7				Barnamol	35.5	13.5	6.5
cv-99-7.31	7	3	13	7.5	17	26	5	28.5	20	6				Barnamol	23.5	7.5	6.5
cv-99-7.32	8	2.5	15	10	13.5	31	6.5	37	23	9				Barnamol	15	3	4
cv-99-7.33	9	2.5	13.5	8	11	33	8	34	23	7				Barnamol	17	5	3
cv-99-7.34	11	5	12	8	13	35	3	31	21	6				Barnamol	22	5	4
cv-99-7.35	8	8	26	1	7	29	9	38	23		7	8		Barnamol	18.5	3	2.5
cv-99-7.36	5	8	27	1	10	29	8	43	22		7	8		Barnamol	12	3	5
cv-99-7.53	8	3.5	10	6.5	6	20	13.5	26	11	8	6			Barnamol	24	12	4.5
cv-99-7.42	16	3	5	13	11	15.5	19	36.5	19		10.5			Bryomol	18.5	4	6.5
cv-99-7.40	5	1	5	18	5	12.5	18.5	23.5	11	9				Bryomol	34	9	2.5
cv-99-7.43	4	3.5	10.5	1.5	7.5									Bryomol			
cv-99-7.45	7	9.5	10	5	12.5									Bryomol			
cv-99-7.47	3.5	5	21.5	1	6.5									Bryomol			
cv-99-7.49	6	2	21	1	14	23.5	6.5	28	23			3		Barnamol	23	15	4
cv-99-7.50	6	4	25	2	15	28	13	29	20		6			Barnamol	18	8	4
cv-99-7.52	2	4	28	1	15	22	17	25	15		5			Bryomol	19	12	5
cv-99-7.1	17	3.5	2.5	7.5	7.5	35	4	40	27		6	4		Barnamol	9	10	2
cv-99-7.2b	8	4	27	1	10	29	8.5	32	16		8	4		Barnamol	18	9	3.5
cv-99-7.3	16	4	3	5	12	29	12.5	34.5	18		10	5		Barnamol	14.5	7	2.5
cv-99-9.18	0.5	2	30.5	3	8									Bryomol			
cv-99-9.17	10	4	13	10.5	5	42	12	38	19	8	10			Barnamol	5	1	2
cv-99-9.16	2.5	3.5	20	9	6.5	52.5	7	29.5	18	4	6			Barnamol	6	3	2
cv-99-9.8	15	7	11	6	8	42	6.5	36.5	26	4	5			Barnamol	6.5	6	2.5
cv-99-9.9	9	4	19	2	8	43	3	33	20	4	7			Barnamol	9	9	3
cv-99-9.10	7	4.5	18.5	5	8	46	6	34	21	4	7			Barnamol	6	5	3
cv-99-9.1	13	8.5	15	1.5	7	43	3	29.5	24	3				Barnamol	8	8.5	3
cv-99-9.23	0.5	2.5	30	2	8									Bryomol			
cv-99-9.28	5	8	28.5	1	1.5	40	6	32	19	4	8			Barnamol	13	7	2

Thin-section ref.	Intrinsic	Extrinsic	Intrinsic ind. Micr.	Porosity 1	Porosity 2	Barnacles	Bryozoans	Other Skeletal gr	Bi	For	Ech	Bra	Alg	Assemblage	Quartz	Other siliciclasts	Glauconite
cv-99-9.29	12	16	14	0	2	45	10	23	16	4	3			Barnamol	13.5	5.5	3
cv-99-9.32	3.5	5.5	21	1	9	15	10	38.5	23	8	5			Bimol	24	6.5	3
cv-99-9.34	0.5	3	26	1	12	24	18	30.5	24	6.5				Barnamol	21	3	3.5
cv-99-9.37	4	2	32	1	10	30	5	31	23	4	3			Barnamol	21	10	3
cv-99-9.44	0	0.5	28	1.5	10	14	4.5	36.5	7	28				Barnafor	29	10	6
cv-99-9.57	3	4	16	10	5	23	16	38	11	20	5.5			Barnamol	12	7	4
cv-99-9.51	0	1.5	31	1	7.5	41	6	33	19	4.5	7			Barnamol	9	5	6
cv-99-9.52	0	2	37	1	3	23	18	37	17.5	12	5	2.5		Bryomol	15	3	4
cv-99-9.53	1	1	37	0	12	14.5	8.5	42.5	13.5	16	12			barnafor	23.5	6	5
cv-99-9.55	5	3	13	16.5	8	16	18	33.5	16	11	6			Bryomol	20	7.5	5
cv-99-9.60	4	4	5	24	2	16	12	36	18	13.5				Bimol	24	9.5	2.5
cv-99-9.63	3	1.5	27.5	1	11	19	8	35.5	15	11	7			Barnamol	22	12.5	3
cv-99-9.69	2.5	3.5	34	0	14.5	33	11	32	15.5	9	5	2.5		Barnamol	16	5	3
cv-99-9.71	9	2.5	42	0	4	43	3	41.5	29.5	5.5	4.5			Barnamol	9	3	0.5
cv-99-9.72	5	2	33	0	3	45	4	39	28		4			Barnamol	8.5	2.5	1
cv-99-9.73	3	1	22	1	20	31	3	27	16	8				Barnamol	29	3.5	6.5
cv-99-9.74	13	3	13	5	11	34	7	34	18	4	9			Barnamol	17	5	3
cv-99-9.75	6	5	20	9	12									Bryomol			
cv-99-9.76	11	3	17	1.5	23.5	37	7.5	31	22		6			Barnamol	17	5.5	2
cv-99-9.78	16	3	0	5	23	37	3	35	24		5			Barnamol	16	5	3.5
cv-99-9.79	16	4	2	12	18	42	4	33.5	20	5	7			Barnamol	12.5	5	3
cv-99-9.113	3	1	27	2	18	34	5	31	21	4.5	4.5			Barnamol	20	5.5	4.5
cv-99-9.119	21	5	12	1	10	45	4	42	29		7			Barnamol	6	2	1
cv-99-9.101	20	27	4.5	0	5.5	48	4	31.5	22	4.5	4			Barnamol	11.5	3	2
cv-99-9.102	14	14	11	1.5	18	42.5	4	33.5	24		7			Barnamol	13	5	2
cv-99-9.103	24	14	7	1	9.5	39	5.5	33	23	5	5			Barnamol	12	5.5	5
cv-99-9.104	12	8	26	0	7	32	5	38	23	6	8			Barnamol	18	4	3
cv-99-9.105	21	20	0	0	9	39	4.5	36	21	3.5	11			Barnamol	12	5	3.5
cv-99-9.106	1	1	35	0	19	20	8	37	18	9	8			Barnamol	24	8	3
cv-99-9.111	2	3	28	1	22	25	8	29	18	3	7.5			Barnamol	21	5.5	11.5
cv-99-9.114	16	4.5	11.5	3	21	39	7	38	23	5.5	8			Barnamol	10	4	2
cv-99-9.115	13	5.5	9.5	1	15	18	5	40	21	9.5	6			Bimol	21	10	6
cv-99-9.80	8	2	7	10	12	48	7	28	20		6			Barnamol	6	7	4
cv-99-9.81	20	5	6	2.5	5	42.5	7	31.5	22	4	4			Barnamol	8	6	5
cv-99-9.83	9	4	0	22	3	38	14	28	17	4	6			Barnamol	8.5	9	2.5
cv-99-9.84	12	5	3	9	10	40	9	36	18	5	11			Barnamol	5	8	2
cv-99-9.85	3.5	0.5	29	0	13	40	8	29	21	4		3		Barnamol	10	9	4
cv-99-9.91	9	4	2	12	18	45	8	37	27	5	3			Barnamol	4	3	3
cv-99-9.90	2	2	33	0	5	41.5	8	34.5	24	3.5	5			Barnamol	8	5.5	2.5
cv-99-9.92	2	3	31	0	12	39	7	34	17	10	7			Barnamol	10.5	6.5	3
cv-99-9.94	6.5	1.5	8	8	13	26.5	5.5	33	13	10	10			Barnamol	19	11	5
cv-99-9.96	12	7.5	14	0	5.5	33.5	2	38	19	11	7.5			Barnamol	18.5	6	2
cv-99-9.97	3	21	38	0	2												

Thin-section ref.	Intrinsic	Extrinsic	Intrinsic ind. Micr.	Porosity 1	Porosity 2	Barnacles	Bryozoans	Other Skeletal gr	Bi	For	Ech	Bra	Alg	Assemblage	Quartz	Other siliciclasts	Glauconite
cv-99-11.7	10	4	30.5	0.5	5	37	7	38	23	4	8			Barnamol	11.5	3.5	3
cv-99-11.8	18	5.5	3.5	2	11	36.5	8	39.5	24		11			Barnamol	12	1	3
cv-99-11.9	8.5	3.5	15	1	19	33.5	6.5	41	28	4	6			Barnamol	14.5	2	2.5
cv-99-11.10	7.5	3	19.5	0	11	37	4.5	42.5	25		7	7		Barnamol	11	2	3
cv-99-11.11	0.5	2.5	39	0	7	35	7	41.5	25	6	7			Barnamol	10.5	3	3
cv-99-11.15	2.5	1.5	33.5	0	13.5	33	10.5	46	24	5	8	5		Barnamol	7	2	1.5
cv-99-11.16	3	2	40	0	9.5	40	6.5	41.5	22	4.5	7.5			Barnamol	10	1	1
cv-99-11.18	2.5	1	37	0	13.5	36	7.5	45.5	29	3.5	6	5		Barnamol	5.5	4.5	1
cv-99-11.20	2.5	1.5	34	0	10	17	14	42	22	6	7			Bryomol	17	5	5
cv-99-11.21	13	3	8	8	18	24	10	43	26	6	7			Bimol	15	5	3
cv-99-11.22	3	3	31	0	14	29	10	44.5	28	4.5	6			Barnamol	8	6	2.5
cv-99-11.23	0.5	1.5	43	0	5	22	10	47	30	4	10.5			Bimol	13	5.5	2.5
cv-99-11.25	21	8	0	3	12	37	4.5	43.5	29	7.5	3.5			Barnamol	6	5.5	3.5
cv-99-11.26	21	5.5	2	1.5	19	26.5	8	40.5	18	11	7			Barnamol	14	6	4
cv-99-11.27	22.5	2.5	4	0	10	32	7	48.5	30	5	8.5	4		Barnamol	7	2.5	3
cv-99-11.28	24	3	2	0.5	19	34	7	43	26	5.5	9			Barnamol	9	5	2
cv-99-11.29	14	1.5	14	1	14.5	33.5	5	42	25	6	7			Barnamol	12.5	2.5	3.5
cv-99-11.33	6.5	4.5	11	1	20	31.5	12	37.5	25	6	5			Barnamol	12.5	2.5	4
cv-99-11.34	27	7	2	0	13	31	14.5	46	21	4	12	4		Barnamol	4	3	1.5
cv-99-11.35	23.5	3	2.5	0.5	17	20	4	50.5	26	13	9			Bimol	16	6	3.5
cv-99-11.36	21.5	2.5	6	0.5	7	23.5	6	43.5	22	12	8			foramol	15	6	6
cv-99-11.39	2	0	31.5	0	19	13.5	8.5	57	19	33				foramol	11.5	6.5	3
cv-99-11.40	1.5	3	30	0	20	23	9	52	24	13	9	4	1.5	Bimol	11.5	2.5	2
cv-99-11.41	0	1	26.5	0	24	15	15	57.5	37	11.5			5	Bimol	4	2.5	1
cv-99-11.42	2	2.5	29	2.5	25.5	23	8	54	31	9	4.5	4.5	4	Bimol	7	3.5	0.5
cv-99-11.44	3.5	5.5	18	0	18	34.5	5	51	29	3	9.5	5	1.5	Barnamol	5	1	2
cv-00-11.51	8	5	36.5	0.5	13	15	15	53	33	11	4			Bimol	11	2	4
cv-00-11.54	18	2	4	1	23	27.5	5	55	35	5	10			Bimol	8	2	2.5
cv-00-11.55	2.5	5.5	31	0	20	23	11	49	34	6.5				Bimol	11	2.5	3.5
cv-00-11.59	4	9	28	0	21.5	28	6.5	46	29	9				Barnamol	11	4.5	4
cv-00-11.58	5.5	4	15	1.5	23	35	7	44.5	24	6.5	8	4		Barnamol	7.5	3	3
cv-00-11.62	0.5	3.5	29	0	16	15	5.5	38.5	20	13				foramol	27.5	8	5.5
cv-00-11.63	12.5	12.5	21.5	3	12.5	23	19	36.5	19	9.5	6			Barnamol	17	2.5	2
cv-00-11.64	20	5	3	0	16	28	6	46	22	9	7.5	7		Barnamol	14	4	2
cv-00-11.65	0	6	48	0	18	20	11	37	24	7				Bryomol	25	2	5
cv-00-11.71	1.5	2	33.5	0	13	21	7.5	44	22	12	6.5	3		Bimol	21.5	2	4
cv-00-11.68	12.5	6	8.5	0.5	27	28	8	43	28	3	10			Barnamol	15	3	3
cv-00-11.81	2	19	29	0	7	11	15	68	38	13.5	8			Bimol	4.5	1	1
cv-00-11.82	2	19	27	0	4	11.5	13.5	70	42	10	12			Bimol	5	0	0
cv-00-11.87	0	14	31.5	0	13.5	12	11	69	35	18	12.5			Bimol	5	3	0
cv-00-11.84	2	16.5	23.5	0	23	9	14	68	40	19				Bimol	7	1	1
cv-00-11.85	2	17	27	0	10	8	17	65	35	16	10			Bimol	6	3	1
cv-00-11.89	4	10	32	0	11	1.5	3	30	19	7				Bimol	51	14	0.5

Thin-section ref.	Intrinsic	Extrinsic	Intrinsic ind. Micr.	Porosity 1	Porosity 2	Barnacles	Bryozoans	Other Skeletal gr	Bi	For	Ech	Bra	Alg	Assemblage	Quartz	Other siliciclasts	Glauconite
cv-00-11.88	1.5	12	35	0	15	11	13.5	64.5	27	18.5	13			Bimol	7	1.5	3
cv-00-11.90	1	6.5	26.5	0	20	5	9	56.5	21	14	13	6.5		Bimol	19	3	7.5
cv-00-11.73	0.5	3.5	33	0	24.5	15	17	49.5	22	13	11			Bryomol	14	1	3.5
cv-00-11.74	6.5	9.5	12.5	0	25	14.5	15	56	26	12	9	4.5		Bimol	9.5	3	2
cv-00-11.75	4.5	4.5	9	14	18	14	12	42	17	13.5	6			foramol	22.5	6	4
cv-00-11.77	2	2	38	0	21	21	11	52	32	6	11			Bimol	10	2	4
cv-00-11.78	1.5	2	43.5	0	18	13.5	19	46.5	19	8.5	12	4		Bryomol	14	3.5	3.5
cv-00-11.79	2.5	5.5	43	0	12	12	16	63	35	13	10			Bimol	7	1	1
cv-99-6.1	12	3	5	5	25	34	5.5	44.5	33	2.5	6.5			Barnamol	11	2	3
cv-99-6.3	7	3	38.5	0.5	6	40	3	37.5	28	2				Barnamol	16	1.5	2
cv-99-6.4	3	1	33	0.5	8	35	4.5	45	30	2	8.5			Barnamol	12	2	1.5
cv-99-6.5	28	7	1	2	3.5	31	3	55	27	2	16			Barnamol	7.5	2.5	1
cv-99-6.6	12	3	29	0	2	31	2	50	36	5				Bimol	11	4	2
cv-99-6.7	7	4.5	21	0	13.5	38	5	39	30	2				Barnamol	16	1	1
cv-99-6.8	7	4	0	14	33	45	3	38	29	2				Barnamol	10	3	1
cv-99-14.1	21	14.5	0	0	5	37.5	0.5	54	41	2	7			Barnamol	4	3	1
cv-00-14.14	18	12	2.5	0	17.5	26	0.5	43	35	4				Bimol	18	9	3.5
cv-00-14.15	16	7	5	0	15	34	2	45	32	4	6			Barnamol	13	3	3
cv-00-14.16	20	5	5	0	12	38	1	37.5	28	3				Barnamol	14.5	7	2
cv-00-14.17	18	11	0	0	25	39	1	50.5	35	1.5	10			Barnamol	5.5	3.5	1.5
cv-00-14.18	25	11	0	2	15	42	1	44.5	33	2	7			Barnamol	7.5	3.5	1.5
cv-00-14.19	7.5	7.5	9	0.5	21.5	23	1	45	32	5	4.5			Bimol	23	5	3
cv-00-14.20	4.5	3	21	0	22	20	3	30.5	18	8	3.5			Barnamol	33	7	6.5
cv-00-14.21	19	8	10	1	6	24	1.5	43	33	2	4			Bimol	21.5	7	3
cv-00-14.24	18	5	31	0	7	28	1	26	13	10	2.5			Barnamol	30	11	4
cv-00-14.25	10.5	5	0	1.5	28	39	1	46.5	35	2.5				Barnamol	8.5	2	3
cv-00-14.26	13	3	4.5	0	29.5	20	7	47.5	28	7.5	8			Bimol	17.5	5.5	2.5
cv-00-14.5	0.5	1.5	29	0	9	16	1	23.5	15	5				Bimol	41	13.5	5
cv-00-14.7	8	1	0	24	5	39.5	3	45	28	5	9			Barnamol	7.5	3.5	1.5
cv-00-14.9	10	4.5	14.5	3	19	26	1.5	33	20	7.5	4			Barnamol	26	9	4.5
cv-00-14.11	21	14	0	0	17	37	3	43.5	30	5.5	6			Barnamol	12	2.5	2
cv-00-14.13	17	17	0	0	14	34	2	39	29	3	5			Barnamol	14	8	3
cv-99-2.1	11	10	8	0	9	22	14	19	10	5	3			Barnamol	29	12	4
cv-99-2.2	11	8	9	0	14	22.5	13	21.5	13	3	4			Barnamol	26	13	4
cv-99-2.3	10	10	9	0	12	25	20	22	11	4	5.5			Barnamol	24	8	1
cv-99-2.4	16	7	9	0	8	38	10	30	22	2				Barnamol	12.5	6.5	3
cv-99-2.5	1	6.5	26.5	0	5	10	29	19	10	5	2			Bryomol	28	8	6
cv-99-2.6	11	11	11	2	11	25	15	21	7.5	2	9.5			Barnamol	23	10.5	5.5
cv-99-2.8	10	7	16	0	9	31	16	22	11	1	8			Barnamol	21	6	4
cv-99-2.7	6	5	29	0	10	15	22	20	11	2	5.5			Bryomol	27	9	7
cv-00-15.22	20	8	4	0	7.5	25	9	36	23	3	6			Barnamol	11	14	5
cv-00-15.23	12	19	3	0	3	22	3	21	12	4	3.5			Barnamol	24	20	10
cv-00-15.24	17.5	7.5	4.5	0	15	20	4	21	14	1	4			Barnamol	33	18	4

Thin-section ref.	Intrinsic	Extrinsic	Intrinsic ind. Micr.	Porosity 1	Porosity 2	Barnacles	Bryozoans	Other Skeletal gr	Bi	For	Ech	Bra	Alg	Assemblage	Quartz	Other siliciclasts	Glauconite
cv-00-15.25	21	10	0.5	0	10	27	3.5	27	20	1.5				Barnamol	20	18.5	4
cv-00-15.27	21	8	0	0	17	33	9	22	16	1	3			Barnamol	12	17	7
cv-00-15.28	15.5	10.5	1	0	6.5	25	5.5	33.5	22	2	8			Barnamol	14.5	14.5	7
cv-00-15.30	11	5	13	0	9.5	21	4	24	16	3	3			Barnamol	29	12	10
cv-00-15.31	7	4.5	17	0	10.5	15	2	19.5	11	3.5	4			Barnamol	35	23.5	5
cv-00-15.32	16	5	14	0	5	19	2	26	16	3	5			Barnamol	21	25	7
cv-00-15.34	19	9	1	0	18	30	5	27	20	2	2.5			Barnamol	13	20.5	4.5
cv-00-15.35	18	4.5	2	0	6	20	3.5	28	19	4	4			Bimol	20	24	4.5
cv-00-15.36	26	2	0	0	1	24	4	38.5	28	3				Bimol	12	18	3.5
cv-00-15.37	15	3.5	1	0	17	20	2	24	18	2				Barnamol	20	30	4
cv-00-15.38	15	3.5	0	0	11.5									Barnamol			
cv-00-15.39	16	4	0	0	14									Barnamol			
cv-00-15.40	14	6.5	3	1	5.5	28.5	1.5	15.5	11	1.5				Barnamol	25	24.5	5
cv-00-15.41	21	9	1	0	4	24	3	28	21	2	4			Barnamol	19	23	3
cv-00-15.42	18	5	0	0	5.5	22	2	24	16	1	4			Barnamol	14	33	5
cv-00-15.43	14	6	3	0	9	18	2	33	21	8				Bimol	18	23	6
cv-00-15.45	14	6	9	0	7.5	23	2.5	28.5	12	4.5	7	2.5		Barnamol	16	25	5
cv-00-15.46	16	9	2	0	15	17	2	23	14	3	4	2		Barnamol	23	28	7
cv-00-15.47	16	5	2	0	10.5	24.5	2	25.5	11	3	7	3		Barnamol	20	23	5
cv-00-15.13	16	4	0.5	0	24.5	27	1	34	27	0.5				Barnamol	12.5	24	1.5
cv-00-15.14	13	6	0	0	17												
cv-00-15.15	13	3	5.5	0	13.5	18	1	31	25	0				Bimol	20	25	5
cv-00-15.17	14	5	0	0	12	21	1.5	33.5	27	0.5				Bimol	14	27.5	2.5
cv-00-15.19	17	7	1	0	9	17	1	29	24	1				Bimol	20	31	2
cv-00-15.20	18	4.5	0	0	18.5	23	2	40.5	33	0.5				Bimol	8.5	24	2
cv-00-15.55	12	18	6	0	8	11	21.5	25	14	5	5			Bryomol	25	14	3.5
cv-00-15.56	12.5	18	1.5	0	8	12	20.5	21	11	3	5.5			Bryomol	26	17	3.5
cv-00-15.57	7	13	8.5	0	7	11	13	20	12	1	4	2		Bryomol	33	20	3
cv-00-16.6	24	11	1	0	16	18	4.5	22	13	3	4	2		Barnamol	21	30	4.5
cv-00-16.7	13	19	2	0	10	17	3	35	19	3.5	10			Bimol	21	19	5
cv-00-16.8	21	14	0.5	0	14.5	22	2	35.5	26	3	4			Bimol	18	18.5	4
cv-00-16.9	19.5	19	0	0	17	21.5	4	39.5	23	1.5	5	8		Bimol	16	14	5
cv-00-16.10	18	5	4	0	16	11	3	15	10	3				Barnamol	38	26	7
cv-00-16.12	1.5	8	29	0.5	4	5	5	17	9	6				Bimol	50	18	5
cv-00-16.13	9	1	16.5	0	13	9	6	16	6.5	6.5	2.5			Bimol	39	23.5	6.5
cv-00-16.14	23	3	4.5	0	4	11	3	18.5	8.5	6	2.5	1.5		Barnamol	28	33	6.5
cv-00-16.15	14	5	18	0	21	20	3.5	19	12	2	1.5	3.5		Barnamol	36.5	17	4
cv-00-16.16	22	6	3	0	16	14.5	7	19	8	6	3	2		Barnamol	29	26	4.5
cv-00-16.17	24	10	1	0	21	18	5	28	13	2	8	4		Barnamol	19	24	6
cv-00-16.1	18	13	0	0	19	23	6	46	32	1.5	8	4.5		Bimol	10.5	11.5	3
cv-00-16.2	16	16	0	0	16.5	27	3	37	20	3	7	5		Barnamol	11.5	17.5	4
cv-00-16.3	21	8.5	8.5	0	12	17	5	39	24.5	4	5	3.5		Bimol	16	20	3
cv-00-16.4	14	14	8.5	0	18	24	4	27.5	15	3.5		6		Barnamol	17.5	23	4

Thin-section ref.	Intrinsic	Extrinsic	Intrinsic ind. Micr.	Porosity 1	Porosity 2	Barnacles	Bryozoans	Other Skeletal gr	Bi	For	Ech	Bra	Alg	Assemblage	Quartz	Other siliciclasts	Glauconite
cv-00-16.5	2	19	30	0	18									Bimol			
cv-00-18.1	5	7	11.5	0	20	11.5	10	38	17.5	12.5	5			Foramol	14	26	1
cv-00-18.2	5.5	5.5	12	0	17.5	20	3	32	21	6	3.5			Barnamol	10	34	2
cv-00-18.3	1	3.5	29	0.5	16.5									Barnamol			
cv-00-18.4	4	6	29	0	18	22	10.5	29	16	6	4.5			Barnamol	13.5	23	2
cv-00-18.5	4	10	24.5	0	26	16	6	28	18	2	5			Bimol	16	32	2
cv-00-18.6	1	3	30	0.5	9.5												
cv-99-13.2	1.5	6.5	23	0	6	56	3.5	21	16	1	2			Barnamol	10	8	1.5
cv-99-13.3	1	6	23	2	7.5	55	4	23	18	2				Barnamol	13.5	4	0.5
cv-99-13.4	0	2	25	0	7									Barnamol			
cv-99-13.5	18	13	0	2	40	58	0.5	36	30	3				Barnamol	4	1	0.5
cv-99-12.8	0	4	36	0	5	8	7	31	17.5	6	3	3		Bimol	35	18	1
cv-99-12.2	4.5	10.5	27	0	10	22	13	42.5	24	4	8	6.5		Bryomol	14.5	5	3
cv-99-12.3	1	9	33	0	13	17	8	28	14.5	4	5	4		Barnamol	33	10	4
cv-99-12.5	7.5	17.5	11.5	0	14	23	14	33.5	22	1	4.5	4.5		Barnamol	21	6.5	2
cv-99-12.6	12	20	14	0	14	20	10	36.5	25	0.5	3.5	7		Bimol	23	8.5	2
cv-99-12.7	13	13	4	3	27	29	15	45	31.5	0	4.5	9		Barnamol	7	3	1
cv-00-17.16	13.5	3.5	9	1	17	21	1.5	42	21	7	7			Barnamol	24	9	2.5
cv-00-17.15	21	8	9.5	0	20	35	4	33	26.5					Barnamol	19	5.5	3.5
cv-00-17.14	30	7	0	0	20	44.5	1.5	41.5	33					Barnamol	9	2	1.5
cv-00-17.13	14	7	0.5	0	25	18	3	50	33	3	12			Bimol	21	7	2.5
cv-00-17.12	16	5	8.5	0	22.5	19.5	2	31	17	7	6			Barnamol	32.5	10	5
cv-00-17.9	21	8	0	0	23	24	1.5	48	30	5	8			Bimol	15	9	2.5
cv-00-17.10	17	7	0	0	29	31	3	41	29.5	4				Barnamol	17	7	1
cv-00-17.1	10	3	15	0	28	22	3	36.5	15.5	10.5	8			Barnamol	29	6	3.5
cv-00-17.2	4.5	6.5	32	0	7	21	4	28	19.5	4				Barnamol	36.5	5	5.5
cv-00-17.3	21	8	0	0.5	26	51	1	38	24	4	7			Barnamol	7	2	1
cv-00-17.4	18	17	1.5	0	14.5	47	1	42	32	3	4.5			Barnamol	6	2	2
cv-00-17.6	10	14	14.5	0.5	20	33	2	30.5	16	9.5	3			Barnamol	24.5	5	5
cv-00-17.7	12	10	12	0	20	38	2	32	19	5	4			Barnamol	19	8	1
cv-00-17.8	17	7	0	0	24	50	2.5	33	25	2.5	3			Barnamol	7	5.5	2

Hierarchical Cluster Analysis of Observations

Squared Euclidean Distance, Complete Linkage

Amalgamation Steps

Step	Number of clusters	Similarity level	Distance level	Clusters joined		New cluster	Number of obs. in new cluster
1	350	100.00	0.000	73	74	73	2
2	349	99.99	0.500	162	319	162	2
3	348	99.99	0.500	15	16	15	2
4	347	99.99	1.000	54	272	54	2
5	346	99.99	1.000	8	11	8	2
6	345	99.98	1.500	158	215	158	2
7	344	99.98	1.500	49	56	49	2
8	343	99.97	2.000	142	223	142	2
9	342	99.97	2.000	61	174	61	2
10	341	99.97	2.000	40	163	40	2
11	340	99.97	2.000	75	153	75	2
12	339	99.97	2.000	60	73	60	3
13	338	99.97	2.000	13	67	13	2
14	337	99.97	2.500	28	310	28	2
15	336	99.97	2.500	218	229	218	2
16	335	99.97	2.500	178	192	178	2
17	334	99.96	3.500	39	161	39	2
18	333	99.95	4.000	290	306	290	2
19	332	99.95	4.000	30	32	30	2
20	331	99.94	4.500	164	198	164	2
21	330	99.94	4.500	97	143	97	2
22	329	99.94	4.500	68	70	68	2
23	328	99.94	5.000	31	49	31	3
24	327	99.93	5.500	277	314	277	2
25	326	99.93	5.500	54	286	54	3
26	325	99.93	5.500	6	8	6	3
27	324	99.92	6.000	302	311	302	2
28	323	99.92	6.000	66	299	66	2
29	322	99.92	6.000	48	208	48	2
30	321	99.92	6.000	166	193	166	2
31	320	99.92	6.500	248	350	248	2
32	319	99.92	6.500	226	280	226	2
33	318	99.92	6.500	158	214	158	3
34	317	99.92	6.500	7	10	7	2
35	316	99.90	7.500	343	344	343	2
36	315	99.90	7.500	177	210	177	2
37	314	99.90	8.000	24	305	24	2
38	313	99.90	8.000	62	304	62	2
39	312	99.90	8.000	91	94	91	2
40	311	99.90	8.000	86	87	86	2
41	310	99.89	8.500	158	202	158	4
42	309	99.89	8.500	186	187	186	2
43	308	99.89	8.500	76	88	76	2
44	307	99.89	9.000	234	249	234	2
45	306	99.88	9.500	29	333	29	2
46	305	99.88	9.500	162	298	162	3
47	304	99.88	9.500	243	250	243	2
48	303	99.88	9.500	25	111	25	2
49	302	99.87	10.000	312	335	312	2
50	301	99.87	10.000	160	188	160	2
51	300	99.87	10.000	72	185	72	2
52	299	99.87	10.000	63	71	63	2
53	298	99.87	10.000	45	46	45	2
54	297	99.87	10.500	28	31	28	5
55	296	99.87	10.500	20	21	20	2
56	295	99.85	11.500	33	328	33	2

57	294	99.85	11.500	171	317	171	2
58	293	99.85	11.500	313	315	313	2
59	292	99.85	11.500	42	290	42	3
60	291	99.85	11.500	271	273	271	2
61	290	99.85	11.500	15	52	15	3
62	289	99.85	12.000	339	341	339	2
63	288	99.84	12.500	281	288	281	2
64	287	99.84	12.500	27	61	27	3
65	286	99.84	12.500	17	30	17	3
66	285	99.83	13.500	51	348	51	2
67	284	99.83	13.500	181	199	181	2
68	283	99.83	13.500	40	66	40	4
69	282	99.83	13.500	1	2	1	2
70	281	99.82	14.000	162	327	162	4
71	280	99.82	14.000	69	302	69	3
72	279	99.82	14.000	270	275	270	2
73	278	99.82	14.000	168	247	168	2
74	277	99.82	14.000	196	205	196	2
75	276	99.82	14.000	190	197	190	2
76	275	99.82	14.000	99	138	99	2
77	274	99.81	14.500	26	340	26	2
78	273	99.81	14.500	103	332	103	2
79	272	99.81	14.500	18	297	18	2
80	271	99.81	14.500	19	44	19	2
81	270	99.80	15.500	195	204	195	2
82	269	99.80	15.500	37	60	37	4
83	268	99.80	16.000	284	292	284	2
84	267	99.79	16.500	217	218	217	3
85	266	99.79	16.500	12	50	12	2
86	265	99.78	17.500	65	200	65	2
87	264	99.78	17.500	101	183	101	2
88	263	99.77	18.000	135	136	135	2
89	262	99.77	18.000	57	107	57	2
90	261	99.77	18.000	9	100	9	2
91	260	99.76	18.500	186	194	186	3
92	259	99.76	18.500	96	98	96	2
93	258	99.76	18.500	3	25	3	3
94	257	99.75	19.500	325	326	325	2
95	256	99.75	19.500	23	116	23	2
96	255	99.74	20.000	43	68	43	3
97	254	99.74	20.500	54	55	54	4
98	253	99.73	21.500	251	255	251	2
99	252	99.73	21.500	19	29	19	4
100	251	99.73	21.500	5	9	5	3
101	250	99.72	22.000	62	308	62	3
102	249	99.72	22.000	256	261	256	2
103	248	99.72	22.000	257	260	257	2
104	247	99.71	22.500	4	76	4	3
105	246	99.71	23.000	6	38	6	4
106	245	99.70	23.500	201	336	201	2
107	244	99.70	23.500	26	321	26	3
108	243	99.70	23.500	36	296	36	2
109	242	99.70	23.500	221	228	221	2
110	241	99.70	23.500	178	181	178	4
111	240	99.69	24.000	13	337	13	3
112	239	99.69	24.000	238	254	238	2
113	238	99.69	24.000	142	225	142	3
114	237	99.69	24.500	95	144	95	2
115	236	99.69	24.500	14	58	14	2
116	235	99.68	25.000	217	230	217	4
117	234	99.67	25.500	17	329	17	4
118	233	99.67	25.500	191	268	191	2
119	232	99.67	26.000	164	167	164	3
120	231	99.67	26.000	43	77	43	4
121	230	99.67	26.000	24	72	24	4
122	229	99.66	26.500	257	258	257	3
123	228	99.66	26.500	203	245	203	2
124	227	99.65	27.500	219	244	219	2

125	226	99.65	27.500	224	243	224	3
126	225	99.65	27.500	59	234	59	3
127	224	99.65	27.500	22	69	22	4
128	223	99.64	28.000	110	173	110	2
129	222	99.64	28.500	84	133	84	2
130	221	99.64	28.500	83	93	83	2
131	220	99.64	28.500	89	90	89	2
132	219	99.62	29.500	95	97	95	4
133	218	99.61	30.500	64	316	64	2
134	217	99.60	31.000	282	322	282	2
135	216	99.60	31.500	266	342	266	2
136	215	99.60	31.500	159	267	159	2
137	214	99.60	31.500	82	152	82	2
138	213	99.59	32.000	207	211	207	2
139	212	99.58	32.500	141	318	141	2
140	211	99.57	33.500	102	276	102	2
141	210	99.57	33.500	157	216	157	2
142	209	99.57	34.000	164	165	164	4
143	208	99.57	34.000	80	121	80	2
144	207	99.56	34.500	48	190	48	4
145	206	99.55	35.500	279	301	279	2
146	205	99.55	35.500	117	177	117	3
147	204	99.53	36.500	237	240	237	2
148	203	99.53	36.500	41	166	41	3
149	202	99.53	37.000	106	334	106	2
150	201	99.52	37.500	160	293	160	3
151	200	99.52	37.500	189	213	189	2
152	199	99.51	38.000	312	320	312	3
153	198	99.51	38.000	269	270	269	3
154	197	99.51	38.000	112	114	112	2
155	196	99.51	38.500	47	346	47	2
156	195	99.51	38.500	271	307	271	3
157	194	99.51	38.500	226	278	226	3
158	193	99.51	38.500	63	172	63	3
159	192	99.49	40.000	179	195	179	3
160	191	99.49	40.000	79	122	79	2
161	190	99.48	41.000	221	239	221	3
162	189	99.47	41.500	274	313	274	3
163	188	99.47	41.500	14	115	14	3
164	187	99.46	42.500	6	7	6	6
165	186	99.44	43.500	287	330	287	2
166	185	99.44	43.500	277	303	277	3
167	184	99.44	44.000	128	150	128	2
168	183	99.44	44.000	126	132	126	2
169	182	99.44	44.000	47	105	47	3
170	181	99.43	44.500	154	231	154	2
171	180	99.43	44.500	103	203	103	4
172	179	99.43	45.000	15	51	15	5
173	178	99.42	45.500	186	209	186	4
174	177	99.41	46.000	212	289	212	2
175	176	99.41	46.000	137	145	137	2
176	175	99.41	46.500	170	222	170	2
177	174	99.39	47.500	96	248	96	4
178	173	99.38	48.500	6	12	6	8
179	172	99.37	49.500	142	347	142	4
180	171	99.37	49.500	323	325	323	3
181	170	99.37	49.500	191	283	191	3
182	169	99.37	49.500	168	227	168	3
183	168	99.37	49.500	117	196	117	5
184	167	99.36	50.000	184	349	184	2
185	166	99.36	50.500	64	171	64	4
186	165	99.36	50.500	109	141	109	3
187	164	99.36	50.500	17	54	17	8
188	163	99.34	51.500	62	162	62	7
189	162	99.34	51.500	34	35	34	2
190	161	99.32	53.500	99	262	99	3
191	160	99.32	53.500	28	42	28	8
192	159	99.31	54.000	157	224	157	5

193	158	99.30	54.500	158	217	158	8
194	157	99.28	56.000	127	130	127	2
195	156	99.28	56.000	96	101	96	6
196	155	99.28	56.500	102	287	102	4
197	154	99.26	58.000	110	118	110	3
198	153	99.26	58.000	39	40	39	6
199	152	99.24	59.500	175	220	175	2
200	151	99.23	60.000	189	294	189	3
201	150	99.23	60.500	291	295	291	2
202	149	99.21	61.500	282	331	282	3
203	148	99.19	63.500	75	351	75	3
204	147	99.19	63.500	102	285	102	5
205	146	99.19	63.500	5	85	5	4
206	145	99.19	63.500	20	39	20	8
207	144	99.18	64.000	81	89	81	3
208	143	99.16	65.500	43	277	43	7
209	142	99.16	66.000	108	182	108	2
210	141	99.15	66.500	191	281	191	5
211	140	99.13	68.500	4	91	4	5
212	139	99.10	70.500	83	139	83	3
213	138	99.09	71.500	137	140	137	3
214	137	99.09	71.500	27	53	27	4
215	136	99.08	72.000	256	259	256	3
216	135	99.07	72.500	26	338	26	4
217	134	99.06	73.500	219	221	219	5
218	133	99.05	74.000	18	22	18	6
219	132	99.05	74.500	323	324	323	4
220	131	99.03	76.000	135	242	135	3
221	130	99.03	76.000	23	63	23	5
222	129	99.01	77.500	146	148	146	2
223	128	98.98	79.500	176	179	176	4
224	127	98.98	80.000	57	300	57	3
225	126	98.97	80.500	266	271	266	5
226	125	98.96	81.500	18	62	18	13
227	124	98.93	83.500	19	201	19	6
228	123	98.93	84.000	252	263	252	2
229	122	98.91	85.500	59	233	59	4
230	121	98.90	86.000	226	269	226	6
231	120	98.90	86.500	48	180	48	5
232	119	98.90	86.500	1	5	1	6
233	118	98.89	87.000	186	284	186	6
234	117	98.85	90.000	14	78	14	4
235	116	98.82	92.500	24	279	24	6
236	115	98.79	94.500	82	84	82	4
237	114	98.78	95.500	23	28	23	13
238	113	98.77	96.000	86	113	86	3
239	112	98.75	97.500	95	104	95	5
240	111	98.75	98.000	65	253	65	3
241	110	98.73	99.500	238	241	238	3
242	109	98.72	100.000	33	43	33	9
243	108	98.70	101.500	36	164	36	6
244	107	98.69	102.500	256	257	256	6
245	106	98.67	104.000	17	312	17	11
246	105	98.67	104.000	206	207	206	3
247	104	98.65	106.000	123	124	123	2
248	103	98.64	106.500	109	119	109	4
249	102	98.60	110.000	13	339	13	5
250	101	98.58	111.500	15	169	15	6
251	100	98.58	111.500	75	155	75	4
252	99	98.56	112.500	170	246	170	3
253	98	98.54	114.500	110	184	110	5
254	97	98.40	125.500	156	186	156	7
255	96	98.38	126.500	37	266	37	9
256	95	98.37	127.500	154	157	154	7
257	94	98.33	130.500	41	160	41	6
258	93	98.32	131.500	159	226	159	8
259	92	98.30	133.500	48	178	48	9
260	91	98.29	134.000	129	146	129	3

261	90	98.28	134.500	48	117	48	14
262	89	98.22	139.500	212	282	212	5
263	88	98.22	139.500	147	149	147	2
264	87	98.14	146.000	176	291	176	6
265	86	98.14	146.000	134	135	134	4
266	85	98.14	146.000	41	57	41	9
267	84	98.12	147.500	3	96	3	9
268	83	98.09	149.500	80	128	80	4
269	82	98.08	150.000	6	23	6	21
270	81	98.04	153.500	47	92	47	4
271	80	98.02	155.000	235	264	235	2
272	79	97.95	160.500	168	236	168	4
273	78	97.94	161.000	18	309	18	14
274	77	97.88	166.000	45	99	45	5
275	76	97.86	167.500	158	219	158	13
276	75	97.83	170.000	17	274	17	14
277	74	97.82	170.500	19	20	19	14
278	73	97.78	173.500	108	343	108	4
279	72	97.62	186.000	65	106	65	5
280	71	97.60	188.000	64	125	64	5
281	70	97.59	188.500	175	232	175	3
282	69	97.59	188.500	120	123	120	3
283	68	97.52	194.000	59	102	59	9
284	67	97.50	196.000	1	26	1	10
285	66	97.37	206.000	81	83	81	6
286	65	97.26	214.500	142	168	142	8
287	64	97.24	216.500	159	265	159	9
288	63	97.18	221.000	189	191	189	8
289	62	97.15	223.500	170	251	170	5
290	61	97.06	230.000	4	37	4	14
291	60	97.06	230.000	13	14	13	9
292	59	97.04	231.500	19	24	19	20
293	58	97.02	233.500	75	154	75	11
294	57	96.90	242.500	109	126	109	6
295	56	96.86	246.000	27	112	27	6
296	55	96.80	250.500	3	103	3	13
297	54	96.71	257.500	3	95	3	18
298	53	96.55	270.000	134	151	134	5
299	52	96.52	272.500	129	131	129	4
300	51	96.42	280.500	237	238	237	5
301	50	96.33	287.500	15	17	15	20
302	49	96.25	294.000	81	82	81	10
303	48	96.20	297.500	158	175	158	16
304	47	96.01	312.500	36	189	36	14
305	46	95.96	316.500	156	345	156	8
306	45	95.84	326.000	127	147	127	4
307	44	95.82	327.500	48	206	48	17
308	43	95.73	334.000	86	110	86	8
309	42	95.47	354.500	45	323	45	9
310	41	95.38	361.500	252	256	252	8
311	40	95.33	365.500	19	41	19	29
312	39	95.29	368.500	1	6	1	31
313	38	95.07	386.000	18	33	18	23
314	37	94.89	400.000	13	47	13	13
315	36	94.84	404.000	134	237	134	10
316	35	94.84	404.000	108	176	108	10
317	34	94.52	429.500	79	80	79	6
318	33	94.48	432.000	59	142	59	17
319	32	94.36	441.500	15	212	15	25
320	31	94.04	466.500	127	129	127	8
321	30	93.67	496.000	48	108	48	27
322	29	93.49	509.500	79	120	79	9
323	28	93.33	522.000	1	3	1	49
324	27	93.24	529.000	64	81	64	15
325	26	92.90	556.000	86	137	86	11
326	25	92.21	610.000	4	34	4	16
327	24	92.15	614.500	65	170	65	10
328	23	92.11	618.000	75	158	75	27

329	22	91.70	650.000	27	86	27	17
330	21	91.65	654.000	45	109	45	15
331	20	91.17	691.500	13	18	13	36
332	19	90.99	705.500	1	15	1	74
333	18	90.02	781.500	36	59	36	31
334	17	90.01	782.500	75	159	75	36
335	16	89.58	816.000	65	235	65	12
336	15	87.40	986.500	48	156	48	35
337	14	86.81	1032.500	4	134	4	26
338	13	86.64	1046.000	1	19	1	103
339	12	85.88	1106.000	27	36	27	48
340	11	84.98	1176.500	79	127	79	17
341	10	84.70	1198.000	13	45	13	51
342	9	82.34	1382.500	48	75	48	71
343	8	79.16	1631.500	1	27	1	151
344	7	75.37	1929.000	65	252	65	20
345	6	74.95	1961.500	64	79	64	32
346	5	66.59	2616.500	4	65	4	46
347	4	57.94	3293.500	1	4	1	197
348	3	43.70	4408.500	1	48	1	268
349	2	34.19	5153.500	13	64	13	83
350	1	0.00	7830.500	1	13	1	351

Final Partition

Number of clusters: 6

	Number of observations	Within cluster sum of squares	Average distance from centroid	Maximum distance from centroid
Barbital	151	27576.457	12.831	26.722
Bimol	26	3544.673	10.937	18.773
Detrital	51	6376.363	10.381	21.951
Barnamol	71	9386.183	10.659	23.401
Bryotal	32	6994.609	13.955	25.202
Mixed skeletal	20	5405.625	15.754	23.239

Cluster Centroids

Variable	Barbital	Bimol	Detrital	Barnamol	Bryotal
barnacle	23.2748	22.7885	13.4706	39.4366	10.2187
bryozoan	7.2219	6.9038	5.5196	6.3732	32.7969
bivalve	21.4967	35.1538	15.5196	25.7042	13.9062
mixed	11.3411	11.0769	8.0686	12.7887	10.6406
detrital	36.6656	24.0769	57.4216	15.6972	32.4375

Variable	Mixed skeletal	Grand centrd
barnacle	13.1500	23.3162
bryozoan	13.7500	9.4829
bivalve	25.3250	22.0171
mixed	26.7250	11.9516
detrital	21.0500	33.2322

Distances Between Cluster Centroids

	Barbital	Bimol	Detrital	Barnamol	Bryotal
Barbital	0.0000	18.5849	24.0056	26.8588	30.0087
Bimol	18.5849	0.0000	39.9394	20.9735	36.7423
Detrital	24.0056	39.9394	0.0000	50.4172	37.2565
Barnamol	26.8588	20.9735	50.4172	0.0000	44.4515
Bryotal	30.0087	36.7423	37.2565	44.4515	0.0000
Mixed skeletal	25.3041	22.1450	42.8362	31.1194	29.8353

	Mixed skeletal
Barbital	25.3041
Bimol	22.1450
Detrital	42.8362

Barnamol	31.1194
Bryotal	29.8353
Mixed skeletal	0.0000

1	Barbital	4	Barnamol
2	Bimol	5	Bryotal
3	Detrital	6	Mixed

cv-4.2	1	cv-99-4.81b	1	cv-99-5.53	1	cv-99-7.16	4	cv-99-9.81	4
cv-4.3	1	cv-99-4.82	1	cv-99-5.56	1	cv-99-7.17	4	cv-99-9.83	4
cv-4.5	1	cv-99-4.83	1	cv-00-5.142	3	cv-99-7.18	4	cv-99-9.84	4
cv-4.6	2	cv-99-4.84	1	cv-00-5.145a	6	cv-99-7.19	4	cv-99-9.85	4
cv-4.7	1	cv-99-4.85	1	cv-99-5.92	1	cv-99-7.20	4	cv-99-9.91	4
cv-99-4.9	1	cv-99-4.86a	1	cv-99-5.93	4	cv-99-7.21	4	cv-99-9.90	4
cv-99-4.10	1	cv-99-4.141	3	cv-99-5.94	3	cv-99-7.22	1	cv-99-9.92	4
cv-99-4.11	1	cv-99-4.93	1	cv-99-5.95	1	cv-99-7.23	1	cv-99-9.94	1
cv-99-4.12	1	cv-99-4.95	2	cv-99-5.99	1	cv-99-7.27	3	cv-99-9.96	1
cv-99-4.13	1	cv-99-4.114	1	cv-99-5.96	1	cv-99-7.31	1	cv-99-11.7	4
cv-99-4.14	1	cv-99-4.115	3	cv-99-5.98	1	cv-99-7.32	1	cv-99-11.8	4
cv-99-4.15	1	cv-99-4.117	1	cv-99-5.97	1	cv-99-7.33	1	cv-99-11.9	4
cv-99-4.16	3	cv-99-4.118	5	cv-99-5.105	3	cv-99-7.34	1	cv-99-11.10	4
cv-99-4.17	3	cv-99-4.119	6	cv-99-5.106	1	cv-99-7.35	1	cv-99-11.11	4
cv-99-4.18	1	cv-99-4.120	1	cv-99-5.102	4	cv-99-7.36	1	cv-99-11.15	4
cv-99-4.19	1	cv-99-4.121	3	cv-99-5.103	1	cv-99-7.53	1	cv-99-11.16	4
cv-99-4.20	1	cv-99-4.122	3	cv-99-5.118	3	cv-99-7.42	6	cv-99-11.18	4
cv-99-4.21	3	cv-99-4.123	3	cv-99-5.119	5	cv-99-7.40	5	cv-99-11.20	6
cv-99-4.22	1	cv-99-4.125	3	cv-99-5.122	5	cv-99-7.49	1	cv-99-11.21	1
cv-99-4.24	1	cv-99-4.126	1	cv-99-5.120	5	cv-99-7.50	1	cv-99-11.22	4
cv-99-4.25	1	cv-99-4.127	1	cv-99-5.124	5	cv-99-7.52	1	cv-99-11.23	1
cv-99-4.26	3	cv-99-4.128	2	cv-99-5.123	5	cv-99-9.17	4	cv-99-11.25	4
cv-99-4.27	1	cv-99-4.129	2	cv-99-5.125	5	cv-99-9.16	4	cv-99-11.26	1
cv-99-4.29	1	cv-99-4.130	4	cv-99-5.127	3	cv-99-9.8	4	cv-99-11.27	4
cv-99-4.31	1	cv-99-4.131	2	cv-99-5.128	5	cv-99-9.9	4	cv-99-11.28	4
cv-99-4.30	1	cv-99-4.132	3	cv-99-5.130	5	cv-99-9.10	4	cv-99-11.29	4
cv-99-4.33	1	cv-99-4.133	3	cv-99-5.129	5	cv-99-9.1	4	cv-99-11.33	4
cv-99-4.32	1	cv-99-4.134	5	cv-99-5.140b	5	cv-99-9.28	4	cv-99-11.34	4
cv-99-4.34	1	cv-99-4.135	5	cv-99-5.131	5	cv-99-9.29	4	cv-99-11.35	1
cv-99-4.35	1	cv-99-4.136	5	cv-99-5.132	3	cv-99-9.32	1	cv-99-11.36	1
cv-99-4.36	1	cv-99-4.137	5	cv-99-5.59	5	cv-99-9.34	1	cv-99-11.39	6
cv-99-4.37	1	cv-99-4.138	5	cv-99-5.61a	2	cv-99-9.37	1	cv-99-11.40	1
cv-99-4.38	3	cv-99-4.140	5	cv-99-5.62	2	cv-99-9.71	4	cv-99-11.41	2
cv-99-4.39	2	cv-99-5.111b	1	cv-99-5.63	2	cv-99-9.72	4	cv-99-11.42	2
cv-99-4.40	2	cv-99-5.112	1	cv-99-5.65	1	cv-99-9.73	1	cv-99-11.44	4
cv-99-4.65	1	cv-99-5.113	1	cv-99-5.66	3	cv-99-9.74	1	cv-00-11.51	2
cv-99-4.66	2	cv-99-5.114	2	cv-99-5.72	5	cv-99-9.76	4	cv-00-11.54	2
cv-99-4.67	1	cv-99-5.116	5	cv-99-5.75	1	cv-99-9.78	1	cv-00-11.55	2
cv-99-4.68	1	cv-99-5.117	5	cv-99-5.76	3	cv-99-9.79	4	cv-00-11.59	4
cv-99-4.69	1	cv-99-5.28	2	cv-99-5.79a	1	cv-99-9.113	1	cv-00-11.58	4
cv-99-4.70	1	cv-99-5.30	3	cv-99-5.81	1	cv-99-9.119	4	cv-00-11.62	1
cv-99-4.71	1	cv-99-5.32c	5	cv-99-5.86	1	cv-99-9.101	4	cv-00-11.63	6
cv-99-4.72a	3	cv-99-5.34	2	cv-99-5.84	1	cv-99-9.102	4	cv-00-11.64	1
cv-99-4.72b	1	cv-99-5.38	1	cv-99-5.135	5	cv-99-9.103	4	cv-00-11.65	1
cv-99-4.72c	3	cv-99-5.44	1	cv-99-7.6	5	cv-99-9.104	1	cv-00-11.71	1
cv-99-4.74	3	cv-99-5.45a	1	cv-99-7.8	5	cv-99-9.105	4	cv-00-11.68	4
cv-99-4.75	3	cv-99-5.46a	1	cv-99-7.9	5	cv-99-9.106	6	cv-00-11.73	6
cv-99-4.76	4	cv-99-5.47	3	cv-99-7.10	5	cv-99-9.111	1	cv-00-11.74	6
cv-99-4.77	1	cv-99-5.48	1	cv-99-7.12	2	cv-99-9.114	4	cv-00-11.75	6
cv-99-4.78	1	cv-99-5.51	1	cv-99-7.14	5	cv-99-9.115	1	cv-00-11.77	2
cv-99-4.81a	1	cv-99-5.52	1	cv-99-7.15	4	cv-99-9.80	4	cv-00-11.78	6

cv-00-11.79	6	cv-00-15.43	1
cv-00-11.81	6	cv-00-15.45	1
cv-00-11.82	6	cv-00-15.46	3
cv-00-11.87	6	cv-00-15.47	1
cv-00-11.84	6	cv-00-15.55	5
cv-00-11.85	6	cv-00-15.56	5
cv-00-11.89	3	cv-00-15.57	3
cv-00-11.88	6	cv-00-16.6	3
cv-00-11.90	6	cv-00-16.7	1
cv-99-14.1	4	cv-00-16.8	1
cv-00-14.14	2	cv-00-16.9	1
cv-00-14.15	4	cv-00-16.10	3
cv-00-14.16	1	cv-00-16.12	3
cv-00-14.17	4	cv-00-16.13	3
cv-00-14.18	4	cv-00-16.14	3
cv-00-14.19	2	cv-00-16.15	3
cv-00-14.20	1	cv-00-16.16	3
cv-00-14.21	2	cv-00-16.17	1
cv-00-14.24	1	cv-00-16.1	1
cv-00-14.25	4	cv-00-16.2	1
cv-00-14.26	1	cv-00-16.3	1
cv-00-14.5	3	cv-00-16.4	1
cv-00-14.7	4	cv-00-18.1	6
cv-00-14.9	1	cv-00-18.2	1
cv-00-14.11	4	cv-00-18.4	1
cv-00-14.13	1	cv-00-15.13	1
cv-00-17.16	1	cv-00-15.15	3
cv-00-17.15	1	cv-00-15.17	1
cv-00-17.14	4	cv-00-15.19	3
cv-00-17.13	1	cv-00-15.20	2
cv-00-17.12	1	cv-99-13.2	4
cv-00-17.9	1	cv-99-13.3	4
cv-00-17.10	1	cv-99-13.5	4
cv-00-17.1	1	cv-99-12.8	3
cv-00-17.2	1	cv-99-12.2	1
cv-00-17.3	4	cv-99-12.3	1
cv-00-17.4	4	cv-99-12.5	1
cv-00-17.6	1	cv-99-12.6	1
cv-00-17.7	1	cv-99-12.7	4
cv-00-17.8	4		
cv-00-15.22	1		
cv-00-15.23	3		
cv-00-15.24	3		
cv-00-15.25	1		
cv-00-15.27	1		
cv-00-15.28	1		
cv-00-15.30	3		
cv-00-15.31	3		
cv-00-15.32	3		
cv-00-15.34	1		
cv-00-15.35	1		
cv-00-15.36	2		
cv-00-15.37	3		
cv-00-15.40	3		
cv-00-15.41	1		
cv-00-15.42	3		

APPENDIX 5

SEQUENCE DIAGRAMS

APPENDIX 5 - SEQUENCE DIAGRAMS

DIAGENETIC SEQUENCE DIAGRAM

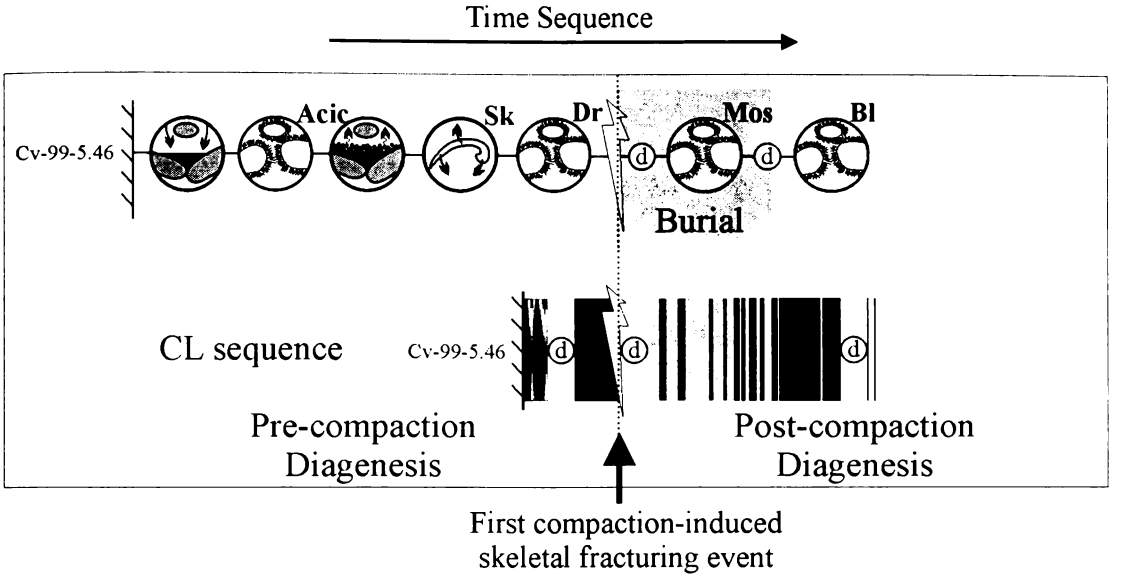

CEMENTS

Dr, Acic, Mos, Dgt, Sc, Syn, Bl

Drusy spar
Acicular
Mosaic spar
Dogtooth spar (**Dgt**)
Scalenohedral spar
Syntaxial overgrowth
Blocky spar

Micritic crust

Micritic meniscus

INTERNAL SEDIMENT

Internal sediment

In situ peloidal sediment

Bm

Collapse of biomolds

Syndepositional micrite

OTHERS

Sk

Leaching of skeletal grains

Ma

Macroboring

Fracturing stage

Encrusting

AG Authigenic glauconite

ⓓ Dissolution stage

ⓐ Abrasion

Key to CL patterns

Patchy-cloudy luminescence

Non-luminescent

Dull brown luminescence

Dull brown luminescence broadly subzoned

Orange luminescence

Bright yellow luminescence

Corroded outer margin of cement

ⓔ Extrinsic cement

ⓓ Dissolution stage

Section: K1 1/2
Locality: Kairakau Beach
Grid reference: V22/457333

IDEALIZED CL SEQUENCE

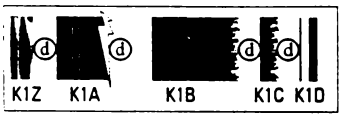

CATHODOLUMINESCENCE-RECORD

DIAGENETIC SEQUENCE

PRE-COMPACTION | SYN/POST-COMPACTION

0 100 µm

S.D.

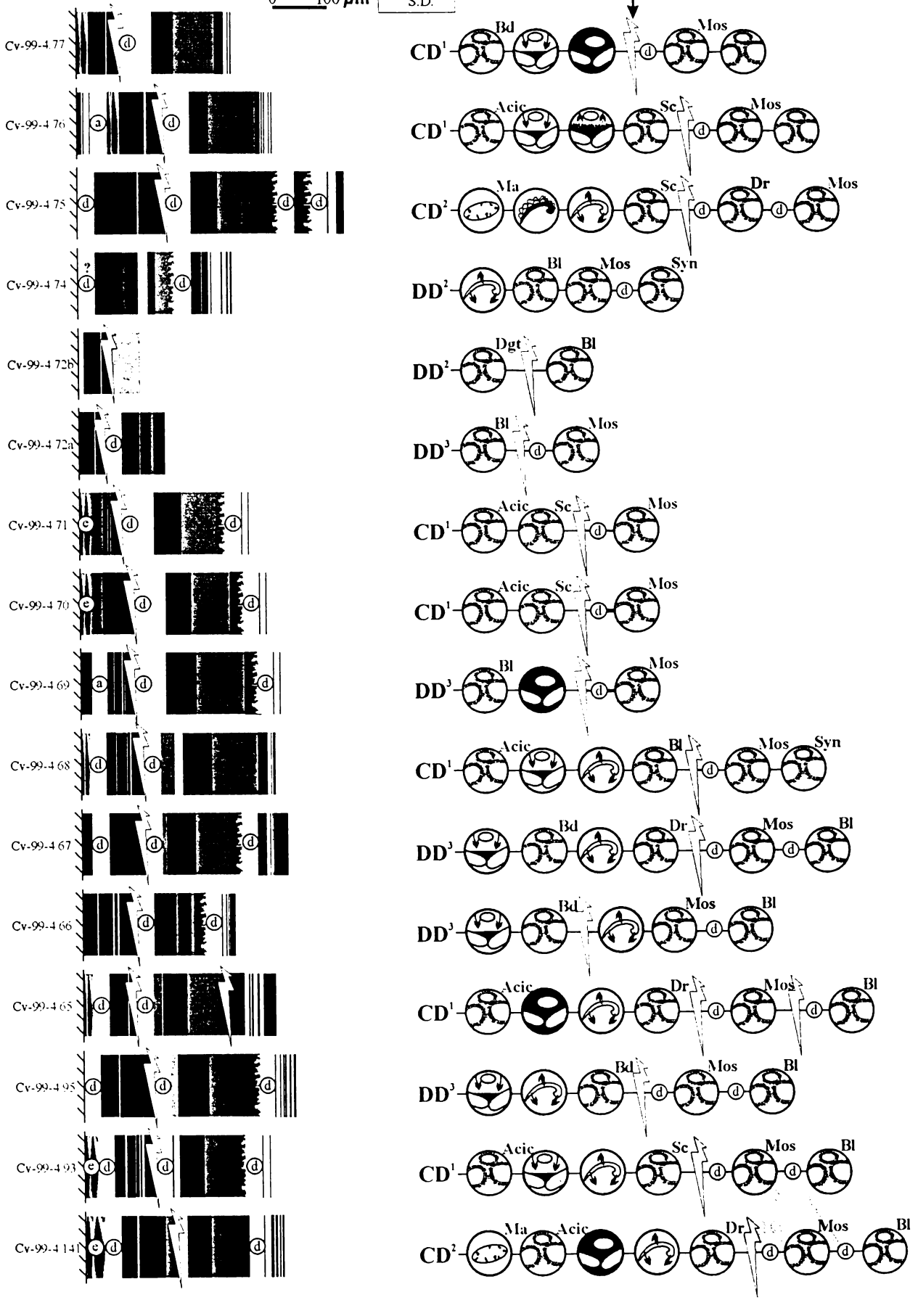

Section: K2
Locality: Taupata
Grid reference: V22/484366

IDEALIZED CL SEQUENCE

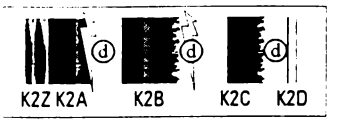

CATHODOLUMINESCENCE-RECORD

DIAGENETIC SEQUENCE

PRE-COMPACTION | SYN POST-COMPACTION

0 100 µm

S.D.

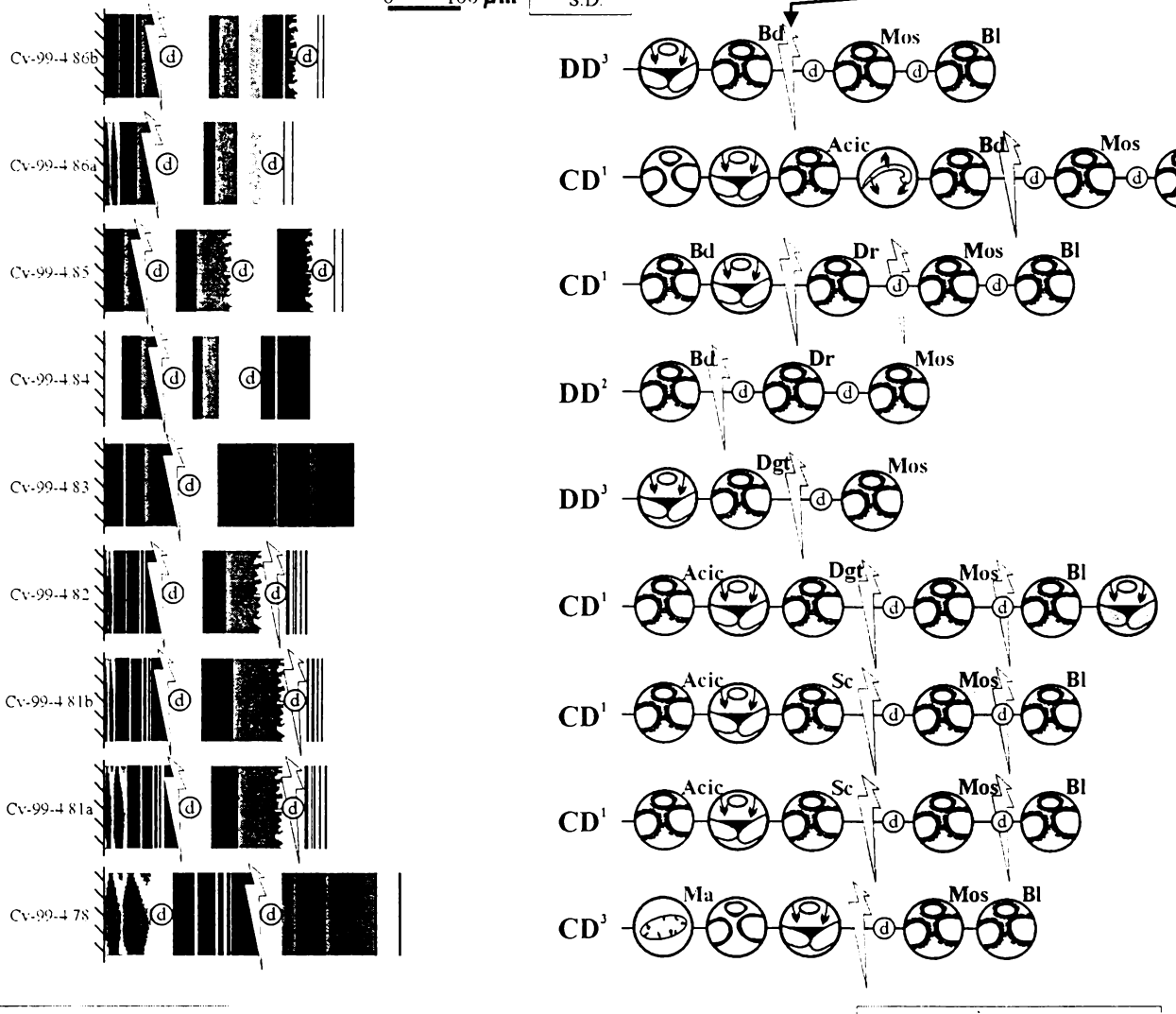

Section: K10
Locality: Apiti
Grid reference: V22/481362

IDEALIZED CL-SEQUENCE

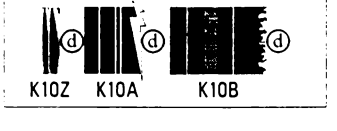

CATHODOLUMINESCENCE-RECORD

DIAGENETIC SEQUENCE

PRE-COMPACTION | SYN POST-COMPACTION

0 100 µm

S.D.

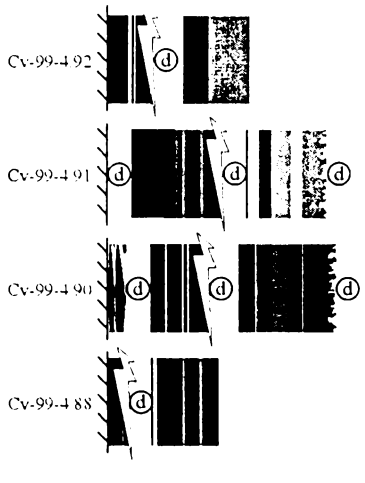


Section: K3
Locality: Cabbage Tree Flat
Grid reference: V22/492467
4
IDEALIZED CL SEQUENCE
K3Z
K3A
K3B
K3C
CATHODOLUMINESCENCE-RECORD
DIAGENETIC SEQUENCE
PRE-COMPACTION
SYN/POST-COMPACTION
0 100 µm
S.D.
Cv-99-4.133
Cv-99-4.132
Cv-99-4.131
Cv-99-4.130
Cv-99-4.128
Cv-99-4.127
Cv-99-4.126
Cv-99-4.125
DD³
CD²
CD¹
DD²
CD¹
CD¹
DD³
DD³
Dr
Mos
Ma
Acic
Sc
Bl
Dgt

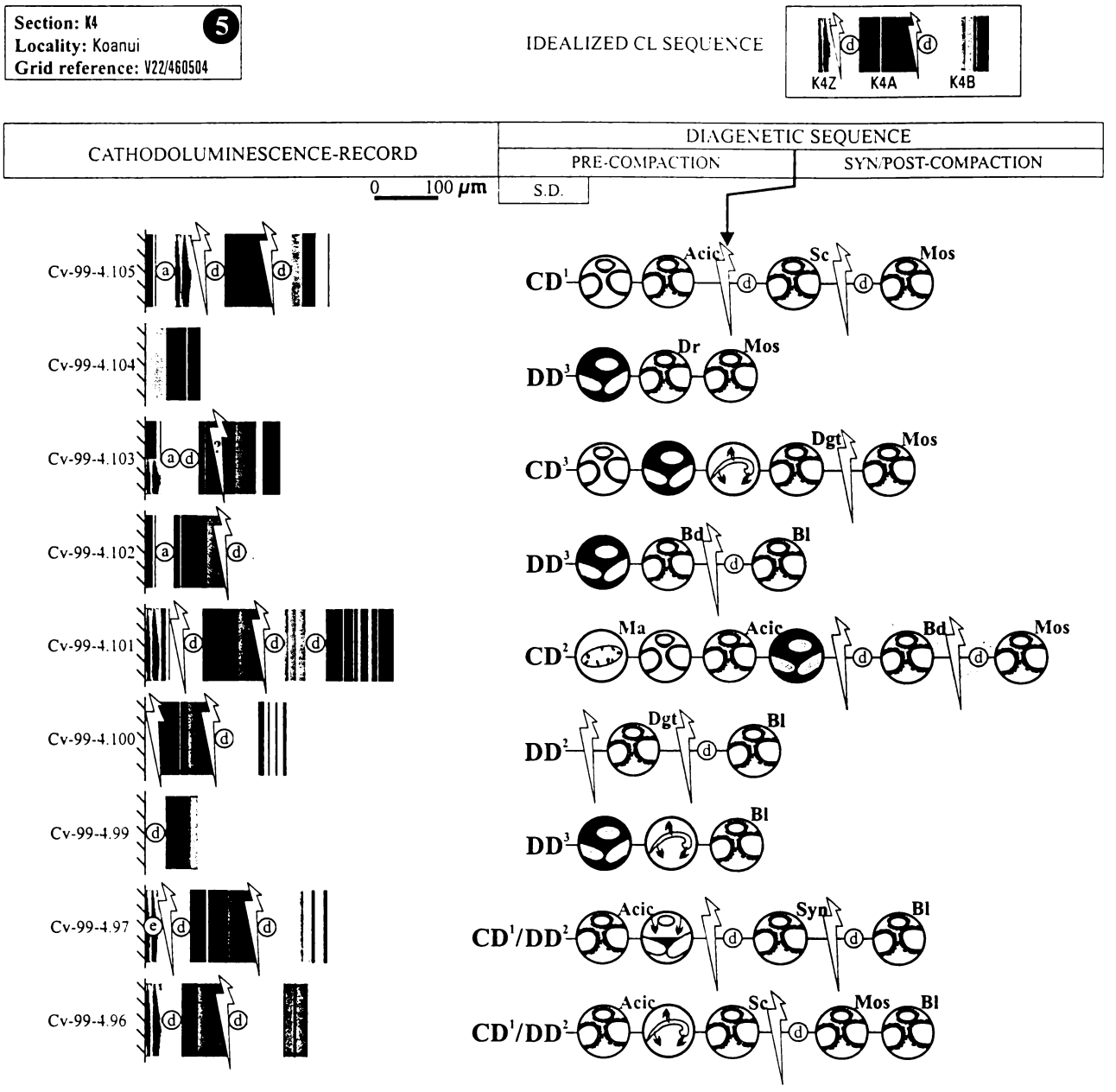
Section: K4
Locality: Koanui
Grid reference: V22/460504
5
IDEALIZED CL SEQUENCE
K4Z
K4A
K4B
CATHODOLUMINESCENCE-RECORD
DIAGENETIC SEQUENCE
PRE-COMPACTION
SYN/POST-COMPACTION
S.D.
0 100 µm
Cv-99-4.105
Cv-99-4.104
Cv-99-4.103
Cv-99-4.102
Cv-99-4.101
Cv-99-4.100
Cv-99-4.99
Cv-99-4.97
Cv-99-4.96
CD1
DD3
CD3
DD3
CD2
DD2
DD3
CD1/DD2
CD1/DD2
Acic
Sc
Mos
Dr
Dgt
Bd
Bl
Ma
Syn

Section: K5a **7**
Locality: Mont Kahuranaki
Grid reference: V22/423515

IDEALIZED CL SEQUENCE

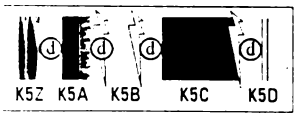

CATHODOLUMINESCENCE-RECORD

0 100 µm

DIAGENETIC SEQUENCE

PRE-COMPACTION | SYN POST-COMPACTION

S.D.

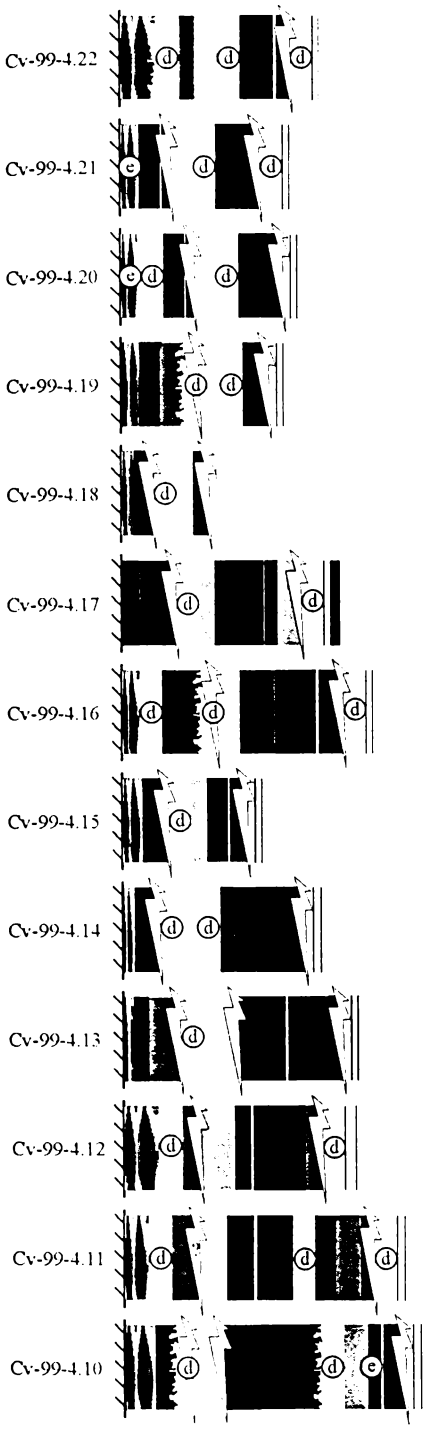

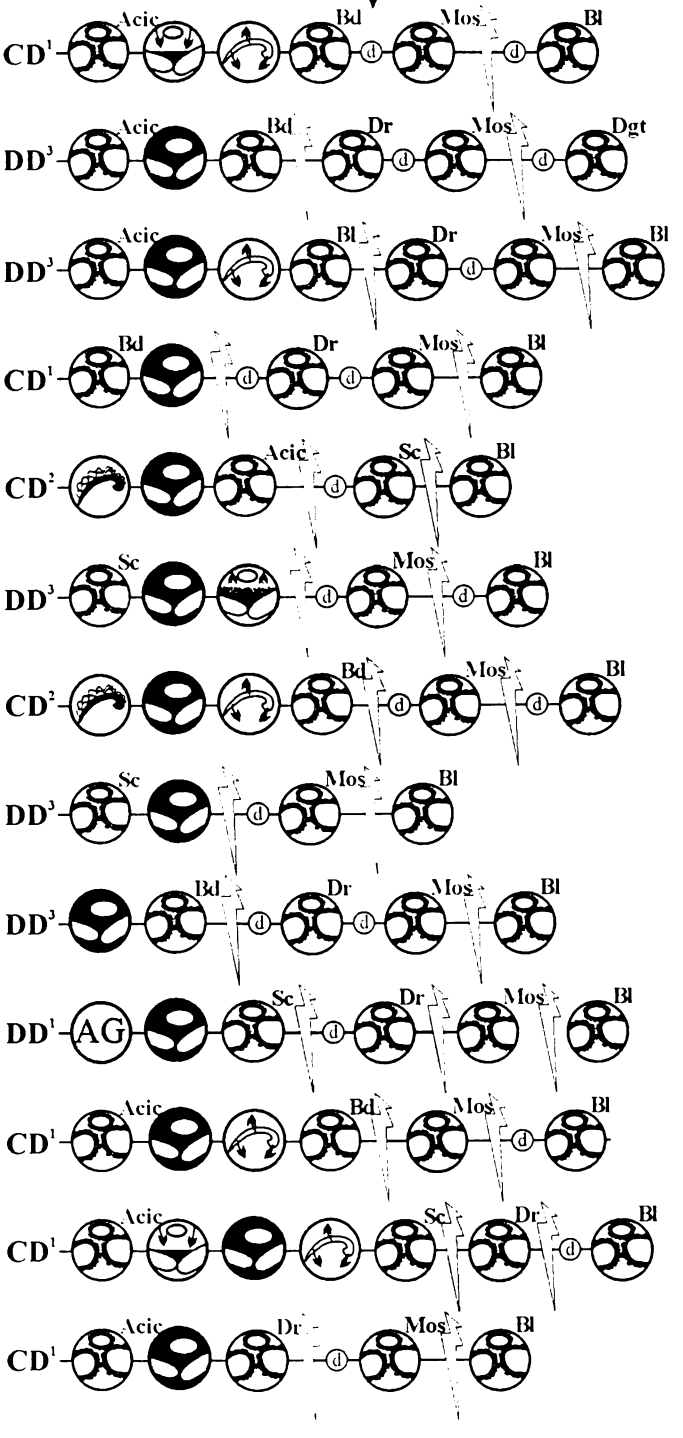

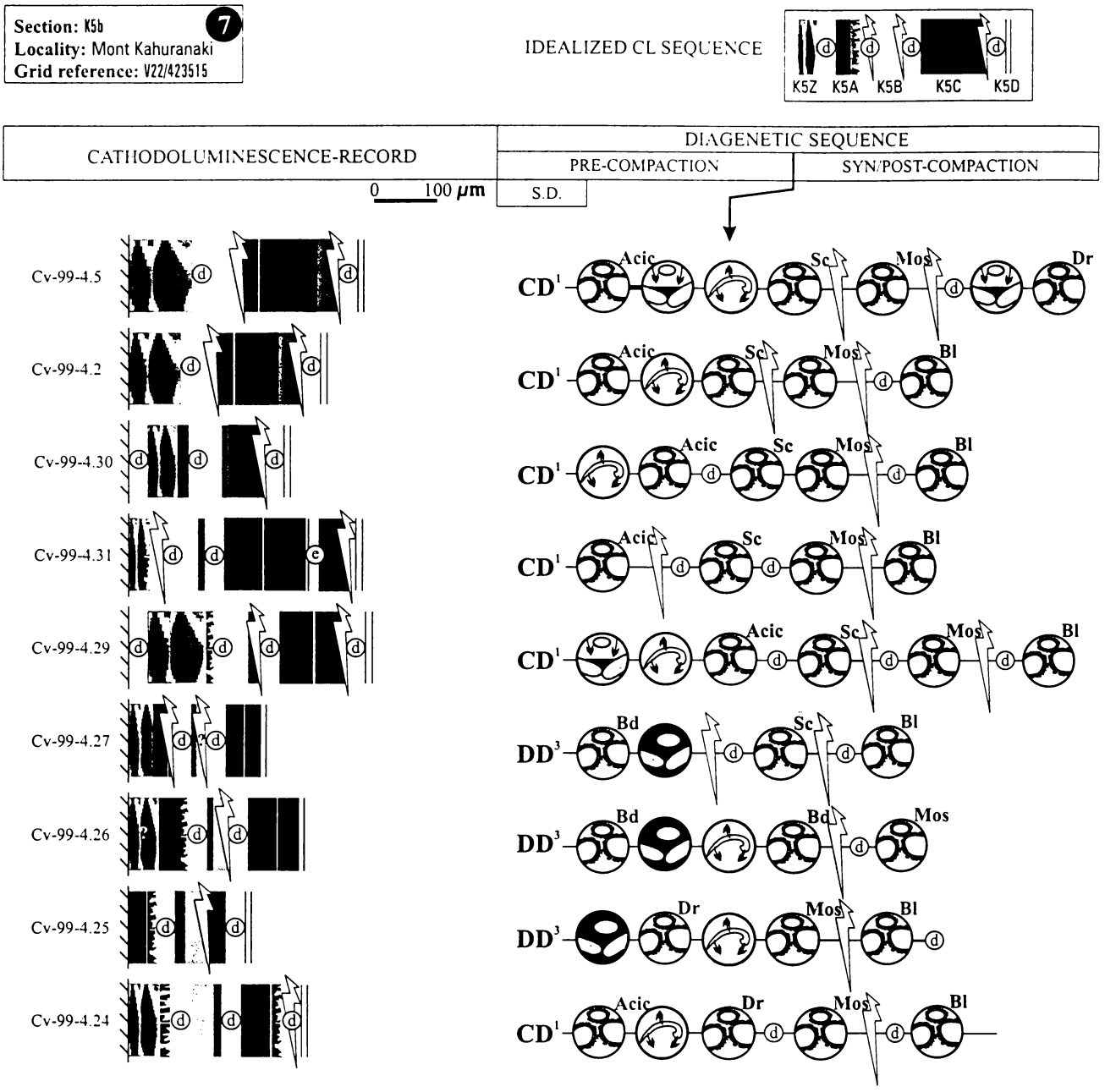
Section: K5b
Locality: Mont Kahuranaki
Grid reference: V22/423515
7
IDEALIZED CL SEQUENCE
K5Z K5A K5B K5C K5D
CATHODOLUMINESCENCE-RECORD
DIAGENETIC SEQUENCE
PRE-COMPACTION
SYN/POST-COMPACTION
0 100 µm
S.D.
Cv-99-4.5
Cv-99-4.2
Cv-99-4.30
Cv-99-4.31
Cv-99-4.29
Cv-99-4.27
Cv-99-4.26
Cv-99-4.25
Cv-99-4.24
CD1
DD3
Acic
Sc
Mos
Dr
Bl
Bd

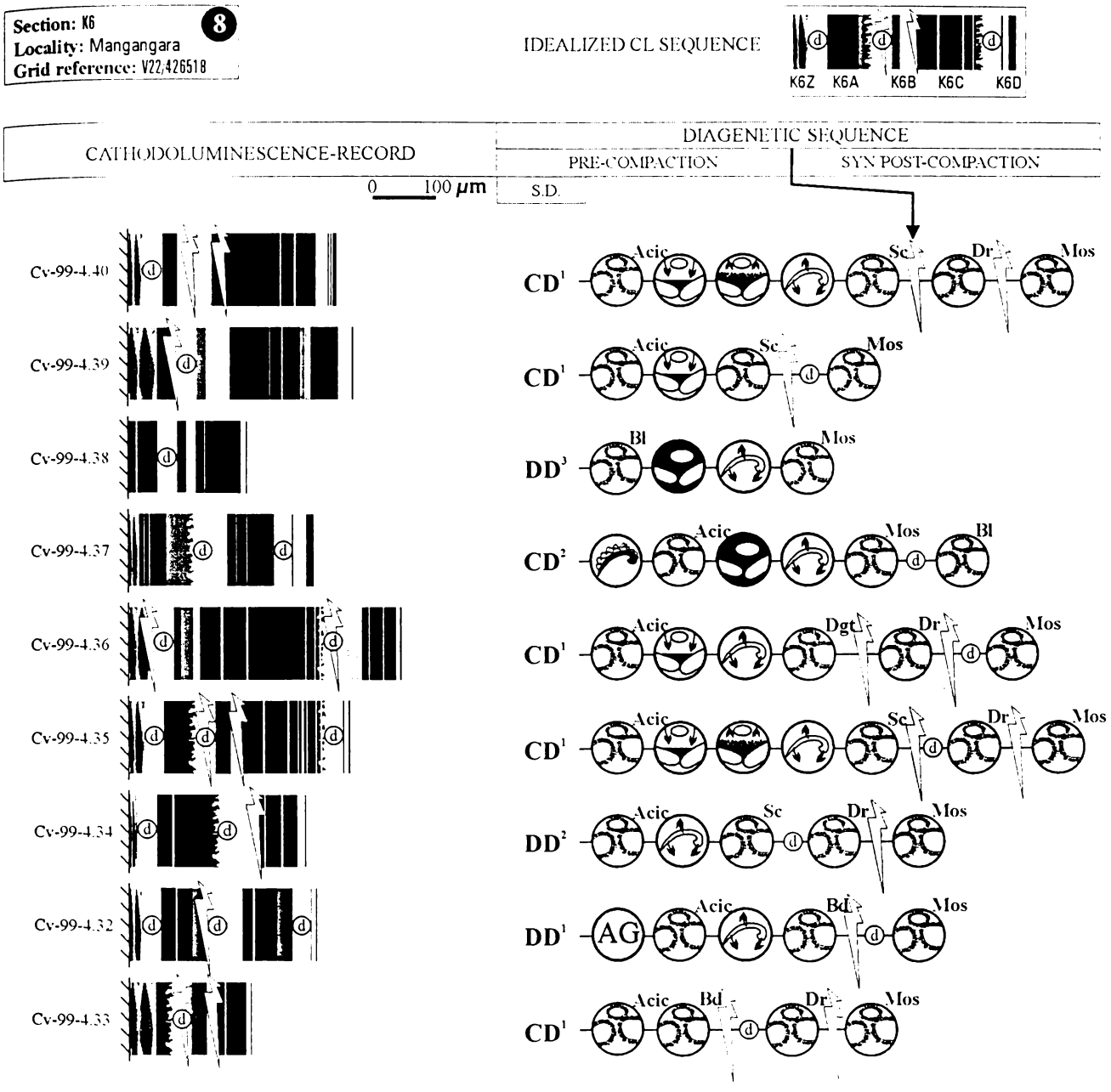
Section: K6
Locality: Mangangara
Grid reference: V22/426518
8
IDEALIZED CL SEQUENCE
K6Z K6A K6B K6C K6D
CATHODOLUMINESCENCE-RECORD
0 100 µm
DIAGENETIC SEQUENCE
PRE-COMPACTION
SYN POST-COMPACTION
S.D.
Cv-99-4.40
Cv-99-4.39
Cv-99-4.38
Cv-99-4.37
Cv-99-4.36
Cv-99-4.35
Cv-99-4.34
Cv-99-4.32
Cv-99-4.33
CD1
CD1
DD3
CD2
CD1
CD1
DD2
DD1
CD1
Acic
Sc
Dr
Mos
Bl
Dgt
Bd
AG

Section: K7 **10**
Locality: Waimarama1
Grid reference: V21/463217

IDEALIZED CL SEQUENCE

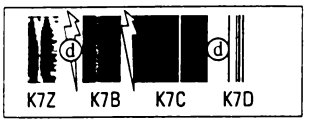

CATHODOLUMINESCENCE-RECORD

0 100 µm

DIAGENETIC SEQUENCE

PRE-COMPACTION | SYN/POST-COMPACTION

S.D.

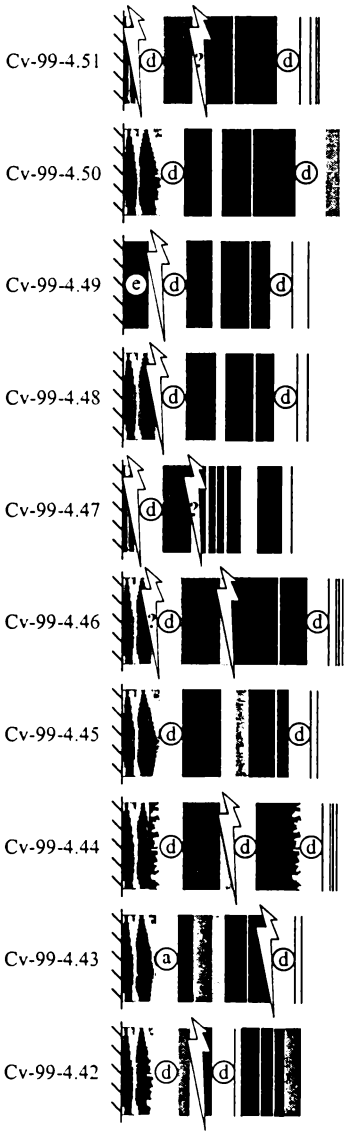

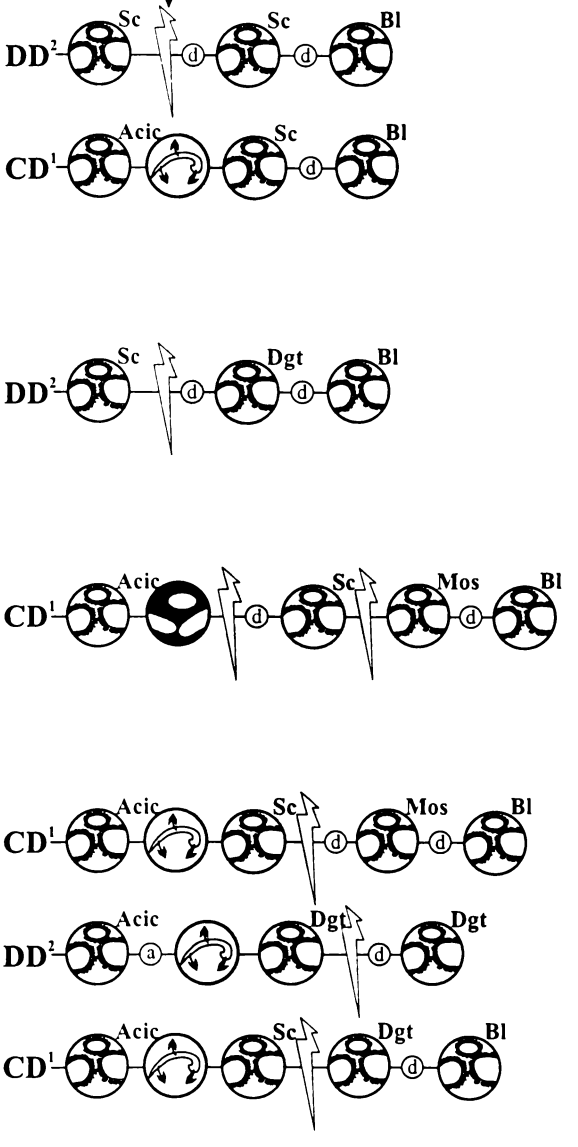

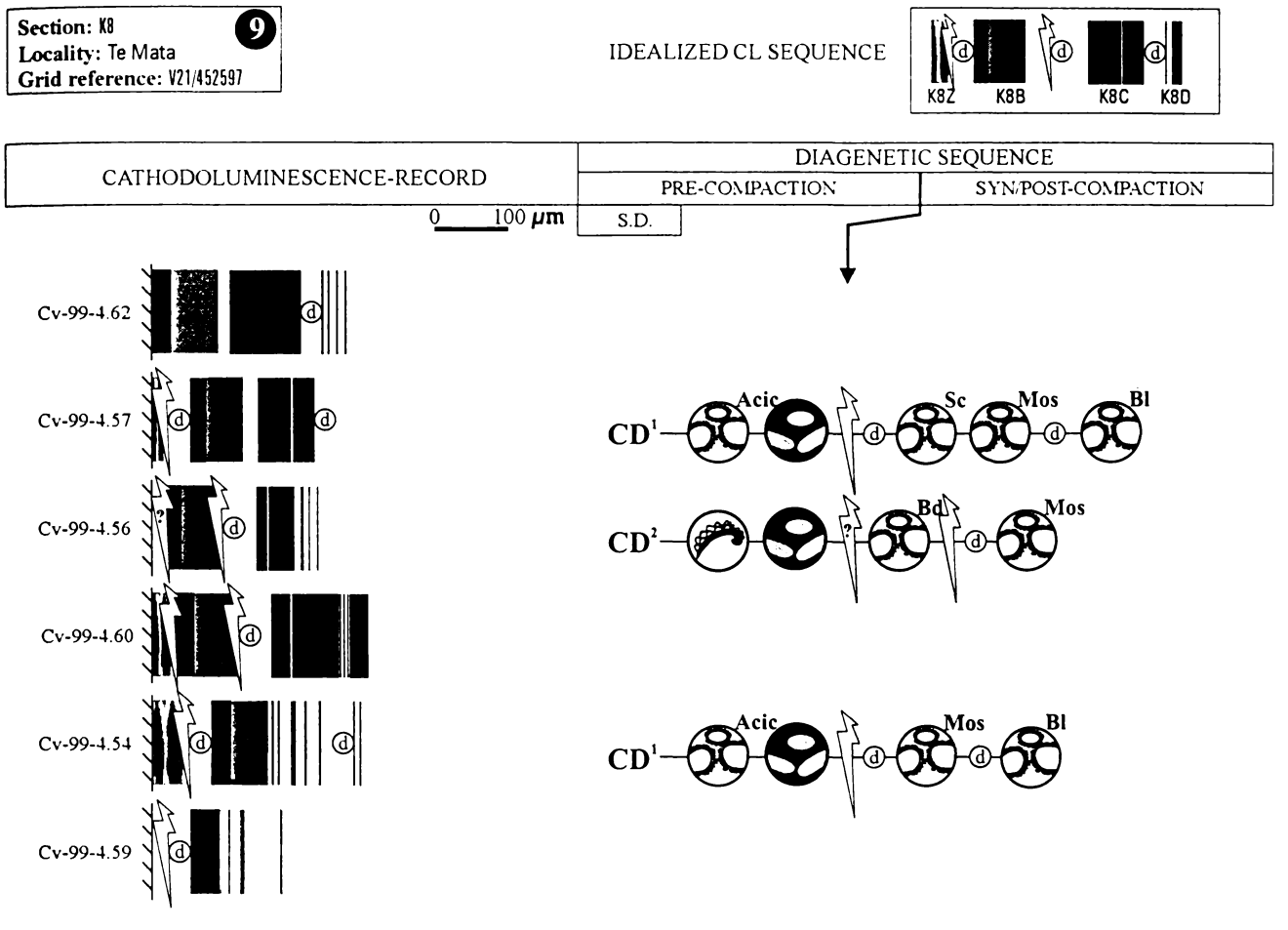
Section: K8
9
Locality: Te Mata
Grid reference: V21/452597
IDEALIZED CL SEQUENCE
K8Z
K8B
K8C
K8D
CATHODOLUMINESCENCE-RECORD
DIAGENETIC SEQUENCE
PRE-COMPACTION
SYN/POST-COMPACTION
0 100 µm
S.D.
Cv-99-4.62
Cv-99-4.57
Cv-99-4.56
Cv-99-4.60
Cv-99-4.54
Cv-99-4.59
CD1
Acic
Sc
Mos
Bl
CD2
Bd
Mos
CD1
Acic
Mos
Bl

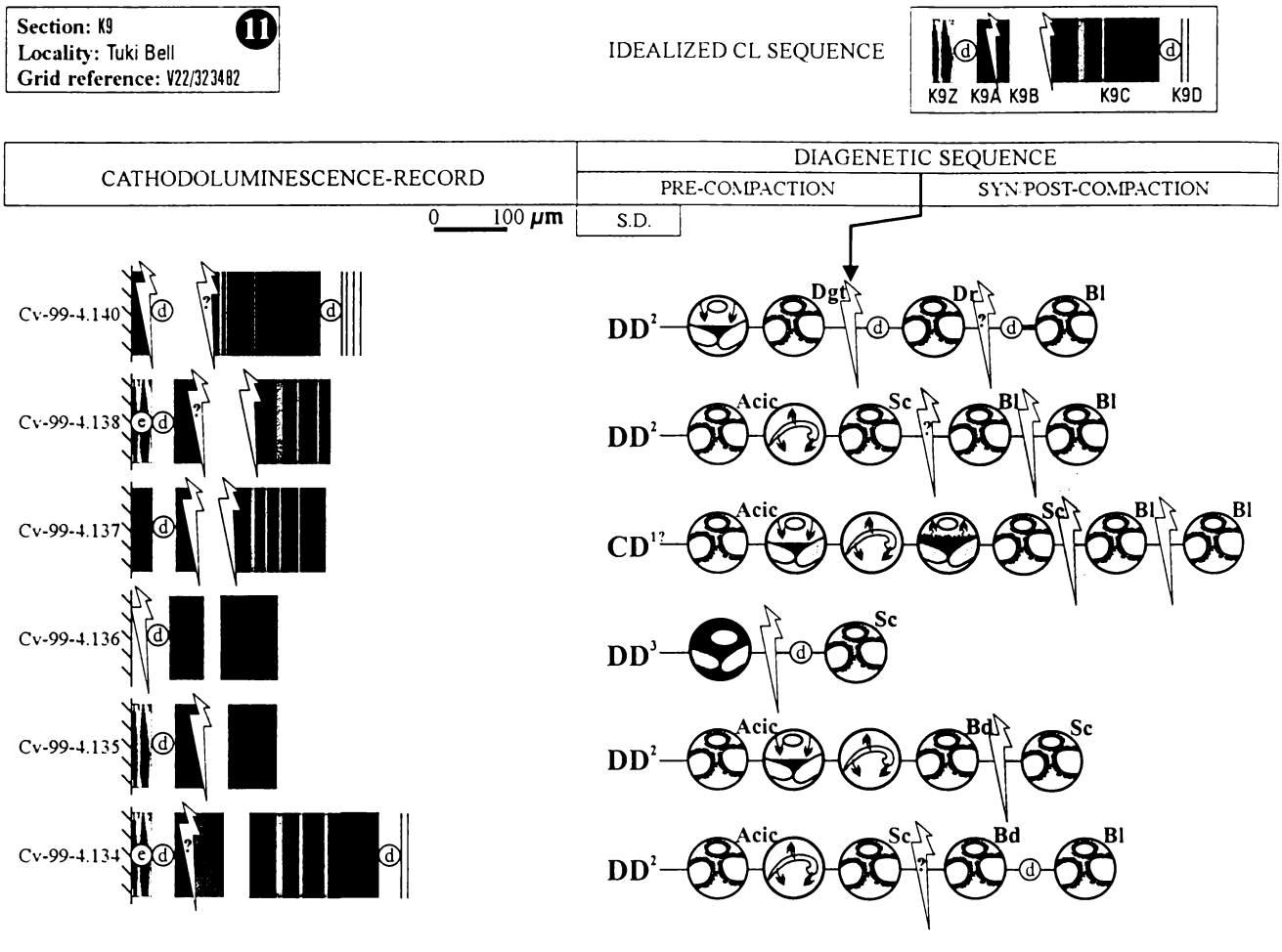
Section: K9
Locality: Tuki Bell
Grid reference: V22/3234B2
11
IDEALIZED CL SEQUENCE
K9Z K9A K9B K9C K9D
CATHODOLUMINESCENCE-RECORD
DIAGENETIC SEQUENCE
PRE-COMPACTION
SYN POST-COMPACTION
0 100 µm
S.D.
Cv-99-4.140
Cv-99-4.138
Cv-99-4.137
Cv-99-4.136
Cv-99-4.135
Cv-99-4.134
DD2
DD2
CD1?
DD3
DD2
DD2
Dgt
Dr
Bl
Acic
Sc
Bd

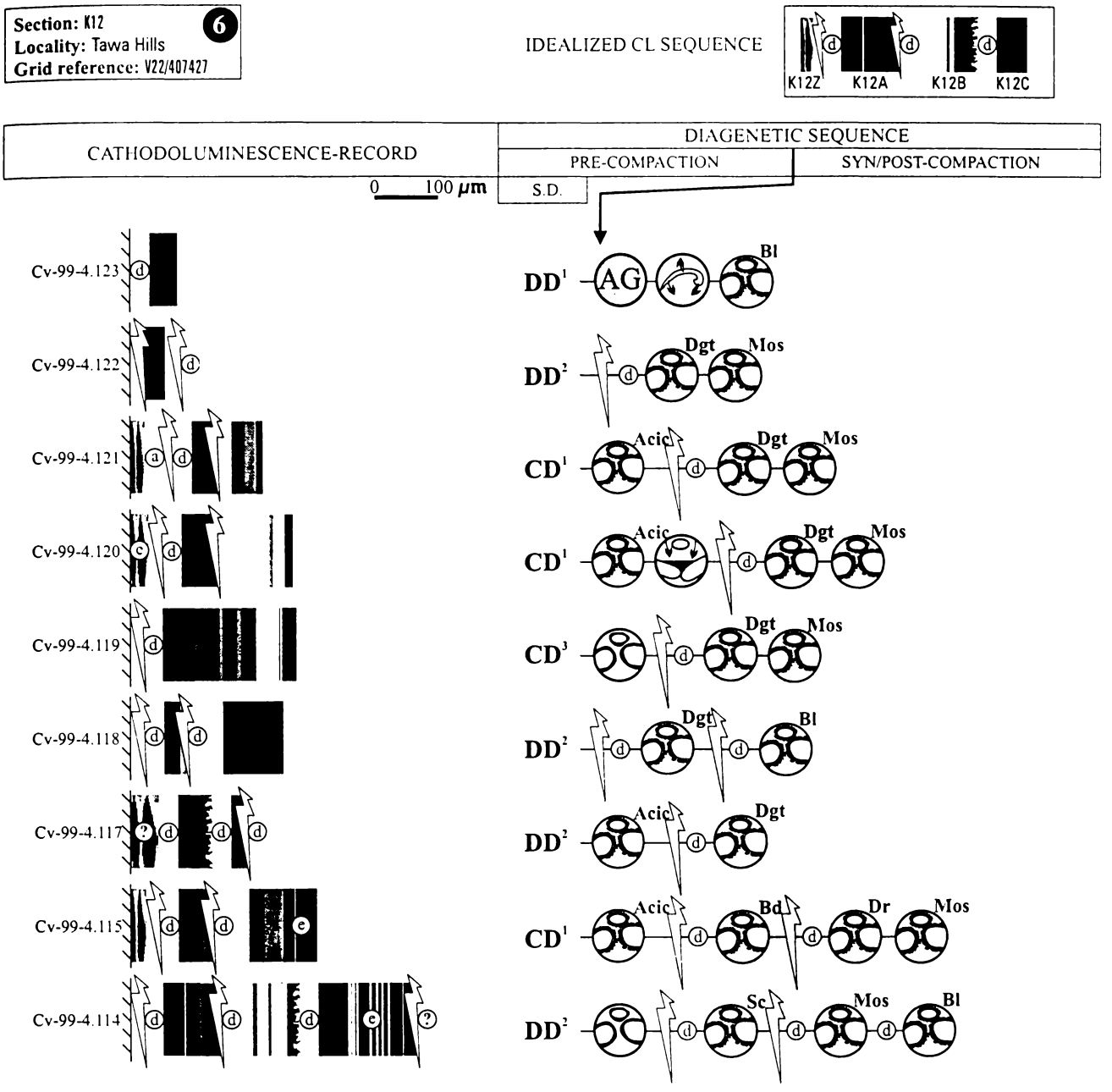
Section: K12
Locality: Tawa Hills
Grid reference: V22/407427
6
IDEALIZED CL SEQUENCE
K12Z
K12A
K12B
K12C
CATHODOLUMINESCENCE-RECORD
DIAGENETIC SEQUENCE
PRE-COMPACTION
SYN/POST-COMPACTION
S.D.
0 100 µm
Cv-99-4.123
Cv-99-4.122
Cv-99-4.121
Cv-99-4.120
Cv-99-4.119
Cv-99-4.118
Cv-99-4.117
Cv-99-4.115
Cv-99-4.114
DD1
DD2
CD1
CD1
CD3
DD2
DD2
CD1
DD2
AG
Bl
Dgt
Mos
Acic
Bd
Dr
Sc

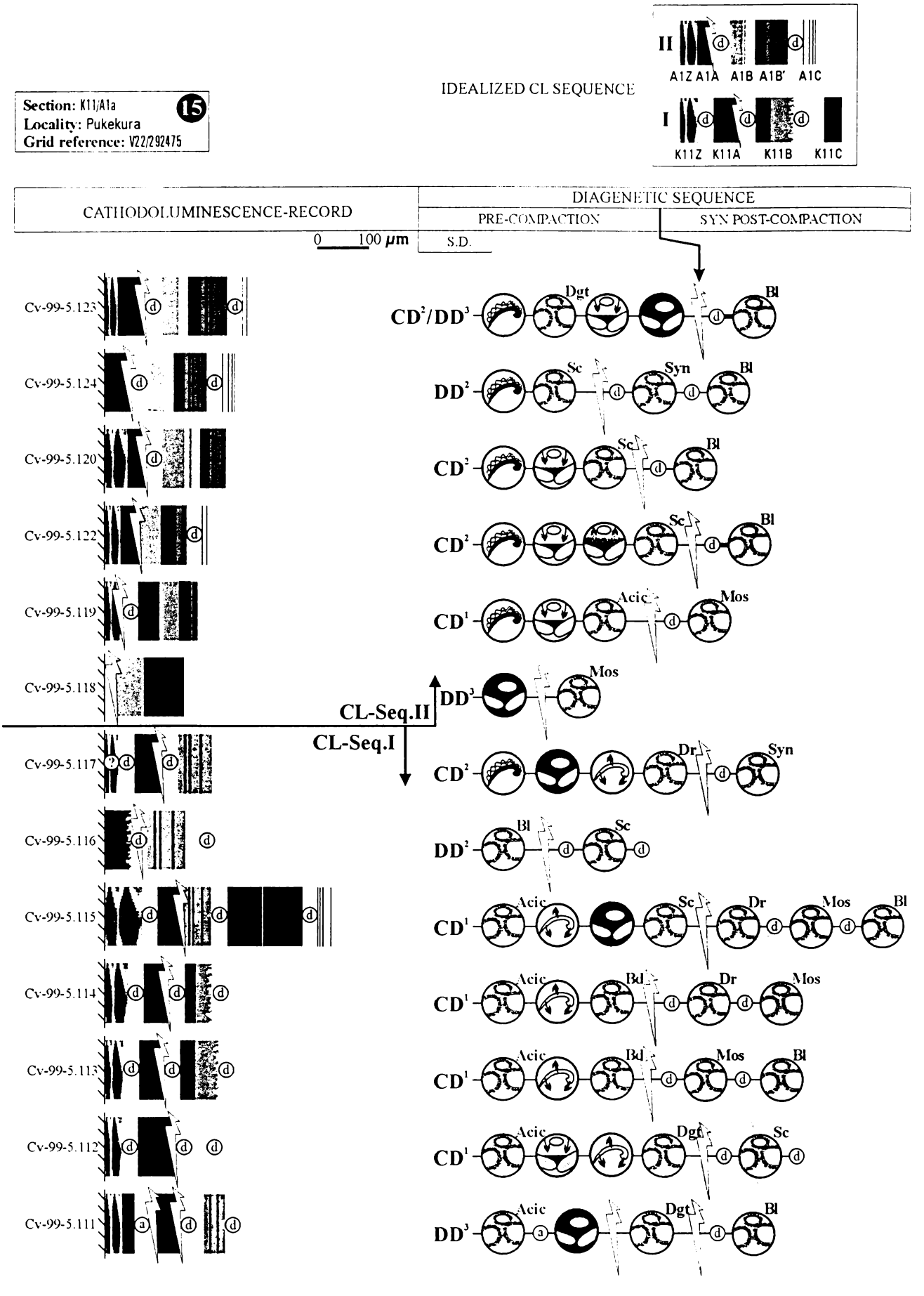
Section: K11/A1a
Locality: Pukekura
Grid reference: V22/292475
15
IDEALIZED CL SEQUENCE
II
A1Z A1A A1B A1B' A1C
I
K11Z K11A K11B K11C
CATHODOLUMINESCENCE-RECORD
DIAGENETIC SEQUENCE
PRE-COMPACTION
SYN POST-COMPACTION
0 100 µm
S.D.
Cv-99-5.123
Cv-99-5.124
Cv-99-5.120
Cv-99-5.122
Cv-99-5.119
Cv-99-5.118
Cv-99-5.117
Cv-99-5.116
Cv-99-5.115
Cv-99-5.114
Cv-99-5.113
Cv-99-5.112
Cv-99-5.111
CL-Seq.II
CL-Seq.I
CD²/DD³
DD²
CD²
CD²
CD¹
DD³
CD²
DD²
CD¹
CD¹
CD¹
CD¹
DD³
Dgt
Bl
Sc
Syn
Acic
Mos
Dr
Bd

Section: K11/A1b
Locality: Pukekura
Grid reference: V22/292475

IDEALIZED CL SEQUENCE

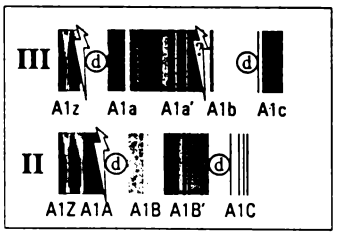

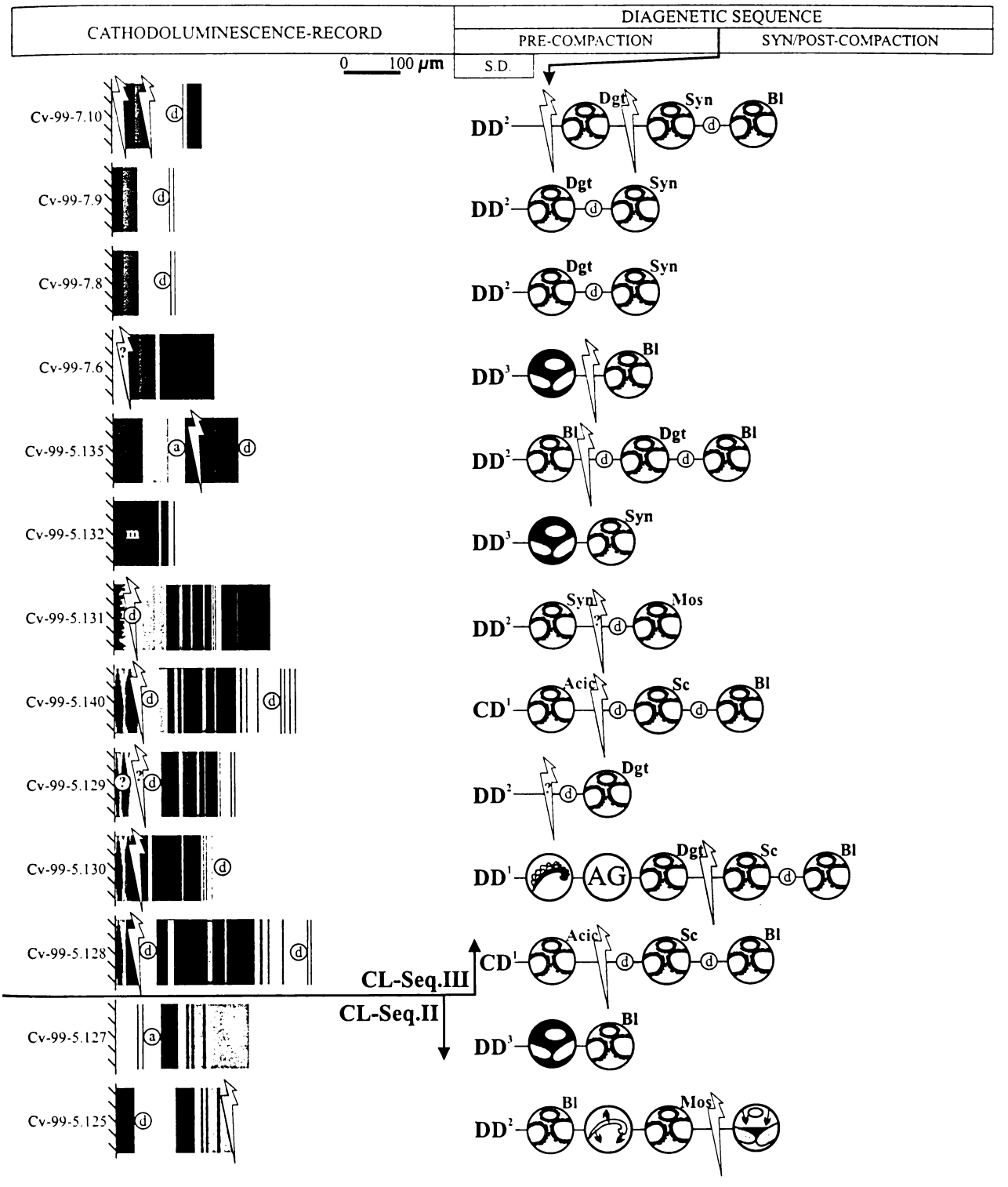

Section: A2a
Locality: Te Mata Peak
Grid reference: V22/451602

9

IDEALIZED CL SEQUENCE

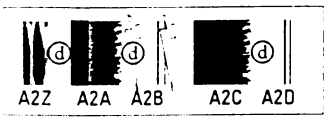

CATHODOLUMINESCENCE-RECORD

0 100 μm

DIAGENETIC SEQUENCE

PRE-COMPACTION | SYN POST-COMPACTION

S.D.

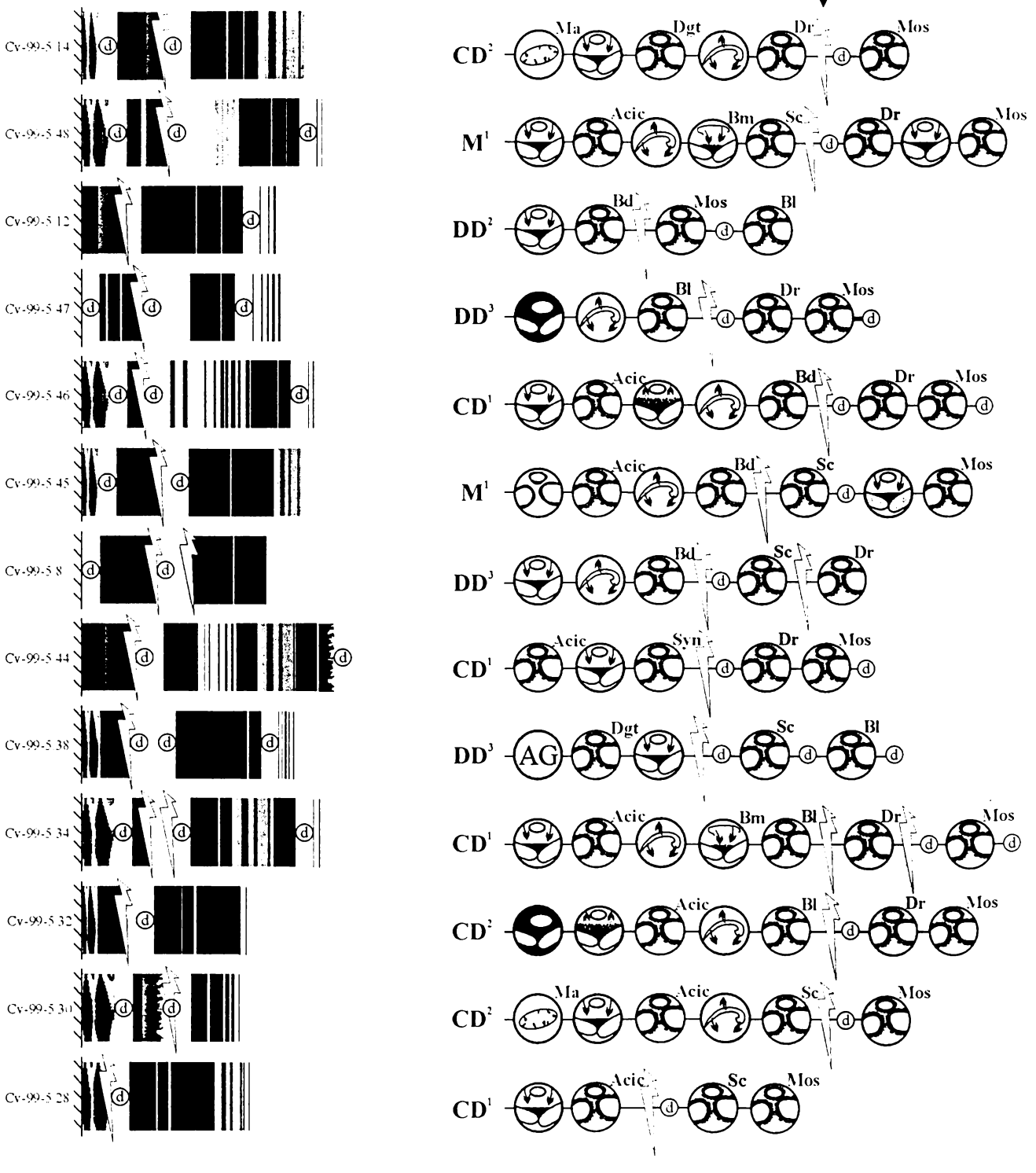

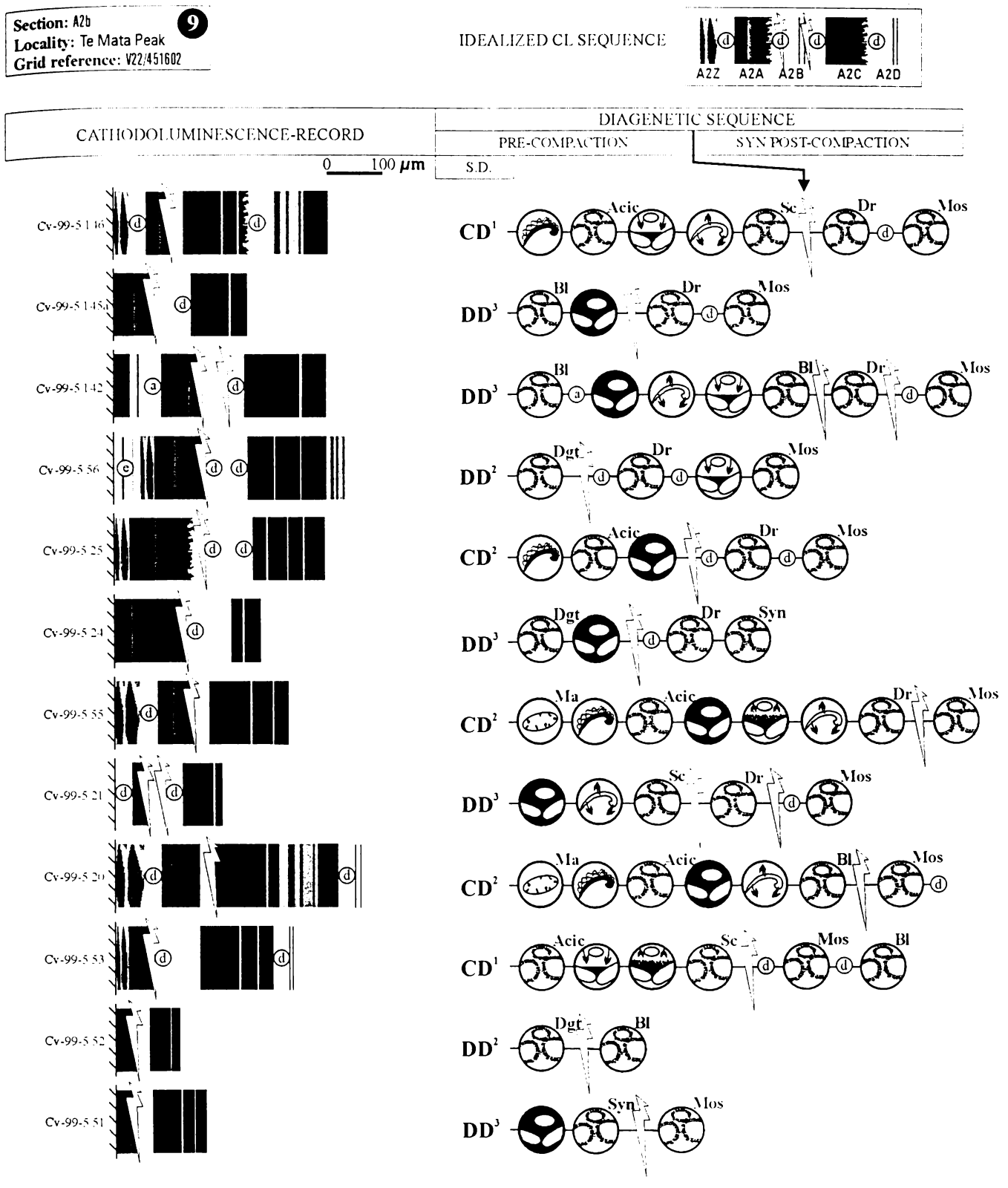
Section: A2b
Locality: Te Mata Peak
Grid reference: V22/451602
9
IDEALIZED CL SEQUENCE
A2Z A2A A2B A2C A2D
CATHODOLUMINESCENCE-RECORD
DIAGENETIC SEQUENCE
PRE-COMPACTION
SYN POST-COMPACTION
0 100 µm
S.D.
Cv-99-5 146
Cv-99-5 145
Cv-99-5 142
Cv-99-5 56
Cv-99-5 25
Cv-99-5 24
Cv-99-5 55
Cv-99-5 21
Cv-99-5 20
Cv-99-5 53
Cv-99-5 52
Cv-99-5 51
CD1
DD3
DD3
DD2
CD2
DD3
CD2
DD3
CD2
CD1
DD2
DD3
Acic
Sc
Dr
Mos
Bl
Dr
Mos
Bl
Bl
Dr
Mos
Dgt
Dr
Mos
Acic
Dr
Mos
Dgt
Dr
Syn
Ma
Acic
Dr
Mos
Sc
Dr
Mos
Ma
Acic
Bl
Mos
Acic
Sc
Mos
Bl
Dgt
Bl
Syn
Mos

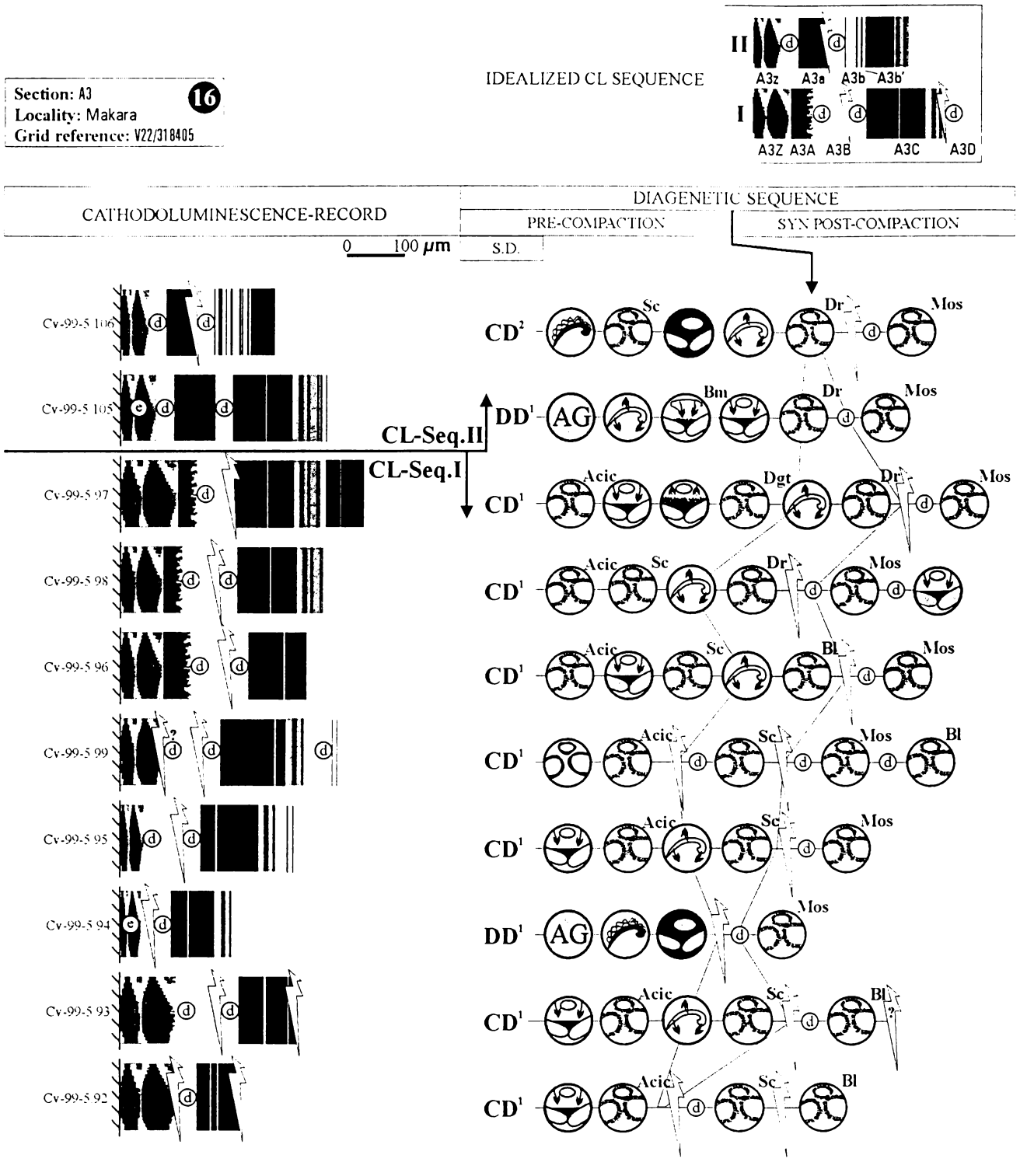
Section: A3
16
Locality: Makara
Grid reference: V22/318405
IDEALIZED CL SEQUENCE
II
A3z A3a A3b A3b'
I
A3Z A3A A3B A3C A3D
CATHODOLUMINESCENCE-RECORD
DIAGENETIC SEQUENCE
PRE-COMPACTION
SYN POST-COMPACTION
0 100 µm
S.D.
Cv-99-5 106
Cv-99-5 105
Cv-99-5 97
Cv-99-5 98
Cv-99-5 96
Cv-99-5 99
Cv-99-5 95
Cv-99-5 94
Cv-99-5 93
Cv-99-5 92
CL-Seq.II
CL-Seq.I
CD²
DD¹
CD¹
DD¹
CD¹
CD¹
CD¹
CD¹
CD¹
CD¹
CD¹
Sc
Dr
Mos
Bm
AG
Acic
Dgt
Bl

Section: A4/A5
Locality: River Bank (Hawea) 13
Grid reference: V22/3444 69 to 3324 82

IDEALIZED CL SEQUENCE

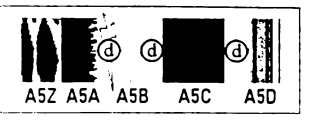

CATHODOLUMINESCENCE-RECORD

DIAGENETIC SEQUENCE

PRE-COMPACTION | SYN POST-COMPACTION

0 100 µm S.D.

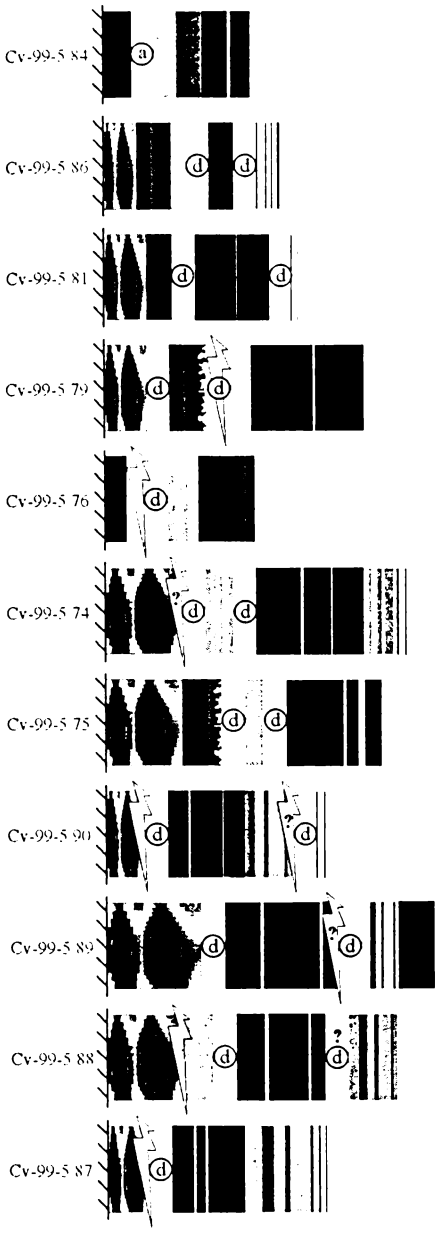

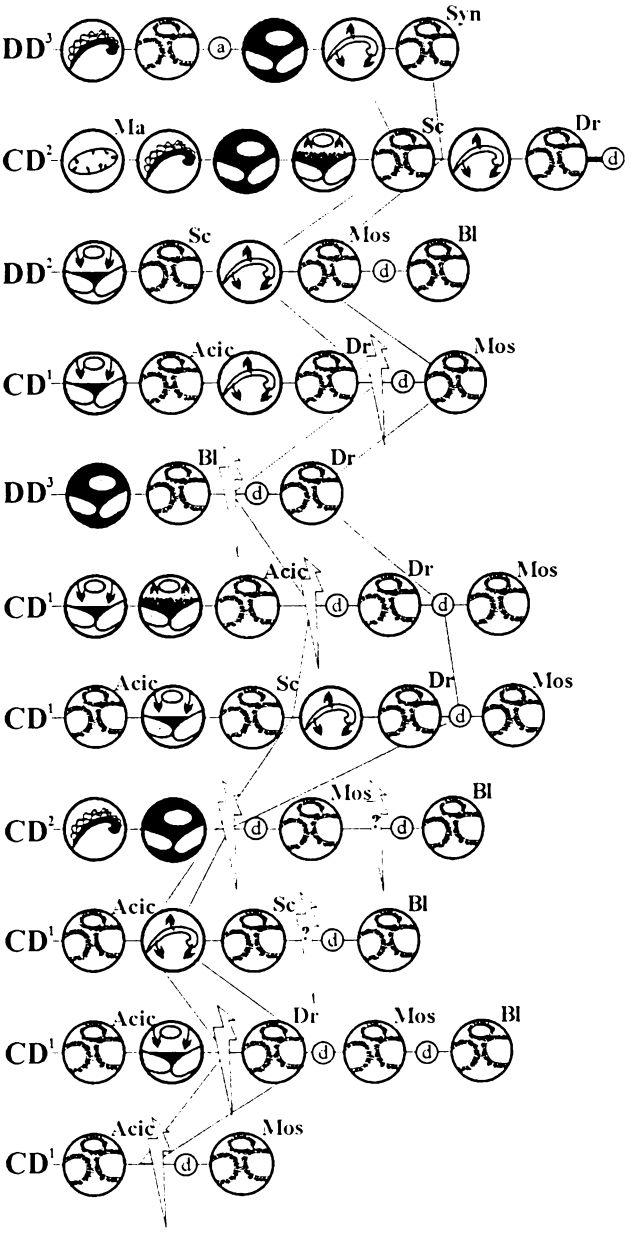

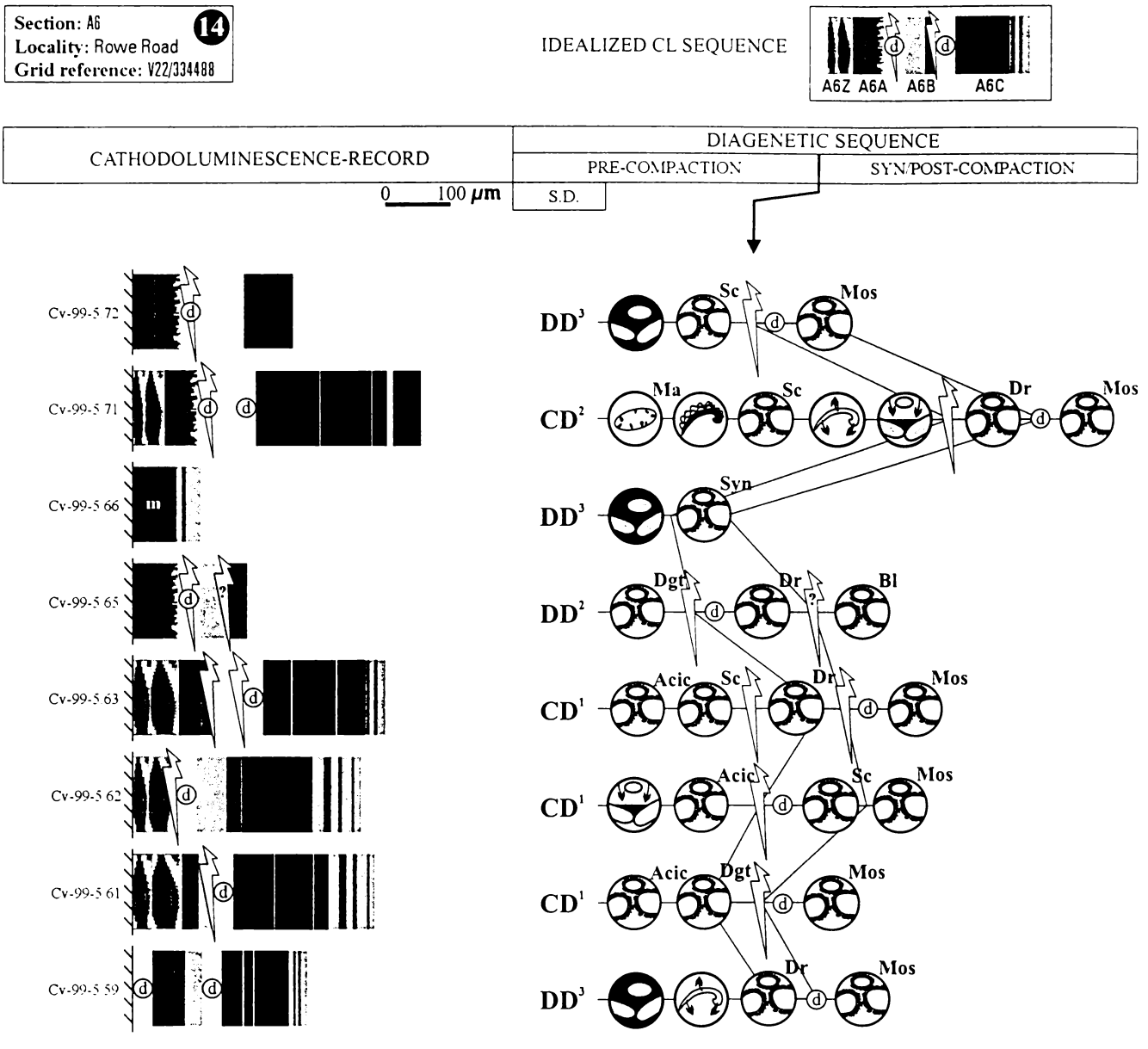
Section: A6
Locality: Rowe Road
Grid reference: V22/334488
14
IDEALIZED CL SEQUENCE
A6Z A6A A6B A6C
CATHODOLUMINESCENCE-RECORD
DIAGENETIC SEQUENCE
PRE-COMPACTION
SYN/POST-COMPACTION
0 100 µm
S.D.
Cv-99-5 72
Cv-99-5 71
Cv-99-5 66
Cv-99-5 65
Cv-99-5 63
Cv-99-5 62
Cv-99-5 61
Cv-99-5 59
DD³
CD²
DD³
DD²
CD¹
CD¹
CD¹
DD³
Sc
Mos
Ma
Sc
Dr
Mos
Syn
Dgt
Dr
Bl
Acic
Sc
Dr
Mos
Acic
Sc
Mos
Acic
Dgt
Mos
Dr
Mos

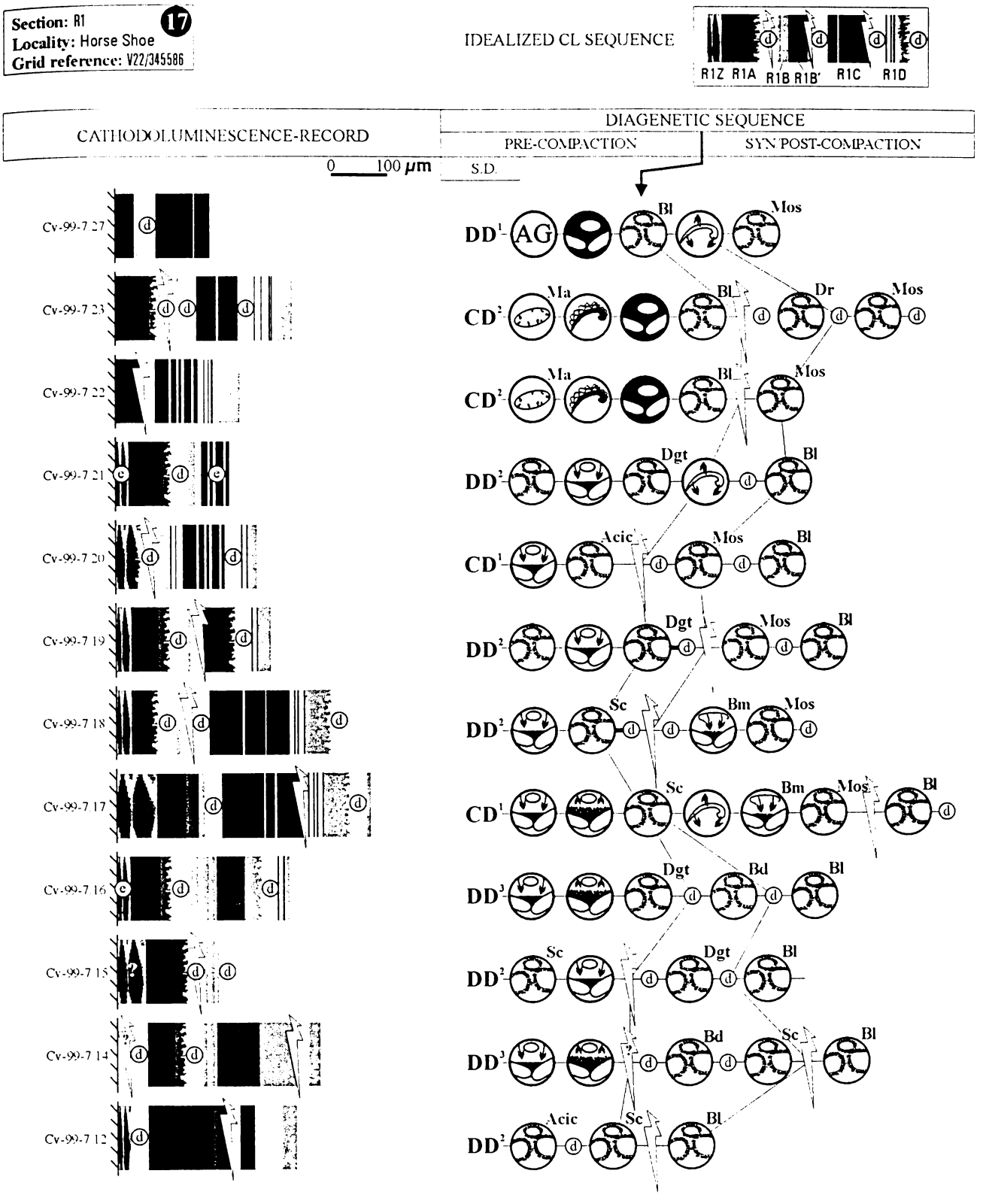
Section: R1
17
Locality: Horse Shoe
Grid reference: V22/345586
IDEALIZED CL SEQUENCE
R1Z R1A R1B R1B' R1C R1D
CATHODOLUMINESCENCE-RECORD
DIAGENETIC SEQUENCE
PRE-COMPACTION
SYN POST-COMPACTION
0 100 µm
S.D.
Cv-99-7 27
Cv-99-7 23
Cv-99-7 22
Cv-99-7 21
Cv-99-7 20
Cv-99-7 19
Cv-99-7 18
Cv-99-7 17
Cv-99-7 16
Cv-99-7 15
Cv-99-7 14
Cv-99-7 12
DD1 AG Bl Mos
CD2 Ma Bl Dr Mos
CD2 Ma Bl Mos
DD2 Dgt Bl
CD1 Acic Mos Bl
DD2 Dgt Mos Bl
DD2 Sc Bm Mos
CD1 Sc Bm Mos Bl
DD3 Dgt Bd Bl
DD2 Sc Dgt Bl
DD3 Bd Sc Bl
DD2 Acic Sc Bl

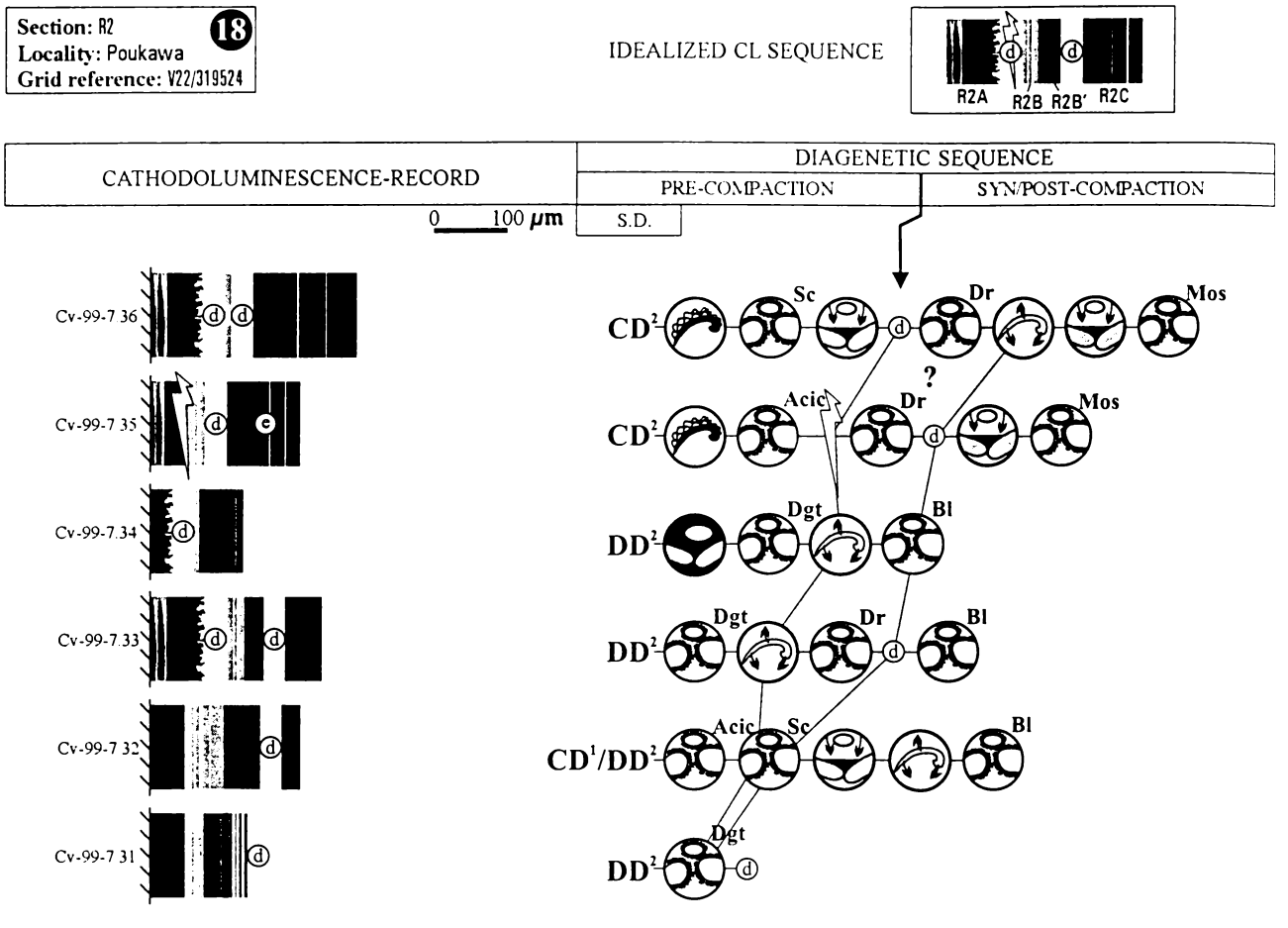
Section: R2
18
Locality: Poukawa
Grid reference: V22/319524
IDEALIZED CL SEQUENCE
R2A
R2B
R2B'
R2C
CATHODOLUMINESCENCE-RECORD
DIAGENETIC SEQUENCE
PRE-COMPACTION
SYN/POST-COMPACTION
0 100 µm
S.D.
Cv-99-7 36
Cv-99-7 35
Cv-99-7 34
Cv-99-7 33
Cv-99-7 32
Cv-99-7 31
CD²
DD²
CD¹/DD²
Sc
Dr
Mos
Acic
Dgt
Bl
?

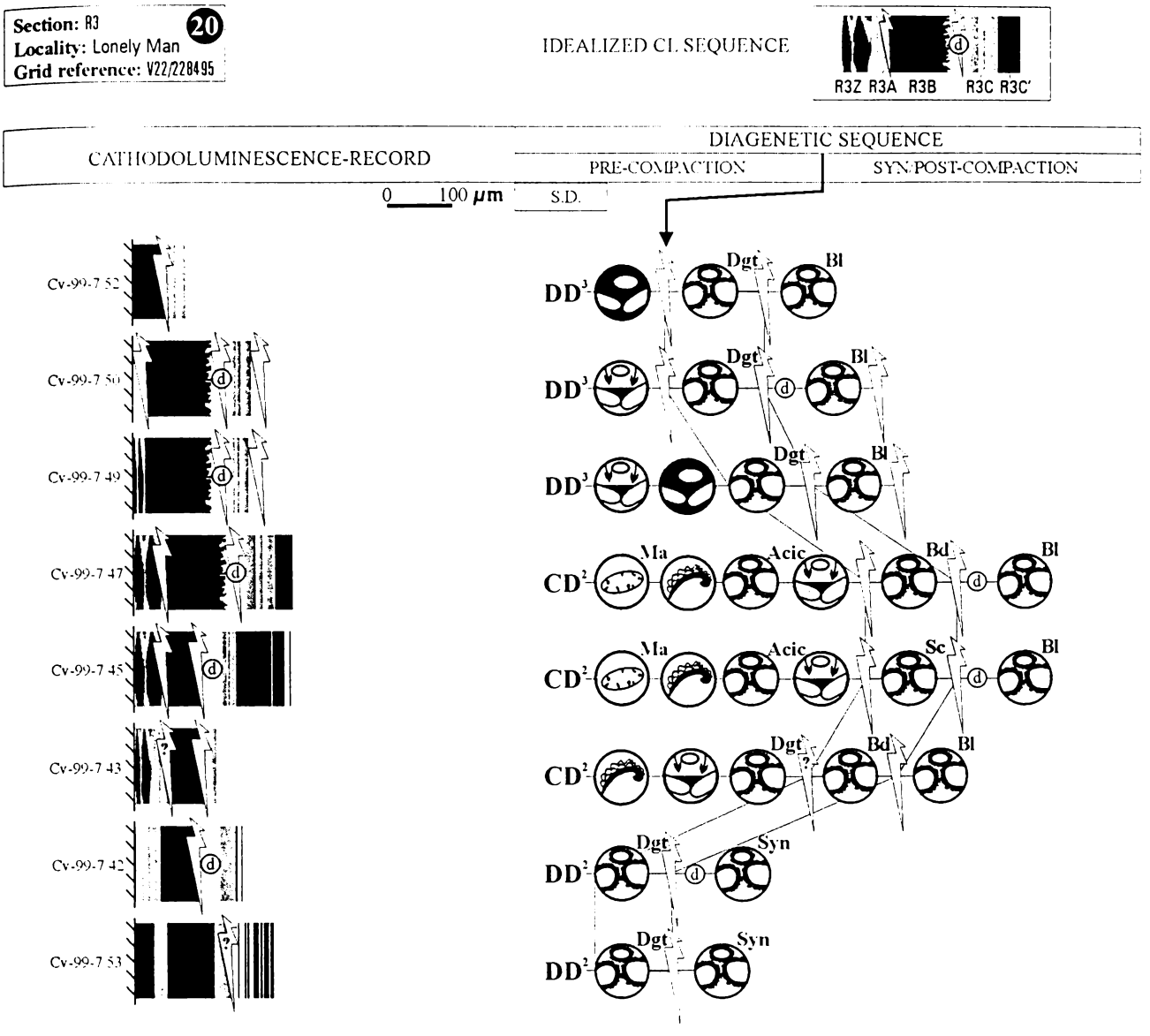
Section: R3
Locality: Lonely Man
Grid reference: V22/228495
20
IDEALIZED CL SEQUENCE
R3Z R3A R3B R3C R3C'
CATHODOLUMINESCENCE-RECORD
DIAGENETIC SEQUENCE
PRE-COMPACTION
SYN/POST-COMPACTION
0 100 µm
S.D.
Cv-99-7 52
Cv-99-7 50
Cv-99-7 49
Cv-99-7 47
Cv-99-7 45
Cv-99-7 43
Cv-99-7 42
Cv-99-7 53
DD³
DD³
DD³
CD²
CD²
CD²
DD²
DD²
Dgt
Bl
Ma
Acic
Bd
Sc
Syn

Section: R4 **19**
Locality: Rotoatara
Grid reference: V22/251451

IDEALIZED CL SEQUENCE

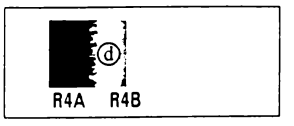

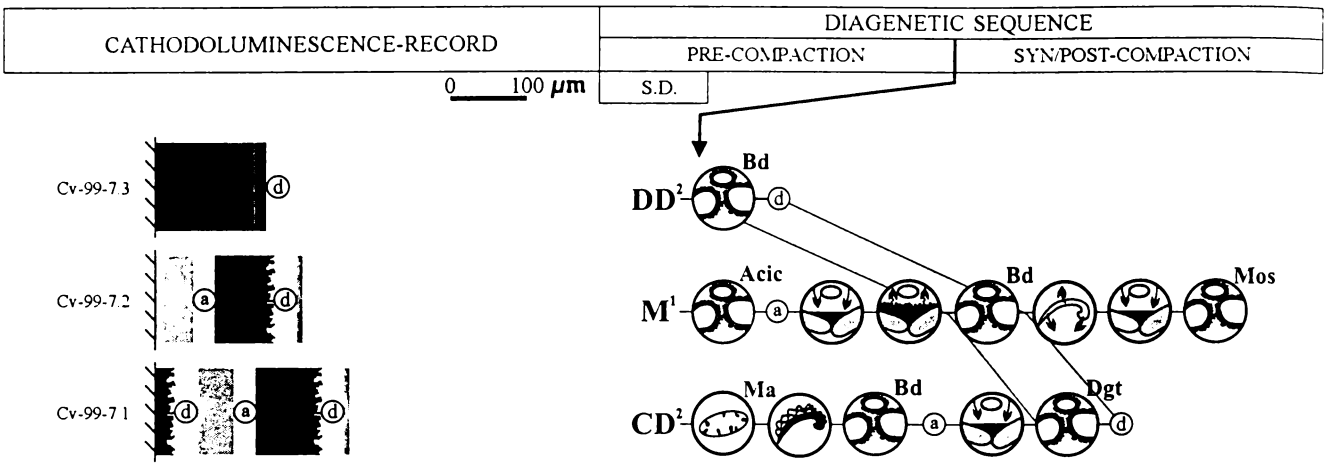

Section: R5
Locality: Ongaonga1 - Core3
Grid reference: U22/107385

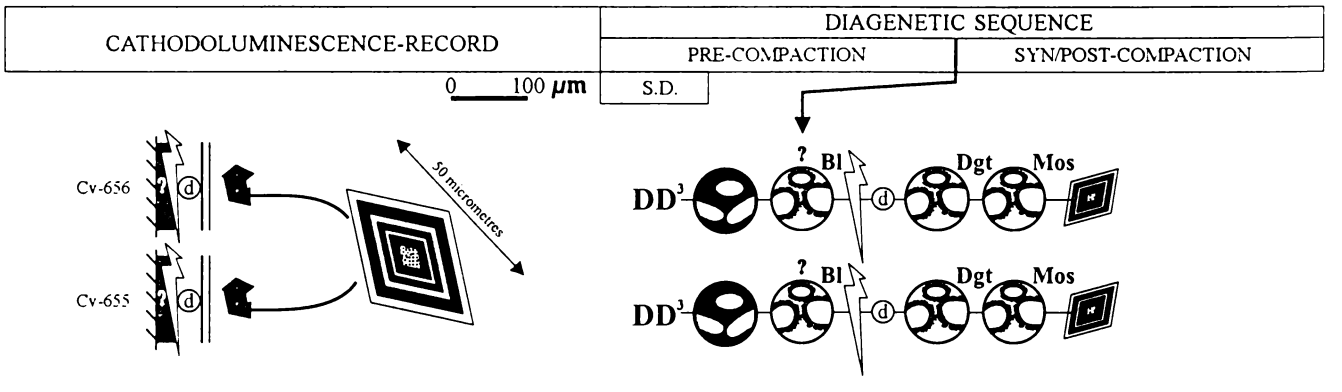

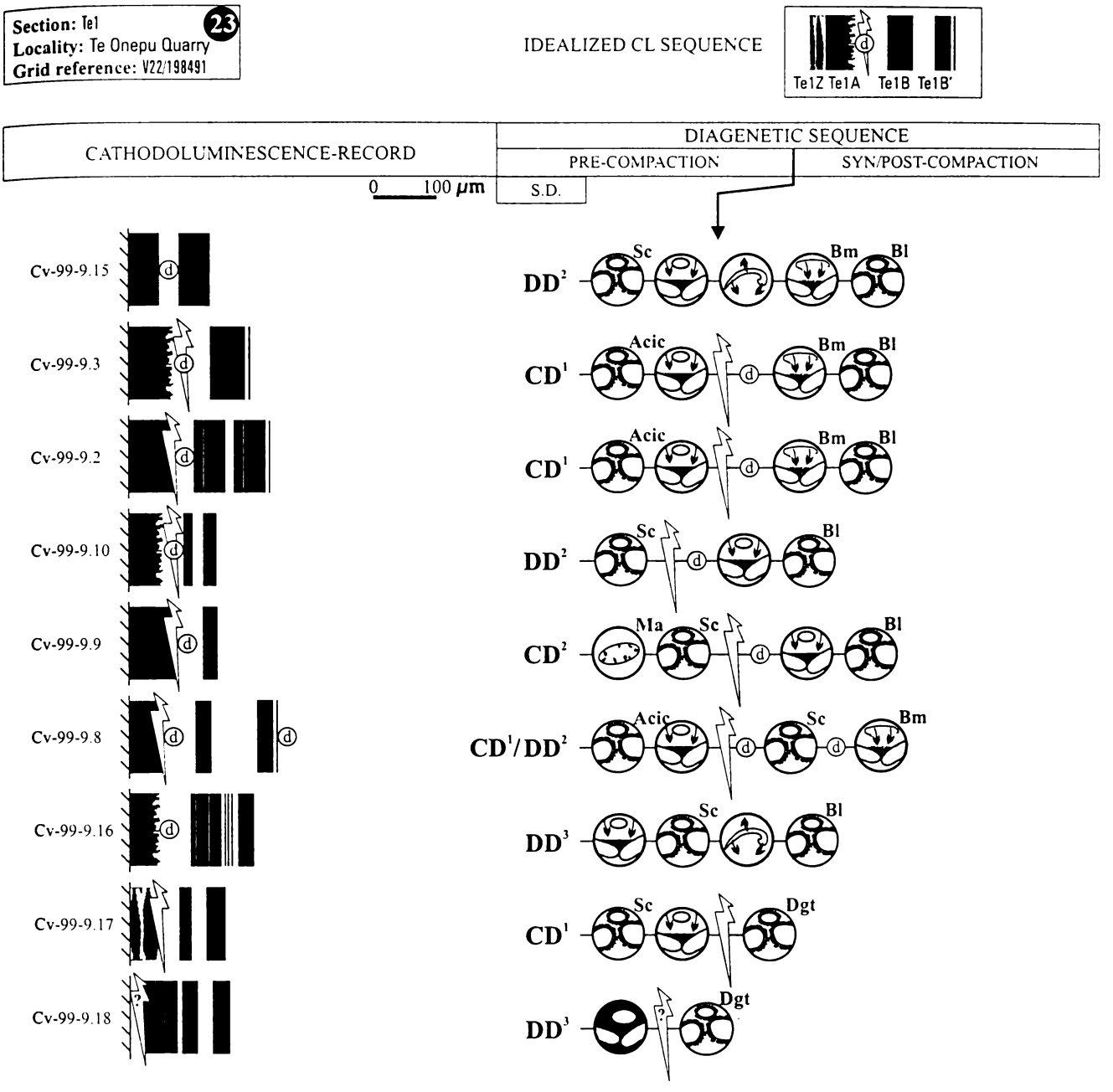
Section: Te1
Locality: Te Onepu Quarry
Grid reference: V22/198491
23
IDEALIZED CL SEQUENCE
Te1Z Te1A Te1B Te1B'
CATHODOLUMINESCENCE-RECORD
DIAGENETIC SEQUENCE
PRE-COMPACTION
SYN/POST-COMPACTION
0 100 µm
S.D.
Cv-99-9.15
Cv-99-9.3
Cv-99-9.2
Cv-99-9.10
Cv-99-9.9
Cv-99-9.8
Cv-99-9.16
Cv-99-9.17
Cv-99-9.18
DD²
CD¹
CD¹
DD²
CD²
CD¹/DD²
DD³
CD¹
DD³
Sc
Bm
Bl
Acic
Ma
Dgt
d

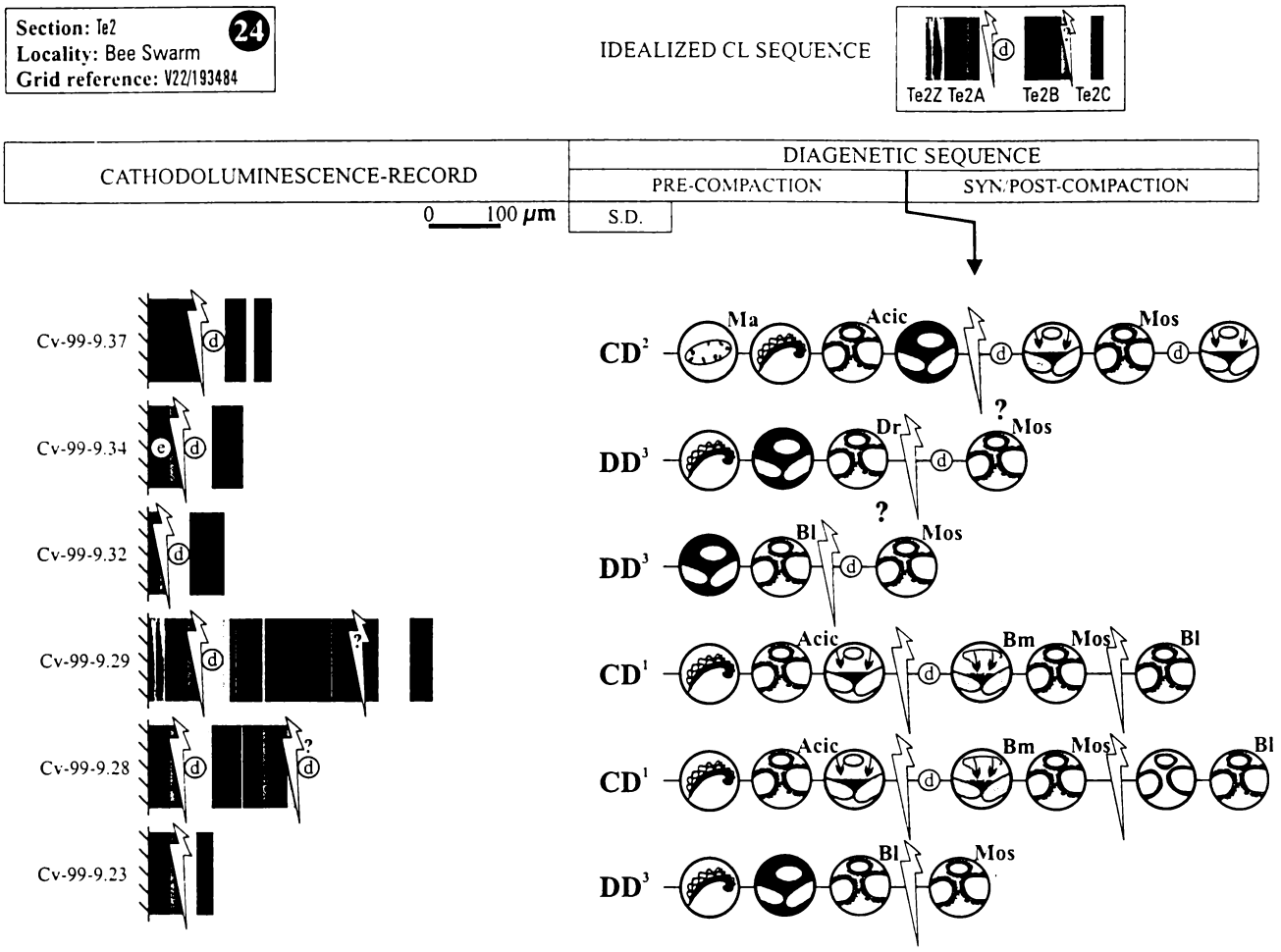
Section: Te2
Locality: Bee Swarm
Grid reference: V22/193484
24
IDEALIZED CL SEQUENCE
Te2Z Te2A
Te2B Te2C
CATHODOLUMINESCENCE-RECORD
DIAGENETIC SEQUENCE
PRE-COMPACTION
SYN/POST-COMPACTION
0 100 µm
S.D.
Cv-99-9.37
Cv-99-9.34
Cv-99-9.32
Cv-99-9.29
Cv-99-9.28
Cv-99-9.23
CD²
DD³
DD³
CD¹
CD¹
DD³
Ma
Acic
Mos
Dr
Mos
Bl
Mos
Acic
Bm
Mos
Bl
Acic
Bm
Mos
Bl
Bl
Mos

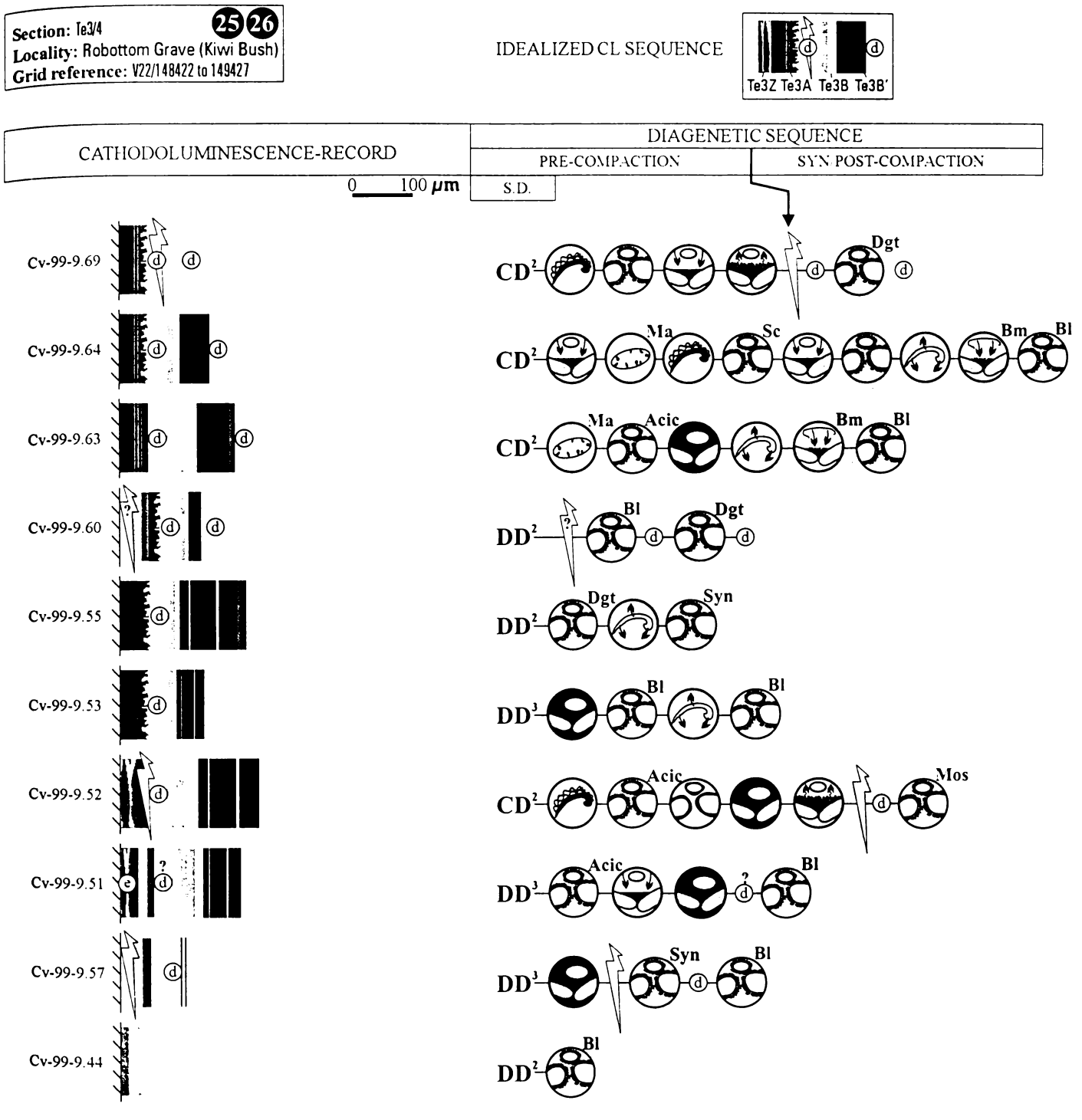
Section: Te3/4
25 26
Locality: Robottom Grave (Kiwi Bush)
Grid reference: V22/148422 to 149427
IDEALIZED CL SEQUENCE
Te3Z Te3A Te3B Te3B'
CATHODOLUMINESCENCE-RECORD
DIAGENETIC SEQUENCE
PRE-COMPACTION
SYN POST-COMPACTION
0 100 µm
S.D.
Cv-99-9.69
Cv-99-9.64
Cv-99-9.63
Cv-99-9.60
Cv-99-9.55
Cv-99-9.53
Cv-99-9.52
Cv-99-9.51
Cv-99-9.57
Cv-99-9.44
CD²
DD²
DD³
Dgt
Ma
Sc
Bm
Bl
Acic
Syn
Mos

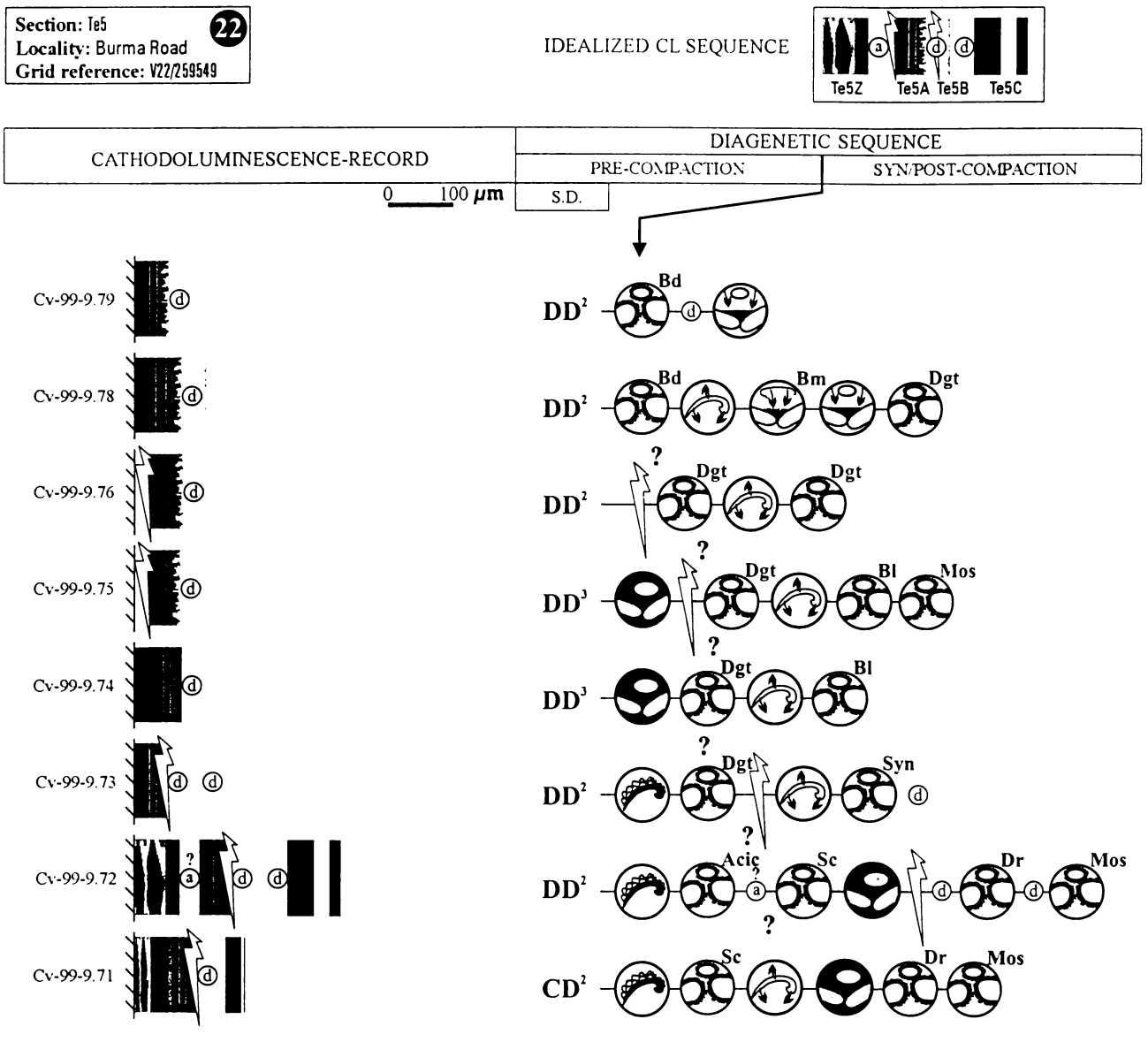
Section: Te5
Locality: Burma Road
Grid reference: V22/259549
22
IDEALIZED CL SEQUENCE
Te5Z
Te5A
Te5B
Te5C
CATHODOLUMINESCENCE-RECORD
DIAGENETIC SEQUENCE
PRE-COMPACTION
SYN/POST-COMPACTION
0 100 µm
S.D.
Cv-99-9.79
Cv-99-9.78
Cv-99-9.76
Cv-99-9.75
Cv-99-9.74
Cv-99-9.73
Cv-99-9.72
Cv-99-9.71
DD²
DD²
DD²
DD³
DD³
DD²
DD²
CD²
Bd
Bd
Bm
Dgt
Dgt
Dgt
Dgt
Bl
Mos
Dgt
Bl
Dgt
Syn
Acic
Sc
Dr
Mos
Sc
Dr
Mos

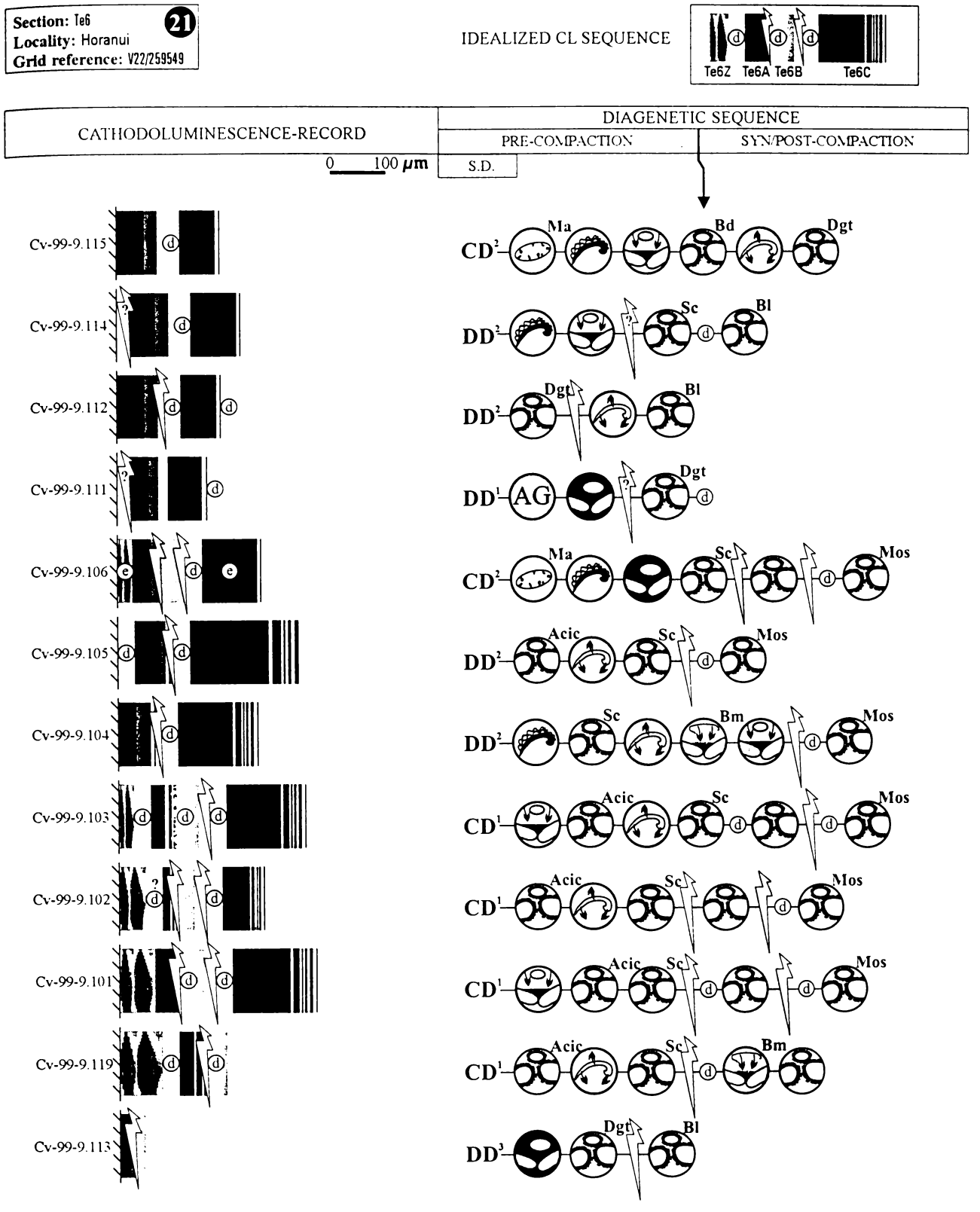
Section: Te6
21
Locality: Horanui
Grid reference: V22/259549
IDEALIZED CL SEQUENCE
Te6Z
Te6A
Te6B
Te6C
CATHODOLUMINESCENCE-RECORD
DIAGENETIC SEQUENCE
PRE-COMPACTION
SYN/POST-COMPACTION
0 100 µm
S.D.
Cv-99-9.115
Cv-99-9.114
Cv-99-9.112
Cv-99-9.111
Cv-99-9.106
Cv-99-9.105
Cv-99-9.104
Cv-99-9.103
Cv-99-9.102
Cv-99-9.101
Cv-99-9.119
Cv-99-9.113
CD2 Ma Bd Dgt
DD2 Sc Bl
DD2 Dgt Bl
DD1 AG Dgt
CD2 Ma Sc Mos
DD2 Acic Sc Mos
DD2 Sc Bm Mos
CD1 Acic Sc Mos
CD1 Acic Sc Mos
CD1 Acic Sc Mos
CD1 Acic Sc Bm
DD3 Dgt Bl

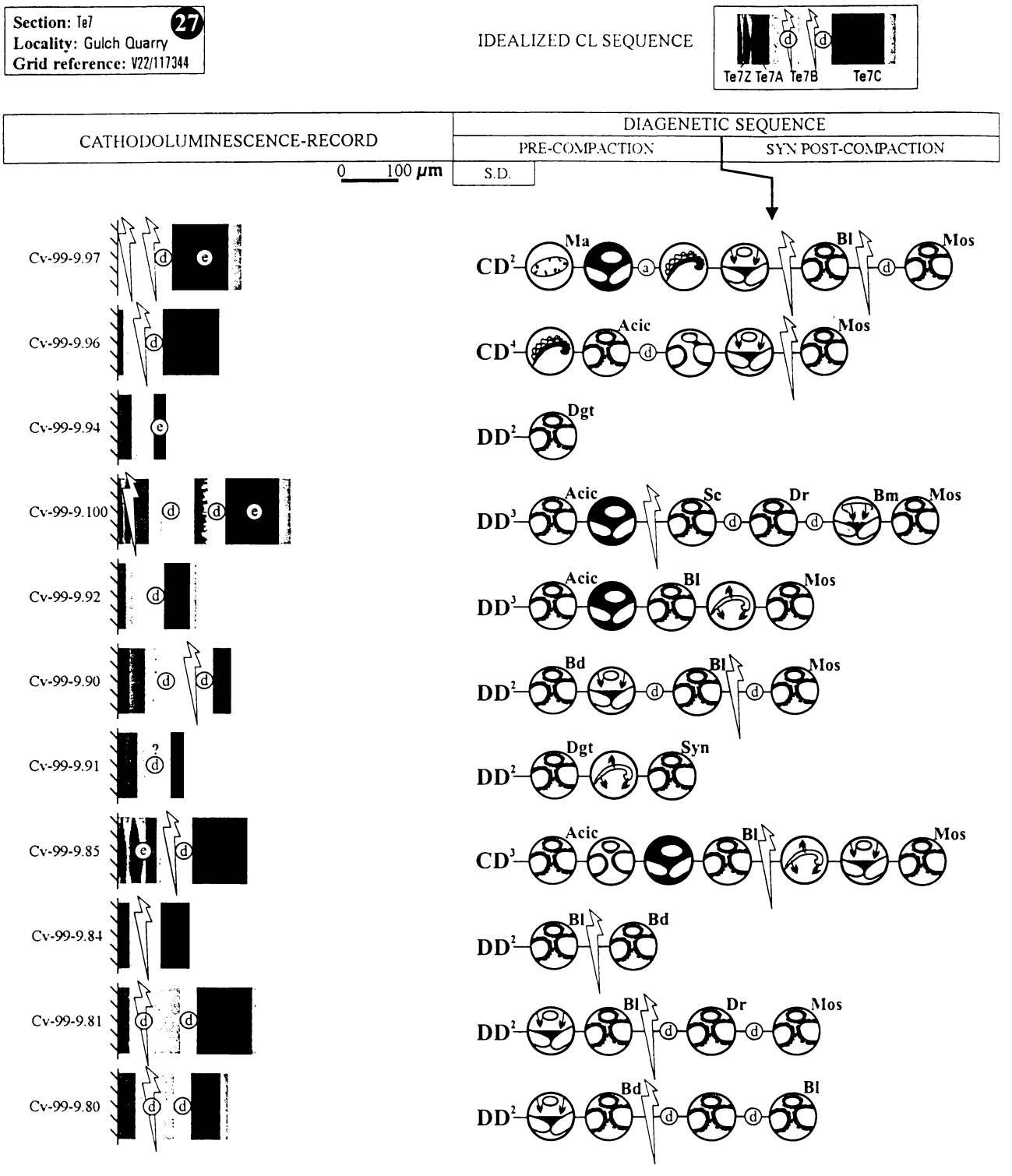
Section: Te7
27
Locality: Gulch Quarry
Grid reference: V22/117344
IDEALIZED CL SEQUENCE
Te7Z Te7A Te7B Te7C
CATHODOLUMINESCENCE-RECORD
DIAGENETIC SEQUENCE
PRE-COMPACTION
SYN POST-COMPACTION
0 100 µm
S.D.
Cv-99-9.97
Cv-99-9.96
Cv-99-9.94
Cv-99-9.100
Cv-99-9.92
Cv-99-9.90
Cv-99-9.91
Cv-99-9.85
Cv-99-9.84
Cv-99-9.81
Cv-99-9.80
CD2 Ma Bl Mos
CD4 Acic Mos
DD2 Dgt
DD3 Acic Sc Dr Bm Mos
DD3 Acic Bl Mos
DD2 Bd Bl Mos
DD2 Dgt Syn
CD3 Acic Bl Mos
DD2 Bl Bd
DD2 Bl Dr Mos
DD2 Bd Bl

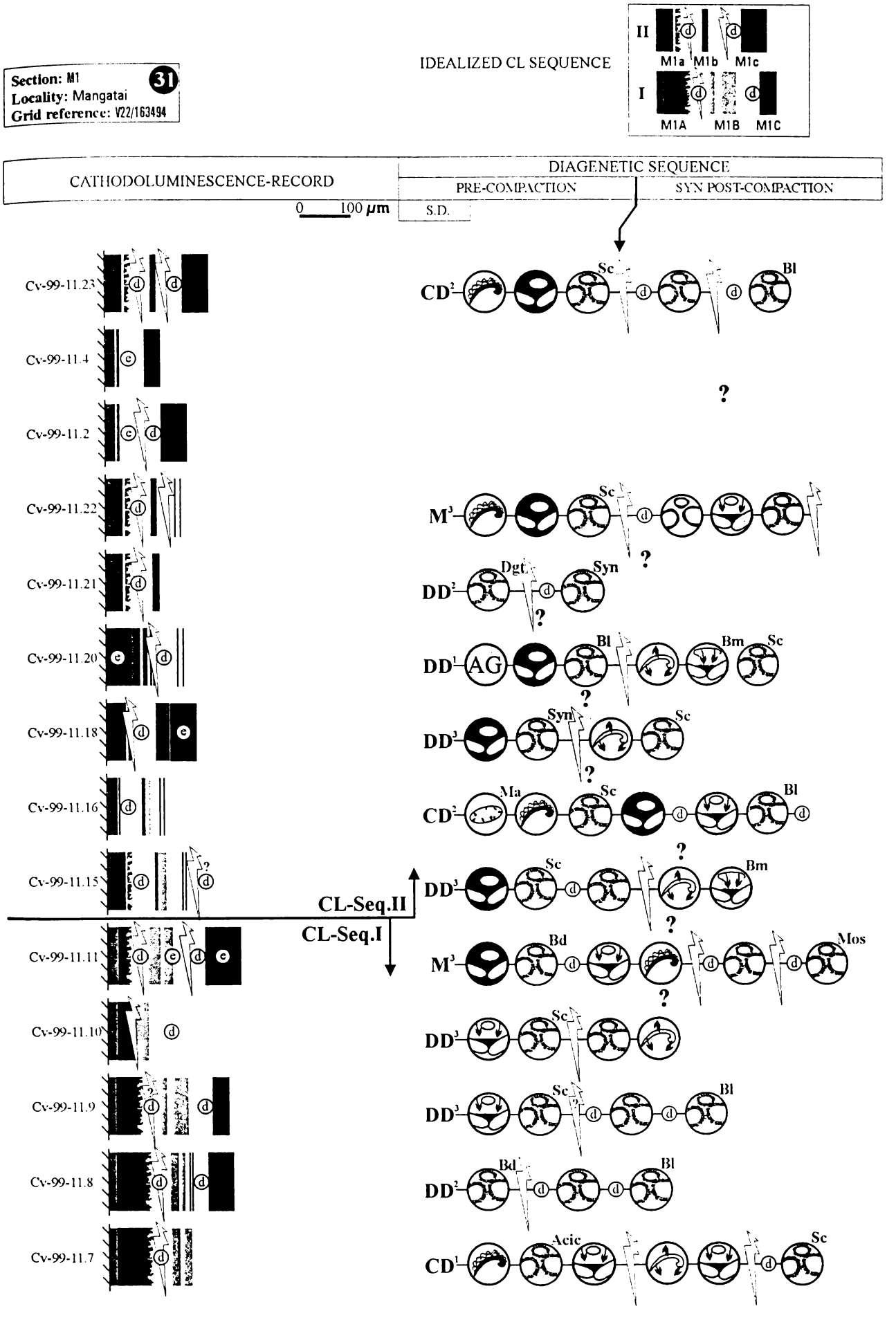
Section: M1
31
Locality: Mangatai
Grid reference: V22/163494
IDEALIZED CL SEQUENCE
II
M1a M1b M1c
I
M1A M1B M1C
CATHODOLUMINESCENCE-RECORD
DIAGENETIC SEQUENCE
PRE-COMPACTION
SYN POST-COMPACTION
0 100 µm
S.D.
Cv-99-11.23
Cv-99-11.4
Cv-99-11.2
Cv-99-11.22
Cv-99-11.21
Cv-99-11.20
Cv-99-11.18
Cv-99-11.16
Cv-99-11.15
CL-Seq.II
CL-Seq.I
Cv-99-11.11
Cv-99-11.10
Cv-99-11.9
Cv-99-11.8
Cv-99-11.7
CD²
Sc
Bl
M³
Dgt
Syn
DD²
DD¹
AG
Bm
DD³
Ma
Mos
Bd
Acic
CD¹

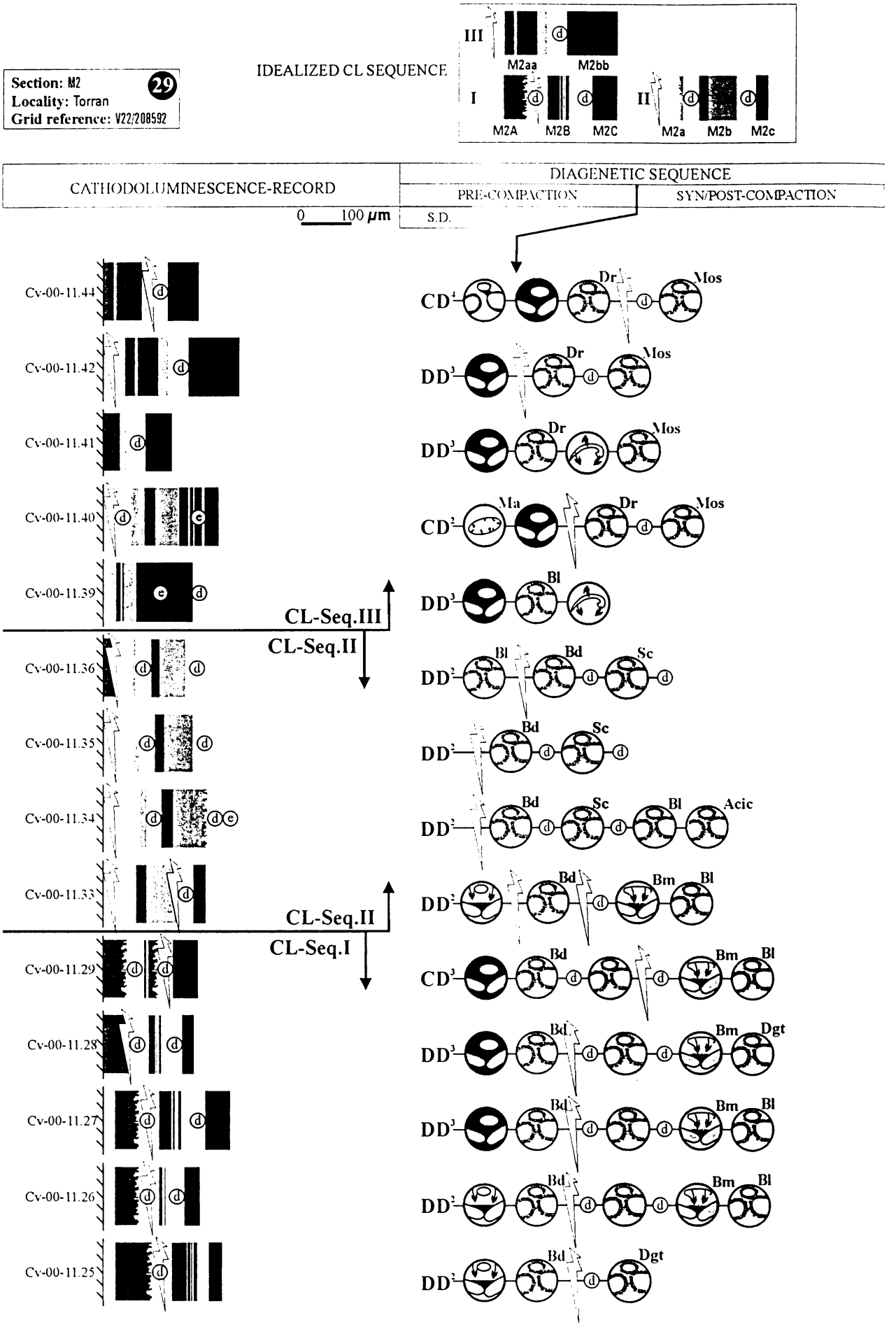
Section: M2
Locality: Torran
Grid reference: V22/208592
29
IDEALIZED CL SEQUENCE
III
M2aa
M2bb
I
M2A
M2B
M2C
II
M2a
M2b
M2c
CATHODOLUMINESCENCE-RECORD
DIAGENETIC SEQUENCE
PRE-COMPACTION
SYN/POST-COMPACTION
0 100 µm
S.D.
Cv-00-11.44
Cv-00-11.42
Cv-00-11.41
Cv-00-11.40
Cv-00-11.39
CL-Seq.III
CL-Seq.II
Cv-00-11.36
Cv-00-11.35
Cv-00-11.34
Cv-00-11.33
CL-Seq.II
CL-Seq.I
Cv-00-11.29
Cv-00-11.28
Cv-00-11.27
Cv-00-11.26
Cv-00-11.25
CD4
DD3
CD2
DD3
DD2
DD2
DD2
DD2
CD3
DD3
DD3
DD2
DD2
Dr
Mos
Ma
Bl
Bd
Sc
Acic
Bm
Dgt

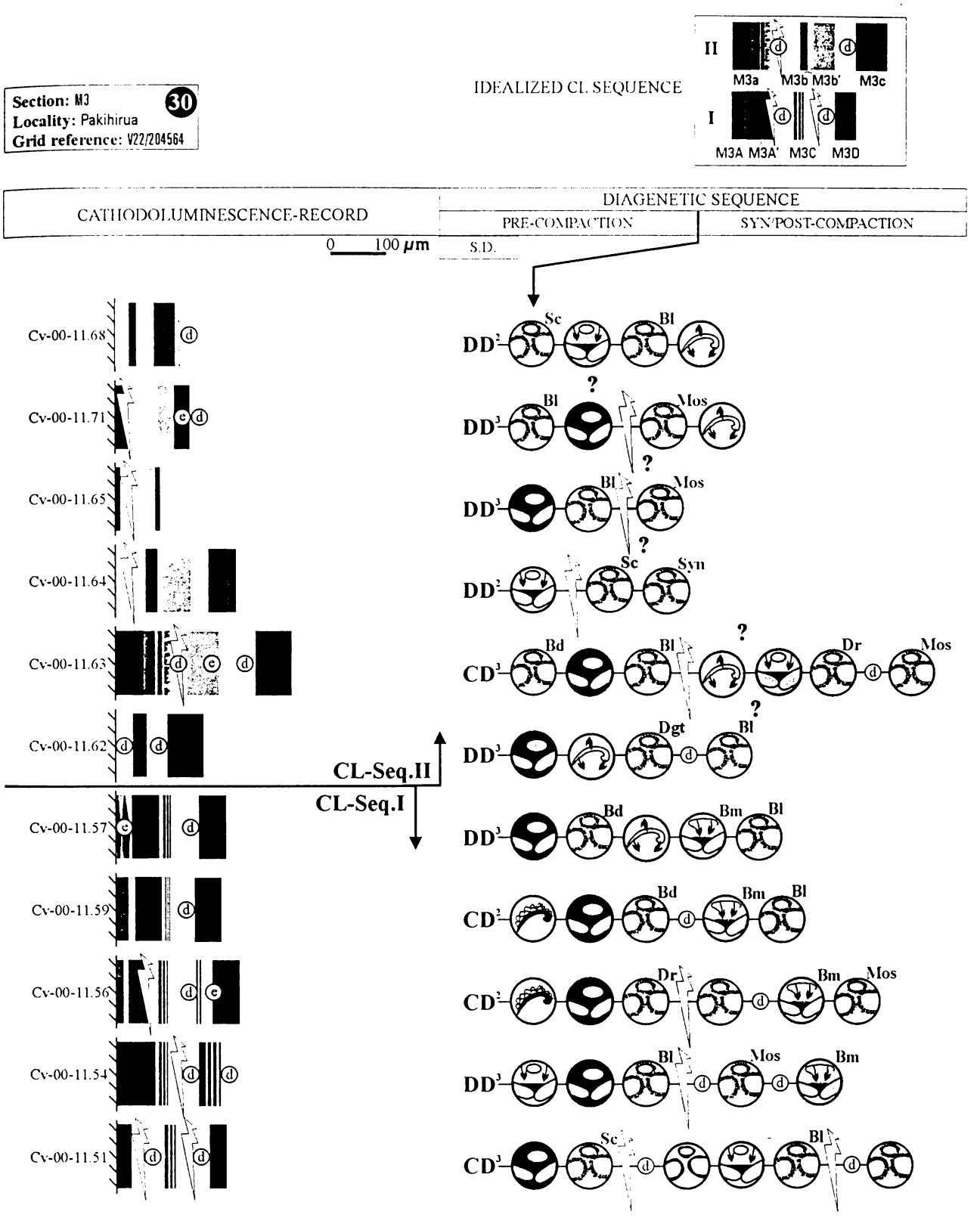
Section: M3
Locality: Pakihirua
Grid reference: V22/204564
30
IDEALIZED CL SEQUENCE
II
I
M3a
M3b
M3b'
M3c
M3A
M3A'
M3C
M3D
CATHODOLUMINESCENCE-RECORD
DIAGENETIC SEQUENCE
PRE-COMPACTION
SYN/POST-COMPACTION
0 100 µm
S.D.
Cv-00-11.68
Cv-00-11.71
Cv-00-11.65
Cv-00-11.64
Cv-00-11.63
Cv-00-11.62
Cv-00-11.57
Cv-00-11.59
Cv-00-11.56
Cv-00-11.54
Cv-00-11.51
CL-Seq.II
CL-Seq.I
DD²
DD³
CD³
CD²
Sc
Bl
Mos
Syn
Bd
Dr
Dgt
Bm

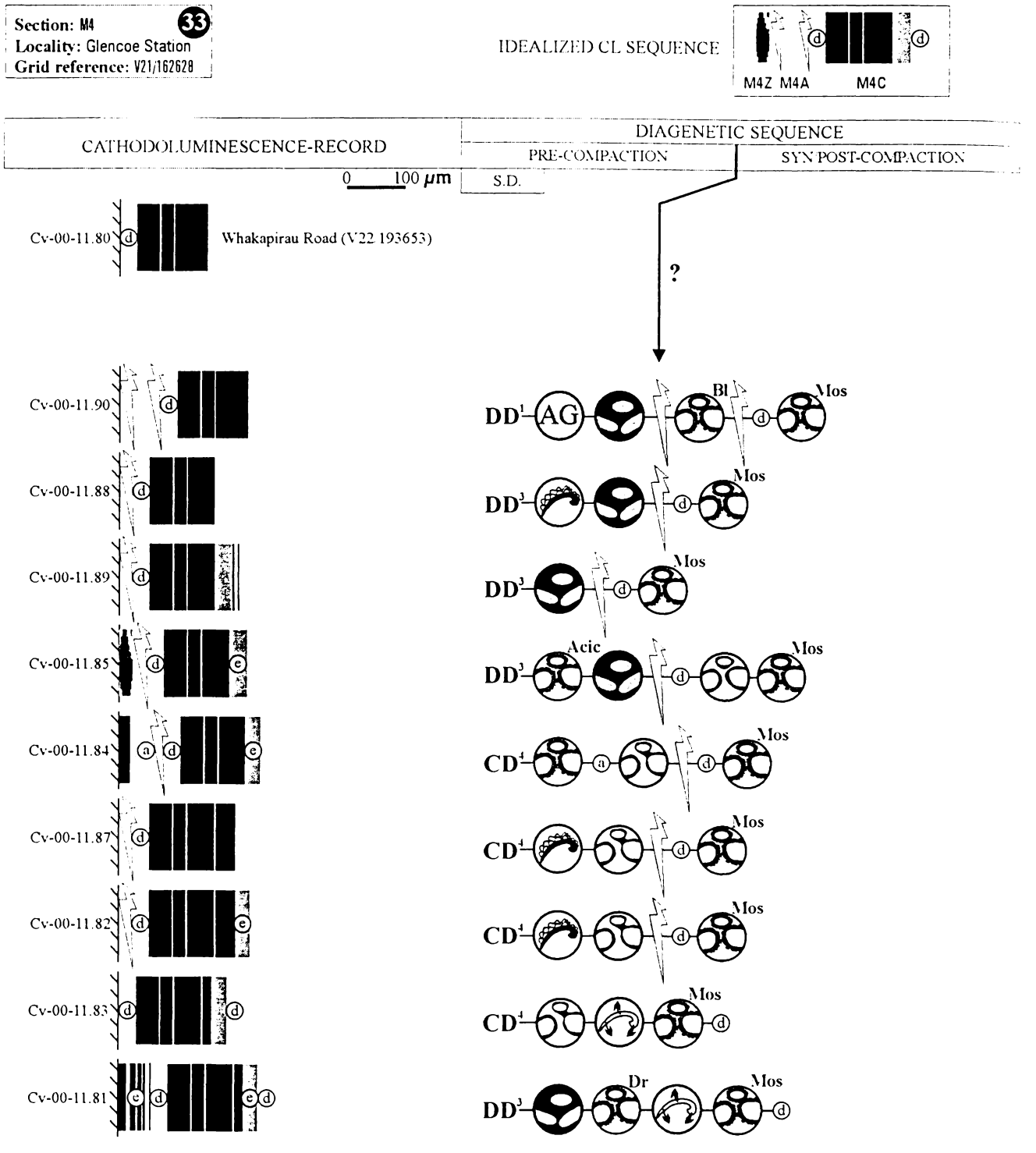
Section: M4
33
Locality: Glencoe Station
Grid reference: V21/162628
IDEALIZED CL SEQUENCE
M4Z M4A M4C
CATHODOLUMINESCENCE-RECORD
DIAGENETIC SEQUENCE
PRE-COMPACTION
SYN POST-COMPACTION
0 100 µm
S.D.
Cv-00-11.80
Whakapirau Road (V22 193653)
?
Cv-00-11.90
Cv-00-11.88
Cv-00-11.89
Cv-00-11.85
Cv-00-11.84
Cv-00-11.87
Cv-00-11.82
Cv-00-11.83
Cv-00-11.81
DD1
AG
Bl
Mos
DD3
Acic
CD4
Dr

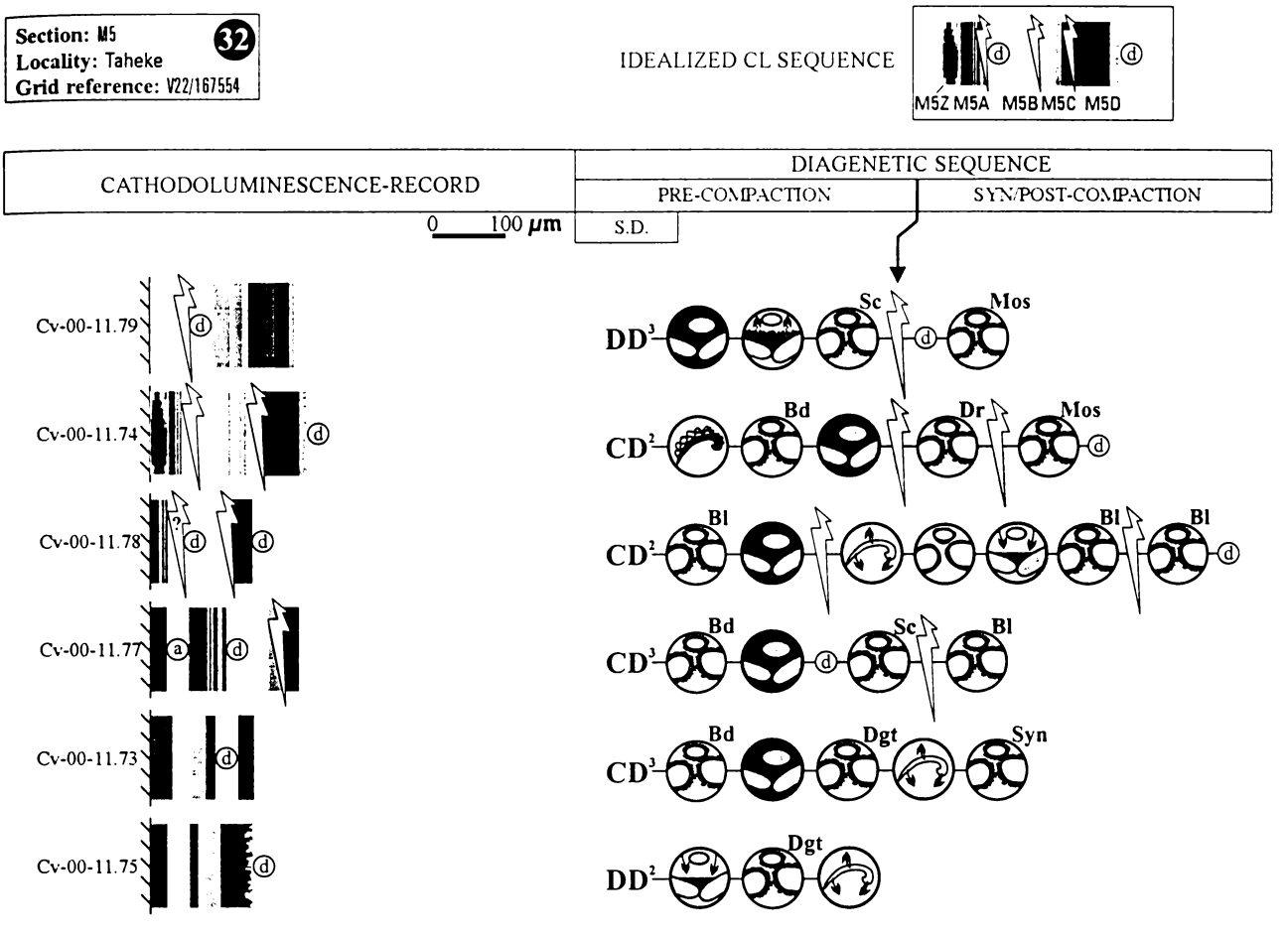
Section: M5
32
Locality: Taheke
Grid reference: V22/167554
IDEALIZED CL SEQUENCE
M5Z M5A M5B M5C M5D
CATHODOLUMINESCENCE-RECORD
DIAGENETIC SEQUENCE
PRE-COMPACTION
SYN/POST-COMPACTION
0 100 µm
S.D.
Cv-00-11.79
Cv-00-11.74
Cv-00-11.78
Cv-00-11.77
Cv-00-11.73
Cv-00-11.75
DD³
Sc
Mos
CD²
Bd
Dr
Mos
CD²
Bl
Bl
Bl
CD³
Bd
Sc
Bl
CD³
Bd
Dgt
Syn
DD²
Dgt

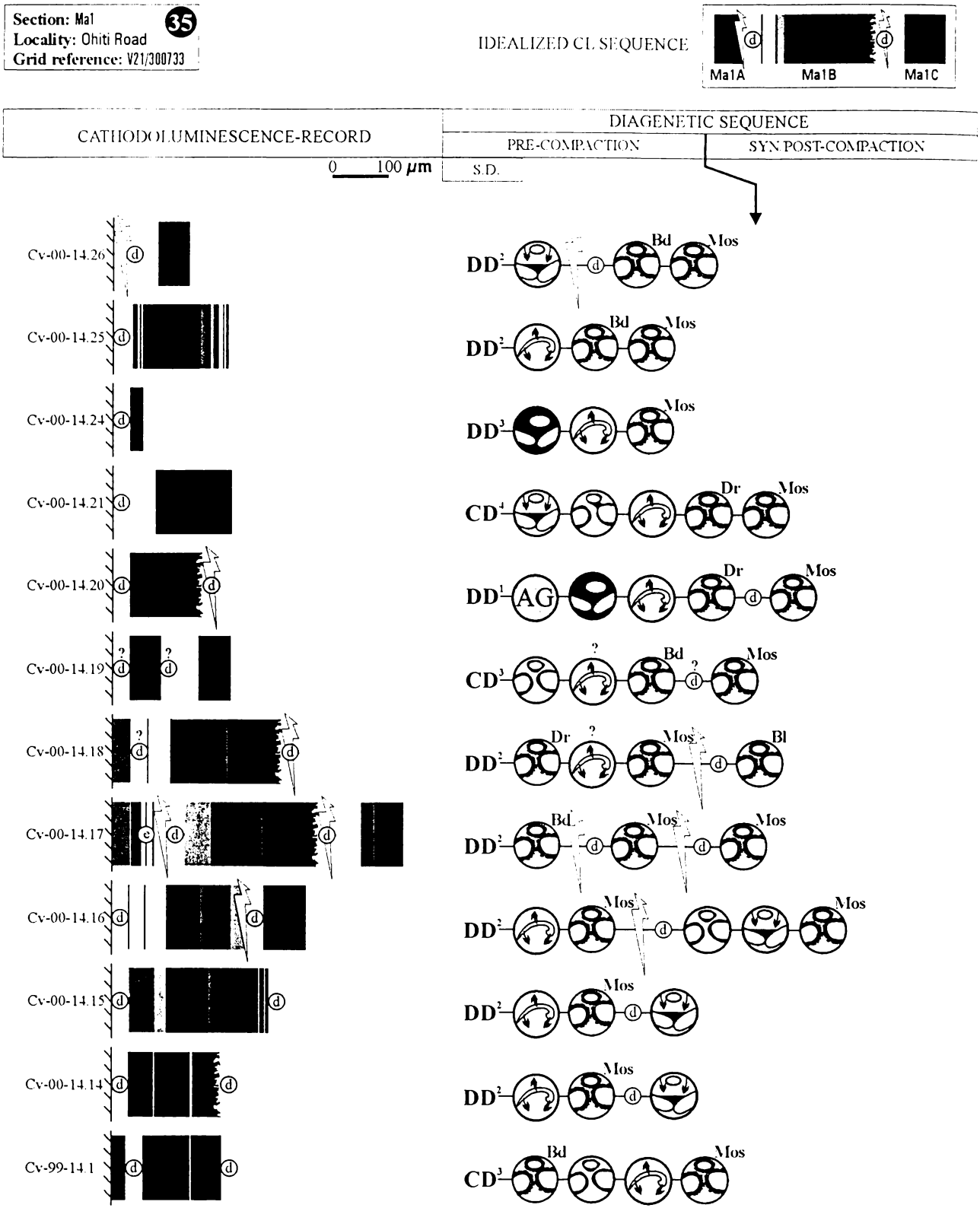
Section: Ma1
35
Locality: Ohiti Road
Grid reference: V21/300733
IDEALIZED CL SEQUENCE
Ma1A
Ma1B
Ma1C
CATHODOLUMINESCENCE-RECORD
DIAGENETIC SEQUENCE
PRE-COMPACTION
SYN/POST-COMPACTION
0 100 µm
S.D.
Cv-00-14.26
Cv-00-14.25
Cv-00-14.24
Cv-00-14.21
Cv-00-14.20
Cv-00-14.19
Cv-00-14.18
Cv-00-14.17
Cv-00-14.16
Cv-00-14.15
Cv-00-14.14
Cv-99-14.1
DD2
DD2
DD3
CD4
DD1
CD3
DD2
DD2
DD2
DD2
DD2
CD3
Bd
Mos
Dr
AG
Bl

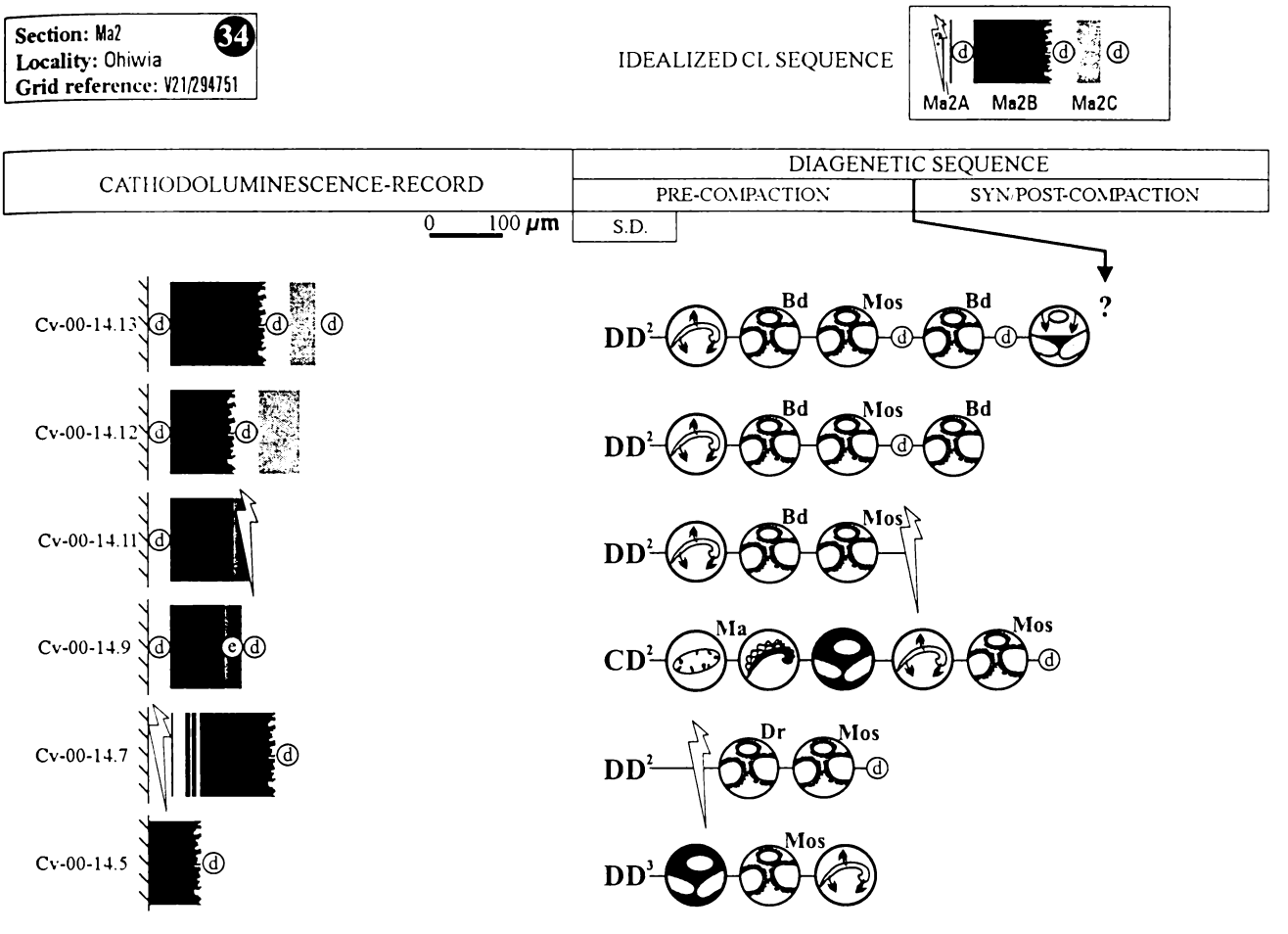
Section: Ma2
34
Locality: Ohiwia
Grid reference: V21/294751
IDEALIZED CL SEQUENCE
Ma2A
Ma2B
Ma2C
CATHODOLUMINESCENCE-RECORD
DIAGENETIC SEQUENCE
PRE-COMPACTION
SYN/POST-COMPACTION
0 100 µm
S.D.
Cv-00-14.13
Cv-00-14.12
Cv-00-14.11
Cv-00-14.9
Cv-00-14.7
Cv-00-14.5
DD²
Bd
Mos
Bd
?
DD²
Bd
Mos
Bd
DD²
Bd
Mos
CD²
Ma
Mos
DD²
Dr
Mos
DD³
Mos

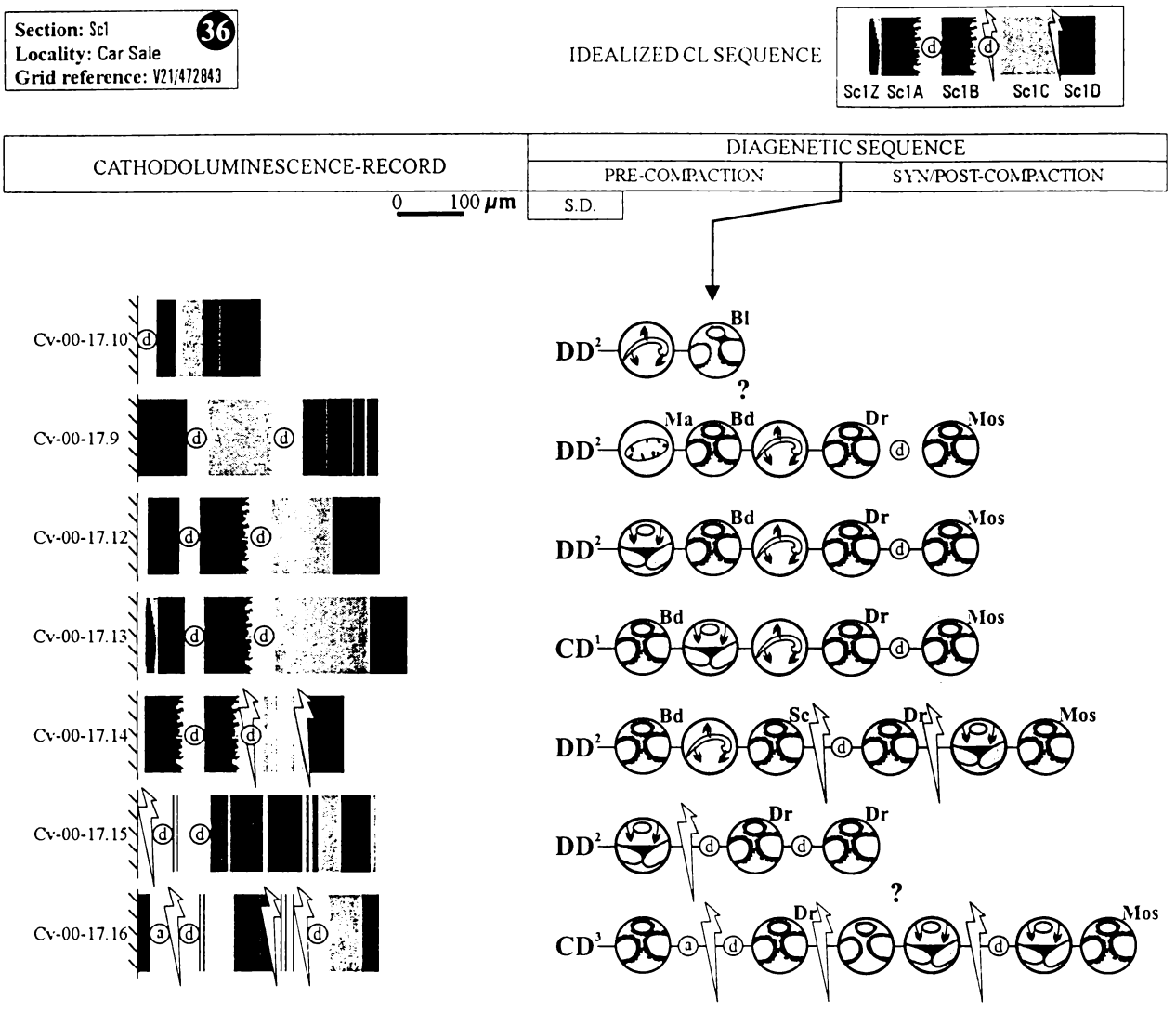
Section: Sc1
36
Locality: Car Sale
Grid reference: V21/472843
IDEALIZED CL SEQUENCE
Sc1Z Sc1A Sc1B Sc1C Sc1D
CATHODOLUMINESCENCE-RECORD
DIAGENETIC SEQUENCE
PRE-COMPACTION
SYN/POST-COMPACTION
0 100 µm
S.D.
Cv-00-17.10
Cv-00-17.9
Cv-00-17.12
Cv-00-17.13
Cv-00-17.14
Cv-00-17.15
Cv-00-17.16
DD²
Bl
?
Ma
Bd
Dr
Mos
CD¹
Sc
CD³

Section: Sc2 **37**
Locality: Milton Road
Grid reference: V21/452833

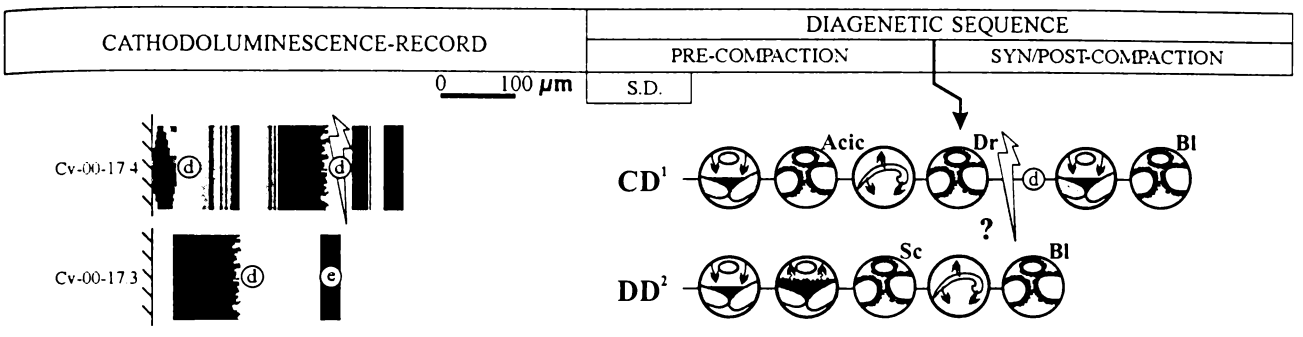

Section: Sc3
Locality: Battery Point
Grid reference: V21/448834

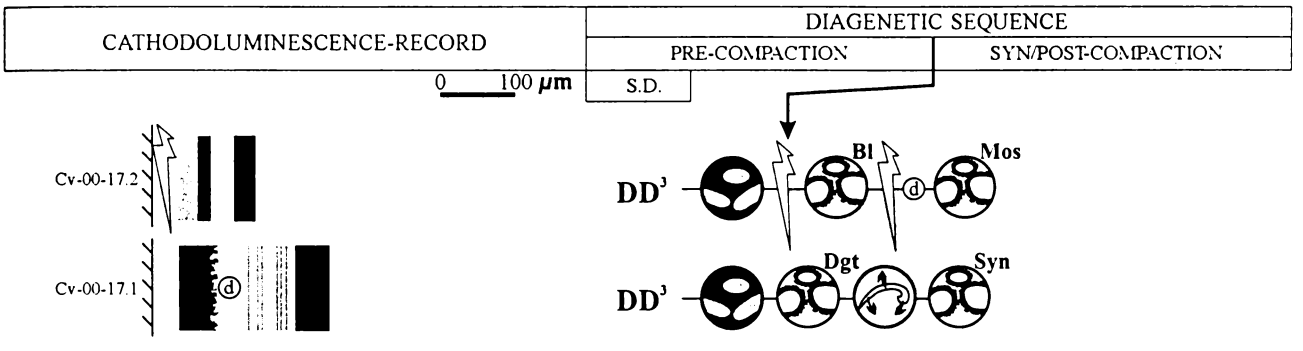

Section: Sc4
Locality: Bluff Hill
Grid reference: V21/472843

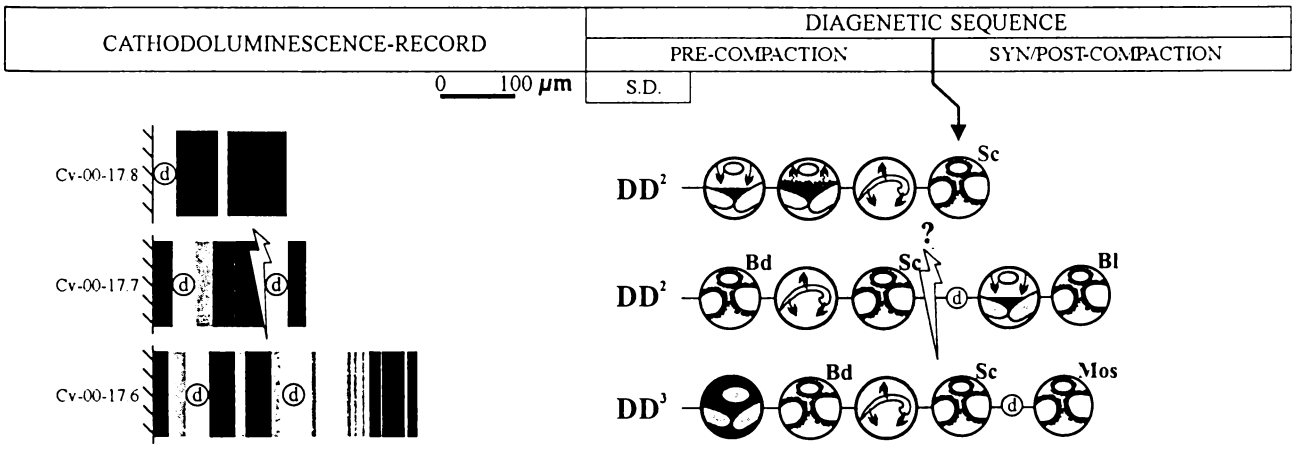

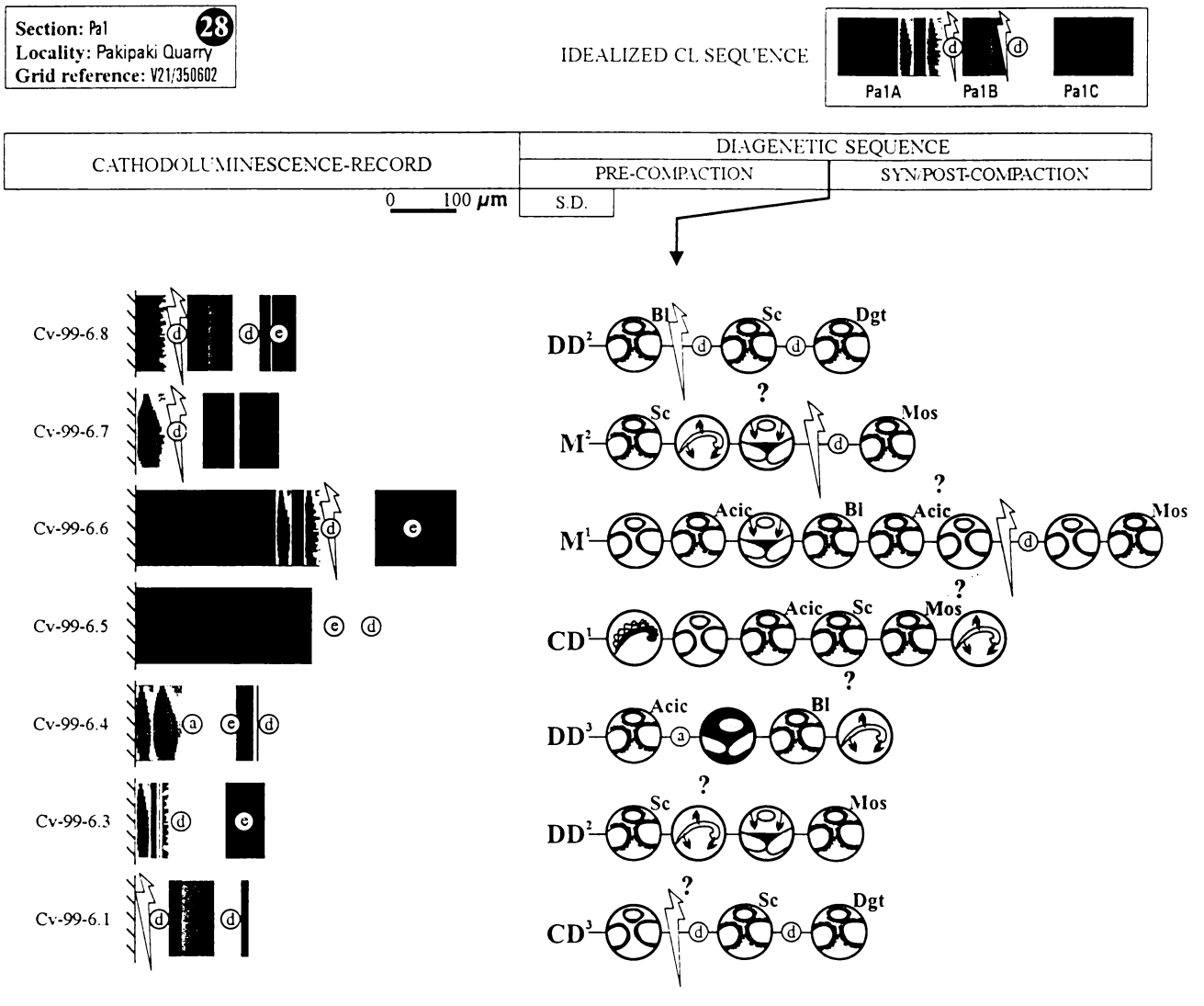
Section: Pal
28
Locality: Pakipaki Quarry
Grid reference: V21/350602
IDEALIZED CL SEQUENCE
Pa1A
Pa1B
Pa1C
CATHODOLUMINESCENCE-RECORD
DIAGENETIC SEQUENCE
PRE-COMPACTION
SYN/POST-COMPACTION
0 100 µm
S.D.
Cv-99-6.8
Cv-99-6.7
Cv-99-6.6
Cv-99-6.5
Cv-99-6.4
Cv-99-6.3
Cv-99-6.1
DD²
Bl
Sc
Dgt
M²
Mos
M¹
Acic
CD¹
DD³
CD³

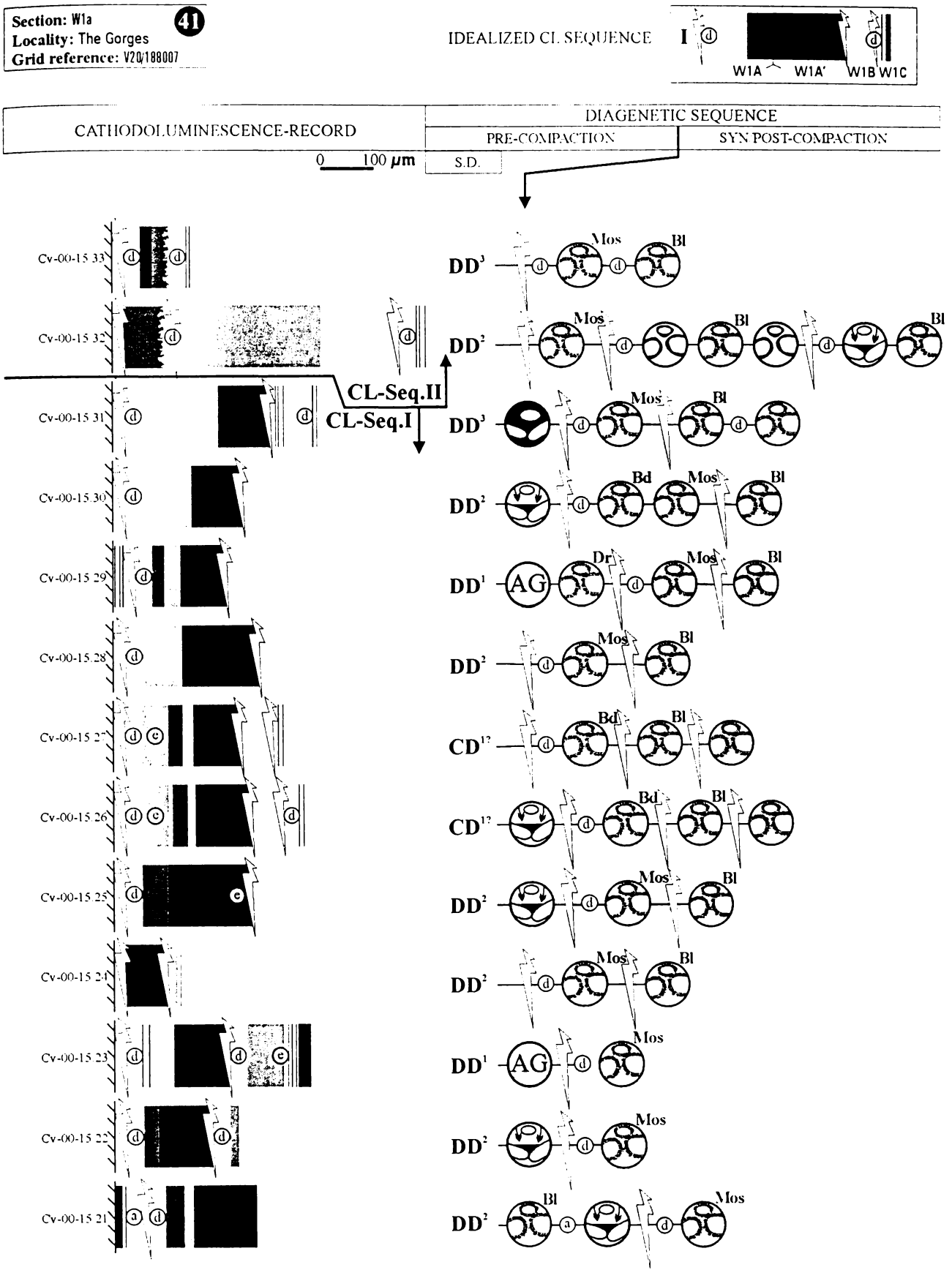
Section: W1a
41
Locality: The Gorges
Grid reference: V20/188007
IDEALIZED CL SEQUENCE
I
d
W1A
W1A'
W1B
W1C
CATHODOLUMINESCENCE-RECORD
DIAGENETIC SEQUENCE
PRE-COMPACTION
SYN POST-COMPACTION
0 100 µm
S.D.
Cv-00-15 33
Cv-00-15 32
Cv-00-15 31
Cv-00-15 30
Cv-00-15 29
Cv-00-15 28
Cv-00-15 27
Cv-00-15 26
Cv-00-15 25
Cv-00-15 24
Cv-00-15 23
Cv-00-15 22
Cv-00-15 21
CL-Seq.II
CL-Seq.I
DD3
DD2
DD3
DD2
DD1
DD2
CD1?
CD1?
DD2
DD2
DD1
DD2
DD2
Mos
Bl
Bd
Dr
AG

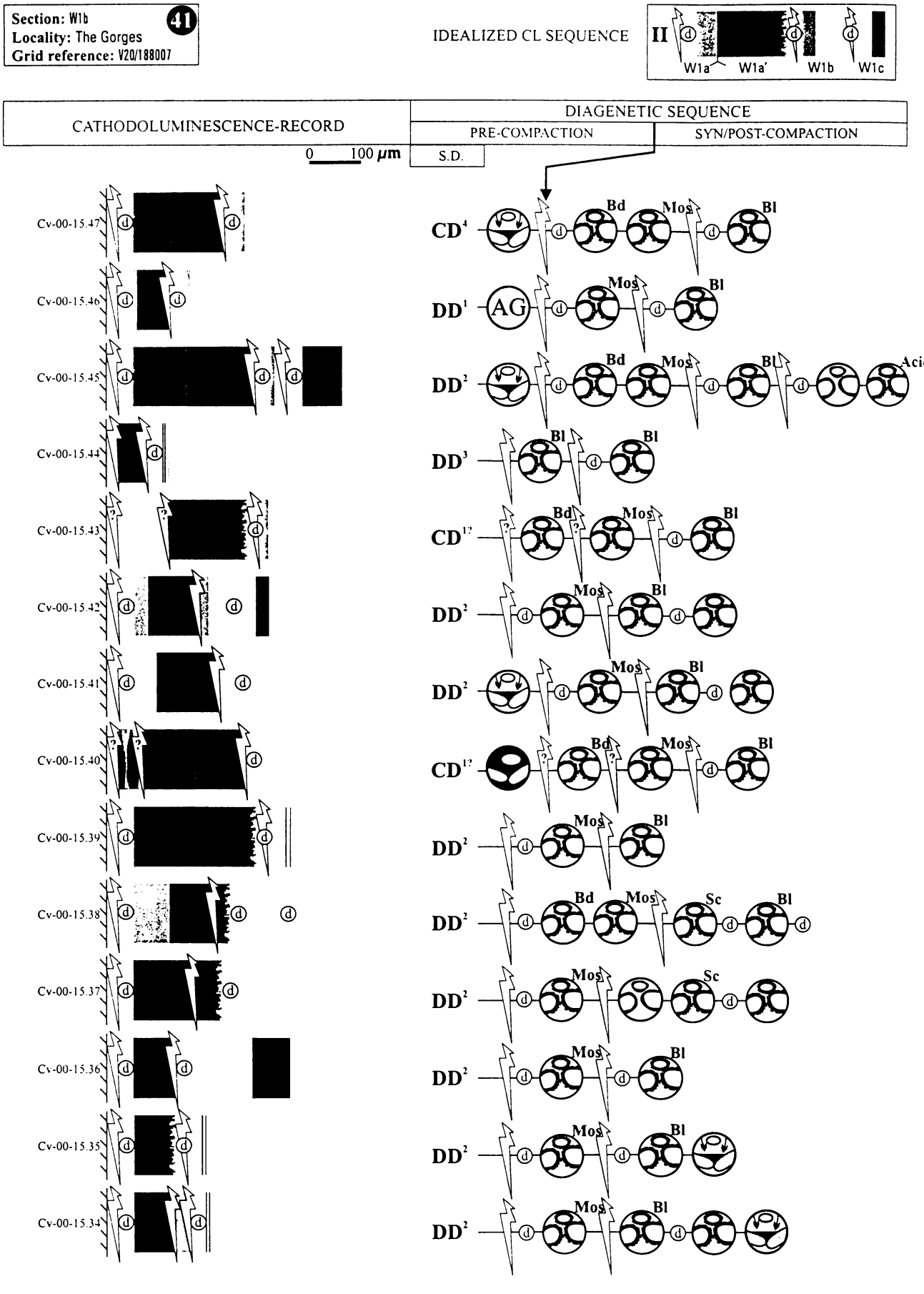
Section: W1b
41
Locality: The Gorges
Grid reference: V20/188007
IDEALIZED CL SEQUENCE
II
W1a
W1a'
W1b
W1c
CATHODOLUMINESCENCE-RECORD
DIAGENETIC SEQUENCE
PRE-COMPACTION
SYN/POST-COMPACTION
0 100 µm
S.D.
Cv-00-15.47
Cv-00-15.46
Cv-00-15.45
Cv-00-15.44
Cv-00-15.43
Cv-00-15.42
Cv-00-15.41
Cv-00-15.40
Cv-00-15.39
Cv-00-15.38
Cv-00-15.37
Cv-00-15.36
Cv-00-15.35
Cv-00-15.34
CD4
DD1
DD2
DD3
CD1?
DD2
DD2
CD1?
DD2
DD2
DD2
DD2
DD2
DD2
Bd
Mos
Bl
AG
Acic
Sc

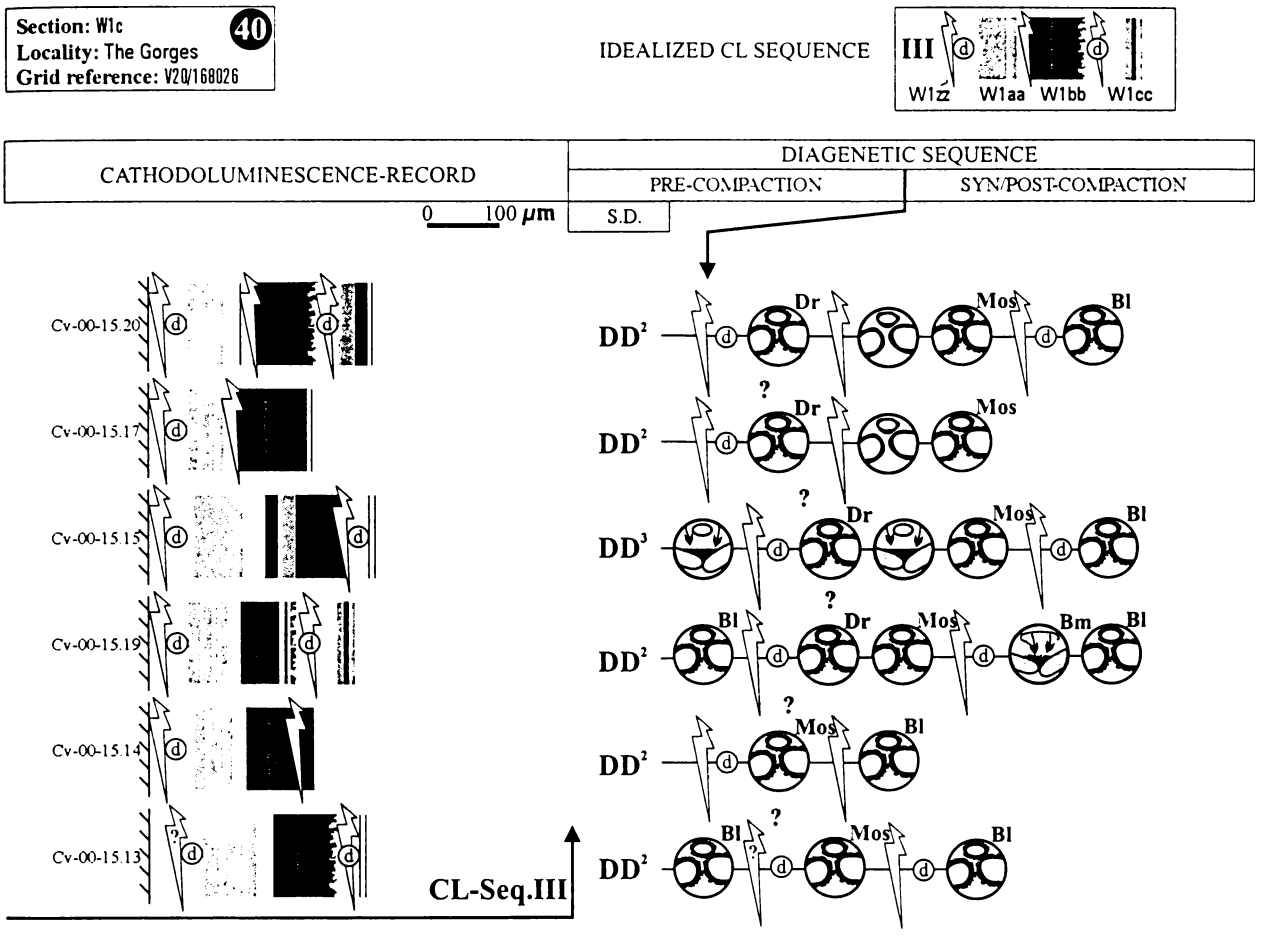
Section: W1c
Locality: The Gorges
Grid reference: V20/168026
40
IDEALIZED CL SEQUENCE
III
W1zz
W1aa
W1bb
W1cc
CATHODOLUMINESCENCE-RECORD
DIAGENETIC SEQUENCE
PRE-COMPACTION
SYN/POST-COMPACTION
0 100 µm
S.D.
Cv-00-15.20
Cv-00-15.17
Cv-00-15.15
Cv-00-15.19
Cv-00-15.14
Cv-00-15.13
CL-Seq.III
DD²
DD²
DD³
DD²
DD²
DD²
Dr
Mos
Bl
Bm

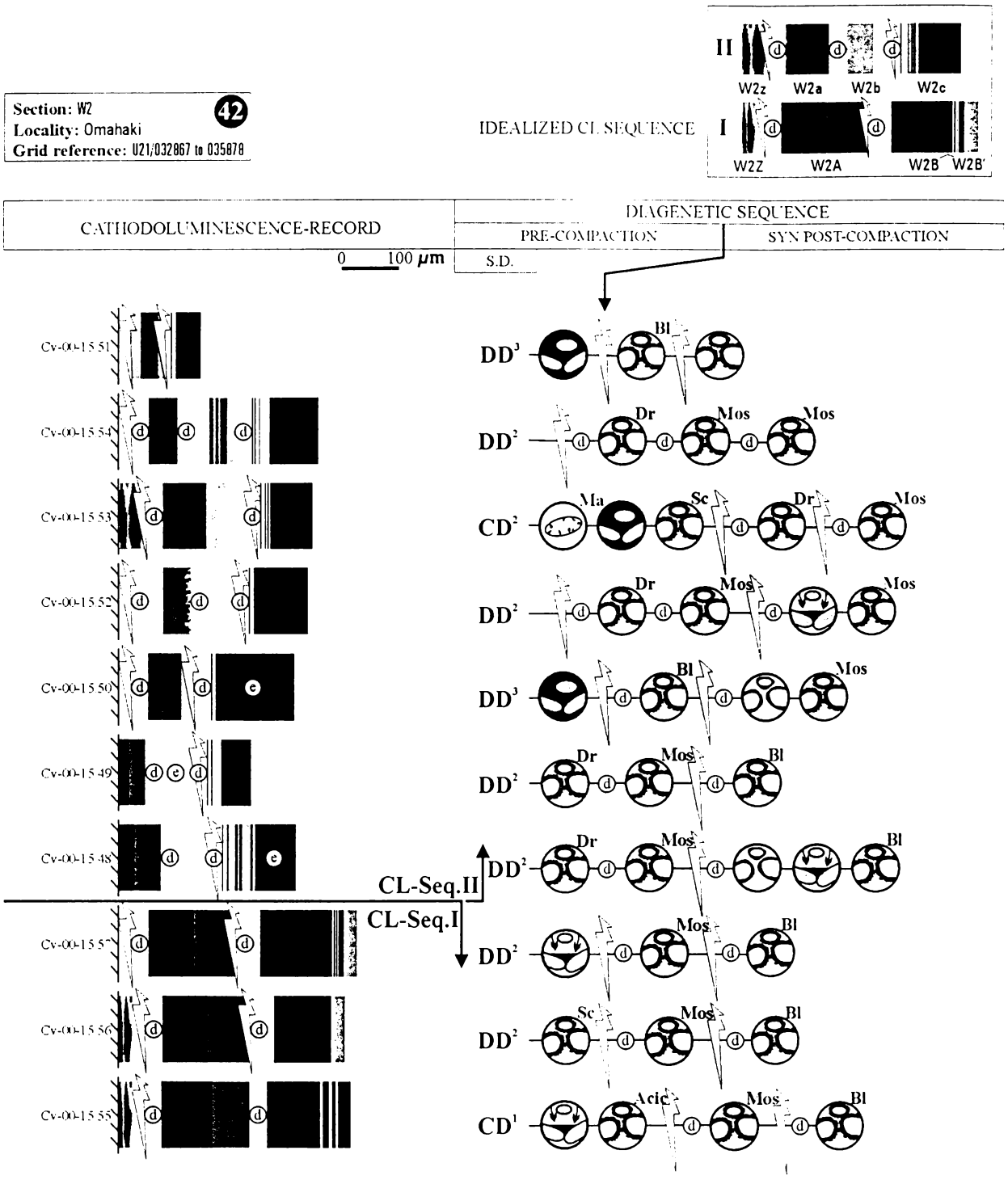
Section: W2
Locality: Omahaki
Grid reference: U21/032867 to 035878
42
IDEALIZED CL SEQUENCE
II
W2z
W2a
W2b
W2c
I
W2Z
W2A
W2B
W2B'
CATHODOLUMINESCENCE-RECORD
DIAGENETIC SEQUENCE
PRE-COMPACTION
SYN POST-COMPACTION
0 100 µm
S.D.
Cv-00-15 51
Cv-00-15 54
Cv-00-15 53
Cv-00-15 52
Cv-00-15 50
Cv-00-15 49
Cv-00-15 48
Cv-00-15 57
Cv-00-15 56
Cv-00-15 55
CL-Seq.II
CL-Seq.I
DD³
DD²
CD²
DD²
DD³
DD²
DD²
DD²
DD²
CD¹
Bl
Dr
Mos
Mos
Ma
Sc
Dr
Mos
Dr
Mos
Mos
Bl
Mos
Dr
Mos
Bl
Dr
Mos
Bl
Mos
Bl
Sc
Mos
Bl
Acic
Mos
Bl

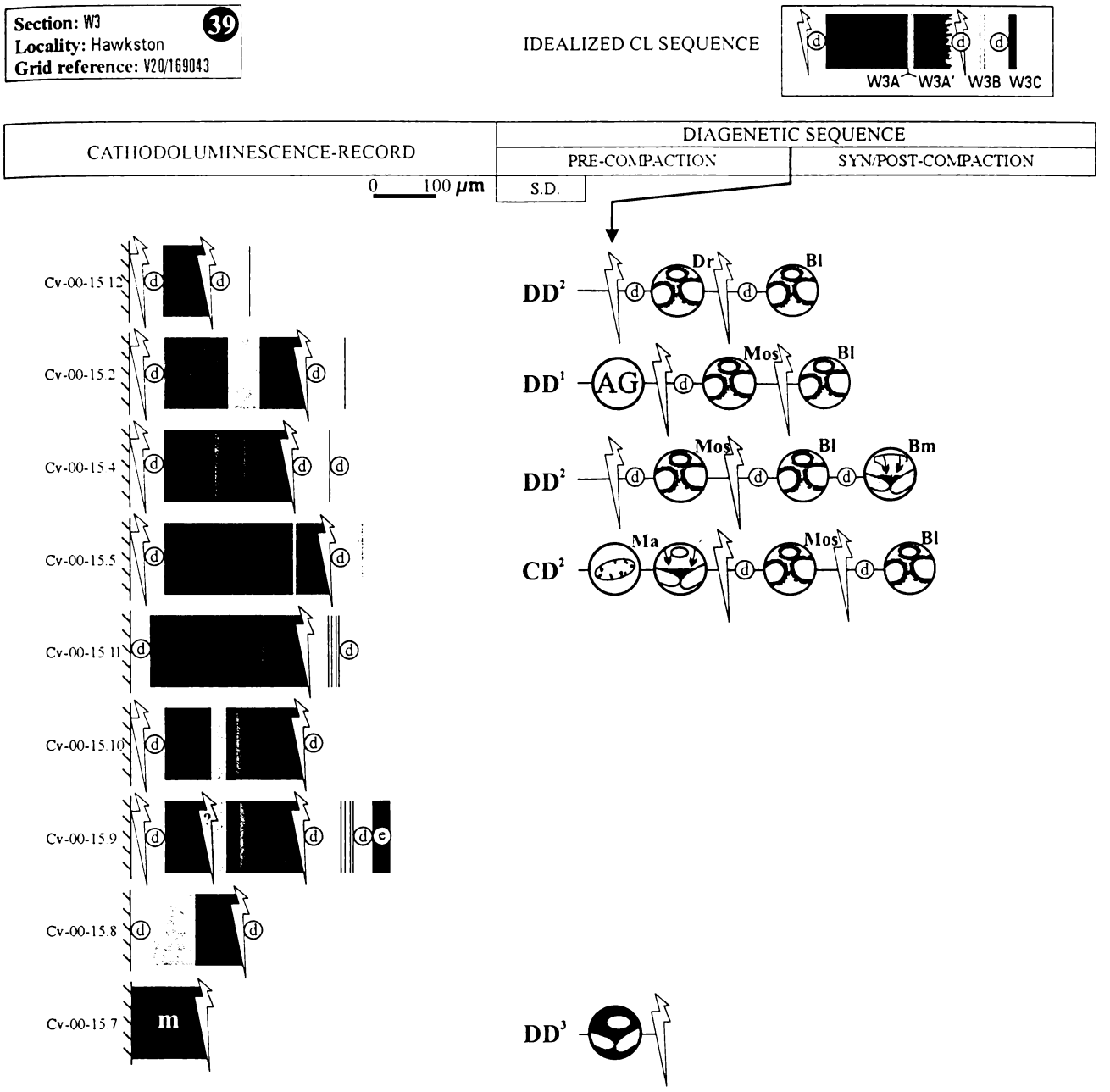
Section: W3
39
Locality: Hawkston
Grid reference: V20/169043
IDEALIZED CL SEQUENCE
W3A
W3A'
W3B
W3C
CATHODOLUMINESCENCE-RECORD
DIAGENETIC SEQUENCE
PRE-COMPACTION
SYN/POST-COMPACTION
0 100 µm
S.D.
Cv-00-15.12
Cv-00-15.2
Cv-00-15.4
Cv-00-15.5
Cv-00-15.11
Cv-00-15.10
Cv-00-15.9
Cv-00-15.8
Cv-00-15.7
m
DD²
Dr
Bl
DD¹
AG
Mos
Bl
DD²
Mos
Bl
Bm
CD²
Ma
Mos
Bl
DD³

Section: W4 (Te Waka Fm.) 38
Locality: Te Pohue
Grid reference: V20/275115

IDEALIZED CL SEQUENCE

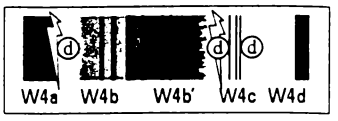

CATHODOLUMINESCENCE-RECORD

DIAGENETIC SEQUENCE

PRE-COMPACTION | SYN/POST-COMPACTION

0 100 µm

S.D.

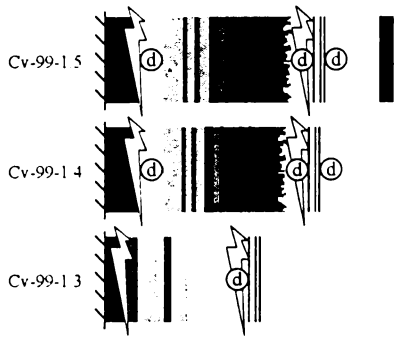

Section: W4 (Titiokura Fm.) 38
Locality: Te Pohue
Grid reference: V20/275115

IDEALIZED CL SEQUENCE

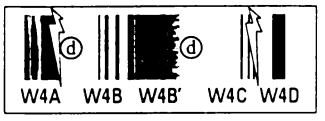

CATHODOLUMINESCENCE-RECORD

DIAGENETIC SEQUENCE

PRE-COMPACTION | SYN/POST-COMPACTION

0 100 µm

S.D.

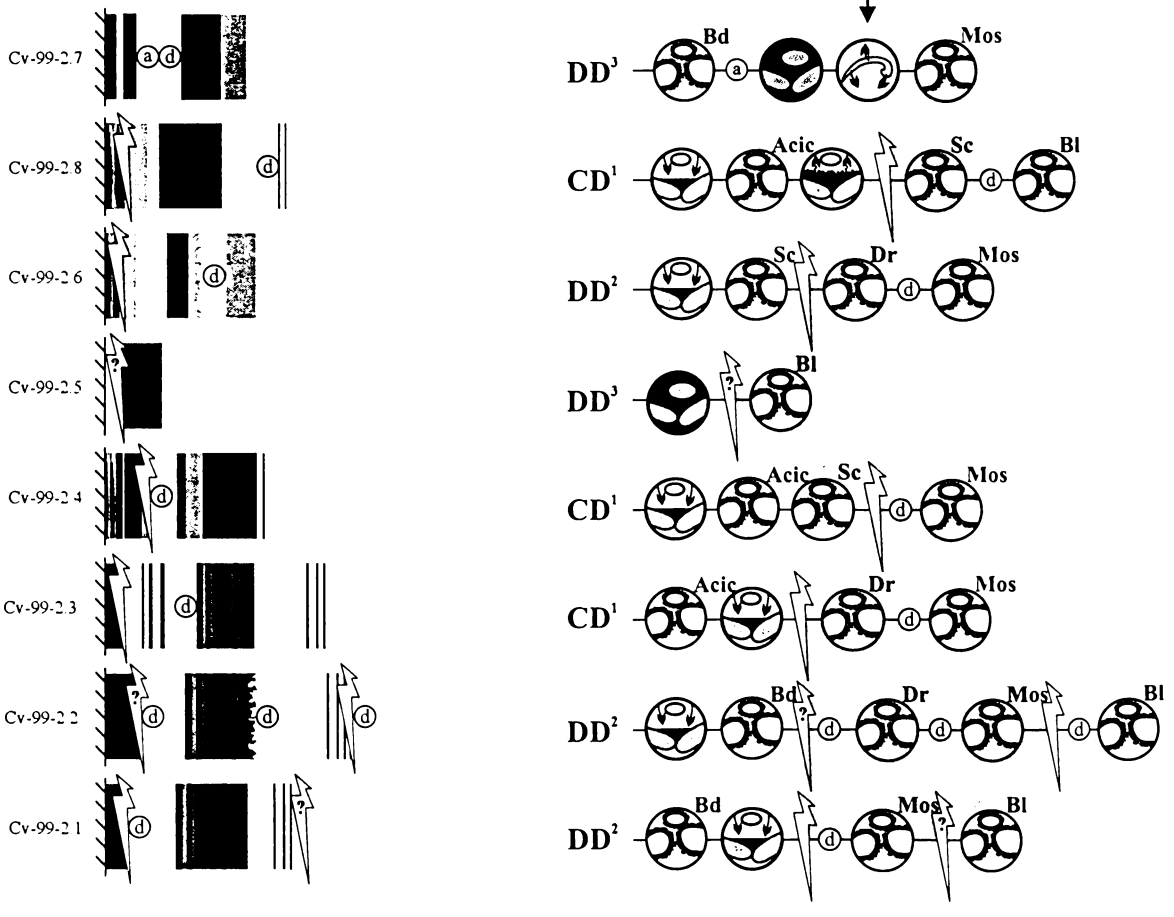

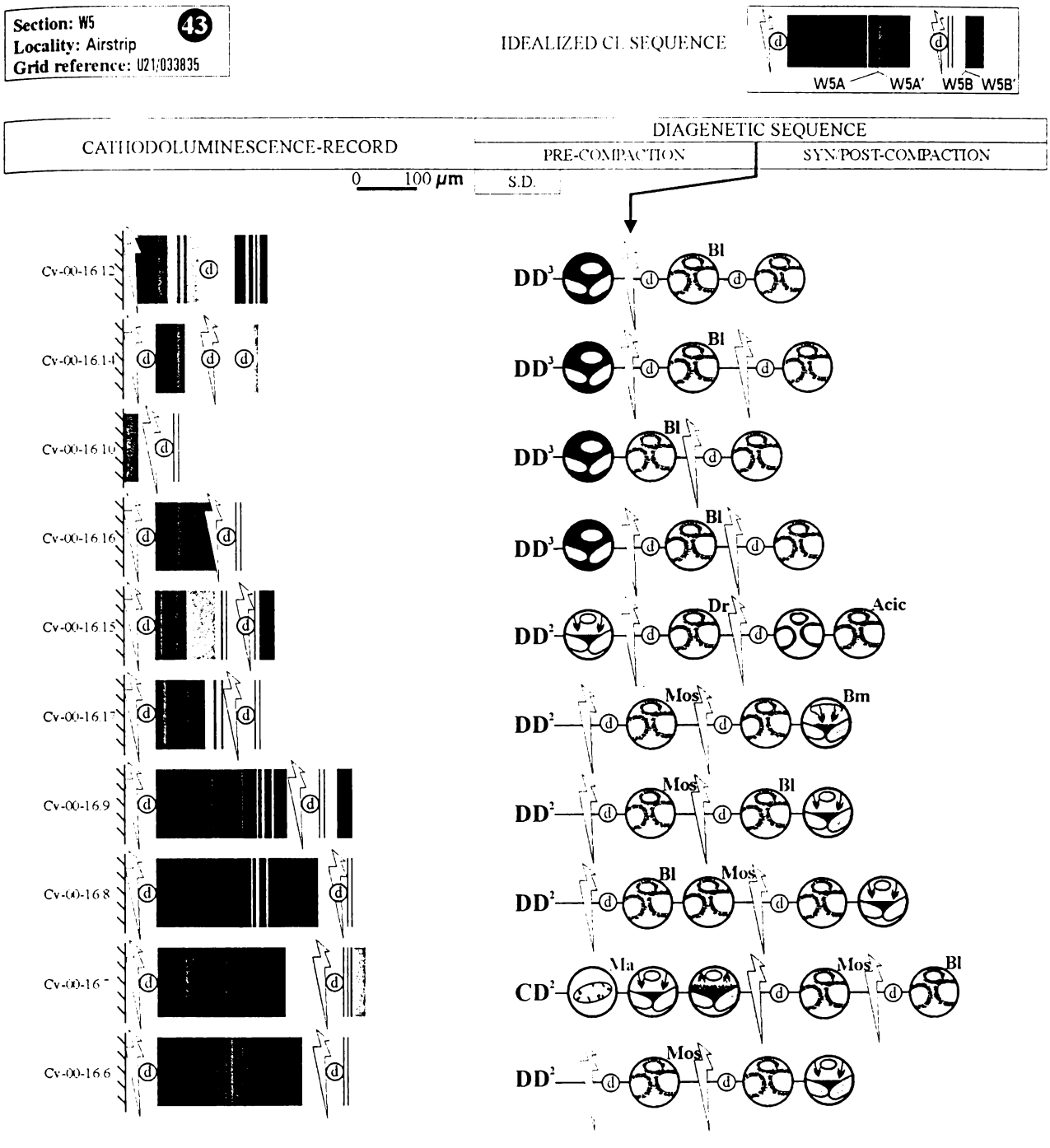
Section: W5
43
Locality: Airstrip
Grid reference: U21/033835
IDEALIZED CL SEQUENCE
W5A
W5A'
W5B
W5B'
CATHODOLUMINESCENCE-RECORD
DIAGENETIC SEQUENCE
PRE-COMPACTION
SYN/POST-COMPACTION
0 100 µm
S.D.
Cv-00-16 12
Cv-00-16 14
Cv-00-16 10
Cv-00-16 16
Cv-00-16 15
Cv-00-16 17
Cv-00-16 9
Cv-00-16 8
Cv-00-16 7
Cv-00-16 6
DD3
DD2
CD2
Bl
Dr
Acic
Mos
Bm
Ma

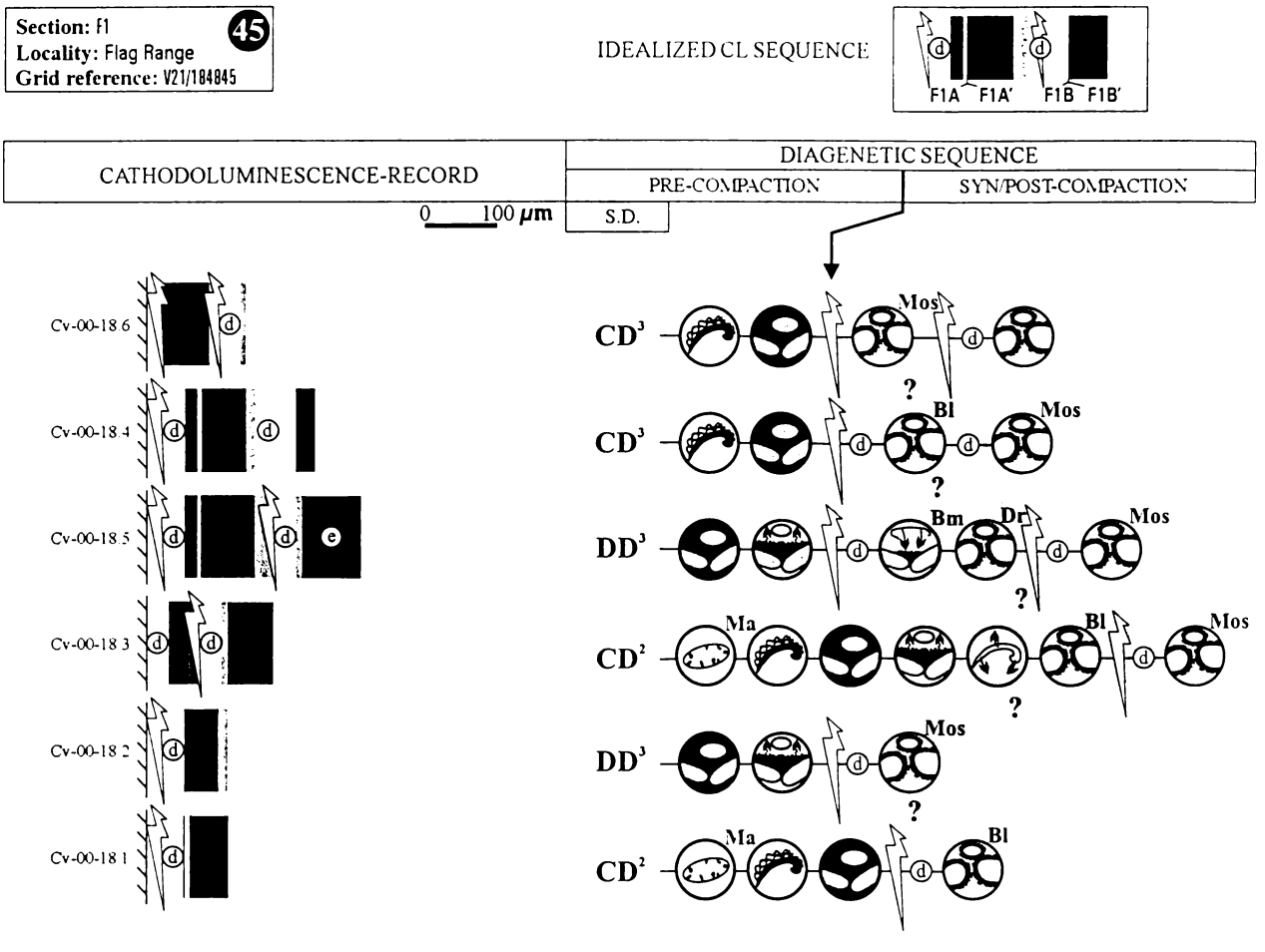
Section: f1
45
Locality: Flag Range
Grid reference: V21/184845
IDEALIZED CL SEQUENCE
d
d
F1A
F1A'
F1B
F1B'
CATHODOLUMINESCENCE-RECORD
DIAGENETIC SEQUENCE
PRE-COMPACTION
SYN/POST-COMPACTION
0 100 µm
S.D.
Cv-00-18 6
Cv-00-18 4
Cv-00-18 5
Cv-00-18 3
Cv-00-18 2
Cv-00-18 1
e
CD³
DD³
CD²
Mos
Bl
Bm
Dr
Ma
?

Section: Ke1 (Kereru Lst.) **46**
Locality: Glendale Farm
Grid reference: U21/964678

IDEALIZED CL SEQUENCE

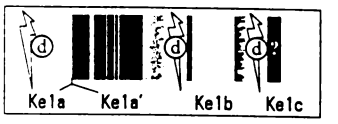

CATHODOLUMINESCENCE-RECORD

DIAGENETIC SEQUENCE

PRE-COMPACTION | SYN/POST-COMPACTION

0 100 µm

S.D.

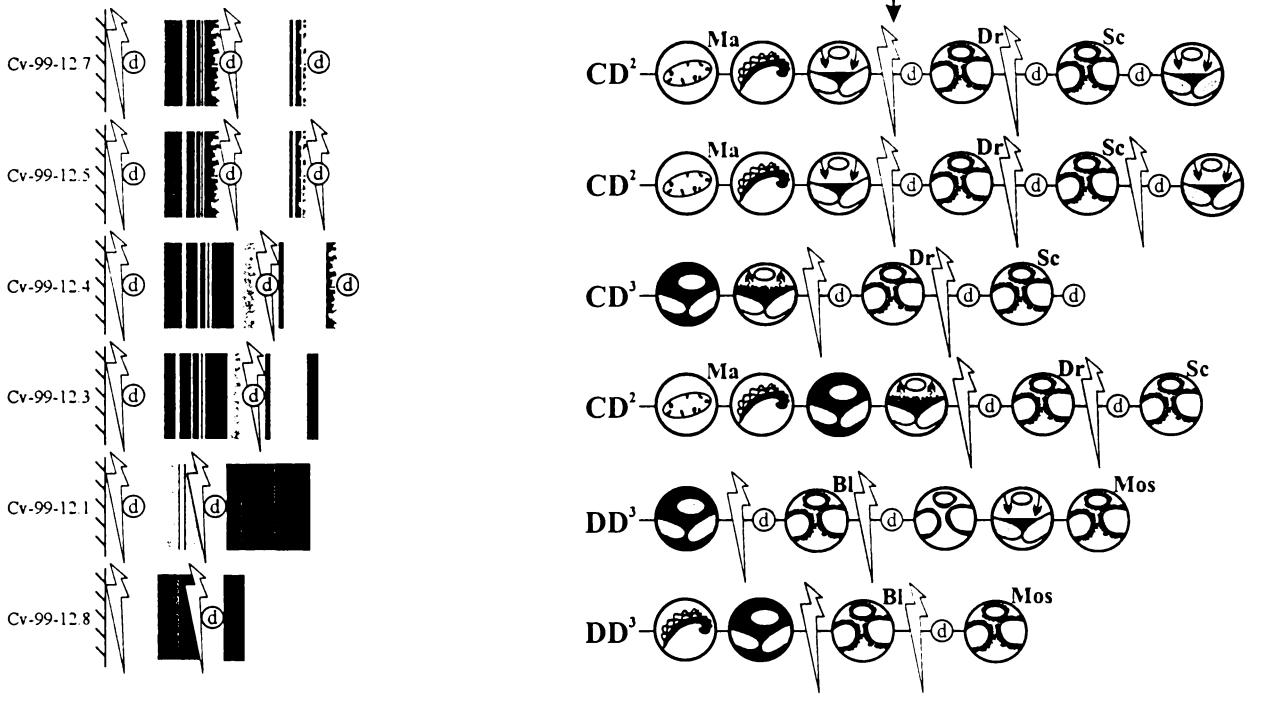

Section: Ke1 (Sentry Box Lst.) **47**
Locality: Jumped Up Stream
Grid reference: U21/934665

IDEALIZED CL SEQUENCE

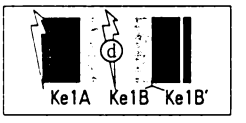

CATHODOLUMINESCENCE-RECORD

DIAGENETIC SEQUENCE

PRE-COMPACTION | SYN/POST-COMPACTION

0 100 µm

S.D.

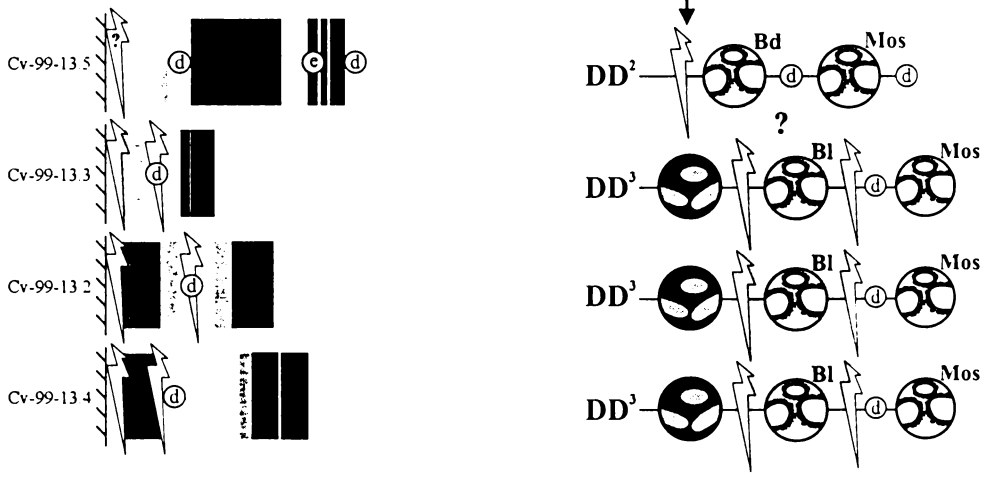

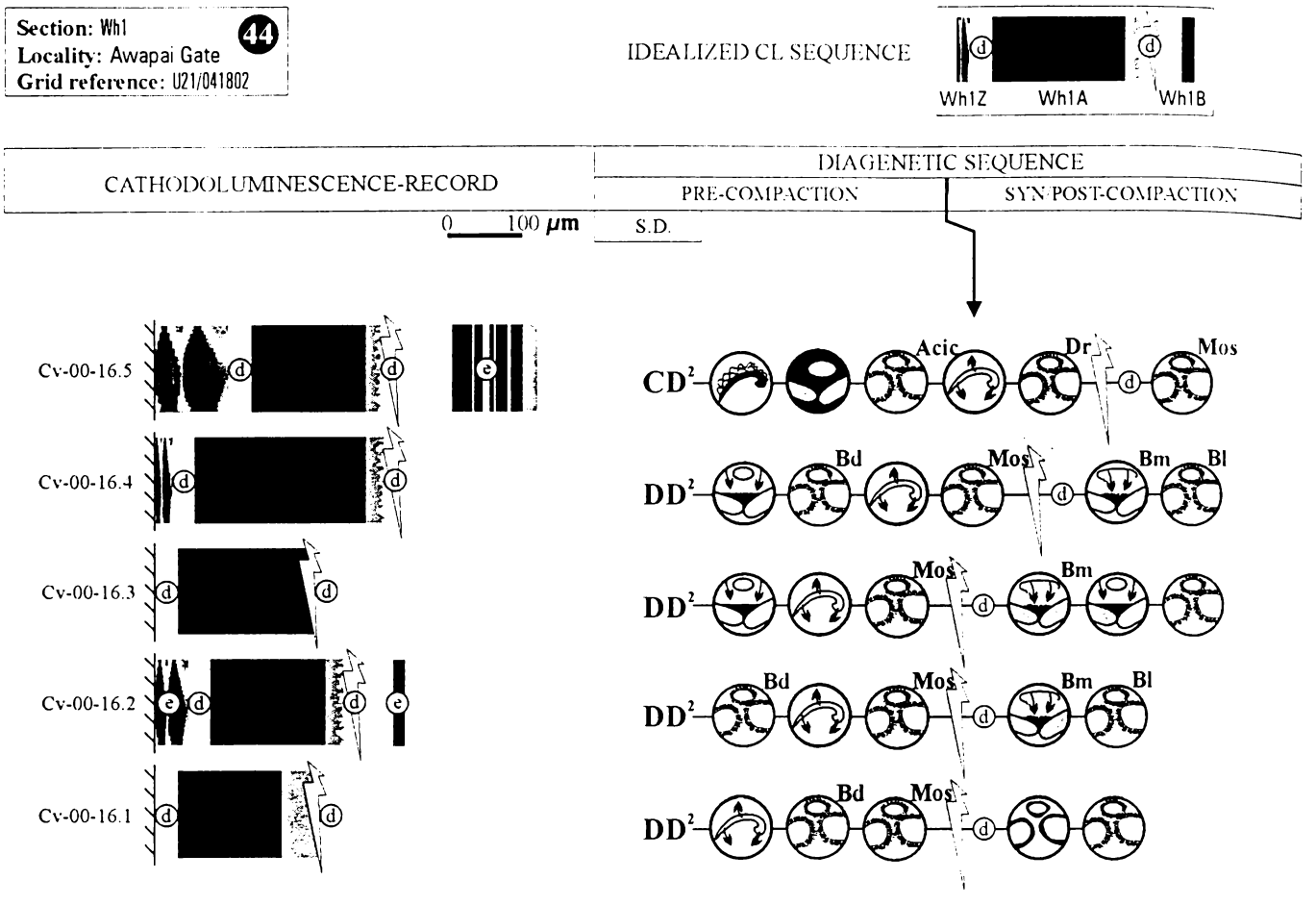
Section: Wh1
Locality: Awapai Gate
Grid reference: U21/041802
44
IDEALIZED CL SEQUENCE
Wh1Z
Wh1A
Wh1B
CATHODOLUMINESCENCE-RECORD
DIAGENETIC SEQUENCE
PRE-COMPACTION
SYN-POST-COMPACTION
0 100 µm
S.D.
Cv-00-16.5
Cv-00-16.4
Cv-00-16.3
Cv-00-16.2
Cv-00-16.1
CD²
DD²
DD²
DD²
DD²
Acic
Dr
Mos
Bd
Mos
Bm
Bl
Mos
Bm
Bd
Mos
Bm
Bl
Bd
Mos

APPENDIX 6

MICROPROBE SPOT ANALYSIS

APPENDIX 6 - MICROPROBE SPOT ANALYSIS

PrC = Pre-compaction clear spar cement (meteoric or mixed marine-meteoric in origin)
PoFC = Post-compaction ferroan cement (burial in origin)
YnfC = Youngest non-ferroan cement (telogenetic/meteoric in origin)

Values are given in wt%

Sample	PrC/SrO	PrC/MgO	PrC/MnO	PrC/FeO	PoFC/SrO	PoFC/MgO	PoFC/MnO	PoFC/FeO	YnfC/SrO	YnfC/MgO	YnfC/MnO	YnfC/FeO
4.22	0.016	0.745	0.007	0.066	0.1	0.26	0	0.35				
4.22	0.1	1.01	0.006	0.024	0.03	0.13	0.65	0.46				
4.22	0.11	1	0	0.212	0.04	0.08	0.01	0.27				
4.22	0.023	0.352	0.01	0.25								
4.22	0.1	0.312	0.02	0.15								
4.44	0.13	0.4	0.04	0.03								
4.36	0.016	0.7	0.02	0.07					0.04	0.37	0.03	0.08
4.36	0	0.47	0.01	0.01					0.24	0.35	0.02	0.12
4.36	0.03	0.3	0.03	0.1					0.02	0.15	0	0
4.36	0.01	0.15	0	0					0	0.17	0.04	0.08
4.36									0.03	0.06	0.03	0.09
4.36									0	0.04	0	0
4.36									0.04	0.23	0.002	0.06
4.36									0.04	0.32	0	0.22
4.36									0.07	0.05	0	0.22
4.36									0.04	0.05	0	0.32
4.36									0.03	0.2	0	0.12
4.36									0.45	0	0.002	0
4.36									0.01	0.12	0.01	0.14
4.68	0.15	0.72	0	0.37	0.56	0.33	0	0.2				
4.68	0.14	0.7	0.04	0.17	0.75	0.34	0.02	0.1				
4.68	0.13	0.5	0	0.12	0.94	0.11	0.03	0.04				
4.68	0.14	0.6	0.02	0.25	0.73	0.22	0.02	0.2				
4.68	0.08	0.78	0.02	0.32	0.22	0.58	0.03	0.31				
4.68	0.18	0.9	0.01	0.39	0.57	0.48	0.03	0.33				
4.68	0.1	0.82	0.02	0.34	1	0.06	0	0.12				
4.68	0.14	0.68	0	0.1	0.7	0.17	0.03	0.11				
4.68	0.22	0.77	0.02	0.4	0.1	0.7	0	0.29				
4.68	0.17	0.69	0	0.06	0.13	0.6	0.02	0.44				
4.68	0.1	0.78	0.05	0.08								
4.68	0.9	0.46	0.01	0.13								
4.68	0.5	0.6	0.03	0.25								
4.68	0.1	0.7	0.02	0.24								
4.105	0.06	0.33	0.045	0.17	2.03	0.3	0.025	0				
4.105	0.2	0.75	0.04	0.19	0.3	0.78	0.008	0.6				
4.105	0.25	0.94	0	0.43	0.2	0.7	0.05	0.15				
4.105	0.19	0.83	0.01	0.42	0.64	0.45	0	0.62				
4.105	0.16	0.51	0.015	0.12	0.1	0.4	0.008	1.25				
4.105	0.2	0.5	0.02	0.1	0.4	0.76	0.005	0.06				
4.105	0.21	0.46	0.03	0.02	0.3	0.94	0.02	0.15				
4.105	0.14	0.4	0	0.2								
4.105	0.54	0.64	0.03	0.23								
4.105	0.23	0.64	0.02	0.14								
4.105	0.16	0.46	0.01	0.11								
4.105	0.24	0.82	0	0.33								
4.6									0	0.2	0.02	0
4.6									0	0.2	0.02	0.08
4.6									0	0.2	0	0.11
4.6									0	0.1	0	0.07
4.6									0.02	0.1	0.01	0.07
4.6									0	0.1	0.03	0.05
4.6									0	0.2	0	0.21
4.6									0	0.2	0.01	0.15
4.6									0	0.2	0.02	0.15
4.6									0	0.1	0	0.05
4.6									0	0.2	0.05	0.23
4.6									0	0.1	0	0.1
4.6									0	0.1	0.03	0.15
4.6									0	0.1	0	0.2
4.6									0.02	0.1	0.02	0.21
4.6									0	0.2	0.02	0.11
5.28									0.0107	0.0943	0	0.0336
5.28									0.029	0.1245	0.0067	0.1058
5.28									0.0009	0.1049	0.0256	0.0393
5.28									0.0201	0.1323	0.0052	0
5.28									0	0.1459	0.0023	0
5.28									0.0191	0.1014	0.0059	0
5.28									0.0199	0.1508	0.0048	0
5.28									0.0053	0.2163	0.0129	0
5.28									0.0097	0.1622	0	0
5.28									0.0068	0.0462	0	0.0094
5.28									0.0399	0.0362	0.0119	0

APPENDIX 6 - MICROPROBE SPOT ANALYSIS

Sample	PrC/SrO	PrC/MgO	PrC/MnO	PrC/FeO	PoFC/SrO	PoFC/MgO	PoFC/MnO	PoFC/FeO	YnfC/SrO	YnfC/MgO	YnfC/MnO	YnfC/FeO
5.28									0	0.1002	0.0362	0.0013
5.28									0.0196	0.1361	0.0253	0
5.28									0	0.135	0	0
5.28									0.0101	0.1104	0.0237	0.0285
5.28									0.0074	0.137	0	0.0043
5.28									0	0.0795	0	0
5.28									0.0121	0.1025	0	0.0315
5.28									0.0076	0.1794	0	0
5.28									0.0058	0.0976	0	0.0014
5.28									0.019	0.1592	0.035	0
5.28									0.0172	0.2188	0.0139	0.0668
5.28									0	0.2427	0.0022	0
5.28									0	0.1488	0	0.0531
5.28									0.009	0.1391	0.0171	0.0139
5.28									0.0213	0.1327	0.0099	0.0343
5.28									0.0078	0.1409	0.0244	0.0023
5.28									0.013	0.1576	0	0.0659
5.28									0	0.1625	0.0089	0.0198
5.28									0	0.1294	0.0209	0.0387
5.28									0	0.0893	0.0087	0
5.28									0.0288	0.1092	0.0278	0.0675
5.28									0.0189	0.0951	0.0127	0.0795
5.28									0.0131	0.0785	0	0.0604
5.28									0.0153	0.1473	0	0.0676
5.46	0	0.2611	0.025	0.0973	0	0.2196	0.0095	0	0.0111	0.268	0	0.0941
5.46	0.0106	0.4743	0	0	0	0.3735	0.0079	0.0551	0	0.5593	0	0.0605
5.46					0.0127	0.3764	0.0242	0	0.0181	0.5234	0.0044	0.0569
5.46					0	0.4932	0.0411	0.2014	0	0.4019	0	0.0101
5.46					0	0.2825	0	0.1423	0	0.4252	0	0.1353
5.46									0.0092	0.5069	0.0195	0
5.46									0	0.459	0.0007	0
5.46									0.008	0.4631	0.0394	0
5.46									0	0.3748	0	0.0173
5.46									0.0073	0.4943	0	0.003
5.46									0.0039	0.4983	0	0
5.46									0	0.4775	0.0281	0.0163
5.46									0	0.3904	0.0162	0
5.46									0.0071	0.3805	0	0.0522
5.46									0	0.4931	0	0.1776
5.46									0.0092	0.3339	0	0
5.46									0.0058	0.4725	0.0016	0.009
5.46									0.0233	0.4646	0.015	0
5.46									0	0.419	0.0113	0.2034
5.46									0	0.2818	0.0088	0.1284
5.46									0.0057	0.4123	0.0293	0.0183
5.46									0	0.265	0	0.1873
5.46									0	0.2929	0	0.0791
5.46									0	0.2753	0	0.0777
5.44	0.003	0.1023	0	0.0105					0.015	0.0305	0.0055	0.0219
5.44	0.4965	0.1395	0.0147	0					0	0.1582	0.0126	0.0249
5.44	0	0.1212	0.0151	0.0325					0	0.1285	0.015	0.008
5.44									0.0146	0.1109	0	0
5.44									0	0.1298	0.0205	0
5.44									0.0081	0.0989	0.0029	0
5.44									0	0.1162	0	0
5.44									0.0156	0.1869	0.0232	0.0166
5.44									0	0.1034	0.0185	0
5.44									0	0.1797	0.0277	0
5.44									0.0078	0.1805	0.0106	0
5.44									0	0.2264	0.0238	0
5.44									0.0081	0.1098	0	0.0331
5.44									0	0.197	0.0485	0.03
5.44									0.0042	0.1021	0.0248	0
5.44									0.0225	0.1311	0.0079	0
5.44									0.0063	0.0849	0	0.0652
5.44									0	0.0531	0.0147	0.061
5.44									0.003	0.0603	0	0.0884
5.44									0.0036	0.0427	0.0038	0
5.44									0.0113	0.0367	0	0.0762
5.44									0.0092	0.0536	0.03	0

APPENDIX 6 - MICROPROBE SPOT ANALYSIS

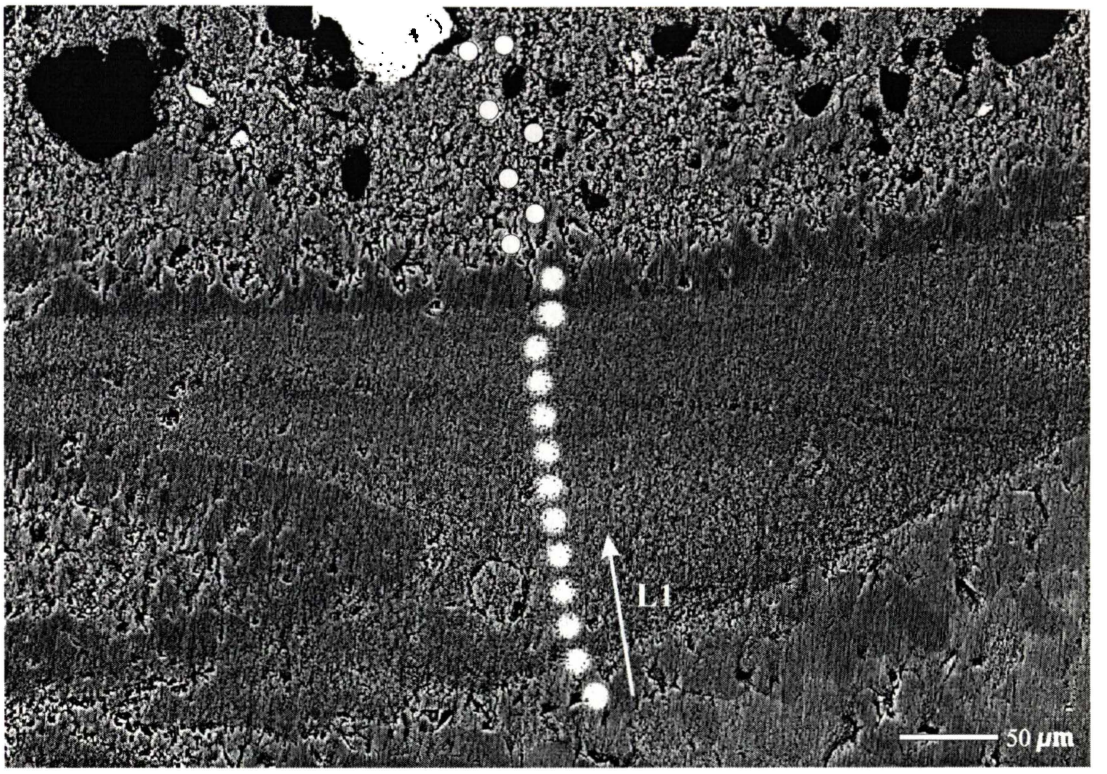

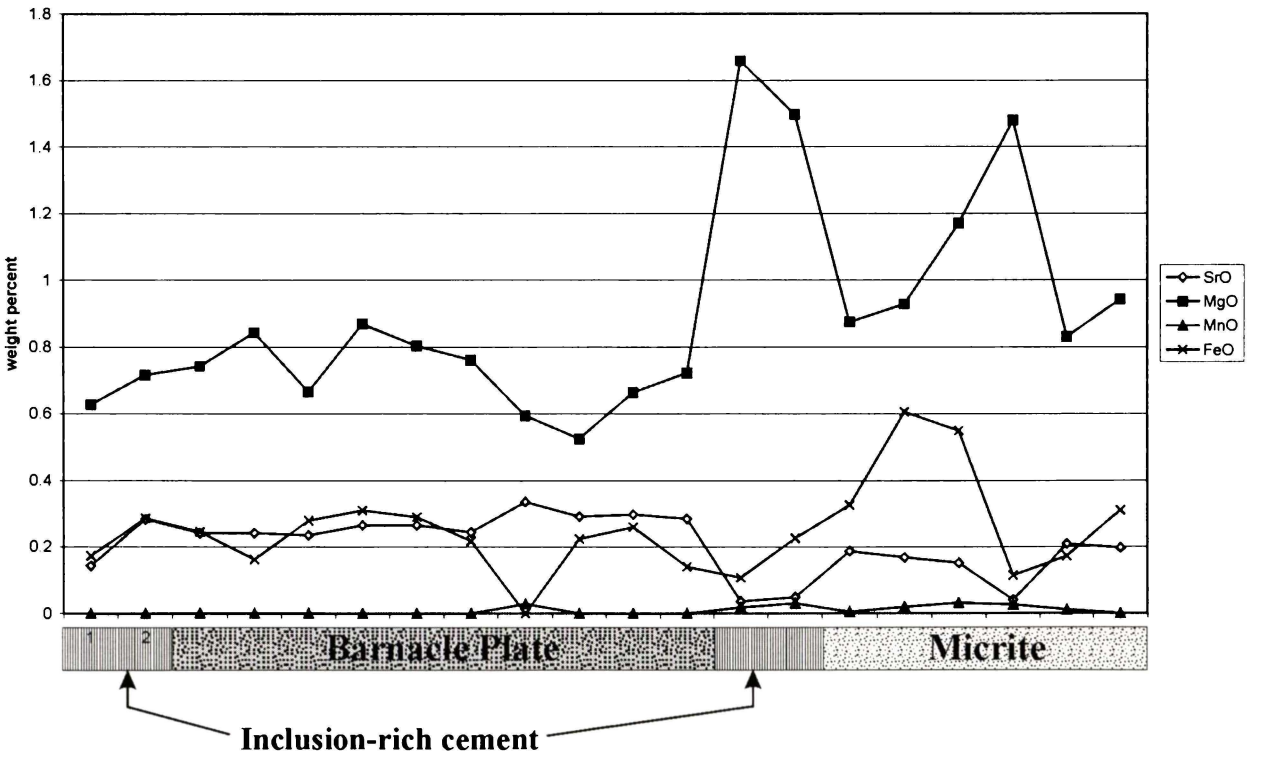

Sample: 4.127
Location: Cabbage Tree Flat
Stratigraphy: Sequence A1 of Kairakau Limestone
Age: Opoitian

APPENDIX 6 -MICROPROBE SPOT ANALYSIS

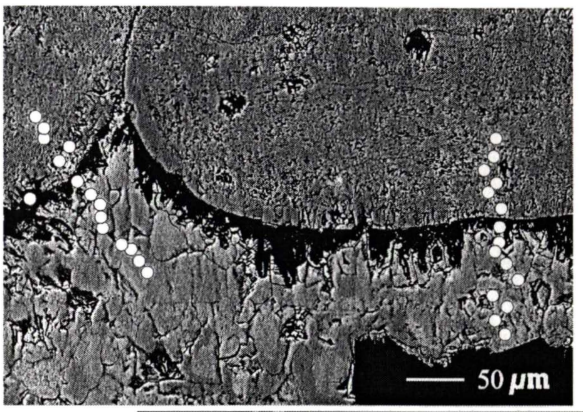

Sample: 4.105
Location: Koanui
Stratigraphy: Base of sequence C1 of Kairakau Limestone
Age: Opoitian

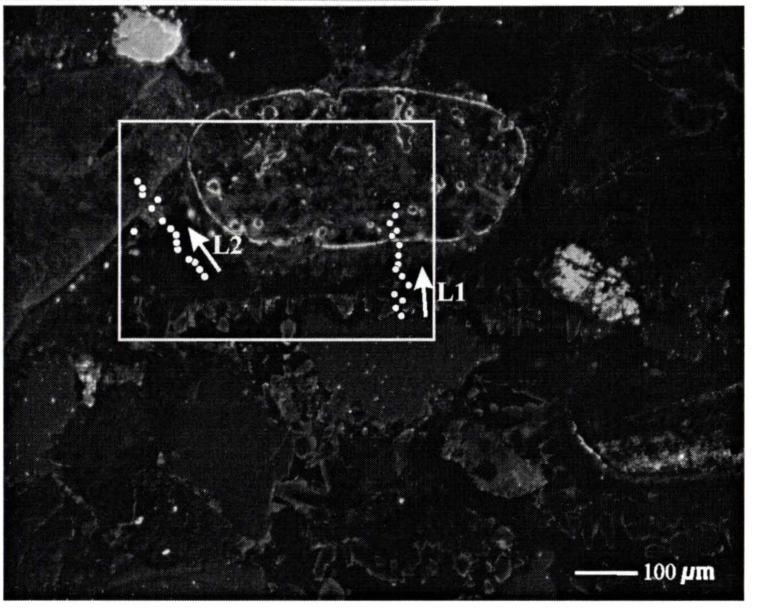

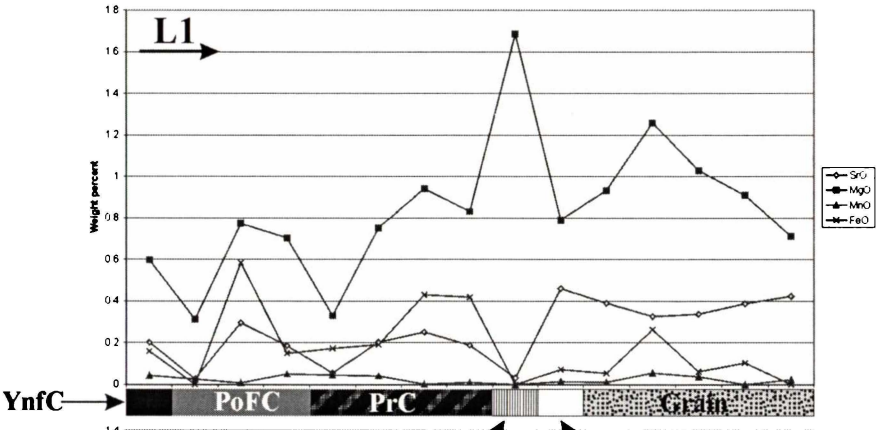

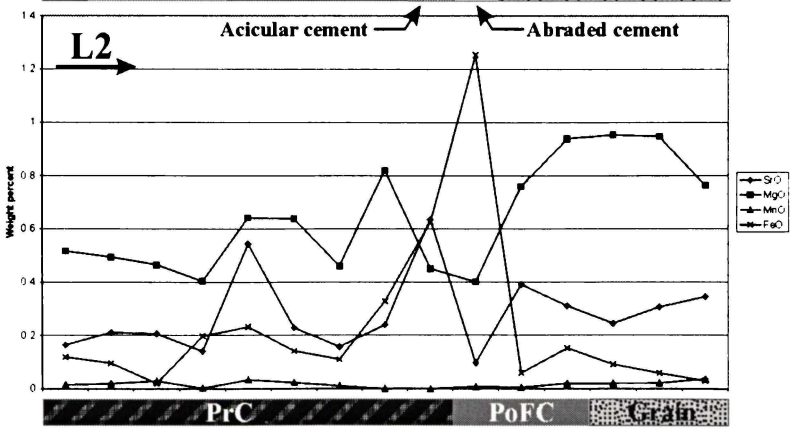

APPENDIX 6 - MICROPROBE SPOT ANALYSIS

Sample: 4.36
Location: North Mount Kahuranaki
Stratigraphy: Sequence A2 of Kairakau Limestone
Age: Opoitian

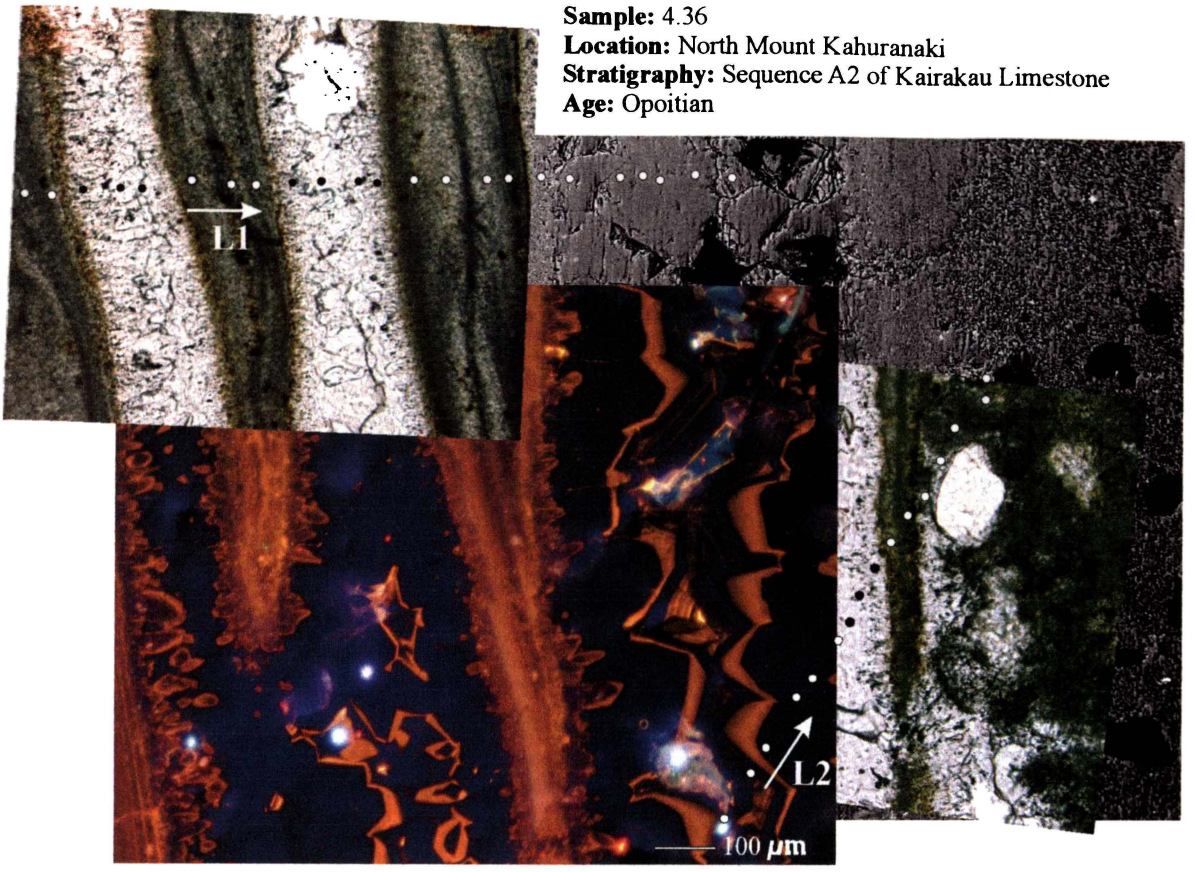

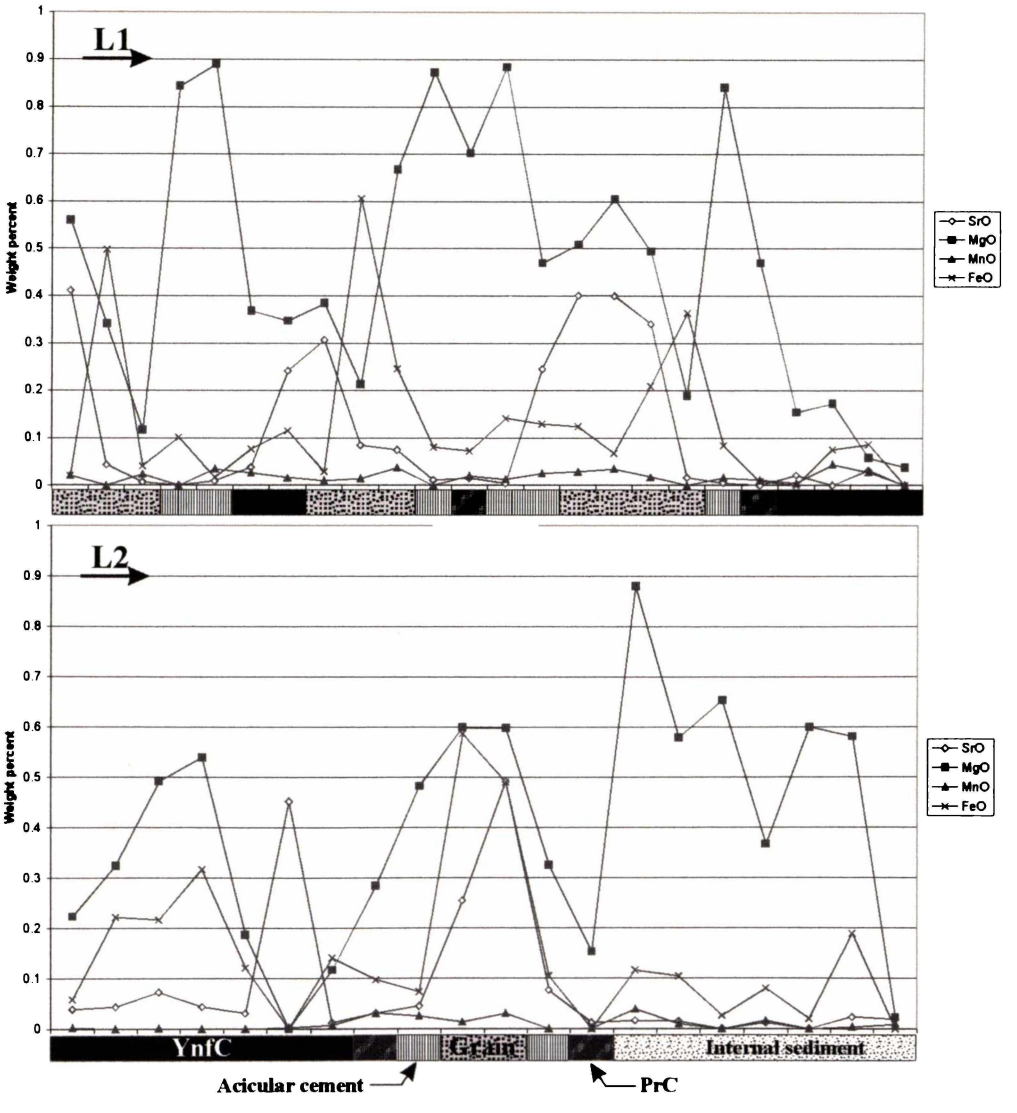

APPENDIX 6 - MICROPROBE SPOT ANALYSIS

Sample: 4.44
Location: Waimarama
Stratigraphy: Sequence B of Kairakau Limestone
Age: Opoitian

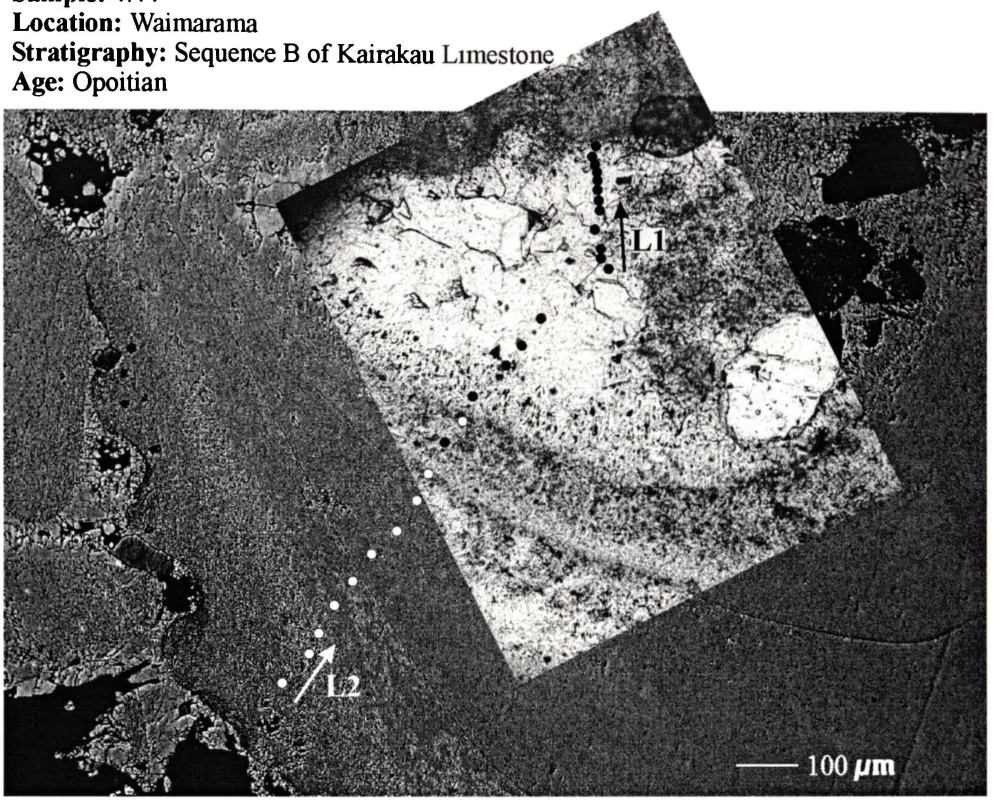

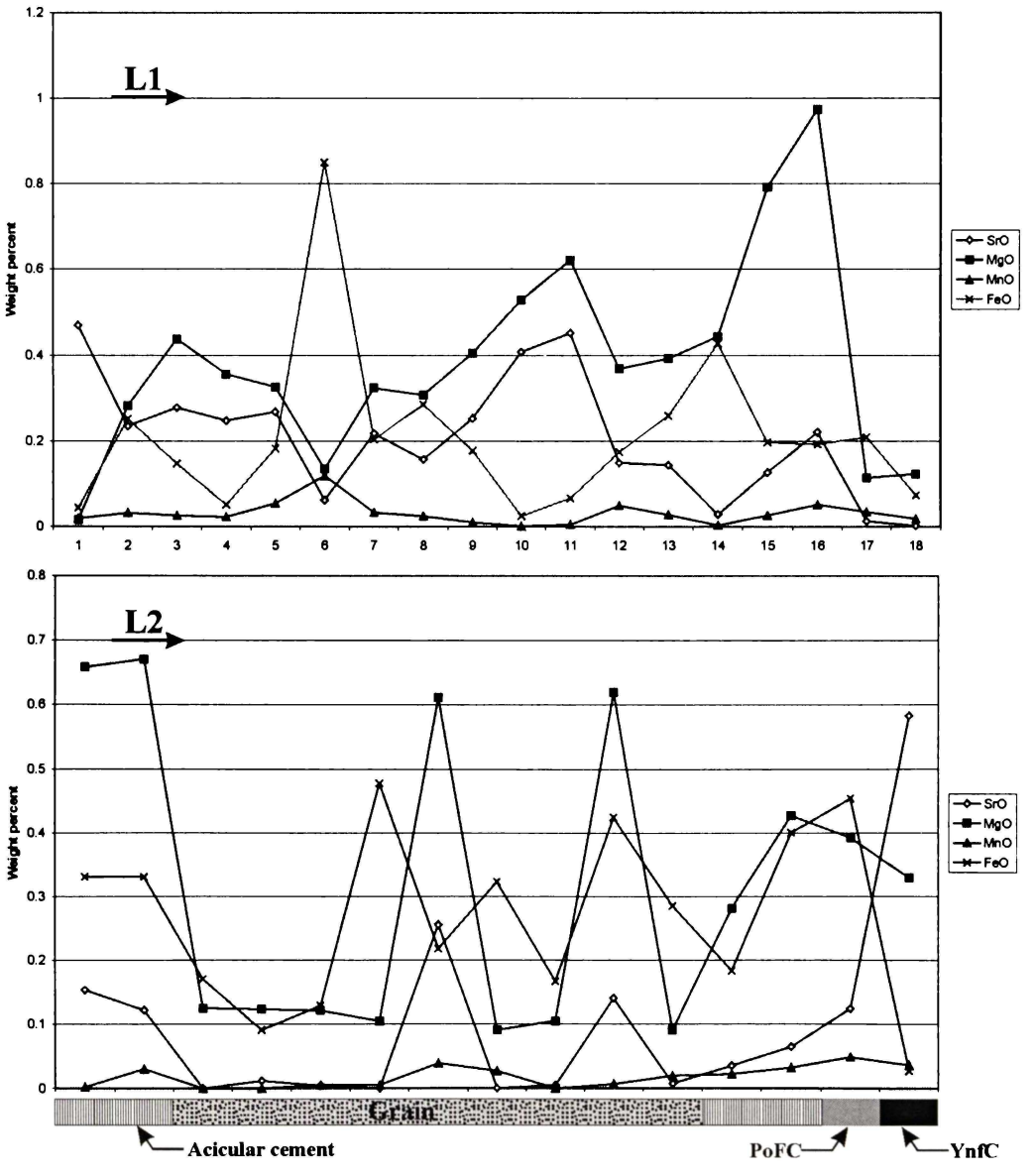

APPENDIX 6 - MICROPROBE SPOT ANALYSIS

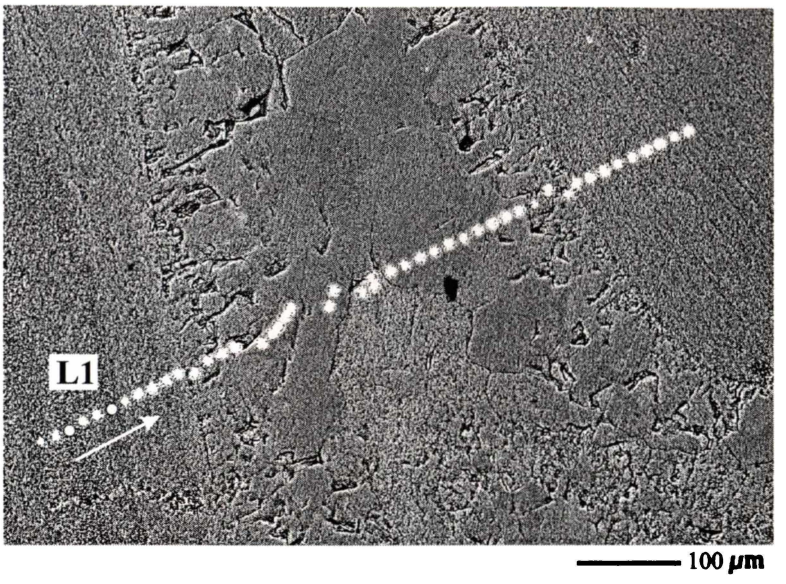

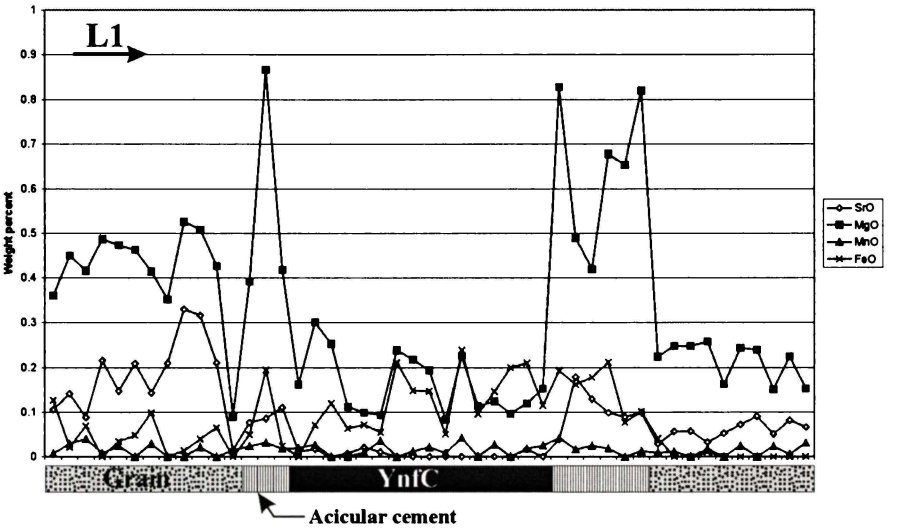

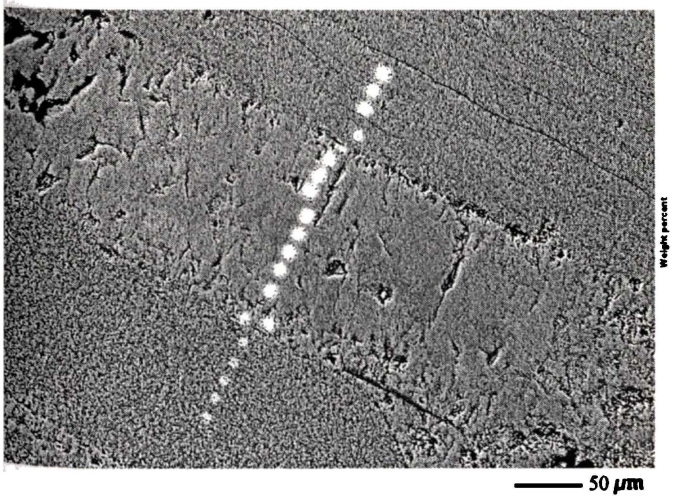

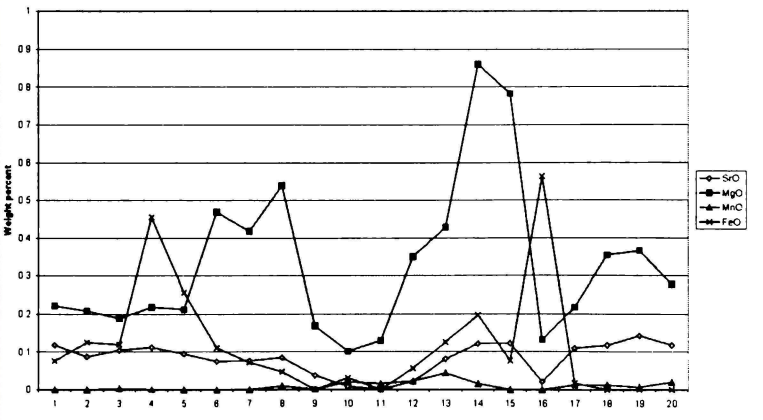

Sample: 4.6
Location: North Mount Kahuranaki
Stratigraphy: Sequence C2 of Kairakau Limestone
Age: Opoitian

APPENDIX 6 - MICROPROBE SPOT ANALYSIS

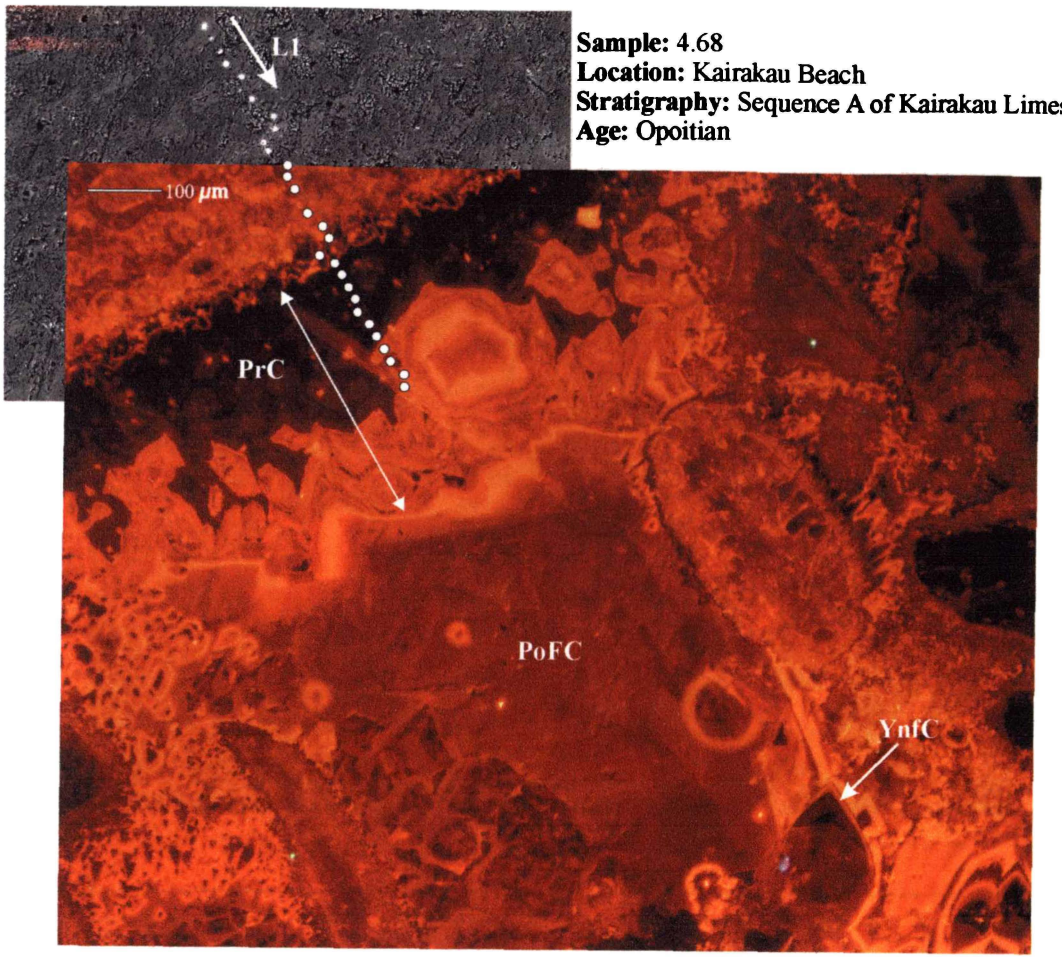

Sample: 4.68
Location: Kairakau Beach
Stratigraphy: Sequence A of Kairakau Limestone
Age: Opoitian

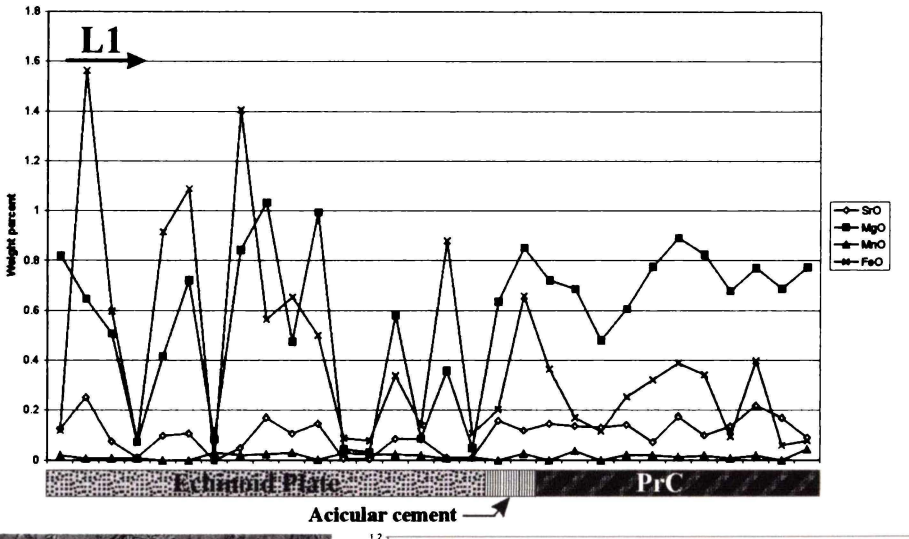

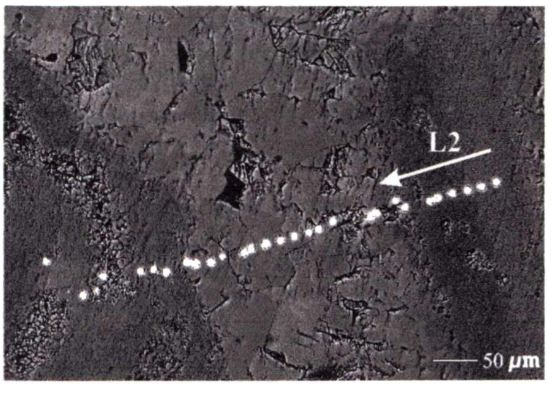

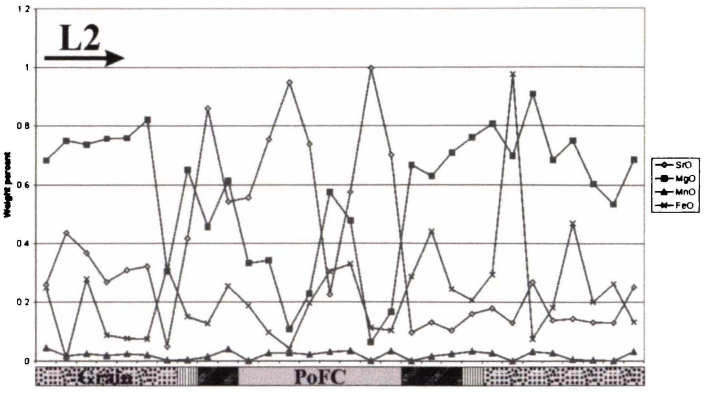

APPENDIX 6 -MICROPROBE SPOT ANALYSIS

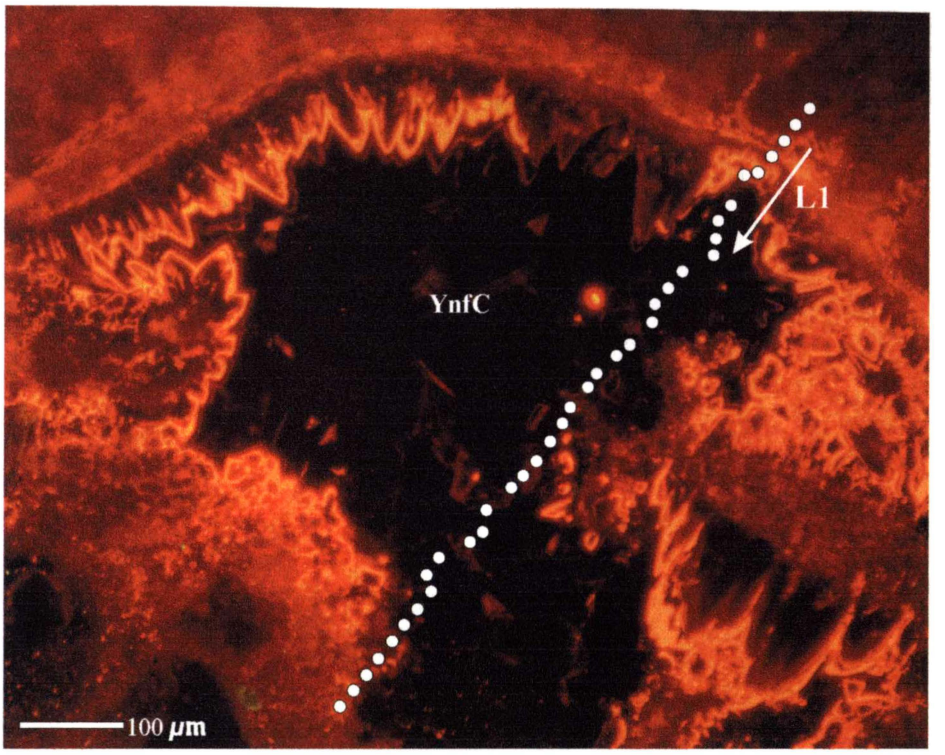

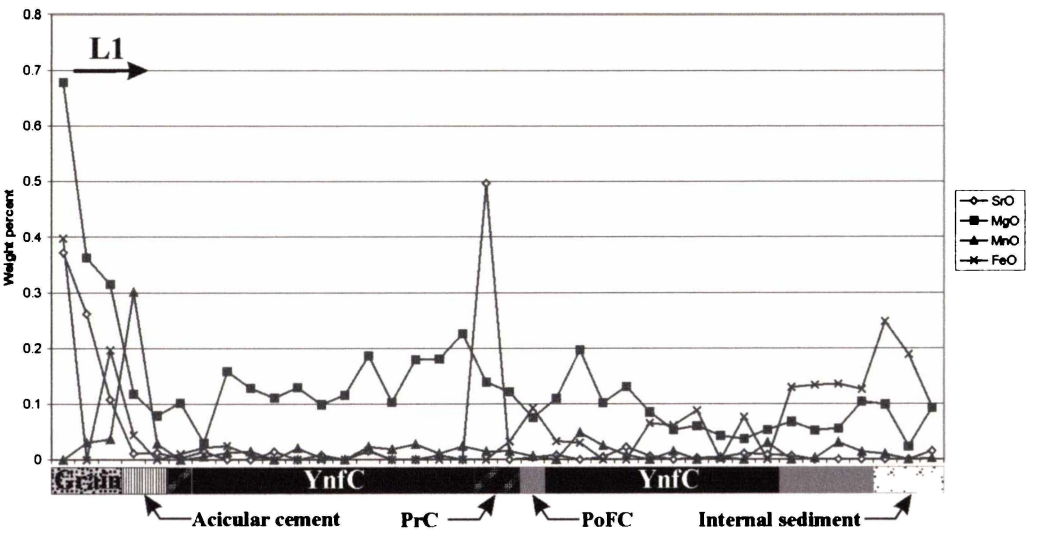

Sample: 5.44
Location: Te Mata Peak
Stratigraphy: Sequence C of Awapapa Limestone
Age: Waipipian

APPENDIX 6 -MICROPROBE SPOT ANALYSIS

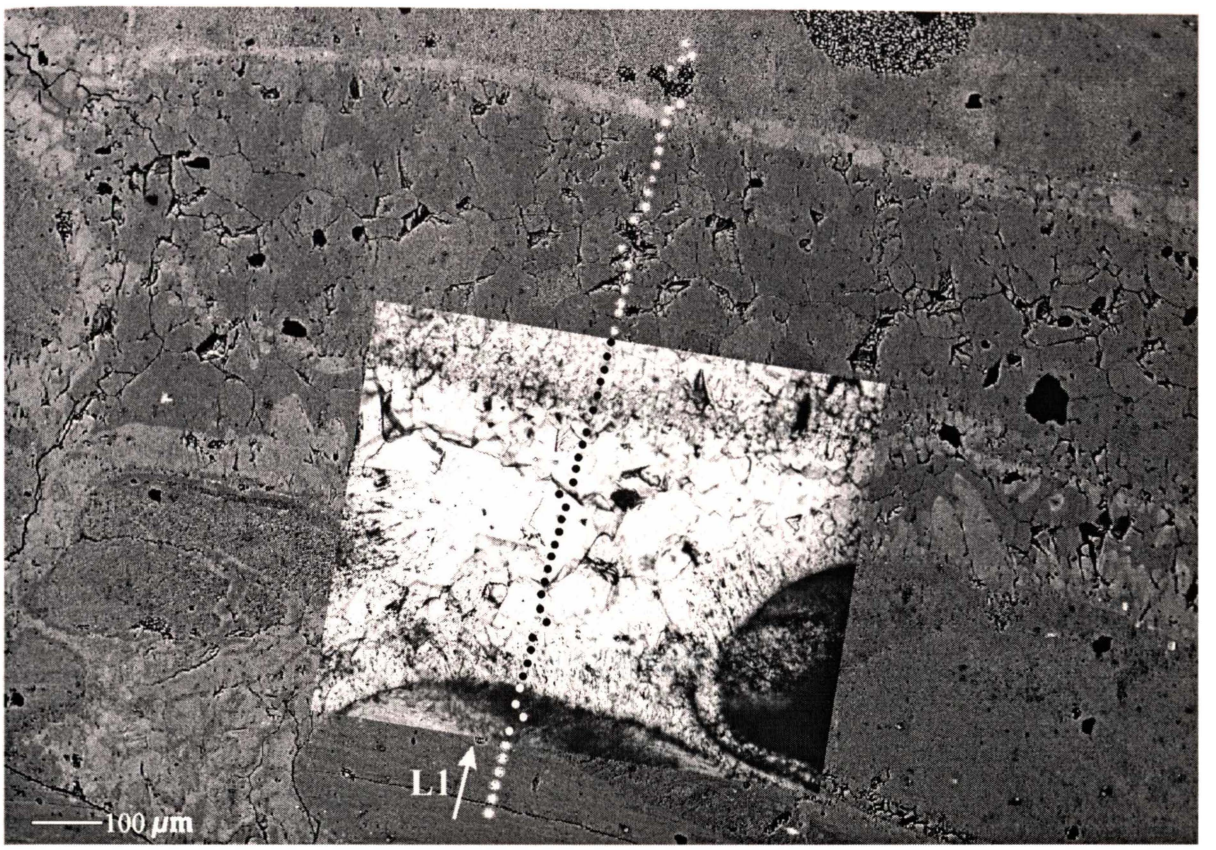

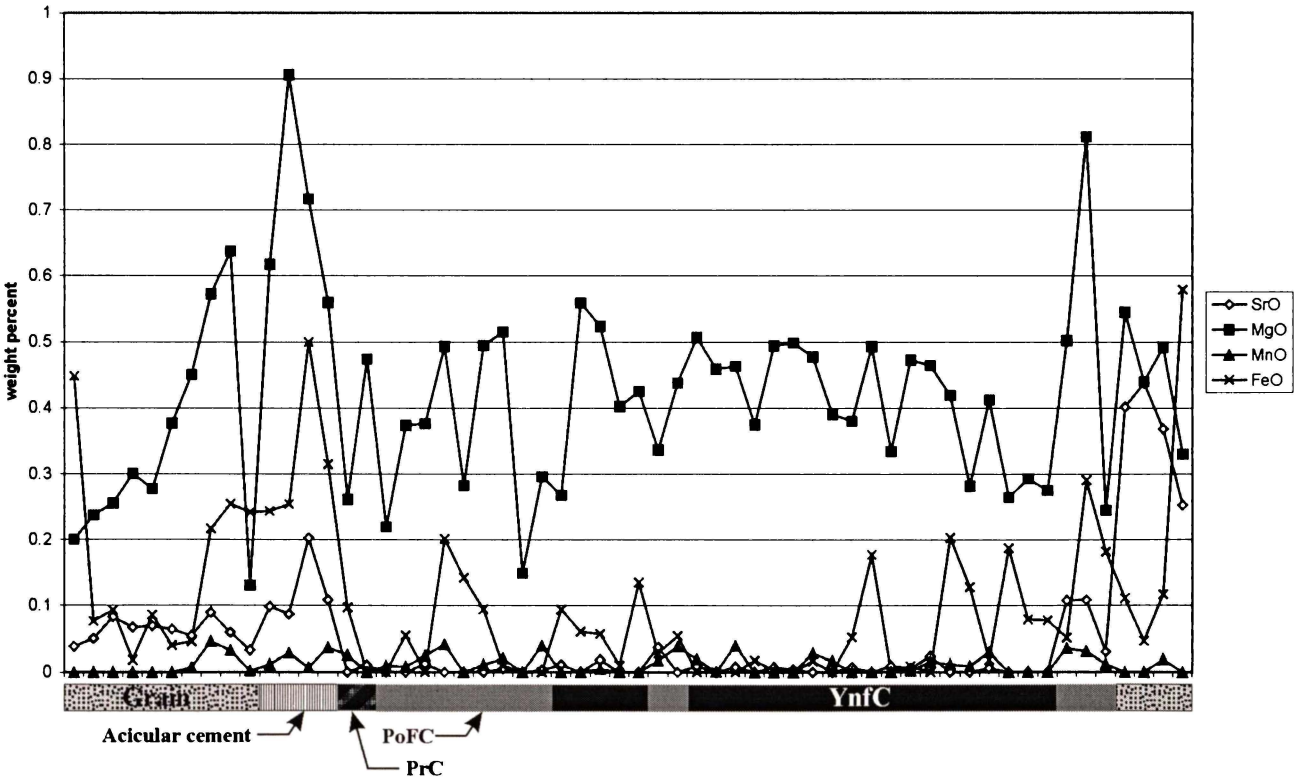

Sample: 5.46
Location: Te Mata Peak
Stratigraphy: Sequence D of Awapapa Limestone
Age: Waipipian

APPENDIX 7

STABLE ISOTOPES

APPENDIX 7 - STABLE ISOTOPES

Sample	Type	δ13C	error	δ18O	error	Age
cv-4.126	bulk	1.13	0.03	-0.30	0.06	Wo
cv-4.133	bulk	1.05	0.03	-0.23	0.06	Wo
cv-5.120	bulk	-1.35	0.03	-1.73	0.06	Wp
cv-5.34	bulk	-2.70	0.03	-2.60	0.06	Wp
cv-5.89	bulk	-2.10	0.01	-3.61	0.02	Wp
cv-5.128	bulk	-1.25	0.01	-1.71	0.01	Wp
cv-5.44	bulk	-1.61	0.02	-1.63	0.01	Wp
cv-9.101	bulk	-4.69	0.01	-2.77	0.01	Wm
cv-5.97	bulk	0.17	0.02	-3.09	0.01	Wp
cv-5.46	bulk	-0.59	0.02	-1.35	0.03	Wp
cv-7.15	bulk	-0.31	0.03	-1.13	0.06	Wp
cv-7.47	bulk	0.23	0.01	-0.07	0.02	Wp
cv-7.20	bulk	-0.92	0.01	-2.30	0.02	Wp
cv-11.35	bulk	-0.66	0.01	-1.13	0.02	Wn
cv-5.45a	bulk	-1.70	0.02	-0.40	0.01	Wp
cv-7.40	bulk	-0.65	0.01	-0.73	0.02	Wp
cv-9.85	bulk	-1.18	0.01	-2.19	0.02	Wm
cv-5.25	bulk	-1.4	0.10	-1.3	0.10	Wp
cv-5.142	bulk	-1.2	0.10	-0.9	0.10	Wp
cv-4.109	bulk	0.7	0.10	-1	0.10	Wo
cv-2.2	bulk	0.5	0.10	-0.4	0.10	Wo
cv-9.64	bulk	0.1	0.10	-1.1	0.10	Wm
cv-11.37	bulk	-1.5	0.10	-3.2	0.10	Wn
cv-11.44	bulk	-1	0.10	-2.8	0.10	Wn
cv-11.85	bulk	-2.6	0.10	-4.3	0.10	Wn
cv-6.6	bulk	-32.9	0.10	1	0.10	Wn
cv-14.14	bulk	-2.3	0.10	-3.9	0.10	Wn
cv-5.75	bulk	-3.2	0.10	-3	0.10	Wp
cv-4.66	bulk	-0.1	0.10	-0.4	0.10	Wo
cv-4.133	bulk	1	0.10	-0.7	0.10	Wo
cv-9.4	bulk	-4.7	0.10	-2.1	0.10	Wm
cv-11.26	bulk	0.8	0.10	0.1	0.10	Wn
cv-11.40	bulk	-0.2	0.10	-1.3	0.10	Wn
cv-11.90	bulk	-1.2	0.10	-4.8	0.10	Wn
cv-11.81	bulk	-3.2	0.10	-4.2	0.10	Wn
cv-15.45	bulk	1.1	0.10	-1.8	0.10	Wp-m
cv-5.120	bulk	-1.5	0.10	-2.1	0.10	Wp
cv-4.35	bulk	-1.4	0.10	-3.1	0.10	Wo
cv-7.15	bulk	-0.3	0.10	-1.3	0.10	Wp
cv-9.97	bulk	-4.9	0.10	-4.5	0.10	Wm
cv-11.29	bulk	0.3	0.10	-1.7	0.10	Wn
cv-11.42	bulk	-1.2	0.10	-3.2	0.10	Wn
cv-11.88	bulk	-1.6	0.10	-4.1	0.10	Wn
cv-15.40	bulk	1	0.10	-0.9	0.10	Wp-m
cv-15.56	bulk	-2.2	0.10	-3.7	0.10	Wp-m

APPENDIX 7 - STABLE ISOTOPES

Sample	Type	δ13C	error	δ18O	error	Age
cv-15.34	bulk	0.9	0.10	-0.9	0.10	Wp-m
cv-15.31	bulk	0.6	0.10	-2.2	0.10	Wp-m
cv-4.5	bulk	-5.25	0.01	-3.98	0.03	Wo
cv-4.29	bulk	-1.04	0.02	-3.05	0.01	Wo
cv-4.10	bulk	-1.67	0.04	-1.78	0.02	Wo
cv-4.29	YnfC	-2.87	0.01	-4.87	0.00	Wo
cv-4.10	YnfC	-5.23	0.03	-4.68	0.05	Wo
cv-4.5	YnfC	-2.073	0.01	-4.60	0.02	Wo
cv-4.67	YnfC	-5.05	0.06	-3.15	0.03	Wo
cv-5.34	YnfC	-7.20	0.03	-4.12	0.06	Wp
cv-5.61	YnfC	-4.60	0.03	-4.24	0.06	Wp
cv-9.101	YnfC	-8.21	0.03	-5.00	0.06	Wm
cv-5.42	brachiopod	1.9	0.10	-0.1	0.10	Wp
cv-5.143	brachiopod	1.1	0.10	0	0.10	Wp
cv-5.64	brachiopod	1.85	0.06	-0.40	0.02	Wo
cv-5.64	brachiopod	1.72	0.05	0.41	0.08	Wo
cv-5.64	brachiopod	1.70	0.03	0.44	0.08	Wo
cv-5.35	brachiopod	1	0.10	0	0.10	Wp
cv-5.60	brachiopod	2.21	0.03	0.75	0.06	Wp
cv-5.121	brachiopod	2.4	0.03	0.9	0.06	Wp
cv-4.75	calcitic bivalve	1.55	0.03	1.27	0.06	Wo
cv-6.6	calcitic bivalve	-1.31	0.03	1.2	0.06	Wn
cv-4.67	inclusion-rich cement	1.17	0.00	-0.44	0.01	Wo
cv-4.5	bulk of pre-compaction	-1.63	0.01	-3.58	0.03	Wo
cv-4.29	bulk of pre-compaction	-1.69	0.04	-4.45	0.02	Wo
cv-4.67	bulk of pre-compaction	-1.30	0.04	-2.11	0.01	Wo
cv-4.53	bulk of pre-compaction	0.06	0.02	-0.78	0.04	Wo
cv-5.46	bulk of pre-compaction	-2.40	0.03	-2.80	0.06	Wp
cv-5.97	bulk of pre-compaction	-0.03	0.03	-3.80	0.06	Wp
cv-5.34	bulk cement	-4.70	0.03	-3.76	0.06	Wp
cv-5.61	bulk cement	-5.02	0.03	-3.63	0.06	Wp
cv-5.89	bulk cement	-2.16	0.03	-4.16	0.06	Wp
cv-6.6	bulk cement	-26.2	0.10	-0.5	0.10	Wn
cv-15.26	bulk cement	1	0.10	-2.4	0.10	Wp-m
cv-15.40	bulk cement	0.8	0.10	-2.3	0.10	Wp-m
cv-4.10	bulk of post-compaction cement	-5.36	0.02	-5.03	0.02	Wo
cv-5.46	bulk of post-compaction cement	-3.60	0.03	-3.00	0.06	Wp
cv-6.6	crust	-31.17	0.03	0.58	0.06	Wn
cv-6.6	crust	-37.06	0.03	1.28	0.06	Wn

APPENDIX 8

XRD ANALYSIS AND DATA

APPENDIX 8 - XRD ANALYSIS AND DATA

1- Equipment

Philips PW1820 vertical goniometer
with PW 1386 automatic divergence slit

Generator type *PW1729 (1730/10(4kw))*
X-Ray tube *PN2273 / 20 Cu long fine focus*
Detector *PW1711 Xe fitted gas proportional*

2- Runs

♪ *Standard:*

QStd = Quartz Standard

From 20 to 21°2θ or 20.5 to 21°2θ

Speed 0.02°2θ/sec.

Range 5,000 c/sec

Chart 10mm/°2θ

♪ *Main run:*

From 18 to 34 °2θ

Speed 0.02 °2θ/sec.

Range 5,000 c/sec

Chart 10mm/°2θ

♪ *Determination of the MgCa rate:*

From 28.5 to 30.5°2θ

Speed 0.01°2θ/sec

Range 5,000 / 10,000 / 20,000 c/sec

Chart 10mm/°2θ or 50mm/°2θ

[+17 samples re-analyzed:

From 28.5 to 30.5°2θ

Speed 0.01°2θ/sec

Range 5 000 or 10 000 or 20 000 c/sec

Chart 50mm/°2θ]

♪ *Determination of the calcite peak height:*

From 28.5 to 30.5°2θ

Speed 0.02°2θ/sec

Range 10,000 / 20,000c/sec

Chart 10mm/°2θ

►► Some other runs made to determinate other peaks.

3- Procedure

►Annotation of the spectrum

►Base line drawn

►Background read at 25°2θ. !! Peaks height is read above background!!

►Determination of the peaks (Ca = calcite; Q = quartz; F = feldspar; A = aragonite; Clays = total clays; Dol = dolomite, Z = Zeolites), and height of each peak.

►Determination of $MgCaCO_3$ rate (chart from Chave, 1952), as follows:

<29.45°2θ	<>	<2%	LM (= low-Mg calcite)
29.45	<>	~2%	LM
29.46-29.48	<>	2-3%	LM
29.49	<>	~3%	LM
29.50-29.51	<>	3-4%	LM
29.52	<>	~ 4%	LM-IM (= intermediate-Mg calcite)
...	<>	~12%	HMC (= high-Mg calcite)

►For indeterminate peaks, value of molecular plane distances (d-spacings in Å) and height noted as in comments.

4- Comments

♪*Values for some minerals:*

d-spacing (Å) and relative intensity (in brackets) between 18 and 34°2θ (from 4.92Å to 2.64Å).

ARAGONITE	3.40Å(100)	3.27Å(50)	2.70Å(46)	
CALCITE	3.04Å(100)	3.86Å(12)	2.85Å(3)	
BIOTITE	3.37Å(100)	2.66Å(80)	3.16Å(20)	2.92Å(20)
PYRITE	2.71Å(84)	3.13Å(36)		
MAGNESIOHORNBLENDE	3.14Å(100)			
HORNBLEND	2.93Å(?)			
GLAUCONITE	4.53Å(80)	3.33Å(60)	3.09Å(40)	3.63Å(40)
DOLOMITE	2.89(100)	2.67Å(10)		

♪*Other comments:*

- Caution, the value read for Quartz (Q (3)) is not the major peak of Quartz (Q (10) at 3.35A).
- When Q (3) is high, the aragonite peak is less well seen, and lower than it should be; as a result, the value is probably underestimated.

5- Database

♪When 0 in a cell ***<it means>*** not observed / when nothing ***<it means>*** undetermined

♪In Comments: **e.g.:** ▪ "4.91Å(4U)/2.96Å(2.5U) = F " <> peak at 4.91Å (height=4 units) = Feldspar and peak at 2.96Å (height = 2.5Units) = F

▪Also "=...= F" <> all the peaks noted before are F.

APPENDIX 8 - XRD Data

Field ref.	Column	Formation	B.Qtd	backg. at 25°2θ	calcite 29.4-30°2θ	aragonite 26.25°2θ	quartz 20.8°2θ	28°	feldspar -	27.5°	clay min. 19.9°2θ	calcite LM-IM-HM	%
1.3	38	Te Waka Fm.	64.0	7.5	108	0	7.0	13.5	3.0	4.0	2.5	LM	2-3%
1.4	38	Te Waka Fm.	-	6	130	0	5.0	5.5	3.0	2.5	1.5	LM	3.0%
1.5	38	Te Waka Fm.	65.0	5.5	138	0	8.0	85??*		2.5	2.0	LM	<2%
2.1	38	Titiokura Fm.	67.0	6.5	116	0	5.5	6.5		2.0	1?	LM	2-3%
2.2	38	Titiokura Fm.	67.0	5.5	130	2	5.0	4.0	3.5	3.0	1.5	LM	3-4%
2.3	38	Titiokura Fm.	-	5.5	142	?	5.0	3.5	1.5	0.0	0.0	LM	3-4%
2.4	38	Titiokura Fm.	66.0	5	144	0	1.5	3.0	2.0	3.0	2.0	LM	2-3%
2.5	38	Titiokura Fm.	64.0	5.5	108	?	5.0	2.0	8.0	5.0	2.5	LM	<2
2.6	38	Titiokura Fm.	-	5	186	0	2.5	14.0		2.5	1.5	LM	2.0%
2.7	38	Titiokura Fm.	67.5	5.5	124	0	6.0	11.0	0.0	8.5	0.0	IM	4-5%
2.8	38	Titiokura Fm.	67.0	5	158	0	2.5	2.5	2.0	7.5	0.0	LM	2-3%
4.2	7	Kairakau Lst.	66.0	4.5	118	0	2.5	4.0		0.0	0.0	IM	4-5%
4.5	7	Kairakau Lst.	67.0	4	208	0	2.0	1.5	1.5	1.5	1.5?	LM	<2%
4.10.	7	Kairakau Lst.	64.5	6	126	0	9.0	8.0		2.0	0.0	LM	<2%
4.12	7	Kairakau Lst.	-	5	168	0	7.0	10.5		4.0	0.0	LM	2.0%
4.13	7	Kairakau Lst.	64.0	7	136		6.5	12.0		4.0	0.0	LM	2.0%
4.14	7	Kairakau Lst.	-	5.5	156	0	6.5	12.0		4.0	0.0	LM	2.0%
4.15	7	Kairakau Lst.	-	6.5	118	0	8.0	8.5		3.0	2.0	LM	<2%
4.16	7	Kairakau Lst.	65.0	5.5	154	0	6.5	4.5		3.0	0.0	LM	<2%
4.17	7	Kairakau Lst.	-	5	152	0	6.0	6.0		2.5	0.0	LM	<2%
4.18	7	Kairakau Lst.	63.5	6	174	0	4.5	5.0		3.5	1.5	LM	
4.19	7	Kairakau Lst.	-	6	138	0	8.5	9.5	5.0	7.0	0.0	LM	<2%
4.20.	7	Kairakau Lst.	-	6.5	182	0	8.5	16.5		2.0	1.5	LM	
4.22	7	Kairakau Lst.	64.5	6.5	152	0	8.5	12.0		3.5	2.0	LM	2-3%
4.24	7	Kairakau Lst.	-	5.5	156	0	13.0	5.0		2.0	2.0	LM	2.0%
4.25	7	Kairakau Lst.	-	7	108	0	9.0	8.5		4.5	2.0	LM	2.0%
4.26	7	Kairakau Lst.	66.0	6	139	0	5.5	8.0	5.5	2.5	1.5	LM	2.0%
4.27	7	Kairakau Lst.	-	6.5	142	0	12.0	17.0		2.5	1.5	LM	2.0%
4.29	7	Kairakau Lst.	-	5	192	0	5.5	3.0		0.0	2.0	LM	<2%
4.30.	7	Kairakau Lst.	64.5	5.5	152	0	6.5	16.0		0.0	0.0	LM	2.0%
4.31	7	Kairakau Lst.	-	5.5	146	0	3.5	17.0		0.0	0.0	LM	<2%
4.32	8	Kairakau Lst.	-	6	134	0	7.0	9.0		4.5	0.0	LM	<2%
4.33	8	Kairakau Lst.	64.0	6	154	0	5.0	4.5		0.0	0.0	LM	2.0%
4.35	8	Kairakau Lst.	66.0	7	173	0	6.5	10.0		11.0	0.0	LM	2.0%
4.36	8	Kairakau Lst.	65.0	6	156	1.5	6.0	4.5		3.0	0.0	LM	2.0%
4.37	8	Kairakau Lst.	65.0	6	142	0	5.0	81.0		0.0	2.0	LM	2.0%
4.38	8	Kairakau Lst.	66.0	7	90	0	21.0	15.0		14.0	2.0	LM	<2%
4.40.	8	Kairakau Lst.	65.0	5	186	0	0.0	0.0		0.0	0.0	LM	<2%
4.42	10	Kairakau Lst.	66.5	7	134	0	12.0	12.0		2.0	0.0	LM	<2%
4.43	10	Kairakau Lst.	65.0	6	112	0	4.5	20.0		83.0	2.0	LM	2-3%
4.44	10	Kairakau Lst.	-	6	160	0	6.5	4.0	3.5	2.0	2.5	LM	<2%
4.45	10	Kairakau Lst.	63.5	7	140	0	7.0	32.0		2.5	2.0	LM	<2%
4.46	10	Kairakau Lst.	66.5	6.5	131	0	8.5	4.5	3.0	3.0	2.5	LM	2.0%
4.49	10	Kairakau Lst.	-	6.5	130	0	4.0	3.5	2.5	3.0	2.5	LM	<2%
4.50.	10	Kairakau Lst.	65.0	6	156	2.5(?)	3.5	3.0	4.5	0.0	0.0	LM	<2%
4.51	10	Kairakau Lst.	-	6.5	148	2	4.0	5.0	2.5	1.5	2.0	LM	2.0%
4.52	10	Kairakau Lst.	65.0	6.5	108	0	14.0	39.5		3.0	2.0	LM	<2%
4.53	10	Kairakau Lst.	65.0	5.5	106	0	?	6.5		2.0	0.0	LM	<2%
4.54	10	Kairakau Lst.	64.5	5.5	98	0	5.0	15.0	7.0	5.0	0.0	LM	2.0%
4.55	10	Kairakau Lst.	63.0	6	115	2	5.0	5.5		6.5	0.0	LM	2.0%
4.56	10	Kairakau Lst.	66.0	7	100		7.0	13.0		2.5	0.0	LM	3-4%
4.57	10	Kairakau Lst.	-	6.5	124	0	4.0	3.5	3.0	1.0	0.0	LM	3-4%
4.65	1	Kairakau Lst.	-	5	202	0	3.0	3.0		0.0	0.0	LM	2.0%
4.66	1	Kairakau Lst.	64.5	6	156	0	5.0	17.0		1.5	0.0	LM	2.0%
4.67	1	Kairakau Lst.	65.0	5	152	0	4.0	8.0	3.0	2.0	0.0	LM	2.0%
4.68	1	Kairakau Lst.	65.0	5	176	0	4.0	7.0		1.5	0.0	LM	2.0%
4.69	1	Kairakau Lst.	67.5	5	151	0	4.0	28.0		0.0	0.0	LM	2.0%
4.71	1	Kairakau Lst.	-	6	110	0	10.0	19.5		2.5	0.0	LM	<2%

Field ref.	Locality	Formation	R.Qtz	backg. at 25°2θ	calcite 29.4-30°2θ	aragonite 26.25°2θ	quartz 20.8°2θ	28°	R.I. pair	27.5°	clay min. 19.9°2θ	calcite LM-IM-HM	%
4.72a	1	Kairakau Lst.	65.0	7.5	100	0	17.0	20.0		4.0	2.0	LM	<2%
4.72b	1	Kairakau Lst.	64.0	7	179	0	13.5	15.0		4.0	1.5	LM	<2%
4.74	1	Kairakau Lst.	63.5	7	161	0	9.0	15.0		7.5	0.0	LM	3-4%
4.75	1	Kairakau Lst.	63.0	6	220	1.5	6.0		14.0	2.5	0.0	LM	2.0%
4.76	1	Kairakau Lst.	65.0	6	148	0	6.5	5.5		0.0	2.0	LM	2.0%
4.77	1	Kairakau Lst.	63.5	6	148	0	5.0	7.0		2.0	0.0	LM	2.0%
4.80.	2	Kairakau Lst.											
4.81a	2	Kairakau Lst.											
4.81b	2	Kairakau Lst.	64.5	6.5	146	0	6.5	17.0	3.5	6.0	1.5	LM	2.0%
4.82	2	Kairakau Lst.	-	6	204	0	3.5	13.5		0.0	0.0	LM	<2%
4.83	2	Kairakau Lst.	65.5	5.5	165	0	9.0	6.0		2.0	0.0	LM	3.0%
4.84	2	Kairakau Lst.	-	6	184	0	8.5	12.0		3.0	2.0	LM	2.0%
4.85	2	Kairakau Lst.	64.0	6.5	133	0	5.0	9.5		3.0	1.5	LM	2.0%
4.86b	2	Kairakau Lst.	-	6.5	125	0	7.5	12.0		7.0	0.0	LM	2-3%
4.88	2	Kairakau Lst.	-	7.5	92		12.0	18.0		6.0	1.5	LM	2-3%
4.90.	2	Kairakau Lst.	63.5	5.5	152	1.5	4.0	4.0	1.50	2.0	0.0	LM	2-3%
4.91	2	Kairakau Lst.	-	5.5	204	0	???20??	3.5		2.0	0.0	LM	2-3%
4.92	2	Kairakau Lst.	64.5	6	150	0	6.0	33.0		11.0	0.0	LM	3.0%
4.93		Kairakau Lst.	-	5	184	0	2.0	2.5	1.0	0.0	0.0	LM	3.0%
4.94		Kairakau Lst.	-	5	192	0	4.0	3.0	2.0	0.0	0.0	LM	3.0%
4.96	5	Kairakau Lst.	64.5	7	146	0	8.0	10.0		4.0	1.5	LM	2-3%
4.97	5	Kairakau Lst.	64.5	6	114	0	7.5	22.0		3.0	0.0	LM	3.0%
4.99	5	Kairakau Lst.	64.5	7.5	88	0	11.0	20.0		4.0	2.5	LM	<2%
4.100.	5	Kairakau Lst.	64.5	6	156	3	12.0	10.0		2.0	0.0	LM	<2%
4.101	5	Kairakau Lst.	63.0	7	142	0	23.0	21.5		4.0	2.0	LM	2-3%
4.102	5	Kairakau Lst.	66.5	7	109	2	24.0	11.0		13.0	0.0	LM	2-3%
4.103	5	Kairakau Lst.	66.5	6.5	104	1.5	31.0	13.5		3.0	0.0	LM	2-3%
4.104	5	Kairakau Lst.	65.5	7	73	0	11.0	9.0		3.0	0.0	IM	5-6%
4.105	5	Kairakau Lst.	67.5	5.5	150	0	2.0	3.0		0.0	1.5	LM	2.0%
4.106		Kairakau Lst.	66.5	5.5	112	0	16.0	7.0		0.0	0.0	LM	2.0%
4.107a		Kairakau Lst.	67.0	5.5	116	0	7.0	13.0		2.0	0.0	LM	2-3%
4.108		Kairakau Lst.	64.0	5.5	134	0	4.0	5.0		4.5	2.0	LM	<2%
4.109		Kairakau Lst.	66.0	6	93	0	6.0	15.0		0.0	1.5?	LM	2-3%
4.110.		Kairakau Lst.	67.0	7	93	3	11.0	43.0		8.5	0.0	LM	2.0%
4.112		Kairakau Lst.	63.0	7	96	0	8.0	10.0		2.0	0.0	LM	2.0%
4.113		Kairakau Lst.	63.0	10	49	0	16.0	0.0	0.0	0.0	2.0	LM	3.0%
4.114	6	Kairakau Lst.	65.5	6	146	2	7.0	8.0		2.0	0.0	LM	2.0%
4.115	6	Kairakau Lst.	63.5	6	106	0	8.0	16.5		9.5	0.0	LM	2-3%
4.117	6	Kairakau Lst.	64.0	6	128	0	7.5	4.0		1.5	0.0	LM	<2%
4.118	6	Kairakau Lst.	66 0	6	120	0	6.0	7.0		0.0	0.0	LM	2.0%
4.119	6	Kairakau Lst.	64.5	6	104	0	5.0	9.0		4.0	0.0	IM	6.0%
4.120.	6	Kairakau Lst.	64.5	6	100	0	4.5	7.0		2.0	2.0	LM	2.0%
4.121	6	Kairakau Lst.	64.0	7	100	0	8.5	13.0		0.0	0.0	LM	<2%
4.122	6	Kairakau Lst.	65.0	7	90	0	13.0	16.0		3.0	2.0	LM	<2%
4.123	6	Kairakau Lst.	65.0	7.5	126	2	8.5	16.0		4.0	0.0	LM	<2%
4.124	6	Kairakau Lst.	65.5	7.5	154	0	14.0	9.0		2.0	2.5	LM	3.0%
4.125	4	Kairakau Lst.	66.0	7	126	2	11.0	12.0		3.0	2.0	LM	2.0%
4.126	4	Kairakau Lst.	-	6	168	0	4.0	0.0		0.0	0.0	LM	2.0%
4.127	4	Kairakau Lst.	67.0	6	142	0	8.0	192.0		0.0	0.0	LM	3.0%
4.129	4	Kairakau Lst.	-	6	192	0	4.0	3.0		2.0	0.0	LM	3.0%
4.130.	4	Kairakau Lst.	67.5	5.5	176	0	2.0	2.5		0.0	0.0	LM	2.0%
4.131	4	Kairakau Lst.	-	5	175	0	2.5	7.0		0.0	0.0	LM	3.0%
4.132	4	Kairakau Lst.	67.5	6.5	124	0	9.0	8.0		3.0	2.5	LM	2-3%
4.133	4	Kairakau Lst.	-	6	108	1.5	9.5	13.0		0.0	2.0	LM	<2%
4.134	11	Kairakau Lst.	65.0	5	118	0	1.5	2.0		0.0	1.0	LM	<2%
4.135	11	Kairakau Lst.	65 5	5.5	142	0	2.5	3 5		2.5	0 0	LM	<2%
4.136	11	Kairakau Lst.	68 0	5.5	124	0	4 0	4 5	3.5	0 0	0.0	LM	2.0%
4.137	11	Kairakau Lst.	64 0	5	136	1 5	3 5	2 0		3.5	0.0	LM	2.0%
4.138	11	Kairakau Lst.	65 0	5	88 5	0	4 5	6.5		2.0	0 0	LM	2.0%

APPENDIX 8 - XRD Data

Field ref.	Locality	Formation	B.Qtd	backg. at 25°2θ	calcite 29.4-30°2θ	aragonite 26.25°2θ	quartz 20.8°2θ	28°	feldspar	27.5°	clay min. 19.9°2θ	calcite LM-EM-IIM	%
5.24	9	Awapapa Lst.	65.0	6.5	140	0	7.0	11.0		2.0	1.5	LM	2.0%
5.28	9	Awapapa Lst.	65.0	6	156	0	4.0	25.5		5.5	1.5	LM	<2%
5.30.	9	Awapapa Lst.	-	7.5	106	0	13.5		22.5	0.0	2.0	LM	<2%
5.31	9	Awapapa Lst.	68.0	6	177	0	4.0	5.0	3.0	4.5	0.0	LM	2.0%
5.32a	9	Awapapa Lst.	66.5	6	138	2?	4.0	6.0	6.0	2.0	1.5	LM	<2%
5.32c	9	Awapapa Lst.	66.0	5.5	148	0	6.0	11.0		3.0	1.5	LM	<2%
5.34	9	Awapapa Lst.	-	5	224	0	4.0	2.0		1.5	0.0	LM	<2%
5.38	9	Awapapa Lst.	68.0	5	138	0	2.5	2.0		0.0	1.5?	LM	2.0%
5.40.	9	Awapapa Lst.	65.0	12	9 or 10.5	0	11.0	20.0	13.5	6.5	6.0	M or IM?	% or 6-7
5.44	9	Awapapa Lst.	68.0	5	140	0	3.0	3.0	1.5	0.0	2.0	LM	3-4%
5.45a	9	Awapapa Lst.	-	5	152	0	2.5	2.0		2.0	1.5	LM	3-4%
5.45b	9	Awapapa Lst.	66.0	6	138	1?	4.5	7.0		3.0	1.5	LM	2.0%
5.46a	9	Awapapa Lst.	68.0	5.5	166	1.5?	3.0	2.0		0.0	0.0	LM	3-4%
5.46b	9	Awapapa Lst.	69.0	5	170	1.5?	1?	9.0		1.5	0.0	LM	3-4%
5.47	9	Awapapa Lst.	67.0	7	124	0	9.5	12.0		10.5	2.0	LM	2.0%
5.48	9	Awapapa Lst.	65.0	5	142	1?	2.5	2.0	2.0	0.0	0.0	LM	<2%
5.49	9	Awapapa Lst.	-	5	168	0	2.0	9.0		2.5	0.0	LM	2.0%
5.51	9	Awapapa Lst.	66.0	5	154	0	2.5	3.0		0.0	2.0	LM	2.0%
5.52	9	Awapapa Lst.	-	5.5	142	0	3.0	3.0		1.5	0.0	LM	<2%
5.53	9	Awapapa Lst.	65.5	6	138	0	5.0	4.0		0.0	2.0	LM	<2%
5.55	9	Awapapa Lst.	66.0	5.5	152	0	6.5	25.0	2.0	1.5	0.0	LM	2.0%
5.56	9	Awapapa Lst.	-	6	182	0	4.0	4.5		2.5	0.0	LM	3-4%
5.65	14	Awapapa Lst.	64.0	5.5	168	0	2.0	1.5	2.0	1.0	0.0	LM	<2%
5.68	14	Awapapa Lst.	-	10.5	43	0	11.5	7.0	15.0	4.0	5.0	LM	2-3%
5.71a	14	Awapapa Lst.	-	6	155	0	4.5	6.0		1.5	1.5?	LM	<2%
5.73	13	Awapapa Lst.	64.0	6	180	0	12.5	5.5		4.0	0.0	LM	<2%
5.74	13	Awapapa Lst.	65.0	5.5	272	0	3.0	2.0	3.0	0.0	1.5	LM	<2%
5.75	13	Awapapa Lst.	66.5	5	192	0	2.5	3.0		6.5	2.0	LM	2-3%
5.76	13	Awapapa Lst.	66.5	6	134	0	6.0	6.0		16.5	2.0	LM	2-3%
5.79a	13	Awapapa Lst.	68.0	4	200	0	1.5	3.0		0.0	1.5	LM	2-3%
5.79b	13	Awapapa Lst.	68.0	4.5	104	0	2.5	3.5	2.0	1.0	2.0	LM-IM	4.0%
5.81	13	Awapapa Lst.	-	5.5	152	0	2.5	2.5		2.0	2.0	LM	<2%
5.83	13	Awapapa Lst.	65.0	5	208	0	3.0	2.0		0.0	0.0	LM	3-4%
5.86	13	Awapapa Lst.	63.5	6	142	0	6.5	6.0		1.0	1.5	LM	<2%
5.87	12	Awapapa Lst.	63.0	5.5	226	2.5?	3.0	2.0	2.0	0.0	1.5	LM	<2%
5.88	12	Awapapa Lst.	66.5	5	196	0	0.0	1.5	1.5	1.5	0.0	LM	2-3%
5.89	12	Awapapa Lst.	65.0	6.5	212	0	3.0	2.5	2.5	0.0	2.0	LM	<2%
5.90.	12	Awapapa Lst.	62.5	6.5	156	0	4.0	6.5		4.0	1.5	LM	<2%
5.93	16	Awapapa Lst.	65.0	5	160	0	2.0	0.0		0.0	1.5	LM	2.0%
5.94	16	Awapapa Lst.	63.5	6	123	0	5.0	14.0	2.0	2.0	1.0	LM	3-4%
5.95	16	Awapapa Lst.	64.0	5.5	180	0	3.5	3.5		1.5	1.0	LM	2.0%
5.96	16	Awapapa Lst.	64.5	5.5	174	0	3.5	4.5	2.0	1.5	2.0	LM	<2%
5.97	16	Awapapa Lst.	65.0	5.5	208	0	3.0	9.0		1.5	1.5	LM	2.0%
5.98	16	Awapapa Lst.	66.5	5	200	0	2.5	0.0		0.0	1?	LM	2-3%
5.99	16	Awapapa Lst.	67.5	5	135	0	8.0	5.0		0.0	0.0	IM	5-6%
5.105	16	Awapapa Lst.	65.0	6.5	81.5	0	8.0	12.0		2.5	1?	LM-IM	4.0%
5.106	16	Awapapa Lst.	65.0	5.5	145	1.5?	5.0	4.5	2.0	0.0	2.0	LM	3-4%
5.111b	15	Kairakau Lst.	67.0	6	106	0	5.0	7.5		0.0	2.0	LM	2.0%
5.112	15	Kairakau Lst.	66.0	5	124	0	2.5	4.0	2.0	1.5	0.0	LM	<2%
5.113	15	Kairakau Lst.	65.0	5	140	0	2.0	2.0	1.5	2.0	0.0	LM	2.0%
5.117	15	Kairakau Lst.	-	5.5	138	0	4.5	0.0	7.0	0.0	1.5	LM	2-3%
5.118	15	Kairakau Lst.	64.0	5.5	109	0	9.0	8.0		3.0	1.5	LM	3-4%
5.119	15	Kairakau Lst.	63.0	5	102	1?	2.0	2.5		1.0	0.0	LM	<2%
5.120.	15	Kairakau Lst.	66.0	5	147	1.5	1.5	4.0	2.0	2.5	0.0	LM	2-3%
5.123	15	Kairakau Lst.	67.0	5.5	128	0	4.0	5.0		0.0	0.0	LM	3-4%
5.124	15	Kairakau Lst.	64.0	5	132	0	1.5	6.0		0.0	1.5	LM	2.0%
5.127	15	Kairakau Lst.	65.0	6.5	111	0	9.0	9.5		10.5	1.5	IM	5.0%
5.128	15	Awapapa Lst.	66.5	6	163	0	3.0	10.0		2.5	1.5	LM	2.0%
5.129	15	Awapapa Lst.	65.5	6.5	136	0	11.0	9.0		1.5	1.5	LM	2.0%
5.130.	15	Awapapa Lst.	65.0	5.5	144	1.5?	4.0	16.0	2.0	0.0	0.0	LM	2-3%

APPENDIX 8 - XRD Data

Field ref.	Locality	Formation	B.Qstp	backg. at 25°2θ	calcite 29.4-30°2θ	aragonite 26.25°2θ	quartz 20.8°2θ	28°	feldspar	27.5°	clay min. 19.9°2θ	calcite LM-IM-HM	%
5.131	15	Awapapa Lst.	64.0	5.5	158	0	4.0	4.0		2.0	1.0	LM	<2%
5.132	15	Pukekura Calc.	67.0	6.5	89	0	13.0	12.0		4.0	2?	LM	2-3%
5.133	15	Pukekura Calc.	65.0	6	78.5	0	8.5	7.0		2.0	2.5	LM	2.0%
5.134	15	Pukekura Calc.	65.0	6.5	69	0	13.5	4.5	12.5	0.0	3.0	LM	2-3%
5.135	15	Pukekura Calcarenite	64.0	6.5	152	0	2.0	4.0		1.5	0.0	LM	<2%
5.139	15	Rotookiwa Lst.?	66.0	8	118	1.5?	11.0	24.5		3.0	2.5	LM	<2%
5.140a	15	Awapapa Lst.	62.0	5.5	153	0	3.0	4.0		2.0	2.0	LM	2-3%
5.142	9	Awapapa Lst.	68.5	5	110	0	2.5	0.0		0.0	0.0	LM	2-3%
5.145a	9	Awapapa Lst.	65.0	5	136	2	2.5	11.0		6.0	2.0	LM	<2%
5.146	9	Awapapa Lst.	67.0	4.5	140	0	4.0	8.0		1.5	0.0	LM	2-3%
6.1	28	Pakipaki Lst.	-	4.5	120	0	2.0	2.0		1.5	1.0	LM	3.0%
6.2	28	Pakipaki Lst.	66.0	4.5	113	0	1.5	2.0		0.0	0.0	LM	<2%
6.3	28	Pakipaki Lst.	65.0	4.5	131	2	0.0	1.5		1.5	0.0	LM-IM	4.0%
6.4	28	Pakipaki Lst.	-	4.5	134	1	1.5	2.0		3.5	1.5	LM	2-3%
6.5	28	Pakipaki Lst.	63.5	4.5	68	16	2.0	2.0		0.0	0.0	LM	2-3%
6.6	28	Pakipaki Lst.	67.0	4.5	62	22	0.0	0.0		0.0	0.0	LM	3-4%
6.7	28	Pakipaki Lst.	67.0	4.5	132	1.5	0.0	2.5		2.5	0.0	LM	2.0%
6.8	28	Pakipaki Lst.	-	4.5	128	0	0.0	0.0		12.5	1.5	LM	2-3%
7.1		Rotookiwa Lst.	65.0	5	134	4	3.0	4.0		1.0	0.0	LM	3.0%
7.2		Rotookiwa Lst.	-	5	132	3.5	2.0	2.0		2.0	0.0	LM	2-3%
7.3		Rotookiwa Lst.	65.0	4.5	131	4	3.0	3.0		2.0	0.0	LM	2-3%
7.6	15	Rotookiwa Lst.	64.0	5.5	216	0	1.5	3.0		0.0	0.0	LM	<2%
7.7	15	Rotookiwa Lst.	66.0	7	124	2.5	10.5	9.5		0.0	1.5	LM	2-3%
7.8	15	Rotookiwa Lst.	67.5	5.5	79	0	11.0	27.5		3.0	1?	LM	2-3%
7.9	15	Rotookiwa Lst.	66.0	5	102	1.5	3.5	3.5		2.5	0.0	LM	3-4%
7.10.	15	Rotookiwa Lst.	67.0	5	132	2	4.0	3.0		1.5	2.0	LM	3-4%
7.12	17	Rotookiwa Lst.	64.0	5.5	158	0	3.5	3.5		2.0	2.5	LM	2-3%
7.14	17	Rotookiwa Lst.	65.0	6	156	1	3.0	2.0		0.0	0.0	LM	2.0%
7.15a	17	Rotookiwa Lst.	61.0	5	145	1.5	0.0	0.0		0.0	0.0	LM	3.0%
7.15b	17	Rotookiwa Lst.	66.5	5.5	167	0	3.0	2.0		1.5	2.0	LM	2-3%
7.16	17	Rotookiwa Lst.	65.0	5.5	160	0	2.5	6.5		1.5	0.0	LM	<2%
7.18	17	Rotookiwa Lst.	-	5	208	0	0.0	1.5		0.0	0.0	LM	<2%
7.19	17	Rotookiwa Lst.	67.0	5	164	0	0.0	1.5		1.5	1.5	LM	<2%
7.20.	17	Rotookiwa Lst.	66.0	5	200	0	1.5	1.5		0.0	1.0	LM	<2%
7.21	17	Rotookiwa Lst.	63.0	5	143	0	0.0	0.0		4.0	0.0	LM	2-3%
7.22	17	Rotookiwa Lst.	66.0	5.5	149	0	4.0	4.0		11.0	2.0	LM	<2%
7.23	17	Rotookiwa Lst.	-	5.5	140	0	4.0	28.0		2.0	0.0	LM	<2%
7.27	17	Sandstone n.f.?	64.0	7	120	0	6.0	16.5		0.0	2.0	IM	4-5%
7.29	18	?	63.0	13.5	0	0	17.0	24.0		3.0	3.5	-	-
7.31	18	Rotookiwa Lst.	66.0	6.5	132	0	3.5	11.0		0.0	1.5	LM	2.0%
7.33	18	Rotookiwa Lst.	-	6	142	0	3.5	5.5		3.0	1.0	LM	<2%
7.35	18	Rotookiwa Lst.	62.5	6	180	0	2.0	14.0		0.0	0.0	LM	3-4%
7.40.	20	Rotookiwa Lst.	64.5	6.5	100	0	16.0	16.5		6.0	1.5	LM	3-4%
7.41	20	Sandstone n.f.?	65.0	5	91	0	6.0	6.5		0.0	0.0	LM	3-4%
7.42	20	Sandstone n.f.?											
7.43	20	Rotookiwa Lst.	62.5	5.5	124	0	3.0	2.0		1.5	1.5	LM	3-4%
7.45	20	Rotookiwa Lst.	65.0	5	132	0	1.0	11.0		2.0	1.5	IM	4-5%
7.46	20	Rotookiwa Lst.	-	5.5	120	2.5?	4.5	6.0		9.5	1.5	LM-IM	4.0%
7.47	20	Rotookiwa Lst.	66.0	6	158	0	4.0	7.0		0.0	0.0	LM	2-3%
7.48	20	Rotookiwa Lst.											
7.49	20	Rotookiwa Lst.	63.0	6	116	2.5?	3.0	5.0	30	2.0	1.5	LM	3-4%
7.50.	20	Rotookiwa Lst.											
7.51	20	Rotookiwa Lst.											
7.52	20	Rotookiwa Lst.											
7.53	20	Sandstone n.f.?	66.0	7.5	77	2?	14.5	19.5		5.5	2.0	LM	2-3%
7.54	20	?	-	7	83.5	0	15.0	18.0		0.0	2.0	LM	3-4%

Field ref.	Locality	Formation	B.Grnd	backg. at 25°2θ	calcite 29.4-30°2θ	aragonite 26.25°2θ	quartz 20.8°2θ	28°	feldspar	27.5°	clay min. 19.9°2θ	calcite LM-IM-HM	%
7.57	23	Waikaraeo Calc.	67.0	8.5	30	3.5	20.0	23.0		0.0	3.0	LM	2-4%
9.1	23	Te Onepu Lst.	63.0	5	167	1.5	0.0	2.0		0.0	0.0	LM	2.0%
9.2	23	Te Onepu Lst.											
9.3	23	Te Onepu Lst.											
9.4	23	Te Onepu Lst.	63.0	5	174	1.5	2.0	2.5		1.5	0.0	LM	<2%
9.8	23	Te Onepu Lst.	64.0	5.5	169	0	1.5	1.0		0.0	0.0	LM	2.0%
9.9	23	Te Onepu Lst.	65.0	5	162	2.5	0.0	1.5		0.0	1.0	LM	2-3%
9.10.	23	Te Onepu Lst.	-	5.5	180	2	1.5?	0.0	0.0	0.0	0.0	LM	<2%
9.11	23	Te Onepu Lst.	66.5	5.5	181	0	0.0	0.0		0.0	0.0	LM	<2%
9.12	23	Te Onepu Lst.	65.5	5.5	184	1.5?	2.0	0.0		0.0	1.5?	LM	2.0%
9.14	23	Te Onepu Lst.	65.5	4.5	110	2.5	0.0	2.0	25	1.5	0.0	LM-IM	4.0%
9.15	23	Te Onepu Lst.	-	5.5	174	2	1.5	2.0		0.0	0.0	LM	2.0%
9.16	23	Te Onepu Lst.	64.5	5.5	174	0	2.0	3.0		1.5	2.0	LM	<2%
9.17	23	Te Onepu Lst.	64.0	5	172	0	0.0	0.0		2.0	0.0	LM	2-3%
9.21	23	Te Onepu Lst.	67.0	5	88	0	8.0	8.5		4.5	2.0	LM	2-3%
9.34	24	Te Onepu Lst.	67.0	5	115	2.5	5.0	3.0	25	2.0	0.0	LM	2-3%
9.36	24	Te Onepu Lst.	-	4.5	112	0	6.0	4.5		2.0		LM	3.0%
9.37	24	Te Onepu Lst.	68.0	5	136	0	2.5	2.0		0.0	2.5	LM	2-3%
9.38	24	Te Onepu Lst.	64.0	5	128	0	1?	5.0		1.5	0.0	LM	3-4%
9.39	24	Te Onepu Lst.	63.0	4.5	104	3	2.5	5.5		1.5	1.5	LM	2-3%
9.41	26	Te Onepu Lst.	63.0	5	84	1.5?	8.0	13.0	50	2.5	2.0	LM	3.0%
9.43	26	Te Onepu Lst.	-	6.5	70	0	12.0	40.0		11.5	3.0	LM	2-3%
9.44	26	Te Onepu Lst.	67.0	7	100	0	9.5	12.0	60	12.0	2.5	LM	2-3%
9.46	26	Te Onepu Lst.	63.0	6	100	2.5?	6.0	6.0	20	2.5	2.0	LM	2-3%
9.48	26	Te Onepu Lst.	65.0	4.5	116	0	2.0	4.0	15	0.0	1.5	LM	2-3%
9.49	26	Te Onepu Lst.	65.0	4.5	120	0	2.5	2.5		0.0	0.0	LM	<2%
9.50.	26	Te Onepu Lst.	69.0	5	162	0	0.0	1.5		1.5	0.0	LM	<2%
9.51	26	Te Onepu Lst.	65.0	4	135	0	0.0	0.0		0.0	0.0	LM	2-3%
9.53	26	Te Onepu Lst.	64.0	6.5	156	?	5.0	6.5	50	3.0	1.5	LM	2-3%
9.55	26	Te Onepu Lst.	65.0	5	110	0	6.0	7.0		6.0	2.0	LM	2-3%
9.58	25	Te Onepu Lst.	-	4.5	129	0	0.0	0.0		0.0	1.5?	LM	2-3%
9.60.	25	Te Onepu Lst.	63.0	5	88	0	8.0	7.0		13.5	2.0	LM-IM	4.0%
9.61	25	Te Onepu Lst.	-	4.5	110	0	3.5	3.5		3.5	0.0	LM	3.0%
9.62	25	Te Onepu Lst.	67.0	5.5	102	0	5.0	18.5	30	3.0	2.5	LM	2-3%
9.64	25	Te Onepu Lst.	-	5	128	2	5.0	5.0	15	2.0	1.5?	IM	6.0%
9.66	25	Te Onepu Lst.	-	5.5	100	1.5	9.5	19.5		3.0	0.0	LM	2-3%
9.68	25	Te Onepu Lst.	65.0	4.5	126	0	1.5	3.0		1.5	1.5	LM	2-3%
9.69	25	Te Onepu Lst.	63.0	5.5	160	0	3.5	5.0		1.5	0.0	LM	2-3%
9.80.	27	Te Onepu Lst.	65.0	5.5	168	2	1.0	1.5		0.0	1.5	LM	<2%
9.81	27	Te Onepu Lst.	65.0	5	180	0	1.5	0.0		0.0	0.0	LM	2-3%
9.83	27	Te Onepu Lst.	65.5	5	128	0	0.0	3.0		2.0	0.0	LM-IM	4.0%
9.85	27	Te Onepu Lst.	-	5	160	0	2.0	1.5	30	0.0	0.0	LM	2-3%
9.90.	27	Te Onepu Lst.	64.0	5.5	174	0	2.0	3.0		0.0	3.0	LM	3.0%
9.91	27	Te Onepu Lst.	-	4.5	134	0	2.0	2.0		0.0	0.0	LM	2-3%
9.92	27	Te Onepu Lst.	65.0	5	156	0	2.0	1.5		1.5	0.0	*LM-IM	3.5-4.5%
9.94	27	Te Onepu Lst.	65.0	6	153	0	3.5	3.5	35	1.5	0.0	LM	2-3%
9.95	27	Te Onepu Lst.											
9.96	27	Te Onepu Lst.	65.0	6	204	2.5	2.5	2.0	20	2.0	1.5	LM	2-3%
9.97	27	Te Onepu Lst.	65.0	5	244	?	1.5	13.0	25	0.0	1.5	LM	2-3%
9.98	27	Te Onepu Lst.	63.0	4.5	136	0	1.5	2.5		1.5	0.0	LM	2-3%
9.101	21	Te Onepu Lst.	-	4.5	175	0	0.0	0.0		0.0	0.0	IM	4-5%
9.102	21	Te Onepu Lst.	63.5	4.5	162	0	1.5	0.0	15	0.0	1.5	LM	2-3%
9.103	21	Te Onepu Lst.	64.0	5	208	1.5	1.5	1.5		0.0	0.0	LM	2-3%
9.104	21	Te Onepu Lst.	66.0	5	180	1.5	0.0	2.0		1.5	1.5	LM	<2%
9.105	21	Te Onepu Lst.	66.0	4.5	212	2	0.0	1.5		1.5	0.0	LM	2-3%
9.106	21	Te Onepu Lst.											
9.107	21	Te Onepu Lst.	65.0	5.5	132	2	4.5	3.0	15	0.0	1.5	LM	3.0%
9.108	21	Te Onepu Lst.	66.0	4.5	122	1.5	1.5	0.0	0.0	0.0	1.5	LM	3-4%
9.110.	21	Te Onepu Lst.	68.0	5	102	0	4.5	9.0	25	3.0	2.0	LM	2.0%
9.112	21	Te Onepu Lst.	-	5	135	2.5	1.5	1.5	20	0.0	0.0	LM	3-4%
9.113	21	Te Onepu Lst.	65.0	4.5	134	0	3.0	3.0	20	4.5	0.0	LM	2-3%
9.114	21	Te Onepu Lst.	65.0	4.5	118	2.5	0.0	0.0		0.0	0.0	LM	3-4%
9.115	21	Te Onepu Lst.	-	5	136	2.5	*14?	2.0	25	2.0	0.0	LM	3-4%
9.117	21	Te Onepu Lst.	65.0	4.5	100	0	4.0	5.0		1.5	1.5	LM	2-3%
9.119	21	Te Onepu Lst.	64.0	4.5	163	0	1.0	0.0		0.0	1.5	LM	2.0%

Field no.	Locality	Formation	BaSO4	backg. at 25°2θ	calcite 29.4-30°2θ	aragonite 26.25°2θ	quartz 20.8°2θ	28°	feldspar	27.5°	clay min. 19.9°2θ	calcite LM-IM-IM	%
9.120.	21	Te Onepu Lst.	-	4	142	0	0.0	1.5	1.5	0.0	0.0	LM	<2%
11.7	31	Mason Ridge Fm.	63.0	5	149	0	0.0	1.0	1.0	1.5	0.0	LM-IM	4.0%
11.8	31	Mason Ridge Fm.	63.0	4.5	150	0	1.5	2.0	5.0	2.0	0.0	LM	2-3%
11.9	31	Mason Ridge Fm.	67.0	5	126	0	2.0	3.0	3.0	1.0	0.0	LM	2-3%
11.10.	31	Mason Ridge Fm.	61.0	5.5	248	2	2.0	2.0	2.0	0.0	0.0	LM	3.0%
11.11	31	Mason Ridge Fm	63.5	5.5	138	2?	2.5	2.0	2.5	0.0	2.0	LM	<2%
11.12	31	Mason Ridge Fm.	63.0	5.5	122	2	3.0	5.5	4.0	2.0	2.0	LM	3.0%
11.13	31	Mason Ridge Fm	63.0	5.5	106	0	6.5	7.0	3.0	0.0	3.0	LM	2-3%
11.14	31	Mason Ridge Fm.	69.0	4.5	130	0	2.0	2.5	1.5	1.5	0.0	LM-IM	4.0%
11.15	31	Mason Ridge Fm	65.0	4.5	123	1.5	2.0	1.5	2.0	0.0	1.5	LM	2-3%
11.16	31	Mason Ridge Fm	64.0	5	140	2.5	2.0	2.0	2.0	0.0	0.0	LM	3-4%
11.18	31	Mason Ridge Fm	63.0	4	120	0	0.0	2.0	2.0	0.0	0.0	LM	2.0%
11.19	31	Mason Ridge Fm	64.0	6	76	0	6.0	8.5	2.0	0.0	2.5	LM	<2%
11.20a	31	Mason Ridge Fm	64.0	5.5	148	0	2.0	3.5	2.0	0.0	1.0	LM	2.0%
11.20b	31	Mason Ridge Fm.	61.0	6	142	0	3.5	3.5	2.0	0.0	1.5	LM	2-3%
11.21	31	Mason Ridge Fm	63.0	5	124	2.5	0.0	7.0	2.0	2.0	0.0	IM	7.0%
11.22	31	Mason Ridge Fm	63.0	5	130	0	0.0	2.0	2.0	0.0	2?	LM-IM	4.0%
11.23	31	Mason Ridge Fm	64.0	5	132	0	1.5?	5.0	2.0	0.0	1.5	LM	2-3%
11.25	29	Mason Ridge Fm.	-	4.5	118	2	2.0	4.5	2.0	2.0	1.5	LM	2-3%
11.26	29	Mason Ridge Fm.	64.0	5.5	144	0	2.0	1.5	2.0	1.5	0.0	LM	2-3%
11.28	29	Mason Ridge Fm.	65.0	5	136	0	1.5	2.5	2.0	0.0	1.5	LM	2-3%
11.29	29	Mason Ridge Fm.	64.0	5	141	2	2.0	2.0	2.0	0.0	1.5	LM	2-3%
11.30.	29	Mason Ridge Fm.	66.0	9	53	5.5	7.0	16.0	2.0	0.0	4.0	*LM	2.0%
11.33	29	Mason Ridge Fm.	65.0	6	148	2.5	3.0	3.0	2.0	1.0	2.0	LM	2-3%
11.35	29	Mason Ridge Fm.	-	5.5	170	3	4.5	7.0	2.0	4.0	0.0	LM	2-3%
11.36	29	Mason Ridge Fm.	-	6	175	2	4.0	23.0	2.0	3.0	0.0	LM	2.0%
11.37	29	Mason Ridge Fm.	67.0	6.5	180	3	6.5	4.0	2.0	0.0	2.5	LM	2-3%
11.38	29	Mason Ridge Fm.	68.0	7.5	83	0	5.5	18.5	2.0	4.0	3.5	LM	2-3%
11.40.	29	Mason Ridge Fm.	62.0	5	122	0	2.0	4.0	2.0	1.5	1.0	LM	3.0%
11.41	29	Mason Ridge Fm.	63.0	5.5	154	0	2.5	3.0	2.0	1.5	1.5	LM	2-3%
11.42	29	Mason Ridge Fm.	67.5	5	144	0	4.0	4.0	2.0	1.5	0.0	LM	3.0%
11.43	29	Mason Ridge Fm.	67.5	6.5	112	?	6.0	13.5	2.0	3.0	2.5	LM	2-3%
11.44	29	Mason Ridge Fm.	66.0	5.5	191	2	2.5	2.5	2.5	0.0	1.5	LM	2.0%
11.45	29	Mason Ridge Fm.	66.5	5.5	128	2.5	3.5	3.0	2.0	3.0	2.0	LM	2.0%
11.50.	30	Mason Ridge Fm.	64.0	6	114	?	3.0	5.0	2.0	3.5	2.0	LM	3.0%
11.51	30	Mason Ridge Fm	-	6	141	3	2.0	3.0	2.0	0.0	0.0	LM	2-3%
11.52	30	Mason Ridge Fm	65.0	5.5	100	11.5	1.5	2.5	2.0	1.5	0.0	LM	<2%
11.54	30	Mason Ridge Fm	-	5	133	3.5	2.0	14.0	2.0	0.0	2.5?	LM	3.0%
11.56	30	Mason Ridge Fm	64.5	5	142	2.5	2.0	1.5	2.0	1.0	2.0	LM	3-4%
11.57	30	Mason Ridge Fm	67.0	5	150	3	3.0	2.5	2.0	1.0	0.0	LM	3-4%
11.59	30	Mason Ridge Fm	63.0	5.5	130	0	2.0	3.0	2.0	2.5	0.0	IM	7.0%
11.62	30	Mason Ridge Fm	-	5.5	118	?	3.5	5.0	2.0	2.0	1.5	LM	3-4%
11.63	30	Mason Ridge Fm	-	4.5	156	0	1.5	0.0	1.5	0.0	1.5	LM	3.0%
11.64	30	Mason Ridge Fm	64.0	5.5	185	2.5	2.0	2.5	2.0	3.5	1?	LM	<2%
11.65	30	Mason Ridge Fm	63.0	5.5	154	0	3.0	2.5	2.0	0.0	2.0	LM	2-3%
11.68	30	Mason Ridge Fm	66.5	5	158	0	0.0	2.5	2.0	2.0	0.0	LM	2-3%
11.70.	30	Mason Ridge Fm	-	7	61.5	4.5	11.5	15.0	2.0	0.0	2.5	LM	2-3%
11.71	30	Mason Ridge Fm	64.0	5.5	140	2	2.5	4.0	2.0	0.0	2.0	LM	2-3%
11.72	30	Mason Ridge Fm	64.0	8	81	2.5	10.0	11.0	2.0	3.5	3.0	LM	2-3%
11.75	32	Mason Ridge Fm.	65.5	5	110	2.5	5.0	7.5	2.0	3.0	1?	LM	2-3%
11.76	32	Mason Ridge Fm	65.0	5	102	3	8.0	4.0	2.0	0.0	2?	LM	2-3%
11.77	32	Mason Ridge Fm	62.5	5	143	3	1.5	5.0	2.0	1.5	1.5	LM	2-3%
11.78	32	Mason Ridge Fm	63.0	5	134	2	0.0	2.5	2.0	0.0	1.5?	LM	3.0%
11.81	33	Mason Ridge Fm.	65.0	4.5	150	3	2.5	2.0	1.5	0.0	1.5	LM	2.0%
11.84	33	Mason Ridge Fm	68.0	5	140	1.5	2?	1.5?	2.0	0.0	2?	LM	2-3%
11.85	33	Mason Ridge Fm	62.0	6	180	2.5	1.5	2.5	2.0	1.5	0.0	LM	2-3%
11.86	33	Mason Ridge Fm	66.0	6	158	2	3.0	6.0	2.0	0.0	2.0	LM	2-3%
11.87a	33	Mason Ridge Fm	63.5	5.5	224	2.5	1.5	2.0	3.0	0.0	2.0	LM	2-3%
11.88	33	Mason Ridge Fm	62.5	4.5	186	2.5	2.5	2.0	1.5	1.5	1.5	LM	2.0%
11.89	33	Mason Ridge Fm	65.0	5.5	204	2.5	4.0	5.5	2.0	0.0	1.5	IM	4-5%
11.90.	33	Mason Ridge Fm	64.0	7	200	4	2.0	7.0	2.0	1.5	1.5?	LM	2-3%

APPENDIX 8 - XRD Data

Field ref.	Locality	Formation	B.Std	backg. at 25°2θ	calcite 29.4-30°2θ	aragonite 26.25°2θ	quartz 20.8°2θ	28°	feldspar -	27.5°	clay min. 19.9°2θ	calcite LM-IM-IIM	%
12.1	46	Kereru Lst.	65.0	5	147	3.5	3.0	2.0		0.0	0.0	LM	2-3%
12.5	46	Kereru Lst.	63.5	5.5	156	2	2.5		3.5	0.0	0.0	LM	2-3%
12.6	46	Kereru Lst.	64.0	5.5	156	2.5	2.5	3.0		0.0	0.0	LM	3-4%
12.7	46	Kereru Lst.	-	5	150	2	2.0	0.0		0.0	2.0	LM	2-3%
12.8	46	Kereru Lst.	63.5	6	118	2.5	5.5	10.0		2.5	2.0	LM	2-3%
13.1	47	Sentry Box Lst.											
13.2	47	Sentry Box Lst.	66.0	5	138	2	2.0	4.0		0.0	1.5	LM	2-3%
13.3	47	Sentry Box Lst.	65.0	5	148	0	3.0	3.5		2.0	0.0	LM	2.0%
14.1	35	Matapiro Lst.	67.0	5	200	5	0.0	0.0	1.5	0.0	1.5	LM	2-3%
14.14	35	Matapiro Lst.	66.0	5.5	240	4	3.0	1.5		0.0	0.0	LM	2-3%
14.15	35	Matapiro Lst.	65.0	5.5	182	2.5	2.5	0.0		0.0	2.5	LM	2-3%
14.16	35	Matapiro Lst.	65.0	5.5	226	2.5	2.5	3.0	9.5	2.0	2.0	LM	2-3%
14.19	35	Matapiro Lst.	67.0	5.5	200	3	3.0	3.5		2.0	0.0	LM	2-3%
14.24	35	Matapiro Lst.	67.0	5	134	2.5	4.0	5.0		2.0	2.0	LM	2-3%
14.25	35	Matapiro Lst.	62.5	5	182	6	0.0	15.0		0.0	0.0	LM	3.0%
14.26	35	Matapiro Lst.	-	5.5	170	6.5	2.5	2.5	3.0	0.0	2.0	LM	<2%
15.25	41	Te Waka Fm.	65.0	6	166	1.5	4.0	5.5		2.0	0.0	IM	4-5%
15.27	41	Te Waka Fm.	63.0	7	162	2.5	3.0	4.0		3.0	2.0	LM-IM	4.0%
15.28	41	Te Waka Fm.	67.0	6.5	150	2	4.0	8.0		5.0	1.5	LM-IM	3-4%
15.29	41	Te Waka Fm.	66.0	6.5	143	2.5	3.5	2.5	3.0	2.0	3.0	LM	3-4%
15.31	41	Te Waka Fm.	67.0	9	81.5	?	11.0	18.0		3.5	2.0	LM	3-4%
15.32	41	Te Waka Fm.	65.0	7.5	125	4	6.0	14.0		2.5	2.0	IM	5.0%
15.34	41	Te Waka Fm.	-	7	134	3	3.5	3.0	4.0	0.0	1.5	IM	4-5%
15.35	41	Te Waka Fm.	66.0	8	85	3	11.0	20.0	8.0	0.0	0.0	LM-IM	4.0%
15.36	41	Te Waka Fm.	-	6.5	109	7.5	3.5	38.0	17.0	4.0	0.0	IM	6-7%
15.37	41	Te Waka Fm.	66.0	7	170	3.5?	9.0	14.0	7.0	4.0	3.0	LM	3.0%
15.38	41	Te Waka Fm.	66.5	7.5	126	4	11.0	12.0	8.0	3.5	1.5	LM-IM	4.0%
15.39	41	Te Waka Fm.	65.0	7	102	5.5	6.5	18.5	18.0	3.5	0.0	LM-IM	3-5%
15.40.	41	Te Waka Fm.	65.0	7	152	6	8.0	13.0	3.5	3.0	0.0	IM	4-5%
15.41	41	Te Waka Fm.											
15.42	41	Te Waka Fm.	65.0	6.5	90	6.5	8.5	19.0		5.0	1.5	IM	5-6%
15.43	41	Te Waka Fm.	-	8.5	74.5	4.5	12.0	4.0	18.0	5.0	2.5	LM	2-3%
15.44	41	Te Waka Fm.	65.0	6.5	142	4	7.5	26.0		3.0	2.0	IM	5-6%
15.45	41	Te Waka Fm.	65.0	7	114	3 (?)	5.0	5.5	4.5	4.0	2.0	IM	5-6%
15.46	41	Te Waka Fm.	66.0	7.5	105	4 (?)	7.5	5.0	4.5	6.5	2.5	LM	3-4%
15.47	41	Te Waka Fm.	63.0	6	128	3 (?)	5.0	5.0		4.0	2.5	IM	5.0%
16.4	44	Whanawhana Lst	65.0	6	140	3?	2.5	4.5	3.0	1.5	0.0	IM	5-6%
16.6	43	Te Waka Fm.	66.0	6	166	2.5	2.5	5.0	4.5	11.0	0.0	IM	4-5%
16.8	43	Te Waka Fm.	67.0	6	172	2	2.0	7.0	3.0	2.0	0.0	IM	4-5%
16.9	43	Te Waka Fm.	63.0	6.5	175	?	6.0	4.5	3.0	2.0	2.0	IM	4-5%
16.10.	43	Te Waka Fm.	66.0	8	89	0	11.0	49.0		6.0	2.5	LM	<2%
16.12	43	Te Waka Fm.	65.0	7	79	0	20.5	31.0		5.0	3.0	IM	4-5%
16.13	43	Te Waka Fm.	67.0	7.5	110	0	10.5	12.5		5.0	2.5	LM	2-3%
16.15	43	Te Waka Fm.	67.5	6	122	0	4.5	6.0		3.5	1.5?	LM	3-4%
16.16	43	Te Waka Fm.	65.0	6.5	101	2.5?	6.0	13.0		3.0	0.0	LM	3.0%
16.17	43	Te Waka Fm.	67.0	6	125	2..5	5.0	8.0	4.0	2.0	2.0	LM-IM	4.0%
17.11	36	Scinde Island Lst	66.0	6.5	112	0	8.0	14.0		2.5	2.5	LM	<2%
17.13	36	Scinde Island Lst	65.0	5	173	12	2.0	3.5		0.0	0.0	LM	2-3%
cv.656		Rotoaira Lst eq ?	65.0	7	110	0	12.0	53.0		9.0	1.5?	LM	3.0%
cv.658		Awapapa Lst eq	66.0	7.5	110	0	16.0	20.0		5.5	2.0	LM-IM	4.0%

APPENDIX 9

ICPOES ANALYSIS AND DATA

APPENDIX 9 – ICPOES ANALYSIS

Carbonate Digestion and analysis method for major and trace elements Elements commonly used: Ca, Mg, Fe, Sr, Na, Mn

Apparatus:
- 50 ml beaker
- 100 ml vol flask
- filter paper, Whatman No. 42 size 9 cm
- distilled and deionised water for ICP
- 100 ml plastic bottle for storage

Procedure:
1 Dry filter at 40°C and weigh

2 Weigh 0.04 g powdered sample into a 50 ml beaker, record weight of sample.

3 Add 8 ml of 8% v/v (1M HCl), swirl occasionally during digestion to mix solution and insoluble material

4 Digest like this for approx 10 – 30 minutes, but no more that 30 minutes.

5 Carefully pour the contents of beaker through filter paper into a 100ml volumetric flask, rinse beaker three times this way, until you are sure that all material has been washed out of the beaker. Use distilled deionised water for this.

6 Fill to 100 ml meniscus line, shake and transfer to storage flask.

7 Dry filter at 40°C again and reweigh to calculate insoluble fraction of carbonate material.

Standards
The standards are to be made up using spectrosol standards, with the addition of 1M HCl to keep the same matrix as the samples.

Standard Range
Ca 0 – 100 ppm
Fe 0 – 25 ppm
Mg 0 – 25 ppm
Mn 0 – 10 ppm
Na 0 – 50 ppm
Sr 0 – 10 ppm

Analysis
Read samples on the ICP with a full range of standards, run a middle standard after every ten samples to check for drift, and include duplicates in every ten as well.

Sample No	El	Concentration Unit	weight inp in g	Weight f1 in g	Weight f2 in g	residue in g f2-f1	CaCo3 in g input-residue	CaCO3 in % CaCO3/input	dilution factor 100/CaCO3	resulting conc in ppm Conc*dilution factor
4.141	Na	1.585 mg/L	0.0411	0.9351	0.9455	0.0104	0.0307	0.74695864	3257.32899	5162.87
	Fe	0.2343 mg/L	0.0411	0.9351	0.9455	0.0104	0.0307	0.74695864	3257.32899	763.19
	Ca	92.1914 mg/L	0.0411	0.9351	0.9455	0.0104	0.0307	0.74695864	3257.32899	300297.72
	Sr	0.1199 mg/L	0.0411	0.9351	0.9455	0.0104	0.0307	0.74695864	3257.32899	390.55
	Mn	0.0461 mg/L	0.0411	0.9351	0.9455	0.0104	0.0307	0.74695864	3257.32899	150.16
	Mg	0.4668 mg/L	0.0411	0.9351	0.9455	0.0104	0.0307	0.74695864	3257.32899	1520.52
4.93	Na	1.5065 mg/L	0.04	0.9288	0.9337	0.0049	0.0351	0.8775	2849.002849	4292.02
	Fe	0.1117 mg/L	0.04	0.9288	0.9337	0.0049	0.0351	0.8775	2849.002849	318.23
	Ca	106.0778 mg/L	0.04	0.9288	0.9337	0.0049	0.0351	0.8775	2849.002849	302215.95
	Sr	0.3429 mg/L	0.04	0.9288	0.9337	0.0049	0.0351	0.8775	2849.002849	976.92
	Mn	0.0346 mg/L	0.04	0.9288	0.9337	0.0049	0.0351	0.8775	2849.002849	98.58
	Mg	0.8618 mg/L	0.04	0.9288	0.9337	0.0049	0.0351	0.8775	2849.002849	2455.27
4.65	Na	1.234 mg/L	0.0408	0.9381	0.9432	0.0051	0.0357	0.875	2801.120448	3456.58
	Fe	0.1568 mg/L	0.0408	0.9381	0.9432	0.0051	0.0357	0.875	2801.120448	439.22
	Ca	115.6784 mg/L	0.0408	0.9381	0.9432	0.0051	0.0357	0.875	2801.120448	324029.13
	Sr	0.3589 mg/L	0.0408	0.9381	0.9432	0.0051	0.0357	0.875	2801.120448	1005.32
	Mn	0.0342 mg/L	0.0408	0.9381	0.9432	0.0051	0.0357	0.875	2801.120448	95.80
	Mg	0.8885 mg/L	0.0409	0.9327	0.9417	0.009	0.0319	0.7799511	3134.796238	2785.27
4.71	Na	1.4435 mg/L	0.0401	0.9305	0.9475	0.017	0.0231	0.57605985	4329.004329	6248.92
	Fe	0.4803 mg/L	0.0401	0.9305	0.9475	0.017	0.0231	0.57605985	4329.004329	2079.22
	Ca	63.813 mg/L	0.0401	0.9305	0.9475	0.017	0.0231	0.57605985	4329.004329	276246.75
	Sr	0.3166 mg/L	0.0401	0.9305	0.9475	0.017	0.0231	0.57605985	4329.004329	1370.56
	Mn	0.0517 mg/L	0.0401	0.9305	0.9475	0.017	0.0231	0.57605985	4329.004329	223.81
	Mg	0.6707 mg/L	0.0401	0.9305	0.9475	0.017	0.0231	0.57605985	4329.004329	2903.46
4.75	Na	1.5554 mg/L	0.0398	0.9285	0.94	0.0115	0.0283	0.71105528	3533.568905	5496.11
	Fe	0.2363 mg/L	0.0398	0.9285	0.94	0.0115	0.0283	0.71105528	3533.568905	834.98
	Ca	89.6188 mg/L	0.0398	0.9285	0.94	0.0115	0.0283	0.71105528	3533.568905	316674.20
	Sr	0.3753 mg/L	0.0398	0.9285	0.94	0.0115	0.0283	0.71105528	3533.568905	1326.15
	Mn	0.0359 mg/L	0.0398	0.9285	0.94	0.0115	0.0283	0.71105528	3533.568905	126.86
	Mg	0.8736 mg/L	0.0398	0.9285	0.94	0.0115	0.0283	0.71105528	3533.568905	3086.93
4.76	Na	1.5483 mg/L	0.0402	0.9253	0.9355	0.0102	0.03	0.74626866	3333.333333	5161.00
	Fe	0.4433 mg/L	0.0402	0.9253	0.9355	0.0102	0.03	0.74626866	3333.333333	1477.67
	Ca	88.9836 mg/L	0.0402	0.9253	0.9355	0.0102	0.03	0.74626866	3333.333333	296612.00
	Sr	0.4678 mg/L	0.0402	0.9253	0.9355	0.0102	0.03	0.74626866	3333.333333	1559.33
	Mn	0.0431 mg/L	0.0402	0.9253	0.9355	0.0102	0.03	0.74626866	3333.333333	143.67
	Mg	0.9484 mg/L	0.0402	0.9253	0.9355	0.0102	0.03	0.74626866	3333.333333	3161.33
4.33	Na	1.5275 mg/L	0.0405	0.9308	0.9354	0.0046	0.0359	0.88641975	2785.51532	4254.87
	Fe	0.2635 mg/L	0.0405	0.9308	0.9354	0.0046	0.0359	0.88641975	2785.51532	733.98
	Ca	104.68 mg/L	0.0405	0.9308	0.9354	0.0046	0.0359	0.88641975	2785.51532	291587.74
	Sr	0.1802 mg/L	0.0405	0.9308	0.9354	0.0046	0.0359	0.88641975	2785.51532	501.95
	Mn	0.0436 mg/L	0.0405	0.9308	0.9354	0.0046	0.0359	0.88641975	2785.51532	121.45
	Mg	0.5625 mg/L	0.0405	0.9308	0.9354	0.0046	0.0359	0.88641975	2785.51532	1566.85
	Na	1.1439 mg/L	0.0401	0.9244	0.9356	0.0112	0.0289	0.72069825	3460.207612	3958.13
4.11	Fe	0.2229 mg/L	0.0401	0.9244	0.9356	0.0112	0.0289	0.72069825	3460.207612	771.28
	Ca	88.9648 mg/L	0.0401	0.9244	0.9356	0.0112	0.0289	0.72069825	3460.207612	307836.68
	Sr	0.0968 mg/L	0.0401	0.9244	0.9356	0.0112	0.0289	0.72069825	3460.207612	334.95
	Mn	0.0591 mg/L	0.0401	0.9244	0.9356	0.0112	0.0289	0.72069825	3460.207612	204.50
	Mg	0.47 mg/L	0.0401	0.9244	0.9356	0.0112	0.0289	0.72069825	3460.207612	1626.30
4.13	Na	1.7642 mg/L	0.0398	0.9231	0.9331	0.01	0.0298	0.74874372	3355.704698	5920.13
	Fe	0.1393 mg/L	0.0398	0.9231	0.9331	0.01	0.0298	0.74874372	3355.704698	467.45
	Ca	84.262 mg/L	0.0398	0.9231	0.9331	0.01	0.0298	0.74874372	3355.704698	282758.39
	Sr	0.0719 mg/L	0.0398	0.9231	0.9331	0.01	0.0298	0.74874372	3355.704698	241.28
	Mn	0.0413 mg/L	0.0398	0.9231	0.9331	0.01	0.0298	0.74874372	3355.704698	138.59
	Mg	0.363 mg/L	0.0398	0.9231	0.9331	0.01	0.0298	0.74874372	3355.704698	1218.12
4.16	Na	1.3788 mg/L	0.0405	0.9341	0.9439	0.0098	0.0307	0.75802469	3257.32899	4491.21
	Fe	0.2758 mg/L	0.0405	0.9341	0.9439	0.0098	0.0307	0.75802469	3257.32899	898.37
	Ca	90.3006 mg/L	0.0405	0.9341	0.9439	0.0098	0.0307	0.75802469	3257.32899	294138.76
	Sr	0.1436 mg/L	0.0405	0.9341	0.9439	0.0098	0.0307	0.75802469	3257.32899	467.75
	Mn	0.0393 mg/L	0.0405	0.9341	0.9439	0.0098	0.0307	0.75802469	3257.32899	128.01
	Mg	0.5596 mg/L	0.0405	0.9341	0.9439	0.0098	0.0307	0.75802469	3257.32899	1822.80
4.17	Na	1.459 mg/L	0.0403	0.9342	0.9416	0.0074	0.0329	0.81637717	3039.513678	4434.65
	Fe	0.3248 mg/L	0.0403	0.9342	0.9416	0.0074	0.0329	0.81637717	3039.513678	987.23
	Ca	96.9942 mg/L	0.0403	0.9342	0.9416	0.0074	0.0329	0.81637717	3039.513678	294815.20
	Sr	0.1798 mg/L	0.0403	0.9342	0.9416	0.0074	0.0329	0.81637717	3039.513678	546.50
	Mn	0.0435 mg/L	0.0403	0.9342	0.9416	0.0074	0.0329	0.81637717	3039.513678	132.22
	Mg	0.5644 mg/L	0.0403	0.9342	0.9416	0.0074	0.0329	0.81637717	3039.513678	1715.50
4.18	Na	1.3814 mg/L	0.0402	0.9333	0.9391	0.0058	0.0344	0.85572139	2906.976744	4015.70
	Fe	0.1643 mg/L	0.0402	0.9333	0.9391	0.0058	0.0344	0.85572139	2906.976744	477.62
	Ca	99.1352 mg/L	0.0402	0.9333	0.9391	0.0058	0.0344	0.85572139	2906.976744	288183.72
	Sr	0.1378 mg/L	0.0402	0.9333	0.9391	0.0058	0.0344	0.85572139	2906.976744	400.58
	Mn	0.0497 mg/L	0.0402	0.9333	0.9391	0.0058	0.0344	0.85572139	2906.976744	144.48
	Mg	0.4941 mg/L	0.0402	0.9333	0.9391	0.0058	0.0344	0.85572139	2906.976744	1436.34
4.20	Na	1.0115 mg/L	0.0407	0.944	0.9625	0.0185	0.0222	0.54545455	4504.504505	4556.31
	Fe	0.2141 mg/L	0.0407	0.944	0.9625	0.0185	0.0222	0.54545455	4504.504505	964.41
	Ca	87.3154 mg/L	0.0407	0.944	0.9625	0.0185	0.0222	0.54545455	4504.504505	393312.61
	Sr	0.109 mg/L	0.0407	0.944	0.9625	0.0185	0.0222	0.54545455	4504.504505	490.99

Sample No	El	Concentration Unit	weight inp in g	Weight f1 in g	Weight f2 in g	residue in g f2-f1	CaCo3 in g input-residue	CaCO3 in % CaCO3/input	dilution factor 100/CaCO3	resulting conc in ppm Conc*dilution factor
	Mn	0.0378 mg/L	0.0407	0.944	0.9625	0.0185	0.0222	0.54545455	4504.504505	170.27
	Mg	0.3858 mg/L	0.0407	0.944	0.9625	0.0185	0.0222	0.54545455	4504.504505	1737.84
4.22	Na	1.4469 mg/L	0.04	0.9284	0.9424	0.014	0.026	0.65	3846.153846	5565.00
	Fe	0.2008 mg/L	0.04	0.9284	0.9424	0.014	0.026	0.65	3846.153846	772.31
	Ca	75.0076 mg/L	0.04	0.9284	0.9424	0.014	0.026	0.65	3846.153846	288490.77
	Sr	0.0963 mg/L	0.04	0.9284	0.9424	0.014	0.026	0.65	3846.153846	370.38
	Mn	0.0561 mg/L	0.04	0.9284	0.9424	0.014	0.026	0.65	3846.153846	215.77
	Mg	0.4298 mg/L	0.04	0.9284	0.9424	0.014	0.026	0.65	3846.153846	1653.08
4.31	Na	1.4013 mg/L	0.0404	0.9476	0.956	0.0084	0.032	0.79207921	3125	4379.06
	Fe	0.1513 mg/L	0.0404	0.9476	0.956	0.0084	0.032	0.79207921	3125	472.81
	Ca	96.8641 mg/L	0.0404	0.9476	0.956	0.0084	0.032	0.79207921	3125	302700.31
	Sr	0.1241 mg/L	0.0404	0.9476	0.956	0.0084	0.032	0.79207921	3125	387.81
	Mn	0.0537 mg/L	0.0404	0.9476	0.956	0.0084	0.032	0.79207921	3125	167.81
	Mg	0.4696 mg/L	0.0404	0.9476	0.956	0.0084	0.032	0.79207921	3125	1467.50
4.24	Na	1.3871 mg/L	0.0399	0.9238	0.9329	0.0091	0.0308	0.77192982	3246.753247	4503.57
	Fe	0.1076 mg/L	0.0399	0.9238	0.9329	0.0091	0.0308	0.77192982	3246.753247	349.35
	Ca	94.063 mg/L	0.0399	0.9238	0.9329	0.0091	0.0308	0.77192982	3246.753247	305399.35
	Sr	0.1157 mg/L	0.0399	0.9238	0.9329	0.0091	0.0308	0.77192982	3246.753247	375.65
	Mn	0.0424 mg/L	0.0399	0.9238	0.9329	0.0091	0.0308	0.77192982	3246.753247	137.66
	Mg	0.4305 mg/L	0.0399	0.9238	0.9329	0.0091	0.0308	0.77192982	3246.753247	1397.73
4.27	Na	-0.1953 mg/L	0.0403	0.9271	0.9391	0.012	0.0283	0.70223325	3533.568905	-690.11
	Fe	-0.1075 mg/L	0.0403	0.9271	0.9391	0.012	0.0283	0.70223325	3533.568905	-379.86
	Ca	-0.1832 mg/L	0.0403	0.9271	0.9391	0.012	0.0283	0.70223325	3533.568905	-647.35
	Sr	-0.0369 mg/L	0.0403	0.9271	0.9391	0.012	0.0283	0.70223325	3533.568905	-130.39
	Mn	0.0274 mg/L	0.0403	0.9271	0.9391	0.012	0.0283	0.70223325	3533.568905	96.82
	Mg	-0.0516 mg/L	0.0403	0.9271	0.9391	0.012	0.0283	0.70223325	3533.568905	-182.33
4.29	Na	-0.3202 mg/L	0.0403	0.917	0.9256	0.0086	0.0317	0.7866005	3154.574132	-1010.09
	Fe	-0.1049 mg/L	0.0403	0.917	0.9256	0.0086	0.0317	0.7866005	3154.574132	-330.91
	Ca	-0.1908 mg/L	0.0403	0.917	0.9256	0.0086	0.0317	0.7866005	3154.574132	-601.89
	Sr	-0.0312 mg/L	0.0403	0.917	0.9256	0.0086	0.0317	0.7866005	3154.574132	-98.42
	Mn	0.03 mg/L	0.0403	0.917	0.9256	0.0086	0.0317	0.7866005	3154.574132	94.64
	Mg	-0.0511 mg/L	0.0403	0.917	0.9256	0.0086	0.0317	0.7866005	3154.574132	-161.20
4.30	Na	-0.3431 mg/L	0.04	0.9457	0.9557	0.01	0.03	0.75	3333.333333	-1143.67
	Fe	-0.1058 mg/L	0.04	0.9457	0.9557	0.01	0.03	0.75	3333.333333	-352.67
	Ca	-0.1947 mg/L	0.04	0.9457	0.9557	0.01	0.03	0.75	3333.333333	-649.00
	Sr	-0.0331 mg/L	0.04	0.9457	0.9557	0.01	0.03	0.75	3333.333333	-110.33
	Mn	0.0276 mg/L	0.04	0.9457	0.9557	0.01	0.03	0.75	3333.333333	92.00
	Mg	-0.0518 mg/L	0.04	0.9457	0.9557	0.01	0.03	0.75	3333.333333	-172.67
4.5	Na	-0.3515 mg/L	0.0399	0.9176	0.9235	0.0059	0.034	0.85213033	2941.176471	-1033.82
	Fe	-0.1061 mg/L	0.0399	0.9176	0.9235	0.0059	0.034	0.85213033	2941.176471	-312.06
	Ca	-0.1957 mg/L	0.0399	0.9176	0.9235	0.0059	0.034	0.85213033	2941.176471	-575.59
	Sr	-0.0304 mg/L	0.0399	0.9176	0.9235	0.0059	0.034	0.85213033	2941.176471	-89.41
	Mn	0.0299 mg/L	0.0399	0.9176	0.9235	0.0059	0.034	0.85213033	2941.176471	87.94
	Fe	0.1379 mg/L	0.0398	0.9337	0.9356	0.0019	0.0379	0.95226131	2638.522427	363.85
	Ca	104.9443 mg/L	0.0398	0.9337	0.9356	0.0019	0.0379	0.95226131	2638.522427	276897.89
	Sr	0.2399 mg/L	0.0398	0.9337	0.9356	0.0019	0.0379	0.95226131	2638.522427	632.98
	Mn	0.042 mg/L	0.0398	0.9337	0.9356	0.0019	0.0379	0.95226131	2638.522427	110.82
	Mg	0.474 mg/L	0.0398	0.9337	0.9356	0.0019	0.0379	0.95226131	2638.522427	1250.66
5.38	Na	2.1871 mg/L	0.0398	0.9401	0.9432	0.0031	0.0367	0.92211055	2724.79564	5959.40
	Fe	0.199 mg/L	0.0398	0.9401	0.9432	0.0031	0.0367	0.92211055	2724.79564	542.23
	Ca	98.5252 mg/L	0.0398	0.9401	0.9432	0.0031	0.0367	0.92211055	2724.79564	268461.04
	Sr	0.2745 mg/L	0.0398	0.9401	0.9432	0.0031	0.0367	0.92211055	2724.79564	747.96
	Mn	0.0415 mg/L	0.0398	0.9401	0.9432	0.0031	0.0367	0.92211055	2724.79564	113.08
	Mg	0.5668 mg/L	0.0398	0.9401	0.9432	0.0031	0.0367	0.92211055	2724.79564	1544.41
5.44	Na	2.9204 mg/L	0.0401	0.9305	0.9336	0.0031	0.037	0.92269327	2702.702703	7892.97
	Fe	0.2332 mg/L	0.0401	0.9305	0.9336	0.0031	0.037	0.92269327	2702.702703	630.27
	Ca	101.3625 mg/L	0.0401	0.9305	0.9336	0.0031	0.037	0.92269327	2702.702703	273952.70
	Sr	0.2712 mg/L	0.0401	0.9305	0.9336	0.0031	0.037	0.92269327	2702.702703	732.97
	Mn	0.0442 mg/L	0.0401	0.9305	0.9336	0.0031	0.037	0.92269327	2702.702703	119.46
	Mg	0.6652 mg/L	0.0401	0.9305	0.9336	0.0031	0.037	0.92269327	2702.702703	1797.84
5.46a	Na	1.7797 mg/L	0.0399	0.9376	0.942	0.0044	0.0355	0.88972431	2816.901408	5013.24
	Fe	0.5011 mg/L	0.0399	0.9376	0.942	0.0044	0.0355	0.88972431	2816.901408	1411.55
	Ca	110.4535 mg/L	0.0399	0.9376	0.942	0.0044	0.0355	0.88972431	2816.901408	311136.62
	Sr	0.3117 mg/L	0.0399	0.9376	0.942	0.0044	0.0355	0.88972431	2816.901408	878.03
	Mn	0.0735 mg/L	0.0399	0.9376	0.942	0.0044	0.0355	0.88972431	2816.901408	207.04
	Mg	0.7737 mg/L	0.0399	0.9376	0.942	0.0044	0.0355	0.88972431	2816.901408	2179.44
5.48	Na	2.0411 mg/L	0.0398	0.9323	0.9389	0.0066	0.0332	0.83417085	3012.048193	6147.89
	Fe	0.3016 mg/L	0.0398	0.9323	0.9389	0.0066	0.0332	0.83417085	3012.048193	908.43
	Ca	107.9275 mg/L	0.0398	0.9323	0.9389	0.0066	0.0332	0.83417085	3012.048193	325082.83
	Sr	0.3351 mg/L	0.0398	0.9323	0.9389	0.0066	0.0332	0.83417085	3012.048193	1009.34
	Mn	0.0529 mg/L	0.0398	0.9323	0.9389	0.0066	0.0332	0.83417085	3012.048193	159.34
	Mg	0.8521 mg/L	0.0398	0.9323	0.9389	0.0066	0.0332	0.83417085	3012.048193	2566.57

Sample No	El	Concentration Unit	weight inp in g	Weight f1 in g	Weight f2 in g	residue in g f2-f1	CaCo3 in g input-residue	CaCO3 in % CaCO3/input	dilution factor 100/CaCO3	resulting conc in ppm Conc*dilution factor
5.51	Na	1.9685 mg/L	0.0397	0.9374	0.9403	0.0029	0.0368	0.92695214	2717.391304	5349.18
	Fe	0.1808 mg/L	0.0397	0.9374	0.9403	0.0029	0.0368	0.92695214	2717.391304	491.30
	Ca	111.8548 mg/L	0.0397	0.9374	0.9403	0.0029	0.0368	0.92695214	2717.391304	303953.26
	Sr	0.3992 mg/L	0.0397	0.9374	0.9403	0.0029	0.0368	0.92695214	2717.391304	1084.78
	Mn	0.037 mg/L	0.0397	0.9374	0.9403	0.0029	0.0368	0.92695214	2717.391304	100.54
	Mg	0.8304 mg/L	0.0397	0.9374	0.9403	0.0029	0.0368	0.92695214	2717.391304	2256.52
5.55	Na	-0.2934 mg/L	0.0404	0.936	0.9423	0.0063	0.0341	0.84405941	2932.55132	-860.41
	Fe	-0.1041 mg/L	0.0404	0.936	0.9423	0.0063	0.0341	0.84405941	2932.55132	-305.28
	Ca	-0.1587 mg/L	0.0404	0.936	0.9423	0.0063	0.0341	0.84405941	2932.55132	-465.40
	Sr	-0.0284 mg/L	0.0404	0.936	0.9423	0.0063	0.0341	0.84405941	2932.55132	-83.28
	Mn	0.026 mg/L	0.0404	0.936	0.9423	0.0063	0.0341	0.84405941	2932.55132	76.25
	Mg	-0.0513 mg/L	0.0404	0.936	0.9423	0.0063	0.0341	0.84405941	2932.55132	-150.44
5.56	Na	2.0121 mg/L	0.04	0.9341	0.9402	0.0061	0.0339	0.8475	2949.852507	5935.40
	Fe	0.2658 mg/L	0.04	0.9341	0.9402	0.0061	0.0339	0.8475	2949.852507	784.07
	Sr	0.3035 mg/L	0.04	0.9341	0.9402	0.0061	0.0339	0.8475	2949.852507	895.28
	Ca	146.8376 mg/L	0.04	0.9341	0.9402	0.0061	0.0339	0.8475	2949.852507	433149.26
	Mn	-0.0563 mg/L	0.04	0.9341	0.9402	0.0061	0.0339	0.8475	2949.852507	-166.08
	Mg	0.8091 mg/L	0.04	0.9341	0.9402	0.0061	0.0339	0.8475	2949.852507	2386.73
	Mg	0.925 mg/L	0.04	0.9341	0.9402	0.0061	0.0339	0.8475	2949.852507	2728.61
5.146	Na	1.4271 mg/L	0.0403	0.9328	0.9405	0.0077	0.0326	0.808933	3067.484663	4377.61
	Fe	0.3196 mg/L	0.0403	0.9328	0.9405	0.0077	0.0326	0.808933	3067.484663	980.37
	Sr	0.2073 mg/L	0.0403	0.9328	0.9405	0.0077	0.0326	0.808933	3067.484663	635.89
	Ca	153.1047 mg/L	0.0403	0.9328	0.9405	0.0077	0.0326	0.808933	3067.484663	469646.32
	Mn	-0.0629 mg/L	0.0403	0.9328	0.9405	0.0077	0.0326	0.808933	3067.484663	-192.94
	Mg	0.4367 mg/L	0.0403	0.9328	0.9405	0.0077	0.0326	0.808933	3067.484663	1339.57
	Mg	0.5166 mg/L	0.0403	0.9328	0.9405	0.0077	0.0326	0.808933	3067.484663	1584.66
5.112	Na	1.9247 mg/L	0.0401	0.9303	0.934	0.0037	0.0364	0.90773067	2747.252747	5287.64
	Fe	0.326 mg/L	0.0401	0.9303	0.934	0.0037	0.0364	0.90773067	2747.252747	895.60
	Sr	0.5963 mg/L	0.0401	0.9303	0.934	0.0037	0.0364	0.90773067	2747.252747	1638.19
	Ca	139.6762 mg/L	0.0401	0.9303	0.934	0.0037	0.0364	0.90773067	2747.252747	383725.82
	Mn	-0.0544 mg/L	0.0401	0.9303	0.934	0.0037	0.0364	0.90773067	2747.252747	-149.45
	Mg	1.3622 mg/L	0.0401	0.9303	0.934	0.0037	0.0364	0.90773067	2747.252747	3742.31
	Mg	1.3784 mg/L	0.0401	0.9303	0.934	0.0037	0.0364	0.90773067	2747.252747	3786.81
5.118	Na	1.3872 mg/L	0.0399	0.9392	0.9537	0.0145	0.0254	0.63659148	3937.007874	5461.42
	Fe	0.4718 mg/L	0.0399	0.9392	0.9537	0.0145	0.0254	0.63659148	3937.007874	1857.48
	Sr	0.0623 mg/L	0.0399	0.9392	0.9537	0.0145	0.0254	0.63659148	3937.007874	245.28
	Ca	95.5336 mg/L	0.0399	0.9392	0.9537	0.0145	0.0254	0.63659148	3937.007874	376116.54
	Mn	-0.0482 mg/L	0.0399	0.9392	0.9537	0.0145	0.0254	0.63659148	3937.007874	-189.76
	Mg	0.674 mg/L	0.0399	0.9392	0.9537	0.0145	0.0254	0.63659148	3937.007874	2653.54
	Mg	0.6896 mg/L	0.0399	0.9392	0.9537	0.0145	0.0254	0.63659148	3937.007874	2714.96
5.124	Na	1.2517 mg/L	0.04	0.9561	0.9593	0.0032	0.0368	0.92	2717.391304	3401.36
	Fe	0.661 mg/L	0.04	0.9561	0.9593	0.0032	0.0368	0.92	2717.391304	1796.20
	Sr	0.3534 mg/L	0.04	0.9561	0.9593	0.0032	0.0368	0.92	2717.391304	960.33
	Ca	146.1236 mg/L	0.04	0.9561	0.9593	0.0032	0.0368	0.92	2717.391304	397075.00
	Mn	-0.0571 mg/L	0.04	0.9561	0.9593	0.0032	0.0368	0.92	2717.391304	-155.16
	Mg	1.3667 mg/L	0.04	0.9561	0.9593	0.0032	0.0368	0.92	2717.391304	3713.86
	Mg	1.2686 mg/L	0.04	0.9561	0.9593	0.0032	0.0368	0.92	2717.391304	3447.28
5.127	Na	1.1296 mg/L	0.04	0.9327	0.9501	0.0174	0.0226	0.565	4424.778761	4998.23
	Fe	1.2209 mg/L	0.04	0.9327	0.9501	0.0174	0.0226	0.565	4424.778761	5402.21
	Sr	0.0614 mg/L	0.04	0.9327	0.9501	0.0174	0.0226	0.565	4424.778761	271.68
	Ca	77.7397 mg/L	0.04	0.9327	0.9501	0.0174	0.0226	0.565	4424.778761	343980.97
	Mn	0.0424 mg/L	0.04	0.9327	0.9501	0.0174	0.0226	0.565	4424.778761	187.61
	Mg	0.4896 mg/L	0.04	0.9327	0.9501	0.0174	0.0226	0.565	4424.778761	2166.37
	Mg	0.514 mg/L	0.04	0.9327	0.9501	0.0174	0.0226	0.565	4424.778761	2274.34
5.128	Na	1.2071 mg/L	0.041	0.9214	0.93	0.0086	0.0324	0.7902439	3086.419753	3725.62
	Fe	0.6149 mg/L	0.041	0.9214	0.93	0.0086	0.0324	0.7902439	3086.419753	1897.84
	Sr	0.3043 mg/L	0.041	0.9214	0.93	0.0086	0.0324	0.7902439	3086.419753	939.20
	Ca	151.7614 mg/L	0.041	0.9214	0.93	0.0086	0.0324	0.7902439	3086.419753	468399.38
	Mn	-0.0535 mg/L	0.041	0.9214	0.93	0.0086	0.0324	0.7902439	3086.419753	-165.12
	Mg	1.2382 mg/L	0.041	0.9214	0.93	0.0086	0.0324	0.7902439	3086.419753	3821.60
	Mg	1.2864 mg/L	0.041	0.9214	0.93	0.0086	0.0324	0.7902439	3086.419753	3970.37
5.129	Na	1.4686 mg/L	0.0405	0.9297	0.9408	0.0111	0.0294	0.72592593	3401.360544	4995.24
	Fe	0.6872 mg/L	0.0405	0.9297	0.9408	0.0111	0.0294	0.72592593	3401.360544	2337.41
	Sr	0.2674 mg/L	0.0405	0.9297	0.9408	0.0111	0.0294	0.72592593	3401.360544	909.52
	Ca	129.6201 mg/L	0.0405	0.9297	0.9408	0.0111	0.0294	0.72592593	3401.360544	440884.69
	Mn	-0.0463 mg/L	0.0405	0.9297	0.9408	0.0111	0.0294	0.72592593	3401.360544	-157.48
	Mg	1.109 mg/L	0.0405	0.9297	0.9408	0.0111	0.0294	0.72592593	3401.360544	3772.11
5.140a	Na	2.1083 mg/L	0.0409	0.931	0.9359	0.0049	0.036	0.8801956	2777.777778	5856.39
	Fe	0.9067 mg/L	0.0409	0.931	0.9359	0.0049	0.036	0.8801956	2777.777778	2518.61
	Sr	0.3216 mg/L	0.0409	0.931	0.9359	0.0049	0.036	0.8801956	2777.777778	893.33
	Ca	152.2486 mg/L	0.0409	0.931	0.9359	0.0049	0.036	0.8801956	2777.777778	422912.78
	Mn	0.0354 mg/L	0.0409	0.931	0.9359	0.0049	0.036	0.8801956	2777.777778	98.33
	Mg	1.3052 mg/L	0.0409	0.931	0.9359	0.0049	0.036	0.8801956	2777.777778	3625.56
	Mg	1.3294 mg/L	0.0409	0.931	0.9359	0.0049	0.036	0.8801956	2777.777778	3692.78

Sample No	El	Concentration Unit	weight inp in g	Weight f1 in g	Weight f2 in g	residue in g f2-f1	CaCo3 in g input-residue	CaCO3 in % CaCO3/input	dilution factor 100/CaCO3	resulting conc in ppm Conc*dilution factor
5.132	Na	1.6556 mg/L	0.0408	0.9333	0.9532	0.0199	0.0209	0.5122549	4784.688995	7921.53
	Fe	0.6547 mg/L	0.0408	0.9333	0.9532	0.0199	0.0209	0.5122549	4784.688995	3132.54
	Sr	0.1718 mg/L	0.0408	0.9333	0.9532	0.0199	0.0209	0.5122549	4784.688995	822.01
	Ca	80.2163 mg/L	0.0408	0.9333	0.9532	0.0199	0.0209	0.5122549	4784.688995	383810.05
	Mn	0.0349 mg/L	0.0408	0.9333	0.9532	0.0199	0.0209	0.5122549	4784.688995	166.99
	Mg	0.8916 mg/L	0.0408	0.9333	0.9532	0.0199	0.0209	0.5122549	4784.688995	4266.03
	Mg	0.8196 mg/L	0.0408	0.9333	0.9532	0.0199	0.0209	0.5122549	4784.688995	3921.53
7.12	Na	2.2015 mg/L	0.0403	0.9232	0.9315	0.0083	0.032	0.79404467	3125	6879.69
	Fe	0.5845 mg/L	0.0403	0.9232	0.9315	0.0083	0.032	0.79404467	3125	1826.56
	Sr	0.4821 mg/L	0.0403	0.9232	0.9315	0.0083	0.032	0.79404467	3125	1506.56
	Ca	151.3243 mg/L	0.0403	0.9232	0.9315	0.0083	0.032	0.79404467	3125	472888.44
	Mn	0.0248 mg/L	0.0403	0.9232	0.9315	0.0083	0.032	0.79404467	3125	77.50
	Mg	1.6696 mg/L	0.0403	0.9232	0.9315	0.0083	0.032	0.79404467	3125	5217.50
	Mg	1.6738 mg/L	0.0403	0.9232	0.9315	0.0083	0.032	0.79404467	3125	5230.63
7.15	Na	2.4848 mg/L	0.0402	0.9344	0.9409	0.0065	0.0337	0.83830846	2967.35905	7373.29
	Fe	0.3642 mg/L	0.0402	0.9344	0.9409	0.0065	0.0337	0.83830846	2967.35905	1080.71
	Sr	0.5134 mg/L	0.0402	0.9344	0.9409	0.0065	0.0337	0.83830846	2967.35905	1523.44
	Ca	155.9276 mg/L	0.0402	0.9344	0.9409	0.0065	0.0337	0.83830846	2967.35905	462693.18
	Mn	0.2489 mg/L	0.0402	0.9344	0.9409	0.0065	0.0337	0.83830846	2967.35905	738.58
	Mg	1.3909 mg/L	0.0402	0.9344	0.9409	0.0065	0.0337	0.83830846	2967.35905	4127.30
	Mg	1.3484 mg/L	0.0402	0.9344	0.9409	0.0065	0.0337	0.83830846	2967.35905	4001.19
7.18	Na	1.8509 mg/L	0.0404	0.9268	0.9343	0.0075	0.0329	0.81435644	3039.513678	5625.84
	Fe	0.2092 mg/L	0.0404	0.9268	0.9343	0.0075	0.0329	0.81435644	3039.513678	635.87
	Sr	0.2812 mg/L	0.0404	0.9268	0.9343	0.0075	0.0329	0.81435644	3039.513678	854.71
	Ca	159.6909 mg/L	0.0404	0.9268	0.9343	0.0075	0.0329	0.81435644	3039.513678	485382.67
	Mn	0.0127 mg/L	0.0404	0.9268	0.9343	0.0075	0.0329	0.81435644	3039.513678	38.60
	Mg	0.6714 mg/L	0.0404	0.9268	0.9343	0.0075	0.0329	0.81435644	3039.513678	2040.73
	Mg	0.711 mg/L	0.0404	0.9268	0.9343	0.0075	0.0329	0.81435644	3039.513678	2161.09
7.20	Na	2.7289 mg/L	0.0399	0.9188	0.9237	0.0049	0.035	0.87719298	2857.142857	7796.86
	Fe	0.2727 mg/L	0.0399	0.9188	0.9237	0.0049	0.035	0.87719298	2857.142857	779.14
	Sr	0.3618 mg/L	0.0399	0.9188	0.9237	0.0049	0.035	0.87719298	2857.142857	1033.71
	Ca	179.447 mg/L	0.0399	0.9188	0.9237	0.0049	0.035	0.87719298	2857.142857	512705.71
	Mn	0.0287 mg/L	0.0399	0.9188	0.9237	0.0049	0.035	0.87719298	2857.142857	82.00
	Mg	0.8189 mg/L	0.0399	0.9188	0.9237	0.0049	0.035	0.87719298	2857.142857	2339.71
	Mg	0.9044 mg/L	0.0399	0.9188	0.9237	0.0049	0.035	0.87719298	2857.142857	2584.00
7.21	Na	2.223 mg/L	0.0396	0.9297	0.938	0.0083	0.0313	0.79040404	3194.888179	7102.24
	Fe	0.2426 mg/L	0.0396	0.9297	0.938	0.0083	0.0313	0.79040404	3194.888179	775.08
	Sr	0.5826 mg/L	0.0396	0.9297	0.938	0.0083	0.0313	0.79040404	3194.888179	1861.34
	Ca	179.1826 mg/L	0.0396	0.9297	0.938	0.0083	0.0313	0.79040404	3194.888179	572468.37
	Mn	0.0219 mg/L	0.0396	0.9297	0.938	0.0083	0.0313	0.79040404	3194.888179	69.97
	Mg	1.278 mg/L	0.0396	0.9297	0.938	0.0083	0.0313	0.79040404	3194.888179	4083.07
	Mg	1.2367 mg/L	0.0396	0.9297	0.938	0.0083	0.0313	0.79040404	3194.888179	3951.12
7.23	Na	1.9648 mg/L	0.04	0.9351	0.9473	0.0122	0.0278	0.695	3597.122302	7067.63
	Fe	0.3694 mg/L	0.04	0.9351	0.9473	0.0122	0.0278	0.695	3597.122302	1328.78
	Sr	0.4714 mg/L	0.04	0.9351	0.9473	0.0122	0.0278	0.695	3597.122302	1695.68
	Ca	148.0226 mg/L	0.04	0.9351	0.9473	0.0122	0.0278	0.695	3597.122302	532455.40
	Mn	0.0217 mg/L	0.04	0.9351	0.9473	0.0122	0.0278	0.695	3597.122302	78.06
	Mg	1.3179 mg/L	0.04	0.9351	0.9473	0.0122	0.0278	0.695	3597.122302	4740.65
	Mg	1.3302 mg/L	0.04	0.9351	0.9473	0.0122	0.0278	0.695	3597.122302	4784.89
7.27	Na	1.8062 mg/L	0.04	0.9301	0.9532	0.0231	0.0169	0.4225	5917.159763	10687.57
	Fe	0.339 mg/L	0.04	0.9301	0.9532	0.0231	0.0169	0.4225	5917.159763	2005.92
	Sr	0.4712 mg/L	0.04	0.9301	0.9532	0.0231	0.0169	0.4225	5917.159763	2788.17
	Ca	106.219 mg/L	0.04	0.9301	0.9532	0.0231	0.0169	0.4225	5917.159763	628514.79
	Mn	0.0207 mg/L	0.04	0.9301	0.9532	0.0231	0.0169	0.4225	5917.159763	122.49
	Mg	1.2893 mg/L	0.04	0.9301	0.9532	0.0231	0.0169	0.4225	5917.159763	7628.99
	Mg	1.2686 mg/L	0.04	0.9301	0.9532	0.0231	0.0169	0.4225	5917.159763	7506.51
7.43	Na	2.0053 mg/L	0.04	0.9556	0.9656	0.01	0.03	0.75	3333.333333	6684.33
	Fe	0.9039 mg/L	0.04	0.9556	0.9656	0.01	0.03	0.75	3333.333333	3013.00
	Sr	0.6053 mg/L	0.04	0.9556	0.9656	0.01	0.03	0.75	3333.333333	2017.67
	Ca	156.5174 mg/L	0.04	0.9556	0.9656	0.01	0.03	0.75	3333.333333	521724.67
	Mn	0.0236 mg/L	0.04	0.9556	0.9656	0.01	0.03	0.75	3333.333333	78.67
	Mg	1.905 mg/L	0.04	0.9556	0.9656	0.01	0.03	0.75	3333.333333	6350.00
	Mg	1.8469 mg/L	0.04	0.9556	0.9656	0.01	0.03	0.75	3333.333333	6156.33
7.49	Na	2.0859 mg/L	0.0405	0.9338	0.9447	0.0109	0.0296	0.7308642	3378.378378	7046.96
	Fe	0.8773 mg/L	0.0405	0.9338	0.9447	0.0109	0.0296	0.7308642	3378.378378	2963.85
	Sr	0.5837 mg/L	0.0405	0.9338	0.9447	0.0109	0.0296	0.7308642	3378.378378	1971.96
	Ca	145.1302 mg/L	0.0405	0.9338	0.9447	0.0109	0.0296	0.7308642	3378.378378	490304.73
	Mn	0.0152 mg/L	0.0405	0.9338	0.9447	0.0109	0.0296	0.7308642	3378.378378	51.35
	Mg	1.6751 mg/L	0.0405	0.9338	0.9447	0.0109	0.0296	0.7308642	3378.378378	5659.12
	Mg	1.7514 mg/L	0.0405	0.9338	0.9447	0.0109	0.0296	0.7308642	3378.378378	5916.89
9.9	Na	2.2318 mg/L	0.0398	0.9259	0.9316	0.0057	0.0341	0.85678392	2932.55132	6544.87
	Fe	0.0739 mg/L	0.0398	0.9259	0.9316	0.0057	0.0341	0.85678392	2932.55132	216.72
	Sr	0.5137 mg/L	0.0398	0.9259	0.9316	0.0057	0.0341	0.85678392	2932.55132	1506.45
	Ca	173.4808 mg/L	0.0398	0.9259	0.9316	0.0057	0.0341	0.85678392	2932.55132	508741.35
	Mn	0.0226 mg/L	0.0398	0.9259	0.9316	0.0057	0.0341	0.85678392	2932.55132	66.28
	Mg	1.6092 mg/L	0.0398	0.9259	0.9316	0.0057	0.0341	0.85678392	2932.55132	4719.06

Sample No	El	Concentration Unit	weight inp in g	Weight f1 in g	Weight f2 in g	residue in g f2-f1	CaCo3 in g input-residue	CaCO3 in % CaCO3/input	dilution factor 100/CaCO3	resulting conc in ppm Conc*dilution factor
9.16	Na	2.3299 mg/L	0.0397	0.9302	0.9354	0.0052	0.0345	0.86901763	2898.550725	6753.33
	Fe	0.1097 mg/L	0.0397	0.9302	0.9354	0.0052	0.0345	0.86901763	2898.550725	317.97
	Sr	0.5509 mg/L	0.0397	0.9302	0.9354	0.0052	0.0345	0.86901763	2898.550725	1596.81
	Ca	178.7613 mg/L	0.0397	0.9302	0.9354	0.0052	0.0345	0.86901763	2898.550725	518148.70
	Mn	0.0169 mg/L	0.0397	0.9302	0.9354	0.0052	0.0345	0.86901763	2898.550725	48.99
	Mg	1.0772 mg/L	0.0397	0.9302	0.9354	0.0052	0.0345	0.86901763	2898.550725	3122.32
	Mg	1.1192 mg/L	0.0397	0.9302	0.9354	0.0052	0.0345	0.86901763	2898.550725	3244.06
9.15	Na	2.5693 mg/L	0.0399	0.9236	0.9245	0.0009	0.039	0.97744361	2564.102564	6587.95
	Fe	0.0695 mg/L	0.0399	0.9236	0.9245	0.0009	0.039	0.97744361	2564.102564	178.21
	Sr	0.4959 mg/L	0.0399	0.9236	0.9245	0.0009	0.039	0.97744361	2564.102564	1271.54
	Ca	179.8564 mg/L	0.0399	0.9236	0.9245	0.0009	0.039	0.97744361	2564.102564	461170.26
	Mn	0.0237 mg/L	0.0399	0.9236	0.9245	0.0009	0.039	0.97744361	2564.102564	60.77
	Mg	1.6217 mg/L	0.0399	0.9236	0.9245	0.0009	0.039	0.97744361	2564.102564	4158.21
	Mg	1.7192 mg/L	0.0399	0.9236	0.9245	0.0009	0.039	0.97744361	2564.102564	4408.21
9.37	Na	2.3564 mg/L	0.0407	0.9318	0.9407	0.0089	0.0318	0.78132678	3144.654088	7410.06
	Fe	0.172 mg/L	0.0407	0.9318	0.9407	0.0089	0.0318	0.78132678	3144.654088	540.88
	Sr	0.4772 mg/L	0.0407	0.9318	0.9407	0.0089	0.0318	0.78132678	3144.654088	1500.63
	Ca	176.3731 mg/L	0.0407	0.9318	0.9407	0.0089	0.0318	0.78132678	3144.654088	554632.39
	Mn	0.0519 mg/L	0.0407	0.9318	0.9407	0.0089	0.0318	0.78132678	3144.654088	163.21
	Mg	1.5901 mg/L	0.0407	0.9318	0.9407	0.0089	0.0318	0.78132678	3144.654088	5000.31
	Mg	1.7691 mg/L	0.0407	0.9318	0.9407	0.0089	0.0318	0.78132678	3144.654088	5563.21
	Na	2.2686 mg/L	0.0397	0.9213	0.93	0.0087	0.031	0.78085642	3225.806452	7318.06
	Fe	0.1751 mg/L	0.0397	0.9213	0.93	0.0087	0.031	0.78085642	3225.806452	564.84
9.64	Sr	0.4428 mg/L	0.0397	0.9213	0.93	0.0087	0.031	0.78085642	3225.806452	1428.39
	Ca	170.3593 mg/L	0.0397	0.9213	0.93	0.0087	0.031	0.78085642	3225.806452	549546.13
	Mn	0.0288 mg/L	0.0397	0.9213	0.93	0.0087	0.031	0.78085642	3225.806452	92.90
	Mg	1.5521 mg/L	0.0397	0.9213	0.93	0.0087	0.031	0.78085642	3225.806452	5006.77
	Mg	1.6086 mg/L	0.0397	0.9213	0.93	0.0087	0.031	0.78085642	3225.806452	5189.03
9.69	Na	2.0528 mg/L	0.0404	0.9338	0.9426	0.0088	0.0316	0.78217822	3164.556962	6496.20
	Fe	0.2009 mg/L	0.0404	0.9338	0.9426	0.0088	0.0316	0.78217822	3164.556962	635.76
	Sr	0.4467 mg/L	0.0404	0.9338	0.9426	0.0088	0.0316	0.78217822	3164.556962	1413.61
	Ca	170.5078 mg/L	0.0404	0.9338	0.9426	0.0088	0.0316	0.78217822	3164.556962	539581.65
	Mn	0.0314 mg/L	0.0404	0.9338	0.9426	0.0088	0.0316	0.78217822	3164.556962	99.37
	Mg	1.4526 mg/L	0.0404	0.9338	0.9426	0.0088	0.0316	0.78217822	3164.556962	4596.84
	Mg	1.6149 mg/L	0.0404	0.9338	0.9426	0.0088	0.0316	0.78217822	3164.556962	5110.44
11.7	Na	2.0652 mg/L	0.0397	0.9256	0.9354	0.0098	0.0299	0.75314861	3344.481605	6907.02
	Fe	0.3369 mg/L	0.0397	0.9256	0.9354	0.0098	0.0299	0.75314861	3344.481605	1126.76
	Sr	0.5416 mg/L	0.0397	0.9256	0.9354	0.0098	0.0299	0.75314861	3344.481605	1811.37
	Ca	187.9342 mg/L	0.0397	0.9256	0.9354	0.0098	0.0299	0.75314861	3344.481605	628542.47
	Mn	0.048 mg/L	0.0397	0.9256	0.9354	0.0098	0.0299	0.75314861	3344.481605	160.54
	Mg	1.7288 mg/L	0.0397	0.9256	0.9354	0.0098	0.0299	0.75314861	3344.481605	5781.94
	Mg	1.7794 mg/L	0.0397	0.9256	0.9354	0.0098	0.0299	0.75314861	3344.481605	5951.17
11.10	Na	2.4188 mg/L	0.0402	0.9292	0.9405	0.0113	0.0289	0.71890547	3460.207612	8369.55
	Fe	0.1825 mg/L	0.0402	0.9292	0.9405	0.0113	0.0289	0.71890547	3460.207612	631.49
	Sr	0.7496 mg/L	0.0402	0.9292	0.9405	0.0113	0.0289	0.71890547	3460.207612	2593.77
	Ca	189.1847 mg/L	0.0402	0.9292	0.9405	0.0113	0.0289	0.71890547	3460.207612	654618.34
	Mn	0.0215 mg/L	0.0402	0.9292	0.9405	0.0113	0.0289	0.71890547	3460.207612	74.39
	Mg	1.9002 mg/L	0.0402	0.9292	0.9405	0.0113	0.0289	0.71890547	3460.207612	6575.09
	Mg	1.9256 mg/L	0.0402	0.9292	0.9405	0.0113	0.0289	0.71890547	3460.207612	6662.98
11.11	Na	2.1372 mg/L	0.0411	0.9146	0.9235	0.0089	0.0322	0.78345499	3105.590062	6637.27
	Fe	0.2457 mg/L	0.0411	0.9146	0.9235	0.0089	0.0322	0.78345499	3105.590062	763.04
	Sr	0.4822 mg/L	0.0411	0.9146	0.9235	0.0089	0.0322	0.78345499	3105.590062	1497.52
	Ca	147.6438 mg/L	0.0411	0.9146	0.9235	0.0089	0.0322	0.78345499	3105.590062	458521.12
	Mn	0.0219 mg/L	0.0411	0.9146	0.9235	0.0089	0.0322	0.78345499	3105.590062	68.01
	Mg	1.2084 mg/L	0.0411	0.9146	0.9235	0.0089	0.0322	0.78345499	3105.590062	3752.80
	Mg	1.2718 mg/L	0.0411	0.9146	0.9235	0.0089	0.0322	0.78345499	3105.590062	3949.69
11.15	Na	2.277 mg/L	0.0404	0.939	0.9456	0.0066	0.0338	0.83663366	2958.579882	6736.69
	Fe	0.196 mg/L	0.0404	0.939	0.9456	0.0066	0.0338	0.83663366	2958.579882	579.88
	Sr	0.5491 mg/L	0.0404	0.939	0.9456	0.0066	0.0338	0.83663366	2958.579882	1624.56
	Ca	174.0282 mg/L	0.0404	0.939	0.9456	0.0066	0.0338	0.83663366	2958.579882	514876.33
	Mn	0.024 mg/L	0.0404	0.939	0.9456	0.0066	0.0338	0.83663366	2958.579882	71.01
	Mg	1.8925 mg/L	0.0404	0.939	0.9456	0.0066	0.0338	0.83663366	2958.579882	5599.11
	Mg	1.8364 mg/L	0.0404	0.939	0.9456	0.0066	0.0338	0.83663366	2958.579882	5433.14
11.18	Na	2.0199 mg/L	0.0399	0.9357	0.9413	0.0056	0.0343	0.85964912	2915.451895	5888.92
	Fe	0.193 mg/L	0.0399	0.9357	0.9413	0.0056	0.0343	0.85964912	2915.451895	562.68
	Sr	0.4288 mg/L	0.0399	0.9357	0.9413	0.0056	0.0343	0.85964912	2915.451895	1250.15
	Ca	173.8389 mg/L	0.0399	0.9357	0.9413	0.0056	0.0343	0.85964912	2915.451895	506818.95
	Mn	0.0665 mg/L	0.0399	0.9357	0.9413	0.0056	0.0343	0.85964912	2915.451895	193.88
	Mg	1.4131 mg/L	0.0399	0.9357	0.9413	0.0056	0.0343	0.85964912	2915.451895	4119.83
11.21	Na	2.5552 mg/L	0.0404	0.9216	0.9287	0.0071	0.0333	0.82425743	3003.003003	7673.27
	Fe	0.2527 mg/L	0.0404	0.9216	0.9287	0.0071	0.0333	0.82425743	3003.003003	758.86
	Sr	0.5697 mg/L	0.0404	0.9216	0.9287	0.0071	0.0333	0.82425743	3003.003003	1710.81
	Ca	172.4956 mg/L	0.0404	0.9216	0.9287	0.0071	0.0333	0.82425743	3003.003003	518004.80
	Mn	0.0344 mg/L	0.0404	0.9216	0.9287	0.0071	0.0333	0.82425743	3003.003003	103.30
	Mg	2.114 mg/L	0.0404	0.9216	0.9287	0.0071	0.0333	0.82425743	3003.003003	6348.35

Sample No	El	Concentration Unit	weight inp in g	Weight f1 in g	Weight f2 in g	residue in g f2-f1	CaCo3 in g input-residue	CaCO3 in % CaCO3/input	dilution factor 100/CaCO3	resulting conc in ppm Conc*dilution factor
11.23	Na	2.0305 mg/L	0.0399	0.9249	0.93	0.0051	0.0348	0.87218045	2873.563218	5834.77
	Fe	0.264 mg/L	0.0399	0.9249	0.93	0.0051	0.0348	0.87218045	2873.563218	758.62
	Sr	0.3753 mg/L	0.0399	0.9249	0.93	0.0051	0.0348	0.87218045	2873.563218	1078.45
	Ca	161.5292 mg/L	0.0399	0.9249	0.93	0.0051	0.0348	0.87218045	2873.563218	464164.37
	Mn	0.0294 mg/L	0.0399	0.9249	0.93	0.0051	0.0348	0.87218045	2873.563218	84.48
	Mg	1.868 mg/L	0.0399	0.9249	0.93	0.0051	0.0348	0.87218045	2873.563218	5367.82
	Mg	1.9069 mg/L	0.0399	0.9249	0.93	0.0051	0.0348	0.87218045	2873.563218	5479.60
7.6	Na	1.516 mg/L	0.0403	0.9303	0.9336	0.0033	0.037	0.91811414	2702.702703	4097.30
	Fe	0.4078 mg/L	0.0403	0.9303	0.9336	0.0033	0.037	0.91811414	2702.702703	1102.16
	Sr	0.2913 mg/L	0.0403	0.9303	0.9336	0.0033	0.037	0.91811414	2702.702703	787.30
	Ca	190.7484 mg/L	0.0403	0.9303	0.9336	0.0033	0.037	0.91811414	2702.702703	515536.22
	Mn	0.0105 mg/L	0.0403	0.9303	0.9336	0.0033	0.037	0.91811414	2702.702703	28.38
	Mg	1.215 mg/L	0.0403	0.9303	0.9336	0.0033	0.037	0.91811414	2702.702703	3283.78
	Mg	1.2618 mg/L	0.0403	0.9303	0.9336	0.0033	0.037	0.91811414	2702.702703	3410.27
11.20	Na	2.0546 mg/L	0.0399	0.9331	0.9439	0.0108	0.0291	0.72932331	3436.426117	7060.48
	Fe	0.3785 mg/L	0.0399	0.9331	0.9439	0.0108	0.0291	0.72932331	3436.426117	1300.69
	Sr	0.3573 mg/L	0.0399	0.9331	0.9439	0.0108	0.0291	0.72932331	3436.426117	1227.84
	Ca	178.6939 mg/L	0.0399	0.9331	0.9439	0.0108	0.0291	0.72932331	3436.426117	614068.38
	Mn	0.0347 mg/L	0.0399	0.9331	0.9439	0.0108	0.0291	0.72932331	3436.426117	119.24
	Mg	1.3246 mg/L	0.0399	0.9331	0.9439	0.0108	0.0291	0.72932331	3436.426117	4551.89
	Mg	1.2882 mg/L	0.0399	0.9331	0.9439	0.0108	0.0291	0.72932331	3436.426117	4426.80
4.27	Na	1.9741 mg/L	0.0403	0.9271	0.9391	0.012	0.0283	0.70223325	3533.568905	6975.62
	Fe	0.3749 mg/L	0.0403	0.9271	0.9391	0.012	0.0283	0.70223325	3533.568905	1324.73
	Sr	0.0929 mg/L	0.0403	0.9271	0.9391	0.012	0.0283	0.70223325	3533.568905	328.27
	Ca	126.2871 mg/L	0.0403	0.9271	0.9391	0.012	0.0283	0.70223325	3533.568905	446244.17
	Mn	-0.041 mg/L	0.0403	0.9271	0.9391	0.012	0.0283	0.70223325	3533.568905	-144.88
	Mg	0.2981 mg/L	0.0403	0.9271	0.9391	0.012	0.0283	0.70223325	3533.568905	1053.36
	Mg	0.4739 mg/L	0.0403	0.9271	0.9391	0.012	0.0283	0.70223325	3533.568905	1674.56
4.29	Na	1.2968 mg/L	0.0403	0.917	0.9256	0.0086	0.0317	0.7866005	3154.574132	4090.85
	Fe	0.1392 mg/L	0.0403	0.917	0.9256	0.0086	0.0317	0.7866005	3154.574132	439.12
	Sr	0.2511 mg/L	0.0403	0.917	0.9256	0.0086	0.0317	0.7866005	3154.574132	792.11
	Ca	143.0668 mg/L	0.0403	0.917	0.9256	0.0086	0.0317	0.7866005	3154.574132	451314.83
	Mn	-0.045 mg/L	0.0403	0.917	0.9256	0.0086	0.0317	0.7866005	3154.574132	-141.96
	Mg	0.7446 mg/L	0.0403	0.917	0.9256	0.0086	0.0317	0.7866005	3154.574132	2348.90
	Mg	0.5795 mg/L	0.0403	0.917	0.9256	0.0086	0.0317	0.7866005	3154.574132	1828.08
4.30	Na	1.1139 mg/L	0.04	0.9457	0.9557	0.01	0.03	0.75	3333.333333	3713.00
	Fe	0.191 mg/L	0.04	0.9457	0.9557	0.01	0.03	0.75	3333.333333	636.67
	Sr	0.2199 mg/L	0.04	0.9457	0.9557	0.01	0.03	0.75	3333.333333	733.00
	Ca	119.861 mg/L	0.04	0.9457	0.9557	0.01	0.03	0.75	3333.333333	399536.67
	Mn	-0.0608 mg/L	0.04	0.9457	0.9557	0.01	0.03	0.75	3333.333333	-202.67
	Mg	0.3006 mg/L	0.04	0.9457	0.9557	0.01	0.03	0.75	3333.333333	1002.00
	Mg	0.4897 mg/L	0.04	0.9457	0.9557	0.01	0.03	0.75	3333.333333	1632.33
4.5	Na	0.7669 mg/L	0.0399	0.9176	0.9235	0.0059	0.034	0.85213033	2941.176471	2255.59
	Fe	0.1142 mg/L	0.0399	0.9176	0.9235	0.0059	0.034	0.85213033	2941.176471	335.88
	Sr	0.1526 mg/L	0.0399	0.9176	0.9235	0.0059	0.034	0.85213033	2941.176471	448.82
	Ca	149.2936 mg/L	0.0399	0.9176	0.9235	0.0059	0.034	0.85213033	2941.176471	439098.82
	Mn	-0.0745 mg/L	0.0399	0.9176	0.9235	0.0059	0.034	0.85213033	2941.176471	-219.12
	Mg	0.6687 mg/L	0.0399	0.9176	0.9235	0.0059	0.034	0.85213033	2941.176471	1966.76
	Mg	0.35 mg/L	0.0399	0.9176	0.9235	0.0059	0.034	0.85213033	2941.176471	1029.41
5.28	Na	1.4312 mg/L	0.0405	0.932	0.937	0.005	0.0355	0.87654321	2816.901408	4031.55
	Fe	0.1599 mg/L	0.0405	0.932	0.937	0.005	0.0355	0.87654321	2816.901408	450.42
	Sr	0.2697 mg/L	0.0405	0.932	0.937	0.005	0.0355	0.87654321	2816.901408	759.72
	Ca	133.6647 mg/L	0.0405	0.932	0.937	0.005	0.0355	0.87654321	2816.901408	376520.28
	Mn	0.0203 mg/L	0.0405	0.932	0.937	0.005	0.0355	0.87654321	2816.901408	57.18
	Mg	-0.1628 mg/L	0.0405	0.932	0.937	0.005	0.0355	0.87654321	2816.901408	-458.59
	Mg	0.6853 mg/L	0.0405	0.932	0.937	0.005	0.0355	0.87654321	2816.901408	1930.42
5.55	Na	2.0513 mg/L	0.0404	0.936	0.9423	0.0063	0.0341	0.84405941	2932.55132	6015.54
	Fe	0.2681 mg/L	0.0404	0.936	0.9423	0.0063	0.0341	0.84405941	2932.55132	786.22
	Sr	0.375 mg/L	0.0404	0.936	0.9423	0.0063	0.0341	0.84405941	2932.55132	1099.71
	Ca	144.1949 mg/L	0.0404	0.936	0.9423	0.0063	0.0341	0.84405941	2932.55132	422858.94
	Mn	-0.0792 mg/L	0.0404	0.936	0.9423	0.0063	0.0341	0.84405941	2932.55132	-232.26
	Mg	0.9123 mg/L	0.0404	0.936	0.9423	0.0063	0.0341	0.84405941	2932.55132	2675.37
	Mg	0.7524 mg/L	0.0404	0.936	0.9423	0.0063	0.0341	0.84405941	2932.55132	2206.45
15.36	Na	4.6544 mg/L	0.0403	0.9159	0.9241	0.0082	0.0321	0.79652605	3115.264798	14499.69
	Fe	4.4404 mg/L	0.0403	0.9159	0.9241	0.0082	0.0321	0.79652605	3115.264798	13833.02
	Sr	1.6451 mg/L	0.0403	0.9159	0.9241	0.0082	0.0321	0.79652605	3115.264798	5124.92
	Ca	106.0735 mg/L	0.0403	0.9159	0.9241	0.0082	0.0321	0.79652605	3115.264798	330447.04
	Mn	1.44 mg/L	0.0403	0.9159	0.9241	0.0082	0.0321	0.79652605	3115.264798	4485.98
	Mg	10.1619 mg/L	0.0403	0.9159	0.9241	0.0082	0.0321	0.79652605	3115.264798	31657.01
12.7	Na	3.4277 mg/L	0.0399	0.9424	0.9507	0.0083	0.0316	0.79197995	3164.556962	10847.15
	Fe	0.906 mg/L	0.0399	0.9424	0.9507	0.0083	0.0316	0.79197995	3164.556962	2867.09
	Sr	1.5861 mg/L	0.0399	0.9424	0.9507	0.0083	0.0316	0.79197995	3164.556962	5019.30
	Ca	193.1876 mg/L	0.0399	0.9424	0.9507	0.0083	0.0316	0.79197995	3164.556962	611353.16
	Mn	1.2149 mg/L	0.0399	0.9424	0.9507	0.0083	0.0316	0.79197995	3164.556962	3844.62
	Mg	10.9257 mg/L	0.0399	0.9424	0.9507	0.0083	0.0316	0.79197995	3164.556962	34575.00

Sample No	El	Concentration Unit	weight inp in g	Weight f1 in g	Weight f2 in g	residue In g f2-f1	CaCo3 in g input-residue	CaCO3 in % CaCO3/input	dilution factor 100/CaCO3	resulting conc in ppm Conc*dilution factor
15.27	Na	4.0426 mg/L	0.0402	0.9267	0.9326	0.0059	0.0343	0.85323383	2915.451895	11786.01
	Fe	3.2083 mg/L	0.0402	0.9267	0.9326	0.0059	0.0343	0.85323383	2915.451895	9353.64
	Sr	1.9841 mg/L	0.0402	0.9267	0.9326	0.0059	0.0343	0.85323383	2915.451895	5784.55
	Ca	154.1824 mg/L	0.0402	0.9267	0.9326	0.0059	0.0343	0.85323383	2915.451895	449511.37
	Mn	1.21 mg/L	0.0402	0.9267	0.9326	0.0059	0.0343	0.85323383	2915.451895	3527.70
	Mg	11.3517 mg/L	0.0402	0.9267	0.9326	0.0059	0.0343	0.85323383	2915.451895	33095.34
	Mg	1.965 mg/L	0.0402	0.9267	0.9326	0.0059	0.0343	0.85323383	2915.451895	5728.86
17.16	Na	4.9154 mg/L	0.0401	0.9627	0.9683	0.0056	0.0345	0.86034913	2898.550725	14247.54
	Fe	0.7242 mg/L	0.0401	0.9627	0.9683	0.0056	0.0345	0.86034913	2898.550725	2099.13
	Sr	1.768 mg/L	0.0401	0.9627	0.9683	0.0056	0.0345	0.86034913	2898.550725	5124.64
	Ca	138.5545 mg/L	0.0401	0.9627	0.9683	0.0056	0.0345	0.86034913	2898.550725	401607.25
	Mn	1.2208 mg/L	0.0401	0.9627	0.9683	0.0056	0.0345	0.86034913	2898.550725	3538.55
	Mg	10.736 mg/L	0.0401	0.9627	0.9683	0.0056	0.0345	0.86034913	2898.550725	31118.84
	Mg	1.212 mg/L	0.0401	0.9627	0.9683	0.0056	0.0345	0.86034913	2898.550725	3513.04
17.9	Na	2.9712 mg/L	0.0408	0.9229	0.9263	0.0034	0.0374	0.91666667	2673.796791	7944.39
	Fe	0.521 mg/L	0.0408	0.9229	0.9263	0.0034	0.0374	0.91666667	2673.796791	1393.05
	Sr	1.8255 mg/L	0.0408	0.9229	0.9263	0.0034	0.0374	0.91666667	2673.796791	4881.02
	Ca	145.5651 mg/L	0.0408	0.9229	0.9263	0.0034	0.0374	0.91666667	2673.796791	389211.50
	Mn	1.2051 mg/L	0.0408	0.9229	0.9263	0.0034	0.0374	0.91666667	2673.796791	3222.19
	Mg	10.3897 mg/L	0.0408	0.9229	0.9263	0.0034	0.0374	0.91666667	2673.796791	27779.95
	Mg	0.7373 mg/L	0.0408	0.9229	0.9263	0.0034	0.0374	0.91666667	2673.796791	1971.39
16.5	Na	3.2818 mg/L	0.0407	0.9398	0.9445	0.0047	0.036	0.88452088	2777.777778	9116.11
	Fe	1.7114 mg/L	0.0407	0.9398	0.9445	0.0047	0.036	0.88452088	2777.777778	4753.89
	Sr	1.7462 mg/L	0.0407	0.9398	0.9445	0.0047	0.036	0.88452088	2777.777778	4850.56
	Ca	149.6048 mg/L	0.0407	0.9398	0.9445	0.0047	0.036	0.88452088	2777.777778	415568.89
	Mn	1.2307 mg/L	0.0407	0.9398	0.9445	0.0047	0.036	0.88452088	2777.777778	3418.61
	Mg	10.7447 mg/L	0.0407	0.9398	0.9445	0.0047	0.036	0.88452088	2777.777778	29846.39
	Mg	0.0447 mg/L	0.0407	0.9398	0.9445	0.0047	0.036	0.88452088	2777.777778	124.17
14.25	Na	-1.2549 mg/L	0.0404	0.9278	0.9281	0.0003	0.0401	0.99257426	2493.765586	-3129.43
	Fe	-0.9093 mg/L	0.0404	0.9278	0.9281	0.0003	0.0401	0.99257426	2493.765586	-2267.58
	Sr	2.1889 mg/L	0.0404	0.9278	0.9281	0.0003	0.0401	0.99257426	2493.765586	5458.60
	Ca	228.0064 mg/L	0.0404	0.9278	0.9281	0.0003	0.0401	0.99257426	2493.765586	568594.51
	Mn	1.216 mg/L	0.0404	0.9278	0.9281	0.0003	0.0401	0.99257426	2493.765586	3032.42
	Mg	10.3679 mg/L	0.0404	0.9278	0.9281	0.0003	0.0401	0.99257426	2493.765586	25855.11
	Mg	-0.4058 mg/L	0.0404	0.9278	0.9281	0.0003	0.0401	0.99257426	2493.765586	-1011.97
7.52	Na	-3.7056 mg/L	0.0403	0.92	0.9215	0.0015	0.0388	0.96277916	2577.319588	-9550.52
	Fe	0.3509 mg/L	0.0403	0.92	0.9215	0.0015	0.0388	0.96277916	2577.319588	904.38
	Sr	1.6293 mg/L	0.0403	0.92	0.9215	0.0015	0.0388	0.96277916	2577.319588	4199.23
	Ca	47.6573 mg/L	0.0403	0.92	0.9215	0.0015	0.0388	0.96277916	2577.319588	122828.09
	Mn	1.2455 mg/L	0.0403	0.92	0.9215	0.0015	0.0388	0.96277916	2577.319588	3210.05
	Mg	10.1672 mg/L	0.0403	0.92	0.9215	0.0015	0.0388	0.96277916	2577.319588	26204.12
	Mg	-0.0537 mg/L	0.0403	0.92	0.9215	0.0015	0.0388	0.96277916	2577.319588	-138.40
14.19	Na	-1.1738 mg/L	0.0406	0.9099	0.913	0.0031	0.0375	0.92364532	2666.666667	-3130.13
	Fe	-1.3701 mg/L	0.0406	0.9099	0.913	0.0031	0.0375	0.92364532	2666.666667	-3653.60
	Sr	2.0105 mg/L	0.0406	0.9099	0.913	0.0031	0.0375	0.92364532	2666.666667	5361.33
	Ca	235.9053 mg/L	0.0406	0.9099	0.913	0.0031	0.0375	0.92364532	2666.666667	629080.80
	Mn	1.2854 mg/L	0.0406	0.9099	0.913	0.0031	0.0375	0.92364532	2666.666667	3427.73
	Mg	10.3543 mg/L	0.0406	0.9099	0.913	0.0031	0.0375	0.92364532	2666.666667	27611.47
	Mg	-0.0856 mg/L	0.0406	0.9099	0.913	0.0031	0.0375	0.92364532	2666.666667	-228.27
12 6	Na	-3.1208 mg/L	0.0398	0.9328	0.9428	0.01	0.0298	0.74874372	3355.704698	-10472.48
	Fe	-0.5637 mg/L	0.0398	0.9328	0.9428	0.01	0.0298	0.74874372	3355.704698	-1891.61
	Sr	1.8127 mg/L	0.0398	0.9328	0.9428	0.01	0.0298	0.74874372	3355.704698	6082.89
	Ca	158.2572 mg/L	0.0398	0.9328	0.9428	0.01	0.0298	0.74874372	3355.704698	531064.43
	Mn	1.2361 mg/L	0.0398	0.9328	0.9428	0.01	0.0298	0.74874372	3355.704698	4147.99
	Mg	10.1208 mg/L	0.0398	0.9328	0.9428	0.01	0.0298	0.74874372	3355.704698	33962.42
	Mg	0.082 mg/L	0.0398	0.9328	0.9428	0.01	0.0298	0.74874372	3355.704698	275.17
13 3	Na	-2.0251 mg/L	0.0404	0.9115	0.9178	0.0063	0.0341	0.84405941	2932.55132	-5938.71
	Fe	-0.8896 mg/L	0.0404	0.9115	0.9178	0.0063	0.0341	0.84405941	2932.55132	-2608.80
	Sr	1.8374 mg/L	0.0404	0.9115	0.9178	0.0063	0.0341	0.84405941	2932.55132	5388.27
	Ca	200.8939 mg/L	0.0404	0.9115	0.9178	0.0063	0.0341	0.84405941	2932.55132	589131.67
	Mn	1.2959 mg/L	0.0404	0.9115	0.9178	0.0063	0.0341	0.84405941	2932.55132	3800.29
	Mg	10.1341 mg/L	0.0404	0.9115	0.9178	0.0063	0.0341	0.84405941	2932.55132	29718.77
	Mg	-0.0102 mg/L	0.0404	0.9115	0.9178	0.0063	0.0341	0.84405941	2932.55132	-29.91
15 34	Na	-3.0528 mg/L	0 04	0.9115	0.9175	0.006	0.034	0.85	2941.176471	-8978.82
	Fe	1.9373 mg/L	0 04	0.9115	0.9175	0.006	0.034	0.85	2941.176471	5697.94
	Sr	1.5306 mg/L	0.04	0.9115	0.9175	0.006	0.034	0.85	2941.176471	4501.76
	Ca	75.2274 mg/L	0.04	0.9115	0.9175	0.006	0.034	0.85	2941.176471	221257.06
	Mn	1.2408 mg/L	0.04	0.9115	0.9175	0.006	0.034	0.85	2941.176471	3649 41
	Mg	10.0354 mg/L	0 04	0.9115	0 9175	0.006	0.034	0.85	2941.176471	29515.88
	Mg	0.251 mg/L	0.04	0.9115	0.9175	0.006	0.034	0.85	2941.176471	738.24
14 16	Na	-3.6949 mg/L	0.0403	0.928	0 9294	0.0014	0.0389	0.96526055	2570.694087	-9498.46
	Fe	-0 8314 mg/L	0.0403	0.928	0 9294	0 0014	0 0389	0 96526055	2570.694087	-2137.28
	Sr	1.8891 mg/L	0.0403	0.928	0 9294	0.0014	0.0389	0.96526055	2570.694087	4856.30
	Ca	59.8013 mg/L	0.0403	0.928	0.9294	0 0014	0.0389	0.96526055	2570.694087	153730.85
	Mn	1.2443 mg/L	0.0403	0 928	0.9294	0.0014	0 0389	0 96526055	2570.694087	3198.71
	Mg	10.2542 mg/L	0 0403	0 928	0.9294	0.0014	0 0389	0.96526055	2570 694087	26360.41

Sample No	El	Concentration Unit	weight inp in g	Weight f1 in g	Weight f2 in g	residue in g f2-f1	CaCo3 in g input-residue	CaCO3 in % CaCO3/input	dilution factor 100/CaCO3	resulting conc in ppm Conc*dilution factor
15.25	Na	-1.7528 mg/L	0.04	0.9299	0.938	0.0081	0.0319	0.7975	3134.796238	-5494.67
	Fe	0.2429 mg/L	0.04	0.9299	0.938	0.0081	0.0319	0.7975	3134.796238	761.44
	Sr	1.6732 mg/L	0.04	0.9299	0.938	0.0081	0.0319	0.7975	3134.796238	5245.14
	Ca	235.9273 mg/L	0.04	0.9299	0.938	0.0081	0.0319	0.7975	3134.796238	739584.01
	Mn	1.2315 mg/L	0.04	0.9299	0.938	0.0081	0.0319	0.7975	3134.796238	3860.50
	Mg	10.1028 mg/L	0.04	0.9299	0.938	0.0081	0.0319	0.7975	3134.796238	31670.22
	Mg	-0.5809 mg/L	0.04	0.9299	0.938	0.0081	0.0319	0.7975	3134.796238	-1821.00
15.32	Na	-2.4661 mg/L	0.0401	0.9362	0.9456	0.0094	0.0307	0.76558603	3257.32899	-8032.90
	Fe	-0.3771 mg/L	0.0401	0.9362	0.9456	0.0094	0.0307	0.76558603	3257.32899	-1228.34
	Sr	1.9053 mg/L	0.0401	0.9362	0.9456	0.0094	0.0307	0.76558603	3257.32899	6206.19
	Ca	96.8094 mg/L	0.0401	0.9362	0.9456	0.0094	0.0307	0.76558603	3257.32899	315340.07
	Mn	1.3399 mg/L	0.0401	0.9362	0.9456	0.0094	0.0307	0.76558603	3257.32899	4364.50
	Mg	10.3858 mg/L	0.0401	0.9362	0.9456	0.0094	0.0307	0.76558603	3257.32899	33829.97
	Mg	0.0777 mg/L	0.0401	0.9362	0.9456	0.0094	0.0307	0.76558603	3257.32899	253.09
16.1	Na	-51.7108 mg/L	0.0402	0.9545	0.9593	0.0048	0.0354	0.88059701	2824.858757	-146075.71
	Fe	-0.3604 mg/L	0.0402	0.9545	0.9593	0.0048	0.0354	0.88059701	2824.858757	-1018.08
	Sr	-5.5277 mg/L	0.0402	0.9545	0.9593	0.0048	0.0354	0.88059701	2824.858757	-15614.97
	Ca	54.2487 mg/L	0.0402	0.9545	0.9593	0.0048	0.0354	0.88059701	2824.858757	153244.92
	Mn	1.1274 mg/L	0.0402	0.9545	0.9593	0.0048	0.0354	0.88059701	2824.858757	3184.75
	Mg	7.5948 mg/L	0.0402	0.9545	0.9593	0.0048	0.0354	0.88059701	2824.858757	21454.24
	Mg	-0.5008 mg/L	0.0402	0.9545	0.9593	0.0048	0.0354	0.88059701	2824.858757	-1414.69
15.29	Na	-67.4641 mg/L	0.0403	0.898	0.903	0.005	0.0353	0.87593052	2832.86119	-191116.43
	Fe	0.4349 mg/L	0.0403	0.898	0.903	0.005	0.0353	0.87593052	2832.86119	1232.01
	Sr	5.006 mg/L	0.0403	0.898	0.903	0.005	0.0353	0.87593052	2832.86119	14181.30
	Ca	49.1055 mg/L	0.0403	0.898	0.903	0.005	0.0353	0.87593052	2832.86119	139109.07
	Mn	1.1466 mg/L	0.0403	0.898	0.903	0.005	0.0353	0.87593052	2832.86119	3248.16
	Mg	7.0221 mg/L	0.0403	0.898	0.903	0.005	0.0353	0.87593052	2832.86119	19892.63
	Mg	-0.6547 mg/L	0.0403	0.898	0.903	0.005	0.0353	0.87593052	2832.86119	-1854.67
15.31	Na	-71.1708 mg/L	0.0398	0.9224	0.938	0.0156	0.0242	0.6080402	4132.231405	-294094.21
	Fe	3.9975 mg/L	0.0398	0.9224	0.938	0.0156	0.0242	0.6080402	4132.231405	16518.60
	Sr	-5.7612 mg/L	0.0398	0.9224	0.938	0.0156	0.0242	0.6080402	4132.231405	-23806.61
	Ca	47.1771 mg/L	0.0398	0.9224	0.938	0.0156	0.0242	0.6080402	4132.231405	194946.69
	Mn	1.1863 mg/L	0.0398	0.9224	0.938	0.0156	0.0242	0.6080402	4132.231405	4902.07
	Mg	7.9426 mg/L	0.0398	0.9224	0.938	0.0156	0.0242	0.6080402	4132.231405	32820.66
	Mg	-0.1607 mg/L	0.0398	0.9224	0.938	0.0156	0.0242	0.6080402	4132.231405	-664.05
12.1	Na	-70.8439 mg/L	0.0404	0.9261	0.9329	0.0068	0.0336	0.83168317	2976.190476	-210844.94
	Fe	0.6252 mg/L	0.0404	0.9261	0.9329	0.0068	0.0336	0.83168317	2976.190476	1860.71
	Sr	-6.3395 mg/L	0.0404	0.9261	0.9329	0.0068	0.0336	0.83168317	2976.190476	-18867.56
	Ca	80.7907 mg/L	0.0404	0.9261	0.9329	0.0068	0.0336	0.83168317	2976.190476	240448.51
	Mn	1.1483 mg/L	0.0404	0.9261	0.9329	0.0068	0.0336	0.83168317	2976.190476	3417.56
	Mg	7.3298 mg/L	0.0404	0.9261	0.9329	0.0068	0.0336	0.83168317	2976.190476	21814.88
	Mg	0.0516 mg/L	0.0404	0.9261	0.9329	0.0068	0.0336	0.83168317	2976.190476	153.57
17.15	Na	-69.1003 mg/L	0.0409	0.9044	0.9087	0.0043	0.0366	0.89486553	2732.240437	-188798.63
	Fe	1.0887 mg/L	0.0409	0.9044	0.9087	0.0043	0.0366	0.89486553	2732.240437	2974.59
	Sr	-10.2476 mg/L	0.0409	0.9044	0.9087	0.0043	0.0366	0.89486553	2732.240437	-27998.91
	Ca	67.1649 mg/L	0.0409	0.9044	0.9087	0.0043	0.0366	0.89486553	2732.240437	183510.66
	Mn	1.3 mg/L	0.0409	0.9044	0.9087	0.0043	0.0366	0.89486553	2732.240437	3551.91
	Mg	6.5916 mg/L	0.0409	0.9044	0.9087	0.0043	0.0366	0.89486553	2732.240437	18009.84
	Mg	-0.4457 mg/L	0.0409	0.9044	0.9087	0.0043	0.0366	0.89486553	2732.240437	-1217.76
9.18	Na	-51.4299 mg/L	0.0401	0.9395	0.9407	0.0012	0.0389	0.97007481	2570.694087	-132210.54
	Fe	0.383 mg/L	0.0401	0.9395	0.9407	0.0012	0.0389	0.97007481	2570.694087	984.58
	Sr	11.2646 mg/L	0.0401	0.9395	0.9407	0.0012	0.0389	0.97007481	2570.694087	28957.84
	Ca	170.6337 mg/L	0.0401	0.9395	0.9407	0.0012	0.0389	0.97007481	2570.694087	438647.04
	Mn	1.2266 mg/L	0.0401	0.9395	0.9407	0.0012	0.0389	0.97007481	2570.694087	3153.21
	Mg	9.7121 mg/L	0.0401	0.9395	0.9407	0.0012	0.0389	0.97007481	2570.694087	24966.84
	Mg	1.2242 mg/L	0.0401	0.9395	0.9407	0.0012	0.0389	0.97007481	2570.694087	3147.04
15.35	Na	-53.4086 mg/L	0.0401	0.9192	0.933	0.0138	0.0263	0.65586035	3802.281369	-203074.52
	Fe	5.5851 mg/L	0.0401	0.9192	0.933	0.0138	0.0263	0.65586035	3802.281369	21236.12
	Sr	-4.1784 mg/L	0.0401	0.9192	0.933	0.0138	0.0263	0.65586035	3802.281369	-15887.45
	Ca	81.8542 mg/L	0.0401	0.9192	0.933	0.0138	0.0263	0.65586035	3802.281369	311232.70
	Mn	1.2281 mg/L	0.0401	0.9192	0.933	0.0138	0.0263	0.65586035	3802.281369	4669.58
	Mg	7.4945 mg/L	0.0401	0.9192	0.933	0.0138	0.0263	0.65586035	3802.281369	28496.20
	Mg	0.0476 mg/L	0.0401	0.9192	0.933	0.0138	0.0263	0.65586035	3802.281369	180.99
11.88	Na	-55.6555 mg/L	0.0396	0.944	0.9494	0.0054	0.0342	0.86363636	2923.976608	-162735.38
	Fe	0.3313 mg/L	0.0396	0.944	0.9494	0.0054	0.0342	0.86363636	2923.976608	968.71
	Sr	5.4337 mg/L	0.0396	0.944	0.9494	0.0054	0.0342	0.86363636	2923.976608	15888.01
	Ca	176.2314 mg/L	0.0396	0.944	0.9494	0.0054	0.0342	0.86363636	2923.976608	515296.49
	Mn	1.2856 mg/L	0.0396	0.944	0.9494	0.0054	0.0342	0.86363636	2923.976608	3759.06
	Mg	9.4184 mg/L	0.0396	0.944	0.9494	0.0054	0.0342	0.86363636	2923.976608	27539.18
	Mg	0.037 mg/L	0.0396	0.944	0.9494	0.0054	0.0342	0.86363636	2923.976608	108.19
11.42	Na	4.6272 mg/L	0.0407	0.949	0.9535	0.0045	0.0362	0.88943489	2762.430939	12782.32
	Fe	0.4927 mg/L	0.0407	0.949	0.9535	0.0045	0.0362	0.88943489	2762.430939	1361.05
	Sr	1.7441 mg/L	0.0407	0.949	0.9535	0.0045	0.0362	0.88943489	2762.430939	4817.96
	Ca	172.8931 mg/L	0.0407	0.949	0.9535	0.0045	0.0362	0.88943489	2762.430939	477605.25
	Mn	1.2351 mg/L	0.0407	0.949	0.9535	0.0045	0.0362	0.88943489	2762.430939	3411.88
	Mg	10.2838 mg/L	0.0407	0.949	0.9535	0.0045	0.0362	0.88943489	2762.430939	28408.29

Sample No	El	Concentration Unit	weight inp in g	Weight f1 in g	Weight f2 in g	residue in g f2-f1	CaCo3 in g input-residue	CaCO3 in % CaCO3/input	dilution factor 100/CaCO3	resulting conc in ppm Conc*dilution factor
12.8	Na	3.9762 mg/L	0.0398	0.9372	0.9546	0.0174	0.0224	0.56281407	4464.285714	17750.89
	Fe	0.5089 mg/L	0.0398	0.9372	0.9546	0.0174	0.0224	0.56281407	4464.285714	2271.88
	Sr	2.0027 mg/L	0.0398	0.9372	0.9546	0.0174	0.0224	0.56281407	4464.285714	8940.62
	Ca	183.8619 mg/L	0.0398	0.9372	0.9546	0.0174	0.0224	0.56281407	4464.285714	820812.05
	Mn	1.2879 mg/L	0.0398	0.9372	0.9546	0.0174	0.0224	0.56281407	4464.285714	5749.55
	Mg	10.4259 mg/L	0.0398	0.9372	0.9546	0.0174	0.0224	0.56281407	4464.285714	46544.20
	Mg	0.0606 mg/L	0.0398	0.9372	0.9546	0.0174	0.0224	0.56281407	4464.285714	270.54
15 43	Na	3.9903 mg/L	0.0396	0.9253	0.9403	0.015	0.0246	0.62121212	4065.04065	16220.73
	Fe	2.1133 mg/L	0.0396	0.9253	0.9403	0.015	0.0246	0.62121212	4065.04065	8590.65
	Sr	1.9768 mg/L	0.0396	0.9253	0.9403	0.015	0.0246	0.62121212	4065.04065	8035.77
	Ca	81.7798 mg/L	0.0396	0.9253	0.9403	0.015	0.0246	0.62121212	4065.04065	332438.21
	Mn	1.3095 mg/L	0.0396	0.9253	0.9403	0.015	0.0246	0.62121212	4065.04065	5323.17
	Mg	10.1166 mg/L	0.0396	0.9253	0.9403	0.015	0.0246	0.62121212	4065.04065	41124.39
	Mg	0.2178 mg/L	0.0396	0.9253	0.9403	0.015	0.0246	0.62121212	4065.04065	885.37
14.14	Na	3.6413 mg/L	0.04	0.8861	0.8909	0.0048	0.0352	0.88	2840.909091	10344.60
	Fe	0.4638 mg/L	0.04	0.8861	0.8909	0.0048	0.0352	0.88	2840.909091	1317.61
	Sr	1.8774 mg/L	0.04	0.8861	0.8909	0.0048	0.0352	0.88	2840.909091	5333.52
	Ca	99.8817 mg/L	0.04	0.8861	0.8909	0.0048	0.0352	0.88	2840.909091	283754.83
	Mn	1.2379 mg/L	0.04	0.8861	0.8909	0.0048	0.0352	0.88	2840.909091	3516.76
	Mg	10.0611 mg/L	0.04	0.8861	0.8909	0.0048	0.0352	0.88	2840.909091	28582.67
	Mg	-0.5019 mg/L	0.04	0.8861	0.8909	0.0048	0.0352	0.88	2840.909091	-1425.85
12.5	Na	3.7036 mg/L	0.0395	0.9258	0.9351	0.0093	0.0302	0.76455696	3311.258278	12263.58
	Fe	0.4773 mg/L	0.0395	0.9258	0.9351	0.0093	0.0302	0.76455696	3311.258278	1580.46
	Sr	1.8684 mg/L	0.0395	0.9258	0.9351	0.0093	0.0302	0.76455696	3311.258278	6186.75
	Ca	195.7728 mg/L	0.0395	0.9258	0.9351	0.0093	0.0302	0.76455696	3311.258278	648254.30
	Mn	1.3116 mg/L	0.0395	0.9258	0.9351	0.0093	0.0302	0.76455696	3311.258278	4343.05
	Mg	10.0557 mg/L	0.0395	0.9258	0.9351	0.0093	0.0302	0.76455696	3311.258278	33297.02
	Mg	0.5911 mg/L	0.0395	0.9258	0.9351	0.0093	0.0302	0.76455696	3311.258278	1957.29
14.15	Na	5.5834 mg/L	0.0398	0.9221	0.9286	0.0065	0.0333	0.83668342	3003.003003	16766.97
	Fe	0.508 mg/L	0.0398	0.9221	0.9286	0.0065	0.0333	0.83668342	3003.003003	1525.53
	Sr	2.3658 mg/L	0.0398	0.9221	0.9286	0.0065	0.0333	0.83668342	3003.003003	7104.50
	Ca	194.5106 mg/L	0.0398	0.9221	0.9286	0.0065	0.0333	0.83668342	3003.003003	584115.92
	Mn	1.3739 mg/L	0.0398	0.9221	0.9286	0.0065	0.0333	0.83668342	3003.003003	4125.83
	Mg	10.2405 mg/L	0.0398	0.9221	0.9286	0.0065	0.0333	0.83668342	3003.003003	30752.25
	Mg	-0.2128 mg/L	0.0398	0.9221	0.9286	0.0065	0.0333	0.83668342	3003.003003	-639.04
11.85	Na	4.1418 mg/L	0.0402	0.9387	0.9449	0.0062	0.034	0.84577114	2941.176471	12181.76
	Fe	0.7096 mg/L	0.0402	0.9387	0.9449	0.0062	0.034	0.84577114	2941.176471	2087.06
	Sr	1.9975 mg/L	0.0402	0.9387	0.9449	0.0062	0.034	0.84577114	2941.176471	5875.00
	Ca	186.5742 mg/L	0.0402	0.9387	0.9449	0.0062	0.034	0.84577114	2941.176471	548747.65
	Mn	1.259 mg/L	0.0402	0.9387	0.9449	0.0062	0.034	0.84577114	2941.176471	3702.94
	Mg	10.285 mg/L	0.0402	0.9387	0.9449	0.0062	0.034	0.84577114	2941.176471	30250.00
	Mg	0.4482 mg/L	0.0402	0.9387	0.9449	0.0062	0.034	0.84577114	2941.176471	1318.24
11.78	Na	5.1123 mg/L	0.0401	0.9499	0.9533	0.0034	0.0367	0.91521197	2724.79564	13929.97
	Fe	0.361 mg/L	0.0401	0.9499	0.9533	0.0034	0.0367	0.91521197	2724.79564	983.65
	Sr	1.9967 mg/L	0.0401	0.9499	0.9533	0.0034	0.0367	0.91521197	2724.79564	5440.60
	Ca	207.0635 mg/L	0.0401	0.9499	0.9533	0.0034	0.0367	0.91521197	2724.79564	564205.72
	Mn	1.2887 mg/L	0.0401	0.9499	0.9533	0.0034	0.0367	0.91521197	2724.79564	3511.44
	Mg	10.6052 mg/L	0.0401	0.9499	0.9533	0.0034	0.0367	0.91521197	2724.79564	28897.00
	Mg	0.942 mg/L	0.0401	0.9499	0.9533	0.0034	0.0367	0.91521197	2724.79564	2566.76
16.3	Na	4.5682 mg/L	0.0398	0.9715	0.9808	0.0093	0.0305	0.76633166	3278.688525	14977.70
	Fe	1.694 mg/L	0.0398	0.9715	0.9808	0.0093	0.0305	0.76633166	3278.688525	5554.10
	Sr	2.4835 mg/L	0.0398	0.9715	0.9808	0.0093	0.0305	0.76633166	3278.688525	8142.62
	Ca	181.597 mg/L	0.0398	0.9715	0.9808	0.0093	0.0305	0.76633166	3278.688525	595400.00
	Mn	1.3371 mg/L	0.0398	0.9715	0.9808	0.0093	0.0305	0.76633166	3278.688525	4383.93
	Mg	10.7783 mg/L	0.0398	0.9715	0.9808	0.0093	0.0305	0.76633166	3278.688525	35338.69
	Mg	0.5448 mg/L	0.0398	0.9715	0.9808	0.0093	0.0305	0.76633166	3278.688525	1786.23
17.10	Na	4.8491 mg/L	0.0399	0.9405	0.9429	0.0024	0.0375	0.93984962	2666.666667	12930.93
	Fe	0.2542 mg/L	0.0399	0.9405	0.9429	0.0024	0.0375	0.93984962	2666.666667	677.87
	Sr	2.4131 mg/L	0.0399	0.9405	0.9429	0.0024	0.0375	0.93984962	2666.666667	6434.93
	Ca	198.3827 mg/L	0.0399	0.9405	0.9429	0.0024	0.0375	0.93984962	2666.666667	529020.53
	Mn	1.3319 mg/L	0.0399	0.9405	0.9429	0.0024	0.0375	0.93984962	2666.666667	3551.73
	Mg	10.363 mg/L	0.0399	0.9405	0.9429	0.0024	0.0375	0.93984962	2666.666667	27634.67
	Mg	-0.3372 mg/L	0.0399	0.9405	0.9429	0.0024	0.0375	0.93984962	2666.666667	-899.20
11.89	Na	4.3518 mg/L	0.04	0.936	0.9421	0.0061	0.0339	0.8475	2949.852507	12837.17
	Fe	0.4724 mg/L	0.04	0.936	0.9421	0.0061	0.0339	0.8475	2949.852507	1393.51
	Sr	1.8599 mg/L	0.04	0.936	0.9421	0.0061	0.0339	0.8475	2949.852507	5486.43
	Ca	162.1425 mg/L	0.04	0.936	0.9421	0.0061	0.0339	0.8475	2949.852507	478296.46
	Mn	1.2415 mg/L	0.04	0.936	0.9421	0.0061	0.0339	0.8475	2949.852507	3662.24
	Mg	10.0896 mg/L	0.04	0.936	0.9421	0.0061	0.0339	0.8475	2949.852507	29762.83
	Mg	-0.3608 mg/L	0.04	0.936	0.9421	0.0061	0.0339	0.8475	2949.852507	-1064.31
11.81	Na	5.2675 mg/L	0.0396	0.9357	0.9409	0.0052	0.0344	0.86868687	2906.976744	15312.50
	Fe	0.4781 mg/L	0.0396	0.9357	0.9409	0.0052	0.0344	0.86868687	2906.976744	1389.83
	Sr	2.0488 mg/L	0.0396	0.9357	0.9409	0.0052	0.0344	0.86868687	2906.976744	5955.81
	Ca	283.4478 mg/L	0.0396	0.9357	0.9409	0.0052	0.0344	0.86868687	2906.976744	823976.16
	Mn	1.2014 mg/L	0.0396	0.9357	0.9409	0.0052	0.0344	0.86868687	2906.976744	3492.44
	Mg	10.4175 mg/L	0.0396	0.9357	0.9409	0.0052	0.0344	0.86868687	2906.976744	30283.43

Sample No	El	Concentration Unit	weight inp in g	Weight f1 in g	Weight f2 in g	residue in g f2-f1	CaCo3 in g input-residue	CaCO3 in % CaCO3/input	dilution factor 100/CaCO3	resulting conc in ppm Conc*dilution factor
14.24	Na	3.8385 mg/L	0.0397	0.9406	0.948	0.0074	0.0323	0.81360202	3095.975232	11883.90
	Fe	0.5414 mg/L	0.0397	0.9406	0.948	0.0074	0.0323	0.81360202	3095.975232	1676.16
	Sr	1.7547 mg/L	0.0397	0.9406	0.948	0.0074	0.0323	0.81360202	3095.975232	5432.51
	Ca	244.2188 mg/L	0.0397	0.9406	0.948	0.0074	0.0323	0.81360202	3095.975232	756095.36
	Mn	1.1764 mg/L	0.0397	0.9406	0.948	0.0074	0.0323	0.81360202	3095.975232	3642.11
	Mg	10.3458 mg/L	0.0397	0.9406	0.948	0.0074	0.0323	0.81360202	3095.975232	32030.34
	Mg	-0.6415 mg/L	0.0397	0.9406	0.948	0.0074	0.0323	0.81360202	3095.975232	-1986.07
15.39	Na	5.2748 mg/L	0.0403	0.9359	0.9462	0.0103	0.03	0.74441687	3333.333333	17582.67
	Fe	1.5835 mg/L	0.0403	0.9359	0.9462	0.0103	0.03	0.74441687	3333.333333	5278.33
	Sr	2.2352 mg/L	0.0403	0.9359	0.9462	0.0103	0.03	0.74441687	3333.333333	7450.67
	Ca	178.8842 mg/L	0.0403	0.9359	0.9462	0.0103	0.03	0.74441687	3333.333333	596280.67
	Mn	1.2234 mg/L	0.0403	0.9359	0.9462	0.0103	0.03	0.74441687	3333.333333	4078.00
	Mg	10.4318 mg/L	0.0403	0.9359	0.9462	0.0103	0.03	0.74441687	3333.333333	34772.67
	Mg	-0.0559 mg/L	0.0403	0.9359	0.9462	0.0103	0.03	0.74441687	3333.333333	-186.33
13.2	Na	3.7399 mg/L	0.0405	0.9183	0.9264	0.0081	0.0324	0.8	3086.419753	11542.90
	Fe	0.5106 mg/L	0.0405	0.9183	0.9264	0.0081	0.0324	0.8	3086.419753	1575.93
	Sr	1.8734 mg/L	0.0405	0.9183	0.9264	0.0081	0.0324	0.8	3086.419753	5782.10
	Ca	224.6558 mg/L	0.0405	0.9183	0.9264	0.0081	0.0324	0.8	3086.419753	693382.10
	Mn	1.2164 mg/L	0.0405	0.9183	0.9264	0.0081	0.0324	0.8	3086.419753	3754.32
	Mg	10.3431 mg/L	0.0405	0.9183	0.9264	0.0081	0.0324	0.8	3086.419753	31923.15
	Mg	0.4544 mg/L	0.0405	0.9183	0.9264	0.0081	0.0324	0.8	3086.419753	1402.47
15.40	Na	3.6377 mg/L	0.0408	0.9196	0.9265	0.0069	0.0339	0.83088235	2949.852507	10730.68
	Fe	1.5347 mg/L	0.0408	0.9196	0.9265	0.0069	0.0339	0.83088235	2949.852507	4527.14
	Sr	1.9077 mg/L	0.0408	0.9196	0.9265	0.0069	0.0339	0.83088235	2949.852507	5627.43
	Ca	840.2626 mg/L	0.0408	0.9196	0.9265	0.0069	0.0339	0.83088235	2949.852507	2478650.74
	Mn	1.2413 mg/L	0.0408	0.9196	0.9265	0.0069	0.0339	0.83088235	2949.852507	3661.65
	Mg	10.4018 mg/L	0.0408	0.9196	0.9265	0.0069	0.0339	0.83088235	2949.852507	30683.78
	Mg	0.0632 mg/L	0.0408	0.9196	0.9265	0.0069	0.0339	0.83088235	2949.852507	186.43
9.33	Na	3.5486 mg/L	0.0393	0.9244	0.9355	0.0111	0.0282	0.71755725	3546.099291	12583.69
	Fe	0.4334 mg/L	0.0393	0.9244	0.9355	0.0111	0.0282	0.71755725	3546.099291	1536.88
	Sr	1.869 mg/L	0.0393	0.9244	0.9355	0.0111	0.0282	0.71755725	3546.099291	6627.66
	Ca	233.0764 mg/L	0.0393	0.9244	0.9355	0.0111	0.0282	0.71755725	3546.099291	826512.06
	Mn	1.1395 mg/L	0.0393	0.9244	0.9355	0.0111	0.0282	0.71755725	3546.099291	4040.78
	Mg	10.2224 mg/L	0.0393	0.9244	0.9355	0.0111	0.0282	0.71755725	3546.099291	36249.65
	Mg	0.0962 mg/L	0.0393	0.9244	0.9355	0.0111	0.0282	0.71755725	3546.099291	341.13
15.28	Na	4.7202 mg/L	0.04	0.9182	0.92	0.0018	0.0382	0.955	2617.801047	12356.54
	Fe	1.0631 mg/L	0.04	0.9182	0.92	0.0018	0.0382	0.955	2617.801047	2782.98
	Sr	2.184 mg/L	0.04	0.9182	0.92	0.0018	0.0382	0.955	2617.801047	5717.28
	Ca	246.1633 mg/L	0.04	0.9182	0.92	0.0018	0.0382	0.955	2617.801047	644406.54
	Mn	1.2229 mg/L	0.04	0.9182	0.92	0.0018	0.0382	0.955	2617.801047	3201.31
	Mg	10.1203 mg/L	0.04	0.9182	0.92	0.0018	0.0382	0.955	2617.801047	26492.93
	Mg	0.2686 mg/L	0.04	0.9182	0.92	0.0018	0.0382	0.955	2617.801047	703.14
15.23	Na	0.6578 mg/L	0.041	0.9438	0.9691	0.0253	0.0157	0.38292683	6369.426752	4189.81
	Fe	1.4332 mg/L	0.041	0.9438	0.9691	0.0253	0.0157	0.38292683	6369.426752	9128.66
	Sr	2.3275 mg/L	0.041	0.9438	0.9691	0.0253	0.0157	0.38292683	6369.426752	14824.84
	Ca	71.6981 mg/L	0.041	0.9438	0.9691	0.0253	0.0157	0.38292683	6369.426752	456675.80
	Mn	-0.0074 mg/L	0.041	0.9438	0.9691	0.0253	0.0157	0.38292683	6369.426752	-47.13
	Mg	0.7174 mg/L	0.041	0.9438	0.9691	0.0253	0.0157	0.38292683	6369.426752	4569.43
	Mg	0.7053 mg/L	0.041	0.9438	0.9691	0.0253	0.0157	0.38292683	6369.426752	4492.36
15.38	Na	0.8360 mg/L	0.041	0.9544	0.982	0.0276	0.0134	0.32682927	7462.686567	6238.81
	Fe	1.7818 mg/L	0.041	0.9544	0.982	0.0276	0.0134	0.32682927	7462.686567	13297.01
	Sr	2.6556 mg/L	0.041	0.9544	0.982	0.0276	0.0134	0.32682927	7462.686567	19817.91
	Ca	75.5564 mg/L	0.041	0.9544	0.982	0.0276	0.0134	0.32682927	7462.686567	563853.73
	Mn	0.0228 mg/L	0.041	0.9544	0.982	0.0276	0.0134	0.32682927	7462.686567	170.15
	Mg	0.5973 mg/L	0.041	0.9544	0.982	0.0276	0.0134	0.32682927	7462.686567	4457.46
	Mg	0.5292 mg/L	0.041	0.9544	0.982	0.0276	0.0134	0.32682927	7462.686567	3949.25
15.42	Na	1.2283 mg/L	0.0399	0.9545	0.9793	0.0248	0.0151	0.37844612	6622.516556	8134.44
	Fe	1.5817 mg/L	0.0399	0.9545	0.9793	0.0248	0.0151	0.37844612	6622.516556	10474.83
	Sr	2.3156 mg/L	0.0399	0.9545	0.9793	0.0248	0.0151	0.37844612	6622.516556	15335.10
	Ca	78.2045 mg/L	0.0399	0.9545	0.9793	0.0248	0.0151	0.37844612	6622.516556	517910.60
	Mn	0.0161 mg/L	0.0399	0.9545	0.9793	0.0248	0.0151	0.37844612	6622.516556	106.62
	Mg	0.5055 mg/L	0.0399	0.9545	0.9793	0.0248	0.0151	0.37844612	6622.516556	3347.68
	Mg	0.4014 mg/L	0.0399	0.9545	0.9793	0.0248	0.0151	0.37844612	6622.516556	2658.28
14.20	Na	1.0310 mg/L	0.0397	0.94	0.9468	0.0068	0.0329	0.82871537	3039.513678	3133.74
	Fe	0.2295 mg/L	0.0397	0.94	0.9468	0.0068	0.0329	0.82871537	3039.513678	697.57
	Sr	2.3471 mg/L	0.0397	0.94	0.9468	0.0068	0.0329	0.82871537	3039.513678	7134.04
	Ca	118.0330 mg/L	0.0397	0.94	0.9468	0.0068	0.0329	0.82871537	3039.513678	358762.92
	Mn	-0.0361 mg/L	0.0397	0.94	0.9468	0.0068	0.0329	0.82871537	3039.513678	-109.73
	Mg	0.3334 mg/L	0.0397	0.94	0.9468	0.0068	0.0329	0.82871537	3039.513678	1013.37
	Mg	0.1326 mg/L	0.0397	0.94	0.9468	0.0068	0.0329	0.82871537	3039.513678	403.04
14.26	Na	1.1224 mg/L	0.0399	0.9442	0.9571	0.0129	0.027	0.67669173	3703.703704	4157.04
	Fe	0.4689 mg/L	0.0399	0.9442	0.9571	0.0129	0.027	0.67669173	3703.703704	1736.67
	Sr	2.3253 mg/L	0.0399	0.9442	0.9571	0.0129	0.027	0.67669173	3703.703704	8612.22
	Ca	155.1638 mg/L	0.0399	0.9442	0.9571	0.0129	0.027	0.67669173	3703.703704	574680.74
	Mn	-0.0188 mg/L	0.0399	0.9442	0.9571	0.0129	0.027	0.67669173	3703.703704	-69.63
	Mg	0.6493 mg/L	0.0399	0.9442	0.9571	0.0129	0.027	0.67669173	3703.703704	2404.81

Sample No	El	Concentration Unit	weight inp in g	Weight f1 in g	Weight f2 in g	residue in g f2-f1	CaCo3 in g input-residue	CaCO3 in % CaCO3/input	dilution factor 100/CaCO3	resulting conc in ppm Conc*dilution factor
cv655	Na	0.6920 mg/L	0.0404	0.9445	0.9725	0.028	0.0124	0.30693069	8064.516129	5580.65
	Fe	1.5160 mg/L	0.0404	0.9445	0.9725	0.028	0.0116	0.29292929	8620.689655	13068.97
	Sr	2.6134 mg/L	0.0404	0.9445	0.9725	0.028	0.0124	0.30693069	8064.516129	21075.81
	Ca	73.4191 mg/L	0.0404	0.9445	0.9725	0.028	0.0124	0.30693069	8064.516129	592089.52
	Mn	0.0160 mg/L	0.0404	0.9445	0.9725	0.028	0.0124	0.30693069	8064.516129	129.03
	Mg	0.9070 mg/L	0.0404	0.9445	0.9725	0.028	0.0124	0.30693069	8064.516129	7314.52
	Mg	0.9026 mg/L	0.0404	0.9445	0.9725	0.028	0.0124	0.30693069	8064.516129	7279.03
cv657	Na	0.1884 mg/L	0.0396	0.9407	0.9682	0.0275	0.0121	0.30555556	8264.46281	1557.02
	Fe	2.6593 mg/L	0.0396	0.9407	0.9682	0.0275	0.0121	0.30555556	8264.46281	21977.69
	Sr	2.3627 mg/L	0.0396	0.9407	0.9682	0.0275	0.0121	0.30555556	8264.46281	19526.45
	Ca	56.3276 mg/L	0.0396	0.9407	0.9682	0.0275	0.0121	0.30555556	8264.46281	465517.36
	Mn	0.0162 mg/L	0.0396	0.9407	0.9682	0.0275	0.0121	0.30555556	8264.46281	133.88
	Mg	0.4960 mg/L	0.0396	0.9407	0.9682	0.0275	0.0121	0.30555556	8264.46281	4099.17
	Mg	0.3504 mg/L	0.0396	0.9407	0.9682	0.0275	0.0121	0.30555556	8264.46281	2895.87

APPENDIX 10

GLOSSARY
CHEMICAL STAINING PROCEDURE
TOPOMAP SERIES 1/50 000
DUNHAM'S CLASSIFICATION SCHEME

APPENDIX 10.1

GLOSSARY FOR THIN-SECTION, CARBONATE CEMENT, AND CRYSTALS DESCRIPTION

acicular Habit in which the crystals are shaped like needles or fibres and often radially arranged.

anhedral Showing no crystal form at all.

blade **(bladed; adj.)** Descriptive of a long narrow crystal with a knife shape.

blocky Equant to subequant crystals with subhedral form.

botryoid **(botryoidal; adj.)** Aggregate with rounded surface.

cement Intergranular precipitate binding grains together.

dogtooth See scalenohedral; cement in sharply pointed crystals of acute scalenohedral habit resembling dog teeth.

drusy Small equant clear spar projecting crystals with euhedral form.

epitaxial Growth of one mineral upon the other or perpendicularly to a substrate.

equant Dimensions of the crystals are about the same in all directions.

euhedral Showing fully developed crystal form.

extrinsic Said of a cement growing within grains (i.e., intraparticle), as within bryozoan zooecia, and is correlated to a cement found within interparticle pore space.

fibrous Habit in which the crystals are shaped like threads.

fitted grain contacts Complexly interpenetrating interfaces involving several grains due to preferential solution at grain contacts.

geopetal Fabric formed by the infilling of the bottom part of a cavity with sediment under the influence of gravity.

HMC High-Mg calcite (>12% mol $MgCO_3$).

IMC Intermediate-Mg calcite (4-12 mol% $MgCO_3$).

inclusion Solid or fluid inclusions trapped in the cements; inclusions often outline the disposition of the crystals (see RFC).

intrinsic Said of a cement growing between grains (i.e., interparticle).

isopachous Refers to a cement maintaining equal thickness about a pore space.

LMC Low-Mg calcite (0-4 mol% $MgCO_3$).

meniscus Texture of the cement at grain contacts that reflects the distribution of pore water between the grains in a meniscus fashion – vadose setting.

micrite Microcrystalline (<0.004mm) to cryptocrystalline calcite making up matrix or cement.

micritic envelope Related to endolithic carbonate grain micritization.

micritic microbial coating Often irregularly shaped and inflated in the direction of the pore space.

mosaic Interlocking crystals of various size, displaying triple-point contacts between them.

mouldic **(moldic)** Secondary porosity developed by the preferential dissolution of shell fragments or other particles.

neomorphism Chemical alteration and transformation of metastable carbonate phases (e.g., aragonite and HMC) into more stable phases (e.g., LMC) with or without retention of primary microarchitectures.

palisadic Arrangement of crystals in a palisade fashion.

pellet Carbonate grains of faecal origin.

peloid **(peloidal; adj.)** Structureless grains resembling pellets which cannot be shown to be of faecal origin.

pendant Texture of the cement that reflects the distribution of pore water as droplets on the underside of grains– vadose setting.

planar/curved grain contact Descriptive of the interface between two grains due to one grain that dissolved, allowing the other grain to penetrate.

precipitate Crystal nucleation phase restricted to intraparticle pores, and as such does not bind grains together.

primary porosity The porosity that developed between grains during sedimentation and/or that was present within sedimentary particles at the time of deposition (see also secondary porosity).

radiaxial Descriptive of a crystal which has grown in a cavity in a fan-like pattern.

repacking Mechanical grain rearrangement in response to compressive stresses.

rim Descriptive of an optically oriented cement surrounding grains.

RFC Radiaxial fibrous calcite, typically cone-shaped arrangement of fibrous crystals showing an undulatory extinction – marine setting.

scalenohedral See scalenohedron.

scalenohedron Closed crystal form whose faces are triangles all with unequal sides, also called "dogtooth spar"(see dogtooth).

secondary porosity All porosity that developed in a sediment subsequent to its deposition through sedimentary, diagenetic, or tectonic processes.

sparite (spar) A descriptive term for the crystalline, clear interstitial component of carbonates, consisting of calcite or aragonite (crystal size>0.004 mm).

stalactitic Arrangement of crystals in a pendant fashion (see pendant).

stubby Small equant clear spar projecting crystals with subhedral form and often irregular shape.

stylolite A complexly shaped seam or interface with a number of roughly columnar extensions that fit in between the columnar extensions of the opposite mass.

subhedral Showing partly developed crystal form.

sutured grain contact Interpenetrating interface between two grains due to irregular solution of both grains.

syntaxial Descriptive of a crystal overgrowing in optical continuity with its substrate (common on echinoids).

APPENDIX 10.2

ETCHING AND STAINING - DICKSON'S PROCEDURE (1965)

Reagents:

(I)

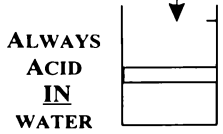

Etching solution
(1.5% HCl solution)

(II)



(III)



This solution must be freshly made

(IV)

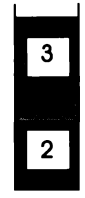

The combined solution lasts
for only one staining session

Staining solution

NB : Avoid contact with the stain: ferricyanide is poisonous
USE RUBBER GLOVES

Procedure :

(I) Immerse thin section face up in the etching solution at 20°C

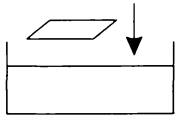

10-15 sec

(II - optional)

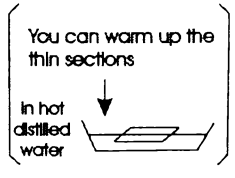

(II) Then immerse in the combined solution at room temperature

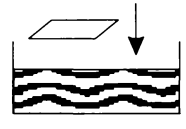

30-45 sec

(III) Better results if you immerse afterward in the Alizarine solution

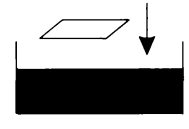

10-15 sec

Te Aute project	*12s*	*No significant change when warmed*	*50s*	*12s*

(IV)

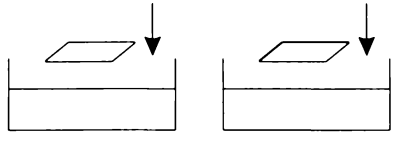

Wash the specimen gently in two changes of distilled water

Only a few seconds each time

(V)

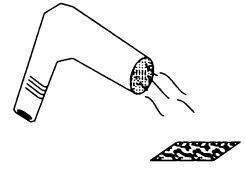

Shake thin section and dry the specimen surface quickly in a stream of warm air

Handle carefully

Colour differentiation:

Calcite	Very pale pink to red	Dolomite	No colour
Ferroan calcite	Mauve, purple to royal blue with increasing Fe content	Ferroan dolomite	Pale to deep turquoise with increasing Fe content

APPENDIX 10.3 - TOPOMAP SERIES 260
1 : 50 000

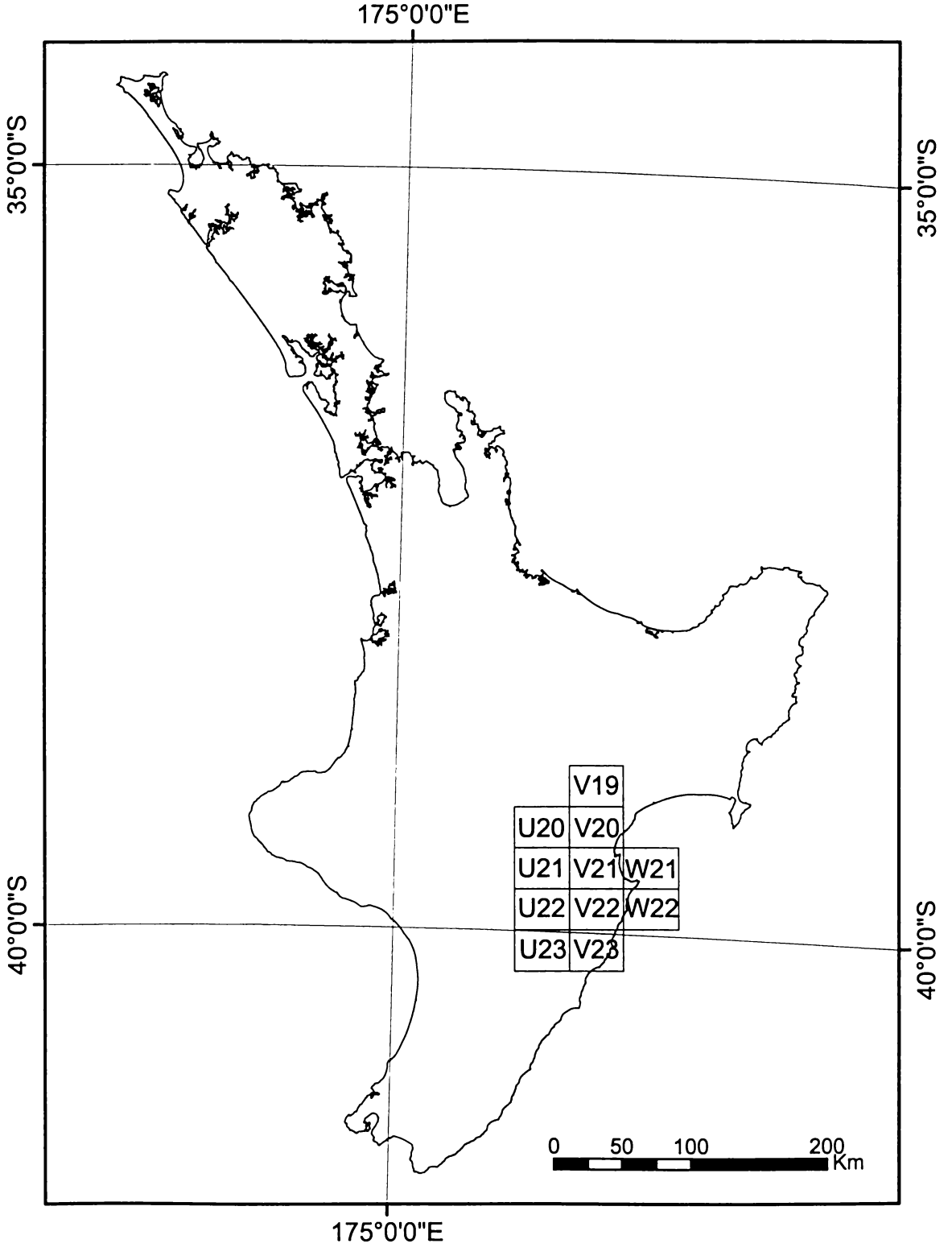

APPENDIX 10.4 – DUNHAM'S (1962) CLASSIFICATION SCHEME

<table>
<tr><td colspan="5">Original components not organically bound during deposition</td><td colspan="3">Original components organically bound during deposition</td></tr>
<tr><td colspan="4">of the allochems, less than 10% > 2 mm diameter</td><td colspan="2">of the allochems, more than 10% >2 mm diameter</td><td colspan="3">Boundstone</td></tr>
<tr><td colspan="3">Contains carbonate mud (particles less than 0.03 mm diameter)</td><td>Mud absent</td><td rowspan="3">Matrix-supported</td><td rowspan="3">Grain-supported</td><td rowspan="3">Organisms acted as baffles</td><td rowspan="3">Organisms encrusting and binding</td><td rowspan="3">Organisms building a rigid framework</td></tr>
<tr><td colspan="2">Mud-supported</td><td rowspan="2" colspan="2">Grain-supported</td></tr>
<tr><td>Less than 10% grains</td><td>More than 10% grains</td></tr>
<tr><td>Mudstone</td><td>Wackestone</td><td>Packstone</td><td>Grainstone</td><td>Floatstone</td><td>Rudstone</td><td>Baffflestone</td><td>Bindstone</td><td>Framestone</td></tr>
</table>

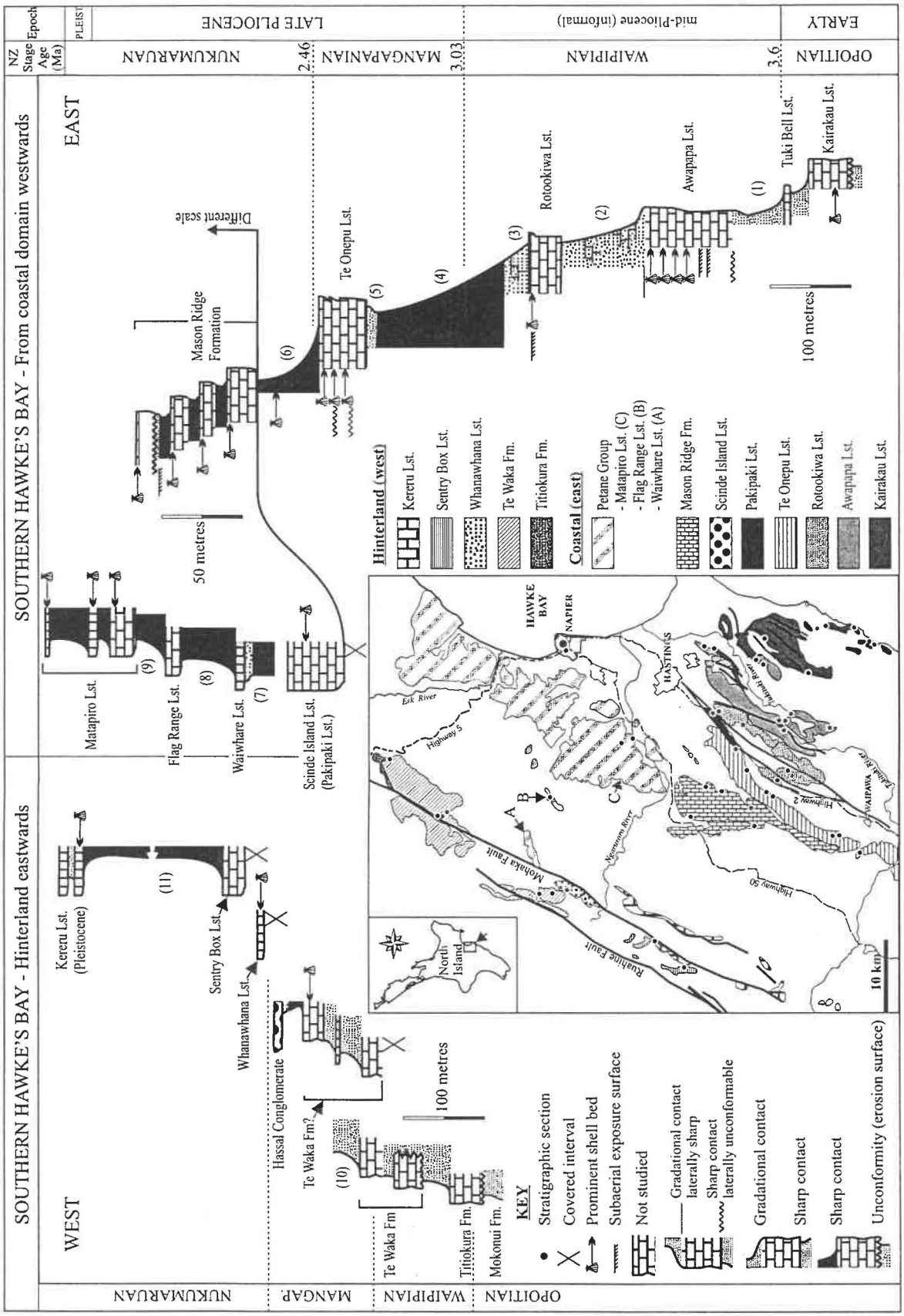

Figure 2- Regional stratigraphic relationships between the various Plio-Pleistocene limestone units in southern Hawke's Bay. The key with limestone names refers to the patterns on the inset geological map enlarged in Figure 1. Interbedded units, typically siliciclastic-dominated, are: (1) Mokopeka Sandstone; (2) Pukekura Calcarenite; (3) Waikareao Calcarenite; (4) Raukawa Mudstone; (5) Argyll Sandstone; (6) Makaretu Mudstone; (7) Willowford Mudstone; (8) Crownthorpe Mudstone; (9) Waitio Mudstone; (10) Pohue Formation (after Bland, 2001); (11) Ohara Mudstone.

Table 1- Summary of facies attributes and their interpretation for the Pliocene sedimentary deposits in southern Hawke's Bay.

Facies and constituents	Physical structures and geometries	Ichnology	Interpretation
Bioclastic Facies			
B1a Fossiliferous rudstone: terrigenous/skeletal matrix (<40% quartz); bivalves (especially oysters, pectinids, brachiopods, bryozoans (encrusting and robust branching), barnacles, rare echinoids, rare gastropods; mud pebbles and occasional bored pebbles	Massive bedding, local trough cross-bedding; medium to thick bedded (<0.5 m up to 4 m); continuous or lensoid	Bioturbation	Shallow water, high energy, intertidal to subtidal *in situ* oyster shell bank and traction emplaced shell beds
B1b Fossiliferous rudstone: silty/muddy matrix (<15% quartz); bivalves (especially oysters), brachiopods, turritellid gastropods, bryozoans (rigid and delicate branching)	Massive bedding, planar cross-bedding; sharp contact with underlying beds; thick bedded (up to 3 m), continuous	Bioturbation	Shallow water, low energy, sheltered subtidal environment oyster shell bank
B1c Pebbly rudstone (fossiliferous): terrigenous/skeletal matrix (<50% quartz) bivalves (especially oysters), pectinids, rare bryozoans (encrusting and robust branching); locally Torlesse pebbles, bored pebbles up to 15 cm in size, locally abundant mud and sand clasts	Massive bedding, flaggy bedding; erosional contact with underlying beds; thick bedded (up to 3 m), continuous or lensoid		Shallow water, high-energy, intertidal, possibly channel-fill deposits
B1d Conglomerate: terrigenous/skeletal matrix, Torlesse boulders and pebbles (average size 2 cm but up to 20 cm), fossiliferous in places	Massive bedding; thick bedded (up to 2 m), tangential and trough cross-bedding in the finer-grained beds	Bioturbation	Fan-delta channel-fill deposits fan delta front
B2a Barnacle-rich grainstone: (<20% quartz); coarse-grained debris; mostly barnacles, oysters, bryozoans and echinoids; locally whole specimens of pectinids and other bivalves; mud clasts in places	Planar cross-stratification, trough cross-bedding, sharp to erosional contact with underlying beds; medium to thick-bedded local mega and so-called giant foresets; continuous, up to 3 m thick sheet-like units	*Thallasinoides* *Skolithos*	Shallow, high energy setting, tidal currents swept sea floor, sand waves
B2b Bioclastic grainstone: (<25% quartz); medium to coarse-grained; barnacles, oysters, various bivalves, bryozoans (encrusting and rigid branching), brachiopods; sand and mud clasts	Planar and tangential cross-stratification, trough cross-bedding; often sharp base; medium-bedded (<1 m); continuous, though laterally discontinuous sheets in places	*Thallasinoides* *Skolithos*	Shallow, high energy setting, tidal or storm-driven currents swept sea floor; sand waves
B3a Bioclastic packstone: (<40% quartz); fine to medium-grained; barnacles, oysters, pectinids, brachiopods (common in places), bryozoans (rigid and delicate branching), rare echinoids; mud clasts	Trough and sigmoidal cross-bedding; ripple structures locally, planar and tangential cross-laminations; local coarse skeletal lenses and common interlayered mudstone sheet-like units (<0.5 m)	Bioturbation *Ophiomorpha* *Planolites*	Moderate energy setting, below fair-weather and above storm wave base (equivalent to mid-shelf deposits)
B3b Bioclastic packstone and wackestone: (<20% quartz); medium to coarse-grained; barnacles, oysters, pectinids, brachiopods, encrusting bryozoans, serpulids, echinoids, red algae, common benthic foraminifers; micritization	Planar and tangential cross-stratification, local small-scale trough and sigmoidal structures; common tabular bedding	Bioturbation *Skolithos*	Moderate energy, shallow water environment, close to fair-weather wave base; embayment
Mixed Facies			
M1 Alternating grainstone and packstone: (<30% quartz); fine to coarse-grained; especially barnacles and oysters, brachiopods, bryozoans (robust and delicate branching), rare echinoids, rare serpulids, pectinids; mud clasts	Trough cross-bedding, sigmoidal and convolute cross-laminations, minor HCS; skeletal lag lenses; sharp-based grainstone; mud layers; laterally discontinuous sheets; thin to medium-bedded (up to 0.25 m)	*Ophiomorpha* *Planolites* rare *Scolicia*	Contrasting conditions; between fair-weather and storm wave base sand dunes
M2 Interbedded grainstone and terrigenous packstone: (<40% quartz); fine to medium-grained; whole barnacles, oysters, brachiopods (abundant in places), bryozoans (delicate and rigid branching, local foliaceous), oysters, echinoids, pectinids, brachiopods; mud clasts	Planar and sigmoidal cross-laminations, HCS; laterally discontinuous, lensoid, sharp-based grainstone; tempestites, thin skeletal lag concentrates, interbedded mudstone lenses; horizontally-bedded sheet units	Dense bioturbation *Ophiomorpha* *Planolites* *Scolicia*	Between fair-weather and storm wave base sand dunes
M3 Interbedded terrigenous packstone and calcareous sandstone: (<50% quartz); lutite-sized debris; barnacles, bryozoans (delicate branching, foliaceous and fenestrate), oysters, echinoids, pectinids, brachiopods; mud clasts	Planar laminations, minor sigmoidal and convolute cross-laminations, ripple structures thin horizontally-bedded discontinuous sheets (5-15 cm); interbedded mudstone lenses	Dense bioturbation *Planolites* *Chondrites*	Moderate to low energy; close to lower storm wave base
Siliciclastic Facies			
S1 Calcareous sandstone: (<50% quartz); lutite-sized debris; bryozoans, Oysters, other bivalves including pectinids	Ripple and convolute structures, horizontal laminations, interbedded mudstone layers, massive to relict horizontally-bedded	Dense bioturbation *Chondrites* *Ophiomorpha*	Moderate to low energy; well-oxygenated; above storm wave base
S2 Siltstone: skeletal hash; rare bryozoans, oysters, pectinids, local Turritellid gastropods	Associated with thin mudstone lenses; medium-bedded (up to 1 m)	*Planolites* *Chondrites*	Quiet waters, more distal setting (equivalent outer shelf)
S3 Mudstone: yellow-grey to blue-grey; uncommon macrofauna (gastropods pectinids)	Lensoid to massive	*Chondrites*	Quiet waters (equivalent outer shelf)

Table 2- Classification of a range of constructive (CD) to destructive (DD) specific diagenetic suites based on petrographic properties of pre-compaction diagenetic features in Te Aute limestones.

Specific diagenetic suite	Facies	Chronological occurrence of diagenetic processes	Interpretation
CD^1 Constructive	Medium- to coarse-grained Clast-supported	- Skeletal grains are variably abraded - Macroboring of shells occurs occasionally; microboring is present to common, microbores penetrate deeply into bioclasts; micritization poor to moderate - Unilaminar encrusting bryozoans occasionally evident - Authigenic glauconite forms but is scattered, moderately evolved (pale green) - Dissolution of aragonite allochems predating marine cements occurs rarely - Internal sediments commonly pre-date and post-date acicular inclusion-rich isopachous cements (up to 100 μm thick). Internal sediments may be microbioclastic or micritic, are geopetally distributed in interparticle pores, but seldom laminated - *In* situ precipitated peloidal micrite (<50 μm in diameter, spherical, nucleus-free peloids)	Near sea floor, marine phreatic environment Marine waters undersaturated enough to dissolve aragonite near sea floor, marine phreatic environment Microbially induced, marine phreatic environment
M^1 Mixed	Medium- to coarse-grained Clast-supported	Same events as in CD^1, but followed by meteoric diagenesis. The capping surface of the sequence is subaerially exposed; neomorphism of metastable mineralogies is the dominant process - Dissolution of skeletal allochems (moldic voids and collapse of weakened shells), the outer margin of acicular cements may be corroded, and cements may be neomorphosed into scalenohedral crystal rims that exhibit internal ghosts of elongate inclusions - Drusy to mosaic clear spar	Phreatic meteoric environment undersaturated waters with respect to $CaCO_3$ percolate from the capping unconformity
M^2 Mixed	Medium- to coarse-grained Matrix-supported	Same events as in M^1, but clast-supported host of CD^1 becomes matrix-supported; clear spar cements are rare; micritic crust may form (iron stained or not); yellowish bioclast- to microquartz-rich homogenous to laminated micrite infiltrates	Phreatic and possibly vadose meteoric environment
CD^2 Constructive	Coarse- to very coarse-grained Matrix-supported	- Skeletal grains are poorly to moderately abraded - Macroboring is common to abundant; microboring is common - Common, well preserved encrusters such as red algae and uni- and multi-laminar bryozoans - Occasional thin isopachous acicular cements - Syndepositional homogenous micrite; *in situ* precipitated peloidal micrite - Matrix may be burrowed; burrows are filled with another generation of internal sediment - Induration of micrite may occur at this stage (seldom)	Near sea floor, marine environment
M^3 Mixed	Coarse- to very coarse-grained Matrix-supported	Same events as in CD^2, but followed by processes related to meteoric diagenesis - Occasional fracturing and micro-brecciation of host rock; rare mud cracks - Dissolution of skeletal allochems; micritic crust (iron-stained or not); yellowish bioclast- to microquartz-rich homogenous to laminated micrite infiltrates - Blocky to mosaic clear spar	Phreatic and possibly vadose meteoric environment
CD^3 Constructive	Medium-grained Clast- to matrix-supported	- Skeletal grains are moderately to well abraded; moderately preserved red algae and bryozoan encrusters - Homogenous syndepositional micrite pre-dated and post-dated by micritization (densely microbored and subsequently micritized margin of shell fragments is up to 200 μm thick) - Induration of micrite may occur at this stage	Near sea floor, marine phreatic environment
CD^4 Constructive	Medium- to coarse-grained Matrix-supported	- Moderately abraded grains - Moderately preserved encrusters (red algae, bryozoans); rare authigenic glauconite - Micritic crust possible; homogenous syndepositional micrite irregularly distributed in pore space (digitations toward pore centre and menisci) - Neomorphism of skeletal allochems may occur (relicts of microstructures common); precipitation of blocky to mosaic clear spar cement may also occur	Vadose marine (though phreatic marine possible) to vadose meteoric environment
DD^1 Destructive	Fine- to medium-grained Clast- to matrix-supported	- Strongly abraded skeletal grains (very well rounded); intensively microbored (multigeneration) - Evolved authigenic glauconite (deep green, brown) and iron oxides fill most intraparticle pores - Uncommon acicular inclusion-rich cement; dissolution of aragonitic shells may also occur - Common intrinsic homogenous micritic sediment seals the sequence	"Starved" sea floor, prolonged exposure of grains on the sea floor
DD^2 Destructive	Fine- to medium-grained Clast-supported	- Moderately to well abraded grains - Encrusting by uni- and multi-laminar bryozoans possible; common microboring - Common thin acicular isopachous extrinsic cement; rare to common authigenic glauconite	Marine phreatic environment
DD^3 Destructive	Fine- to medium-grained Matrix-supported	- Poorly to moderately abraded grains - Microboring is common; authigenic glauconite is common - Extrinsic thin (<50 μm) acicular cement is possible - Homogenous syndepositional micrite - Burrowing common; burrows are filled with clast-supported internal sediment (microquartz, planktic foraminifers, etc.)	Marine phreatic environment